UNIVERSITY OF DEBRECEN
Faculty of Engineering
Department of Mechanical Engineering

PROCEEDINGS OF THE 4th INTERNATIONAL SCIENTIFIC CONFERENCE ON ADVANCES IN MECHANICAL ENGINEERING (ISCAME 2016)

13-15 October, 2016

Debrecen, Hungary

organized by

Department of Mechanical Engineering
Faculty of Engineering, University of Debrecen

and

Working Commission in Mechanical Engineering
Specialized Committee in Engineering
Regional Committee in Debrecen, Hungarian Academy of Sciences

PROCEEDINGS OF THE
4th INTERNATIONAL SCIENTIFIC CONFERENCE ON ADVANCES IN MECHANICAL ENGINEERING

Edited by Sándor BODZÁS PhD
Tamás MANKOVITS PhD

Technical editors Sándor PÁLINKÁS PhD
Sándor HAJDU
Dávid HURI
Péter BALSA
Tamás Antal VARGA

Publisher: Department of Mechanical Engineering
Faculty of Engineering
University of Debrecen
2-4 Ótemető str. Debrecen, Hungary
Phone: +36 52 415 155
Web page: www.eng.unideb.hu/userdir/gepesz

ISBN 978-963-473-944-9

PROCEEDINGS

4th INTERNATIONAL SCIENTIFIC CONFERENCE ON ADVANCES IN MECHANICAL ENGINEERING (ISCAME 2016)

13-15 October, 2016

Debrecen, Hungary

PROCEEDINGS OF THE 4th INTERNATIONAL SCIENTIFIC CONFERENCE ON ADVANCES IN MECHANICAL ENGINEERING

CONTENTS

INTERNATIONAL SCIENTIFIC CONFERENCE ON ADVANCES IN MECHANICAL ENGINEERING

13-15 October 2016, Debrecen, Hungary

EXPERIMENTAL, MODELLING AND APPLICATION OF TIMBER BEAMS REINFORCED WITH CARBON FIBRE

[1]ANDOR Krisztián PhD, [2]LENGYEL András PhD, [3]KARÁCSONYI Zsolt PhD, [4]BELLOVICS Bertalan

[1]Institute for Applied Mechanics and Structures, University of West Hungary, H-9400 Sopron, Bajcsy-Zsilinszky u. 4., Hungary
E-mail: andor.krisztian@nyme.hu
[2]Department of Structural Mechanics, Budapest University of Technology and Economics, H-1521 Budapest, Műegyetem rkp. 3., Hungary
E-mail: lengyel@eik.bme.hu
[3]Institute for Applied Mechanics and Structures, University of West Hungary, H-9400 Sopron, Bajcsy-Zsilinszky u. 4., Hungary
E-mail: karacsonyi.zsolt@nyme.hu
[4]Institute for Applied Mechanics and Structures, University of West Hungary, H-9400 Sopron, Bajcsy-Zsilinszky u. 4., Hungary
E-mail: bertalan.bellovics@student.nyme.hu

Abstract
Enhancement of timber beams with fibre reinforced materials gained momentum in the last few decades producing a wide range of materials, techniques and modelling methods. Experiments show that the potential improvement of structural behaviour is greatly affected by the type of reinforcement, wood species, etc. In this study a series of experiments were conducted on sawn Norway spruce beams reinforced with various amounts of CFRP sheets (carbon fibre reinforced plastic) followed by a statistical analysis. A moderate increase of load-bearing capacity and ductility and a small increase of elastic stiffness can be achieved. The FEM model of the reinforced timber beam were made, with results showing high correspondence with experimental results. We can use our experiences in the practice well. Timber beams in wooden floors we examines and the control measurements of the practical application support the results of the laboratory measures.

Keywords: *CFRP, reinforced timber beam, modelling of the reinforcing by CFRP; application of the CFRP on built-in wood construction*

1. INTRODUCTION

Application of fibre reinforced plastic materials for reinforcement in structural engineering has now a history of several decades, however, reinforcing timber structures in this way has come in focus in the last twenty years. Use of FRP materials proved a promising approach in various engineering problems, e.g. enhancing structural performance of sawn timber beams or glued-laminated (glulam) beams, and also for repairing or strengthening old historic beams in existing structures or bridges. An important aspect of the behaviour of the composite material is the bond between wood and the fibre reinforced plastic. Investigation started several years ago. The objective of our research was to examine the composite structure of a timber beam made of spruce, which is commonly available worldwide, and flat fibre reinforced plastic lamellae fitted to the tensile side, an arrangement which is easily applicable in various mechanical problems. The species chosen for the experiments is Picea abies (Norway spruce) native to Europe while other species of the genus Picea are found in

several regions worldwide, and the reinforcement is composed of several amount of carbon fibre fabric embedded in epoxy resin. This research aims to determine the increase of the flexural capacity and the stiffness of the composite beams when reinforced with CFRP through a number of experiments and thus to verify the efficiency of reinforcement. The experimental results are supported by example of modelling and practice object-lesson.

2. MEASUREMENTS IN LABORATORY – MATERIALS, MEASUREMENTS SET-UP, EXPERIMENT RESULTS

Timber for the beams was sawn of Norway spruce (Picea abies) in rectangular solid cross-sections of 95 mm-by-95 mm with random orientation with respect to growth-rings (i.e. R and T directions were not aligned with the contour of the cross-section). All specimens were dried to moisture content of 12%. Via visual inspection and non-destructive tests it was ensured that the test specimens had no major visible defects or damage, such as drying splits, biological deterioration, etc. Presence of knots was allowed as a natural feature of the species. Fibre reinforcements were prepared in situ using unidirectional (99% of fibres with respect to surface in warp, 1% in weft) carbon fibre fabric of 300 g/m2 weight and a two-component epoxy resin applied manually in approximately 0.5 kg/m2 amount. The epoxy resin was applied on the surface in the prescribed amount following manufacturer's instruction using rollers. The fabric was then placed and impregnated with resin completely manually such that the strengthening took place simultaneously with the bonding to the wood.

Four-point bending tests of a series of specimens have been prepared with supports of 1800 mm span. The geometric parameters of the beams were set to comply with the European standards regarding testing. The experiments were conducted in a laboratory accredited for timber structural testing using a standard MTS testing device with capacity of 250 kN. Load was applied by a single actuator and transmitted to the test specimens at two points via an intermediate beam of 600 mm span centrally aligned.

A total of forty-four specimens were prepared, of which eight without any reinforcement and thirty-six with various amounts of CFRP fabric. Twenty and eight specimens were fitted with a single and a double layer of fabric on the entire width of cross-section, respectively, while the remaining eight specimens were reinforced with a narrower strip (50 mm) of single layer CFRP fabric centrally aligned with respect to the vertical symmetry plane. In all cases the CFRP fabric was glued to the tensile face of the beam at full length and then were cut through just near the supports. The four types of test specimens are denoted by S0, S1, S2, and SN, respectively. A summary of the data and results are shown in Table 1.

The density of the wood of all specimens were measured giving an average of 476 kg/m^3 with relative standard deviation of 8.5%. The data were grouped and analysed with respect to the division into groups S0, S1, S2, and SN, yielding averages and relative standard deviations as 456 kg/m^3 (5.4%), 495 kg/m^3 (9.2%), 465 kg/m^3 (7.5%), and 459 kg/m^3 (5.6%), respectively. The data are in correspondence with usual values associated with the species.

Table 1 Results of the measurement – summary of ultimate load

Test group and number of specimens	Reinforcement and amount	Ultimate load (kN)	Increment (%)	Standard deviations	
				(kN)	(%)
S0 (8 PCs)	None	23,220		7,696	33,14
S1 (20 PCs)	CFRP, 1 layer, full width	30,527	+ 31,47	5,673	18,58
S2 (8 PCs)	CFRP, 2 layers, full width	30,959	+ 33,33	3,831	12,37
SN (8 PCs)	CFRP, 1 layer, 50 mm width	27,448	+ 18,21	5,933	21,62

Table 2 Results of the measurement – summary of ultimate load

Test group and number of specimens	Reinforcement and amount	Max. deflection (mm)	Increment (%)	Standard deviations	
				(kN)	(%)
S0 (8 PCs)	None	41,312		15,438	37,37
S1 (20 PCs)	CFRP, 1 layer, full width	49,106	+ 18,87	11,019	22,44
S2 (8 PCs)	CFRP, 2 layers, full width	53,378	+ 29,21	12,999	24,35
SN (8 PCs)	CFRP, 1 layer, 50 mm width	44,857	+ 8,58	8,408	18,74

3. MODELLING OF THE REINFORCED TIMBER BEAM

By the laboratory measurement we do not have satisfactory information about the internal stress distribution, because according to the results, there is no balance between the inner and the outer forces. Therefore, it was necessary to finite element modeling of the CFRP-reinforced timber beam *(Figure 1)*. The modeling has two basic steps: building the FEM model, and running the simulation.

The building of FEM model has the following steps:

- *Choosing element type*: to the modeling the ANSYS general FEM software was used. The ANSYS applies different finite element types depending on the model type. To the timber beams, and the CFRP-reinforced timber beams modeling the most useful element type is the

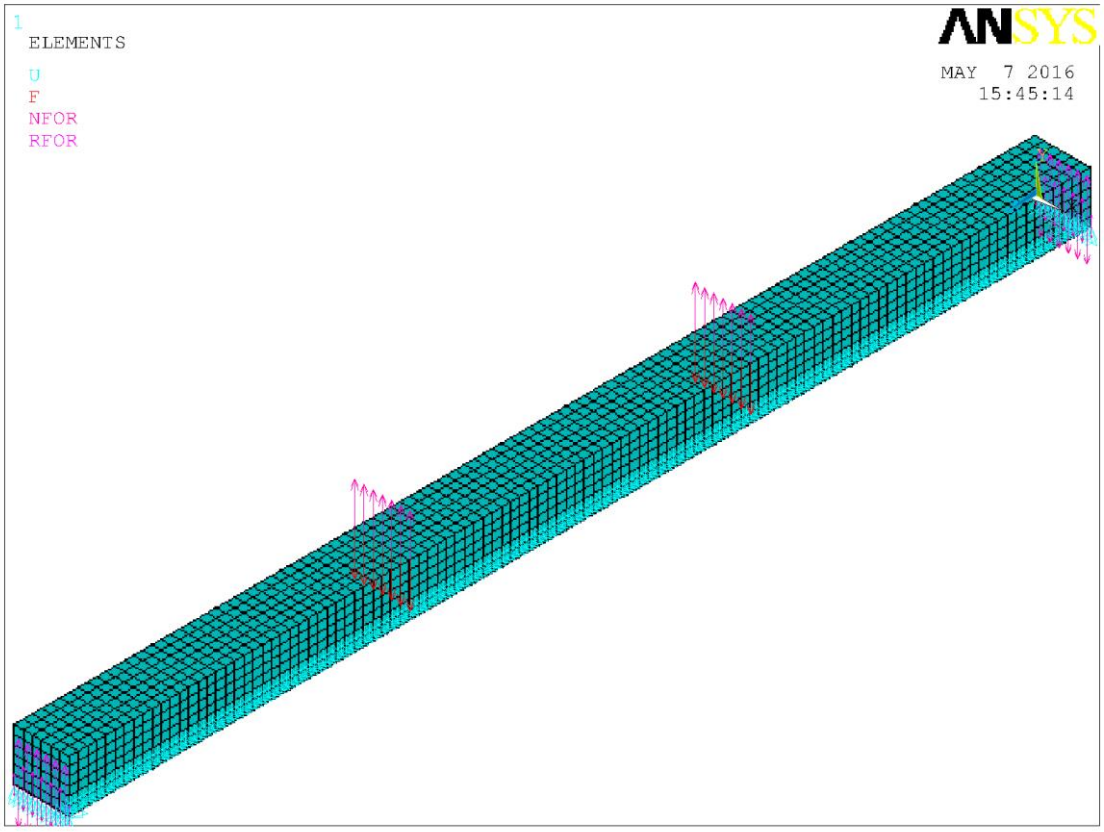

Figure 1 Finished FEM model

- SOLID95 *(Figure 2)*. It's a cuboid with 20 nodes which is able to model internal stresses and strains.
- *Defining material models*: we have to define the strength model and the parameters of the strength model. The timber has orthotropic material model so we must define 9 independent material parameters. These are the moduli of elasticity on 3 axes and Poisson-ratios and shear moduli on 3 plains. In the case of the carbon fibre we use an elasticity modulus on longitudinal axis, and a Poisson-ratio on perpendicular plain.
- *Making geometry*: that is based on the various model shape which was used to the laboratory measurements.
- *Generating mesh*: in this step the program divides the 3D model for finite elements. The density of mesh is regulated if we are defining the edge length of finite element (in this situation this is a cube). The density is increased until the simulation results show little difference.
- *Defining loads*: with load definition we apply displacements and forces to the model like in the MTS testing. The forces are defined as the ultimate force, where the failure occurred in the laboratory.

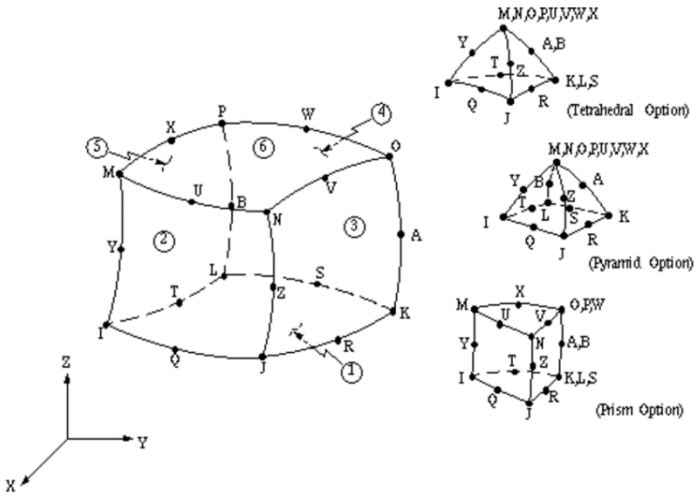

Figure 1 SOLID 95 element

After building the FEM model the results of simulation are compared with the laboratory results and manual calculating results.

Table 3

ANSYS	LABORATORY	CONTROL CALCULATION
41,97 N/mm^2	42,22 N/mm^2	42,12 N/mm^2

As see on *Table 3.* the differences between the dates are not significant. The efficiency of FEM model is proved by comparing the strain distribution which are obtained by the FEM simulation and laboratory measurements *(Graph 1).*

Garph 1

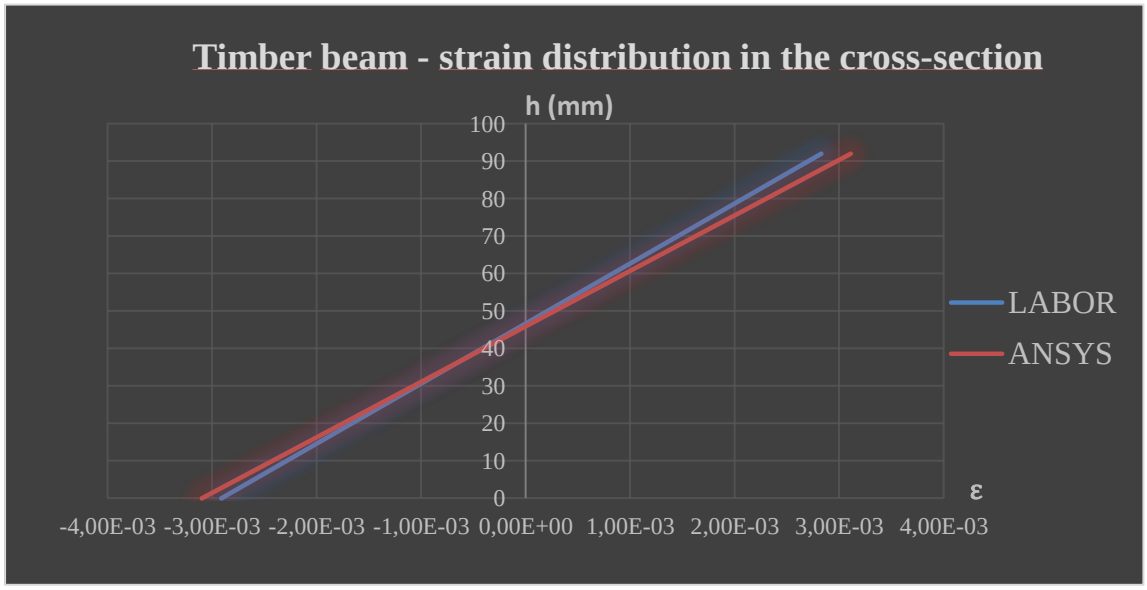

Graph 1. shows that the differences are not significant as well, therefore the model works for the real case of the timber beam.
The main question is the behavior of the CFRP reinforced FEM model. After running the simulation we get the stress distribution in the cross section *(Figure 3.)*

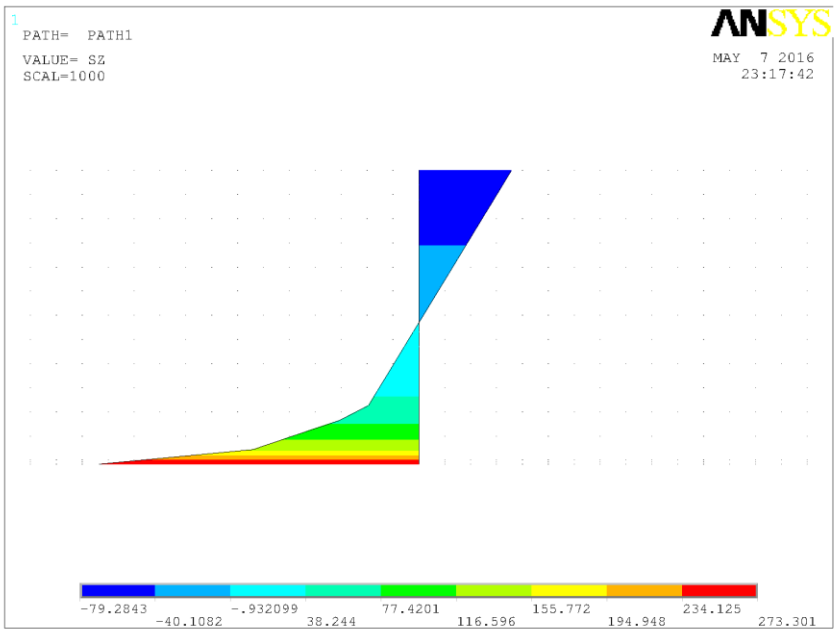

Figure 2 Stress distribution of CFRP reinforced timber beams in the cross section

Graph 2

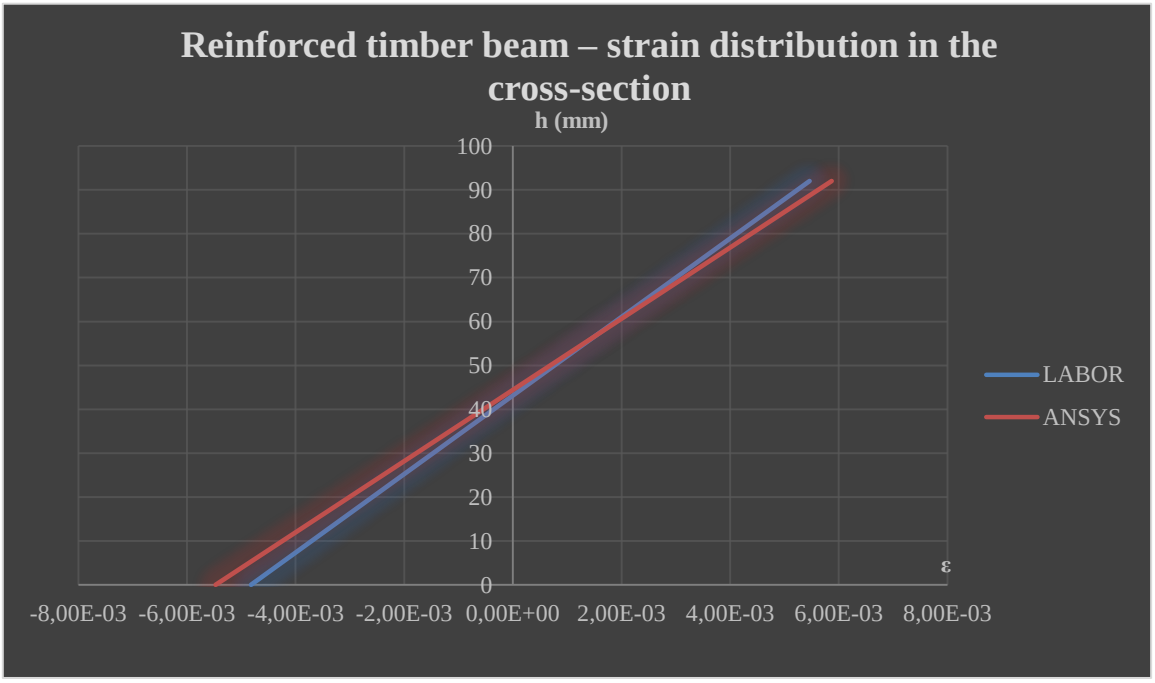

The results show that the carbon fiber takes on a large part of the stresses. This corresponds to the reality. Here the strain data are also compared (*Graph 2)*. Note that the difference is minimal. This statement is valid for the majority of strain data.
There were some data where there were significant differences. In the laboratory testing was used strain gauges. The strain gauges positioning might be problematic, mainly because of the gluing. This problem perhaps generated some false data. But based on the comparison of strain data we determined that the CFRP reinforced model works as well. Owing to the finite element model, we could analyze the internal stresses and strains. With the strain gauge this was not possible, because the gauges are not able to measure in 3D. The stress analysis showed that the carbon fabric had the largest stress. Knowing the stress distribution, in the next phase of the research we can make a calculation method for the carbon reinforced wood constructions.

4. APPLICATION OF THE CARBON FIBRE REINFORCING IN CASE BUILT-IN WOOD CONSTRUCTION

There are three main problems with wooden floor structures of old buildings.

1. Damaged structural material: damages due to insects or funghi decrease the strength of wood
2. Insufficient capacity: Cross-section dimensions are not sufficient to carry loads arising from the new functions of the building, fails for load-bearing capacity.
3. Insufficient stiffness: floor structure responds with large vibrations to dynamic loading, fails for serviceability criteria.

Various techniques are in use currently in the renovation of old timber structures:

1. New reinforced concrete structure over the old timber floor: The old floor structure is kept as a formwork or for practical purposes, e.g. support for suspended ceiling. It is regarded as a waste since it does not utilize the capacity of the old floor structure.
2. Combined timber and reinforced concrete floor system: A reinforce concrete slab made in situ on top of the old timber floor. The interaction of the two structures is secured by bolts.

Reinforcement with reinforced concrete generates 3 main problems:

- The reinforced concrete slab adds a significant extra weight to the floor.
- Concrete is one the most environmentally hazardous construction material. During cement production clinker minerals are ground at 1500 degrees of temperature.
- Risk of biological deterioration due to wet technology. Wet timber is a suitable medium for wood-destroying funghi.

Reinforcement with carbon fibre composites:

The combination of FRP materials with timber structures is not yet well developed, mainly because of the complex, inhomogeneous structure of wood. Technological application of CFRP reinforcement for an old existing building was performed as follows.
The renovation of an old industrial building is designed to function as an office block and we wished to improve the behaviour of the structure by the application CFRP reinforcement. The area of a floor in the building is approximately 300 square meters. It consists of a large part in the front and a smaller one in the rear. The floor is supported by a longitudinal main girder and a number of transverse beams. The building has three storeys. The upper two floors are made of timber.

The exploration was done using a non-destructive test method called FAKOPP. The non-destructive testing was performed on the structural elements of the building. The device measures the modulus of elasticity by the propagation of sound in the material. A tapping on the transmitter pin of the device generates a sound, which is detected at the receiving pin. The elapsed time is measured and the velocity of the sound is determined, which is proportional to the modulus of elasticity of the material. The aim of the test is to determine the modulus of elasticity and the flexural strength of the selected beams. There is a close relationship between the modulus of elasticity and the dynamic modulus of elasticity.

Figure 4 Non-destructive method FAKOPP

The results have shown that the beams in the floor structure fail to satisfy strength and serviceability criteria. In a part of the building the application of CFRP reinforcement seemed to be an ideal solution.
Analysis of timber beams reinforced with CFRP was performed to verify the reinforcement provided by the CFRP fabric. The details of the analysis are as follows.

- Timber gained from demolition: During the renovation a considerable amount of timber was left. A part of them was reinforced by us with CFRP, and the other part was left as it was. The beams formed three groups by their dimensions.
- 4-point bending: loading at two points at the thirds of the span.
- E modulus without CFRP: Beams were loaded up to 5kN, deflections were measured by a videoextensometer, and the modulus of elasticity was computed.
- Determination of E modulus with CFRP: Beams were fitted with CFRP fabric on the tensile face, loaded up to 5kN, deflections were measured by a videoextensometer, and the modulus of elasticity was computed.

Table 4 Summary of samples gained from demolition

Series	Span [mm]	Width [mm]	Height [mm]	Load span [mm]	Number of specimens	Reinforced
A	1800	157 (6%)	89 (5%)	600	11	6
B	2500	138 (2%)	138 (2%)	833	8	4
C	2900	206 (1%)	163 (1%)	967	10	5

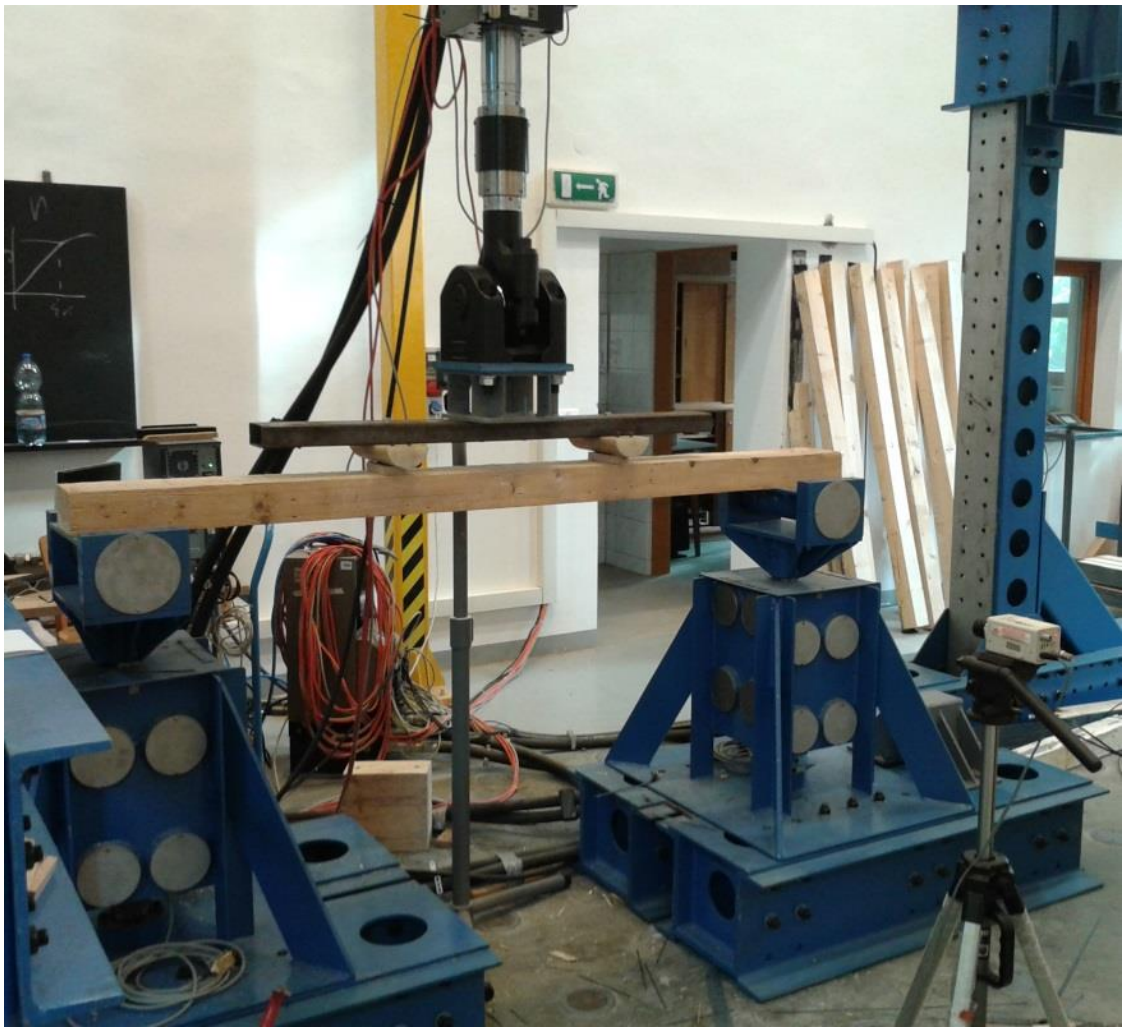

Figure 5 4 points bending test (MTS)

Examination of the strength of the samples showed more than 50% increase in load-bearing capacity as well as increase of stiffness shown in the table below.

Table 5 Increase of stiffness

A			B			C		
w/o CFRP	w/ CFRP		w/o CFRP	w/ CFRP	incr.	w/o CFRP	w/ CFRP	incr.
6.844			5.953			10.042		
8.559			8.240			7.832		
13.619			4.885			7.092		
8.173			8.060			6.609		
7.150						10.443		
8.427	9.209	+9.27%	9.821	10.052	+2.35%	7.213	7.573	+5.00%
12.762	13.440	+5.32%	8.769	8.861	+1.05%	8.314	9.471	+13.91%
12.298	12.140	-1.28%	8.963	9.559	+6.64%	9.228	9.616	+4.20%
9.625	10.030	+4.20%	10.165	11.285	+11.02%	9.446	10.887	+15.26%
10.247	12.092	+18.01%				9.699	10.191	+5.08%
8.159	9.147	+12.12%						
9.624		*+7.94%*	*8.107*		*+5.27%*	*8.592*		*+8.69%*
24.15%			*22.54%*			*15.82%*		

The increase of stiffness was also verified by in situ measurements of the deflection. We examined the deflection of the floor beams in the building by performing a test loading of the completed building. With this examination we determined the deflections due to loading with an accuracy of 0.01mm and scaled them to the design limit deflections. The values remained under the acceptable limits in the case of the reinforcement.

Figure 6 Old timber beams before and after reinforcement

CONCLUSIONS

We can conclude that the CFRP reinforcement is a viable approach, because (1) it provides material efficiency, (2) easy applicability, and (3) improved behaviour. We reached an increase in stiffness ranging between 0% and 18% with an average of 6-8%. It is also an important observation that inhomogeneity of wood causes variations in elastic moduli.

REFERENCES

[1] Malkus, D.S.: *Finite Element with Penalties in Nonlinear Elasticity*. International Journal for Numerical Methods in Engineering, 16, 121-136., 1980.
[2] Swanson, S., Christensen, L., Ensing, M.: *Large Deformation Finite Element Calculations for Slightly Compressible Hyperelastic Materials*. Computers & Structures, 21(1-2), 81-88., 1985.
[3] Zienkiewicz, O.C, Qu, S., Taylor, R.L., Nakazawa, S.: *The Patch Test for Mixed Formulations*. International Journal for Numerical Methods in Engineering, 23, 1873-1883., 1986.
[4] Krisztián Andor, András Lengyel, Rudolf Polgár, Tamás Fodor, Zsolt Karácsonyi: *Experimental and statistical analysis of spruce timber beams reinforced with CFRP fabric* CONSTRUCTION AND BUILDING MATERIALS 99: pp. 200-207. (2015) (ISSN: 0950-0618)

THIN-LAYER DRYING CHARACTERISTICS OF PLUM DURING HYBRID- AND FREEZE-DRYING

[1]ANTAL Tamás PhD, [2]SIKOLYA László PhD

[1]University of Nyíregyháza, Institute of Engineering and Agricultural Sciences, Nyíregyháza, HU
E-mail: antal.tamas@nye.hu
[2]University of Nyíregyháza, Institute of Engineering and Agricultural Sciences, Nyíregyháza, HU
E-mail: sikolya.laszlo@nye.hu

Abstract
The plum slices were dried under mid-infrared- (MIR), freeze- (FD), and intermittent mid-infrared & freeze (MIR-FD) conditions at 40, 50 and 60°C in order to determine the drying characteristics and energy consumption of drying systems. The moisture ratios changes during the drying time were compared by four different mathematical models – Page, Henderson & Pabis, third-degree polynomial, Sigmoid – and evaluated by two statistical criteria for example coefficient of determination (R^2) and root mean square error (RMSE). The results showed that operational time and energy consumption decreased significantly at MIR-FD. Considering the energy factors and product appearance, the optimum drying condition was at MIR-FD with drying temperature of 50°C. The Page and third-degree polynomial models gave the best results and showed a good agreement with experimental data of drying.

Keywords: *combined drying, freeze drying, thin-layer drying model, energy uptake.*

1. INTRODUCTION

Freeze-drying or lyophilization is a dehydration process in which water is removed by sublimation of ice from frozen biomaterials. Freeze-drying, although costly method, is the best way for drying foods with regards to its quality. Preservation of most of the initial raw material properties such as shape, appearance, taste, color, flavor, texture, biological activity etc. makes it one of the best dehydration methods [1].
Drying is the most energy intensive process in food industry. Therefore, new drying techniques – e.g. hybrid drying – must be designed and studied to minimize the energy cost in drying process [2]. Infrared drying is well established in food. The infrared drier heats the sample by transmission of electromagnetic radiation [3]. The infrared drying has many advantages, such as: decreased drying time, high energy efficiency, high quality finished products, and uniform temperature in the product [4].
The aim of this paper was to evaluate the effect of different drying technics, i.e. mid-infrared-, mid-infrared-freeze, freeze drying on drying characteristics and energy consumption.

2. METHODS

2.1. Moisture content

Prior to the drying experiment, the plum (*Prunus domestica* L.) was washed and damaged fruits were discarded. Afterwards, the plums were manually cut into slices having dimensions of 1 cm length, 1 cm width and 0.5 cm thickness using a sharp stainless steel knife. Each drying condition

used a 50 g sample of plum for the experiment. The samples weight was determined by means of an electronic balance (JKH-500, Jadever Co., New Taipei, Taiwan). Ten portions were used in every drying process.
The oven method was used to determine the initial moisture content. A sample of about 10 g of plum was taken and dehydrated in an experimental dryer (model LP306, LaborMIM, Budapest, Hungary) at 105°C for 10 h. The initial moisture content of the plum sample was 4.376 g water/g dry matter expressed in dry basis (d.b.). The plum was stored at 5°C in a refrigerator until used.

2.2. Drying experiments

The samples were spread on drying trays in a single layer and dried in infrared- and freeze dryers. The drying process would not stop until the equilibrium moisture content (M_e) was achieved. All the drying experiments were replicated three times and the average values reported. The dehydrated samples were packed immediately into nylon bags after drying.
The following three different drying programs were implemented in the course of this research:

1. MIR – pure mid-infrared drying under the total process with drying temperature (dt) of 40-60°C.
2. FD – pure freeze drying under the total process.
3. MIR-FD or hybrid – intermittent mid-infrared pre- (dt=40-60°C) and freeze finish-drying.

Mid-infrared drying (MIR)
The medium infrared drying (wavelength of radiation: 1-4 μm) experiments were performed in a pilot infrared dryer (model Precisa, Precisa Instruments AG, Dietikon, Switzerland) (*Figure 1*). In the drying chamber, a pair of quartz glass emitters (220 V, maximum power of per lamp 300 W) was positioned above the sample support. The drying temperature was set in keyboard of the equipment as 40, 50 and 60°C in each experiment. The drying temperature which was set in keyboard section was converted suitable radiation power (3-5.5 kW/m^2) values in control unit of the dryer.
The mass of the plum was measured by a digital electronic balance (a precision of ± 0.1 g, model Precisa, Precisa Instruments AG, Dietikon, Switzerland) at interval of 1 min during the drying test. The temperature of the sample and drying air was measured continuously using type-K thermocouples (Testo GmbH, Lenzkirch, Germany).

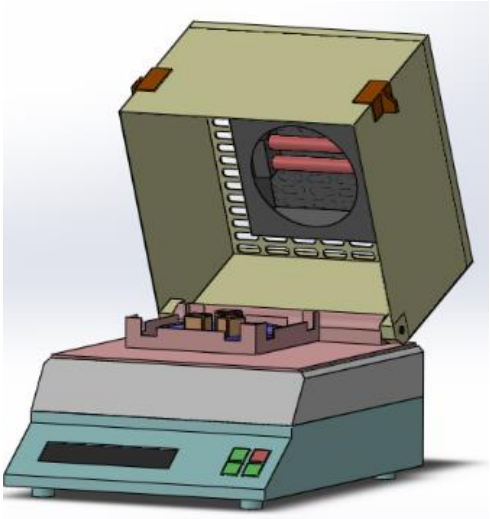

Figure 1 Schematic view of the infrared dryer

Freeze drying (FD)

For vacuum-freeze drying, a laboratory-scale freeze dryer (model Armfield FT33, Armfield LTD, Ringwood, England) was used (*Figure 2*). The drying was carried out by maintaining the chamber pressure at 80-90 Pa, chamber temperature at 20°C and condenser temperature at -45°C for a period 25h. At an interval of 1h, the mass of samples were recorded to determine the moisture removal from material. The weight loss of the samples was followed by a data logger (ES-138, Emalog, Budapest, Hungary) and a RS-232 attached to a PC computer, acquired the data readings from platform cell (PAB-01, Emalog, Budapest, Hungary), which is placed within the sample chamber.

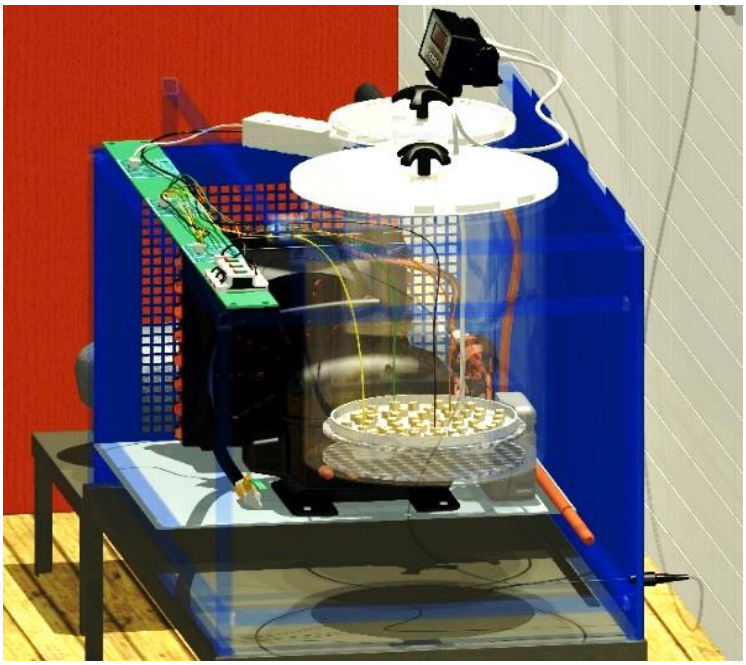

Figure 2 X-ray of Laboratory-scale freeze dryer

Hybrid dehydration (MIR-FD)

A hybrid drying process consisting of mid-infrared drying (40, 50 and 60°C) followed by freeze-drying was carried out. Different trials consisted of a decrease in the mid-infrared stage (5 and 4 min) followed by increase in the freeze-drying stage (17, 18; 15, 17 and 12, 14 h).

2.3. Mathematical models

The drying curves were fitted with four different commonly used thin-layer empirical models given in *Table 1*.

Table 1 Thin-layer mathematical models applied to the drying kinetics

Name of model	Model equation	Fitting of drying curve	Reference
Page	$MR = \exp\left(-kt^n\right)$	MIR	[5]
Henderson and Pabis	$MR = a\exp\left(-kt\right)$	MIR	[6]
Sigmoid	$MR = a + \frac{b}{1+e^{k\cdot(t-c)}}$	FD and MIR-FD	[7]
Third-degree polynomial	$MR = at^3+bt^2+ct+1$	FD and MIR-FD	[8]

The moisture ratio (MR) of the plum samples during drying was calculated using the following equation (1):

$$MR = \frac{M - M_e}{M_0 - M_e} \quad , \tag{1}$$

MR is the moisture ratio, *M* is the moisture content (g water/g dry matter), M_e is the equilibrium moisture content (g water/g dry matter) and M_0 is the initial moisture content (g water/g dry matter). The sample moisture content – *M* – was calculated on a dry basis (d.b.) according to Eq. (2):

$$M = \frac{W_t - W_k}{W_k}, \tag{2}$$

W_t is the sample weight at a specific time (g) and W_k is the sample dry weight (g).
The performance of the empirical models was evaluated using various statistical parameters such as the coefficient of determination (R^2) and the root mean square error (RMSE). These criterions can be calculated as following (Eqs 3, 4):

$$R^2 = 1 - \left[\frac{\Sigma_1^n \left(MR_{\exp_i} - MR_{pre_1}\right)^2}{\Sigma_1^n \left(MR_{ave} - MR_{pre_i}\right)^2} \right], \tag{3}$$

$$RMSE = \sqrt{\frac{1}{n} \cdot \sum_{i=1}^{N} (MR_{\exp_i} - MR_{pre_i})^2} \quad , \tag{4}$$

n is the number of observations, *exp* is the experimental data, *pre* is the predicted data, *ave* is the average data, and *MR* is the dimensionless moisture ratio.
The lower the RMSE values (close to zero) and the higher the R^2 values indicate the high fit of the model.

2.4. Measuring of specific energy consumption

An energy-cost-checker (model EKM 265, Conrad Electronic GmbH, Hirschau, Germany) during drying process was used to measure the energy consumption of the dryer. The energy uptake measured was converted into the energy required to evaporate 1 kg of water (so-called specific energy consumption - SEC).

2.5. Data analysis

The significance of differences between treatments was determined by ANOVA using the Duncan's test ($p<0.05$). The calculations were performed using PASW Statistics 18 (IBM Corp., Armonk, USA) software.

3. RESULTS

3.1. Drying characteristics of plum

The effect of MIR, MIR-FD and FD on the moisture content of final product and operational time are shown in *Table 2.* It should be noted that the drying time at MIR-FD is greatly decreased while

increasing the drying temperature and MIR pre-drying time. Therefore the MIR power level and MIR temperature has an important effect on the drying time. The initial moisture content of the plum 81.4% (w.b.) and was reduced to the final moisture content ranged from 1.87 to 2.81% (w.b.)

Table 2 Effect of different drying methods on the drying time and moisture content

Drying method (Symbol)	Infrared pre-drying period [min]	Freeze finish-drying period [h]	Product moisture content [%, w.b.]	Total drying time [min]	Reduction in FD drying time [%]
FD	-	25	2,56	1500^{i}	-
MIR40°C/4-FD	4	17,93	2,33	1080^{gh}	28^{e}
MIR50°C/4-FD	4	16,93	2,67	1020^{g}	32^{d}
MIR60°C/4-FD	4	13,93	2,55	840^{e}	44^{b}
MIR40°C/5-FD	5	16,92	2,81	1020^{g}	32^{d}
MIR50°C/5-FD	5	14,92	2,12	900^{ef}	40^{c}
MIR60°C/5-FD	5	11,92	2,07	720^{d}	**52**^{a}
MIR40°C	24	-	1,89	24^{c}	-
MIR50°C	20	-	1,93	20^{b}	-
MIR60°C	16	-	1,87	16^{a}	-

Means with different letters in the same column were significantly different at the level ($P<0.05$)

3.2. Modelling of drying process

Four empirical drying models – namely Page, Henderson-Pabis, Sigmoid and third-degree polynomial – have been used to describe mid-infrared-, hybrid- and freeze-drying curves. The results of the statistical calculation are shown in *Table 3*. The values of R^2 and RMSE of the all models were suitable for describing the drying characteristics of the plum during drying. Among the applied mathematical models, the Page and third-degree polynomial models were provided the best fit to the MIR and MIR-FD, FD drying kinetics of plum slices as indicated by a higher R^2 and lower RMSE values than those of the other models.

Table 3 Statistical results obtained from the thin-layer drying models

Drying method (Symbol)	Name of thin-layer drying model							
	Page		Henderson-Pabis		Sigmoid		3rd deg. polynomial	
	R^2	RMSE	R^2	RMSE	R^2	RMSE	R^2	RMSE
FD	-	-	-	-	0,99906	0,03448	0,99977	0,01332
MIR40°C/4-FD	-	-	-	-	0,99914	0,03154	0,99943	0,02213
MIR50°C/4-FD	-	-	-	-	0,98991	0,12462	0,99956	0,01745
MIR60°C/4-FD	-	-	-	-	0,98888	0,14588	0,99929	0,02767
MIR40°C/5-FD	-	-	-	-	0,99922	0,02901	0,99969	0,01601
MIR50°C/5-FD	-	-	-	-	0,99941	0,02356	0,99951	0,01889
MIR60°C/5-FD	-	-	-	-	0,99877	0,04922	0,99919	0,02994
MIR40°C	0,98921	0,13356	0,98195	0,19337	-	-	-	-
MIR50°C	0,99110	0,10833	0,97926	0,25232	-	-	-	-
MIR60°C	0,98677	0,15984	0,98291	0,18722	-	-	-	-

3.3. Specific energy consumption of driers

Figure 3 shows the amount of energy needed by the dryers to preserve plum slices. As shown in *Figure 3* and *Table 2*, FD had the longest drying time and highest specific energy consumption (SEC), with drying time of 25h and SEC of 121.5 MJ/kg H_2O.

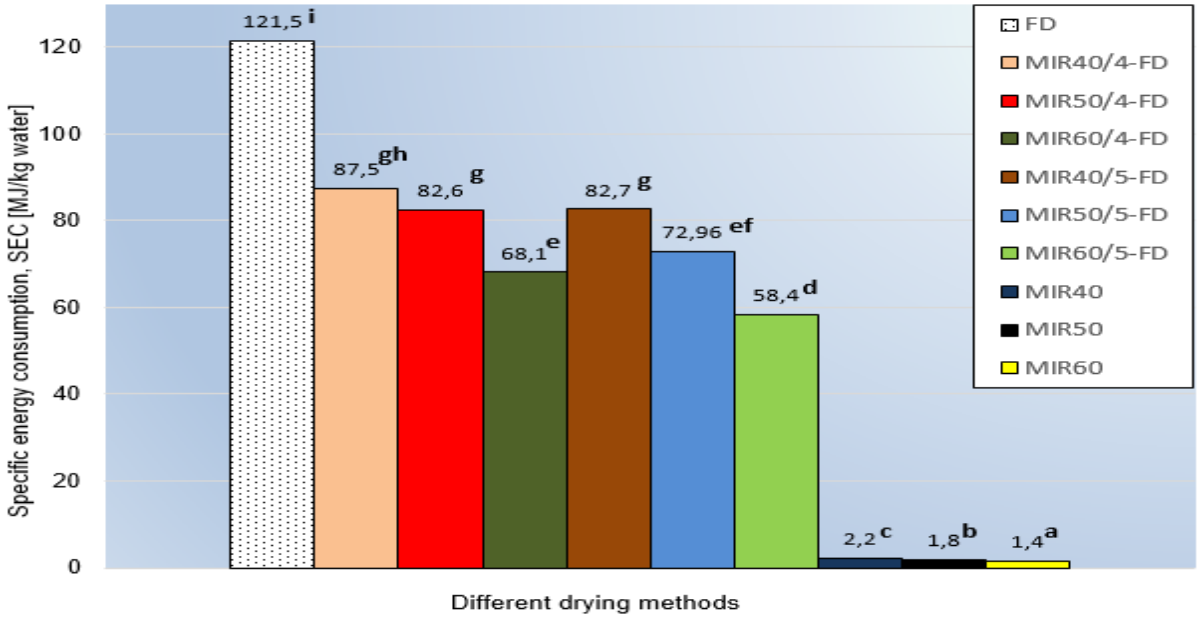

Means with different letters were significantly different at the level (*P<0.05)*

Figure 3 Effect of different drying technics on the SEC

The specific energy consumption decreased with the increase in drying temperature (infrared intensity) and MIR pre-drying time from 4 to 5 min at MIR-FD. Similar trends have been observed by [9]. The energy savings using MIR-FD with respect to FD were in the range from 27.9 to 51.9%. The specific energy consumption at MIR60°C/5min-FD was more than two times that at FD.
The MIR had both significantly lower (P<0.05) operational time and SEC compared with other drying methods.

CONCLUSIONS

Based on the experimental results of the present work, the following conclusions can be drawn:

1. Drying time was significantly lower (P<0.05) in the combination mid-infrared pre- and freeze finish-drying compared to freeze-drying. Drying time used in MIR-assisted FD drying was 48-72% of that in FD drying.
2. In the hybrid (mid-infrared freeze-drying) method: the specific energy consumption decreased with increasing MIR temperature and MIR pre-drying time.
3. The Page and third-degree polynomial models gave the best fit to drying curves for all the experimental data points.
4. The best drying method – the optimum – in terms of treatment duration, specific energy consumption and product appearance (color, shrinkage and texture) is the MIR50°C/5min-FD.
5. Further research about effect of hybrid drying on drying characteristics and quality of plum is necessary for optimization of plum drying.

REFERENCES

[1] George, J.P., Datta, A.K.: *Development and Validation of Heat and Mass Transfer Models for Freeze-Drying of Vegetable Slices*. Journal of Food Engineering, 52, 89-93., 2002.
[2] Kocabiyik, H., Tezer, D.: *Drying of Carrot Slices using Infrared Radiation*. International Journal of Food Science and Technology, 44(5), 953–959., 2009.
[3] Fenton, G.A., Kennedy, M.J.: *Rapid Dry Weight Determination of Kiwifruit Pomace and Apple Pomace Using an Infrared Drying Technique.* New Zealand Journal of Crop and Horticultural Science, 26, 35-38., 1998.
[4] Doymaz, I.: *Infrared Drying of Sweet Potato* (*Ipomoea batatas L.) Slices*. Journal of Food Science and Technology, 49(6), 760-766., 2012.
[5] Page, G.E.: *Factors Influencing the Maximum Rates of Air Drying Shelled Corn in Thin Layers.* M.Sc. thesis, Department of Mechanical Engineering, Purdue, USA, 1949.
[6] Henderson, S.M., Pabis S.: *Grain Drying Theory II: Temperature Effects on Drying Coefficients.* Journal of Agricultural Engineering Research, 6(3), 169-174., 1961.
[7] Figiel, A.: *Drying Kinetics and Quality of Vacuum-Microwave Dehydrated Garlic Cloves and Slices*. Journal of Food Engineering, 94, 98-104., 2009.
[8] Antal, T., Kerekes, B.: *Investigation of Hot Air- and Infrared-Assisted Freeze-Drying of Apple*. Journal of Food Processing and Preservation, 40(2), 257-269., 2015.
[9] EL-Mesery, H.S., Mwithiga, G.: *Specific Energy Consumption of Onion Slices during Hot-Air Convection, Infrared Radiation and Combined Infrared-Convection Drying*. Journal of Applied Science and Agriculture, 9(20), 13-22., 2014.

EVALUATION OF THE IMPACT OF CUTTING FLUIDS ON THE COURSE OF CUTTING FORCES DURING MACHINING

[1]BACHRATÝ Michal PhD [2]KRÁLIK Marian CSc, [3]TOLNAY Marián PhD, [4]TEKULOVÁ Zuzana PhD

[1,2,3,4] Institute of manufacturing systems, environmental technology and quality management, Slovak University of Technology in Bratislava, Faculty of Mechanical Engineering
E-mail: michal.bachraty@stuba.sk, marian.kralik@stuba.sk, marian.tolnay@stuba.sk, zuzana.tekulova@stuba.sk

Abstract
Article deals with the results of research in monitoring of friction properties of the most widely used cutting fluids. Measured components of cutting forces and cut-off pressure were used as criteria for formula to calculating each components of cutting forces with allowance of cutting liquid influence.

Keywords: *cutting fluids, friction properties, measurement cutting force*

1. INTRODUCTION

Currently we are looking for ways to make the process of machining the most economically profitable. One of the possibilities is the use of cutting fluids. The use of the cutting fluids is reducing of the cutting forces, which increases life of the tool, reduces the temperature at the place of cutting and improves the roughness of machined surface. Cutting medium also has the function of the chip the place of cutting and ensures the protection of corrosion [4], [5]. The goal of the research was to extend the calculation of cutting forces on impact of cutting fluid by means of the cut-off pressure - P_{max}:

$$F_z = C_{F_z} * a_p^{x_{Fz}} * f^{x_{Fz}} * P_{max}^{z_{Fz}} \quad (1)$$

$$F_x = C_{F_x} * a_p^{x_{Fx}} * f^{x_{Fx}} * P_{max}^{z_{Fx}} \quad (2)$$

$$F_y = C_{F_y} * a_p^{x_{Fy}} * f^{x_{Fy}} * P_{max}^{z_{Fy}} \quad (3)$$

$$F_y = \sqrt{F_z{}^2 + F_x{}^2 + F_y{}^2} \quad (4)$$

C_F – constant of the material
F_z – the main component of the cutting force
F_y – the feed component of the cutting force
F_x – passive component of the cutting force
F_v – the resultant of the cutting force
P_{max} – the cut-off pressure
x_{Fz}, x_{Fx}, x_{Fy} – exponents impact of the depth of cut
y_{Fz}, y_{Fx}, y_{Fy} – exponents of influence of feed
z_{Fz}, z_{Fx}, z_{Fy} - exponents of impact of the cut-off pressure (cutting fluid)

2. ANALYSIS OF THE IMPACT OF CUTTING FLUIDS ON THE MACHINING PROCESS

The cutting process usually can be evaluated of the size of cutting forces, of the durability of cutting edge, of the roughness of the surface, of the forming of the chip and of the creation of vibration. Some authors associate with these indicators also the accuracy. The numerical values of these parameters depend mainly on the type of machining and of cutting material, the geometry of the cutting edge of tool and cutting conditions (the feed, the depth of cut and the cutting speed).
The temperature and pressure are in the cutting area too high, so that the cutting fluid is unable to avoid the hydrodynamic effects of direct contact between the workpiece and the tool. This the unfavorable state can be effectively prevented by the presence of chemically active components in the cutting fluid - emulsion or cutting oil, so called EP (extreme pressure) additives.
Cutting fluid in the machining process reduces the size the cutting forces [3]. The effect is the expression of physical, chemical, and tribological factors for changes in the cutting zone. The effect is the expression of physical, chemical, and tribological factors for changes in the cutting zone [1].
Differences in the roughness of surface were observed during machining low alloy steel AISI 9310 with the cutting tool from the sintered metal carbides in a certain file of the cutting speed, feed and depth of cut for dry, wet and MQL (minimum quality lubrication) machining environment. For the MQL conditions, the surface roughness increases very slowly, we can therefore say that the MQL medium is effective in reducing of the surface roughness.
Temperature of the workpiece during the process cutting reaches by type of material, cutting speed and the chip dimensions of approximately 200 - 500 ° C. The strength of the material for carbon steels roses with the temperature to about 300 ° C, then decreases. If the temperature is above 300 ° C, during the cooling increases the strength of the material and the cutting resistance, and thereby increasing the deformation work by the formation of the chip. If the material temperature is below 300 ° C, during the cooling occurs to a reduction of the strength of the material and the deformation work is reduced [6] [7].
During cutting with the tools with the definable cutting geometry wedge is a main function of cutting fluid the protection of the tool - eliminating the built up edge (BUE) on the face of the tool (which under certain circumstances may damage the surface of the workpiece) and reduce the premature wear of the cutting edge.

3. METHODOLOGY DESIGN AND EXPERIMENTAL VERIFICATION OF IMPACT OF CUTTING FLUIDS ON THE COURSE OF CUTTING FORCES DURING MACHINING

The parameters of the experiment:

- Machine - Lathe SN 50
- Tool - knife holder + replaceable cutting plate SUMO TEC 5010 from ISCAR (see figure 1)
- Workpiece - pipe TR 135 x 12 STN 42 5715.01 – 11523.1
- Preparation - multi-component dynamometer with piezoelectric sensor KISTLER 9257B
- Cutting medium - 5% concentrate of selected cutting fluids

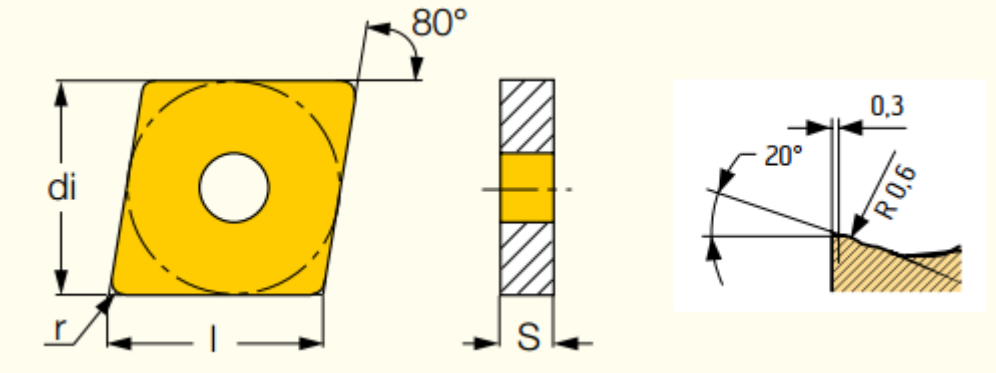

Figure 1 Geometry of cutting plate SUMO TEC 5010 [ ]
l = 12,9 mm, di = 12,7 mm, S = 4,76, r = 0,8 mm

Figure 2 Clamping of the workpiece – pipe and dynamometer Kistler 9257B

For each type of cutting fluid has performed an experiment with nine combinations of cutting conditions. They were used three different feed – f and 3 different depths of cut - a_p. Cutting conditions were selected based on recommendations of the manufacturer of the cutting tool. The cutting conditions and the points on matrix are shown in figure 3.

Point	*f [mm/ot]*	*a_p [mm]*
1	0,16	0,5
2	0,16	1
3	0,16	1,5
4	0,36	0,5
5	0,36	1
6	0,36	1,5
7	0,56	0,5
8	0,56	1
9	0,56	1,5

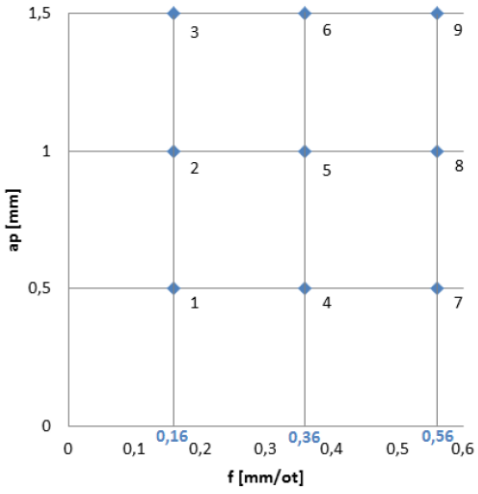

Figure 3 Table of the cutting conditions and points of matrix

Cutting fluids

For the experiment were used 16 kinds of cutting emulsion at various specified cutting conditions. Machining emulsions were earning 5% concentrate. From container of concentrate to the point of cutting were fed by a pump and tubing.

Figure 3 The supply of the cutting emulsion into the place oj cutting

An overview of used cutting fluids with the cut-off pressure is given in table 1. Detection cut-off pressure was made on the tribological measurements in another research process [2].

Table 1 The measured values of the cut-off pressure P_{max} for different liquids:

K	P_{max} [MPa]	Code	K	P_{max} [MPa]	Code
01	4,94	KAA	09	7,42	KAI
02	7,69	KAB	10	7,79	KAJ
03	14,77	KAC	11	8,15	KAK
04	13,54	KAD	12	7,81	KAL
05	7,4	KAE	13	10,9	KAM
06	9,7	KAF	14	6,14	KAN
07	6,39	KAG	15	8,06	KAO
08	7,47	KAH	16	5,61	KAP

Measurement of the cutting forces

Workpiece during the machining of the experiment was machined on a lathe SN 50 with methods of frontal area. Orientation of components of the cutting forces in the coordinate system of the machine is shown in the figure 4.

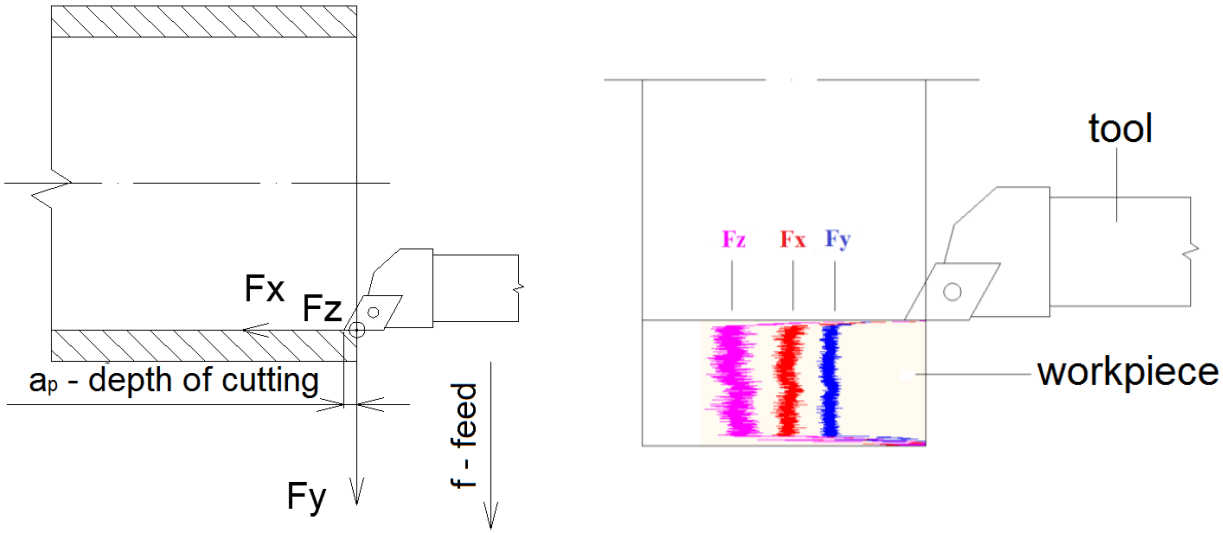

Figure 4 Orientation of components of the cutting forces in the coordinate system of the machine and process of cutting forces during machining

DynoWare program from Kistler is used for recording and analysis of cutting forces. The program can determine the minimum, maximum and average value of each cutting forces during machining times.

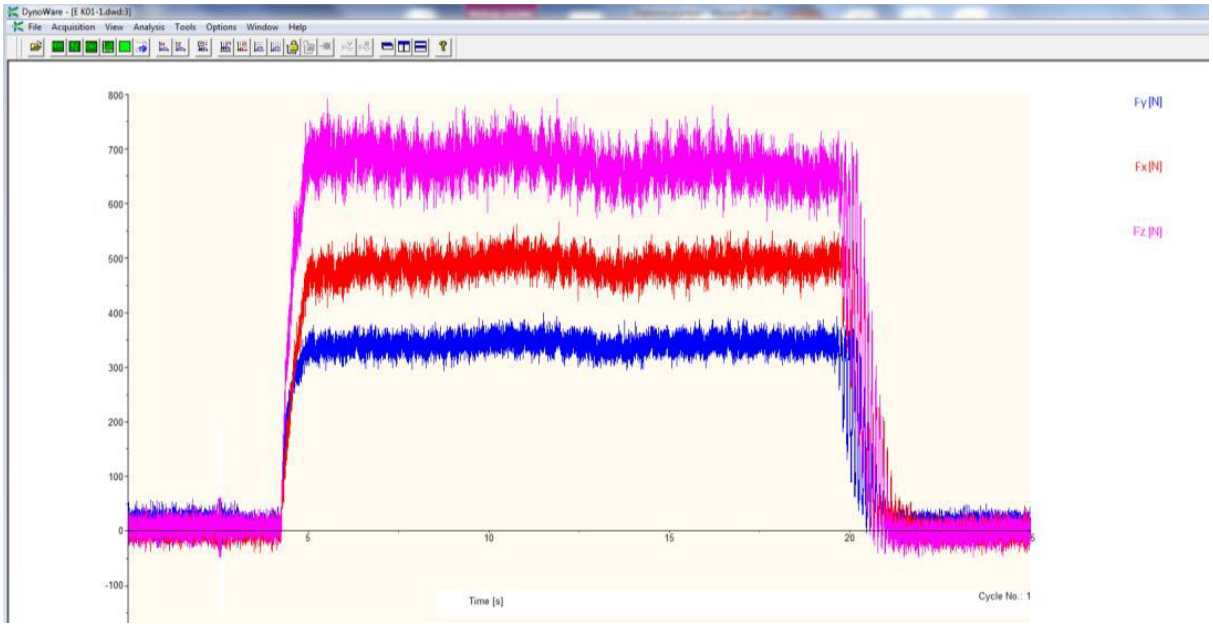

Figure 5 An example of a cutting force analysis in the program DynoWare

Using the measured values of the individual cutting forces and cutting conditions are specified functions for calculating of cutting forces for different cutting fluids (see table 2).

Table 2 Functions for calculating cutting forces for different cutting fluids

K	Fz [N]	Fx [N]	Fy [N]	Fv [N]
01	$Fz = 4958{,}78.ap^{0.89}.f^{0.72}$	$Fx = 1606{,}22.ap^{0.23}.f^{0.56}$	$Fy = 1437{,}24.ap^{0.98}.f^{0.24}$	$Fv = 5287{,}70.ap^{0.82}.f^{0.61}$
02	$Fz = 4833{,}19.ap^{0.87}.f^{0.70}$	$Fx = 1582{,}65.ap^{0.25}.f^{0.54}$	$Fy = 1469{,}38.ap^{0.99}.f^{0.27}$	$Fv = 5196{,}02.ap^{0.81}.f^{0.60}$
03	$Fz = 4577{,}42.ap^{0.89}.f^{0.67}$	$Fx = 1576{,}88.ap^{0.24}.f^{0.53}$	$Fy = 1407{,}11.ap^{1.05}.f^{0.27}$	$Fv = 4969{,}99.ap^{0.83}.f^{0.58}$
04	$Fz = 4155{,}09.ap^{1.00}.f^{0.61}$	$Fx = 1581{,}65.ap^{0.23}.f^{0.53}$	$Fy = 1404{,}21.ap^{1.00}.f^{0.24}$	$Fv = 4646{,}49.ap^{0.89}.f^{0.53}$
05	$Fz = 4899{,}40.ap^{0.94}.f^{0.72}$	$Fx = 1615{,}20.ap^{0.03}.f^{0.57}$	$Fy = 1404{,}54.ap^{1.05}.f^{0.26}$	$Fv = 5288{,}88.ap^{0.83}.f^{0.62}$
06	$Fz = 4951{,}90.ap^{0.85}.f^{0.71}$	$Fx = 1643{,}07.ap^{0.21}.f^{0.57}$	$Fy = 1429{,}88.ap^{0.95}.f^{0.24}$	$Fv = 5288{,}64.ap^{0.79}.f^{0.61}$
07	$Fz = 4748{,}36.ap^{0.89}.f^{0.70}$	$Fx = 1485{,}42.ap^{0.19}.f^{0.47}$	$Fy = 1358{,}20.ap^{1.02}.f^{0.20}$	$Fv = 5026{,}82.ap^{0.82}.f^{0.58}$
08	$Fz = 4800{,}09.ap^{0.96}.f^{0.70}$	$Fx = 1617{,}75.ap^{0.23}.f^{0.55}$	$Fy = 1164{,}03.ap^{0.73}.f^{0.16}$	$Fv = 5110{,}23.ap^{0.84}.f^{0.60}$
09	$Fz = 4549{,}46.ap^{0.84}.f^{0.64}$	$Fx = 1612{,}89.ap^{0.19}.f^{0.54}$	$Fy = 1372{,}65.ap^{0.99}.f^{0.20}$	$Fv = 4915{,}07.ap^{0.78}.f^{0.55}$
10	$Fz = 4684{,}77.ap^{0.92}.f^{0.67}$	$Fx = 1569{,}90.ap^{0.25}.f^{0.53}$	$Fy = 1379{,}14.ap^{1.07}.f^{0.22}$	$Fv = 4395{,}22.ap^{0.94}.f^{0.49}$
11	$Fz = 4642{,}17.ap^{0.89}.f^{0.67}$	$Fx = 1505{,}11.ap^{0.24}.f^{0.50}$	$Fy = 1340{,}48.ap^{0.84}.f^{0.22}$	$Fv = 4981{,}69.ap^{0.80}.f^{0.57}$
12	$Fz = 4880{,}18.ap^{0.90}.f^{0.71}$	$Fx = 1548{,}06.ap^{0.23}.f^{0.51}$	$Fy = 1348{,}52.ap^{0.98}.f^{0.20}$	$Fv = 5152{,}96.ap^{0.83}.f^{0.59}$
13	$Fz = 4927{,}11.ap^{0.86}.f^{0.71}$	$Fx = 1559{,}73.ap^{0.22}.f^{0.52}$	$Fy = 1416{,}96.ap^{0.99}.f^{0.24}$	$Fv = 5234{,}60.ap^{0.80}.f^{0.60}$
14	$Fz = 4849{,}44.ap^{0.89}.f^{0.70}$	$Fx = 1541{,}36.ap^{0.22}.f^{0.51}$	$Fy = 1328{,}82.ap^{0.99}.f^{0.19}$	$Fv = 5127{,}69.ap^{0.82}.f^{0.58}$
15	$Fz = 4631{,}74.ap^{0.90}.f^{0.66}$	$Fx = 1569{,}85.ap^{0.23}.f^{0.53}$	$Fy = 1390{,}19.ap^{1.01}.f^{0.23}$	$Fv = 4995{,}18.ap^{0.83}.f^{0.57}$
16	$Fz = 4788{,}72.ap^{0.89}.f^{0.70}$	$Fx = 1536{,}87.ap^{0.21}.f^{0.49}$	$Fy = 1406{,}14.ap^{0.97}.f^{0.21}$	$Fv = 5091{,}42.ap^{0.81}.f^{0.58}$

An example of chart for the cutting force F_z is shown in figure 6.

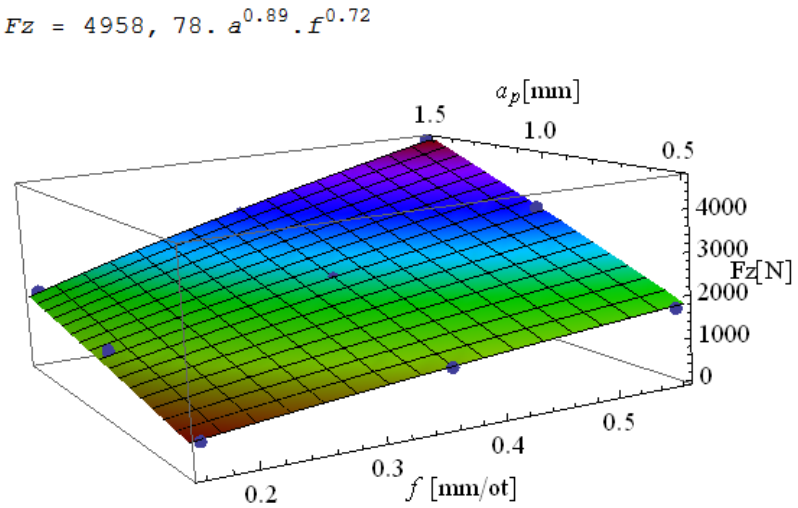

Figure 5 An example of chart for the cutting force F_z in the program DynoWare

Using the measured cutting forces from the intended matrix of cutting conditions and the inclusion of the selected evaluation criteria of cutting environment - a cut-off pressure P_{max} were using the Wolfram Mathematica 7 for the calculating of cutting forces for different cutting fluids:

$$F_z = 5070{,}42 * a_p^{0,90} * f^{0,69} * P_{max}^{-0,032}$$

$$F_x = 1550{,}39 * a_p^{0,21} * f^{0,53} * P_{max}^{0,007}$$

$$F_y = 1419{,}43 * a_p^{0,98} * f^{0,23} * P_{max}^{-0,014}$$

$$F_v = 5358{,}84 * a_p^{0,0,82} * f^{0,58} * P_{max}^{-0,026}$$

CONCLUSIONS

The goal of research was to express the functions for calculating cutting forces with the impact of cutting fluid. For the experiment were used 16 kinds of cutting fluids, which were used as a 5% concentrate. During the experiment they were measured cutting forces F_x, F_y, F_z using multi-component piezoelectric dynamometer KISTLER 9257B. The measured values are further processed in the program from Kistler - DynoWare. To include the impact of cutting fluid in the calculation of cutting forces was chosen parameter P_{max} - cut-off pressure.
The values of cut-off pressures were the subject of research in tribology (Table1). The measured value of the components of the cutting forces and cut-off pressures were then processed in the program Mathematica 7th.

ACKNOWLEDGEMENT

This work was supported by the Scientific Grant Agency of the Ministry of Education under contract no. VEGA 1/0670/15 Impact of assessment of the cutting environment to balance of energy of the machining process.

REFERENCES

[1] Bachratý, Michal - Jedinák, Michal - Javorek, Ľubomír - Králik, Marián - Tolnay, Marián. *Evaluation of cutting fluids quality using energy.* In Scientific Proceedings Faculty of Mechanical Engineering STU Bratislava. Vol. 22, (2014), s. 1-7. ISSN 1338-1954.
[2] Bachratý, Michal - Králik, Marián - Tolnay, Marián - Tekulová, Zuzana - Kováč, Pavel - Pucovský, Vladimir. *Test equipment for measuring of friction factor of cutting environment*. In Scientific Proceedings Faculty of Mechanical Engineering STU Bratislava. Vol. 23, iss. 1 (2015), s. 69-77. ISSN 1338-1954.
[3] Bachratý, Michal - Jedinák, Michal - Tolnay, Marián - Javorek, Ľubomír - Richtáriková, Daniela - Králik, Marián. *The influence of cooling fluids to energy consumption during transversal turning.* In Proceedings of the Annuals session of scientific papers: vol. 14. Oradea: University of Oradea publishing house, 2015, S. 265-268. ISBN 978-606-10-1537-5.
[4] Kocman Karel - Prokop Jaroslav., *Technologie obrábění*. Brno : CERM, 2005, ISBN 80-214-3068-0.
[5] Buda Ján - Souček Ján - Vasilko Karol: *Teória obrábania,* Alfa,Bratislava (1988)
[6] Buda, Ján. - Békés, Ján: *Teoretické základy obrábania kovov.* Bratislava: ALFA, 1977
[7] Neslušan, M. - Čilliková, M.: *Teória obrábania, EDIS Žilina,* 2007, ISBN 978-80-8070-790-3, 167 s

DYNAMIC MODELING OF HYDROCARBON RESERVOIRS USING FINITE DIFFERENCE METHODS AND DERIVATION OF ANALYTIC FORMULAE FOR EASIER FORECASTING

[1]BÁNKI Dániel, [2]JOBBIK Anita PhD

[1]Research Institute of Applied Earth Sciences, Miskolc, Hungary
E-mail: banki@afki.hu
[2]Research Institute of Applied Earth Sciences, Miskolc, Hungary
MTA-ME Geoengineering Research Group University of Miskolc
E-mail: jobbik@afki.hu

Abstract
In order to understand and optimise hydrocarbon reservoirs, simulation gained a vast role in reservoir management in the past decades. As far as the reservoirs are very complex hydrodynamical systems, the full mathematical description is impossible; the only way is to use numerical simulation and iterational calculations. In order to forecast the behaviour of a petroleum field, continuous data implementation and model rerunning is needed. This article deals with the basics of finite difference modeling on an example of an artificial model. The dynamic modeling of a reservoir is based on the governing equations of flow in porous media, and the behaviour of the wells drilled into it. At first, an artificial model was built mimicing a closed system consisting of an oil body and depleted with a five-spot one production four injection well pattern. The software used throughout the process is an industry reference simulator. In the dynamic model building phase, there is an opportunity to test the behavior of the reservoir and build analytical formulae for easier prediction. The phenomenon examined is the forecasting of water breakthrough time of the wells in a water flooded artificial reservoir.

Keywords: *reservoir modeling, simulation, finite difference, analytic*

1. INTRODUCTION

The petroleum resources of the world are porous rock-formed underground storage layers, which are capped with an impermeable formation to ensure the accumulation and to prevent further migration. These porous storages are called reservoirs. Adding the frequently jointed water bodies, the aquifers, these hydrodynamical systems became even more complex, with multiple phases and inner energy sources present in situ.

For describing this behaviour and the flow of the phases present, reservoir simulation is responsible. Most common softwares used for simulation are based on numerical modeling, and using the so-called finite difference method. [1] In the past few decades finite element methods gained place in solving various engineering problems, but for reservoir simulation the finite difference method is standing still as a good opportunity. In the past years finite volume methods appeared, which could be appliable, but the uncertainty is high and the methods need a lot of refinement yet. The second “type” of modeling used in the petroleum industry is the introduction of analytical formulae. These approaches do not separate the space into cells or calculate the attributes with iterative methods, but tries to match the examined phenomena with one exact mathematical solution. [2] By analytical models the border of application and validity should always be defined, as these are not total

equivalent pairings, just useful tools for fast calculations, which do not describe reality on the whole range of recognition. An other important characteristic of analythical formulae is that these cannot describe a system as a whole, thus all these formulae will be reservoir-, drive mechanism-, wellpattern-, and fluid-specific. Beside this, application of analytical approaches is widely used in the petroleum industry or in Experimental Design (or DOE). According to accuracy, one can reach a good answer with analythics when the start and the end points are important and the way inbetween can be treated as "one" process, ruled by only the most significant parameters.

During natural energy depletion of hydrocarbon reservoirs, the processes of natural driving mechanisms are able to move the hydrocarbons up to the surface, these systems and wells are called "flowing". As soon as the pressure and volume properties change to a level where the energy needed to produce the fluids to the surface is more than the total effect of the driving mechanisms, production stops, leaving vast amounts of hydrocarbon in the reservoir. The most common method afterwards, is to invest energy into the hydrodynamical system, using injection wells for the sake of pressure upkeeping. The injected fluid can be water or gas, or in case of WAG methods, both alternating in one well as plugs or at the same time from two wells. Location and injection rate determination of these wells are crucial, one always has to take the density differences, the permeability, the transition zone, and so many other factors into consideration. The easiest energy supply is the water flooding method due to the very very low compressibility of the water, and the relative ease of the treatment and well completion. [3] In the life of a reservoir, monitoring and simulation is omnipresent throughout the whole production cycle. First decesions are made after building the dynamic model upon the reservoirgeological static model, and the new data are always implemented for refinement and forecasting. The total understanding of the processes happening inside a porous rock is the most important step of knowing and modeling the behaviour of a reservoir. These modeling processes are conducted with finite difference modeling, and analytical approaches can be used for forecasting the more crucial events, such as water breakthrough of the production wells, more easily.

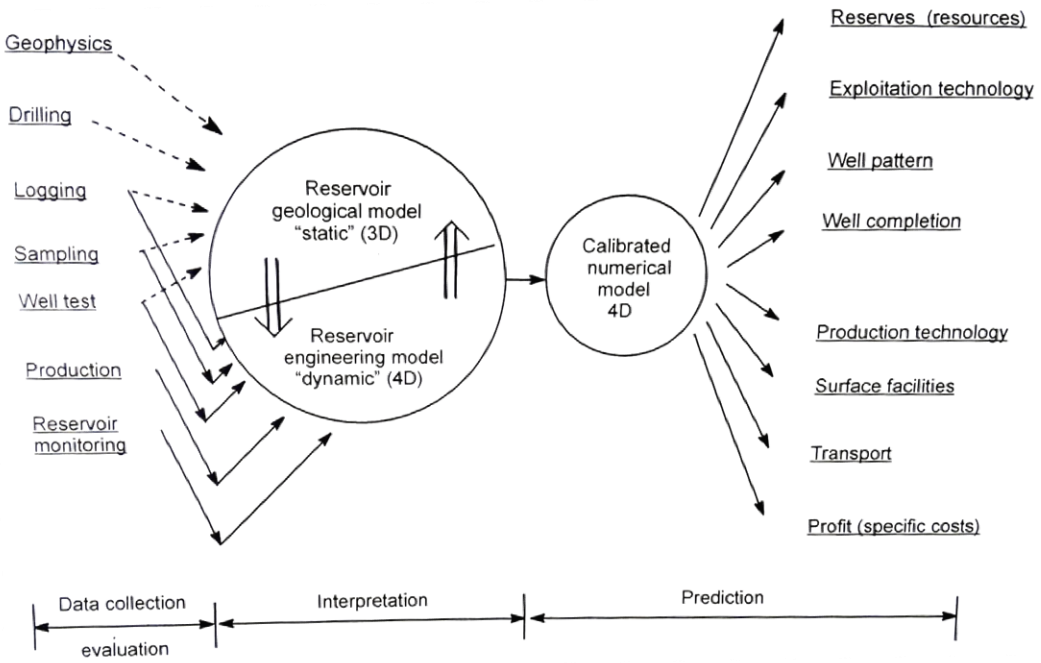

Figure 1 Flow diagram of the application of numerical simulation [4]

As seen on *Figure 1*, the application of the simulation is a very complex method in the petroleum industry. First, all the accessible petrophysical data are needed and gathered from laboratory measurements, borehole geophysics, analogous fields, well tests etc. Then, as a second phase, all these properties are matched and calibrated with the stratigraphy and the geological structure of the reservoir, in order to form a 3D static reservoir geological model. The welltests, production data and any other dynamic variables and results are used in the second phase where a reservoir engineering model is established onto the reservoirgeological one. [4] These two are in constant connection and when the model is sufficiently accurate, it comes to 4D calibrated numerical modeling, which means the saturation and quantity changes of the present phases throughout the time as a function, according to production and other depletion methods. At this point the simulation is suitable for the solution of several reservoir engineering problems, however model developement never stops, and every process is revised in 4-5 years, to reestimate reserves, saturations, to match history, and to predict/suggest new production rates and lifetime.

2. METHODS

In order to be able to describe the flow occuring in a hydrodynamical system of a porous rock mass one has to gather the equations used to describe each process, and generate a base simulator equation. There are three types of flow in techinal view occuring in a reservoir model; flow from one grid block to another, flow from the grid block to the well completion and flow within the wells and surface networks. The governing equations used for numerical simulation of a hydrocarbon reservoir are introduced in the following. [5]

Darcy's equation of fluid flow through porous media:

$$q = -\frac{k}{\mu}\nabla P \qquad Q = -\frac{kA}{\mu}\frac{(P_b - P_a)}{L} \tag{1}$$

Where q is mass flow, Q is velocity of flow, k is permeability, Pb and Pa are the in- and outlet pressures, L is the length of the sample, and μ is the viscosity of the flowing fluid. Darcy's equation *(Equation 1.)* describes the occuring mass flow in a porous media, and that this flow is a function of the pressure drop along the sample, the viscosity of the fluid, the area for crossflow and the rockphysical resistance to flow ("equivalent" cross section area). This equation is valid for isothermal conditions and single phase steady state flow of an incompressible and Newtonian fluid with 100% saturation within the pores.

Mass flux conseravtion equation:

$$-\nabla \cdot M = \frac{\partial}{\partial t}(\phi\rho) + Q \tag{2}$$

The modified version of the law of continuity *(Equation 2.)*, essential for every material balance involved process. States that mass flux equals the sum of the accumulation and the production/injection. If a given amount of fluid enters the system, the same amount will leave it.

Simulator flow equation:

$$\nabla \cdot [\lambda(\nabla P - \gamma \nabla z)] = \frac{\partial}{\partial t}\left(\frac{\phi}{\beta}\right) + \frac{Q}{\rho} \qquad \lambda = \frac{k}{\mu\beta} \tag{3}$$

It contains the mass balance equation and Darcy's law, extended with a gravity term. This formula *(Equation 3.)* describes the flow of fluids in porous media suitably for modeling, the velocity of flow between cells and the continuity is included.

Well modeling equation:

First we have to introduce the terms mobility and transmissibility. Mobility *(Equation 4.)* is the ability of flow of each phase depending on fluid properties, where k is the relative permeability of the phases present, μ is the viscosity of the phases, β is the formation volume factor of each phase, and Rv and Rs are solution gas ratios.

$$\text{Mobility}_{\text{phase,connection}}$$

$$M_{o,j} = \frac{k_{o,j}}{\beta_{o,j} \cdot \mu_{o,j}} + R_v \frac{k_{g,j}}{\beta_{g,j} \cdot \mu_{g,j}}$$

$$M_{g,j} = \frac{k_{g,j}}{\beta_{g,j} \cdot \mu_{g,j}} + R_s \frac{k_{o,j}}{\beta_{o,j} \cdot \mu_{o,j}} \tag{4}$$

$$\text{Transmissibility}_{\text{connection}}$$

$$T_{wj} = \frac{c\theta \cdot Kh}{\ln(r_o / r_w) + S} \tag{5}$$

Transmissibility *(Equation 5)* is also the ability to flow but according to rock and well properties, such as radii, skin effect, horizontal permeability etc. Using these two, the well equation *(Equation 6.)* can be written, where P denotes pressure values, and H denotes hydraulic head:

$$q_{p,j} = T_{wj} M_{p,j} (P_j - P_w - H_{wj}) \tag{6}$$

The process of solution is started with dividing the reservoir into several cells, making a grid to achieve separate elements for each simultaneous calculation then providing basic data for each cell, such as petrophysical properties of the reservoir rock, stratigraphycal differences, faults, aquifers, etc. Then positioning and description of wells is the next one, with specifying production rate also. The second main part is called equlibration where the governing equations are solved for t=0 in order to know the saturation of each cell.

According to the artificial model the phenomenon of watering was examined. First a 5 spot pattern black oil reservoir model was established with extrem permeable zones called thief zones. Afterwards, 7 years of simulation were run, along with sensitivity and scoping runs needed for the analytical model. After the numerical simulation, the data from it were processed further into an analythical formula which predicts the water breakthrough time of the production well with 5% error as a funtion of well distance and production rate.

3. RESULTS

After building the static part of the model, conduction of the dynamic and generation of the data for post processing were made. *Figure 2* shows the schematics of the reservoir model. The length, width and height of the artificial model was 3630x3630x120 in units of feet, with a top layer at 7900 ft and an oil water contact at 8200 ft. The production well is located in the middle and four water injection wells are placed on the borders in order to keep up the pressure and to purh the oil towards the production well. The system operates on voidage replacement method which means that total production equals total injection in terms of volume at reservoir conditions.

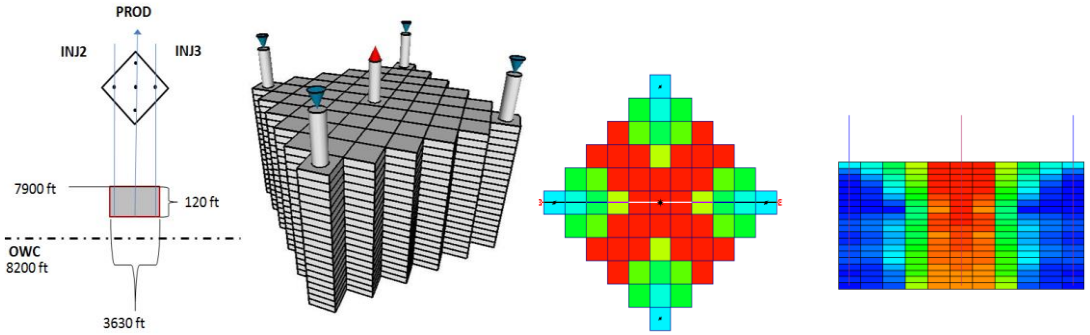

Figure 2 The artificial model and the saturation distribution of a sensitivity run

The saturation of the phases is also visualised, after 3,5 years of production. Thief zones are clearly visible, as the water propagates through the porous system. The sensitivity runs were made for determining the effect of well distance and production rate on the water breakthrough time of the wells.

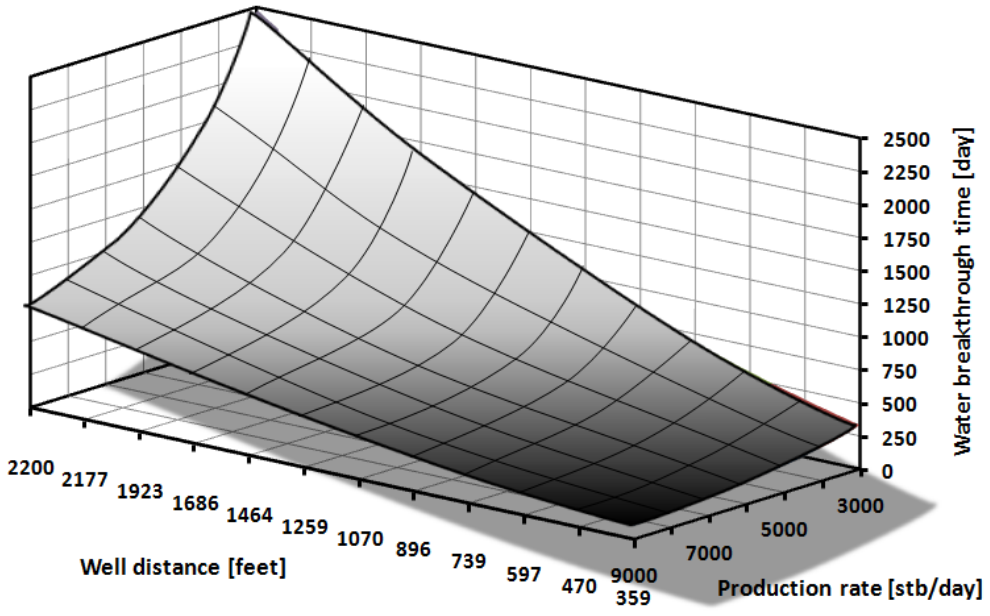

Figure 3 Visualisation of a response surface in 3D

After the fitting of the analytical model with regressional methods and choosing the correct

mathematical type of correlation, charts can be made for graphical solution to make forecasting easier. A 3D response surface *(Figure 3)* can be constructed for estimation, as it represents the contribution of the most significant parameters to the waterbreakthrough time. It can be deducted that for high production rates, the distance of the wells is crucial because water needs time to settle towards the bottom, thus if the spacing is small, water channels through the thief zones, and disturbs the production of the middle well almost immediately. The formula itself can also be used to predict the water breakthrough behaviour of this artificial model with the given accuracy. The 3D plot is also suitable for rough prediction.

CONCLUSIONS

Dynamic modeling of a reservoir is an important tool, if we know how to use it. A well established model needs continuous calibration, history matching, and a vast gathering and preprocessing of petrophysical data. A dynamic reservoir model cannot be accurate or effective unless the static reservoir geological model is suitable and well established. With a basis of numerical modeling, analytical formulae can be used in conjunction with the classical reservoir engineering solutions in order to estimate faster, reduce the PC demand and to mobilise the technology as no licence is needed after the sensitivity and scoping analysis.

ACKNOWLEDGEMENT

The research was carried out in the framework of the GINOP-2.3.2-15-2016-00010 "Development of enhanced engineering methods with the aim at utilization of subterranean energy resources" project in the framework of the Széchenyi 2020 Plan, funded by the European Union, co-financed by the European Structural and Investment Funds.

REFERENCES

[1] Robinson S.: *Simulation: The Practise of Model Development and Use*, Palgrave Macmillan, 2014.
[2] Gokhale S. S.–Trivedi K. S.: *Analythical Modeling, Encyclopedia of Distributed Systems*, Kluwer Academic Publishers, 1998.
[3] Lucas S. K.: *Maximising output from oil reservoirs without water breakthrough*, The Anziam Journal, ISSN: 1446-1811, 401-422, 45, TeXAdel Scientific Publishing, 2004
[4] Pápay J.: *Development of Petroleum Reservoirs*, Akadémiai Kiadó, 420-430, Budapest, 2003.
[5] Schlumberger Inf. Solutions: *ECLIPSE Blackoil Reservoir Simulation*, Schlumberger, 2008

SPECIFIC ASPECTS CONCERNING THE DAMAGES OF COMPONENTS FROM REFIGERANT SYSTEM UNITS

[1]BELÉNYI Alpár, [2]GYENGE Csaba DSc, [3]ACHIMAS Gheorghe DSc

[1,2,3]InstituteDepartment of Manufacturing Engineering, Technical University of Cluj-Napoca
E-mail:alpar_belenyi@yahoo.com , csaba.gyenge@tcm.utcluj.ro , gheorghe.achimas@tcm.utcluj.ro

Abstact
Within the confines of work, appear the practical diagnoses of authors concerning the characteristical usage and deteriorations of semi-hermetic compressors used for refrigerating unit.From a technical point of view these equipments can fail, wear and deteriorate after some specific hours of functioning. We can name failures, deteriorations as: hydraulic hits(slugging), lubrifacation problems(loss of lubrifacation), overwheating etc. These defects and damages could be evaded with a maintenance program with which we can discover that these compressors aren't functioning at the given parameters but the advantages of these compressors are that they can be disassembled in parts, and the hampered and weared parts can be reconditioned and repaired.

Keywords: *compressor semi-hermetic,damages,failure,wear,deterioration,recondition*

1. INTRODUCTION

Semi-hermetic compressors are specific to the technic of refrigerating, because refrigerants are protecting the electric coverings which allows the introduction of an engine in the flux of refrigerant, vehiculated by the compressor. The main advantage of these compressors is that on the same axis we can find the electric engine and the winch of the compressor. Aditionally the assamebly is introduced into a single dense carcass for the refrigerant, such problems disappear as aligning of the engine with the compressor and the problem of traversing of the case via the vibrochen as well as the problem of mechanic gasket. The maximum power of such a semi-hermetic compressor is allowed maximum until 45 kW and they are used for averige power in the industry.

Semi-hermetic compressors can be of two types [1]:

- Volumic- with piston;
- Rotative -eliocid; -with spirals; -centrifugal;

These compressors are used in diverse factors which are presented in *Table 1.*

Table 1 Types of semi-hermetic compressors

Semi-hermetic Compressor	Volumic	Rotative		
	with Piston	Elicoid	with Spirals	Centrifuga
	Haushold	-	-	-
	Commercial	Commercial	-	-
	Air Conditioning	Air Conditioning	Air Conditioning	Air Conditioning
	Cooling	Cooling	-	-

Semi-hermetic compressors can be disassembled as much the engine as well as the compressor part, making possible mechanic interventions for maintenance and repairs. The compressor's component parts are presented in *Figure 1*.

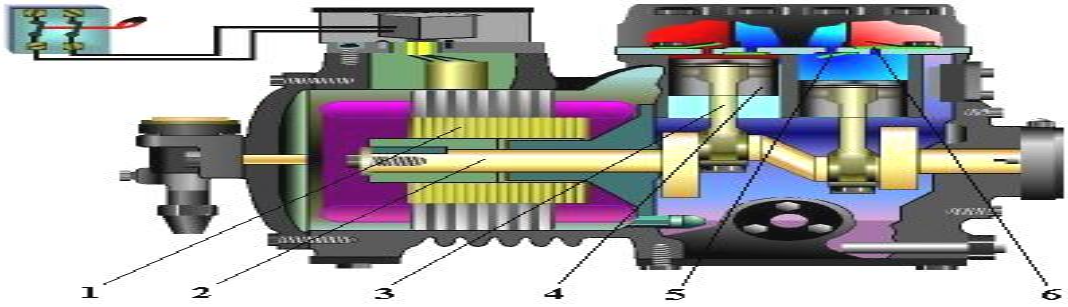

Figure 1 Component pieces of semi-hermetic compressors
a-stator; b- rotor crankshaft; c-winch; d-piston; e-inlet valve; f-relief valve;

2-THE MAIN COMPONENTS OF SEMI-HERMETIC COMPRESSORS

Valves(*Figure 1e,f*) are in general with the razors. Needs noticed though that modern machines are using more and more valves resembling those of industrial compressors'. Such an example is presented by the DISCUS system. The sucking of vapors is realized by traversing the board of valves. The valve of sucking is cyclic while the one for repression valve DISCUS, is a piece of cylinder-cone made of a plastic material having the following properties: it's lightweight, elastic, resistant to oils and refrigerant at high temperatures.
Case is tuned from a single piece and contains the compressor's body as well as that of the engine, sometimes also featuring cooling winglets. It's closed on the compressor's side by the support of the bearings chamber and of the oil pomp while on the engine's side by a cover on which is a sucking faucet and inside a filter for the sucked vapors.
Cylinders are in general in a number of 2-3 lines, 4 in V and 6 in W. They are premade directly in the case's body. The cylinders' covers are from the same cast iron as the case and the entrance is to be found on the compressor's side. Two compressors can also be assembled in tandem, in which case there is an additional part between the two engines holding them together back to back.

3. MAINTENANCE OF A SEMI-HERMETIC COMPRESSOR

From a technical point of view just like any other equipment, a compressor too needs maintenance or preventive maintenance which consists the followings [2]:

- monthly check of the quantity of refrigerant and oil;
- at least twice a year the tightness of nipple needs to be checked, the functioning of high pressure pressure switch and the oil differential pressure switch;
- changing the valve board after at most 5000 hours of functioning;
- checking the vibrations every 6 months.

After circa 10.000 hours of functioning a general technical revision needs to be done for the group components (preventive maintenance) while in function of technical status, the compressor components will be repaired, replaced or reassembled and the greasing oil will be completely changed.
If these preventive interventions for the semi-hermetic compressors are not respected, they can wear, fail or deteriorate.If the compressor is not functioning at the optimal parameters, some noises can be heard because of the maintenances were not respected or caused by a hidden error, the component elements of the compressor needs to be identified and inspected during disassembly, also analyzing the relative positions of these components one in front of the other. Each part needs to be verified and noted in a diagnostics book (the quality of the surface, the level of cleanness or dirtiness etc.). Most failures with the exception of those deteriorated by the hidden foulness of materials and they can be listed in one of the following categories [3][4][5]:

- Loss of lubrifacation, lubrifacation problems. reasons: faulty lubrication;
- Hydraulical hits(slugging)-reasons: low refrigerant velocity, low load, etc;
- Overheating-reasons: due to a cause.

4. WEARS AND DAMAGES APPEARING AT THE PARTS OF SEMI-HERMETIC COMPRESSORS

From a technical point of view at semi-hermetic compressors two types of failures and deteriorations can appear: mechanic and electrical (*Figure2*). Mechanical failures(a) include: broken valves, scored shaft, broken rods and overheating. Electrical failure(b) includes: single phasing, overheating and system control problems.
So in this study we will study the three biggest deteriorations of semi-hermetic compressors which are damaging and wearing the component pieces:
-loss of lubrifacation, lubrifacation problems; - slugging, hydraulical hits; -overheating;

Figure 2 Semi-hermetic compressor failure
a-Mechanical failures (broken and wear valves); b-Electrical failure (overheatings);

4.1. Loss of lubrifacation and greasing problems

The most common greasing problem of freezing compressors are the followings:

- dilution of the oil by the refrigerant;
- decreasing of the oil's level;
- reduction of the oil's viscosity by excessive heating;

Dilution of the oil is one of the most common lubrification problem of refrigeranting unit. While the oil is showing a greater affinity compared to the refrigerant, being miscibile with this, in the case of an elongated stopping, it's possible of becoming dilueted enough with the refrigerant as to lose its lubing properties. In *Figure 3* and *4* we can see a crankshaft being exposed to the lubrification of oil by the refrigerant. The abresion of the aluminum can be observed from which the hinge was made of, on the surface of the crankpin's chamber, without this showing even the slightest lose of color produced by heating, the deterioration causing itself practically instantly, and the biggest part of the heat caused by scrubbing was absorbed by the vaporization of the refrigerant.

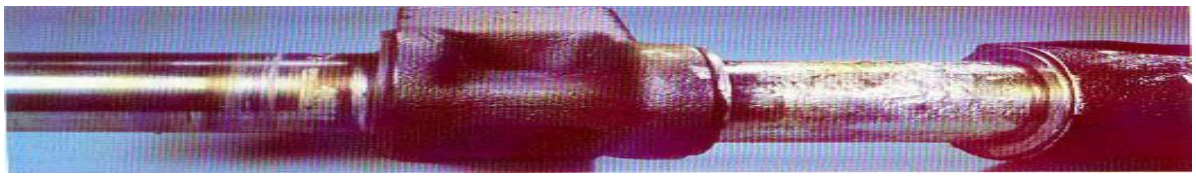

Figure 3 Typical deterioration,an cranckshaft submissive washing with oil by refrigereant

The same specific particularity of the surface's deterioration is presented by the aluminum hinge of the same compressor presented in *Figure 4*.

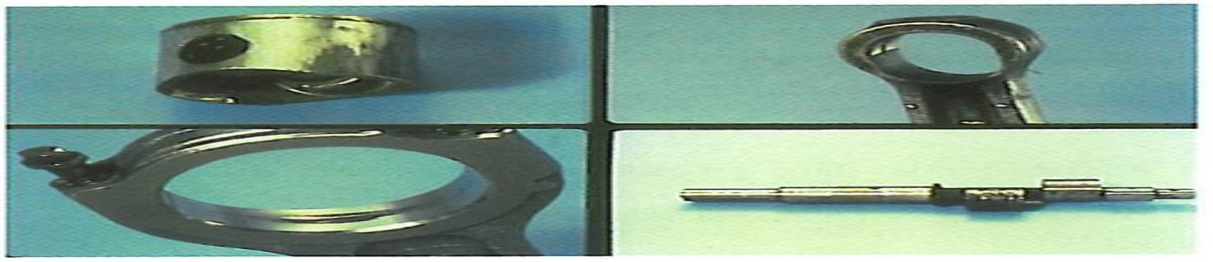

Figure 4 A piston,worn and crakshaft submissive wasching with an impropper oil

When a discharge valve has failed or a valve plate gasket has blown, the pressure on the top of the piston remains high and the bottom of the wrist pin never gets lubrificated. The friction causes the bottom of the wrist pin hole to wear (*Figure 5).*

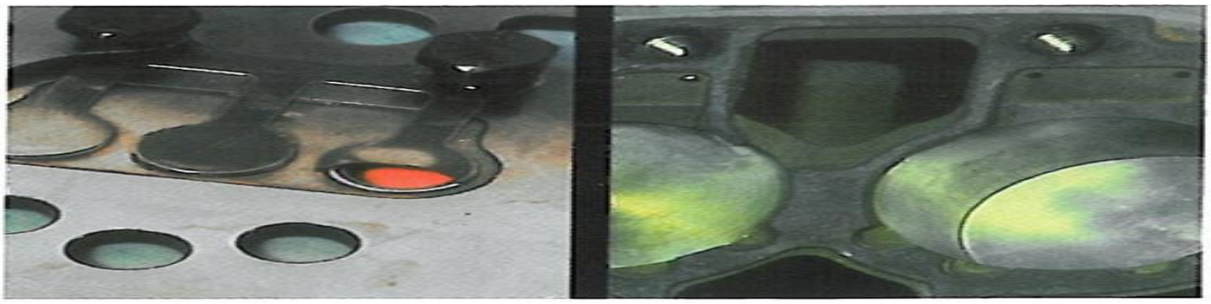

Figure 5 The wrist pin hole wear

4.2. Slugging, hydraulical hits

The main producing cause of hydraulic hits are:

- the thermostatic regulating valve is selected wrongly;
- reducing the thermal strain;
- unequal distribution of air over the surface of the vaporizer;
- sucking of the oil.

A compressor at which hydraulic hits were found, a deterioration of the sucking valve can be observed, which is exposed to a very strong pressure and shock. In *Figure 6* we can observe that detached pieces of the sucking valve have embedded in the repression valve and on the channel. It is possible that the sucking valve not to be destroyed completely like the one in *Figure 6* but it manifests radial fissures on the surface, which at an additional hydraulic hit may end up in the breaking of the valve.
The piston and the hinge of the same compressor are presented in *Figure 8*. The destruction of the compressor was provoked by contact with the broken pieces of the sucking valve. Of course in such a situation the cylinders are deteriorated as well and they need to be repaired.

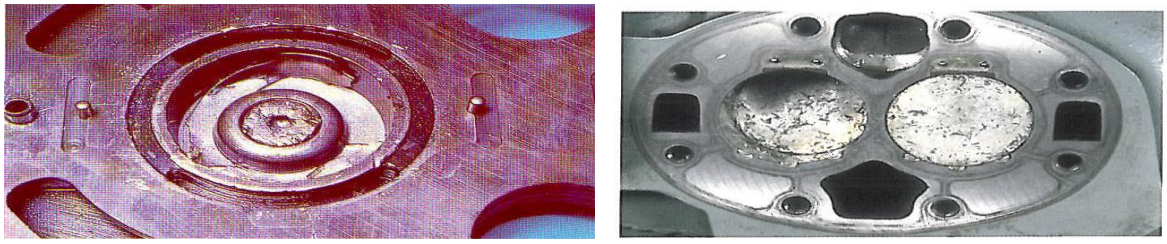

Figure 6 Block of valves submisive of hydraulic hit and pistons deteriorations

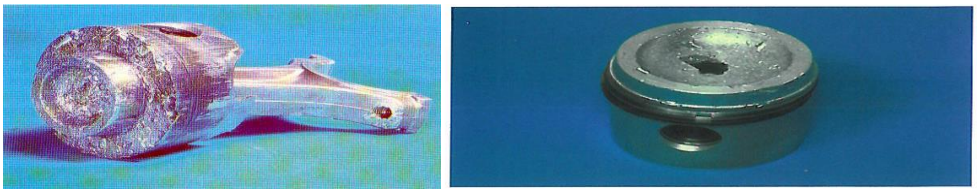

Figure 7 Damages of piston after hydraulical hits

If a piston survived a slug ,the suction or discharge valves probably did not. The slugs are capable of causing damage to the valves when they try to push them trough the port. Damage can range from dented valves to complete punctures at the ports.This pieces of the compressor can become lodged in the stator and it can eventually cause a stator failure (*Figure 9*).

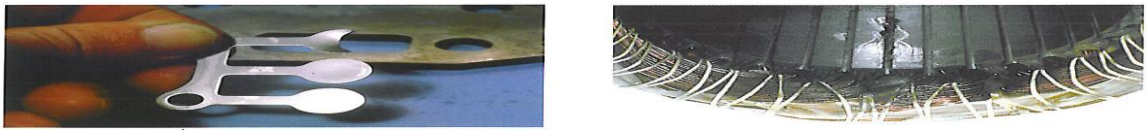

Figure 8 Damaged valves and pieces in the stator

4.3. Overheating

The causes of excessive overheating of the compressor can be the followings:

- a rapport too big compression;
- a too small quantity of freezing agent in the cylinders;
- the functioning in reduction mode of the freezing power under the allowed limits;

Overheating of the compressor, determines the reduction of oil viscosity and concomitant the reduction of greasing capacity. In even graver phases of carbonization of the greasing oil, carbonized particles can also make the functioning of the valve harder, determining leakiness of the cylinders and escaping of agent which will have the tendency to spread again in the cylinder, during the sucking process. Hinge of darker color in *Figure 9*.

Figure 9 Damaged piece-winch from an overheated compressor

Winch from figure 10 was extracted from a compressor which's oil pomp was intact and appeared to function correctly. This caused the winch to overheat.

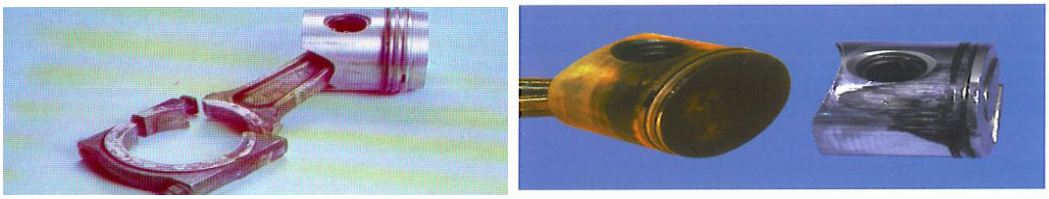

Figure 10 Damaged pieces-broken winch and piston from an overheated compressor

In *Figure 11*. is shown another disassembled winch from the compressor. We can see the aspect of the winch head's surface. A winch exposed to scrubbing and overheating. The portion exposed to scrubbing show fine scratches, which have nothing in common with the aspect of surfaces applied for scrubbing thanks to the washing of greasing oil by the refrigerant. Dry scrubbing, caused by lubing failure, produced overheating of the winch's leg. Production of this phenomenon is confirmed by the dark color of aluminum from which the piston is made.

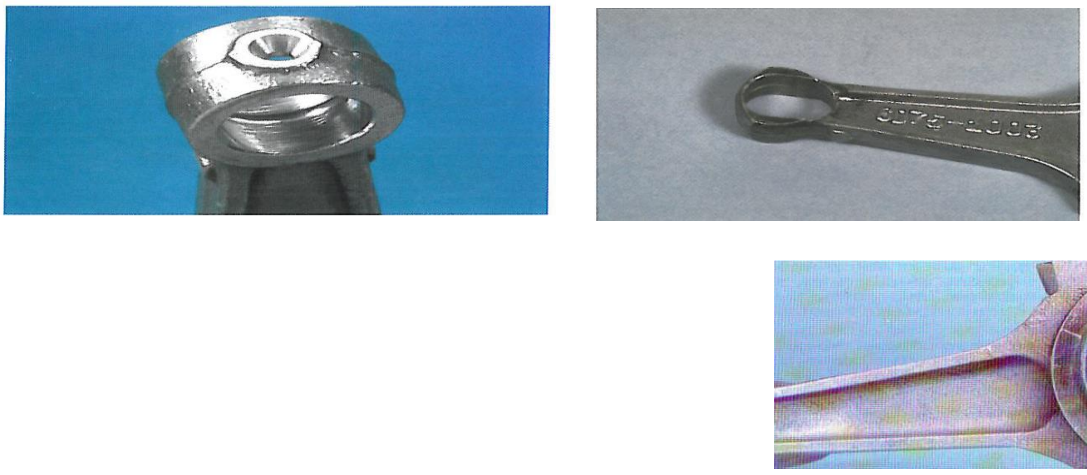

Figure 11 Deterioration of winch due overheating

CONCLUSIONS

In this study I have highlighted the main causes of deterioriation of the semi-hermetic compressors.The bibliographical studies helped me to understand which are the most frequently appeared defects over the last few years: hidraulic hits, problems with lubrication

and overheating. These are the most severe defects of a semi-hermetic compressor, and these can be pointed as the main causes of their deterioration. In the future we will set creating a program of maintenance as a goal,so that we can reduce the possibility of the deterioration. We will also make a plan for reparing and reconditioning the malfunctioned components.

REFERENCES

[1] M. Bălan, *Instalaţi frigorifice.Construcţie,funcţionare şi calcul*, Editura tehnica
[2] N. Purice, *Exploatarea şi întreţinerea utilajelor frigorifice comerciale,* Editura Bucureşti
[3] www.termo.utcluj.ro/ufa/ufapdf/ufa14.pdf
[4] Tech Service-Training,*Why Compressors* fail II,Carrier Corporation 1998 I.Culinescu, *Manualul mecanicului Frigotehnist,*Editura Bucureşti

COMPOSITE FRICTION MATERIALS OF COUPLINGS

[1]BICZÓ Roland, [2]KALÁCSKA Gábor DSc

[1]Szent István University, Gödöllő, Hungary, Páter Károly st., 1.
E-mail: rolbicz@gmail.com
[2]Szent István University, Gödöllő, Hungary, Páter Károly st., 1.
E-mail: kalacska.gabor@gek.szie.hu

Abstract
This paper deals with composite friction materials used mainly in automotive clutch applications. With listing their main types and differences in manufacturing, it reviews components used for production showing material and construction development trends in the past. Finally it reflects on some present and near future investigations and experiments to answer questions and solve problems of this field of frictional material science.

Keywords: *polymer, composite, frictional material, clutch*

1. INTRODUCTION

Typical components of polymer composite friction materials for clutches can be classified in the following groups: reinforcements, binders, friction modifiers, and fillers. The friction materials are deformable, their task is to maintain a sufficiently high and stable friction coefficient and a good wear resistance during operation. They should possess the ability to resist heat induced deterioration, impact, and centrifugal force during friction.
Requirements of composite friction materials derive from the operating characteristics of their applications. A clutch transfers the kinetic energy of a rotating crankshaft – coupled to a power source – to the transmission and wheels. Slippage results in the generation of heat, which is absorbed and eventually dissipated to the atmosphere by the clutch [2].
Couplings have dry and wet operation types. In dry applications, heat is removed by conduction to the surrounding air and other assembly members. When the application operates in fluid, for instance oil, this liquid absorbs the heat and maintains low operating temperatures while trapping the wear debris [2].

2. MANUFACTURING STEPS

Clutch facing types – for main types see *Figure 1* – have some diversities in manufacturing steps, as a consequence that three basic types of clutch facing materials are available on the market nowadays. They are fibre reinforced woven clutch facings – some bonded onto a steel carrier plate –, paper based friction materials usually for oil-immersed clutches, and cermet segments for heavy duty and high velocity applications [2].
The manufacturing steps for the first type are wire preforming, dry mixing of fillers and modifiers, molding of mix around strand or wire preforms (coating), weaving according to a specified pattern, then hot pressing, curing and grinding. The recipe for wet mixing types contains an additional drying step. Paper based materials use a core plate to carry the frictional layer, which comes from a soaked roll taken up onto a winder. The final steps are similar to the former type without the need of grinding. Cermet segment ingredients are mixed, compacted and sintered, and finally grinded to final geometry.

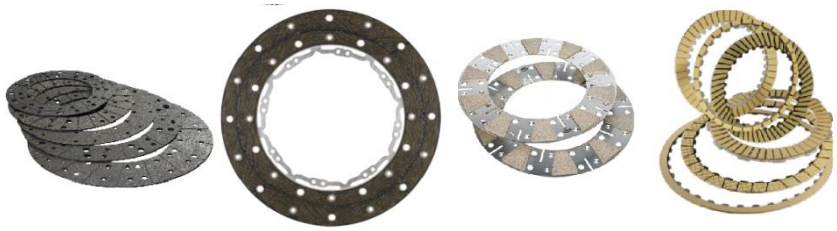

Figure 1 Typical clutch facing types (from left to right): Schaeffler woven clutch facings; Schaeffler woven facing with steel carrier plate, cermet segmented facing with steel carrier plate by Miba; Schaeffler paper based friction materials

3. COMPONENTS AND MATERIALS

Table 1 Clutch friction materials vs constructions

	Year	1886	1889 - 1920's	1918 - 1920's	-1920's	1900 - 1918	1900's -	('04) 1920's -
	Type of clutch	transmis-son belt clutch	friction clutch					
Year	Friction material		cone/ bevel friction clutch	NAG cone	Daimler Al-cone	Daimler/ Mercedes spring band clutch	Weston multidisc oiled/ dry	single clutch disk
1886	leather belts	x						
1889	camel hair		x	x				
after 1889	leather belt soaked into castor oil		x					
after 1889	spring loaded pins/ leaf spring + leather		x					
1918	metal		x			x		
1918 -	oiled aluminium				x			
1900's -	oiled bronze and steel						x	
1900's -	riveted friction lining						x	
1920's -	graphite lubricated							x
1920's -	ferodo asbestos							x
1990's -	asbestos free (NAO) linings							x

Tribological performances and mechanical properties of these materials depend on their components. Fibres play a critical role in determining the mechanical strength, thermal resistance, and friction and wear properties of the materials [3]. Typical fibres are aramid, glass, carbon, steel,

cellulosic fibre, thermoplastic fibre, and asbestos (now banned). The latter became popular due to its high strengths and modulus, thermal stability, good wear properties and the possibility to be used also as a filler. Regarding strength and modulus aramid, glass, carbon, and steel can be taken into account as a substitution. Aramid also has high thermal stability, good wear properties and stable coefficient of friction. Glass fibre is relatively cheap. In terms of thermal stability aramid, carbon, and steel fibres became popular [1].
Taking a look at the development regarding constructions along with friction materials in use, – see *Table 1* –there are some dates assuming a common influence compared to other application fields of friction materials – for instance efforts to replace asbestos – that affected the goals of the whole friction material industry. Although fibre reinforced materials were present since the beginning of the twentieth century, only after the discovery of flexible resins could they spread widely on the market. Another change in trends began in the 60's with the growing number of reports about the hazardous effects of asbestos. Sweeping out the material from all newly developed applications took more than thirty years. *Table 1* also shows that the construction and material development trends regarding clutches became parallel only with single clutch discs going through milestones in fields like lubrication improving possibilities and utilization of newly discovered friction material components, then taking healthcare and environmental protection into consideration. Most of the basic designs were developed early, but only the availability of new materials and machining methods allowed them to be realized.

4. DEVELOPMENT TRENDS

Working with polymer composites opens a wide range of opportunities to develop new or better materials experimenting with amounts of ingredients, untested, new components or expanding or narrowing down manufacturing steps. All of this however needs comprehensive analysis.
Searching through the scientific literature of the mentioned materials one can find that studies are circling around three basic topics in accordance with the requirements, loads and operating conditions, namely mechanical properties, thermal phenomena and tribology, and parameters influencing and governing them.

4.1. Mechanical aspects

The main mechanical topic can be divided into the following subtopics: 1) fibre – matrix adhesion and parameters affecting it, fibre – fibre friction relations; 2) Effect of waving parameters; 3) warpage, shrinkage, residual stress and parameters affecting it; 4) mechanical tests for justification of properties.
For inner friction characterisation de Lange *et al*. [4] investigated the properties of the interface between aramid fibres with and without surface treatment and matrices. From structural differences and pull-out tests by composites with treated fibres they concluded that curing makes the adhesion stronger due to stronger dispersive and polar interactions. Xie *et al*. dealt with the problem of using natural fibres in composites, because they need silane coupling agents for the creation of adhesion with the matrix. According to Xie proper treatment of fibres with silane can increase the interfacial adhesion to the target polymer matrices and improve the mechanical and outdoor performance of the resulting composites [5].
From manufacturing side Bigaud *et al*. studied 3D braiding technic in order to find relation between process parameters and mechanical properties. Different braiding angles of carbon fibre woven with PA12 have been found to result in different stiffness and strength values [6].
Investigating manufacturing failures Zarelli *et al*. [7] created a model based on the changing geometrical and mechanical properties due to curing. It was a novel resin sensitivity model

considering effects of heat treatment - a common step in all matrix composite material manufacturing - and polymerization happening during that. They concluded that among others chemical shrinkage, heat expansion and the change of viscoelastic modulus affects the most significantly spring-in phenomena, warpage and residual stresses. Similar investigation concerning the consequences of residual thermal stress in carbon fibre thermoplastics went down by Greisel *et al*. They found that the process-induced residual thermal stress can be reduced by annealing the untreated composite at temperatures beyond the glass transition temperature of the matrix. It leads to a change in failure behaviour due to an increase in interfacial fracture toughness [8].
Kravchenko *et al*. [9] created a multi-scale model for the response of a bi-material "thermostat", in order to measure thermal strains during a prescribed, but arbitrary thermal history. Their achievement was to separate different stresses caused by shrinkage and thermal expansion, and to be able to control curing temperatures so that shrinkage remains as minimal as possible.
Daniel *et al*. [10] managed to develop test methods for complete mechanical characterization of textile composites in three dimensions. They proposed three types of failure criteria in three dimensions: limit criteria (maximum stress), fully interactive criteria (Tsai–Hill, Tsai–Wu), and failure mode based and partially interactive criteria (Hashin–Rotem, Sun, NU).
Manufacturing hybrid composites, in most cases, the main difficulty can be found in achieving the required geometry (shape, dimensions etc.). A wise selection of manufacturing parameters is not only capable of cost reduction, but could also prevent problems like warpage, residual stress, micro cracks, and fibre-matrix failures [7]. Being successful with that can lower manufacturing costs.

4.2. Thermal aspects

In thermal cases studies usually deal with 1) effects of material and manufacturing parameters on thermal properties with 2) hot spots – small areas where extreme high temperatures and pressures occure if speed is higher than a critical value –, TEI (thermo elastic instability), third body phenomena or with 3) shrinkage during cure
The dependence of thermal properties with respect to material formulation and manufacturing parameters was investigated by Khamlichi *et al.* [11] Their study concluded that when only a single clutch engagement is considered, the temperature rise is hardly affected by the ratio of fibres to matrix. However, when repeated cyclic engagements are performed, higher fibre to matrix ratios can evacuate rapidly the frictional generated heat.
The modulus of elasticity can control the creation of hot spotting. Zagrodzki *et al*. dealt with hot spots resurfacing in wet multidisc clutches due to unstable thermoelastic friction system behaviour as a consequence of material composition and geometry failures. Simulation results have shown that reduction of the thickness of the steel disk can substantially improve thermoelastic stability, but it has limitations due to manufacturing reasons [12]. Majcherczaka *et al*. [13] developed a thermal numerical model, the third body was introduced as a uniform layer with energy storage and conduction. Ahn *et al*. created transient finite element simulation in order to solve the two-dimensional contact problem involving thermo-elastoplastic instability (TEPI) in a frictional sliding system presenting the change of hot spot location after cooling [14].
Chemical shrinkage of thermoset polymers was investigated by Nawab *et al*. for modelling residual strains and stresses, by taking into account the coupling between volume variation and thermal gradients. They found that for an equal mass, chemical shrinkage of resin carrying fibres is lesser than the shrinkage of neat resin. Assuming that a part of the shrinkage has been hindered by the fibres, it can reside as residual stresses in the composite part [15].

4.3. Tribological aspects

From tribological aspects papers also can be categorized into subtopics like 1) effects of components on the tribological behavior, 2) friction film development, 3) gas induced fading etc.
Chang *et al*. [16] used pin on disc setup with composite pins against polished steel counterparts within moderate pv-ranges at room and elevated temperatures, and microscopic observations to investigate the tribological properties of two kinds of high temperature resistant thermoplastic composites with short carbon fibre (SCF), graphite flakes, and sub-micro particles. It was found that conventional fillers could effectively enhance both the wear resistance and the load-carrying capacity of the base polymers. The frictional coefficient and wear rate of the composites were further reduced especially at elevated temperatures with the addition of sub-micro particles. Dominant wear mechanisms were discussed based on microscopic observation of worn surfaces.
Fernandes *et al*. compared friction films observed on clutches with results from laboratory tests and found that sliding conditions influence the stability of multi-layer friction films. It was also found that removing wear debris increases the friction level and reduces the wear rate [17].
The influence of a phase transition from solid organic material to gas on the contact behaviour in dry clutches was investigated by Fidlin *et al*. [18] The phase transition can result in a decrease in transmissible torque, which is known as fading-effect. A new model for the effect of outgassing on the dynamical behaviour of a dry clutch was developed taking into consideration asymptotic expansion for the pressure field, enabling to overcome numeric problems. They gave qualitative explanation of both fading and recovery effects finding permeability of the contact layer as the main parameter.

CONCLUSIONS

Coupling composite friction materials' history developed alongside with the evolution of clutch construction. Milestones that pushed it forward were the discovery and utilization of flexible resins, the growing popularity then the banning of asbestos considering healthcare. Nowadays trends turn in the direction of environmental protection experimenting with environmental friendly components such as plant fibres and fillers or bio-degradable friction materials.
However there are still open questions about friction behaviour under different conditions, wear characteristic sensitivity, thermal loads and responses, manufacturing steps etc. The field of composite frictional materials is so wide-spread and still an undeveloped land, that it grants a wide range of research opportunities for present and future investigations, experiments and studies.
In our future investigations, we are planning to deal with the thermal and tribological interactions and mechanical aspects of the different components in hybrid matrix friction materials for dry clutches in order to support material and finite element model development.

REFERENCES

[1] Bijwe, J.: *Composites as friction materials: Recent developments in non-asbestos fibre reinforced friction materials—a review*, Polymer Composites, 18 (3), 378–396, 1997
[2] Jacko, M. G. and Rhee, S. K.: *Brake Linings and Clutch Facings*. Kirk-Othmer Encyclopedia of Chemical Technology, 144-154, 2000
[3] Zhang, X., Li K.-Z., Li, H.-J., Fu, Y.-W., Fei, J.: *Tribological and mechanical properties of glass fibre reinforced paper-based composite friction material*, Tribology International, 69, 156–167, 2014

[4] P.J. de Lange, E. Mäder, K. Mai, R.J. Young, I Ahmad: *Characterization and micromechanical testing of the interphase of aramid-reinforced epoxy composites*, Composites Part A: Applied Science and Manufacturing, 32 (3–4), Pages 331–342, 2001
[5] Yanjun Xie, Callum A.S. Hill, Zefang Xiao, Holger Militz, Carsten Mai: *Silane coupling agents used for natural fibre/polymer composites: A review*, Composites Part A: Applied Science and Manufacturing, 41 (7), 2010, 806–819, 2010.
[6] D. Bigaud, L. Dréano, P. Hamelin: *Models of interactions between process, microstructure and mechanical properties of composite materials—a study of the interlock layer-to-layer braiding technique*, Composite Structures, 67 (1), 99–114, 2005
[7] Mauro Zarrelli, Ivana K. Partridge, A. D'Amore: *Warpage induced in bi-material specimens: Coefficient of thermal expansion, chemical shrinkage and viscoelastic modulus evolution during cure*, Composites Part A: Applied Science and Manufacturing, 37 (4), 565–570, 2006.
[8] M. Greisel, J. Jäger, J. Moosburger-Will, M.G.R. Sause, W.M. Mueller, S. Horn: *Influence of residual thermal stress in carbon fibre-reinforced thermoplastic composites on interfacial fracture toughness evaluated by cyclic single-fibre push-out tests*, Composites Part A: Applied Science and Manufacturing, 66, 117-127, 2014.
[9] O. G. Kravchenko, C. Li, A. Strachan, S. G. Kravchenko, R. B. Pipes: *Prediction of the chemical and thermal shrinkage in a thermoset polymer*, Composites Part A: Applied Science and Manufacturing, 66, 35–43, 2014.
[10] I. M. Daniel, J.-J. Luo, P. M. Schubel R. R. McCormick: *Three-dimensional characterization of textile composites*, Composites Part B: Engineering, 39 (1) Pages 13–19, 2008
[11] A. Khamlichi, M. Bezzazi, M.A. Parrón Vera: *Optimizing the thermal properties of clutch facings*, Journal of Materials Processing Technology, 142 (3), 634–642, 2003.
[12] P. Zagrodzki, S. A. Truncone: *Generation of hot spots in a wet multidisk clutch during short-term engagement*, Wear, 254, (5–6), 474–491, 2003
[13] D. Majcherczaka, P. Dufrenoya, Y. Berthierb: *Tribological, thermal and mechanical coupling aspects of the dry sliding contact*, Tribology International, 40 (5), 834–843, 2007.
[14] S. Ahn, Y. H. Jang: *Frictionally excited thermo-elastoplastic instability*, Tribology International, 43, (4), 779–784, 2010.
[15] Y. Nawab, X. Tardif, N. Boyard, V. Sobotka, P. Casari, F. Jacquemin: *Determination and modelling of the cure shrinkage of epoxy vinylester resin and associated composites by considering thermal gradients*, Composites Science and Technology 73 (23) 81–87, 2012.
[16] L. Chang, Z. Zhang, L. Ye, K. Friedrich: *Tribological properties of high temperature resistant polymer composites with fine particles*, Tribology International, 40 (7), 1170–1178, 2007.
[17] G.P. Fernandes, P.S. Zanotto, A. Sinatora: *Contribution on understanding the friction film development in the performance of a dry automotive clutch system*, Wear, 342–343 364–376, 20015.
[18] A. Fidlin, S. Bäuerle, F. Boy: *Modelling of the gas induced fading of organic linings in dry clutches*, Tribology International, 92, 559–566, 2015.

MANUFACTURING ANALYSIS OF GRINDING TECHNOLOGY OF CONICAL WORM SHAFT

BODZÁS Sándor PhD

Department of Mechanical Engineering, University of Debrecen
E-mail:bodzassandor@eng.unideb.hu

Abstract
The geometric correct production of conical thread surfaces is very complex and difficult task. In this publication a manufactruing technology of a new geometric worm shaft will be analysed using grinding wheel banking angle correction without centre stoppage. We introduce the geometric establishment of worm shaft and determine the necessary connections for the technological analysis. Based on the connections we model the technology and determine the necessary grinding wheel profiles for the manufacturing process.

Keywords: *spiroid, center distance, grinding wheel banking angle correction, manufacturing*

1. INTRODUCTION

Based on the advantages of cylindrical worm gear drive having arched profile [1, 4] and spiroid worm gear drive having linear profile [4, 8] in axial section we have developed a new geometric worm gear drive, that is the spiroid worm gear drive having arched profile in axial section [7].

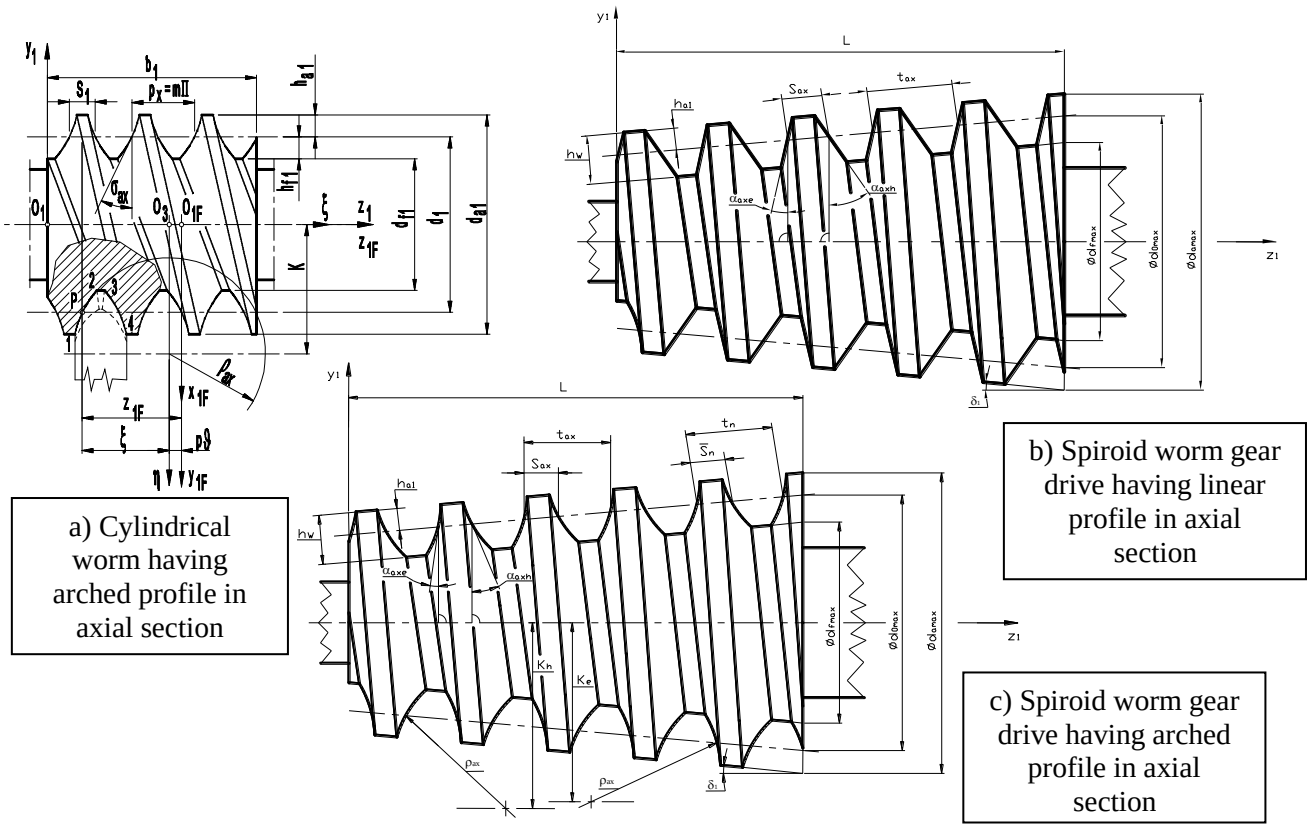

Figure 1 The geometric establishment of worm shafts [1, 3, 4, 8]

The parametric equation of the spiroid worm having arched profile is the following without derivation [3]:

$$\left.\begin{aligned} x_{1F} &= -\eta \cdot \sin \vartheta \\ y_{1F} &= \eta \cdot \cos \vartheta + p_r \cdot \vartheta \\ z_{1F} &= p_a \cdot \vartheta + \sqrt{\rho_{ax}^2 - (K_e - \eta)^2} \end{aligned}\right\} \qquad (1)$$

2. THE KINEMATIC ANALYSIS OF THE PRODUCTION TECHNOLOGY

Because of the geometric establishment of conical thread surfaces the lead angle is continuously changing. In consequence the conical worm profile in axial section is continuously changing in case of manufacturing [3]. For the worm profile is kept on the prescribed profile tolerance zone the optimal wheel extraction position has to be determined. Grinding of the spiroid worm with the wheel profile of this the worm profile in axial section is on the prescribed tolarance zone [3].
On Figure 1 because of the diameter changing of the spiroid worm the γ_0 lead angle on the mid – circle is changed on behalf of the assurance of the constant axial lead of thread.
In case of a new kinematical grinding wheel banking spindle case, as a function of the change of the centre distance [1, 2], $\pm B_2$ the value of wheel banking angle correction is constantly changed along the pitch length of the worm (Figure 2) [3, 4, 6].
The wheel is banked accordingly the γ_{0opt} lead angle on the mid-circle in case of manufacturing. During the process $\gamma_{0opt} \pm B_2$ grinding wheel banking angle correction is applied [3, 4, 6].
Based on the Illés Dudás – type general mathematical model [4, 5] the movements of the manufacturing process could be determined by the coordinate systems and the positions of these which are correlated each other (Figure 3).

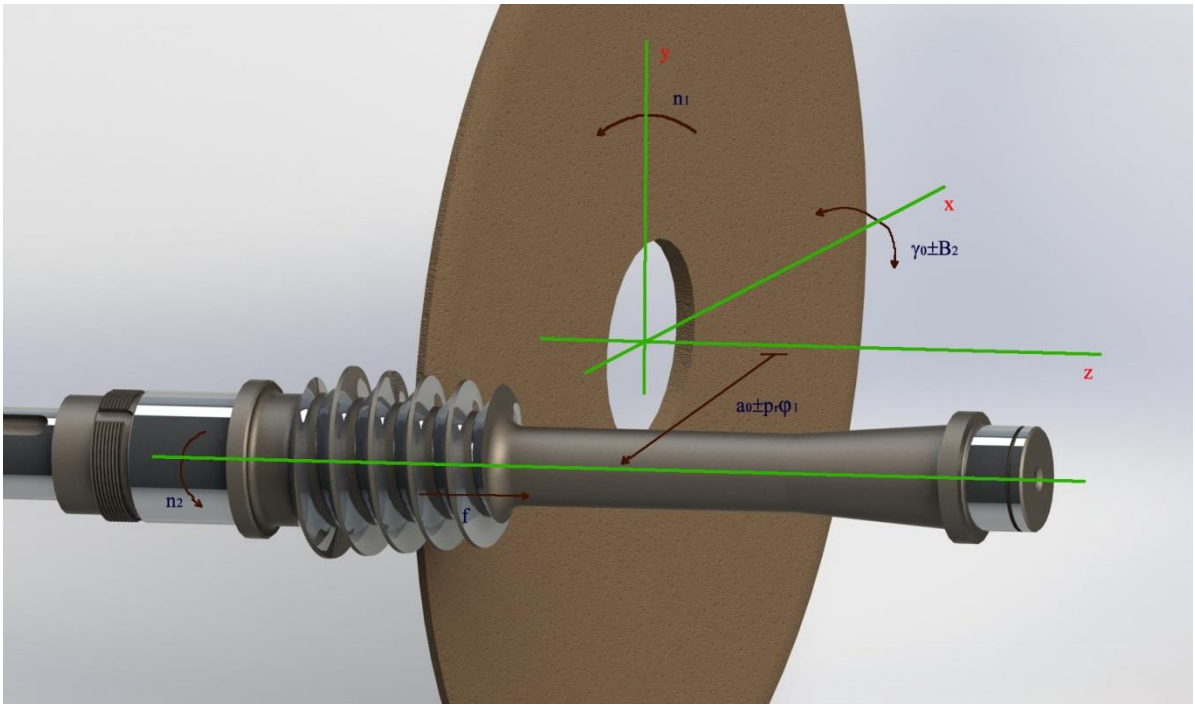

Figure 2 The grinding of the spiroid worm by computer aided modelling (CAM)

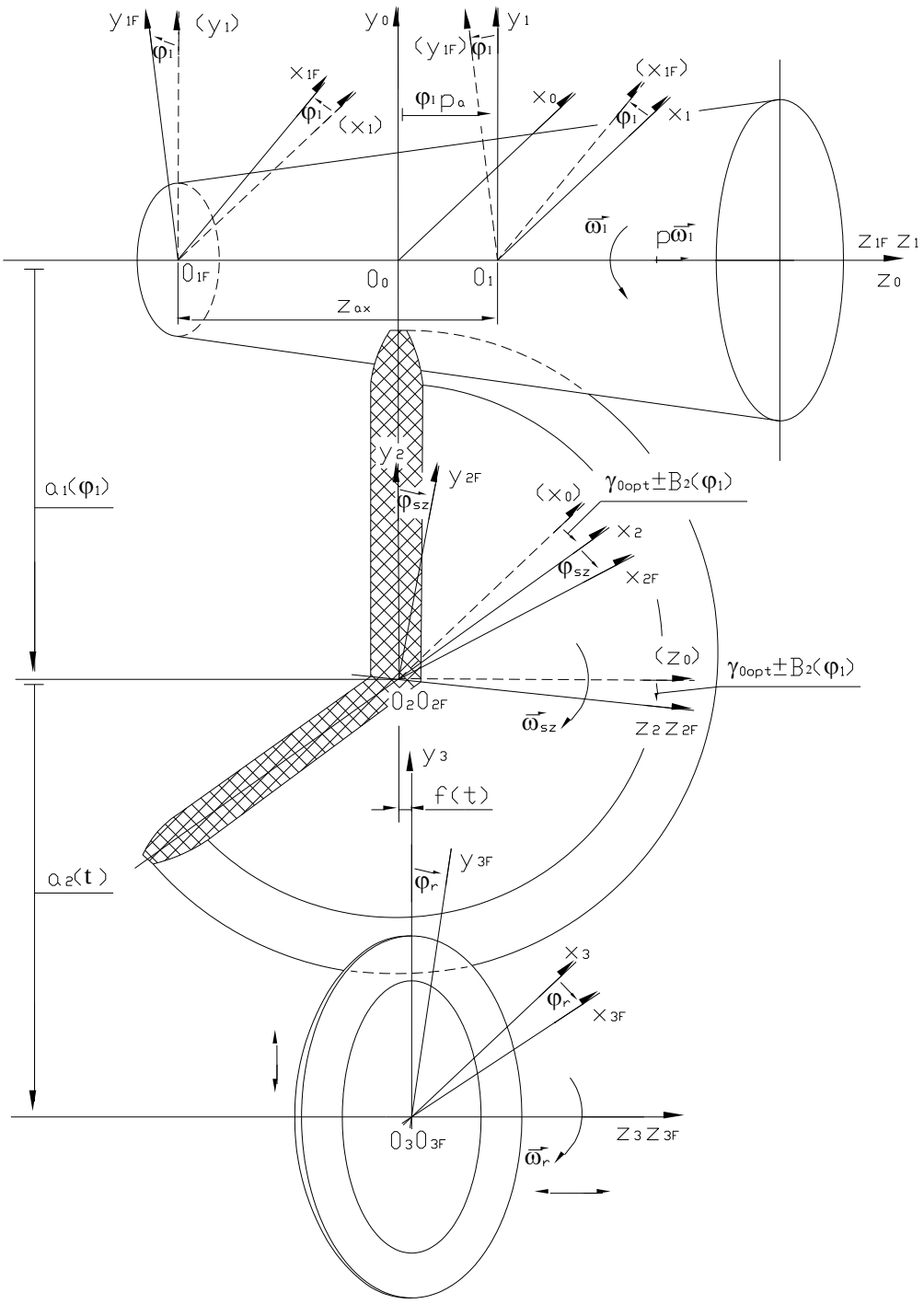

Figure 3 The coordinate systems in case of the manufacturing process of conical thread surface

The a_0 starting centre distance of the manufacturing process [3, 6]:

$$a_0 = \frac{d_{a\max}}{2} - \frac{h_w}{\cos\delta_1} + \frac{d_{akorong}}{2} \tag{2}$$

The a_1 centre distance in any given place [3, 6] (Figure 3):

$$a_1 = a_0 - p_r \cdot \varphi_1 \tag{3}$$

The grinding wheel banking angle correction could be determined based on (4) expression:

$$\gamma_0 = \gamma_{0opt} \pm B_2 = \arctan\left(\frac{H}{2 \cdot \pi \cdot \left(a_0 - p_r \cdot \varphi_1 + \frac{h_w - h_{a1}}{\cos \delta_1} - \frac{d_{akorong}}{2} \right)} \right) \tag{4}$$

The given two parametric vector – scalar $\vec{r}_{1F} = \vec{r}_{1F}(\eta, \vartheta)$ equation of spiroid worm the necessary grinding wheel profile for the manufacturing process could be determined by the theorem of double wrapping [4, 8, 9]:

$$\left.\begin{aligned} \vec{n}_{1F} \cdot \vec{v}_{1F}^{(12)} &= 0 \\ \vec{r}_{1F} &= \vec{r}_{1F}(\eta, \vartheta) \\ \vec{r}_{2F} &= M_{2F,1F} \cdot \vec{r}_{1F} \end{aligned}\right\} \tag{5}$$

The transformation matrix between the spiroid worm and the grinding wheel is the following:

$$M_{2F,1F} = \begin{bmatrix} \cos\varphi_1 \cdot \cos\gamma_0 \cdot \cos\varphi_{sz} - \sin\varphi_1 \cdot \sin\varphi_{sz} & -\sin\varphi_1 \cdot \cos\gamma_0 \cdot \cos\varphi_{sz} - \sin\varphi_{sz} \cdot \cos\varphi_1 & \sin\gamma_0 \cdot \cos\varphi_{sz} & -z_{ax} \cdot \cos\varphi_{sz} \cdot \sin\gamma_0 + \varphi_1 \cdot p_a \cdot \sin\gamma_0 \cdot \cos\varphi_{sz} - a_0 \cdot \sin\varphi_{sz} - \varphi_1 \cdot p_r \cdot \sin\varphi_{sz} \\ \cos\varphi_1 \cdot \cos\gamma_0 \cdot \sin\varphi_{sz} + \cos\varphi_{sz} \cdot \sin\varphi_1 & -\sin\varphi_1 \cdot \cos\gamma_0 \cdot \sin\varphi_{sz} + \cos\varphi_1 \cdot \cos\varphi_{sz} & \sin\gamma_0 \cdot \sin\varphi_{sz} & -z_{ax} \cdot \sin\varphi_{sz} \cdot \sin\gamma_0 + \varphi_1 \cdot p_a \cdot \sin\gamma_0 \cdot \sin\varphi_{sz} + a_0 \cdot \cos\varphi_{sz} + \varphi_1 \cdot p_r \cdot \cos\varphi_{sz} \\ -\sin\gamma_0 \cdot \cos\varphi_1 & \sin\gamma_0 \cdot \sin\varphi_1 & \cos\gamma_0 & -z_{ax} \cdot \cos\gamma_0 + p_a \cdot \varphi_1 \cdot \cos\gamma_0 \\ 0 & 0 & 0 & 1 \end{bmatrix} \tag{6}$$

The transformation matrix between the grinding wheel and the regulating wheel is the following:

$$M_{3F,2F} = \begin{bmatrix} \cos\varphi_r \cdot \cos\gamma_0 \cdot \cos\varphi_{sz} + \sin\varphi_r \cdot \sin\varphi_{sz} & \cos\varphi_r \cdot \cos\gamma_0 \cdot \sin\varphi_{sz} - \sin\varphi_r \cdot \cos\varphi_{sz} & -\cos\varphi_r \cdot \sin\gamma_0 & -a_2 \cdot \sin\varphi_r \\ \sin\varphi_r \cdot \cos\gamma_0 \cdot \cos\varphi_{sz} - \cos\varphi_r \cdot \sin\varphi_{sz} & \sin\varphi_r \cdot \cos\gamma_0 \cdot \sin\varphi_{sz} + \cos\varphi_r \cdot \cos\varphi_{sz} & -\sin\varphi_r \cdot \sin\gamma_0 & a_2 \cdot \cos\varphi_r \\ \sin\gamma_0 \cdot \cos\varphi_{sz} & \sin\gamma_0 \cdot \sin\varphi_{sz} & \cos\gamma_0 & -f \\ 0 & 0 & 0 & 1 \end{bmatrix} \tag{7}$$

3. THE CALCULATED RESULTS FOR A CONCRETE WORM GEOMETRY

Using the received equations a computer aided program has been developed for the determination of the necessary optimal grinding wheel profile. The calculations have been done for a concrete worm geometry.

Table 1 Calculated results of the manufacturing process (m_{ax}=5 mm, $d_{akorong}$=400 mm)

Low side d_{0opte}=58,328 mm, φ_{1opte}=730,9°, γ_{0opte}=4,8995°, K_e=37,615 mm			**High side** d_{0opth}=59,032 mm, φ_{1opth}=600,962°, γ_{0opth}=4,841°, K_h=45,305 mm		
Angular displacement φ_1 [°]	**Centre distance a_1 [mm]**	**Banking angle correction B_2 [°]**	**Angular displacement φ_1 [°]**	**Centre distance a_1 [mm]**	**Banking angle correction B_2 [°]**
0	225,6420	-0,4233	**0**	225,6420	-0,3648
180	224,9549	-0,3253	**180**	224,9549	-0,2668
360	224,2678	-0,2229	**360**	224,2678	-0,1644
540	223,5806	-0,1158	**540**	223,5807	-0,0573
720	222,8936	-0,0037	**φ_{1opth}=600,962**	223,3480	0
φ_{1opte}=730,9	222,8520	0	**720**	222,8936	+0,0548
900	222,2065	+0,1137	**900**	222,2065	+0,1722
1080	221,5194	+0,2369	**1080**	221,5194	+0,2954
1260	220,8323	+0,3663	**1260**	220,8323	+0,4248
1440	220,1452	+0,5023	**1440**	220,1452	+0,5608
1583,2	219,5986	+0,6157	**1583,2**	219,5986	+0,6742

On Table 1 the variations of centre distance and grinding wheel banking angle correction are in case of the two tooth sides.
On Figure 5 the motion cycles of the manufacturing steps of the calculated grinding wheel profile could be seen for both tooth sides by the regulating wheel.

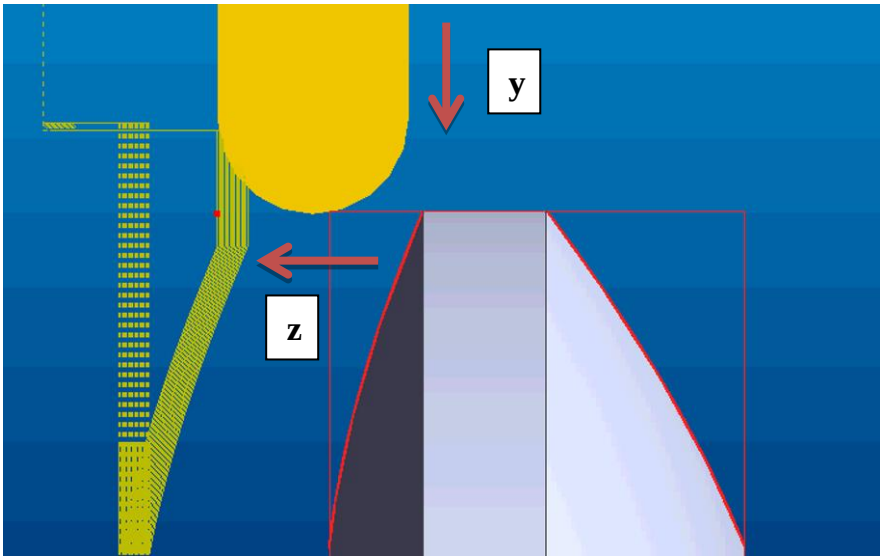

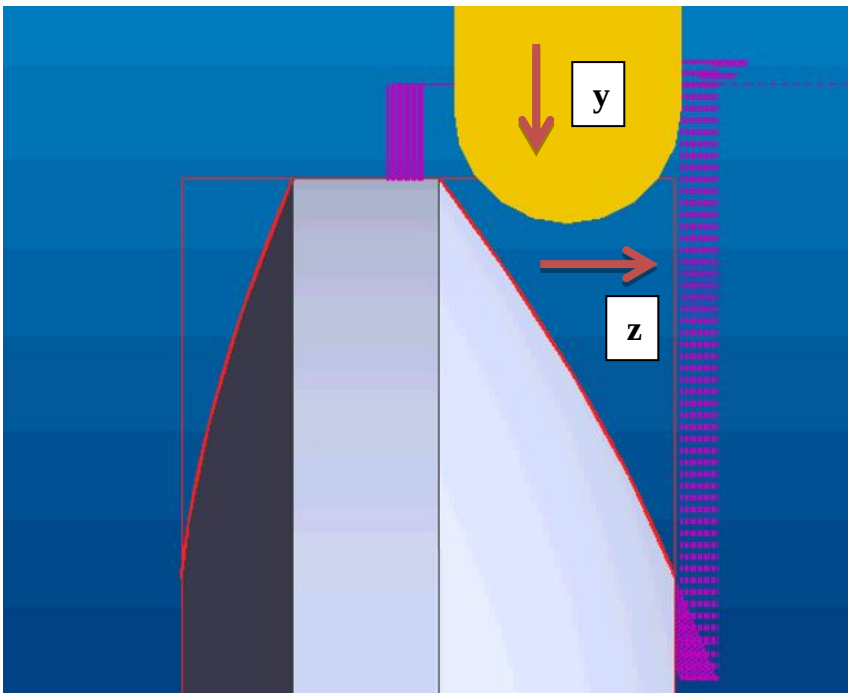

Figure 5 The manufacturing simulation of the necessary wheel profiles

CONCLUSIONS

We have worked out a new geometric spiroid worm gear drive that is the spiroid worm gear drive having arched profile in axial section [7].
In case of the finishing manufacturing technology of the spiroid worm the centre distance between the worm axis and the grinding wheel axis are continuously changing. Because of the geometry of the conical thread surface the lead angle is continuously changing that is why during the manufacturing process grinding wheel banking angle correction is also applied [3, 4, 6].
We have determined the necessary mathematical correlations for the manufacturing analysis. We have analysed the manufacturing technology in case of concrete worm geometry.

REFERENCES

[1] Balajti Zs.: *Kinematikai hajtópárok gyártásgeometriájának fejlesztése*, Ph.D. dissertation, Miskolc, University of Miskolc, 2007., Research Leader: Prof. Dr. Dudás Illés
[2] Bányai, K., Dudás, I.: *Analysis of the spiroid drivings having new production geometry*, Production Process and Systems, Miskolc, University Press, Volume 1, 2002, pp. 177-185., ISSN 1215-0851
[3] Bodzás, S.: *Connection analysis of surfaces of conical worm, face gear and tool*, Ph.D. dissertation, University of Miskolc, 2014., p. 154., Research Leader: Prof. Dr. Illés Dudás, DOI 10.14750/ME.2014.006
[4] Dudás, I.: *The Theory and Practice of Worm Gear Drives* Penton Press, London, 2000., ISBN 1877180295
[5] Dudás, I.: *The extension of the general mathematical model developed for helical surfaces to the whole system of manufacturing technology and production geometry (ProMAT)*, International Journal of Advenced Manufacturing Technology, Springer, ISSN 0268-3768

(Online), 2016. 01. 12. (Online), Volume 82, Number 1 – 4. (2016), (IF 1.458), DOI 10.1007/s00170-015-8233-5

[6] Dudás, I., Bodzás, S.: *The kinematical model for the geometrically appropriate production of cylindrical and conical helicoidal surfaces having unvaried lead*, International Journal of Advenced Manufacturing Technology, Springer, ISSN 0268-3768 (Online), 2015. 04. 17. (Online), Volume 78, Number 1 – 4. (2015), (IF 1.458), DOI 10.1007/s00170-015-7088-0

[7] Dudás I., Bodzás S., Dudás I. Sz., Mándy Z.: *Konkáv menetprofilú spiroid csigahajtópár és eljárás annak köszörüléssel történő előállítására*, The day of the patent registration: 2012.07.04., Patent number: 229 818

[8] Hegyháti, J.: *Untersuchungen zur Anwendung von Spiroidgetrieben*. Dissertation, TU Dresden, 1988.

[9] Litvin, F. L., Fuentes, A.: *Gear Geometry and Applied Theory*, Cambridge University Press, 2004., ISBN 978 0 521 81517 8

APPLICATION OF INDUSTRY 4.0 IN THE MATERIAL HANDLING

[1]BOHÁCS Gábor PhD, [2]RINKÁCS Angéla

[1,2]Department of Materials Handling and Logistic Systems; Faculty of Transportation Engineering and Vehicle Engineering; Budapest University of Technology and Economics
[1]E-mail: gabor.bohacs@logisztika.bme.hu
[2]E-mail: angela.rinkacs@logisztika.bme.hu

Abstract
In today's manufacturing systems change is a constant issue. Smart, automated production systems, appearance of novel production technologies and assembly systems together with the modern supply chains applying computers in all areas enabled new possibilities in the industry. Application of these new possibilities in a mass resulted in the born of the Industry 4.0 – the fourth industrial revolution. This novel business model didn't leave untouched material handling either. This paper introduces the related most important issues between the two areas, and point out the most significant directions for further development.

Keywords: *material handling, smart production, Industry 4.0, cyber-physical systems, logistics*

1. INTRODUCTION

Modern production systems must be adaptable to variable market needs, trend changes and new technologies. The product variety constantly increases, which led to smaller production volumes, even a lot of one product is getting common. Parallel the product's lifecycle is decreasing. There are opinions that conventional Computer Integrated Manufacturing (CIM) systems are over [1]. In the 1990s appeared the Lean Production which changed the existing production principles by its flexibility and effectiveness. Later Lean evolved into a much wider spectrum, enabling e.g. Lean automation [1] which is a combination of automation technology and Lean production. The results of this are widely used, examples like the digitized Kanban or the automatic reordering of materials using mini cameras attached to storage boxes [2]. Born of Industry 4.0, which is a relevant German project [3] on the application of Cyber-physical systems in the industry is the next decisive game changer. Industry 4.0 describes principles of production processes based on the tight connection of physical and digital components. The system components autonomously communicating with each other making decentral decisions along the value chain. Industry 4.0 takes account of the increased computerization of the manufacturing industries where physical objects are seamlessly integrated into the information network. As a result, "manufacturing systems are vertically networked with business processes within factories and enterprises and horizontally connected to spatially dispersed value networks that can be managed in real time – from the moment an order is placed right through to outbound logistics [4].
Materials handling is a key element of production systems. It plays an important role in enhancing productivity and flexibility of the entire system as well as effective utilization of resources. The cost of material handling constitutes15% to 70% of the total manufacturing cost of a product [5]. There are several typical machines applied in material handling: these are cranes industrial trucks, floor and overhead conveyors, automatic guided vehicles, robots and other transfer devices and manuals. As being a collaborative part to manufacturing systems, material handling should strongly be affected by Industry 4.0. This paper surveys the most important trends and effects between them.

2. CHARACTERISTICS OF CURRENT MATERIAL HANDLING RESEARCH

Material handling research has extensive areas of interest. Matson et al. [6] in their paper surveyed the most relevant research areas. However this publication is not fresh, this listing is broadly valid even today. First there is an ongoing research on the transported materials as their specifics are decisive on the material handling capacity and required power. Certainly mechanical constructional issues in material handling from various aspects have always an important focus. Besides the mechanical part, control – first of all motion control - issues of materials handling machines are strongly addressed by research ever since. System control of the machinery is also a central question
as the optimal utilization of these has a significant effect on the competitiveness of a company. Selection of material handling systems and integration of them with other components of manufacturing has also been researched for a long time but mainly from economical aspects. Simulation model developments have also a long record in the research. Former optimization of these models was dominant, but for now there is an increasing number of research are focusing on automatic data transfer from the real system into the model [7]. Additionally, research has focused on designing ergonomically sound material handling systems. In material handling systems 'scheduling' problems such as the flow path and the number of equipment are also matter of research.
The above research directions are valid for today too. Industry 4.0 research has already been appeared in many areas, but explicitly for materials handling only a few topics can be pointed out.

3. ACTUAL TRENDS OF MATERIAL HANDLING SYSTEMS WITH I4.0 RELEVANCE

Industry 4.0 appears in the material handling first via the realization of intelligent components. In this context the emphasis altered compering to the current systems, where the main goal is to have an intelligent system as a whole. Industry 4.0 focuses on each component to be intelligent. This way these components can be easier matched to changing demands. Figure 1. gives two examples for it. In Figure 1 a) intelligent roller conveyor components are depicted. In Figure 1 b) modular drive components for conveyors are shown, where the control logic and the motion control electronic are integrated. This way a holistic intelligent actuator function is realized. Similar solutions will enable that in the future the realization of material handling systems can be made in a „plug & work" way.

a) from [8] b) from [9]

Figure 1 Intelligent material handling components

Above components come primarily in conveyors systems forward. The area of forklifts and transfer devices is effected by another technology: robotics. Automatic guided vehicles (AGVs) are operating as part of automated materials handling systems since several decades. In the AGV technology there are two trends which helps robotics in this area. First there are more and more suppliers on AGV components from which customized machines can be built. These are not only functional elements but such intelligent components which help to reconfigure the machine on changing needs. The various components enable to turn even a conventional forklift truck into a service robot (Fig. 2 a). Secondly, there are AGVs which are equipped with industrial robotic arms, in order to be able to facilitate handling operations (Fig. 2 b.). This makes the AGV as a material handling machine very much adaptable and flexible thus one major component to implement the Industry 4.0's objectives.

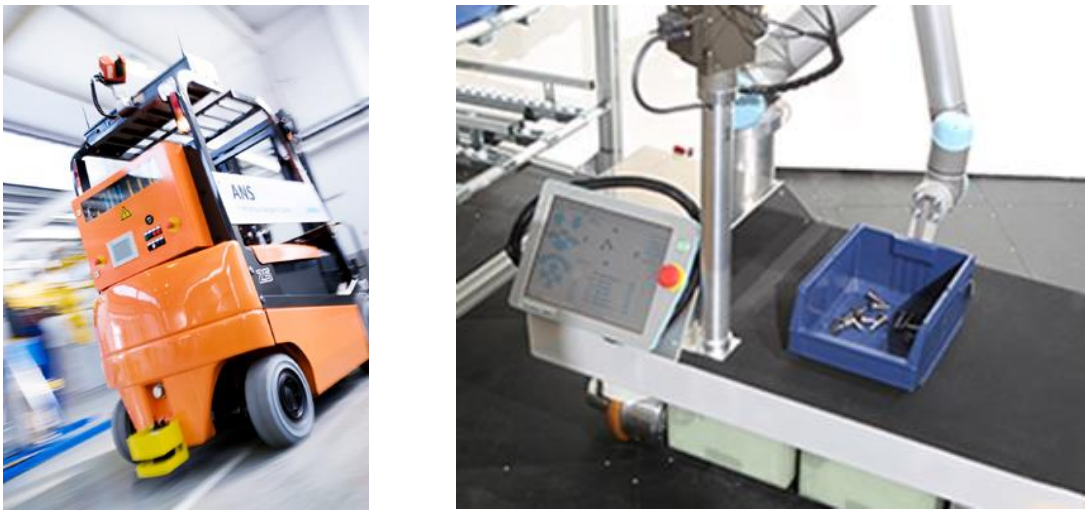

a) Autonomous forklift components [10] b) AGV with a robotic arm [11]

Figure 2 Industry 4.0 relevant AGV developments

Besides the above two there are several other areas, where material handling is subject to changes in order to comply to Industry 4.0. These are for example the extensive use of sensors and general application of localization systems for the material handling system components.

CONCLUSIONS

If a conclusion should be drawn, what will be the most decisive area in material handling research to reach the objectives of Industry 4.0, we would name a research area which hasn't been mentioned yet. In [12] a Reference architecture model of Industry 4.0 (RAMI 4.0) has been described. It is an information model for Industry 4.0 components and their handling from various aspects (e.g.: business, constructional, functional, localization, network layer, human machine interface). Creation of these RAMI 4.0 models enables systematic, quick planning activity even by multiple experts using existing or new components. From this point these information models are extremely interesting for material handling. In our opinion without the creation of these models for material handling components, and applying them strongly together the material handling machines will be interpreted in a different way as has been in the past or nowadays. In the past material handling machines were (frequently unique) solutions for the task of transferring material from a point to another in a production facility. Current stand of the technology says machines are components of a highly optimized material handling system. Due to the integrated use of the physical and information models the material handling machines will turn more and more into 'Apps' (like

Applications on the computers) with special interfaces, such as physical, human, informatics. Only this way can it be ensured that these machines can actively fulfill their tasks in the rapidly changing environment made by Industry 4.0.

REFERENCES

[1] Dennis Kolberg, Detlef Zühlke: *Lean Automation enabled by Industry 4.0 Technologies. IFAC-PapersOnLine 48-3 (2015) 1870–1875*

[2] Würth Industrie Service GmbH & Co. KG (2013) *iBin(R) stocks in focus - the first intelligent bin*. https://www.wuerth-industrie.com/web/media/pictures/master/press_information_master/EN_P_iBin_Stocks_in_Focus.pdf

[3] Bundesministerium für Bildung und Forschung: Zukunftsbild „Industrie 4.0“ https://www.bmbf.de.

[4] Smit et al.: Industry 4.0., a Study for the ITRE Comittee, http://www.europarl.europa.eu/RegData/etudes/STUD/2016/570007/IPOL_STU(2016)570007_EN.pdf

[5] Behzad Esmaeilian, Sara Behdad, Ben Wang: *The evolution and future of manufacturing: A review*, Journal of Manufacturing Systems 39 (2016) 79–100.

[6] Matson, J. O., & White, J. A. (1982). *Operational research and material handling*. European Journal of Operational Research, 11(4), 309–318. doi:10.1016/0377-2217(82)90196-5

[7] G. Bohács, D. Gáspár, B. Kádár, A. Pfeiffer. Simulation Support in Construction Uncertainty Management: a Production Modelling Approach. Periodica Polytechnica Transportation Engineering, Vol. 44, No. 2, pp. 115-122, 2016. DOI: 10.3311/PPtr.8547

[8] Furmans, K: Industrie 4.0 und cyberphysische Systeme: *Kurzlebiger Trend oder Arbeitswelt von morgen?* Fachtagung Sicherheit und Gesundheitsschutz in der Warenlogistik 2015,BGHW, 14. September 2015, Dresden

[9] Weidmüller GmbH: MSF-Vathauer Antriebstechnik präsentiert neue Motorsteuereinheiten auf Basis des „FieldPower® Drive“ Konzeptes von Weidmüller. http://www.weidmueller.de/de/presse/produktmeldungen/msf-vathauer-antriebstechnik

[10] Siemens: *Fahrerlose Freiheit: Autonomous Navigation System für Transportsysteme*. https://www.industry.siemens.com/verticals/global/de/automobilproduktion/anlagenloesungen/foerdertechnik-automobilfertigung/Documents/e20001-a780-p200.pdf

[11] Fraunhofer IPA: *ROB@WORK 3*. http://www.ipa.fraunhofer.de/fileadmin/user_upload/Kompetenzen/Roboter-_und_Assistenzsysteme/Industrielle_und_gewerbliche_Servicerobotik/English_Documents/productsheet_rob@work_3.pdf

[12] VDI: *Fortentwicklung des Referenzmodells für die Industrie 4.0 – Komponente*. https://www.vdi.de/fileadmin/vdi_de/redakteur_dateien/gma_dateien/6146_PUB_GMA_ZVEI_Statusreport_-_RAMI_4-0_Struktur_der_Verwaltungsschale_Internet.pdf

FUNDAMENTAL PLASMA PROCESSES IN THE NEXT GENERATION OF COMBINED PIII-HIPIMS IMPLANTATION AND DEPOSITION TECHNIQUE

[1]BÓNOVÁ Lucia PhD, [2]BOHOVIČOVÁ Jana PhD, [3]HALANDA Juraj, [4]IVAN Jozef, [5]MEŠKO Marcel PhD

[1]Slovak University of Technology in Bratislava, Faculty of Materials Science and Technology in Trnava, Advanced Technologies Research Institute, J. Bottu 25/8857,917 24 Trnava, Slovakia
E-mail: lucia.bonova@stuba.sk
[4]Slovak University of Technology in Bratislava, Faculty of Electrical Engineering and Information Technology in Bratislava, Institute of Electronics and Photonics, Ilkovičova 3, 812 19, Bratislava, Slovakia
E-mail: jozef.ivan@stuba.sk

Abstract
In this contribution we have considered the role of energetic ions transport in HiPIMS post discharge. By using variable pulse magnetron current durations, the contribution of the elementary time step of the magnetron post-discharge to the ion transport toward a biased substrate located at various distances from the magnetron was analyzed. Moreover, a short reviews of PIII and HiPIMS plasma technologies are also given in this work.

Keywords: *Plasma ion immerse implantation, magnetron sputtering, drift velocity.*

1. INTRODUCTION

Plasma immersion ion implantation (PIII) can be considered as a mature technology for thin film modification. The application of PIII in earlier times was directed to the surface modification by implantation of gaseous ions; for example, hardening of machine tools and mechanical parts [1,2], formation of oxide layers on metal and semiconductor surfaces [3,4], the delamination of semiconductor wafer [5] and so on. Recently, PIII&D (plasma immersion ion implantation and deposition) is being extended to deal with various metallic ions to make hard and wear-resistant coating layers of metal carbides (TiC, TaC, SiC, WC), metal nitrides (BN, AlN, Si_3N_4, CrN, TiN, TiCN, TiAlN, TaN), and metal oxides (Al_2O_3, SiO_2, TiO_2, ZrO_2) on the workpiece. The merit brought by ion implantation is the excellent adhesion of the coating layer caused by the ion-collision-induced interface mixing [6].The main advantage of PIII&D is the ability of implanting 3-dimensional targets with complicated geometries, because electrical field between plasma sheath and target is ending perpendicular everywhere with the target surface.

2. PIII PRINCIPLES

Usually, the plasma is generated by RF-power (13.56 MHz) which is coupled to the plasma by means of matched antennas or coils, which are either placed inside the chamber or outside with a suitable glass window. Typical values for the plasma density and neutral gas pressure are 10^9–10^{11} cm^{-3} and 10^{-1}–10 Pa, respectively. A schematic drawing of the PIII system is shown in Figure 1(a). When a rectangular high voltage negative pulse is applied to a conducting substrate immersed in plasma, an ion sheath develops around the substrate and the ions are accelerated towards the

substrate surface, where they are implanted as it can be seen on Figure 1(a). The sheath dynamics has already been extensively studied [8–11] and is now well understood. When a substrate or target is immersed into a plasma, it is pulsed biased to high negative potential ϕ, typically many kilovolts, such as to repel electrons on a timescale of the inverse electron plasma frequency ω_{pe}^{-1}, which is given as follows: $\omega_{pe} = (n_e e^2/m_e\varepsilon_0)^{1/2}$. After ω_{pe}^{-1}, a sheath of ions is formed between the plasma and the biased substrate, usually referred to as the ion matrix sheath [7]. The ion matrix sheath, free of electrons is formed around the substrate on the time scale of the inverse ion plasma frequency,$\omega_{pi} = (n_i e^2/m_i\varepsilon_0)^{1/2}$, the ions in the matrix sheath close to the substrate are accelerated towards the substrate and the ion current density reaches a sharp maximum, before decreasing. Typical time evolution of the sheath thickness and the ion current during the pulse is illustrated in Figure 1(b). The sheath thickness $s(t)$ rapidly increases from its initial matrix sheath thickness s_0 toward the steady-state thickness s_c that changes in proportion to $V^{3/4}$ for the negative applied voltage $-V$. These s_0 and s_c are given as follows: $s_0 = (2\varepsilon_0 V/en)^{1/2}$and $s_c = (2/9)^{1/2}(2eV/kT_e)^{1/4}s_0$, where ε_0 is the permittivity of vacuum, e is the elementary charge, n is the plasma density, k is the Boltzmann constant and T_e is the electron temperature. During this period, the ion current I_i and equivalently dose rate rapidly decreases as $I_i \propto V^{3/2}/s^2 \propto s^{-2}(t)$ with increasing the sheath thickness, according to the Child-Langmuir law.

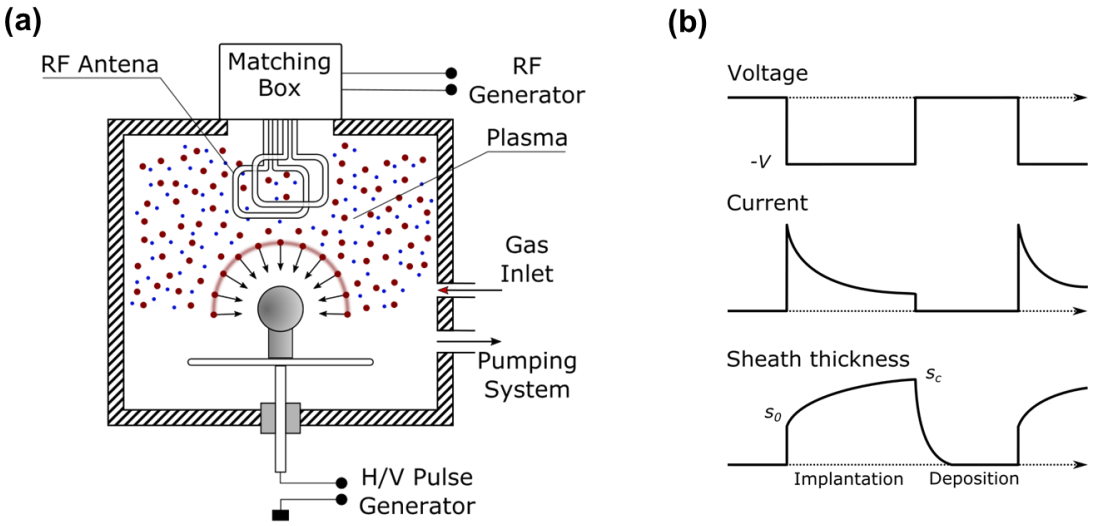

Figure 1 (a) Schematic drawing of the PIII system using RF antenna, (b) voltage, current and sheath thickness as a function of time.

Since in PIII, the duration of negative pulses is much longer than the inverse ion plasma frequency, we can generally consider that the steady-state sheath thickness, s, is that given by the steady-state Child–Langmuir law, $s = \left(2^{5/2}\varepsilon_0^{1/2}/3exp(-1/4)\right)\left(V_0^{3/4}/e^{1/4}n_e^{1/2}(kT_e)^{1/4}\right) \approx \lambda_{De}(eV_0/kT_e)^{3/4}$ where V_0 is the potential of the substrate during the pulse (as a first approximation, the plasma potential is assumed to be equal to the ground potential), T_e is the electron temperature of the plasma, k the Boltzmann constant, and λ_{De} the electron Debye length. As shown in equation above, s is independent of the ion mass, depends little on the electron temperature, and is inversely proportional to the square root of the plasma density. When considering plasmas with a density n_e equal to 10^{10} cm^{-3} and an electron temperature kT_e = 1 eV, the sheath thickness, for example, exceeds 40 cm for V_0 = 100 kV. This result has strong implications for the design of PIII reactors. To enter the plasma, ions have to satisfy the Bohm criterion. Typical value of Bohm criterion is

$\sim 10^5$ cm.s^{-1}. Finally, the ion current density j is related to the diffusive flux of ions from the plasma, which is given by the product of the plasma density and the ion acoustic or Bohm velocity, $v = \sqrt{kT_e/m_i}$.Regarding the size of the plasma, which must be much larger than the sheath thickness in order to avoid total depletion of the plasma between the substrate and the vessel walls. Implantation of monoenergetic ions using PIII requires that ion transit in the sheath must be collision less, i.e. an ion mean free path λ in of the order of or larger than the sheath thickness, s. Under these conditions, monoenergetic ion bombardment can be obtained.

3. HIGH POWER IMPULSE MAGNETRON SPUTTERING (HiPIMS)

HiPIMS is defined as pulsed magnetron sputtering, where the peak power exceeds the time-averaged power by 2 orders of magnitude [12]. During HiPIMS, a short impulse of power with very high amplitude is applied to the cathode and a long pause exists between the pulses resulting in low duty cycle [13]. Thanks to that, the average power is low enough to prevent target melting, but it simultaneously results in high plasma density and high degree of ionization of the sputtered material. HiPIMS brings several principal advantages: i) plasma densities approximately two orders of magnitude higher than in DC magnetron discharge (i.e. around 10^{13} cm^{-3}) [14], ii)substantial increase of the ion vs neutrals ratio from several percent in the case of DC magnetron sputtering over 70% depending on the electron impact cross section and ionization potential of the corresponding target material and sputtering conditions the HiPIMS regime [15], iii) possibility for self-sustained sputtering [12]. Higher densities result from the increase of surface mobility of the adatoms due to enhanced ion flux and subsequent reduction of coating porosity [16]. The prospects for the increase of the level of ionization can be estimated from the following calculation: if the electron density in the ionization region close to the target surface is around 10^{13} cm^{-3}, the ionization mean free path is about 1 cm. In DC magnetrons, the electron density is typically 10^{11} cm^{-3}. Then, the ionization mean free path would be ~50 cm [17]. The peak power density during the pulse is in the range of a few kW cm^{-2} while the time-average power is kept at the level of several W cm^{-2} similarly as in conventional DC magnetrons [18]. The length of the pulse is usually in the range 10-500 μs while the pulse frequency may cover the range from Hz to several kHz. The voltage during the pulse is usually 500-1000 V and the peak current density reaches a few A.cm^{-2}. Each period consists of several stages: i) electrical breakdown, ii) gas plasma, iii) metal plasma, and iv) steady state, which may be reached if the metal plasma is dense enough to effectively dominate over the gas plasma [18].

4. PIII&D BASED ON PIII AND HIPIMS

PIII is usually carried out with isotropic gaseous plasma, such as discharge in nitrogen. In contrast, gas and metal ions have different behaviors when implanted. Metallic ions have a high bonding affinity and can be incorporated at lattice sites of the substrate as replacements [19]. The most widely used device for metal PIII&D was introduced by Brown *et al*. [20]. In this technique, a pulsed cathode arc plasma source is used to produce a plasma with metal ions, which are implanted when high-voltage pulses are applied to the samples. However, the cathode spot of a vacuum arc generates a spray of liquid droplets, which condensate in macroparticles on the sample surface [21]. These macroparticles having size of 0.1 – 10 μm. Presence of the nanoparticles are highly undesirable because they degrade properties of thin films and coatings. Macroparticle inclusions can be reduced by substrate biasing and by concentrating the plasma flow with magnetic fields by using a curved magnetic plasma duct [22]. However this filtering arrangement implies large plasma losses [23].Wu *et al.* [24] have introduced a novel metal plasma immersion

implantation method, where PIII and HPPIMS is merged. Such PIII-HiPIMS&D arrangement is shown in Figure 2 (a). The metal plasma is produced by HiPIMS using a common magnetron sputtering target instead of ionizing atoms from a pulsed cathodic arc plasma source. This method combines the advantages of PIII and HiPIMS, and there are very few macroparticles in the high density plasma. Since the target used to produce the plasma in a common magnetron sputtering target, it is easy to scale up to process large samples.

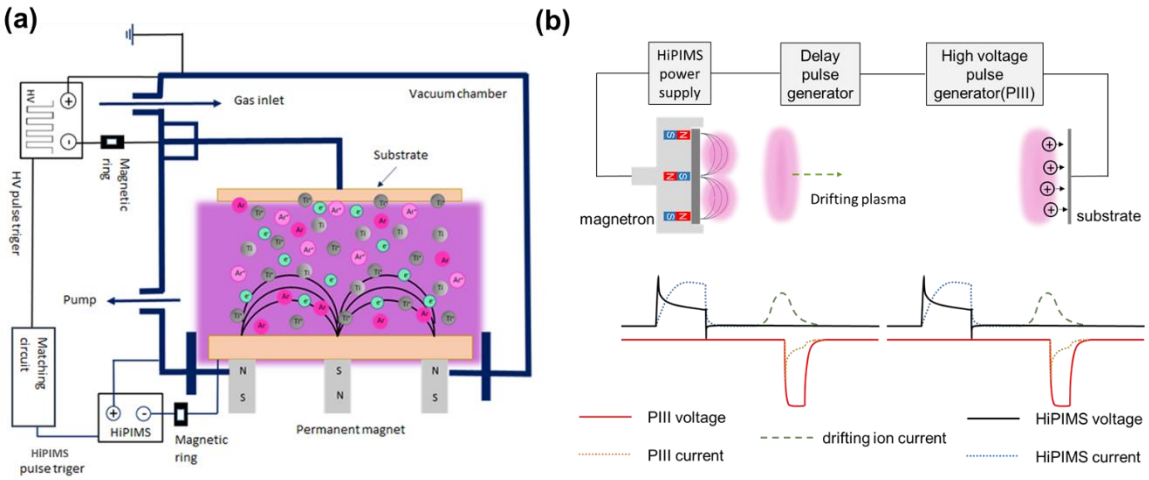

Figure 2 (a) Schematic drawing of the PIII-HiPIMS&D, (b) Synchronization hardware requirements with transient I-V characteristics

However detailed studies regarding the ion transport from HiPIMS onto the high voltage biased substrate are missing. Furthermore, it is necessary to synchronize pulses in order to implant metallic ions solely. Synchronization hardware requirements together with pulse sequences of PIII-HiPIMS&D are shown in Figure 2 (b). HiPIMS discharges are featured by an initial pressure-dependent current peak followed by a second phase which is power and material dependent. This suggests that the initial phase of a HiPIMS discharge pulse is dominated by gas ions, whereas the latter phase has a strong contribution from self-sputtering, indicating the latter phase of a HiPIMS discharge pulse is dominated by metal ions. This gives an opportunity of selective metallic ions implantation by synchronized PIII biasing. In order for the sheath to exist with a monotonic potential, ions must arrive at the sheath edge at least with the velocity of ion acoustic waves. A conventional interpretation for stationary, non-flowing plasma is, that ions gain this directed velocity via a small voltage drop in the ‘pre-sheath’, a quasi-neutral transition layer between the space-charge sheath and the undisturbed, quasi-neutral plasma. For cathodic arcs, ions are already supersonic before they are accelerated in the sheath. The Bohm criterion is over satisfied, with important consequences for the pre-sheath - sheath structure. In the case of HiPIMS discharge, these conditions have to be verified.

5. RESULTS

Knowledge of the mass, flux, and energy distribution of each ion species incident at the film growth surface is essential for establishing the relationship between plasma process parameters and the properties of resulting thin films. In the case of pulsed-plasmas such as HiPIMS, the time evolution of ion fluxes is also important. The detailed experimental set-up together with the corresponding emissions lines for Ar and Cu atoms and ions together with various phase of HiPIMS discharge are described elsewhere [25]. In Figure 3 (a) the time evolutions of magnetron currents are plotted

when the pulse duration was varied from 10 μs to 55 μs for a repetition frequency of 11 Hz. With increasing magnetron pulse the peak of the ion substrate current broadens indicating the time separation of metal- and gas-ion fluxes incidence at the substrate. The substrate holder currents measured at the distances varied from 3 cm up to 10 cm from the magnetron at a repletion frequency of 30 Hz are shown in Figure. 3 (b). As it can be calculated, the propagation velocity of the propagation velocity of the ion peak current is about $2x10^5$ $cm.s^{-1}$. This value is sufficiently large in order to satisfied Bohm criterion.

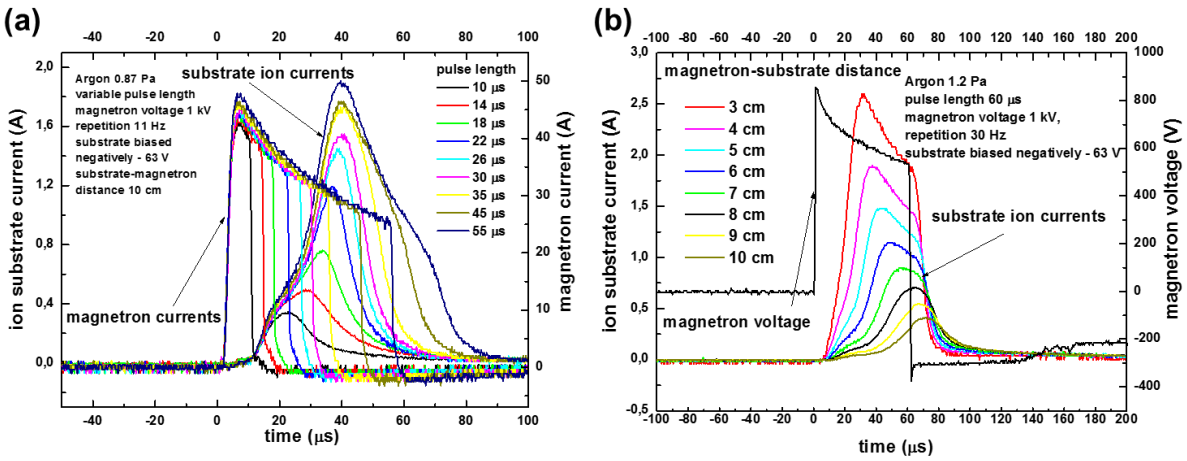

Figure 3 (a) Dependence of magnetron and ion substrate currents on the pulse length, (b) dependence of ion substrate currents on the magnetron-substrate distance

CONCLUSIONS

In this work we analyzed the contribution of the elementary time step of the magnetron post-discharge to the ion transport toward a biased substrate located at various distances from the magnetron by using variable pulse magnetron current durations. We have found that a large fraction of sputtered particles remains ballistic. We have observed a broadening in measured ion current indicating the time separation of metal- and gas-ion fluxes incident at the substrate. Consequently, this gives opportunity to synchronize PIII pulses with transient HiPIMS ion post-discharge currents in order to implant metallic ions solely. Short reviews of PIII and HiPIMS plasma technologies are also given.

ACKNOWLEDGEMENTS

The authors would like to thank for financial contribution from the STU Grant scheme for Support of Young Researchers, grant no. 1359 and from the STU Grant scheme for Support of Excellent teams of young scientists, grant no. 1372.This work was also funded by the ERDF, Project CAMBO, ITMS: 2622022079, and by Slovak grant agency VEGA, project no.1/0503/15.

REFERENCES

[1] Wei, R.: *Low energy, high current density ion implantation of materials at elevated temperatures for tribological applications.* Surf. Coat. Technol., 83, 218-227., 1996.
[2] Williamson, D. L., Davis, J. A., Wilbur, P. J., Vajo, J. J., Wei, R., Matossian, J. N.: *Relative roles of ion energy, ion flux, and sample temperature in low-energy nitrogen ion implantation*

of Fe-Cr-Ni stainless steel. Nucl. Instrum. Methods B, 127/128, 930-934., 1997.
[3] Cerofolini, G. F., Bertoni, S., Meda, L., Spaggiari,C.: *Silicon on thin insulator: prediction of the oxygen fluence required for the formation of a continuous buried oxide.* Mat. Sci. Eng. B, 22, 172-180., 1994.
[4] Jaussaud, C., Margail, J., Stoemenos, J., Bruel, M.: *High temperature annealing of simox layers physical mechanisms of oxygen segregation.* MRS Proc., 107, 17, 1988.
[5] Bruel, M.: *Application of hydrogen ion beams to Silicon On Insulator material technology*. Nucl. Instrum. Methods B, 108, 313-319., 1996.
[6] Günzel, R., Shevshenko, N., Matz, W., Mücklich, A., Celis, J. P.: *Structural investigation and wear resistance of submicron TiN coatings obtained by a hybrid plasma immersion ion implantation process.* Surf. Coat. Technol., 142-144, 978-983., 2001.
[7] Anders, A.: *Width, structure and stability of sheaths in metal plasma immersion ion implantation and deposition: measurements and analytical considerations*. Surf. Coat. Technol., 136, 85-92., 2001.
[8] Lieberman, M A.: *Model of plasma immersion ion implantation*. J. Appl. Phys., 66, 2926, 1989.
[9] Scheuer, J.T., Shamim, M., Conrad, J.R.: *Model of plasma source ion implantation in planar, cylindrical, and spherical geometries.* J. Appl. Phys., 67, 1241, 1990.
[10] Collins, G.A., Tendys, J.: *Sheath development around a high-voltage cathode.* Plasma Sources Sci. Technol., 3, 10-18., 1994.
[11] Brutscher, J., Gunzel, R., Moller, W.: *Sheath dynamics in plasma immersion ion implantation*. Plasma Sources Sci. Technol., 5, 54-60., 1996.
[12] Helmersson, U., Lattemann, M., Bohlmark, J., Ehiasarian, A. P., Gudmundsson, J. T.: *Ionized physical vapor deposition (IPVD): A review of technology and applications.* , Thin Solid Films, 513, 1–24., 2006.
[13] Kouznetsov, V., Macák, K., Schneider, J., Helmersson, U., Petrov, I.: *A novel pulsed magnetron sputter technique utilizing very high target power densities.* , Surf. Coat. Technol., 122, 290–293., 1999.
[14] Macák, K., Kouznetsov, V., Schneider, J., Helmersson, U., Petrov, I.: *Ionized sputter deposition using an extremely high plasma density pulsed magnetron discharge.*, J. Vac. Sci. Technol. A., 18, 1533 – 1537., 2000.
[15] Bohlmark, J., Alami, J., Christou, C., Ehiasarian, A. P., U. Helmersson, U.: *Ionization of sputtered metals in high power pulsed magnetron sputtering.*, J. Vac. Sci. Technol. A., 23, 18, 2005.
[16] Samuelsson, M., Lundin, D., Sarakinos, K., Björefors, F., Walivaara,B., Ljungcrantz, H. Helmersson, U.: *Influence of ionization degree on film properties when using high power impulse magnetron sputtering.*, J. Vac. Sci. Tech. A. 30, 031507, 2012.
[17] Lundin, L.: The HiPIMS Process, PhD Thesis, Linkoping University, Linkoping, Sweden, 2010.
[18] Sarakinos, K., Alami, J., Konstantinidis, S.: *High power pulsed magnetron sputtering: A review on scientific and engineering state of the art.*, Surface & Coatings Technology., 204, 1661-1684, 2010.
[19] Ehiasarian A. P., Wen, J. G., Petrov, I.: *Interface microstructure engineering by high power impulse magnetron sputtering for the enhancement of adhesion.*, J. Appl. Phys., 101, 054301, 2007.
[20] Brown, I. G., Godechot X., Yu, K. M.: *Novel metal ion surface modification technique.* Appl. Phys. Lett., 58, 1392, 1991.
[21] Boxman, R. L., Goldsmith, S.: *Macroparticle contamination in cathodic arc coatings: generation, transport and control.*, Surface and Coatings Technology, 52, 39 – 50, 1992.

[22] Takikawa, H., Tanoue, H.: *Review of cathodic arc deposition for preparing droplet free thin films.*, IEEE Trnsactions on Plasma Science, 35, 992 – 999., 2007.

[23] Anders, A.: *Metal plasmas for the fabrication of nanostructures.*, J. Phys. D: Appl. Phys., 40, 2272 – 2284., 2007.

[24] Wu, Z., Tian, X., Shi, J., Wang, Z., Gong, C., Yang, S., Chu, P. K.: *Novel plasma immersion ion implantation and deposition hardware and technique based on high power pulsed magnetron discharge.*, Rev. Sci. Instrum., 82, 033511, 2011.

[25] Vašina., P., Meško, M., Imbert, J. C., Ganciu, M., Boisse-Laporte, C., de Poucques, L., Touzeau, M., Pagnon D., Bretagne, J.: *Experimental study of a preionized high power pulsed magnetron discharge.*, Plasma Sources Sci. Technol., 16, 501-510., 2007.

EVALUATION OF TRUCK VIBRATION LEVELS FOR PACKAGING TESTING PURPOSES IN HUNGARY

BÖRÖCZ Péter PhD

Institute: Széchenyi István University, Department of Logistics and Forwarding
E-mail: boroczp@sze.hu

Abstract
In the past decades with an increase in globalization and international trade, the economic and transportation links between various regions and economies have increased both in size and efficiency. This study measured the transportation vibration levels that occur during truck shipment in Hungary using the most popular mode of shipping as semi-trailer truck. The aim of this paper is to provide vibration levels in truck during delivery and to analyse vibration intensity in 1-200Hz frequency bands that can be a primary source of damages in packaged products. The measured acceleration-time data were analysed in the form of power spectral densities (PSD). As a result of this study a composite PSD spectra of averaged intensity have been provided, which can be used to simulating vertical vibration levels on vibration table in packaging laboratories.

Keywords: *vibration, power spectral density (PSD), truck, Hungary, packaging*

1. INTRODUCTION

Truck transport is the most widely form of transportation used for the shipment of goods in Hungary. Today, among the countries in Central Europe, Hungary has become a distribution logistics hub for truck shipping due to its geographical location. Four vital European transport corridors pass through Hungary, providing unparalleled access to all parts of Europe, from the north to south and from the west to east.

Truck vehicles produce vibration as a consequence of their motion. Naturally, several kinds of factors including vehicle speed, road conditions, load conditions and vehicle suspension system have impact to the vibration. The vibration during transportation can be a primarily source of damages for packaging and its contents [1]. This research attempts to measure and analyse the vibration levels and intensity on truck shipments on the major distribution roads in Hungary using accelerometer data recorder to measure and record vibration events and present them in the form of PSD. The data from this study can be compared to vibration test profiles recommended in popular, widely used packaging vibration test standards such as American Society for Testing and Materials (ASTM) and International Safe Transit Association (ISTA). The data and results from this study can be used to compare packaging vibration test methods used by packaging engineers to develop optimized packaging for shipment in Hungary.

Previous studies have also measured and analysed the vibration levels and developed power spectral density (PSD) for trucks in various continents and regions such as i.e. North America [2] mounted with air-suspension or leaf spring. Data has also been previously collected on comparing vibration levels in small and medium package delivery vehicles including small-sized and medium-sized trucks and automobiles [3]. There are studies, which also have measured the truck vibration levels as a function of truck speed, weight of payload [4, 5] and road conditions [6]. There are two

measurements on vibration levels concerning railcar [7] and multi mode of transportation [8], which used a very short segment in Hungary, but author of this paper could not find any published research that presented the vibration levels for truck transportation in Hungary and development of test methods.

2. MEASUREMENTS AND EVALUATION

2.1. Data analysis using power spectral density

A typical PSD function shows the strength of the variations (energy) as a function of frequency. The average power density within a narrow band of frequencies of a given spectrum can be determined by G_{rms} values based on the number of samples for a given bandwidth. In this way G_{rms} is determined as the root mean square value of the acceleration in G's in the given bandwidth of frequency, based on a number of (N) samples. The unit of PSD is energy, namely PD in acceleration squared divided by frequency (g^2/Hz) versus frequency (Hz). The energy within a specific frequency range can be obtained by integrating PSD within that frequency range and is usually represented as overall G_{rms} for the examined spectrum. A PSD plot is an important tool in simulating real life transportation conditions on vibration equipment in packaging laboratory [9]. Figure 1 shows a typical PSD plot used to simulate truck random vibration and Figure 2 shows a typical truck vertical vibration signal recording.

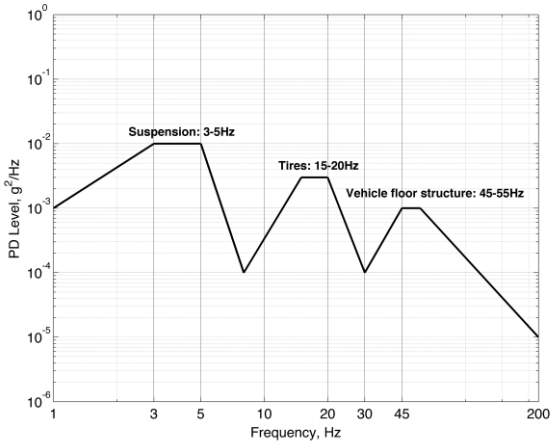

Figure 1 Typical PSD spectrum for truck vehicle vibration

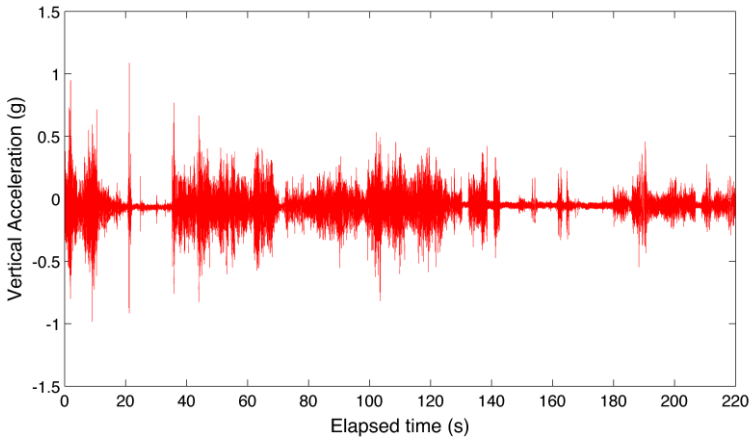

Figure 2 Sample of vertical vibration signal recorded

2.2. Instrumentation and methodology

The vibration events for transportation were measured in vertical axis using Lansmont SAVER™ 3X90 (Shock and Vibration Environment Recorder, Lansmont Corp., CA, USA) to collect the data (Figure 3). Then SaverXwareTM software and MathLab software were also used for analysing the data. The settings of the recorder used in this study are shown below:

- Recording Time: 2.048 s
- Sample/sec: 500 Hz
- Sample size: 1024
- Frequency resolution for PSD: 0.48 Hz
- Timer trigger: 1 min
- Signal trigger: 2.0 G
- Anti-alias filtering: 250Hz

Because the main purpose of this survey is to characterize the distribution environment on truck in Hungary the survey used time-based triggering and relatively high signal trigger level. The SAVER^{TM} was mounted at the rear location of the longitudinal I-beam ensuring that the equipment can record the direct input excitation of the semi-trailer's suspension.

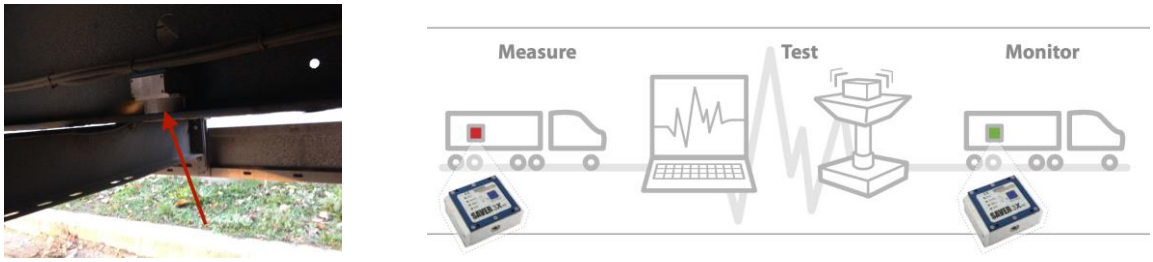

Figure 3 Data logger (SAVERTM 3X90) used in this study (right picture source Lansmont brochure, lansmont.com)

In this study, the PD data are presented from 1 to 200 Hz. The vibration data were filtered to remove all undesirable events such as any noise or non-vibration featured movements from the analysis. This way data below 0.01 G_{rms} were filtered out.

2.3. Data collection

The measurements for this study were conducted in May 2016. The vehicle was an IVECO Stralis truck with Fliegl SDS semi-trailer, which was monitored on a daily trip, then on a weekly route, could be seen on Figure 5. The average trucks speeds in this study were 57-63 km/h. The entire vibration measurement was conducted with loaded trailer and with the density ranging from 1,500 kg to 23,600 kg. The truck semi-trailers that were studied had air ride suspension system. The length of the observed route was 1.966km including motorway, limited access highway, main road and city road.

Figure 4 Truck used in this study

Figure 5 Shipping route measured (red: daily LTL collecting, blue: FTL and LTL weekly distribution with freight exchange tool)

3. RESULTS

6 198 samples were used to analysis, this is the total number of events recorded over 0.01 G_{rms}. Figure 6 shows the vertical PSD spectrum for all truck shipments. Figure 5 also shows ISTA 3A air-ride [10], ISO 13355 [11] and ASTM D7386 [12] spectra for heavy truck random vibration testing. As shown on the PSD spectrums, the measured vibration intensity in the low-frequency range (1–5 Hz). After 20Hz the PD levels decrease rapidly, and in the higher frequency band (over 60 Hz) the data show very low intensities. The intensity (overall G_{rms}) of vibration level on field measurement was 0.212 in 1 to 200Hz.

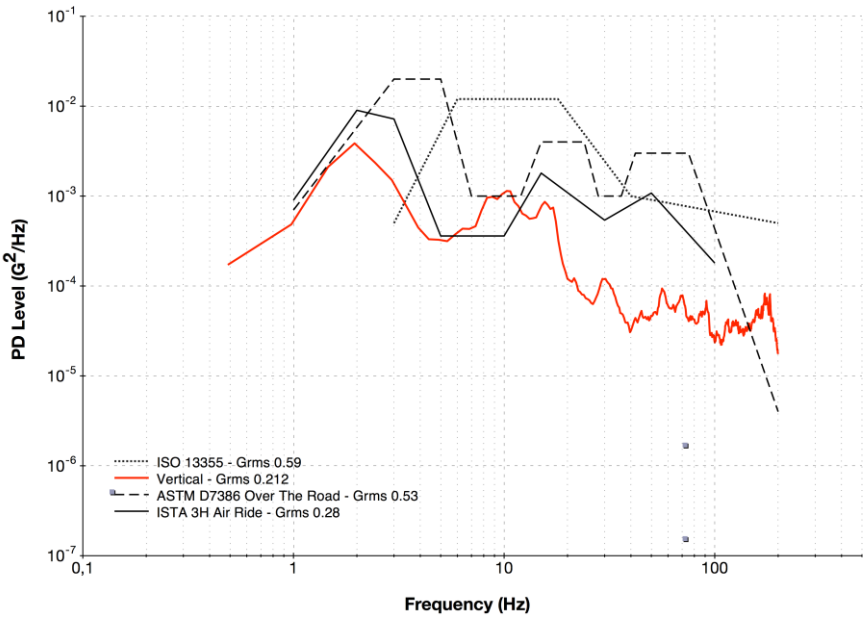

Figure 5 Air-Ride Truck Semi-Trailer Vertical vibration levels with PSD spectrum in Hungary in vertical axe

Table 2 describes composite spectrums for truck semi-trailer shipments in the vertical axis based on measured and averaged data in Hungary. The spectrum was developed using PD levels for 100% of all events and conditions between 1 and 200 Hz. These breakpoints and PD levels are informative and recommended to be used for simulating the truck transportation in truck and van in Hungary.

Table 6 Recommended test spectrum for vertical vibration in Hungary

Air-ride Semi-Trailer Truck	
Frequency (Hz)	PD level G^2/Hz
1	0,0004
2	0,005
3	0,005
4	0,001
6	0,001
10	0,005
20	0,0004
50	0,0004
200	0,00002

CONCLUSIONS

The study concludes the following. Composite spectrum from vibration profiles created through this study can be compared with test levels recommended in existing American Society of Testing and Materials (ASTM), International Safe Transit Association (ISTA) an ISO protocols for air-ride truck vibration testing methods.

REFERENCES

[1] Böröcz P, Vastag Gy. *Good Vibrations: Lessons from Packaging for the Global Supply Chain.* In: Sriram Narayanan POMS 26th Annual Conference, Washington, USA 2015, p. 1318.
[2] Singh J, Singh SP, Joneson E. *Measurement and analysis of US truck vibration for leaf spring and air ride suspensions, and development of tests to simulate these conditions.* Packaging Technology and Science 2006; 19: 309–323. DOI: 10.1002pts.732
[3] Chonhenchob V, Singh SP, Singh J, Stallings J, Grewal G. *Measurement and analysis of vehicle vibration for delivering packages in small-sized and medium-sized trucks and automobiles.* Packaging Technology and Science 2012; 25: 31–38. DOI:10.1002/pts.955.
[4] Zhou R, Yan L, Li B, Xie, J. *Measurement of Truck Transport Vibration Levels in China as a Function of Road Conditions, Truck Speed and Load Level*. Packaging Technology and Science 2015; 28: 949-957, DOI:10.1002/pts.2176
[5] Singh SP, Marcondes J. *Vibration levels in commercial truck shipments as a function of suspension and payload.* Journal of Testing and Evaluation 1992; 20(6): 466–469.
[6] Garcia-Romeu-Martinez MA, Singh SP, Cloquell-Ballester VA. *Measurement and analysis of vibration levels for truck transport in Spain as a function of payload, suspension and speed.* Packaging Technology and Science 2008; 21: 439–451. DOI:10.1002/pts.798.
[7] Böröcz P, Singh SP. *Measurement and Analysis of Vibration Levels in Rail Transport in Central Europe*. Packaging Technology and Science, 2016, DOI: 10.1002/pts.2225
[8] Böröcz P, Singh SP, Singh J: *Evaluation of Distribution Environment in LTL Shipment between Central Europe and South Africa*, Journal of Applied Packaging Research, Vol. 7, No. 2, Article 3, 2015. DOI: 10.14448/japr.04.0003
[9] Singh SP, Singh J, Saha K. *Measurement and Analysis of Physical and Climatic Distribution Environment for Air Package Shipment*. Packaging Technology and Science 28.8 (2015): 719-731.
[10] ISTA Procedure 3H. *Performance Test for Products or Packaged-Products in Mechanically Handled Bulk Transport Containers*. International Safe Transit Association: East Lansing, 2006.
[11] ISO 13355:2001. *Complete, filled transport packages and unit loads - Vertical random vibration test.* International Organization for Standardization, ICS 55.180.40, 2001
[12] ASTM Standard D7386 - 16. *Standard Practice for Performance Testing of Packages for Single Parcel Delivery Systems.* Annual Book of ASTM Standards, vol. 15.10. American Society of Testing and Materials: West Conshohocken, 2016.

INTERNATIONAL SCIENTIFIC CONFERENCE ON ADVANCES IN MECHANICAL ENGINEERING
13-15 October 2016, Debrecen, Hungary

OBJECTIVE DRAUGHT COMFORT INVESTIGATIONS IN A SINGLE OFFICE MODEL ROOM

[1]BOTH Balázs, [2]SZÁNTHÓ Zoltán PhD, [3]GODA Róbert PhD

[1,2,3]Budapest University of Technology and Economics, Department of Building Service and Process Engineering
[1]E-mail: both@epget.bme.hu
[2]E-mail: szantho@epget.bme.hu
[3]E-mail: goda@epget.bme.hu

Abstract
Draught is one of the most disturbing discomfort parameters in buildings, because the working performance of people may decrease. Furthermore, due to the draught, people require higher indoor air temperature, which increases the energy consumption of the building.
In this article, a full-scale single office model room's draught environment is investigated experimentally, using slot air diffuser device. Air velocity and turbulence intensity – like the most important features of the turbulent airflow – were measured on a constant air temperature at various inlet Reynolds-numbers. The measurement results were evaluated with statistical methods and compared to the relevant international standards and technical reports. These standards offer some turbulence intensity and velocity for indoor air comfort design, but does not take into consider the type of the inlet device and Reynolds-number's effect on room's draught comfort.
The results showed some differences between the standardized design values and the measured draught parameters in the room. The draught environment was evaluated with Fanger's model, which is an internationally known and accepted draught model in Europe.

Keywords: *Reynolds-number; draught comfort; single office room; slot-diffuser.*

1. INTRODUCTION

People spend most of their life in closed spaces so it is important to provide acceptable microclimate parameters in rooms. The single offices are widely used in HVAC designing practice, where the primary direction of the air inlet is often vertical. In these ventilated spaces a linear slot-diffuser is often used as the air inlet. This diffuser is usually located next to a wall surface as it is shown in Fig. 1. The main advantage of such slot-diffuser placement is that supply air is injected outside of the occupied zone of the room, so the draught risk can be decreased in the space [1], [2], [3]. Technical report CEN CR 1752 contains some requirements for the cellular offices [s1].
The inlet (or slot) Reynolds-number of the air injection is:

$$Re_0 = \frac{v_0 \cdot s_0}{\nu_0}, [1] \quad (1)$$

In Eq. 1 v_0 is the inlet air velocity, s_0 is the width of the slot and ν_0 is the kinematic viscosity.
The air velocity is a time-dependent quantity, which has an average and a fluctuating value.

$$v(time) = v_{mean} + v_{RMS}, \left[\frac{m}{s}\right] \quad (2)$$

In Eq. 2 v_{mean} is the mean air velocity, v_{RMS} is the root mean square velocity component, which equals with the standard deviation of the sample.

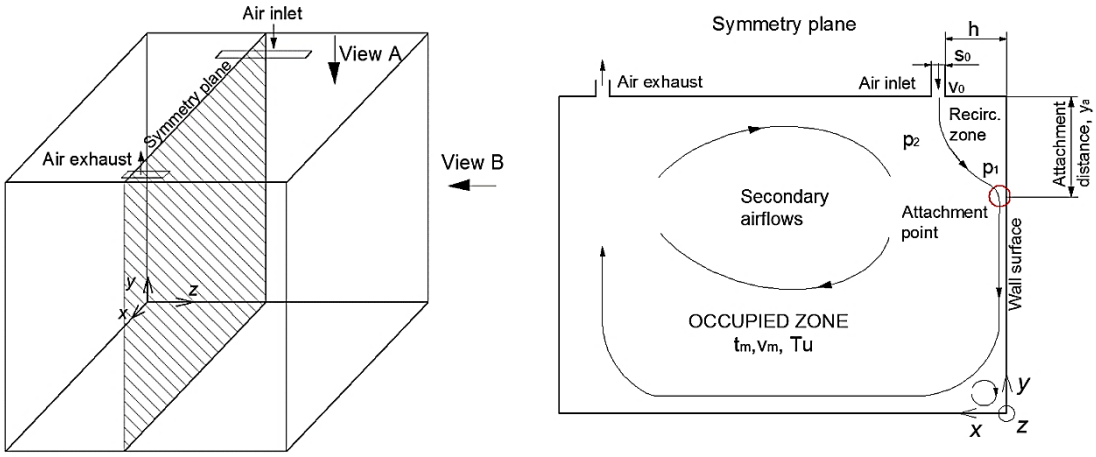

Figure 1 Sketch of the single office model room

The turbulence intensity of the airflow can be calculated with the following formula:

$$Tu = \frac{v_{RMS}}{v_{mean}} \cdot 100, [\%] \tag{3}$$

Average air velocity, turbulence intensity and temperature are the main features of draught comfort in rooms. The most common and internationally accepted model to predict draught environment in Europe is Fanger's model, which is based on a semi-empirical formula and describes draught comfort in the room [6]:

$$DR = (34 - t_{mean}) \cdot (v_{mean} - 0.05)^{0.62} \cdot (0.37 \cdot Tu \cdot v_{mean} + 3.17), [\%] \tag{4}$$

In Eq. (4) t_{mean} is the mean air temperature in the room. This Eq. can be valid for one point in the room and also it can be used for the whole occupied zone. According to technical report CEN CR 1752:2000 [s1], the occupied zone of the ventilated room can be categorized from the aspect of draught comfort. Category A is the best (DR ≤ 15 [%]) and it is followed by category B (15 < DR ≤ 20 [%]) and finally category C (20 < DR ≤ 25 [%]). It is important to predict DR in the room to describe draught environment. Several researchers have investigated draught comfort in the past decades. The most accepted and well-known researches of draught comfort in closed spaces come from Fanger et al. [1], [6], [7]. They have investigated the main parameters of draught like air velocity, turbulence intensity and air temperature in whole rooms. The investigations based on experimental methods including measurements in rooms. The exact type of the applied room air distribution – especially the single office's room air distribution – was not considered in these researches. They have only made the difference between displacement and mixing ventilation systems. Magyar, Goda et al. [2], [3], [8], [9], [10] took experimental and numerical investigations on single office models to describe draught comfort. Cao [11], Rohdin and Moshfegh [12] used experimental method and numerical simulation to model room airflow. Moureh and Flick [13], [14] also took experimental and numerical researches in slot-ventilated rooms. All of the previously introduced authors investigated room airflow in the occupied zone of the ventilated space. In most of these investigations the inlet Reynolds-number was the changing parameter.

Some researchers like Nozaki et al. [4], [15], Nasr and Lai [5], Rathore and Das [16] only investigated injected air jets and their attachment process near the air inlet and did not take into consider the airflow inside the room. In these researches the inlet aspect ratio, offset ratio and Reynolds-number were the changing parameters.
The primary aim of this paper is to investigate the draught parameters in a single office full-scale model room and comparing the results to the international standards.

2. METHODS

Air velocity and turbulence intensity measurements were performed in a full-scale single office test room in the Ventilation Laboratory of Budapest University of Technology and Economics, according to the relevant standards [s2], [s3], [s4] [s5]. The measurements were performed in four relevant heights of the occupied zone in the test room, according to standard EN ISO 7726 [s4]: at ankle height (y = 0.1 [m] from floor), at knee height (y = 0.6 [m] from floor) and at head height of seated person (y = 1.1 [m] from floor) and at head height of standing person (y = 1.7 [m] from floor) as it can be seen in Fig. 2. At each height 29 measurements points were used, which meant 116 measurement points in the whole occupied zone at one inlet Reynolds-number.
Air velocity (v_i) and temperature (t_i) were measured by an omni-directional hot sphere probe at the relevant point (i) in each height. The omni-directional sensor was compared to a higher sampling frequency hot-wire anemometer from the aspect of turbulence intensity measurement accuracy. The turbulence intensity was measured with the omni-directional and hot-wire probes in the same conditions. The sample size was 40 [pcs] using a sampling interval 180 [s] according to the relevant standards [s4], [s5]. It resulted two independent samples measured with two different probes. Due to the Abbe-test, F-test, and the two sample t-test there was not any significant difference between the standard deviation and the average of the two samples. It meant that the omni-directional sensor could be also used for the turbulence measurements in the present office model room.
The inlet Reynolds-number was the only changing parameter during the measurements in the range of Re_0 = 1500÷3500. The measured data were evaluated with statistical methods on probability level 95 [%] [17]. Geometry of the slot diffuser device was constant (1 [m] long and 0.012 [m] wide), the diffuser was located h = 0.26 [m] from the wall. The constant average inlet air temperature's confidence interval was $P(23.4 \leq t_0, [°C] \leq 24.0) = 95$ [%] while the constant average indoor air temperature's confidence interval was $P(24.3 \leq t_m, [°C] \leq 25.1) = 95$ [%].

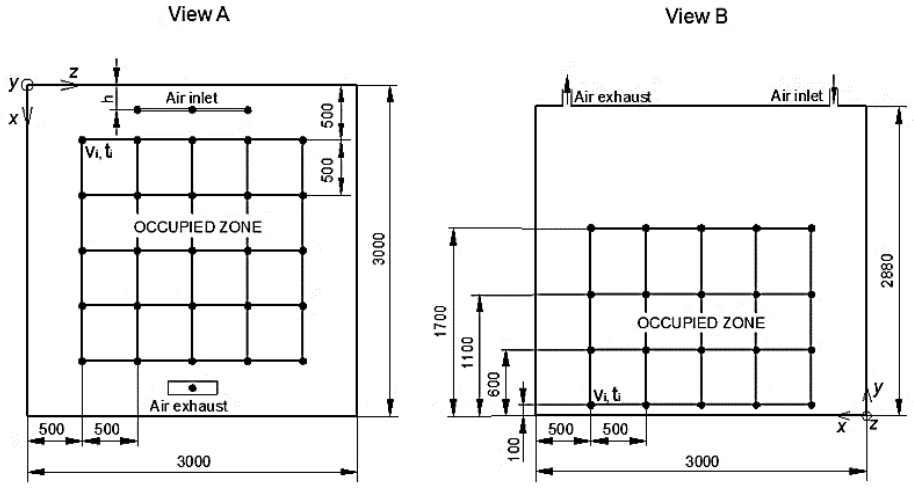

Figure 2 Measurement points in the occupied zone of the test room

3. RESULTS

The average air velocity (v_{mean}) was calculated in each measurement height using the measured data and the results are plotted in Fig. 3. It can be seen that the air velocity was increasing in each height as a function of the inlet Reynolds-number. This tendency complies with the results in Awbi's book [18]. The maximum recommended velocities are shown in this figure for winter and summer state suggested by CEN CR 1752 and ISO 7730 in category A, B and C. Category A is the best with the lowest air velocity and it is followed by category B and C. In summer condition, most of the average air velocities were less, than the allowable values (Fig. 3 left), expect two average velocities in the ankle height between Re_0 = 3000 and 3500. In winter state, some average velocities were higher than the recommended values in the ankle height between Re_0 = 2500 and 3500 (Fig. 3 right).

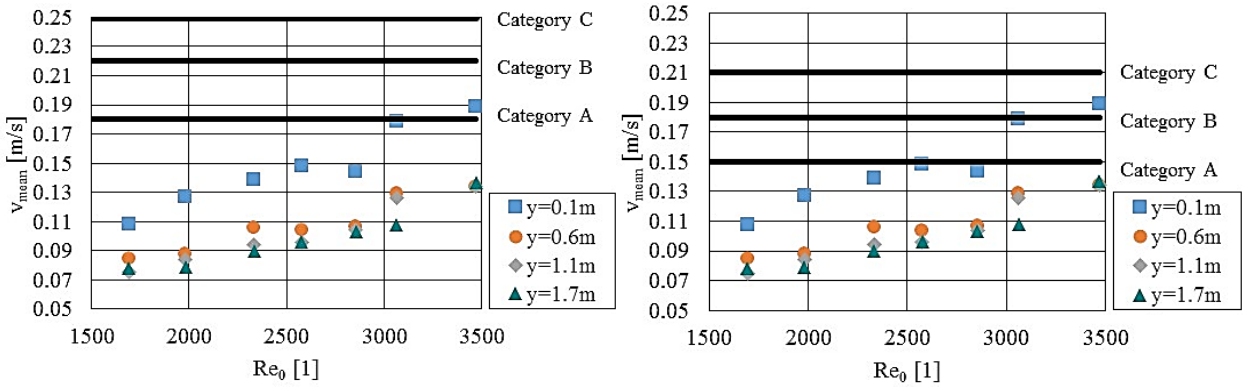

Figure 3 Average air velocity and the standardized values in summer (left) and winter (right)

Fig. 4 shows the average turbulence intensities calculated from the measured points in the four heights. The Abbe test resulted that the average turbulence intensity was independent from the inlet Reynolds-number in the investigated range. The standardized reference 40 [%] turbulence intensity is suggested by CR 1752, EN 13779 and EN ISO 7730 for the DR calculation in mixing ventilation systems. In Fig. 4 it can be seen that most of the average turbulence intensities were less than this reference value. In the head height of seated and standing persons were observed some higher value than 40 [%].

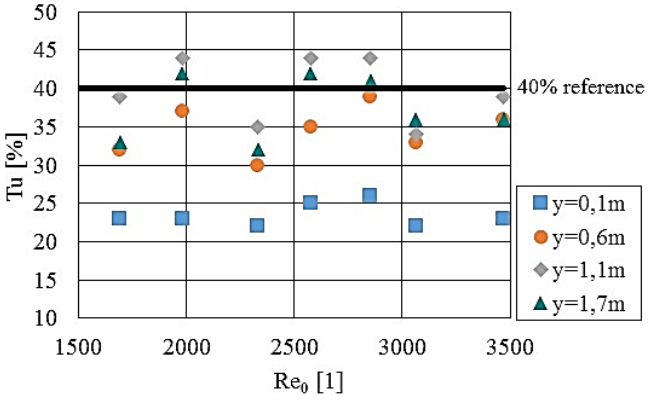

Figure 4 Turbulence intensities

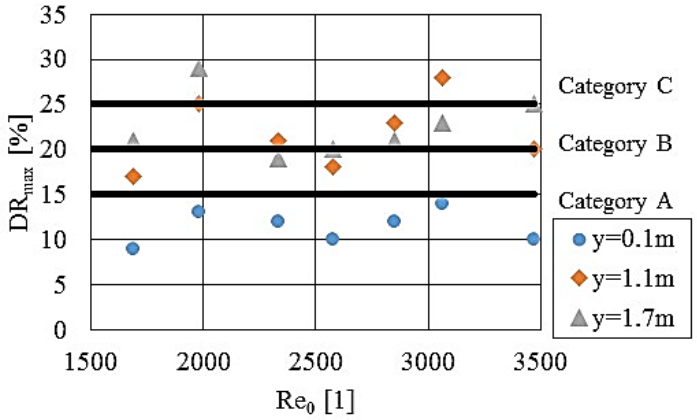

Figure 5 Draught Rate numbers

The maximum values of DR are plotted in Fig. 5 in the three most important heights from the aspect of draught comfort. In the ankle height, all points belonged to category A. In the height of seated and standing persons, most of the points belonged to category B and C, expect two inlet Reynolds-numbers: 2000 and 3000, because at this values the DR was higher than 25 [%]. Note that these DR numbers were calculated on a constant indoor air temperature described in the Methods section.

CONCLUSIONS

In this paper the draught environment of a single office model room was investigated objectively with experimental method. The investigations included air velocity and turbulence intensity measurement on constant inlet and indoor air temperature at seven various inlet Reynolds-numbers. The measurements were conducted in four heights of the occupied zone of the test room.
The results showed that most of the average air velocities in the different measurement heights were less than the standardized recommended values in winter and summer cases, except some values in the ankle height. The reason of this was that in single offices, where a slot-diffuser is located next to the wall – like in this case – the primary air flows on the boundaries of the room so near the floor in the ankle heights higher air velocities can be observed. The air velocity was increasing in every height as a function of the inlet Reynolds number in the investigated range $Re_0 = 1500 \div 3500$.
The average turbulence intensity in the four measurement heights was found to be independent from the inlet Reynolds-number. Some international standards for draught comfort design suggest a 40 [%] reference turbulence intensity. The results showed smaller turbulence intensities in the bigger part of the occupied zone, except some averages values in the head heights.
Using Fanger's model the draught environment was evaluated objectively in the occupied zone of the test room. Most point belonged to draught comfort category A and B, while some to C, which meant acceptable category. The DR values were calculated on constant indoor air temperature.
The results showed some significant differences from the standardized design values, because these standard do not take into consider the type of the air diffuser device and the other inlet parameters like Reynolds-number. These result may help designers to predict the draught environment on a more accurate way in single offices.

REFERENCES

[1] Fanger, P. O., Christensen, N. K.: *Perception of draught in ventilated spaces*. Ergonomics, 29:2, 215-235, 1986.

[2] Magyar, T.: *Helyiségek légvezetési rendszerei és a hőérzeti méretezés kapcsolata*. Ventilation Symposium, Budapest, Budapest University of Technology and Economics, 16–43, May 1993.
[3] Magyar, T., Goda, R.: *Laboratory modelling of tangential air supply system*. Periodica Polytechnica Ser. Mech. Eng., 44 No. 2, 207–215, 2000.
[4] Nozaki, T., Hatta, K., Nakashima, H., Matsumura, H.: *Attachment flow issuing from a finite width nozzle*. Bull JSME, 22, 340–347, 1979.
[5] Nasr, A., Lai, J. C. S.: *A turbulent plane offset jet with small offset ratio*. Experiments in Fluids, 24, Springer-Verlag, 47–57, 1998.
[6] Fanger, P. O., Melikov, A. K., Hanzawa, H.: *Air turbulence and sensation of draught*. Energy and Buildings, 12, 21-39, 1988.
[7] Hanzawa, H., Melikow, A. K., Fanger, P. O.: *Airflow characteristics in the occupied zone of ventilated spaces*. ASHRAE Trans., 93, Part 1, 524-539, 1987.
[8] Magyar, T.: *Qualification of the occupied zones of different types of air supply systems on the basis of measurements*. Periodica Polytechnica, 44, No. 2, 217-227, 2000.
[9] Goda, R.: *Measurement and Simulation of Air Velocity in the Test Room with Slot Ventilation*. In: Clima2010: Sustainable Energy Use in Building. Antalya, Turkey, 2010.05.09-2010.05.12. Antalya: Paper R6-TS46-PP03.
[10] Goda, R.: *Turbulence intensity and air velocity characteristics in a slot ventilated space*. Periodica Polytechnica-Mechanical Engineering, 58:(1), 1-6, 2014.
[11] Cao, G., Sivukari, M., Kurnitski, J., Ruponen, M.: *PIV measurement of the attached plane jet velocity field at a high turbulence intensity level in a room*. International Journal of Heat and Fluid Flow, 31, 897–908, 2010.
[12] Rohdin, P., Moshfegh, B.: *Numerical modelling of industrial indoor environments: A comparison between different turbulence models and supply systems supported by field measurements*. Building and Environment, 46, 2365-2374, 2011.
[13] Moureh, J., Flick, D.: *Airflow characteristics within a slot-ventilated enclosure*. International Journal of Heat and Fluid Flow, 26, 12–24, 2005.
[14] Moureh, J., Flick, D.: *Wall air–jet characteristics and airflow patterns within a slot ventilated enclosure*. International Journal of Thermal Sciences, 42, 703–711, 2003.
[15] Nozaki, T.: *Attachment flow issuing from a finite width nozzle (report 4: Effects of aspect ratio of the nozzle)*. Bulletin of the JSME, 26, No. 221, 1884–1890, 1983.
[16] Rathore, S. K., Das, M. K.: *Comparison of two low-Reynolds number turbulence models for fluid flow study of wall bounded jets*. International Journal of Heat and Mass Transfer, 61, 365–380, 2013.
[17] Kemény, S., Deák, A.: *Kísérletek tervezése és értékelése*. Műszaki Könyvkiadó, Budapest, Hungary. ISBN 963 16 3073 0. 2000.
[18] Awbi, H.: *Ventilation of Buildings*. Second Edition, Spon Press, London and New York, ISBN 0-203-63782-8. 2005.

STANDARDS

[s1] CEN CR 1752:2000. Ventilation for buildings. Design criteria for the indoor environment.
[s2] EN ISO 5167-1:2003. Measurement of fluid flow by means of pressure differential devices inserted in circular cross-section conduits running full. Part 1: General principles and requirements.
[s3] EN 24006:2002. Measurement of fluid flow in closed conduits; vocabulary and symbols.

[s4] EN ISO 7726:2003. Ergonomics of the thermal environment. Instruments for measuring physical quantities.
[s5] ASHRAE. 1992. ANSI/ASHRAE Standard 55-1992.
[s6] EN 13779:2007. Ventilation for non-residential buildings. Performance requirements for ventilation and room-conditioning systems.
[s7] EN ISO 7730:2006. Ergonomics of the thermal environment. Analytical determination and interpretation of thermal comfort using calculation of the PMV and PPD indices and local thermal comfort criteria.

INTERNATIONAL SCIENTIFIC CONFERENCE ON ADVANCES IN MECHANICAL ENGINEERING
13-15 October 2016, Debrecen, Hungary

HEAT TRANSFER CONDITIONS IN SCRAPED SURFACE HEAT EXCHANGERS

BOTH FEHÉR Kinga PhD

Budapest University of Technology and Economics
E-mail: feher@mail.bme.hu

Abstract
The food industry requires handling of products that are sensitive to high temperature for long periods of time. Scraped surface heat exchangers are widely used in technologies, where products of high viscosity or non-Newtonian liquids have to be heated up or cooled down. Scraping blades prevent material from burning or creating a layer on the heat transfer surface. Experiments were carried out to analyse heat transfer conditions in scraped surface heat exchanger. On the basis of the results a dimensionless equation was determined to make simpler the dimensioning process of heat transfer area of scraped surface heat exchangers.

Keywords: *scraped surface exchanger, heat transfer coefficient, dimensionless correlation*

1. INTRODUCTION

Scraped surface heat exchangers (SSHEs) are used in food, chemical and pharmaceutical industry first of all for heat treatment of liquids with high viscosity or non-Newtonian ones. These products are usually very heat-sensitive materials. Another application can be the cooling viscous, sticky and lumpy products and crystallisation of solutions. In this case due to cooling or increasing concentration, components in the fluid change to the solid state and deposit on the heat exchanger surface.
Scraped surface heat exchanger is a double pipe heat exchanger with a rotor in the inner space. Process fluid flows in the inner pipe. Scraper blades mounted on the rotating shaft continuously remove layer of the product created on the heat transfer surface, insuring good mixing and avoiding thermal damage of the product. Heating or cooling medium flows in the annulus between the outer and inner pipe. (*Figure 1*)

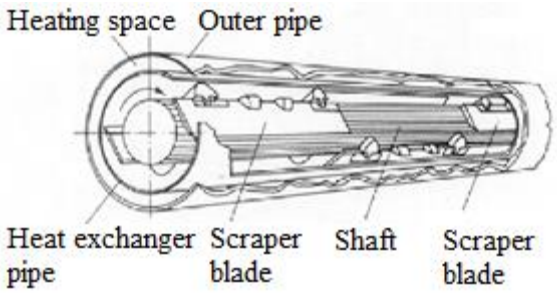

Figure 1 Scraped surface heat exchanger

High viscous fluids require very large heat transfer areas due to low heat transfer coefficient. Scraped surface heat exchangers mix the fluid vigorously. This intense mixing helps to promote transport of the fluid to and from the heat exchange surface. This increases the heat transfer rates

and the required heat exchange area is reduced.
The first scraped surface heat exchanger was constructed and registered as a patent in 1928. Scraped surface heat exchangers have been applied for high temperature – short time sterilization since 1946. Since then a lot of experiments were carried out by researchers in order to describe flow and heat transfer phenomena in SSHE.

2. LITERATURE REVIEW

Process fluid flow in SSHE is induced by the pump (axial flow) and the rotating blades (rotational flow). On the basis of studying heat transfer phenomena most authors found the following equation suitable to describe process fluid side heat transfer coefficient:

$$Nu = A \cdot Re_{ax}^{B} \cdot Re_{r}^{C} \cdot Pr^{D} \cdot \left(\frac{\mu}{\mu_w}\right)^{E} \quad (1)$$

where Nusselt number, axial Reynolds number and rotational Reynolds number:

$$Nu = \frac{h_{pf} \cdot d_{eq}}{k_{pf}}; \quad Re_{ax} = \frac{v_{ax} \cdot d_{eq} \cdot \rho_{pf}}{\mu_{pf}}; \quad Re_{r} = \frac{d_t^2 \cdot N \cdot \rho_{pf}}{\mu_{pf}} \quad (2)$$

These authors have used a dimensional analysis in order to compute the heat transfer coefficient under various experimental parameters. Exponents for dimensionless numbers found by different authors and their validity range can be seen in *Table 1*.

Table 1 Exponents for dimensionless numbers

Data source	Exponents of the dimensionless model					
	A	B	C	D	E	
Cuevas-Cheryan-Porter [1]	0,30	0,50	0,32	0,33	0,18	Re<1800, water
	4,59E-04	0,94	0,64	0,33	0,18	Re>1800, water
Sykora [7]	0,57	-0,01	0,48	0,40	0,00	water, glycerine
Skelland [2]	3,26	0,57	0,17	0,47	0,00	low viscosity
	0,03	1,00	0,06	0,70	0,00	high viscosity
Ramdas [5]	57,00	0,06	0,11	0,06	-0,02	
Maingonnat-Corrieu [4]	5,86	0,29	0,32	0,33	0,00	low viscosity, 4 rows of blades
	3,10	0,40	0,36	0,33	0,00	low viscosity, 2 rows of blades
	2,24	0,02	0,56	0,33	0,00	high viscosity, 4 rows of blades
	2,04	0,16	0,52	0,33	0,00	low viscosity, 2 rows of blades
Uhl [6]	1,00	0,00	0,50	0,33	0,18	10<Re<300
	0,36	0,00	0,67	0,33	0,18	300<Re<40000
Penney-Bell [3]	0,12	0,00	0,78	0,33	0,18	
Sykora [7]	4,09	0,00	0,48	0,24	0,00	
Latinen [9]	$2/\sqrt{\pi \cdot n_b}^{0,5}$	0,00	0,50	0,50	0,00	

In opinion of other authors, the axial velocity of the liquid through the exchanger does not influence the process since the frequency of surface removal is high. [9] On the basis of these considerations theoretical relationships were derived (see last 5 rows in *Table* 1).
It can be stated that there is a wide variation in the values of the exponents for the dimensionless numbers used.

3. EXPERIMENTS

Experiments were carried out for studying heat transfer phenomena in SSHE. My aim was to work out a new correlation which takes account of both axial and rotational motion.
Educational and experimental station was established for studying heat transfer and flow processes of Newtonian and non-Newtonian materials of low and high viscosity and also for dynamic studies of SSHE system. The units are fitted with four rows of blades which are, as a result of rotation, centrifugally forced to the inner wall, mechanically induce turbulence, film removal and mix the product. The system consists of a heater and two cooler units. Heating medium was saturated steam, cooling medium was cold water.
Process fluid used in measurements: water, yoghourt, tomato puree (15, 20, 23, 24, and 25% concentrations), CMC (carboxymethylcellulose) solution 1, 2, 3% concentrations. Mass flow rate of process fluid: $\dot{m}_{pf}$ = 500-2500 kg/h. Rotational speed of blades: N=0-300 rpm. Unit length: 1,85 m, shaft diameter: d_s = 0,06 m, tube inner diameter: d_t = 0,098 m, tube thickness: x_w =0,002 m, 4 rows of blades.
Measuring temperature, mass flow rate in scraped surface heat exchanger units and using physical properties of process fluid, heat flow rate can be calculated. Overall heat transfer coefficient can be determined from the average values of heat flow rates, logarithmic mean temperature difference and heat transfer area of the heat exchanger:
Heat flow rate on process fluid and steam side:

$$\dot{Q}_{pf} = c_{pf} \cdot \dot{m}_{pf} \cdot \Delta T_{pf}; \qquad \dot{Q}_{st} = \dot{m}_{st} \cdot \Delta h_{st} \tag{3}$$

Overall heat transfer coefficient:

$$U = \frac{\dot{Q}}{A \cdot \Delta T_{lm}} \tag{4}$$

h_{cond} condensation side heat transfer coefficient can be calculated from steam flow rate and saturation pressure. Heat transfer coefficient on process fluid side:

$$h_{pf} = \frac{1}{\frac{1}{U} - \frac{1}{h_{cond} \cdot \frac{A_o}{A_i}} - \frac{1}{\frac{k_w}{x_w} \cdot \frac{A_{wm}}{A_i}}} \tag{5}$$

4. RESULTS

Correlations of earlier theories listed in *Table1* include an axial and a rotational Reynolds number that means influence of axial and rotational flows on heat transfer process are taken account separately.

Nevertheless it may be hypothesized that process fluid flow in SSHE can be characterized by one velocity and consequently in dimensionless correlation only one Reynolds number can be used. Mean velocity of the fluid can be calculated as the vector sum of the two proper velocities.
Axial and rotational velocities:

$$v_{ax} = \frac{\dot{m}_{pf}}{\rho_{pf} \cdot \frac{d_t^2 - d_s^2}{4}}; \qquad v_r = 2\pi \cdot N \cdot \frac{d_t + d_s}{2} \tag{6}$$

Vectors of axial and rotational velocities are at 90-degrees to each other so the magnitude of the total velocity vector can be calculated by Pythagorean Theorem:

$$v = \sqrt{v_{ax}^2 + v_r^2} \tag{7}$$

There was a new combined Reynolds number defined instead of two separate Reynolds numbers. In combined Reynolds number mean velocity is equal with the sum velocity, d_{eq} is the hydraulic equivalent diameter of the annulus:

$$Re = \frac{v \cdot d_{eq} \cdot \rho_{pf}}{\mu_{pf}} \tag{8}$$

Nusselt number, calculated from h_{pf} process fluid side heat transfer coefficient, can be plotted against combined Reynolds number in logarithmic scale (*Figure 2*). It can be seen that points relative to different process fluids create separable groups.

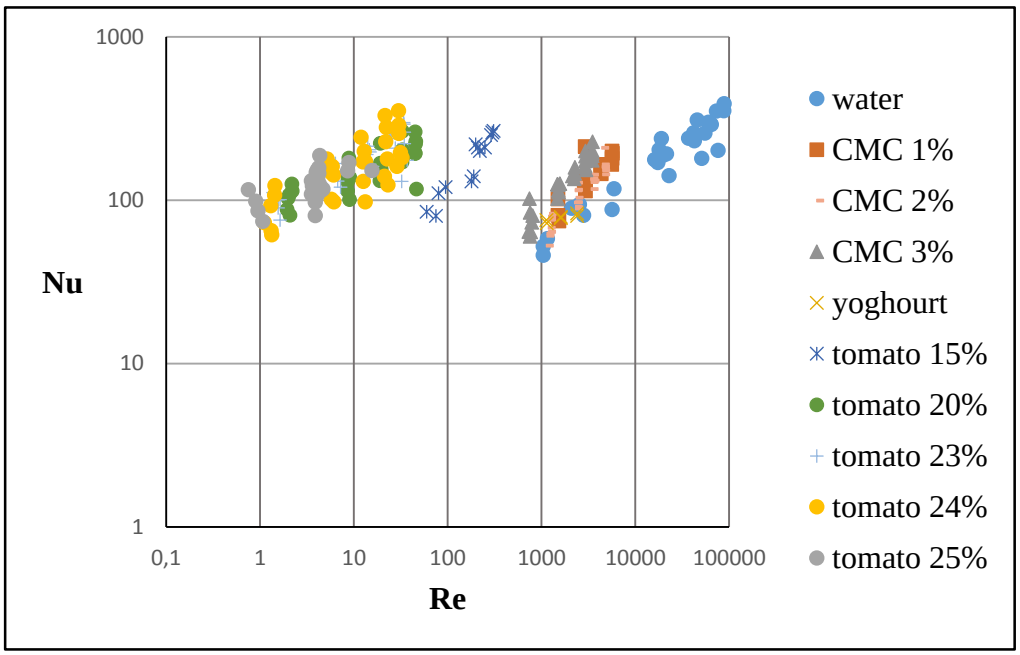

Figure 2 Nusselt number vs. combined Reynolds number

The aim of our investigation was to describe process fluid side Nusselt number in the following form:

$$Nu = G \cdot Re^H \cdot Pr^D \cdot (\frac{\mu}{\mu_w})^E \quad (9)$$

According to literature review exponents of Prandtl number and viscosity ratio:

$$D = \frac{1}{3}; \qquad E = 0{,}18 \quad (10)$$

In order to determine G and H exponents, Eq. (9) has to be transformed into the following form:

$$Y = \frac{Nu}{Pr^D \cdot (\frac{\mu}{\mu_w})^E} = G \cdot Re^H \quad (11)$$

With the exponents of (10):

$$Y = \frac{Nu}{Pr^{1/3} \cdot (\frac{\mu}{\mu_w})^{0{,}18}} = G \cdot Re^H \quad (12)$$

Values of Y were plotted against combined Reynolds numbers in *Figure 3.* In this diagram set of points relative to different process fluids seem to be heading the same lines.

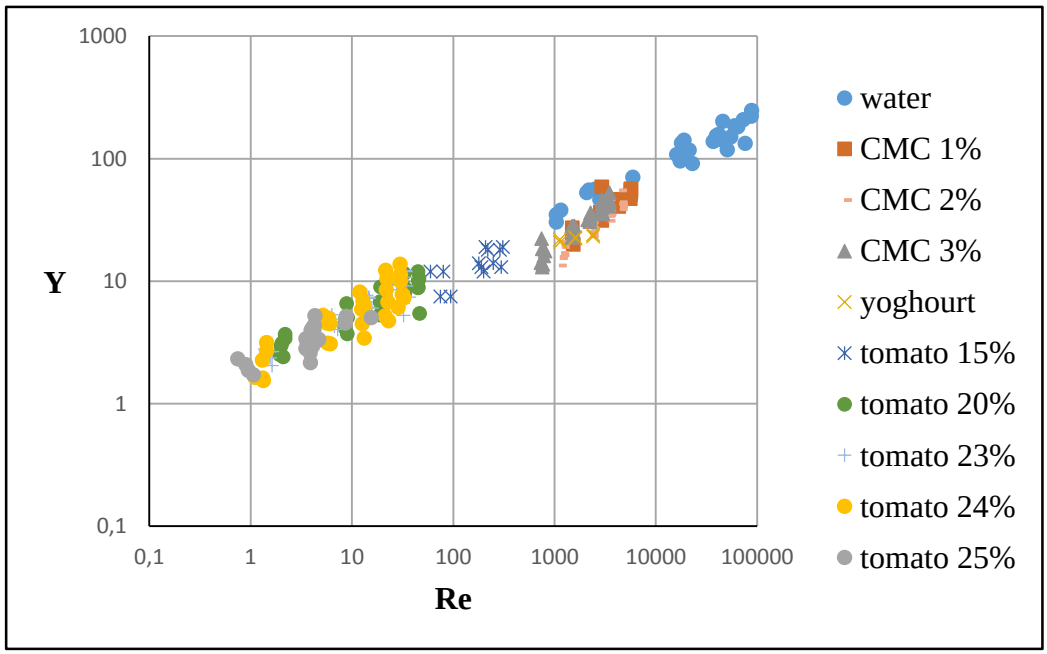

Figure 3 Y vs. combined Reynolds number

Points in *Figure 4* are divided into two groups according to laminar and turbulent Reynolds number regimes.

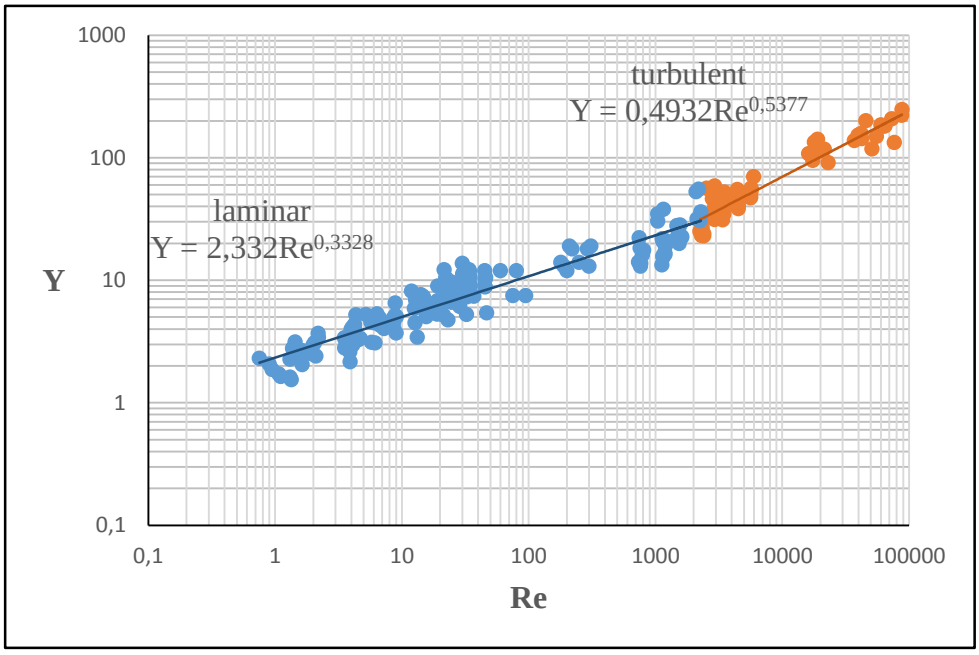

Figure 4 Y vs. combined Reynolds number with trend lines in laminar and turbulent regimes

On the basis of trend lines fitted to sets of points the following dimensionless correlations were determined:

$$Nu = 2{,}332 \cdot Re^{0{,}3328} \cdot Pr^{\frac{1}{3}} \cdot \left(\frac{\mu}{\mu_w}\right)^{0{,}18} \qquad 0{,}5 < Re \leq 2000 \qquad (13)$$

$$Nu = 0{,}4932 \cdot Re^{0{,}5377} \cdot Pr^{\frac{1}{3}} \cdot \left(\frac{\mu}{\mu_w}\right)^{0{,}18} \qquad 2000 < Re < 10^5 \qquad (14)$$

CONCLUSIONS

On the basis of investigations a new combined Reynolds number was defined. It has been determined that in SSHE similar to flow phenomena in empty tube or annulus there are two different flow regimes. The dimensionless correlations worked out makes simpler the dimensioning process of heat transfer area of SSHE.

REFERENCES

[1] Cuevas, R., Cherian, M., Porter, V.L.: *Performance of a Scraped-Surface Heat Exchanger under Ultra High Temperature Conditions: A Dimensional Analysis*. Journal of Food Science, 47, 619-625., 1982.
[2] Skelland AHP.: *Correlation of scraped film heat transfer in the votator*. Chem. Eng. Sci. 7, 166–75., 1958.
[3] Penney, W.R., Bell K.J.: *Close clearance agitators. Part 2. Heat transfer coefficients*, Ind. Eng. Chem., 4, 47-54., 1967.
[4] Maingonnat JF, Benezech T, Corrieu G. : *Performances thermiques d'un échangeur de chaleur à surface raclée traitant des produits alimentaires newtoniens et non-newtoniens.* Rev. Générale de Thermique, 279, 299–304., 1985.

[5] Ramdas V, Uhl VW, Osborne MW, Ortt JR.: *Heat transfer to viscous materials in continuous-flow, scraped-wall, commercial-size heat exchanger*. AIChE Nat. heat transfer conference, 24–31., 1977.
[6] Uhl VW.: *Mechanically aided heat transfer*; Mixing Theory and Practice, 1, 279. Academic Press New York, 1966.
[7] Sykora S, Navratil B, Karasek O.: *Heat transfer on scraped walls in the laminar and transitional regions*. Collect Czechoslovak Chem Commun, 33(2), 518–28., 1968.
[8] M. Yataghene, J. Pruvost, F. Fayolle, J. Legrand: *CFD analysis of the flow pattern and local shear rate in a scraped surface heat exchanger.* Chem. Eng. Process, 47, 1550–1561., 2008.
[9] Latinen G.A.: *Discussion of the paper Correlation of scraped film heat transfer in the Votator (A.H. Skelland).* Chem. Eng. Sci. 9, 263-266. 1959.
[10] Härröd M.: *Flow patterns, mixing effects and heat transfer in scraped surface heat exchangers.* Thesis at the Department of Food Science and SIK, The Swedish Institute for Food Research, Göteborg Sweden 1988.

INTERNATIONAL SCIENTIFIC CONFERENCE ON ADVANCES IN MECHANICAL ENGINEERING

13-15 October 2016, Debrecen, Hungary

PENDULAR SYSTEMS A NONCONVENTIONAL INTERDISCIPLINARY VARIABLE STRUCTURE SYSTEM

[1]CALISTRU Cătălin Nicolae PhD, [2]TIMOFTE Dan PhD

[1]Faculty of Automatic Control and Computers Engineering, "Gheorghe Asachi" Technical University of Iaşi, Romania
E-mail: calistru@ac.tuiasi.ro
[2]"Gr. T. Popa" Medicine and Pharmacy University of Iaşi, Romania
E-mail: danieltimofte@yahoo.com

Abstract
The paper deals with a particular class of nonlinear control system, PENDULAR Control Systems. This class of systems have the basic idea origin in some interdisciplinary observations concerning the "good-bad" unity and fight of contraries. From the systems point the feedback game, i. e. positive versus negative feedback has its relevance. PENDULAR (Pendulum Efficiency with Nonlinear Dynamics and Unconventional Law in Achievement of Robustness) systems are Variable Structure Systems (VSS) with a simple structure. The systems are divided into two subsystems one system with positive feedback the other with negative feedback. Short description of PENDULAR systems, the study of stability and the essential PENDULAR system is presented in the paper. Certain illustrative examples are detailed. Simulation and experimental results show the efficiency of the PENDULAR systems.

Keywords: *variable structure system, control systems, optimization, PENDULAR control*

1. INTRODUCTION

The word PENDULAR comes from the Romanian verb "a pendula" that means the pendulum movement. PENDULAR systems (mnemonic Pendulum Efficiency with Nonlinear Dynamics and Unconventional Law in Achievement of Robustness) are a class of nonlinear control systems with variable structure.Variable structure systems (VSS) are very interesting to be studied because often reveal surprises. Usually, the feedback control systems are closing the loop via a negative feedback. In this manner it is assumed the fact that the control system is robust (stable and efficient even if different exogenous will disturb: reference variations, external disturbances, measurement noises, and plant uncertainties). The question is: "Is positive feedback always bad for a control system?" For the positive feedback systems the input has a cumulative aspect that intuitively leads the system to instability. In the classical negative feedback control systems where output *y* is kept close to the reference *r*, the negative feedback could delay the system response.
For example, let assume is analysed "a level control system" with "automation at level 0". In other terms, a human operator supervises the level in the tank closing the tap whenever the water will reach the reference level.For efficiency (and if the tank volume is large), the operator does not proceed like this: leave the tap on the drop by drop position and when the level reaches the reference value turn off the tap. He proceeds like this: turn on the tap at a large flow and when the level is near to the reference point turn the tap at a small value tending to zero. Then, by intuition, positive feedback means a large flow, negative feedback a small flow.
Extending this very simple idea to the control loops, the PENDULAR system is a feedback system that starts with positive feedback and, at a certain time, changes its structure becoming a negative

feedback control system Next step in the research is to find which of these systems are stable or stabilizable? Since these systems may contain PID controllers how to tune these controllers for proper performances achievement?[1]
Other practical questions may occur are: the switching time, the number of commutations (because of the chattering the actuator can be damaged). At these questions the answer is the Essential PENDULAR Control System (EPCS). EPCS theoretically changes its structure one time and has a very simple structure [2]-[4].
The paper is organized as following: introduction, a brief introduction to pendular control systems (PCS), the stability of PCS, Essential PCS (EPCS) are detailed and various aspects are emphasized and analyzed by a comparative simulation study EPCS-classical control system.
Next section deals with some experiments made on a laboratory setup and illustrative experimental results are presented. Finally, conclusions and references are given.

2. PENDULAR CONTROL SYSTEMS

Let the control system depicted in *Figure 1*.

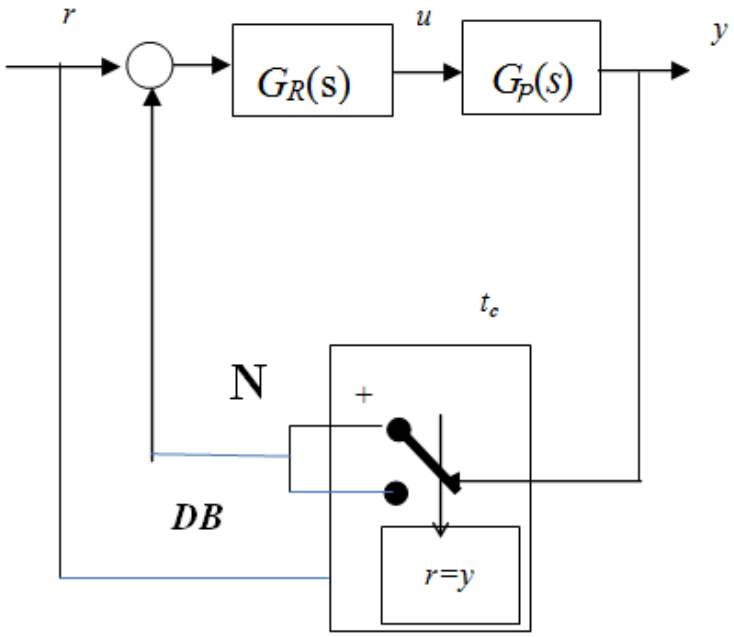

Figure 1 PENDULAR Control System (PCS) structure

PCS obtained introducing a nonlinear element ***N*** on the conventional system feedback loop. The signals r, u, y, G_R and G_p are respectively the reference, command, the controlled output, controller transfer function and the plant transfer function. The nonlinear element ***N*** contains a decision block and a switch K.
Initially the switch is on "+" position. The decision block DB commands the switch**,** "+" to **"-"** for the very first time t_c. The system changes its structure at time t_c. The system became now a negative feedback loop system. At this time the simple switch condition is fulfilled:

$$y(t_c)=r \tag{1}$$

The nonlinear element N is characterized by:

$$\tilde{y}(y)=\begin{cases}+y, & y\in[0,r]\\ -y, & y\in(r,\infty)\end{cases} \tag{2}$$

Definition. The nonlinear element expressed by the relation (2) is called PENDULAR nonlinear element.
N leads the system to the following behavior:

- till the moment t_c,
  $\tilde{y}(y)=y,\quad y\in[0,r],\ y(t_c)=r$,
  system has a positive feedback with closed loop transfer function:

$$G_{0+}(s)=\frac{G_R(s)G_p(s)}{1-G_R(s)G_p(s)}=\frac{G_d(s)}{1-G_d(s)} \tag{3}$$

•for $t>t_c$, system has a negative feedback ($\tilde{y}(y)=-y$) *only if* $y(t)\geq r$. The closed loop transfer function is:

$$G_{0-}(s)=\frac{G_R(s)G_p(s)}{1+G_R(s)G_p(s)}=\frac{G_d(s)}{1+G_d(s)}. \tag{4}$$

However, $y(t),\ t\geq t_c$ represents the differential equation Cauchy problem for the negative feedback system (the conventional one), initial condition $y(t_c)=r$. If for $t_{c1}>t_c$, $y(t_{c_1})=r$ and for $t>t_{c1}$, $y(t)<r$ the system will behave as positive feedback system (switch "-" to "+") and so on. In this manner, the controlled variable *y*, may be considered as output signal for the positive feedback system, then at the moment t_c, after the very first commutation, output signal for the negative feedback system; eventually for the moment t_{c1}, again output signal for the positive feedback system, etc. till the controlled signal variable is stabilized at the value *r*. The pendulum image for the output *y* reflects the movement between the two classes of differential equations solutions: S_+ (for positive feedback sub-system) and S_(for negative feedback sub-system) is represented in Figure 2.

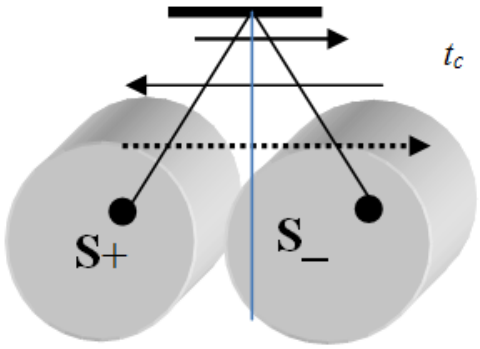

Figure 2 The y oscillatory "movement"

Definition. The system obtained introducing a nonlinear element N on the feedback loop of a classical control system is called PENDULAR control system (PCS).
*Illustrative example.*Let assume that the reference *r=1*, the controller is a proportional type with *k>0*, the plant is a simple integrator and no disturbance. One obtains directly from (3) and (4):

$$G_{0+}(s)=\frac{\frac{k}{s}}{1-\frac{k}{s}}=\frac{k}{s-k};\ G_{0-}(s)=\frac{\frac{k}{s}}{1+\frac{k}{s}}=\frac{k}{s+k} \tag{5}$$

Let us analyze the PCS system behavior:

- $t \in [0, t_c]$.System starts with positive feedback and is characterized by the differential equation :

$$\frac{dy_+}{dt} - ky_+ = k,\ y_+(0) = 0,\ t \in [0, t_c] \tag{6}$$

with the solution

$$y_+(t) = e^{kt} - 1,\ \ t \in [0, t_c] \tag{7}$$

From the relations (1) and (7) the switching time t_c is given by:

$$y_+(t_c) = r = 1 \Leftrightarrow e^{kt_c} - 1 = 1 \Leftrightarrow t_c = \frac{1}{k}\ln 2 \tag{8}$$

From (7), when $t \geq t_c \Rightarrow y_+(t) \geq 1 = r$, and according to (2) the switching condition "+"to "-" is fulfilled.

- $t > t_c$.System has now a negative feedback, being characterized by:

$$\frac{dy_-}{dt} + ky_- = k,\ y_-(t_c+) = 1,\ \ t > t_c\,, \tag{9}$$

One can see here the *nonzero initial condition.*What is remarkable from the mathematical point of view is that the solution of the Cauchy problem is

$$\begin{cases} y_-(t) = 1 + ce^{-kt}, t > t_c \\ y_-(t_c+) = 1 \Rightarrow c = 0 \end{cases} \Leftrightarrow y_-(t) = 1, t > t_c. \tag{10}$$

*The relation (10) shows that the system was stabilized only after one switch and stays in this state if no disturbance is reported.*The system global response is:

$$y(t) = \begin{cases} e^{kt} - 1, t \in [0, t_c] \\ 1, \quad t \in (t_c, \infty) \end{cases} \tag{11}$$

Computer simulation. Let us consider the above PCS with *k=1*. At t_p*=10* sec disturbances-*0.5 are applied.* Using *Matlab* , PCS response (*y*) with bold dotted line and conventional system (*y_*) with continuous line are depicted. The command *u* is also depicted One observe the chattering phenomenon *in Figure 3*.

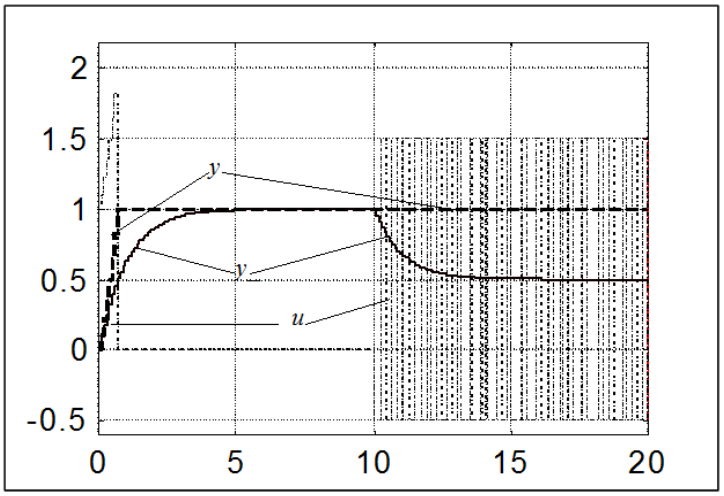

Figure 3 PCS with disturbance applied= -0.5

The chattering phenomenon is characteristic for variable structure systems (VSS). In practical applications chattering has to be as little as possible to not damage the actuator.

3. STABILITY OF PCS

The stability of PCS is an important point that was analysed in previous works [2]-[4].
Theorem. PCS is globally asymptotic stable if:

$$F(s)=\frac{1-G_d(s)}{1+G_d(s)} \tag{12}$$

is a real positive function [3].
The theorem leads to an important observation: not all PCS are stable but for a well now structure of the plant characterized by G_p one can choose a proper controller as (12) to be fulfilled.

4. ESSENTIAL PENDULAR CONTROL SYSTEM

Let now consider a PCS with PI controller and a first order plant (referring to Figure 1):

$$G_R(s)=k_R(1+\frac{1}{T_i s});\quad G_P(s)=\frac{k_P}{Ts+1};\quad T_i=T\,. \tag{13}$$

The closed loop transfer function *for a conventional negative feedback system* should be:

$$G_{0-}(s)=\frac{G_d(s)}{1+G_d(s)}=\frac{k}{Ts+k} \tag{14}$$

The system response for unitary r=1:

$$h_-(t)=1-e^{-\frac{k}{T}t},\quad \forall t>0 \tag{15}$$

The time response 5% t_{r-} for the conventional system:

$$h_-(t_{r-})=0{,}95 \Leftrightarrow e^{-\frac{k}{T}t_{r-}}=0.05 \Leftrightarrow t_{r-}=\frac{T}{k}\ln 20\cong 3\frac{T}{k} \tag{16}$$

Let now return to PCS. PCS has for $t\in[0,t_c]$ a transfer function (positive feedback case)
Definition. PCS that switches *only* one time when *no* disturbance is applied is called *essential pendular control system* (EPCS).
Theorem The system described above is EPCS. Its step response is given by:

$$y(t)=\begin{cases}h_+(t), & t\in[0,t_c)\\ 1, & t\in[t_c,\infty)\end{cases}. \tag{17}$$

Demonstration. For $t\in[0,t_c)$, the response is given by (11).For $t\ge t_c$ (after one commutation) the system response is obtained solving the following Cauchy problem:

$$T\frac{dh_-}{dt}+k\,h_-=k,\quad h_-(t_c)=1,\quad \forall t\ge t_c\,. \tag{18}$$

The general solution for (32) is $h_-(t)=1+c\,e^{-\frac{k}{T}t}$, $t\ge t_c$, $c\in R$ and imposing the initial condition, one obtains c=0. Mathematically speaking EPCS reaches and stays in r=1 after one commutation. From the control system point of view this is very important. In Figure 4 the responses for the classical system y_ (with conventional negative feedback) versus EPCS system y are depicted. The responses were obtained by simulation via Matlab-Simulink environment. For simplicity k=T=1.

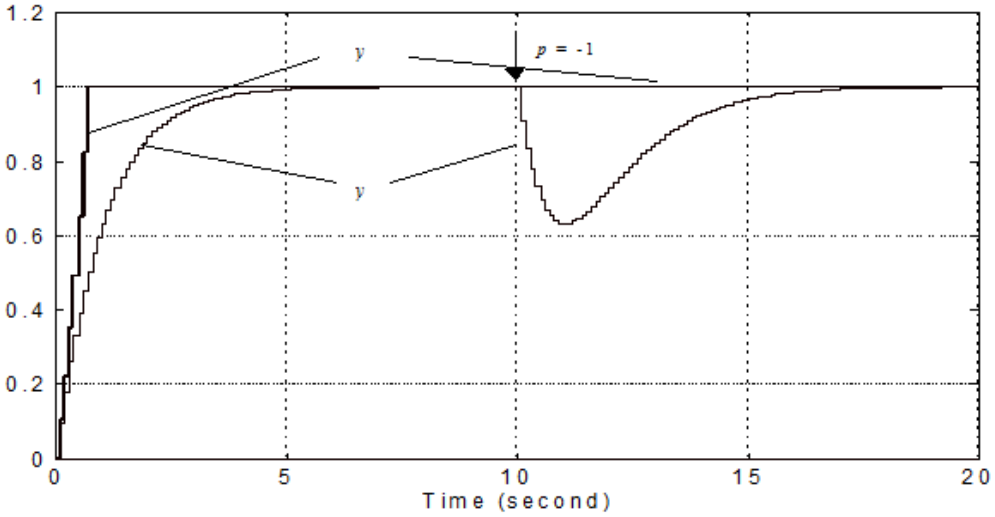

Figure 4 Simulation results for $k=T=1$

If a unitary step disturbance will be applied (at $t=10$ sec $p=-1$) an excellent behavior is reported for EPCS. In fact the disturbance being negative the system commutes on positive feedback and stays in 1.

5. EXPERIMENTAL SETUP

The setup consists in a Feedback® Discovery Product for temperature and flow control. In this paper were made tests only for the flow control. The plant is a heat changer and the controlled variable is the hot water flow that entered the heat changer. The flow is measured and converted with a flow transducer and adapted with an adaptor. Using a PCL-812 board the signal is acquired in order to be processed. As actuator a servo-valve was used. The servo-valve was commanded by a signal from acquisition board output channel. A rectangular reference was used. Because the process is strongly affected by disturbances, the controller used is a PI type Using the PENDULAR control methodology, the response is obtained as in Figure 5.

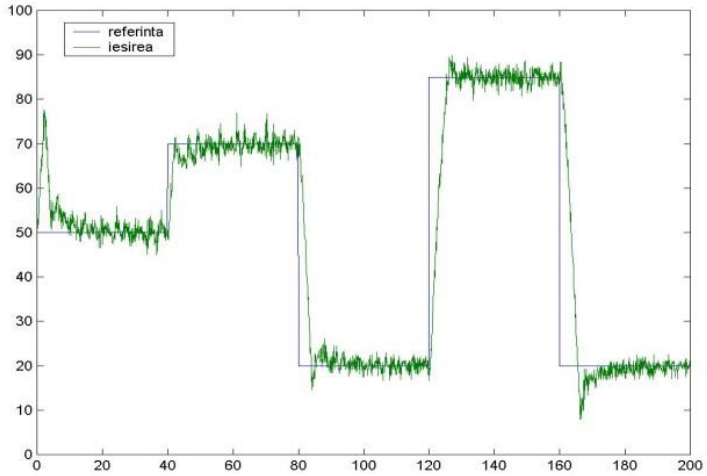

Figure 5 Flow control via PCS

CONCLUSIONS

The paper presents the PENDULAR control systems concept. The PENDULAR control principles are sustained by a stability study. PCS are in fact a Variable Structure System with a simple structure. The main idea is to optimize conventional structures with negative feedback using a nonlinear element on the feedback loop. In this manner positive feedback plays an import role in control. EPCS systems were detailed and the simulation results are illustrative. The research is also sustained by experimental results made on flow control setup. This new control methodology seems to have some impact over the control strategies.

REFERENCES

[1] K.J. Aström and T. Hägglund, *PID Controllers: Theory, Design and Tuning,* Research Triangle Park, USA, 2nd Ed. 1995.
[2] C.N. Calistru, A symbolic optimization approach to tuning PID controllers, *Proceedings of the 4th IEEE Conf. on Control Applications, CCA'95*, Albany, NY, pp.174-175, 1995.
[3] C.N. Calistru, *Increasing Control Systems Robustness Using Integral Criteria and Alternate Feedback*, (in Romanian), Matrix Rom Publ. House, 2004.
[4] C.N. Calistru, Optimization of control structures via the PENDULAR concept, *Proceedings of the 3rd European Conference on the Use of Modern Information and Communication Technologies*, ECUMICT'2008, Gent, pp. 18-29, 2008.

INTERNATIONAL SCIENTIFIC CONFERENCE ON ADVANCES IN MECHANICAL ENGINEERING

13-15 October 2016, Debrecen, Hungary

THE DESIGN AND REALIZATION OF THE MC MANIPULATION STRUCTURE FOR MICROFACTORIES

[1]CĂȘVEAN Marius, [2,3]LATEȘ Daniel PhD, [3]CIOLOCA Flaviu

[1] *Master Student, Technical University of Cluj-Napoca*
E-mail: marius.casvean@yahoo.com
[2]*Associate professor, "Petru Maior", University of Târgu Mureș*
E-mail: ddan005@gmail.com
[3] *Mechanical Designer, IRUM, Târgu Mureș*
E-mail: cioloca.flaviu@irum.ro

Abstract
In this work will be designed and realised a micromanipulator named MC, for microfactories keeping in account the command and control technology from the last generations. The work will begin with the introduction in the microfactory domain touching the conditions which these need to achieve. It will present also the actual stage of the micromanipulators researched and designed from more worldwide universities. The second part of the work will focus on the analisys and design of the manipulation physically design. In the end of the work will present the practical realisation of the MC micromanipulator and the conclusions.

Keywords: *micromanipulation, microfactory, precision, constructive analisys, 3D design.*

1. INTRODUCTION

Microfactories concept first appeared around 1990 in Japan, where they implemented various methods to miniaturize machines and equipment needed in production line with the objective to reduce costs. This field of research was further developed in Europe, in the US and globally, through various projects that were initiated, thus trying to realise production by another concept, respectively small factory, to be able to save resources such as energy consumption in production process, raw material, the working space necessary for the functioning of the production line, execution time, etc. [1].

Equipment and accessories needed a small factory, are in generally similar in terms of tasks that must meet with the ones in a traditional factory (of classical size), the difference being in terms of how to achieve the tasks, size, mass and precision. Precision micromanipulation tasks are required in a wide range of applications such as microassembly, surgeries or positioning of parts for various verification operations. Thus, many micromanipulation systems can be found in the specialised literature [2]. The size of the end effector may vary from micrometers to a few tens of millimeters [2], [3]. While micrometer structures are suitable for high-precision positioning, the advantage of millimeter is larger displacements. In most cases, the sound and vibrations are the main factors that reduce system performance micromanipulation, which leads to poor reproducibility and loss of accuracy [4], [5]. When you need a high precision positioning, measures must be taken on these perturbations. There are various possible solutions: design isolation environment platforms [6], [7], or using controllers suitable for noise rejection [8].

2. EXAMPLES OF EXISTING MICROFACTORIES

Microfactory notion roots are in Japan. In Mechanical Engineering Laboratory in Japan was realised a micro-manipulator with two grippers [9].
Within the firsts concepts of microfactory, appeared outside Japan were TOMI, developed by TOT in Finland in 2000. This project was aiming to develop an efficient assembly system for small products [10]. In Germany they have done different positioning modules for microfactories.
In Switzerland at the EPFL Lausanne, Zurich ETHZ, EMPA Dübendorf, where they developed models for microfactories in vertical structure [11]. In Finland also, at Tampere University of Technology (TUT), production engineering department is performing research micromanipulation technology for over 10 years and is one of the world's leading research units in this area.
The concept of microfactory, TUT, is constituted by a series of compact modules that can be assembled, for example in a robotic assembly cell, a cell of laser processing a 3D printer or a machine tool. These production cells can be integrated to build a whole production line in a very small space [12]. In the US, the University of Illinois, Department of Mechanical and Industrial Engineering, a microfactory has been realised, and the University of Louisville, Kentucky, has developed a microfactory, called Opal [13]. In Romania, Valahia University has patented a device for micromanipulation with magneto-piezoelectric actuation [14].
Research miniaturization of systems are conducted also in universities in Belgium (ULB Brussels), Italy (University of Pisa, ITIA-CNR), England (Cambridge University, University of Nottingham), Vanderbit University, Brigham Young University, Cornell University, The Chinese University of Hong Kong, National Key Laboratory of Manufacturing Systems in Xi'an Jiaotong University, Tsukuba Mechanical Engineering Laboratory [15] but are supported also by agencies such as NASA, ESA.

3. ANALISYS OF THE MANIPULATION SYSTEM

In order to precede the design, a block diagram of such a complex technical system for handling was performed. This is shown in Figure 1.
The manipulator mechanism is a system mechanically mobile, having a fixed base and the possibility to move of his elements in a variety of positions.
The tool is attached jointly to the effector manipulator element and is designed to perform application-specific operation. The actuators are electrical and attached to the mobile mechanical system and are the mechanical energy source of the robot. Their movement is planned and followed in real time by the control system. Sensors are devices transducers of physical parameters into digital information used for command and control system. Most often, the parameters are such cinematic track (position and velocity) and mechanical (force). The command and control system consists of a computer with specific software and interfaces for the transfer of information between it and the sensor system on the one hand and controls the motor on the other hand. The role of this system is to program the desired action and to pursue its development [16].

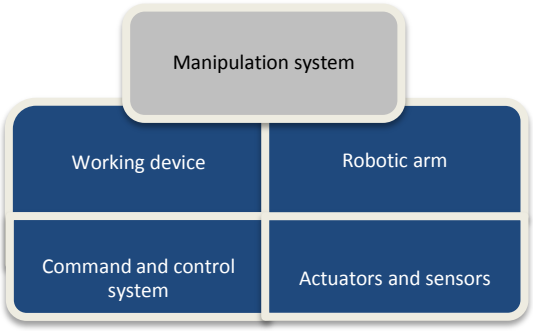

Figure 1 Block diagram of the handling system

4. THE DESIGN OF THE PROTOTYPE STRUCTURE IN VIRTUAL ENVIRONMENT

For the mechanical structure is realized the 3D model with SolidWorks software, implementing geometric and material properties. Finite element analysis is carried out in the same software, the optimum mesh, that is to say in areas with smaller sizes the number of finite elements was higher, the aim being to increase the accuracy of the calculation of the areas of interest. The analysis conducted in elastic mesh uses for finite elements "Solid theta 92", which adapts very well to this type of calculation. Boundary conditions imposed to the gripper with movements in the axial direction by FEM simulation that is as close to reality, are given by recessed areas screw fixing or cancellation of all degrees of freedom. The micromanipulation in Figure 2 was designed as a cell with the following modules: serial mechanism (1), servomotors (2) gearbox, gear rack (3) gripper mechanism (4), actuator for gripper mechanism (5).

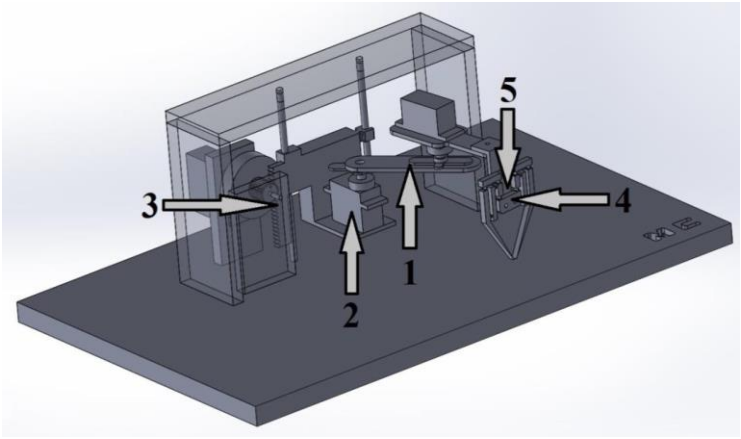

Figure 2 The CAD model of the MC structure

5. RESULTS

In Figure 3 you can see the practical realization of MC designed system. After modelling, all the parts necessary for the system were brought to the stage to be made practical. All pieces of the system structure, which required certain processing were performed in the laboratories of the Technical University of Cluj Napoca.

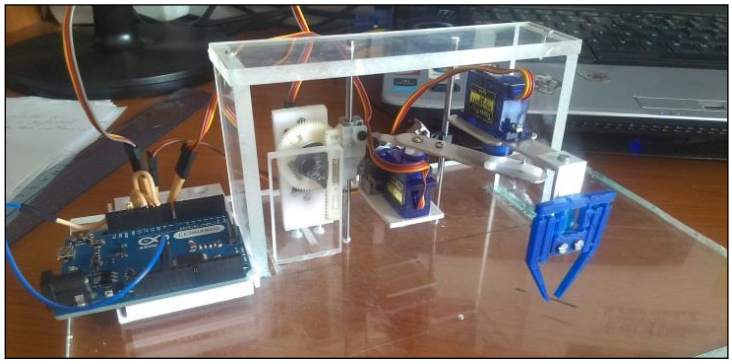

Figure 3 The phisycal realization of the MC structure with command elements

To program the system was used Arduino programming environment adapted for Leonardo plate and it was written a program with which you can simultaneously control three actuators in any sense with a certain number of steps. In this programming environment, appropriate settings are made and then the design code, to control actuators. Once the code has been correctly written, it loads in the plate Arduino Leonardo followed the actuators to perform movements by logic implemented in the written code.

CONCLUSIONS

The different nature of the handling subsystems as specific problems of each, makes this interdisciplinary field to be developed as applications in various fields of activity. Handlers are defined and developed according to the needs of the assembly procedure and designed as miniaturized systems, to a certain scale, considering the precision and accuracy of the application at which are used requires.
MC manipulator shown is used for high-precision operations and some of high speed. It can be developed in parts, as separate components of a more complex device, of a work station and these assembling cells are continuously evolving to express as accurately the microfactories modular concept.
The manipulator is designed as miniaturized systems to a certain scale of dimensions, taking into account the objective of their use, accuracy, speed work or other items to be imposed on them to meet the requests.

REFERENCES

[1] http://static.aminer.org/pdf/PDF/000/353/685/
[2] Beyeler F., Neild A. P., Oberti S., Bell D. J., Sun Y., Dual J., Nelson B. J., *Monolithically Fabricated Micro-Gripper with Integrated Force Sensor for Manipulating Micro Objects and Biological Cells Aligned in an Ultrasonic Field*, IEEE/ASME Journal of Microelectromechanical Systems (JMEMS), Vol. 16, Number 1, pp. 7-15, 2006.
[3] Jain R. K., Patkar U. S., Majumdar S., *Micro gripper for micromanipulation using IPMCs (ionic polymer metal composites),* Journal of Scientific and Industrial Research, Vol. 68, pp. 23-38, 2009.
[4] Anis Y., Cleghorn W. L., Mills J. K., *Modal Analysis of Microgrippers used in Assembly of MEMS Devices,* International Conference on MEMS, NANO and Smart Systems, Banff, Alberta, Canada, 2005.
[5] Martinez J., Panepucci R., *Design, Fabrication and Characterization of a Microgripper*

Device, Proceeding of the Florida Conference on Recent Advances in Robotics, 2007.
[6] Zhou Q., Aurelian A., Del C. C., Esteban P. J., Kallio P., Bo C., Koivo H. N., *A microassembly station with controlled environment,* Microrobotics and microassembly, Vol. 4568, pp. 252-260, 2001.
[7] Brenan C. J., Charette P. G., Hunter I. W., *Environmental isolation platform for microrobot system development,* Review of Scientific Instruments, Vol. 63, issue 6, pp.3492-3498, 1992.
[8] Rakotondrabe M., Agnus J., Rabenorosoa K., Chaillet N., *Characterization, modeling and robust control of a nonlinear 2 DOF piezocantilever for micromanipulation/microassembly,* IEEE/RSJ – IROS, International Conference on Intelligent Robots and Systems, St. Louis MO, USA, 2009.
[9] Mishima, N., : *Development of a Design Tool for conceptual Design Stages of Machine Tools*. ASPE 16th Annual Meeting. Arlington, p.184, 2001.
[10] Yi Qin, *Micromanufacturing Engineering and Technology,* Second Edition, Elsevier, ISBN: 978-0-323-31149-6, 2010.
[11] Verettas I., Clavel R., Codourey A., *Pocket Factory: Concept of miniaturized modular cleanrooms*
[12] http://www.tut.fi/en/about-tut/news-and-events/international-visibility-for-tut-s-microfactory-research-p043466c1
[13] http://www.gereports.com/post/125266029665/the-dawn-of-a-new-ice-age-meet-opal-firstbuilds/
[14] Alexandru I., Mihaita A., Veronica D., *Dispozitiv de actionare magneto-piezoelectric pentru micromanipulare,* OSIM, nr. Cerere: a 00471, RO 129160 A2, 2012.
[15] Mishima, N., Shinsuke, K., Masui, K. : *A Study Efficiency Analysis of Micro Manufacturing Systems.* Proceedings of the 2007 IEEE International Conference on Mechatronics and Automation. Harbin, China, p.51, 2007.
[16] http://www.mec.ugal.ro/pdf/Robotica.pdf

STUDY ON OPERATING RISKS IN DIESEL ENGINES AT 060-DA RAILWAY ENGINE

COROIAN Olimpia PhD

Technical University of Cluj-Napoca
E-mail: olimpiatutas@yahoo.com

Abstract
The 060-DA diesel-electric railway engine is the most ussed in Romanian Railways network. It is equipped with a high power motors of 2100 HP. In time, all the parts of diesel engine acquires wears and defects that diminish their performance and can endanger traffic safety, so risk analysis is an essential operation

Keywords: maintenance, diesel engine, inspection, repairs, risks

1. 12 LDA 28 DIESEL ENGINE CHARACTERISTICS

The diesel-electric 060-DA railway engine is equipped with an SULZER engine having 12 cylinders mounted on two distributions in line and arranged vertically mounted in the space between the two management positions, being insulated and soundproofed to these.

Figure 1 The 12 LDA diesel engine

2. MAINTENANCE AND REPAIRS MADE TO THE 060-DA RAILWAY ENGINE

Maintaining the railway engine in a safe running is made by execution on time and at a corresponding quality level of revisions and planned repairs, moments in which we eliminate the normal wear of the parts.

In Romania the type hauls and repairs planned faced rail vehicles succession of their norms of time (days, months, years) or norms of kilometers from railway vehicles are out of service for revisions and planned repairs are set by ministerial order 1359 / 30.08.2012, namely the railway norm "railway vehicles. Types of planned inspections and repairs. Time and mileage standards for revisions and planned repairs. " systematized in figure 2.

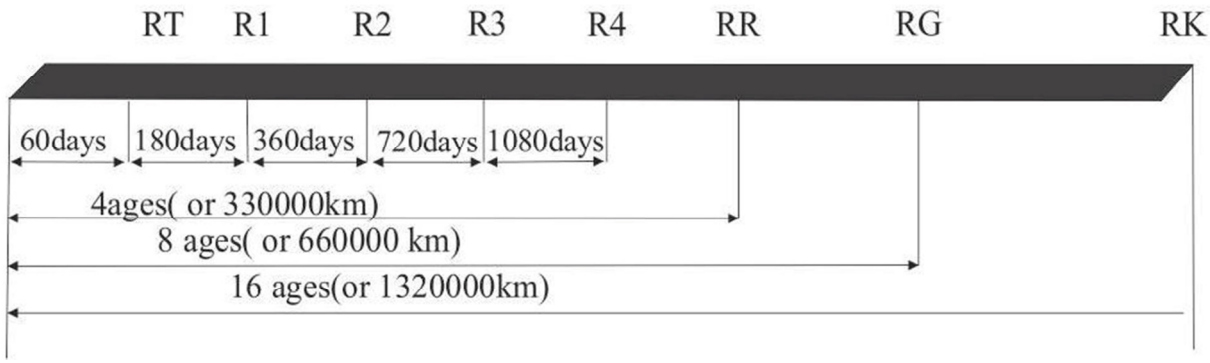

Figure 2. The diagram of diesel-electric locomotives revisions

Any diesel electric locomotive has a life service of 35 years. Maintaining operational locomotives have exceeded the normal service is performed only after the vehicles have undergone technical assessments to establish the technical condition of the structure strength (chassis, chassis). Evaluation of technical condition of vehicles is made in relation to a repair with lifting axle / bogies.
In the following we will focus on in-service behavior of the diesel engine crankshaft and associated risks.

3. THE BEHAVIOR IN SERVICE OF THE 12 LDA 28 CRANCKSHAFT ENGINE AND ASSIMILATED RISKS

Figure 3 Grinder - SC Remarul February 16 Cluj Napoca

The crankshafts brought for examination and repair at the SC Remarul SA February 16, are rectified in most cases (over 90%). In figure 3 is presented the grinder that is running the operation.
Analysing the activity from the repair plant we can say that the most frequent defects are micro fissures, fissures, cracks, the wear of bearing spindles and crankpins, ovality and taper of bearing spindles and crankpins , deflection of crankshaft , seizure and breakage.
Between november 2013 and december 2015 were brought for reparation, 8 diesel electric 060-DA railway engines, on which operations were performed, especially grinding crankshafts, major affected by wear and deformation. We can see the activity of "Engine" department of SC Remarul February 16 SA between November 2013 – December 2015 in table 1.

Table 1 The activity of "Engine" department of SC Remarul February 16 SA between November 2013 – December 2015

Date	Railway engine	Performed operations
November 2013	DA-1593	1st Distribution –Crankshaft grinded at crankpins 2nd Distribution –No operation made
February 2014	125-805	Crankshaft grinded at spindle bearing no.7 and lapped at crankpins
March 2014	DA-1617	1st Distribution –Crankshaft lapped 2nd Distribution Crankshaft lapped
Iuly 2014	DA-1243	1st Distribution- Spindle bearings and crankpins lapped 2nd Distribution –Spindle bearings lapped and crankpins grinded
September 2014	DA-063	1st Distribution - Crankshaft lapped 2nd Distribution - Crankshaft lapped
Ianuary 2015	DA-1651	1st Distribution –Crankshaft grinded 2nd Distribution –Spindle bearings lapped and crankpins grinded
February 2015	DA-1695	1st Distribution –Crankshaft changed 2nd Distribution - Crankpins lapped
April 2015	DA-460	1st Distribution - Spindle bearings grinded and crankpins lapped 2nd Distribution –Spindle bearings grinded and crankpins lapped

The defects are strictly related to operating conditions of the engine and the conditions of their maintenance or heandling on time the revisions.
In table 2 we can see the possible defects and the frequency which they occure, frequency observed during repaires carried out.

Table 2 Possible defects of crankshafts

Possible defect	The frequency	Defect consequences	Prevention manner	Material risk
Wear of spindles bearing and crankpins	90%	Seizure Breakage	Proper operation and maintenance	Bearings change
Ovality of spindles bearing and crankpins	80%	Unusual wear Microfissures Seizure	Proper operation and maintenance	Bearings change
Taper of spindles bearing and crankpins	80%	Unusual wear Microfissures Seizure	Proper operation and maintenance	Bearings change
Crankshaft deflection	80%	Unusual wear Microfissures Seizure	Proper operation and maintenance	Bearings change
Microfissures	70%	Unusual wear Fissures	Proper operation and maintenance	Bearings change
Fissures	90%	Unusual wear Seizure	Proper operation and maintenance	Bearings change
Cracks	90%	Unusual wear Seizure	Proper operation and maintenance	Bearings change
Seizure	30%	Breakage	Proper operation and maintenance	Bearings change
Breakage	5%	Unable to be used	Proper operation and maintenance	Crancksha ft change

Analyzing in terms of the risks these weaknesses, using FMEA method was established for each of a RPN (Risk Priority Number) based on coefficients of severity (S), probability of occurrence (O) and probability of detection (D) of the defect, as it is showen in table 3.

Table 3 Applied F.M.E.A. on the possible defects of the crankshaft

Possible defect	Severity (S)	Occurrence (O)	Detection (D)	Risk Priority Number (RPN=S*O*D)
Wear of spindles bearing and crankpins	4	9	3	108
Ovality of spindles bearing and crankpins	4	8	2	64
Taper of spindles bearing and crankpins	4	8	2	64
Crankshaft deflection	4	8	2	64
Microfissures	2	9	3	54
Fissures	3	9	2	54
Cracks	3	9	2	54
Seizure	8	3	1	24
Breakage	10	2	1	20

Considering that the wear of spindles bearing and crankpins it has the biggest RPN it is neccesary to take proper measures to reduce it. The biggest point is 9, for occurence, so measures must be taken to reduce this probability, reduce the frequency of occurrence.
As emerges from the risk analysis, wear of spindles bearing and crankpins is important due to the fact that neglected entail some serious defects and also harder to control.
The interdependence relation between the possible defects is presented in the next graphic (Figure 4).

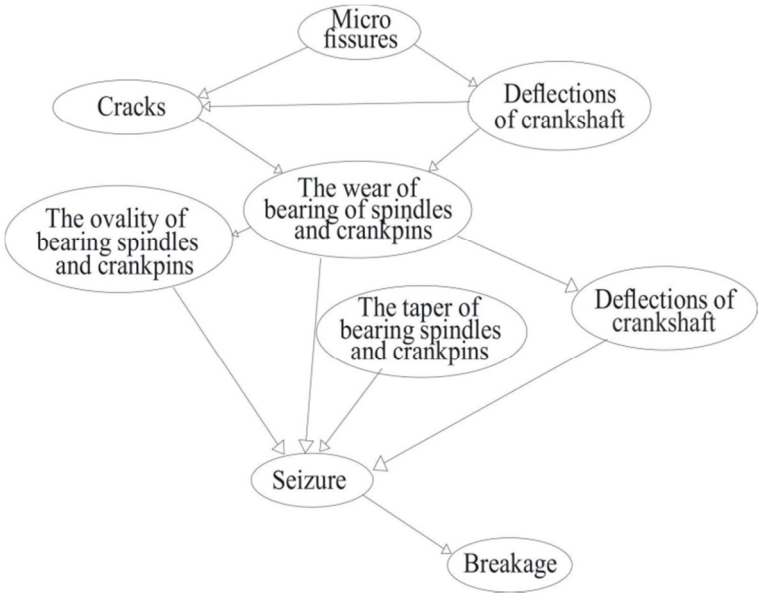

Figure 4 The relation of defects interdependence

The measures to be taken in this case related to the operation and maintenance of the engine crankshaft which includes namely the timely revision and repair works. So:
- At the daily overhaul it must be checked without disassembly of the engine subassemblies and performing the necessary anointings. It will take sample from the engine oil sump and sent to the laboratory for analysis. Daily oil level should be checked and if necessary supplementing it;
- At the technical inspection it will be revied the working fine fuel filters, oil centrifuges cleaning and checking the injectors;
- At the the revision type 1 it will be carried out the work provided at the technical inspection and it will be checked and replaced the fine oil filters;
- During revision type 2 it will necessarily replace the oil;
- During repair lift (RR) is very important to analyze in detail each component after dismantling. Where appropriate components that do not match will be repaired or replaced.
As you can deduce an important role in wear bearing spindles and crankpins it has the adequate lubrication that leads to radically decrease wear. In this sense anointing of 12 LDA-28 diesel engine is ensured by a system of forced lubrication, wet sump type.
Oil consumption of a diesel engine is between 4-10% of the fuel consumption and increase oil consumption shows that the engine has reached an advanced stage of wear and requires revision.

CONCLUSION

Studying the behavior in service of the crankshaft, we can conclude that they have a functioning cycle, as required in the phase of manufacturing, but by analyzing the frequency of occurrence of defects crankshaft and risks involved occurrence of these defects apparent either maintenance is inadequate or not carried out on time.
To optimize the proces of maintenance, repair and reducing the risks, we propose drawing up a maintenance plan customized for each locomotive in part, plan in whicj the work done both in depots and in factories to be linked and have fluency in order to reduce maintenance costs and increase traffic safety.

REFERENCES

[1] Băţagă, N.,Cazila, A., heart N. - *Running-in, wear testing and regulating heat engines,* Technical Publishing House, Bucharest, 1995
[2] Bonta, D. - *060 diesel electric locomotives of DA-2100 HP, construction, maintenance and operation*, ASAB Publisher, Bucharest, 2003
[3] Coroian, O., Gyenge, C. – *Patterns of analysis and risk interpretation for the rolling stock repair process*, HD-45-Stud, Hunedoara, 2015
[4] Coroian, O., Gyenge, C. – *Analysis the risc factor at repair process of rolling stock using modelling methods*, National Multidisciplinary Conference, professor Ion D. Lazarescu, 3rd Edition , Cugir 2015
[5] Coroian, O. – *Study on behavior in service of diesel engines and aspects concerning their maintenance*, K.O.D., 2016
[6] Coroian, O. – *Study on behavior in service of diesel engines fitted to locomotives*, National Multidisciplinary Conference, professor Ion D. Lazarescu, 4th Edition , Cugir 2016
[7] Isac, C., Popoviciu, G. – *Diesel Electric Locomotive Technical Book*, Vol. I - Mechanical and thermal, Ministry of Transport and Telecommunications, Technical publications and documentation center, Bucharest, 1973
[8] Muresan, A. - *Contributions to the development of modern technologies for reconstructing Some parts of the engine-transmission ensemble for diesel locomotives*, PhD Thesis, Cluj Napoca, 2010
[9] OM 1359 / 08.30.2012, *Railway vehicles. Types of planned inspections and repairs. Time and mileage standards for revisions and planned repairs*
[10] Zglavuţă, E., Croitoru, M., Mark, M. - *Troubleshooting for diesel-hydraulic locomotives, publications and technical documentation center*, M.T.Tc.
[11] *Master, operation and maintenance of diesel electric locomotive 060-DA-2100 CP*, Ministry of Railways, the Centre for Documentation and technical publications Bucharest, 1969
[12] *The list of works executed during revisions and repairs, LDE 2100 HP diesel engine 28 12 LDA*, Romanian Railway Register 2011
[13] www.remarul.eu

THEORY OF ACOUSTIC METAMATERIALS

[1]CVETICANIN Lívia DSc, [2]CVETICANIN Dragan PhD

[1]University of Novi Sad, Novi Sad, Serbia
Obuda University, Budapest, Hungary
E-mail: cveticanin@uns.ac.rs, cpinter.livia@bgk.uni-obuda.hu
[2]REMMING, Novi Sad, Serbia
E-mail: dragan.cveticanin@remming.co.rs

Abstract
In this paper the novel acoustic absorbers based on acoustic metamaterials are considered. Instead of acoustic isolators these absorbers improve the reduction of the acoustic effect in buildings, machinery, ships and other applications and so on. Their working mechanism is based on the concept of conventional vibration absorbers. The basic unit of the acoustic metamaterial is a mass-in-mass system which works as vibration absorber. In the paper the effective mass of the unit is calculated. Conditions for negative effective mass are discussed. The advantage and disadvantage of the metamaterial in comparison to the conservative acoustic absorber is underlined.

Keywords: *Acoustic absorber; metamaterial beam; spring-mass systems; negative effective mass.*

1. INTRODUCTION

One of the requirements of environmental and occupant health protection is the noise reduction and elimination of the sources of sound pollution. Various methods are developed to damp and reduce the acoustic influence on the health of population. One of the most often applied methods is based on the use of materials for acoustic isolation which absorb the acoustic energy. It is known that acoustic waves which come to the wall generate waves in the wall itself and these waves transmit sound power through the wall to the other side [1]. To reduce the transmitted energy a partition is settled on the wall. In [1] it is stated that at a given frequency the level of sound transmitted through a partition will be reduced by 5-6 dB for every doubling of the mass of the partition. Unfortunately, it means that the considerable noise reduction requires the significant mass of isolator. It was the reason that the new kind of absorber which is much lighter has to be designed. One of them is the acoustic metamaterial beam. Based on the concept of conventional mechanical vibration absorbers the metamaterial beam is proposed. The metamaterial beam consists of a uniform isotropic beam with many small spring-mass-damper subsystems integrated at separated locations along the beam to act as vibration absorbers (*Figure 1*). The elastic wave in the beam force the integrated spring-mass-damper absorbers to vibrate at frequencies close to but above their local resonance frequency and to create shear forces and bending moments to straighten the beam and stop the wave propagation. Thus, the spring-mass-damper subsystems create a stop-band in which no elastic waves in this frequency range can propagate forward.

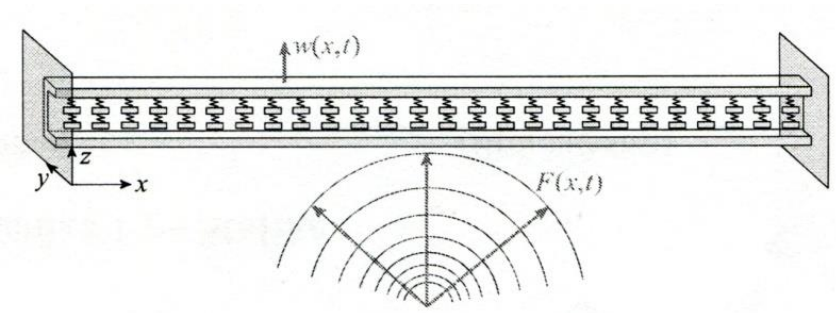

Figure 1 Model of a metamaterial beam for vibration absorption [2]

In this paper the mechanism of action of the acoustic absorber is discussed.

2. CONCEPT OF CONVENTIONAL VIBRATION ABSORBER

As it is well known, the conventional vibration absorber consists of a lumped mass m_2 attached with a linear spring k_2 to the mechanical system with mass m_1 (see *Figure 2*).

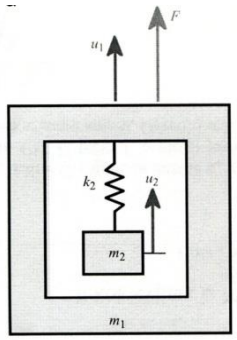

Figure 2 Mass-in-mass model [3]

If the excitation force acts on the mass m_1 differential equations of motion are:

$$m_1\ddot{u}_1 + k_2(u_1 - u_2) = F_0\exp(i\omega t) \tag{1}$$

$$m_2\ddot{u}_2 + k_2(u_2 - u_1) = 0 \tag{2}$$

Solutions of (1) and (2) have the form:

$$u_1 = a_1\exp(i\omega t)\,, \qquad u_2 = a_2\exp(i\omega t) \tag{3}$$

where:

$$a_1 = \frac{F_0(k_2 - m_2\omega^2)}{(k_2 - m_1\omega^2)(k_2 - m_2\omega^2) - k_2^2}, \qquad a_2 = \frac{F_0 k_2}{(k_2 - m_1\omega^2)(k_2 - m_2\omega^2) - k_2^2} \tag{4}$$

and i=$\sqrt{-1}$ is the imaginary unit. For this model only one local resonance frequency exists. The vibration absorber uses the 1:1 external resonance between the forcing frequency on the main

system ω and the local resonance frequency of the absorber $\omega_2 = \sqrt{k_2/m_2}$ to transform the vibration energy to the absorber and stop the main system motion (u_1=0). Based on this conception an idea of a new material, which would be the acoustic absorber is developed. Besides, motivated by the mathematical analogy between acoustic and electromagnetic waves the investigation were directed toward so called metamaterials which exhibit exceptional properties not observed in nature or in the constituent materials [2]. Namely, the acoustic (elastic) metamaterials have to be the counterpart to electromagnetic metamaterials. The main property of electromagnetic metamaterials is that they have negative permittivity and magnetic permeability which result in a negative refractive index. According to analogy it has to be asked the acoustic metamaterial to be with negative mass density and negative modulus. The negative effective mass/mass density is not the physical property of the material but is the result of inaccurate modelling of acoustic metamaterials.

3. EFFECTIVE MASS DENSITY FOR MASS-IN-MASS SYSTEM

Let us consider the mass-in-mass model (*Figure 2*) as a subunit of a metamaterial which is suggested to be identified with a single mass with effective mass m_{eff} whose motion is the same as that of m_1. The effective mass is defined by treating this two-degree-of-freedom system as a one-degree-of-freedom one by assuming the internal absorber being unknown to the observer. In other words, the identity of the internal mass m_2 would be ignored and its effect would be absorbed by the introduction of an effective mass m_{eff} as shown in *Figure 3*.

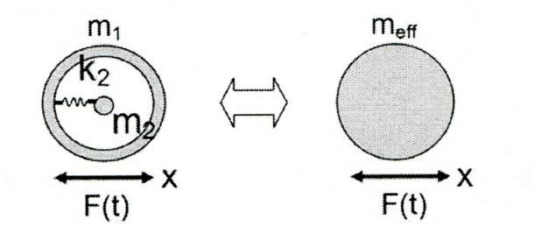

Figure 3 Identity of the mass-in-mass model and of the model with effective mass [4]

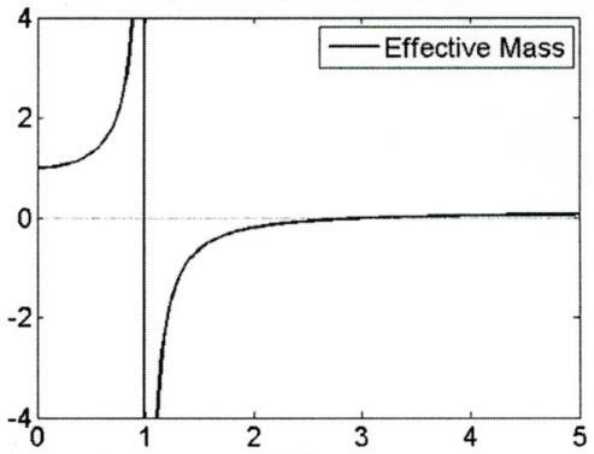

Figure 4 Dimensionless effective mass m_{eff}/m_1 as a function of ω/ω_2 [6]

If the motion of the mass m_1 is u_1, the effective mass has also the motion u_1. Linear momentums for the both models given in *Figure 3* have to be equal, i.e.:

$$m_{eff}\frac{du_1}{dt} = m_1\frac{du_1}{dt} + m_2\frac{du_2}{dt} \tag{5}$$

Substituting the assumed solution (3) into (5) it is:

$$m_{eff}a_1 = m_1a_1 + m_2a_2 \tag{6}$$

Motion of the mass m_2 is given with the equation (2). Substituting the assumed solutions (3) we have

$$-m_2\omega^2a_2 + k_2(a_2 - a_1) = 0 \tag{7}$$

After some modification equations (8) and (9) yield the effective mass [4-6]:

$$m_{eff} = m_1 + m_2\frac{k_2}{k_2 - m_2\omega^2} \tag{8}$$

which is for: $\omega_2 = \sqrt{k_2/m_2}$

$$m_{eff} = m_1 + m_2\frac{\omega_2^2}{\omega_2^2 - \omega^2} \tag{9}$$

Analyzing the relation (9) it is obvious that the effective mass depends on the ration between the excitation frequency ω and natural frequency of the system ω_2.
For the system three modes of motion are evident: 1) acoustic mode when $\omega<\omega_2$, 2) resonant mode when $\omega=\omega_2$ and 3) optic mode when $\omega>\omega_2$. For the acoustic mode the effective mass is positive. In the resonant mode the effective mass is theoretically infinite. In the optical mode the effective mass is negative for:

$$m_1 + m_2\frac{1}{1-\frac{\omega^2}{\omega_2^2}} < 0. \tag{10}$$

Otherwise, it is positive. In *Figure 4*, according to (9) the effective mass - frequency diagram is plotted.
Differentiating the relation (5) we have:

$$(m_{eff} - m_1)\ddot{u}_1 = m_2\ddot{u}_2 \tag{11}$$

Substituting (11) into (2) we obtain:

$$k_2(u_2 - u_1) = -(m_{eff} - m_1)\ddot{u}_1 \tag{12}$$

Equation (1) and (12) give:

$$-m_{eff}\ddot{u}_1 = F_0\exp(i\omega t) \tag{13}$$

The effective mass is the ratio between the excitation force and acceleration of the mass m_1:

$$m_{eff} = \frac{F}{\ddot{u}_1} = \frac{F_0}{-\omega^2 a_1} = -\frac{F}{\omega^2 u_1} \tag{14}$$

According to *Figure 4* it is obvious that for $\omega_2=\omega$ the effective mass tends to infinity. For that value the motion of mass m_1 is zero and the inertial force of the mass m_2 is equal to the excitation force: $F(t) = m_2\ddot{u}_2$. So, the external force is eliminated with the inertia force -$m_2\ddot{u}_2$ through the spring k_2. This is the concept of vibration absorbers. Finally, the following is concluded:
In the acoustic mode, when $\omega<\omega_2$, the effective mass m_{eff} is positive and the motions u_1 and u_2 are in phase. For the optical mode, when $\omega>\omega_2$, the effective mass m_{eff} may be positive or negative, while the displacements u_1 and u_2 are 180^0 out of phase. Then, the absorber works efficiently in the optical mode against the external acting on the mass m_1. The excitation is absorbed with the inertial force.

4. MECHANICAL STRUCTURE WITH NEGATIVE EFFECTIVE MASS

Mechanical structures are designed by incorporating of the previously mentioned mechanical subunits in a natural material with the aim to resonate during mechanical wave propagation in it. For the local mechanical resonance the designed structures have negative effective masses. The negative mass behavior is generated by oscillating of resonant structures within the material with 180^0 out of phase to the acoustic waves which apply to surface. It causes existence of frequency bands where wave propagation is theoretically impossible. These bands are usually called band gaps. The aim of the designed structure is to overcome the limitations of the mass law for solids by creating engineered materials with useful acoustic band gaps, and the key to the generation of these band gaps is an inhomogeneous structure. Huang et al. [6] composed a one-dimensional lattice which contains mass-in-mass lattices (*Figure* 5). The model is based on those with negative mass as explained in previously. Equations of motion for the unit cell are:

$$\begin{gathered} -m_{eff}\ddot{u}_1 = F_0 e m_1^{(j)}\ddot{u}_1^{(j)} + k_2\left(u_1^{(j)} - u_2^{(j)}\right) + k_1\left(2u_1^{(j)} - u_1^{(j-1)} - u_1^{(j+1)}\right) = 0 \\ m_2^{(j)}\ddot{u}_2^{(j)} + k_2\left(u_2^{(j)} - u_1^{(j)}\right) = 0 \end{gathered} \tag{15}$$

where k_1 is the rigidity of connection.

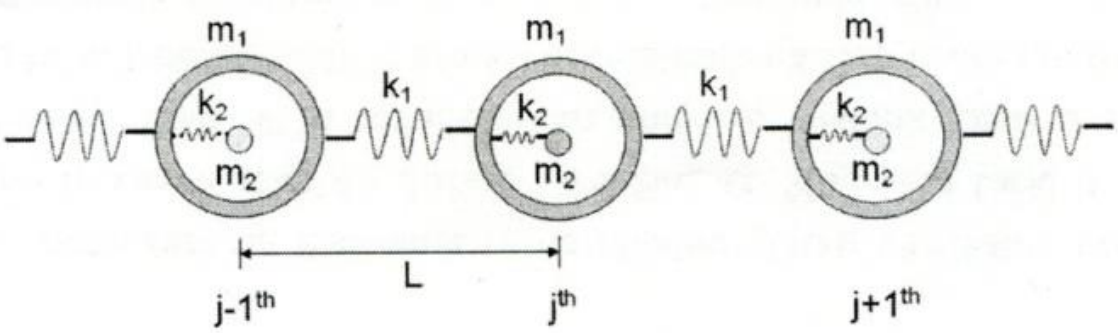

Figure 5 Model of subunits connected in lattice [7]

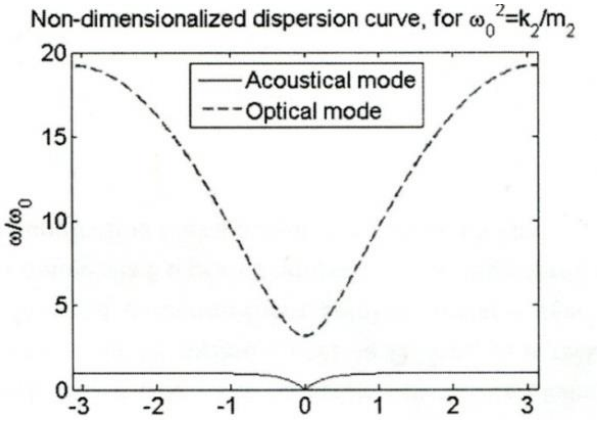

Figure 6 Nondimensional dispersion curve

The harmonic wave solution for (15) is assumed in the form:

$$\begin{aligned} &u_1^{(j)} = U_1 \exp(i\beta x - i\omega t), \quad u_2^{(j)} = U_2 \exp(i\beta x - i\omega t), \\ &u_2^{(j)} = U_2 \exp(i\beta x - i\omega t), \quad u_2^{(j)} = U_2 \exp(i\beta x - i\omega t), \\ &u_1^{(j+1)} = U_1 \exp(i\beta x - i\omega t)\exp(i\beta L), \quad u_1^{(j-1)} = U_1 \exp(i\beta x - i\omega t)\exp(-i\beta L) \end{aligned} \tag{16}$$

Substituting (16) into (15) two homogenous equations for U_1 and U_2 follow which give the dispersion equation:

$$m_1 m_2 \omega^4 - [(m_1 + m_2)k_2 + 2m_2 k_1(1 - \cos(\beta L))]\omega^2 + 2k_1 k_2(1 - \cos(\beta L)) = 0 \tag{17}$$

In *Figure 6*, both branches of the band structure (17) which correspond to the optical mode, when $\omega > \omega_0$, and to the acoustic mode, when $\omega < \omega_0$, are plotted. The parameter values are m_2/m_1=9, k_2/k_1=0.1 and $\omega_0 = \sqrt{k_2/m_2}$=149.07s^{-1}. The frequency distribution is given as a function of the wave number βL.

The displacements in (16) are functions of $\exp(i\beta x)$. For the case when the wave number has a complex form:

$$\beta L = \gamma + i\alpha \tag{18}$$

it is

$$u \propto \exp\left(\frac{i\gamma x}{L}\right)\exp\left(-\frac{\alpha x}{L}\right). \tag{19}$$

The amplitude of the displacement decays as the exponential function $\exp(-\frac{\alpha x}{L})$ if the attenuation factor γ is positive. It is of interest to analyze the case when wave frequency approaches the local resonance frequency ω_0 and the attenuation factor γ theoretically becomes unbounded.

If the lattice system is reduced to a homogenous mono-atom lattice system in which only effective masses m_{eff} are connected by springs with rigidity k_1, the homogenous lattice system has the dispersion equation:

$$\omega^2 = \frac{2k_1}{m_{eff}}(1 - \cos(\beta L)) \tag{20}$$

The suggested model is equivalent to the original mass-in-mass system if their dispersion equations (17) and (20) are identical. Substituting (20) into (17) the effective mass (9) is obtained.
Analyzing relations (9) and (20) in the resonant regime it is obvious that the effective mass is negative only if (1-cos(βL)) is negative and when k_1 and ω^2 are positive. It means that the dimensionless wavenumber βL has to be complex. Thus, frequencies corresponding to the negative mass are in the stopping band. In other words, a negative effective mass in the equivalent mass-spring lattice system yields spatial attenuation in wave amplitude. For a material with a negative mass density the speed of sound is imaginary, and therefore only evanescent waves, which decay exponentially from the surface, can exist.

CONCLUSIONS

Based on the developed theory it can be concluded that beams with acoustic metamaterial are very efficient in absorption of acoustic waves of certain frequencies. Unfortunately, manufacturing acoustic metamaterials with tiny mass-in-mass subunits in order to have stop-bands, require expensive manufacturing techniques which include micro and nano-manufacturing technologies.
Future investigation would be directed toward widening the frequency band for which the acoustic wave can be stopped and also treating the subunits as nonlinear systems [7-9].

ACKNOWLEDGEMENT

The investigation is the part of the COST Action CA15125: Design for Noise Reducing Materials and Structures (DENORMS) and financially supported by the project of the Faculty of Technical Sciences in Novi Sad, Serbia.

REFERENCES

[1] Calius, E.P., Bremaud, X., Smith, B., Hall, A.: *Negative Mass Sound Shielding Structures: Early Results.* Physica Status Solidi B 246 (9), 2089-2097., 2009.
[2] Sun, H., Du, X., Pai, P.F.: *Theory of Metamaterial Beams for Broadband Vibration Absorption*. Journal of Intelligent Material Systems and Structures, 21, 1085-1101., 2010.
[3] Pai, P.F, Peng, H., Jiang, S.: *Acoustic Metamaterial Beams Based on Multi-Frequency Vibration Absorbers*. International Journal of Mechanical Sciences, 79, 195-205., 2014.
[4] Milton, G.W., Willis, J.R.: *On Modifications of Newton's Second Law and Linear Continuum Elastodynamics.* Proceedings of the Royal Society A, 463, 855-880., 2007.
[5] Milton, G.W.: *New Metamaterials with Macroscopic Behavior Outside that of Continuum Elastodynamcs*. New Journal of Physics, 9, 1-13., 2007.
[6] Huang, H.H., Sun, C.T., Huang, G.I.: *On the Negative Effective Mass Density in Acoustic Metamaterials.* International Journal of Engineering Science, 47, 610-617., 2009.
[7] Mester, Gy.: *Distance Learning in Robotics*. Proc. Third Int. Conf. on Informatics, Educational Technology and New Media in Education, 239-245, ISBN 86-83097-51-X, Sombor, Serbia and Montenegro, 01-02.04.2006.
[8] Mester, Gy.: *Improving the Mobile Robot Control in Unknown Environments*. Proc. Conf. YUINFO' 2007, 1-5., ISBN 978-86-85525-02-5, Kopaonik, Serbia, 11-14.03.2007.
[9] Cveticanin, L., Kalami-Yazdi, M., Askari, H.: *Analytical Approximations to the Solutions for a Generalized Oscillator with Strong Nonlinear Terms*. Journal of Engineering Mathematics, 77(1), 211-223., 2012.

INTERNATIONAL SCIENTIFIC CONFERENCE ON ADVANCES IN MECHANICAL ENGINEERING
13-15 October 2016, Debrecen, Hungary

VIBRATION TESTING IN THE EVALUATION OF PACKAGING PERFORMANCE

CSAVAJDA Péter

Széchenyi István University, Department of Logistics and Forwarding
E-mail: csavajda.peter@sze.hu

Abstract
Markets and consumers are located widely separated areas from manufacturers. That is why products became subject to transportation, handling and warehousing during the physical distribution. Each element includes hazard to the products such as vibration, shock or static and dynamic load. Packaging helps products arrive in good condition to the consumers. Use of packaging pre-shipment testing is performed to check and control the ability of packaging exposed to real physical stresses in the distribution environment. Furthermore, this can be considered as the most complicated. Vibration always occurs during shipping by any mode of transport. It can cause varied damages of product i.e. abrasion, bruising or fatigue. The simulation of vibration is not obvious due the various external and internal sources of vehicle vibrations. This paper summarizes the key principles of vibration testing in the evaluation of packaging performance.

Keywords: *vibration, packaging, testing*

1. INTRODUCTION

Three logistic activities create the physical distribution. Transportation moves products from point to point using different modes and equipment. Warehousing helps ensure availability to satisfy demand. Handling connects the parts of the logistics system, which include the following elements: manufacture to warehouse, warehouse to shipping equipment, shipping equipment to retailer. Each activity includes hazards to the products and packages. Shocks, static and dynamic loads are also able to damage the goods, but vibration is the only one, which always occurs during the distribution.
Vibration is a periodic input, with a generally low level of intensity. This continuous input is generated by the transport vehicles. The inputs can be categorized into external and internal sources. Road pavements, rail tracks and ocean waves are external sources. Examples of internal sources are rotating parts such as unbalanced wheels and the engine.
One of the most important aims of packaging engineers is to design packages that reduce vibrations. Usually cushions are used to eliminate this effect.
Vibration testing is usually the last step of the design process. It determines the potential for packaged product to survive the hazards of the transport environment. The basics of vibration and the different testing methodologies are presented in the following sections [1].

2. FUNDAMENTALS OF VIBRATION

Generally, a simple spring-mass system is applied to represent the vibrating system. *Figure 1* shows the fundamental analysis of the motion of a single degree of freedom (SDOF) spring-mass system. The Figure shows a simple harmonic motion, which are represented by a stretched spring.

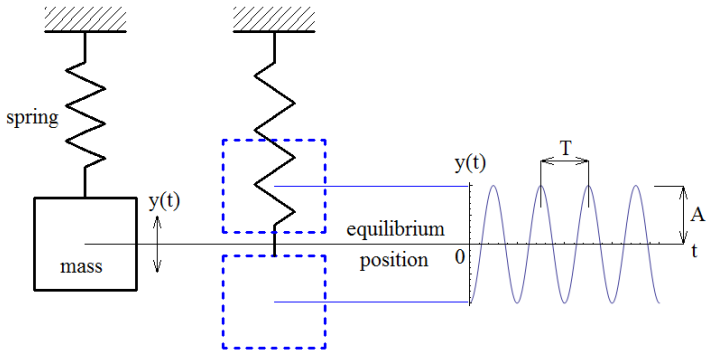

Figure 1 Motion of a SDOF spring-mass system [2]

The mass begins to rotate at the equilibrium position, and first reaches the positive peak amplitude (A) and later reaches the negative peak amplitude. The period of vibration (T) is the required time to take a complete one vibration cycle and return to the initial position. Another important parameter of vibration is Hertz (Hz). It is the unit for frequency, with one cycle/sec equal to one Hertz. The natural frequency ($f_{n)}$ is the frequency at which a given spring-mass system vibrates, when set into free motion. Natural frequency is the reciprocal of the natural period, T, which is the time required for the vibrating system to complete one cycle.
Figure 2 shows a simple vibration system in field of packaging. It contains the line (road, rail etc.), the platform and the products. The basics of the motions are similar to the above expounded spring-mass system. The differences are from the damping and the complexity of the line-platform-product system.

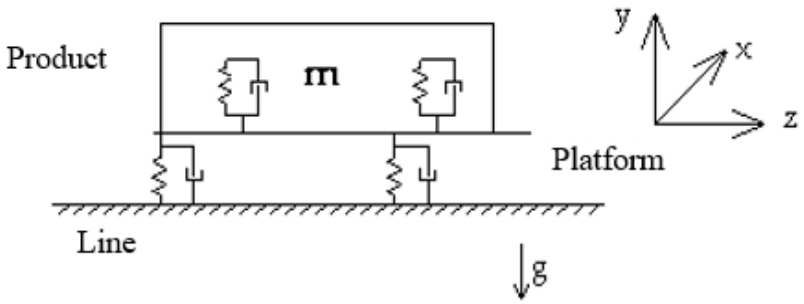

Figure 2 Vibration of the line-platform-product system [3]

Forced (when there is a continuous input source) and free (input source discontinued) are the two main categories of vibration. The type of vibration usually is forced vibration in field pf packaging, because a source continuously drives the system to vibrate. The system will continually decrease its vibration level (free vibration now) after the stop of the source of vibration, until a full stop, when the energy is totally dissipated. An obstacle such as a pothole, also cause forced vibration. The vibration that occurs without external excitation is called free vibration. Whenever a system is vibrating freely, the movement will decrease and the vibration will eventually cease, because of damping. Damping is always present in mechanical systems, and it dissipates the energy that keeps the system vibrating. Both types, free and forced, occur in all vehicles during transport.
During the logistic processes, the packaged products usually ride in a truck trailer, container or in other transport vehicles. It means, they sustain forced vibration. The external forces here are the moving and the contents (suspension systems, wheels etc.) of the vehicle. The package system

vibrates at the forcing frequency of the external input, instead of their own natural frequency. The response of the package system will depend on the ratio of that forcing frequency to the natural frequency of the product/package. This is defined as the transmissibility of the system. It is also influenced by the damping ratio [1], [4].

3. VIBRATION IN PACKAGING TESTING

Vibration tests are performed to check the suitability of a packaging. During these tests, different levels of stresses are simulated, which are corresponding to the expected stresses of the real transport environment. Different experimental methodologies have been employed over the years, but ASTM D 999 contains the most common test methods for vibration testing in field of packaging.

The two main performed tests are the sinusoidal and the random. Sinusoidal tests (repetitive shock, resonance search and dwell) are used to identify resonant frequencies of a product, a packaging material, or a complete package. This is not the most suitable method to evaluate the packaging, because the transport environment rarely generates pure sinusoidal motion. Simulating the real transport environments (random vibration) requires field measurements. Usually special data logger is used to determine the vibration inputs during the shipping. Based on the collected data, the real stresses can be reproducing in the laboratory. The analysis of these information shows that, the random vibration has two main differences from the sinusoidal vibration. The waveform is complex and the instantaneous value of the vibration amplitude is unpredictable. This complex waveform is created by the mixed effects to the vibration of all the component of the transport vehicles. If a truck trailer is traveling along the highway, various components of the vehicle are vibrating, in sinusoidal modes, at their respective natural frequencies. The suspension system will generate a frequency between 1-10 Hz, depending on the trailer being fully loaded or empty. Tire frequencies generally fall within the 15-20 Hz range, based on low to high tire pressure. Chasis and structural components of the vehicle range from 50-100 Hz. Other inputs can be measured, including engine revolutions and wheel imbalances. The latter inputs will vary with engine and vehicle speed. All inputs to the trailer cargo occur simultaneously and create the complex waveform. *Figure 3* shows a random signal, such as one might record in an over-the road truck. It can be observed that the amplitude of the signal varies over time. The statistical properties of these acceleration-time records are related to their probability distribution. The probability distribution most commonly examined in random vibration analysis is the Gaussian or normal distribution [4].

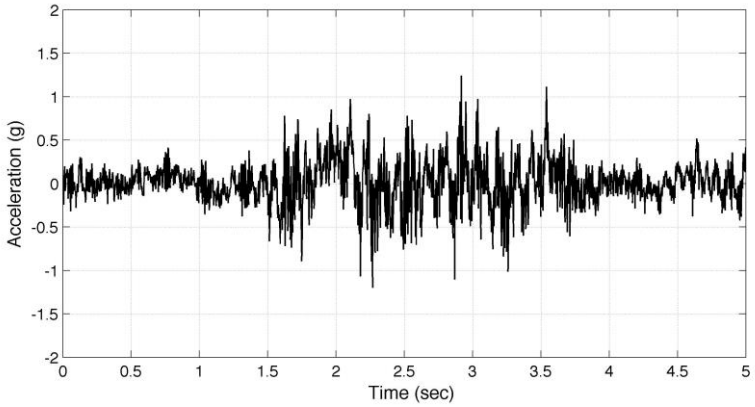

Figure 3 Acceleration versus time in random vibration

The complex waves have to break down to determine power spectral density. This can be performed with the application of Fast Fourier Transform (FFT). This algorithm is able to break down the continuous random signal into its sinusoidal components and transforms the signal from the time domain to the frequency domain, by simultaneously filtering narrow bands of frequencies. The overall intensity of the complex signal can be determined for each discrete frequency in the spectrum.
Decomposition process can be accomplished by sampling to analyse random signal at even intervals and examining the distribution of the amplitude values. Given that the amplitudes are usually recorded as acceleration levels, units of 'g' will normally be the basis for mathematical evaluation. The standard deviation for this distribution is defined as the root mean square average acceleration (RMS value), which is determined to be the square root of the variance, for a Gaussian distribution. The standard deviation of the distribution of g-values, G, for a sample size, n, will be as follows [4].

$$s = \sqrt{\frac{\sum_{i=1}^{n}(G - mean\ acceleration)^2}{n-1}} \tag{1}$$

where
s = standard deviation
G= acceleration level (g's)
n= sample size.

Given the large sample sizes recorded and a mean value of zero, the standard deviation then becomes Equation 2.

$$s = \sqrt{\frac{1}{n}\sum_{i=1}^{n} {G_i}^2} = G_{rms} \tag{2}$$

The result of the equation is the G_{rms} (RMS average of the acceleration values). It is the statistical measure of the amplitude of random signal at a specific frequency band, and can be thought of as the effective energy of the vibration. As this information is captured over the entire spectrum (usually 1-200 Hz) of the measured transportation environment, additional mathematical operations can be performed to represent the amplitude in a different format. The PSD plot is a representation of changing amplitude power normalized to the frequency bandwidth of 1 Hz, over the frequency spectrum. Electronic analysers calculate the PSD from samples of the measured amplitudes captured at a given frequency, using Equation 3 [4].

$$PD = \frac{\sum_{i}^{n} \frac{{(G_{rms})_i}^2}{N}}{BW} \tag{3}$$

where
PD= power density, G^2/Hz
G_{rms} = root mean square average acceleration (g) within the bandwidth BW
N= number of samples
BW = bandwidth for which the RMS was evaluated, Hz.

Figure 4 shows a typical PSD plot. It is ISTA (International Safe Transport Association) Steel Spring Truck Random Vibration Spectrum with an overall G_{rms} level of 0.54.

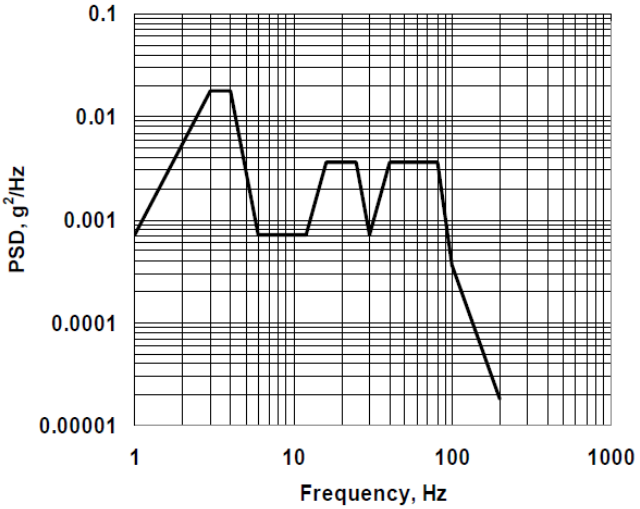

Figure 4 ISTA Steel Spring Truck Random Vibration Spectrum [5]

Research into measured transportation environments has developed a vast data base for analysis. Since the power density (PD) values are an approximation for the severity of the various transport modes, the packaging professional can try to choose those modes which will expose their product to the least hazardous transport inputs. The data base has also provided an extensive set of profiles for laboratory-based transport simulations. As stated earlier, the distributions measured in the transportation environment are usually treated as normal or Gaussian distributions. Based on filed-measured data, individual PD levels can be recommended. For example, *Figure 5* shows PSD spectra for vertical rail vibration tests in different regions.

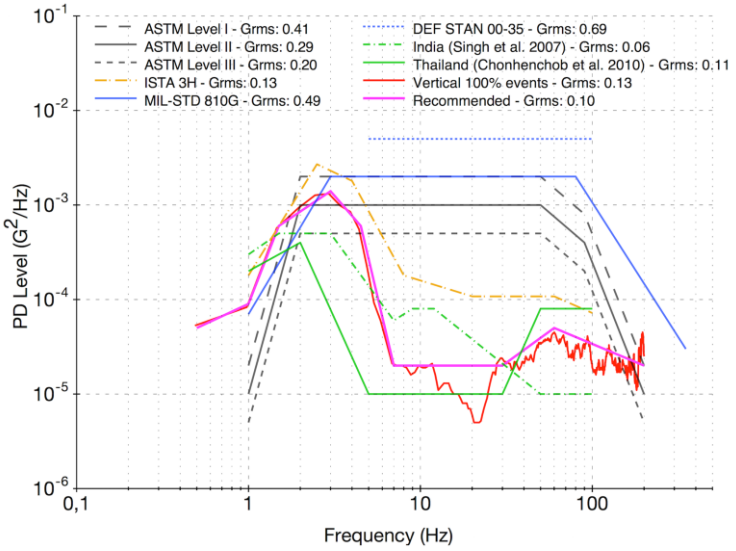

Figure 5 Recommended PSD spectrums for vertical rail vibration tests [6]

The graph contains the recommendation of the test standards and the most significant result of other researchers. With developing random vibration profiles, the evaluation process of packaging can be

performed with good correlation to the real stresses. This way the over-packaging is avoidable and the product damage (in connection with packaging) is minimized. *Figure 6* shows the two main categories of vibration equipment.

Figure 6 Hydraulic and electrodynamic vibration system with packaging testing purposes [7]

CONCLUSIONS

Products have to be moved during the logistic processes. Transportation generates different hazards to the products, one of these is vibration. Packaging engineers have to be developing packaging systems, which decrease the effect of this hazard. Therefore, define the parameters and effects of vibration are necessary. Based on these, suitable test programs can be developed and the evaluation of packaging system can be performed. Organizations, such as ISTA, ASTM, ISO issue standards with test programs, but the own-developed vibration test profiles from field-measured data could be much more adequate. Accelerated testing is one of the most important part of these profiles.

REFERENCES

[1] Kit, L.Y.: *The Wiley Encyclopedia of Packaging Technology, 3rd Edition*. John Wiley & Sons, ISBN: 978-0-470-08704-6, 2009.
[2] Goga, V.: *Mechanical vibration*. http://www.posterus.sk/?p=14142, [accessed: 26. 09. 2016.].
[3] Böröcz P, Vastag Gy: *Good Vibrations: Lessons from Packaging for the Global Supply Chain*, POMS 26th Annual Conference, Washington, USA, Production and Operations Management Society, pp. 1318, 2015
[4] Goodwin, D., Young, D.: *Protective Packaging for Distribution*. DEStech Publications, ISBN: 978-1-60595-001-3, 2011.
[5] *Procedure ISTA 3E: Unitized Loads of Same Product***.** International Safe Transit Association, East Lansing, MI, USA
[6] Böröcz, P., Singh, S. P.: *Measurement and Analysis of Vibration Levels in Rail Transport in Central Europe*. Packaging Technology and Science, in Press, 2016., DOI: 10.1002/pts.2225
[7] Böröcz P, Singh SP, Singh J.: *Evaluation of Distribution Environment in LTL Shipment between Central Europe and South Africa.* Journal of Applied Packaging research, 7 (2), Paper 3, 2015., DOI: 10.14448/japr.04.0003

INTERNATIONAL SCIENTIFIC CONFERENCE ON ADVANCES IN MECHANICAL ENGINEERING

13-15 October 2016, Debrecen, Hungary

EFFECT OF FIBRE LASER WELDING ON MICROSTUCTURE AND MICROHARDNESS OF DP600-DP980 STEEL JOINTS

[1]CSICSÓ Tomáš, [1]ŠVEC Pavol CSc, [2]DŘÍMAL Daniel PhD

[1]Institute of Technologies and Materials, Faculty of Mechanical Engineering, Slovak University of Technology in Bratislava, Pionierska 15, 831 02 Bratislava, Slovakia
E-mail: tomas.csicso@stuba.sk, pavol.svec@stuba.sk
[2]First welding company, Inc., Kopčianska 14, 851 01 Bratislava, Slovakia
E-mail: drimal.daniel@pzvar.sk

Abstract
Fibre laser was used for welding of tailor welded blanks composed of thin steel sheets. The effects of laser welding parameters on microstructure and microhardness of welded joints were evaluated. Welding process was realized by YLS 5000 type fibre laser at various beam powers and welding speeds. The microstructures and microhardness were studied in the fusion and heat affected zones of butt joints.

Keywords: *Laser welding, DP600 steel, DP980 steel, microhardness, microstructure*

1. INTRODUCTION

The production and development of new materials such as dual phase steels play an essential role in the transportation industries for the 21st century. The characterization of laser welding process of DP steels as new automotive material represents one of the most forward looking aims for many researchers in the last 20 years. The term dual phase steels, or DP steels, refers to a class of high strength steels which is composed of two phases, usually a ferrite matrix and a dispersed second phase of martensite, retained austenite and/or bainite. DP steels were developed in the 1970's. The development was driven by the need for new high strength steels without reducing the formability or increasing costs. In particular, the automotive industry has demanded steel grades with high tensile elongation to ensure formability, high tensile strength to establish fatigue and crash resistance, low alloy content to ensure weldability without influencing production costs. For years later, the demand for DP steels is still strong. Materials that can combine high strength and good formability and thus reduce the weight of vehicles and other products give an environmental and economic advantage. Comparing DP steels with other high strength low alloy steels, DP steels show superior properties [1-5].
Thanks to the combination of high strength, good formability and low cost as well as high deformation hardening, which implies a high energy absorbing ability or crashworthiness, DP steels are mainly used by the automotive industry primarily for safety parts in car bodies, e. g. bumpers, B-pillars, side impact beams, etc., see *Figure 1* [6-8].

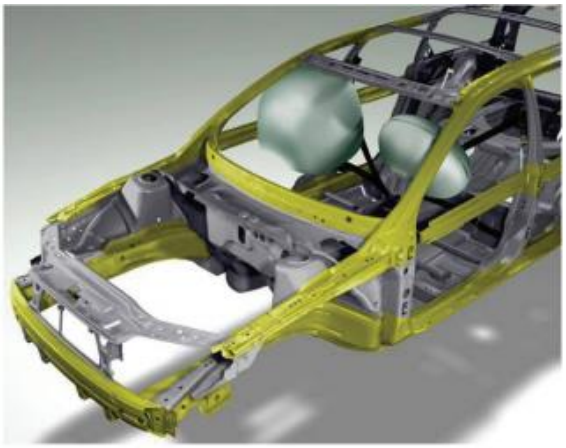

Figure 1 Example of using of DP steels as safety parts in car bodies

Laser welding is the most used joining operation when applying DP steels in car bodies, which can be made of tailor welded blanks. Tailor welded blanks made of DP steel and welded using fibre laser process enable good ratio of strength deformation properties. They enable reducing of forming operations and enhanced use of material that leads to lower production costs [9-11].

2. EXPERIMENTAL DESIGN

The characterization of fibre laser welding of DP600-DP980 steel sheets was studied with concentration on microstructure and microhardness of butt joints

2.1. Materials selection

Two commercially available types of DP steels, DP600 and DP980, were used in this work. These steels are ideal for meeting auto industry requirements for weight reduction and safety. DP steels were received in a hot-rolled, galvanized condition and with a thickness of 1.2 mm. The chemical composition of the investigated steels is listed in Table 1. Mechanical properties of DP steels are compared in *Table 2*.

Table 1 Chemical compositions (wt. %) of DP steels

Element	**C**	**Si**	**Mn**	**P**	**S**	**V**	**Al**	**B**	**Cr+Mo**	**Ti+Nb**
DP600	0.17	0.8	2.2	0.08	0.02	0.2	2.0	0.01	1.0	0.15
DP980	0.23	0.8	2.5	0.08	0.015	0.2	0.2	0.005	1.0	0.15

Table 2 Mechanical properties of DP steels

Steel	**Ultimate strength, MPa**	**Elongation, %**
DP600	600	20
DP980	980	10

2.2. Description of the fibre laser welding process

DP600-DP980 steel sheet joints were produced with YLS 5000 type fibre laser with a maximal beam power of 5kW, a wavelength of 1.06 μm and diameter of fibre of 0.1 mm. The spot diameter was focused into 0.3 mm with lens of 250 mm focal length. The laser welding process was realized without shielding gas. Welding speed was varied from 5mm/s to 100 mm/s. Applied beam power was changed from 550 W to 4300 W. Parameters of fibre laser welding process are shown in a Table 3.

Table 3 Parameters of fibre laser welding

	Joint 1	Joint 2	Joint 3	Joint 4	Joint 5	Joint 6
Beam power, [W]	550	900	1500	2200	2760	4300
Welding speed, [mm/s]	5	10	30	50	70	100
Focusation, [mm]	+7	+7	+10	+10	+10	+10
Heat input, [J/mm]	110	90	50	44	39.5	43

2.3. Microstructure of joints

Metallographic samples of weld cross sections were prepared following standard procedures of mounting, grinding and polishing. The microstructures of DP600-DP980 steel joints were investigated using JEOL JSM-IT300 scanning electron microscope. It is found that the DP600 steel typically has a microstructure of mainly soft ferrite, with islands of hard martensite with volume fraction of 25 % dispersed throughout (*Figure 2*). The DP980 steel has the same microstructure, but with a martensitic volume fraction of 50 %, see *Figure 2.* The ferrite grain size in DP600 is more or less between 7-10 μm and in DP980 between 2-5 μm.

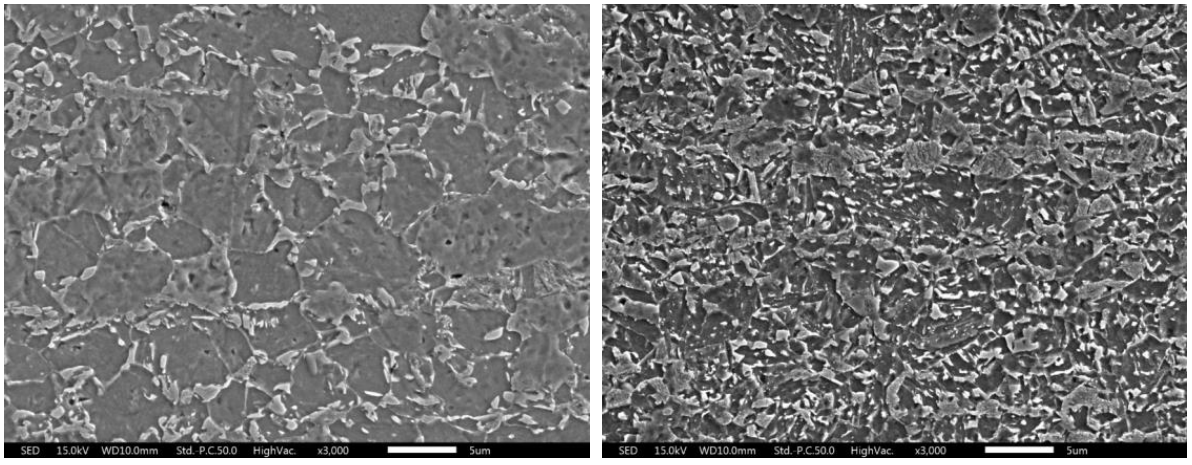

Figure 2 Microstructure of DP600 (left) and of DP980 (right) steel BMs

Welding speed and applied beam power influenced the microstructure of fusion zone (FZ) and heat affected zones (HAZ) of fibre welded joints. The Microstructures of FZ, HAZ of DP600 steel, and HAZ of DP980 steel consist of the same structural components, acicular ferrite, upper bainite, lower bainite and martensite, but with different volume fractions. The heat input (ration of applied beam power and welding speed) influenced the geometry of each zones of welded joints. When the welding speed was the lowest, the FZ and both HAZs were the brightest and respectively in reverse.

The microstructure in fusion zone is documented in *Figure 3*. It consists mainly of acicular ferrite, but upper bainite, lower bainite and martensite was observed too. As is possible to see, the microstructure was composed of small laths of low aspect ratio which occur in several distinct orientations which give the appearance of an interlocking microstructure.

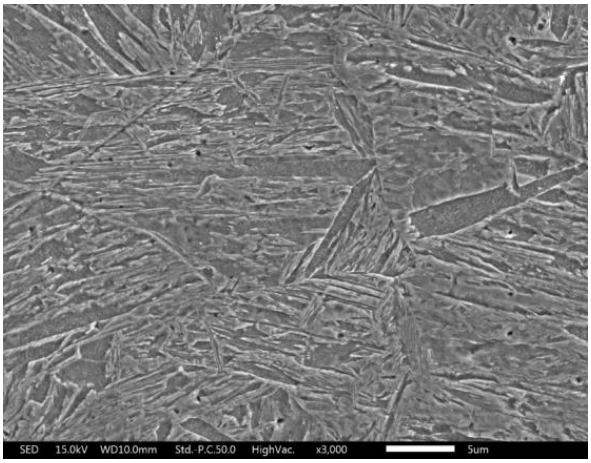

Figure 3 Microstructure of FZ of joint

The microstructure of both HAZs changed with the distance from the weld centre as can be seen in *Figure 4 and 5*. The coarse grained microstructure was observed in the vicinity of the FZ and fine grained microstructure in vicinity of both BMs, because of the decrease of temperature peaks during the laser welding process. The microstructures in both HAZs consisted of larger ratio of bainite and martensite in comparison to the FZ.

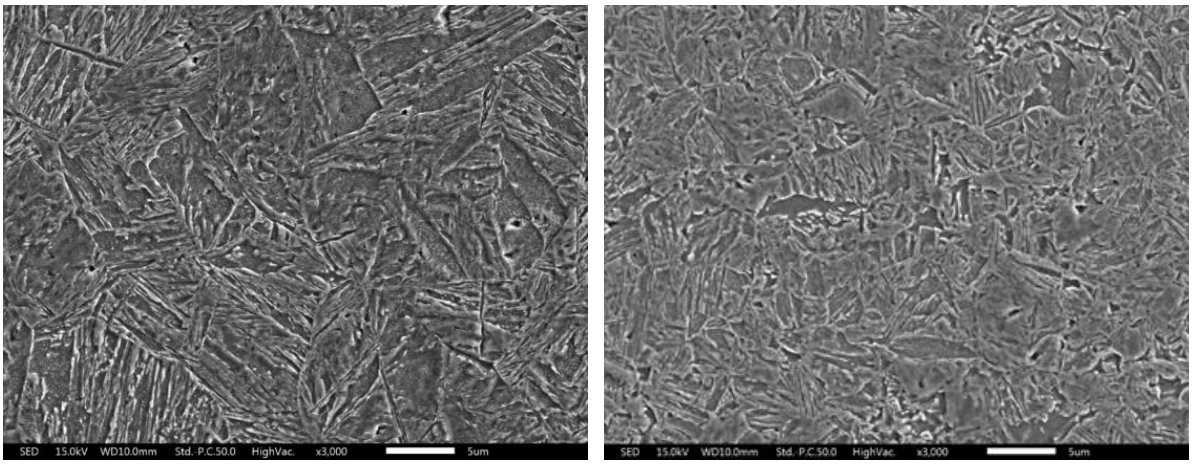

Figure 4 Microstructure of coarse grained (left) and fine grained (right) region of HAZ of DP600 steel

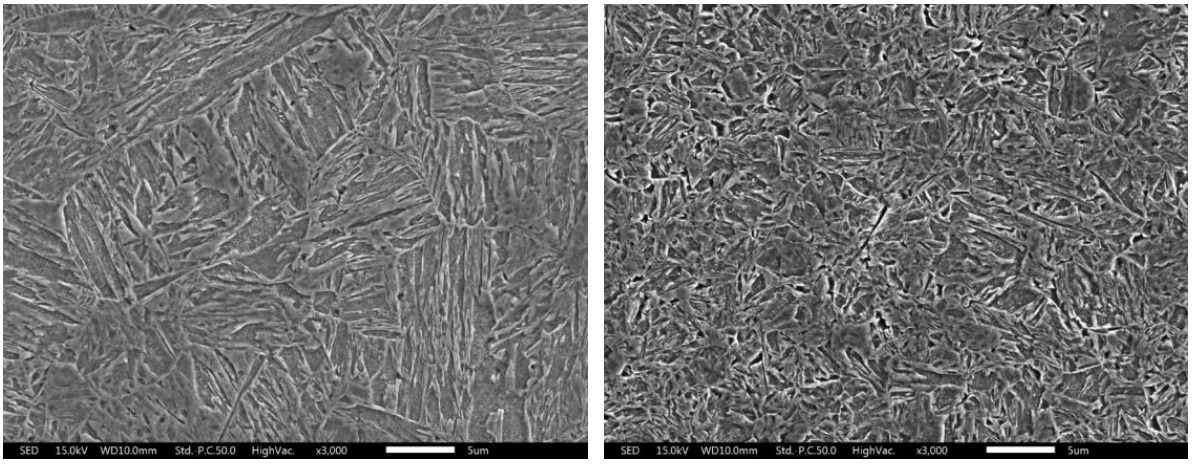

Figure 5 Microstructure of coarse grained (left) and fine grained (right) region of HAZ of DP980 steel

2.4. Microhardness profiles

Vickers microhardness profiles of fibre laser welded joints were determined using load of 100 g and dwell time of 15 s. The microhardness profile of joint welded at beam power of 2200 W and welding speed of 50 mm/s is documented in *Figure 6.* The microhardness increases in FZ and both HAZs in comparison with basic materials. This is because the high alloying content of DP steels increases the carbon equivalent and the rapid solidification process observed at laser welding process generally increases the potential for the formation of bainite and martensite. The martensite structure gives the FZ and HAZs near the FZ the maximum hardness. The decrease in the hardness of HAZs near the base metals results from relatively soft ferrite having a low hardness.

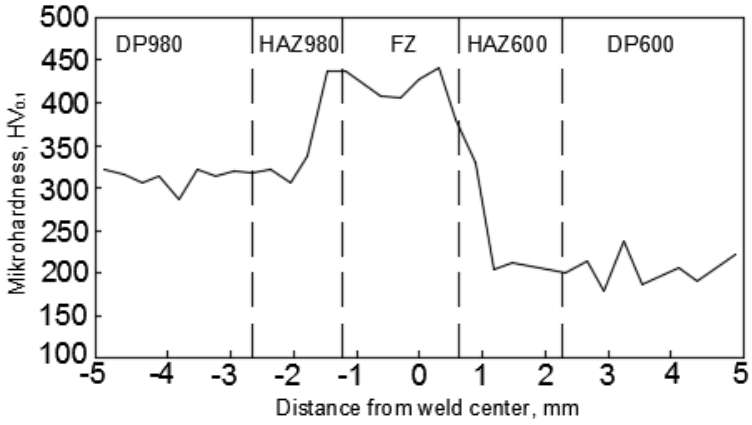

Figure 6 Microhardness profile of welded joint

The effects of welding speed on microhardness in particular joints zones are given from *Figure 7* to *Figure 9*. The measured values are compared with average hardness of DP600 steel (210 $HV_{0.1}$) and DP980 steel (320 $HV_{0.1}$). The same tendency is observed at all figures. The hardness values scatter. The lowest values are measured at the welding speed of 5 mm/s with the highest heat input (see Tab. 3) and the maximal hardness values are measured at the welding speed of 70 mm/s with the lowest heat input (see *Table 3*).

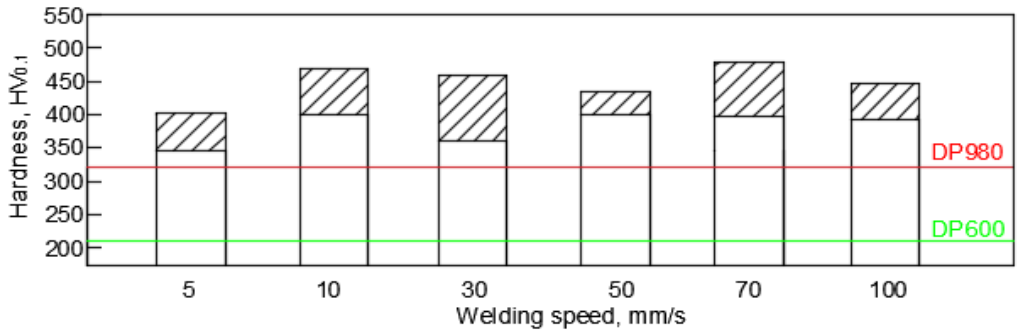

Figure 7 The effect of welding speed on microhardness in FZ of joints

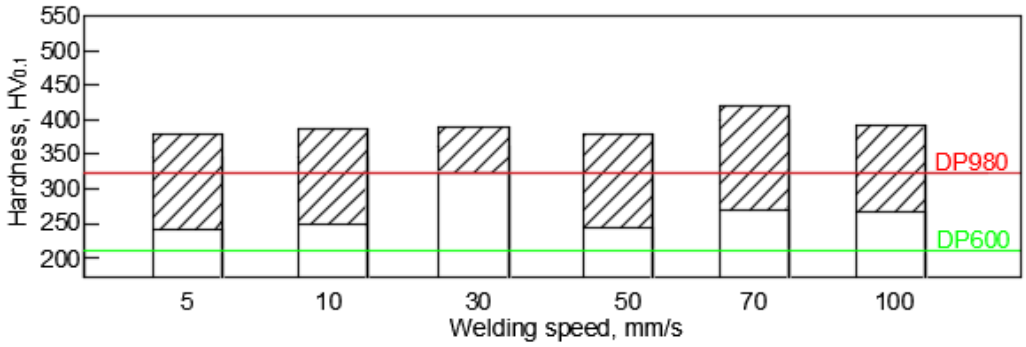

Figure 8 The effect of welding speed on microhardness in HAZ of DP600 steel

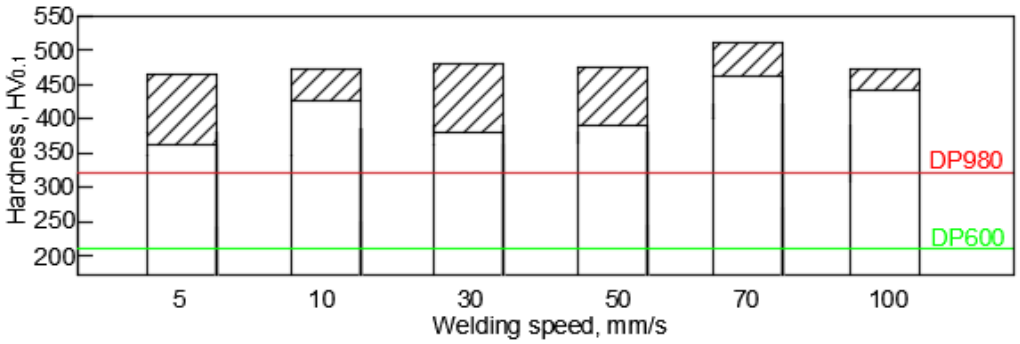

Figure 9 The effect of welding speed on microhardness in HAZ of DP980 steel

CONCLUSIONS

The microstructure and microhardness of fibre laser welded joints of DP600-DP980 steel sheets prepared with different applied beam powers and welding speeds were investigated. Microctructures in the FZ, HAZ of DP600 and HAZ of DP980 steel consisted of the same structural components, acicular ferrite, upper bainite, lower bainite and martensite, but with the different portion of these structures. The high alloying contents of DP steels stand for increased carbon equivalent and the rapid solidification process also increased the potential for the formation of bainite and martensite in the FZ and both HAZs. The microhardness increased in the FZ and both HAZs near the FZ. It decreased when approaching the BMs. The welding parameters had the effect

on microhardness values in particular zones of welded joints. The highest microhardness values were measured at the welding speed of 70 mm/s and it was in the consequences of the lowest heat input.

ACKNOWLEDGEMENTS

This work was supported by the Slovak Research and Development Agency under the contract No. APVV-0281-12.

REFERENCES

[1] Jinfeng, W., Lijun, Y., Mingsheng, S., Tong, L., Huan, L.: *Effect of energy input on the microstructure and properties of butt joints in DP1000 steel laser welding*, Materials & Design, Volume 90, 642-649., 2016
[2] Meško, J., Zrak, A., Mulczyk, K., Tofil S.: *Microstructure analysis of welded joints after laser welding.* Manufacturing Technology, Vol. 14, No. 3, 355-359., 2014
[3] Qian, S., Hong-Shuang, D., Jun-Chen, L., Xiao-Nan, W.: *Effect of pulse frequency on microstructure and properties of welded joints for dual phase steel by pulsed laser welding*, Materials & Design, Volume 105, 201-211., 2016
[4] Rossini, M., Russo Spena, P., Cortese, L., Matteis, P., Firrao, D.: *Investigation on dissimilar laser welding of advanced high strength steel sheets for the automotive industry*, Materials Science and Engineering: A, Volume 628, 288-296., 2015
[5] Nayak, S.S., Biro, E., Zhou, Y.: *Laser welding of advanced high-strength steels* (AHSS), Welding and Joining of Advanced High Strength Steels (AHSS), 71-92., 2015
[6] Miyayaki, Y., Hashimoto, K., Kuriyama, Y., Kobayashi, J.: *Welding methods and forming characteristics of tailored blanks.* Nippon Steel Technical Report No. 88, 65-72., 2003
[7] Wu, Q., Gong, J., Chen, G., Xu, L.: *Research on laser welding of vehicle body.* Optics and Laser Technology, Vol 40, Issue 2, 420-426., 2008
[8] Seang, C., Kouadr David, A., Ragneau, E.: *Effect of Nd:YAG laser welding parameters on the hardness of lap joint: experimental and numerical approach.* SciVerse Sciensdirect, 38-40., 2013
[9] Mingsheng, X., Biro, E., Tian, Z., Zhou, Y. N.: *Effects of heat input and martensite on HAZ softening in laser welding of dual phase steels.* ISIJ International 48 N. 6, 809-814., 2008
[10] Hartley, B., Ono, M.*: Laser weldability of dual phase steels in tailored blank applications.* SAE Technical Paper Series, -01-15., 2002
[11] Ma, C., Chen, D.L., Bhole, S.D., Boudreau, G., Lee, A., Biro, E.: *Microstructure and fracture characteristics of spot –welded DP600 steel.* Materials Science and Enginiering: A Vol 484, ISSUES 1-2, 334-346., 2008

INTERNATIONAL SCIENTIFIC CONFERENCE ON ADVANCES IN MECHANICAL ENGINEERING
13-15 October 2016, Debrecen, Hungary

APPLIED VIBRATION MEASUREMENT METHODS AND DATA EXTRACTION FOR BEARING FAULT DIAGNOSIS

[1]DEÁK Krisztián, [2]KOCSIS Imre PhD

[1]Department of Mechanical Engineering, Faculty of Engineering, University of Debrecen
E-mail: deak.krisztian@eng.unideb.hu
[2]Department of Basic Technical Studies, Faculty of Engineering, University of Debrecen
E-mail: kocsisi@eng.unideb.hu

Abstract
Roller bearings are critical and important parts of most industrial machines. It is important to reveal their problems in early stage to prevent further serious damages. Review of vibration and acoustic measurement methods for the detection of defects in rolling element bearings is presented in this paper. Detection of both localized and distributed categories of defect has been considered. An explanation for the vibration and noise generation in bearings is given. Bearing faults derive from mostly wear, plastic deformation, corrosion, brinelling, improper mounting, design and manufacturing processes, fatigue problems. Vibration measurement in both time and frequency domains along with signal processing techniques such as the high-frequency resonance technique have been covered. For diagnosis of bearings wavelet transform gained remarkable roles in the previos years.

Keywords: vibration, bearing, manufacturing, diagnosis

1. INTRODUCTION

Typically, a rolling element bearing consists of two rings with a set of elements running in the tracks between the rings. The standard shapes of a rolling element include ball, cylindrical roller, tapered roller, needle, and barrel roller, encased in a cage that provides equal spacing and prevents internal strikes. Bearings consist of some basic parts, inner ring, outer ring, cage, sealing that prevent contaminations to get to the bearing. As for types of bearings, ball bearings fall roughly into three classes: radial, thrust, and angular-contact. Angular-contact bearings are used for combined radial and thrust loads and where precise shaft location is needed. Deep-groove bearings are the most widely used ball bearings. In addition to radial loads, they can carry substantial thrust loads at high speeds, in either direction. They require careful alignment between shaft and housing. Self-aligning bearings come in two types: internal and external. In internal bearings, the outer-ring ball groove is a ground as a spherical surface. The principal types of roller bearings are cylindrical, needle, tapered, and spherical. In general, they have higher load capacities than ball bearings of the same size and are widely used in heavy-duty, moderate-speed applications.
Even a normally loaded, properly lubricated, and correctly assembled bearing fails due to material fatigue after a certain running time. This is referred as fatigue life of a bearings, it can be significantly shortened due to manufacture defects, improper handling and installation, or lack of lubrication. The result is either a localized or a distributed defect in the components of the bearings. The determining bearing faults and their causes are briefly discussed next. Bearings during operation suffer damages which significantly reduce its life time even a normally loaded, properly lubricated, and correctly assembled state. It generates fatigue problems inside the material at first under the surfaces then subsurface cracks propagate towards the surface creating well visible cracks

that are the initial local areas of spalling. Furthermore, manufacturing problems, improper handling and installation, or lack of lubrication can result in both localized or a distributed defects in the components of the bearings
Bearing defects have two main groups: manufacturing defects: material problems, cracks inside the material, grinding problems, pulling difficulties, improper handling of the bearing parts
Operational defects as wear, impact marks, smearing, spalls, fatigue craks, corrosion, electric faults.

2. VIBRATION MEASUREMENT METHODS FOR BEARINGS

Detection of previous mentioned defects at an early stage without machine disassembly is vital for condition monitoring and predictive maintenance. Various methods are used for the diagnosis and prognosis of bearing defects. The methods could be grouped as acoustic measurements, current and temperature monitoring, wear debris detection, and vibration analysis etc. Next, acoustic and vibration monitoring are described.
Acoustic Measurement
Bearings generate noise during operation common bearing health monitoring is acoustic emission. Cracks are detected by this method, basically a transient impulse generated by the rapid release of strain energy in solid material under mechanical or thermal stress. Early time initial faults can be revealed usually at high frequencies above 100 KHz. Accuracy highly depends on sound pressure and sound intensity data versus energy attenuation in material.
Vibration Measurement
Since the abnormal vibration of rotary machines is the first sensory effect of rotary component failure, vibration analysis is widely employed in the industry. The fault vibration signal generated by the interaction between a damaged area and a rolling surface occurs regardless of the defect type. Consequently, a vibration analysis can be employed for the diagnosis of all types of faults, either localized or distributed.
Furthermore, low-cost sensors, accurate results, simple setups, specific information on the damage location, and comparable rates of damage are other benefits of the vibration measurement method.
Vibration is generated by both localized and distributed faults on bearing rings and raceways. If rolling elements hit spalls, initial surface cracks, short time impulses are induced creating vibration. Vibration monitoring is wide spread method because of its simplicity and cost-effectiveness. Both velocity and acceleration sensors are attached on the machine/ bearing house to obtain signals. It is important to fix the sensors properly either with glue or magnet or screw with regards to the frequency limit requirements. For data acquisition, DAQ units are used, sometimes compact units like National Instrument CompactRio (*Figure 1*) is propagated with Labview software application (*Figure 2*) where virtual instruments (VIs) could be built. CompactRio has an own computer, FPGA unit, Ethernet connection up to 8 slots for DAQs creating a versatile, flexible measurement. Basically, raw signal is in time domain, amplitude is given every time of period. After Fourier transform, filtering typical faults are visible on the spectrogram.

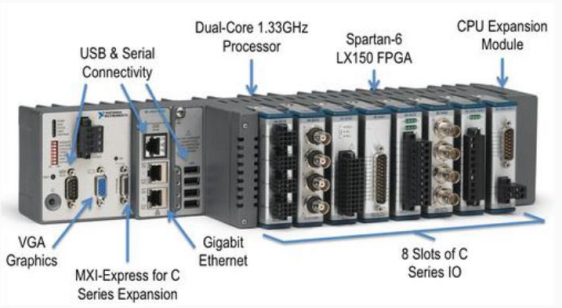

Figure 1 NI CompactRio measurement device

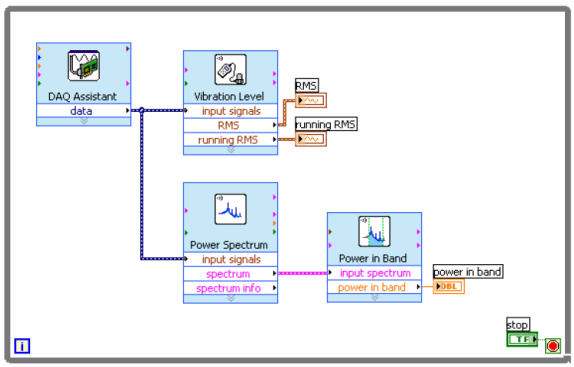

Figure 2 NI Labview Sound and Vibration VI

Time domain analysis is widely used monitoring method. Mostly Root Mean Square (RMS) [1], Kurtosis [2], skewness, peak value, Crest Factor (CF), and synchronous averaging [5] are applied in the low frequency range of <5 kHz.
The Kurtosis, the fourth normalized statistical moment, corresponds to the peak value of the data. For an undamaged bearing, the value is equal to three in frequencies. Some researchers [15] have found kurtosis value more useful, when it is compared with the RMS, crest factor, and peak value.
The Crest Factor is the ratio of the peak acceleration to the RMS value. Crest factor is a good indicator of small size defects; although, when localized damage grows, the value of the crest factor decreases significantly because of the increasing RMS.
Time domain analysis and its spectrum (*Figure 3*) have some great advantage of simple calculations and signal pre-processing, speed independency. However, insensitivity to early stage faults and deeply distributed defects are drawbacks of this approach.

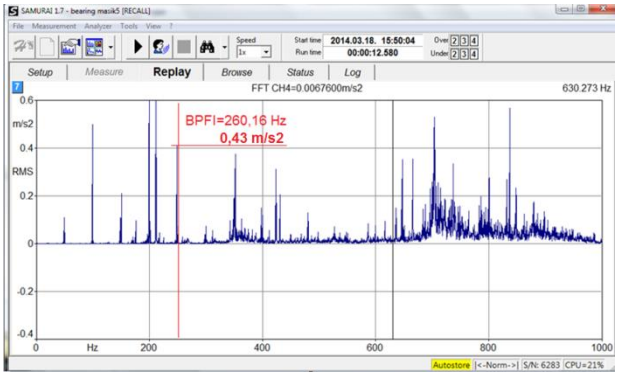

Figure 3 NI Labview Sound and Vibration VI

Frequency domain analysis, also called spectral analysis, is the most widely used signal processing method for bearing diagnosis. The characteristic frequency of the bearings is a vital parameter, which can be calculated from bearing data. Monitoring these frequencies or their harmonics at a low frequency range (< 5 kHz) has been successful in bearing diagnosis; however, some research pointed the weakness of this method for detecting small defects, spallings.
Enveloped or demodulated signals have higher efficiency because basically raw signals are noisy, SNR ratio is bad. Frequency domain analysis is referred as effective way for analyzing bearing state. Simple or more sophisticated signal processing methods such as power cepstrum [1], adaptive noise cancellation [4], and denoising, are also proposed for bearing diagnosis. The frequency domain approach is sensitive and robust to detect bearing defects and to identity the localized damage location. However, the accuracy of this method highly depends on the bearing dimensions

and rotational speed. Moreover, frequency domain methods need an intelligent selection of the frequency band in order to make proper analysis.

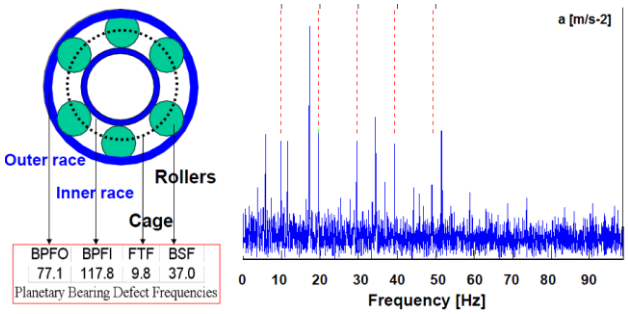

Figure 4 Frequency-domain spectrum

Time-frequency methods are very useful for obtaining the energy distribution over frequency bands. Many methods are used in digital signal processing, the most conventional method is the Fourier transform that give the frequency spectrum (*Figure 4*) more sophisticated methods are Wigner-Ville distribution, wavelet transforms, and basis pursuit [5]. Wavelet transform is a versatile, effective method for processing of noisy signals in bearing diagnosis and prognosis, wavelet decompositions, and wavelet packets [5].Wavelets have been established as more effective tools in machine fault diagnosis.

Envelope of a signal can give important information for the presence of faults. Morlet wavelets are used with success. The Short-time Fourier transform (STFT) is similar to the wavelet transform, it is also time- and frequency localized, but there are issues with the frequency/time resolution trade-off.

High Frequency Resonance Technique (HFRT) based on impulse measurement, namely all roller elements create short impacts by hitting the surface fault on the raceways, each have short durations with a low energy level that is distributed over a broad-band. These faults are spalls and cracks that reach the surface of the raceways. Signal is band pass filtering is applied to modify raw signals, amplitude demodulation technique by Hilbert transform is widely used to identify fault frequencies. Band pass filter frequency is usually 22-26 KHz.

Wavelet transforms have advantages over traditional Fourier transforms for representing functions that have discontinuities and sharp peaks, and for accurately deconstructing and reconstructing finite, non-periodic and/or non-stationary signals. Both discrete wavelet transform (DWT) and continuous wavelet transform (CWT) are continuous-time transforms. These transforms can be used to represent continuous-time (analog) signals. CWTs operate over every possible scale and translation whereas DWTs use a specific subset of scale and translation values or representation grid. *Figure 5*. shows the wavelet decomposítion tree to devide the full frequency bands to sub-bands.

Lot of wavelet types exist: Haar, Daubechies, Legendre, Symlet and som other with their own advantages and disadvantages in certain applications.

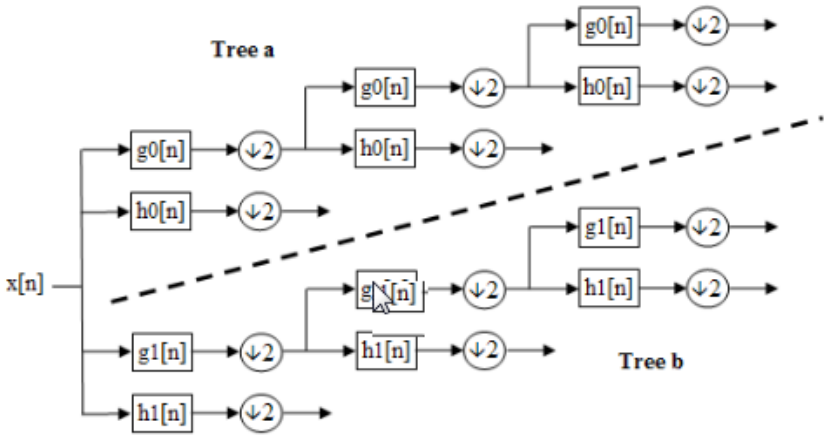

Figure 5 Wavelet decomposition tree [5]

CONCLUSIONS

In this paper tappered roller bearing faults and their diagnosis methods were overviewed. These faults can be classified as production and operational faults. Manufacturing faults are investigated from the raw material handling to the end product. Condition monitoring is vital part of machine diagnosis and prognosis. Sophisticated machines have large number of machine elements, among others bearings represent important role in mechanical engineering. Vibration diagnosis is a wide spread method to determine the machine condition because of its simplicity and reliability. For faster and complicated measurements FPGA based units are applied due to their high speed parallel operation.. Time domain analysis based on statistical parameters, kurtosis, crest factor, RMS is usually monitored. For frequency domain measurement the traditional Fourier transform is generally used. Time-frequency methods like wavelet transform, Wigner-Ville distribution, STFT mostly applied in noisy environment. Wavelet analysis is an efficient method to detect sharp edges in the vibration signal generated by tiny defects which emerge in the form of transient impulses.

REFERENCES

[1] Avraham H.: *Bearing Design in Machinery – Engineering Tribology and Lubrication*. Marcel Dekker Inc, New York, 323-329, 2003.
[2] Xiao,-S.S., Wenbin, W., Chang,-H.H., Dong, H.Z.: *Remaining useful life estimation – A Review on the statictical data driven approaches*. Europen Journal of Operational Research, 2010.
[3] Medjaher, K., Tobon-Mejia, D.A., Zerhouni, N.: *Remaining useful life estimation of ctritical components whit application to bearings*. IEEE Transactions on Reliability, 292-302, 2012.
[4] Edwin, S., Hyunseok, Arvind, S.S.V., Michael, P.: *Estimation of Remaining Useful Life of Ball Bearings using Data Driven Methodologies*. Center of Advanced Life Cycle Engineering (CALCE), 2012.
[5] Tandon, N..: *Acomparison of some vibration parameters for the condition monitoring of rolling elements bearings*. Measurement, 12, 385-289, 1994.

INTERNATIONAL SCIENTIFIC CONFERENCE ON ADVANCES IN MECHANICAL ENGINEERING

13-15 October 2016, Debrecen, Hungary

SELECTION OF WAVELET FUNCTION FOR DETECTION OF BEARING DEFECTS BY SHANNON ENTROPY

[1]DEÁK Krisztián, [2]KOCSIS Imre PhD

[1]Department of Mechanical Engineering, Faculty of Engineering, University of Debrecen
E-mail: deak.krisztian@eng.unideb.hu
[2]Department of Basic Technical Studies, Faculty of Engineering, University of Debrecen
E-mail: kocsisi@eng.unideb.hu

Abstract

Diagnosis of bearings is vital for modern maintenance strategy. Detection of both localized and distributed categories of defect is made by mostly vibration measurement methods. Bearing faults derive from mostly wear, plastic deformation, corrosion, brinelling, improper mounting, design and manufacturing processes, fatigue problems. This article focuses on the detection of manufacturing defects. Vibration measurement in both time and frequency domains along with signal processing techniques such as the high-frequency resonance technique have been covered. For diagnosis of bearings wavelet transform gained remarkable roles in the previos years. Wavelet transform is an efficient tool for analyzing the vibration signal of the bearings because it can detect the sudden changes and transient impulses in the signal caused by faults on the bearing elements. In this article manufacturing faults on the outer ring of tapered roller bearings due to the grinding process in manufacturing are investigated. Nine different real values wavelets, Symlet-2, Symlet-5, Symlet-8, db02, db06, db10, db14, Meyer and Morlet are compared according to the Energy to Shannon Entropy ratio criteria and it is determined which is efficient for detecting the manufacturing faults

Keywords: vibration, bearing, manufacturing, diagnosis, wavelet, entropy

1. INTRODUCTION

Researches of different bearings defects by vibration analysis mostly focus on operational defects caused by wear and cracks. Patel et al. used envelope methods to reveal local faults on the races of deep groove ball bearings [1]. Kalman and H filter were applied by Khanam et al. to measure bearing faults especially in noisy condition with low signal-to-noise ratio when it was difficult to identify the useful components of the vibration signal [2]. Some studies used acoustic signal instead of vibration to indentify bearing faults [3,4]. Acoustic emission measurement is a powerful method to detect cracks inside the bearing material which are the initial reasons of fatigue spallings Al-Ghamd and Mba applied this method combined with the traditional vibration analysis to determine the bearing outer race defect width directly from the raw signal [3]. Sawalhi and Randall made their researches to determine the fault size of the bearings from the vibration signal by analyzing the entry and exit impulses [5].
Because of its flexibility and computational efficiency several studies applied the wavelet analysis in bearing fault diagnosis [7-12]. Wavelets are perfect tools for fault feature extraction, singularity detection for signals, denoising and extraction of the weak signals from the vibration signals. These applications were presented by Peng and Chu [6]. Combination of envelope spectrum and wavelet transform for extraction of defect problems in bearings were used by Shi et al. [8]. Discrete wavelet

transform with Daubechies-4 (db04) mother wavelets to analyze the combination of different faults on the races of ball bearings were used by Prabhakar et al. [7].
Wavelet filter based denoising is suitable method for detection of weak signatures in bearing fault diagnosis. This experiment was presented by Qiu et al. [10]. Symlet wavelets were used efficiently in the study of Kumar et al. [12]. In their study tapered roller bearings were analyzed to determine the fault size on the outer ring.
Symlet wavelets were used in several papers [7-11] to determine the problems of bearings and machines since its shape is adequate to solve the problem. Symlet-5 wavelet represents the entry and impact events as the roller hits the defects during operation of the bearing. A detailed study was presented about the decomposition of the vibration signals using discrete wavelet transform with Symlet-5 by Kumar et al. [14]. Moreover, Symlet wavelet is a good tool for noise reduction in ECG signals because it could filter out the useful components of the complex signal from the noisy background [13].
Analytical Wavelet Transform (AWT) based acoustic emission technique for identifying inner race of radial ball bearing were applied by Kumar et al. [15].
Machine learning methods for optimization of parameteres such as support vector machines were used by Mankovits et al. [16].

2. WAVELET TRANSFORM FOR FAULT DETECTION

Wavelet transform is continuous or discrete and it is calculated by the convolution of the signal and a wavelet function. A wavelet function is a small oscillatory wave, which contains both the analysis and the window function. Continuous wavelet transform (CWT) generates the two dimensional maps of coefficients that is called scalogram.

$$CWT_f(a,b) = \frac{1}{\sqrt{a}} \int_{-\infty}^{\infty} f(t) \cdot \psi^* \left(\frac{t-b}{a} \right) dt \tag{1}$$

where a is the scale parameter, b is the translation parameter, f(t) is the signal in time domain, ψ is the 'mother' wavelet and ψ^* is the complex conjugate of ψ [19].
Discrete wavelet transform (DWT) applies filter banks for the analysis and synthesis of a signal. Filter banks contain wavelet filters and extract the frequency content of the signal in the pre-determined subbands. The discrete wavelet transform is derived from the discretization of continuous wavelet transform by adopting the dyadic scale and translation to reduce the computational time and can be expressed by the following equation [20]:

$$DWT_s(j,k) = \frac{1}{\sqrt{2^j}} \int_{-\infty}^{\infty} s(t) \cdot \psi^* \left(\frac{t-2^j k}{2^j} \right) dt \tag{2}$$

where j and k are integers, 2^j and $2^j k$ represent the scale and translation parameter respectively. The original signal $s(t)$ passes through a set of low pass and high pass filters emerging as low frequency (approximations, a_i) and high frequency (details, d_i) signals at each decomposition level n. They are usually finite impulse response filters whose impulse response (or response to any finite length input) is of finite duration, because it settles to zero in finite time. Therefore, the original signal $s(t)$ can be written as [4]:

$$s(t) = a_n + \sum_{i=1}^{n} d_i \tag{3}$$

3. WAVELET SELECTION ON SHANNON ENTROPY

Fault detection procedures based on time-frequency methods usually rely on visual observation of contour plots. It is also known that if the wavelet matches well with the shape of the signal at a specific scale and location a large transform value is obtained. However, a low transform value is obtained if the signal and wavelet do not correlate well. To avoid defects of visual observation a more precise way of determining the best suited wavelet is presented here.
The combination of the energy and Shannon entropy content of the wavelet coefficients of the signal, denoted by Energy to Shannon Entropy ratio is an appropriate indicator to choose the best wavelet for diagnosis and it can be calculated in the following form [21, 22]:

$$\xi(n) = E(n) / S_{entropy}(n) \tag{4}$$

The energy content of signal wavelet coefficients is given by:

$$E(n) = \sum_{i=1}^{m} \left| C_{n,i} \right|^2 , \tag{5}$$

where m is the number of wavelet coefficients, $C_{n,i}$ is the i th wavelet coefficient of n th scale.
The entropy of signal wavelet coefficients is given by:

$$S(n) = -\sum_{i=1}^{m} p_i \log_2 p_i \tag{6}$$

where $(p_1,...,p_n)$ is the energy probability distribution of the wavelet coefficients, defined as:

$$p_i = \left| C_{n,i} \right|^2 / E(n) \tag{7}$$

4. EXPERIMENT

In this study an experimental test rig (*Figure 1-2*) has been constructed to measure properly vibration signatures of the tapered roller bearings.
The shaft in the test rig is supported by two tapered roller bearings. The one under investigation is No. 30205 tapered roller bearing. Four tapered roller bearings with different manufacturing defect width on the outer race (OR1-4) were investigated in our experiments (*Table 1*). Defect on the outer race is a line (rectangular) shape grinding defect (*Figure 3*) The shaft is driven by an alternating current motor of 0.75 kW (made by Cemer), frequency of 50 Hz, and nominal speed of 2770 rpm which is reduced to 1800 rpm with variable speed drive device. Rubber V-belt between the electric engine and the shaft provides smooth running and low vibration which help accurate and precise measurements. Rubber bumpers are installed to reduce vibration of the electric motor to the bearing housing in order to minimize harmful vibrations. The arrangement provides option of different speeds controlled by Schneider ATV32HU22M2 variable speed drive device. In the experiment the

speed of the shaft is measured using an optical tachometer with digital display to check the speed fluctuations. Additionally, the test rig can be used for acoustic measurements as well because an anechoic chamber is installed around the test bearing house with an appropriate features to suppress outside noises and reduce echo time. Test bearing is spanned by screw mechanism to supply the sufficient axial force to the measurements. Constant spanning force during the measurements is measured by strain gauges in Wheatstone-bride mode on the basis of difference in voltage measurement.

NI 9234 dynamic signal acquisition is used in the experiments with 4-channels to vibration measurements from integrated electronic piezoelectric (IEPE) and non-IEPE sensors. The NI 9234 delivers 102 dB of dynamic range. Input channels simultaneously digitize signals at rates up to 51.2 kHz per channel with built-in anti-aliasing filters [17]. PCB IMI 603C01 vibration transducer is used which is an industrial type platinum stock piezoelectric sensor with low noise level, sensitivity of 100 mV/g and frequency range of 0.27 to 10 kHz with top exit 2-pin connector [18]. The accelerometer is placed right above the previously ground surface of the top of the bearing house with screw mechanism perpendicular to the axis of the rotation of the shaft. 32 bit AMD Athlon II X2 M300 2.0 GHz processor is used for data processing which is carried out in Matlab and Labview environment. For visual validation of the defect sizes on the bearing rings Garant MM1-200 video microscope is applied that is an incremental measuring system, built-in image processing with 1.3 megapixel colour camera. Furthermore, Mahr MMQ 200 with precision roundness measuring axis, motorized vertical and horizontal measuring axis is used for roundness deviation measurement to determine both width and depth of the grinding marks.

In the experiments the energy contect of the transient impulse and the signal-to-noise ratio are sufficiently large but additional effects of the structural and environmental vibrations could emerge despite of the vibration isolation system of the test rig.

Figure 1 Test rig for tapered roller bearing measurement

Figure 2 Test rig for tapered roller acoustic chamber

Table 1 Geometrical parameters of grinding defects of outer rings (OR)

Type	Width(mm)	Depth (μm)
OR1 defect	0.6311	6.5
OR2 defect	1.2492	33.6
OR3 defect	1.4751	42.3
OR4 defect	1.6236	51.4

Figure 3 Outer ring of the tapered roller bearing with grinding defect of 1.6236 mm

5. RESULTS

Figure 5 presents the spectra of outer race defect of 0.6311 mm. The highest periodic transient impulse related energy content of the burst occurs at 2.09 kHz that causes 5 ms rate of periodicity which is equal to 206.18 Hz BPFO frequency (*Figure 6*). The spectrum was measured in all outer rings with different fault sizes and they showed similar manner around the peak of 2.09 kHz.

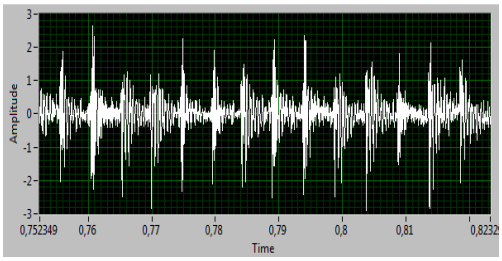

Figure 4 Typical raw time domain signal of bearing having 0.6311 mm of ground fault width on the outer race

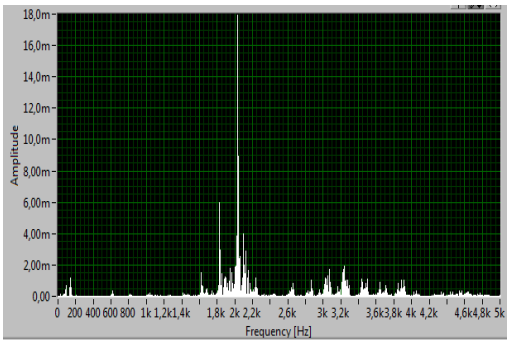

Figure 5 Frequency domain spectrum of bearing having 0.6311 mm of ground fault width on the outer race, transient frequency of 2.09 kHz

Total nine different wavelets are considered for the present study. An appropriate base wavelet should extract the maximum amount of energy, with minimizing the Shannon entropy of the corresponding wavelet coefficients. Calculated values of the Energy to Shannon Entropy ratios are in *Table 2-4*.
E/S values are calculated from the vibration signal at the wavelet center of 2.08 kHz. (*Table 2*).

Table 2 Calculated values of Energy to Shannon Entropy ratios of wavelet functions, F_c=2.08 kHz

E/S	OR1	OR2	OR3	OR4	Mean
Sym2	59.86	82.69	103.26	112.52	89.58
Sym5	69.58	98.31	114.01	112.34	98.56
Sym8	79.43	117.24	120.56	113.51	107.69
db02	59.86	82.69	103.26	112.54	89.59
db06	72.64	95.03	116.37	121.17	101.30
db10	77.69	101.8	121.01	123.05	105.89
db14	85.81	118.47	123.14	124.31	112.93
Meyer	97.56	160.37	127.08	103.33	122.09
Morlet	114.01	194.25	144.72	142.14	148.78

Values, after calculating the mean values of E/S ratio, are presented in *Figure 4*. It is observed that Morlet wavelet gives the highest value that indicates to be the most efficient wavelet for both fault detection and possibly fault size estimation.

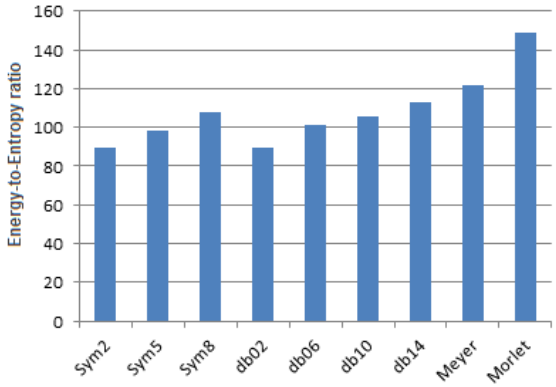

Figure 5 Energy to Shannon Entropy ratio values of wavelet functions, F_c=2.08 kHz

CONCLUSIONS

Condition monitoring is vital part of machine diagnosis and prognosis. Sophisticated machines have large number of machine elements, among others bearings represent important role in mechanical engineering. Vibration diagnosis is a wide spread method to determine the machine condition because of its simplicity and reliability.
A technique based on wavelet transform using nine different real-valued wavelets has been proposed for measuring outer race manufacturing defect width of tapered roller bearings. Wavelet analysis is an efficient method to detect sharp edges in the vibration signal generated by tiny defects which emerge in the form of transient impulses.
Wavelet coefficients were determined at constant scale value of the scalograms of four outer rings with grinding manufacturing defects. Then, wavelet coefficients at the highest local maxima of the scalograms were calculated. Nine real-valued wavelets were analyzed and it was determined that

Morlet wavelet was the best for the manufacturing fault detection in all cases on the basis of the Shannon Entropy Criteria. Furthermore, the width measurement of the outer ring grinding fault was executed with all nine wavelets. The best wavelet previously chosen by Shannon Entropy Criteria creates the opportunity to determine the manufacturing defect width in the most accurate way because it presents the best correlation with the transients.

REFERENCES

[1] Patel, V. N., Tandon, N., Pandey, R., K.: *Defect Detection in Deep Groove Ball Bearing in Presence of External Vibration Using Envelope Analysis and Duffing Oscillator.* Measurement, 45, 960., 2012.
[2] Khanam, S., Tandon, N., Dutt, J. K.: *Fault Identification of Rolling Element Bearings from Vibration Signals: An Application of Kalman and H Filters.* LOWHUV 10th International Conference on Vibrations in Rotating Machinery (VIRM10), 703-713., 2012.
[3] Al-Ghamd, A.M., Mba, D.: *A Comparative Experimental Study on the Use of Acoustic Emission and Vibration Analysis for Bearing Defect Identification and Estimation of Defect Size.* Mechanical Systems and Signal Processing, 20, 1537., 2006.
[4] Elforjani, M., Mba, D.: *Accelerated Natural Fault Diagnosis in Slow Speed Bearings with Acoustic Emission.* Engineering Fracture Mechanics, 77, 112., 2010.
[5] Sawalhi, N., Randall, R.B.: *Vibration Response of Spalled Rolling Element Bearings: Observations, Simulations and Signal Processing Techniques to Track the Spall Size.* Mechanical Systems and Signal Processing, 25, 846., 2011.
[6] Peng, Z.K., Chu, F.L.: *Application of the Wavelet Transform in Machine Condition Monitoring and Fault Diagnostics.* Mechanical Systems and Signal Processing, 18, 199., 2004.
[7] Prabhakar, S., Mohanty, A.R., Sekhar, A.S.: *Application of Discrete Wavelet Transform for Detection of Ball Bearing Race Faults.* Tribology International, 35, 793., 2002.
[8] Shi, D. F., Wang, W. J., and Qu, L. S.: *Defect detection for bearings using envelope spectra of wavelet transform.* ASME Journal of Vibration and Acoustics, 126(4), 567., 2004.
[9] Nikolaou, N. G., Antoniadis, I. A.: *Demodulation of Vibration Signals Generated by Defects in Rolling Element Bearings Using Complex Shifted Morlet Wavelets.* Mechanical Systems and Signal Processing, 16(4), 677., 2002.
[10] Qiu, H., Lee, J., Lin, J., Yu, G.: *Wavelet Filter-Based Weak Signature Detection Method and its Application on Rolling Element Bearing Prognostics.* Journal of Sound and Vibration, 289, 1066., 2006.
[11] Junsheng, C., Dejie, Y., Yu, Y.: *Application of an Impulse Response Wavelet to Fault Diagnosis of Rolling Bearings.* Mechanical Systems and Signal Processing, 21, 920., 2007.
[12] Kumar, R., Singh, M.: *Outer Race Defect Width Measurement in Tapered Roller Bearing using Discrete Wavelet Transform of Vibration Signal.* Measurement, 46, 537., 2013.
[13] Awal, M. A., Mostafa, S. S., Ahmad, M.: *Quality Assessement of ECG Signal Using Symlet Wavelet Transform.* Proceedings of International Conference on Advances in Electrical Engineering, 129-134., 2012.
[14] Chavan, M. S., Mastorakis, N., Chavan, M. N., Gaikwad, M. S.: *Implementation of SYMLET Wavelets to Removal of Gaussian Additive Noise from Speech Signal.* Recent Researches in Communications, Automation, Signal Processing, Nanotechnology, Astronomy and Nuclear Physics, 37-41., 2012.
[15] Kumar, R., Jena, D.P., Bains, M.*: Identification of inner race defect in radial ball bearing using acoustic emission and wavelet analysis.* Proceedings of ISMA 2010 including USD 2010 Leuven (Belgium), 2883–2891., 2010.

[16]Mankovits, T., Szabó, T., Kocsis, I., Páczelt, I.: *Optimization of the Shape of Axi-Symmetric Rubber Bumpers.* Strojniski vestnik-Journal of Mechanical Engineering, 60(1), 61-71., 2014.
[17]NI 9234 datasheet: http://www.ni.com/datasheet/pdf/en/ds-316, accessed on 2016-02-04.
[18]PCB IMI 603C01 transducer, from https://www.pcb.com/contentstore/docs/PCB_Corporate/IMI/Products/Manuals/603C01.pdf, accessed on 2016-02-04.
[19]Michel, M., Yves, M., Georges, O., Jean-Michel, P.: *Wavelets and their Applications.* ISTE Ltd., 2007.
[20]Salguerio, J., Persin, G., Vizintin, J., Ivanovic, M., Dolenc, B.: *On-line Oil Monitoring and Diagnosis.* Strojniski vestnik-Journal of Mechanical Engineering, 59(10), 604-612., 2013.
[21]Kankar, P.K., Sharma, S.C., Harsha, S.P.: *Fault diagnosis of ball bearings using continuous wavelet transform.* Applied Soft Computing, 11, 2300–2312., 2011.
[22]Kankar, P.K., Sharma, S.C., Harsha, S.P.: *Fault diagnosis of rolling element bearing using cyclic autocorrelation and wavelet transform.* Neurocomputing, 110, 9-17., 2013.

INTERNATIONAL SCIENTIFIC CONFERENCE ON ADVANCES IN MECHANICAL ENGINEERING
13-15 October 2016, Debrecen, Hungary

ADDITIONAL PROBLEM OVERVIEW OF FLUID FLOW IN POROUS SYSTEMS

[1]DÓCS Roland, [2]JOBBIK Anita PhD

[1]Research Institute of Applied Earth Sciences, University of Miskolc
E-mail: docs@afki.hu
[2]Research Institute of Applied Earth Sciences,
MTA-ME Geoengineering Research Group University of Miskolc
E-mail: jobbik@afki.hu

Abstract
The task of describing fluid flow in porous media rather than in solid pipes is a much more difficult one. In order to define flow in these particular systems Darcy equation is required, in which at certain given criteria flow of fluids can be described. Although the equation is rather simple in order to be used, petrophysical parameters have to be determined. These can only be obtained throughout laboratory measurements for each individual rock sample. In case of this paper those problems which are present regarding fluid flow in porous media will be observed. The importance of petrophysical property measurements will be mentioned in detail. Furthermore calculations of pressure drops will be included for steel pipe, theoretical and real porous systems with equal cross sectional area and length of one meter.

Keywords: *porous system, Darcy's equation, porosity, permeability, pressure drop*

1. INTRODUCTION

Description of fluid flow in solid pipes is a rather simple task in which not much needs to be known in order to calculate pressure drop of liquid flowing inside of the cylindrical volume with given inner radius. Regarding of fluid flow in horizontal pipe lines besides irreversible energy losses caused by friction, changes in potential and kinetic energies are also present, but can be neglected for a short section (1m) of the total pipe length. Thus only frictional pressure drop will be taken into consideration from the general equation of single phase flow.

$$\frac{dp}{dl} = \frac{g}{g_c}\rho \sin\alpha + \frac{\rho v dv}{g_c dl} + f\frac{\rho v^2}{2g_c d} \tag{1}$$

Assuming the previous equation only the frictional factor covered by Darcy and Weisbach has to be obtained throughout measurements, all other parameters are known. In Darcy's equation regarding flow in porous media only forces of compression, gravity and friction are taken into consideration, (capillary- and forces of inertia are not). In order to use its differential form the following statements have to be made [1]:

- A certain volumetric element with known dimensions is considered in space with fix boundaries, in a way that random effects may be statically eliminated.
- Stream lines are building up the surface so that its base surfaces are perpendicular to it.
- Forces acting on the fluid volume inside the control volume are equal.
- Regarding to Newton's Law of motion, fluid body will accelerate until resultant acceleration is larger than zero, but will keep its velocity (u_i).

- We seek a value for u_i such that the resultant acceleration equals the null vector.

In order to simplify without losing the generality a cylindrical element was taken as shown in the following figure.

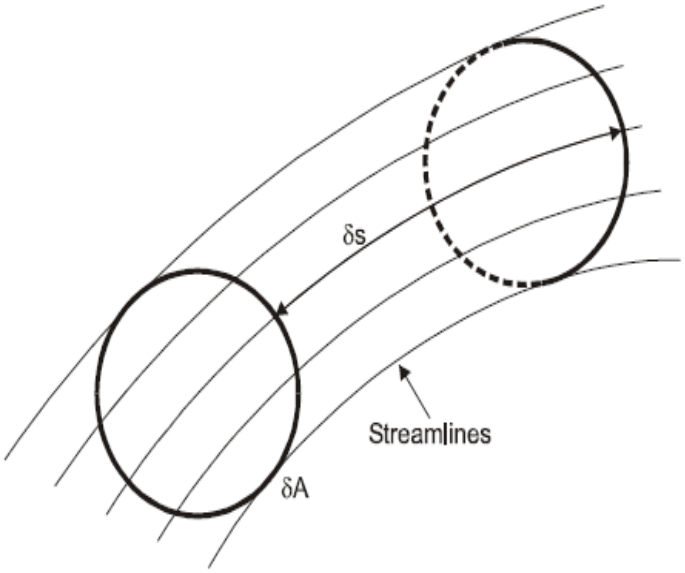

Figure 1 Control volume determined by Darcy [1]

As the equation of single phase flow by Darcy and Weisbach is written up considering those statements made previously, the equation of single phase filtration is described as following.

$$F_p + F_g + F_\mu = 0 \tag{2}$$

$$-\Phi\delta A\nabla p\delta s - \rho g\Phi\delta A i_3\delta s - B\mu\delta A u\delta s = 0 \tag{3}$$

$$-\left(\nabla p + \mu\frac{B}{\Phi}u + i_3\rho g\right)\Phi\delta A\delta s = 0 \tag{4}$$

In the previous equation two parameters have to be introduced regarding porous media, its porosity (Φ) and a coefficient (B). According to this, ΦδA describes the cross sectional area in which flow is possible, B/Φ can be written up as the so called permeability (k), a parameter that describes resistance present during flow inside a given porous media saturated only with that given fluid. Both parameters could only be obtained during petrophysical measurements. After determination of these parameters Darcy's Law is given as the differential of the previous equation.

$$u = -\frac{k}{\mu}(\nabla p + i_3\rho g) \tag{5}$$

Flow behaviours of consolidated rock materials, as can be seen are rather difficult to be described by calculations. In order to be able to determine these, methods are being used at the Research Institute of Applied Earth Sciences-University of Miskolc are listed in the following.

2. METHODS

In order to describe the effective pore space in which flow happens, porosity (Φ), the ratio of pore volume (V_p) to total bulk (V_b=samples measurable volume) volume has to be determined.

$$\Phi = \frac{V_p}{V_b} = \frac{V_b - V_s}{V_b} \tag{6}$$

Porosity can be measured by multiple methods, one of them used by our institute works on the basis of Boyle's Law for ideal gases. Using Helium which has the finest particles of all non reactive gases is used to measure the solid volume (V_s) of samples. In the procedure, an apparatus consisting of two chambers (sample and reference) of known volumes is used to measure pressure difference reached by existing Helium quantity in given volumes at isothermal conditions (T_a). If both chambers are empty, the previously adjusted pressure (p_1) at reference volume (V_R) after expansion between both reference and sample chambers (V_R+V_C) will drop to a certain (p_2) pressure.

$$V_s = V_c - V_R \left[\left(\frac{p_1}{p_2}\right) - 1\right] \tag{7}$$

Solid volume of rock inside the sample chamber decreases volume where gas can expand to resulting in higher p_2 for same p_1 in case of an empty sample chamber. Regarding the measurement procedure reference- and expansion pressures are recorded 3 times resulting in 3 calculated solid volumes for each sample. From each solid volume and the samples dry weight, solid densities of each measurement is calculated, then standard deviation of the three values is determined. At standard deviation values higher than 0,003 g/cm^3, measurements are repeated until satisfactory conditions reached. At lower standard deviation values, average of the calculated volumes determines the solid volume of the given sample with sufficient accuracy. As previously discussed, in knowledge of both solid and bulk volumes pore volume also porosity can be calculated.

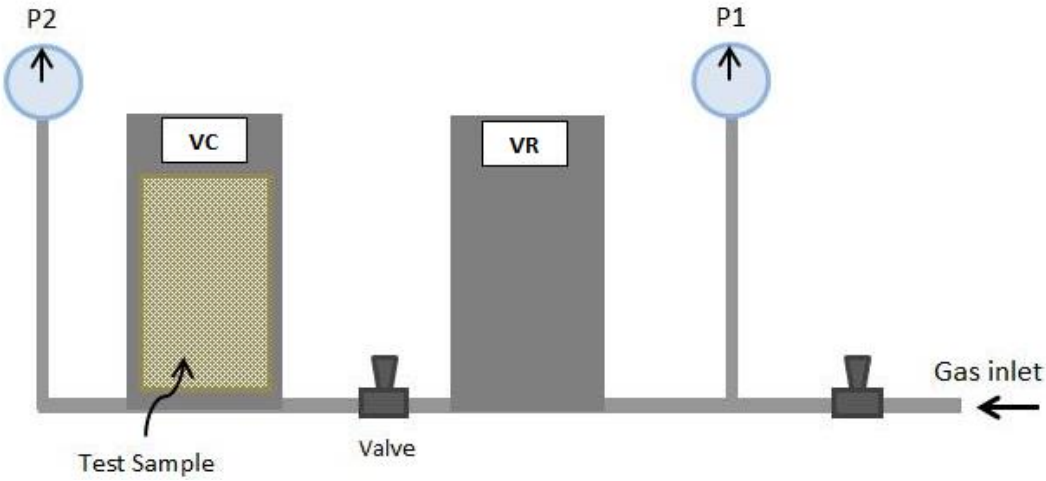

Figure 2 Schematic figure of the Helium pycnometer

Problem is, that even in knowledge of effective pore volume a porous system cannot be modelled as a pipe with an inner diameter equal to the original, corrected ($d_i\Phi$) by porosity. Resistance of fluid flow in porous media depends not only on porosity but also on much more.

Permeability is a parameter which describes the reciprocal value of this resistance if flow of incompressible fluid occurs in a porous sample of A cross sectional area and l length in horizontal position. If at constant pressure difference flow rate obtained through the sample is known, then the only unknown parameter will be permeability.

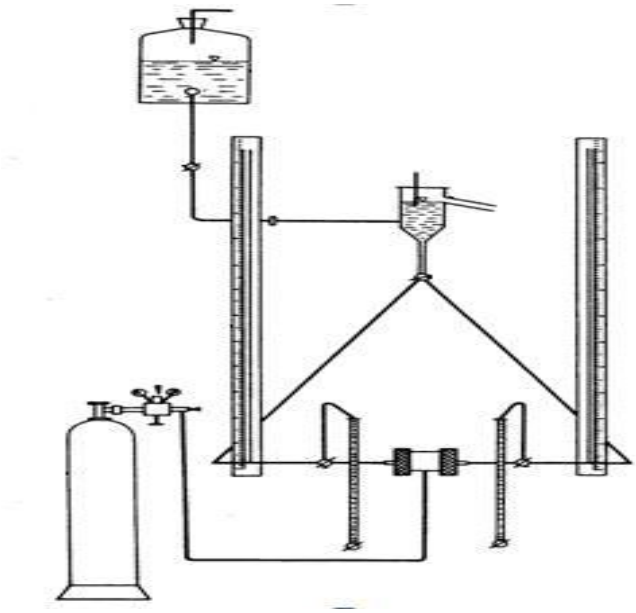

Figure 3 Schematics of the water permeability measurement

By monitoring pressure difference, and keeping it constant between the inlet (p_1) and outlet side (p_2=atmospheric pressure), time is measured which is required for a given volume of fluid to pass through the sample of known volume (A, l), then permeability can be calculated. Because of constant pressure difference throughout the entire measurement, time periods for equal amount of fluid volume accumulation should be constant as well. Permeability of the sample regarding that given fluid will be calculated as the average of each measured point.

$$k = \frac{q\mu\Delta l}{A\Delta p} \tag{8}$$

To introduce the importance of flow resistance measurements of porous samples, the following three calculations were made on standard conditions. Systems of equal diameters and lengths (1m) were taken into consideration. First, a solid pipe, then a porous system of same diameter (corrected by porosity) and finally a porous sample of equal diameter as in case of the solid pipe. Flow rates were equal (25 ml/h) and were chosen in order to stay at the laminar flow region in all three cases. Water was used as an incompressible fluid with a dynamic viscosity (μ) of 1cP.

Table 1 Parameters of the observed systems

	d_i, [cm]	Φ
Steel pipe	3,762	0,0000
Theoretical porous system	0,2879*3,762=1,0831	0,2879
Porous sample	3,762	0,2879

3. RESULTS

Pressure drop calculations regarding the steel pipe was made using those described by Gábor T. [3]. First, calculation of flow velocity was required, where parameter B_w is the so called Formation Volume Factor of water, which describes the ratio of water volume at standard and at given pressure and temperature conditions. In our case because of standard conditions B_w was equal 1.

$$v = 0.0119 \frac{q_w B_w}{d_i^2} \tag{9}$$

After flow velocity was known, calculation of the Reynolds number was required to ensure that flow was indeed Laminar. In our case flow was indeed at Laminar conditions (N_{Re}<2300), which means that the flow rate for our given inner pipe diameter was chosen efficiently. Friction factor at Laminar flow can easily be calculated by *Equation 11*. Lastly, pressure drop caused by friction was calculated by *Equation 12*. All calculations regarding the steel pipe were made in field units and converted into SI.

$$N_{Re} = 124 \frac{\rho v d_i}{\mu} \tag{10}$$

$$f = \frac{64}{N_{Re}} \tag{11}$$

$$\Delta p_f = 1.294\ 10^{-3} f \frac{l}{d_i} \rho v^2 \tag{12}$$

In case of the theoretical porous system, which was modelled as if it was a solid pipe with decreased inner diameter, calculation of frictional pressure drop was exactly the same because of Laminar flow also.

Pressure differences between inlet and outlet side of the porous sample regarding the 25 ml/h flow rate were measured during permeability measurement at laboratory conditions. After elimination of false pressure values resulting of not yet stable dynamic conditions, reached pressure drop of the system was determined as average of the considered points. Results of pressure drops are summed in the following table.

Table 2 Pressure drops of the systems

Pressure drop of	Steel pipe [MPa]	Theoretical porous system [MPa]	Porous sample [MPa]
	1,4099E10-7	2,0522E10-5	0,4053

It can be clearly seen that difference in pressure drops regarding these systems were multiple of magnitudes. As predicted, lowest value was present at the steel pipe and highest at the porous rock sample with a total difference of six magnitudes. Also as predicted, pressure drop of the theoretical porous system was nowhere near that present in an actual porous system, which had effective flow volume equal to it.

CONCLUSIONS

In order to describe flow restrictions in porous media our only solution is to measure the permeability of a cylindrical sample taken from it. Unique properties of consolidated rocks such as porosity, pore size distribution, capillary forces and wettability make pressure drop calculation a rather impossible task. Modelling porous systems as they were constructed from many individual capillaries are also rather rare. Even in possession of the correct values these models would not represent what truly happens in consolidated porous rock materials.

ACKNOWLEDGEMENT

The research was carried out in the framework of the GINOP-2.3.2-15-2016-00010 "Development of enhanced engineering methods with the aim at utilization of subterranean energy resources" project in the framework of the Széchenyi 2020 Plan, funded by the European Union, co-financed by the European Structural and Investment Funds.

REFERENCES

[1] Zoltán, E., Heinemann: *Fluid Flow In Porous Media*. Textbook Series Volume 1, Montanuniversitat Leoben Petroleum Engineering Department 2005. page 12-97.
[2] Béla, M., Tibor, B.: *Rezervoármechanika I.* Oktatási segédanyag, Miskolci Egyetem Olajmérnöki Tanszék 1997 45. old.
[3] Gábor, T.: *Production Engineering Fundamentals Vol. 1.* University of Miskolc Petroleum Engineering Department 2012. page 19-23.

INTERNATIONAL SCIENTIFIC CONFERENCE ON ADVANCES IN MECHANICAL ENGINEERING

13-15 October 2016, Debrecen, Hungary

APPLICATION OF ON-LINE VIBRATION MONITORING IN A ROLLING MILL

[1]DÖMÖTÖR Ferenc PhD, [2]ÁCS János, [3]SZÖRÉNYI Norbert

[1]BME Budapest University of Technology and Economics, Faculty of Transport Engineering and Vehicle Engineering (1111 Budapest, Stoczek Str. 4.)
E-mail: ferenc.domotor@gjt.bme.hu
[2]Schaeffler Magyarország Ipari Kft. (1118 Budapest, Rétköz Str. 5.)
E-mail: Acsjno@schaeffler.com
[3]Alcoa-KÖFÉM Kft. (8000 Székesfehérvár, Verseci Str. 1-15.)
E-mail: Norbert.szorenyi@alcoa.com

Abstract
Rolling is one of the most important manufacturing procedures, during which both structural and bearing vibrations play an important role from the quality assurance and reliability point of view. On-line condition systems, using vibration measurement methods have been installed recently on the hot rolling mill stand, and on three cold mill stands at the Alcoa-KOFEM plant in Székesfehérvár (Hungary). Signals for the monitoring system are provided by piezoelectric accelerometers, manufactured by the FAG as well. Goal of the monitoring system is to provide a reliable operation of the bearings, and the prediction of a potential failure. Good results contribute to the success of predictive maintenance and the manufacturing of high quality products.

Keywords: *Rolling mill, condition monitoring, vibration measurements*

1. NEW TENDENCIES OF ROLLING BEARING SURVEILLANCE

Rolling is one of the most important manufacturing procedures, during which both structural and bearing vibrations have an important role from the quality assurance and reliability point of view. One of these giant, super modern rolling mills is at the Alcoa-KOFEM plant in Székesfehérvár, where an on-line vibration monitoring system, manufactured by FAG/Schaeffler has been installed recently.

2. ON-LINE CONDITION MONITORING SYSTEM

On-line condition systems, using vibration measurement methods have been installed on the hot rolling mill stand, and on three cold mill stands at the Alcoa-KOFEM plant in Székesfehérvár (Hungary). The most important features of the system are as follows:

- there is a FAG DTECT X1 measurement system on each of the stands,
- there are two accelerometers on each pairs of rolls,
- sensing and tracking of rotational speed.

Location and arrangement of the condition monitoring system can be seen on the *Figure 1*.

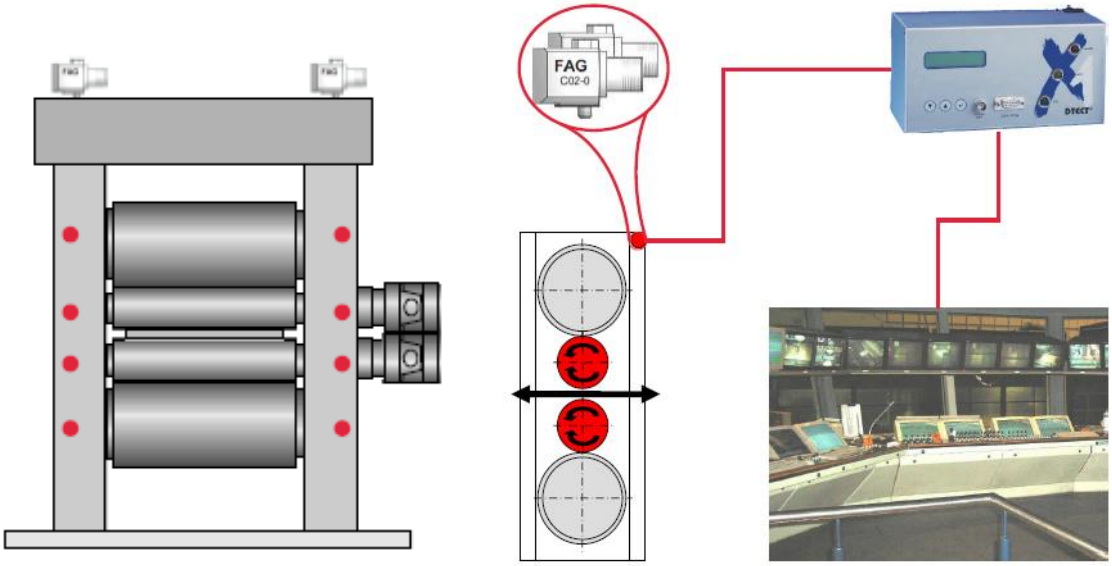

Figure 1 Location of vibration sensors on the stand of rolling mill [1]

Signals for the monitoring system are provided by piezoelectric accelerometers, manufactured by the FAG as well. Goal of the monitoring system is to provide a reliable operation of the bearings, and the prediction of a potential failure. The most important features of the on-line monitoring system are as follows:

- vibration measurement, and tracking of rotational speed,
- configuration of the signal processing as necessary,
- display both in time and frequency domain (FFT spectrum),
- trend, analysis, waterfall diagram,
- remote distance diagnostics.

FAG DTECT X1 allows connection of all common acceleration, velocity and displacement sensors. The signal of these sensors is recorded and processed by FFT method. It is possible to monitor amplitudes within fixed and very narrow frequency bands for specified limit values. An alarm is triggered when these are exceeded. Using FAG DTECT X1 two different parameter types can be recorded from the vibration acceleration signal. Firstly the RMS value, which is detected from the spectrum of the raw signal, and secondly the LDZ value (a bearing diagnostic parameter), which is generated from the envelope signal.

FAG DTECT X1 can calculate various parameters, like RMS, peak value, peak-to-peak value, steady component, crest factor. FAG DTECT X1 has two additional channels. They can be used to record process variables (speed, torque, temperature, pressure, etc.). FAG DTECT X1 allows remote monitoring of the plant and machinery.

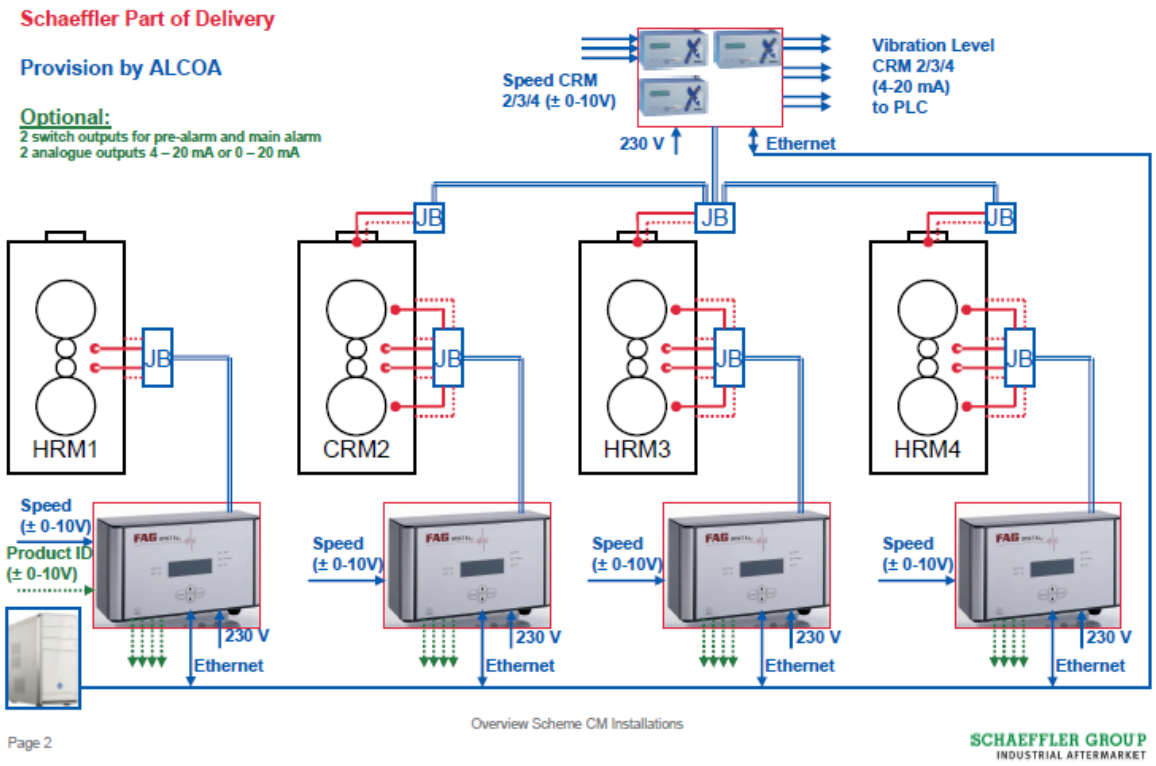

Figure 2 Schematic view of the connection of the elements of the measurement system [1]

3. PREDICTION OF THE BEARING FAULT USING VIBRATION MEASUREMENT

Results of the measurements and the data processing are available both in time and frequency domain. Time signals of the vibration measurements can be seen at the *Figure 4.*, while the spectrum of the same signal can be seen at the *Figure 3*. The monitored signal is a so called enveloped acceleration curve. On the spectrum of the signal the peaks, typical for inner ring defects can be seen. Also the cursor position is pointing to the fault.

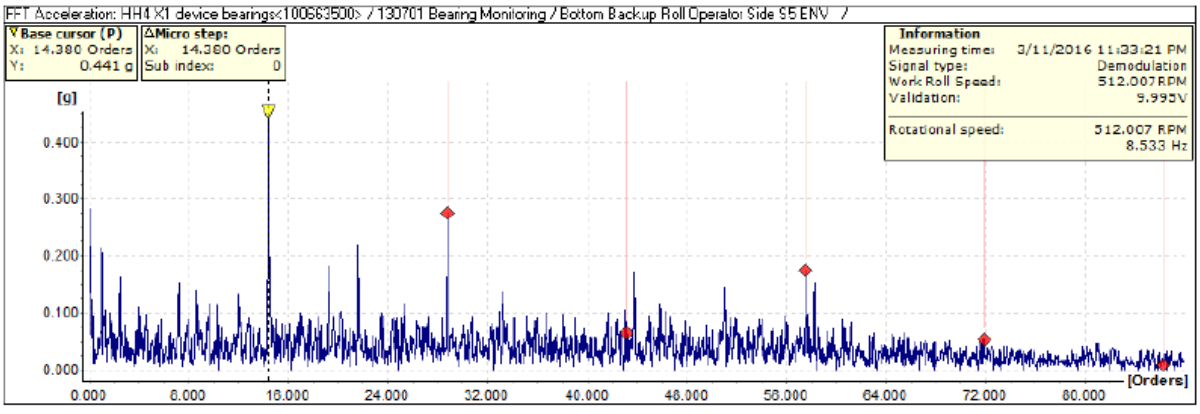

Figure 3 Frequency spectrum of the vibration at one of the cold mill bearings [1]

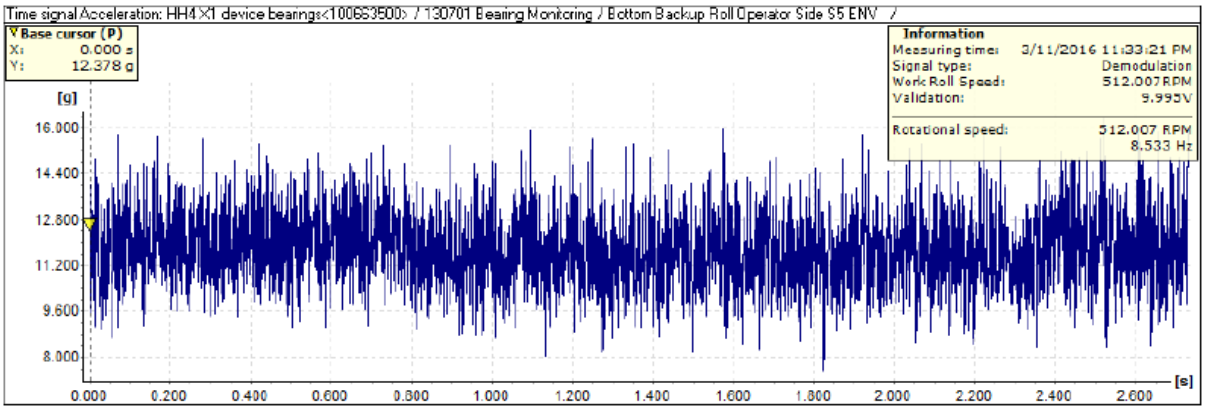

Figure 4 Time signal of the same bearing on the cold mill [1]

CONCLUSIONS

On-line condition systems, using vibration measurement methods provide a reliable operation of the plant. One of the proofs is the new on-line syyste, which has been installed on the hot rolling mill stand, and on three cold mill stands at the Alcoa-KOFEM plant in Székesfehérvár (Hungary).

REFERENCES

[1] *Monitoring Report for the Aluminum Rolling Mills MH, HH2, HH3, and HH4 at the Alcoa KOFEM Plant in Hungary*
[2] *Condition Monitoring on a Hot Strip Mill*, Brochure of the Schaeffler Global Technology Solutions GTS 0006/ 01 / GB-D / 201304
[3] FAG DTECT X1 s *Continuous Monitoring of Plant and Machinery*, Brochure, © Schaeffler Technologies AG & Co. KG, Issued: 2015, December, TPI 170 GB-D
[4] FAG Vibro *Check, Online-Monitoring System for the Heavy Industry*, Brochure
[5] Dömötör, F. (edited by): „*Vibration diagnostics" for students of technical universities*, Volume I. Publishing House of the Dunaújváros University, Dunaújváros, 2008., ISBN: 978-963-87780-0-0
[6] Dömötör, F. (edited by): „*Vibraton diagnostics" for students of technical universities*, Volume II. Publishing House of the Dunaújváros University, Dunaújváros, 2011., ISBN 978-963-9915-43-5

DIGITAL IMAGE CORRELATION TECHNIQUE APPLICATION ON WELDED JOINT - ADVANTAGES AND DISADVANTAGES

[1]ĐORĐEVIĆ Branislav, [1]TATIĆ Uroš, [1]SEDMAK Simon, [1]MILOŠEVIĆ Miloš, [2]SEDMAK Aleksandar PhD

[1] Innovation Center of Faculty of Mechanical Engineering, Kraljice Marije 16, 11120 Belgrade
[2] Faculty of Mechanical Engineering, Kraljice Marije 16, 11120 Belgrade
E-mail: b.djordjevic88@gmail.com

Abstract
Presented in this paper is the application of a non-contact digital image correlation (DIC) measuring method, including the methodology for non-contact testing technique with two cameras (stereometric method). Different examples of optical measuring methods used on welded joints are presented, along with its results, possibility of results presentation, advantages and disadvantages which can somewhat limit the application of this measuring technique to objects with a heterogeneous structure i.e. welded joint. The application of this method is shown on two welded plate specimens made of micro-alloyed steel P460NL1 during their deformation. Obtained results were analyzed and can indicate the further detailed examinations of specified parts of welded joint.

Keywords: *Digital image correlation, tensile testing, deformation, welded joint*

1. INTRODUCTION

A clear and completely accurate image of a deformed machine part, structure or a real object was always difficult to determine, and measuring techniques were focused on finding ways to display the strain field as a whole, which could be measured and evaluated as simply as possible. Stereometric strain measuring represents one such method. This measuring technique found a broad application in experimental measuring, since it is able to record the observed local part of the volume during deformation in high resolution. Use of ARAMIS software enables the displaying of a complete 3D surface, 3D displacements and strain with their values (both large and small), as well as the rate at which displacement takes place. This system can replace all traditional measuring devices typically used in experiments (strain gauges, extensometer, etc).
Stereometric measuring technique can be used to:

- determine the mechanical properties of a structure, its parts or a machine part,
- examine the possibilities and limitations of tested material application,
- analyze the effects of vibrations,
- perform durability studies,
- perform tests for the purpose of determining fracture mechanics parameters or failure conditions in general,
- verify results obtained by conventional test methods, numerical calculations or by using finite element method,
- gather results which can be used for further material analysis.

The ARAMIS system represents a suitable and reliable technique of verifying results obtained by finite element method simulations [1-2]. With its aid, material properties can be determined and existing material models can be improved.
Insight, possibilities and results shown in this paper can be used for further research, application and improvement of the optical stereometric method. In addition, results of its application to welded joints emphasize its significance even more, due to the direct application of this measuring technique on materials with a non-homogeneous structure caused by the complexity of the welding process itself.

2. STEREOMETRIC MEASURING PROCEDURE

Digital image correlation technique is widely used in experimental mechanics. The monitoring system consists of two cameras which provide a synchronized stereo view of the specimen or a real object (*Figure 1*). The system also includes a stand which provides sensor stability, a control power supply unit, a unit for storing of recorded images and a system for data processing, i.e. a computer.

Figure 1 Experimental setup for the DIC technique

The surface of the specimen must be carefully prepared before measuring, so that the results obtained are valid. A stochastic pattern of contrasting colors is sprayed onto the specimen surface. After that, and before the experiment, it is necessary to adjust the required parameters in order to record the specimen with cameras. Parameters which must be taken into account include: determining of the measured volume, hardware adjustments (which includes calibration of measured volume, adjusting of the sensor unit, software calibration using calibration objects), measured surface lighting, defining of "facets", defining of the calculation mask, etc. During the experiment, the loaded specimen is recorded before and after deforming and the ARAMIS software calculates individual displacements and strain for each point on the measured volume, based on the non-deformed specimen image.
After the calculation is complete, obtained data are available in 2D and 3D forms for every load step during the experiment. Before the post-processing of results, it is necessary to define the adequate means of 3D results presentation. For the purpose of displaying results in diagrams and the 3D model, step points, sections (planar sections, circular sections, curved plane sections) and primitives can be made. It is possible to show Misses strain, principal strain, Tresca strain, etc. In engineering practice, Misses' calculation of equivalent strain is the most widely applied method [1, 3-5].

3. RESULTS

General research related to welded joints, involves the testing of cracks in welds, i.e. determining of how dangerous they are in exploitation [2, 6, 7], however such a study was not performed as part of this paper. As is known, welding represents a complex process during which various physical, chemical and metallurgical processes take place, and the weld metal and parent material are characterized by different chemical compositions and mechanical properties. It is extremely difficult to determine the properties and behavior of welded joints due to their complexity, and such joints can play a crucial role in determining of structural integrity. Use of digital image correlation enables the determining of critical fields within a welded joint subjected to load.
In the following part of the paper, two examples of this technique's application are presented, along with its possibilities. Specimens were obtained from two plates made of micro-alloyed steel P460NL1. Plates were 14 mm thick. Load levels were different for every specimen. Test plates were welded using the MAG procedure, in 12% Ar + 82% CO_2 shielding atmosphere. VAC 65 wire with a diameter of $\phi 1{,}6$ mm, manufactured by Zelezarna Jesenice [8] were used as additional material. The geometry of both tested specimens is shown in the *figure 2*.

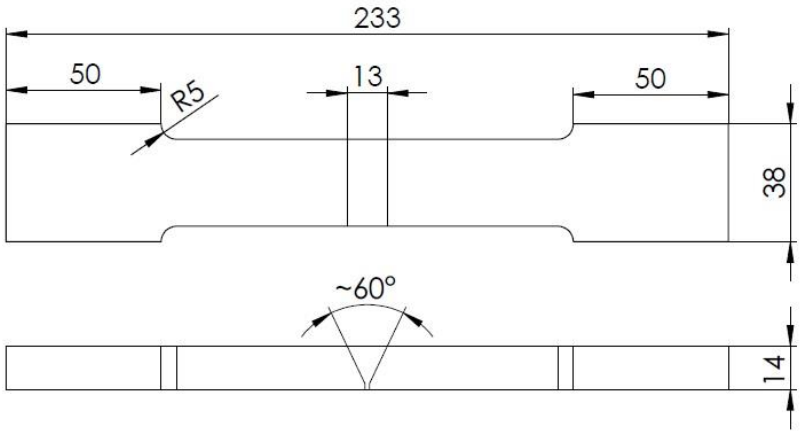

Figure 2 Specimen geometry

The first example can be seen in *figure 3*. Shown in this figure is one of the possible ways of displaying strain in a specimen which was loaded up to a plastic strain of 5%. Accurate values of major strain are shown in points 0-17. As can be seen from the figure, smallest strain was located in the heat affected zone (point 12). Largest strain was located in the parent material, in areas further away from the weld metal, which indicated that the weld metal had higher strength compared to the parent material. The strain field in the HAZ area can also be seen.
In practice, load can be defined as maximum displacement in order to limit the strain or the force acting on the structure and prevent large-scale failure. The following DIC application example involves a specimen with a given strain of 16 mm. Shown in *figure 5a* is the force-displacement diagram.
Calculation results are given in form of Misses strain, which represents yet another way of displaying results in ARAMIS (*figure 4b*). Shown in points 0-13 are the exact values of displacement and strain. Smallest strain was in point 9, within the HAZ.

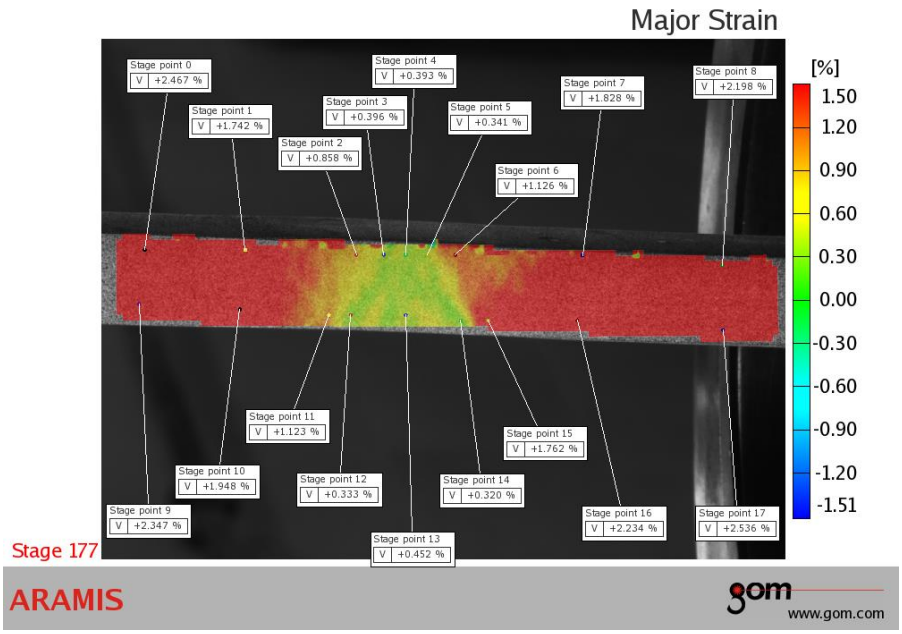

Figure 3 Major strain in a specimen loaded up to a plastic strain of 5%

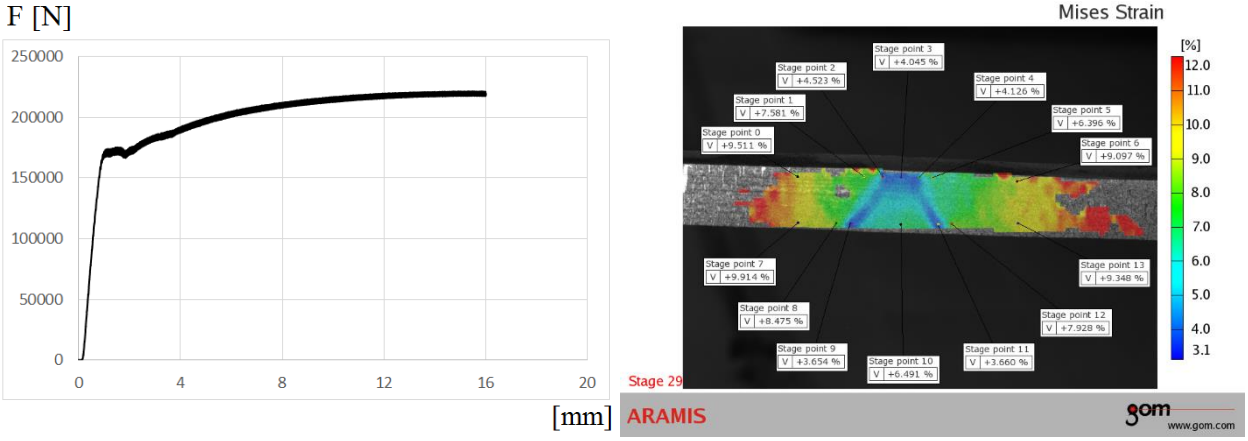

a) b)

Figure 4 a) Force-displacement diagram up to 16 mm *b)* strain field of the tested specimen

Apart from the display shown above, the ARAMIS system also enables direct comparison of strain along sections. Thus it is possible to directly compare strain values of individual welded joint and parent material zones.

Sections denote lines which include different welded joint zones. Section 0 includes the parent material, HAZ and weld root, whereas section 1 includes part of the PM near the HAZ, the HAZ and weld metal (*figure 5a*). Strain is displayed along defined sections in *figure 5b*, where it can be clearly seen that smallest strain due to tensile load was located in the welded joint root and HAZ.

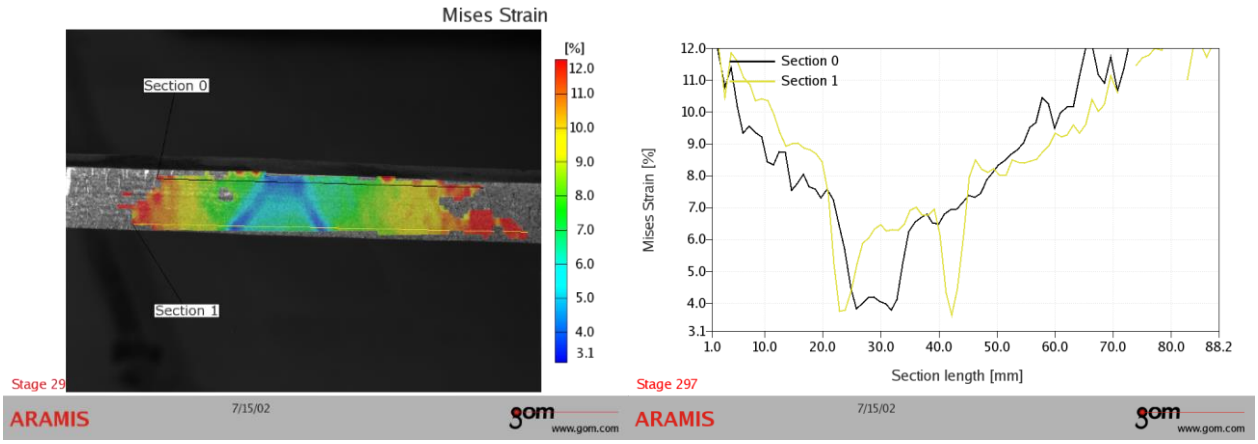

a) b)

Figure 5 a) View of sections 1 and 2 and *b)* diagram of strain distribution along the tested specimen sections

DISCUSSION AND CONCLUSIONS

Due to the welding process, during which various physical, chemical and metallurgical processes occur, welded joints represent complex problems in terms of stress calculation, determining of mechanical properties, etc. Testing of welded joints made of steel P460NL1 resulted in complete displacement and strain fields, which provide complete insight into the behavior of a welded joint subjected to tensile loads. Strain and displacement were shown for various load levels and different behavior of the welded joint as a whole. Most importantly, concrete and accurate values of the entire observed strain fields are obtained, as opposed to a selected representative part which would be examined by using a strain gauge in a single location.

Results of the first tested specimen indicated which zones within the welded joint had the largest and which had the smallest strain. Highest strain under tension was in the parent material, and the lowest values were in the HAZ. In addition, it can be seen that the strain was not equal in HAZ on both sides of the weld metal, which may have been caused by non-uniform heat input, which was likely higher on one side. Results of the third tests confirmed that the smallest strain was in the weld root and the HAZ. In the case of this specimen, forming of a slight neck and cross-section contraction in the parent material can be observed. By using the stereometric method, behavior of all zones in the weld metal during strain caused by tension can be seen, and also compared directly via selected sections.

This technique also has certain flaws which could result in errors. When measuring small strain, ARAMIS can make errors in calculation, which also affects the strain values and incorrect conclusions could result from this. In addition, specimen preparation plays an extremely important role. A small zone in the strain field wherein ARAMIS was not able to determine the values of strain can be seen on the second tested specimen. This could have been caused by the increased reflection due to non-uniform lighting of the measuring surface and/or test specimen preparation.

ACKNOWLEDGEMENT

The authors of this paper acknowledge the support from Serbian Ministry of Education, Science and Technological Development for projects TR35040 and TR35011.

REFERENCES

[1] Simon Sedmak, Uroš Tatić, Radomir Jovičić, Aleksandar Sedmak, Miloš Milošević, Ramo Bakić, Stojan Sedmak: *Numerical Modeling of Austenite-Ferrite Weldment Tensile Test*, 20th European Conference on Fracture (ECF20), Procedia Materials Science, ISSN 2211-8128, 2014

[2] Isamu Oda, Andrew Willett, Mitsuharu Yamamoto, Takeshi Matsumoto, Yasuhide Sosogi: *Non-contact evaluation of stresses and deformation behaviour in pre-cracked dissimilar welded plates*, Engineering Fracture Mechanics 71, ISSN 1453–1475, 2004

[3] Aleksandar Sedmak, Milos Milosevic, Nenad Mitrovic, Aleksandar Petrovic, Tasko Maneski: *Digital image correlation in experimental mechanical analysis*, Structural Integrity and Life Vol.12, No.1, pp 39-42, ISSN 1451-3749, 2012

[4] Nenad Gubeljak: *Application of stereometric measurement on structural integrity,* Structural integrity and life, Vol. 6, No.1-2, pp 65-74, ISSN 1451-3749, 2006

[5] Tatić, U., Đorđević, B., Sedmak, S., Milošević, M., Sedmak, A: *Stereometric methods of measuring strain and displacement in welded joints subjected to tensile load;* 32nd Danubia Adria Symposium Advances in Experimental Mechanics, Slovakia, pp. 86-87, ISBN 978-80-554-1094-4, 2015

[6] S. Sedmak, Lj. Milovic, R. Jovicic, B. Djordjevic, E. Dzindo, M. Zrilic, T. Maneski: Use *Of Digital Image Correlation In Measuring Of Crack Propagation In A Three Point Bending Specimen,* 16th International Conference On New Trends In Fatigue And Fracture (NT2F16), Book of Abstracts, ISBN 978-7738-39-6, Dubrovnik, Croatia, 2016

[7] Radomir Jovičić, Simon Sedmak, Uroš Tatić, Uroš Lukić, Musraty Walid: *Stress state around imperfections in welded joints,* Structural Integruty and Life, Vol. 15, No.1, pp.27–29, ISSN 1451-3749, 2015

[8] http://www.honex.rs/sites/default/files/jesenice/elektrode_web.pdf

INTERNATIONAL SCIENTIFIC CONFERENCE ON ADVANCES IN MECHANICAL ENGINEERING
13-15 October 2016, Debrecen, Hungary

EFFECT OF GRADUAL AMPLITUDE INCREASE ON FLOW AROUND A CYLINDER OSCILLATED IN LINE

[1]DOROGI Dániel, [2]BARANYI László CSc

[1,2]Universtity of Miskolc
E-mail: aramdd@uni-miskolc.hu, arambl@uni-miskolc.hu

Abstract
The present study deals with the numerical simulation of the flow around a circular cylinder oscillated in-line with the main stream. The primary aim of this paper is to investigate the effect of altering oscillation amplitudes during the course of computations on the time-mean values of force coefficients and to compare results with those of constant amplitudes. The two-dimensional computations are carried out at Re*=80 and at 80% of the natural vortex shedding frequency, while the oscillation amplitude is varied in the lock-in regime. The results show that for constant amplitudes there are several switches in the vortex structure, in contrast with altering amplitude solutions, where the solution can remain in one of the two state curves when the amplitudes are increased rapidly. Another finding is that the lock-in domain is substantially wider for the amplitude alteration model than for the constant amplitude case.*

Keywords: *amplitude alteration, circular cylinder, fluid flow, in-line oscillation, vortex switches*

1. INTRODUCTION

Fluid flow around an oscillating cylinder is a well-known fluid-solid interaction problem that is widely investigated due to its academic and practical importance, using numerical and experimental approaches. When a structure is exposed to wind or waves, vortices shed from the body induce a periodic load on the structure. When the vortex shedding frequency is near the natural shedding frequency of the structure and the damping is small, high amplitude oscillation can occur. Chimney stacks, transmission lines and offshore structures are good examples for this phenomenon.
Numerical studies often place a cylinder in forced motion in order to gain an approximation of this fluid-structure interaction. In this study we concentrate on forced oscillations, which can occur transverse or in-line to the main stream or in both directions. Until the early 1970s most researchers dealt with transverse oscillations. However, [1] showed that streamwise oscillation can occur in full scale piles, while [2] reported that the damage at the Monju nuclear power plant was caused by in-line oscillations.

The cylinder oscillation is characterized by the oscillation amplitude A and frequency f. The forcing frequency is often represented by the frequency ratio $FR=f/St_0$ where St_0 is the natural shedding frequency. The effect of the frequency ratio in the range of FR=0.44-3 was investigated in [3] using experimental techniques at medium Reynolds numbers. A similar frequency ratio range was investigated numerically in [4] at Reynolds number Re=200 and dimensionless oscillation amplitudes A=0.1 and 0.3, and found abrupt changes in the vortex structure. In [5] computations were carried out at low and medium amplitude values at FR=1. In [6] in-line cylinder oscillation was analyzed at frequency ratios 0.8 and 0.9, where the oscillation amplitude was varied between 0.1 and 0.7. A large number of jumps were identified in the time-mean values of lift and torque coefficients, indicating vortex switches. An amplitude alteration model was introduced in [7] where

the amplitude was varied with time for both streamwise and transverse cylinder oscillations. Results showed that for in-line oscillation with abrupt amplitude changes the vortex switches were avoided.

In this study an amplitude alteration model is presented which is tested for in-line cylinder oscillations. The Reynolds number and the frequency ratio are kept constant at Re=80 and FR=0.8, respectively. The oscillation amplitude is varied in the regime where the vortex shedding frequency synchronizes with the frequency of the cylinder motion, called locked-in regime. The results of the amplitude alteration and constant amplitude models are compared.

2. COMPUTATIONAL METHOD

The dimensionless governing equations for an incompressible, constant property, Newtonian fluid flow around a circular cylinder are the two components of the Navier-Stokes equations, the continuity equation and a Poisson equation for pressure. The equations of motion are written in a non-inertial system fixed to the moving cylinder. *Figure 1* shows the physical and computational domains where R_1 is the cylinder radius and R_2 is that of the far field. Undisturbed velocity field is assumed in the far field and no-slip boundary conditions are used on the cylinder surface for the velocity. Neumann type boundary conditions are used for pressure on both R_1 and R_2.

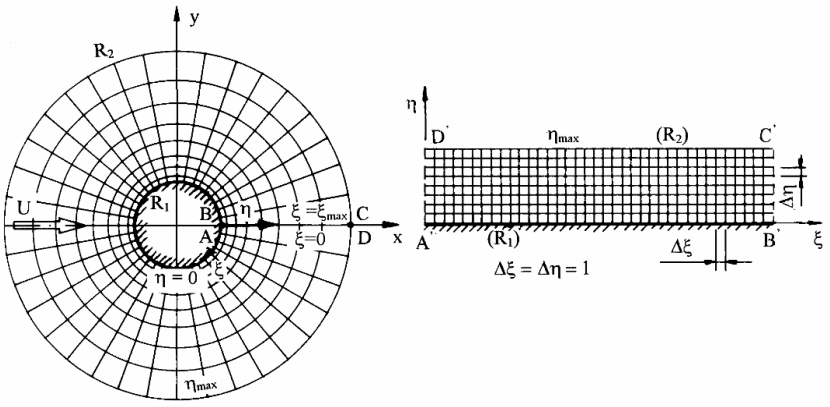

Figure 1 The physical and computational domains

In order to be able to impose boundary conditions accurately and to avoid numerical inaccuracies, boundary-fitted coordinates are used. The physical domain is transformed into a rectangular computational domain applying linear mapping functions [8]. The properties of the mapping functions ensure that the grid on the physical plane is very fine in the vicinity of the cylinder surface and coarse in the far field, while the grid is equidistant on the computational domain. The transformed governing equations with the boundary conditions are solved applying finite difference method [8]. The space derivatives are discretized using fourth order schemes except for the convective terms which are approximated by a third order upwind difference scheme. The Poisson equation is solved using successive over-relaxation, the equation of motion is integrated explicitly and continuity equation is satisfied at every time step.

The computational code was tested thoroughly against results in the literature for stationary and moving cylinders and very good agreement was found [8]. During the computations the radius ratio R_2/R_1=160 and the computational grid is characterized by grid points 360×292 (peripheral × radial) and the dimensionless time step Δt is 0.0005. Applying these parameters the code results in a solution independent from the domain, grid and time step. Following [6-7] the vortex switches are analyzed using lift and torque. From their time histories the time-mean (mean) values are computed.

3. RESULTS

The non-dimensional displacement of the center of the cylinder

$$x(t) = A\,cos(2\pi f t), \tag{1}$$

where t, A and f are the dimensionless time, amplitude and frequency of the cylinder.

Flow around a circular cylinder is a typical non-linear problem with two solutions. There are two attractors in this system (see [9]), each with a basin of attraction. If the set of parameters is near the boundary which separates the two basins of attraction, then even a tiny change in a single parameter is sufficient to change the attractor, yielding a switch in the solution. For example, [6,7] found large jumps in the time-mean values of lift and torque, indicating switches in vortex structure.

3.1. Constant amplitude solutions

In Figs. 2(a) and (b) the time-mean values of lift C_L and torque tq coefficients (see [6]) are plotted against oscillation amplitude A_0, while A_0 does not change with time. During these computations the Reynolds number and frequency are kept at constant values of Re=80, f=0.8St$_0$ (where St$_0$=0.15229 taken from [10]). It can be seen that (1) lock-in takes place between A_0=0.48–0.94 which agrees well with results in [6]; (2) the number of the jumps increases with A_0; (3) the locations of jumps are identical for the time-mean of lift and torque but their signs are opposite.

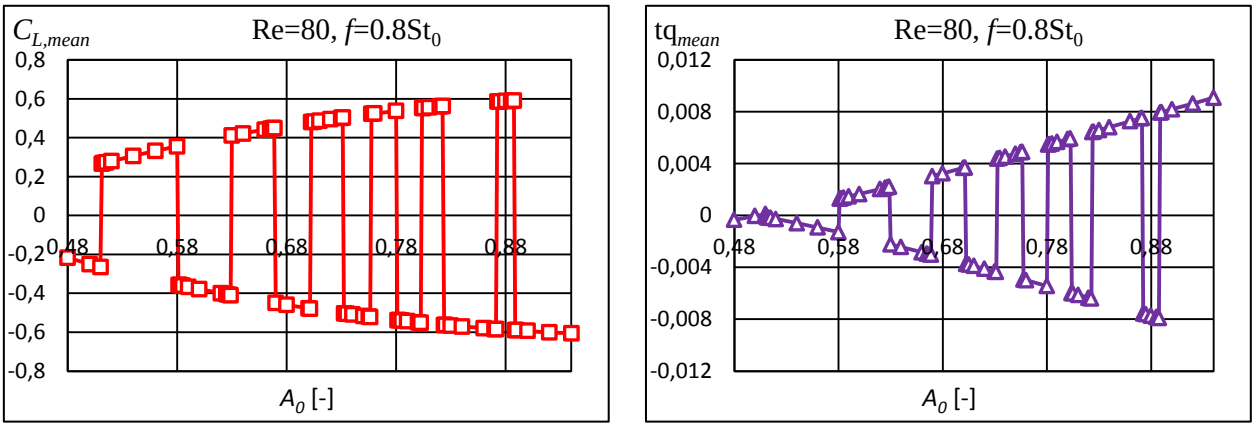

(a) (b)

Figure 2 Time-mean values of lift (a) and torque (b) for A=A_0=const. oscillation amplitude

Both state curves, which form the envelope, are clearly visible in the figure. As also found in [6,7], the state curves are mirror images. While the curves can be determined using different initial conditions, repeating the set of computations for several initial values is computationally expensive.

3.2. Altered amplitude solutions

In order to reduce the computational cost, [7] suggests that by applying amplitude alteration the solutions can be kept in one state curve. In the model applied in [7] the cylinder started to oscillate at an amplitude of A_{x1}, which was altered with time to a higher A_{x2} value either abruptly or gradually. The rate of change between A_{x1} and A_{x2} was linear. Here, a more gradual rate of increase is used, as shown in *Figure 3*.

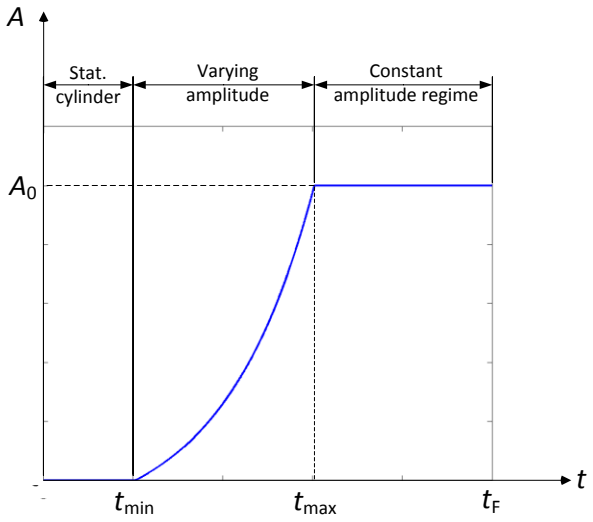

Figure 3 The amplitude alteration model based on equation (2)

It can be seen that the full investigation time t_F is divided into three parts: (a) $0<t<t_{min}$ the cylinder is stationary; (b) $t_{min}<t<t_{max}$ the amplitude is altered from $A=0$ to A_0 using an exponential function; (c) $t_{max}<t<t_F$ constant amplitude regime of $A=A_0$. This can be written mathematically as

$$A = \begin{cases} 0, & if\ 0 < t < t_{min} \\ A_0 \dfrac{e^{n(t-t_{min})} - 1}{e^{n(t_{max}-t_{min})} - 1}, & if\ t_{min} < t < t_{max} \\ A_0, & if\ t_{max} < t < t_F \end{cases} \quad (2)$$

where A_0 is the maximum amplitude, n influences the slope of the curve, t_{min} and t_{max} are the start and the end of the alteration, respectively. Compared to [7], small n values correspond to gradual amplitude alteration. However, when the alteration is abrupt the value of n is relatively high. The course of amplitude alteration can be controlled using t_{min} and t_{max}. In order to avoid discontinuity in the velocity and the acceleration of the cylinder, at the start of the alteration (t_{min}) the cylinder has to be in the origin, i.e, condition $cos(2\pi ft) = 0$ is satisfied, and at the end of the amplitude alteration the cylinder has to be in the position of $x= A_0$. At this instant the condition of $cos(2\pi ft) = 1$ is satisfied. In the further part of this study the effect of t_{min} is investigated. The end point of the alteration was fixed at t_{max}=205.2005 and parameter n is chosen to be n=0.024375. The starting point of the alteration t_{min} was varied between 0 and t_{max}.

In *Figures 4 and 5* the time-mean values of lift are shown for different t_{min} values. It can be observed that compared with *Figure 3(a)* the number of jumps is significantly smaller. In *Figure 4(a)* only two jumps occur. Increasing t_{min} the location of jumps from the upper state curve to the lower shift to higher amplitude values. *Figure 4(b)* shows that for t_{min}=133.3805, there is only one jump. For t_{min}=149.796 shown in *Figure 5(a)* two jumps occur again. However, in *Figure 5(b)*, there are no jumps at all, and the solutions lay on the lower state curve. This is probably due to the short alteration time, which in this case is only t_{max}-t_{min}=14.3635.

In *Figure 6* a comparison of the constant and altered amplitude solutions using the time-mean of lift and torque coefficients is shown. It can be seen that (1) the number of jumps is much smaller for the altered amplitude than for the constant amplitude case shown earlier, and (2) using the altered amplitude model the locked-in regime can be made substantially wider. In case of constant amplitudes, synchronization takes place between A_0=0.48–0.94, but with altering amplitudes this regime is almost twice as wide, A_0=0.48–1.31.

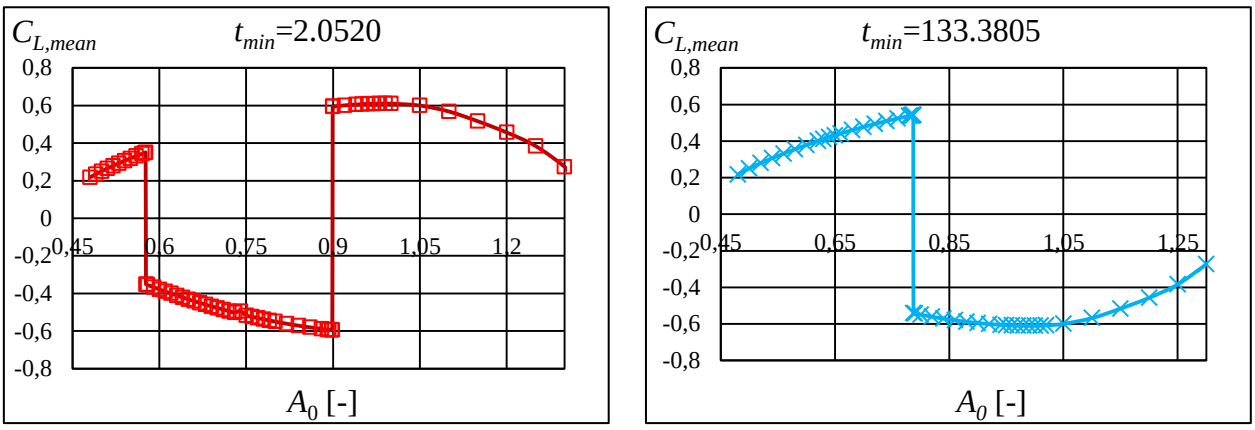

(a) (b)

Figure 4 Time-mean of lift vs. amplitude for (a) t_{min}=2.0520 (b) t_{min}=133.3805

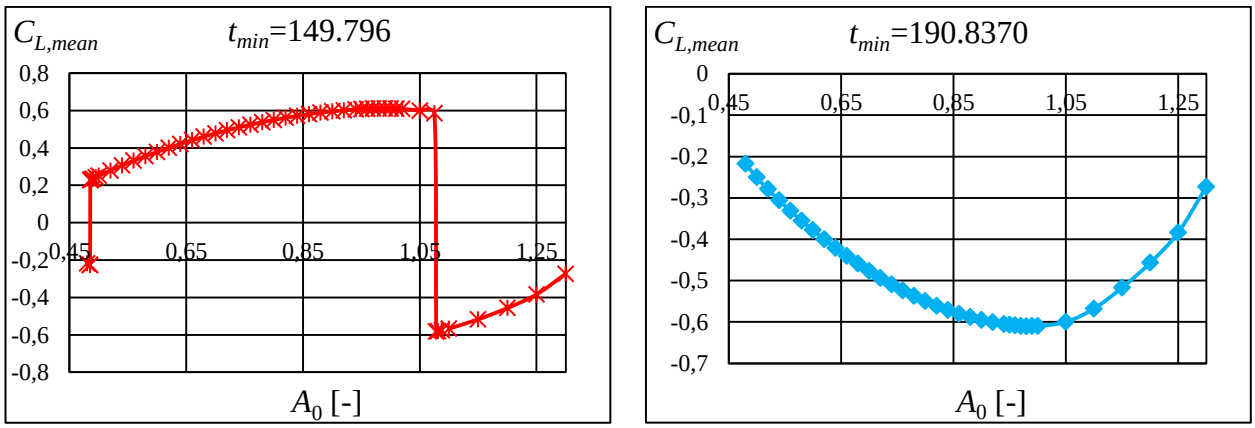

(a) (b)

Figure 5 Time-mean of lift vs. amplitude for (a) t_{min}=149.796 (b) t_{min}=190.8370

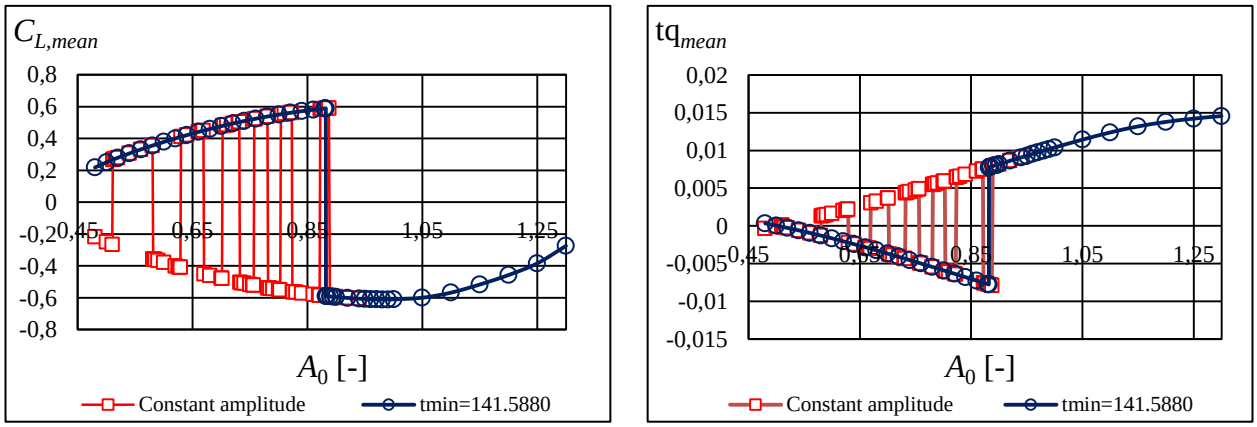

(a) (b)

Figure 6 Comparison of constant and altered amplitude solutions (a) lift and (b) torque

CONCLUSION

In this study the flow around a circular cylinder oscillated in-line with the main stream was investigated using a numerical approach. The time-mean values of the force coefficient were plotted against the oscillation amplitude. The comparison of the constant and altering amplitude solutions show that

1) using the constant amplitude model several jumps between the upper and lower state curves in the time-mean of lift and torque coefficients were identified, indicating switches in the vortex structure;
2) applying the altering amplitude model a maximum of two jumps was detected. For t_{min}=190.8370 no jump was observed, with all of the solutions staying on a single state curve;
3) the locked-in regime at constant amplitudes was A_0=0.48-0.94 and at altering amplitudes the synchronization regime extended considerably to A_0=0.48-1.31.

In the near future an investigation into the effect of initial conditions is planned.

REFERENCES

[1] Wootton, L.R.: *Resume on full-scale tests on oscillation of piles in marine structures.* Construction Industry Research & Information Association (CIRIA), 1972, London

[2] Nishihara, T., Kaneko, S., Watanabe, T.: *Characteristics of fluid dynamic forces acting on a circular cylinder oscillated in the streamwise direction and its wake patterns*. Journal of Fluids and Structures **20** (2005), 505–518.

[3] Cetiner O., Rockwell, D.: *Streamwise oscillation of a cylinder in a steady current. Part 1. Locked-on states of vortex formation and loading*. Journal of Fluid Mechanics **427** (2001), 1-28.

[4] Al-Mdallal, Q.M., Lawrence, K.P., Kocabiyik, S.: *Forced streamwise oscillation of a circular cylinder: Locked on modes and resulting fluid forces*. Journal of Fluids and Structures **23** (2007), 681-701.

[5] Leontini, J.S., Jacono, D.L., Thompson, M.C.: *A numerical study of an inline oscillating cylinder in a free stream*. Journal of Fluid Mechanics **688** (2011), 551-568.

[6] Baranyi, L., Huynh, K., Mureithi, N.W.: *Dynamics of flow around a cylinder oscillating in-line for low Reynolds numbers*. Proc. FEDSM2010-ICNMM2010 ASME Conference 2010, Montreal, Québec, Canada, (2010), on CD ROM, pp. 1-10, Paper No. FEDSM-ICNMM2010-31183

[7] Baranyi, L.: *Sudden and gradual alteration of amplitude during the computation for flow around a cylinder oscillating in transverse or in-line direction*. Proc. PVP2009 ASME Conference 2009 Prague, (2009), on CD ROM, pp. 1-10, Paper No. PVP2009-77463

[8] Baranyi, L.: *Numerical simulation of flow around an orbiting cylinder at different ellipticity values*. Journal of Fluids and Structures **24** (2008), 883-906.

[9] Strogatz, S.H.: *Nonlinear Dynamics and Chaos***.** Cambridge, MA, Westview Press, 1994.

[10] Posdziech, O., Grundmann, R.: *A systematic approach to the numerical calculation of fundamental quantities of the two-dimensional flow over a circular cylinder*. Journal of Fluids and Structures **23** (2007), 479-499.

INTERNATIONAL SCIENTIFIC CONFERENCE ON ADVANCES IN MECHANICAL ENGINEERING
13-15 October 2016, Debrecen, Hungary

GENERATION AND ANALYSIS OF A NEW HOURGLASS-LIKE WORM GEARING

[1]*DUDÁS László PhD*

[1]*University of Miskolc*
E-mail: iitdl@uni-miskolc.hu

Abstract
The paper introduces a new type gearing. This type characterised by a hourglass form worm and the mating worm gear, but the generation of the worm and the properties of the mating are different from the well-known globoid gearing features. The advantage of the gearing is that the worm generation can be performed on a normal lathe and does not apply circular motion of the generating edge. Instead a linear motion used, but it is not parallel to the axis of the worm. The form of the worm is a hyperbolic surface of revolution. The paper presents the applied generation method, the used coordinate systems and the generation of the worm gear. The analysis of the mating accomplished by the Surface Constructor software application reveals the characteristic lines of the mating surface pair. A short comparison to globoid and to cylindrical drives is also included in the paper.

Keywords: *Hourglass-like worm, worm generation, globoid gearing, mating properties.*

1. INTRODUCTION

The advantageous and disadvantageous properties of globoid gearing are well-known. Among the advantages the long summated contact lines, the large load capacity, the robustness, the small wear and the precise motion transfer can be mentioned. The known disadvantages are the high cost of the machining because of the required excellent precision, the need of special teething machine and the expensive assembly process can be mentioned. The original Cone- or Hindley-type worm gear shown in *Figure 1* suffered from undercut on the surface of the gear and from a surface-edge contact [1].

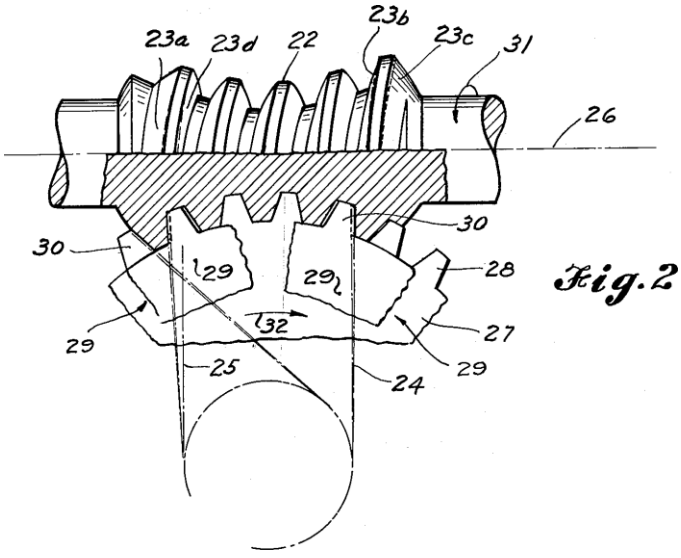

Figure 1 The circular motion of the generating edge in case of Cone-type globoid worm [1]

The improved constructions decreased or eliminated this drawback, like the Wildhaber shaping [2], moreover special machining-oriented constructions that applied rotary tool for generation of the worm surface instead of a discrete edge made possible grinding in the finishing process resulting in improved mating properties, surface quality and precision such a way [3]. See *Figure 2*.

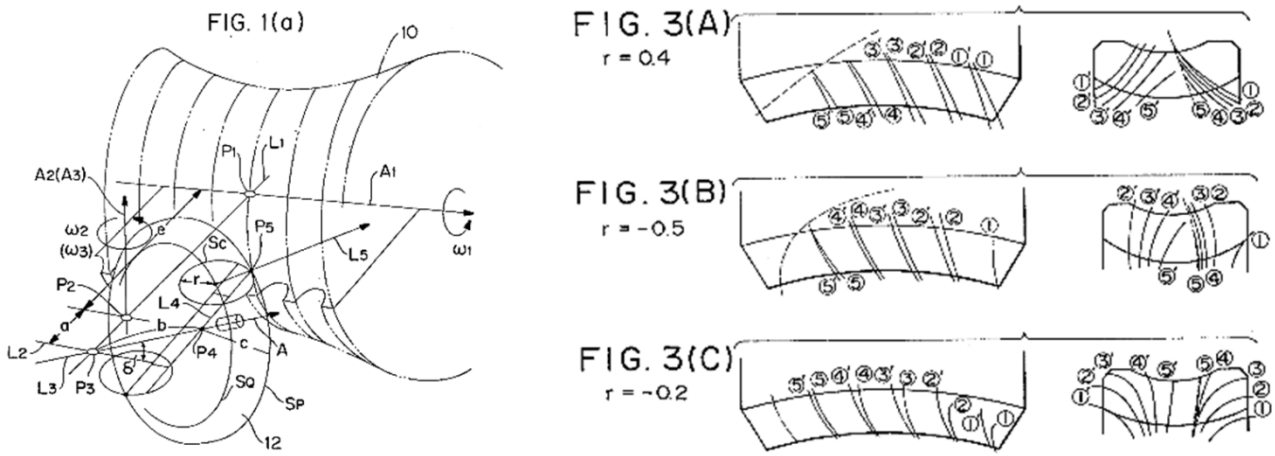

Figure 2 Globoid worm generation method suggested by *Kobayashi* and the improved characteristic lines [3]

But all these types require the special circular motion of the tool that means applying special teething machine for producing the worm. The cutting of the gear can be made using normal hobbing using radial feed in the process.
Lunin from the ZAKGEAR presented interesting new constructions that apply skew axes and hyperbolic surface of momentary axes, so axoid, see *Figure 3*. These complicated constructions have extremely long summated contact lines and costly manufacturing properties [4].

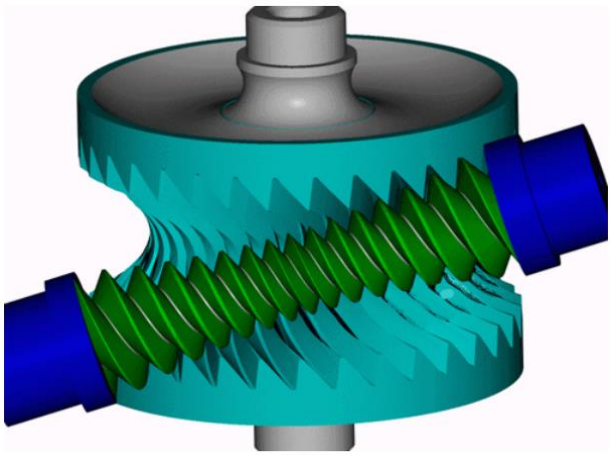

Figure 3 Lunin's special drive characterised by skew axes and hyperbolic axoids [4]

The expensive producing of the mentioned worms induced the development of a substituting cutting process that can be performed on a normal lathe using an additive fixture and simple cutting methods. This new technology also includes the possibility of applying the modern generating

methods of the worm that use surface of revolution shaped tools, like disk form milling cutters and grinding wheels.
The paper will introduce the inexpensive generating method of the worm, the enveloping process of the worm gear and the analysis of the mating properties through the form and wandering of the characteristic lines. For all these processes the Surface Constructor kinematical modelling and surface generator software tool will be used [5]. Short listings of the advantages and disadvantages of the proposed new gearing type are also included in the content of the analysis with an inclusive comparison to globoid and cylindrical worm gearings. The concluding remarks will close the paper.

2. THE QUASI-GLOBOID WORM GEARING

The generation of the worm surface and the enveloping of the worm gear will be presented in this section.

Worm surface generation

The surfaces of the worm are swept by the edge of the cutting tool as shown in *Figure 4* in two views. The co-ordinate system of the worm is CS100, while the edges of the cutting tool are given in the CS70 co-ordinate system. The tool moves along the z70 direction and sweeps the tooth surfaces of the worm. The hyperbolic head surface is generated with similar motion.

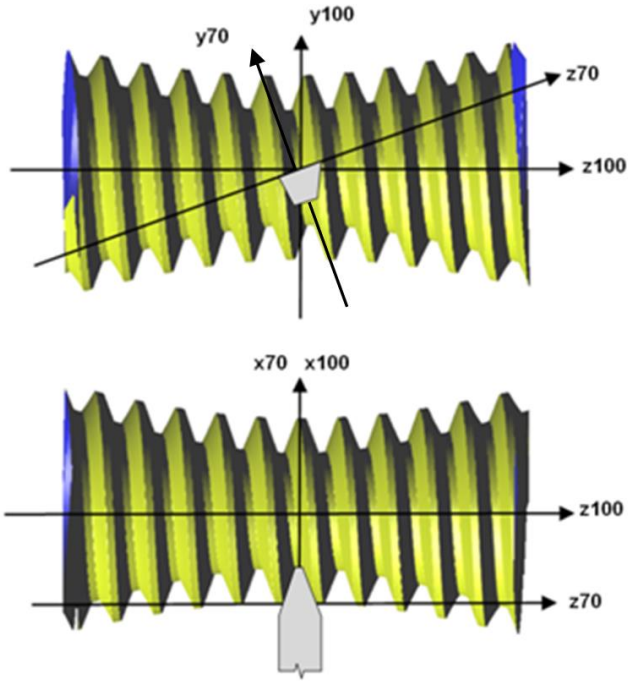

Figure 4 The generation of the tooth surface of the worm

In the practice an additional machine part applied that makes possible to set the rotational angle of the workpiece in the angle of z70-z100 axes and to hold it between a live centre and a dead centre. The driving comes from the main spindle through a Cardano-type mechanism providing errorless angle speed transfer.

Worm gear surface generation

The worm gear working tooth surface is enveloped by the worm surface. The relative position of the worm and worm gear is sketched in *Figure 5*. The co-ordinate system CS100 holds the worm while CS230 frame is fixed to the worm gear surface. The CS201 co-ordinate system is connected to the housing. The figure shows only a three teeth segment of the gear.

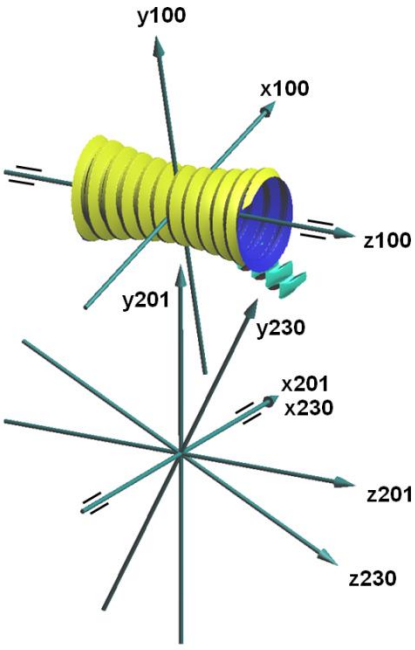

Figure 5 The applied co-ordinate systems for the gear teeth enveloping process

As every tooth of the gear has same geometry, only three of the 82 teeth were generated. The resulted in segment can be seen in *Figure 6*.

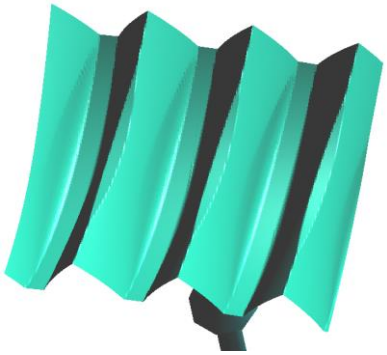

Figure 6 Teeth of the gear

The figure shows that the geometry of the prototype was not determined correctly because there is undercut at the dedendum of the gear. The diameter of the base circle has to be decreased. As this gearing was the first modelled version, it was very interesting what will the shape of the contact lines look like? As the form of the characteristic lines is very informative and determines the quality of the mating properties of the gearing, the next step was the analysis of them. For this three connecting moment was united to get a nine teeth segment of the gear.

3. ANALYSIS OF THE MATING PROPERTIES

The set of the characteristic lines are shown in *Figure 7*. It is a good property that every teeth of the worm is in contact with the gear. This feature reminds us to the globoid worms and means high load carrying capability, low wear and precise working. On the other side this property needs precise manufacturing and assembly in case of this type of gearing, similarly to globoid gearing.

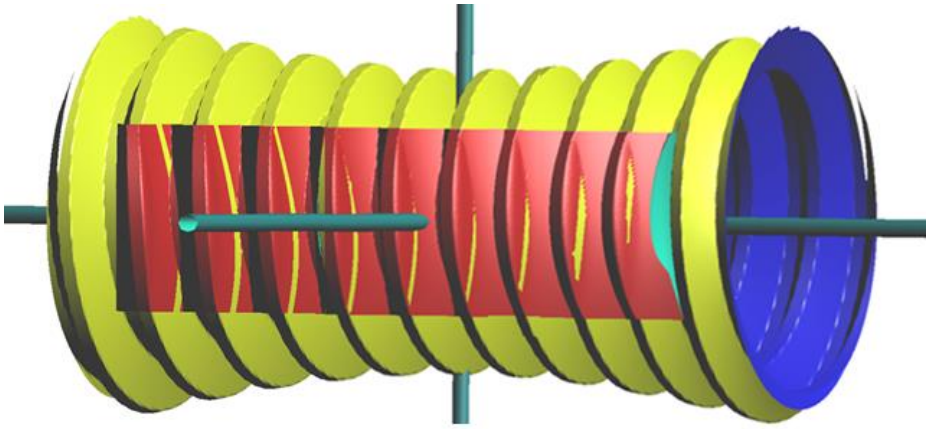

Figure 7 The contact lines shown from the inside of the gear

The tangential shape of the characteristic lines is not advantageous to provide loadable oil film, similarly to the contact lines of the cylindrical worm gearings that have linear tooth profile in the axial section. From the previous experience of the author is known that this drawback can be eliminated easily modifying the tooth profile section curve in the tilted x70-z70 plane. This easy modification possibility anticipates the possible use of all the advantageous modifications that were successful in case of cylindrical worm gearings. These modifications can be realised easily using the Surface Constructor kinematical modelling and surface generator software tool. The software proved its suitability for innovation of gearings many cases. The power of the application comes from its high level of modelling capabilities, the designer needs not performing any calculation, these accomplished behind the scenes, the designer can concentrate on the surfaces, kinematical relations, movements and animations, so can study and analyse the developed and investigated new gearing type. The application can visualise the modelled gearing in eleven windows, every window has own visualisation parameters and the motions can be animated in every window independently. This makes easy to analyse the features of the modelled gearing from different sights. Moreover it has special visualisation capabilities not detailed here to check for local undercuts. The numerical parameters of the model can be modified easily, moreover the kinematical model itself can be modified easily as the application uses symbolic representation of the surfaces and kinematical relations, so these can be entered with expressions. The Surface Constructor models the kinematical modelling process itself giving a maximum freedom for modelling. This can be checked in this case in Fig 8. where the software application is shown in the midst of the development. Previous modelling results were presented e.g. in [6].

CONCLUSIONS

The paper introduced a new worm gearing having hourglass-like worm. Despite of high similarity to globoid form, this type of worm can be generated without circular tool motion with a simple linear feed and as a consequence it can be produced even on a normal lathe equipped with a tilted

worm holder. The advantages and disadvantages of the gearing are similar to globoid drives, but it has additional advantages, like easy and cheap machining and the possibility of using the well-tried modification methods of cylindrical worm drives. In the future the improvement of the presented prototype construction will be accomplished and the effect of profile modifications on the characteristic lines will be analysed.

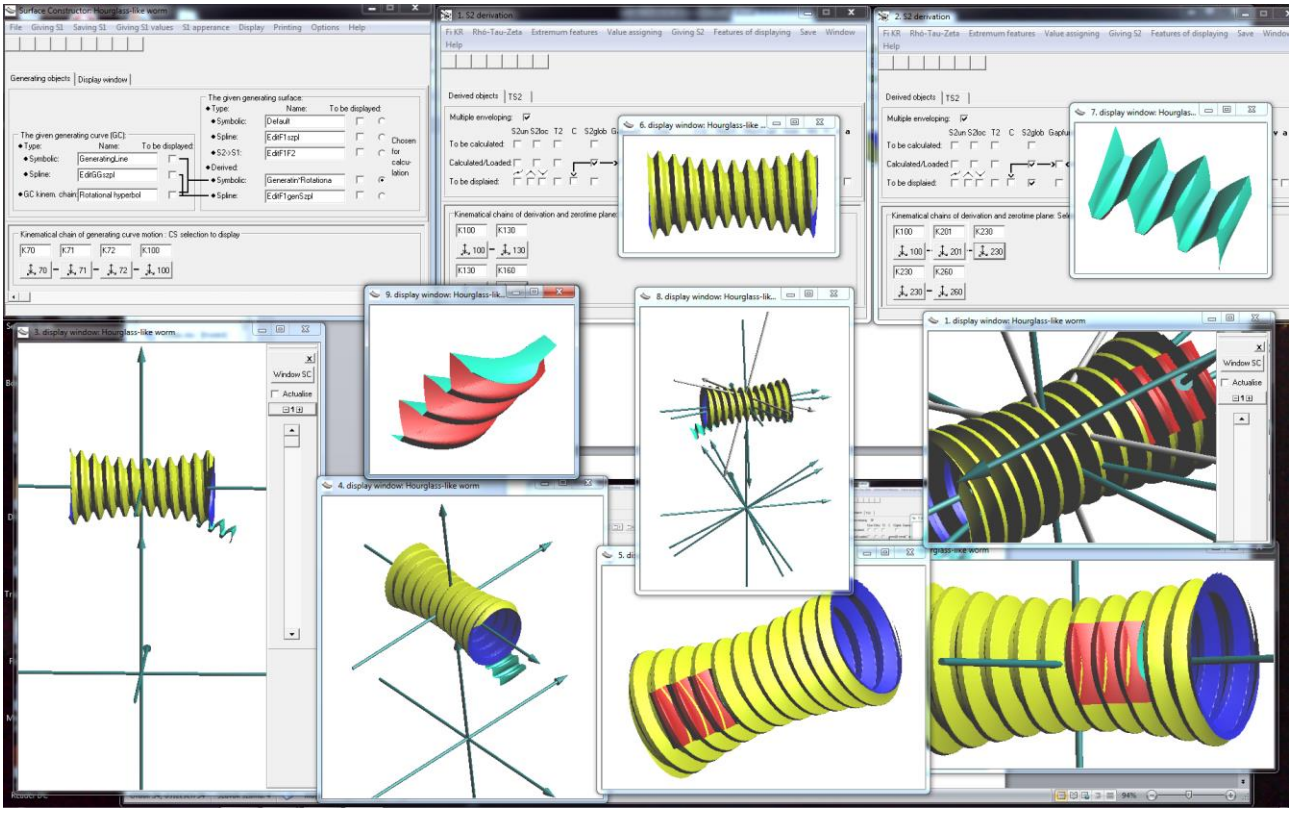

Figure 8 Snapshot of the computer screen in the midst of the analysis accomplished with Surface Constructor

ACKNOWLEDGMENTS

This research was partially carried out in the framework of the Center of Excellence of Mechatronics and Logistics at the University of Miskolc. The financial support is acknowledged.

REFERENCES

[1] Skog, G.: *Gear worm thread generating machine*. US 2756641 A patent, 1956.
[2] Wildhaber, E.: *Enveloping worm gearing*. US 2935886 A patent, 1960.
[3] Kobayashi, T.: *Hourglass worm gear*. US 5325634 A patent, 1994.
[4] Lunin, S. V.: *Globoid gear technology from ZAKGEAR* http://www.zakgear.com/Wormoid.html, Accessed: 10.10.2016.
[5] Dudás, L.: *Advanced Software Tool for Modelling and Simulation of New Gearings*. Int. J. Des. Eng. vol. 3, no.3, 289–310, 2010.
[6] Dudás, L.: *New Way for the Innovation of Gear Types*. Engineering the Future, L. Dudas (Ed.), InTech, 111–140, 2010.

INTERNATIONAL SCIENTIFIC CONFERENCE ON ADVANCES IN MECHANICAL ENGINEERING
13-15 October 2016, Debrecen, Hungary

DIVIDING BOX FROM 10 TO 210

ENYEDI László

Department of Mechanical Engineering, Faculty of Mechanical Engineering, Technical University of Cluj-Napoca
E-mail: evolventa2015@gmail.com

Keywords: *dividing box, gearbox, transmission ratio, dividing head, gear hobbing machine*

1. INTRODUCTION

This invention is registered at the Romanian State Office for Inventions and Trademarks the OSIM (Oficiul de Stat pentru Inventii si Marci) with Nr. a201400193 and was published in the Official Industrial Property Bulletin (BOPI), Patents Section Nr 9/2015 (RO-BOPI 9/2015) on page 16 and 17.

2. PRESENTATION

This is a gearbox with which is feasible 201 transmission ratio (i = ni/ne), (any whole number from 10 to 210, in arithmetical progression), using 3 gear shifters: M1, M2, M3 (*Figure 1*). On *Figure 2* you can see the kinematic diagram of the dividingbox. Here it is in neutral position, M1, M2, M3 gear shifters are in 0 position (*Figure 1*).

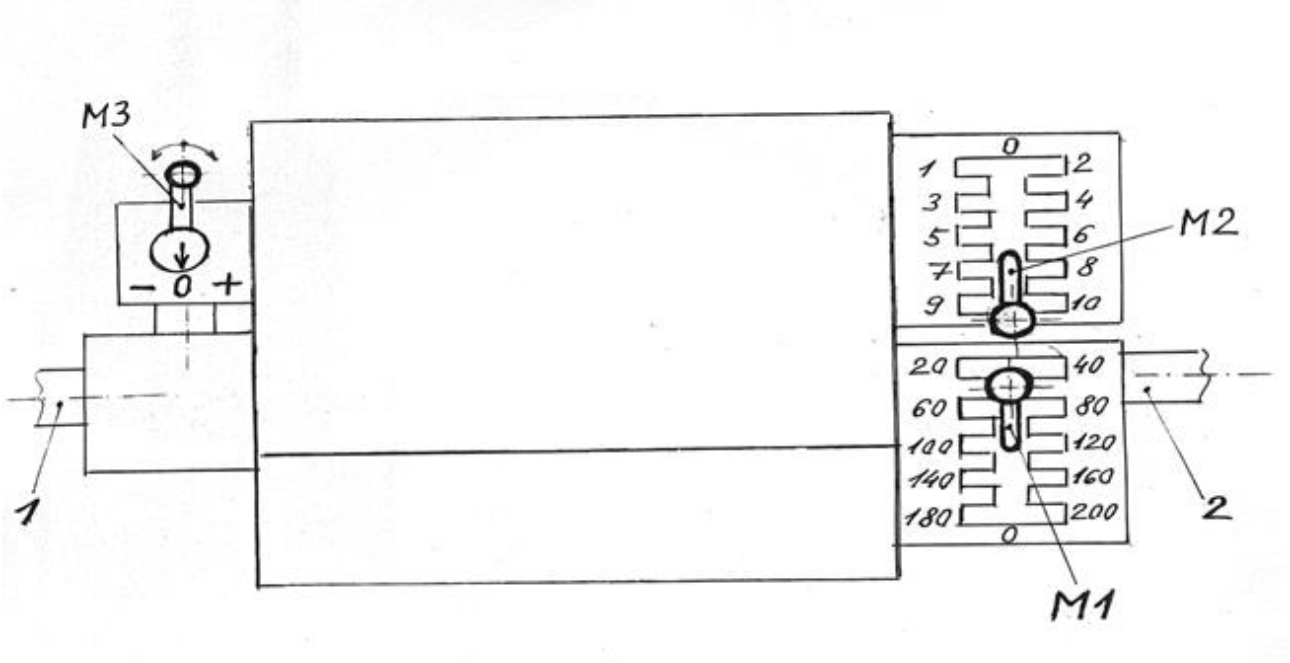

Figure 1

For **i = ni/ne = 20**, Z_{11} gear is engaged with Z_{21} gear, using M1 gear shifter (the 20 position on *Figure 1*)
For **i = 40**, Z_{12} gear is engaged with Z_{22} gear, using M1 gear shifter (the 40 position on *Figure 1*)

For **i = 60**, Z_{13} gear is engaged with Z_{23} gear, using M1 gear shifter (the 60 position on *Figure 1*)
For **i = 80**, Z_{14} gear is engaged with Z_{24} gear, using M1 gear shifter (the 80 position on *Figure 1*)
For **i = 100**, Z_{15} gear is engaged with Z_{25} gear, using M1 gear shifter (the 100 position on *Figure 1*)
For **i = 120**, Z_{16} gear is engaged with Z_{26} gear, using M1 gear shifter (the 120 position on *Figure 1*)
For **i = 140**, Z_{17} gear is engaged with Z_{27} gear, using M1 gear shifter (the 140 position on *Figure 1*)
For **i = 160**, Z_{18} gear is engaged with Z_{28} gear, using M1 gear shifter (the 160 position on *Figure 1*)
For **i = 180**, Z_{19} gear is engaged with Z_{29} gear, using M1 gear shifter (the 180 position on *Figure 1*)
For **i = 200**, Z_{110} gear is engaged with Z_{210} gear, using M1 gear shifter (the 200 position on *Figure 1*)

If the transmission ratio (i) is a different whole number than 20; 40; 60; 80; 100; 120; 140; 160; 180; 200 in the 10-210 interval, the differencial case will rotate.

For modification with **+1 or –1** any before mentioned transmission ratio, Z_{31} gear is engaged with - Z_{21} gear, using M2 gear shifter (the 1position on *Figure 1*).
For modification with **+2 or –2** any before mentioned transmission ratio, Z_{32} gear is engaged with Z_{22} gear, using M2 gear shifter (the 2position on *Figure 1*).
For modification with **+3 or –3** any before mentioned transmission ratio, Z_{33} gear is engaged with Z_{23} gear, using M2 gear shifter (the 3position on *Figure 1*).
For modification with **+4 or –4** any before mentioned transmission ratio, Z_{34} gear is engaged with Z_{24} gear, using M2 gear shifter (the 4position on *Figure 1*).
For modification with **+5 or –5** any before mentioned transmission ratio, Z_{35} gear is engaged with Z_{25} gear, using M2 gear shifter (the 5position on *Figure 1*).
For modification with **+6 or –6** any before mentioned transmission ratio, Z_{36} gear is engaged with Z_{26} gear, using M2 gear shifter (the 6position on *Figure 1*).
For modification with **+7 or –7** any before mentioned transmission ratio, Z_{37} gear is engaged with Z_{27} gear, using M2 gear shifter (the 7position on *Figure 1*).
For modification with **+8 or –8** any before mentioned transmission ratio, Z_{38} gear is engaged with Z_{28} gear, using M2 gear shifter (the 8position on *Figure 1*).
For modification with **+9 or –9** any before mentioned transmission ratio, Z_{39} gear is engaged with Z_{29} gear, using M2 gear shifter (the 9position on *Figure 1*).
For modification with **+10 or –10** any before mentioned transmission ratio, Z_{310} gear is engaged with Z_{210} gear, using M2 gear shifter (the 10position on *Figure 1*).

Depending of **+ or –** modification, Z_8 gear is sliding to engage with Z_9 gear using M3 gear shifter (+ and – position on *Figure 1*). And so, the differencial case will rotate with n_5 in the same direction or invers with n_i.

1. Example : i = 127

M1 is in the 120 position, M2 is in the 7 position and M3 is in + position. By that, Z_{16} engage Z_{26} , Z_{37} engage Z_{27} and Z_8 engage Z_9 , the differencial case will rotate with n_5 in the same direction with n_i

2. Example: i =113

M1 is in the 120 position, M2 is in the 7 position and M3 is in – position. In this situation the differential case will rotate with n_5 , invers like at i = 127.

3. Example: i = 210

M1 is in the 200 position, M2 is in the 10 position, M3 is in + position. By that Z_{110} engage Z_{210}, Z_{310} engage Z_{210} and Z_8 engage Z_9. The differential case will rotate with n_5 in the same direction with n_i.

3. UTILISATION

3.1 On the gear hobbing machine in the dividing Kinematic chain, because it does not need to change gears, depending the number of teeth that we have to mill.

3.2 On the dividing head and rotary table, because it does not need to use indexing plates. In all situations, indexing is 1 revolution on the input shaft ($n_i = 1$).

3.3 If we engage 2 dividing boxes (*Figure 3*), will work like a gearing (invisible gears).

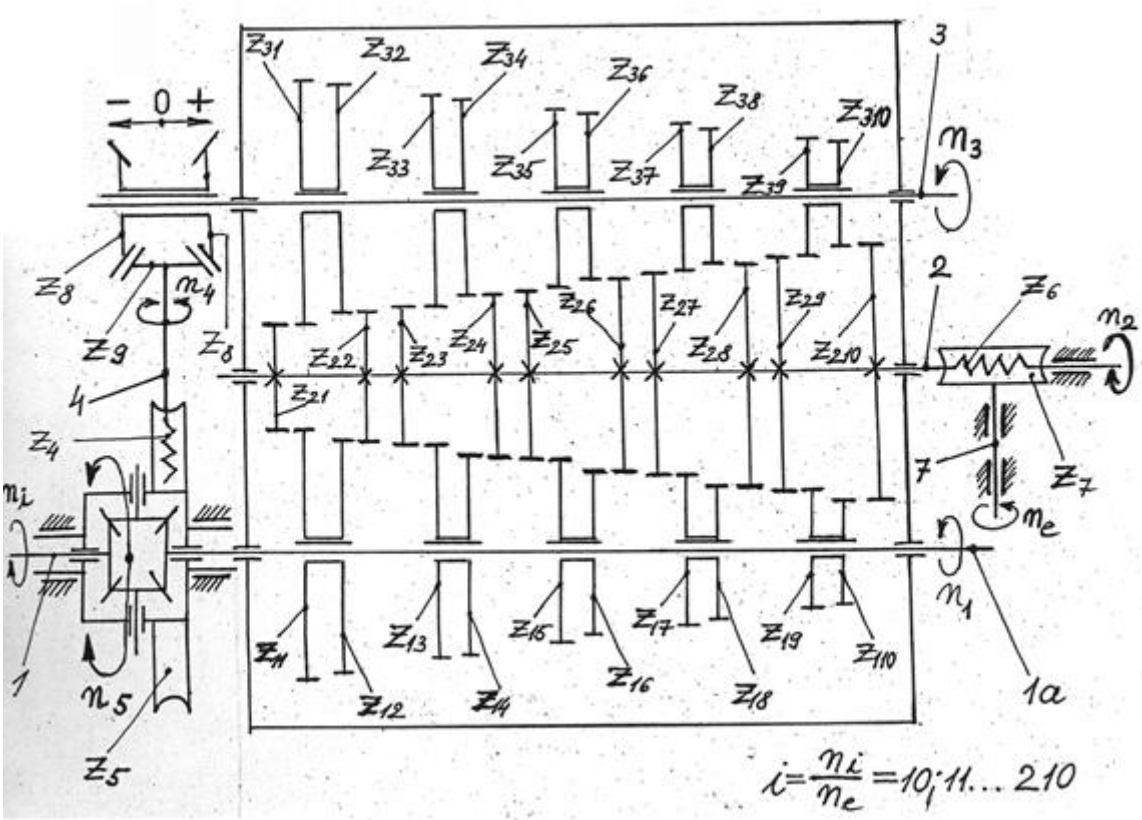

Figure 2

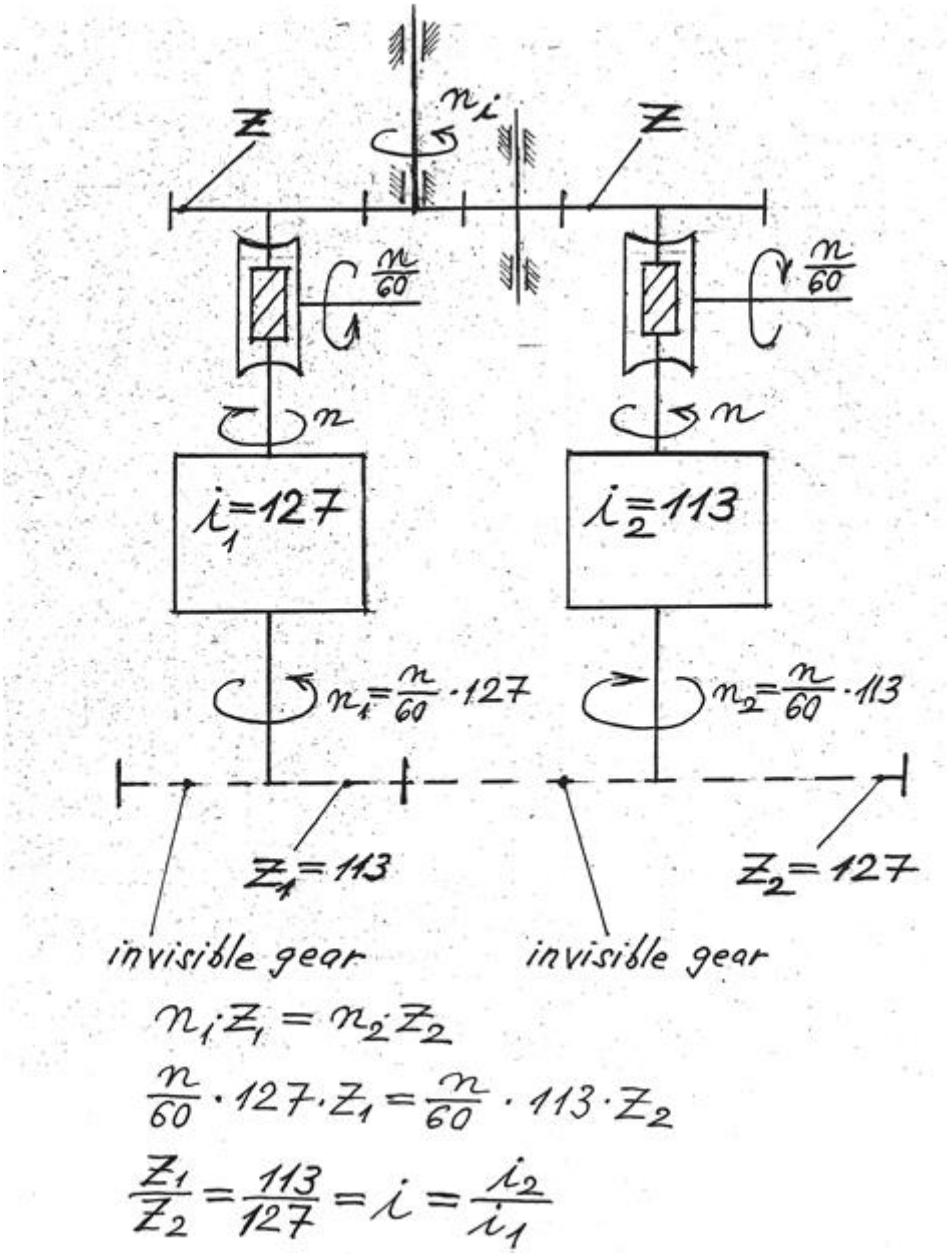
Z
n_i
Z
$\frac{n}{60}$
$\frac{n}{60}$
n
n
$i_1=127$
$i_2=113$
$n_1=\frac{n}{60}\cdot 127$
$n_2=\frac{n}{60}\cdot 113$
$Z_1=113$
$Z_2=127$
invisible gear
invisible gear
$n_1 Z_1 = n_2 Z_2$
$\frac{n}{60}\cdot 127\cdot Z_1 = \frac{n}{60}\cdot 113\cdot Z_2$
$\frac{Z_1}{Z_2}=\frac{113}{127}=i=\frac{i_2}{i_1}$

Figure 3

SMART LIVESTOCK FARMING
IN THE FOOTSTEPS OF INDUSTRY 4.0

[1]ERDÉLYI Viktor, [2]JÁNOSI László CSc

[1]Department of Mech. Eng. Faculty, Dept. of Mechatronics, Szent István University
E-mail: erdely.viktor@gmail.com
[2]Department of Mech. Eng. Faculty, Dept. of Mechatronics, Szent István University
E-mail: janosi.laszlo@gek.szie.hu

Abstract
Today, using smart technologies are very prosperous field in the industry. This paper highlights the possibilities of application of this smart concept in the field of Agriculture, based on the literature. As technology advances, the electromechanical systems are increasingly shifted toward mechatronics, since the electromechanical equipment slowly became more and more „intelligent". In a modern, complex agricultural facility we can find plenty of embedded systems, such as microcomputers, and microcontrollers. These autonomous units are the building blocks of a modern agricultural complex. However, these embedded systems has been used just in singular subdivisions of livestock farming, and they have not been connected to a bigger network. This paper presents the historical development of the synergistic cooperation of agriculture and mechatronics, highlights the current tendencies in the industry and adumbrates the possibly advantageous effects of these trends in the agriculture.

Keywords: *Smart Agriculture, IoT, Industry 4.0, Smart Farming, Agromechatronics*

1. INTRODUCTION

The aim of this paper is to investigate the possibilities of smart agriculture based on the industry 4.0 architecture, enumerating the today existing technologies, and to forecast the system structure of a future smart livestock farming system.

Nowadays – because of the overpopulation of the world - it is too pressing to permit a longer delay [10] mitigating food crisis. More than 1.9 billion people exists on the Globe of 6.7 billion who are suffering of malnutrition. The number of people existing near to critical starvation exceeds 600 million [15].

At a guess the population of the World could reach 9.6 billion inhabitants by the time 2050. This increase requires to enlarge the food production by 70 % [8] and still we will be able to keep only the present condition.

Besides we are in a shortage of food in the World we have less and less area where we could produce that [6]. The better utilization of arable land seems to be a good solution.

This paper highlights the already existing solutions of better utilization, and shows what is currently going on in the industry, to revolutionize the manufacturing.

Precision farming, animal husbandry and biomass usage are all distinct and long time researched

areas of the agriculture. These fields gained increased production very adequately [16]. However, in agriculture, there are no, or very little use of complex integrated solutions. All solutions focusing only a small part of the whole system [17-19].

Only Precision crop farming approaches to cloud thinking, but this also does not extend to the entire crop production sector.

2. METHODS

The acronym IoT comes from the English phrase; Internet of Things. This concept is still a little known idea, but it is very prospering one in industry, in particular. In another terminology IoT is the "Cyber Physical Systems" [2]. These two concepts have virtually the same meaning; cooperation among devices with its own "intelligence" connected in networks.

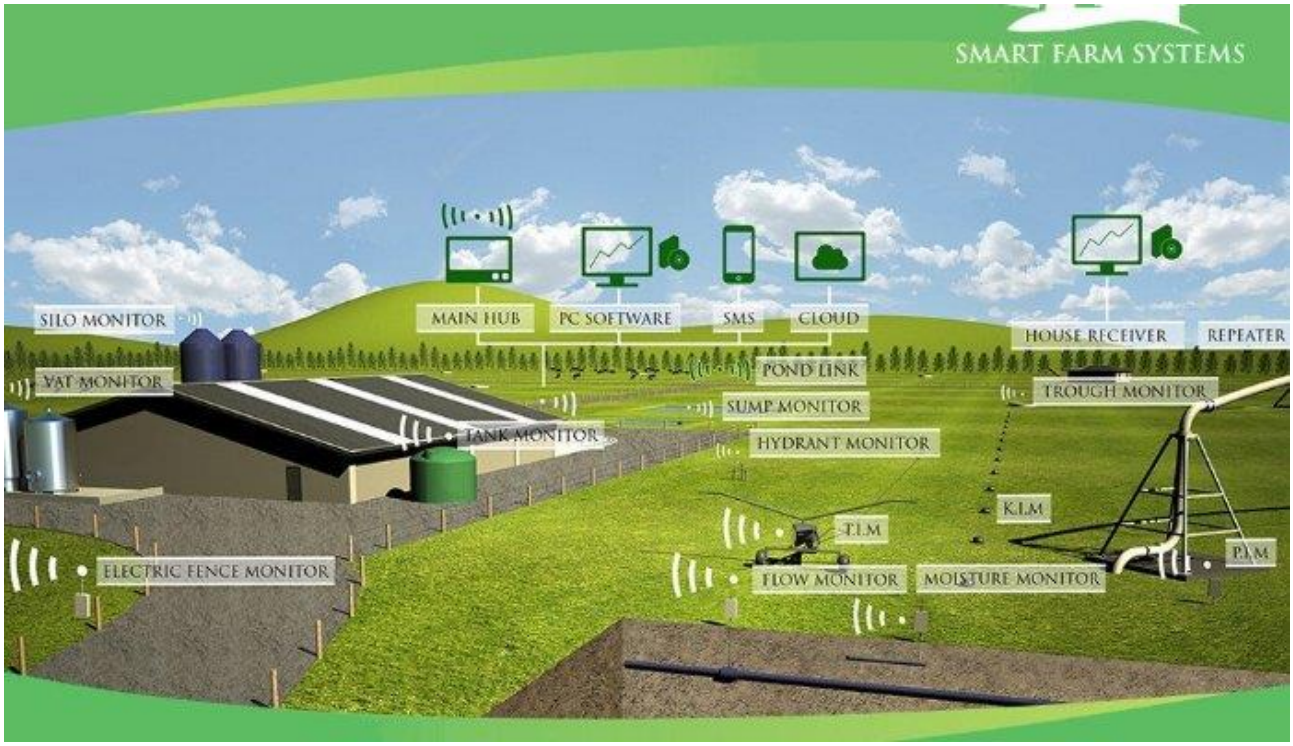

Figure 1 IoT, in Agriculture. Source: smartfarmsystems.co.nz [21]

The Internet of Things (IoT) is an umbrella term that covers a variety of typically interconnected network elements, as well as a network of sensors, and which is often uses cloud to compute the enormous amount of data, which is collected. (Cloud Computing, Big Data) [9] In fact IoT is a network between different physical network-compatible devices, and it does not necessarily include humans [11].

We can consider Internet of Things as a new paradigm, not only in agriculture, but in all fields of our life as well [7].

The usage of Internet of Things is widespread in the area of crop production. For example, there are plenty of wireless sensors to measure the moisture of soil, which are located like a grid on the agricultural lands. Or there is a network of weather forecasting stations of various points of some vineyards. But there are also more and more co-working machineries, which can be used for

ploughing, seeding or planting or fertilizing, and sometimes they are automatically controlled [13].

In contrast, in the Industry there is a huge movement towards manufacturing based on cyber-physical systems. This movement is powered mostly by the German Federal Government. The phrase, "Industrie 4.0" was shown on the Hannover fair in 2011. In 2016 whole Europe supported Industry 4.0. The main driving forces of the *fourth industrial revolution* are the artificial intelligence, robotics, and other advanced technological solutions, and naturally, the new business models that came possible by these technologies. Nowadays, the digital technology, and the network based productions are the key to stay alive in the market. The digitalisation of manufacturing, the M2M communication, the IoT can improve significantly the efficiency of the production [5].

In the agricultural field we could use some of the ideas and experience coming from the industry could be of assistance of building a new system in livestock farming. Many industrial examples show extraordinary data and could give assistance to the development.

In the western world, the greatest amounts of animal husbandry are poultrys (mainly chicken, broiler, and layer), cattle (meat, milk), and pigs (meat). We can distinguish several subtypes within these breeds as well (depending on the animal type; milk, meat, egg, breeding, or reproduction).

Cattle breeding is the simplest technically. The cattle are much less sensitive as poultry or pigs. This is especially true of the animal's babies. While the little chicken, and piglet needs very strictly controlled environment to survive, the calf is able to adapt its environment much better.

With the exception of cattle breeding there is almost no cold breeding, at least not in industrial grade production. Most livestock farms use barns to house the animals continuously. A modern livestock barn houses usually 1200-2500 pigs, or 25000-50000 broiler, or up to 250000 layer. The operation of these buildings are necessarily automated, or at least highly mechanized. Automated systems controlling the climate, lighting, feeding, watering, manure management, egg, and animal handling [20].

Although the stables were built to protect the animals against the effects of weather, today they are the criteria to gain high animal density. With higher animal density we should consider the increased humidity, temperature, carbon dioxide, and ammonia levels in the stables. To overcome these problems, there are many sophisticated solutions. The key element in these solutions to find the optimum between the conditions of animal growth and energy usage [1].

Feeding, medication, and watering systems can be very diverse. (Dry, wet, and liquid feeding.) Typically these in pork and poultry houses are automated, while in cattle husbandry are manual methods in use.

These systems (mainly in pork industry) are so automated, that the device can feed the animals separately. With this method the feed intake and the weight gain can be also monitored.

It can be seen, that in the livestock farming are already a lot of automated systems, however these are only dealing with unique tasks. Separately, we can talk major level solutions but these are not

connected to a network. According to the industrial example, they could be able to work together for a common goal significantly more efficiently if they were connected into a network.

As all major changes, the shift of agriculture to Cyber Physical space is accompanied by fears. One such fear is the cyber-crime. Obviously, if there is a large amount of data stored and processed in the cloud it can come in wrong hands, at least easier as if all these data would be stored offline or wouldn't be stored at all [14].

The other problem is with this enormous data collecting from various fields, that the data storage and process has to be enormous too. The rapid development of computing technology can't even keep up with the dramatically increased volume of data [4], so the solution can be the cloud computing, and cloud storages (many computers co-operation) [3].

3. RESULTS

It is clear, that in agriculture developers and researchers have only solved specific sub-tasks even under the umbrella of IoT.

In the Industry, this is a whole other story. In the industry they try to apply the idea of IoT to the whole system, including the supply chain, and even the end-users. This can be very perspective to agriculture as well, since agriculture is basically the same production system as the industry. In industry the use of IoT and mechatronic systems are very effective to build cyber physical systems, in order to gain more productivity, while lowering the stocks [12]. The base of the German initiatives development of industry 4.0 is to track the whole production from the suppliers to the end-users with using "smart" devices, and systems.

The global architecture of the smart pig farming should be like this. All of the elements, and subsystems have their own IDentification tag, which contains the capabilities of the system or sensor and the history and needs of the product. These components should connect via universal ports to each other and to the system, and this connection would be the key of the Plug and Produce concept.

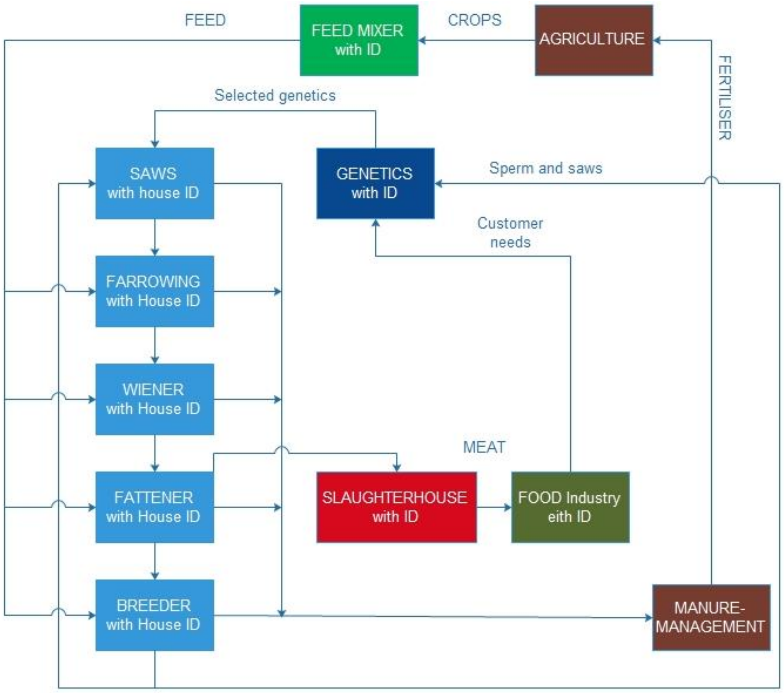

Figure 2 The structure of a subsystem

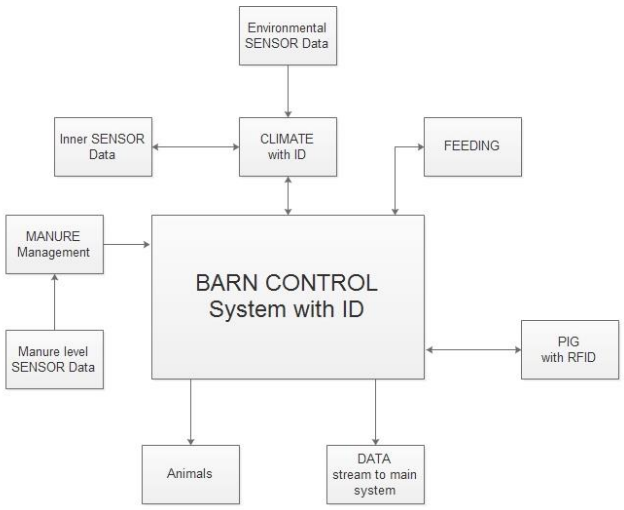

Figure 3 The structure of a subsystem

Figure 3. shows a more detailed view of one subsystem (presented on *Figure 2*). It is clear, that one subsystem has its own identification tag, but this subsystem contains more subsolutions, which are tagged as well. In that way, all subsystems could be tailor made.

The Pig itself can be observed, on Figure 4. as a member of the whole network. If the pig has its own identification tag, the pig can be kept by the individual demands of the customer. So the pig can be fed and be medicated individually and to some level it can be kept in unique environmental conditions. If all the parameters of these circumstances are stored in a cloud service, bonded to the pig's RFID tag, then the pig can be tracked down to its roots. This way we could produce meat based on customer's demands in automated mass production, which could lead to a massive improvement in the Input-Output balance.

Figure 4 Pig as the part of the network

CONCLUSIONS

Based on the literature, the crop farming side of precision agriculture is a well-developed, and researched field. Precision livestock farming however is not a well-researched field but it has serious potential in it.

The articles show the relationship between agriculture and mechatronics and clearly highlights that both in crop farming and livestock farming uses mechatronics in order to achieve better output rates, but industry 4.0 grade integration cannot be found. Although industry 4.0 is still in its infancy, has already achieved a several promising results, by integrating existing systems into larger systems and networks. Based on these observations, our main goal is to elaborate a system structure of livestock farming to achieve Industry 4.0 grade improvement in the field of agriculture.

REFERENCES

[1] Albright, L.D. (1990.): *Environment Control for Animals and Plants.* St. Joseph, ML: ASABE

[2] Baheti Radhakisan, Helen Gill. (2011): *"Cyber-physical systems."* The impact of control technology 12 pp.: 161-166.

[3] Christian Schulze, Joachim Spilke, Wolfgang Lehner, (2007.): *"Data modeling for Precision Dairy Farming within the competitive field of operational and analytical tasks,"* Computers and Electronics in Agriculture, pp. 39-55

[4] David Bradley, David Russell, Ian Ferguson, John Isaacs, Allan MacLeod, Roger White, (2015.):*"The Internet of Things – The future or the end of mechatronics,"* Mechatronics, pp. 57-74

[5] Dr Sipos Mihály (2016.): *A negyedik ipari forradalom – fel kell rá készülni!* Elektronet magazine

[6] EEA Report (2006): *Urban sprawl in Europe, The ignored challenge*, European Environment Agency Report, No 10 ISSN 1725-9177

[7] Eleonora Borgia, (2014.): *"The Internet of Things vision: Key features, applications and open issues,"* Computer Communications, pp. 1-31

[8] FAO (Food and Agriculture Organisation of the United Nations) (2015):2050: *A third more mouths to feed*

[9] Farah Hussein Mohammed, Roslan Esmail, (2013.): *"Survey on IoT Services: Classifications and Applications,"* International Journal of Science and Research, pp. 2124-2127

[10] Glaeser, Bernhard (1989*): Umweltpolitik zwischen Reparatur und Vorbeugung. Eine Einführunh am Beispiel Bundesrepublik im internationalen Kontext.* Westdeutscher Verlag GmbH. Oplade, p.14-15

[11] In Lee, Kyoochun Lee, (2015.): "*The Internet of Things (IoT): Applications, investments, and challenges for enterprises,"* Business Horisons, pp. 431-440, 2015.

[12] Jay Lee, Behrad Bagheri, Hung-An Kao (2015.): *A Cyber-Physical Systems architecture for Industry 4.0-based manufacturing systems* Manufacturing Letters. pp.: 18-23.

[13] Miao, Chaodong, (2015.):*"The Intelligent Supervision of The Agriculture Production Based on Internet of Things and Cloud Service Platform,"* International Conference on Information Sciences, Machinery, Materials and Energy,

[14] S. Sicari, A. Rizzardi, L.A. Grieco, A. Coen-Porisini, (2015.): *"Security, privacy and trust in Internet of Things: The road ahead,"* Computer Networks, pp. 146-164

[15] Szakály Sándor (2004): *Táplálkozási dilemmák és az élelmiszerek fejlesztésének világstratégiai irányai, Élelmiszer,* Táplálkozás és Marketing, Évf. 1, Szám 1-2.

[16] Tóth László (2002): *Elektronika és automatika a mezőgazdaságban* ISBN:9638617063

[17] Yao Shifeng,Feng Chungui,He Yuanyuan,Zhu Shiping (2011): *Application of IOT in Agriculture,* Journal of Agricultural Mechanization Research

[18] Yifan Bo, Haiyan Wang (2011): *The Application of Cloud Computing and the Internet of Things in Agriculture and Forestry*, Service Sciences

[19] Yuan Chen, Lihua Zheng, Changyi Xiao, Wei Yang, Minzan Li (2014): *An Information Acquisition System of Vegetable Safety Based on Web Service* American Society of Agricultural and Biological Engineers

[20] Zhang. Q. (20O3.): *Agricultural infotronic systems*. Resource. 10 pp.:29.

[21] http://www.smartfarmsystems.co.nz/images/hero-image-new.jpg

INTERNATIONAL SCIENTIFIC CONFERENCE ON ADVANCES IN MECHANICAL ENGINEERING

13-15 October 2016, Debrecen, Hungary

AN INSIGHT INTO NON-CONTACT ASSESSMENT OF HUMAN SKIN MICROCIRCULATION

[1]FINŽGAR Miha, [2]PODRŽAJ Primož PhD

[1]Faculty of Mechanical Engineering, University of Ljubljana
E-mail: miha.finzgar@fs.uni-lj.si
[2]Faculty of Mechanical Engineering, University of Ljubljana
E-mail: primoz.podrzaj@fs.uni-lj.si

Abstract
Many diseases have their origin in microcirculation. Therefore the assessment of human skin microcirculation, which is readily accessible and provides a representative index of microcirculation function, is of big clinical importance. In order to obtain objective results it is necessary to use methods, which do not additionally disturb the state of a human body. In order to achieve this the use of non-invasive and non-contact methods is mandatory. The aim of this article is to provide insight into these methods. Their improved versions will most likely play an important role in numerous disciplines outside clinical environment, where these methods are currently used.

Keywords: *microcirculation, skin blood flow, medical imaging, optical measurements*

1. INTRODUCTION

Numerous diseases as well as physiological aging are associated with changes in microcirculation [1]. Microcirculation is a term for blood vessels sized less than 100 μm in diameter in which exchange of numerous substances (e.g. nutrients and waste products) is taking place [2]. Assessment of microcirculation is defined by morphological and functional measurements [3]. The latter provide information about the endothelial function of microcirculation (by observing reactions to different provocation tests, e.g. pharmacological tests and post-occlusive reactive hyperaemia test), while the former include measurements of blood vessels density and diameter, rate of perfused vessels, blood flow velocity and blood cell concentration [3]. Accessibility and possibility of non-invasive approaches make human skin an important site for the assessment of microcirculation [4]. It has been shown that skin microcirculation can be used as a reliable model for the assessment of generalized microcirculatory dysfunction [5]. Numerous methods, from invasive to non-invasive, contact to non-contact and based on optical and non-optical principles have been developed in order to provide as much information about the observed microcirculation as possible. Out of all the proposed methods non-contact optical based methods seem to be the most promising, when it comes to the implementation of these methods outside the clinical environment. Absence of contact between probes and human skin additionally offers more objective assessment of human skin microcirculation: when pressure is applied to the skin vasodilation occurs [6]. This serves as a protective mechanism [6], but it changes the physiological state of human body and therefore biases the measurements.

2. LITERATURE REVIEW

2.1. Laser Doppler flowmetry

Laser Doppler flowmetry (LDF), also known as laser Doppler velocimetry or laser Doppler anemometry, systems can be divided into two categories: contact, probe-based systems (laser Doppler perfusion monitoring or LDPM) and non-contact imaging system (laser Doppler perfusion imaging or LDPI or LDI) [2]. When an incident laser beam hits the area of a skin, photons are scattered by static and moving particles present in the skin. Only moving particles (mainly red blood cells; hereinafter RBC) impart a Doppler frequency shift to the photons. The scattering angle, wavelength of incident light and the velocity of the scatterers are factors that determine this shift [7]. Laser Doppler methods do not offer absolute measurements of skin blood flow, but provide an index of skin perfusion (defined as the product of average RBC velocity and their concentration), known as flux [1, 8]. Flux is measured in arbitrary perfusion units or PUs, where 1 PU equals 10 mV [1]. It can also be expressed as cutaneous vascular conductance or CVC (ratio of flux and arterial pressure) [9]. It is however possible to obtain speed distributions (in absolute units) by decomposition of spectrum of laser Doppler signal [7]. LDF is mostly used to assess microvascular reactivity by applying different provocation tests [1]. General disadvantages of LDF are [3, 10]: dependence of skin optical properties on perfusion signal, sensitivity to motion, arbitrary units, biological zero, no possibility of absolute measurements.

2.1.1. Laser Doppler perfusion imaging (LDPI) – conventional system

In general, LDPI consists of three basic elements: laser, scanner (lenses and mirror) and detector [11]. Laser beams are of low intensity and red or near-infrared spectra [11]. Light penetration into the skin is defined as the path at which intensity of incident light falls to 1/e [12]. Penetration depth can influence the output results and it depends on skin thickness, vascular geometry and distribution, tissue absorption and scattering characteristics, laser wavelength and configuration of the beam and detector [11]. The conventional LDPI technique is time consuming, due to mapping and long processing times, and the need for processing of raw data [3]. This results in low temporal resolution, which makes LDPI unsuitable for functional test. Times for LDPI were decreased with development of high-speed complementary metal-oxide semiconductor (CMOS) cameras and new mapping algorithms [2]. Measuring of large areas with good spatial resolution is possible, which results in good reproducibility [2]. Noise in the Doppler signal (biological zero), present even in complete occlusion of the flow is due to the local redistribution of cells [13] within the vessels and due to the Brownian motion [9].

2.1.2. Laser Doppler perfusion imaging (LDPI) - CMOS camera based system

In CMOS camera based LDPI systems the entire tissue of interest is illuminated at the same time which allows faster acquisition of the entire image of the tissue [2]. An important disadvantage of this technique is camera frame rate [2]. If it not sufficient, the expected perfusion value can be underestimated or it may even decrease when the velocity of the moving particles increases. There are various types of noise influencing CMOS based LDPI measurements: variations in background light intensity, common mode noise, shot noise and thermal noise [2].

2.2. Laser speckle contrast imaging

Laser speckle contrast analysis (LASCA), also known as laser speckle contrast imaging (LSCI) or laser speckle imaging (LSI), is a technique that uses coherent laser light for illumination and CCD camera for imaging of the tissue of interest. Speckle is a random pattern produced by scattered light

from illuminated optically rough surface [14]. When time-integrated image of a moving tissue is taken it is blurred, which appears as a reduction in the speckle contrast. Time analysis of speckle fluctuations therefore provides information regarding the motion of the scatterers. The main problem is the same as in the temporal frequency measurement techniques (e.g. laser Doppler) – relating the correlation time to velocity profile [2]. Obtaining this relation is influenced by the following parameters [2]: multiple scatter events, size, shape and spin of scatterrers, non-Newtonian flow etc. As a result LASCA relies on relative measurements, which are however obtainable in real-time [14].

2.3. Tissue viability imaging

In tissue viability imaging (TiVi), a digital camera equipped with polarization filters used for generation of cross- and/or copolarized images is used [2]. In order to obtain cross-polarized images, orthogonal polarization direction of filters is used. Light that is reflected from the surface does not depolarize, while highly scattered light does. Concentration of RBC can be assessed by subtraction of pixel intensity value in red channel from pixel intensity value in green channel (since RBC absorb more green light than red) [15]. This offers mapping of local RBC concentration in microcirculation of the observed tissue. Change of RBC concentration in short time is most likely associated with change of blood flow as a result of vasoconstriction or vasodilation. Blood flow changes associated with these two processes can be visualized and objectively quantified with TiVi [2].

2.4. Infrared thermography

Infrared thermography is used for the assessment of body functions related to the thermal homeostasis and temperature [16]. It is also suitable for the power spectral density analysis of arteriolar microcirculation in real time [16]. Periodic oscillations in microcirculation blood flow cause small temperature changes in the skin, which can be seen as oscillations of heat-emission intensity values. Two-dimensional maps of regional temperature distribution across the skin can be used as an indirect measure of skin blood flow [7]. Although, temperature oscillations fall behind the blood flow oscillations by 10-20 s [17], it is still possible to reconstruct skin blood flow based on temperature oscillations (value of correlation coefficient is up to 0.63 for digital skin blood flow [17]). The method is relatively easy to use and has good spatial resolution [7].

2.5. Imaging photoplethysmography

Imaging photoplethysmography (iPPG) is an optical method for detection of blood volume changes in microcirculation of an observed tissue [18]. With each heart beat the volume of blood in skin microcirculation changes, which results in different amounts of reflected light. Higher reflectance and consequent stronger iPPG signal are associated with smaller blood volume change. Non-cardiovascular changes in skin reflectivity might be a result of redistribution of blood in venous system [19]. A new model for light skin interaction in iPPG has been proposed recently [12], which might alter the generally accepted underlying mechanism of iPPG signal formation. For iPPG signal detection a light source and a digital camera are needed. Two important characteristics of this technique are that it can operate in environment with only ambient light [20] (no additional dedicated light is needed) and that even consumer grade digital cameras [20] or even smartphone cameras [21] can be used. Two main PPG modes exist [22]: transmission mode, in which the transmitted light is detected (the observed tissue is placed between light source and camera), and reflection mode, in which the reflected light is detected. The majority of the proposed iPPG systems operate in reflection mode system. Imaging photoplethysmography offers 2D mapping of iPPG signal [20] and relative assessment of blood flow with results comparable to LDPI [23].

Additionally, it also offers assessment of heart rate and heart rate variability [24, 25]. It has two very prominent disadvantages: sensitivity to lighting variation and to motion [26].

2.6. Non-optical methods

The majority of the non-optical non-contact methods for assessment of microcirculation (computer tomography, magnetic resonance, positron emission tomography, single photon emission computed tomography) are less attractive due to the use of contrast agents (labels) and/or ionizing radiation [2] and will not be discussed in this paper.

3. DISCUSSION

Literature review, focused on the non-contact methods for the assessment of human skin microcirculation, revealed important disadvantages of these methods. The first one is their sensitivity to motion. This can be reduced by tracking, lateral synchronization of consecutive frames [20], by using vacuum cushion for reducing motion of the subjects [27] etc. The second one is the lack of standardization and lack of absolute calibration of the signals, which prevents reliable comparison between different studies using the same measurement methods. Third one is lack of generally accepted data on agreement between different methods, however a lot of attempts have been done in this direction [2] (it is however possible for example to obtain with LASCA power spectrum equivalent to the one obtained with laser Doppler based methods by using multiple exposure [28]). Finally yet importantly, the presented methods differ in imaging resolution, sampling depth [7] and main output result, which must be taken into account when choosing the most appropriate system for the chosen application. Based on the literature review iPPG appears the most attractive, since it does not require dedicated lighting and is affordably priced, since it can work by using consumer grade digital cameras.

CONCLUSIONS

The field of non-contact assessment of human skin microcirculation offers promising methods for the implementation outside the research-based clinical environment. Out of all the presented methods it seems that iPPG is the most promising one. In order to implement iPPG or any other of the presented methods in as many fields as possible it would be necessary to reduce sensitivity to motion and ambient light variation. Additionally, standardization and absolute calibration of these methods should also be properly addressed.

REFERENCES

[1] Roustit, M., Cracowski, J.L.: *Non-invasive assessment of skin microvascular function in humans: an insight into methods*. Microcirculation, 19(1), 47-64., 2012.
[2] Leahy, M.J.: *Microcirculation Imaging*. John Wiley & Sons, 2012.
[3] Eriksson, S., Nilsson J., Sturesson C.: *Non-invasive imaging of microcirculation: a technology review*. Medical Devices (Auckland, N.Z.), 7, 445-452., 2014.
[4] Minson, C.T.: *Thermal provocation to evaluate microvascular reactivity in human skin*. Journal of Applied Physiology, 109(4), 1239-46., 2010.
[5] Holowatz, L.A.,Thompson-Torgerson C.S., Kenney W.L.: *The human cutaneous circulation as a model of generalized microvascular function*. Journal of Applied Physiology, 105(1), 370-372., 2008.
[6] Fromy, B., Abraham P., Saumet J.L.: *Non-nociceptive capsaicin-sensitive nerve terminal stimulation allows for an original vasodilatory reflex in the human skin*. Brain Research, 811(1-2), 166-168., 1998.

[7] Daly, S.M., Leahy M.J.: *'Go with the flow ': a review of methods and advancements in blood flow imaging.* Journal of Biophotonics, 6(3), 217-255., 2013.
[8] Leahy, M.J., et al.: *Principles and practice of the laser-Doppler perfusion technique*. Technology and Health Care, 7(2-3), 143-162., 1999.
[9] Cracowski, J.-L., et al.: *Methodological issues in the assessment of skin microvascular endothelial function in humans*. Trends in Pharmacological Sciences, 27(9), 503-508., 2006.
[10] Rajan, V., et al.: *Review of methodological developments in laser Doppler flowmetry*. Lasers in Medical Science, 24(2), 269-283., 2009.
[11] Hayat, M.A.: *Cancer imaging: Lung and breast carcinomas*. Academic Press, 2007.
[12] Kamshilin, A.A., et al.: *A new look at the essence of the imaging photoplethysmography*. Scientific Reports, 5, 10494., 2015.
[13] Zhong, J., et al.: *A mathematical analysis on the biological zero problem in laser Doppler flowmetry*. IEEE Transactions on Biomedical Engineering, 45(3), 354-64., 1998.
[14] Draijer, M., et al.: *Review of laser speckle contrast techniques for visualizing tissue perfusion*. Lasers in Medical Science, 24(4), 639-651., 2008.
[15] McNamara, P.M., et al.: *Tissue viability (TiVi) imaging: temporal effects of local occlusion studies in the volar forearm*. Journal of Biophotonics, 3(1-2), 66-74., 2010.
[16] Szentkuti, A., Kavanagh, H.S., Grazio S.: *Infrared thermography and image analysis for biomedical use.* Periodicum biologorum, 113(4), 385-392., 2011.
[17] Sagaidachnyi, A.A., et al: *Correlation of skin temperature and blood flow oscillations*. Saratov Fall Meeting 2011: Optical Technologies in Biophysics and Medicine XIII, 83370A-83370A., 2012.
[18] Challoner, A.: *Photoelectric plethysmography for estimating cutaneous blood flow*. Non-invasive physiological measurements, 1, 125-151., 1979.
[19] Aarts, L.A., et al.: *Non-contact heart rate monitoring utilizing camera photoplethysmography in the neonatal intensive care unit - a pilot study.* Early Human Development, 89(12), 943-948., 2013.
[20] Verkruysse, W., Svaasand L.O., Nelson J.S.: *Remote plethysmographic imaging using ambient light*. Optics Express, 16(26), 21434-21445., 2008.
[21] Huang, R.Y., Dung L.R.: *Measurement of heart rate variability using off-the-shelf smart phones*. Biomed Engineering OnLine, 15(1), 11., 2016.
[22] Allen, J.: *Photoplethysmography and its application in clinical physiological measurement.* Physiological Measurement, 28(3), R1-39., 2007.
[23] Marcinkevics, Z., et al.: *Imaging photoplethysmography for clinical assessment of cutaneous microcirculation at two different depths*. Journal of Biomedical Optics, 21(3), 35005., 2016.
[24] Poh, M.Z., McDuff D.J., Picard R.W.: *Non-contact, automated cardiac pulse measurements using video imaging and blind source separation*. Optics Express, 8(10), 10762-10774., 2010.
[25] McDuff, D., Gontarek S., Picard R.: *Remote measurement of cognitive stress via heart rate variability*. Conference proceedings: 36th Annual International Conference of the IEEE Engineering in Medicine and Biology Society, 2957-29560., 2014.
[26] Kumar, M., Veeraraghavan A., Sabharwal A.: *DistancePPG: Robust non-contact vital signs monitoring using a camera.* Biomedical Optics Express, 6(5), 1565-1588., 2015.
[27] Millet, C., et al.: *Comparison between laser speckle contrast imaging and laser Doppler imaging to assess skin blood flow in humans*. Microvascular Research, 82(2), 147-151., 2011.
[28] Thompson, O.B., Andrews M.K.: *Tissue perfusion measurements: multiple-exposure laser speckle analysis generates laser Doppler-like spectra*. Journal of Biomedical Optics, 15(2), 027015., 2010.

INTERNATIONAL SCIENTIFIC CONFERENCE ON ADVANCES IN MECHANICAL ENGINEERING

13-15 October 2016, Debrecen, Hungary

TESTING ADHESION OF THE COATING WITH THIN LAYERS BY THE INCLINED CYCLIC IMPACT

[1]FLORESCU Virgil PhD, [2]CAPITANU Lucian PhD, [3]BADITA Liliana-Laura PhD

[1]Mechanical Engineering Department, Institute of Civil Engineering, Bucharest, Romania
E-mail: florescuvirgil@yahoo.com
[2]Tribology Department, Institute of Solid Mechanics of the Romanian Academy, Bucharest, Romania
E-mail: lucian.capitanu@yahoo.com
[3]National Institute of Research and Development in Mechatronics and Measurement Technique, Bucharest, Romania
E-mail: badita_l@yahoo.com

Abstract
In this paper, the authors try to evaluate some contact mechanism characteristics at the interface between a cylindrical indenter with spherical head that exercises repeated inclined impacts at an angle of 30^0 over some thin layers from TiN. The coatings with thin layers were obtained by laser pulses deposition process and had different thickness, depending on the number of pulses at that were made the coatings. Two impact testers were used, one at low frequency and other at high frequency. It was analysed the evolution of the failure process of coatings, as well as the appearance and development of critical events. By chance, after a cyclic inclined impact test at 30^0 over 10^4 cycles, it has produced a long imprint of wear, very similar to that obtained by another author, and declared as resulting as a consequence of an "inclined cyclic impact test with sliding".

Keywords: *TiN coating, PLD, inclined impact, failure process of coatings, inclined cyclic impact test with sliding*

1. INTRODUCTION

Pioneers of instrumented indentation technique, W. C. Oliver and G.M. Pharr introduced in 1992 the measuring of hardness and elastic modulus by instrumented indentation technique that was adopted and widely used in mechanical behaviour characterization of materials at the small scales [1]. Also, K.-D. Bouzakis et. al. [2] have examined the stresses – deformation laws of treated substrates by means of a finite element method (FEM) based on evaluation of the coating nano-indentation and adhesion results through the inclined impact test. The continuous improvement of technologies of PVD (physical vapour deposition), chemical or mechanical treatments of cemented carbide substrates, such as microblasting, have contributed to the significant growth of the cutting performance [3, 4]. Studying the effect of mechanical treatment on the topography of cemented carbide inserts and resistance properties of the surface, was polished micro-sandblasting substrates at different process pressures and roughness data, for two lengths of cutting. To count the stress – deformation laws and properties of hardness in the exposed layers of the material, the measurements were made of nano-hardness at different indent loads, and the corresponding results were evaluated using the methods described in [5].
In the nano-indentation procedures, because deviations of the indenter tip shape from its ideal geometry and indentation depth limited, the contact region between indenter and sample cannot be determined accurately [6]. Thus, the contact area between the indenter and sample during the phases

of loading and downloading of nano-indentation are defined by calculations based on FEM, thus allowing the determination of hardness from different methods. Methods used until now to assess the results of the nano-indentation to determine the hardness values are based on empirical equations describing the course of loading of indentation versus indentation depth during nano-indentation stages of loading [4] and unloading [6]. These methodologies involve among other things that the material under examination provides uniform mechanical properties compared to the depth of the indentation, which excluded the determination of hardness of thin films, due to the effects of the substrate, or materials with surface classified mechanical properties. The nano-deviations due to the limits of the accuracy of indenter manufacturing are difficult to accurately record. Even through the observations of atomic force microscopy (AFM) of the tip, real geometry cannot accurately be mathematically described and is treated as a spherical surface. The perpendicular impact test was documented as an effective and convenient methodological tool for the characterization of the fatigue properties of coatings. In addition, the cohesive and adhesive failure models of PVD coatings can be investigated by this test. Adhesion strength at coating - substrate was described in, through a simulation based on FEM, using the corresponding contact elements. In this paper we report about the testing in inclined cyclical normal impact or, with high frequency and the results obtained on two thin coatings deposited on SS316 stainless steel, medical grade. The authors try to evaluate some contact mechanism characteristics at the interface between a cylindrical indenter with spherical head that exercises repeated inclined at an angle of 30^0 and over some thin layers from TiN.

2. METHODS

To characterize the cohesion and adhesion strength of coatings, many tests of normal impact and inclined impact with a cylindrical pin with spherical head were made. Impact test is a more accurate simulation of a real situation that affects the life of the material. There are two common test procedures at multiple impact, namely the cyclic impact testing of low frequency and impact testing of high frequency. In this paper we report about a new setup for the cyclic impact testing, normal or inclined, with high frequency and the results obtained on three thin coatings of TiN deposited on stainless steel SS 316L, medical degree.
Samples used as substrates for TiN thin films deposition were 316L stainless steel discs with a diameter of 22.5 mm, height of 10 mm and hardness of 464 HV30. The hardness measured values of 316L stainless steel samples before coating and layers of TiN micro-hardness were:
- Sample TIN/316L stainless steel; 5000 pls: Substrate material hardness: 277; 299; 286 *HV* 5 gf, HV_5; Average hardness: 287 HV_5; Coating micro-hardness: 352; 345 *HV* 50 gf; Average micro-hardness: 348.5 $HV_{0.5}$.
- Sample TIN/316L stainless steel; 10000 pls: Substrate material hardness: 407; 429; 423 *HV* 5 kgf, HV_5; Average hardness: 420 HV_5; Coating micro-hardness: 532; 545 *HV* 50 gf; Average micro-hardness: 539 $HV_{0.5}$.
- Sample TIN/316L stainless steel; 20000 pls: Substrate material hardness: 453; 473; 423 *HV* 5 kgf, HV_5; Average hardness: 420 HV_5; Coating micro-hardness: 748; 727 *HV* 50 gf; Average micro-hardness: 737.5 $HV_{0.5}$.
In the case of the normal impact, where a target suffering from plastic straining, the largest part of the initial kinetic energy W_1 is dissipated in target, as mechanical work, W_p, with small amounts recovered by the elastic forces, at the kinetic energy of indenter W_2. In addition, a possible source of this energy loss seems to lie in the dissipation of energy into the test piece, in the form of elastic vibrations W_v caused by transient nature of collision. An expression of this energy can be written as follows:

$$W_1 = W_2 + W_v + W_p \quad (1)$$

W_v estimation was derived theoretically, assuming that contact pressure that acts on the contact area is constant and then:

$$W_v = \frac{\beta(1+\nu_d)}{\rho_d C_d^3} \cdot \left(\frac{1-\nu_d^2}{1-2\nu_d}\right)^{1/2} F_z^2 \omega_d \alpha \quad (2)$$

where:

$$C_d = \left(\frac{E_d}{\rho_d}\right)^{1/2};\ \omega_d = \frac{2\omega}{1+e};\ e = \left(\frac{W_2}{W_1}\right)^{1/2} \text{ and } \omega = \frac{\pi}{2t},$$

where ν_d is Poisson's ratio for substrate; ρ_d and E_d are the density and Young's modulus. F_z is the maximum load of normal impact, e is the coefficient of restitution, and t is the loading time obtained from the relation of the curve between load and time. β is a dimensionless amount which depends only on the Poisson's ratio. For $\nu = 0.25$, $\beta = 0.537$ and for $\nu = 0$, $\beta = 0.639$.
The scheme of the inclined impact exercised by a cylindrical pin made of Cr carbide, with spherical head of 3 mm diameter is presented elsewhere [7]. Normal force initially produces an elastic deformation of the coating and of the base material, which respond as a whole. To study the evolution of coating failure, an impact force (F_i) of 40 N has been applied, resulting in a compression component F_c ($F_c = F_i \cdot \cos 30^0 = 40$ N $\cdot$ 0.866 = 34.64 N) and a tangent component F_t ($F_t = F_c \cdot$ tg $30^0 = 40$ N $\cdot$ 0.5774 = 23.1 N), at 5 Hz and at three different impact cycles (200, 400 and 600). Appeared tangential force, (F_t) exerts an additional important stress on the ball-coating contact. The tangential force increases, as the angle of inclination is larger (*Figure 1*). *Figure 1* shows the forces that act upon the sample surface during cyclic impact with an inclination angle of 30^0 front of the sample surface.

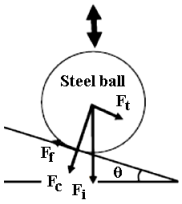

Figure 1 The forces that act upon the inclined cyclic impact plane.

In this situation, dislocation of the coating will take place, initially by agglomeration of its material in front of the contact mark, and then by piercing the coating and its removal by peeling. *Figures 2* show two images of this impact tester with mechanical driving (a), where the impact is applied to the sample with a Cr carbide pin with spherical head, clamped in a chucking (b).

(a)

(b)

Figure 2 Images of the impact tester with mechanical driving (a), where the impact is applied to the sample with a Cr carbide ball, clamped in a chucking (b).

For the impacts at very high frequency it was built another tester, that in principle consists in a *X* – *Y* table where a sample of different materials is fixed. The sample will be hit (impacted) by a large number of times, but always monitored by a cylindrical impactor, with spherical head, extremely hard, mechanically actuated by knocking with a hammer, presented elsewhere [7].

3. RESULTS

Figures 3 show the depths of some remaining craters on TiN/ SS316L determined by measurements of confocal 3D microscopy (left) and profilometry (right), depending on the duration of the impact.

10^4 impacts at 1400 N impact force; impact duration: 5 ms; scar depth: ≈ 1.75 µm

Figure 3 Depth of remaining crater on TiN/ SS316L determined by measurements of confocal 3D microscopy (left) and profilometry (right), depending on the duration of the impact

Primary data collected included measurements of volume and depth and radius ratio of the residual impact crater, h_r depth and residual radius of coating impact crater were measured directly from a cross topography image. Cross image, parallel to the *y* axis was taken into the impact crater center. To calculate the residual impact crater, have used primary data of the residual imprint impact profile. In this study was analyzed and a new method of testing reported in [8], the "cyclic inclined impact test with sliding", to investigate the failure behaviour of various types of biomaterials, (SS316L, Ti6Al4V and CoCr) with different coatings (TiN and CoCr), in terms of extremely high sliding contact dynamic stresses.
Figure 4 shows the registration curve of cyclic impact with sliding force depending on the time for one cycle, as in [8].

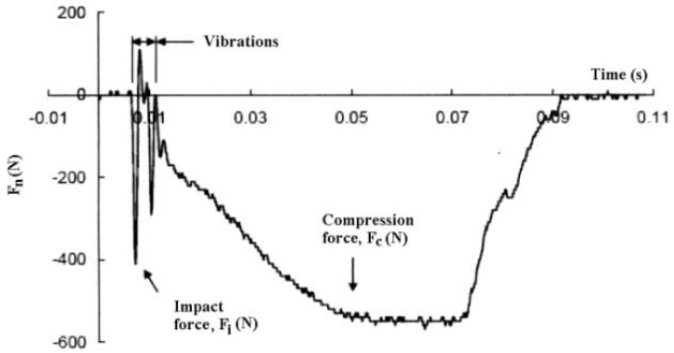

Figure 4 Time dependence of the impact force with sliding curve, for a cycle F_i / F_c = 40 N/34.64 N

The loading curve shows that there are three stages in each inclined impact cycle, i.e., that is the stage of the impact loading, vibrating stage and stage of static loading. After the stage of vibrations, the load continues to increase gradually up to the pre-configured load of compressing (F_c), and then the indenter began to move upward.

It was called the compression stage, in which was formed a long trace (tail) with sliding failures. When the indenter hits the surface of the test sample for the first time, it produces the first peak load, which is the effective impact load, F_i. Once the spherical indenter has completed his first complete contact with coating surface and formed an impact deep impact crater, the indenter had a recoil and again impact the sample. *Figure 5* shows the appearance of the impact and sliding imprint and the distribution of fatigue cracks on the coated surface, after 10000 impact cycles on the SS316L sample coated by the PLD procedure, at 10000 pls. Cross section diagram of the impact scar in the longitudinal direction is illustrated in *Figure 6* [7].

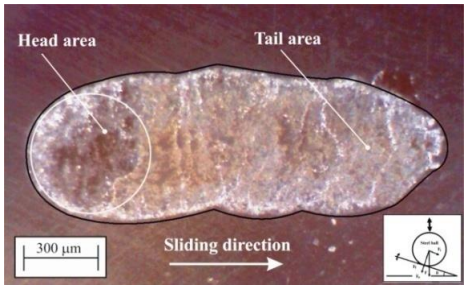

Figure 5 Microphotography of cyclic impact with sliding scar after 10000 inclined impacts at 30^0.

According to the loading curve in *Figure 4*, there are two peaks of signal monitored in vibrating stage, which means that there are two distinct impacts, before to be sliding wear. This is due to lack of the imposed stiffness of the ensemble impactor - sample, so that after the initial impact, the indenter continues to contact the sample. In this case, after the first full contact between the two surfaces has been completed, the sample has been pushed down and lost the contact with the spherical indenter. However, along with the continuing downward movement of the indenter, formed a second impact crater with a smaller diameter compared to the first, due to the decreasing impact energy. The longitudinal section scheme of the inclined cyclic impact at 30^0 imprint, adapted from [8], is presented in *Figure 6*.

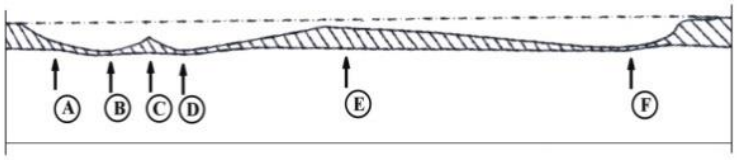

Figure 6 The longitudinal section scheme of the inclined cyclic impact at 30^0 imprint, that is presented in *Figure 5*, adapted from [8]

Due to of the tilted angle of the sample, area where is exerted the greatest impact force was not the focus in the centre of first impact crater, but it has gone slightly towards the head of the central area (point A). The normal component F_n of the impact force F_i, caused the bending stress on the edge of the impact - sliding scar, where they were seen in a series of severe cracks (point A). In the area located behind the centre of the first impact crater (point B), could be seen cohesive failures with a network of cracks due to elastic deformation of spherical indenter and combined results of the static friction force and normal component F_n of the impact force. Between the two impact craters, there is a ridge point C which delineates an area with fewer failures compared to adjacent areas B and D, because it has a lower bending deformation due to the "shots" of indenter. From *Figure 6*, it may be noted that there are a number of cracks formed in the D - E zone, which intersect with each other. Suppose that they were formed by bi-directional bending deformations in the overlapping impact

craters zone. There is no bending deformation in the initial part of the tail (point E). However, once the downward-moving of the spherical indenter, the normal component has kept growing following the load curve in the compression loading stage, until it reaches its maximum value (the point F) that is equal to the maximum compressive load, F_c (*Figure 4*).

CONCLUSIONS

It is very clear that the test of impact provides coatings with thin layers testing of materials (substrate) to moderate mechanical loadings similar of endoprosthesis, but also to large and very large loads, as in the case of tools for cutting and mining of constructions machines.
Wear mechanisms by impact of hard metallic coatings is a current concern regarding the process of breakage of the cover due to propagate cracks in severe wear conditions. However, research reports do not discuss how impact wear mechanisms of coating acts in mild conditions. In terms of impact, it is well known that plastic deformation should appear before impact wear. Impact with sliding stresses is a by chance case, due to situations in which there it has not provided the necessary structural rigidity of the indenter - sample. It cannot be considered to be an evaluation test, but a failed test by cyclically inclined impact at large angle.
In the case presented in this paper, the indenter with spherical head had a diameter of 3 mm and a length of 30 mm high, due to constructional constraints. This means a ratio between the width and height of 1/10. In this case, the impact on SS316L sample coated with TiN after 10000 inclined impacts at 30^0 caused that long imprint presented in *Figure 5*, due to the lack of stiffness of the indenter - sample assembly that allowed the indenter recoil after initial shot.

REFERENCES

[1] Oliver. W.C., Pharr. G.M.: *An improved technique for determining hardness and elastic modulus using load and displacement sensing indentation experiments*, Journal of Materials Research, 7, 1564-1583, 1992.
[2] Bouzakis, K.D., Skordaris, G., Michailidis, N., Asimakopoulos, A., Erkens, G.: *The Effect on PVD coated cemented carbide inserts cutting performance of micro-blasting and lapping of their substrates.* Surface & Coatings Technology 200 (1-4), 128-132, 2005.
[3] Toensoff, H.K., Mohlfield, A.: *Surface treatment of cutting tool substrates*. International Journal of Machine Tools and Manufacture, 38 (5-6), 469-476, 1998.
[4] Bouzakis, K.D., Michailidis, N., Hadjiyanis, S., Efstaniou, K., Erkens, G., Rambadt, S.,Wirth, I.: *Improvement of PVD coated inserts cutting performance, through appropriate mechanical treatments of substrate and coating surface*, Surface and Coatings Technologies, 146–147, 443-450, 2001.
[5] Bouzakis, K.D., Asimakopoulos, A., Skordaris, G., Pavlidou, E., Erkens, G.: *The inclined impact test: A novel method for the quantification of the adhesion properties of PVD films*, Wear, 262, 1471–1478, 2007.
[6] Bouzakis, K.D., Michailidis, N., Hadjiyanis, S., Skordaris, G., Erkens, G.: *The effect of specimen roughness and indenter tip geometry on the determination accuracy of thin hard coatings stress–strain laws by nanoindentation*, Materials Characterization 49, 149-156, 2002.
[7] Tiganesteanu, C., Capitanu, L., Badita, L.L.: *Optimizing the relationship between hardness and modulus at cohesion and adhesion of thin coatings by cyclic inclined impact test*, Proceedings SISOM 2015, Bucharest, 309-321.
[8] Ying, C., Nie, X.: *Study on fatigue and wear behaviours of a TiN coating using an inclined impact-sliding test*, Surface and Coatings Technologies, 206, 1977–1982, 2011.

INTERNATIONAL SCIENTIFIC CONFERENCE ON ADVANCES IN MECHANICAL ENGINEERING

13-15 October 2016, Debrecen, Hungary

PROTOTYPE BATTERY ELECTRIC CAR DEVELOPMENT FOR SHELL ECO-MARATHON® COMPETITION

[1]GÁBORA András, [2]MAGYARI Attila, [3]VARGA Tamás Antal, [4]BALÁZS Dávid, [5]LEMPERGER László, [6]IGAZ Tamás, [7]DIÓSI István, [8]VESZELSZKI Krisztián József, [9]SIMON Attila, [10]JAKABÓCZKI Gábor, [11]NÉMETH Anikó Barbara, [12]KOVÁCS Viktória Ilona, [13]LOVADI Gyula Dávid, [14]ZILAHI Krisztián László, [15]SIPOS Kristóf Balázs

[1,2,3,5,6,8,13]Department of Mechanical Engineering, University of Debrecen, Hungary
andrasgabora@eng.unideb.hu
[4,9,10,14,15]Department of Electrical Engineering and Mechatronics, University of Debrecen, Hungary
bal.david.94@gmail.com
[7]Department of Engineering Management and Enterprise, University of Debrecen, Hungary
istvan.diosi87@gmail.com
[11,12]Department of Civil Engineering, University of Debrecen, Hungary
nemethniko942@gmail.hu

Abstract
Shell Eco-marathon is a unique competition that challenges students around the world to design, build and drive the most energy-efficient car. With three annual events in Asia, Americas and Europe, student teams take to the track to see who goes further on the least amount of fuel. This paper summarize the most of technical expectations to participate at the competition.

Keywords: *prototype, electric, efficient, car, competition*

1. INTRODUCTION

This unique competition brings together around 200 teams and 3,000 students from across Europe to battle for ultra energy efficiency on the road. In 2016, Shell Eco-marathon Europe was in London, UK at the Queen Elizabeth Olympic Park from June 30 to July 3rd.

2. VEHICLE DESIGN

The drive train in the 'Battery Electric' category is restricted to a maximum of one electric storage device, and up to two electric motors, with associated control units. The electric motors may be purchased, purchased-and-modified, or purpose-built. The motor controller must be purpose-built for the Shell Eco-marathon. Only Lithium-based batteries are permitted as electric storage devices. The vehicle must be equipped with a Battery Management System (BMS) to control and protect the battery against risk of fire. All vehicles must be equipped with one joulemeter located between the battery and the motor controller to measure the vehicle propulsion energy consumption. A successful run will be classified in descending order of fuel economy, expressed in km/kWh.
During vehicle design, construction and competition planning, participating Teams must pay particular attention to all aspects of safety. Prototype vehicles must have three or four running wheels. Any sharp points must have a radius of 5 cm or greater, alternatively they should be made of foam or similar deformable material. Vehicle body panels must be rigid with an appropriate stiffness not to be prone to changing shape due to wind. Windows must not be made of any material which may shatter into sharp shards. All objects in the vehicle must be securely mounted. All

vehicles must have a solid floor and frame that prevents any part of the driver's body from contacting the ground. All vehicles must be fully covered. Open top vehicles are not allowed. The vehicle chassis must be equipped with an effective roll bar that extends 5 cm around the driver's helmet when seated in normal driving position with the safety belts fastened. Any roll bar must be capable of withstanding a static load of 700 N (~ 70 kg) applied in a vertical, horizontal or perpendicular direction, without deforming. A permanent and rigid Bulkhead must completely separate the vehicle's propulsion and energy storage systems from the driver's compartment. This bulkhead must be of fire retardant material and construction. The Driver must have access to a direct arc of visibility ahead and to 90° on each side of the longitudinal axis of the vehicle.

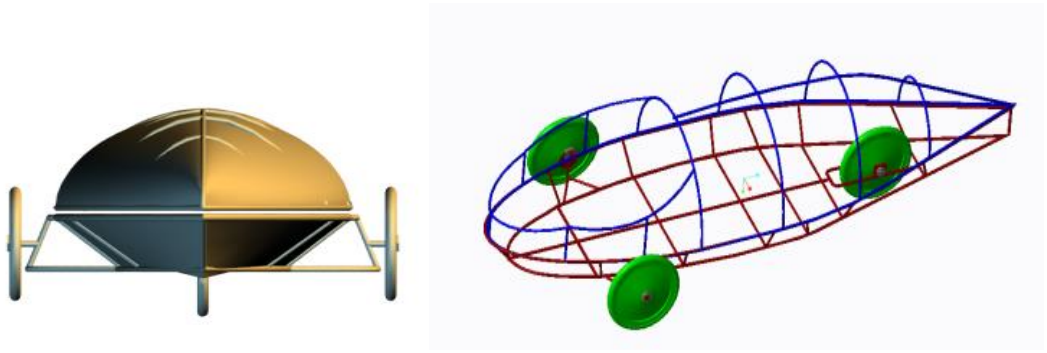

Figure 1 Perspective and frame design

The vehicle must be equipped with a rear-view mirror on each side of the vehicle, each with a minimum surface area of 25 cm² (e.g. 5 cm x 5 cm). In technical inspection visibility will be checked in order to assess on-track safety by using 60 cm high poles spread out every 30° in a half-circle, with a 4 m radius in front of the vehicle. The five independent belts must be firmly attached to the vehicle's main structure and be fitted into a single buckle, specifically designed for this purpose. It is imperative for Drivers, fully harnessed, to be able to vacate their vehicles at any time without assistance in less than 10 seconds. Each vehicle must be equipped with an electric horn mounted towards the front of the vehicle, in such a manner that is effectively audible to other vehicles and track marshals. With the vehicle in normal running condition, it must emit a sound greater than 85 dBA when measured 4 meters horizontally from the vehicle. Only front wheel steering is permitted. The turning radius must be 8 m or less. The external wheel of the vehicle must be able to follow a 90° arc of 8 m radius in both directions. Vehicles must be equipped with two independently activated brakes or braking systems; each system comprising of a single command control. One system has to act on all front wheel(s), the other on all rear wheel(s). In addition, the right and left brakes must be properly balanced. For safety reasons, the maximum voltage on board of any vehicle at any point must not exceed 48 Volts nominal and 60 Volts max.

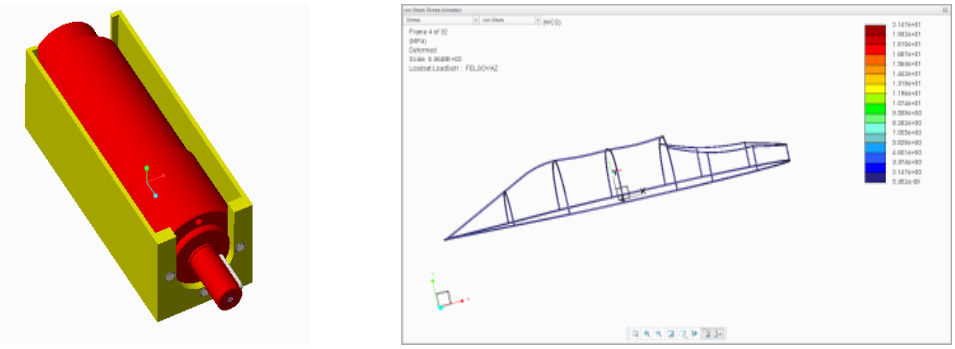

Figure 2 Motor suspension and load simulation

The vehicle maximum height must be less than 100 cm. The vehicle track width must be at least 50 cm, measured between the midpoints where the tyres of the outermost wheels touch the ground. The ratio of maximum height divided by track width must be less than 1.25. The vehicle wheelbase must be at least 100 cm. The maximum total vehicle width must not exceed 130 cm. The maximum total length must not exceed 350 cm. The maximum vehicle weight, without the Driver is 140 kg. [1]

3. RESULTS

With a team involving more than 20 people, engineers and students from different departments, we design and build the vechicle, we participate at the competition. After we passed the very serious technical inspection, at the last attemp, we complete a succesful run with **101.8 km/kWh** efficiency.

Figure 3 The car and the team

Figure 4 The recognition

REFERENCES

[1] *SHELL ECO-MARATHON*. 2016 OFFICIAL RULES CHAPTER I, 2016.

INTERNATIONAL SCIENTIFIC CONFERENCE ON ADVANCES IN MECHANICAL ENGINEERING
13-15 October 2016, Debrecen, Hungary

HOT-DIP GALVANIZING IN ZINC-MANGANESE BATH

[1]GODZSÁK Melinda, [2]LÉVAI Gábor PhD, [3]VAD Kálmán CSc, [3]CSÍK Attila PhD, [3]HAKL József PhD, [4]KULCSÁR Tibor, [5]KAPTAY George DSc

[1]Institute of Physical Metallurgy, Metalforming and Nanotechnology, University of Miskolc
E-mail: godzsak.melinda@gmail.com
[2]Innocenter Nonprofit Ltd., Miskolc
E-mail: levai.gabor@gmail.com
[3]Institute for Nuclear Research, Hungarian Academy of Sciences, University of Debrecen
E-mail: vad@atomki.hu, csik@atomki.hu, jshakl@gmail.com
[4]Institute of Metallurgical and Foundry Engineering, University of Miskolc
E-mail: femestorres@gmail.com
[5]Institute of Physical Metallurgy, Metalforming and Nanotechnology, University of Miskolc, Bay Zoltán Nonprofit Ltd. for Applied Research
E-mail: kaptay@hotmail.com

Abstract
A theoretical analyzes and experiments have been performed for producing colored hot-dip galvanized steel sheets in zinc bath alloyed with manganese. Manganese, dissolved in zinc bath creates a thin manganese-oxide film on the surface of the zinc coating on top of the galvanized steel sheet. Due to interference this coating seems to be colored.

Keywords: *coloring hot-dip galvanizing, Zn-Mn hot-dip galvanizing bath, zinc-manganese system, color oxide film, light interference MnO layer*

1. INTRODUCTION

The hot-dip galvanizing is one of the most important and the most effective methods of the corrosion protection of iron and steel products. However it can be mentioned among other disadvantageous properties the monotonous grey color of the final product,that makes the technology less popular in many cases. The most wide-spread solution to this problem is the so called duplex coating, during the galvanized surface get an optional color topcoat, such as organic painted coating. The colorfulness of the hot-dip galvanized coating in one step can be achieved by the so called coloring hot-dip galvanizing. During this process a thin oxide film is forming on the hot-dip galvanized surface due to the alloyed element into the zinc bath and its oxidation on the surface in air atmosphere. Because of constructive and destructive light interference this oxide layer can be seen colorful, and these colors change with the thickness of the layer. Some publications of first of all researchers from the Far East [1] [2] [3], furthermore a doctoral thesis written recently in Hungary [4] and an article [5] based on this doctoral thesis were researched before the experiments.

2. METHODS

Detailed theoretical analysis was carried out before the experiments, then the experiments between laboratory conditions were fulfilled, with self built hot-dip galvanizer equipment. The manganese concentration was 0.25 wt pct, the hot-dip galvanizing was made in seven different temperatures (*Table 1*). The dipping time of steel sheets was always 30 s, the dipping and removal speed were 50

mm/s. The samples were 0.8 and 1.5 mm thick, low alloyed cold rolled DC04 (St14 according to DIN) steel sheets (*Table 2*). The SHG zinc base material comes from the Hungarian NAGÉV Zinc Ltd.

Table 1 Variable parameters of the hot-dip galvanizing experiments

Mn concentracion in zinc bath, wt pct	**0.25**	**Temperature of coloring hot-dip galvanizing, °C**						
		430	450	480	510	540	570	600

Table 2 Chemical composition of DC04 (St14) steel sheet (wt pct) [6]

DC04 / St14	**C**	**P**	**S**	**Mn**
	0.08	0.030	0.030	0.40

3. RESULTS

The hot-dip galvanized steel sheets were qualified with colorful surface according to various aspects. It was chosen from at variable temperature coloring hot-dip galvanized steel sheets (*Table 1*) to particular investigation those,that were at 430- 450 and 510 °C hot-dip galvanized. Their surface quality and colors were the most homogenous:

- at 430 °C hot-dip galvanized 1.5 mm thick steel sheet: blue
- at 450 °C hot-dip galvanized 1.5 mm thick steel sheet: yellow
- at 510 °C hot-dip galvanized 1.5 mm thick steel sheet: green
- at 510 °C hot-dip galvanized 0,8 mm thick steel sheet: purple

Comparing our own results to the experimental results of Le and Cui [1] from the Far East can be determined that also they produced at 430 °C temperature, between 0.20 – 0.30 wt pct manganese concentration, blue hot-dip galvanized steel sheets (*Figure 1*). However near 450 °C temperature they produced still blue hot-dip galvanized steel sheets, different from our results. In the results of Le and Cui around 510 °C are first of all still yellow measuring points, but can be detected some purple and green measuring points also. The impurity element of the zinc bath may have an influence on the visual perception caused by interference, therefore might be differences between our experimental results and the results of literature.

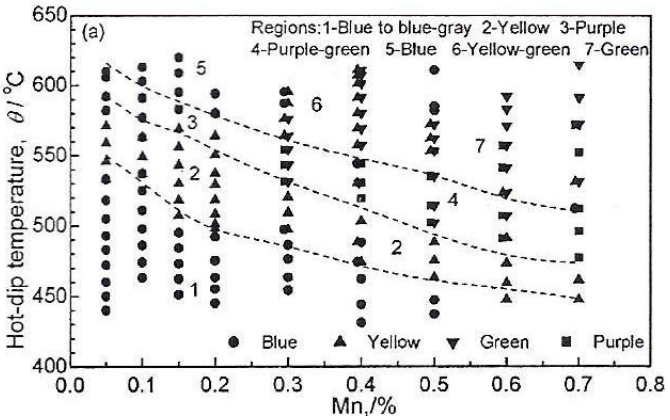

Figure 1 Colors forming on hot-dip galvanized steel sheets in the Zn-Mn bath, cooling by air [1]

It was coloring hot-dip galvanized at 430 °C to prove or to negative that at quite low temperature it is managed or not to get colorful hot-dip galvanized surface. Despite of hot-dip galvanizing of steel sheets the lowest temperature as possible, the hot-dip galvanized surface has become colorful (*Figure 2a*). However this light blue color was not full and high color, but the surface hadn't still the normal silvery and bright color. So it was ascertained, that silvery color steel sheet in zinc bath with minimum 0.25 wt pct manganese content can't be produced at 430 °C not yet. At 450 °C the color of the surface was high yellow instead of light blue color (*Figure 2b*). The quality of hot-dip galvanized surface and the evenness of color were quite good. It can be determined that the colors of the hot-dip galvanized surfaces will be different in case of different temperature and by the same manganese content.

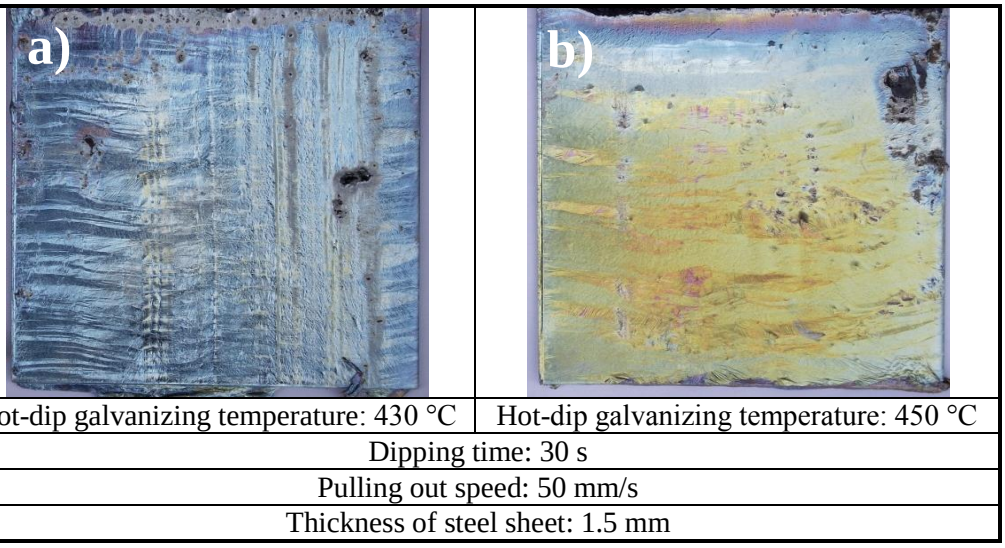

Hot-dip galvanizing temperature: 430 °C	Hot-dip galvanizing temperature: 450 °C
Dipping time: 30 s	
Pulling out speed: 50 mm/s	
Thickness of steel sheet: 1.5 mm	

Figure 2 At 430 °C (a) and 450 °C (b) hot-dip galvanized 1.5 mm thick steel sheet, 0.25 wt pct Mn concentration

The coloring hot-dip galvanizing at 510 °C has resulted again a changing in the color tone on the surface. In case of the 0.8 mm thick steel sheet at 510 °C dipping temperature the new color is purple. However it should be noted, that the color is not even, somewhere is mostly iridescent, so more colors are appearing simultaneously on the surface, but mostly with purple color tone (*Figure 3a*). At the same hot-dip galvanizing temperature, but in case of a 1.5 mm thick steel sheet the color of the surface is mostly green, but also some iridescence can be discover. Despite of the same hot-dip galvanized parameters the different thicknesses of steels have resulted the changes of colors.
The thicker steel sheet has higher heat capacity, so there is more time for the diffusion and oxidation of manganese to the surface, therefore the oxide layer can become thicker and change the result of interference (*Figure 3b*).

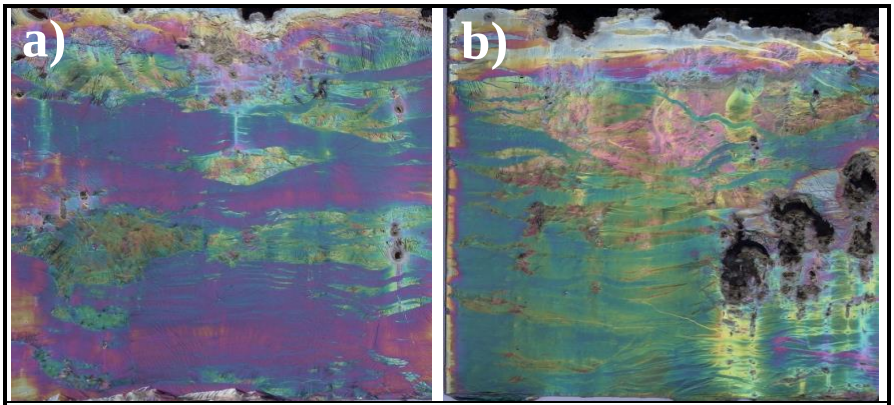

Hot-dip galvanizing temperature: 430 °C	
Dipping time: 30 s	
Pulling out speed: 50 mm/s	
Thickness of steel sheet: 0.8 mm	Thickness of steel sheet: 1.5 mm

Figure 3 At 510 °C hot-dip galvanized 0.8 (a) and 1.5 mm (b) thick steel sheet, 0.25 wt pct Mn concentration

To prove that there are differences in the colors of the 0.8 and 1.5 mm thick hot-dip galvanized steel sheets not only at 510 °C dipping temperature, comparative examinations were performed at 430-450-and 480 °C. It was concluded that at 430 °C there isn't significant color difference between 0.8 and 1.5 mm thick steel sheets, but at 450 and 480 °C dipping temperature can be observed different colors. In case of 450 °C coloring hot-dip galvanizing temperature by the 0.8 mm thick steel sheet can be obtained a light yellow color, however by 1.5 mm thick steel sheet an intensive yellow (*Figure 4a*). At 480 °C dipping temperature the thinner, 0.8 mm thick steel sheet was yellow-purple, while on the surface of the the thicker, 1.5 mm thick steel sheet was dominated the purple color (*Figure 4b*).

Mn concentration: **0.25 wt pct** Hot-dip galvanizing temperature: **450 °C** 0.8 mm (left) 1.5 mm (right)	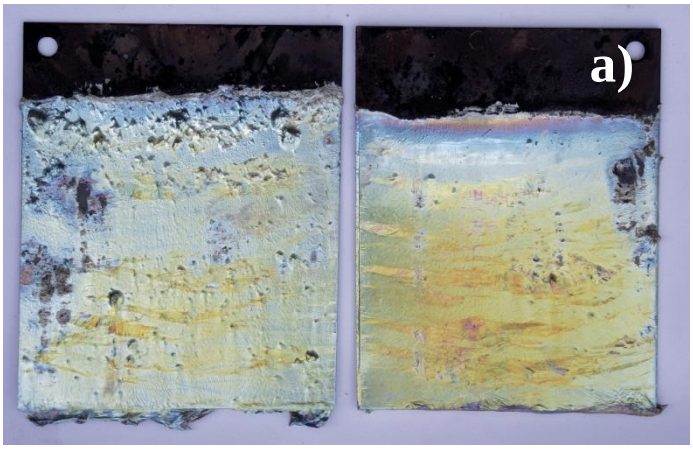

Mn concentration: **0.25 wt pct** Hot-dip galvanizing temperature: **480 °C** 0.8 mm (left) 1.5 mm (right)	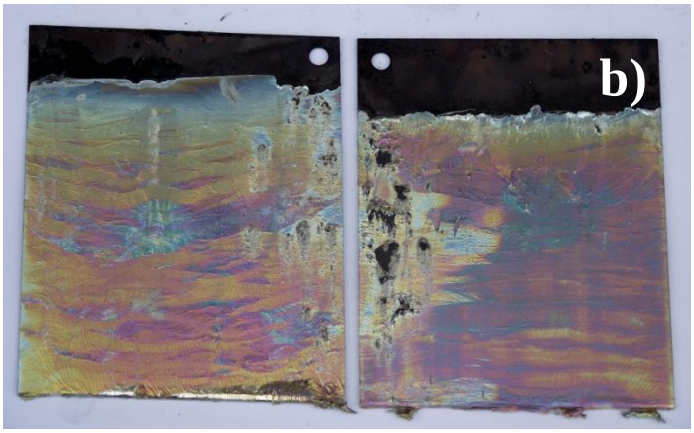

Figure 4 At 450 (a) and 480 °C (b) hot-dip galvanized 0.8 (left) and 1.5 mm (right) thick steel sheet, 0.25 wt pct Mn concentration

From these results it was concluded, that the thicker sheets with greater heat capacity really had an influence on the coloring processes: in case of thicker sheets more intensive colors were formed and sometimes color changes were occurred comparing to the thinner sheets. The reason is that in case of the two thicknesses of sheets is forming different manganese-oxide layer thicknesses on the surface. The thicker sheet has a disadvantage: while in case of the thinner 0.8 mm sheet the color formed a few second after pulling out from the zinc bath hasn't changed during cooling at room temperature in air atmosphere, then in case of the thicker 1.5 mm sheet the color was changing during cooling after pulling out from the zinc bath.

The forming colors on the surface depend on the thickness of the manganese-oxide layer. Optical analysis was carried out to predict what kind of manganese-oxide layers are going to cause the certain colors. Later we would like to control this analysis with GD-OES and SNMS measures.

In the optical analysis first it was assumed that the flat surface of metal is covered by dielectric coating with thickness "d" and with refractive index "n", which is manganese-oxide. In this case the incident light is partly reflected from its surface and partly transmitted through. The transmitted part of the light reflects fully back from the metallic layer – in our case from the zinc layer – underneath. A part of this reflected light is transmitted through the upper surface of the manganese-oxide film and interferes with the originally reflected light. In case when these lights are projecting through the eyepiece to the retina of our eyes, each beam of light is running different distances until our retina, and due to this processes destructive or constructive interference is generated. Consequently, both constructive and destructive interference will take place at special wavelengths. In our case, when the refractive index of MnO layer is higher (n_{MnO} = 2.16), than the refractive index of air (n_{air} = 1.0002926), and the refractive index of zinc under the oxide film (n_{Zn} = 15,3) is the highest, than will be occured a totally destructive interference, if the following equation is true [7, 8]:

$$\lambda_{dest} = \frac{2 \cdot n \cdot d}{m - 0{,}5}$$

where λ_{dest} (m) is the special wavelength of destructive interference, d (m) is the thickness of the MnO layer with two, parallel Zn/MnO and MnO/air interfaces, n (dimensionless) is the refractive index of MnO, m = 1, 2, …. (dimensionless) is the order of interference.

Maximally constructive interference is occuring for the following wavelength light [7, 8]:

$$\lambda_{const} = \frac{2 \cdot n \cdot d}{m}$$

It is important to emphasize that the destructive and the maximally constructive interference equations concern only perpendicularly incident beam, and also that if the MnO layer is on a surface with less refractive index than the MnO's, such as glass, then the equations of destructive and constructive wavelengths change each other. In *Figure 5* it is shown the dependence of destructive and maximally constructive wavelength on the thickness of the MnO layer. In diagram (*Figure 5)* can be seen on the y-axis the wavelength of light marked only in the visible region, on the upper x-axis the scale of visible colors is appearing, on the under x-axis the thickness of MnO layer. To understand the results also the *Figure 6* is needed. In *Figure 5* the destructived colors in y-axis due to " "Destr./1" line are resulting the colors in the upper x-axis, in function of the thickness of MnO layer in the under x-axis.

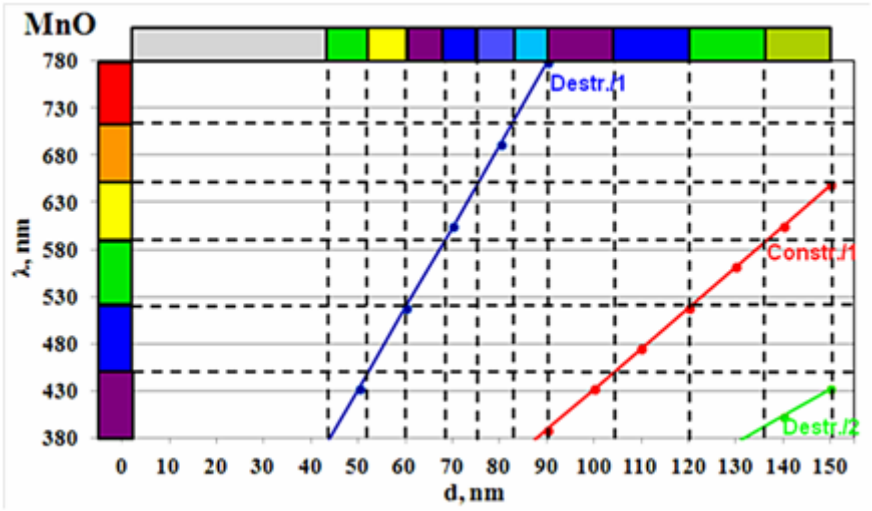

Figure 5 The dependence of the maximally constructive ("const") and destructive ("dest") wavelengths on the MnO layer thickness (the numbers next to the destructive and constructive values are the "m" parameter). The color scale on the left side shows the colors in the visible light wavelength, the color scale on the top of the diagram shows the colors depending on the thickness of the forming MnO layer

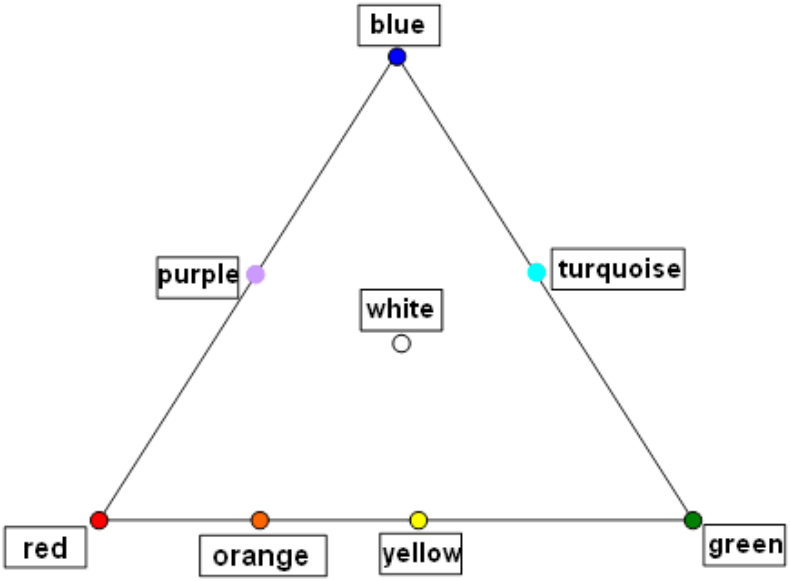

Figure 6 The triangle diagram of the color mixing [7]

CONCLUSIONS

With the same experimental parameters hot-dip galvanized steel sheets were produced with colourful surface, in yellow, pink, purpose, blue and iridescent (mixed) colors. The hot-dip galvanizing experiments were carried out at 7 temperatures: at 430 °C to prove that at quite low temperature and using manganese alloying element into the zinc bath, it is managed to get not colorful hot-dip galvanized surface, at 450 °C according to the industrial conditions, and at 480 °C-510 °C -540 °C -570 °C -600 °C. The three constant experimental parameters were the manganese concentration of the zinc bath (0,25 wt pct), the dipping time (30 s) and the pulling out speed (50 mm/s). The base material was low alloyed cold rolled DC04 (St14 according to DIN) steel, the sheets were 0.8 and 1.5 mm thick. The coloring hot-dip galvanized steel sheets were analyzed mostly by human eye but in the future we would like to make GD-OES and SNMS depth profile analyzes to identify the oxide layer on the surface.
By the visual evaluation of our experiments it was determined, that the colors are:

- at 430 °C light blue,
- at 450 °C yellow,
- at 480 °C purple,
- at 510 °C green.

in case of 0.25 wt pct manganese content zinc bath.

It was concluded furthermore that the colors of the coloring hot-dip galvanized steel sheets depend not only on the temperature of the hot-dip galvanizing, but also on the thickness of the steel sheets.
In our experiments it was confirmed that in case of the same hot-dip galvanizing parameters but using thicker steel sheets, the colors were more intensive or even sometimes color changes were occurred comparing to the thinner sheets.
Finally an optical analysis was carried out to predict the colors of the forming different manganese-oxide layers thicknesses. By this theoretical prediction in the future the results of the SNMS depth profile analyzes can be checked.

ACKNOWLEDGEMENT

Special thank to **NAGÉV Cink Ltd**. – experimental conditions and base material
Dr. Olivér Bánhidi (University of Miskolc) – ICP measurements
Institute of Physical Metallurgy, Metalforming and Nanotechnology and Institute of Metallurgical and Foundry Engineering (University of Miskolc) and their workshops - experimental and measurement conditions

REFERENCES

[1] Le, Q.C., Cui, J.Z.: *Investigation on colorization regularity of coloring hot-dip galvanization processing*, Surface Engineering, 2008, 24 (1): 57-62.
[2] Le, Q.C., Cui, J.Z., Houg, C.H.: *Optimization of coloring galvanization baths*, 2007.
[3] Chen Jinhong, Lu Jintang, Xu Qiaoyu, Zeng Guangliang: *Colored hot-dip galvanized research*, South China University of Technology, Materials Protection, Vol 29. No. 7. 1996.
[4] Lévai Gábor PhD dissertation: *Acéllemezek színező tűzihorganyzása cink-titán fémolvadékkal (Coloring hot-dip galvanizing of steel sheets with zinc-titanium liquid metal)*, University of Miskolc, 2013.
[5] G.Lévai, M.Godzsák, T.I.Török, J.Hakl, V.Takáts, A.Csik, K.Vad, G.Kaptay: *Designing the color of hot-dip galvanized steel sheet through destructive light interference using a Zn-Ti liquid metallic bath*, Metallurgical and Materials Transactions A, 2016, doi: 10.1007/s11661-016-3545-0 (2014-IF = 1.703)
[6] Website of Dunaferr: http://www.dunaferr.hu/documents/hun/aceltermekek-ertekesitese/aceltermekek/hidegen_heng.pdf
[7] Ábrahám György: *Optika*, Panem –McGraw-Hill, Budapest, 1998.
[8] S. Van Gils, P.Mas, E.Stijns, H.Terryn: *Surface Coating Technology*, 2004, vol.185, pp.303-310.

INTERNATIONAL SCIENTIFIC CONFERENCE ON ADVANCES IN MECHANICAL ENGINEERING
13-15 October 2016, Debrecen, Hungary

MAIN RESULTS OF 50 YEARS RESEARCHES IN THE FIELD OF GEAR TRANSMISSIONS DEVELOPMENT

[1]GYENGE Csaba CSc

[1]Technical University of Cluj-Napoca
E-mail: Csaba.Gyenge@tcm.utcluj.ro

Abstract
In this paper I present the main results of theoretically and practically researches oriented for developing the modern gear transmissions. Practically researches were made at UM.Cugir, TEHTRANS Oradea, UNIO Satu-Mare and NEPTUN Campina factories. In these activities I developed the following main transmissions: helical pumps and compressors, DUPLEX and CAVEX worms, special worm hobs, environmental gearing , profile modified gears, CNC hobbing and grinding of gears. The theoretically researches was made at T.U.Cluj-Napoca Department of Manufacturing Engineering.

Keywords: *Gearing, gears transmissions, gear manufacturing*

1. INTRODUCTION

After finished the university studies, I started the industrial activities in Mechanical Factory from Cugir (RO), where I studied and realized a lot of new gears transmission and needed tools. After 9 years I continued my activities in T.U.Cluj-Napoca, where in cooperation with Professor Maros.D. was made a lot of theoretically and applicative researches in the field of design and manufacturing the special gears.

2. DEVELOPING THE MANUFACTURING TECHNOLOGY OF THE FIRST ROMANIAN HELICOIDALLY PUMPS

In cooperation with professor D. Maros, we developed the geometry and technology of helicoidallyal pumps (*Figure 1*) and compressors which was manufactured firstly in Romania.

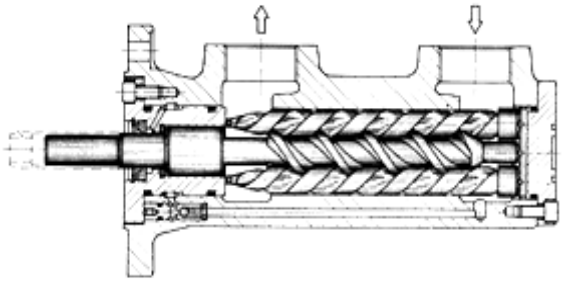

Figure 1 Axial section of helicoidally pump

We analyzed the theoretically and two modified variants (*Figure 2*) of reciprocal enveloping curves. For variant 2, the equations of axial reciprocally enveloping surfaces are :

$$x = 2R\sin(\alpha' + \varphi) - (R + f)\sin(\alpha + 2\varphi),$$
$$z = 2R\cos(\alpha' + \varphi) - (R + f)\cos(\alpha + 2\varphi) \quad (1)$$

For practically manufacturing we analyzed two technological variants (*Figure 3*).

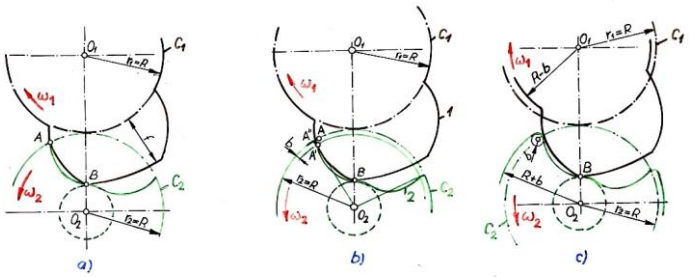

Figure 2 Different variants of reciprocal enveloping curves of helicoidally pumps

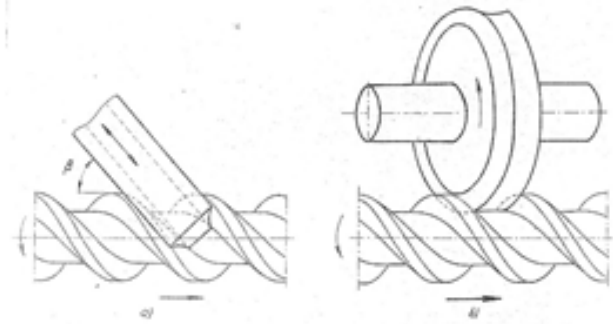

Figure 3 Two possibilities of manufacturing by meshing of helicoidally pump parts

For disc type tools the relative position of coordinate systems can see on *Figure 4*.

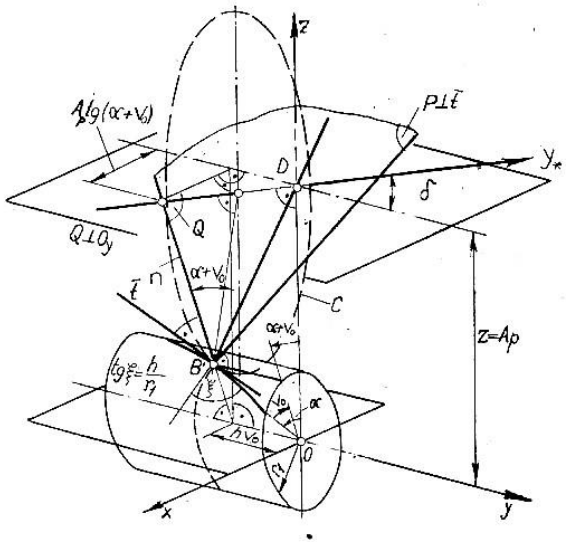

Figure 4 Determination of relative enveloping surfaces in the case of manufacturing the helicoidally pump parts with profiled disc tools

The realised complex tools for these pumps can see on *Figure 5*.

Figure 5 The tools materialized on the base of the developed methodology

3. ACCURATE CALCULATION OF WORM HOBS FUNCTIONAL GEOMETRY AND NEW METHOD FOR OPTIMIZATION OF LATERAL ACTIVE CLEARANCE ANGLES.

It is well known that in the case of the worm hob, one of the difficult problems is the wear of cutting edges, which are mainly due to the inappropriate lateral clearance angle. In order to accurate calculation of this angle I developed a new methodology based on accurate theoretically and practical study.

Based on the *Figure 6*, I define the constructive lateral clearance angel α_l as the angle between the normal $\overline{N_0}$ at the spatial imaginary envelope surface and normal $\overline{N_\alpha}$ to the lateral surface of the tool, in any point of the cutting edge.

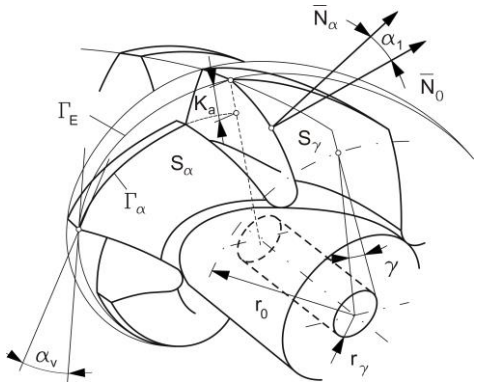

Figure 6 The constructive geometry of worm-hob

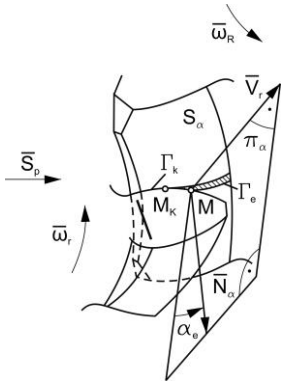

Figure 7 The active lateral clearance angle

The **functional lateral clearance angel**, was define like the complement of the spatial angel between the normal $\overline{N_\alpha}$ and relative speed, from the cutting process. (*Figure 7*)

In order to accurate determination of the constructive lateral clearance angel, I used the cutting triangular planes of generating cutting process with worm-hob (*Figure 8*).Using the previsions definition:

$$\alpha_l = \arccos \frac{\overline{N_0}.\overline{N_\alpha}}{\left|\overline{N_0}\right|.\left|\overline{N_\alpha}\right|} \tag{2}$$

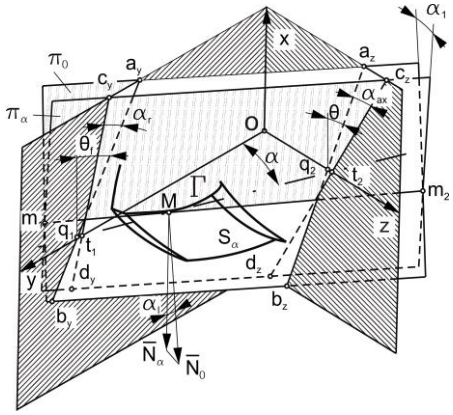

Figure 8 The characteristic triangular planes of generating cutting processes

4. USING THE FRENET'S TRIHEDRON FOR STUDY OF HELICOIDALLY SURFACE TECHNOLOGIES

It is known that the most commonly used procedure for helicoidally surfaces finishing is their grinding. The successes of these depend at wheel axis correct adjustment. Only the ZI involutes worm gears can be grind with planar front surface of tool. Traditional definition of the adjustment parameters leads to quite complicated and not always correct results.

I proved theoretically that the grinding wheel axes must be oriented on direction of binormal at base cylinder's helix line of worm.(*Figure 9*).

The direction cosines of this vector are:

$$\cos\lambda_x = \frac{r_b}{r_0}\sin\theta_b ; \cos\lambda_y = \frac{\sqrt{r_0^2 - r_b^2}}{r_0}\sin\theta_b ; \cos\lambda_z = \cos\theta_b \tag{5}$$

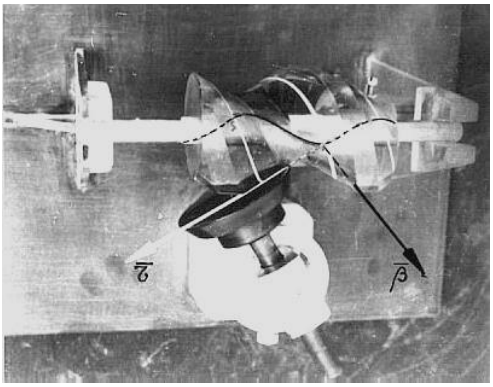

Figure 9 The binormal of base cylinder's helix line and the ZI worm surfaces manufacturing tool axe

5. NEW METHOD FOR TECHNOLOGY DEVELOPMENT OF HIGH QUALITY WORM HOBS

In order to increase the performance of worm gears used in various industrial field it is necessary the continuous development of the computational and design methods, as well as the manufacturing and control techniques. Of curse, the complexity of problems leads to a correlation between design, technology and control.
In order to determine the relative speed is considered relative position of the technological system elements from *Figure 10*, was used the matrix method of **Litvin**.

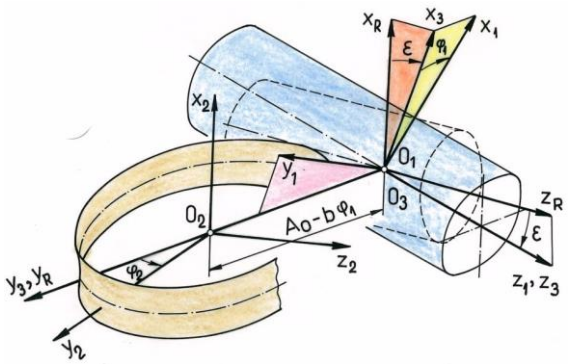

Figure 10 The relative position of the cylindrical helicoids of the worm hob and worm wheel in relative motion during processing.

The relative speed between virtual enveloping surfaces in rotation with angular velocity ϖ_1, and the worm wheel rotating with angular velocity ϖ_2 and radial feed movement s_R is:

$$\overline{v}_{12} = \begin{Vmatrix} [(A_0 - b\varphi_1)\cos\varphi_1 - y_1]\sin\varepsilon - z_1\sin\varphi_1\cos\varepsilon + (y_1 - b\sin\varphi_1)i_{12} \\ [(A_0 - b\varphi_1)\sin\varphi_1 + x_1]\sin\varepsilon + z_1\cos\varphi_1\cos\varepsilon - (y_1 - b\sin\varphi_1)i_{12} \\ (A_0 - b\varphi_1 + x_1\sin\varphi_1 - y_1 c\cos\varphi_1)\cos\varepsilon \\ 0 \end{Vmatrix} \quad (6)$$

The relative speed determined by this algorithm can be use in the computing processes of high precision hobs, optimization of cutting parameters and accurate definition of active lateral relief angle.
It is well-known the fact that manufacturing of high quality worm gears imposes the use of highly-accurate tools and o good correlation of their geometry with the parameters of the gearing process. Except some special cases, the tools are radial relieving (mostly by grinding).
In order to obtain the good localization of the contact path, and to allow the necessary resharpening, the reference diameter of hob is greater than that of the worm gear. Thus the cutting edges of the worm hob will be located on a virtual enveloping surfaces persevering the helical parameter of the worm, but having a reference radius increased with 3...5%. Of curse after resharpening both the reference diameter and the cutting edges profile are modified (*Figure 11*).

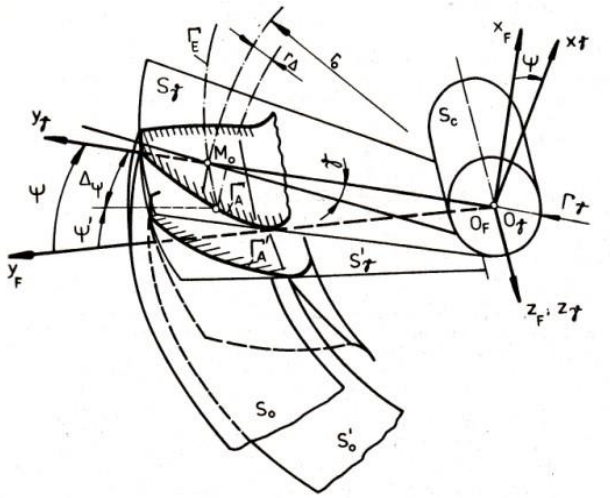

Figure 11 Modification of the cutting edge as a consequence of resharpening

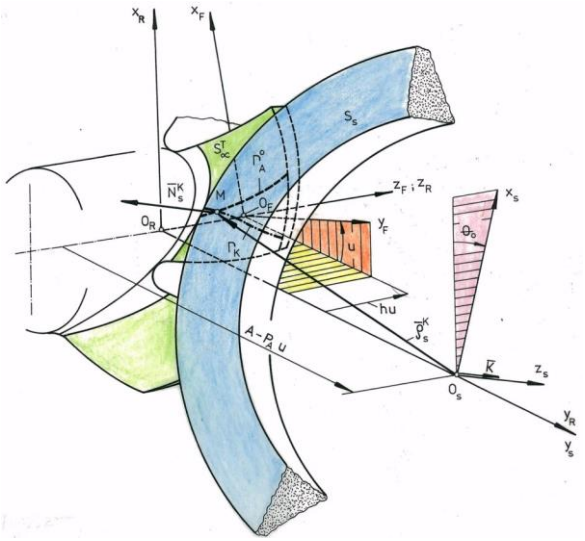

Figure 12 Determination of radial relieving tool profile

The problem of optimization consist in finding a method ensuring a minimum modification of the tool profile after resharpening and consequently a uniform precision of the manufactured worm wheels.

In order to determine the tool profile for radial relieving of hobbing cutter I considered the hob and the relieving tool in an intermediary position (*Figure 12*).

The theoretical accurate lateral surface S_L^T is in contact with the S_S active surface of the grinding tool across the characteristically curve Γ_K.

Based on the general equation of meshing, over the characteristically curve, the normal vector is perpendicular on the relative speed v_{FS}, which mathematically is expressed by the equation:

$$\left(y_\alpha^T - P_A.\sin u\right).n_{\alpha x}^T - \left(x_\alpha^T - P_A.\cos u\right).n_{\alpha y}^T + h.n_{\alpha z}^T = 0 \tag{7}$$

With the parameter, determined by this way, the grinding tool profile for relieving, under a general form, can write:

$$\overline{\rho_S} = M_{SF}.\overline{\rho_\alpha^T} = \overline{\rho_S}(p,\psi), \tag{8}$$

where M_{SF} -is the transfer matrix between coordinates systems $O_S X_S Y_S$ and $O_F X_F Y_F$.

The real lateral surface is the surface cinematically enveloped by the grinding tool.
If we intersect the lateral surface of the hob) with the rake face, we obtain the real cutting edges Γ_A^R.
The both cutting edges, theoretic and real obtained by these ways, have different positions and shapes, depending on the measure of rescharpening (*Figure 13*).
According to the [2] *theoretical errors of hob edges profile* are defined as a difference between the profile of real cutting edges Γ_A^R -and the profile of theoretical cutting edge Γ_A.
The ***local deviation of the profile*** is determined with following equation:

$$\varepsilon_i = z_c(p) + h.v - z_{\alpha i}^R = \varepsilon_i(p, p_i). \tag{9}$$

The ***cumulated deviation*** is given by the relation:

$$\Phi = MAX[\varepsilon_i] - MIN[\varepsilon_j], \tag{10}$$

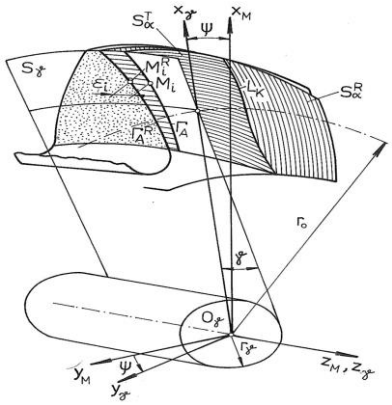

Figure13 The relative position of the theoretically and real cutting edges

In the process of worm hob precision optimization the object function is the cumulated deviation defined by relation (16). On purpose analyzing the variation of function with respect of resharpening parameter ψ, as well as side relief angle α_l, it was tested in a real case. *Figure 14* shows the convex form of function as well as the linear dependence.
From the previous researches [2] it is known that the function Φ, also depends on rake angle γ (*Figure 15*).

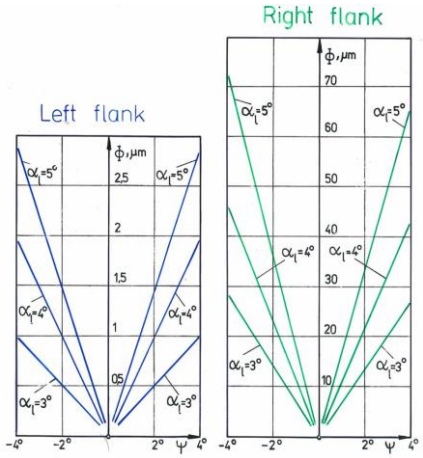

Figure 14 Variation of Φ function for $\gamma = 0$.

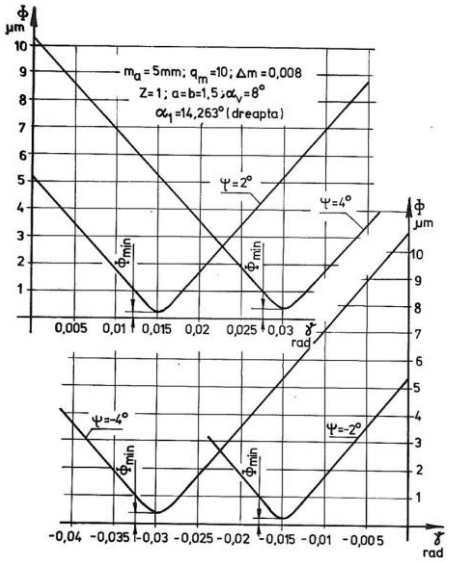

Figure 15 Variation of Φ function for relative with resharpening parameter ψ, and rake angle γ.

One sees that for every stage of resharpening there is an optimum value for which the function Φ is minimum.
For optimization the hob geometry according to variations of function T, I considered a number of cutting edges defined by n discrete points. Based on figure 13 for each of $\Psi(\gamma)$ curve, we can find a parabola given by following formula:

$$\Phi = \Phi(\gamma, \psi) \tag{11}$$

The **local error** can be calculated with following equation:

$$\delta_q = B_1.\gamma_q^2 + B_2.\gamma_q + B_3 - \Phi_q \tag{12}$$

The square average error is defined by :

$$\Delta = \frac{1}{Q}\sum_{q=1}^{Q}(\delta_q)^2 = \frac{1}{Q}\sum_{q=1}^{Q}(B_1.\gamma_q^2 + B_2.\gamma_q + B_3 - \Phi_q)^2 \tag{13}$$

Theoretical and technological research results have been tested numerically for different types of precision worm gears manufactured at enterprise UMCugir(Romania).
On further, I present, for example, the results obtained in the case of a worm gear type ZA duplex with the following definition parameters:
$m_a = 5mm; q = 10; \Delta m = 0{,}008mm,$
$z = 2; a = b = 1{,}5; \alpha_v 8^0; \alpha_1 = 14{,}263^0; \alpha_2 = 10^0; \alpha_l = 4^0.$
Theoretical and real axial profiles of the new tool, and the tool after resharpening with $\psi = -4^0$, are shown in *Figure16*.

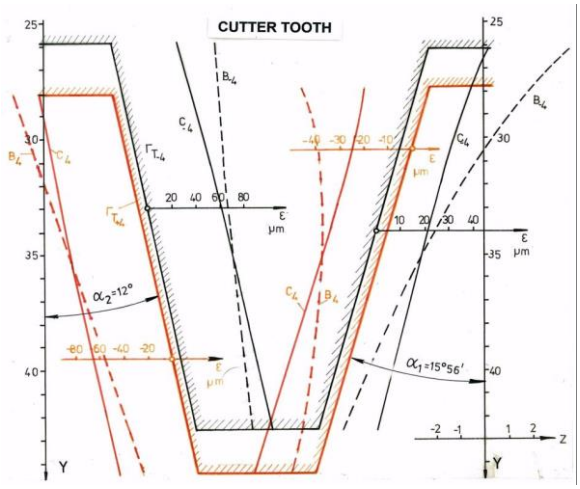

Figure 16 The axial profiles of the new and resharpened duplex hob developed

Analyzing the profiles from figure 16, one can see the followings:

- - the profile deviation of the left flank (α_2), in all cases are very small and the real profile of this flank remain approximately parallel to the theoretical profile, in any stage of resharpening;
- on the right flank , the axial profile of non optimized hob (curves B_{+4}) is convex and concave after the last resharpening;
- the profile deviation of right flank of the non optimized cutting tool have over fulfilled the width of tolerance range of AA precision clas (DIN 3968).

Using the two methods for establishing the profile error, we have realized a hob with alternative cutting (*Figure 17*), which has been used for manufacturing the precision worm wheels of the indexing system of gear milling machine-tool.
The manufacturing of wheels has been performed on a PHAUTER P900S machine. The control of realized worm gears has been made using the equipment Dr.Höfler (*Figure 18*).

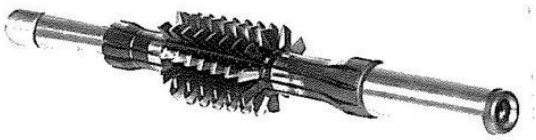

Figure.17 General view of the new duplex hob developed

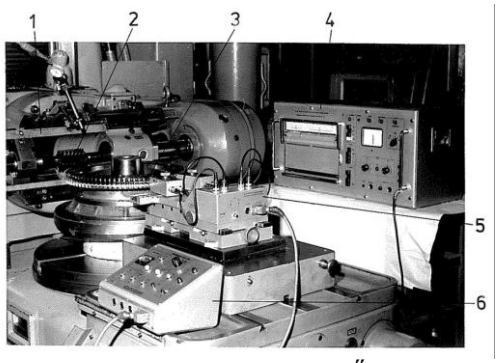

Figure 18 The worm hob and measurement device Dr.HŐFLER installed on a PHAUTER 900S machine tool.

6. CNC GEAR GRINDING

For grinding various profile modifications spur gears from different transmissions, we modernized one NILES type grinding machine with FANUC numerical control equipment (*Figure 19*).

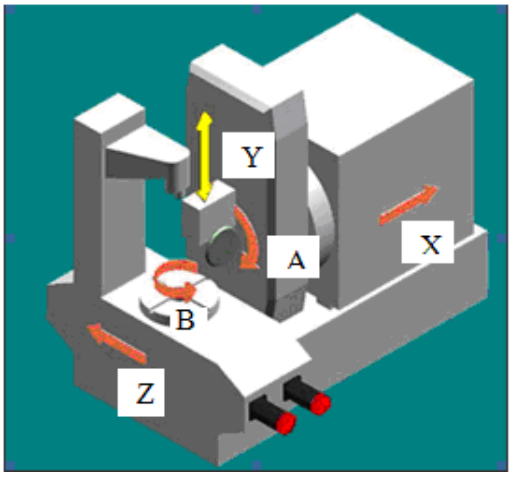

Figure 19 The orientation of the coordinate axes of the CNC gear grinding machine

Movement of gear over flanks of reference rack materialized by the grinding wheel is made of Z and B axes. The X-axis is also controlled by the machine's CNC system, ensuring radial positioning of the tool. For CNC generating of this teeth profile we used the variable speed meshing method. Thus the pitch line is made up from three portions and the generating process are achieving at bases circles R_{bf}, R_b, R_{ba} (*Figure 20*).

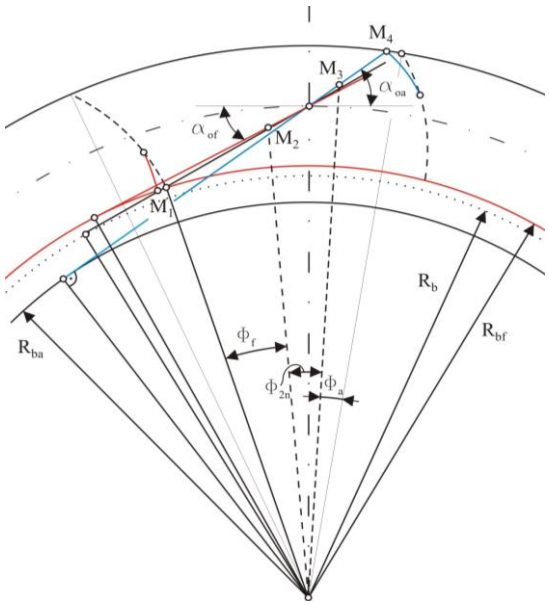

Figure 20 Generating the tooth's flank with three involute parts

Thus, for calculating the programming parameters needed for grinding the three portions of the flank (respectively to cover the pitch line), were developed the necessary algorithms, for gears defined on different norms (STAS, DIN, AGMA, etc).

The measurements made on GHIBLI TRAX - CNC apparatus, show that the different parameters of gears manufactured with developed CNC method are appropriate at precision class 5-after DIN 3962. After our modest opinion it is one good result.

7. ENVIRONMENT FRIENDLY CUTTING OF CYLINDRICAL GEARS

In order to estimate the effects of some environment friendly techniques. We made some theoretical and practical researches in the field of cylindrical gear milling using several kinds' tools, lubrication and cooling methods.
The main part of experimental researches has been done on the Gear Milling Machine Pfauter PE 500 CNC (*Figure 21*).

Work piece parameters Material: 16 Mn Cr15 , Modulus: 2.75 mm, Number of teeth: 37, Diameter: 110 mm, Teeth breadth: 19 mm

Used tools: Worm hob from EMo5Co5 with TiN coating Lubricants

Figure 21 Environmetal lubricant devices on Phauter PE-500 CNC milling machine

We tested the following cooling methods:

- Minimal Quantity Lubrication (MQL) with a mixture of air and vegetable oil
- Classical Flood (CF) of soluble oil Rotanor with a flow rate of 100 l/min.
- Minimal Quantity Lubrication (MQL) with a mixture of air and vegetable oil
- (0.4 ml/min) pulverized in airflow by 5 bar of pressure using a device with 2 nozzles.
- Minimal Quantity Cooling (MC) with emulsion (15ml/min) in airflow by 5 bar.
- Minimal Lubrication and Cooling (MQL+MC) – a combination between minimal lubrication and minimal cooling.
- Dry Cutting (DC) (without fluid).

CONCLUSIONS

The conclusions of our researches in this field was that MQL represents itself as a viable alternative for gear milling with respect to tool wear, heat dissipation, and machined surface quality.

REFERENCES

[1] Gyenge, Cs.: *A Frenet –féle triéder alkalmazása a csavarfelületek gyártástervezében*. Gépgyártástechnológia, Budapest, 5-6, 191-194., 1992.

[2] Gyenge, Cs.: *Some Contribution to the improvement of the Accuracy of Worm Hobs for DUPLEX Worm Wheel*. PhD. Thesis, Cluj-Napoca.1979.

[3] Gyenge, Cs.: *Nagypontosságú csigakerék lefejtőmarók tervezése és gyártása*. Gép. 11-12, 385-394, 1991.

[4] Gyenge, Cs.: *Lefejtőmarók oldalhátszögeinek pontos meghatározása és optimálása*. Gép Budapest, 48, 38-42., 1996.

[5] Gyenge, Cs**.**, Ros, O., Frăţilă, D.: *Researches Concerning the Minimal Lubrification Technique in the Gear Cutting.* Acta Mechanica Slovaca, 2, 49-54., 2002.

INTERNATIONAL SCIENTIFIC CONFERENCE ON ADVANCES IN MECHANICAL ENGINEERING

13-15 October 2016, Debrecen, Hungary

EXAMINATION OF THE FERTILIZER DISTRIBUTOR USING GPS GUIDANCE SYSTEM

[1]HAGYMÁSSY Zoltán PhD, [2]PÁLINKÁS Sándor PhD, [2]GINDERT-KELE Ágnes PhD

[1]Department of Agrotechnology, Institute for Land Utilization, Technology and Regional Development, Faculty of Agricultural and Food Sciences and Environmental Management, University of Debrecen
E-mail: hagymassy@agr.unideb.hu
[2]Department of Mechanical Engineering, Faculty Engineering, University of Debrecen
E-mail: palinkassandor@eng.unideb.hu, battane@eng.unideb.hu

Abstract
In University of Debrecen, Department of Agrotechnology different type's fertilizer distributor was examined by authors within the framework of precision farming. The examinations were conducted partly in the Department test track and partly in field conditions. The unevenness of fertilizer dosage quantity is an important aspect due to the application analyzes, while the transversal unevenness of spreading is an important aspect due to the even fertilizer distribution. The tractor was equipped with Trimble EZ Guide 500 GPS guidance system device. For this reason, the tractor was moved much straighter and more accurately. Based on our measurements we concluded that the fertilizer spreaders transversal unevenness of spreading significantly influence the work quality.

Keywords: *Fertilizer distribution, GPS guidance system*

1. INTRODUCTION

The modern agro-food sector has to meet society demands like food safety, sustainability and the aim that there should be enough food production. This implies the needs of high efficient use of nutrients in production processes. This includes cost price efficiency and reduction of environmental losses. Development of high tech mechanics in agricultural equipment is a continuous process of innovation [2].
Distributing different types of fertilizer accurately and evenly is necessary in experimental plots. In the parcels the more precise labour quality demands require mechanization of experiments. The examinations are preceded by control measurements of the fertilizer granules which basically affected the machine settings. The examination content is triggered by usage of GPS in agriculture to improve efficiency by reduction of losses, both in usage of fertilizers and pesticides or herbicides. Nevertheless it can not only be a high tech oriented examination. The end-users of the high tech applications are farmers and contractors [2].

2. METHODS

The examinations were carried out at the University of Debrecen, Faculty of Agricultural Sciences, Experimental Field Station of Látókép and the Department of Agrotechnology. Fertilizer type which was used during the tests: Salt of Pét (ammonium nitrate limestone 27 % N, Nitrogénművek Rt. Pétfürdő). The examination of the transversal unevenness of spreading was conducted at the flat parcel of the Látókép Experimental Field Station.
The tractor and fertilizer spreader (*Figure 1*) setting data:

- The tractor: John Deere 6620
- The fertilizer spreader: Spinning disc type fertilizer distributor Amazon ZAM 900
- Running speed: 8 km/h
- Working width: 18m
- Spreading discs: OM18 / 24 , Blade positions: 24/47 , Valve position is (36)
- The distributed amount of fertilizer per hectare is: 400 kg / ha
- Limiter: spreading A8, A13 Boundary spreading
- Parcel Length: 600m

Figure 1 The spinning disc fertilizer distributor in the field

The definition of the unevenness of spreading gives CV as the variety factor. [1]

$$CV = \frac{100}{\bar{x}} \sqrt{\sum_{i=1}^{n} \frac{(x_i - \bar{x})^2}{n-1}} \quad (1)$$

where:

1. x_i – the average amount of collected fertilizer at a certain test place during three measurements
2. $\bar{x}$ – the average amount of collected fertilizer at all test places during three measurements
3. n - the number of test places

3. RESULTS

The standard size and shape of the parcel trays were put down 50 meters away from the edge of the parcel, the direction of the measuring way was transversal. The parcel trays sizes were: 500 x 500 mm, the trays were equipped with anti-bounce grid, in order to prevent the trays from rebounding. (*Figure 2*) The working width was B = 18m. The spreading width was W=36m. The type of distribution pattern was triangular. The parcel trays allocation was: 1.636 m x (12 trays -1) = 18m [2].

Figure 2 Testing trays on the field

At first, the examination was performed in the traditional way. The fertilizer was distributed forward and backward. During the first test the working width was measured manually, the tractor was driven without GPS guidance system. After the test the fertilizer was picked out of the test trays, and the fertilizer was measured by a digital scale. The digital scale accuracy was 0.1 gram. The mass of fertilizer was illustrated. The diagram shows the fertilizer distribution in the parcel, the examined direction way was transversal. (*Figure 3*)

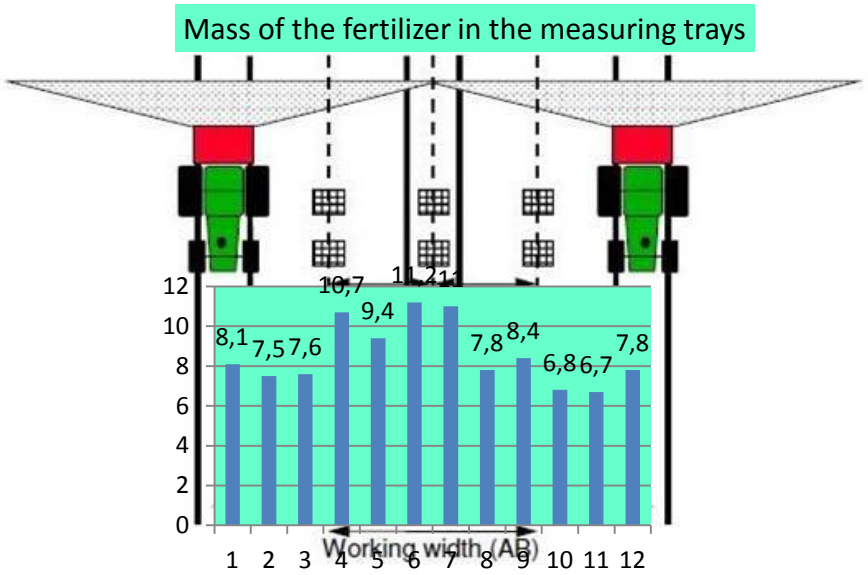

Figure 3 Distributing rate when the working width measured manually

It can be stated that the transversal coefficient of variation is CV=18.65. It is more than the maximum limit CV > 15%. Therefore the evenness of spreading was not satisfying. In the middle of the working width the distributed volume of the fertilizer was greater, than the volume at the edge of the area. It can be concluded that straight driving line of the tractor should be more accurate, because it is making more precise balance rate. Afterwards, the set up of the spinning disc fertilizer spreader was corrected. (*Figure 3*)

Figure 4 Trimble EZ Guide 500 GPS guidance device in the tractor

The John Deere tractor was equipped with Trimble EZ Guide 500 GPS guidance device. For this reason, the tractor was moved much straighter and more accurately. Based on our measurement the driving accuracy was approximately 30cm driving with GPS guidance device. (*Figure 4*)

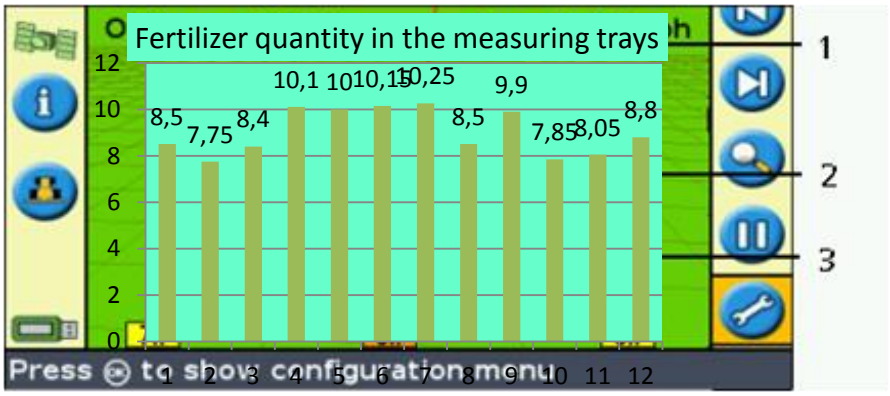

Figure 5 Distributing rate when the working width measured by GPS guidance system [2]

During the field experiments, the setting parameters were changed. The measuring trays were placed transversally, and the fertilizer was distributed. The tractor route was led by EZ Guide 500 GPS guidance system equipment. The differences of the tractor path straightness were less than 30 cm. After the distribution the fertilizer was collected and every tray of fertilizer was measured by a digital balance. The result of the measurement is shown in *Figure 5*. The transversal coefficient of variation was calculated CV=10.8%. It can be stated that the transversal coefficient of the variation CV <15%. Therefore, the unevenness of distribution was acceptable. (*Figure 5*)

CONCLUSIONS

The measurement proved that the manually measured working width is inaccurate and results the unevenness of spreading. We can conclude that the deviation of evenness of spreading is not visible without proper measurement. It can be monitored by correct measurements. The test experiment demonstrated that the EZ Guide 500 guidance system significantly improved the tractor path straightness and the evenness of spreading was significantly increased.

REFERENCES

[1] Csizmazia, Z.: *Technical Conditions Of Equalized Fertilizer Applications*. Hungarian Agricultural Research, 1993/12. p. 16-22

[2] Hagymássy, Z., Ancza, E.: *Experience of an Intensive Program Course on Utilization of High Technology Equipment*, Agrárinformatika 2011, Agricultural Informatics Debrecen, Hungary. 2011. p. 80-86., 2011

INTERNATIONAL SCIENTIFIC CONFERENCE ON ADVANCES IN MECHANICAL ENGINEERING

13-15 October 2016, Debrecen, Hungary

FRICTION TESTS OF DIFFERENT POLYMERS TREATED BY PLASMA TECHNOLOGY

[1]AL-MALIKI Hayder, [2]ZSIDAI László PhD, [3]KALÁCSKA Gábor DSc, [4]KERESZTES Róbert PhD, [5]SZAKÁL Zoltán PhD

[1,2,3,4,5]Szent István University, Faculty of Mechanical Engineering, Institute for Mechanical Engineering Technology, Gödöllő H-2100. Páter K. út 1.
E-mail: zsidai.laszlo@gek.szie.hu

Abstract
Our study is connected with the research of sliding tribological properties of untreated and nitrogen PIII-treated polymers against conventional low carbon structural steel S235 under dry and water-lubricated conditions. However tribology investigations are very difficult and expensive, consequently, standards recommend simplified laboratory tests with small-scale specimens. An individual measuring system and the method are presented in the next. During this work we used a standardised Pin on Disc test with special features. These papers contain a selection of the test category, some technical innovations in connection with test rig, and an individual testing method to study the effects of the different lubrications.

Keywords: tribology, tribotest, Pin On Disc, polymer, PIII

1. INTRODUCTION

Plasma-based ion implantation (PIII) has been applied to improve the material surface in several different applications in the machine-, electrical-, biology- and medical-industry also [1–5]. In this work we present an adequate method to investigate the sliding tribological properties of nitrogen PIII treated polymers by a pin-on-disc tribometer as a function of sliding distance, with various loads and sliding velocities, under dry, water- and oil-lubricated conditions.
We plan to continue our earlier study in connection with the sliding tribological properties of untreated and nitrogen PIII-treated polymers against conventional low carbon structural steel S235 under dry and water-lubricated conditions. The measuring system and the method are presented in the next. I deviate on the row of the main features of the measurements for this and the presentation of the tribotest rig also.
Our work gives a new direction to the examination of the reliability of modified polymer surfaces in sliding (tribology) polymer-metal contact systems, through the complex tribology exploration of characteristics.

2. THE SELECTION OF THE TEST CATEGORY

In most cases, the tribological investigations are very difficulties and expensive, since many times one–one tests are not enough for accurate determination of the tribological behaviour. Therefore recommend simplified laboratory tests with small-scale specimens. The reasons for these so-called small-scale tests are quite obvious, e.g. simple test rig with low forces and power, reduced cost for preparing test specimens, easy of control of environment. Moreover many small-scale results are available in literature to be referenced e.g. [6, 7]. They are useful to compare the properties of different materials, but could induce unrealistic edge effects.

The tribological investigations were carried out by the VI. level of the *Figure 1* according to the German standard DIN 50322 [8].

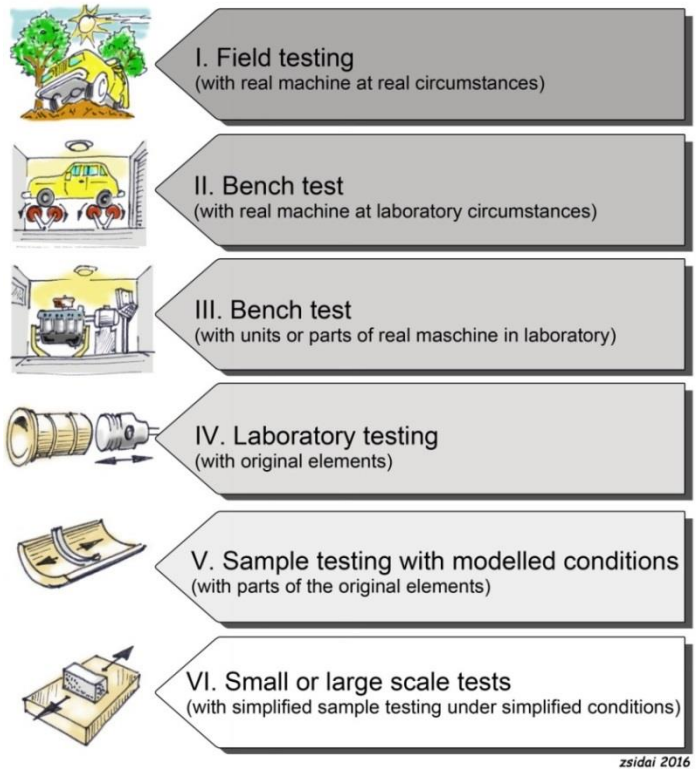

Figure 1 Overview of the tribology test categories of DIN 50322 [base on 8]

From among the several standardised small scale tests method the pin-on-disc (POD) type we elected it. Give reasons for this, the model system insuring the continuous one-way sliding friction adjusting well to the practical applications. The POD module of the dynamic tribotester of Szent István University was used.

3. THE PIN ON DISC TRIBO-TEST RIG AND THE METHOD

The *Figure 2* shows the original construction of the (Dynamic) PIN ON DISC tribometer. We may observe the position of the specimens, the driving system the way of load transfer and the positioning arm mechanism on the photo. Vibrations of the test equipment are reduced by a massive cast support (1). With a turn-free attachment in order to ensure a homogeneous contact surface, the cylindrical polymer sample is fixed into a clamp head (2), what is mechanically pushed against the mating steel disc. The test rig is equipped with a manual loading system, where a constant (or changeable) load by means of a lever system (3) and dead weights. The radius of the frictional track is determined by the position of the cross guiding rail (4). The end surface of the polymer cylinder is facing the metal counter face plate (5), providing continuous sliding friction [9]. The rotating metal counter face (original steel plate or polymer plate) is fixed to the supporting table, providing a continuous rotational motion. In this way, a conformal contact is ensured between the end surface of the polymer cylinder and the steel or polymer disc. The friction force is determined by a special measuring head what is stocked round strain gauged to measure bending moments in more positions. The wear is characterised by the drop in height of the polymer cylinder, and is measured with a contactless proximitor. The so-called bulk temperature is measured in the bulk of polymer with a thermocouple.

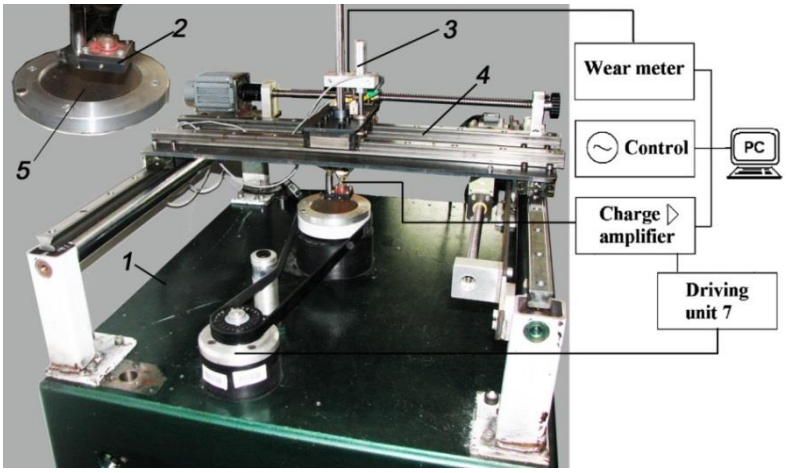

Figure 2 Experimental set-up of the Pin on Disc (POD) tribotester

We applied a special holder to the fixture of the polymer specimens (*Figure 3*). Because of the disc form of the polymer specimens, we have to guarantee the parallel contact surfaces in the sliding zone. The small steel ball in the head, gives a self-aligning possibility of the polymer specimen during the test. The figure shows a needle in the polymer also, it can keep without turning the polymer during the sliding.

Figure 3 The fixed specimen holder and his main parts

The polymer specimens with diameter 10 mm and thickness 4 mm were used as pin (disc) and the mating surface was S235 steel disc with an average surface roughness R_a=0.07- 0.1 μm. In addition to the compare the POD test under dry sliding conditions, tests were done with water and oil (run out) lubricants as well. In case of the hydrophilic (distilled) water, the liquid was added drop wise into the contact zone, with a drop volume= 10 μl and drop frequency = 2 min^{-1}. In oil (hydrophobic) lubricant condition commercial gearbox oil (SAE 80W90) was used (*Figure 4*) [10].

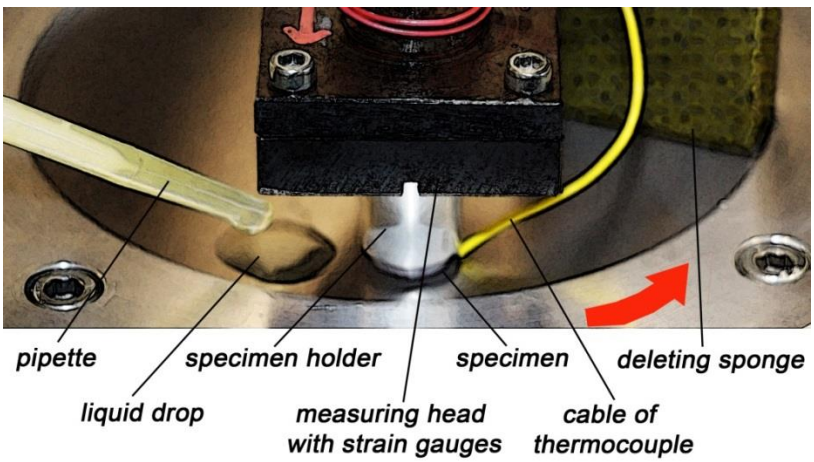

Figure 4 The fixed specimen holder and his main parts

I will use the examination logical order used in the course of my earlier researches that is shown on the *Figure 5*.

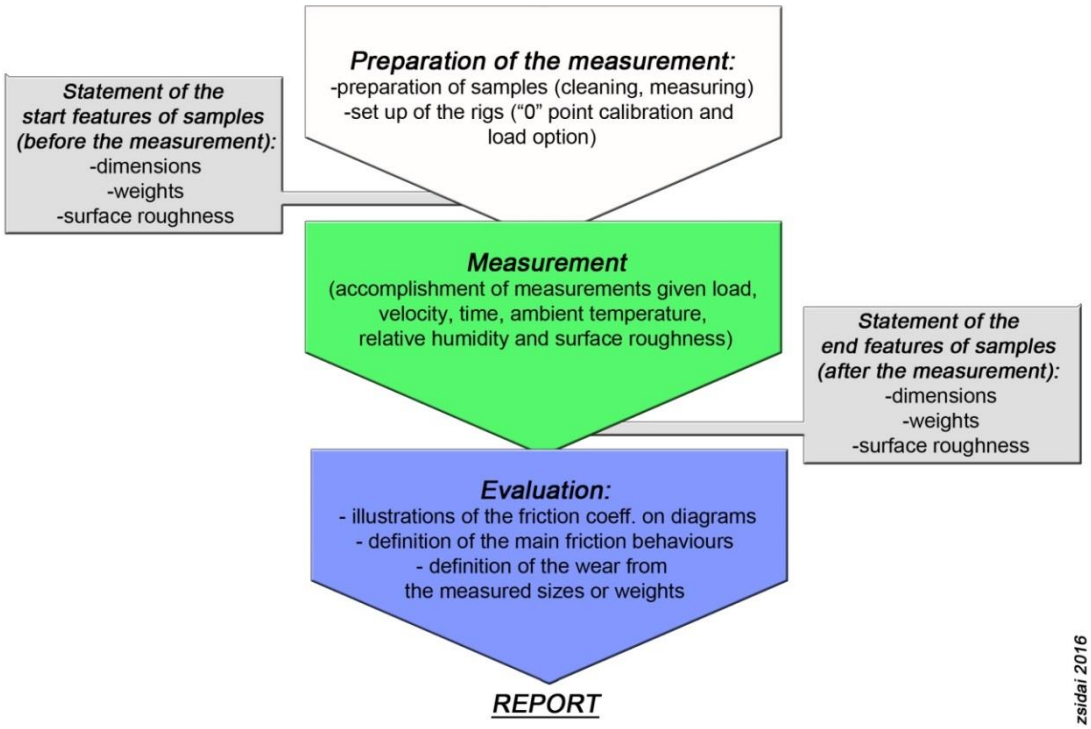

Figure 5 The order of the logical steps of the tribological measurement process

The sliding test conditions are as follows:

Sliding Velocity	v=0.05 m s-1 and v=0.025 m s^{-1}
Load	stepwise increase from P=0.5, 1 and 2 MPa
Pv factors	0.025, 0.05 and 0.1 MPa m s^{-1}

The initial phase of the sliding tribological behaviour of samples is also studied under the conditions of low sliding velocity (v=0.025 m s^{-1}) and low load (P=0.3 MPa), resulting in a very low *Pv* factor. Every test was repeated three times and the results were compared with the trends of changes in μ, *d* and *T*. *(Figure 6)*

-Tests with water lubrication

The aim of tribotests performed under water-lubricated conditions was to compare the results with those of the dry friction measurements and to establish a relationship between the modified surface properties and the altered friction behaviour. The basic test conditions were similar to those of the pin-on-disc tests performed under dry sliding conditions, the only difference was the dropwise addition of distilled water into the contact zone. (*Figure 6*)

- Tests with continuous oil lubrication

These measurements were imported to find an eventual relationship between the altered surface energy and the tribological behaviour of the N PIII-modified surface under hydrophobic lubrication. In addition, we intended to compare the results to those obtained under dry and water lubrication conditions. The basic test parameters were identical to those applied for the dry and water

lubrication tests. The only difference was the drop wise addition of SAE 80W90 gearbox oil into the contact zone. (*Figure 6*)

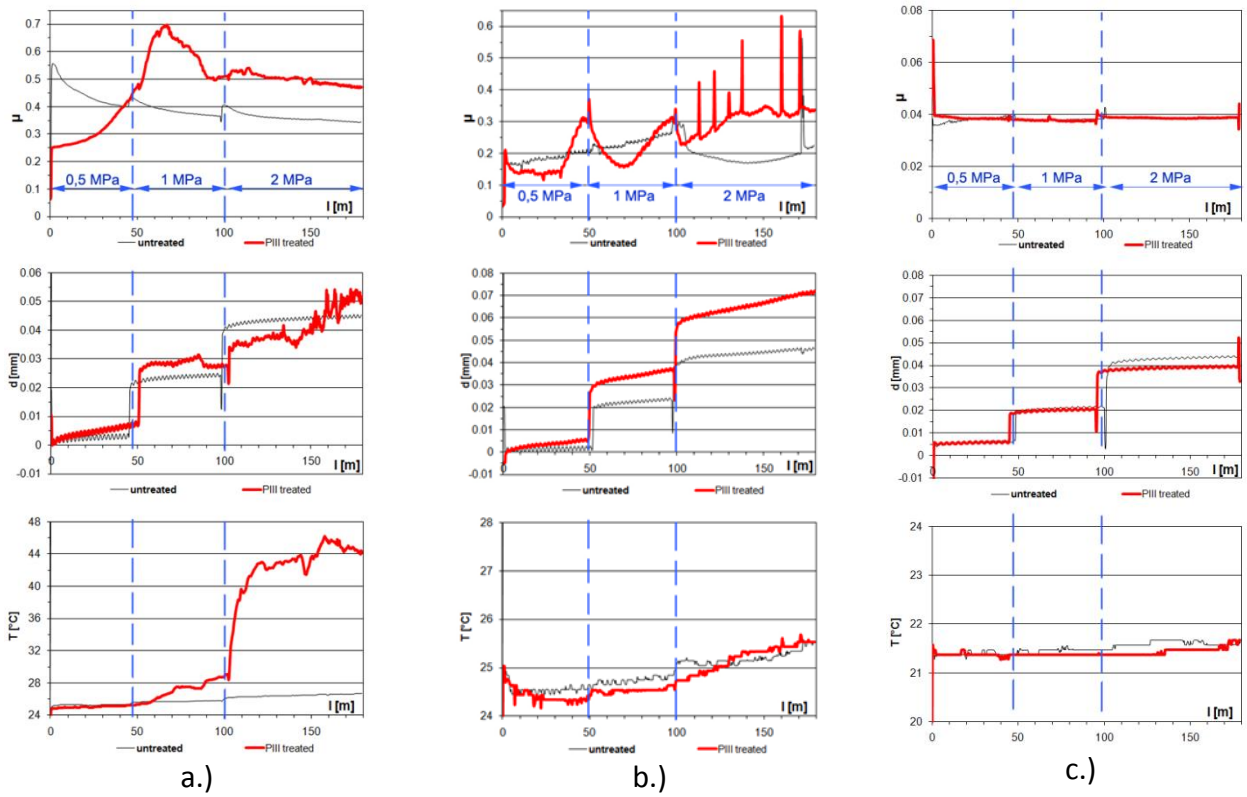

Figure 6 Some example early tribology results of the PA6 (untreated and PIII treated) under different lubricant conditions (P=0,5-1-2 MPa, v=0,05 m/s, l=180 m)
a) under dry sliding b) with water lubrication c) with continuous oil lubrication

- *Run-out oil lubrication tests*

In this case, each step of controlled automatic lubrication carried out by the next. The addition of an oil drop was followed by a cleaning performed by wiping the lubricated surface with a cleaning head covered by a filter sponge. It means, that the first part of the running pertains to an oil-lubrication regime and it is followed by a next phase, characterised by sliding on a cleaned track.

CONCLUSIONS

The aim of our study was to present an appropriate testing method to a given surface modified polymers with different lubricated conditions. From the research expected results may serve as a basis reliable, modern, developments of materials and surfaces on the different areas of the industry. During this work we used a standardised Pin on Disc test with special features. I mean a new specimen holder to ensure the self-aligning position of the specimens, and an individual testing method to study the effects of the different lubrications.

The largest significance of the given results their informative role furthering the practical application, based on which is increasable the reliability of tribology features. Beside the technical viewpoints, we wait the results about the environment protection one (lubricant reduction –self lubrication) and the economic benefits (exchanging more expensive polymer for cheaper one) also. For example, the results of the run out oil tests can be considered to belong to a mixed/ boundary lubrication regime. The application of such a thinned lubricating film proved to be suitable for

establishing a difference between the tribological properties of the untreated surface and those of the treated one.

ACKNOWLEDGEMENT

The research is supported by OTKA K 113039 and one of the authors (László Zsidai) would like to thank MTA (Hungarian Academy of Sciences) for supporting this work in the frame of the research fellowship BOLYAI (BO/00127/13/6).

REFERENCES

[1] Sakudo, N., Mizutani, D., Ohmura, Y., Endo, H., Yoneda, R., Ikenaga, N., Takikawa, H.: Nucl. Instrum. Method. B 206, 687., 2003.
[2] Ueda, M., Kostov, K.G., Beloto, A.F, Leite, N.F., Grigorov, K.G.: Surf. Coat. Technol. 186 295., 2004.
[3] Lee, Y., Han, S., Lim, H., Kim, Y., Kim, H.: Anal. Bioanal. Chem. 373, 595., 2002.
[4] Wang, J., Huang, N., Yang, P., Leng, Y.X., Sun, H., Liu, Z.Y., Chu, P.K.: Biomaterials 25, 3163., 2004.
[5] Wang, J., Chen, J.Y., Yang, P., Leng, Y.X., Wan, G.J., Sun, H., Zhao, A.S., Huang, N., Chu, P.K.: Nucl. Instrum. Method. 242, 12., 2006.
[6] Sukumaran, J., Ando, M., De Baets, P., Rodriguez, V., Szabadi, L., Kalacska, G., Paepegem V.: *Modelling gear contact with twin-disc setup.* Tribology International 49, 1-7., 2012.
[7] Zsidai L., et al.: *The tribological behaviour of engineering plastics during sliding friction investigated with small-scale specimens.* Wear, 253 673-688., 2002.
[8] DIN 50322. *Kategorien der Verschleißprüfung, Deutsche Norm 50322*. Beuth Verlag, 1986.
[9] Kalacska, G., et al.,: *Műszaki műanyagok gépészeti alapjai (Mechanical Basics of Polymers).* Minervasop Bt. Sopron, 1997
[10] Kalácska, G., Zsidai, L., Keresztúri, K., Mohai, M., Tóth A.: *Sliding tribological properties of untreated and PIII-treated PETP*. Applied Surface Science 255 5847–5850., 2009.

COMPUTER AIDED PRODUCT DEVELOPMENT OF BALL SCREW DRIVE

HEGEDŰS György PhD

University of Miskolc, Institutional Department of Miskolc
E-mail: hegedus.gyorgy@uni-miskolc.hu

Abstract
This paper presents computer aided product development of ball screw drive returns. Ball screw drives have different solutions for the balls recirculation depending on the screw and ball diameters pitch and length. In CNC machines high-lead ball screw drives are used due to the increasing manufacturing speeds and time reducing. However in the recent years low-lead screws are appeared in automotive applications as a driving system in electrically operated steering systems (Electric Power Steering, EPS). The article demonstrates the results of CAD development of returns built in high-lead and low-lead ball screw drive mechanisms.

Keywords: *ball screw, product development, CAD*

1. INTRODUCTION

Several factors affect the precision of machine tools, for instance manufacturing tolerances and technology, quality insurance, reliability of production, etc. The ball screw transmission mechanisms have been widely used their advantageous properties in modern NC and CNC machine tools (however, the application of linear motors is increasing). The gothic-arc profile ball screw motion transforming mechanisms are commonly used in machine tools, measuring devices, linear actuators and EPS steering drives. A ball screw drive mechanism basically consists of a screw, a nut, a returning (recirculating) guide and balls. It is frequently used to convert rotary motion to linear motion or torque to thrust, and vica versa. The product development processes on these drive mechanisms focus on the generation method of profiling tool of high-lead ball nut and the designing of recirculation parts.

1. TYPES OF RECIRCULATING PARTS

One of the challenge in the design of ball-screw drive mechanisms is the type of ball recirculation. Previously the most common design applied tubes, where the recirculating tubes were mounted outside the ball nut. This type of return forces each ball to change motion direction by 90 degrees at the end of each returning tube. This extreme change in motion causes higher frictional losses and also increases the risk of balls jamming. It also increases the variation in frictional torque. Tube returns also suffer a loss of lubricant. The port where the tube enters or leaves the nut body is difficult to seal. As a result, tube-return ball screws tend to leak, a costly and messy maintenance problem. Tubes are also generally incompatible with rotating nut configurations [1].
To avoid the extreme change in motion internal returns are used, where the recirculating path follow the natural trajectory of the ball. Generally this type of returns are based on tangential deflection. This minimizes the required deflection forces, resulting in higher efficiencies and reliability, furthermore without tube connection, no lubricant leakage from the nut. The internal returns can be grouped to six different format:

1.) *Track-to-track*: this return is still the widely used. It is available on the widest range of shaft diameters and nut types. It uses ball deflectors to lift balls across the shaft's outer diameter and guide them directly into the next (or previous) track. Each deflector serves one turn, which corresponds to one ball circuit.
2.) *Liner*: this format of returns is a variation on track-to-track deflectors. The liner essentially consists of several deflectors arranged and manufactured as a single component. It is placed entirely inside the nut, eliminating the need for bore holes. It was developed for the aerospace industry where coarse-positioning ball screws must reliably control aerodynamic surfaces, cargo doors, and cockpit-seat adjustments. None of these applications require pre-loading, so tube returns dominate older, legacy designs. Liner returns provide both safety and reliability. Unlike tube returns, balls cannot leave the nut if a deflector or the liner fails.
3.) *Through-the-nut*: these returns were originally developed for high-speed operation of high-lead ball screws. This return uses deflectors at each end of the nut. Balls get lifted off the shaft, guided through a bore inside the nut body, and set back onto the shaft. One pair of deflectors serves one circuit, which includes several turns. This nut design is normally used for lead/diameter ratios greater than *0.5* and dual start threads (that is, two separate thread paths on the shaft).
4.) *Z-Deflector* is another version of the through-the-nut return. It was designed for shafts with solid bearing shoulders on both ends of the threaded shaft.
5.) *Endcap*: The endcap return is similar to the *through-the-nut* return, except that caps at both ends of the nut serve as ball deflectors. This design is normally used for lead/diameter ratios greater than *0.5*, and nuts with two or more start threads for high load capacity in a short nut. The endcap is usually made of plastic, which lowers weight and keeps the ball screw 50% quieter when operating. Furthermore, the extra length of the endcaps accommodates combination wipers, which include both a felt ring and plastic fingers.
6.) *Track-to-track with oversized balls*: To increase the load capacity of ball screws, oversized balls are built (*15 – 19 mm*) in the standard track-to-track return. The resulting ball screws had dynamic capacities up to about *800 kN*. Plastic deflectors move balls tangentially out of the nut raceway. The main purpose of this return is to let ball screws replace hydraulics in a greater number of applications. Electromechanical drives offer improved efficiency and lower environmental impact, which is leading to an increasing demand for high-thrust screws.

Types of internal returns can be determined by the application where it is used and the critical driving speed value of ball-screw drive.

2. DEVELOPMENT OF RECIRCULATING PART FOR HIGH-LEAD BALL NUT

In the past decades the demand for high-lead ball screw drive mechanisms is increasing due to high-speed manufacturing. These ball screw types are generally manufactured by form grinding, where the tool has a corresponding profile [2], while for ultra-precision ball screws sometimes a lapping method is performed after grinding process [3, 4]. Novel manufacturing processes apply hard turning to produce the final form of the ball-nuts and decrease production time [5, 6]. Generally the thread surface of ball-nuts is finished by profiled abrasive tools on internal thread grinding machines. In the case of a long and high lead threaded ball-nut the grinding wheel is not tilted at the lead angle of the thread in order to avoid collision between the quill and workpiece. Due to these conditions the profile obtained is not gothic-arc, because the grinding wheel tends to overcut the thread surface. The problem of over- and undercutting is well known in gear and worm manufacturing, and several methods have been worked out to solve this task [7–9].
For high-lead ball screw drives a novel internal return part has been developed. The principal design

criteria was the ball nut downsizing, while the changing of the rate of transmissible power is negligible.
Figure 1 shows a solution for an internal return built into a high-lead ball nut.

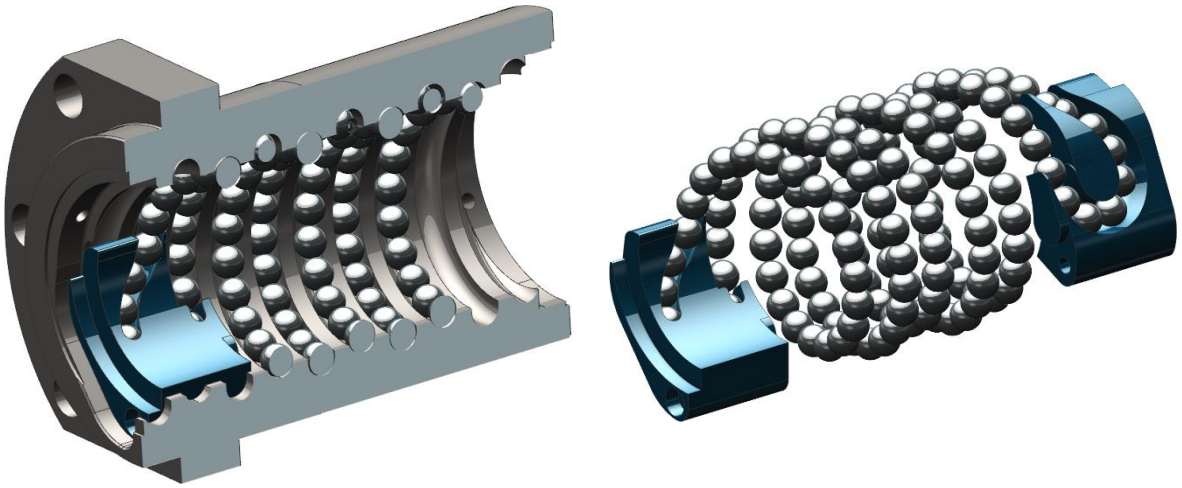

Figure 1 Novel internal returns in high-lead ball nut

The advantage of this arrangement is that the recirculating path formed inside the nut. This type of internal returns is possible, when the balls diameter between *8 – 12 mm*.

3. DEVELOPMENT OF RECIRCULATING PART FOR LOW-LEAD BALL NUT

The problem on low-lead ball screw drives the number of returns. If track-to track or liner returns are used, the number of balls which do not participate in load capacity higher. To avoid this disadvantageous condition the working length of the nut thread has to be lengthened. Due to this problem resolving method, the mass of ball screw drive mechanisms will be greater. The solution of the problems mentioned above through-the-nut returns are used.

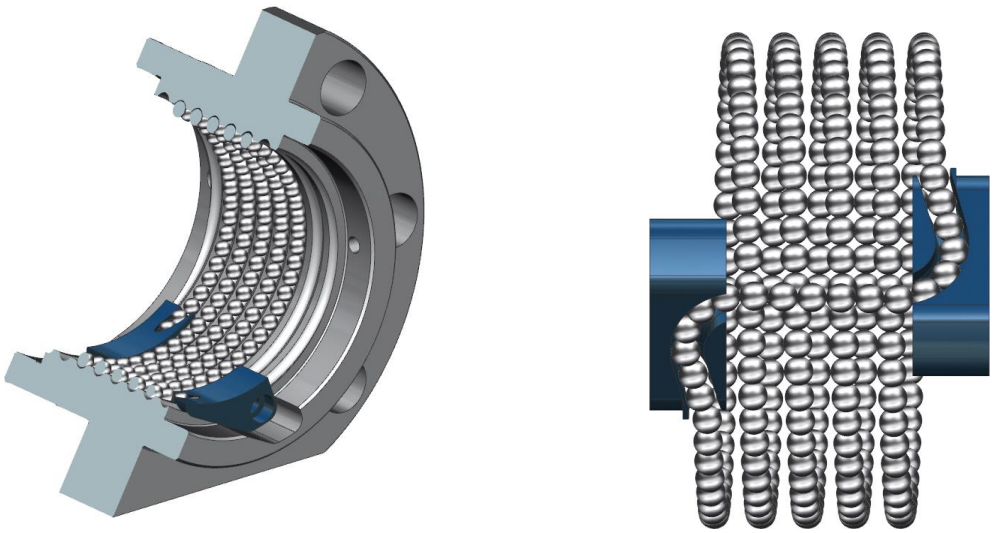

*Figure 2 I*nternal returns in low-lead ball nut

Figure 2 represents an optimised through-the-nut returns in low-lead ball nut. The dimensions are *50x5 mm*. The viper and the preloader are built inside the nut (not shown on *Figure 2*).

CONCLUSIONS

This paper presents the returns part generally used in ball screw drive mechanisms. The customers' demands require the development of new solutions for high-lead and low-lead ball screw drives returns. To find an optimal design variant for the new solution computer aided design environment was used. The future works will be the manufacturing of newly developed returns and testing and measuring of the ball screw drive mechanisms.

ACKNOWLEDGMENTS

This research was carried out as part of the TÁMOP-4.2.1.B-10/2/KONV-2010-0001 project with support by the European Union, co-financed by the European Social Fund. This research was supported by the European Union and the State of Hungary, co-financed by the European Social Fund in the framework of TÁMOP-4.2.4.A/ 2-11/1-2012-0001 'National Excellence Program'.

REFERENCES

[1] Gretz, B.: *Ball-Screw Design: The Advantages of Internal Ball Returns*. Machine Design, 2016 (2), ISSN 0024-9144
[2] Harada, H., Kagiwada, T.: *Grinding of high-lead and gothic-arc profile ball-nuts with free quill-inclination.* Precision Engineering 28(2), 143–151 (2004). ISSN 0141-6359. doi: 10.1016/j. precisioneng.2003.07.003
[3] Guevarra, D.S., Kyusojin, A., Isobe, H., Kaneko, Y.: *Development of a new lapping method for high precision ball screw (1st report)-feasibility study of a prototyped lapping tool for automatic lapping process*. Journal of the International Societies for Precision Engineering and Nanotechnology 25(1), 63–69 (2001). ISSN 0141- 6359. doi: 10.1016/S0141-6359(00)00059-3
[4] Guevarra, D.S., Kyusojin, A., Isobe, H., Kaneko, Y.: *Development of a new lapping method for high precision ball screw (2nd report) Design and experimental study of an automatic lapping machine with in-process torque monitoring system*. Journal of the International Societies for Precision Engineering and Nanotechnology 26(4), 389–395 (2002). ISSN 0141-6359. doi:10.1016/S0141-6359(02)00122-8
[5] Alexander, B.: *Hard thread turning shortens the process chain*. Fabricating & Metalworking F & M. 13(3), 32–34 (2014). ISSN 1541-2415
[6] Kiss, D., Csáki, T.: *Investigating the machining possibilities of a ball nut*. Proceedings CADAM 2012: 10th International Conference on Advanced Engineering, Computer Aided Design and Manufacturing. pp. 51-54. (ISBN:978-953-57074-2-4)
[7] Litvin, F.L.: *Gear Geometry and Applied Theory*. Cambridge Univ. Press, Cambridge (2004). ISBN 978-052-181-517-8
[8] Berbinschi, S., Teodor, V., Oancea, N.: *3D graphical method for profiling gear hob tools*. The International Journal of Advanced Manufacturing Technology 64(1-4), 291–304 (2013). ISSN 0268-3768. doi: 10.1007/s00170-012-3989-3
[9] Dudás, L.: *Modelling and simulation of a new worm gear drive having point–like contact*. Engineering with Computers 29(3), 251–272 (2013). ISSN 0177-0667. doi: 10.1007/s00366-012-0271-0

INTERNATIONAL SCIENTIFIC CONFERENCE ON ADVANCES IN MECHANICAL ENGINEERING
13-15 October 2016, Debrecen, Hungary

BATCH EXTRACTIVE DISTILLATION WITH OFF-CUT AND ENTRAINER RECYCLE

HÉGELY László PhD, LÁNG Péter DSc

Budapest University of Technology and Economics, Faculty of Mechanical Engineering, Department of Building Services and Process Engineering
E-mail: hegely@mail.bme.hu, lang@mail.bme.hu

Abstract
The influence of off-cut and entrainer recycle are studied by dynamic simulation for a batch extractive distillation process. The mixture acetone-methanol is separated by using water as entrainer. The production cycle consists of processing three consecutive batches. The influence of preloading of the entrainer is also studied. The different operational policies are compared. For the calculations a professional flow-sheet simulator is used.

Keywords: *batch distillation, extractive distillation, off-cut recycle, entrainer, dynamic simulation.*

1. INTRODUCTION

Distillation is the most frequently used method to separate liquid mixtures, based on the differences in the volatility of the components. *Batch distillation* (BD) can be used to separate mixtures of varying quantity and composition (flexibility of operation), and it is frequently used in the fine chemical, spirit and pharmaceutical industry, as well as in solvent recovery.
The main components to be recovered are produced in the *main cuts* (products). The polluting components and azeotropes are removed in off-cuts (fore-, intermediate and/or after-cut). The *off-cuts* may contain the main components in considerable quantity. The off-cuts can either be disposed of by incineration or can be recycled to the next batch in order to reduce the loss of the main components. Recycle of the final hold-up serves for the same goal. However, the cuts recycled diminish the amount of the fresh feed in the next batch and vary the composition of the mixture (charge) to be separated.
For the separation of *azeotropic mixtures* a special distillation method must be applied. In *batch extractive distillation* (BED, Yatim et al. [1]), an entrainer is fed continuously into the column. The separation of an equimolar mixture acetone(A)-methanol(B) with BED by applying pure water as (heavy) entrainer (E) in a batch rectifier was studied among others by Lang et al. [2], Lelkes et al. [3]. The mixture A-B forms a minimum boiling azeotrope, but by using water (E) the relative volatility $\alpha_{A,B}$ can be increased and the azeotrope can be broken [2]. On the basis of industrial experiences Lang et al. [4] suggested a new operational policy, with entrainer feeding already during the heating-up of the column. Yao et al. [5] maximised the efficiency of the entrainer usage and optimised its amount preloaded to the binary charge. For increasing the effectiveness of the BED, process control structures were also suggested.
Hegely et al. [6] investigated the effects of *off-cut recycle* for six-batch BD and BED waste solvent regeneration processes. Hegely and Lang [7] performed the optimization of the above processes.
Entrainer recycle, on one hand, reduces the amount of fresh pure entrainer needed, but on the other hand the pollutant content of the entrainer might have adverse effects on the separation process. Water is frequently used as an entrainer due to its favourable properties. In this case, the still residue is handled by waste water treatment, the cost of which can also be reduced by entrainer recycle.

Luyben and Chien [8] studied dehydration of acetic acid via heteroazeotropic batch distillation. The light entrainer (vinyl acetate) was recycled to the next batch.
The aim of this work is to study by simulation the influence of the off-cut and entrainer recycling on a three-batch BED separation process, where an equimolar acetone-methanol mixture is separated with water as entrainer. The influence of the preloading of entrainer is also investigated.

2. THE SEPARATION PROCESS

The separation process consists of three consecutive batches.
The processing of the *Batch I* has the following steps:
-Step 0: *Warming up* of the charge (fresh feed) onto its boiling point without entrainer (E) feeding. Some E can be added (preloading). The amount of E added (SF_0) can be optimised.
-Step 1: *Heating-up* of the column under total reflux ($R=\infty$) with continuous E-feeding (molar flow rate: F_1), whose aim is to purify the distillate by retaining B. This step is finished when the distillate (condensate) is pure enough for A: $x_{D,A}$ reaches the specified purity of product A (PA). The flow rate of E can be equal to that applied in Step 2 ($F_1= F_2$).
-Step 2: *Production of A* under finite reflux ratio ($R_2<\infty$) with continuous E-feeding ($F_2>0$). This step is finished when the specified purity of PA cannot be maintained more with the given F and R. The location of E-feeding (f_2) can be optimised. R_2 and F_2 can be also optimised.
If the entrainer contains some B, this can influence the optimal value of f_2, R_2 and F_2.
-Step 3: *Off-cut A+B (OAB) collection* under $R_3<\infty$ and $F_3=0$. OAB can be recycled to the next batch, Step 3 is finished when the distillate is pure enough for B: $x_{D,B}$ reaches the specified purity.
-Step 4: *Production of B (PB)* under $R_4<\infty$ and $F_4=0$. This step is essentially a binary B/E separation. This step ends when the specified purity of PB cannot be maintained more with the given R_4. R_4 can be optimised. At the end the reboiler and the column hold-ups (residue, W_4+U_4) contain some B.
Step 5: *Off-cut B+E (OBE) collection (optional,* under $R_5<\infty$ and $F_5=0$). There are two cases:
1. The entrainer is purified further. The distillate (OBE), which contains considerable amount of B, can be incinerated or recycled and fed before Step 4 of the next batch. The residue (W_5+U_5) containing much less B is collected and can be recycled (or be sent for incineration or biological purification if E is water).
2. The batch is already finished at the end of Step 4 and the residue (W_4+U_4) is recycled to the next batch (or it is incinerated), that is, Step 5 is omitted.

For *Batches II and III* Steps 0, 1 and 2 are slightly different from those of Batch I.
The residue of the previous batch can be recycled and used as entrainer in the next batch. There are two options: the whole amount of the regenerated entrainer is fed continuously in Steps 1-2 or one part of it is added to the next charge (SF_0) together with the off-cut(s) of the previous batch. The ratio $SF_0/(W_5+U_5)$ can be optimised.
When processing this batch, it is expedient at least to replace the amount of E lost in the previous batch in the products (PA and PB) and eventually OBE with fresh E. The fresh E make-up can be
- mixed together with the previous residue or
-can be fed from a separate tank when the regenerated solvent ran out. (In this case even more than the minimum can be used from it.) This option will be called sequential feeding from now on.
Steps 3-5 are similar to those of Batch I.

Four *separation policies* were investigated:
- Policy 1: No preloading of E, neither off-cut nor entrainer recycle.
- Policy 2: Preloading of E, neither off-cut nor entrainer recycle.

- Policy 3: No preloading, recycle of OAB only.
- Policy 4: No preloading, recycle of OAB and of the entrainer. Two variants are distinguished based on whether the recycled and fresh entrainer is mixed (4a) or fed sequentially (4b).

By Policies 1 and 2, the individual batches are independent from each other. For Policies 3 and 4, where recycle is applied, the state-task-network is shown in *Figure 1*. OBE is also taken, but it is stored for further treatment (distillation or incineration) instead of recycling.

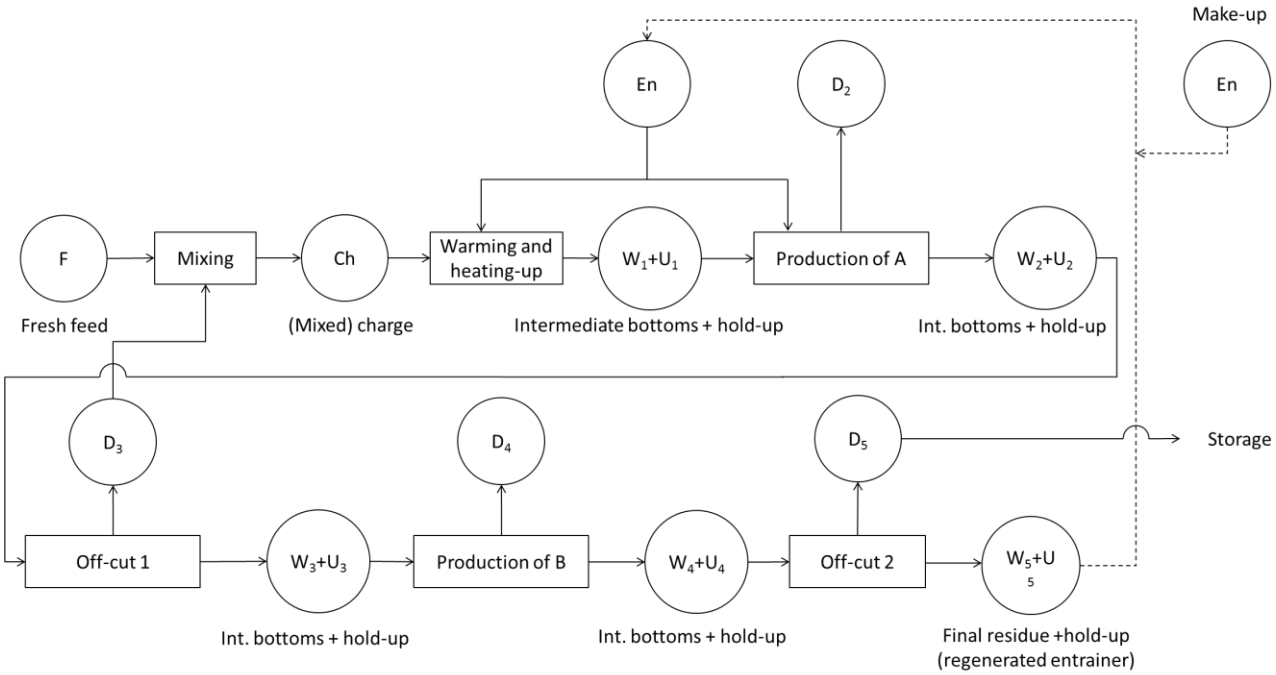

Figure 1 The state-task-network of the BED process (dashed line: for entrainer recycling only)

3. CALCULATION RESULTS

First the calculation method and input data, then the results are presented.

3.1. Calculation method and input data

The data of the separation process (including the NRTL model parameters) are based on the example of Yao et al. [6] (published also in the book [9]), though they studied only one batch without off-cut and entrainer recycle. For the rigorous calculations the dynamic simulator (CC-DCOLUMN) of the CHEMCAD 7.0 is applied.

The fresh feed is equimolar mixture A-B. The prescribed purities are 95 mol% for A, 92 mol% for B and 99 mol% for E. The amount of the charge is 16 kmol in each batch. The temperature of both the charge and entrainer is 25°C. The column has 30 theoretical stages (including the condenser and the reboiler) and is operated at atmospheric pressure. The hold-up of the condenser was 40 dm^3, that of the column 2 dm^3/stage. The heat duty of the reboiler is 400 MJ/h. Reflux ratios in the different steps: R_1=2.5, R_2=5, R_3=17.5 and R_4=5. The position of entrainer feeding is changed after Step 1: f_1=4 (without E recycle) or 5 (with E recycle), f_2=11. The flow rate of the entrainer: F_1=F_2=10 kmol/h. The amount of entrainer preloading is SF_0=8 kmol, when applied.

4. RESULTS

Before performing calculation with recycled entrainer, *the effect of the B-content of the entrainer* (z_B) is investigated on Batch II of Policy 3. The B-content is varied between 0 and 1 mol% (z_A=0). On the increase of z_B, the duration of Step 1 increases (*Figure 2a*), that of Step 2 (and hence the amount of PA) decreases (*Figure 2b*). The A/B separation is sensible to the value of z_B; by increasing it only to 0.5 mol%, PA is reduced by 10%. Moreover, there is a z_B value above which $x_{D,A}$ in Step 1 never reaches the specified value (95 mol%) due to the increase of $x_{D,B}$. In this case, the location of the entrainer feeding stage must be lowered from f_1=4 to 5.

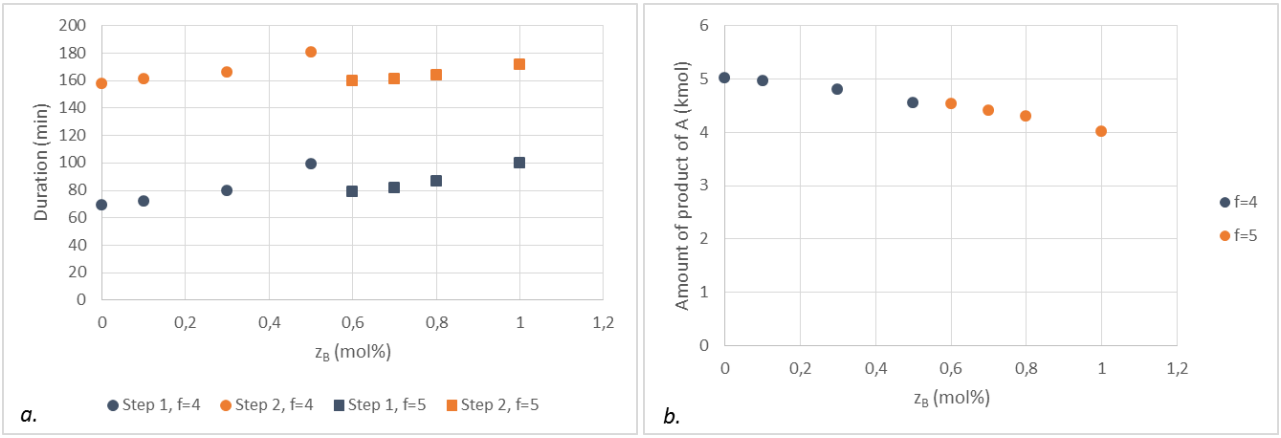

Figure 2 The effect of z_B on (a) the duration of Steps 1 and 2, (b) the amount of PA (Batch 2)

The most important *results for the different policies* are shown in *Table 1*. *Preloading* of E (Policy 2) decreases the recoveries (η) of the products by 0.9% (A) and 3.6% (B), respectively, but at the same time the duration of the process is also decreased by 3.8%. This results in slightly increased specific product flow rates (SPF), defined as the ratio of PA or PB and the duration of the process. However, both the amount of the fresh E used, and that of the still residue increase significantly (by 35% and 57%, respectively). Therefore, preloading of the entrainer is not recommended.

Table 1 Results obtained for different recycling policies

Policy	Duration, [min]	Fresh feed, [kmol]	PA, [kmol]	PB, [kmol]	Fresh E used, [kmol]	Still residue, [kmol]	η_A, [%]	η_B, [%]	SPF_A, [kmol/h]	SPF_B, [kmol/h]
1	2688	48	11.43	13.91	65.01	44.42	45.23	53.32	0.255	0.310
2	2586	48	11.31	13.36	88.00	69.93	44.78	51.23	0.262	0.310
3	2569	34.06	13.53	12.90	71.00	51.19	75.49	69.69	0.316	0.301
4a	2611	33.32	12.59	12.81	29.74	19.95	71.77	70.74	0.289	0.294
4b	2624	33.40	12.46	12.82	30.17	20.27	70.88	70.61	0.285	0.293

The *recycle of the off-cut A+B* decreased the amount of fresh feed processed, as expected, both with and without entrainer recycling. The amount of the off-cut is between 6 and 7.5 kmol. The A-content of the off-cut is between 57 and 60 mol%, that is, higher than in the fresh feed. The off-cut recycling reduces the loss of A and B, thus the recoveries show an important increase. The recycling is more favourable for A, as explained by the composition of the off-cut. The increase of η_A is so high that the total amount of product A is increased even though less fresh feed is processed. PB is reduced, but only by less than 8%.

By Policy 3 (no E recycle), the production process is faster by 4.4% than without off-cut recycle. SPF_A is significantly higher (35%), while SPF_B is only slightly lower (3%). However, the amount of fresh E and still residue increases by 9 and 15%, respectively.

When *E recycle* is applied, the amount of the still residue and final hold-up is not enough for the next batch, and fresh E make-up is necessary. By Policy 4a (mixing of fresh and recycled entrainer), Batch II requires 5.73, Batch III 2.34 kmol fresh E. These are 22% and 9% of the total amount of entrainer fed at the respective batches. By Policy 4b (sequential feeding), 7.83 kmol (39%) 0.67 kmol (3%) fresh E is needed. The composition of the recycled entrainer (both for 4a and 4b) is in the range: 0.05-0.07% A, 0.7-1% B, 99-99.25% E. As presented in Section 3.2, these B concentrations are high enough to appreciably influence the separation process. *Figure 3* presents the effect of entrainer recycle on the evolution of the distillate composition. In Steps 0-2, $x_{D,A}$ reaches higher values without entrainer recycle, while $x_{D,B}$ and $x_{D,E}$ are lower. By entrainer recycling, the production steps are shifted, resulting in longer duration of the process.

By comparing Policy 4 to Policy 3 and 4, it can be stated that the production becomes slower, although it is still faster than with neither off-cut nor E recycle. The amount of fresh feed, PA and PB is slightly lower. The recovery of A is reduced (by 5-6%) as expected, but that of B is slightly increased due to the additional amount of B recycled. Due to the entrainer recycle, the amount of fresh E used is less than half, and only the still residue of the last batch has to be treated.

The two variants of Policy 4 give very similar results; those of 4a are more favourable, but as sequential entrainer feeding is easier to realize in a practical way, Policy 4b is recommended for entrainer recycling.

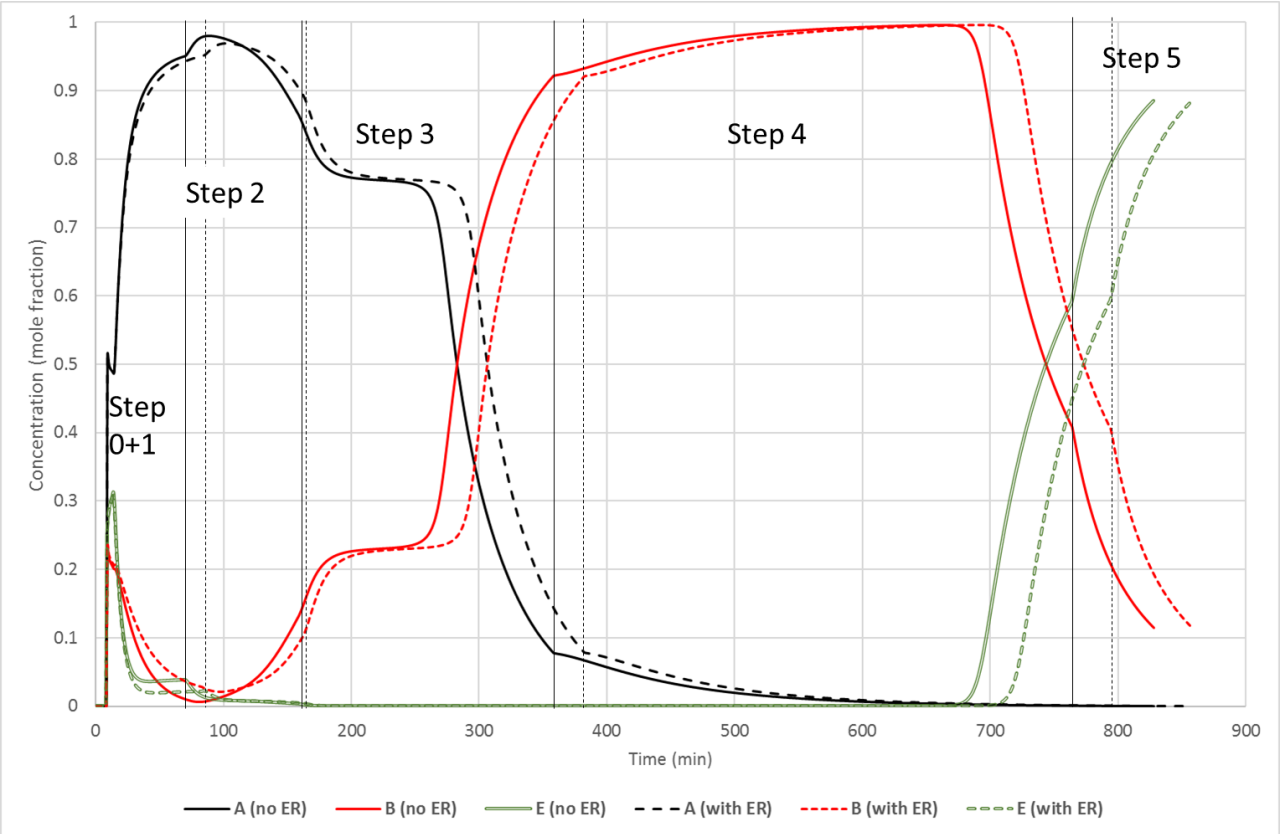

Figure 3 Evolution of condensate composition without and with entrainer recycle (Batch 2)

Off-cut recycle changes the composition of the charge (*Figure 4*). The water content is negligible (40-50 ppm) in all the cases, thus it is enough to present the change in the A-content. Due to the increase A-content of the off-cut A+B, $x_{Ch,A}$ is increasing. In Batch III, the A-content decreases, but it is still higher than in the fresh feed. By E recycling this decrease does not occur.

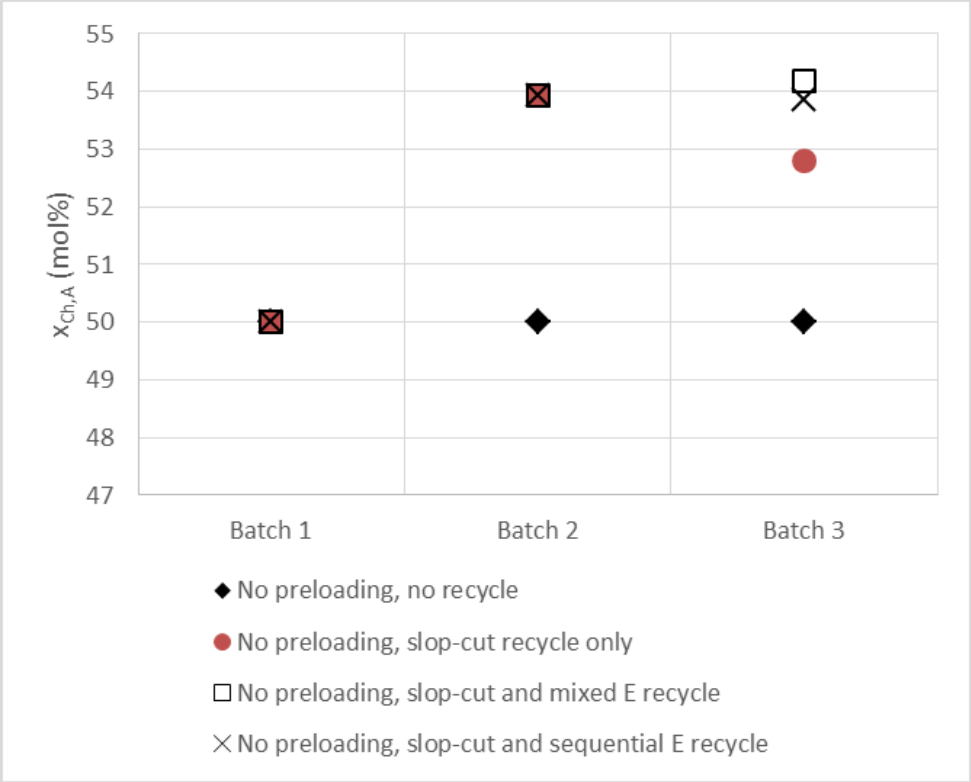

Figure 4 The variation of the charge composition as a function of the serial number of batch

CONCLUSIONS

The effects of entrainer preloading, off-cut and entrainer recycle on a batch extractive distillation process were investigated by dynamic simulation with the ChemCad software. Equimolar mixture of acetone(A)-methanol(B) was separated using water as entrainer(E). The production cycle consisted of processing 3 batches.

By the results preloading of the water to the binary charge had no positive effect. Recycling the off-cut A+B significantly increased the A-content of the charge and the recoveries. The capacity decreased, but the specific product flow rates were higher (for A) or similar (B).

The B-content of the recycled entrainer had an important effect on the production of A. Entrainer recycling greatly reduced the amount of fresh entrainer needed and that of still residue, but the recovery of A decreased. From among the two entrainer recycle versions the sequential one (feeding first the recycled entrainer then the fresh one) was slightly less favourable than premixing it with the fresh entrainer, but it is easier to realize.

REFERENCES

[1] Yatim, H., Moszkowicz, P., Otterbein, M., Lang, P.: *Dynamic simulation of a batch extractive distillation process*. Comput. Chem. Eng. 17, S57-62., 1993.

[2] Lang P., Yatim H., Moszkowicz P., Otterbein M.: *Batch extractive distillation under constant*

reflux ratio. Comput. chem. Engng. 18, 1057–1069., 1994.
[3] Lelkes, Z., Lang, P., Benadda, B., Moszkowicz, P.: *Feasibility of extractive distillation in a batch rectifier.* AIChE J. 44, 810-822., 1998.
[4] Lang, P., Kovacs, G., Kotai, B., Gaal-Szilagyi, J., Modla, G. : *Industrial application of a new batch extractive distillation operational policy*. IChemE Symp. Ser., 152. 830-839., 2006.
[5] Yao J.Y., Lin S.Y., Chien I. L.: *Operation and control of batch extractive distillation for the separation of mixtures with minimum-boiling azeotrope*, J. Chin. Inst. of Chem. Eng., 38, 371–383., 2007.
[6] Hegely, L., Lang, P., Gerbaud, V.: *Off-cut recycle for batch and batch extractive distillation separation of a multicomponent azeotropic mixture*. Chem. Eng.Trans. 35, 967-972, 2013
[7] Hegely L., Lang P.: *Optimization of a batch extractive distillation process with recycling off-cuts.* Journal of Cleaner Production,136, 99-110., (2016)
[8] Luyben, W.L., Chien, I.L., Design and Control of Distillation Systems for Separating Azeotropes. John Wiley & Sons, Inc., Hoboken, New Jersey, 421-422., 2010.

INTERNATIONAL SCIENTIFIC CONFERENCE ON ADVANCES IN MECHANICAL ENGINEERING
13-15 October 2016, Debrecen, Hungary

SIMULATION OF CO_2 ABSORPTION WITH DIFFERENT AMINE SOLVENTS

[1]LÁNG Péter DSc, [2]HÉGELY László PhD, [3]DÉNES Ferenc PhD

[1,2]Budapest University of Technology and Economics, Faculty of Mechanical Engineering, Department of Building Services and Process Engineering
E-mail: hegely@mail.bme.hu, lang@mail.bme.hu
[3]Budapest University of Technology and Economics, Faculty of Mechanical Engineering, Department of Energy Engineering
E-mail: denes@energia.bme.hu

Abstract
For the capture of CO_2 the most promising method is the chemical absorption in aqueous amine solutions. The most common solvent recycled in the absorber-stripper system is the aqueous monoethanolamine (MEA). However other amines such as diethanolamine (DEA) and methyldiethanolamine (MDEA) are also considered as potential suitable solvents. The reduction of the CO_2 emission of a coal fired power plant by absorption is studied by simulation with a professional flow-sheet simulator. The effectiveness and the characteristics of the three different amine solvents are compared.

Keywords: *CO2 capture, absorption-desorption, simulation, MEA, DEA, MDEA.*

1. INTRODUCTION

From all the greenhouse effect gases, the atmospheric concentration of carbon dioxide shows the most significant increase. Several methods exist for the capture of CO_2 from flue gases, such as water or amine scrubbing, or membrane separation. The most promising method is the chemical absorption in aqueous amine solutions. The most common solvent recycled in the absorber-stripper system is aqueous solution of monoethanolamine (MEA). Though the absorption process is efficient but the energy demand of the stripping is very high and this considerably decreases the efficiency of power plants. Therefore other solvents must be also taken into consideration in order to decrease the energy demand of the process and to eliminate the other disadvantages of the MEA (e.g. danger of corrosion). From among the other potential solvents the aqueous solution of diethanolamine (DEA) and that of methyldiethanolamine (MDEA) were also frequently studied.
The goals of this paper:
- to describe the criteria for solvent selection and the characteristics of the solvents studied,
- to study the operation of the absorber-stripper system by rigorous simulation with the professional flow-sheet simulator ChemCad,
- to create the open and closed loop models of the absorber-stripper system,
- to compare the effectiveness of the three different amine solvents.

For the vapour-liquid equilibrium and enthalpy calculations the “AMINE” model of the simulator was applied, which was validated for measurement data.

2. THE PROCESS

Before entering the absorber the flue gas must be purified (desulphurisation, denitrification,

removal of fly ash), saturated with water (in order to decrease the loss of solvent), cooled down and slightly compressed (the pressure drop of the absorber must be covered).
The removal of CO_2 from the pre-treated flue gas is performed in an absorber-stripper system (*Figure 1*). The CO_2 is absorbed from the flue gas by the solvent lean in CO_2 in the absorber, operating at nearly atmospheric pressure. In the case of MEA the gas leaving the column is washed by water in a washing section, in order to reduce solvent loss. For the DEA and MDEA there is no need for washing sections. With the water make-up fed to the washing section the water loss of the system can be compensated. The solvent rich in CO_2 leaves the bottom of the absorber and after being preheated by the lean solvent in the cross (rich/lean) heat exchanger, enters the stripper, which is operated under pressure. The vapour generated in the reboiler strips the CO_2 out of the solvent. The warm lean solvent leaving the bottom of the stripper is cooled down by the rich solvent and then in an aftercooler and it is recycled to the absorber. The stripped gas can be washed in a washing section, after which its water content is condensed in a partial condenser. The condensate can serve as the washing liquid and one part of it can be withdrawn.

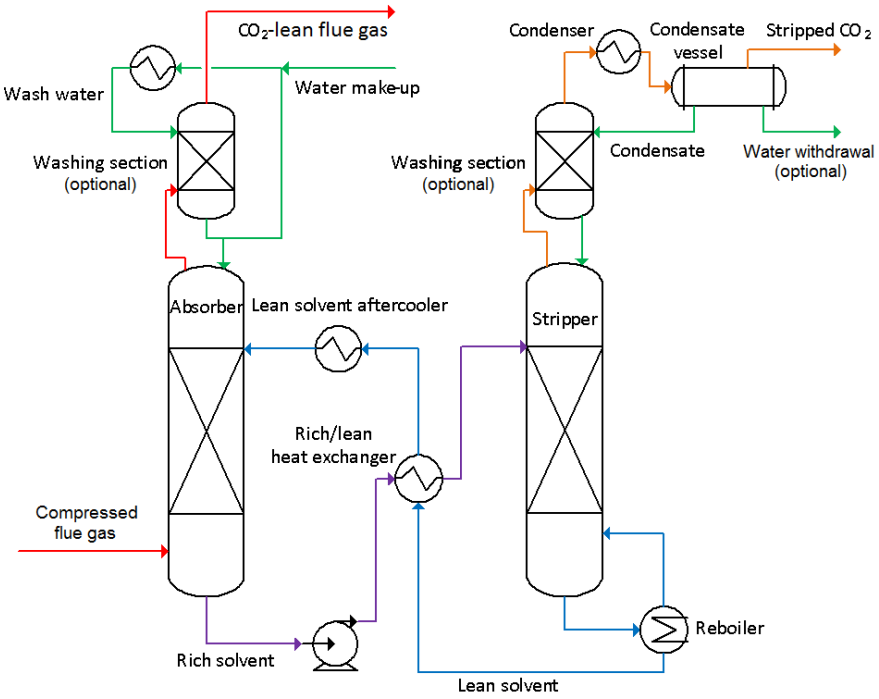

Figure 1 The absorber-stripper system (with washing sections)

3. CRITERIA FOR THE SOLVENT SELECTION

The design and operation parameters of the columns are determined by the following parameters:
- Reaction rate with CO_2: In the case of low reaction rate the residence time of the liquid on the plate and therefore the diameter of the column and the height of the overflow weir of plates must be increased.
- Absorption ability of CO_2: The higher, the less solvent must be circulated in the system. It is advantageous, if the (theoretical) loading capacity of the solvent is high (e.g. for tertiary and sterically hindered amines: 1 mol CO_2/mol amine, for secondary amines: 0.5 mol CO_2/mol amine).
- Heat of reaction, regenerability: The energy demand of the stripping of CO_2 cannot be too high. In the case of high heat of reaction the energy demand of the regeneration is also high.
- Thermal and chemical stability: The solvent, which is used several times, can degrade because of

thermal and chemical effects, and environmentally harmful and corrosive decomposition products can be formed. In order to reduce the degradation it is necessary to use materials as stable as possible.
- Environmental effect: It must be as slight as possible (e.g. toxicity).
- Corrosivity: If the solvent is strongly corrosive, its concentration is maximized in the aqueous absorbent solution.

The following *physical* parameters also must be taken into consideration:
- Volatility: The high volatility means potentially high solvent loss. It can be characterized by the vapour pressure (p^0) and/or the boiling point (T_{BP}).
- Density (ρ_L), viscosity (η_L), surface tension (σ_L): The higher density results in a lower solvent volumetric flow rate, therefore also a smaller apparatus is sufficient. However, the surface tension and the viscosity must be low for the good mass transfer.
- Melting point (T_{MP}): In the absorber higher temperature must be kept than the melting points of the components of the liquid mixture.

Table 1 The most important physical parameters of the amines studied (T = 50 °C)

Component	M_w g/mol	T_{MP} °C	T_{BP} °C	p^0 mbar	ρ_L kg/m^3	η_L Pas	σ_L N/m
MEA	61.1	10	171	3.39	993	8.0x10^{-3}	0.046
DEA	105.1	28	268	0.01	1077	0.0105	0.047
MDEA	119.2	-21	247.3	0.104	1010	0.027	0.036

4. METHOD OF SIMULATION

From the pre-treated flue gas of the lignite fueled power plant 85% of the CO_2 is removed, applying MEA, DEA and MDEA solvents. First for the different solvents all input parameters are the same except for the lean solvent flow rate, which is determined with open-loop simulation by the aid of a controller (*Figure 2*). The recycling of the lean solvent and of the washing liquid was cut. Hence the flow rate, the solvent and CO_2 contents of the lean solvent when it is fed to the absorber and the recovery of CO_2 can be specified directly.

In the second stage closed-loop simulation is performed, that is,
- the solvent is recycled to the absorber, eliminating the controller manipulating its flow rate in the open-loop simulation,
- the washing water is also recycled to the top of the absorber,
- the mass balance of water is ensured with either a make-up fed to the recycled lean solvent or a withdrawal from the condensate of the stripper,
- a separate partial condenser (FLASH+DIVIDER) is simulated for the stripper,
- the solvent loss is compensated with a make-up if necessary (in our case there is no need for this).

The closed-loop ChemCad model suitable for simulating all the three cases is shown in *Figure 3.* Both columns are simulated on the basis of the theoretical plate model with the module SCDS.

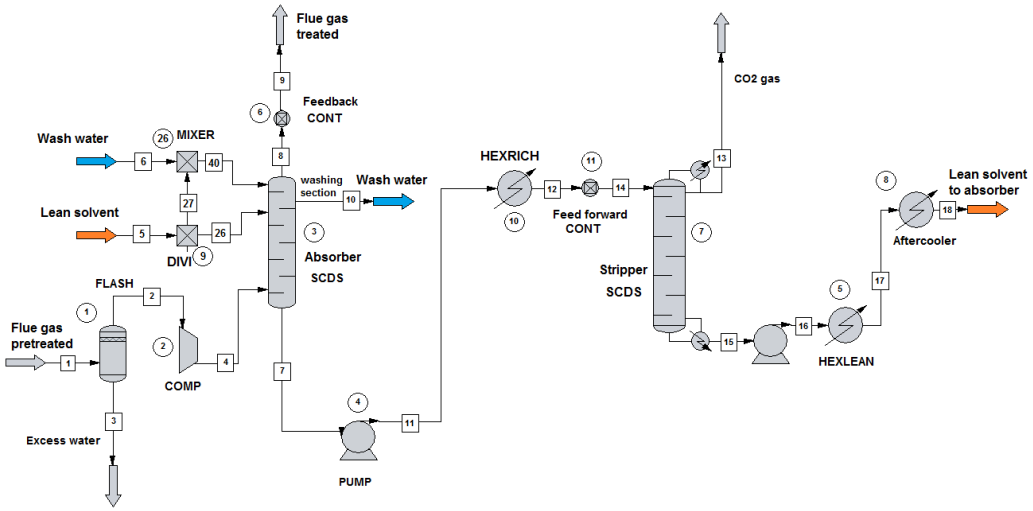

Figure 2 The general open-loop ChemCad model

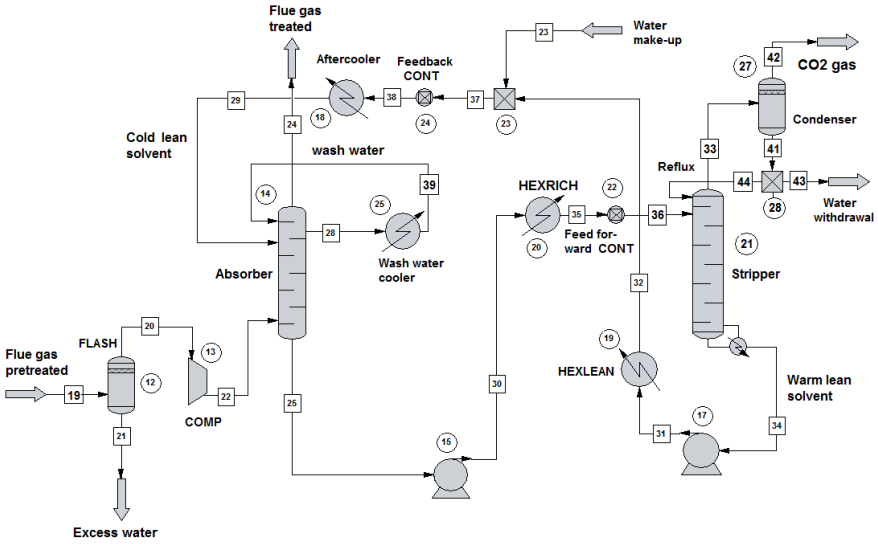

Figure 3 The general closed-loop ChemCad model

5. CALCULATIONS

The simulation is begun with the cooling of the flue gas onto 40 °C. The excess water is separated and the flue gas leaving is saturated with water vapour. In the compressor the pressure of the gas is increased onto the bottom pressure of the absorber, and its temperature also increases onto 49.4 °C. The flow rate of the gas entering the absorber: 13.00 kmol/s (389.01 kg/s). Its composition (mol%): CO_2: 15.34, water: 7.32, amine: 0.0, nitrogen: 74.65, oxygen: 1.81, argon: 0.88

The number of theoretical plates is 15 for the absorber (for the MEA including a washing section containing 2 plates), that of the stripper is 12. The top pressures are 1.013 bar (absorber) and 2 bar (stripper). The bottom pressures are 1.1 bar (absorber) and 2.1 bar (stripper).

The cold lean solvent enters the absorber at 40 °C. For the MEA (in the open-loop simulation) the lean solvent contains 30 mass% of the reagent and also 4 mass% of CO_2, hence its composition (mol%): CO_2: 2.14, water: 86.29, amine: 11.57. For DEA and MDEA the same molar composition is specified. The flow rate of the cold lean solvent is manipulated by a controller, so that the purified flue gas contains only 15% of the amount of CO_2 arriving at the bottom. For the MEA the

data of the wash water at the inlet: 66.9 kg/s (240.8 m^3/h), 40 °C (pure in the open-loop simulation) and its whole quantity is withdrawn at the bottom of the washing section. In the stripper CO_2 in a purity of 95 mol% must be produced. The temperature of the warm rich solvent entering the stripper is 100 °C.

The lean solvent flow rates calculated, kmol/s: MEA: 42.88 (1010 kg/s), DEA: 61.95 (1775 kg/s), MDEA: 107.04 (3240 kg/s). For the MDEA the temperature of the cold lean solvent had to be reduced to 25 °C and that of the warm one to 80 °C. The results of the open-loop simulations (begun with specified reflux ratio and bottom mole flow rate in the stripper) are shown in *Table 2*.

Table 2 Results of the open-loop simulations

Solvent	ABSORBER				STRIPPER					
	Top gas		Temperature		R	Q_N MW	Top gas		Temperature	
	kmol/s		°C				kmol/s		°C	
	water	amine	top	bottom			CO_2	water	top	bottom
MEA	3.5702	1.86E-09	65.8	46.0	0.65	257.05	1.6872	0.0843	44.8	120.3
DEA	1.8729	1.08E-05	54.6	53.2	0.63	239.66	1.6801	0.0912	46.3	113.7
MDEA	0.3712	1.08E-05	26.6	38.3	0.213	277.83	1.6818	0.0898	46.0	93.2

Solvent	Cross heat exchanger		After-cooler	Loss	
	Q MW	ΔT_{min} °C	Q MW	kmol/s	
				water	amine
MEA	207.4	15.2	72.8	2.6764	3.80E-09
DEA	306.9	8.7	132.6	0.9859	1.08E-05
MDEA	476.9	12.8	125.0	-0.5172	1.08E-05

The solvent losses are negligible. For the MEA and DEA water make-up must be applied and whilst for the MDEA water must be withdrawn (since the flue gas outlet temperature is lower than 40 °C). In the cross heat exchanger the heat duty is the highest for the MDEA because of the highest rich solvent flow rate caused by the highest lean solvent flow rate.

In the closed-loop simulations the water make-up is manipulated by a controller keeping constant the flow rate of the cold lean solvent (equal to that of the open-loop simulation). For the MDEA a separate partial condenser is used in the ChemCad model. In the stripper for the condenser the reflux ratio (MEA) or the distillate temperature (dew point of CO_2 product of prescribed purity) whilst for the reboiler the bottoms component flow rate of CO_2 are specified. For the MDEA the ratio of the reflux and liquid distillate flow rates is still fixed (1/9). The results are shown in *Table 3*.

Table 3 Results of the closed-loop simulations

Solvent	ABSORBER								
	Lean solvent				Top gas			Temperature	
	kmol/s	mol%			kmol/s			°C	
		CO_2	water	amine	CO_2	water	amine	top	bottom
MEA	42.8941	2.14	86.35	11.51	0.3114	3.5528	6.13E-04	65.7	46.0
DEA	61.9507	2.14	86.29	11.57	0.3496	1.5430	9.76E-06	54.4	54.9
MDEA	110.1095	2.07	86.73	11.20	0.2634	0.3077	9.80E-06	26.0	38.6

Solvent	STRIPPER						Cross heat exchanger		After-cooler	Make-up/ Withdrawal	
	R	Q_N MW	Top gas		Temperature		Q MW	ΔT_{min} °C	Q MW	kmol/s	
			kmol/s		°C					water	amine
			CO_2	water	top	bottom					
MEA	0.650	256.7	1.6828	0.0846	44.9	120.3	207.2	14.8	71.7	2.6402	0
DEA	0.488	251.8	1.6450	0.0866	45.8	116.6	289.2	14.8	180.8	0.6782	0
MDEA	0.111+	297.5	1.7308	0.0911	45.8	94.7	484.1	14.1	314.7	-0.2802	0

+ liquid/liquid reflux ratio

The recovery of CO2 is near to 85% (MEA: 84.4, DEA: 82.5, MDEA: 86.8). By increasing the flow rate of the lean solvent the recoveries could be increased. The specific energy consumptions in MJ/kg CO_2: MEA: 3.47, DEA: 3.48, MDEA: 3.90.The heat duty of the cross heat exchanger is the lowest for MEA and the highest for MDEA. This is also true for the after-cooler. On the basis of the results in the case studied the best solvent is MEA.
The performance of the absorber-desorber systems could be improved by exploiting better the cross heat exchanger (decreasing ΔT_{min}). The following parameters can be also optimised: the temperature, flow rate and composition (CO_2 and amine content) of the cold lean solvent, for the stripper: top pressure, location of the feed stage.

CONCLUSIONS

The reduction by 85% of the CO_2 emission of a coal fired power plant by absorption was studied by simulation with a professional flow-sheet simulator ChemCad. The effectiveness and the characteristics of three different amine solvents (MEA, DEA, MDEA) were compared. First the simulation was performed for open-loop systems then on the basis of their results for closed-loop ones. In the case studied the best performance was obtained for the MEA. In the future the systems must be still optimised.

ACKNOWLEDGEMENTS

This work was supported by OTKA. project No.: K- 120083 and TÁMOP - 4.2.2.B-10/1-2010-0009. The authors are grateful to Károly Moser PhD and Bálint Vörös MSc for their valuable help.

DESIGN OF ADAPTER FOR FIRE FIGHTING OF FOREST FIRES

[1]HNILICOVÁ Michaela PhD, [2]CHROMEK Ivan PhD, [3]HNILICA Richard PhD, [3]DADO Miroslav PhD

[1]Department of Forest Harvesting, Logistics and Ameliorations, Faculty of Forestry, Technical University in Zvolen
E-mail: michaela.hnilicova@gmail.com
[2]Department of Fire Protection, Faculty of Wood Sciences and Technology, Technical University in Zvolen
E-mail: chromek@tuzvo.sk
[3]Department of Manufacturing Technology and Quality Management, Faculty of Environmental and Manufacturing Technology, Technical University in Zvolen
E-mail: hnilica@tuzvo.sk, dado@tuzvo.sk

Abstract
An important role in manage the forest fires in difficult terrain is mobile fire equipment. The content of this article is design and construction of the fire bodywork to off-roader which will ensure the expansion of their use to fighting forest fires. The Fire and Rescue Service of the Slovak Republic as easy to use off-road vehicles Nissan Navara 4x4 and Land Rover Defender. The result is the design and construction of the fire bodywork for those vehicles, thereby widening their usefulness for fighting forest fires.

Keywords: *adapter, off-roader, fire body system, difficult terrain, forest fires.*

1. INTRODUCTION

The Slovak Republic covers an area of 49 035 km^2. It ranks among European countries with the highest forest coverage. The area of forest in the Slovak Republic, according to forest management in 2014 was 2 014 259 ha and forest stand area was 1 941 992 ha. Forest coverage has reached 41 %. In Slovak forests predominate in term of tree composition of tree species 61,85 % deciduous and coniferous trees make up 38,15 %. Beech has the largest representation (33 %), spruce (23,7 %), oak (10,6 %) and pine (6,8 %) [1].
From the aspect of forest protection, forest fire is the most drastic method of forest destruction. It has a huge impact for the whole forest ecosystem, especially plants and animals living here. Technically is a sudden, partly or wholly uncontrolled casualty delimited time and space which has a negative impact on all social function of the forest (commercial and non-commercial). It is a complex of physical and chemical effect which are based on non-stationary processes (space-time variable) of burning, gas exchange and heat transmission [2].
Generally we can say that the cause of forest fires are especially natural conditions and man himself. In European countries human factor involved in causing of fires from 80 % to 98 %. This most frequently arise from the negligence, non-observance of fire prevention measures, or underestimation of fire danger in the use of open flame - burning of grass burning of brushwood, setting a fire, smoking and children play with matches.
Based on the statistics [3], at the present time not coming a significant reduction in risk of forest fires, caused mainly by the following factors:

- increase of forest areas affected by the calamity caused by bark beetles, which exceeds the consequences of windthrow disaster of the 2004,
- underestimation of the factors identified in the period to 2007,
- lack of funds for consistent monitoring (aero, aboveground), focused on early detection of forest fires in the early stages,
- no-build enough dense forest road network in risk areas for different reasons,
- constant shortage of aboveground fire-fighting mechanisms, intended for localization and liquidation of forest fires in difficult ground in Slovakia.

Based on these results, we can say that mainly the last three factors have a significant influence on the extent of forest fires, which depends on the of late detection of forest fires and the problem of availability of ground for interference of fire brigades.

The basic condition for successful localization and liquidation of fire is continuity of supply of extinguishing medium. Without this condition can´t do fire-fighting one of the biggest of fires, which include forest fires. Forest fire conceals a many unknown quantities. The correct defining of these parameters is on intervention commander. One parameter is water resources and transport of water to fire-fighting of forest fire. Follows from the above the necessity of search for possibilities assurance of water and its transport in difficult conditions of forest operations, with the available techniques at the appropriate adaptation at forest fire fighting.

2. METHODS

Fire and Rescue Service SR today has off-road cars, whose body is not appropriate for conditions for forest fires in difficult terrains. Specifically the automobiles brands of Nissan Navara 4x4 and Land Rover Defender 130 with a loading area. The following automobiles have very excellent use for interventions and exceptional cases of different types due to the excellent patency difficult terrain. Loading area, which is on these vehicles are used to transport different material (equipment for lake system of water relay of forest fires-fighting, rock-climbing and speleology material, material for the establishment of general staff, flood-protection material) on food distribution, approach injured people to ambulances as well search for people in difficult terrain [4].

Designed body systems will increase usability of specified cars to forest fires-fighting, monitoring fireplace and monitoring increased risk of fire at the time. In the design of body systems we coming out with condition that in making use load capacity of off-road cars used in Fire and Rescue Service SR and Forests SR is possible place to body systems 400 litres of extinguishing medium useable for forest fires-fighting. Then, when choosing the type of car for the design body systems we coming out of three basic criteria:

- availability of cars within the Fire and Rescue Service SR and in the forestry sector,
- clearance height in the middle and difficult terrain,
- reserve in capacity weight minimum 800 kg for the need to achieve the objective of work.

A basic condition for design concept of the body is the use of reserves capacity weight with a focus on:

- centre of gravity of vehicle depending on changes in vehicle driveability,
- strength properties of the materials used for each part of the body,
- select the type of pump,
- choice of material elements increasing effectiveness of utilization body for forest fires-fighting and monitoring,
- design and scheme dimensions of body in view of the loading area cars,
- design water tank of minimum water volume 400 liters,
- design and scheme breakwaters into tank body,

- design protective frame of body,
- determine the mass of body.

3. RESULTS

Designed fires body systems are constructed and adapted to the parameters of the selected cars and will be placed on the loading area of these vehicles. Further body systems will be mobile, so the loading area of the cars will be demounting. Equipment proposed facility will serve the needs for efficient intervening cause in forest fires and monitoring of forests. Machine design concept we provide for condition is not exceeded capacity weight vehicles. Studying and searching we come to the conclusion that the proposed body systems will have the following basic parameters:

- the same material of construction of tank,
- fast assembly and disassembly of the vehicle loading area,
- the largest possible volume of water from the point of view load capacity,
- breakwater designed for maintaining vehicle driveability of car,
- motor pump.

The body system on the Nissan Navara 4x4 we designed only one configuration. This body has additional equipment for fire-fighting forest fires, designed as a flow winch. Equipment for fire-fighting forest fires are not included in equipment of body from the point of view capacity weight of car Nissan Navara 4x4. Transport of body systems is intended only car loading area. Body for Nissan Navara 4x4 therefore consists of:

- feed-tank,
- motor pump with equipment,
- flow winch.

The body system for the Land Rover Defender 130 we designed in two versions (variants A and B), by reason of various equipment. Transport of body systems over the previous body systems extended to transport in the underslung of helicopter. For the expansion of transport of body systems in underslung of helicopter must have body designed protective frame, which allows the transportation options and while protecting tank of body systems from mechanical damage during transport helicopter in underslung. Body for Land Rover Defender 130 therefore consists of:

variant A

- feed-tank,
- protective frame of body,
- motor pump with equipment,
- box with additional equipment (hose "C", "D"; branchpipe; dividing breeching; adapter of type "C" - "D", ax-hoe).

variant B

- feed-tank,
- protective frame of body,
- motor pump with equipment,
- flow winch.

For the needs of body systems was necessary to choose the basic material of the water tank, which would be resistant to accidental impact and simultaneously was the most light. Based on these needs and mutual consultation with producers of various tanks for our case we chose composite materials. Composite materials are known to the general public as glass fiber (carbon) materials and the profile can have different shapes.

The advantages of composite materials generally are based mainly on their weight. The proportion of strength and density a composite material advance steel many times. The important properties of

the composite is anisotropy, i.e. different mechanical properties for various load directions [5]. For complex loads are used composites consist of multiple layers with different orientation of fibers or fabric reinforced [6].

Fire body system for Nissan Navara 4x4

In the design of body systems go out of the parameters of car at which basic conditions for the machine design concept of the body were:

- the greatest possible volume of water in the tank,
- equipment of body system needed to fire-fighting forest fires, monitoring fireplace and forests in times of increased risk of forest fire,
- quick assembly and attachment of body system to the car loading area.

After the determination of conditions for the machine design concept of body system and given the load of car was body designed follows:

- volume approximately 400 litres of water,
- equipment of body system (high pressure motor pump and flow winch),
- principle of attachment the body to the loading area of the car through the anchor points,
- manipulation with tank (tank transferring, lifting tank) by the handles.

The tank of body system is made of fibreglass laminate (polyester). Tank is thickness of 5 mm. Fire body system (*Fig. 1*) was designed for the loading area of car such that the bottom of the tank is located between the fenders. The walls of tank copied fenders and continue around the side of the loading area and are ended along with the top edge sidewalls. Water inflow into the tank is handled through a draft tube of pump. On the draft tube of pump are located spherical valves using which we control water, which absorption the pump.

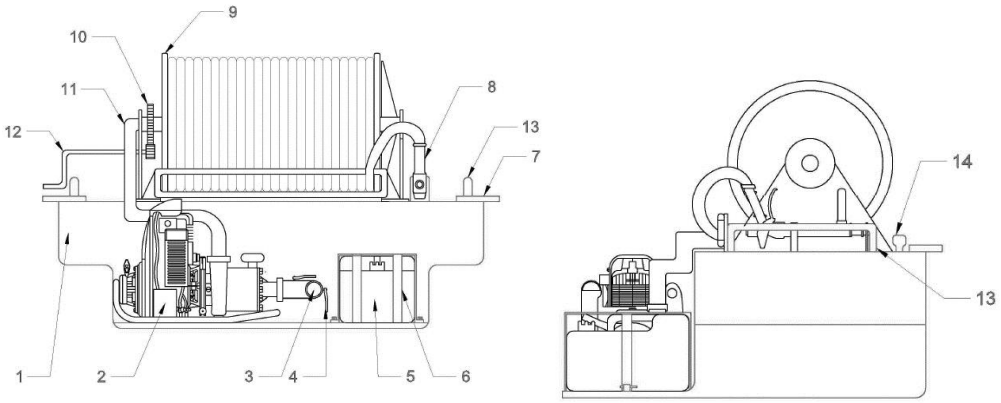

Figure 1 Fire body system for Nissan Navara 4x4

(1) tank of bodywork, (2) pump, (3admission and intake line, (4) spherical valve, (5) gas tank, (6) anchoring + protective frame for the gas tank, (7) anchoring of bodywork, (8) high pressure line of flow, (9) flow winch, (10) transmission of winch, (11) admission line, (12) winding handle on the flow tube, (13) handle on lift tank, (14) air eliminator

Fire body system for Land Rover Defender

In the design of the body system go out of the same conditions as the body on the Nissan Navara 4x4 whereby the conditions for design have been extended by alternative transport the body to the locality of the forest fire in underslung of helicopter.

After determination of conditions for the design of the body system for Land Rover Defender and given the load capacity this car, body has been designed as follows:

- volume approximately 600 litres of water,

- equipment of body system (high pressure motor pump, box with additional equipment in variant A, flow winch in variant B),
- principle of attachment the body to the loading area of the car through the anchor points,
- protective frame which provide for manipulation with body (tank transferring, lifting tank) and transport the body to the locality of the forest fire in underslung of helicopter.

Concept proposal of body system - version A

The body system type A for Land Rover Defender is specially adapted to fire-fighting of forest fire. This body type is designed with a box in which will deposited equipment to fire-fighting of forest fire and protective metal frame that allows its transport in underslung of helicopter, where must resist dynamic stresses and under shocks while saving helicopter on the ground (*Fig. 2*). The type of the body system is designed so that the car gets the highest possible location, as close to the fire and after that fire lines pulled from a car or engage in the lake system of water relay.

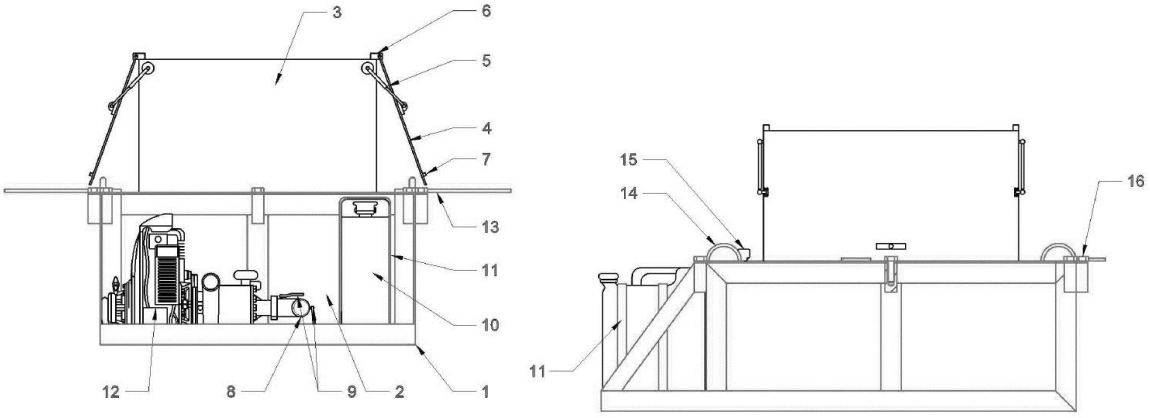

Figure 2 Fire body system for Land Rover Defender (variant A)

(1) protective frame of bodywork, (2) the tank of bodywork, (3) bodywork for firefighting tools, (4) door of bodywork, (5) piston door opening of bodywork, (6) hinge join door of bodywork, (7) hand grip door of bodywork, (8) admission and intake line, (9) spherical valves, (10) gas tank, (11) anchoring + protective frame for the gas tank, (12) pump, (13) anchoring of bodywork, (14) anchoring eye for fixing the bodywork to underslung, (15) air eliminator, (16) screw for fixing of the top protective frame on construction of protective frame

Concept proposal of body system - version B

The body system type B for Land Rover Defender is of the same design as the body of type A. The main difference is in location of flow winch instead of box for equipment, thereby ensuring direct of fire-fighting (*Fig. 3*).

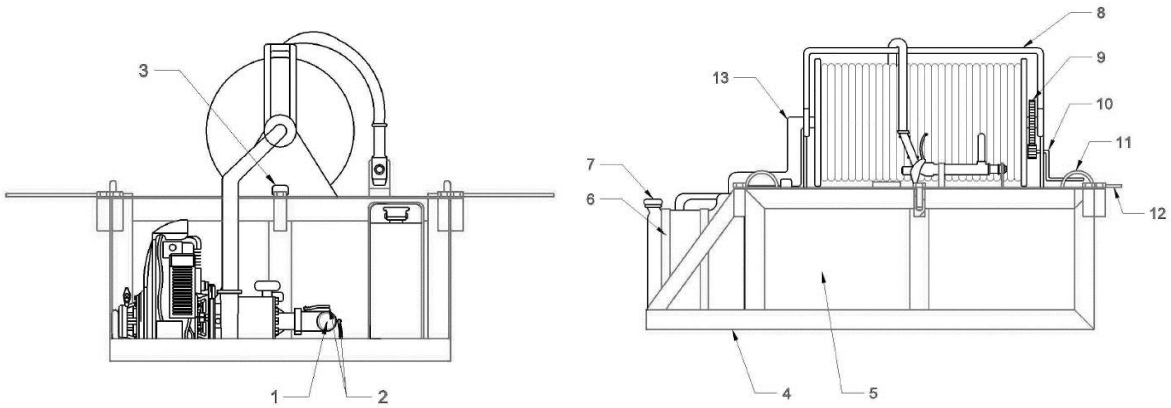

Figure 3 Fire body system for Land Rover Defender (variant B)
(1) admission and intake line, (2) spherical valves, (3) air eliminator, (4) protective frame, (5) the tank of bodywork, (6) anchoring + protective frame for the gas tank, (7) gas tank, (8) flow winch, (9) transmission of winch, (10) winding handle on the flow tube, (11) anchoring points for fixing the bodywork to underslung, (12) anchoring of bodywork, (13) admission line

The tank of the body system is the same for variant A and variant B, specifically of fiberglass laminate (polyester). Tank is thickness of 5 mm. The shape of tank is accommodate the loading area of a car and automobile equipment, where had to balance with dimensions of the loading area, location of fenders in the loading area and location of the spare tire, which is located on the loading area and location of the motor pump.

CONCLUSIONS

The main content and aim of this work is the design of the body system for off-road car used in Fire and Rescue Service SR and Slovak forests. Designed of the body system are engineered so that its equipment and layout do not exceed the capacity weight. The aim of this work we complete task and exceed designed of the body systems of capacity weight of cars.
Another working hypothesis was condition when using of capacity weight of the cars we placed in the body system a minimum of 400 liters of water. Definition of the work hypothesis we confirmed. In regard to capacity weight of cars we are able to pour into tank of body systems minimum amount of water (400 liters). Next we confirmed that the amount of water in the adapter is dependent on the capacity weight of the car and the equipment designed of body system.
The designed bodies we have expanded efficiency of these cars to fire-fighting forest fires in difficult terrain, the monitoring activity of fireplace and monitoring of forests in times of increased risk of fire.
Taking into consideration that at present Fire and Rescue Service SR and Forests SR dispose of indicated types of cars but does not have the type of bodies designed in this paper, it would be advisable to process of design based on this design incorporate to carriage stock also this type of cars with similar body systems or it started with production of types of body systems. The designed body systems will increase the usability of the mentioned cars to fire-fighting forest fires. Processed idea of design solutions can be useful for companies that handle the design fire-fighting body systems.

ACKNOWLEDGEMENT

This work was supported by the Slovak Research and Development Agency under the contract No. APVV-14-0468 „Development of an auxiliary device and its technological employment to increase the efficiency of extinguishing forest fires“.

REFERENCES

[1] Green report 2015. Report on forest management in the Slovak Republic 2014. Bratislava, 2015.
[2] Hlaváč, P., Chromek, I.: Forest fires in Slovakia. In *Forest protection 2015 :* Proceedings of the reviewed original scientific and profesional papers. - Zvolen : Technical University in Zvolen, ISBN 978-80-228-2835-2, s. 109-116., 2015.
[3] Statistical Yearbook 2013. Požiarnotechnický a expertízny ústav MV SR v Bratislave (PTEÚ).
[4] Hudáč, J.: Proposal firefighting superstructure for off-road vehicle. Diploma thesis, Technical University in Zvolen, DF-5811-16262, 115 s., 2016.
[5] Kořínek, Z.: Kompozity. [online]. [cit. 2016-07-09]. <http://mujweb.cz/zkorinek/>. 2016.
[6] Bezecny, J.: Composites. Study materials for students. AIS Fakulta výrobných technológií TnUAD, [online]. [cit. 2016-07-09]., <http://www.fpt.tnuni.sk/index.htm>., 2016.

INTERNATIONAL SCIENTIFIC CONFERENCE ON ADVANCES IN MECHANICAL ENGINEERING

13-15 October 2016, Debrecen, Hungary

EXTENDED OPERATING MAINTENANCE MODEL FOR MODERN PRINTING MACHINES, NEW INITIATIVES

HORVÁTH Csaba PhD

Institute of Media Technology and Light Industry Engineering, Rejtő Sándor Faculty of Light Industry and Environmental Engineering, Óbuda University, Budapest, Hungary
E-mail: horvath.csaba@rkk.uni-obuda.hu

Abstract
The author outlined a model to examine unexpected breakdowns in modern printing machines. They were analyzing the different downtimes for years. The results of the researches help to organize the pro-active maintenance at the graphic arts industry.
During the study, the operation of characteristic printing machines was monitored in two steps, primarily to analyze unexpected breakdowns. From 1988 until 2004, i.e. for 17 years a database of unexpected breakdowns was structured with respect to 65 modern printing machines. The associated theoretical and practical conclusions drawn from the study were presented in 2008, in Valencia (Spain) at the 35th IARIGAI (International Association of Research Organizations for the Information) Conference. This publication is a summary of the observations of an additional period of 10 years (2005–2014). In this latter period, 71 mechanical printing equipment units were studied; some of them were identical to the machines investigated earlier, but a significant part of them were newly commissioned machines. Resulting from the study, the database of unexpected breakdowns was compared to the earlier results to highlight similarities, changes and development. One of the major conclusions of the study that is reflected from the results of the full-scale (27-year) monitoring effort is that in the world of printing machines a large proportion of unexpected breakdown, failures are technical or technological errors that can be quickly tackled. This fact entails specific maintenance and machine surveillance demands that the professionals of the industry who are involved in maintenance operations have to be aware of. The processing of the failure database has yielded numerous other results and conclusions that the authors detail in their work. Special attention has been paid to the impacts and demands that the technological development of the past quarter of a century has brought about in the organization of maintenance activities for characteristic equipment.

Keywords: *printing machines, unexpected breakdown, preventive maintenance*

1. INTRODUCTION

Maintenance techniques have changed over time from correction (breakdown) to prevention to prediction and pro-active continuous improvement. Effective maintenance is a series of progressive steps to improve operational effectiveness and the key step in this process is the transition of pro-active working. Companies that optimize their maintenance select and combine the techniques that match the needs of their equipment and operations. Moving up the maintenance stairway requires a planned approach that brings together the right procedures, tools, training and the knowledge the feature and history of our machines' breakdowns [4].

2. THE OBJECTIVES OF THE RESEARCH

The results of authors' survey – covering 25 leading Hungarian printing offices – suggest that the major cause (46%) of maintenance issues is events of unexpected breakdowns. Consequently, the high ratio is the most influential factor of the design and management of maintenance tasks. The objective of the research is to critically map and discover the characteristics of unexpected breakdowns of printing machines in order to facilitate proper maintenance management [2].

3. RESEARCH METHODS - OPERATING MAINTENANCE MODEL

Despite the possible big differences between printing machines we treat them with a united approach based on their fundamentally common characteristics. One of the major reasons for the synthesis originates from maintenance practice. Generally, the printing offices perform the maintenance duties with staff small in number. Consequently, there is a little chance to gain special knowledge and subdivide the maintenance approach and practice. The machines, which are different in structure and technological tasks, have a lot of common characteristics from the operational and maintenance point of view in case of printing office applications, which makes the united approach acceptable (Claypole, 2005; Wells, 2003).
The technological elements of modern printing machines unite two equally important operations. The major operation, which performs informational types of formation on the product, is based on a highly accurate transmitting operation of the processing material (mostly paper). Therefore, the input and the output units are very important elements of printing machines. These elements ensure the assembly of machine systems. Moreover, if the bigger systems were divided into elements we would always get division three, in the model. The units of operation, management and supply set the same claims up for the technological units regarding their structural form, complexity and especially their maintenance requirements.
The author outlined a model (*Figure 1*) to examine the unexpected breakdowns of modern printing machines.

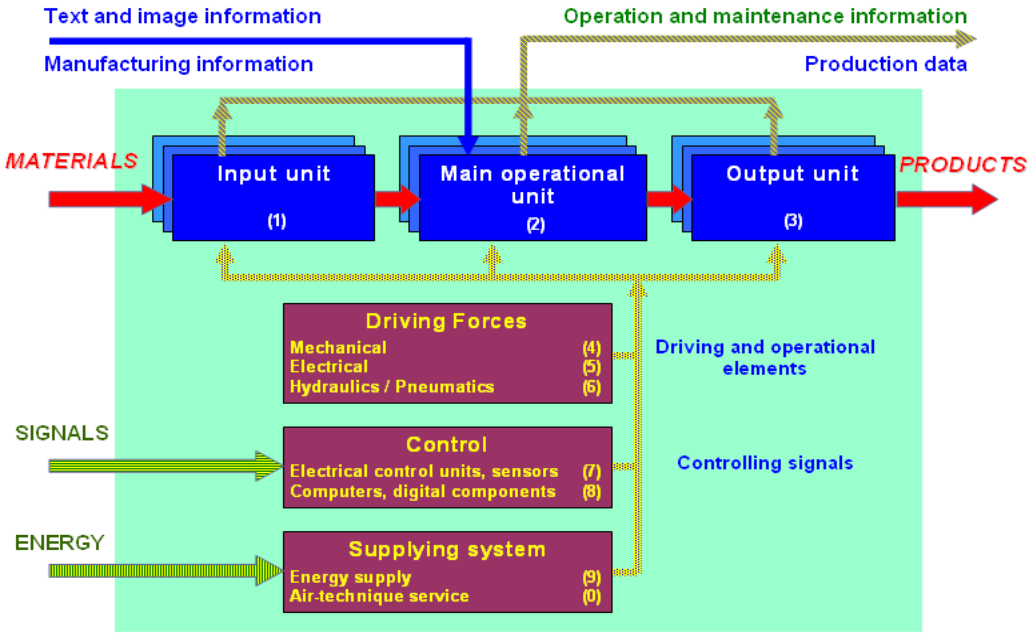

Figure 1: Extended operating maintenance model for the printing machines

The model reflects the general structure of printing machines, which is needed to analyse the features of maintenance and maintenance management. The modeling analysis focused on various types of downtimes of 65 different printing machines representing the previous, current and future generations.
The data of unexpected breakdowns were derived from an extensive period of time.

4. MAINTENANCE FEATURES OF PRINTING MACHINES

While providing analysis for the typical features of the troubleshooting and detailed information of repairing operations, the results of the researches outline the maintenance characteristics of the modern printing machines' unexpected breakdowns.
The similarities between the manufacturing processes, raw materials and products of printing machines result in similar defective, corrective and maintenance features, which should be considered during management and organizational tasks. Therefore, thoroughly analyzed those sources of faults and damaging processes, with which we struggle during the operation of printing machines.
The authors collected data on unexpected breakdowns of printing machines for a long period of time at Alfoldi Printing Plant Plc., Hungary's largest book printing plant. A computer-assisted system could continuously record the basic data of the important processing machines. The historical datasets were set as the starting point for our analysis. The continuous data collection was carried out on the most important processing machines of Alfoldi Printing Plant Plc. During the monitoring the machines were replaced from time to time following the technological development. We monitored 65 printing machines. These represent the previous, current and following generations. Their age varied between 1 and 27 years and 22 completely new machines were purchased during our monitoring. Every machine was operated at a specific site, the centre site of Alfoldi Printing Plant.
The data of unexpected breakdowns what they used are from a wide period of time (data of 17 years of full operation between 1988 and 2004).
The extent of generalization based on the characteristics of printing machines might obviously raise a few questions from the reader. The printing machines and the relatively complex technology of Alfoldi Printing Plant and their loading give an extensive cross-section of today's typical printing machines. It was a limiting factor that there were only a few similarly detailed and accessible historical databases even for a shorter period of time. However we could make a comparison with the data of similar Hungarian printing plants; like Szikra Lapnyomda., Revai. and Petofi Printing Plant. The data on downtime and reparation time showed similarities with the calculations from our database.
Figure 2 shows the major conclusions and the calculated characteristics. The 65 printing machines ran nearly 1.7 million operating hours, while 58317 maintenance events originated from unexpected breakdowns were recorded. The reparation of the machines caused more than 105,000 operational hours of dropout in the production and more than 130,000 reparation hours.

The calculated mean values	Mean	*Standard deviation*
Restoration time	**1.80 hours**	0.47 hours
Repair time of a breakdown	**2.24 hours**	0.54 hours
Characteristic data of printing machine		
Operational time in a year	**2 883 hours**	**617 hours**
The expected number of unexpected breakdowns during the operational period (rounded values)		
yearly	**87 occasions**	**24 occasions ***
monthly	**7 occasions**	**3 occasions ***
weakly	**2 occasions**	**1 occasions ***

* Rounded values for the easier understanding

Figure 2 Most relevant data characterizing the unexpected breakdowns of printing machines (Examination period: 1. January 1988. – 31. December 2004.)

The unexpected breakdowns of printing machines are quickly reparable; these generally require small maintenance events. The downtime, which is not more than two hours, caused by operational failure is more than 80%, which generates more than 50% of this kind of troubleshooting. The originated reduction of losses requires concentration to details and predictive organization. The relatively low average value might just well have a great influence on the future developmental concepts of maintenance systems. The relatively short reparation times typically contain several elements that are not actual professional work (reaction time, approaching the reparation scene, information transfer etc.). The relative frequency of values characterizing the reparation times of unexpected breakdowns is shown on a histogram of *Figure 3.* These data contain extremely important information for maintenance managers.

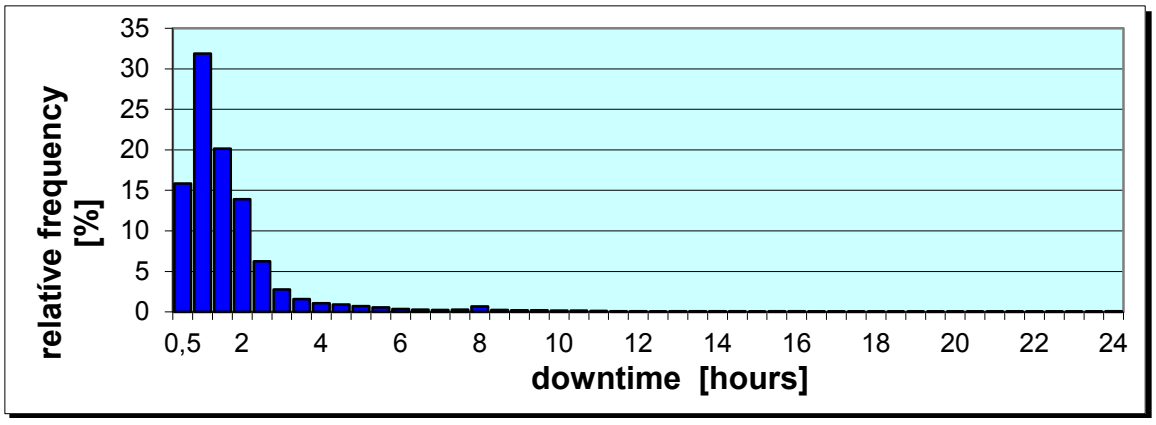

Figure 3 Histogram of the relative frequency of time needed to troubleshoot the unexpected breakdowns of printing machines (Examination period: 1. January 1988. – 31. December 2004.)

5. THE „REFURBISHED" MONITORING AND EXAMINATION BETWEEN JANUARY 1, 2005 AND DECEMBER 31, 2014

The finishing of the last investigation of the monitoring mentioned above was teen years ago. The monitoring of the printing machines of Alfoldi Printing Plant was continuously during this period of time. The "newer" 10 years is more than enough to repeat the investigation.
Even the company has partly changed its machinery and technology during the 10 years of examination. The average number of the running machine was 77. They have taken 38 machines out of order and have bought and took in operate 24 pieces new ones. The summary of the operating time was 611 326 hours while 18 585 maintenance events originated from unexpected breakdowns were recorded. It can be seen the number of unexpected breakdown was considerable reduced. The Figure 5 shows the character of the histogram hasn't changed, but the average time for the trouble-shot and repairing of the unexpected breakdowns increased. Only 60% of the breakdown is repairable within 2 hours.

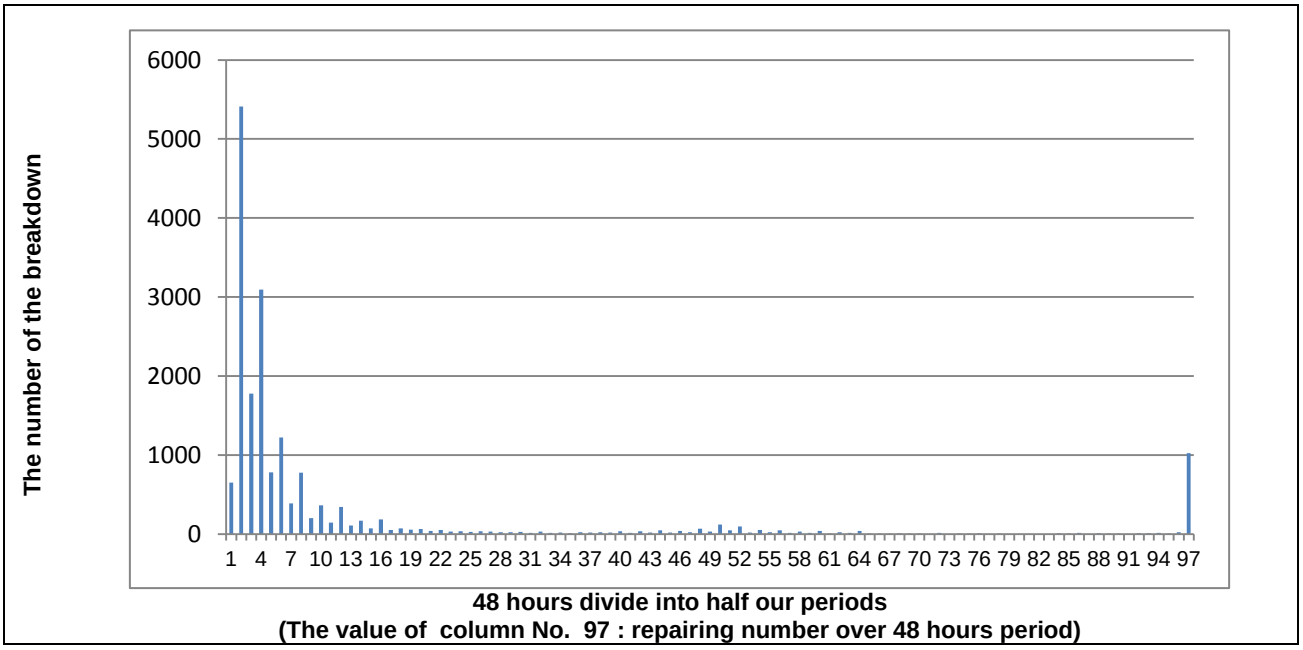

Figure 5 Histogram of the relative frequency of time needed to troubleshoot the unexpected breakdowns of printing machines
(Examination period: 1. January, 2005 – 31. December, 2014)

CONCLUSIONS

For maintaining the productivity of printing machines, the detailed knowledge of relations between failures is crucial. Aversion of unexpected breakdowns generally requires short/reactive reparative action. The knowledge about the typical failure rates of major parts of printing machines is the fundamental pillar to apply pro-active maintenance management. The strategy of the maintenance in Alfoldi Printing plant has also been changed to prefer the pro-active management.

REFERENCES

[1] Claypole T. – Wells N.: *Productivity maintenance in the UK Printing Industry*, pp. 84, Vision in Print, March, 2005, www.visioninprint.co.uk
[2] Gaál Z.: *Karbantartás-menedzsment*, Pannon Egyetemi Kiadó, Veszprém, 2007, pp. 236
[3] Horváth Cs. – Gaál Z. – Kerekes, K.: *Extended operating Maintenance Model for Modern Printing Machines*, 35th International Research Conference of Iarigai, Valencia, Spain, 7-10 September, 2008**,** Vol. XXXV of the Advances in Printing and Media Technology (published in November 2008), pp. 129-136, ISBN 987-3-9812704—0-2
[4] Tsang, A.: *Strategic dimension of maintenance management*, Journal of Quality in Maintenance Engineering, 2002/1 pp. 7-39
[5] Wells, N.: *Best Practice: Maintenance*, PrintWeek, December, 2003, pp. 24-31, www.visioninprint.co.uk

INTERNATIONAL SCIENTIFIC CONFERENCE ON ADVANCES IN MECHANICAL ENGINEERING
13-15 October 2016, Debrecen, Hungary

INCOMPRESSIBILITY ANALYSIS OF RUBBERS USING FEM

[1]HURI Dávid, [2]MANKOVITS Tamás PhD

[1,2]Department of Mechanical Engineering, Faculty of Engineering, University of Debrecen
E-mail: huri.david@eng.unideb.hu, tamas.mankovits@eng.unideb.hu

Abstract
Non-linear finite element calculations are indispensable when important information of the material response under load of a rubber component is desired. Although the material characterization of a rubber component is a demanding engineering task, the changing contact range between the parts and the incompressibility behaviour of the rubber further increase the complexity of the investigations. In this paper the effects of the choice of the numerical material parameters (e.g. bulk modulus) are examined with regard to numerical stability, mesh density and calculation accuracy. As an example, a compressed rubber spring is chosen in ideal conditions.

Keywords: *rubber, finite element method, numerical stability, incompressibility*

1. INTRODUCTION

Rubber products are widely used in industry due to their special mechanical and physical properties and the technological development in producing artificial rubber raw materials. As a structural element, rubber can be found in several fields, such as building industry, agriculture, engineering, etc. Although the extensive usage and the proper design of rubber parts are still demanding engineering tasks due to several factors that determine their behaviour.
One is the production of the rubbers, where the wide range of the applied components strongly influence the property. Thanks to the different rubber recipes, the components percentage are handled as an industrial secret so the important material constants must be determined in laboratorial environment.
On the other hand, during the design phase the incompressibility of rubber must be taken into consideration. Incompressibility as an auxiliary condition can be enforced by penalty method [1-3]. Rubbers may undergo large deformations under load and their characteristics show non-linear behaviour. The changing contact range between the parts and the incompressibility of the rubber further increase the non-linear behaviour. Numerous papers are devoted to the finite element analysis of rubber materials [4-9]. In [10] the bulk modulus and Poisson's ratio of incompressible materials are investigated. The incompressibility of rubber-like material was analyzed in [11]. The material parameters of rubber-like materials bonded to rigid surfaces were evaluated by [12, 13].
In this paper a numerical analysis determining the numerical material parameters are presented, which ensures the numerical stability, the accuracy and the incompressibility during the finite element calculations. A numerical evaluation is also performed to estimate the optimal input parameters for the finite element analysis such as mesh density. As an example, a compressed rubber spring is chosen in ideal conditions.

2. THE THEORETICAL BACKGROUND OF THE RUBBER INCOMPRESSIBILITY

The material models for rubbers are generally given by the strain energy density function. A successful finite element simulation of rubber parts hinges on the selection of an appropriate strain

energy function and on the accurate determination of material constants. The available strain energy functions have been represented in terms of the strain invariants which are functions of the stretch ratios.

The strain energy function is defined by this specific decomposition

$$W = W_V(J) + W_D(\boldsymbol{C}), \tag{1}$$

where $W_V(J)$ denotes the strain energy due to the volumetric change and J is the Jacobian and $W_D(\boldsymbol{C})$ is the strain energy determined by volume preserving deformation [1,2,14]. The $\boldsymbol{C}$ right Cauchy-Green deformation tensor

$$\boldsymbol{C} = \boldsymbol{F}^T \boldsymbol{F} \tag{2}$$

where $\boldsymbol{F}$ is the so called deformation gradient. A number of material models can be found in literature for the volume preserving part of strain energy density. The two-parameter Mooney-Rivlin material model is applied to describe the material behaviour

$$W_{D\,MR} = C_{10}(I_I - 3) + C_{01}(I_{II} - 3) \tag{3}$$

where C_{10} and C_{01} are the material constants, I_I and I_{II} are the first and second invariants of the right Cauchy-Green tensor, respectively.

It is well known that rubbers are regarded as incompressible or nearly incompressible materials. Total incompressibility means that the material suffers zero volumetric change under hydrostatic pressure. The incompressibility of the material can be represented by $det\boldsymbol{F} = 1$, so the Poisson's ratio is $\nu = 0.5$. It should be noted that engineering rubbers may be regarded as nearly incompressible materials due to additives. Accordingly, the Poisson's ratio is between $0.49 < \nu < 0.5$.

The strain energy density resulting from the change in volume is often defined in the simplest way [14]

$$W_V(J) = \frac{1}{2}\kappa(J-1)^2, \tag{4}$$

where κ is the bulk modulus which can be interpreted as a penalty parameter in the finite element calculations. The bulk modulus using [14] can be calculated as

$$\kappa = \frac{2G(1+\nu)}{3(1-2\nu)} = \frac{E}{3(1-2\nu)}, \tag{5}$$

where E is the Young's modulus and G is the shear modulus. Reordering (5)

$$\nu = 0.5 - \frac{E}{6\kappa} \tag{6}$$

Poisson's ratio can be determined for different bulk modulus values at $E = 1.5$, see in Table 1.

Table 1 The values of the Poisson's ratio

$\kappa\ [MPa]$	$E\ [MPa]$	ν
1	1.5	0.25
10	1.5	0.475
100	1.5	0.4975
1000	1.5	0.49975
10000	1.5	0.49998

It can be observed that different bulk modulus values have influence on the strain measures of the continuum element. So it is important to investigate the relationship between the deformed volume element dV in the current configuration with the original volume element dV_0 in the reference configuration. In order to be able to compare the calculated result, unit values have to be introduced,

$$\varepsilon_{dV} = \frac{\Delta dV}{dV_0} = \frac{dV - dV_0}{dV_0} \tag{7}$$

and

$$\varepsilon_V = \frac{\Delta V}{V_0} = \frac{V - V_0}{V_0} = \frac{V}{V_0} - 1 \tag{8}$$

where ε_{dV} is the unit volume change calculated for volume elements and ε_V is the unit volume change for the investigated body in the current configuration. For the solid body this volume change can be determined directly, when the rubber spring is in ideal conditions.

3. NUMERICAL EXAMPLE

A cylindrical rubber spring is chosen for analysis, see in *Figure 2.* The governing input data of the finite element analysis can be seen in *Table 2.*

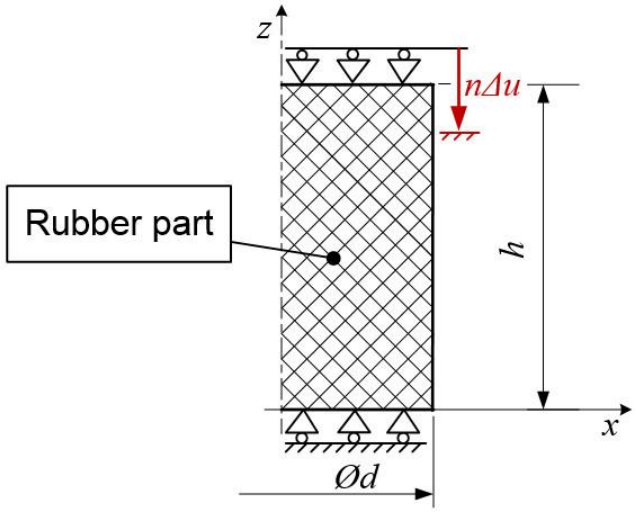

Figure 2 The meridian section of the rubber spring

Table 2 The input data of the simulations

Geometry	
Diameter of the rubber spring (d)	20 $[mm]$
Height of the rubber spring (h)	20 $[mm]$
Material parameters	
Mooney-Rivlin material constants (C_{10})	0.6 $[MPa]$
Mooney-Rivlin material constants (C_{01})	0.15 $[MPa]$
Bulk modulus (κ)	2^i $(i = 1, \dots 13)$ $[MPa]$
Finite element settings	
Supports	frictionless
Displacement increment (Δu)	1 $[mm]$
Number of loading steps (n)	10

The purpose of the first investigation was to analyze the effect of the bulk modulus change for the unit volume change. It can be stated that higher bulk modulus value results in smaller volume change and converge to zero, therefore, the incompressibility can be ensured, see in *Figure 3*.

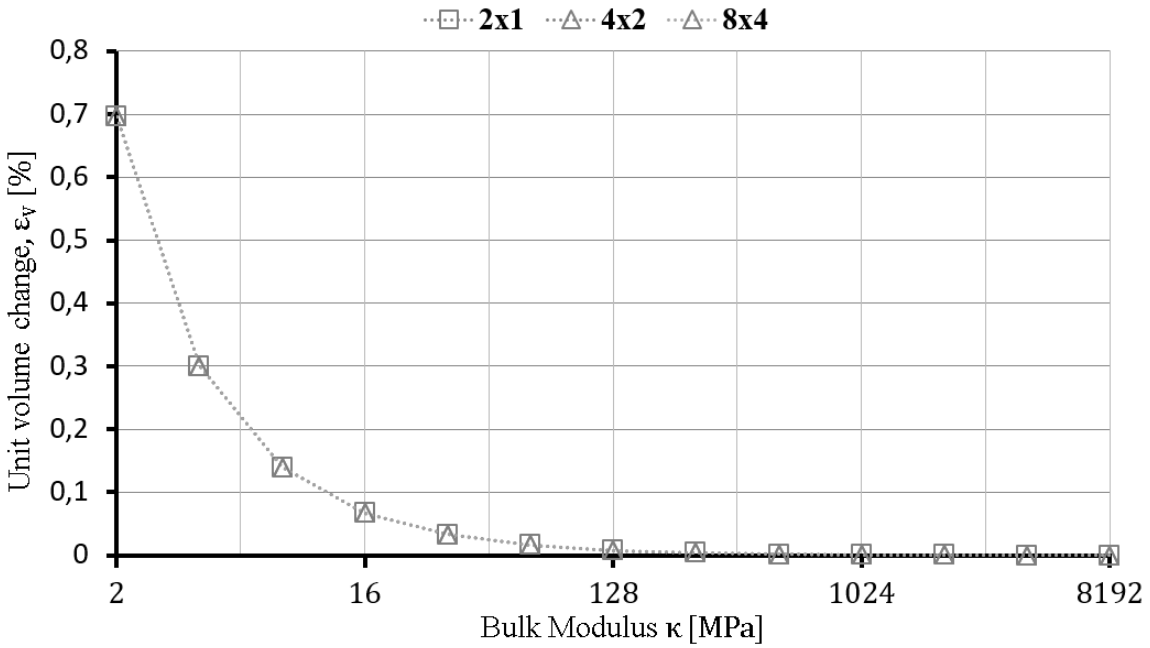

Figure 3 The effect of the mesh density and the bulk modulus for the incompressibility

At the same mesh density the volume change of the elements were analyzed using different bulk modulus, see in *Figure 4*. It can be stated that the bulk modulus value strongly influences the deformation.

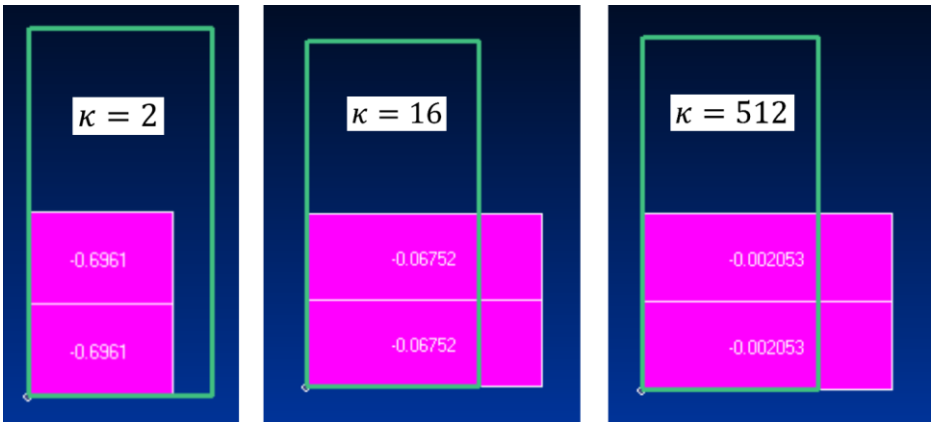

Figure 4 Volume change of the element for different bulk modulus

At different mesh density the volume change of the elements were analyzed using $\kappa = 64\ MPa$ bulk modulus value. It can be observed that in ideal conditions no real effect of the mesh density for the unit volume change, see in *Figure 5*.

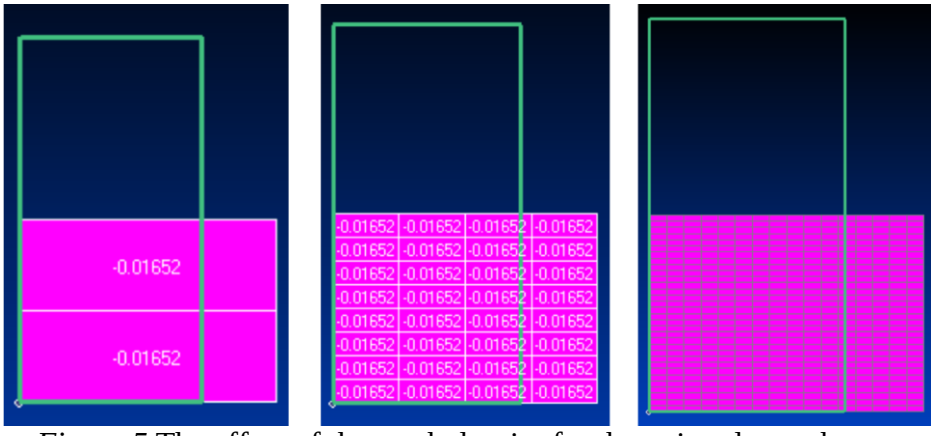

Figure 5 The effect of the mesh density for the unit volume change

Using different mesh density and bulk modulus values the resulted force for 50% compression was determined, see in *Figure 6*.

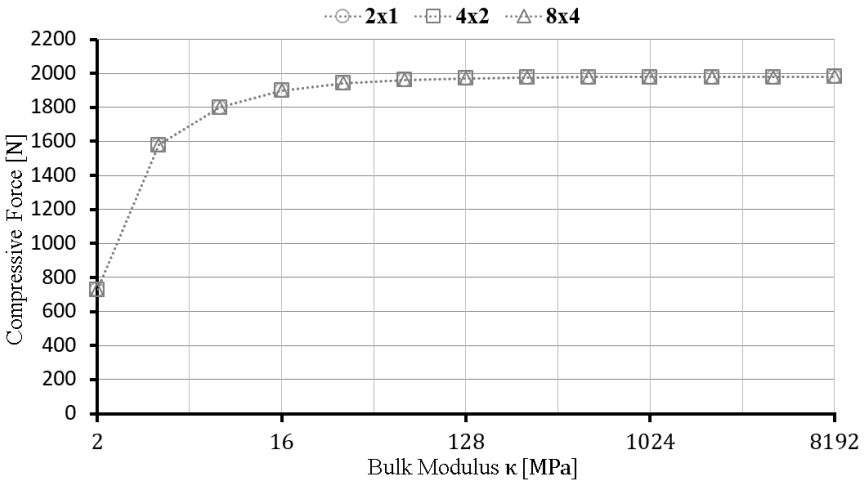

Figure 6 The effect of the bulk modulus for the resulted compressive force

In order to be able the determine the goodness of resulted forces an error analysis was performed introducing the error

$$e[\%] = \frac{|F_{ref} - F|}{F_{ref}} 100, \tag{9}$$

where F_{ref} is the reference compressive force resulted using $\kappa = 8192$ and F is the actual compressive force. Although small deviations can be observed mesh density has no real influence on accuracy, see in *Figure 7*.

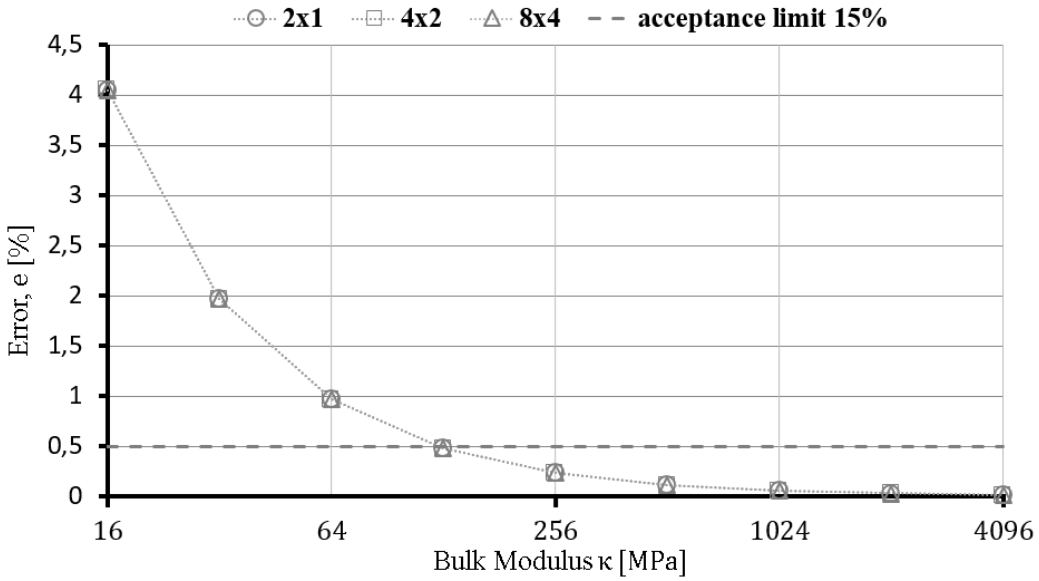

Figure 7 Error analysis

The investigations have shown that by choosing $2x1$ mesh and the $\kappa = 128$ the calculated results are appropriate.

Table 3 The results of the simulations

$\kappa\ [MPa]$	16	32	64	128	256	512	1024
ν	0,47959	0,48969	0,49482	0,49740	0,4987	0,49935	0,49968
ε_V [%]	-6,7522	-3,3271	-1,6519	-0,82311	-0,41085	-0,20525	-0,10258
e [%]	4,04914	1,96819	0,96797	0,47722	0,23411	0,11310	0,05275

CONCLUSIONS

Non-linear finite element calculations are indispensable when important information of the material response under load of a rubber component is desired. In this paper a numerical analysis of determining the numerical material parameters are investigated. The correct choice of the material parameters ensures the numerical stability, the accuracy and the incompressibility during the finite element calculations. A numerical evaluation was also performed to estimate the optimal input parameters for the finite element analysis, such as mesh density.

ACKNOWLEDGEMENT

The described work was carried out as part of a project supported by the National Research, Development and Innovation Office – NKFIH, K115701.

REFERENCES

[1] Mankovits, T., Szabó, T., Kocsis, I., Páczelt, I. (2014), *Optimization of the Shape of Axi-Symmetric Rubber Bumpers*. Strojniski vestnik-Journal of Mechanical Engineering, 60(1), 61-71.
[2] Mankovits, T., Kocsis, I., Portik, T., Szabó, T., Páczelt, I. (2013), *Shape Design of Rubber Part Using FEM*. International Review of Applied Sciences and Engineering, 4(2), 85-94.
[3] Páczelt, I., Baksa, A., Szabó, T. (2007), *Product Design Using a Contact-optimization Technique*. Strojniski vestnik-Journal of Mechanical Engineering, 53(7-8), 442-461.
[4] Kim, J.J. and Kim, H.Y. (1997), *Shape Design of an Engine Mount by a Method of Parameter Optimization*. Computers & Structures, 65(5), 725-731.
[5] Ramachandran, T., Padmanaban, K.P. and Nesamani, P. (2012), *Modeling and Analysis of IC Engine Rubber Mount using Finite Element Method and RSM. Procedia Engineering*, 38, 1683-1692.
[6] Lee, J.S. and Kim, S.C. (2007), *Optimal Design of Engine Mount Rubber Considering Stiffness and Fatigue Strength*. Journal of Automobile Engineering, 221(7), 823-835.
[7] Mankovits, T. and Szabó, T. (2012), *Finite Element Analysis of Rubber Bumper Used in Air-springs*. Procedia Engineering, 48, 388-395.
[8] Vámosi, A., Mankovits, T., Huri, D., Kocsis, I., Szabó, T. (2015), *Comparison of Different Data Acquisition Techniques for Shape Optimization Problems*. International Journal of Mechanical, Aerospace, Industrial, Mechatronic and Manufacturing Engineering, 9(3), 458-461.
[9] Mankovits, T., Huri, D., Kállai, I., Kocsis, I., Szabó, T. (2014), *Material Characterization and Numerical Simulation of a Rubber Bumper*. International Journal of Mechanical, Aerospace, Industrial, Mechatronic and Manufacturing Engineering, 8(8), 1367-1370.
[10] Mott, P.H., Dorgan, J.R., Roland, C.M. (2008), *The Bulk Modulus and Poisson's Ration of Incompressible Materials*. Journal of Sound and Vibration, 312, 572.572.
[11] Giannakopoulos, A.E., Panagiotopoulos, D.I. (2009), *Conical Indentation of Incompressible Rubber-like Materials*. International Journal of Solids and Structures, 46(6), 1436-1447.
[12] Koblar, D., Skofic, J., Boltezar, M. (2014), *Evaluation of the Young's Modulus of Rubber-like Materials Bonded to Rigid Surfaces with Respect to Poisson's Ratio*. Strojniski vestnik-Journal of Mechanical Engineering, 60(7-8), 506-511.
[13] Huri D. (2016), *Incompressibility and mesh sensitivity analysis in finite element simulation of rubbers*, International Review of Apllied Sciences and Engineering 7
[14] Bonet, J. and Wood, R.D. (1997), *Nonlinear Continuum Mechanics for Finite Element Analysis*. Cambridge University Press.

INTERNATIONAL SCIENTIFIC CONFERENCE ON ADVANCES IN MECHANICAL ENGINEERING

13-15 October 2016, Debrecen, Hungary

STUDY OF TECHNICAL SYSTEMS AND OF INTEGRATED WASTE MANAGEMENT ACTIVITIES OF PROCESSING AND STORING THE MUNICIPAL WASTE

JOLDES Nicolae PhD

Technical University of Cluj-Napoca,
E-mail: joldes_nicolae@yahoo.com

Abstract
It is well known that in entire world there are serious problems in the management of waste. Before the change of regime in Romania is quite primitive waste treatment plants were operating. After 1990's changes through local and European financial support relatively acceptable results were obtained in order to improve the situation. Of course, there is still much to be done in this area. In this paper, the authors describe the Salaj County (Romania) waste actual situation, and the result of latest regional and European projects in this direction.

Keywords: *Waste Management, Waste storage, Sustainable Development Strategy*

1. INTRODUCTION

Harmonization our national policies and legislation on waste management with European policies and legislation and the provisions of international agreements and conventions to which Romania is a party, establish and use economic and financial mechanisms for waste management, while respecting all general principles, especially the principle of "polluter pays", is the **main objective** for our project.

2. SPECIFIC OBJECTIVES

For our project the specific objectives are:

- To ensure the compliance with national and European legislation, under the transitional periods agreed between Romania and the EU in the environmental sector;
- To prepare the project to the point that should be proposed for EU co-financing;
- To ensure optimum use of funds;
- To help the project promoters to develop local capacity for further development of the project and provide training in the workplace for staff to final beneficiaries, responsible for implementing the project in all its stages, from the initial phase of the project at the preparatory studies feasibility and development to the tender documents;
- To provide assistance in establishing PIUs;
- To define a long-term investment program;
- To ensure that an effective system of procurement and implementation plan and tender documents are prepared so that the basis for implementation of the project before starting this task, design, cost and objectives must have been already defined;
- Human Resources: availability of sufficient personnel with appropriate training.

3. TECHNICAL ANALYSIS OF INTEGRATED WASTE MANAGEMENT SYSTEM IN SALAJ COUNTY – CURRENT SITUATION

In the present, in Salaj County, the waste problem can be showed in the next 3 graphics.

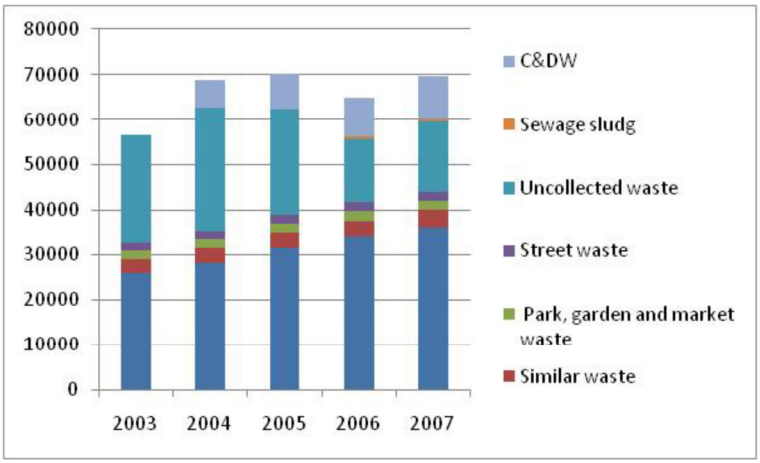

Figure 1 Solid waste generation in Salaj county

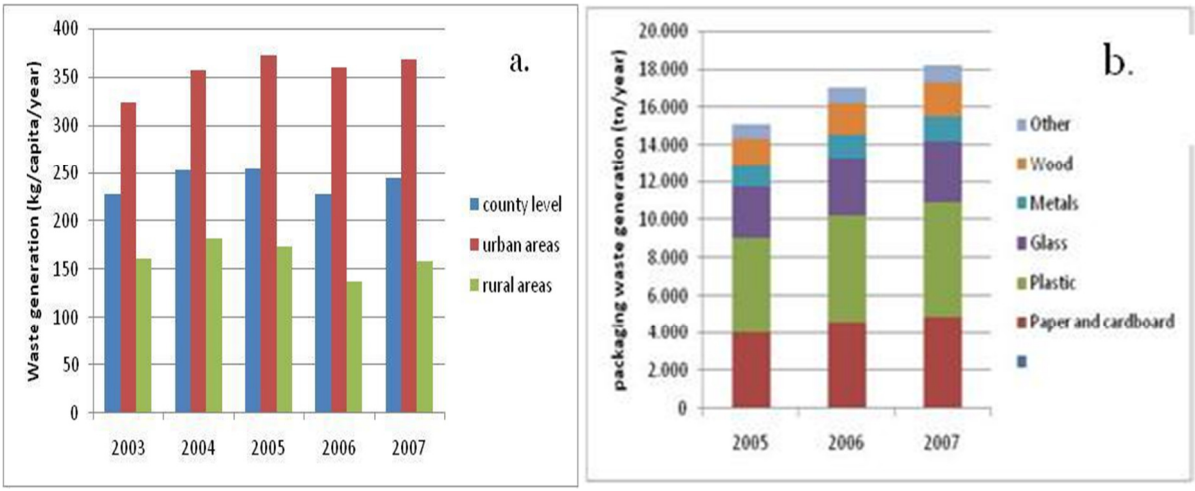

Figure 2 a. Waste generation in households in Salaj county, *b.* Packaging waste generation in Salaj county

Developing a new waste management projects covering all aspects, will include:

- Technical aspects: infrastructure design required;
- Financial aspects and economics: calculating the project investment and operating and maintenance costs and tariffs to be charged both people and businesses;
- Environmental issues: the description of the environmental impacts of waste management and rehabilitation measures;
- Institutional aspects: creation schemes required administrative capacity building of persons involved in the implementation of an integrated waste management system.

The study will be developed in Salaj County, located in the North-West of Romania, and his time horizon is 30 years.
Analysis of the situation related to the relationship with management and waste generation provided the following results:

- The amount of municipal waste generated annually is about 60,000 t / year, of which about 62% comes from urban areas and 38% in rural areas. Furthermore, almost 61% of waste is generated by households, while the rest comes from commercial activities, parks, streets, etc;
- The total amount of municipal solid waste is about 244 kg / capita / year, and is higher in urban areas (368 kg / capita / year).

The technical objectives of the integrated system covers

- Waste prevention;
- Maximizing a waste prevention;
- Optimize the amount of packaging a product packed;
- Reduce the quantity of packaging waste generated by product unit;
- Collection and transportation of waste.
- Providing a collection and transport to a larger number of waste producers, creating new systems covering the whole area of waste generators.

The conclusion is that the current system of waste management in Salaj doesn't meet national objectives and European waste management strategy (with the exception of rural deposits closure of non-compliant and non-compliant urban Şimleu Silvaniei).

4. OPTIONS ANALYSIS. METHODOLOGY ANALYSIS. TECHNICAL DESCRIPTION OF THE WASTE MANAGEMENT INFRASTRUCTURE

By implementing integrated waste management, waste utilization can be achieved, and storage of waste quantities reduced safely, without any harm to the environment and public health, an analysis of options in order to choose the best variant for integrated waste management system.

Figure 3 a. Intermediate stage in the preparation of central warehouse, b. New equipment proposed for the central warehouse

Dividing the county into 4 areas of waste management:

• 1st Zone covers the central part of the county served by central waste management facility;

• 2nd Zone covers the western part of the county served by CRASNA transfer station (this zone will also be covered by small transfer stations developed by PHARE);
• 3rd zone covers the northern part of the county served by the transfer station SURDUC;
• 4th zone 4 covers the eastern part of the county served by the transfer station SÂNMIHAIU ALMAŞULUI.
Technical highlights of the new system should include:

- Modernize the system for the collection by acquiring new trucks and bins - wide implementation of selective collection;
- Construction and operation the transfer stations for waste collection optimizing logistics;
- Construction and operation of a sorting station for the recovery and use of recyclable materials to be collected separately;
- Construction and operation of treatment plants biodegradable fraction of waste, to reduce environmental impact (leach ate and biogas) related to the elimination of this fraction;
- Promoting individual composting of organic material to prevent waste and reduce the amount of biodegradable waste to be treated;
- Termination of operation and rehabilitation of existing non-compliant landfills urban and rural;
- Construction and operation of a landfill for the disposal of waste; residues from the treatment of waste. Landfill should be built in accordance with strict specifications of the legislation.

CONCLUSIONS

The conclusion that can be drawn is that current waste management system is deficient and not compliant with national and European legislation regarding waste management.
The solution to the main problems identified in Salaj municipal waste management is promoting an Integrated Waste Management System funded by the SOP: increase and upgrade existing equipment collection and transport (vehicles, bins, etc.), expansion of selective collection system at the county level and promotion of household composting, improved waste management through the construction and operation of transfer stations for optimizing logistics waste collection, sorting station for the recovery and use of recyclables, to be collected separately MBT station and a controlled storage of waste within the regional landfill waste

REFERENCES

[1] Antonescu, N. - Energy *recovery from waste*, Bucharest: Technical Publishing House, 1988
[2] Bold O.V.,Mărăcineanu G.A. - *Municipal solid waste management and industrial*, Matrix Rom Publishing House, Bucharest 2003.
[3] Bold O.V., Mărăcineanu G.A. - *Storage, treatment and recycling of waste and materials*, Matrix Rom Publishing House, Bucharest 2004.
[4] Căpătână C., Racoceanu C. – *Waste*, Matrix Rom Publishing House, Bucharest 2003
[5] Commission of European Communities – *Document de travail de la Commission – Integration des considerations environnementales dans les autres politiques - bilan du Processus de cardiff. Towards sustainability. A european community programme of policy and action inrelation to the enviroment and sustainable development* – Com 2004
[6] Council of the European Union - *Green Paper on biowaste management in the EU*, Brussels, December 19, 2008

[7] Dumitru, Camelia – *Ecological Management and Marketing - a strategic approach*, Tehnopress Publishing House, Iasi 2009
[8] European Commision, *Organisation of awareness – raising events concernig the implementation of Directive 1999/31/EC on the landfill of waste*, Final Report, Bruxelles, 2007
[9] Fizesanu, S., s.a.- *Science and Engineering, vol. 5, "Improve the quality of life by providing renewable energy from organic waste"*, AGIR Publishing House, Bucharest, 2004
[10] *Guidance on waste collection, developed through Project Packaging and packaging waste Recovering and recycling systems (MAT03 / RM / 9/1),* funded by the Dutch government / EVD International Cooperation - Agency.
[11] *Guidance on regionalization localities sanitation*, drafted by Law Office "Catalina Mark" 2009
[12] *Government Decision 162/2002 on waste disposal*
[13] Marinescu D., - *The right environment*, Publishing house and press SRL, Bucharest, 1996
[14] Păunescu, I.; Atudorel, A. – *Urban waste management* , Matrix Rom Publishing House, Bucharest 2002
[15] Păunescu I., Paraschiv G. – *Environmental management and biogas farms suinicole*, Biotechnical Faculty of Engineering - UPB
[16] *Implementation Plan for Directive 2002/96 / EC on waste electrical and electronic equipment*, the Government of Romania, 2004

INTERNATIONAL SCIENTIFIC CONFERENCE ON ADVANCES IN MECHANICAL ENGINEERING

13-15 October 2016, Debrecen, Hungary

TEST METHOD FOR BRITTLENESS TEMPERATURE OF TPU ELASTOMERS BY IMPACT

[1]IMRE Kállai, [2]JÜRGEN Holzweber, [3]ZOLTÁN Major PhD

[1,2,3]Institute of Polymer Product Engineering, Johannes Kepler University Linz
E-mail: imre.kallai@jku.at, jürgen.holzweber@jku.at, zoltan.major@jku.at

Abstract
TPUs are widely used in the automotive industry like damping materials. In case of automotive use, the environmental temperature is very important regard to choose a right material. It is therefore important, to determine the minimum service temperature of the material. In this work, we must be defined two different TPU materials brittleness temperature, because for the future use, we must choose the right material which has better low-temperature flexibility. To determine the T_g temperature, we can use a DSC, DTMA, and a Charpy or Izod test method. If the polymer component working on low-temperature and during the use reach impact loading, we must prefer a Charpy or Izod test methods. However, there is a less well known standard test method, wherewith we can determine the minimum service temperature. This test method covers the determination of the temperature at which plastics and elastomers exhibit brittle failure under specified impact conditions.

Keywords: *TPU, Brittleness Temperature, Impact.*

1. INTRODUCTION

TPU has many applications including automotive instrument panels, caster wheels, power tools, sporting goods, medical devices, drive belts, footwear, inflatable rafts, and a variety of extruded film, sheet and profile applications.[1][2] TPU is also a popular material found in outer cases of mobile electronic devices, such as mobile phones. It is also used to make keyboard protectors for laptops. [3] TPU is well known for its applications in performance films, wire and cable jacketing, hose and tube, in adhesive and textile coating applications and as an impact modifier of other polymers. These materials are distinguished by the following properties, high wear and abrasion resistance, high tensile strength and outstanding resistance to tear propagation, excellent damping characteristics, high resistance to oils, greases, oxygen and ozone, very good low-temperature flexibility. [4] This is the reason, that TPUs are widely used in the automotive industry like damping materials. In case of automotive use, the environmental temperature is very important regard to choose a right material. It is therefore important, to determine the minimum service temperature of the material. Damping materials reduce or eliminate the damaging forces caused by mechanical energy (i.e., vibrations, movement, or noise). The performance of a damping material depends on the combined characteristics of the material and the environment in which it is used. It is important to choose the best damping material for a specific environment (temperature) to maximize its performance. The TPUs and the elastomers can be good damping materials, because this group of materials have great elasticity. But the damping has no constant value. It depends on the grade of the rubber, temperature, strain rate (velocity) and acceleration, shape, and type of stress (compression, tensile, or shear).

1.1. Thermoplastic elastomers

Thermoplastic elastomers combine elastomeric properties with thermoplastic characteristics. For most TPE's, new generation materials were developed to deliver the required mechanical, physical and chemical requirements for the industry. [5]. TPE's can be separated in different areas in terms of material structure, which can be seen in figure 1.

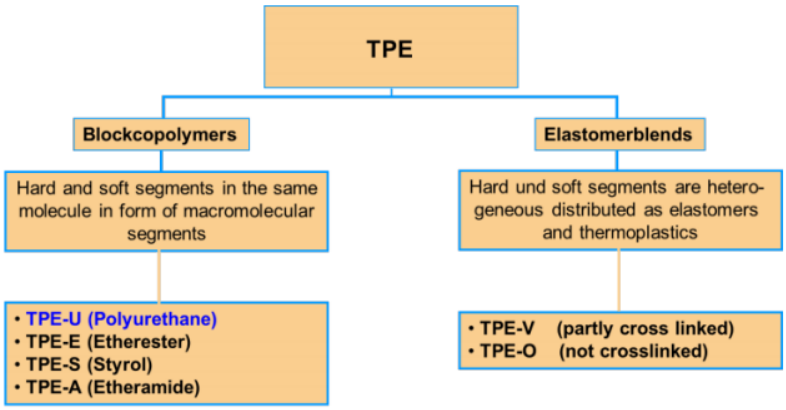

Figure 1 Classification of TPE's [6]

In this paper, thermoplastic polyurethanes are interesting. TPU's are block copolymers, where the "hard" block is formed with an additional chain extender, e.g. butanediol, to a diisocyanate. The "soft" block consists out of long flexible polyether- or polyester-chains. The two segments of this polymer can be seen as incompatible at room temperature due to their different polarity. A simple model of a TPU can be seen in figure 2. The micro-phase separation depends on the crystallinity of the hard segments. When its melting temperature is reached, a homogeneous melt accrues, which can be processed as common thermoplastic materials [7].

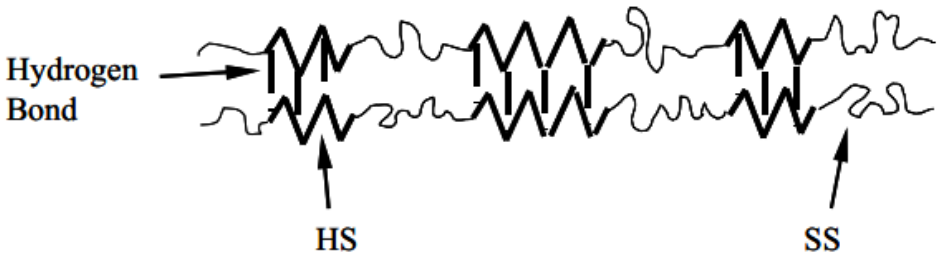

Figure 2 Structure of TPu's; HS: hard segment, SS: soft segment [8]

TPUs are mainly consisting of two domains, a hard and a soft domain. The hard phase is responsible for the “plastic” properties as the thermoplastic process ability, the high-temperature performance as well as for the tensile strength. [5], [6], In contrary the soft phase is for elastomeric properties as the low-temperature behavior and the flexibility and compression set. One can say that the boundary condition of the temperature range is in between of the melt temperature of the hard phase and the temperature of the glass transition of the soft phase. (Figure 3.) [9], [8].
The two-segment system means, that the glass transition temperature of the "soft" block is the minimum service temperature. The service temperature is between the glass transition temperature of the elastomeric phase and the glass transition temperature, or melting temperature of the hard phase.

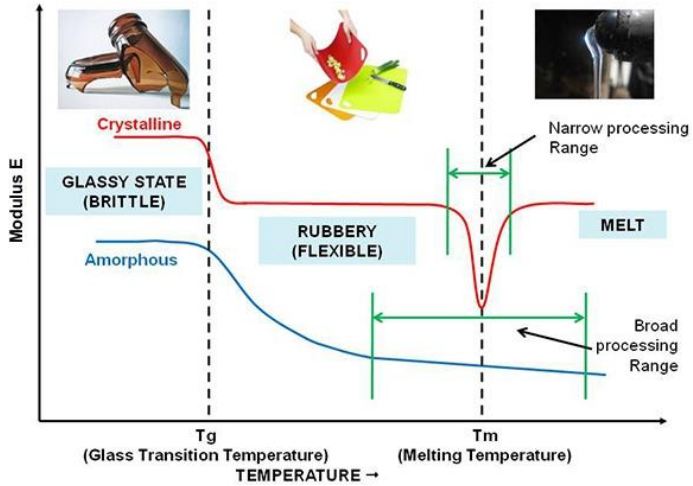

Figure 3 Useful state of polymers

1.2. Thermoplastic Polyurethane

Thermoplastic polyurethane (TPU) is any of a class of polyurethane plastics with many properties, including elasticity, transparency, and resistance to oil, grease and abrasion. Technically, they are thermoplastic elastomers consisting of linear segmented block copolymers composed of hard and soft segments. They have a quite long history. TPUs are the first commercial thermoplastic elastomers and were established by the Goodrich, US and Bayer-Farbenfabriken in Germany in the 1950s. (Schollenberger 1948) TPUs are block copolymers which are randomly segmented. (Hepburn, 1982) They have an alternating structure of hard and soft segments. With the ratio of the hard and the soft segments the hardness of the material can be adapted. It is a big advantage of the TPUs that the specific properties can be customized very easy by varying the ratio of the different segments. TPU consists of polyaddition from Polyisocyanat and Polyoles. The diissozianat and the short chains of diols forming the hard segment which are responsible for the thermomechanical properties. The soft segments consist of the long chain diols (Polyester or Polyether) [10], [11].

2. METHODS

We have a standard test method for brittleness temperature of plastics and elastomers by impact. This test method (ASTM D 746-07) covers the determination of the temperature at which plastics and elastomers exhibit brittle failure under specified impact conditions.
To determine the brittleness temperature, specimens are secured to a specimen holder with a torque wrench, and they are struck at a specified linear speed and then examined. The brittleness temperature is defined as the temperature at which 50% of the specimens fail.
Plastics and elastomers are used in many application requiring low-temperature flexing with or without impact. Use data obtained by this method to predict the behaviour of plastic and elastomeric material at low temperatures only in applications in which the conditions of deformation are similar to those specified in this test method [12].

2.1 Procedure

In establishing the brittleness temperature of a material, it is recommended that the test be started at a temperature at which 50% failure is expected. We must test a minimum of ten specimens at this temperature. If all of the specimens fail, increase the test temperature by 10°C and repeat the test

using new specimens. If none of the specimens fail, decrease the temperature by 10°C and repeat the test with new specimens. If we don't know the approximate brittleness temperature, we can select the start temperature arbitrarily. The specimens are struck at impact conditions with a speed of 2000mm/sec and then examined. If we find the minimum or maximum temperature where all of or none of the specimens fail, we must increase or decrease the temperature in uniform increments of 2°C and repeat the procedure until the lowest temperature at which none of the specimens fail and the highest temperature at which all of the specimens fail is determined. A minimum of four tests shall be conducted in that temperature range, and we must use new specimens for each test!

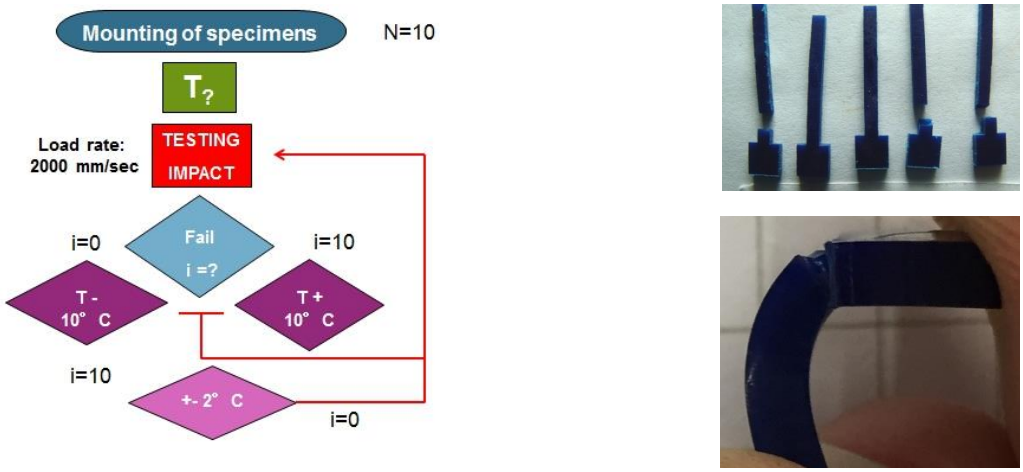

Figure 4 Procedure and failure inspection

After the test remove the individual specimens from the clamping device. Allow the specimens to warm up prior to being bent for inspection of cracks by leaving the specimens at room temperature for 1 min or by placing them in lukewarm water for 10 to 15 sec. examine each specimen to determine whether or not it has failed. Failure is defined as the division of a specimen into two or more completely separated pieces or as any crack in the specimen which is visible to the unaided eye. Where a specimen has not completely separated, it shall be bent to an angle of 90° in the same direction as the bend caused by the impact and examined for cracks at the bend. We must record the number of failures and temperature at which they were tested. [12]

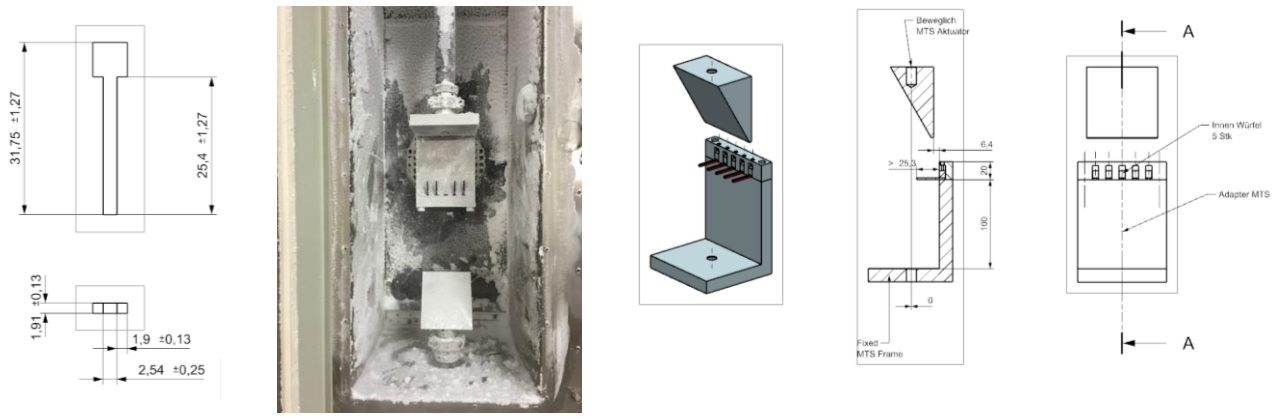

Specimen type II. Test Setup Apparatus type A

Figure 5 Specimen geometry and clamping setup

3. CALCULATION AND RESULTS

If we want to calculate the brittleness temperature of the material, we must use the number of specimens that failed, and calculate the percentage of failures at each temperature. For the calculations use the following formula: (1)

$$T_b = T_h + \Delta T\,[(S/100)-(1/2)] \quad (1)$$

where:
T_b = brittleness temperature, °C ; T_h = highest temperature at which failure of all the specimens occurs, °C ; ΔT = temperature increment, °C ; S = sum of the percentage of breaks at each temperature
Material: TPU-1 and TPU-2

At -80°C ; 10 failed
At -78°C ; 8 failed
At -76°C ; 6 failed
At -74°C ; 4 failed
At -72°C ; 2 failed
At -70°C ; 1 failed
At -68°C ; 0 failed

TPU-1 T_b = -74,8°C

At -90°C ; 10 failed
At -88°C ; 9 failed
At -86°C ; 8 failed
At -84°C ; 6 failed
At -82°C ; 5 failed
At -80°C ; 4 failed
At -78°C ; 2 failed
At -76°C ; 0 failed

TPU-2 T_b = -82,2°C

The evaluation with the graphic mode, we must plot the data on probability graph paper with temperature on the linear scale and percent failure on the probability scale. The temperature indicated at the intersection of the data line with 50% probability line shall be reported as the brittleness temperature. Figure 6. [12]

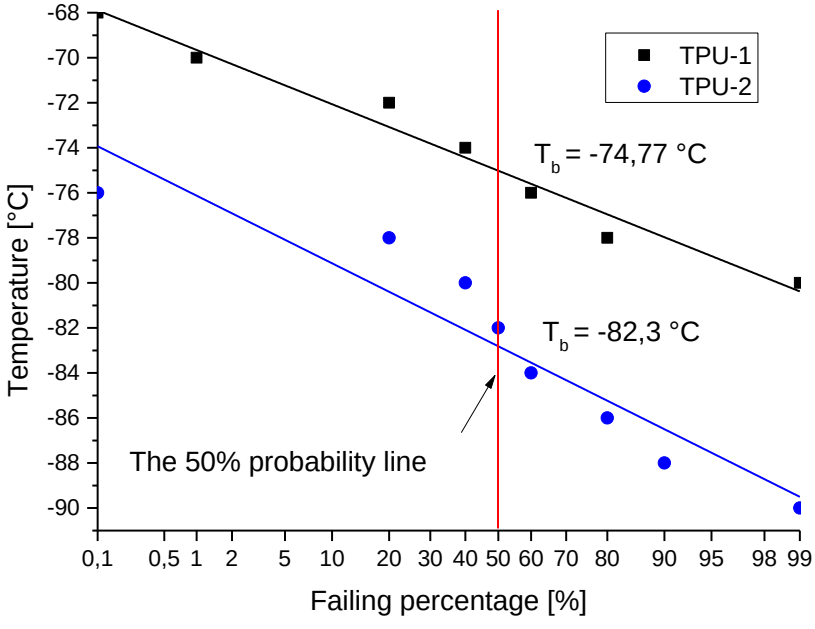

Figure 6 Graphic method

CONCLUSIONS

Whit this standard test method we were able to define the brittleness temperature for both TPU materials. Both of them have good low temperature flexibility, but the TPU-2 material has little bit better resistance against the cold temperature.
Why use this test method instead of Izod? Because we don't need a special test machine. (It is true, if we have an impact test machine.) We don't need a sensor technic, because we don't measure the force or energy. (At impact load rate and extremely low temperature the force measurement is not so easy.) This test method is faster, several specimens can be measured simultaneously. Whit this method we have immediately statistical data.

REFERENCES

[1] Texin® thermoplastic polyurethane (TPU) resin. *Bayer Material Science. Retrieved 2012.02.26.*
[2] Thermoplastic Polyurethane. American Chemical Council. *Retrieved 2012.02.26.*
[3] Michael, John. TPU Cases. *Cellz. Retrieved 13 November 2014*
[4] PEARLTHANE. *Merquinsa, A Lubrizol Company. Retrieved 2013-01-31*
[5] Mark, James E.; Erman, Burak; Roland, Michael C.: The Science and Technology of Rubber. *Oxford, 2013*
[6] Muehren, Oliver; Westerdale, Sarah: Thermoplastic Polyurethane (TPU) for high performance cable applications: current applications and future development. In: Proceedings of the 61s6 IWCS Conference, *International Wire&Cable Symposium, 2012*
[7] Qi, H.J, Boyce, M.C: Stress-Strain Behavior of Thermoplastic Polyurethane. *Cambridge, Massachusetts Institute of Technology, 2004*
[8] Treloar, L.R.G: The Physics of Rubber Elasticity. *Oxford, 1975*
[9] Houwink, R.; De Decker, H.K.: Elasticity, Plasticity and Structure of Matter. Third Edition, *London, 1971*
[10] M. Metten, Veränderung der Verbundfestigkeit von Hart/Weich-Verbunden und die mechanischen Eigenschaften von thermoplastischen Elastomeren durch eine Elektronenbestrahlung, *Technische Universität Darmstadt, Darmstadt, 2002.*
[11] T. Zysk, Zum statischen und dynamischen Werkstoffverhalten von Thermoplastischen Elastomeren, *LKT - Universität Erlangen-Nürnberg, 1992.*
[12] ASTM D746-07 Standard test method for brittleness temperature of plastics and elastomers by impact

INTERNATIONAL SCIENTIFIC CONFERENCE ON ADVANCES IN MECHANICAL ENGINEERING
13-15 October 2016, Debrecen, Hungary

INFORMATION TECHNOLOGIES MANAGEMENT SYSTEM FOR MEDIUM-SIZED COMPANIES IN MECHANICAL ENGINEERING

[1]KARTUNOV Stefan DSc, [2]DRUMEV Krasimir PhD, [3]STOEV Iliyan

[1,2]Institute Technical University of Gabrovo, Bulgaria
E-mail: skartunov@abv.bg, kid@tugab.bg
[3]Institute Technical University of Gabrovo, Filial Fioniks, Weliko Tarnovo, Bulgaria,
E-mail: ilian100ev@gmail.com

Abstract
The article indicates the introduction of Information Technologies - System in the Enterprise of Mechanical Engineering. Few steps are needed for creation of the entire IT environment of an enterprise: Planning, Implementing, Testing and Support of the hardware and the software, the work of IT specialists with needed experience and qualification.

Keywords: *Information Technologies Management System, Enterprise of Mechanical Engineering.*

1. INTRODUCTION

1.1. Information Technologies

1.1.1. What is Information Technologies - IT

Humans have been storing, retrieving, manipulating and communicating information since the Sumerians in Mesopotamia developed writing in about 3000 BC, but the term information technology in its modern sense first appeared in a 1958 article published in the Harvard Business Review. Authors Harold J. Leavitt and Thomas L. Whisler commented that "…the new technology does not yet have a single established name. We shall call it information technology (IT) [1]." Their definition consists of three categories: techniques for processing, the application of statistical and mathematical methods to decision-making, and the simulation of higher-order thinking through computer programs. Based on the storage and processing technologies employed, it is possible to distinguish four distinct phases of IT development: pre-mechanical (3000 BC – 1450 AD), mechanical (1450–1840), electromechanical (1840–1940) electronic (1940–present), and more over, IT as a service. By today's authors IT is the broad subject concerned with all aspects of managing and processing information, especially within a large organization or company. IT is generally not used in reference to personal or home computing and networking.
While IT is often used to describe computers and computer networks, it actually includes all layers of all systems within an organization - from the physical hardware to the operating systems, applications, databases, storage, servers, the support of those systems and more. Telecommunication technologies, including Internet and business phones are also part of an organization's IT infrastructure.

1.1.2. IT process

The main product of every IT process is the Information product. It is the wanted information in an appropriate form for particular working process. The next three steps are the shortest path of

creating this information. In practice to be reached the final result, the process goes through this cycle many times. After the early 1990s a group of IT processes and tools, based on RDBS (Relational Data Base System), becomes naturally a main system for enterprises [2]. Those were the ERP - Enterprise Resource Planning systems.

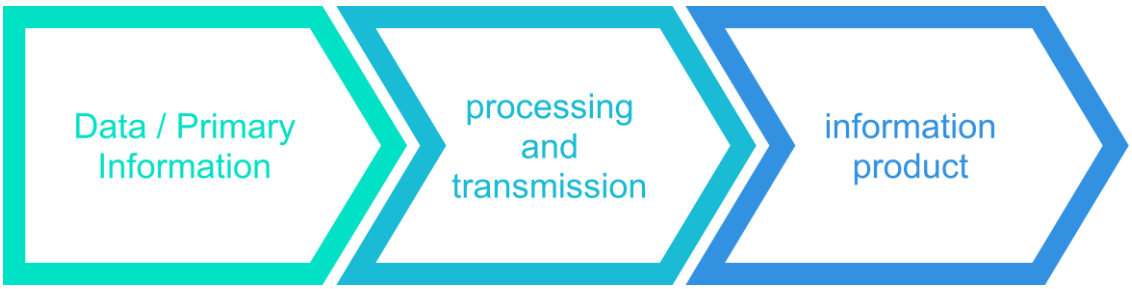

Figure 1 IT – process

1.2. Enterprise Resource Planning systems

1.2.1. What is Enterprise Resource Planning systems - ERP

Enterprise resource planning (ERP) is a category of business-management software—typically a suite of integrated applications—that an organization can use to collect, store, manage and interpret data from many business activities, including: product planning, purchase, manufacturing or service delivery, marketing and sales, inventory management, shipping and payment.
ERP provides an integrated view of core business processes, often in real-time, using common databases maintained by a database management system. ERP systems track business resources—cash, raw materials, production capacity—and the status of business commitments: orders, purchase orders, and payroll. The applications that make up the system share data across various departments (manufacturing, purchasing, sales, accounting, etc.) that provide the data. ERP facilitates information flow between all business functions, and manages connections to outside stakeholders.
Enterprise system software is a multibillion-dollar industry that produces components that support a variety of business functions. IT investments have become the largest category of capital expenditure in United States-based businesses over the past decade. Though early ERP systems focused on large enterprises, smaller enterprises increasingly use ERP systems.
The ERP system is considered a vital organizational tool because it integrates varied organizational systems and facilitates error-free transactions and production. However, developing an ERP system differs from traditional system development. ERP systems run on a variety of computer hardware and network configurations, typically using a database as an information repository.

1.2.2. ERP - Modules

ERP systems are made up of many different software modules. Each of the modules in ERP module is specialized to handle specific business processes. In this guide to ERP modules and software, you'll find introductions to the various components of ERP and learn how each module can benefit your organization.

Figure 2 Enterprise Resource Planning systems

- ERP supply chain management; ERP customer relationship management
- ERP product lifecycle management; ERP human capital management
- ERP warehouse management; ERP asset management
- ERP financial management; ERP order management
- ERP project management; ERP inventory management

Supply chain management (SCM) is one of the most important software modules for manufacturers. SCM gives provides visibility into the entire supply chain, from start to finish. ERP SCM modules typically include components for forecasting, demand management, procurement and planning; delivery modules such as logistics; and components for after-market issues like returns, installations and contracts.

Manufacturers can use customer relationship management (CRM) software to organize and view data on individual customer transactions in one accessible place. ERP CRM modules provide customer data integration, or master data management (MDM), which keeps track of customers across all the sales channels from in-person (field sales) to phone (including telemarketing) to online (teleservice and support).With product lifecycle management (PLM) software, manufacturers can track the design and attributes of a product throughout its lifecycle, from concept to end-of-life. The components that make up ERP PLM modules include product data management (PDM), product design, portfolio management, direct materials sourcing and customer needs management.

Human capital management is another one of the common ERP modules. ERP HCM modules function as the core employee record, which details personnel actions, benefits administration and payroll, position management and compliance with government regulations. ERP HCM covers three areas of employee management: transactional, talent management and extended management.

Warehouse management systems (WMS) software is a must-have for manufacturers. ERP WMS modules follow the distribution process involved with finished goods or materials from delivery into the warehouse for storage through replenishment and picking for shipment to fulfill orders. WMS modules also help synchronize and control stock on the shop floor.

Manufacturers can track physical manufacturing assets involved in production - the plant itself and equipment - using ERP asset management modules. Some of the daily functions that ERP asset management handles are maintenance schedules, equipment uptime and downtime, inventory and warranty management and compliance with hazardous materials and waste tracking regulations.

Financial management is a critical business function for manufacturers. ERP financial management modules include functionality for general ledger, which is the core of ERP financial management.

These modules also handle functions for accounts payable and receivable, fixed assets, financial reporting and treasury management.
Order management systems take in data from orders on the front end - such as customer number and product part number - and make sure that orders get filled on the back end. Manufacturers use ERP order management modules to fill product orders at the lowest possible cost. These modules are equipped to handle functions such as automated order entry, viewing and tracking; order status; canceled transactions; order and credit limit validation and checking for duplicate orders.
With project management software, manufacturers can organize and review the data around project timelines and costs. These software systems are geared toward organizations that bill clients based on the time their employees spend working on individual projects. ERP project management modules handles project definition, project costing and accounting, project portfolio management, resource management and project billing.
ERP inventory management modules move finished goods through the production cycle. They are often tied into other functions, including shipping, logistics, orders, billing and, on a broader scale, warehouse management. ERP order management software includes functionality for inventory control, serial number tracking, bar code printing, build materials and kitting, inventory valuation and SKU management.

2. METHODS FOR IMPLEMENTATION OF THE IT-SYSTEM

Few steps are needed for creation of the entire IT environment of an enterprise: Planning, Implementing, Testing and Support of the hardware and the software, the work of IT specialists with needed experience and qualification.

2.1. Hardware

The following is a description of the core elements of the hardware.

2.1.1. Data Center

A data center is a facility used to house computer systems and associated components, such as telecommunications and storage systems. It generally includes redundant or backup power supplies, redundant data communications connections, environmental controls (e.g., air conditioning, fire suppression) and various security devices. Large data centers are industrial scale operations using as much electricity as a small town. Mostly in the enterprises the data center is arranged as Private Cloud. A private cloud is a particular model of cloud computing that involves a distinct and secure cloud based environment in which only the specified client can operate. As with other cloud models, private clouds will provide computing power as a service within a virtualized environment using an underlying pool of physical computing resource. However, under the private cloud model, the cloud (the pool of resource) is only accessible by a single organization providing that organization with greater control and privacy. The technical mechanisms used to provide the different services which can be classed as being private cloud services can vary considerably and so it is hard to define what constitutes a private cloud from a technical aspect. Instead such services are usually categorized by the features that they offer to their client. Traits that characterize private clouds include the ring fencing of a cloud for the sole use of one organization and higher levels of network security. They can be defined in contrast to a public cloud which has multiple clients accessing virtualized services which all draw their resource from the same pool of servers across public networks. Private cloud services draw their resource from a distinct pool of physical

computers but these may be hosted internally or externally and may be accessed across private leased lines or secure encrypted connections via public networks.
The additional security offered by the ring fenced cloud model is ideal for any organization, including enterprise, that needs to store and process private data or carry out sensitive tasks. For example, a private cloud service could be utilized by a financial company that is required by regulation to store sensitive data internally and who will still want to benefit from some of the advantages of cloud computing within their business infrastructure, such as on demand resource allocation. The private cloud model is closer to the more traditional model of individual local access networks (LANs) used in the past by enterprise but with the added advantages of virtualization. The features and benefits of private clouds therefore are: Higher security and privacy; public clouds services can implement a certain level of security but private clouds - using techniques such as distinct pools of resources with access restricted to connections made from behind one organization's firewall, dedicated leased lines and/or on-site internal hosting - can ensure that operations are kept out of the reach of prying eyes. More control; as a private cloud is only accessible by a single organization, that organization will have the ability to configure and manage it online with their needs to achieve a tailored network solution. However, this level of control removes some the economies of scale generated in public clouds by having centralized management of the hardware.
Cost and energy efficiency; implementing a private cloud model can improve the allocation of resources within an organization by ensuring that the availability of resources to individual departments/business functions can directly and flexibly respond to their demand. Therefore, although they are not as cost effective as a public cloud services due to smaller economies of scale and increased management costs, they do make more efficient use of the computing resource than traditional LANs as they minimize the investment into unused capacity. Not only does this provide a cost saving but it can reduce an organization's carbon footprint too. Improved reliability; even where resources (servers, networks etc.) are hosted internally, the creation of virtualized operating environments means that the network is more resilient to individual failures across the physical infrastructure. Virtual partitions can, for example, pull their resource from the remaining unaffected servers. In addition, where the cloud is hosted with a third party, the organization can still benefit from the physical security afforded to infrastructure hosted within data centers.

2.1.2. Networking

An enterprise network is an enterprise's communications backbone that helps connect computers and related devices across departments and workgroup networks, facilitating insight and data accessibility. An enterprise network reduces communication protocols, facilitating system and device interoperability, as well as improved internal and external enterprise data management.
The key purpose of an enterprise network is to eliminate isolated users and workgroups. All systems should be able to communicate and provide and retrieve information. Additionally, physical systems and devices should be able to maintain and provide satisfactory performance, reliability and security. Enterprise computing models are developed for this purpose, facilitating the exploration and improvement of established enterprise communication protocols and strategies.
In scope, an enterprise network may include local and wide area networks (LAN/WAN), depending on operational and departmental requirements. An enterprise network can integrate all systems, including Windows and Apple computers and operating systems (OS), Unix systems, mainframes and related devices like smartphones and tablets. A tightly integrated enterprise network effectively combines and uses different device and system communciation protocols.

2.1.3. Workstations

A workstation is a special computer designed for technical or scientific applications. Intended primarily to be used by one person at a time, they are commonly connected to a local area network and run multi-user operating systems.

2.1.4. Printing Devices

A print device is a hardware device used for printing. Print device resolution is measured in dots per inch (DPI) The higher the DPI, the finer the resolution. A print client is an application on a user's computer that submits print jobs to a print device.

2.1.5. Mobile Devices

Mobile devices
Mobile computers, tablets, phones, portable scanners and other.
MDM - Mobile Devices Management
Mobile device management (MDM) is the administrative area dealing with deploying, securing, monitoring, integrating and managing mobile devices, such as smartphones, tablets and laptops, in the workplace. The intent of MDM is to optimize the functionality and security of mobile devices within the enterprise, while simultaneously protecting the corporate network.
Mobile device management software allows distribution of applications, data and configuration settings and patches for such devices. Ideally, MDM software allows administrators to oversee mobile devices as easily as desktop computers and provides optimal performance for users. MDM tools should include application management, file synchronization and sharing, data security tools, and support for either a corporate-owned or personally owned device.
The ideal mobile device management tool is compatible with all common handheld device operating platforms and applications, can function through multiple service providers, can be implemented directly over the air, targeting specific devices as necessary, can deploy next-generation hardware, operating platforms and applications quickly and can add or remove devices from the system as necessary to ensure optimum network efficiency and security.

2.1.6. Telephony

Enterprise standard for telephony is the VoIP. Voice over IP (VoIP) is a methodology and group of technologies for the delivery of voice communications and multimedia sessions over Internet Protocol (IP) networks, such as the Internet. Other terms commonly associated with VoIP are IP telephony, Internet telephony, broadband telephony, and broadband phone service.
The term Internet telephony specifically refers to the provisioning of communications services (voice, fax, SMS, voice-messaging) over the public Internet, rather than via the public switched telephone network (PSTN). The steps and principles involved in originating VoIP telephone calls are similar to traditional digital telephony and involve signaling, channel setup, digitization of the analog voice signals, and encoding. Instead of being transmitted over a circuit-switched network, however, the digital information is packetized, and transmission occurs as IP packets over a packet-switched network. Such transmission entails careful considerations about resource management different from time-division multiplexing (TDM) networks.

2.2. Software

2.2.1. Server operating system - OS

A server operating system, also called a server OS, is an operating system specifically designed to run on servers, which are specialized computers that operate within a client/server architecture to serve the requests of client computers on the network. The server operating system, or server OS, is the software layer on top of which other software programs, or applications, can run on the server hardware. Server operating systems help enable and facilitate typical server roles such as web server, wail server, wile server, watabase server, application server and print server. Popular server operating systems include Windows Server, Mac OS X Server, and variants of Linux such as Red Hat Enterprise Linux (RHEL) and SUSE Linux Enterprise Server.

2.2.2. Workstations OS

The most popular OS for the client stations are: Windows from Microsoft Corporation, RedHat Enterprice Linux Desktop, by RedHat Inc., Ubuntu Desktop, Linux Mint and others.

2.2.3. Domain Controller

A very special and useful server software, for controlling shared network resources inside the enterprise. On Microsoft Servers, a domain controller (DC) is a server that responds to security authentication requests (logging in, checking permissions, etc.) within a Windows domain. A domain is a concept introduced in Windows NT whereby a user may be granted access to a number of computer resources with the use of a single username and password combination. As defined by Microsoft, in Active Directory server roles, computers that function as servers within a domain can have one of two roles: member server or domain controller. Abbreviated as DC, domain controller is a server on a Microsoft Windows or Windows NT network that is responsible for allowing host access to Windows domain resources. The domain controllers in your network are the centerpiece of your Active Directory directory service. It stores user account information, authenticates users and enforces security policy for a Windows domain. Currently there in no substitutions for AD as a DC in the enterprise environment.

2.2.4. Virtualisation

In computing, virtualization refers to the act of creating a virtual (rather than actual) version of something, including virtual computer hardware platforms, operating systems, storage devices, and computer network resources. Virtualization began in the 1960s, as a method of logically dividing the system resources provided by mainframe computers between different applications. Since then, the meaning of the term has broadened. Desktop virtualization is the concept of separating the logical desktop from the physical machine. One form of desktop virtualization, virtual desktop infrastructure (VDI), can be thought of as a more advanced form of hardware virtualization. Rather than interacting with a host computer directly via a keyboard, mouse, and monitor, the user interacts with the host computer using another desktop computer or a mobile device by means of a network connection, such as a LAN, Wireless LAN or even the Internet. In addition, the host computer in this scenario becomes a server computer capable of hosting multiple virtual machines at the same time for multiple users.

As organizations continue to virtualize and converge their data center environment, client architectures also continue to evolve in order to take advantage of the predictability, continuity, and quality of service delivered by their converged infrastructure. For example, companies like HP and IBM provide a hybrid VDI model with a range of virtualization software and delivery models to improve upon the limitations of distributed client computing. Selected client environments move workloads from PCs and other devices to data center servers, creating well-managed virtual clients, with applications and client operating environments hosted on servers and storage in the data center. For users, this means they can access their desktop from any location, without being tied to a single client device. Since the resources are centralized, users moving between work locations can still access the same client environment with their applications and data. For IT administrators, this means a more centralized, efficient client environment that is easier to maintain and able to more quickly respond to the changing needs of the user and business. Another form, session virtualization, allows multiple users to connect and log into a shared but powerful computer over the network and use it simultaneously. Each is given a desktop and a personal folder in which they store their files. Thin clients, which are seen in desktop virtualization, are simple and/or cheap computers that are primarily designed to connect to the network. They may lack significant hard disk storage space, RAM or even processing power, but many organizations are beginning to look at the cost benefits of eliminating “thick client” desktops that are packed with software (and require software licensing fees) and making more strategic investments. Desktop virtualization simplifies software versioning and patch management, where the new image is simply updated on the server, and the desktop gets the updated version when it reboots. It also enables centralized control over what applications the user is allowed to have access to on the workstation.
Moving virtualized desktops into the cloud creates hosted virtual desktops (HVDs), in which the desktop images are centrally managed and maintained by a specialist hosting firm. Benefits include scalability and the reduction of capital expenditure, which is replaced by a monthly operational cost.

2.2.5. Intranet

An intranet is a network based on TCP/IP protocols (an internet) belonging to an organization, usually a corporation, accessible only by the organization's members, employees, or others with authorization. An intranet's Web sites look and act just like any other Web sites, but the firewall surrounding an intranet fends off unauthorized access. Like the Internet itself, intranets are used to share information. Secure intranets are now the fastest-growing segment of the Internet because they are much less expensive to build and manage than private networks based on proprietary protocols.

2.2.6. Utility Applications

Utility software is system software designed to help analyze, configure, optimize or maintain a computer. Utility software, along with operating system software, is a type of system software used to support the computer infrastructure, distinguishing it from application software which is aimed at directly performing tasks that benefit ordinary users. Good examples are: Anti-virus, Archivers, Backup software - can make copies of all information stored on a disk and restore either the entire disk (e.g. in an event of disk failure) or selected files (e.g. in an event of accidental deletion), Clipboard managers, Cryptographic utilities encrypt and decrypt streams and files, Data compression utilities output a shorter stream or a smaller file when provided with a stream or file, Data synchronization utilities establish consistency among data from a source to a target data storage, Debuggers, Disk checkers, cleaners, compression, defragmenters, space analyzers, Disk storage utilities, File managers, Hex editors directly modify the text or data of a file. These files

could be data or an actual program, Memory testers check for memory failures, Network utilities analyze the computer's network connectivity, configure network settings, check data transfer or log events, Package managers are used to configure, install or keep up to date other software on a computer, System monitors for monitoring resources and performance in a computer system.

2.2.7. VoIP Software

Voice over IP (VoIP) is a methodology and group of technologies for the delivery of voice communications and multimedia sessions over Internet Protocol (IP) networks, such as the Internet. Other terms commonly associated with VoIP are IP telephony, Internet telephony, broadband telephony, and broadband phone service. The term Internet telephony specifically refers to the provisioning of communications services (voice, fax, SMS, voice-messaging) over the public Internet, rather than via the public switched telephone network (PSTN). The steps and principles involved in originating VoIP telephone calls are similar to traditional digital telephony and involve signaling, channel setup, digitization of the analog voice signals, and encoding. Instead of being transmitted over a circuit-switched network, however, the digital information is packetized, and transmission occurs as IP packets over a packet-switched network. Such transmission entails careful considerations about resource management different from time-division multiplexing (TDM) networks.
Because of the bandwidth efficiency and low costs that VoIP technology can provide, businesses are migrating from traditional copper-wire telephone systems to VoIP systems to reduce their monthly phone costs. In 2008, 80% of all new Private branch exchange (PBX) lines installed internationally were VoIP. VoIP solutions aimed at businesses have evolved into unified communications services that treat all communications—phone calls, faxes, voice mail, e-mail, Web conferences, and more—as discrete units that can all be delivered via any means and to any handset, including cell phones. Two kinds of competitors are competing in this space: one set is focused on VoIP for medium to large enterprises, while another is targeting the small-to-medium business (SMB) market. VoIP allows both voice and data communications to be run over a single network, which can significantly reduce infrastructure costs. The prices of extensions on VoIP are lower than for PBX and key systems. VoIP switches may run on commodity hardware, such as personal computers. Rather than closed architectures, these devices rely on standard interfaces. VoIP devices have simple, intuitive user interfaces, so users can often make simple system configuration changes. Dual-mode phones enable users to continue their conversations as they move between an outside cellular service and an internal Wi-Fi network, so that it is no longer necessary to carry both a desktop phone and a cell phone. Maintenance becomes simpler as there are fewer devices to oversee.

2.3. ERP system implementation

There are 6 phases that make up an ERP implementation project: Discovery and Planning, Design, Development, Testing, Deployment, and Ongoing Support. Though this is an iterative process, there will be a tendency for phases to overlap, and for movement back and forth between phases.
1. Discovery and Planning
This first phase begins during the sales process and then continues post-sale. During this period, the project team will be created. There will be initial meetings and documentation developed as the team works to identify current issues and potential solutions. An important part of this phase is constructing the project plan, which will serve as a guide throughout the rest of the project.
2. Design

In the ERP Design phase, the project team and implementation team will be working out the various configurations for the new system, defining roles, and documenting standard procedures.

3. Development

The purpose of the development phase is to prepare the entire system for going live. This includes activities such as completing any necessary customizations, developing user trainings, and importing data. With ERP implementations, like any custom software development projects – "First, Solve the problem. Then, write the code."

4. Testing

Is the system's functionality aligning with the set requirements for the project? The Testing and Development phases will often overlap, as the implementation and project teams jump between the two – constantly fine tuning the configuration. By the end of this phase, project team members will be comfortable doing their job s in the new system. This is the final step before diving into the live system.

5. Deployment

The project team and implementation team will assess the situation and make the final go or no-go decision. Prior to going live, the final data will be loaded and validated. The project team will train other employees who will then start working in the new system, and completely stop using the old one.

6. Support

Once the ERP system has gone live, the purpose of the project team will shift. Over time, as the way the users work within the system evolves, adjustments and changes to the system configuration may be needed.

2.4 Support

There is not a standard for the support processes and systems, but some practices are common for all of the big companies. These are Help Desks, Ticket systems and other.

2.4.1. Help Desk

A help desk is a resource intended to provide the customer or end user with information and support related to a company's or institution's products and services. The purpose of a help desk is usually to troubleshoot problems or provide guidance about products such as computers, electronic equipment, food, apparel, or software. Corporations usually provide help desk support to their customers through various channels such as toll-free numbers, websites, instant messaging, or email. There are also in-house help desks designed to provide assistance to employees.

2.4.2. Specialists

System Administrator

A system administrator, or sysadmin, is a person who is responsible for the upkeep, configuration, and reliable operation of computer systems; especially multi-user computers, such as servers. The system administrator seeks to ensure that the uptime, performance, resources, and security of the computers he or she manages meet the needs of the users, without exceeding the budget.

To meet these needs, a system administrator may acquire, install, or upgrade computer components and software; provide routine automation; maintain security policies; troubleshoot; train and/or supervise staff; or offer technical support for projects.

IT Specialists

An information technology specialist applies technical expertise to the implementation, monitoring, or maintenance of IT systems. Specialists typically focus on a specific computer network, database, or systems administration function. Specialty areas include network analysis, system administration, security and information assurance, IT audit, database administration, web administration and more.

IT Support

A technical support specialist is someone who provides assistance and technical support to either businesses or consumers that are experiencing technical, hardware, or software issues. Some examples of these issues are slow performance, connection problems, and an inability to access data. Technical support specialists are able to deal with most customer issues over the telephone or through email, however some issues need to be dealt with on site, especially if the computer software and hardware needs to be modified, cleaned, or repaired. A computer repair technician would typically be sent out to take care of any repairs.

3. RESULTS

After implementation of the system should be carried out tests to assess its performances. Measure the traffic in centers for data and end-client devices. The data of *Table 1* indicate measurements at the test start of the system and the total traffic for 24 hours in example enterprise Pharmalog. The cost of implementing a full license system for one user and usefulness to other systems on the market are shown in *Table 2*.

Table 1 Results of the measurement

Devices	Average traffic, [MB/s]	Peak traffic, [MB/s]	Total, [MB/s]	Traffic, [MB/24h]	Traffic, [GB/24h]
Mobile bar-code devices	0,121	0,31	4,235	365904,00	357,33
Wireless routers	0,168	0,42	5,88	508032,00	496,13
Workstation-store	0,218	2,5	7,63	659232,00	643,78
Workstation office	0,356	2,5	12,46	1076544,00	1051,31
Telephone exchange	0,728	2,3	25,48	2201472,00	2149,88
					Total 4698,42

Table 2 The cost of implementing

ERP System	Cost of implementing a full license system for one user, [lv]	Cost of implementing a limit license system for one user, [lv]	Speed data processing/base SAP, [%]	Completeness of developed modules, [%]	Utility cost, [%]
SAP	4500	2250	100	98	110,89
Pharmalog	37,5	-	180	92	2308
Oracle	5250	1155	100	97	109,24
Microsoft	225	120	75	78	230
Infor	1875	-	98	96	125,09

CONCLUSIONS

There is no other process that is related to everyone else as IT processes. ERP systems provide continuous access to accurate information about all business functions in the organization and provide it at the right time to the right people to make effective and informed decisions. Here is an example of implementation of such a system in the example enterprise in Mechanical Engineering.

REFERENCES

[1] Leavitt H. J., Whisler T. L.: *Information technologyes*, Harvard Business Review, 1958
[2] Kartunov S.K., Rachev P.T.: *Автоматизирано планиране и управление на производството. CIM.* Gabrovo, TU - Gabrovo, 1997, ISBN 954-683-057-7

INTERNATIONAL SCIENTIFIC CONFERENCE ON ADVANCES IN MECHANICAL ENGINEERING

13-15 October 2016, Debrecen, Hungary

BEHAVIOUR OF METAL MATRIX SYNTACTIC FOAMS UNDER CYCLIC LOADING

[1]KATONA Bálint, [2,3]SZEBÉNYI Gábor PhD, [1,3]ORBULOV Imre Norbert PhD

[1]Budapest University of Technology and Economics, Faculty of Mechanical Engineering, Department of Materials Science and Engineering
E-mail: katona@eik.bme.hu
[2]Budapest University of Technology and Economics, Faculty of Mechanical Engineering, Department of Polymer Engineering
E-mail: szebenyi@pt.bme.hu
[3]Budapest University of Technology and Economics, Faculty of Mechanical Engineering, MTA–BME Research Group for Composite Science and Technology

Abstract
Metal matrix syntactic foams consisting of aluminium alloys and oxide ceramic hollow spheres were investigated under compressive cyclic loading with load asymmetry factor of 0.1. The results ensured full reliability design data for the investigated material in the lifetime region, while the fatigue limits were determined by staircase method. The Wöhler curves of the foams were also constructed, including the median curves, their confidence boundaries and the fatigue strength. The softer Al99.5 matrix ensured higher load levels for the fatigue strengths than the more rigid AlSi12matrix. Considering the size of the ceramic hollow spheres, the large spheres with thick wall performed better than the more vulnerable smaller ones with thinner wall. The general failure mode was identified as a cleavage along a well determined shear band, similar to the case of quasi-static loading.

Keywords: *metal matrix syntactic foams, composites, fatigue, cyclic loading.*

1. INTRODUCTION

High strength, closed cell metallic foams, as ceramic hollow sphere reinforced metal matrix syntactic foams (MMSFs) are promising materials to build lightweight structural parts. Their can range from load bearing structures to vibration damping structural parts etc. In such cases, their fatigue properties are needed for proper design calculations.
The mechanical properties of MMSFs have been widely studied. The publications focus mainly on the compressive behaviour of the foams, but tensile and wear properties [1, 2] as well as structure reconstruction methods [3] have been published too. For example, the compressive properties of Al-Al_2O_3 MMSFs at different loading rates were monitored and predicted considering the strength of the matrix material and the size of the hollow spheres [4-6]. Other researchers [7-10] characterized glass microsphere reinforced iron based syntactic foams. Besides their production, the quasi-static mechanical properties and the strain-rate dependency of these them were investigated up to 10^3 s^{-1}). The strain-rate influence observed for the MMSFs was mainly connected to the matrix. Taherishargh et al. [11, 12] provided cost effective production method by using low-density perlite as filler material. Because of the high porosity of the filler (~95%), the porosity of the foam was ~60%. Under compression, these MMSFs showed common stress–strain curves consisting of elastic, plateau and densification regions. Because of their consistent plateau stress (average value ~30 MPa), large densification strain (almost 60%), and high-energy absorption efficiency (~90%)

the produced MMSFs are effective energy absorbers. Besides the above mentioned and similar works, only a moderate effort was focused on the fatigue properties.
Vendra et al. studied the fatigue behaviour of different MMSFs that built up from steel hollow spheres in aluminium matrix (gravity casting) or in steel matrix (powder metallurgy). Under cyclic compressive loading, the MMSFs showed high cyclic stability and the deformation of the composite foam samples could be divided into three stages – linear increase in strain with fatigue cycles (stage I), steady state section with minimal strain accumulation in large number of cycles (stage II) and rapid strain accumulation within few cycles up to complete failure (stage III) [13].

2. METHODS

Standard Al99.5 and AlSi12 alloys were applied as matrix materials, while Globocer (GC) grade ceramic hollow spheres were applied as filler, provided by Hollomet GmbH. [14]. The material of the hollow spheres consists of 38 wt% Al_2O_3, 43 wt% SiO_2 and 19 wt% $3Al_2O_3 \cdot 2SiO_2$. The hollow spheres show a normal distribution regarding their diameter (1425±42 μm) and wall thickness (60±1.7 μm), while their density is 0.816 gcm^{-3}. The amount of the filler material was maintained at ~65 vol%. The MMSFs were produced by pressure infiltration. During the infiltration 400 kPa infiltration pressure was applied for the infiltration time of 30 s. The infiltration temperature was always set to 50°C above the melting temperature of the matrix materials (660°C for Al99.5 and 575°C for AlSi12). The produced foams were designated after their constituents, for example Al99.5-GC stands for an MMSF sample with Al99.5 matrix and ~65 vol% of Globocer filler material. Cylindrical samples with diameter of Ø8.5 mm and height of 12.75 mm (1.5 aspect ratio) were machined from the produced blocks. For classic fatigue tests, load levels (k) should be determined, that describe the maximum load (σ_{max}) during each fatigue cycle in a relation to a limit strength. In the case of conventional metals, the load levels are usually related to the proof strength ($R_{p0.2}$) that is measured by simple tensile tests. In the case of MMSFs the proof strength can be substituted by the compressive strength (σ_c, the first local maximum in the engineering compressive stress – strain diagram, that causes irreversible failure, see *Fig. 1*).

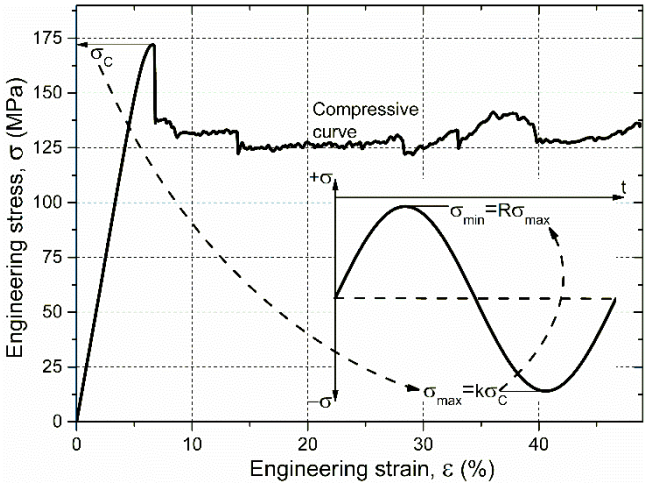

Figure 1 Typical quasi-static compressive curve of MMSFs and the derivation of the cyclic loading parameters σ_{min} and σ_{max} (inset figure)

The compressive strength (σ_c) of the foams, was measured for each material type on six samples (Table 1). On this basis the load levels can be defined as the ratio of the maximal load and compressive strength within the loading cycle (Eq. 1) and expresses similar load intensity, for the investigated materials that may have different compressive strength.

$$k = \frac{\sigma_{max}}{\sigma_C} 100\ (\%) \quad (1)$$

In our case the load level was altered between 60-100%. Fatigue tests were performed on an Instron 8872 type closed loop servo-hydraulic testing machine under force control and in compression-compression mode (stress asymmetry factor of R=0.1). The frequency of the fatigue tests was set to f=10 Hz and the load form followed a sine curve (inset of *Fig. 1*). The cylindrical specimens were carefully lubricated and placed between hardened and polished plates in a four bar upsetting tool.

Table 1 Compressive strength, sample number and time

Foam	Compressive strength, σ_c (MPa)	Number of samples at load level			SUM
		k=80%	k=85%	k=90%	
Al99.5-GC	19.7	3	9	9	
AlSi12-GC	40.0	9	9	9	
Overall number of samples		12	18	18	48
Overall number of cycles		6966673	28377	3320	6998370
Overall duration of tests (hours)		193.52	0.79	0.09	194.40

3. RESULTS

During the fatigue tests, the maximum values of the compressive engineering deformation were recorded in the function of cycles (*Fig. 2*). The curves can be divided into two parts. In stage I, the strain remains relatively constant over a large number of cycles. This stage is known as incubation period. A higher load ratio increases the overall strain in stage I. Stage II is accompanied by densification of the material and a rapid strain accumulation after a critical number of cycles. Higher load ratios shift the onset of stage II towards lower numbers of cycles.

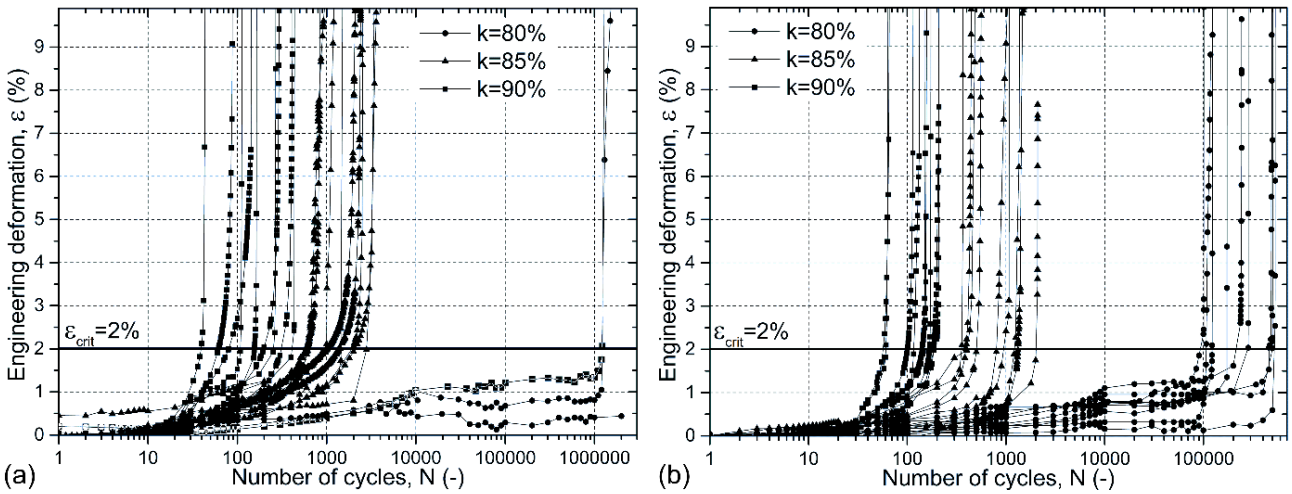

Figure 2 The measured compressive engineering deformation – number of cycles curves of (a) Al99.5-GC and (b) AlSi12-GC

For the correct evaluation of the deformation – cycle curves a failure criterion needs to be defined, that is always depending on the desired application. As there is no conventional criterion limit for the failure, the obtained deformation – number of cycle curves were evaluated at an arbitrarily chosen ε_{crit}=2% (*Fig. 2a*) in order to get the failure cycles (N_F). It should be emphasized that

ε_{crit}=2% engineering deformation corresponds to a macroscopically observable failure in the specimen. The obtained failure cycles showed large scatter, as it is usual in the case of fatigue test, therefore mathematical statistics, namely the Weibull distribution function (Eq. 2) was used to determine the expected number of cycles up to failure at a survival level (or probability, P_S) of 50%.

$$P_S = 1 - e^{-\left(\frac{N-N_0}{\alpha}\right)^{\beta}} \quad (2)$$

Where N is the independent variable, for which the equation should be evaluated to get the number of cycles up to the failure, N_0 is the threshold parameter, α is the scale parameter and β is the shape parameter of the function.

The next step is to construct the Wöhler-curve of the materials, that consists of two main parts. The first, endurance (or finite lifetime) part establish a relationship between the load level and the expected lifetime of the material. The second part represents the fatigue strength of the material. Considering the first part, the above derived results of the described mathematical statistic method are valid for the endurance range and the fitted line on them represents the endurance part of the Wöhler curve. By using this curve in the case of a given part and a given loading, the expected lifetime of the part can be predicted at the 50% survival probability (P_S).

Regarding the second part, the load level corresponds to the fatigue strength can be determined by the staircase method. First, the load level corresponds to the mean fatigue limit has to be estimated, and a fatigue life test is then conducted at a little higher load level than the estimated mean. If the specimen fails prior to the life of interest ($2 \cdot 10^6$ cycles in our case), the next specimen has to be tested at a somewhat lower load level. If the specimen does not fail within this life of interest, a new test has to be conducted at a higher stress level. Therefore, each test depends on the previous test results, and the test continues with a load level increased or decreased. The load level increments are usually taken to be less than about 5% of the initial estimate of the mean. The staircase method resulted in the load levels of 78.44% and 73.75%, that corresponds to the fatigue strength of 15.45 MPa and 29.50 MPa for the Al99.5-GC and AlSi12-GC MMSFs, respectively.

In the possession of the finite lifetime data and fatigue limit it is possible to construct the Wöhler curves of the MMSFs (*Fig. 3*). In Fig. 3 the measured points are shown by hollow squares, while the evaluated points are designated by black squares.

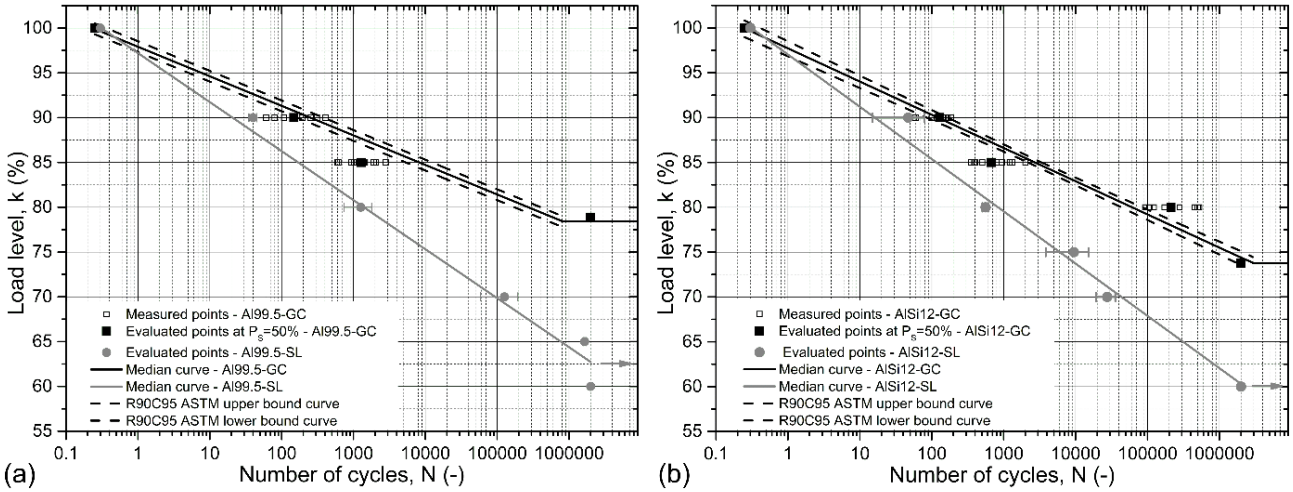

Figure 3 Wöhler curve for Al99.5-GC (a) and AlSi12-GC (b) MMSFs

The endurance part start from k=100% as that correspond to a single (1/4 cycle) uploading to the compressive strength. In the finite lifetime region, the black line was fitted on the evaluated points

by the least square method (R^2=0.976 and R^2=0.978 for the Al99.5-GC and AlSi12-GC foams, respectively). The load levels corresponding to the fatigue limits and obtained by the staircase method are also plotted by black line in the diagrams. The finite lifetime regions are supplemented by 90% reliability bands at 95% confidence level according to the ruling ASTM method (black dashed lines) [15]. Considering the identical scales and comparing Figs. 3a and 3b the technical purity Al99.5 matrix material ensured higher fatigue limit and higher lifetimes for a given load level. This phenomenon can be explained by the more or less pronounced rigidity of the high Si content eutectic Al matrix and by the presence of the Si lamellae in the matrix resulting in a moderate stress concentrating effect. On the other hand, the more ductile and soft technical purity Al matrix could hinder the incidental crack propagations resulting in a higher lifetime. These curves can be directly used to predict the expected lifetime of the MMSF parts based on their maximum permitted loading during operation, that could be determined by measurements on actual parts or can be estimated by finite element methods.
For comparison and to investigate the size effect of the hollow spheres preliminary measurements on MMSFs reinforced by smaller hollow spheres with identical chemical composition were performed. The smaller hollow spheres are commercially available under the SL300 grade name (provided by Envirospheres Pty. Ltd. [16], designated by SL in the diagrams). The average diameter (150±4.1 μm) and wall thickness (6.75±0.2 μm) of the smaller, SL grade hollow spheres were about one tenth of the GC grade spheres, while their density was slightly lower (0.691 gcm^{-3}). The preliminary tests were performed on fewer samples and the results were evaluated by simpler statistics (average and scatter). However, two important trends can be clearly observed: (i) in the case of the smaller hollow spheres similar relationship can be seen regarding the matrix material: the softer Al99.5 matrix ensured higher expected lifetimes at certain load levels and (ii) the lifetime region of the smaller spheres always run well below the curves of the GC spheres.

CONCLUSIONS

From the above investigations and analysis of the MMSFs, the following conclusions can be drawn:

- The Wöhler curve of the hollow sphere reinforced MMSFs were constructed according to the ruling ASTM standard for the case of compressive cyclic loading. The results include the median curves, their 95% confidence boundaries and the fatigue strength.
- The softer, technical purity Al99.5 matrix ensured higher load levels for the fatigue strengths than the more rigid, eutectic AlSi12 matrix.
- Regarding the size of the reinforcing ceramic hollow spheres, the larger, GC grade spheres performed better, because the smaller spheres are more vulnerable and the cracks have to propagate shorter distances within the ductile matrix to the next rigid ceramic sphere.

ACKNOWLEDGEMENTS

This paper was supported by the János Bolyai Research Scholarship of the Hungarian Academy of Sciences (Imre Norbert ORBULOV, Gábor SZEBÉNYI).

REFERENCES

[1] Májlinger, K., Bozóki, B., Kalácska, G., Keresztes, R., Zsidai, L.: *Tribological properties of hybrid aluminum matrix syntactic foams.* Tribology International, 99, 211-223., 2016.
[2] Májlinger, K.: *Wear properties of hybrid AlSi12 matrix syntactic foams.* International Journal of Materials Research. 106(11), 33-37., 2015.

[3] Kozma, I., Zsoldos, I., Dorogi, G., Papp, S.: *Computer tomography based reconstruction of metal matrix syntactic foams.* Periodica Polytechnica Mechanical Engineering, 58, 87-91., 2014.
[4] Santa Maria, J. A., Schultz, B. F., Ferguson, J. B., Rohatgi, P. K.: *Al-Al_2O_3 syntactic foams - Part I: Effect of matrix strength and hollow sphere size on the quasi-static properties of Al-A206/Al_2O_3 syntactic foams.* Materials Science and Engineering A. 582, 415-422., 2013.
[5] Ferguson, J. B., Santa Maria, J. A., Schultz, B. F., Rohatgi, P. K.: *Al-Al_2O_3 syntactic foams - Part II: Predicting mechanical properties of metal matrix syntactic foams reinforced with ceramic spheres.* Materials Science and Engineering A. 582, 423-432., 2013.
[6] Ferguson, J. B., Santa Maria, J. A., Schultz, B. F., Gupta, N., Rohatgi, P.K.: *Effect of hollow sphere size and size distribution on the quasi-static and high strain rate compressive properties of Al-A380–Al_2O_3 syntactic foams.* Journal of Materials Science. 49(3), 1267-1278., 2014.
[7] Weise, J., Lehmhus, D., Baumeister, J., Kun, R., Bayoumi, M., Busse, M.: *Production and Properties of 316L Stainless Steel Cellular Materials and Syntactic Foams.* Steel Research International. 85(3), 486-497., 2013.
[8] Peroni, L., Scapin, M., Avalle, M., Weise, J., Lehmhus, D., Baumeister, J., Busse M.: *Syntactic iron foams – on deformation mechanisms and strain-rate dependence of compressive properties.* Advanced Engineering Materials. 14, 909-918., 2012.
[9] Peroni, L., Scapin, M., Avalle, M., Weise, J., Lehmhus, D.: *Dynamic mechanical behavior of syntactic iron foams with glass microspheres.* Materials Science and Engineering A. 552, 364-375., 2012.
[10] Peroni, L., Scapin, M., Fichera, C., Lehmhus, D., Weise, J., Baumeister, J., Avalle, M.: *Investigation of the mechanical behaviour of AISI 316L stainless steel syntactic foams at different strain-rates.* Composites Part B. 66, 430-442., 2014.
[11] Taherishargh, M., Belova, I. V., Murch, G. E., Fiedler, T.: *Low-density expanded perlite–aluminium syntactic foam.* Materials Science and Engineering A. 604, 127-134., 2014.
[12] Taherishargh, M., Belova, I. V., Murch, G. E., Fiedler, T.: *On the mechanical properties of heat-treated expanded perlite–aluminium syntactic foam.* Materials Design. 63, 375-383., 2014.
[13] Vendra, L., Neville, B., Rabiei, A.: *Fatigue in aluminum–steel and steel–steel composite foams.* Materials Science and Engineering A. 517, 146-153., 2009.
[14] Hollomet GmbH. www.hollomet.com/home.html, last accessed 5th September 2016.
[15] ASTM International, ASTM E739-10 (2015) Standard Practice for Statistical Analysis of Linear or Linearized Stress-Life (S-N) and Strain-Life (ε-N) Fatigue Data, ASTM International, West Conshohocken, PA, 2015.
[16] Envirospheres Pty. Ltd. www.envirospheres.com, last accessed 5th September 2016.

INTERNATIONAL SCIENTIFIC CONFERENCE ON ADVANCES IN MECHANICAL ENGINEERING

13-15 October 2016, Debrecen, Hungary

AN IMPROVED COARSE-FINE SEARCHING SCHEME FOR FAST DISPLACEMENT MEASUREMENT

KOMPOLŠEK Melita

School of Electrical and Computer Engineering and Technical Gymnasium, Vegova ulica 4, 1000 Ljubljana, Slovenia
E-mail: melita.kompolsek@gmail.com

Abstract
In the field of experimental mechanics, the coarse-fine searching scheme is stated as one of the most rarely used sub-pixel registration procedures for measurement of displacement through the sequence of deformed images. The main reason for this lies in the fact that its computational efficiency is basically more demanding compared to the other existing registration procedures. Consequently, this has direct influence on higher execution time. In order for a coarse-fine searching scheme to become more frequently applied in the future, a novel, more efficient coarse-fine searching scheme is presented in this paper. Based on deep theoretical derivation of presented novelty, it turns out that it is approximately 600 times faster in comparison with traditional coarse-fine searching scheme. In addition, the theoretical results were further proved by numerical experiment. The obtained results showed that the proposed searching scheme significantly outperforms the traditional one as well.

Keywords: *Coarse-fine searching scheme, displacement measurement, digital image correlation.*

1. INTRODUCTION

In the field of experimental mechanics, the measurement of displacement based on the visual information obtained by the digital camera is known as digital image correlation (DIC). The basic idea behind the standard and most widely used subset-based DIC approach [1] is to track the actual subset located in reference image through the sequence of deformed images. The obtained result is motion for each individual subset and full-field motion in the case of large number of subsets which define region of interest (ROI). It is obvious that the basic idea is rather simple and intuitive however some care must be taken regarding to sub-pixel registration accuracy and computational efficiency for fast and reliable displacement calculation. In the most cases, both of them are placed at the opposite sides of the spectrum, which implies that reduction of computational complexity has usually direct influence on decreasing accuracy of the actual sub-pixel registration method and vice-versa. Due to this fact, the different types of DIC methods have been developed in literature.
One of the most widely used sub-pixel registration algorithms is an iterative spatial domain cross-correlation approach (for example a Newton-Raphson [2] (NR) approach) which is receiving a lot of modification from the theoretical and practical point of view [3]. In hindsight, the original NR approach was first presented in [2] and it has been extensively improved regarding to reducing computational complexity [4], increasing robustness [5] and extending applicability in various fields of science [6]. The NR approach has attracted quite a lot of attention in the field of solid mechanics as well, where it is commonly accepted as a golden standard for robust and reliable deformation measurement in digital images. The main reason for its wide applicability lies in the fact that it can take into account relative deformations of target subset beside its translation components. This results in the fact that the NR's sub-pixel accuracy is one of the best compared to

the other existing methods. On the other hand, calculation of displacement based on the NR approach needs the correlation function which is basically by nature nonlinear with respect to the desired mapping parameters vector. Due to this fact, it implies to using nonlinear numerical optimization techniques. However, the initial value [7] of mapping parameters vector is needed as well, which presents initial guess in the correlation procedure. The accurate estimation of the initial guess is one of the most challenging steps for guarantee of fast and reliable convergence of NR approach. Therefore, the large translation through the sequence of deformed images can easily induce that the convergence of the NR approach is not completely fulfilled and thus its applicability is immediately restricted.

In situations where deformation can be neglected it is promising to use the sub-pixel registration approach which is not so demanding from mathematical and programming point of view. In many situations, this fact provides the possibility to use a method which will be very simple from the theoretical point of view, and very straightforward for implementation. This means that it can be computationally efficient if it is appropriately modified. In order to meet all the foregoing requests, the coarse-fine search algorithm [8] is well suited for such task. However, one of the well-known disadvantages of it is a very high computational complexity which is probably the main reason why it was not given enough attention to be improved. This fact was our starting point to developing a novel coarse-fine searching approach which outperforms conventional ones [6], [8] and solves the problem of high computational load.

2. CONVENTIONAL COARSE-FINE SEARCHING STRATEGY

The basic idea behind the conventional coarse-fine search strategy can be described by the following steps [6]. In the first step, it calculates the predefined correlation coefficient for all points of interest in the searching area, usually with 1 pixel step. In order to improve its accuracy it is logical to reduce the searching step, for example to 0.1 pixel or 0.01 pixel. If the value of a searching step is less than 1 pixel, the grey level at sub-pixel locations must be reconstructed and for this purpose a certain interpolation scheme is needed [9]. If searching area of $m \times m$ pixels is assumed, the coarse-fine searching approach first calculates the predefined correlation coefficient for all points of interest in the actual searching area with 1 pixel step. The pixel with the highest correlation presents the best match and its location is a starting point for fine searching approach. Thus the computation complexity of such searching method is combined by $(m \times m)$ coarse searching steps and $(x_{step}^{-1} + 1) \times (y_{step}^{-1} + 1)$ fine searching steps for each sample point, where x_{step} and y_{step} present number of fine searching steps in the *x* and *y* direction, respectively. To be more precise, if the coarse searching area $m = 5$ and the fine searching steps $x_{step} = y_{step} = 0.01$ pixel in both directions, the algorithm has to be executed $(5 \times 5) + (101 \times 101) = 10226$ times for each sample pixel. It is obvious that the presented scheme is very time consuming, since for each sample pixel, a great number of the correlation coefficients must be calculated.

3. AN IMPROVED COARSE-FINE SEARCHING SCHEME

A starting point for a proposed scheme is a coarse searching area of $m\,x\,m$ pixels where actual displacement is predicted to be located. This step is the same for all coarse searching schemes. For simplicity, we suppose that the accuracy of the proposed scheme is of the form $m\,x\,2^{-n}$ $(n = 1, 2, \ldots)$ and it is evident that the parameter *n* defines desired resolution which can be at sub-pixel location. To make it more clear, the idea behind the proposed searching scheme for coarse searching area $m = 3$ is presented in *Figure 1*.

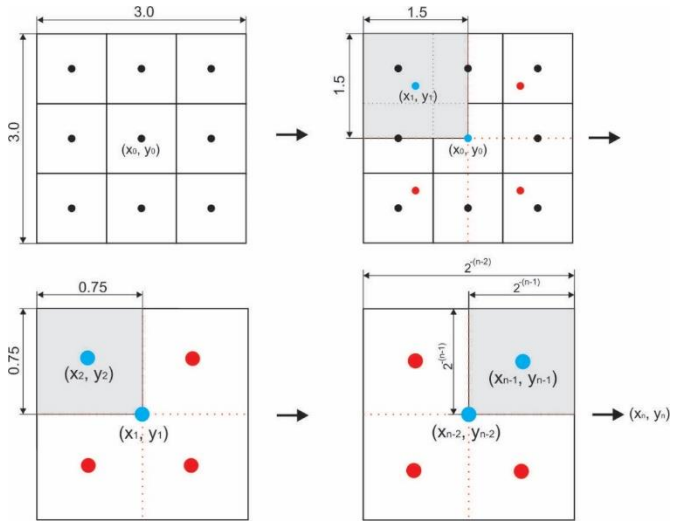

Figure 1 Schematic diagram of a novel combined coarse-fine search scheme

As shown in *Figure 1*, the coarse searching area of $3\ x\ 3$ pixels centered at (x_0, y_0) is divided into four subsets centred at four sub-pixel locations (four red dots in the top right image in *Figure 1*). For each of them normalized sum of squared differences (NSSD) correlation coefficient is calculated and the location of the point with the best match is denoted as (x_1, y_1). At this stage, the accuracy is defined as $3\ x\ 2^{-1} = 1.5$ pixels. In the next iteration, the searching procedure is performed in the same manner as in the first one, but in this case a square subset of $1.5\ x\ 1.5$ centred at (x_1, y_1) is used for searching area (grey square in the top right image in *Figure 1*). Thus, the new location of the best match is denoted as (x_2, y_2) (bottom left image in *Figure 1*), where the actual accuracy is $3\ x\ 2^{-2} = 0.75$ pixels. In this iteration, the accuracy is reduced from 1.5 pixels to $3\ x\ 2^{-1} = 0.75$ pixels in *x* and *y* direction. This procedure is repeated until the actual accuracy is better than the predefined threshold. If the accuracies are assumed to be $m\ x\ 2^{-n}$ pixels in *x* and *y* direction, then one of the four sub-pixel locations in a square subset of $m\ x\ 2^{-n+1}\ x\ 2^{-n+1}$ pixels centred at (x_{n-1}, y_{n-1}) presents the best match which is denoted as (x_n, y_n). From *Figure 1*, it is obvious that the proposed scheme needs to be executed $n\ x\ 2\ x\ 2$ times, if the desired accuracies are assumed to be $m\ x\ 2^{-n}$ pixels in *x* and *y* direction, respectively. Based on the presented theoretical background, number of iterations which need to be calculated for each sample point at various predefined accuracies with coarse searching area $m = 1$ are presented in *Table 1*.

Table 1 The number of iterations in the case of *m* = 1 for conventional and proposed scheme

Accuracy [pixel]	Number of iterations	
	Conventional scheme	Proposed scheme
0.25	25	8
0.125	64	14
0.0625	289	16
0.0312	1027	20
0.0156	4238	24
0.0078	16694	28

It can clearly be seen, that the obtained number of iterations by the proposed scheme increases much more slowly compared to the conventional scheme when the desired accuracy has to be improved. For example, if the actual accuracy is required to be 0.0078 pixels in both directions, then the conventional scheme needs to be executed 16694 times for each sample point. Consequently, this means that additional 16666 iterations are needed if compared to the proposed

searching scheme. This result confirms that the proposed scheme drastically reduces computational cost.

4. EXPERIMENTAL RESULTS

The proposed searching scheme was evaluated using computer-generated speckled images. The computational complexity of the proposed scheme are presented in *Table 1*, where it is evident that conventional coarse-fine searching scheme needs to execute much larger number of iterations for a certain accuracy. For example, if the actual accuracy is required to be 0.0078 pixels then the proposed searching scheme needs to be executed only 28 times at each sample point. This means that it significantly outperforms conventional searching scheme which is 596 times slower. Beside the estimated computational complexity, the experimental test was focused on the obtained accuracy of the proposed scheme in the case of different known translations between the reference and deformed images as well.
In our experiment, proposed method was evaluated on sequences of computer-generated speckled images which were translated in relation to the previous one for some predefined values of the displacement vector. Applied displacement vectors together with two different coarse searching areas m are presented in the second column of *Table 2*. In each image 256 points were used for tracking through the sequence of deformed images. Their mean values and standard deviations in x and y directions for various displacement vectors were calculated. The obtained results are listed in the third and fourth columns of *Table 2*. Based on the obtained results, it can be concluded that the proposed searching scheme achieves mean displacements which are almost identical with the preassigned ones. Likewise, their standard deviations for all 256 points are comparable with the results of conventional coarse-fine searching schemes [6], [8].

Table 2 Obtained accuracy for pure translations together with various initial searching areas

Mask $(m \times m)$	Exact values (x, y)	Mean values $(E(x), E(y))$	Standard deviations $(\sigma(x), \sigma(y))$
3 x 3	$(0.3, 0.3)$	$(0.3017, 0.3018)$	$(0.00020, 0.00010)$
3 x 3	$(0.6, 0.6)$	$(0.5990, 0.5989)$	$(0.00016, 0.00016)$
3 x 3	$(0.9, 0.9)$	$(0.8986, 0.8985)$	$(0.00016, 0.00012)$
3 x 3	$(1.2, 1.2)$	$(1.2019, 1.2020)$	$(0.00022, 0.00016)$
3 x 3	$(1.5, 1.5)$	$(1.4999, 1.4999)$	$(0.00006, 0.00006)$
5 x 5	$(0.3, 0.3)$	$(0.3015, 0.3022)$	$(0.00040, 0.00360)$
5 x 5	$(0.6, 0.6)$	$(0.5988, 0.6018)$	$(0.00086, 0.00818)$
5 x 5	$(0.9, 0.9)$	$(0.8985, 0.8985)$	$(0.00016, 0.00013)$
5 x 5	$(1.2, 1.2)$	$(1.2021, 1.2027)$	$(0.00052, 0.00310)$
5 x 5	$(1.5, 1.5)$	$(1.4999, 1.5000)$	$(0.00015, 0.00014)$
5 x 5	$(1.8, 1.8)$	$(1.7985, 1.7985)$	$(0.00020, 0.00052)$
5 x 5	$(2.1, 2.1)$	$(2.1014, 2.1015)$	$(0.00017, 0.00013)$
5 x 5	$(2.4, 2.4)$	$(2.4009, 2.4010)$	$(0.00017, 0.00015)$

CONCLUSIONS

The presented theoretical background and corresponding numerical experiment of the proposed scheme clearly show that it significantly outperforms the conventional scheme especially in the term of computational load. The novel developed scheme turns out to be roughly 600 times faster when the actual accuracies are 0.0078 pixels in x and y direction, respectively. It can be seen, that this ratio depends on the required accuracy of displacements. For instance, it will be larger if the actual accuracy is required to be better and vice-versa. This fact vastly extends the set of

applicability of the proposed scheme for real time applications, because the execution time was drastically reduced meanwhile the accuracy remained the same.

REFERENCES

[1] Tong, W.: *Formulation of Lucas-Kanade Digital Image Correlation Algorithms for Non-contact Deformation Measurements: A Review*. Strain, 49, 313-334., 2013.
[2] Bruck, H., McNeill, S., Sutton, M., Peters III, W.: *Digital image correlation using Newton-Raphson method of partial differential correlation*. Experimental Mechanics, 29(3), 261-267., 1989.
[3] Wang, Z., Wang, S., Wang, Z.: *An analysis on computational load of DIC based on Newton-Raphson scheme*. Optics and Lasers in Engineering, 52, 61-65., 2014.
[4] Pan, B., Li, K., Tong, W.: Fast, *Robust and Accurate Digital Image Correlation Calculation Without Redundant Computations*. Experimental Mechanics, 53, 1277-1289., 2013.
[5] Pan, B.: *Recent Progress in Digital Image Correlation*. Experimental Mechanics, 51, 1223-1235., 2011.
[6] Zhang, Z.-F., Kang, Y.-L., Wang, H.-W., Qin, Q.-H., Qiu, Y., Li, X.-Q.: *A novel coarse-fine search scheme for digital image correlation method*. Measurement, 39(8), 710-718., 2006.
[7] Simončič, S., Klobčar, D., Podržaj, P.: *Kamlan filter based initial guess estimation for digital image correlation*. Optics and Lasers in Engineering, 73, 88-88., 2015.
[8] Peters, W., Ranson, W.: *Digital Imaging Techniques in Experimental Stress Analysis*. Optical Engineering, 21(3). 1982.
[9] Pan, B., Li, K.: *A fast digital image correlation method for determination measurement*. Optics and Lasers in Engineering, 49(7), 841-847., 2011.

INTERNATIONAL SCIENTIFIC CONFERENCE ON ADVANCES IN MECHANICAL ENGINEERING

13-15 October 2016, Debrecen, Hungary

DIELECTRIC PARAMETERS OF MEAT INDUSTRY WASTEWATER

[1]KOVÁCS Róbertné, [2] KESZTHELYI-SZABÓ Gábor DSc[3], SZENDRŐ Péter DSc

[1] Technical Department, Faculty of Engineering, University of Szeged
E-mail: veszelov@mk.u-szeged.hu
[2]Department of Process Engineering, Faculty of Engineering, University of Szeged
[3]Institute of Mechanics and Machinery, Faculty of Mechanical Engineering, Szent István University

Abstract
Microwave (MW) irradiation has gained a great deal of attention owing to the molecular level heating. In addition to heating the materials consistently electromagnetic treatment can disrupt cell membrane and change biological structure increasing degradability. In our studies we were carried out pre-treatment of food industrial waste water (WW). However, the commercialization of MW technology for real-time WW treatment requires the understanding of basic mechanism of MW method. Determination of dielectric properties can provide the electrical or magnetic characteristics of the materials, which useful in many research and development fields improving design, processing, quality and control of product. Dielectric materials placed in electromagnetic field can change the nature of the field and changes can occur in the material itself. This changing ability of the materials can be characterised by dielectric parameters. Dielectric parameters of the material were determined by methods elaborated earlier based on the changing electric parameters measured by the unit attached to the pretreating system. Dielectric parameters of meat industry WW follow the trend of parameters of water, however in case of ε" at a critical temperature (52 ^{o}C) it began to increase. In addition to MW at this temperature cell membranes can rupture and cell sap releases. Because of increasing concentration of ions releasing with cell sap in the free water ionic conductioncome to the fore increasingly affect dielectric loss factor, increasing its value.

Keywords: *wastewater, microwave pretreatment, dielectric parameters*

1. INTRODUCTION

Sludge treatment is often resolved by product producer companies themselves due totightening of the rules on WW disposal and increasing cost of destruction by specialized companies. In this respect, anaerobic digestion of WW is a cost-effective configuration for industrial companies who owe to dispose the wastewater safely and, at the same time, could benefit directly from the energy recovered in the form of biogas. Most soluble organic materials which can be converted into biogas are produced during hydrolysis process, but it is identified as the rate-limiting step [4]. Consequently, the biogas production depends for the most part on the biodegradability and hydrolysis rate [3].
Pre-treatment of sludge to break down its complex structure can be used for enhancing anaerobic digestibility in order to lyse sludge cells further to facilitate hydrolysis. Thermal, chemical, biological and mechanical processes as well as different combinations of them have been studied as possible pre-treatments. Thermal treatments can be highlighted as no additional chemicals needed and they can be controlled easily. Microwave pre-treatment was found to be superior over the thermal treatment with respect to sludge solubilisation and biogas production [2].
Measuring of dielectric properties of materials has gained increasing importance in many research and development fields, especially in material science, microwave treating system design and

operation, absorber development, biological research. There are many methods developed for measuring dielectric properties but each method is limited to specific frequencies, materials, applications. At University of Szeged measuring equipment was developed using reflection method. Voltage Standing Wave Ratio (VSWR), as the ratio of the maximum to the minimum voltage in the standing wave is measured. Results of our measurements were evaluated by three methods.

2. METHODS

Meat industry WW was treated by the microwave system *Fig. 1*. Microwave pre-treating system contains a water-cooled, variable-power magnetron operating at 2450 MHz. Electromagnetic energy of the magnetron travels through a rectangular waveguide and spread over a resonant slot. Getting through this slot the energy gets in the toroidal resonator. During the operation of toroid resonator energy is given to the treated material. As a result of energy transmission the temperature of the material rises and the dielectric properties change continuously.
The material can flow through the waveguide of dielectrometer attaching to the system in a Teflon tube. Electric signal of the dielectrometer, the inlet and outlet temperature of the material are received by the measurement data collector and recorded on-line by software and displayed in the computer screen.

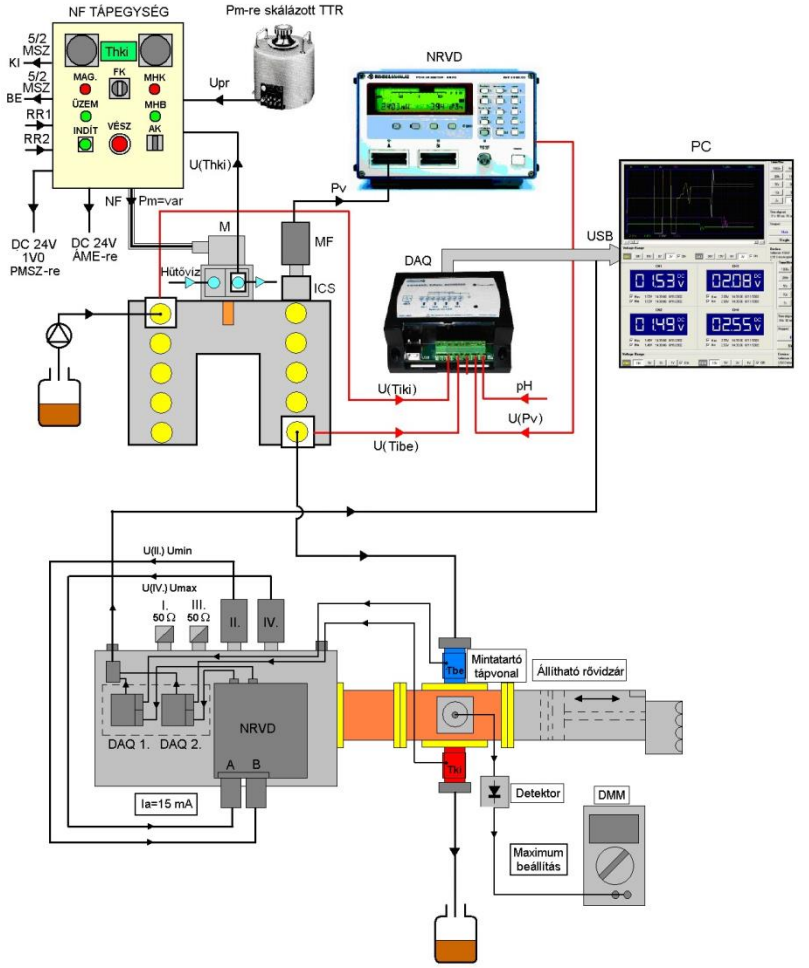

Figure 1 Microwave treating system

Three methods were developed for evaluating the measured electrical parameters. In case of

Method1 from electrical parameters Voltage Standing Wave Ratio, phase shift, and voltage reflection coefficient are counted. Dielectric parameters can be determined on their basis.

The ratio of the maximum to minimum voltage is known as Voltage Standing Wave Ratio (VSWR) [1].

$$r = \frac{U_{\max}}{U_{\min}} \tag{1}$$

If the signals from the diode detectors are quadratic, as is typical, the standing wave ratio will be:

$$r = \sqrt{\frac{U_{\max}}{U_{\min}}} \tag{2}$$

The relationship between VSWR and reflection coefficient is the following:

$$|\Gamma| = \frac{r-1}{r+1} \tag{3}$$

Phase shift

$$\Gamma_0 e^{-2\gamma l} = |\Gamma| e^{j\varphi} \tag{4}$$

$$-2\gamma l = j\varphi \tag{5}$$

$$\varphi = \frac{-2\gamma l}{j} = (-j)\cdot -2\gamma l = j2\gamma l \tag{6}$$

where γ is the complex propagation constant.
In case of Method2 travelling-wave coefficient is calculated first, then impedance of the short-circuited line and its real and imaginary part can be determined. According to these and the geometry of the waveguide dielectric parameters are determinable.

Travelling-wave coefficient that is calculated when $K_t \geq 0.4$ as

$$K_t = \sqrt{\frac{E_{\min}}{E_{\max}}} \tag{7}$$

where E_{min} and E_{max} are the minimum and maximum values of electric field amplitude.
Input impedance of the short-circuited line:

$$Z_{in} = \frac{K_t^2 + tg^2\left(\frac{2\pi}{\lambda_g} l\right)}{K_t\left[1 + tg^2\left(\frac{2\pi}{\lambda_g} l\right) + j\left(l - K_t^2\right) tg\left(\frac{2\pi}{\lambda_g} l\right)\right]} \tag{8}$$

where *l* is the distance between the dielectric surface and the first minimum of the standing wave, λ_g is the wavelength in unloaded part of transmission line.

$$\varepsilon' = \left(\frac{\lambda}{2\pi d}\right)^2 (x^2 - y^2) + \left(\frac{\lambda}{\lambda_{qc}}\right)^2 \tag{9}$$

$$\varepsilon'' = \left(\frac{\lambda}{2\pi d}\right)^2 2xy \qquad (10)$$

where λ is the free-space wavelength, λ_{qc} is the quasicutoff wavelength, d is the sample thickness x=Re(Z_{in}), and y=Im(Z_{in})Ţ, and Z_{in} is the input impedance of the short-circuited line.
In case of Method3 Voltage Standing Wave Ratio, phase shift, and voltage reflection coefficient are counted as in Method1, but on their basis complex permittivity can be determined.

3. RESULTS

As we expected dielectric parameters of meat industry WW follow the trend of parameters of water, however in case of ε" at a critical temperature (52 °C) it began to increase. In addition to MW at this temperature cell membranes can rupture and cell sap releases. Because of increasing concentration of ions releasing with cell sap in the free water ionic conduction come to the fore increasingly affect dielectric loss factor, increasing its value.

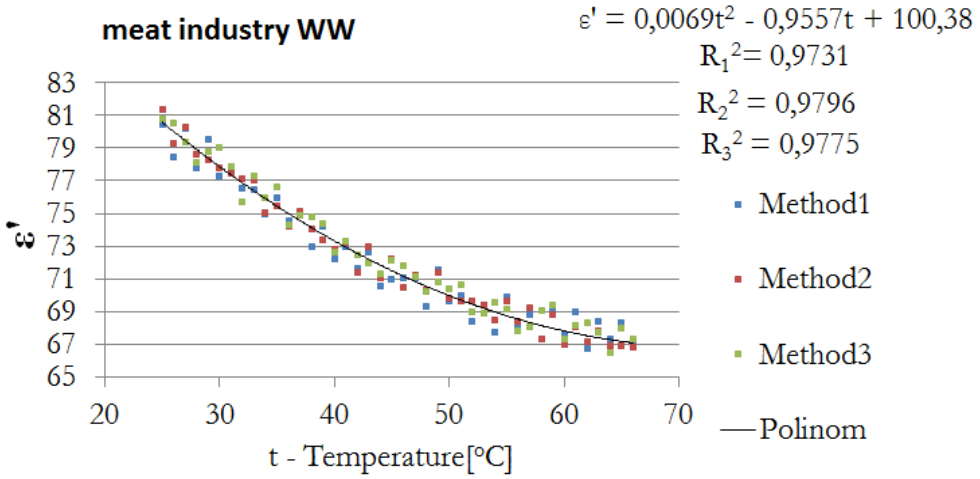

Figure 2 Dielectric constant of meat industry WW

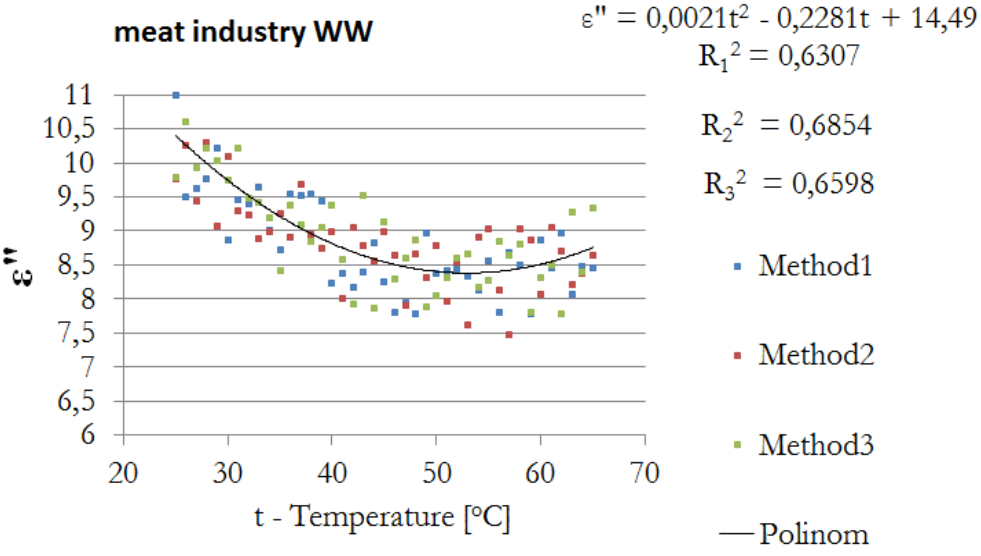

CONCLUSIONS

Results representing the three evaluating methods fit better the approximate polynomic in case of ε' than in case of ε". Changing the range of measurement results can be improved.

REFERENCES

[1] J. Baker-Jarvis, M. D. Janezic, J. S. Grosvenor, R. G. Geyer, Transmission/ Reflection and Short-Circuit Methods for Measuring Permitivity and Permeability, NIST Technical Note 1355-R, December 1993
[2] Beszédes S, László Z, Horváth Z H, Szabó G, Hodúr C (2011), Comparison of the effects of microwave irradiation with different intensities on the biodegradability of sludge from the dairy- and meat-industry BIORESOURCE TECHNOLOGY 102:(2) pp. 814-821.
[3] El-Mashad, H.E.-M.H. (2003). Solar Thermophilic Anaerobic Reactor (STAR) for Renewable Energy Production Agrotechnology and Food Sciences.Wageningen University, Wageningen.p. 238.
[4] Ghyoot W, Verstraete W. (1997). Anaerobic digestion of primary sludge from chemical pre-precipitation. Water SciTechnol; 6-7:357-65.

INTERNATIONAL SCIENTIFIC CONFERENCE ON ADVANCES IN MECHANICAL ENGINEERING

13-15 October 2016, Debrecen, Hungary

ANALYSIS OF REQUIREMENTS CORRESPONDING TO DEVELOPMENT OF MODERN PRODUCTS

[1]KUZMANOVIĆ Siniša PhD, [1]RACKOV Milan PhD, [2]VERES Miroslav PhD

[1]*University of Novi Sad,* Faculty of Technical Sciences,
E-mail: kuzman@uns.ac.rs, racmil@uns.ac.rs
[2]*Slovak University of Technology in Bratislava, Faculty of Mechanical Engineering*
E-mail: miroslav.veres@stuba.sk

Abstract
The paper deals with the problem of shaping and designing machines and machine parts with a particular focus which customers expect of products nowadays. Today, it is not enough that cheap product has a good quality (which is hard to achieve), but the product should be innovative, i.e. it should have some elements which will make the product different from the other similar products already existed on the market. This innovation is often manifested in slightly different form (design) which will make product more interested and will stimulate customer to purchase that particular product.

Keywords: *Design, modern look of product, market, product characteristics.*

1. INTRODUCTION

Nowadays, it is very hard to make some new product, which is cheaper and better than that solution which exists on the market. Also, new solution is not easy to sell, but if it is sold, it's hard to collect the payment, so any thought of creation some new product is suppressed at the beginning. However, possibility of making some new innovative product always exists, something different from the others, with different forms and shapes which will attract the customers to buy the product.

2. PROBLEM DESCRIPTION

Beside functional, structural, technical, exploitation, aesthetic and environmental characteristics, modern products have to meet specific market characteristics, which are manifested only when the product appears on the market. Market characteristics consist of all features of product which can attract the customer to buy it, but designer cannot do much to satisfy them. Since one of the fundamental roles of industrial design is to "sell" the product, these characteristics will be paid the greatest attention in this paper.
Market characteristics of products are: the type and complexity of product, specific characteristics (technical and exploitation), innovative characteristics, simplicity of using the product, assortment, quality, environmental characteristics, energy efficiency, design (shape, colour, graphic ways of information), product brand, the image of product, country of origin, emphasizing that the product has domestic origin, the price, the method and deadline for payment, packing and packaging of product, date of production, operating life of product, producing method, serial number, recognition and product protection, year of foundation of company, prospects and catalogue materials, directions for use and maintenance, marketing support, availability, period of delivery, terms, place and method of delivery, guarantees, technical support, service, possibility of trial period, possibility of free assembly, possibility of replacing and restoring gear reducer [1].

2.1. The Type and Complexity of Product

The type and complexity of product depends on development policy and technological capability of manufacturer, as well as on market demands. In fact, the products of the same type can be designed in different degrees of complexity. For example, in machine industry there are different levels of complexity [2]: (1) keys, bolts, shafts, (2) gears, mechanical transmissions, (3) electric motors, (4) washing machines, refrigerators, vacuum cleaners, (5) simple machine tools, (6) cars, (7) robots and machining centres, (8) ships, (9) jet aircraft and (10) spacecraft. Products of higher level of complexity requires more complex manufacturing technology which is possessed by only some manufacturers, so the price of these products is higher and competition is much lower. Therefore, most of manufacturers try to produce more complex (more expensive) products which enable higher profit. For example, manufacturers of keys earn significantly less profit than aircraft manufacturer.

2.2. Specific (Usually Technical and Exploitation) Characteristics of Product

Specific product characteristics depend on product type. So, (1) the most important characteristics of generators and power converters are power and efficiency degree (which shows efficiency of converting input energy into consumed), projected lifetime, etc. (2) For operating machines, the most important characteristics are capacity, accuracy, automation degree, efficiency of machines, etc. (3) Sensitivity, accuracy and stability of indication, the methods of reading, possibility of making records, etc. are very important for measuring equipment. (4) For transport vehicles, the most important characteristics are design, easy operation, low fuel consumption, high degree of efficiency, the lower the level of environmental pollution (exhaust and noise), safety, comfort, light weight, easy maintenance, etc. (5) Specific characteristics of household appliances are design, simple operation, easy disassembly and assembly, easy maintenance, safety, low noise, high efficiency, low cost, etc. (6) However, design, comfort, low cost, easy maintenance, durability are important specific characteristics for sports equipment. Better position at the market is taken by those products that work with, for example, higher efficiency or lower noise, etc. [1].

2.3. Innovative Characteristics

Figure 1 Innovative car Nissan IDS

Innovative characteristics depend on type of product, but they involve introduction of certain new solution compared to the old product which should be more attractive to customers. For example, in automotive industry, there is installation of start stop system which stops the engine when the car is stopped. For customers it is also attractive installation of camera for reversing driving, installation of system for slowing down and stopping the car when approaching some obstacle, installation of system for automatic parking, etc. (Fig.1).

2.4. Simplicity of Using the Product

It a lot of depends on type of the product, but in principle it means simple product application which should be attractive for customers. For example simple entering to vehicle could encourage some potential buyer to buy particular car.

2.5. Product Assortment

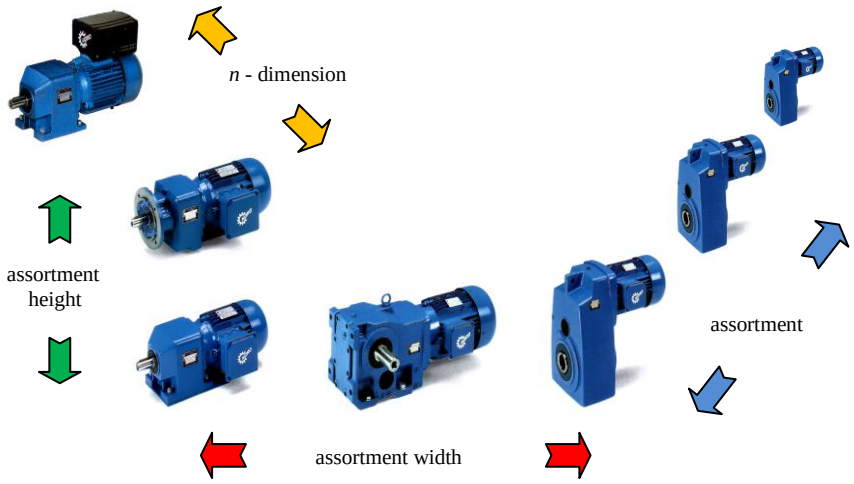

Figure 2 Graphic display of motor gear reducer assortments [6]

Product assortment represents a set of products that manufacturer can offer at the market. Customers would like to purchase all possible product type, so producers try to have wide assortment product range (usually with more product lines and within each line as many sub-lines). This increases production costs due to large number of raw materials, semi-products, tools, storage of final products, etc. Therefore, manufacturers are interested in short-range assortment, but with larger series, so they constantly seek some compromise. Product assortment varies in more dimensions: width, depth and height, although it practically can have n-dimensions (*Fig. 2*) [3, 4]. If motor gear reducer is observed, it can be produced in several lines, as helical motor gear reducer, worm motor gear reducer, helical-worm motor gear reducer, etc., and it is called "assortment width". In the frame of every line of these gear reducers, there are several sizes (product family) and it is called "assortment depth" or length of the line. Since these motor gear reducers are produced in different product variants: foot-mounted variant, large and small flange-mounted variant, foot and flange-mounted variant, flange-mounted variant with extended bearing hub, it is called "assortment height". However, if these motor gear reducers are offered with electric motor, with IEC adapter, with solid input shaft, with brake, or variator, or with electric control unit (slow start, revolution frequency regulation, etc.), then it is called "n-dimensions of assortment" (*Fig. 2*). Important characteristics of assortment observed during production and distribution of spare parts are assortment length (the range between the first and last product in the frame of product line), assortment density (number of products within a single line or number of product lines) and assortment consistency (connection between different product lines) [5]. For example, if the same gears are used in various types of gearboxes, then it can be confirmed that product assortment is consistent. All manufacturers try to give their products specific design feature in order to ensure easy recognition of their products on the market.

2.6. Quality of Product

Product quality represents the ability of products to meet customers' requirements and expectations. It can be low, average, high and superior. Product quality depends completely on the manufacturer, i.e. its professional and technological capabilities, as well as its market orientation and target customer groups for which the product is intended. High-quality products are always given a special design which attract attention of potential customers of these products and point to their speciality.

2.7. Environmental Characteristics

Environmental characteristics (no possibility of water, air or land pollution) start to be significant factor to much more customers on the selection of gear reducers. Also, a lot of positive legislations do not allow bringing to the market product that can pollute or excessively pollute the environment [7]. Beside other things, this was the main reason for appearance of ecological plastic bags, development of hybrid cars, development of cars with electric drive and other similar products.

2.8. Energy Efficiency

Rational use of energy has very important impact on market placement, not only because of lower exploitation costs, but also due to lower environmental pollution. Nowadays many positive low regulations do not allow bringing to the market products with low energy efficiency. Because of energy shortages, this was the main reason for development of energy-saving light bulbs and many other similar products.

2.9. Design

Shape, colour and graphic ways of information are included in the general frame of design. For almost all products, it has become a crucial factor which affects attractiveness and product placement on the market. However, it is not enough that the product is attractive, but it should be easy to use. Nowadays, design is very important since it is better to see nice and attractive product, than the product which is not. Attractiveness is especially pronounced for jewellery, clothing, shoes and all products intended for wide market of vehicles, cell phones, televisions, CD players, washing machines, refrigerators, furniture, etc. However, design is not so significant for machine tools, electric motors, plumb and gas installation, while for steel profiles and bolts, it is not important, but it cannot be ignored.

2.10. Product Brand

Product brand (brand or trade mark) represents a short name or logo of some product, or some manufacturer, easy to remember, pronunciation and reading and is used to distinguish products from different manufacturers. One company can have multiple brands. If the customer is able to buy product of particular brand per the same or some higher price of the product of unknown or less known brand, certainly he will decide to purchase the product of the known product brand. Therefore, it should constantly work on building product brand image [7].

2.11. The Image of Product, or Brand

Product image represents a positive opinion about the product which is built up by advertising or established by high product quality, good design or fine packaging, which helps the customers to

decide for purchasing the product of certain brand [7]. Product image should be distinguished from the brand image, although they are in a tight mutual connection. Product image has a great influence on its market placement [1]. Product image is created through modern methods of marketing and it can be affected by appropriate promotion, good service support, providing the warranty of gear reducer quality, providing the credit loans, etc. All manufacturers have to continually work on improving the product image and brand image.

2.12. Country of Origin

The country of origin has a very large impact on product placement on the market, since there's existing opinion that some countries produce high quality products, while some other countries are not able to do that. If it is estimated that declaring of country would have positive impact on product placement, then it is specially noticed, although it is also legal obligation [6].

2.13. Emphasizing that the Product has Domestic Origin

Information that the product has domestic origin can have great impact on product placement, since majority of customers are prepared to support action "buy domestic".

2.14. The Price of Product

The price is certainly one of the most important factor that influences the purchasing of products. However, if products have good quality and design, it isn't a problem for customers to pay that price, so great attention is paid to increasing of quality and improving design. The product price is a market category and designers can have great influence over product quality, production costs, but they do not define it. The price depends on orientation and goals of company, so when there is no competition, price could be much higher than actual production costs and higher price will obtain higher profits [1, 6]. Also, when there is a large competition, price could be lower, with any or small profit, if the manufacturer wants to force its products at a new market.

2.15. The Method and Deadline for Payment

Method and deadline for payment can also influence on purchasing gear reducers, since it is very important for customer should the payment must be in cash, immediately or delayed payment, or with credit. In many cases, crediting the customers represents the basic condition for successful product realization. Significant number of customers would not be able to appear as buyers of certain gear reducers if they are not allowed to buy on credit or delayed. In this way, some manufacturers of gear reducers provide themselves regular customers [6].

2.16. Packing and Packaging of Product

Packing (way of putting the product in the packaging) and packaging represent very important instrument of marketing. Good implemented packing (individual or group) and fine designed packaging attract customers' attention and can have a great influence on product placement. Special attention is paid to design of the packaging which aim is to attract the customers' attention. Also, it should provide visibility of the contents of the packaging on those places where it is necessary and possible. In the same time, packaging should be designed to provide easy transport and relocating the product, simply unpacking, etc.

2.17. Date of Production, or the Date until the Product can be Used

This date is very important for a wide range of products, not only for the food industry, so it is specially marked on the product or packaging. Date or year of production does not tell only about freshness of product, but also about its actuality, so the customers, when choosing the product, pay a great attention on this detail. Expiration date of product, or the expiration time after opening the package, can have a great influence on the safety and market placement of some products.

2.18. Operating Life of Product

Operating life of product gives information about time intended for exploitation and about its durability and has a great influence on customer's decision, so it should be accentuated on product, packaging and its documentation.

2.19. Producing Method

Information that the product is made or assembled manually can be very important for customers. Usually, hand-made or manually assembled products are considered as products produced with great care and therefore, they have higher quality and price. It is specially highlighted for products made in a small series, for example for prestigious type of vehicles, shoes, cigars, soaps, etc.

2.20. Serial Number

For many products, serial number represents important information in the case of reclamations or product recognition, but also it can be a case of prestige, when the products are produced in limited series.

2.21. Recognition and Product Protection

Recognition and product protection represent specific characteristic or product feature which is different from other (for example origin country or way of delivery). Manufacturers try to protect their products from copying by using special symbols on product or on packaging, or by creating special shape of product. They usually make it by holograms or other protection methods, for example special shape of product or packaging, etc.

2.22. Year of Foundation of Company

With specifying the year of company foundation, printed on product or packaging, manufacturer would like to announce its experience and this certainly can attract the customers' attention.

2.23. Prospects and Catalogue Materials

Prospects and catalogue materials represent important documentation without which marketing and selling is not possible nowadays, so it is paid great attention to the preparation of these documents. Creating on-line catalogues by Internet, development of these materials reached unimaginable proportions.

2.24. Directions for Use and Maintenance

Legal obligation of every manufacturer is creating directions for use and maintenance accompanied with every product on the market. Without these instructions, it is impossible to send product to the market. Documentation can be given in the form of specific documents, or it can be printed on products as a text, picture or pictogram.

2.25. Marketing Support

Marketing support includes continual promotional activities carried out with product in order to increase its support at the market and better product placement. Successful placement at the market cannot be expected without these activities.

2.26. Availability

Availability represents the possibility that gear reducer can be bought at any place where there are interested customers. Providing high availability is very important, since this increases possibility of their sales.

2.27. Period of Delivery

Period of delivery can be often crucial factor which attract the customers' attention. When it is made sales contract not intended for wide market, i.e. when it is not required prompt delivery, it is very important to define exact delivery time because these products usually requires strict respecting of contracted delivery terms and complete the work on time. Contract usually defines so-called penalty (which is paid in the event the agreed period is not respected), or premium (which is obtained if the work is done before agreed period). This can influence on successful company business, or ruin the business if the deadlines are not agreed.

2.28. Terms, Place and Method of Delivery

Terms, place and method of delivery can have great influence on choosing the product. Some products can be delivered only after whole amount is paid, or after some payment in advance. Method of delivery (by plane, truck, railway, ship, etc.) and place of delivery (from manufacturer's storage, dealer's storage, or with a possibility of delivering on a given address) can be important information for customers, especially for large products, such as household appliances, furniture, etc. Therefore, all manufacturers and dealers have to pay a great attention to this factor.

2.29. Guarantees

Guarantee represents special kind of sales service which advertises new product and protects the buyer. Guarantee is a formal statement that the product will meet basic customers' expectations in predicted time period. It confirms the product level and tells about the expected period during which customer can have confidence in product [6]. According current law regulation, warranty covers period of two years, i.e. manufacturer guarantees that the product will operate two years with no failure and all possible failures occurred as a result of manufacturing errors will be serviced and repaired by his own expense. If the failure cannot be fixed in reasonable time, the manufacturer is required to replace the customer's product by new one. In some cases, manufacturer gives longer

warranties, since it wants to convince the customers about high quality of its product and to attract the customers' attention. Longer guarantees period can be also used for formation higher selling price.

2.30. Technical Support

Technical support represents providing of technical advices during purchasing, mounting, starting and running in the product, service, maintenance and the product repair. It is usually carried out by direct contact, by phone, or internet between customer and seller or customer and manufacturer. Technical support for most of products can have a big influence on product placement.

2.31. Service

Service provide to the customer all necessary service or operation of purchased product during its installation, starting, running, and in the event of any failure or defect in the period of its warranty. Similar as guarantee, its role is to attract the product, in indirect way, and to protect the costumer. For many products service is important factor which influence the customers to buy certain product (vehicle, television, refrigerator, etc.). It's hard to believe that customer will decide to buy new product if it hasn't provided good service. In many cases fast and good service has greater importance to the customers than the product price. Well-organized customer service and timely response to customer's complaints represent the largest sales support.

2.32. Possibility of Trial Period

Possibility of trial period can have big influence on final customer's decision which product to buy, not only in food industry, for example chocolate, but also for buying technical equipment, for example vehicle. Therefore producers must dedicate a great attention to this marketing possibility, since it can increase the purchasing.

2.33. Providing Gifts and Organizing Prize Contests

Providing gifts and organizing prize contests with purchasing some product can also stimulate selling and it should kept in mind when forming the strategy of selling the products. These activities are particularly interested for new products or for buying the product for the first time in order to make the product attractive as more as possible.

2.34. Possibility of Free Assembly

If the product is delivered in parts - disassembled, it could be very important for customers to have free assembling of product. Therefore, for every complex product which is delivered disassembled, the costumers should be offered by free assembly of product. This opportunity should be announced to customer on time, before making a final decision about purchasing the product. Certainly, the price of assembling is included in the product price.

2.35. Possibility of Replacing or Returning the Product

If a customer is not satisfied with bought product, possibility of replacing or its returning can be very important factor that customer decides to buy particular product. If a customer is not satisfied with purchased product or it does not fulfil his expectations, in a specified period of time customer could ask to replace the product, or to return it and get money back.

Beside these listed characteristics, there are a lot of characteristics specific for each product individually. For example, energy value, not included preservatives and additives are important for food; pH-value is interested for soaps (which determine whether the soap is acidic or alkaline); octane number interested for petrol, etc., but they will not be discussed separately here.

3. THE WAY OF SOLVING PROBLEMS

Designer task is oriented to identify costumers' needs and create the products that will meet these requirements as much as possible. These are primarily included: function, purpose, structure, size, material, weight, ergonomic requirements, safety, functionality safety, aesthetic requirements, forms (composition, compositional balance, symmetry, proportion, harmony, rhythm, accent, ornament, plasticity, shadows, etc.), colors and graphic media, series size (unification), time of delivery, the agreed quality, service life, efficiency, degree of automatization, energy consumption, agreed prices, ways of manufacturing (castings, pressings, forgings, etc.), clamping methods, measuring, assembling, marking, testing, conservation, packing, packaging, storage, transport, unpacking, deconservation, mounting, exploitation, service, maintenance, repair, atmospheric and biological factors, recycling, ecology, special requests (low regulations, standards, contracts, licenses, financing capabilities, possibility of high temperature, low temperature, high vibration, sealing, centricity, elasticity, rigidity, easy disassembly, anti-explosive protection, protection against vandalism, theft, disaster - fire, flood, earthquake, work in emergency conditions, hygiene requirements, upgrading ability, etc.) and personal requests (tastes, habits, customs, prestige, fashion, comfort, quality, size, gender, age, occupation, marital status, lifestyle, ethnicity, race, religion, pregnancy, handicap, etc.).

CONCLUSIONS

Based on given data, final choice of product, or producer, depends on all presented factors, but also on ability/capability of marketing managers, sellers and customers to adequately emphasize and utilize these characteristics in forming final price and other condition of sale (payment in rates, credit, compensation, etc.).

REFERENCES

[1] S. Kuzmanović (2012): *Industrial Design*. 3rd ed. Faculty of Technical Sciences, University of Novi Sad.
[2] M. Rackov (2013): *Conceptions of Development of Universal Gear Reducers*. Ph.D. thesis (in Serbian), University of Novi Sad, Faculty of Technical Sciences.
[3] S. Kuzmanović (2009): *Universal Helical Gear Reducers*. 2nd ed. Faculty of Technical Sciences, University of Novi Sad.
[4] S. Kuzmanović, M. Vereš, M. Rackov (2010): *Product Design as the Key Factor for Development in Mechanical Engineering*, Mechanical Engineering in XXI Century, University of Niš, Faculty of Mechanical Engineering, Niš, Serbia, 25-26 November 2010, str. 113-116, ISBN 978-86-6055-008-0
[5] S. Kuzmanović, M. Rackov(2010): *Design Analysis of Housings of Universal Multistage Helical Motor Gear Units*, 5th International Symposium on Graphic Engineering and Design – GRID'10, University of Novi Sad, Faculty of Technical Sciences, Novi Sad, Serbia, 11-12 November 2010, pp. 255-260, ISBN 978-86-7892-294-7.
[6] S. Kuzmanović (2009): *Product Management*. Economic Faculty, University of Novi Sad.
[7] S. Kuzmanović, M. Rackov (2009): *Directions of Development of Universal Speed Reducers*, International Conference General Machine Design 2009, Rousse, Bulgaria, 15-16. October 2009, ISSN 1313-9193; University of Ruse „Angel Kanchev" / Transport Faculty of University of Ruse / Union of Scientists – Branch Rousse; pp. 31-34.

INTERNATIONAL SCIENTIFIC CONFERENCE ON ADVANCES IN MECHANICAL ENGINEERING
13-15 October 2016, Debrecen, Hungary

INNOVATIVE METHOD FOR HYDRAULIC FRACTURING OPTIMIZATION

[1]LENGYEL Tamás, [2]PUSZTAI Patrik, [3]JOBBIK Anita PhD

[1,2]Petroleum Engineering Department, University of Miskolc
E-mail: lengyel@afki.hu , pusztai@afki.hu
[3]Research Institute of Applied Earth Sciences, MTA-ME Geoengineering Research Group University of Miskolc
E-mail: jobbik@afki.hu

Abstract
As it is well-known, the well stimulation methods are getting more popular recently due to the increased significance of unconventional hydrocarbon resources. The hydraulic fracturing is one of the most frequently used treatments because of its large impact on the productivity index of the well. This paper presents a fracturing optimization algorithm which can be used effectively in evaluation period of the projects since it needs only the most important parameters of the given reservoir. This method provides both technical and economical optimization in hydraulic fracturing point of view. It is able to determine the most important fracking parameters which could provide the maximum NPV of the project with this algorithm.

Keywords: *hydraulic fracturing, optimization, unconventional hydrocarbon, NPV*

1. INTRODUCTION

The hydraulic fracturing is a multidisciplinary science, it needs very complicated engineering skills and in addition it is a quite expensive treatment therefore all effects should be considered in a fracking design procedure. It is obvious that the greater the treatment the greater the treatment's effect will be however there is a point considering the "size" of the treatment after that the profit resulted by the fracturing will be less than the costs of the procedure. Fig. 1 illustrates the NPV values of the fracking treatment as the function of the fracture half-length which is representing the size of the fracturing.

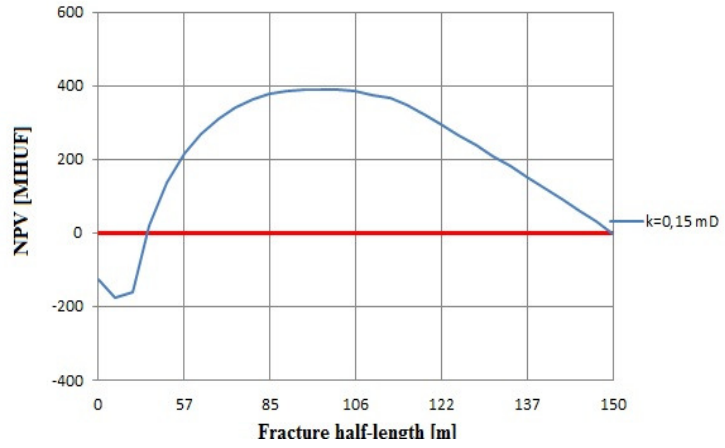

Figure 1 NPV of Treatment

Investigating the fracturing, a huge number of parameters might be taken into account. On one hand

it depends on which period of the project is actual, on the other hand how many data are available. As it was mentioned before this type of algorithm offers an optimization method in the early period of the project thus it integrates approximations, simplifications to be able to determine optimal parameters of fracturing. However a very important parameter was also integrated in the algorithm by which the application of the process was extremely extended. Well path is one of the most influencing parameter considering any kind of problem in petroleum engineering, therefore this optimization method can be applied also in case of vertical, deviated and horizontal wells providing diversification for the algorithm. As the results proved significant differences can be observed in variant cases.

2. MODEL

Considering the versatility and the complexity of the fracturing and the behaviour of several reservoirs, the operation of the algorithm was interpreted in relatively short range. However it must be emphasized that the process could be used for any kind of reservoirs and fluids with the necessary modifications. In the following the most important model properties are introduced.

Fracture geometry

The improved productivity of the well is closely related to the increased inflow surface which is in fact the fracture surface. Fracture opens always in the least resistance direction, in a given stress field fracture tries to propagate so as to avoid the greatest stress and it creates width in direction that requires the least force. It means that fracture propagates parallel to the maximum horizontal stress and perpendicular to the minimum horizontal stress. As the service companies, this model also assumes that fracture is created in the whole height of the layer. Fig. 2 represents the fracture geometry in vertical wells.

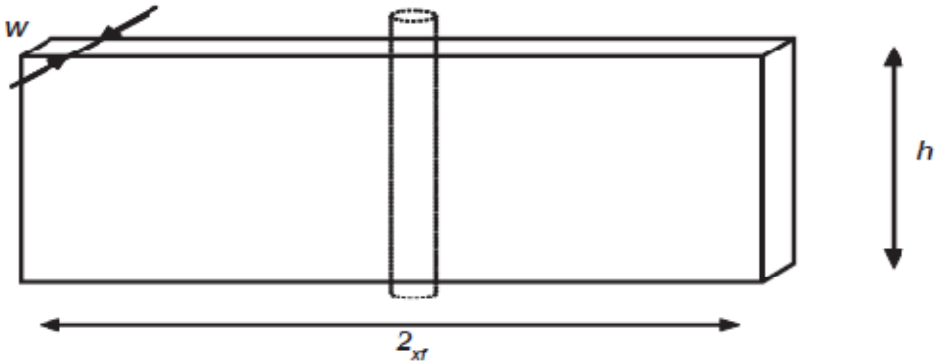

Figure 2 Fracture geometry in vertical well

Compared to vertical wells, fracture geometry in horizontal wells is completely different. Basically two types of fracture geometry can be defined in case of horizontal wells. If the well path is parallel to the maximum horizontal stress longitudinal fracture will be created, if the well is perpendicular to the maximum horizontal stress (parallel to the minimum horizontal stress) transverse fracture(s) will be created. In the longitudinal case, the facture properties are the same as in the vertical well case. However the transverse fractures play a more significant role in the fracturing treatment. Although the inflow parameters of a transverse fracture are less favourable, this kind of treatment has the possibility to create more parallel transverse fractures (multi-fractured horizontal well) providing a significantly better inflow condition. Fig. 3 illustrates the fracture geometry in horizontal wells.

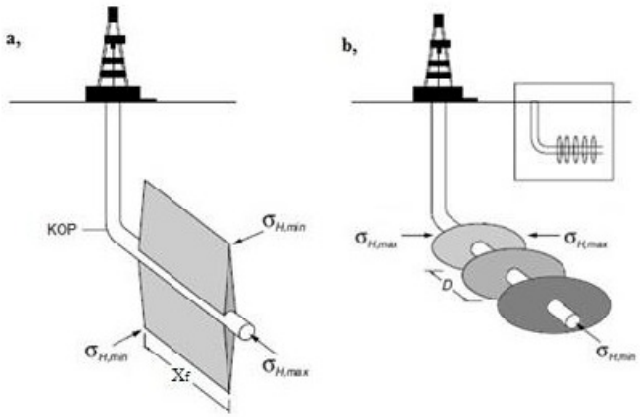

Figure 3 Fracture geometries in horizontal wells

According to the quite different fracture geometry in transversely fractured well several other effect has to be considered. Especially the limited contact area between the well and the reservoir that results a huge velocity increase in the inflow which requires another flow theory to consider correctly the flow.

Proppant distribution

One of the most important segment of fracking is the so-called proppant which propped the created fracture and provides a support not to collapse the fracture. Without going into details, the proppant distribution is a critical point considering the effectiveness of the treatment because it provides the conductivity of the flow pattern. The algorithm considers the proppant distribution on inhomogeneous way (as shown in Fig. 4) which makes the model much more realistic.

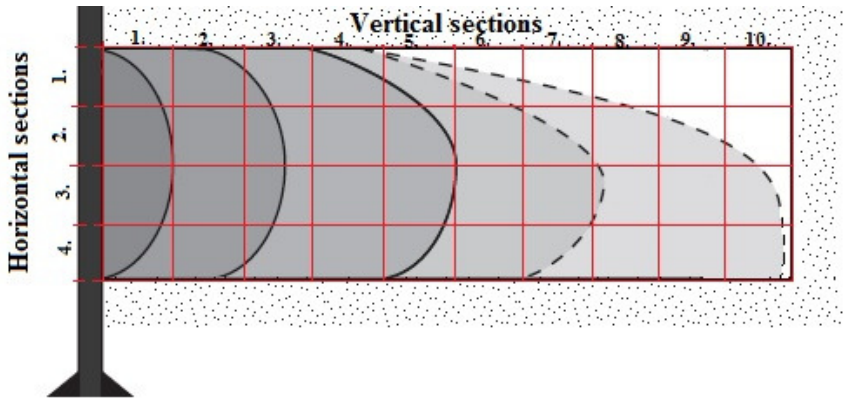

Figure 4 Proppant distribution

The cross section of the fracture is divided into vertical and horizontal cells thus the inhomogeneity due to the loss in proppant transport and the gravitational segregation can be considered as a proppant pack permeability decrease.

Other parameters

According to the high flow rates, the effect of turbulence has to be taken into account. This non-Darcy flow concept was also integrated into the algorithm as a separated small cycle. In addition in case of transversely fractured horizontal wells a choke skin effect was also considered due to the converging radial flow which results a significant drop in the flow rates.

To demonstrate the results on a relatively simple way, a closed dry gas reservoir was chosen. As the production is run, the reservoir pressure drops which results a production drop also in the flow rates considering a constant depression. A material balance equation was used to cope with this problem, Fig. 5 shows this perfectly.

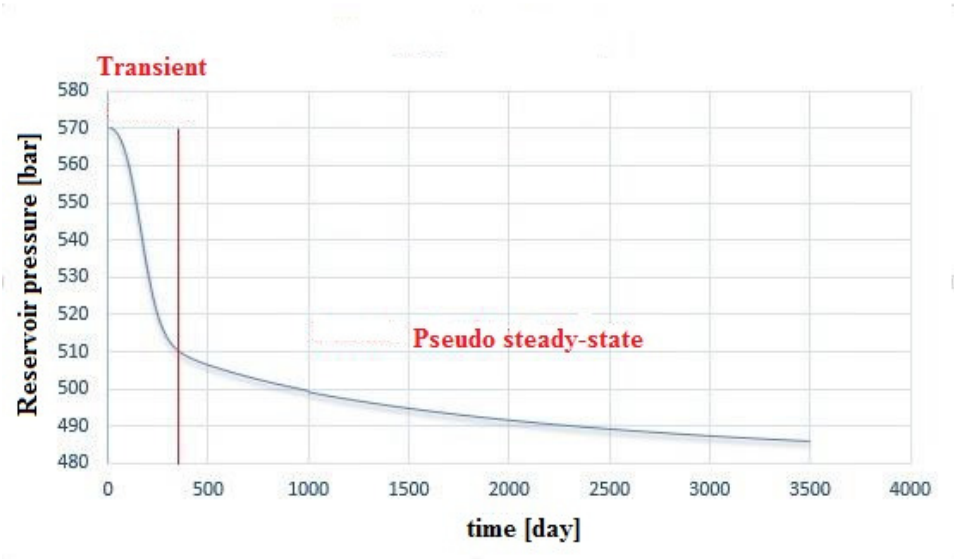

Figure 5 Pressure decrease in a closed reservoir

3. ALGORITHM

The optimization method presented in this paper is based on a multistage algorithm which includes main cycles. The main cycles contain more small cycles and calculations. The technical optimization is made by the so-called UFD (Unified Fracture Design) model which gives the maximum productivity indexes in function of the proppant masses. The economical optimization and the solution of other petroleum engineering problems are based on personal considerations. Table 1 summarizes the most important input parameters while Fig. 6 illustrates the operation of the algorithm with a flow chart, it symbolizes the main cycles of the algorithm.

Table 1 Input Parameters

Parameter	Symbol [dimension]	Parameter	Symbol [dimension]
Reservoir height	h [m]	Gas specific density	γ [-]
Reservoir permeability	k [mD]	Proppant pack permeability	k_f [mD]
Reservoir pressure	P_r [bar]	Proppant bulk density	ρ [kg/m^3]
Bottom hole pressure	P_{wf} [bar]	Original gas in place	G_i [nm^3]
Drainage area length	X_e [m]	Well radius	r_w [inch]
Reservoir temperature	T [K]	Crash factor	C_r [%]
Gas dynamic viscosity	μ [cP]	Treatment costs	$\$_t$ [MHUF]

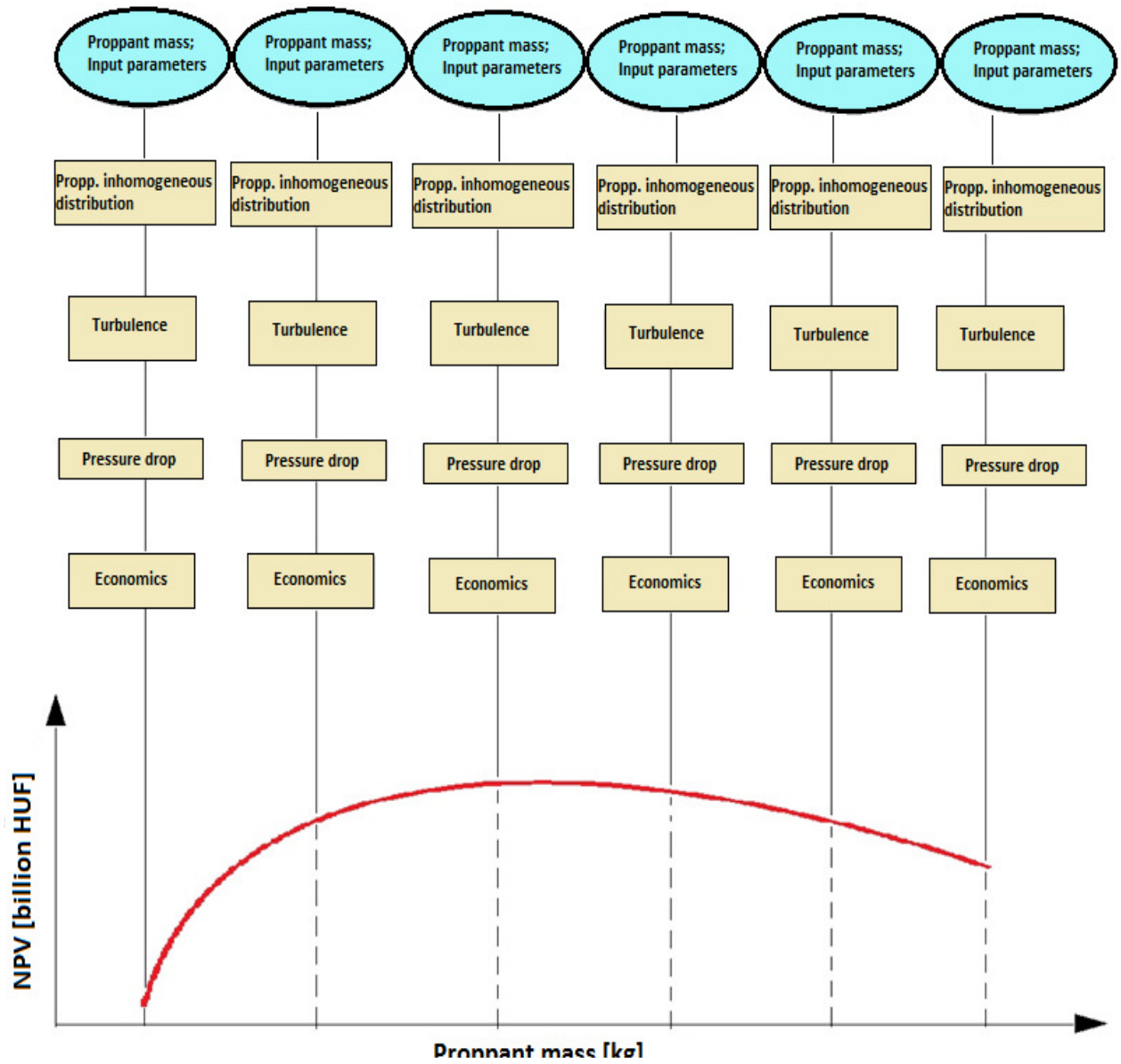

Figure 6 Flow chart

4. RESULTS

To show the operation of the optimization method, the algorithm was run with Hungarian input parameters which represent a typical tight gas reservoir in a Hungarian field. Different proppants were chosen to demonstrate the impact of proppant properties. Fig. 7 shows the NPV curves in function of proppant masses pumped down into a vertical well. As the flow chart illustrates (Fig. 6) the actual treatment parameters like fracture half-length, fracture conductivity, improved productivity index etc. can be also determined. In addition varying technical (fluid type, reservoir pressure and temperature, drainage area, well data, proppant size, OGIP or OOIP) and economical (drilling cost, treatment cost, CAPEX, OPEX) parameters sensitivity tests can be carried out and several significant and interesting effects can be concluded.

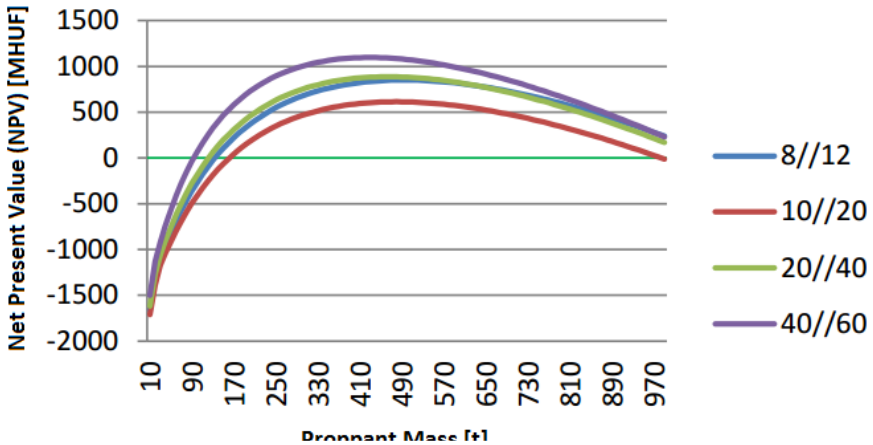

Figure 7 NPV curves

CONCLUSION

Applying the developed multistage algorithm fracturing projects can be prejudged and the profitability of the investment can be evaluated. With this method, the optimal treatment parameters can be determined. It also provides a kind of economical and technical optimization. In addition several types of sensitivity tests can also be conducted, thus the impact of technical (like proppant properties, reservoir parameters etc,) and economical (like gas or oil prize, OPEX, CAPEX) parameters can be investigated.

ACKNOWLEDGEMENT

The research was carried out in the framework of the GINOP-2.3.2-15-2016-00010 "Development of enhanced engineering methods with the aim at utilization of subterranean energy resources" project in the framework of the Széchenyi 2020 Plan, funded by the European Union, co-financed by the European Structural and Investment Funds.
Furthermore Tamás Lengyel and Patrik Pusztai appreciate the support of The New National Excellence Program granted by the Ministry of Human Capacities.

REFERENCES

[1] ADVANTI, S. H.–KHATTIB, H.–LEE, J. K.: Hydraulic Fracture Geometry Modeling, Prediction and Comparisons, In: paper SPE, 13863, 1985.
[2] ECONOMIDES, Michael J.–MARTIN, Tony: Modern Fracturing. Enhancing Natural Gas Production, 2007.
[3] LENGYEL, T.: *Horizontális kút hidraulikus rétegrepesztés optimalizálása,* Thesis, Miskolc, 2015.
[4] PUSZTAI, P.: *Ferdített kút hidraulikus rétegrepesztés optimalizálása,* Thesis, Miskolc, 2015.
[5] ZHANG, Y.–EHLIG-ECONOMIDES, C. A.: Inflow Performance for a Hydraulic Fracture in a Deviated Well. In: paper SPE, 119345, 2009.

INTERNATIONAL SCIENTIFIC CONFERENCE ON ADVANCES IN MECHANICAL ENGINEERING
13-15 October 2016, Debrecen, Hungary

THE EFFECT OF AMBIENT TEMPERATURE ON PARTS DIMENSIONAL CONTROL AT REPAIRING OF LOCOMOTIVES COMBUSTION ENGINES

[1]ĽUPTÁČIKOVÁ Veronika, [1]ŤAVODOVÁ Miroslava PhD

[1]Faculty of Environmental and Manufacturing Technology, Technical University in Zvolen, Študentská 26, 960 53. Slovak Republic.
E-mail: xluptacikova@tuzvo.sk, tavodova@tuzvo.sk

Abstract
The article is focused on the determination of the ambient temperature influence on parts dimensional control at repairing of combustion engines. The oil pump of the K6S230-DR locomotive engines was a chosen node of the combustion engine. Dimensions of chosen parts were controlled by workshop gauges and instruments. The aim of the measurement was to determine whether the ambient temperature has a major influence on the parts size change at repairing of combustion engines. Measured dimensions were being compared with the required dimensions. In the results and in the conclusion, we analysed the expansion of the material and the measurement errors that may occur when measuring.

Keywords: *combustion engine, oil pump, control, temperature, expansion.*

1. INTRODUCTION

Repairs of the rolling stock are aimed on diesel locomotives, railcars, personal cars according to the customer requirements and railway bogies. When repairing the railcars, the calibrated gauges are used. Metrology is a scientific and technology discipline which deals with various findings and activities related to a measurement. The basis is a consistent and accurate measurement in all fields of science, economy, public administration, defence, health and environment. Metrology in a quality management system must be understood as a set of activities related to keeping, filing, calibration and verification of measuring instruments, namely a creation and adherence of the metrology regulations [1]. In this article, we focus on the measurement of the oil pump elements size in the K6S230-DR locomotive engine and their change which is affected by the ambient temperature. In the broad sense, thermal effects are those caused by a redistribution of internal energy in a system, and they may be grouped in natural and artificial [2].

2. METHODS

Combustion engines of locomotives and railcars are principally consistent with automobile engines (or better with engines of trucks). Some locomotives and railcars use the automobile engine directly. Today, diesel engines are used exclusively; the period of petrol (gasoline) aggregates passed during the first half of the 20th century. In comparison with the gasoline engine, the diesel engine has a higher efficiency which ranges from 30 to 42% while the efficiency of gasoline engines reach only 20-33% [3].
The term measurement means the experimental procedure, where we find out a specified value of a physical quantity as a multiply of the unit or assigned value. Measuring the sizes of parts, the quantitative characteristics are being found out. For each measurement, there are some errors. They are caused by the imperfection of our senses, inaccuracies of the measuring instruments and impossibility to meet the same measurement conditions for example local and time temperature

stability, invariability of air pressure etc. Unlike regular errors, random errors always occur there and their existence is manifested by the fact that the results obtained by repeated measuring with the same conditions are always different. These differences among the results of the repeated measurements give us the possibility to estimate the size of random errors or their order at least, and according to them, the accuracy of the measurements is reviewed. From the statistical character of normal law, we can see that it does not give us the possibility to determine the real measurement error, nor find out the true value of a measured quantity. From that, we can determine a probability of the errors occurrence in selected limits and it allows to determine the most likely value of a measured quantity. If a value is calculated as an average, we can expect that we are closer to a correct value more often by any calculation. In the other words, the average gives the most likely measured value; it gives us the greatest hope that we will come to the correct value [4], [7].
Thermal expansion of the material is a volume material response to a temperature increase. Increasing a temperature, material atoms oscillate in greater distances from the equilibrium position and thus the material volume is changed [5].
The linear coefficient of length expansion α is defined by the expression (1):

$$\alpha = \frac{1}{L_0}\frac{dL}{dt} \tag{1}$$

in a small temperature range, α is a constant, so (2):

$$L = L_0.(1 + \alpha.t) \tag{2}$$

where L_0 is the length at the reference temperature. When measuring the geometrical quantities, the reference temperature r = 20 ° C, and L is the length at a temperature t (° C) [6].
The average value of the measurements was calculated by the formula (3):

$$\bar{x} = \frac{1}{n}\sum_{i=1}^{n} x_i \tag{3}$$

where:
x_i – measured value of the i-th measurement
$\bar{x}$ - average value from n measured values
n – number of independent measurements.

2.1. Experiment

Locomotive combustion engine consists of several parts and subassemblies. For the experiment, a part of the locomotive engine K6S230-DR, namely the oil pump was chosen (*Figure 1*).

Figure 1 Assembled and distributed oil pump [8]

The measurement was performed in the engineering workshop. The parts of the oil pump were prepared on the desk and the specified dimensions were checked according to the specific sheet. The following four parts were chosen for the measurement:
- Front cover,
- Tailgate.
- Driving wheel,
- Driven wheel.

The measurement of the A dimension on the driven sprocket is shown in *Figure 2*.

Figure 2 Measurement of the A dimension on the driven sprocket [8]

The measurements were performed by chosen workshop gauges and instruments. The length dimensions were measured by Subito SOMET with the range of 55-155 mm and the accuracy of 0.01 mm, MITUTOYO with the range of 250-400 mm and the accuracy of 0.01 mm, microns SOMET with different ranges (for example with the range of 125-150 mm and the accuracy of 0.01 mm) and by the dial indicator SOMET with the range of 0-3 mm and the accuracy of 0.01 mm. Fluke multimeter with the range of 200-1350 °C and the basic accuracy of 1.0 % was used for the temperature measurement. All workshop gauges and measuring devices had been calibrated. The ambient temperature in the workshop was 26 °C. In the *Figure* 3, the dimensions of measured parts are shown.

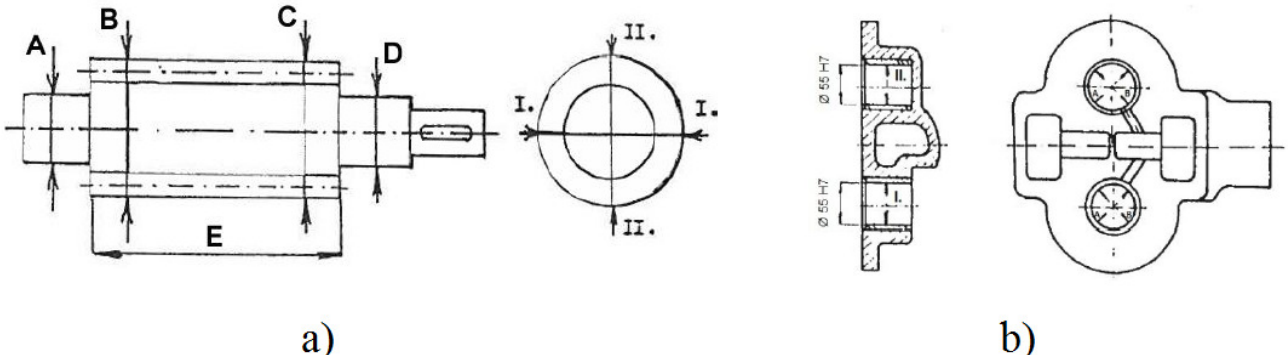

Figure 3 The measured dimensions of the parts a) driving wheel b) front cover [8]

3. RESULTS

Dimensions and the material of the measured components are shown in *Table 1*.

Table 1 Dimensions and the material of the measured parts [8]

Part	Material	Label of the measured dimension	Dimension (mm)	Maximum dimension (mm)	Minimum diameter (mm)	OK/NOK
Driving wheel	17 346	A	$\emptyset\ 55\ ^{-0,06}_{-0,075}$	Ø 54.94	Ø 54.925	OK
		B	$\emptyset\ 137.5\ ^{-0,45}_{-0,5}$	Ø 137.05	Ø 137.00	OK
		C	$\emptyset\ 137.5\ ^{-0,45}_{-0,5}$	Ø 137.05	Ø 137.00	OK
		D	$\emptyset\ 60\ ^{-0,06}_{-0,075}$	Ø 59.94	Ø 59.925	OK
Driven wheel	17 346	A	$\emptyset\ 55\ ^{-0,06}_{-0,075}$	Ø 54.94	Ø 54.925	OK
		B	$\emptyset\ 137.5\ ^{-0,45}_{-0,5}$	Ø 137.05	Ø 137.00	OK
		C	$\emptyset\ 137.5\ ^{-0,45}_{-0,5}$	Ø 137.05	Ø 137.00	OK
		D	$\emptyset\ 55\ ^{-0,06}_{-0,075}$	Ø 54.94	Ø 54.925	OK
Front cover	11 600	A	$\emptyset\ 55\ H7$	Ø 55.03	Ø 55.00	OK
		B	$\emptyset\ 55\ H7$	Ø 55.03	Ø 55.00	OK
Caseback	11 600	A	$\emptyset\ 55\ H7$	Ø 55.03	Ø 55.00	OK
		B	$\emptyset\ 60\ H7$	Ø 60.03	Ø 60.00	OK

During the measurement, there were simulated the conditions which may occur in the lobby during the year. The temperature of the parts was being changed, while the ambient temperature remained to be constant - 26 °C. Found out dimensions were recorded to the tables. The average values of the measurements are shown in *Table 2*.

Table 2 The measured dimensions of parts - normal conditions, simulated warming and cooling [8]

Part	Label of the measured dimension	Normal conditions		Simulated warming		Simulated cooling	
		Part temperature (°C)	Average dimensions (mm)	Part temperature (°C)	Average dimensions (mm)	Part temperature (°C)	Average dimensions (mm)
Driving wheel	A	23.7	Ø 54.935	33.1	Ø 54.938	12.2	Ø 54.928
	B		Ø 137.047		Ø 137.047		Ø 137.032
	C		Ø 137.037		Ø 137.043		Ø 137.03
	D		Ø 59.93		Ø 59.937		Ø 59.928
Driven wheel	A	24.9	Ø 54.93	33.4	Ø 54.938	12.5	Ø 54.927
	B		Ø 137.037		Ø 137.047		Ø 137.033
	C		Ø 137.04		Ø 137.045		Ø 137.03
	D		Ø 54.932		Ø 54.938		Ø 54.927
Front cover	A	25.3	Ø 55.025	33.0	Ø 55.028	13.1	Ø 55.013
	B		Ø 55.022		Ø 55.027		Ø 55.003
Caseback	A	25.3	Ø 55.025	33.3	Ø 55.027	13.3	Ø 55.012
	B		Ø 60.023		Ø 60.020		Ø 60.017

The temperature of parts was measured by Fluke millimetre. After measuring of all values, a meeting of prescribed tolerances was verified by the elementary calculations (4) - (11).
The average dimension of the part A at the ambient temperature (4):

$$\bar{x} = \frac{\sum_i^n x}{n} = \frac{54.95 + 54.92 + 94.93 + 54.95 + 54.93 + 54.93}{6} = 54.935\ mm \quad (4)$$

The average dimension of the part A at simulated warming (5):

$$\bar{x} = \frac{\sum_i^n x}{n} = \frac{54.93 + 54.94 + 54.94 + 54.93 + 54.94 + 54.95}{6} = 54.938\ mm \quad (5)$$

The average dimension of the part A at simulated cooling (6):

$$\bar{x} = \frac{\sum_i^n x}{n} = \frac{54.92 + 54.92 + 54.93 + 54.95 + 54.93 + 54.90}{6} = 54.928\ mm \quad (6)$$

Calculation of the upper tolerance for the size A (7):

$$55 - 0.06 = 54.94\ mm \quad (7)$$

Calculation of the lower tolerances for the size A (8):

$$55 - 0.075 = 54.925\ mm \quad (8)$$

Comparison of the average size with the upper and lower tolerance at normal temperature (9):

$$54.925 < 54.935 < 54.94 \rightarrow OK \quad (9)$$

Comparison of the average size with the upper and lower tolerance at simulated warming (10):

$$54.925 < 54.938 < 54.94 \rightarrow OK \quad (10)$$

Comparison of the average size with the upper and lower tolerance at simulated cooling (11):

$$54.925 < 54.928 < 54.94 \rightarrow OK \quad (11)$$

Findings, whether the dimensions meet the prescribed tolerances or not are shown in *Table* 1.

CONCLUSIONS

An observance of the regular controls of engine part dimensions is very important part of the combustion engine maintenance. It is necessary for ensure the smallest possible number of failures. During the measurement and control, the surrounding environment including the temperature affects the components. Temperature can affect dimensional changes to the point where the components stop to meet the required function and may jeopardize the operation of the combustion engine.

By the measurements, we found out that the components meet the prescribed tolerances at changed temperatures as well. A dimension change at a low temperature range does not have a significant influence on resizing and does not affect the functionality of the oil pump as a whole.

REFERENCES

[1] Tichá, Š.: *Strojírenská metrologie.* Ostrava. 2004. 110 p. ISBN 978-80-248-0671-6.
[2] Martínez, I.: *Thermal effects on Materials.* 2016. [online]. [cit. 25. 9. 2016]. Availability on the Internet: http://webserver.dmt.upm.es/~isidoro/ot1/Thermal%20effects%20on%20materials.pdf
[3] Švestka, D.: *Atlas lokomotiv: Spalovací motory, přenosy výkonu* [online]. [cit. 26. 9. 2016]. Availability on the Internet:<http://www.atlaslokomotiv.net/page-motory.html>.
[4] Mikleš, M.: *Metrológia.* Zvolen. 1996. 196 p. ISBN 80-228-0496-7.
[5] Oslanec, P.: *Teplotná rozťažnosť materiálov.* 2008. [online]. [cit. 26. 9. 2016]. Availability on the Internet: <http://www.materialing.com/teplotna_roztaznost_materialov>.
[6] Labuda, J.: *Metrológia a skúšobníctvo.* 2014. [online]. [cit. 27. 9. 2016]. Availability on the Internet: <https://www.sutn.sk/files/Spravy/Metrologia/Prispevky_Metrologia_1_2014_web.pdf>.
[7] Ťavodová, M.: *Kalibrácia meradiel ako nástroj zabezpečovania kvality. In Acta facultatis technicae.* ISSN 1336-4472. 13th year, 1. n. (2009), p. 113-123.
[8] Ľuptáčiková, V.: *Vplyv teploty okolia na rozmerovú kontrolu dielov pri opravách spaľovacích motorov.* Diploma thesis, Zvolen. 2016. 55 p.

INTERNATIONAL SCIENTIFIC CONFERENCE ON ADVANCES IN MECHANICAL ENGINEERING
13-15 October 2016, Debrecen, Hungary

TIG WELDING OF ADVANCED HIGH STRENGTH STEEL SHEETS

[1]MÁJLINGER Kornél PhD, [2]BORÓK Alexandra, [3]PASQUALE Russo Spena PhD, [4]VARBAI Balázs

[1]Institute: BME Department of Materials Science and Engineering
E-mail: welding@att.bme.hu , [*]corresponding author
[2]Institute: BME Department of Materials Science and Engineering
E-mail: borokalek@gmail.com
[3]Institute Free University of Bozen-Bolzano, Faculty of Science and Technology
E-mail: pasquale.russospena@unibz.it
[4]Institute: BME Department of Materials Science and Engineering
E-mail: varbai@eik.bme.hu

Abstract
To reduce self-weight, car manufacturers and machine part producers tend to parts made of high strength steels and advanced high strength steels. The load bearing capacity of these components depends largely on the quality of the welds, therefore the joining of such high strength steels sheets by automatized tungsten inert gas (TIG) welding without filler metal was investigated. The selected steel grades were transformation induced plasticity (TRIP) steel (with 1000 MPa ultimate tensile strength) and twinning induced plasticity (TWIP) steel (with 800 MPa ultimate tensile strength). The weldability of both steel grades without filler metal and without pre heating and post weld heat treatment was investigated also in dissimilar joints. The visual and metallographic examinations, hardness measurements and tensile testing showed that the usability of this welding process to weld good TWIP-TWIP joints is good, to TRIP-TRIP joints is limited and to TRIP-TWIP joints is poor.

Keywords: *Advanced high strength steel, Transformation induced plasticity steel, Twinning induced plasticity steel, Tungsten inert gas welding, Quantitative metallography.*

1. INTRODUCTION

To decrease self-weight of steel structures and machine parts manufacturer tends to use steel grades with higher and higher strength. Although structural steels can have very high ultimate tensile strength (S700, S960...S1300QL [1]) their welding is difficult, and the formability and fatigue properties of the joints are not very high [2-5]. At applications where safety and toughness is especially important -like in car bodies- other types of high strength steels (HSS) or advanced high strength steels (AHSS); like dual phase, transformation induced plasticity (TRIP) and twinning induced plasticity (TWIP) steel grades are used [6, 7].
The TRIP and TWIP AHSS grades have large plasticity which makes them ideal for the production of difficult car body parts and they have also very good tensile properties to increase passenger safety and to decrease the weight of the vehicle. However the welding of these steel grades has challenges because of the high alloying element content and small grain size and in case of TRIP steel the four-phasic microstructure[8]. So far gas metal arc welding (GMAW) [9] also with flux cored wire [10] resistance spot welding [11-13] and laser beam welding [14-18]of these AHSS sheets have been studied. But studies about the tungsten inert gas welding (TIG) or gas tungsten arc (GTA) welding of AHSS steels is rear and their mostly about low alloy HSSs [19]. Therefore in our current study we intend to determine the weldability of high alloy TRIP and TWIP steels.

2. MATERIALS AND METHODS

To investigate the possibility of robotized TIG welding neither filler metal (142 process) nor preheating or post weld heat treatment was used during the tests.
The AHSS types investigated in this study were one TRIP steel and one TWIP steel. The steel grades were: Zn-coated HCT800T (1.0948) steel, commercial name TRIP 800 and 22Mn0.6C steel, commercial name TWIP 1000 with the nominal 800 MPa and 1000 MPa ultimate tensile strength (UTS) respectively. The chemical composition and main properties of the used AHSSs are listed in *Table 1*. The TWIP steel had fully austenitic microstructure, the trip steel contained 60.2% ferrite, 25.4% bainite, 2.4% martensite and 12.2% austenite. The microstructure of the used base AHSSs are shown in *Figure 1*.

Table 1 Chemical composition and main properties of the used materials

Materials	Chemical composition [wt. %]							Sheet thickness [mm]	Tensile properties				grain size, d [µm]
	C	Mn	Si	Al	Ni	Cr	Fe		UTS [MPa]	YS [MPa]	$A_{11.3}$ [%]	Z [%]	
TRIP 800	0.27	2.1	1.52	0.25	-	-	bal.	1.5 ± 0.05	795±6	490±14	21±1	9±1.5	2.6
TWIP 1000	0.51	15.0	0.46	1.00	-	13.0	bal.	1.0 ± 0.05	1030±12	540±15	52±2	8.5±1	4.9

For the welding tests 100×50 mm pieces were cut mechanically from the sheets without edge chamfering. The AHSS sheets were cleaned before the welding with acetone. The sheets were mechanically clamped and butt welded perpendicular to the roll direction to 100×100 mm specimens. For the welding tests a REHM Invertig.Pro® digital 350 AC/DC welding machine automated with a Yamaha F1405-500 type linear drive was used. The welding torch was perpendicular to the sheets the working distance to the thicker sheet was 4 mm. The tungsten electode was Ø 2.4 mm, WT20 type (~2% ThO_2) with 30º bevel-angle. As shielding gas 99.996 % argon was used both face and root side. During the welding process the sheets were not in direct contact to each other, at the end of the sheets 1 mm gap was left to provide co-axial joints and the sheets were mechanical clamped during welding. The height step (in case of the TWIP-TRIP joint) was on the torch side. The polarity for the welding tests was DC+. Preliminary welding tests were made with different parameters, than visually examined. During parameter optimization the specimens were evaluated on the basis of the macroscopic joint appearance, full weld penetration and absence of visible weld defects (cracks, burn through etc.). The welding parameters which were evaluated to be the best according to the visual examinations are listed in *Table 2*.

Table 2 The TIG welding parameters for the AHSSs

Joint type		Current [A]	$V_{welding}$ [cm·min^{-1}]	Ar_{face} [l·min^{-1}]	Ar_{root} [l·min^{-1}]
TRIP	**TRIP**	35	8	12	8
TRIP	**TWIP**	39	8	12	8
TWIP	**TWIP**	39	8	16	8

The specimens for microscopic examination were mechanically cut in cross sections, mounted in metallography resign and mechanically grinded on SiC papers P80, P120, P320, P600, P1200, and P2500 with continuous water rinsing. Finally the specimen were polished with 1 µm and 0.5 µm particle size Al_2O_3 suspension. After etching the specimens were investigated with Olympus PMG3 optical microscope. Tensile tests were made with MTS 810 universal materials testing machine. To

prepare the tensile specimen the sheets were grinded to achieve even sheet thickness and cross section area. Hardness measurements were made with Buehler 1010 Vickers hardness tester on specimens prepared for metallographic investigations. Nickel and chromium equivalents ($Ni_{eq.}$, $Cr_{eq.}$) were determined according to *Equation 1 and 2.*

$$Ni_{eq.}=\%Ni + 30\times\%C + 0.5\times\%Mn + 30\times\%N \quad (1)$$

$$Cr_{eq.}=\%Cr + 1.4\times\%Mo + 1.5\times\%Si + 0.5\times Nb + 2\times\%Ti \quad (2)$$

The $Ni_{eq.}$ and $Cr_{eq.}$ values and the predicted phases after welding according to Schäeffler diagram – presuming 50-50% intermixture of the two sheet parts in the weld pool – are listed in *Table 3*.

Table 3 The $Ni_{eq.}$ and $Cr_{eq.}$ values and the predicted phases of the weldments

Joint type	$Cr_{eq.}$	$Ni_{eq.}$	predicted microstructure
TRIP TRIP	0,69	9,15	austenite+martensite
TRIP TWIP	7,19	15,98	martensite
TWIP TWIP	13,69	22,80	austenite

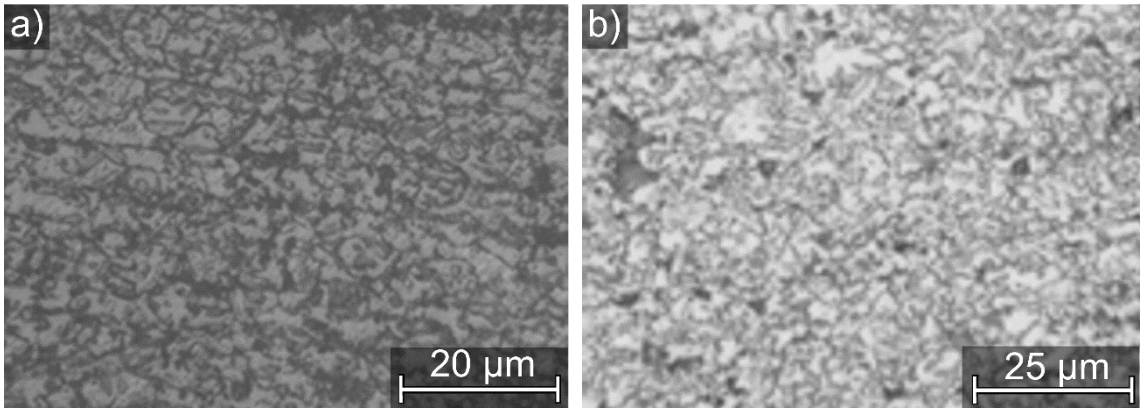

Figure 1 Light microscope micrographs of the: a) TRIP 800 and b) TWIP 1000 AHSSs

3. RESULTS AND DISCUSSION

The visually best looking joints of each type (welded according the parameters of *Table 2*) are shown in *Figure 2*. No visible weld defects could be detected, therefore these joints were investigated further in details. The microhardness profiles and the corresponding micrograps of the selected joints are shown in *Figure 3* and the results of the tensile tests are listed in *Table 4*.

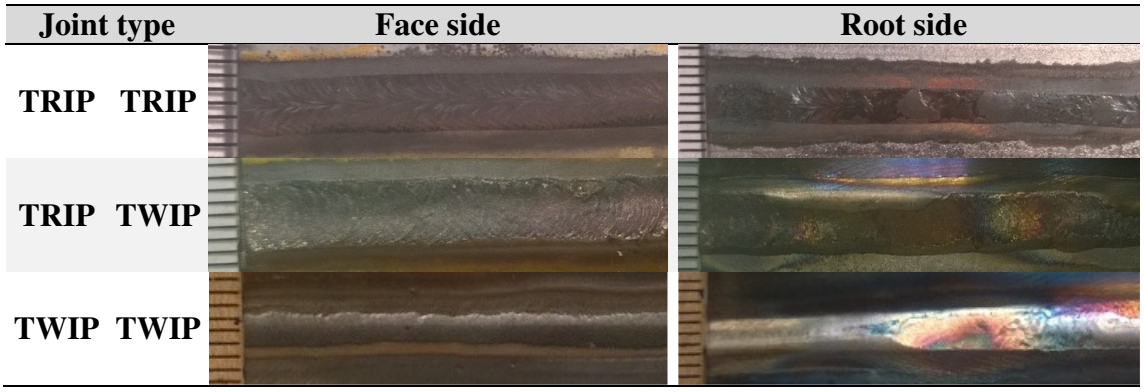

Figure 2 Macroimages of the weld beads

In case of the TRIP-TRIP joints the weld metal in the fusion zone had fine martensitic microstructure (as expected from Table 3) with considerable hardness of ~500 HV01. The heat affected zone (HAZ) had coarser grain structure with martensite and retained austenite. The tensile properties of the joints showed decreased UTS~760 MPa (due to coarse grain structure in the HAZ) with ~8% fracture elongation which is lower than the base material but for most engineering applications it could be acceptable. Note that at lower root side shielding gas flow rates $< 7\ l \cdot s^{-1}$ a slight discoloration alongside the weld occurred originating from the Zn-coating of the sheets and at too high flow rates $> 9\ l \cdot s^{-1}$ the melt-through was not sufficient. Altogether it is possible to automatize the welding of TRIP to TRIP steel sheets for mass production.

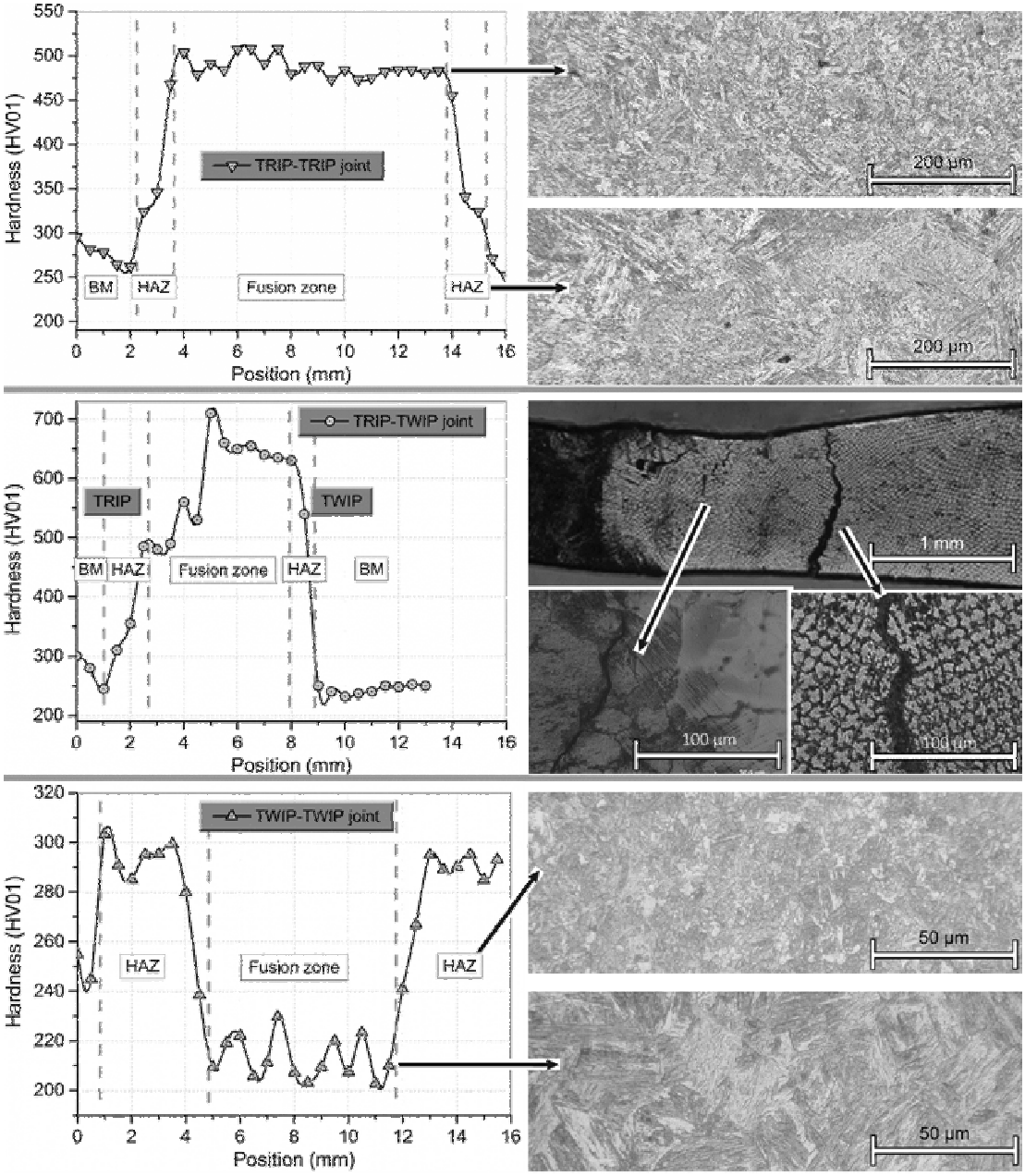

Figure 3 The hardness profiles of the welded joints and the corresponding optical microscope micrographs of the different zones

In case of the TRIP-TWIP weld metal, coarse dendritic microstructure was found and although they appeared visually good there were intergranular cracks in the weldment indicating cracking while solidification. The hardness profile showed excessive increase in hardness up to 700 HV01 in the weld metal. Tensile specimens cold not been made from the joints, because they broke brittle during machining. As a conclusion it is not recommended to weld this combination of AHSSs without any filler metal or special heat treatment considerations.
In case of the TWIP-TWIP joint the fusion zone contained some bainite and had a lower hardness values (~ 210 HV) than the base material. The HAZ had finer grains also with some bainite and had higher hardness values (~290 HV) than the base material. The tensile tests showed about 950 MPa UTS with considerable (~22 %) fracture elongation (about 43% of the base material), and ductile fracture. Therefore the weld can be qualified as a good joint and it is most suitable for robotized TIG applications.

Table 4 The Tensile properties of the TIG welded specimens for the AHSSs

Joint type		**UTS [MPa]**	**$A_{11.3}$ [%]**
TRIP	TRIP	762± 20	8.16±1.37
TRIP	TWIP	-	-
TWIP	TWIP	949±105	21.59±6.31

CONCLUSIONS

In our research the applicability of TIG welding without filler material (142 welding process) without excess preheating or post weld heat treatment to join TRIP 800 and TWIP 1000 thin AHSS sheets was investigated for the purpose of future robotization for mass production (for e.g. car body parts welding). From the above mentioned investigations the following conclusions can be drawn:

- TRIP-TRIP joints can be made with adequate quality but the welding process is sensitive to the shielding gas flow rate.
- To weld TRIP-TWIP joints 142 process is not recommended, to achieve crack free joints special heat treatment sequence needs to be developed, but it will be most likely not economic for mass production
- TWIP-TWIP welds had the best mechanical and ductile properties, it is the easiest to make therefore recommended for automation.

ACKNOWLEDGEMENTS

This paper was supported by the János Bolyai Research Scholarship of the Hungarian Academy of Sciences grant number: BO/00294/14 and by The Hungarian Research Fund, NKTH-OTKA PD 120865 (K. Májlinger). The authors are grateful for the financial support of the Free University of Bozen-Bolzano (P. Russo Spena), grant number: TN2001. Moreover, special thanks go to Enikő Réka FÁBIÁN for her help with the metallographic sample preparation.

REFERENCES

[1] SSAB *Strenx 1300 The ultra-high-strength steel at 1300 MPa.* Available from: http://www.ssab.com/products/brands/strenx/products/strenx-1300. – 2016.09.01.
[2] Gáspár, M., A. Balogh, Dobosy, Á.: *Effect of postweld heat treatment on HAZ toughness of Q+T high strength steels*, in XXX. microCAD International Multidisciplinary Scientific Conference, University of Miskolc: Miskolc, Hungary.

[3] Zhang, Z., Skallerud, B., Thaulow, C., Ostby, E., He, J., Berg, J., Stranghoener, N.: *20th European Conference on Fracture Fatigue Strength of Welded Ultra High Strength Steels Improved by High Frequency Hammer Peening.* Procedia Materials Science, 3, 71-76., 2014.
[4] Gáspár, M., Lukács, J.: *Fatigue crack growth resistance of S960QL high strength steel and its GMAW welded joints.* Production Processes and Systems, 7(1), 41-52., 2014.
[5] Lukács, J., Kuzsella, l., Koncsik, Zs., Gáspár, M., Meilinger, Á.: *Role of the physical simulation for the estimation of the weldability of high strength steels and aluminum alloys*. Materials Science Forum, 149-154., 2015.
[6] *AHSS Application Guidelines*. Available from: http://www.worldautosteel.org/projects/advanced-high-strength-steel-application-guidelines/. – 2016.09.01.
[7] *Evolving Use of Advanced High-Strength Steels for Automotive Applications*. Available from: http://www.autosteel.org/global/document-types/news/2012/auto---gdis-ahss-101-release.aspx?siteLocation=5e03a9ae-8b3f-4f35-a746-995afbf525e2. – 2016.09.01.
[8] Shome, M., Tumuluru, M.: *1 - Introduction to welding and joining of advanced high-strength steels (AHSS)*, in Welding and Joining of Advanced High Strength Steels (AHSS). Woodhead Publishing. 1-8., 2015.
[9] Májlinger, K., Kalácska, E., Russo Spena, P.: *Gas metal arc welding of dissimilar AHSS sheets*. Materials & Design, 109, 615-621., 2016.
[10] Gáspár, M., Balogh, A.: *Efficient Increase of the Productivity of GMA Welding of AHSS Using Flux Cored Wire, in Design, Fabrication and Economy of Metal Structures*: International Conference Proceedings 2013, Miskolc, Hungary, April 24-26, 2013, K. Jármai and J. Farkas, Editors. Springer Berlin Heidelberg: Berlin, Heidelberg. 463-468. 2013.
[11] Kong, J.P., Han, T.K., Chin, K.G., Park, B.G. Kang, C.Y.: *Effect of boron content and welding current on the mechanical properties of electrical resistance spot welds in complex-phase steels*. Materials & Design 54, 598-609., 2014.
[12] Hayat, F.: *Comparing Properties of Adhesive Bonding, Resistance Spot Welding, and Adhesive Weld Bonding of Coated and Uncoated DP 600 Steel*. Journal of Iron and Steel Research International. 18(9), 70-78., 2011.
[13] Russo Spena, P., De Maddis, M., Lombardi, F., Rossini, M.: *Investigation on Resistance Spot Welding of TWIP Steel Sheets*. steel research international, 86(12), 1480-1489., 2015.
[14] Bandyopadhyay, K., Panda, S.K., Saha, P., Baltazar-Hernandez, V.H., Zhou, Y.N.: *Microstructures and failure analyses of DP980 laser welded blanks in formability context.* Materials Science and Engineering: A, 652, 250-263., 2016.
[15] Spena, P.R., Rossini, M., Cortese, L., Matteis, P., Scavino, G., Firrao, D.: *Laser Welding between TWIP Steels and Automotive High-Strength Steels*, Characterization of Minerals, Metals, and Materials 2015, John Wiley & Sons, Inc.11-20., 2015.
[16] Spena, P.R., De Maddis, M., Lombardi, D'Aiuto, F.: *Resistance spot welding of advanced high strength TWIP steels.* Applied Mechanics and Materials. 876-880., 2013.
[17] Correard, G.C.C., Miranda, G.P., Lima, M.S.F.: *Development of laser beam welding of advanced high-strength steels*. International Journal of Advanced Manufacturing Technology, 83(9-12), 1967-1977., 2016.
[18] Farabi, N., Chen, D.L., Zhou, Y.: *Microstructure and mechanical properties of laser welded dissimilar DP600/DP980 dual-phase steel joints*. Journal of Alloys and Compounds, 509(3) 982-989., 2011.
[19] Joshi, J.R., Potta, M., Adepu, K., Gankidi, M. R., Katta, R. K.: *Influence of Welding Techniques on Heat Affected Zone Softening of Dissimilar Metal Maraging Steel and High Strength Low Alloy Steel Gas Tungsten Arc Weldments*. Transactions of the Indian Institute of Metals, 1-13., 2016.

THE VISUAL LANGUAGE OF A FORM

MARKOVA Kremena PhD

Technical University -Varna
E-mail: kremenacankova@abv.bg

Abstract
This article focuses mainly on the quality characteristics of the product's form – in consequence of the applied forming methods. These characteristics are obtained by applied concepts, forming methods and standards and their expression can be designated as "visual language".
In this case the marketing and advertisement methods do not apply.

Keywords: *form, product, visual*

1. INTRODUCTION

The main part of the information that one receives is perceived by the human eye (about 75%). That makes the visual observation so important that it could not lead to the wanted result if the wrong message is encoded in the forming process. The language that is used by the product's form can be reviewed as a system of characteristics, indications and limits, that implement the non-verbal contact between the item and the consumer.
Indications – signs – titles, logos that render the working behavior, usage safety and storing requirements.
Limits – linked to the material and the quality of the material, the item's behavior when it's on and its functions.

2. METHODS AND RESULTS

2.1. Purpose of informational expression

Possessions are produced to be used. That is why their functional designation is so important. The **tradition** in operating products from the same of similar nature acts as **memory**, nothing more – one is supposed to count on it. Even if during the implementation of the formal (from "form") and technological evolution the adaptation of the basic configuration and function of a product stay unaffected, the memory of the traditional usage would be reason enough for the product to be used as it supposed to. But if it's input an innovative alteration in its functioning, then the traditionally used informational expression would be not only insufficient, but also inappropriate.
Objects rely on another type of informational expression – mystery, objects, sphinxes. Their function is conveyed within the traditional activities, but the approach in their forming, and respectively in their application, lay an untraditional and abnormal contact and exploitation, that cannot be realized in an average case without the instructions. This type of products/appliances could exist by several reasons – functional perfection, resources savings or generating of benefits, following a certain trend, concept, provocation etc.

Figure 1

Figure 1 From left to right
Evolution of the telephone's shape, where both appliances are separated by almost a 100 years. The innovative change in the function of mobile phones leads to a new form and type of informational expression;
Philippe Starck - **Hot Bertaa Ketle** - Object – sphynx; Abstract shape, doesn't relate to the traditional shape of the teapot. Even after knowing its designation, the consumer still has questions about the elements of the form and their function – which one is the handle and which one is the spout, where do you pour the water from and whether the handle gets hot enough to burn one's hand and so on;
GruppoStrum - **Torneraj** - The established look of a concrete piece, covered in tiles deceivingly covers the soft and elastic nature of the armchair made of cotton; this purposeful confrontation between seen and tangible defines the dynamic in provocation in visual and notional;

2.2. Simplicity as a factor

The simplicity of a visual stimulus has its adequate impact on the opportunity of it being recognized and compared with known samples, its classification and retention. The simple form, close to the basic geometric shapes is easily recognizes by the human eye and its permanently memorized, because of the comparison with basic thought models. This specification of the human visual perceptions is the reason why the simplicity of the form is one of the most searched for qualities in designing the elements of our artificial environment.
Dimensions – proximity to the basic geometric models; few forming elements; relation to the "clarity" quality; modularity

Figure 2

Figure 2 From left to right:
Dieter Rams - **606 Universal Shelving System** - Underlined geometric model of every element in the module system;
Le Corbusier, Jeanneret, Perriand **- Grand Confort Armchair -** The chair's simplified cubic structure helps its shape to be easily perceived, easily distinguished among other similar items – a condition for a permanent memorization;
Mies van der Rohe - **Weissenhof B42 Chair** - Small number of forming elements – a condition to achieve simplicity;
Gerrit Ritveld - **Zig Zag Chair** - Geometric expression, small number of the shape's elements; the name of the chair doubles the input in the visual dynamic meaning.

Rodolfo Bonetto - **Quatro Qarti** - Geometric system of a module type; there is no doubt about its purpose;

2.3. Static/dynamic

The idea of static and dynamic is inevitably set in every form, because of its tectonics, construction, material, function, appurtenance of style, comparison with certain behavior/qualities/natural phenomena/mature cultural models, a certain trend.
Straightforwardness in the ration "visible-suspected-proven", i.e. when there's no mistake in the visual evaluation of a type, suspected behavior and function of the product. (Rams, Hadid)
Intentional deception – of the senses, of the meaning – postmodern, playful situation, desire for financial profit.
Deception because of novelty/innovation – the senses cannot compare with known samples/phenomena.

Figure 3

Figure 3 From left to right:
Dieter Rams, Hans Gugelot - **Radio-Phonograph SK 4 -** There is no mistake in the visual evaluation about the type, set designation and function of the product;
Zaha Hadid - **Liquid Glacial Table -** Purposefully set deception of the senses, static object that provokes a feeling of movement in the form itself;
Memphis Gruppe - **Tawaraya** - Meaningful dynamic – conflict between visible and notional – a couch that look like a boxing ring;
Gaetano Pesce - **Golgotha Chair -** Meaningful dynamic, purposefully set deception of the senses;
Buckminster Fuller - **Geodesic Dome -** Innovation, the informational expression is unclear, because the is an opportunity to compare with other samples missing;

2.4. Contrast

In the process of designing the elements of the material setting contrast can be view both as a method and as a quality. The method suggests building and adding of a system of actions, which will lead to certain characteristics of the shape and function of the products. Contrast as a quality is the availability of the desired characteristics in the products in precise formal (from "form") dimensions, evoking respective sensory and thought reactions.
This is why the visual evaluation is so important.
Material contrast. Organic/synthetic – This is the most obvious type of contrast. The human, as a being, has a natural visual filter towards different materials and natural preference towards these that are organic in their origin. The differences in materiality are momentarily observed, but also carry thoughtful evaluation of what has been seen, including senses, based on past experiences. Past experiences have defining importance in observation, because they include the necessity of definitive proof of quality characteristics such as hard, soft, liquid, cold, smooth, red etc.

Semantic contrast – Semantic or meaningful contrast is based on the difference between observation and what is already known by past experiences. "The deception" of the visual senses is usually linked to the conceptual and innovative ideas by designers, whose purpose is to prove a certain thesis. Often used method is the quote, which aims to compare, to dethrones, ridicule and so on cultural phenomena, perceived as mature cultural models or classic in design. There could be a demand of meaning in the paradoxical ideas.
Plastic contrast – This type of contrast is related to the plastic state of the shapes, the applied methods of forming, the processing of the surface and texture. In this case, of course, the essence of the input materials, their properties and qualities could also be defining.
Scaling contrast – It signifies the ratio between the size of the different elements in the product. The small elements are usually present in repeatedly larger number than the bigger ones.

Figure 4

Figure 4 From left to right:
Oil Monkey - **Plastic Wood Chair** - The contrast between organic (a tree) and synthetic (an acrylic glass) is fortified by the contrast in the qualities of the used materials – transparent/non-transparent. The contrast is input in the spatial orientation of the different elements of the materials – all acrylic glass elements are mutually parallel and perpendicular to the wood material;
Stiletto Studio (Frank Schreiner) - **Comsumer's Lounge Rest Chair -** The trolley in the supermarket is transformed into a means of rest and relaxation (semantic contrast);
Greg Klassen - **River Table** - Plastic contrast, set in the forming process – geometric model of the whole and its pieces; only the glass gets a "natural" shape, that defines the "organic" curves of the tree in the places where it meets the glass.
Jurgen Bey - **Tree Trunck Bench** - The contrast is put on a lot of levels – semantical, moral, material, plastic. The last one is in consequence of the visual confrontation of the natural surface of the log's crust and the stuck in it polished brass chair backrests.
Emile Jacques Ruhlman - **Cabinet -** Classic art deco chef-de-oeuvre; inlaid bone and metal elements, which decorate the furniture's look have a strong contrast in size and number of elements of the construction – ratio contrast.

CONCLUSIONS

The language of the forms helps us to make a satisfactory contact with our possessions. The well achieved and inventive shape relies on the intellect of its user, it doesn't ignore their intelligence. On the other hand, if the consumer is "taught" through the design of the products that can help balance the relation between the person and items that one uses.

References

[1] Маркова, К., Доврамаджиев , Т.: *THE VISUAL DYNAMIC OF THE PRODUCT'S SHAPE. IS IT FUNCTIONAL, STRUCTURAL, LOGICAL OR JUST A TREND?* XIII International Scientific Congress Machines. Technologies. Materials. 2016 SUMMER SESSION 14–

17.09.2016 VARNA, BULGARIA VOLUME III SECTION "MACHINES" SECTION "INDUSTRIAL DESIGN ENGINEERING & ERGONOMICS 2016" ISSN 1310-3946, 46-48., 2016.

[2] *Better Buy Design - 606 Universal Shelving System//* uk.staging.phaidon.com , 24.01,2012 <http://uk.staging.phaidon.com/agenda/design/articles/2012/january/24/better-buy-design-606-universal-shelving-system/>(11.10.2016).

[3] *Bukminster Fuller's Home in a Dome//* sometimes-interesting.com, 18.06.2015 <http://sometimes-interesting.com/2015/06/18/buckminster-fullers-home-in-a-dome/>(11.10.2016).

[4] *ETTORE SOTTSASS: MEMPHIS RETROSPECTIVE EXHIBITION//* designboom.com, 06.08,2009< http://www.designboom.com/design/ettore-sottsass-memphis-retrospective-exhibition/> (11.10.2016).

[5] *GERRIT RIETVELD// http://*deconlinemadrid.blogspot.bg, 4.09.2012 < http://deconlinemadrid.blogspot.bg/> (11.10.2016).

[6] Ker, A.: *The Design Legacy Of Dieter Rams//*ignant.de, 20.05,2016 <http://www.ignant.de/2016/05/20/the-design-legacy-of-dieter-rams/> (11.10.2016).

[7] *Le Corbusier// iconicinteriors.com < https://iconicinteriors.com/about_us/meet_the_designers/le_corbusier/>*(11.10.2016).

[8] *LIQUID GLACIAL TABLE BY ZAHA HADID//* designboom.com, 16.01.2013 < http://www.designboom.com/design/zaha-hadid-liquid-glacial-table/> (11.10.2016).

[9] Nazarali, R.:*Oil Monkey's Curene Seating Design Combines Plastic & Wood* // trendhunter.com, 20.05.2009 < http://www.trendhunter.com/trends/oil-monkey-plastic-wood-chair > (30.09.2016).

[10] Make sure your home phone service can reach 911// consumerreports.org, 03.09.2013< http://www.consumerreports.org/cro/news/2013/09/make-sure-your-home-phone-service-can-reach-911/index.htm> (11.10.2016).

[11] Pesce, Gaetano (1939)// theredlist.com <http://theredlist.com/wiki-2-18-393-1391-view-memphis-design-profile-pesce-gaetano-3.html>(11.10.2016).

[12] Rotary Dial Telephones // anteeart.com.cn < http://www.anteeart.com.cn/productgrouplist-221956471/Rotary_Dial_Telephones.html> (11.10.2016).

[13] Special guest: Jurgen Bey// lodzdesign.com < http://2014.lodzdesign.com/en/special-guest-jurgen-bey/> (30.09.2016).

[14] Weissenhof B42 Chair - design Mies Van Der Rohe - Tecta//https:// classicdesign.it <classicdesign.it/B42-tecta-en-1955.html>(11.10.2016).

[15] http://findicons.com/search/iphoneFuller's Home in a Dome

INTERNATIONAL SCIENTIFIC CONFERENCE ON ADVANCES IN MECHANICAL ENGINEERING
13-15 October 2016, Debrecen, Hungary

A POSSIBLE MODELING OF THE CONSTRUCTIVE CUTTING GEOMETRY OF THE GEAR HOBS

MÁTÉ Márton PhD

Sapientia Hungarian University of Transylvania
E-mail: mmate@ms.sapientia.ro

Abstract
Gear-hobs are the most often used cutting tools in cylindrical gear manufacturing processes due to their productivity and precision. The relative motion of the cutting edge to the workpiece is a high complexity spatial motion. As a consequence, precise computing of the cutting geometry requires an adequate mathematical model. The computing of the geometry is based on a vectorial geometrical model, where the rake and relief angle values are obtained using the normal vectors of the rake and relief faces in the considered edgepoint as well as the vector base of the constructive and effective frames. The investigation of the model leads to conclusions regarding the change of the geometry depending on the position of the edge point of the cutting edge, and the position of the cutting edge related to the machined gear. The conclusion that succeeds from the application of the model is that in case of classical gear hobbing process the effective geometry changes insignificantly in comparison with the values computed using classical methods. It is also to mention that in case of diagonal hobbing the model can be useful for avoiding the presence of zero relief angle on the edge.

Keywords: *gear-hob, cutting geometry, rake-angle, relief-angle.*

1. INTRODUCTION

Gear hob is without any doubt the most productive cylindrical gear cutting tool. There exist a lot of valorous works focused on the mathematical deduction of the cutting edge delimiting surfaces [1, 4, 5, 6, 7], on the exact calculus of relief angles [3], studies regarding the grinding of the side relief faces and re-sharpening [6,7] of the hob. Here is an excellent opportunity to mention the valorous results of the gear theory schools from the University of Miskolc, The Polytechnic Institute of Cluj-Napoca.
In the following it will be considered that the provenience surface of the gear hob is an involute worm. The edges will result as the intersection between the involute worm surfaces and the helical rake face. Rake face is a straight line generated helical surface whose generatrix crosses the axis of worm helices. The edge equations related to a frame whose *z0* axis overlaps the axis of the worm surfaces and x_0 axis crosses the top edge in its midpoint are as follows,

$$\begin{aligned} x_0(\varphi_1;j) &= R_b(\cos B(\varphi_1)+\varphi_1 \sin B(\varphi_1)) \\ y_0(\varphi_1;j) &= j\,R_b(\sin B(\varphi_1)-\varphi_1 \cos B(\varphi_1)) \\ z_0(\varphi_1;j) &= \frac{p_C p_{ax}}{2\pi(p_c+p_{ax})}(\zeta+\operatorname{arctg}\varphi_1-\varphi_1)\,,\; B(\varphi_1;j)=\frac{p_{ax}}{p_c+p_{ax}}(\varphi_1-\zeta)+\frac{p_C}{p_c+p_{ax}}\operatorname{arctg}\varphi_1 \end{aligned} \quad (1)$$

where parameter *j* hits -1 for the left and +1 for the right sided edge.

Relief faces are obtained through helical relieving. Here is considered that the relief faces are described by the corresponding cutting edges through their motion over a conical helix leading curve.

2. THE VECTORIAL MODEL OF THE CONSTRUCTIVE GEOMETRY

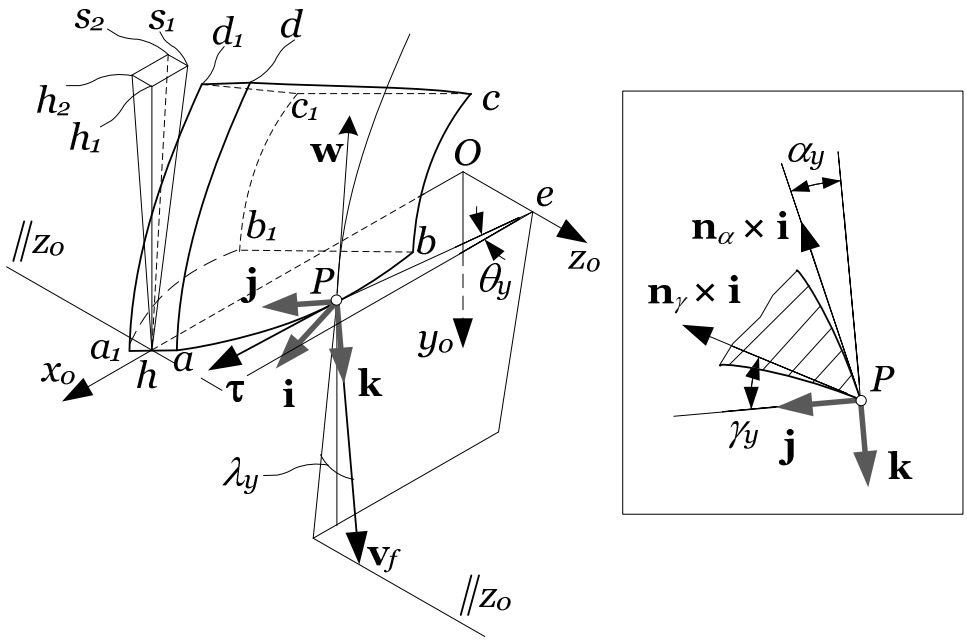

Figure 1 The vectors used in the constructive geometry model

The vectors used for the computing of the constructive geometry are presented in figure 1. The calculus is focused on the arbitrary *P* point situated on the right edge (j=+1 in equations (1)). Let **k** the unit vector of the main cutting velocity vector $\mathbf{v}_f$. The basic plane is passing through *P* and its normal unit vector is **k**. Let $\boldsymbol{\tau}$ the tangent of the edge in *P*. Thus, **k** and $\boldsymbol{\tau}$ define the tangential plane of the cutting edge, whose normal unit vector is **j**. Evidently it can be written through the cross product $(\mathbf{k}\times\boldsymbol{\tau})/|\mathbf{k}\times\boldsymbol{\tau}|$. The constructive frame's third normal unit vector, **i** is the normal vector of the measuring orthogonal plane where rake and relief angles are defined. The frame on the right side of figure 1 shows the orthogonal section and the vectors involved in the definition of the rake and relief angles. The tangent vector to the intersection curve between the rake face and the orthogonal plane is defined as the cross product of the normal of the intersecting surfaces, thus result $\mathbf{n}_\gamma\times\mathbf{i}$. Similarly is written the tangent vector of the print of the relief face in the orthogonal plane as $\mathbf{n}_\alpha\times\mathbf{i}$.

The calculus is started with the localization of the constructive frame in point *P*. Therefore is necessary to compute the components of the tangent vector by deriving position parametric functions (1) in dependence to φ_1. It is to remark that $\boldsymbol{\tau}$ must be oriented like in figure1, thus its *x* component must be positive.

$$\underline{\boldsymbol{\tau}}^{(T)} = \operatorname{sgn}(\dot{x}_0)(\dot{x}_0\ \dot{y}_0\ \dot{z}_0) \tag{2}$$

The rake and relief face normal vectors and the main cutting velocity vector can be written using the geometric dependences shown in figure 2.

First it is necessary to compute the angle θ_y defined by plane $(x_0 z_0)$ and the plane passing by *P* and axis Oz_0:

$$\theta_y = \arctan \frac{y_0^{(P)}}{x_0^{(P)}} \tag{3}$$

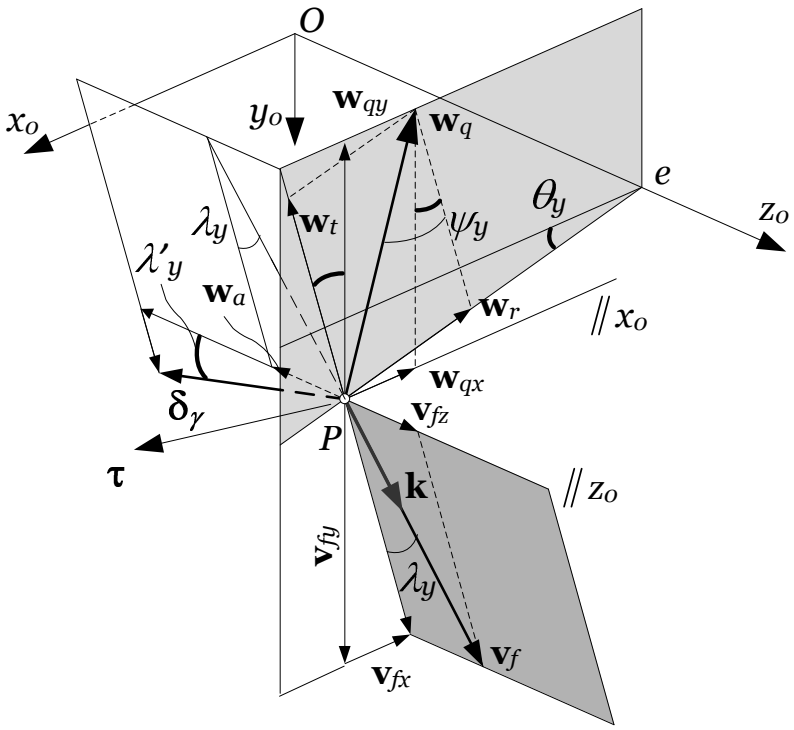

Figure 2 The computation of $\mathbf{v}_f$, $\mathbf{n}_\alpha$ and $\mathbf{n}_\gamma$

Figure 2 shows two components of the main cutting velocity vector: the radial component normal to the radius *eP* and the helical component $\mathbf{v}_{fz}$ parallel to the helix axis Oz_0. Considering the angular velocity of the hob $\omega = 1\text{s}^{-1}$, and the radial component decomposed in $\mathbf{v}_{fx} + \mathbf{v}_{fy}$ the main velocity vector can be written as follows:

$$\underline{\mathbf{v}}_f = \begin{pmatrix} -Pe\sin\theta_y \\ Pe\cos\theta_y \\ Pe\tan\lambda_y \end{pmatrix} = \begin{pmatrix} -\sqrt{\left(x_0^{(P)}\right)^2 + \left(y_0^{(P)}\right)^2}\sin\theta_y \\ \sqrt{\left(x_0^{(P)}\right)^2 + \left(y_0^{(P)}\right)^2}\cos\theta_y \\ R_0\tan\lambda_0 \end{pmatrix} = \begin{pmatrix} -y_0^{(P)} \\ x_0^{(P)} \\ R_0\tan\lambda_0 \end{pmatrix} \tag{4}$$

The normal vector $\mathbf{n}_\alpha$ of the relief face will be primed as the cross product of the edge tangent vector $\boldsymbol{\tau}$ and the tangent vector $\mathbf{w}$ to the conical helix trajectory of the relieving motion while relief surface was generated by the edge of a turning tool. On figure 2 three kinematic components of $\mathbf{w}$ are emphasized: the tangential component $\mathbf{w}_t$ that results from the rotation of the hob, the radial component $\mathbf{w}_r$ that results from the radial relieving penetrative motion and finally the axial component $\mathbf{w}_a$ that appears as a consequence of helical motion. It is also to remark that $\mathbf{w}_t + \mathbf{w}_r = \mathbf{w}_q$ –a component normal to the axis Oz_0. Considering the angular velocity of the hob in relieving equal to the unity the expressions of the components mentioned above can be primed as follows:

$$\begin{cases} w_t = \omega Pe = 1 \cdot \sqrt{\left(x_0^{(P)}\right)^2 + \left(y_0^{(P)}\right)^2} \\ w_r = \omega \dfrac{kz_m}{2\pi} = \dfrac{kz_m}{2\pi} \\ w_a = \omega \dfrac{p_{ax}}{2\pi} = \dfrac{p_{ax}}{2\pi} \\ w_q = \sqrt{w_t^2 + w_r^2} = \sqrt{\left(x_0^{(P)}\right)^2 + \left(y_0^{(P)}\right)^2 + \dfrac{kz_m}{2\pi}} \end{cases} \tag{5}$$

The angle ψ_y can be primed through the components w_t and w_r:

$$\psi_y = \arctan\frac{w_r}{w_t} \tag{6}$$

Using (5) and (6), the components of vector **w** hit the following form:

$$\underline{\mathbf{w}} = \begin{pmatrix} -w_q \sin\left(\psi_y - \theta_y\right) \\ -w_q \cos\left(\psi_y - \theta_y\right) \\ -w_a \end{pmatrix} \tag{7}$$

Using expressions (2) and (7), relief face normal vector will be primed as:

$$\mathbf{n}_\alpha = \boldsymbol{\tau} \times \mathbf{w} \tag{8}$$

The normal vector of the rake face is similarly primed using the edge tangent vector $\boldsymbol{\tau}$ and the tangent vector $\boldsymbol{\delta}_y$ of that rake helix line that passes through the considered point *P*. $\boldsymbol{\delta}_y$'s components can be deduced on figure 2:

$$\underline{\boldsymbol{\delta}}_y = \begin{pmatrix} -\sin\lambda_y \cos\theta_y \\ \sin\lambda_y \sin\theta_y \\ -\cos\theta_y \end{pmatrix}, \qquad \lambda_y = \arctan\frac{\sqrt{\left(x_0^{(P)}\right)^2 + \left(y_0^{(P)}\right)^2}}{R_0} \tan\lambda_0 \tag{9}$$

Using (2) and (9), rake face normal vector can be computed from the formula

$$\mathbf{n}_\gamma = \boldsymbol{\tau} \times \boldsymbol{\delta}_y \tag{10}$$

Finally, the expressions of the constructive rake and relief angles in the arbitrary edgepoint *P* are [2]:

$$\begin{aligned} \gamma_y &= \arcsin\frac{-\left(\mathbf{n}_\gamma \times \mathbf{i}\right) \cdot \mathbf{k}}{\left|\mathbf{n}_\gamma \times \mathbf{i}\right|} = \arcsin\frac{\mathbf{n}_\gamma \cdot \mathbf{j}}{\left|\mathbf{n}_\gamma \times \mathbf{i}\right|} \\ \alpha_y &= \arcsin\frac{\left(\mathbf{n}_\alpha \times \mathbf{i}\right) \cdot \mathbf{j}}{\left|\mathbf{n}_\alpha \times \mathbf{i}\right|} = \arcsin\frac{\mathbf{n}_\alpha \cdot \mathbf{k}}{\left|\mathbf{n}_\gamma \times \mathbf{i}\right|} \end{aligned} \tag{11}$$

3. NUMERICAL INVESTIGATION

The model presented above is applied to a hob having the following parameters: $m_n = 5\,\text{mm}$, $\lambda_0 = 2°30'$, $z_m = 12$, $\alpha_{0n} = 20°$, $\gamma_V = 0°$, $\alpha_V = 8°$, $k \approx 4.7\,\text{mm}$. The variation of the constructive geometry for the right edge is shown in figure 3.

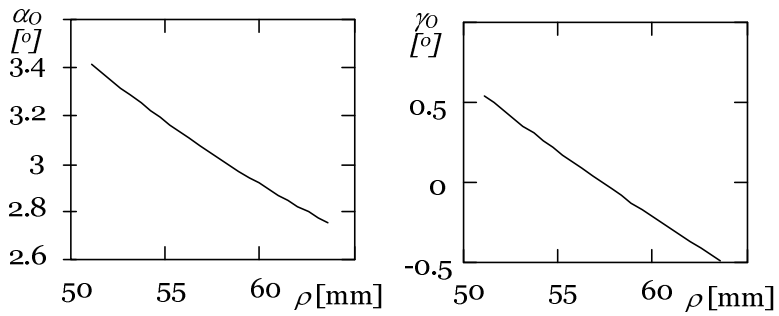

Figure 2 The variation of the constructive relief and rake angles in dependence with the distance ρ of the edgepoint to the axis of the hob

It is to observe that both angles present a light decreasing with the axis distance. Practically this variation is nonimportant. Interesting is the fact that rake angle becomes both positive and negative values. If edge positioning angle κ is considered equal to α_{0n}, the difference between relief angles computed with the classical formula $\tan\alpha_y = \tan\alpha_r \sin\kappa = \frac{kz_m}{2\pi r_y}\sin\alpha_{0n}$ [7] and the model based formula doesn't exceed 0.6 degrees.

In case of the rake face the same classical formula couldn't show the sign change of the rake angle. The effective cutting geometry presents a more complicated variation due especially to the position of the considered edgepoint in the intersection volume of the addendum cylinder of the machined gear and the hob. Main cutting velocity can be primed as the relative velocity of the considered edgepoint to the point coincident with it at the considered moment but relative to the workpiece [1]. Its expressions will be used instead those written in (4). After that, formulae (2-11) lead to the effective values of the rake and relief angle.

CONCLUSIONS

The computational model of the cutting geometry returns the exactly rake and relief angle values in conformity with their exact definition. The model is easily applicable to any relative motion between the hob and machined gear, including diagonal hobbing.

NOTATIONS

α_0 – gear generating rake profile angle;
λ_0 – hob helix angle on the pitch diameter;
λ_y – hob helix angle on arbitrary diameter;
α_V – top relief angle;
γ_V – top rake angle;
k – radial relieving parameter value;
m_n – normal module;
R_b – basic cylinder radius;
p_{ax} – helix pitch of the hob;
p_C – helix pitch of the rake face;
z_m – number of teeth of the hob;

k – basic plane's normal unit vector;
j – tangential plane's normal unit vector;
i – orthogonal plane's normal unit vector;
α_y – constructive relief angle in the arbitrary edgepoint;
γ_y – constructive rake angle in the arbitrary edgepoint;
τ – edge tangent vector in the arbitrary point;
$\mathbf{n}_\alpha$ – relief face normal vector in the arbitrary edgepoint;
$\mathbf{n}_\gamma$ – rake face normal vector in the arbitrary edgepoint;

REFERENCES

[1] Dudás, I. The Theory and Practice of Worm Gear Drives. ISBN9781857180275. Penton Press, 2000.
[2] Máté, M. Contribuții la optimizarea parametrilor constructivi-funcționali ai cuțitelor-roată cu dinți înclinați. *PhD Thesis.* „Transilvania" University of Brașov, Romania, 1999.
[3] Gyenge Csaba. Lefejtőmarók oldalhátszögeinek pontos meghatározása és optimálása. GÉP 48:(10) pp. 38-40. (1996)
[4] Gyenge Csaba Determinarea profilului sculelor abrazive la detalonarea radiala a frezelor-melc In: Buzatu Vasile, Ionescu Maria Antoinette (szerk.) Tehnologii Calitate Masini Materiale Vol.7. Bucuresti: Editura Tehnica, 1990. pp. 92-115. (ISBN:973-31-0240-7)
[5] Gyenge Csaba, Pacurar Ancuta, Olah László, Pacurar Razvan. New Manufacturing Technology for Variable Pitch and Variable Screw Profile Worms. In: Nicolae Balc (szerk.) Modern Technologies in Manufacturing. 394 p. Cluj-Napoca, România, 2015.10.14-2015.10.16. Zürich: Trans Tech Publications, 2015. pp. 48-53. (Applied Mechanics and Materials; Vol. 808.) (ISBN:978-3-03835-653-0).
[6] Gyenge Csaba, Mihai M, Ros O. Relativ sebesség és forgácskeresztmetszet meghatározása globoidkerekek fogazásánál. In: Lehoczky László, Kalmár László (szerk.) microCAD 2004 International Scientific Conference. Miskolc: Miskolci Egyetem Innovációs és Technológia Transzfer Centrum, 2004. pp. 73-76. (ISBN:963-661-608-6)
[7] Pálffy Károly, Prezenszky T, Csibi Vencel, Antal B, Gyenge Csaba, Balogh F. Fogazott alkatrészek tervezése, szerszámai és gyártása. Kolozsvár: Gloria Kiadó, 1999. 435 p. (ISBN:973-9203-46-9)

INTERNATIONAL SCIENTIFIC CONFERENCE ON ADVANCES IN MECHANICAL ENGINEERING
13-15 October 2016, Debrecen, Hungary

INVESTIGATION OF DEFLECTOR PLATES IN CASE OF GAS EXPLOSION

[1]MIKÁCZÓ Viktória, [2]SIMÉNFALVI Zoltán PhD, [3]SZEPESI L. Gábor PhD

[1]Institute of Energy Engineering and Chemical Machinery, University of Miskolc
E-mail: mikaczo.viktoria@uni-miskolc.hu
[2]Institute of Energy Engineering and Chemical Machinery, University of Miskolc; Head of Institute
E-mail: simenfalvi@uni-miskolc.hu
[3]Institute of Energy Engineering and Chemical Machinery, University of Miskolc
E-mail: szepesi@uni-miskolc.hu

Abstract
Dust and gas explosions occur in a wide range of industrial segments. Explosion vents can be installed into enclosure walls, and in case of explosion, they open in their full area, and let flames with other materials into the environment. For proper direction of these burnt and unburnt materials, deflector plates can be used. Deflector plates change direction of flow, besides stand against force and heat of outflow. During design process, dynamic forces should be taking care. This article investigates the effects of deflector plates distances between vent area and for reduced pressure based on experimental data. Static activation overpressure of explosion vent was previously measured, and determined of 0.475 bar_g. Numerous vented explosions of 5 vol. % propane-air mixture were conducted, using a 20-liter spherical explosion chamber. Distances between round vent area of 30 mm diameter and square deflector plate of 0.4 m, 0.45 m, 0.5 m and 0.7 m were selected.

Keywords: *gas explosion, deflector plate, dynamic force, venting, distance.*

1. INTRODUCTION

Disasters and accidents caused by dust or gas explosions occur from the beginning of industrial activity, and occur in a wide range of industrial segments, for example food industry, pharmaceutical industry, timber industry, etc. [1, 2, 3, 4] First documented case happened in Italy at the 18th century [5] and ever since circumstances and causes are available in written form for making some safety analysis or improve manufacturing process safety.
Dust and gas explosion phenomenon has been studied for decades, although results are still far from their required level. Lots of ordinary summarizing publication can be found in the literature which are clearly negotiate cases and causes of explosions, rule standards and opportunities of safety. [1, 6, 7]
The first line of safety is prevention, which means avoidance of explosions. Some opportunities and devices are commercially available; however combination of circumstances should results disaster. Practically, there is impossible to completely avoid explosions. So, safety systems are under construction to make industry more reliable and safe. Parts of these systems can be explosion vents which can be installed into enclosures walls, and in case of explosion, they open in their full area, and let flames with burnt and unburnt gases into the environment. [2, 8, 9, 10, 11] *Figure 1* shows the effect of venting to explosion overpressure in enclosures. [5]

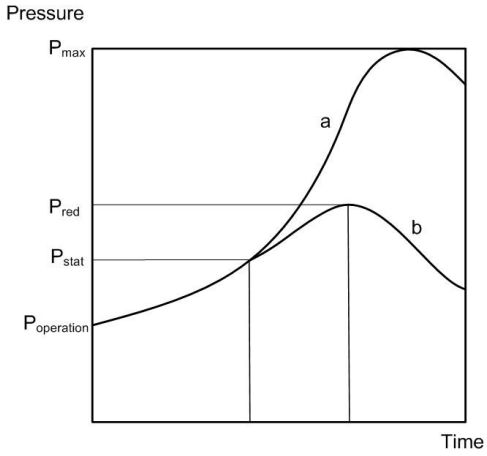

Figure 1 Pressure rise in vessels during explosion
a) without venting; b) with venting

To protect the working area, deflector plates can be used to change direction of material outflow. *Figure 2* shows the correct assembly regarding to MSZ EN 14491 standard, which describes the following instructions:

- the area of the deflector plate should be at least three times the area of the vent, and
- dimensions of the deflector plate should be 1.6 times the dimensions of the vent;
- the plate should deflect outflowing materials and flames at least 45 to 60 degrees to the horizontal;
- the axis of the venting centre should be the axis of the deflector plate;
- the distance of the plate and venting area should be 1.5 D, where D is the diameter of the vent, but in some cases it can be modified in practice, depending on circumstances. [12]

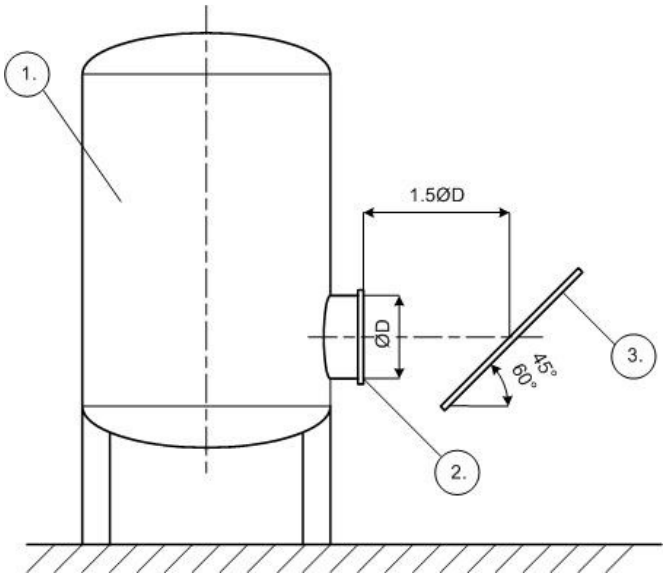

Figure 2 Design of blast deflector plate,
where 1. enclosure, 2. rupture panel, 3. deflector plate [12]

Equation which is appropriate for estimating recoil force of deflector plate according to this standard is the following [12]:

$$F_R = 0.52 \cdot 119 \cdot A \cdot p_{red,max} \quad (1)$$

where

F_R	recoil force	kN
A	geometric area of the vent	m^2
$p_{red,max}$	maximum reduced overpressure	bar_g

It clearly seems, that the *Equation 1* does not contain or refers to distance between deflector plate and venting area, however the standard allows to modify it.
Some previous studies investigated venting processes in numerous types of enclosure. At the early times, most common of them was silo which combustible powders handle in, so this equipment means the base of some article. Hauert measured pressure rise in silos in case of dust explosions [13], and Hey investigated effect of ignition position for explosion overpressure in vented silos [14]. Some other author tried to generalize their research, and started to investigate explosion in standard enclosures. Holbrow studied small tank venting [15], and Proust investigated 20-litre sphere compared to 1 m^3 enclosure [16]. This 20-litre sphere with high pressure bearing capacity gets a growing interest from researchers, because it allows selecting elevated static activation overpressures and high peak pressures during burst. However, investigation of deflector plates' effect had not been a popular scope in the explosion venting topic. For this reason, effect of vent duct distance to recoil force and maximum reduced overpressure were investigated in current study.
This paper describes the venting experimental results in standard 20-litre explosion chamber in case of propane-air mixture with different distance of deflector plate. The aim of this research is to discuss the possible vent sizing problems in the protection of enclosures in situation of different distances of deflector plates.

2. METHODS

The experimental set-up and picture are shown in *Figure 3*. It includes a 20-litre spherical combustion chamber which designed by principles of standard E 1226-10, and in certain cases, includes venting devices.
The chamber is a hollow 20 litre volume sphere with double stainless steel wall. The double wall serves as water jacket to transfer the heat of explosions and to thermostatically control test temperatures. [17]
For testing, the gas in proper concentration is dispersed into the vacuumed chamber via outlet nozzle. The ignition source is located in the centre of the sphere. For gases, source is electric spark, with arbitrarily changed energy. For installing additional measuring elements, aperture of sight glass can be used. In current experiments, rupture foils and a venting nozzle were setting up.
Venting nozzle length of 0.2 m and inner diameter of 30 mm was selected. An electric igniter with 10 kJ energy was used in every experiment. Applied deflector plate had square shape with 48 mm side length and 45° to the horizontal. Distance of the plate is variable with a special rail, which can be fixed in selected positions. These distances were 40 mm, 45 mm, 50 mm and 70 mm.
Propane-air mixture with 5 vol. % was used in experiments. Propane was commercially available by Linde in 99.5% purity. Air was applied from the environment and compressed air tanks for more realistic measurements. Experimental circumstances were atmospheric pressure (0 bar_g) and ambient temperature (293 K), which are priority important in case of gases. Maximum explosion overpressure in closed vessel was 7.79 bar_g, and with venting nozzle without deflector plate was

5.38 bar_g, which were previously measured.
As the venting device, round aluminium foil with 43 mm total diameter was installed to the sight glass of the chamber between special clamping tools. Venting diameter of foil was 30 mm (which area can tear in its whole cross-section). Its thickness was 0.01 mm, and previously it had been exposed homogenization heating in 573 K for 15 minutes. Static activation overpressure of the foils was 0.476 bar_g ± 5%, which was previously measured value.
Pressures in the vessel during explosion were recorded with high speed pressure sensors with a frequency of 9600 Hz. Recoil forces were measured on the opposite side of deflector plate with a load cell, a frequency of 9600 Hz, too. The entire control unit and data logger unit operated on the computer with data collection function.
Figure 4 shows simplified scheme of measuring set-up.

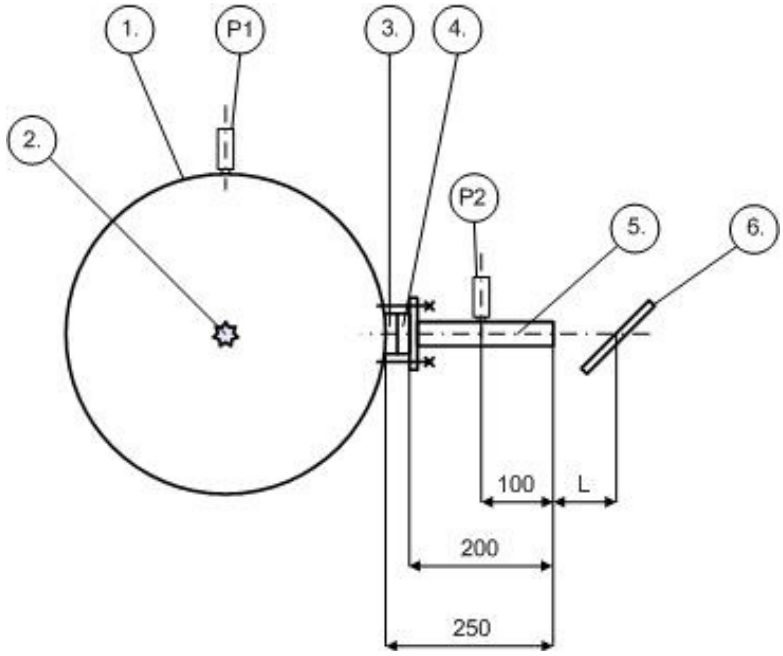

Figure 3 Measuring set-up
1. explosion chamber, 2. ignition point, 3. and 4. rupture foil clamping devices,
5. venting nozzle, 6. deflector plate, P1 and P2 pressure transducers,
L is the variable distance of deflector plate

3. RESULTS

Deflected venting experiments for 5 vol. % propane-air mixture were performed after these tests described above. As mentioned previously, four distances of deflector plate were selected: 40 mm, 45 mm, 50 mm and 70 mm. As the MSZ EN 14491 standard recommends, distance of 45 mm were measured and ±5 mm to observe the effect of distance. 70 mm distance gave significantly different values, and measuring without deflector plate gave value for “infinite distance”.
Table 1 shows the average of deflagration properties and recoil forces which were measured and estimated by *Equation 1*; and – for controlling purposes – explosion properties for closed vessel, and vented vessel without deflector plate.

Table 1 Results of the measurement

Distance	Maximum overpressure [bar_g]	Recoil force	
		measured [N]	calculated [N]
0 mm (closed vessel)	7.79	-	-
40 mm	5.52	188.22	210.68
45 mm (recommended)	5.61	189.45	213.66
50 mm	5.46	191.62	208.01
70 mm	5.35	185.98	203.67
∞ (without deflector)	5.38	-	-

For easier understanding, *Figure 4* shows the diagram of results. Experimental results indicated that the distance of deflector plate has an influence on the peak pressure on the vessel during explosion, and recoil force on the plate. However, the position besides peak of overpressure (45 mm) is not overlaps with the position of peak recoil force (50 mm). Current experimental data show that venting to deflagration panels can cause higher recoil forces than recommended by MSZ EN 14491 standard. Although, measured data significantly less than estimated ones in case of each distance.

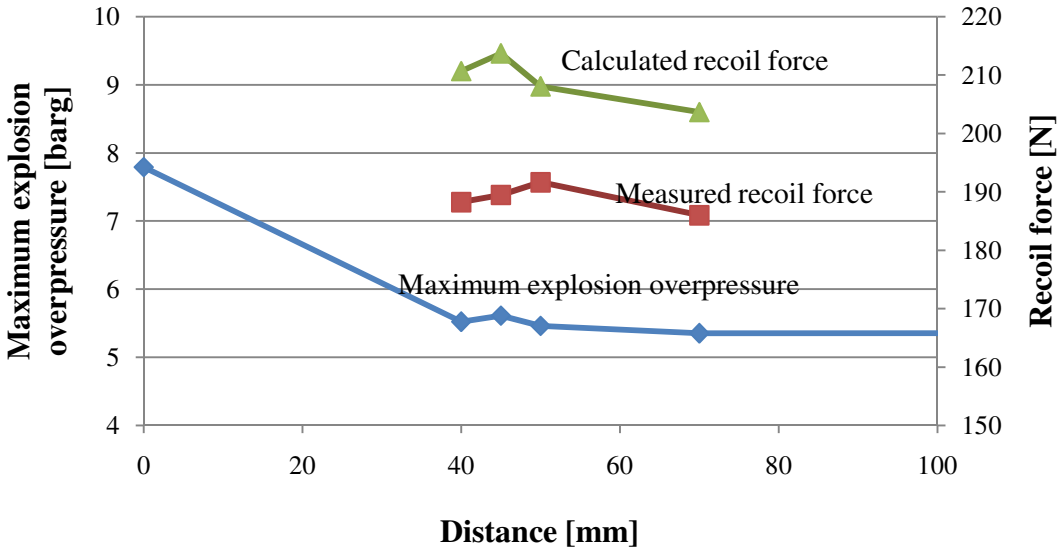

Figure 4 Diagram of results

CONCLUSIONS

Vented explosions to deflector plate experiments were studied in the 20-litre apparatus, with different vent distances between venting nozzle and the plate of 40 mm to 70 mm. The main results are listed as follows:

(1.) The maximum overpressures of 5 vol. % propane-air mixture were measured in the confined 20-litre combustion chamber in case of closed vessel, and different distances.
(2.) The maximum recoil forces of 5 vol. % propane-air mixture venting were measured in the opposite side of deflector plate in case of different distances.
(3.) The distance of deflector plate has an influence on the peak pressure on the vessel during

explosion.

(4.) The distance of deflector plate has an influence on the peak recoil force on the deflector plate during explosion.

(5.) Maximum values of pressure in the vessel and recoil forces are not occur at the same distance.

(6.) Increasing deflector plate distance, effect of reduced explosion overpressure and recoil force became constant.

(7.) Measured recoil force values had not reached what had been calculated by MSZ EN 14491 standard.

More tests should be performed to evaluate the accuracy of current results. With them, correlations, equations and constraints of standards should become more reliable and improvable. The best method to solve this problem is to establish some semi-empirical, empirical or theoretical equations for description of explosion venting.

REFERENCES

[1] Barton: *Dust explosion prevention and protection: A practical guide*. Gulf Professional Publishing, 2002, ISBN 0-7506-7519-3

[2] Blair: *Dust explosion incidents and regulations in the United States*, Journal of Loss Prevention in Process Industries, No. 20, 2007, pp. 523-529

[3] Abbasi, Abbasi: *Dust explosions – Cases, causes, consequences and control*, Journal of Hazardous Materials, No. 140, 2007, pp. 7-44

[4] Bokros, Mannheim, Siménfalvi, Szepesi: *Por- és gázrobbanás elleni védelem*, Nemzeti Tankönyvkiadó, 2009, TÁMOP-4.1.2-08/1/A-2009-0001

[5] Grimvall, Holmgren, Jacobsson, Thedéen: *Risks in technological systems*, Springer, 2010. doi: 10.1007/978-1-84882-641-0

[6] Eckhoff: *Dust explosions in process industries – Third edition*, Gulf Professional Publishing, 2003, ISBN 0-7506-7602-7

[7] Amyotte, Eckhoff: *Dust explosion causation, prevention and mitigation: An overview*, Journal of Chemical Health and Safety, 2010. jan/febr, pp 15-28

[8] Bartec: *Dust explosion protection*, 2005, 03-0330-0338-08/05-BCS-A220236/1E

[9] Bjerkvedt, Bakke, Wingerden: *Gas explosion handbook*, Journal of hazardous Materials, No. 1, 1997.

[10] Fike: *Explosion venting – product guide*, 2009, Form No. B9100 1209

[11] Snoeys: *Dust explosion protection using flameless venting*, Fike Corporation

[12] MSZ EN 14491-1 standard

[13] Hauert, Vogl, Radandt: *Dust cloud characterization and the influence on the pressure-time history in silos*, Process Safety Progress, Vol. 15, No. 3, 1995, pp. 178-184, ISSN: 1547-5913

[14] Hey: *Pressure relief of dust explosions through large diameter*, Journal of Loss Prevention in the Process Industries, No. 4, 1991, pp. 217-222

[15] Holbrow: *Dust explosion venting of small vessels and flameless*, Process Safety and Environmental Protection, No. 91, 2013, pp 183-190

[16] Proust, Accorsi, Dupont: *Measuring the violence of dust explosions with the "20 l sphere" and with the standard "ISO 1 m3 vessel". Systematic comparison and analysis of the discrepancies*, Journal of Loss Prevention in the Process Industries, No. 20, 2007, pp. 599-606

[17] Cesana: *Operating instructions 20 l apparatus*, Kühner AG, 23.04.01 CC

INTERNATIONAL SCIENTIFIC CONFERENCE ON ADVANCES IN MECHANICAL ENGINEERING
13-16. October 2016, Debrecen, Hungary

PROPERTIES OF COLD GAS DYNAMIC SPRAYED COATINGS

[1]MOLNÁR András, [2]FAZEKAS Lajos PhD, [3]CSABAI Zsolt PhD, [4]PÁLINKÁS Sándor PhD

[1]*University of Miskolc*
E-mail: a.molnar2007@gmail.com
[2]*University of Debrecen*
E-mail: fazekas@eng.unideb.hu
[3]*Csabai Pharma AG Svitzerland, Zug,*
E-mail: dr.csabai@csabai.de
[4]*University of Debrecen*
E-mail: palinkassandor@eng.unideb.hu

Abstract
Cold gas dynamic spray or simply cold spray (CS) is a process in which solid powders are accelerated in a de Laval nozzle toward a substrate. If the impact velocity exceeds a threshold value, particles endure plastic deformation and adhere to the surface. Different materials such as metals, ceramics, composites and polymers can be deposited using CS, creating a wealth of interesting opportunities towards harvesting particular properties. CS is a novel and promising technology to obtain surface coating, offering several technological advantages over thermal spray since it utilizes kinetic rather than thermal energy for deposition. As a result, tensile residual stresses, oxidation and undesired chemical reactions can be avoided. Development of new material systems with enhanced properties covering a wide range of required functionalities of surfaces and interfaces, from internal combustion engines to biotechnology, brought forth new opportunities to the cold spraying with a rich variety of material combinations.

Keywords: Cold spray, Metal matrix composite, Polymer, Ceramic, Powder

1. INTRODUCTION

Cold spray technology: basic principles CS is a process in which solid powder particles are accelerated over the sonic velocity through a de Laval nozzle with a convergent-divergent geometry. Particles have ballistic impingement on a suitable substrate at speeds ranging between 300 and 1200 m s^{-1}. The nozzle geometry as well as the characteristics of feedstock powders is fundamental to determine the final temperature and velocity of sprayed particles which is strictly related to coating microstructure, physical and mechanical properties.

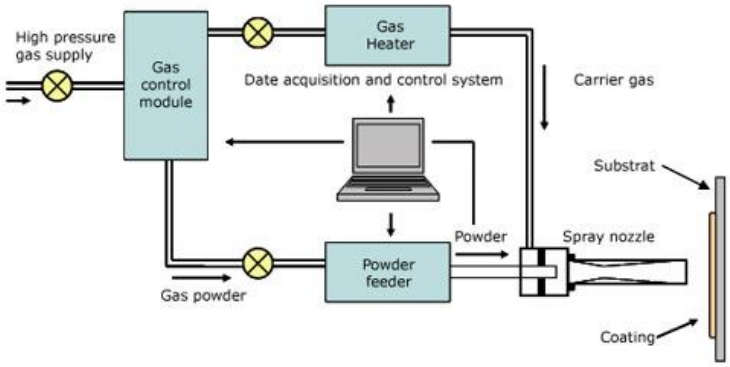

Figure 1 The principle of the cold gas dynamic spray process (CGDSP) is to accelerate a gas supersonic velocities in the „De Laval" nozzle.

The temperature of the gas stream is always below the particle material's melting point. Therefore, CS could be effectively defined as a solid state deposition process. As the coating deposition is accomplished at the solid state, it has characteristics that are quite unique compared to other traditional thermal spray techniques. There are currently two main types of CS systems: a/ low pressure cold spray (LPCS) in which powders are injected in the diverging section of the spray nozzle from a low pressure gas supply. LPCS systems are typically much smaller, portable, and are limited to 300–600 m s^{-1} particle velocities and b/ high pressure cold spray (HPCS) in which particles are injected prior to the spray nozzle throat from a high pressure gas supply. They are used in the application of lighter materials and they generally utilise readily available air or nitrogen as propellant gases.

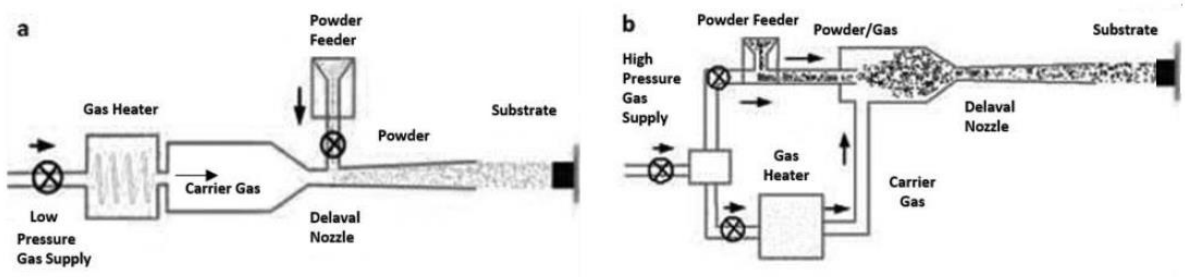

Figure 2 Schematic of different CS systems: a low pressure cold spray (LPCS) ; b high pressure cold spray (HPCS)

High pressure systems instead, use higher density particles. They utilise higher pressure gases, are stationary and typically generate particle velocities of 800 – 1400 m s^{-1}. Lower weight gases, such as nitrogen or helium, are the preferred propellant gases for HPCS. Figure 3 compares the coating thickness capabilities of the cold spray process to other surfacing technologies including surface conversion/modification and deposition methods. The cold spray process covers a vast range of possible coating thicknesses.

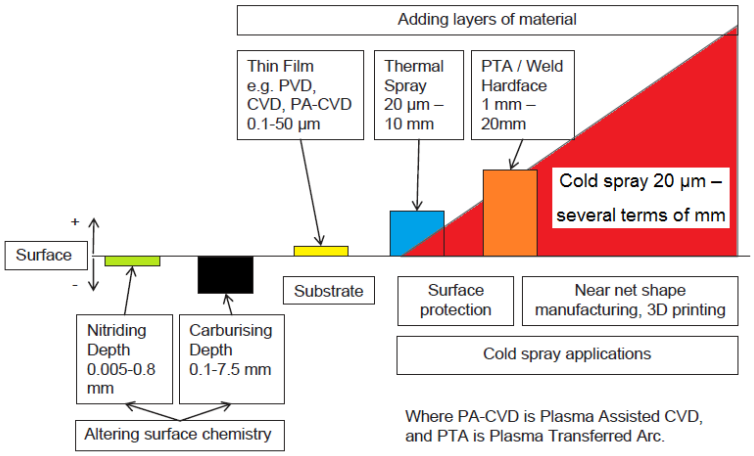

Figure 3 Cold spray in the surface engineering space. *CS* cold spray, *PVD* physical vapor deposition, *CVD* chemical vapor deposition [35]

Hence, due to the importance of two-phase flows in aerospace optimal design and safety operations, it was normal for the Russian scientists at the Institute of Theoretical and Applied Mechanics of the Siberian Branch of the Russian Academy of Science (ITAM SB RAS) in Novosibirsk to perform, in

the mid-1980s, wind tunnel experiments and study the influence of particles on flow structure and their interaction with a body [1]. However, apart from other results, the original carefully planned and controlled conditions of wind tunnel experiments at ITAM SB RAS also led to the observation for the first time of deposition of aluminum on a body in a "cold" (280 K) supersonic two-phase flow with aluminium particle at a velocity of 400–450 m/s [1]. This was the "happy accident" of observing a new phenomenon. However, it was the scientist who actively created the conditions for discovery and the "prepared minds" of scientists, such as Professor Papyrin and his colleagues, who properly identified and understood the importance of the unforeseen incident, used creative analogies, and, using the incident constructively, transformed it into what we call today the cold spray process. The scientific and practical importance of the discovery of the cold spray process stimulated further experiments for a more detailed study of the observed phenomenon and the establishment of the basic physical principles of the process. The wide spectrum of research conducted include, in no particular order: experimental studies, modelling of the process, gas dynamics inside and outside the supersonic nozzle, optimization of the nozzle, the impact of a supersonic jet on a substrate, deformation of particles and bonding mechanisms, coating properties, and equipment and applications development [1]. All these studies led to a large number of initial patents in Russia;

2. PROPERTIES OF COLD SPRAYED COATINGS

2.1 Deposited Material Property Advantages

Cold spray coating property advantages are summarized in Figure 3. Many of these properties are interrelated; for example, cold-sprayed characteristics such as high density, low porosity, and no oxidation maximize both thermal and electrical conductivity, and, depending on the corrosion environment, may be conducive to improved corrosion resistance.

2. 1. 1 No Powder Melting

The key physical difference between cold spraying and more conventional thermal spraying methods is that, in cold spray, material consolidation occurs entirely in the solid state [1] which requires enough impact energy (particle velocity) to stimulate bonding by rapid plastic deformation. Therefore, to achieve higher gas flow velocities in the DeLaval nozzle, the compressed carried gas is often preheated. However, while preheated temperatures as high as 1000 °C or more may be used, the fact that contact time of spray particles with the hot gas is quite short and that the gas rapidly cools as it expands in the diverging section of the nozzle, the temperature of the particles actually remains substantially below the initial gas preheat temperature, hence, below the melting temperature of the spray material [2].

2. 1. 2 No Grain Growth

During other material consolidation processes, such as powder metallurgy and conventional thermal spray processes, grain re-crystallization and coarsening is a fact of life which is unacceptable in many instances [3]. In contrast, during cold spraying, the net heat input into the material is low enough that extensive grain growth and re-crystallization do not typically happen; this is largely beneficial as the consolidated material may be able to retain desirable mechanical and physical properties of the feedstock material [4], such as fatigue strength, which strongly depends on surface microstructure and grain size [5]. After cold spraying, the grain microstructure of the consolidated

material remains largely equaxial contrary to the splat-like microstructure typical of conventional thermal spray [7]. Others have even reported fine grain microstructures with ultimate tensile strength and hardness always higher than the equivalent properties in equivalent wrought materials - attributed to the high degree of plastic deformation during cold spraying [8].

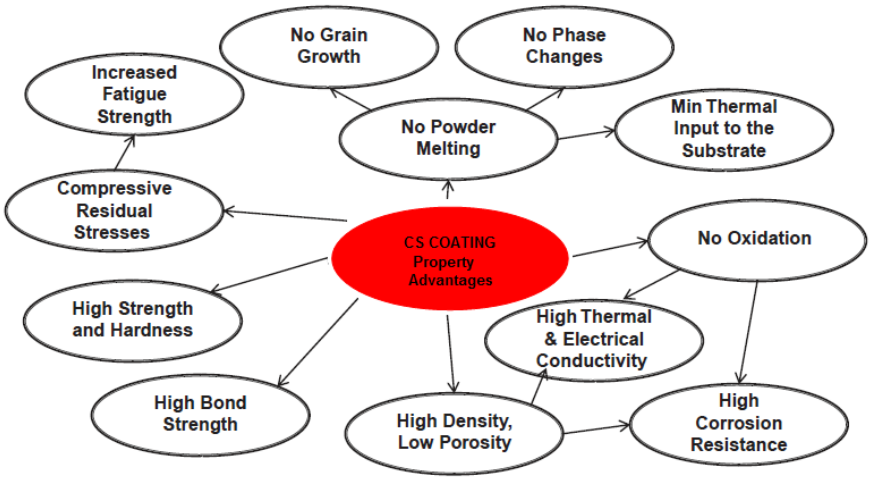

Figure 3 Cold spray coating property advantages [13]

[9]; [10-11]. At a more micro-structural level, rapid plastic deformation during cold spraying may also result in the formation of nano-sized grain zones at the interfacial regions between particles, which may have further implications on mechanical properties of cold spray deposits [12]. In summary, the low-temperature solid-state condition of the cold spray technique makes this method attractive to process temperature-sensitive materials, such as nano-structured and amorphous materials [3]; [7].

2. 1. 3 No Phase Changes

The properties of all materials are affected by the chemical, micro-structural, and phase compositions of the processed material. In most cases, these properties have been engineered through material processing techniques that, at some point, involved high-temperature phase transformations [13]. In high-temperature processes, such as plasma spraying, molten species (including ceramic species) can react during their very short fly from the spray gun to the substrate. For example, NiAl plasma-sprayed powder can show all possible phases in the deposit, including Ni, alpha-Ni, NiAl, Ni_2Al_3, $NiAl_3$, and Al; AI_2O_3 and TiO2 plasma-sprayed powder blends can result in deposition of Al2O3 significantly enriched with TiO2 [13]. Even during lower-temperature spray processes, such HVOF, WC–Co powders tend to undergo detrimental decarburization, with by-products of reactions that are fundamentally undesirable, such as $W2_C$, W, and WO_3 [3]; [15]. In the cold spray process, thermally induced phase transformations are avoided. Researchers have used cold spray to consolidate WC-based powders. Using X-ray diffraction (XRD), it has been confirmed that cold spray does not induce changes to the chemistry, phase composition, or grain structure [3]; [14]; [4]. Yet, another classical example refers to the preservation of nanocrystalline microstructure, which yields exceptional mechanical properties [15]. The cold spray process has been successfully used to consolidate nanostructured powder materials into useful forms without destroying their fine grain size [6].

2. 1. 4 Minimum Thermal Input to the Substrate

Repairing damaged ion vapor deposition (IVD) aluminium coatings on high-strength steel substrates, such as 300M, 4340 or 4130, requires better than 99 wt.% aluminium coatings along with a coating process that does not raise the substrate temperature to 8 I. Botef and J. Villafuerte more than 204 °C (per MIL-DTL-83488D). Because of its low-temperature deposition, cold spray has become the ideal process to repair damaged IVD aluminium on thin plates. Qualification tests have demonstrated that during the cold spray coating process, the temperature at the reverse side of steel sheets (as thin as 1 mm) did not reach more than 120 °C [16]. In addition to IVD, cold spray can also be used to repair damaged aluminium plate, sputter aluminium, chemical vapor deposition (CVD) aluminium, and ionic liquid aluminium coatings [16]. Furthermore, cold spray could be used to spray any temperature-sensitive materials such as magnesium, nano-structured materials, amorphous materials, carbide composites, and many polymers. According to experts, cold spray technology could be used for almost 70 % of materials that could be spray coated but that are ruled out because of the high-process temperatures associated with traditional thermal spray processes [17].

2. 1. 5 No Oxidation

In-process oxidation constitutes one of the main limitations of most traditional thermal spray processes. In-flight oxidation of particles results in internal oxide inclusions, while postimpact oxidation produces surface oxide layer between splat layers [18]. Low-cost processes such as air plasma spray (APS) and wire arc spray produce coatings with the most oxidation and porosity compared to, for example, HVOF [18]. Yet, the increased particle velocity in HVOF generally correlates well with improved splat deformation and less porosity but unfortunately has no effect on oxidation [19]. Oxidation is particularly critical when spraying oxygen-sensitive materials such as aluminum, copper, magnesium, titanium, and others as small amounts of undesirable oxygen may degrade the physical properties of the deposits [15].

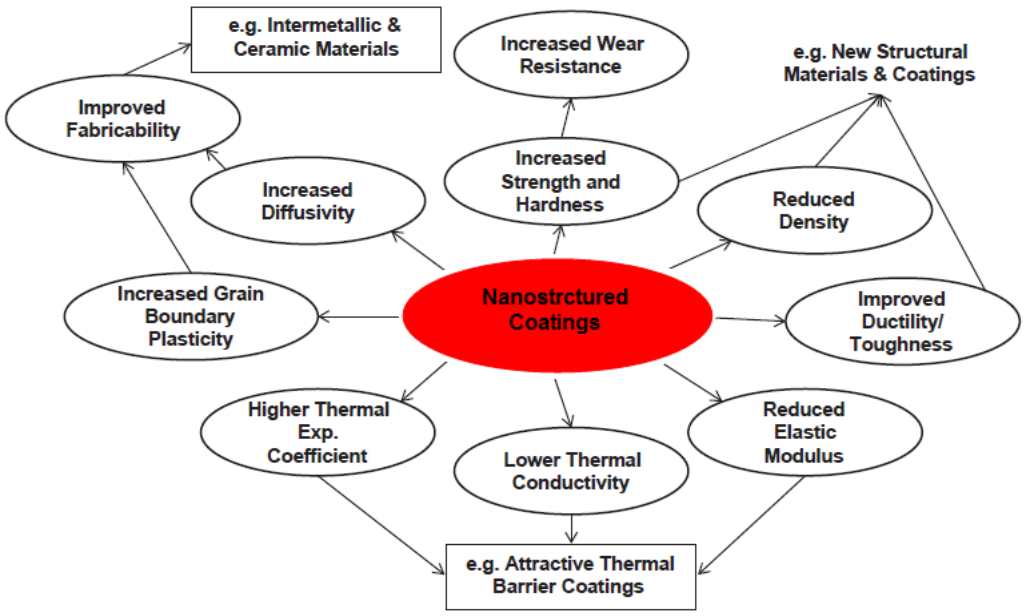

Figure 4 Cold spray nanostructured coating advantages [13]

One example is alloy 600, a nickel-based alloy used in heat exchangers in the nuclear industry, which is prone to stress corrosion cracking (SCC), one of the most challenging modes of material failure. SCC failures have been directly associated with the presence of Fe- and Cr-rich oxide films along grain boundaries [20]. During particle impact in cold spraying, the brittle oxide skin that covers most metal surfaces shatters, making the oxide swept away by the high-velocity gas jet and readying the bare surface for a clean bond with particles coming behind; in practice, it has been demonstrated that cold spray deposits show same or lower oxygen content than the starting powder material [6]. Figure 5 illustrates textures of Cu, Sn, and Al when sprayed by conventional thermal spray versus cold spray. The ability of cold spray not to introduce but rather diminish oxide content in the deposit is very appealing for a number of exciting future applications. One example is the deposition of inter-metallic compounds such as FeAl-based inter-metallic alloys, which exhibit good mechanical properties and excellent corrosion resistance in oxidizing and sulfidizing atmospheres at elevated temperatures. These materials are lighter (5.56 g/cm^3) than steels or Ni-based alloys, have a high melting point, high creep strength, excellent thermal conductivity, and are relatively inexpensive.

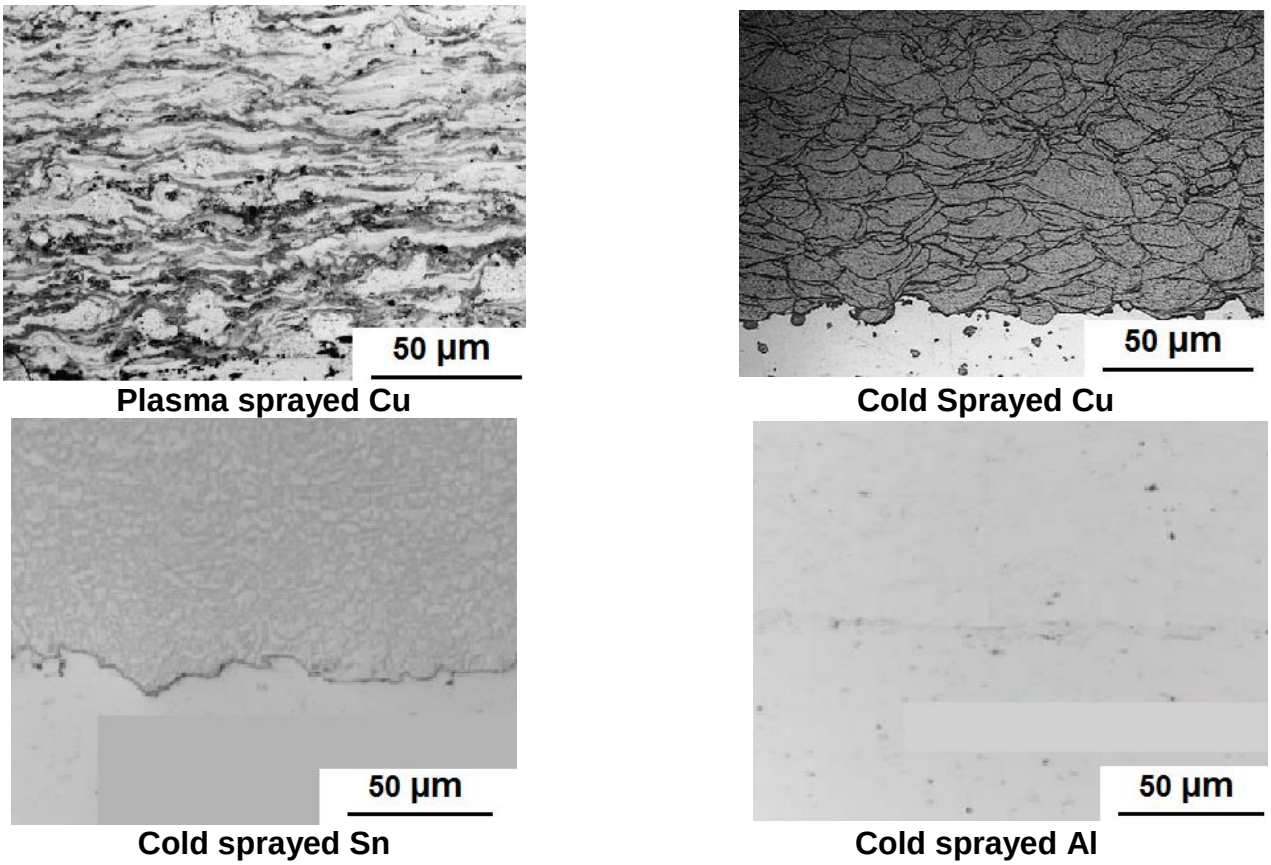

Figure 5 Sprayed different metal coatings

Because of these attributes, they have been considered as a substitute for stainless steels or Ni-based super-alloys for high-temperature service [21]. Fe–Al inter-metallics show limited ductility at low temperatures, and their mechanical strength degrades at temperatures higher than 600 °C. Thermal spray processes, such as plasma spray, HVOF, wire arc, or flame spray, have been used to spray with FeAl-based alloys for corrosion protection of carbon steels. However, such deposits end up with excessive oxide content which leads to poor corrosion performance and other problems,

emphasized by the significant difference in melting points between Al and Fe as well as the exothermic nature of formation of iron aluminides [22]; [21]. Cold spraying of Fe–Al-based materials can be achieved by utilizing powder blends, which then, with an appropriate annealing post-spray treatment [22] can induce the complete transformation of Fe(Al) solid solution into FeAl intermetallics [21]. Other powder mixtures, such Al/Ni, Al/Ti, W/Cu, Zn/Al, Ti/Al, and Ni/Al can be cold sprayed and then annealed to form a dense well-dispersed distribution of their intermetallics [21]; [22].

2. 1. 6 High Density, Low Porosity

The outer zone of the typical lamellar structure of a thermal spray deposit shows splats that are not well bonded together and that, in their turn, lead to many micronsized pores [23]. A high level of porosity—such as 5–15 % for flame and arc spray and 3–8 % for plasma spray—may lead to corrosion [24]. Cold spraying is a solid-state process with no splashing. When particles impact the substrate at speeds higher than the material's critical velocity, they plastically deform at high strain rates and bonding occurs. Highstrain rate deformation produces additional thermal energy at interfaces, which
may lead to the generation of interfacial metal vapor jet. This jet in effect produces "vapor deposition" of material at the inter-particulate interfaces which fills any pores and cracks that exist. In this respect, it has been suggested that cold spray can be viewed as a combination of a particulate and microscopic vapor deposition processes [25]. On top of that, every subsequent pass of the spray plum effectively "shot peens" the underlying layers, thus increasing their density. The combination of all these phenomena in cold spray produces near-theoretical density coatings [25]. Furthermore, when post-spray heat treatments (such as annealing) are applied, the deposits experience even further consolidation and densification approaching ideal levels due to closure of pores, inter-splat boundaries, and cracks [26]; (Figure 5).

2. 1. 7 High Thermal and Electrical Conductivity

Electrical conductivity is a good indicator of coating quality in terms of material density and presence of dispersed oxide phases [10]. Because of its exceptional electrical and thermal conductivities combined with its commercial availability, copper represents a key material in today's industrialized world [9]. It has been demonstrated that the presence of oxide inclusions in plasma- sprayed copper coatings lowers the electrical conductivity of the deposits down to about 15 % of the conductivity of oxygen-free high-conductivity (OFHC) copper [15]. In contrast, dense cold-sprayed copper coatings may display conductivities better than 85 % OFHC copper [15]; [6] similar copper material would typically display conductivities of about 40–63 % OFHC copper when sprayed by conventional thermal spray processes. If the process can afford it, post-annealing after cold spraying will further increase the conductivity of the deposits by densification and re-crystallization [9]; [10]. Figure 6 compares the "as-sprayed" electrical conductivity of copper coatings using upstream injection (high gas pressures, HP) and downstream injection (lower gas pressures, LP) cold spray systems. International Annealed Copper Standard (IACS) values were given as an average of values measured by using four-point measurements for the following sample conditions: (c1) on steel as-sprayed, (c2) on steel heat treated at 400 °C, (c3) on ceramic heat treated at 280 °C, and (c4) on ceramic heat treated at 280 °C. Upstream injection cold spray systems operating at HP would produce copper coatings with higher electrical conductivities than downstream injection systems operating at LP. However, when using downstream injection systems in combination with powder blends (such as Cu + Al_2O_3), the deposits can be sufficiently densified as to attain electrical conductivities that are acceptable for most electrical applications. The main

function of Al_2O_3 particle additions, in this case, is to activate (cleaning/roughening) the underlying surfaces as well as hammer-deposited particles so that a high-density low-oxygen deposit is built up, become more receptive to adhesion, fresh impact of sprayed particles and better adhere to the surface.

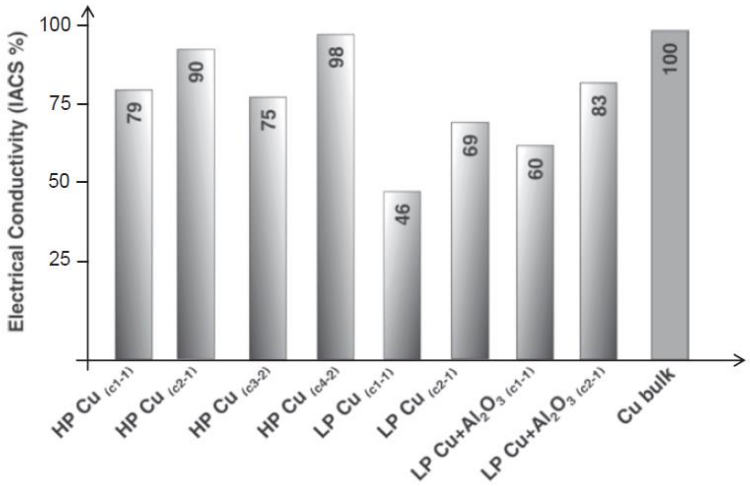

Figure 6 Electrical conductivity for cold-sprayed copper coatings. *IACS* International Annealed Copper Standard, *HP* high gas pressure, *LP* low gas pressure [35]

2. 1. 8 Bond Strength

Both adhesive and cohesive strengths of a deposit are key to determine its usefulness within any particular application [27]. In general, average adhesive/cohesive strengths are determined by spraying the top surface of a cylindrical tensile sample, then gluing the sprayed area to a respective counter-body of the same size, and finally pulling the assembly in tension to failure (ASTM C633). Using this method with certain materials combinations, it has been shown that deposits may fail cohesively (fracture inside the deposit [10] or adhesively (fracture at the deposit/substrate interface; [28]. In other cases, the addition of ceramic particles, such as Al2O3, to pure aluminium can significantly increase adhesive/cohesive strength [27]; [22]. There are cases where the test results are limited by the strength of the glue itself. To overcome the latter, others [27] have attempted other testing techniques, which have indicated that cold-sprayed deposits can display high adhesive strengths (as high as 250 MPa for aluminium alloys [8].

2. 1. 9 Compressive Residual Stresses

It is generally accepted that the presence of surface tensile stresses may contribute to the formation and propagation of micro-cracks, which may accelerate fatigue failure. Because of thermal expansion and contraction during melting and solidification, deposits made by thermal spray may develop surface residual tensile stresses [24]. A distinct feature of the cold spray process is the development of superficial compressive residual stresses instead [29]. Compressive stresses have the opposite effect on fatigue life. Because of the importance of this subject, has been entirely dedicated to discuss the topic of the formation of residual stresses during cold spraying. Through modeling and experimentation, it has been shown that the cold spray process can generate desirable surface compressive stresses which are responsible for improvements in fatigue life of certain materials. For example, cold-sprayed Al7075 over Al5052 substrates, using downstream injection system at low pressure, showed an improvement of close to 30 % in fatigue life [30]. Others have

reported a fatigue life improvement of 10 % for cold-sprayed aluminium over AZ31B magnesium substrates [31]. Compressive residual stresses generated during the cold spray process also contribute to the possibility of producing ultra-thick, well-bonded, and near-room-temperature coatings for near net - shape manufacturing of components made of metallic, composite, and polymeric materials [24].

2. 1. 10 Corrosion Resistant

Conventional thermal spray processes such as flame spray, twin-wire arc spray, and air plasma spraying (APS) represent some of the common methods to deposit aluminium over steel and other materials for corrosion protection. Although they are typically less expensive compared to cold spraying, the severe oxidation, phase transformations, and high porosity are conducive to relatively poor corrosion performance compared to fully dense materials [23]; [32], not to mention some of the environmental challenges associated with the processes [33]. The high density, phase purity, and homogeneous microstructure of cold-sprayed coatings are characteristics that yield exceptional corrosion resistance [8]. Consequently, cold spray is increasingly becoming a preferred method to provide localized corrosion repair and protection in a vast number of applications, many without other means available [33]. Some of these applications include aircraft as well as automotive magnesium castings [33]; [34]. Others [11]. have experimented mixing stainless steel 316L particles with particles made of Co–Cr alloy L605; the latter known to display superior corrosion resistance than 316L alone but difficult to manufacture. These studies suggested that cold spray may be used to consolidate these metals as a blend (67 % 316L—33 % L605), then post-heat treated so that both corrosion and mechanical properties of the resulting composite are better than 316L alone, potentially becoming a new class of metallic biomaterial [11].

CONCLUSION

The explored cold spray technology in the context of the much wider thermal spray family, its beginnings as well as its relative advantages and limitations. An attempt was made at discussing cold spray as a single component of a more complex multidisciplinary surface engineering field, aimed at solving engineering problems. It is indeed, both theoretically and practically, possible to use the cold spray process as a method to solve a number of modern surface engineering challenges including recyclability, life cycle, remanufacturing, emissions, energy consumption, and environmental friendliness. Cold spray was presented as a challenger to traditional problem-solving approaches, drawing attention to the need for new methods that allow us to continue developing and implementing advanced materials for aerospace, electronics, information technology, energy, optics, tribology, and bioengineering applications. Finally, this study served as a brief introduction to the vast amount of current information to be presented in subsequent study by well-known professionals in the field of thermal and cold spray.

ACKNOWLEDGEMENT

This paper was prepared using Julio Villafuerte Modern Cold Spray Materials, Process, and Applications title book.

REFERENCES

[1] Papyrin, A., V. Kosarev, S. Klinkov, A. Alkhimov, and V. Fomin. 2007. *Cold spray technology*, 1st ed. Oxford: Elsevier.

[2] Grujicic, M., C. Tong, W. DeRosset, and D. Helfritch. 2003. Flow analysis and nozzle-shape optimisation for the cold-gas dynamic-spray process. *Proceedings of the Institution of Mechanical Engineers* 217:1603–1613.
[3] Kim, H. J., C. H. Lee, and S. Y. Hwang. 2005. Fabrication of WC–Co coatings by cold spray deposition. *Surface & Coatings Technology* 19:335–340.
[4] Al-Mangour, B., R. Mongrain, E. Irissou, and S. Yue. 2013. Improving the strength and corrosion resistance of 316L stainless steel for biomedical applications using cold spray. *Surface &Coatings Technology* 216:297–307.
[5] Luzin, V., K. Spencer, and M. X. Zhang. 2011. Residual stress and thermo-mechanical properties of cold spray metal coatings. *Acta Materialia* 59:1259–1270. Maev, R. Gr., and V. Leshchynsky. 2008. *Introduction to low pressure*
[6] Karthikeyan, J. 2007. The advantages and disadvantages of cold spray coating process. In *The cold spray materials deposition process: fundamentals and applications*, 1st ed., ed. V. K. Champagne. Cambridge: Woodhead.
[7] Luzin, V., K. Spencer, and M. X. Zhang. 2011. Residual stress and thermo-mechanical properties of cold spray metal coatings. *Acta Materialia* 59:1259–1270.
[8] Karthikeyan, J. 2007. The advantages and disadvantages of cold spray coating process. In *The cold spray materials deposition process: fundamentals and applications*, 1st ed., ed. V. K.Champagne. Cambridge: Woodhead.
[9] Phani, P. S., D. S. Rao, S. V. Joshi, and G. Sundararajan. 2007. Effect of process parameters and heat treatments on properties of cold sprayed copper coatings. *Journal of Thermal Spray Technology* 16:425–434.
[10] Koivuluoto, H., and P. Vuoristo. 2010. Effect of powder type and composition on structure and mechanical properties of Cu+ Al2O3 coatings prepared by using low-pressure cold spray process. *Journal of Thermal Spray Technology* 19 (5): 1081–1092.
[11] Al-Mangour, B., R. Mongrain, E. Irissou, and S. Yue. 2013. Improving the strength and corrosion resistance of 316L stainless steel for biomedical applications using cold spray. *Surface & Coatings Technology* 216:297–307.
[12] Jahedi, M., S. Zahiri, P. King, S. Gulizia, and C. Tang. 2013. "Cold spray of Titanium", ASM International, Aeromat 2013 Conf. Proc., Apr 2–5, Belleview, Washington.
[13] Chraska, P., J. Dubsky, B. Kolman, J. Ilavsky, and J. Forrnan. 1992. Study of phase changes in plasma sprayed deposits. *Journal of Thermal Spray Technology* 1:301–306.
[14] Melendez, N. M., and A. G. McDonald. 2013. Development of WC-based metal matrix composite coatings using low-pressure cold gas dynamic spraying. *Surface & Coatings Technology* 214:101–109.
[15] Smith, M. F. 2007. Comparing cold spray with thermal spray coating technologies. In *The cold spray materials deposition process: Fundamentals and applications*, 1st ed., ed. V. K. Champagne. Cambridge: Woodhead.
[16] Gaydos, S. 2011. Qualification of cold spray for repair of MIL-DTL-83488 aluminum coatings.ASETS defense workshop, Boeing, US.
[17] Kaye, T., and Thyer, R. 2006. Spray coatings: Cold gold—cool moves. Solve Issue 6, CSIRO. Kestler, R. 2011. NAVAIR cold spray efforts, cold spray action team presentation, Fleet Readiness Center East.
[18] Gan, J. A., and Christopher C. Berndt. 2013. Review on the Oxidation of Metallic Thermal Sprayed Coatings: A Case Study with Reference to Rare-Earth Permanent Magnetic Coatings. *Journal of Thermal Spray Technology* 22:1069–1091.
[19] Hanson, T. C., and G. S. Settles. 2003. Particle temperature and velocity effects on the porosity and oxidation of an HVOF corrosion-control coating. *Journal of Thermal Spray Technology* 12:403–415.

[20] Dugdale, H., D. Armstrong, E. Tarleton, S. G. Roberts, and S. L. Perez. 2013. How oxidized grain boundaries fail. *Acta Materialia* 61:4707–4713.
[21] Wang, H. T., C. J. Li, G. J. Yang, and C. X. Li. 2008. Cold spraying of Fe/Al powder mixture: Coating characteristics and influence of heat treatment on the phase structure. *Applied Surface Science* 255:2538–2544.
[22] Lee, H. Y., S. H. Jung, S. Y. Lee, K. H. Ko. 2006. Fabrication of cold sprayed Al-intermetallic compounds coatings by post annealing. *Materials Science and Engineering A* 433:139–143.
[23] Dong, S-J., B. Song, G. Zhou, C. Li, B. Hansz, H. Liao, and C. Coddet. 2013. Preparation of aluminium coatings by atmospheric plasma spraying and dry-ice blasting and their corrosion behaviour. *Journal of Thermal Spray Technology* 22:1222–1228.
[24] Maev, R. Gr., and V. Leshchynsky. 2008. *Introduction to low pressure gas dynamic spray, physics and technology*. Weinheim: Wiley-VCH.
[25] Papyrin, A. 2006. Cold spray: State of the art and applications. European Summer University, St-Etienne, Sept 11–15.
[26] Chavan, N. M., B. Kiran, A. Jyothirmayi, P. S. Phani, and G. Sundararajan. 2013. The corrosion behaviour of cold sprayed zinc coatings on mild steel substrate. *Journal of Thermal Spray Technology* 22:463–470.
[27] Huang, R., and R. Fukanuma. 2012. Study of the influence of particle velocity on adhesive strength of cold spray deposits. *Journal of Thermal Spray Technology* 21:541–549. coatings formation and properties. *Journal of Thermal Spray Technology* 16:661–668..
[28] Irissou, E., J. G. Legoux, B. Arsenault, and C. Moreau. 2007. Investigation of Al-Al_2O_3 cold spray
[29] Spencer, K., V. Luzin, N. Matthews, M. X. Zhang. 2012. Residual stresses in cold spray Al coatings: The effect of alloying and of process parameters. *Surface & Coatings Technology* 206:4249–4255.
[30] Ghelichi, R., D. MacDonald, S. Bagherifard, H. Jahed, M. Guagliano, and B. Jodoin. 2012. Microstructure and fatigue behavior of cold spray coated Al5052. *Acta Materialia* 60:6555–6561.
[31] Shayegan, G., H. Mahmoudi, R. Ghelichi, J. Villafuerte, J. Wang, M. Guagliano, H. Jahed. 2014. Residual stress induced by cold spray coating of magnesium AZ31B extrusion. *Materials and Design* 60 (2014): 72–84.
[32] Chavan, N. M., B. Kiran, A. Jyothirmayi, P. S. Phani, and G. Sundararajan. 2013. The corrosion behavior of cold sprayed zinc coatings on mild steel substrate. *Journal of Thermal Spray Technology* 22:463–470.
[33] Villafuerte, J., and Zheng, W. 2011. Corrosion protection of magnesium alloys by cold spray. In *Magnesium alloys corrosion and surface treatments*, 1st ed., ed. F. Czerwinski, 185–194. Croatia: InTech.
[34] Suo, X. K., X. P. Guo, W. Y. Li, M. P. Planche, and H. L. Liao. 2012. Investigation of deposition behaviour of cold-sprayed magnesium coating. *Journal of Thermal Spray Technology* 21:831–837.
[35] Villafuerte, J. Modern Cold Spray Material process and Application Springer Canada 2014, ISBN 978-3-319-16771-8

INTERNATIONAL SCIENTIFIC CONFERENCE ON ADVANCES IN MECHANICAL ENGINEERING

13-15 October 2016, Debrecen, Hungary

DURABILITY IMPROVEING OF AGRICULTURAL MACHINES PARTS WITH HARD COATINGS

[1]MOLNÁR András, [2]FAZEKAS Lajos PhD, [3]CSABAI Zsolt PhD, [4]PÁLINKÁS Sándor PhD

[1]*University of Miskolc*
E-mail: a.molnar2007@gmail.com
[2]*University of Debrecen*
E-mail: fazekas@eng.unideb.hu
[3]*Csabai Pharma AG Svitzerland, Zug,*
E-mail: dr.csabai@csabai.de
[4]*University of Debrecen*
E-mail: palinkassandor@eng.unideb.hu

Abstract
Wear is known to be as the degradation of material under plethora of service conditions and is considered as one of the major issue of the material used in engineering. Many types of wear have been recognized such as abrasive, erosive, corrosion, oxidation etc. Abrasive wear is probably the most significant cause of mechanical damage of equipment components coming in contact with abrasive bodies. For combating with wear problem various methods have also been developed such as hardfacing, cryogenic treatment, coating and heat treatment of components which are chosen on the basis of various conditions under which the component has to perform the desired work. The wear of the component depends on its surface characteristics like roughness, microstructure and hardness. The abrasive wear in agriculture equipments is the most common problem. The high wear rate of ground engaging tools led to huge loss of material, recurring labor, downtime and replacement costs of worn out parts. Hardfacing is commonly employed method to improve surface properties of tillage tools.

Key Words: *wear, abrasive wear, agricultural equipments, ground engaging tools*

1. INTRODUCTION

Surface engineering is one of the most relevant current fields of research. The events that occur on the surface, such as wear, corrosion or stress concentration create regions prone to crack nucleation, which under static or dynamic loading will eventually lead to most components and structures failures [1]. Wear is the degradation of metal surface, showing a continuous loss of material, due to relative motion between that main metal surface and another materials or substances whichever come in the contact with the original one. Wear is a major problem in industry and its direct cost is estimated to vary between 1 to 4% of gross national product [2].
Wear is a major problem in the excavation, earth moving, mining, automobiles, machines and mineral processing industries and occurs in a wide variety of items, such as bulldozers blades, excavator teeth, drill bits, crushers, slusher, ball and roll mills, chutes, slurry pumps and cyclones [3]. The wear behaviour of material is related to parameters such as shape, size of component, composition and distribution of micro constituents in addition to the service conditions such as load, sliding speed, environment and temperature [4]. The complex nature of wear has delayed its investigations and results in isolated studies towards specific wear mechanisms. The wear of the component depends on its surface characteristics like roughness, microstructure and hardness. Friction and wear of materials are generally considered important properties in engineering practice [5]. Many types of wear have been recognized such as abrasive, erosive, adhesive, corrosion, oxidation and surface fatigue wear etc. Wear of solids is treated as the mechanical process. However, other chemical processes, oxidation and corrosion are exceptions of this rule. The abrasive wear and the contact fatigue are the most important from technological point of view. It

was estimated that the total wear of component can be identified 80-90% as abrasion and 8% as fatigue wear. Contribution of other types of wear is small [6]. So, abrasive wear is probably the most significant cause of mechanical damage of equipment components coming in contact with abrasive/erosive bodies. The abrasive wear is caused by sharp particles sliding or flowing across a metal surface at varying speeds and pressure, thereby grinding away material like small cutting tools.

It has been estimated that 50% of all wear problems in industry are due to abrasion, and as such, much laboratory work has examined and sought to rationalise the abrasive wear behaviour of a wide range of material [8]. However two body abrasive wear generally arise when particles are in sliding movement, between hard and rough surface, and are able to move freely. Machinery that is operating in sandy environment is vulnerable to sand particles entering and becoming entrapped between components, causing abrasive wear [9]. In a study Hokkirigawa et al (1978) observed three abrasive wear mechanisms using scanning electron microscopy (SEM): microcutting, microploughing and wedge formation. Fig.1 (a) shows the microcutting mechanism, whereas Fig.1 (b) shows the microcutting with less deep grooves. Fig.1(c) shows the micro-ploughing mechanism and Fig.1 (d) shows the wedge formation.

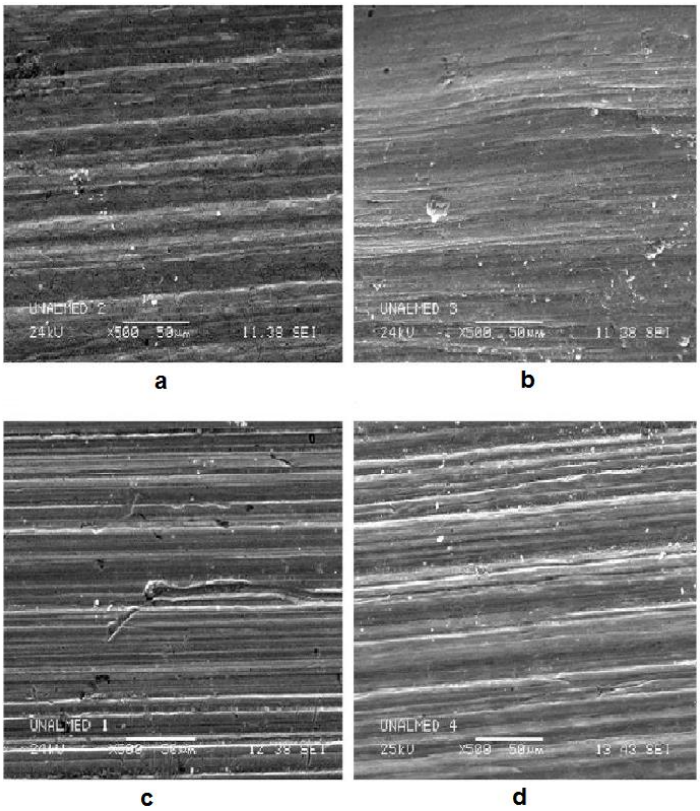

Figure 1 Abrasive wear mechanisms; (a) and (b) microcutting, (c) microploughing, (d) wedge formation.

2. ABRASIVE WEAR IN AGRICULTURAL EQUIPMENTS

The problem of wear has mainly been concentrated on industrial related to large industries, but the interaction between agricultural tillage equipment and soil constitutes a complicated tribological problem [10]. In addition the optimizing tillage is one of the major objectives in mechanized farming to achieve economically viable crop production system [11]. Farmers and equipment

operators often complain about high wear rate of ground engaging tools in some dry land agricultural areas. The problems faced with recurring labour, downtime and replacement costs of exchanging the worn out ground engaging components like ploughshares [12]. Worn out tools results in poor tillage or seeding efficiency, poor weed control and higher fuel penalties. Carbon or low alloy steels are generally preferred to make tillage tool under low stress abrasive wear [13]. Tillage having composites with alumina ceramics and boron, medium and high carbon heat treated steels offers great potential the severity of abrasive wear in soil-engaging components [14]. Hardness of tillage tool, grain structure and its chemical composition are also the influential factors in determination of wear rate. Wear due to highly abrasive soils have surface damage characterized by scoring, cutting, deep grooving and gauging, and micro machining caused by soil constituents moving on a metal surface [15].

The wear of tillage implements in most soils is caused by the stones and gravel content. In addition wear on parts of a plough body, more systematically, depends on the wear resistance of the plough parts which in term is dependent on their thermal processing and shape, the tillage conditions, as plough area (or time), plough speed and tillage depth, the normal forces between the soil and the surfaces of the plough area, the proportion, hardness, sharpness and shape of soil particles, the moisture content of the soil, the density and mechanical properties of the soil (hardness, shear strength and brittleness) and environmental effects and weather changes [16]. Wear resistance of plough is mainly associated with their surface hardness and shape of ploughshare, which in turns related to the soil type and the cutting edge thickness. The wear and wear rate determination of tillage tool is necessary because it seriously affects production planning, tillage quality, repair cost of tillage component, energy consumption for tillage process each time performed and finally the production cost of agricultural product [17]. Several studies on the evaluation of abrasive wear resistance have found that using hard deposits in welding processes is a good alternative to recover parts under abrasive wear [18].

3. GROUND ENGAGING TOOLS

The mouldboard „flat feet" hoes is the most widespread tillage tool in the world and the biggest consumer of energy in agriculture [19]. For the design of an energy efficient mouldboard „flat feet" hoes in different operating conditions, an understanding of the interactions of different „flat feet" hoes, soils and operational parameters is essential [20]. The „flat feet" hoes and the mouldboard are the main soil engaging parts of the mouldboard „flat feet" hoes hare is the part with the highest wear rate [21]. The „flat feet" hoes wear not only effects its working life but directly changes its initial shape, which is one of the most important factors influencing ploughing quality. The comparison between a new and a worn out ploughshare with changes in initial shape is shown in Fig. 2. The wear of the „flat feet" hoes also lead to frequent work stoppages for replacement, downtime and results in direct costs through the important effects of higher fuel consumption and lower rates of work [22].

4. REMEDIAL MEASURES

Wear is considered a genuine problem with engineering material globally, for instance, it has been reported that there is total losses in agricultural sector due to wear is about $940 million every year in Canada [23] the similar losses costing about $4.4 million in Turkey every year [24]. Research is going on over the years to reduce the wear either in the form of using a new wear resistance material or by improving the wear resistance of the existing material by addition of any wear resistance alloying element etc.

Figure 2 A new and a worn out „flat feet" hoes

In order to combat with problem of wear several attempts have been made, and surface treatment has been considered as the most appropriate method [25].In this various surface modification processes has been found so far, such as carborizing, boriding, nitridng, cryogenic treatment, heat treatment processes, coating and hardfacing. Hardfacing and coating are generally preferred for abrasion wear as cryotreatment found its application in the high-cycle fatigue fields [26]. Hardfacing process is considered as the effective and economical method to reduce wear problem by increasing hardness of the component [27]. Hardfacing is commonly employed method for functionalizing surfaces subjected to severe wear, corrosion or oxidation, which has transformed itself into a field of broad application and development, both in manufacturing of new components and in the repair and extension of useful life across a vast range of industries [28]. The hardfacing not only has a high wear and impact resistance, anti-corrosive behavior of deposited metal, but also can restore the dimensions of worn out components. In addition, the hardfacing may produce a thick deposited layer with a high deposition rate and resulting hardened layer has a high bonding strength with the matrix [29]. Hardfacing can be deposited by various welding methods (Figure 3)

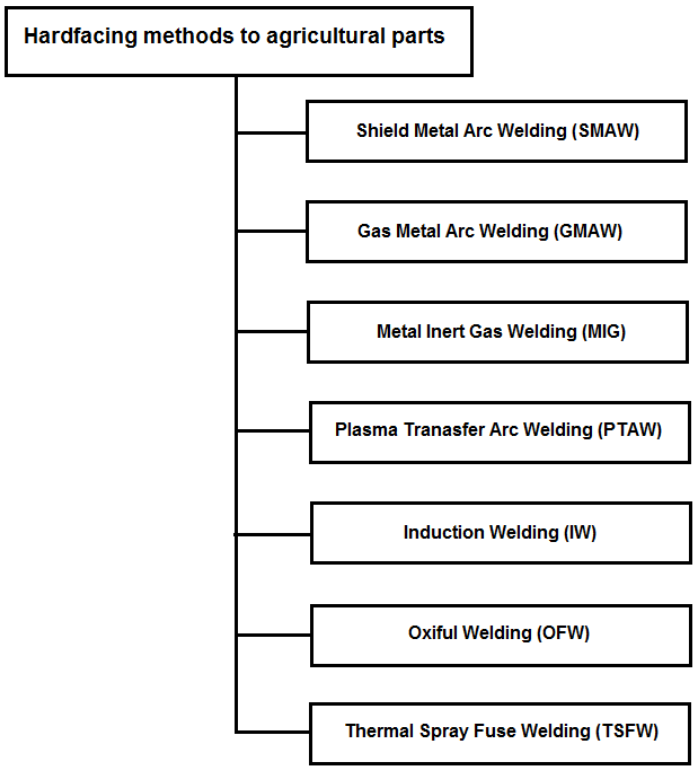

Figure 3 Different hardfacing methods for agricultural parts

The systematic study of various consumable and welding processes applied to hardfacing, is of great interest for the optimization of the design of the consumables and for the evaluation of fine tuning of the welding procedures. The working life of equipment or of a mechanical component exposed to mechanical wear on its surface has been prolonged through the use of wear resistance alloys. Greater benefits can be and of the deposition process. We tried to encrease of „flat feet" hoes life time with spray fuse welding methods (Figure 4 and Figure 5).

Figure 4 Spray fused „flat feet" hoe

Figure 5 Spray fused „flat feet" hoes

The selection of deposition process is as important as the selection of the alloy to be deposited, i.e it must be based on various factors such as the operating conditions, characteristics of the base material, the geometry and dimensions of the part, the cost/benefit ratio of the component to be coated and processing cost. The wear resistance of tillage tools depends mainly upon surface hardness. We presenting our results in Table 1 and Figure 6.

Table 1 Mass changeing of spray fused hoes in g before- and after useing

Number of pieces	Practical work	Mass of piece in [g]		
		Before useing	After useing	Different
1.	Normalised	226,44	118,42	108,02
2.	Hardened of sharps	232,85	163,34	69,51
3.	Double heat treated of sharps	230,74	157,72	73,02
4.	Hardened of full surface	234,93	142,32	92,61
5.	Double heat treated of full surface	231,63	119,71	111,92
6.	Hardfacing with GMAW	252,68	134,78	117,9
7.	Spray fused welding with Deloro (60 HRC) powder	247,23	153,54	93,69
8.	Spray fused welding with N 40 powder	244,58	167,35	77,23
9.	Spray fused welding with N 50 powder	240,25	169,06	71,19
10.	Spray fused welding with N 60 powder	249,43	206,08	43,35

Figure 6 Mass changeing of spray fused hoes in g before- and after useing

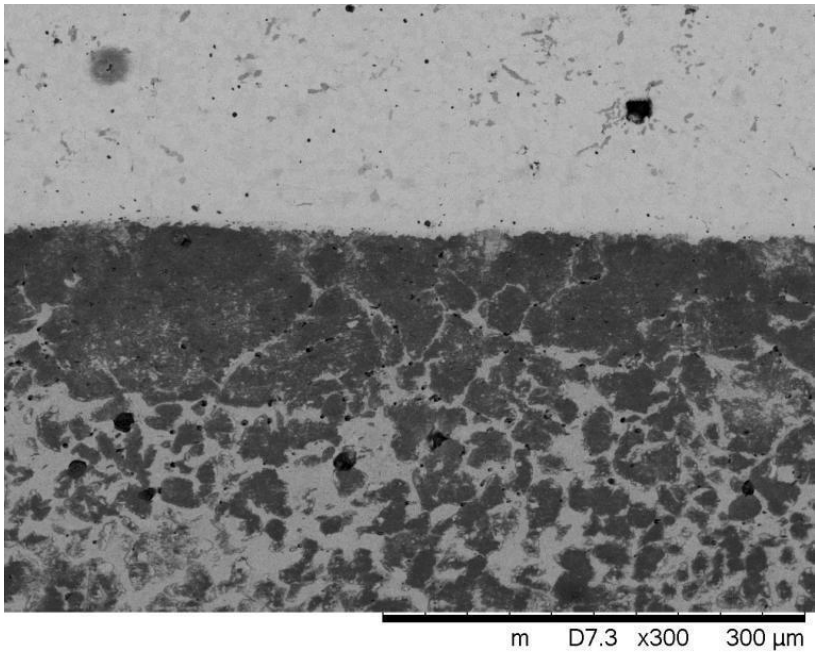

Figure 7. Intermediate laye at number of 8 probe piece (M=300X)

The increase in material hardness results in decrease in wear rate. We showed the intermediate layer on Figure 7 – when we made a hard coating spray fused NiCrBSi coating on steel substrate. Certainly, there has to be a relationship between tool hardness and hardness of particles in order to keep effective wear resistance but also to be borne in mind is the fact that high hardness implies brittleness [30]. Studies on the wear resistance of the materials subjected to the impact of abrasive particles are usually carried out at many research centres. The research determined the wear

resistance of material under laboratory conditions and includes selection of adequate grades of steel [31]. On the other hand, determination of effect different implement designs and different working conditions on the wear and its distribution on a given element requires field testing. This is due to the difficulties in laboratory simulation of changes in load, which occur during work in soil [32]. In laboratory conditions several methods are employed to determine the wear resistance of materials like dry sand rubber wheel test, pin on disc test etc. When comparison is made between the laboratory and in field experiments, it can be concluded that the actual field environment, in which the impacts or contacts to the tillage tool components occurs due to factors such as hard soil particles as the stones, gravels, rocks and roots during working in field could not be achieved satisfactorily in the laboratory merely through wear test machine [33-34].

CONCLUSION

Wear is considered as the major problem in engineering and agricultural components. To combat with wear problem, hardfacing is the most versatile process among many alternatives to improve the life of the worn out components and reducing the cost of replacement. Hardfacing reduces the downtime because parts last longer and fewer shutdowns are required to replace them. To determine wear in agricultural sector, in-field tests are necessary due to the difficulties in laboratory simulation of changes in load, which occur during work in soil. The performance of the components variations in conditions in actual environment could not be achieved through laboratory tests. in accordance to the variations in conditions in actual environment could not be achieved through laboratory tests.

ACKNOWLEDGEMENT

This paper was prepared using by Parvinkal Singh Mann and Navjeet Kaur Brar: Tribological aspects of agricultural equipments [34]. :

REFERENCES

[1] J. Gandra, D. Pereira, R.M. Miranda, R.J.C. Silva and P. Vilaça, "*Deposition of AA6082-T6 over AA2024-T3 by friction surfacing - Mechanical and wear characterization"*, Surface & Coatings Technology, vol. 223, pp. 32–40, 2013.

[2] Philip D Goode, Nuclear Instruments and Methods in Physics Research Section B: *Beam Interactions with Materials and Atoms*, Volume 39, Issues 1–4, Pages 521–530,1989.

[3] Sarkar AD, ClarkeJ , Friction and wear of aluminium silicon alloys, *Wear*,Volume 61, Issue 1, Pages 157–167,1980.

[4] Al-Mangour, B., R. Mongrain, E. Irissou, and S. Yue. 2013. Improving the strength and corrosion resistance of 316L stainless steel for biomedical applications using cold spray. *Surface &Coatings Technology* 216:297–307.

[5] S. Ma, S. Zheng, D. Cao and H. Guo, *"Anti-wear and friction performance of ZrO2 nanoparticles as lubricant additive"*, Particuology, vol. 8, pp. 468–472, 2010.

[6] Alfred Zmitrowicz, "Wear patterns and laws of wear", *A Review Journal of Theoretical and Applied Mechanics*, Warsaw, vol. 44, no. 2, pp. 219-253, 2006.

[7] K. Hokkirigawa, K. Kato, "An experimental and theoretical investigation of ploughing, cutting and wedge formation during abrasive wear", *Tribol international*, vol. 39, no. 6, pp. 570-574, 2006.

[8] Eyre T S , Wear characteristics of metals ,*Tribol. Int.* 10 , 203-212,1976.

[9] WoldmanM,van der Heide E ,Schipper D J ,Tinga T, Masen M A, Investigating the influence of sand particle properties on abrasive wear behaviour,294-295,Page 419-426,2012.
[10] Natsis A, Petropoulaos G , Pandazaras C, Influence of local soil conditions on mouldboard ploughshare abrasive wear,*Tribology International*,41, 151-157,2008.
[11] Jayasuriya H P W, Salokhe V M ,SW—Soil and Water: A Review of Soil–tine Models for a Range of Soil Conditions,*Soil and Water*,doi:10.1006/jaer.2000.0692.
[12] G.R. Quick, "Tillage tool wear – some governing factors, measuring techniques and materials for wear resistance", *Agricultural Engineering Development International Rice Research Institute.* Phillipines, 1989.
[13] H-J Yu ,Bhole SD ,Development of a prototype abrasive wear tester for tillage tool materials.*Tribol Int*,23(5):309-16,1990.
[14] Foley AG , Lawton PJ ,Mclees VA .The use of alumina ceramic to reduce wear of soil-engaging components. J *AgricEngRes* ,30(1):37-46,1984.
[15] S.A. Ferguson, J.M. Fielke, T.W. Riley, "Wear of cultivator shares in abrassive south Australian soils", *J. Agric. Engg. Res.,* vol. 69, pp. 99-105, 1998.
[16] Bayhan Y, Reduction of wear via hardfacing of chisel ploughshare,Tribology International 39 ,570-574,2006.
[17] A. Natsis, G. Papadakis, J. Pitsilis, "The influence of soil type, soil water, and share sharpness of mouldboard plough on energy consumption, rate of work and tillage quality", *J Agric. Engg. Res.*, vol.72, pp. 171-176, 1999.
[18] I.M. Hutchings, Tribology : "Friction and wear of engineering materials", *Cambridge University Press ;* 1992.
[19] V. Cracium, D. Leon, "An analytical method for identifying and designing a mouldboard plough surface", *Trans. ASAE,* vol. 41, no. 6, pp. 1589-1599, 1998.
[20] D.S. Shrestha, G. Singh, G. Gebresenbet, "Optimizing design parameters of mouldboard plough", *J Agric. Engg. Res.*, vol. 78, no. 4, pp. 337-389, 2001.
[21] G. Wiese, E.H. Bourarach, "Handbook of agricultural engineering", *Plant Production Engineering,* vol. 3, pp. 184-217, 1999.
[22] E.Y.H Bobobee, K. Sraku-Lartey, S.C. Fialor, E.A. Canacoo,S.K. Agodzo, A. Yawson, "Wear rate of animal drawn ploughshares in selected Ghanian soils", *Soil Tillage Res.*, vol. 93, no. 2, pp. 299-308, 2007.
[23] Ulusoy E. A research on determination of wearing of some tillage tool shares. Ege University. J AgricFac (390),1981.
[24] Gupta D ,Sharma A K , Investigation on sliding wear performance of WC10Co2Ni cladding developed through microwave irradiation,*wear*,271, 1642-1650, 2011.
[25] Ivusic V, Jakovljevic M. Protection of agricultural machinery from wear. In: Proceedings of the international conference "*Science and Practice of Agricultural Engineering*," Djakovo, Croatia, p. 275-83,1992.
[26] Bayhan Y, Reduction of wear via hardfacing of chisel ploughshare,*Tribology International* 39 ,570-574,2006.
[27] Buchely M F , Gutierrez J C , Leon L M, Toro A , The effect of microstructure on abrasive wear of hardfacing alloys,*Wear* 259, 52-61,2005.
[28] Agusti'n Gualco, Herna'n G. Sroboda, Estela S. Surian and Luis A. deVedia, "Effect of post weld heat treatment on the wear resistance of hardfacing martensitic steel deposits", *Welding International,* vol. 24, no. 4, pp. 258-265, 2010.
[29] CHEN Bing-quan CHAI Cang-xiu PENG JUN-bo, "A high Fe-Aluminium matrix welding filler metal for hardfacing aluminium-silicon alloy", *Journal of Wuhan University of Technology – Mater. Sci. Ed.,* vol. 18, no. 1, pp. 25-28, 2003.

[30] Y. Bayhan, "Reduction of wear via hardfacing of chisel ploughshare", *Tribol. Int.,* vol. 39, no. 6, pp. 570-574, 2006..
[31] Zygmunt Owsiak, "Wear of spring tine cultivator points in sandy loam and light clay soils in southern Poland", *Soil and Tillage Research,* vol.
[32] A.G. Folay, P.J. Lawton, A.W. Barker, V.A. McLees, 1984. "The use of alumina ceramic to reduce wear of soil engaging components", *J Agric. Engg. Res.,* vol. 30, pp. 37-46, 1984.
[33] B Par, U Er, "Wear of ploughshare components in SAE 950 C steel surface hardened by powder boriding", *Osmangazi University*, Bati Meselik , 26480 – Eskishir, Turkey, Wear 261, pp. 251-255, 2005.
[34] Parvinkal Singh Mann and Navjeet Kaur Brar: Tribological aspects of agricultural equipments a review International Research Journal of Engineering and Technology (IRJET) Volume: 02 Issue: 03 | June-2015

INTERNATIONAL SCIENTIFIC CONFERENCE ON ADVANCES IN MECHANICAL ENGINEERING

13-15 October 2016, Debrecen, Hungary

METHODEN DER LIEFERANTENAUSWAHL IN DER AUTOMOBILINDUSTRIE IN UNGARN

[1]MORAUSZKI Kinga, [2]LAJOS Attila PhD

[1]PhD School in Business and Management, Szent István University
2100 Gödöllő, PáterKároly u. 1. Tel.: (28) 522-000
E-mail: morauszki.kinga@gtk.szie.hu
[2]Faculty of Economics and Social Sciences, Szent István University
2100 Gödöllő, Páter Károly u. 1. Tel.: (28) 522-000/2034
E-mail: lajos.attila@gtk.szie.hu

Abstrakt
Die vorliegende Arbeit stellt dar, was für Auswahlmethoden es gibt natürlich die sowohl ungarische, als auch ausländische Fachliteratur anwenden. Wir haben Zusammenhänge und Verbindungspunkte gesucht, um begründete Schlüsse ziehen zu können. Andererseits haben wir für wichtig gehalten das vorzustellen, wie die Kunden über das Auswahlthema meinen und warum sie solche Entscheidungen treffen wie wir es eben erfahren. Unser Ziel war die Methoden zu zeigen, die im Beruf meistens benutzt werden.

Stichwörter: Auswahlmethoden, Lieferanten

1. EINLEITUNG

In der Mitte des 20. JH-s gab es eine Vorstellung über die Qualität, dass das Produkt zur Anwendung geeignet sein und den technischen Parametern entsprechen soll. Später ist der Bedarf an Qualitätsverbesserung erschienen, d.h. es wurde erwartet, dass das Produkt die Kundenanforderungen während seinem ganzen Leben übertreffen muss. Vor kurzem ist es auch eine Vorstellung der Qualität in den Vordergrund getreten, dass die vor allem die Kundenansprüche erfüllen muss [3].
In der letzten Zeit haben sich die Erwartungen der Kunden geändert, sie ändern sich zurzeit und werden sich auch noch ändern, wie sich die Industrie kontinuierlich entwickelt. Das Ziel ist jetzt nicht nur das Folgende: die gewünschten und bestellten Waren rechtzeitig ausliefern zu können und sie den Kunden zur Verfügung zu stellen, sondern auch „kleine Anforderungen“ haben sich diesen Ansprüchen angeschlossen. In unserer heutigen Welt ist es nicht mehr genug, wenn die Kunden mit unseren Produkten oder Dienstleistungen zufrieden sind. Wie die Konsumgewohnheiten immer anspruchsvoller werden, so erwartet man Dienstleistungen von den Unternehmen auf einem höheren Niveau [7].
Der Begriff Lieferanten–Management kann durch die Lieferantenbeziehungen eines Unternehmens als Entwicklung, Führung und nicht zuletzt als Resultat effizienter Gestaltung der Lieferantenbasis bestimmt werden [9]. Vor einigen Jahren wurde der Lieferant für einen potentiellen Feind gehalten, und wurde durch die ständigen Preisverhandlungen gegen andere Lieferanten ausgespielt. Dadurch ergaben sich negative Folgen bezüglich der Lieferantenzuverlässigkeit, bzw. hat das zu hohen Kosten geführt. Heutzutage behaupten immer mehr Firmen, dass der Preis nur eines von den wichtigen Kriterien ist. Vor allem geht es jedoch um die Gesamtleistung des Lieferanten. Es ist immer wichtiger, den besten und zuverlässigsten Lieferanten auszuwählen, bzw. eine langfristige Geschäftsbeziehung auszubauen. Ein unerlässliches Mittel dazu ist aber die Lieferantenbewertung [6].

2. AUSWAHLMETHODEN

Es gibt viele Methoden zur Lieferantenauswahl. Diese werden im Hinblick auf die Umfangsgrenze von uns nur erwähnt und nur werden die Methoden ausführlicher dargestellt, die von den ungarischen Unternehmen angewendet werden. Die konkrete Auswahlmethode oder –Mittel müssen aufgrund dessen gestaltet werden, was das Ziel der Firma mit der Lieferantenbewertung ist. Man kann das auch sagen, dass die gleiche Methode auf andere Weise von 2 verschiedenen Unternehmen angewendet wird. Es gibt kein im Voraus bestimmbares Rezept dafür, welche die beste Lösung wäre. Über die benutzte Methode muss von dem Einkaufsleiter des Unternehmens entschieden werden [13].
Im Falle der Automobilzulieferer wurden die zusammengehörigen Kundenanforderungen, Wertdimensionen und die dazu gehörenden notwendigen Fähigkeiten und Teilfähigkeiten von GELEI (2006) bestimmt, durch die Kompetenzen beeinflusst werden. So können diese Unternehmen zu stabilen Lieferanten der Lieferkette werden. Es gibt mehrere verschiedene Klassifizierungen der Auswahlmethoden. Durch die *Tabelle 1* wird die von GLANTSCHNIG (1994) erstellte Klassifizierung dargestellt. Im Laufe der Analyse der Lieferantenauswahl, bei der Analyse der angewendeten Methoden können nur wenige ungarische Hinweise gefunden werden. Anhand der vorherigen Forschungen haben wir die Folgerung gezogen, dass es viele Auswahlmethoden gibt, über die in der heimischen Fachliteratur nur teilweise oder überhaupt nicht gelesen werden können.

Tabelle 1 Verfahren, Methoden zur Lieferantenbewertung

<table>
<tr><td rowspan="4">Qualitative Methoden</td><td rowspan="4"><u>a) Verbale Verfahren</u>
- Checklistenverfahren
- Lieferantentypologien
- Portfolio – Methode
- Notensysteme

<u>b) Numerische Verfahren</u>
- Punktbewertungsverfahren
- Matrix Approach
- Nutzwertanalyse

<u>c) Graphische Verfahren</u>
- Profilanalyse
- Lieferanten – Gap – Analyse</td><td rowspan="2">Quantitative Methoden</td><td>Bilanzanalyse
Preis – Entscheidungsanalyse
Kosten – Entscheidungsanalyse
Mathematische Programmierung
Kennzahlenverfahren</td></tr>
<tr><td rowspan="2">Konventionelle Methoden</td></tr>
<tr><td>Einfache kategorische Methode
Gewichtete Methode
Kostenaufstellungsmethode
Komplex Beurteilungsmethode</td></tr>
<tr><td>Sonstige Methoden</td><td>Fuzzy Logic
AHP
Principal Component Analysis
Activity – Based – Costing
Klasteranalyse</td></tr>
<tr><td colspan="3">Multiple attribute decision making (MADM)</td></tr>
</table>

Quelle: nach GLANTSCHNIG (Eigene Darstellung., 2012)

Wie man es sieht, die Literatur erwähnt bzw. präsentiert viele vorhandene Bewertungs- und Auswahlmethoden, aber – anhand der vorherigen Forschungen – ihr Nachteil ist das, dass sie nicht richtig behandeln können, dass unter den Bewertungskriterien auch Ursache-Wirkung Zusammenhänge existieren können. Es kann viele Verbindungen geben, wo ein Kriterium ohne das andere nicht existiert. Nach einer anderen Klassifizierung können die Methoden in drei größeren Gruppen geteilt werden, wie einfache, klassische und moderne Mittel (*Tabelle 2*).

Tabelle 2 Einfache, klassische und moderne Methoden zur Lieferantenauswahl

EINFACHE METHODEN	KLASSISCHE METHODEN	MODERNE METHODEN
Fragebogen ausfüllen durch Lieferanten Besuch vor Ort Referenzen Informationen auf der Lieferanten Webseite Interviews	SWOT-Analyse Portfolio- Analyse ABC- Analyse XYZ- Analyse LMN- Analyse	BSC (Balanced Scorecard)

Quelle: Eigene Darstellung (2016)

2.1. Einfache Methoden

Zu dieser Kategorie gehören z. B das Interview oder das persönliche Treffen. Durch einfache Fragen kann ein Blick über die Schwachpunkte und Stärken der potentiellen Lieferanten bekommen werden. Das Ziel ist wie bei allen anderen Bewertungsmethoden, eine Beurteilung zu geben. Die Fragen können das Engagement der teilnehmenden Unternehmen oder die Wichtigkeit der Forschung enthalten. Die Fragen müssen einfach, ohne jegliche Forschung beantwortet werden. Verschiedene Methoden können angewendet werden, zur Antwort auf die Fragen können, wie z. B

- die betroffenen Abteilungen fragen
- Fragebogen von den Lieferanten ausgefüllt
- persönliches Treffen
- Unternehmensberichte
- Referenzen, usw.

Das Vorteil des Interview ist das, dass es geeignet ist die Erfahrungen zu generalisieren und wenn offene Fragen geblieben sind, kann sich dadurch so die Fragen stellende Peron neue Kenntnisse erwerben. Wir müssen aber auch die Nachteile erwähnen, weil durch die Auslegung der Fragen bzw. durch die Struktur der Fragen ein Ergebnis verursacht werden kann. Nicht zuletzt zeigen die teilnehmenden Firmen größere Bereitschaft im Rahmen eines persönlichen Treffens, ein günstigeres Bild über den befragten Bereich, die Prozesse zu geben.

2.2. Klassische Methoden

Zur Lieferantenbewertung können auch klassische Controllingsmittel angewendet werden. Dadurch bedeutet das Controlling nicht nur Steuerung und Kontrolle, sonder auch Leitung, Entscheidung und Entwicklung [5].

SWOT – Analyse

Diese Methode ist aber für die Unternehmen ein sehr hilfreiches Hilfsmittel der strategischen Planung, um Chancen und Risiken identifizieren zu können.

Der Begriff stammt aus dem englischen Akronym für **S**trengths (Stärken), **W**eaknesses (Schwächen), **O**pportunities (Chancen) und **T**hreats (Gefahren). Diese Methode kann zur Lösung technischer Probleme erfolgreich benutzt werden, ihr Wesen ist die zur Verfügung stehenden Methoden zu analysieren und die schwachen und starken Faktoren mit den Möglichkeiten und Gefahren zu vergleichen. Für jede Gruppe können kurz- und langfristige Maßnahmen getroffen werden, wie z. B. die Schwäche verstärken, die Stärke weiterentwickeln, die Möglichkeiten ausnutzen und die Gefahren neutralisieren.

Portfolio – Analyse

Der Grundgedanke der Portfolio-Analyse stammt aus der finanziellen Welt, wo das Risiko mit Hilfe der finanziellen Indizien von den Investoren beurteilt werden. Das Portfolio enthält diese addierten

Daten. Die Analyse ist nicht anders, als die „Gesamtheit der SWOT-Analysen". Der Grundgedanke ist, dass die Geschäftseinheiten in ein zweidimensionales Koordinatensystem gesetzt werden müssen, auf dessen horizontaler Achse ein oder mehrere zusammenhängende firmenspezifische Faktoren dargestellt werden, aber auf der vertikalen Achse können ein oder mehrere externe Faktoren Platz haben [7]. Anhand der entdeckten Zusammenhänge gibt die Analyse zusätzliche Information, wenn es graphisch dargestellt wird, können die verschiedenen Möglichkeiten, Methoden verglichen werden [11]. Mit dieser Methode kann auch die Änderung oder Entstehung der Wettbewerbslage der einzelnen Unternehmen geprüft werden [2].

ABC – Analyse

Die ABC-Analyse ist eine Methode für die Auswahl besonderer Produktgruppen, dass zur Analyse der homogen Menge dient, wie z. B. zur Analyse einer Produktfamilie oder eines Kundenkreises. Es hilft der Produktstruktur des Unternehmens beim besseren Kennenlernen. Die ABC-Analyse zeigt, welche Produkte nach einem gewissenen Aspekt berücksichtigt werden müssen. Es kann unter ihren Vorteilen erwähnt werden, dass ihre Anwendung einfach ist und es eine Möglichkeit gibt, die Ergebnisse graphisch darzustellen. Ihr Nachteil ist aber, dass keine qualitativen Faktoren berücksichtigt werden. Die ABC-Analyse ist weit verbreitet und findet Anwendung inner- und außerhalb der Betriebswirtschaft.
Die Klassifizierung erfolgt in drei Gruppen (ABC):
A – hoher Wert und sehr kleine Menge
B – mittlerer Wert und geringe Menge
C – kleiner Wert und große Menge
Das Ergebnis der Analyse bedeutet, dass die „A – Lieferanten" in Lieferantenmanagement unbedingt berücksichtigt werden müssen, weil sie eine bedeutende Quote des Umsatzes betragen. Das bedeutet, dass bei den einzelnen „A – Lieferanten" die komplette Leistungsfähigkeit bzw. das Risiko und das Potenzial der Bewertung gründlich geprüft werden müssen. Dieser Lieferantentyp bildet für einen Kunden die wichtigste Lieferantengruppe und die etwaige Vorschriftswidrigkeit muss mit Umsicht geprüft werden.

XYZ – Analyse

Die Lieferanten werden anhand der Regelmäßigkeit der Lieferungen [4] und der Menge [1] durch die XYZ – Analyse aufgeteilt. Zusammengefasst gestalten sich die Klassen wie folgt:
X - konstanter Verbrauch,
Y - stärkere Schwankungen im Verbrauch,
Z - unregelmäßiger Verbrauch**.**
Nur mit Hilfe dieser Analyse kann eine 100%-e Lieferantenbewertung nicht durchgeführt werden. Infolge dessen wird diese Analyse mit der Kombination der anderen Beurteilungsmethoden angewendet, z. B. mit ABC – Analyse.

LMN – Analyse

Die Lieferanten können durch LMN-Analyse in drei Gruppe aufgeteilt werden. Im Gegensatz zu den o.g. Methoden (ABC-Analyse, bzw. XYZ-Analyse) wird hier in diesem Fall das Volumen als Kriterium angewendet oder gewählt und dementsprechend diese 3 Gruppe sieht so aus L (großvolumige Teile), M (mittelvolumige Teile) und N (kleinvolumige Teile). Nach einer Klassifizierung, wenn eine kleine Anzahl von Lieferanten große Volumen oder sogar n.i.O. Teile liefert, während die Mehrzahl der Lieferanten kleinvolumig sind [4]. Die LMN-Teile sind dementsprechend einzeln, in kleinen bzw. in großen Verpackungseinheiten ein-und auszulagern [10].

2.3. MODERNE METHODE

Balanced Scorecard (BSC)
Der Begriff BSC wird irrtümlich für verschiedene Arten von kennzahlenbasierten Systemen verwendet. Die BSC, die eine Ursache-Wirkung-Analyse verlangt, ist aber eine originär andere Managementmethode als die deskriptive Prozesskostenrechnung oder das klassische monetäre Kennzahlensystem. In der BSC wird es möglich, die Entwicklung der Geschäftsvision zu verfolgen. Mit dieser Methode kann man nicht nur die finanziellen Aspekte zu betrachten, sondern auch strukturelle Frühindikatoren für den Geschäftserfolg zu steuern.BSC kann ein umfassendes Bild über die Funktion des Unternehmens.

3. RESULTATE

Im Laufe unserer Forschung sind viele Fragen aufgetaucht, auf die wir die Antwort gesucht haben. Einerseits haben wir die Zusammenhänge, Verbindungspunkte gesucht, um irgendwelche – wenn auch nicht statistische aber begründete Schlüsse ziehen zu können. Andererseits haben wir das für wichtig gehalten zu ermitteln, wie die Kunden über das Auswahlthema denken und warum sie ebenso Entscheidungen treffen wie sie eben Entscheidungen treffen. Im Laufe der Zusammenstellung unseres Fragebogens war unser Ziel, die meisten Auswahlmethoden zu erfassen, die darzustellen, die im Beruf benutzt werden. Im Besitz von diesen Informationen haben wir unseren Fragebogen erstellt, der 13 Auswahlmethoden enthält. Wir haben nicht für wichtig gehalten, die Methoden in diesen Fragebogen hineinzunehmen, die wir in der ungarischen Fachliteratur eigentlich nicht gefunden haben

Großunternehmen
Im Falle von den Großunternehmen können wir keine großen Abweichungen finden, was die zwei Lieferantentypenanbetrifft – sie bewerten die Wichtigkeit der Methoden fast ähnlich, das bedeutet, obwohl sie zwischen den zwei Lieferantentypen Unterschied machen, es ist aber nicht bedeutend. Bezüglich des Themas der Lieferantenauswahl, ist die Frage aufgetaucht, d.h. wenn wir über den vorhandenen Lieferanten sprechen, warum müssen sie wieder zu einem nächsten Projekt oder zur einen Bestellung ausgewählt werden?
Die Frage ist berechtigt, da der jeweilige Lieferant in die Lieferantenbasis des Kunden ja schon hineingekommen ist, in die es schwierig ist hinzukommen und es immer schwieriger heutzutage wird hineinzukommen. Aber halten wir die Tatsache vor Augen, dass die Kunden irgendwie „befangen" mit schon vorhandenen und bewährten sind, weil sie schon geleistet haben. Aber auch solche Projekte können vorkommen, die doch nicht von diesen Zulieferer-Firmen erhalten werden. Aber sie können weiterhin Mitglieder dieser Lieferantenbasis bleiben. Die schon bewährten Lieferanten bekommen das nächste Projekt nicht in allen Fällen. Es kann vorkommen, dass sie in vergangenen Monaten, Jahren mit irgendwelchen Problemen gekämpft haben, wie z. B. Qualitäts-, Logistikproblem oder etwas anders.
Der Kunde will natürlich über ein Problem nicht hören. Es ist ja vorgekommen, wie z. B. bei einem Automobilzulieferer, dass er das „Partner-Projekt" (es gab nur Maßabweichungen im Vergleich zum ersten Projekt) nicht gewonnen hat, da mehrere Qualitätsprobleme zum Vorschein gekommen sind, die mehrere Monate lang nicht gelöst werden konnten, obwohl alle möglichen Lösungen zur Sprache gekommen sind. Es geht um eine empfindliche Konstruktion. Die Kosten sind gestiegen, natürlich zugunsten dem Lieferanten – Sortierkosten, Investition, Mehrüberstunden, usw. Die definierten Maßnahmen wurden beim Lieferanten verifiziert, aber der Endkunde war nicht mehr

bereit trotz der Maßnahmen mit diesem Unternehmen zusammenzuarbeiten. Demzufolge hat der Lieferant das „Partner-Projekt" nicht erhalten. Deswegen habe ich auch zwischen den schon vorhandenen von dem neuen Lieferanten unterschieden. Ja, die vorhandenen Lieferanten müssen auch zum nächsten Projekt ausgewählt werden. Es ist nicht selbstverständlich, dass sie die Möglichkeit bekommen können, die nächstfolgenden Produkte mit ähnlicher Struktur herstellen zu dürfen. Wenn wir die nächste Tabelle (*Tabelle 3*) gründlicher betrachten, kann man die früher erwähnten Beispiele sehen, d.h. die verschiedenen Portfolio-, ABC-, SWOT-Analysen sind im Laufe der Auswahl weniger wichtig. Die Großunternehmen bevorzugen lieber die Besuche (71% der Unternehmen wählen diese Methode), das Lieferantenaudit (76% der Firmen entscheiden sich für diese Methode), wobei sie die eventuell für die früheren Probleme getroffenen Maßnahmen persönlich verifizieren und anhand dieser Ergebnisse bezüglich der neuen Projekte Entscheidungen treffen können.

Tabelle 3 Rangliste von Großunternehmen bevorzugter Auswahlmethoden

METHODEN	VORHANDENE LIEFERANTEN	NEUE LIEFERANTEN
SWOT-Analyse	23%	10%
Portfolio- Analyse	10%	9%
ABC- Analyse	33%	14%
Besuch vor Ort	71%	81%
Referenzen	24%	62%
Lieferantenaudit	76%	76%

Quelle: Eigene Darstellung (2016), N=212

Natürlich gibt es in der Praxis auch positive Beispiele. Es gibt solche OEMs, die den gut bewährten, die etwas beweisen und etwas leisten wollen Lieferanten treu sind. Sie wollen weiterhin in der Lieferantenbasis bleiben und dafür tun auch etwas. Es gibt auch solche OEMs, den gleichen Lieferanten – ohne darüber nachzudenken – für das nächste Projekt auswählen. Es ist „genug", wenn der Lieferant gut leistet, d.h. er kann die Anforderungen der Kunden vollständig erfüllen, es gibt keine Beanstandungen, oder wenn es doch welche gibt, können sie die Probleme sofort lösen. Diese Bemühungen werden von dem Kunden hochgeschätzt. Er drückt seine Anerkennung mit einem neuen Vertrag oder mit einem Projekt aus. So konnte es auch passieren, dass ein OEM mit 4 neuen Projekten den Lieferanten beauftragt hat, da es in den alten „Partner-Projekten" keine Qualitätsreklamationen gab.

Mittlere Unternehmen

Über die mittleren Unternehmen kann man das gleiche sagen, wie über die Großunternehmen. Es gibt Abweichungen bezüglich der 2 Lieferantentypen, aber sie sind unbedeutend. Diese Unternehmen halten auch persönlich für wichtig ihre Lieferantenpartner kennenzulernen, zu erfassen, was sieeigentlich (Lieferantenaudit 93-95%) können. So können wir das anhand den Daten behaupten, dass sie bei den neuen Unternehmen die Referenz (33% - 16%), bzw. die Daten und die Informationen von der Webseite (50% - 33%) für wichtiger halten, als bei den vorhandenen Partnern. Es ist ja aber zu verstehen (*Tabelle 4*.).

Tabelle 4 Rangliste der von mittleren Unternehmen bevorzugten Auswahlmethoden

METHODEN	VORHANDENE LIEFERANTEN	NEUE LIEFERANTEN
Besuch vor Ort	83%	100%
Referenzen	16%	33%
Lieferantenaudit	93%	95%
Information auf der Lieferanten Webseite	33%	50%

Quelle: Eigene Darstellung (2016), N=212

83% von den mittleren Unternehmen, die den Fragebogen ausgefüllt haben, halten im Falle der vorhandenen Lieferanten für wichtig sie zu besuchen und sie besuchen 100 prozentig die neun Lieferanten, die in die Lieferantenbasis aufgenommen werden wollen (*Abbildung 1.*).

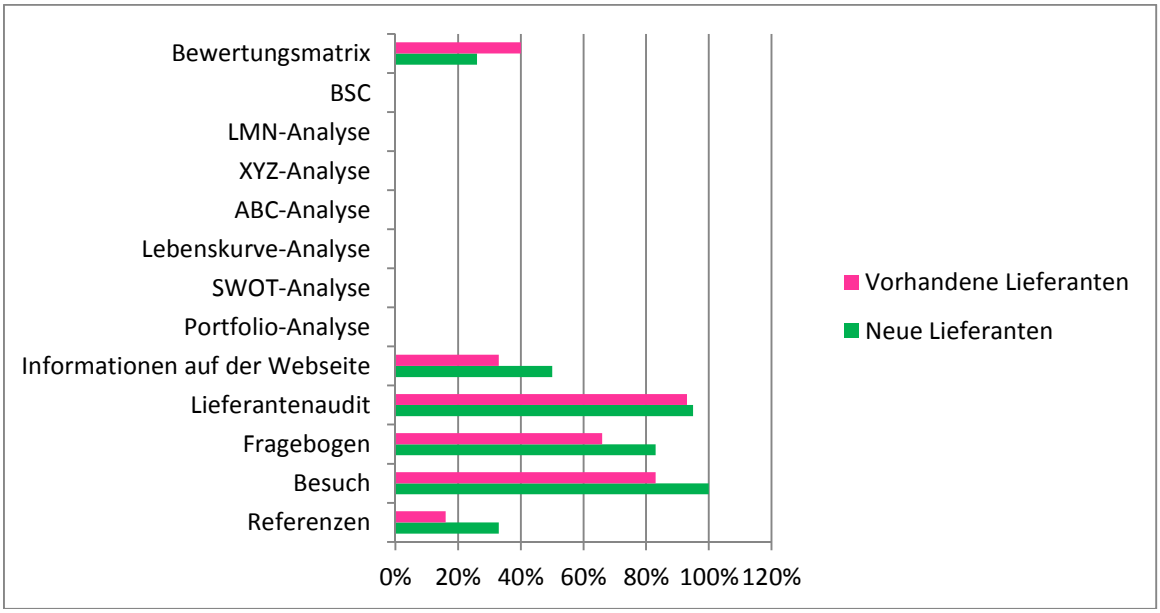

Abb. 1 Rangliste der von mittleren Unternehmen bevorzugten Auswahlmethoden

Quelle: Eigene Darstellung (2016), N=212

Anhand der Ergebnisse des Diagramms kann man feststellen, dass diese Unternehmen gleiche Methoden für die Lieferantenauswahl anwenden, nur die Gewichtigkeit der Faktoren kann dieses Verhältnis beeinflussen. Sie benutzen lieber die Methoden, die keine große Fachkenntnisse, keine Formeln, keine Überblick über die Zusammenhänge benötigen. Den Bewerbern werden einfache Fragen gestellt, um die entsprechendste Antwort bekommen zu können. Es bedeutet aber nicht, dass sie nicht alles berücksichtigen, bzw. nicht mit Vorsicht vorgehen würden. Bei diesen Unternehmen kommt es selten vor, dass sich eine besondere Abteilung mit den Lieferanten beschäftigt. Anhand dieser Auswertung kann man auch feststellen, dass die Kunden die Methoden vorzugsweise anwenden, die schon bewährt, bekannt und seit langem benutzt sind. Andere Methoden oder Verwendungsalternativen probieren sie nicht gerne aus, die für sie fremd sind, obwohl sie im Beruf schon bekannt sind. Es würde für die Unternehmen sowohl einen finanziellen als auch einen Zeitaufwand bedeuten. Ob die Firmen eigentlich diese Methoden kennen, werden wir es später detailiert analysieren.

Das Ziel ist am Leben zu bleiben, die auf dem Markt gegenüber den „Großen“ zu behalten. Es gibt einige Methoden wie bei den mittleren Unternehmen, die schon gut bewährt sind und funktionieren. Warum müsste man sie dann wechseln? Es bedeutet Geld- und Zeitaufwand. Alle Unternehmen (100%), die an dieser Forschung teilgenommen haben, halten die Informationen für wichtig die auf den Webseiten der Lieferantengefunden werden können und anhand dieser Angaben können sich diese Firmen über den Lieferantenpartner informieren. Die erste Frage ist, ob die Produktpalette des Lieferanten ins Produktspektrum hineinpassen kann, das von den Kundenfirmen gesucht wird. Auf der Firmenwebseite können die folgenden Informationen gefunden werden, wie z. B Unternehmensstruktur, Unternehmensgeschichte, Referenzen, Produktpalette, angewendete Verfahren und nicht zuletzt die Erreichbarkeit.

Kleinunternehmen

Anhand der *Abbildung 2* kann man sagen, dass die Kleinunternehmen keinen Unterschied machen, was die zwei Lieferantentypen angeht.

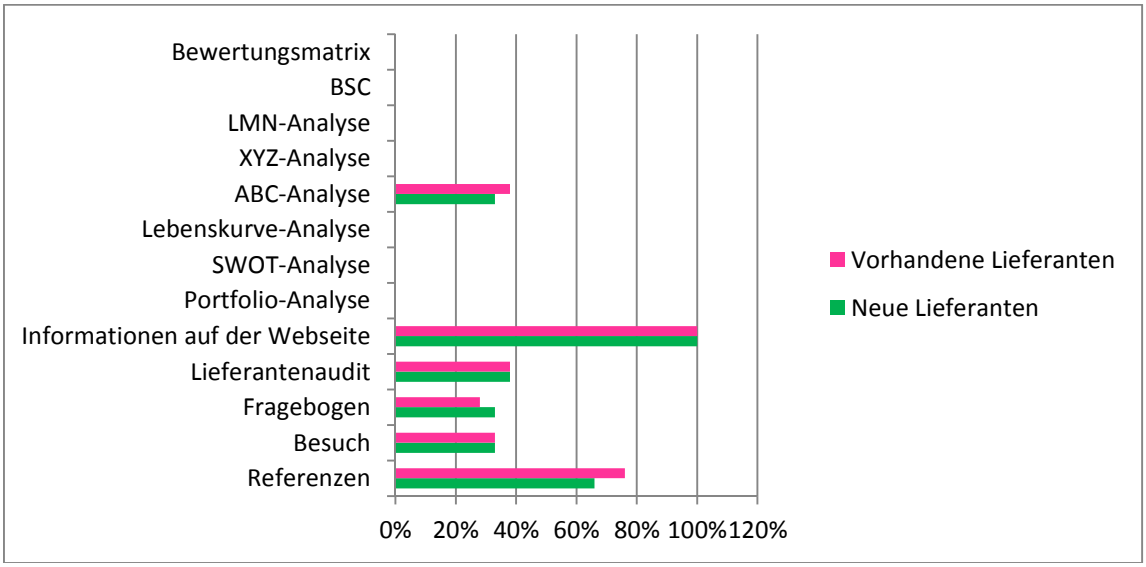

Abb. 2 Rangliste der von Kleinunternehmen bevorzugten Auswahlmethoden

Quelle: Eigene Darstellung (2016), N=212

Im Falle von beiden „Gruppen“ werden die folgenden Methoden, oder irgendeine der Methoden angewendet: Referenzen, Besuch, ein von den Lieferanten ausgefüllter Fragebogen Lieferantenaudit, Informationen auf der Lieferantenwebseite, bzw. ABC-Analyse (*Tabelle 5*.).

Tabelle 5 Von den Kleinunternehmen bevorzugte Auswahlmethoden (%)

METHODEN	VORHANDENE LIEFERANTEN	NEUE LIEFERANTEN
ABC – Analyse	38%	33%
Referenzen	76%	66%
Lieferantenaudit	38%	38%
Information auf der Lieferanten Webseite	100%	100%

Quelle: Eigene Darstellung (2016), N=212

Die oben angegebene Tabelle kann es auch gut darstellen, welche Auswahlmethoden am häufigsten von den Kleinunternehmen angewendet werden. In diesem Fall können wir auch den gleichen

Schluss ziehen, wonach sich diese Unternehmen nicht streben, komplizierte Formeln anzuwenden oder Zusammenhänge aufzubauen. In den Kleinunternehmen, die Auswahl der Lieferanten erfolgt durch den Geschäftsführer im Allgemeinen, der auch noch andere Aufgabe erledigen muss. Es gibt keine besondere Abteilung zur Erledigung dieser Aufgabe. Infolgedessen wenden diese Firmen im Laufe des Prozesses die einfachsten Methoden an.
Von den Auswahlmethoden, die im Fragebogen aufgelistet wurden, wenden keine Firmen die LMN-Auswahlmethode an. Während der Abfragung wurde diese Frage nicht diskutiert, d.h. es wurde auf die Frage keine Antwort gesucht, warum man diese Analyse nicht anwendet. Aber es wäre doch interessant doch zu wissen warum. Vielleicht müsste man die Antwort unter den Eigenschaften der Methode suchen. Über die anderen Methoden kann auch das gleiche festgestellt werden. In allen Fällen kann man behaupten, dass nur die Großunternehmen die folgenden Methoden ausnahmsweise anwenden, wie z. B Portfolio-, SWOT-, XYZ-, Lebenskurve-Analyse, BSC. Natürlich, nicht in hoher Prozentzahl aber sie werden angewendet. Von den erwähnten haben die Lebenskurve und das BSC den gleichen Wert erreicht (19%) (*Tabelle 6*). Die Bewertungsmatrix, deren Benutzung nicht zu kompliziert ist und kein größeres Fachwissen erfordert, wird auch von den mittleren Unternehmen vorzugsweise benutzt (26-40%).

Tabelle 6 Von den Unternehmen bevorzugte Auswahlmethoden (%)

	METHODEN	**Groß-Unternehmen**	**Mittlere Unternehmen**	**Klein-unternehmen**
VORHANDENE LIEFERANTEN	ABC – Analyse	33%	-	38%
	Lebenskurve-Analyse	19%	-	-
	BSC	19%	-	-
	Information auf der Webseite	10%	35%	100%
	Bewertungsmatrix	38%	40%	-
	METHODEN	**Groß-Unternehmen**	**Mittlere Unternehmen**	**Kleinunternehmen**
NEUE LIEFERANTEN	ABC – Analyse	17%	-	33%
	Lebenskurve-Analyse	19%	-	-
	BSC	19%	-	-
	Information auf der Webseite	30%	50%	-
	Bewertungsmatrix	38%	26%	100%

Quelle: Eigene Darstellung (2016), N=212

Wir müssen auch noch über die ABC-Analyse reden, ihre Anwendung ist lieber bei den Kleinunternehmen verbreiteter (33-38%). Wenn wir die Vorteile dieser Methoden berücksichtigen, können wir berechtigt feststellen, dass die ABC-Analyse im Kreis der Kleinunternehmen eine Methoden von denen ist, die am besten und am leichtesten benutzt werden können. Wenn wir aus diesen Methoden eine Rangliste aufstellen, wird sie dann folgendermaßen aussehen, was auch in der *Abbildung 3-4*dargestellt wird.

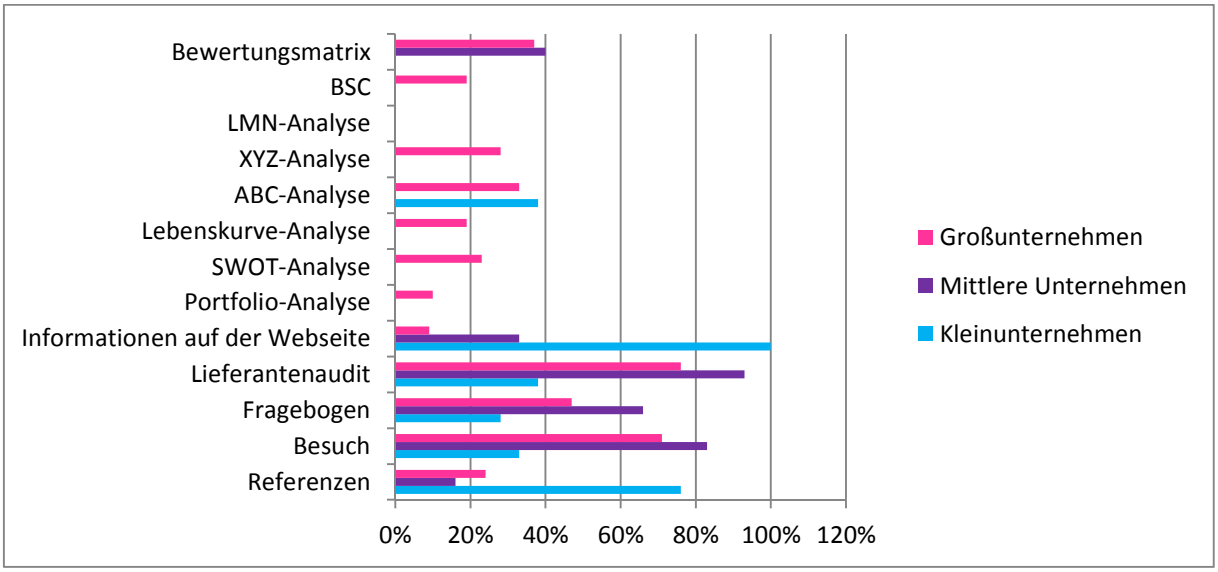

Abb. 3 Anwendung der Auswahlmethoden im Fall der vorhandenen Lieferanten (%)
Quelle: Eigene Darstellung (2016), N=212

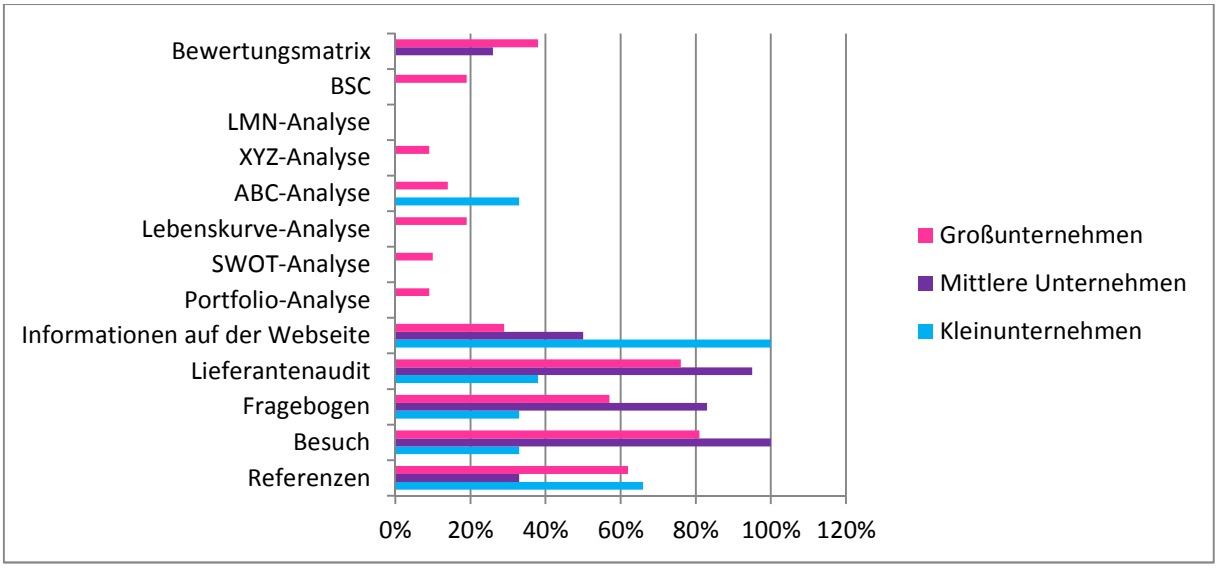

Abb. 4 Anwendung der Auswahlmethoden im Fall der neuen Lieferanten (%)
Quelle: Eigene Darstellung (2016), N=212

Kenntnisse der Auswahlmethoden

Der Fragebogen hat auch Fragen enthalten, wie gut die Firmen die Auswahlmethoden kennen, wie gut sie über die Methoden informiert sind, die in der Fachliteratur gefunden werden können. Kennen sie diese Methoden, oder kennen sie, aber sie werden von ihnen nicht angewendet, bzw. haben wie letzten Endes über die gegebene Methode nicht einmal gehört. Die zu diesem Thema gehörende Bewertung wird in der *Abbildung 5* veranschaulicht.

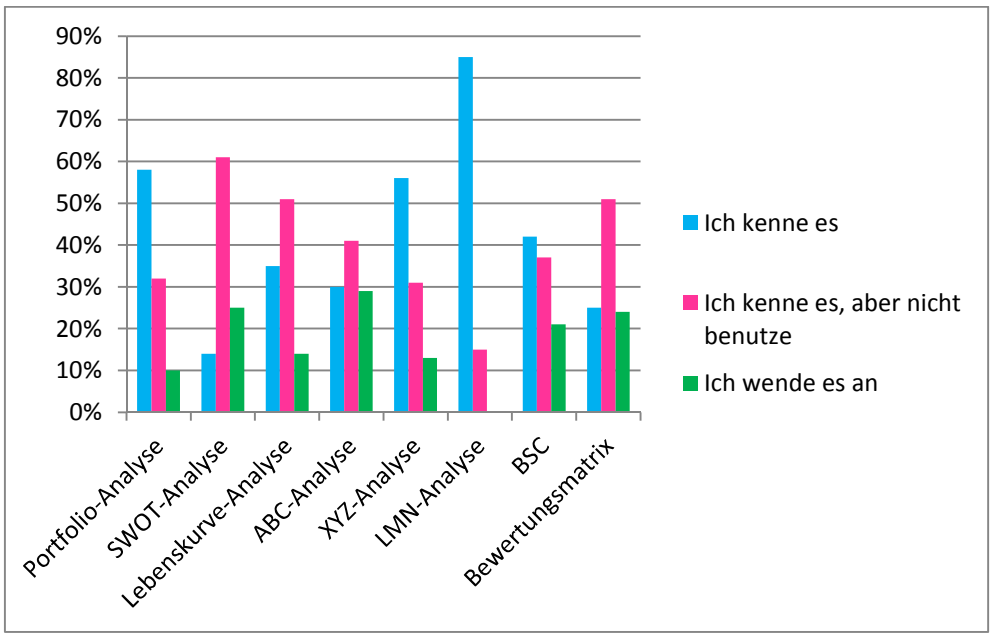

Abb. 5 Kenntnis der Auswahlmethoden im Kreis der Unternehmen

Quelle: Eigene Darstellung (2016), N=212

Anhand der zusammengezogenen Ergebnisse die 3 am meisten nicht gekannten Auswalmethoden, die Portfolio-Analyse (58%), XYZ-Analyse (56%) und die LMN-Analyse. Die kennen 85% der Firmen gar nicht. Nur 15% der Unternehmen haben gesagt, dass sie die LMN-Methode kennen, aber benutzen sie nicht. In der 2. Kategorie („ich kenne, aber nicht benutze diese Methode“) der Forschungsfrage hat die SWOT-Analyse 61% erreicht, die ziemlich gut gekannt ist und zur Aufdeckung des Problems benutzt werden kann. An der zweiten Stelle stehen, obwohl die Lebenskurve als auch die Bewertungsmatrix mit 51%. Nur 29% der Unternehmen, die an der Forschung teilgenommen haben, benutzt die ABC-Analyse, 25% von ihnen wenden die SWOT-Analyse an und 24% von diesen Unternehmen verwendet die Bewertungsmatrix. Wie es früher erwähnt wurde, benutzt keines von diesen Unternehmen die LMN-Analyse und nur 10% dieser Firmen wenden die Portfolio-Analyse an.

KONKLUSION

Wir wollten mit dieser Fallstudie, ein aktuelles Bild über den Status der Lieferantenauswahl in der Automobilindustrie in Ungarn geben. Es kann festgestellt werden, dass die Unternehmen den Methoden treu sind die schon gut bewährt sind und sie wollen sie nicht gerne wechseln. Es bedeutet finanziellen Aufwand und auch Zeitaufwand. Es gibt in der Fachliteratur viele Methoden, die anhand der verschiedenen Schemen aufgebaut werden, aber das Wesen ist gleich, man will den geeignetsten den geeigneten Lieferanten finden. Es gibt Methoden, die überhaupt nicht angewendet werden, und es gibt auch solche, die unbekannt sind.
Alles in allem können Folgerungen gezogen werden, es kann auch festgestellt werden, dass die Methoden von den Unternehmen angewendet werden, am einfachsten sind und am leichtesten zur Lieferantenauswahl benutzt werden können. Es gibt Unternehmen, in denen diese Aufgaben zum Geschäftsführer gehören und es gibt auch solche Firmen, wo eine besondere Abteilung zur Erledigung dieser Aufgaben zustande gebracht worden ist. Natürlich ist im zweiten Falle ist das Know-How auch höher, was sicherlich im Zusammenhang mit dem Vorhandensein der finanziellen Quellen stehen kann (Lehrgänge, Erweiterung und Entwicklung der Kenntnisse). Aber das Ziel ist

für alle Kunden gleich, den entsprechendsten Lieferanten für das nächste Projekt finden und auswählen zu können.

LITERATURVERZEICHNIS

[1] Aberle, G.: *Transportwirtschaft*, 3. überarbeitete Auflage, R. Oldenbourg Verlag, München, Wien, p. 474., 2000
[2] Balogh, T.: *Tudománypolitika, A szakértői bírálattól a portfólió-elemzésig*, Magyar Tudomány, 2001. március (2001/3.) http://epa.oszk.hu/00700/00775/00028/index.htm Letöltés: 2012.január 18.
[3] Busics, Gy.: *Minőségbiztosítás*, Nyugat-Magyarországi Egyetem, Székesfehérvár, 2005
[4] Disselkamp, M. – Schüller, R.: Lieferantenrating, Instrumente, Kriterien, Checklisten, Gabler Verlag, 1. Auflage, Wiesbaden; p. 48., 2004
[5] Domschke, W. – Scholl, A.: *Grundlagen der Betriebswirtschaftslehre, Eine Einführung aus entscheidungsorientierter Sicht*, Springer Verlag, Berlin, Heidelberg, New York, p. 180, 2000
[6] Eyholzer, K.: *Effizientes Lieferantenmanagement als Erfolgsfaktor* In: Beschaffungsmanagement 04/2003, SVME Schweizerischer Verband für Materialwirtschaft und Einkauf, Aarau, 2003
[7] Eyholzer, K. – Münger, T.: *Endlich Transparenz im Lieferantenmanagement* In: Beschaffungsmanagement 04/2004, SVME Schweizerischer Verband für Materialwirtschaft und Einkauf, Aarau, 2004
[8] Gelei, A.: *Beszállítói típusok a hazai autóipari ellátási láncban –kompetencia alapú megközelítés*. Budapesti Corvinus Egyetem, Műhelytanulmányok Vállalatgazdaságtan Intézet, 74. sz. műhelytanulmány, HU ISSN 1786-3031, pp. 11-34., 2006
[9] Glantschnig, E.: *Merkmalsgestützte Lieferantenbewertung*. Zugl. Diss., Universität zu Köln: FördergesellschaftProdukt-Marketing, Düsseldorf, 1994
[10] Kortus-Schultes, D. – Ferfer, U.: Logistik und Marketing in Supply Chain, Gabler Fachverlage gmbH, Wiesbaden, 100 p., 2015
[11] Roussel, PH. A., Saad, K. N., Erickson, T. J., (Arthur D. Little Inc).: *Third Generation R&D, Managing the Link to Corporate Strategy*, Harvard Business School Press, Boston, Massachusett, 1991
[12] Sibbel, R. – Hartmann, F.: *Lieferanten unter der Lupe* In: Beschaffung aktuell, 11/2005, p. 72., 2005
[13] Szegedi, Z. –Prezenszki, J.: *Logisztika-menedzsment*, Kossuth Kiadó, Budapest, p. 452., 2003
[14] Vollmuth, H. J.: *Controllinginstrumente von A - Z*, 6. Auflage, Verlag Haufe, Freiburg, 2002

INTERNATIONAL SCIENTIFIC CONFERENCE ON ADVANCES IN MECHANICAL ENGINEERING
13-15 October 2016, Debrecen, Hungary

ENERGY EFFICIENT FEASIBLE AUTONOMOUS MULTI-ROTOR UNMANNED AERIAL VEHICLES TRAJECTORIES

[1]NEMES Attila, [2]MESTER Gyula PhD

[1,2]Óbuda University, Doctoral School on Safety and Security Sciences, Budapest, Hungary
E-mail: [1]mr.attila.nemes@gmail.com, [2]drmestergyula@gmail.com

Abstract
In this paper an energy efficient multi-rotor autonomous unmanned aerial vehicles trajectory design is presented. Multi-rotors like quad- and hexa-rotors are popular representatives of unmanned aerial vehicles (UAVs) as they are relatively simple to build and easy to control, while being of versatile applicability, capable of vertical take-off and landing. Also the UAVs architecture has simple mechanics, high relative payload capability and good maneuverability. Disadvantages are the increased helicopter weight and increased energy consumption due to extra motors.
Keywords: *quad- and hexa-rotors, unmanned aerial vehicles, energy efficient trajectory design.*

1. INTRODUCTION

Small model vehicles are harder to control than the full sized real vehicles as the models have significantly lower mass, lower inertia, which induces much shorter time constants. Control mechanisms as PID, back stepping (computed torque) and their fuzzy variants have been well studied and successfully used on many systems [1]. Benchmarking and qualitative evaluation of different autonomous quadrotor flight controllers was presented in [2]. Three characteristic representatives of flight control techniques were considered: PID, back stepping and fuzzy. Dynamic performances, trajectory tracking precision, energy efficiency and control robustness upon stochastic internal and/or external perturbation was considered. Two experimental scenarios were constructed for a characteristic benchmarking procedure: dynamic quadrotor flight in a 3D loop manoeuvre and a typical cruising flight along the trajectory introduced by setting waypoints with pre-defined GPS coordinates. Through analysing simulation results the back stepping method presented the best control performances in sense of trajectory tracking precision. The other two algorithms had presented slightly better characteristics in sense of energy efficiency. By increasing the flight speed dynamic effects become influential on the system performances: the back stepping method was more sensitive to increased flight speeds than the PID and the fuzzy logic controller – as studied in [2], where the dominant chattering characteristics of actuator signals is obvious; the system has significant difficulties in precisely tracing the designated trajectories. As all three control algorithms are mature, proven on many real life and simulation environments, it is probable that the prescribed path is not suitable for multi-rotors. The state space trajectory has to be more carefully designed than connecting control points of desired body position coordinates.

2. OVERVIEW OF OPTIMAL TRAJECTORY DESIGN METHODS

The basic problem to solve is moving a body of mass m from point A to point B. In general there are set boundaries of the trajectory in terms of allowed geometrical regions or obstacles, velocity, acceleration or even jerk (third time derivative of displacement) limits are defined. Usually time optimality and/or energy optimality requirements set. The theoretical approach starts with plotting a 3D geometric path curve from A to B. The time optimal solution is then selecting the shortest

geometric displacement curve s and traveling along this path with v_{max} the maximum allowed velocity for $t_f = s/v_{max}$. A trajectory for mass m where instant v_{max} maximum speed is planned from point A and instant stop to zero at t_f in point B is not feasible: there has to be acceleration and deceleration period. This realization was adopted in „bang-bang" trajectory plans, where the first part of the trajectory was planned for a_{max} constant maximal acceleration until reaching v_{max}, then traveling with v_{max} for the appropriate distance and finally decelerating with a constant maximal deceleration $-a_{max}$ to reach the target. These "bang-bang" trajectories were dubbed „time optimal" trajectories, though obviously for $a_{max} = v_{max}/(t_f/2)$ we get $\sqrt{s/a_{max}} > s/v_{max}$. These „bang-bang" trajectories imply that we plan for using discontinuous force actions $F(t_0) = 0$, then in the next infinitesimally close time $F(t_0 + \varepsilon) = F_{max} = m \cdot a_{max}$; also when reaching the target it plans for an instant drop from $F(t_f - \varepsilon) = F_{max}$ to $F(t_f) = 0$, which is also not feasible in real life for non-rigid bodies. For these trajectories the best we can do is to apply fast and strong enough control loops so that the controlled system transient period is acceptably small, while the overshoot and the settling time also remains "controlled". Still well noticeable remain the immense energy spikes used for achieving these fast discontinuous transients, compensating for overshoots and the resulting vibrations, oscillations after the rise time – be it mechanical or electrical in nature. These effects increase wear and reduce the life span of physical systems. Vibrations are also highly undesirable for precise path tracking. For robotic manipulators (RM) the lowest vibration levels were identified to correspond to the magnitude of the second time derivative of the torque, while an appropriately constructed trajectory can decrease oscillations and energy consumption by a factor of 10 [3].

To have smooth acceleration its rate of change has to be continuous. The term (n times) smooth is used as in being equivalent to having continuous (n^{th}) time derivative. The first derivative of acceleration, which is the third time derivative of the displacement is called jerk $j = d^3s/dt^3 = \dddot{s}(t)$. Minimum jerk trajectories are constructed by minimization of a cost function like $C(s) = \frac{1}{2}\int_0^{t_f} \dddot{s}(t)^2 dt$. Calculus of variation or Hamiltonian with Lagrange functions is the usual tool to solve this mathematical problem, where a perturbation function $\delta(t)$ is added with a constant multiplier α in the form of $s(t) + \alpha \cdot \delta(t)$, such that for boundary conditions the perturbation and its derivatives are 0 like $\delta(x) = \dot{\delta}(x) = \ddot{\delta}(x) = \dddot{\delta}(x) = 0$ for $x = 0$ and $x = t_f$. Based on calculus of variations instead of minimizing $C(s(t) + \alpha \cdot \delta(t)) = \frac{1}{2}\int_0^{t_f} (\dddot{s}(t) + \alpha \cdot \dddot{\delta}(t))^2 dt$ the zero point of its partial derivative for $\alpha = 0$ is calculated like $\partial C(s + \alpha\delta)/\partial\alpha|_{\alpha=0} = \int_0^{t_f} (\dddot{s}(t) + \alpha \cdot \dddot{\delta}(t)) \cdot \ddot{\delta}(t) dt\big|_{\alpha=0} = \int_0^{t_f} \dddot{s}(t) \cdot \ddot{\delta}(t) dt$. Using boundary conditions the result is $-\int_0^{t_f} s^{(6)}(t) \cdot \delta(t) dt = 0$, which according to the calculus of variations is equivalent to the requirement of having the sixth derivative of the displacement equal to zero: $s^{(6)}(t) = 0$. Knowing the boundary conditions of the trajectory $s(x) = \dot{s}(x) = \ddot{s}(x)$ at $x = 0, x = t_f$ the a, b, c, d, e parameters can be calculated as a polynomial trajectory $s(t) = a + bt + ct^2 + dt^3 + et^4 + ft^5$, $s(t) = b + 2ct + 3dt^2 + 4et^3 + 5ft^4$, $s(t) = 2c + 6dt + 12et^2 + 20ft^3$. For such trajectories jerk $j(t = 0) = s(t = 0) = 6d$, obviously starts with an instantaneous jump from 0 to $6d$, also at the final moment $t = t_f$ there is a jump from a non-zero to 0; again planning for discontinuity in a physical quantity. Even for the simplest direct electro-motor actuator considering $i_e(t) \cong const_1 \cdot \tau(t) = const_2 \cdot a(t)$ model the discontinuity in jerk means a discontinuity in $di_e(t)/dt$, which is nonsense, since in an electro-motor the armature voltage depends on $di_e(t)/dt$. Also if we accept the paradigm of not planning for a discontinuity of the second derivative of the linear displacement (acceleration), we have to accept the same for the rotation displacement as well, and we have $di_e(t)/dt = 1/K_\tau \cdot (J_m\ddot{\omega} + \mu_m\dot{\omega})$, where ω is the rotation speed, the time derivative of the rotor position, K_τ is the torque constant, J_m is the motor inertia, and μ_m is the rotor friction coefficient.

In [4] Pontryagin defined the notion of mathematical theory of optimal processes. To minimize the total used energy E_{t_f} of moving mass m from A to B, a cost function like $E_{t_f} = \int_0^{t_f} P_{abs}(t)dt$ is devised by cumulating the absolute value of the instantaneous applied power $P_{abs}(t) = |F(t)v(t)| + |\tau(t)\omega(t)|$ through which the product of the absolute acceleration and velocity function profile of the shortest geometric path is minimized. Since $P_{abs}(t) = \sum_i m_i \cdot |a_i(t)| \cdot v_i(t)$ this minimization process is very similar to looking for the minimal jerk trajectory, only that here we are actually looking for a kind of minimal acceleration trajectory, which results in a polynomial trajectory of order 5, with a discontinuity in acceleration for $t = 0$ and $t = t_f$. As we have previously discussed: this induces oscillations. A sudden jerk induces vibrations and in case of vehicles like elevators, high speed trains, rolocosters the ride is very uncomfortable at those points.
For electrical systems the energy minimum cost function is devised with electric voltage and current like $P_{abs}(t) = |v_e(t) \cdot i_e(t)|$. For electro-motor torque actuated mechanical systems like RMs or multi-rotor unmanned aerial vehicles (UAVs) cost functions like $E_{t_f} = \int_0^{t_f} \tau_{abs}(t)dt$ are also used to minimize the total used actuator energy (torque) as in a stationary state of the actuators it is common to use a simplified motor torque model, where the applied current is linearly proportional to the resulting torque $i_e(t) \cong const \cdot \tau(t)$ [5]. Limiting the actuator torque vibration must not be considered only as a mathematical problem of limiting $|\ddot{q}|$. In trajectory plans not the extent of discontinuity in a physical quantity is the problem, but the existence of a discontinuity itself.
Researches [6-7] are pointing out that applying input shaping instead of direct step change, for example in BLDC rotor speed control both the unwanted oscillations and the energy consumption can be reduced and responsiveness of the system can be increased; when there are no current spikes, much less energy used [8]. The pioneering work of [9] relying on [4] presents a time optimal trajectory design method for RMs, which accounts for pre-defined torque limits, while the optimisation problem is transferred to the trajectory space. Torque limits are transformed to acceleration limits. As the path $\boldsymbol{f}(s)$ describes the position of the end effector in the task coordinates, so state variables became parameterised functions $q = f(s), \dot{q} = f'(s)\dot{s}, \ddot{q} = f''(s)\dot{s}^2 + f'(s)\ddot{s}$. Finding optimal trajectories becomes finding the appropriate parametrisation s for $\boldsymbol{f}(s)$, given the pre-defined feasibility limits on torque in system dynamic equations. There are multiple approaches for multi-rotor UAV applications, starting from simple path plotting up to complete trajectory generation [10-13] describes the possibility of defining the major path milestones by visual fuzzy servoing, also any map based three search algorithm can be applied to define the next major target point during a flight mission. To facilitate both time and energy efficiency of flight the major path milestones are best connected with continuous curvature functions $\boldsymbol{f}(s)$ [14].

3. OVERVIEW OF MULTI-ROTOR UAV NAVIGATION DYNAMICS

Multi-rotors are popular representatives of UAVs as they are relatively simple to build and easy to control, while being of versatile applicability, capable of vertical take-off and landing. Also the multi-rotor architecture has simple mechanics, high relative payload capability and good manoeuvrability. The study of multi-rotor kinematics and dynamics is based on the physics of aerial platforms [15]. The kinematics and general force and torque dynamics of any symmetric multi-rotor (quad- or hexa- rotors) is the equivalent 6DOF dynamic system of mass m moved against the gravity acceleration g. Generalised translational forces: $m\left(\ddot{\boldsymbol{\xi}} + g[0\ 0\ 1]^T\right) = \boldsymbol{F}_{\xi}$; and generalised body torques are: $\boldsymbol{J}(\boldsymbol{q})\ddot{\boldsymbol{q}} + \boldsymbol{C}(\boldsymbol{q}, \dot{\boldsymbol{q}})\dot{\boldsymbol{q}} = \boldsymbol{\tau_B}$, where in analogy with robotic manipulators: $\boldsymbol{J}\ddot{\boldsymbol{q}}$ is the inertia matrix, $\boldsymbol{C}\dot{\boldsymbol{q}}$ is the Coriolis term, the state vector is composed from the Euler angles for roll, pitch and jaw $\boldsymbol{q} = [\phi, \theta, \psi]$. The roll and pitch of a multi-rotor UAV can be calculated from the path curve vector function $\boldsymbol{f}(t)=(x(t),y(t),z(t))$ and the required yaw motion $\psi(t)$ as presented in [14]:

$$\phi = asin\left(\frac{\dot{x}sin\psi - \dot{y}cos\psi}{\ddot{x}^2+\ddot{y}^2+(\ddot{z}+g)^2}\right), \theta = atan\left(\frac{\dot{x}cos\psi - \dot{y}sin\psi}{(\ddot{z}+g)}\right) \quad (1)$$

Minimum-snap polynomial trajectories are proven good for quadrotors, "since the motor commands and attitude accelerations of the vehicle are proportional to the snap, or forth derivative, of the path" [16]. In [16] the rotor blade velocity is considered as an arbitrary control input. As minimum-snap polynomial trajectories are discontinuous in displacement crackle, fifth derivative of displacement, this is a sub-optimal approach; again: the rotor blade velocity is not an arbitrary theoretical control signal, but a real electro-mechanical physical system under aerodynamically load conditions.
The goal of this paper is to present a new method for efficient real-time direct path parametrisation, which is capable of generating physically feasible, time-and energy optimal, bounded, continuous trajectories for autonomous navigation [17]. The notion of time and energy optimality is not used in mathematics theory manner, but in real life physically feasible engineering manner. Finding optimal trajectories is focused on finding the appropriate parametrisation for the path vector function ***f(t)***, given the pre-defined feasibility limits on the displacement time derivatives, in conjunction with the effects of the path curvature. The defined boundary conditions of the trajectory have to be satisfied. The defined limits on maximum values for arbitrary time derivatives of the displacement have to be obeyed. Continuity and smoothness of every trajectory component has to be ensured up to the predetermined order (5 in case of multi-rotors). As described in [17-19] to have realistic, feasible torques along a trajectory, which are efficiently controllable without chattering, we need smooth torque changes. For indirect rotor-blade propulsion systems (ships, multi-rotors) we have the propulsion motor force or torque $M_M(t) \approx const \cdot \omega(t)^2$ proportional to the square of the rotor angular velocity. The applied mechanical force or torque $M_B(t) \approx m * \ddot{\boldsymbol{\mu}}(t)^2$ excreted onto the body is proportional with the second derivative of the linear position or rotation angle $\ddot{\boldsymbol{\mu}}(t)$ of the body. As the body is driven by a rotor blade, $\omega(t)$ is proportional to $\ddot{\boldsymbol{\mu}}$, the body acceleration. In reality no discontinuities can physically occur, not even in third time derivatives of a displacement.
Multi-rotor UAVs introduce yet another layer of complexity: their torque dynamics is similar to RMs, while they are propelled by a lift force of rotating blades fixed to the body $\vec{z}$ axes. Paths $[\boldsymbol{\xi}(t), \boldsymbol{\mu}(t)] = \big[\big(x(t), y(t), z(t)\big), \psi(t)\big]$defined along earth coordinate $\vec{x}, \vec{y}, \vec{z}$ axes extended with the desired jaw rotation angle $\psi(t)$ translate to body rotation coordinates $\boldsymbol{\mu}(t) = \big(\varphi(t), \theta(t), \psi(t)\big)$ as defined by equation (2) like $\varphi(t) = \varphi\big(\ddot{x}(t), \ddot{y}(t), \ddot{z}(t)\big)$, and $\theta(t) = \theta\big(\ddot{x}(t), \ddot{y}(t), \ddot{z}(t)\big)$, which means $\boldsymbol{\mu}(t) = \boldsymbol{\mu}\left(\ddot{\boldsymbol{\xi}}(t)\right)$. Thus from the torque equation we can conclude $\boldsymbol{\tau_B}(t) = \boldsymbol{\tau_B}\big(\boldsymbol{\xi}^{(4)}\big)$, where $\boldsymbol{\xi}^{(4)} = d^4\boldsymbol{f}(\boldsymbol{t})/dt^4$ is the fourth time derivative of the displacement curve vector function ***f(t)***. This means that we have the body torque being a function of the displacement snap, the fourth time derivative of the displacement. This is the point where [15] draws the conclusion to use minimum snap trajectories. But this is not the complete picture! For multi rotors the control signal is the angular velocity of the rotor blade, which is not an arbitrary 'just a mathematical' function; it is a real physical system! For BLDC actuators $i_e(t) \approx const_2 \cdot \tau_{Bi}(t) = const_2 \cdot (\boldsymbol{J_i}(\boldsymbol{\mu}) \cdot \ddot{\boldsymbol{\mu}} + \dot{\boldsymbol{\mu}}^T \cdot \boldsymbol{C_i}(\boldsymbol{\mu}) \cdot \dot{\boldsymbol{\mu}}) = const_2 \cdot \tau_{Bi}\big(\boldsymbol{\xi}^{(4)}\big)$ the discontinuity in snap ($\xi^{(4)}$) means a discontinuity in the electric current $i_e(t)$, which is physically not possible. Since the complete electrical and torque equation of an electric motor for rotor blade load is:

$$v_e(t) = L_e\frac{di_e}{dt} + R_e i_e + K_b\omega,\ K_\tau i_e - \tau_L = J_M\frac{d\omega}{dt} + \gamma_M\omega,\ \tau_L = J_R\frac{d\omega}{dt} + K_d\omega^2, \quad (2)$$

where the rotation velocity of the rotor is ω, and L_e, R_e are the electrical inductance and resistance of the armature, K_b is the back EMF parameter. K_τ is the torque constant, J_m is the motor inertia, and γ_M is the rotor friction coefficient. K_d is the rotor drag parameter and J_R the rotor blade inertia. So neither $\frac{d\omega}{dt}$ nor $\frac{di_e}{dt}$ is allowed to be discontinuous in real life. Further on from equation (2) we have: $\frac{di_e}{dt} = \frac{1}{K_\tau}\left((J_M + J_R)\frac{d^2\omega}{dt^2} + (\gamma_M + 2K_d\omega)\frac{d\omega}{dt}\right)$, which means that even $\frac{d^2\omega}{dt^2}$ has to be continuous. As τ_L dominantly depends on ω ($\tau_L \approx K_d\omega^2$), and we have already concluded that $\boldsymbol{\tau_B}(t) = \boldsymbol{\tau_B}\left(\boldsymbol{\xi}^{(4)}\right)$, **we can conclude that for a realistic, feasible control input of multi-rotor UAVs the designed path has to be such that the displacement snap ($\boldsymbol{\xi}^{(6)}$) must be continuous and $\boldsymbol{\xi(t)^{(4)} \sim \omega(t)}$.!** The major driving force behind the proposal of this paper is that by acknowledging the obligatory physical requirement of the actuator torque and the actuator electric motor current being at least 2 times smooth – so the actuator rotor displacement jerk ($\frac{d^2\omega}{dt^2}$) has no discontinuities: we must respect a physical requirement to have the $\boldsymbol{\xi}(t)$ multi-rotor displacement continuous up to pop, its 6th time derivative $\boldsymbol{\xi}^{(6)}(t) = d^6\boldsymbol{\xi}/dt^6$. Another observation is that since body torques $\boldsymbol{\tau_B}\left(\boldsymbol{\xi}^{(4)}\right)$ are induced by the combined electric motor torque equations (2), they cannot change at an arbitrary pace, the torque changes must obey the capability of the electric motor in terms of transient behaviour at changing the rotation speed $\tau_B\left(\boldsymbol{\xi}(t)^{(4)}\right) \approx K_d\omega^2(t)$.
After algebraic manipulations of equations (3-5) by Laplace transformations we conclude:

$$-Bs^2W - sW(C + DW) = KV_e - W(K^2 + R_e\gamma_M + R_eK_dW), \tag{3}$$

where $(J_M + J_R) = J, K_T = K_b = K$, $B = L_eJ, C = R_eJ + L_e\gamma_M, D = L_eK_d$. The right hand side represents the stationary mode of the electric motor, and the left hand side represents the dynamic transient mode. For the stationary case we can directly calculate the required v_e for an arbitrary stationary ω_{stat}. The solution of the left hand side, keeping the right hand side zero, defines the transient mode characteristic of the rotation speed $\omega_t(t)$ as $\omega_t(t) = \frac{\omega_{stat}}{2}\left(1 + tanh\left(\frac{\pi}{P}\left(t - \frac{P}{4}\right)\right)\right)$ where ω_{stat} is the targeted stationary rotation speed, P is the settling time of the transient [17].
The important message of the proposal of this paper based on [16] is that we must not overlook the physical capabilities, constraint of neither the system nor the actuator itself. For multi-rotors the body torques and matching rotation speed of rotors and their transient behaviour is limited – these constraints are proportional to properties of the trajectory displacement snap $\boldsymbol{s}(t) = \boldsymbol{\xi}^{(4)}(t)$. The snap is required to be 2 times smooth, which is equivalent to pop $\boldsymbol{p}(t) = \boldsymbol{\xi}^{(6)}(t)$ being continuous. Also the transient behaviour of rotor $\omega_t(t)$ has to be proportional to $1 + tanh\left(\frac{\pi}{P}\left(t - \frac{P}{4}\right)\right)$.

4. NEW ENERGY EFFICIENT, FEASIBLE, TIME OPTIMAL TRAJECTORY DESIGN RESULTS

The proposal is to use for the snap transient a base function in the form of:

$$\boldsymbol{c_t}(t) = \boldsymbol{\xi_t^{(5)}}(t) = \left(1 - cos\left(\frac{2\pi}{P}t\right)\right), \tag{4}$$

where P is equal to half of the settling time of the $\omega_t(t)$ actuated system [17]. By this we obtain pop base transient function as $\boldsymbol{p_t}(t) = \boldsymbol{\xi_t^{(6)}}(t) = \frac{2\pi}{P}\sin\left(\frac{2\pi}{P}t\right)$, actually all further derivatives of displacement will be continuous The detailed algorithm to generate arbitrary bounded, arbitrary

smooth trajectories is presented in [17]. The basic smooth trajectory parametrization curve used is presented for $P = 1$, sampling time $dt = 0.01$[s], which results in a feasible time optimal trajectory with dynamic boundaries for maximum of $pop = 2\pi$ [m/s^6] sinus wave of 1[s] period, maximum of $crackle = 2$[m/s^5], $maximum\_snap = 1$[m/s^4], $maximum\_jerk = 1$[m/s^3], $maximum\_acceleration = 2$[m/s^2], $maximum\_velocity = 8$[m/s], $displacement = 64$[m], within $duration = 16$[sec]. The integral of absolute jerk is 8[m/s^2], what is proportional to the expended energy (as mass and desired displacement we consider to be constant). This base trajectory parametrisation is projected to the training path, which results in training data worth of ~55 seconds of flight time along the major diagonals and edges of a 100m sized cube, while performing rotations around the z axes. For the general case of $P=1$ trajectory plots and corresponding smooth UAV body torques are:

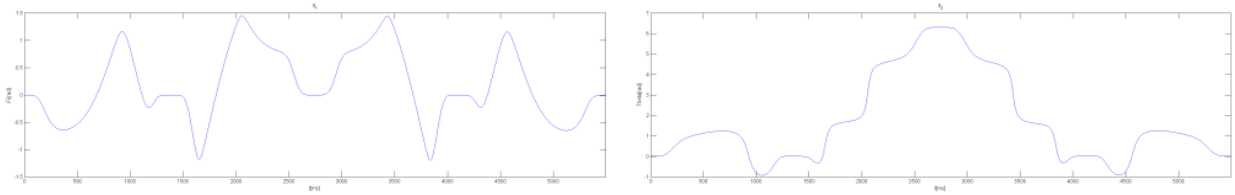

Figure 1,Trajectory – UAV body roll $\phi(t)$ and pitch $\theta(t)$

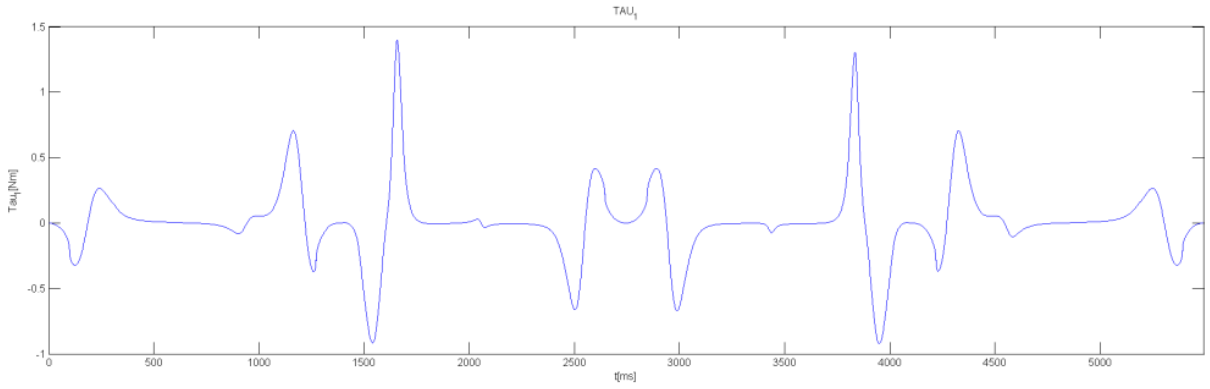

Figure 2, Trajectory – UAV body torque around the x axis.

CONCLUSIONS

The proposed trajectory design method is capable of forming bounded, smooth, energy efficient and time optimal trajectories with a single pass algorithm using closed formulas [17]. The design method is defined and validated on an example for a multi-rotor UAV path planning, where a single parameter controls the trajectory dynamics. The proposed trajectory design method results in real-life feasible smooth, limited torque transients, which is energy efficient for control signal design; while providing a flexible interface to arbitrary velocity, acceleration, jerk and snap limit enforcement. Dynamic transient properties and energy efficiency of the trajectory can be tuned with a single parameter, while the feasibility of torque transients is maintained. The resulting trajectory for the properly selected parameter is always the time optimal feasible solution, which complies with all defined limits. This paper presents a novel direct path construction algorithm [17] for generating physically feasible, time-and energy optimal, bounded, continuous trajectories, which are smooth up to the 5th time derivative of displacement for multi-rotor UAV trajectories introduced in [18-19] and used for multi-rotor UAV genetic fuzzy system identifications in [20-22].
Reduction of the method is strait forward to systems with simpler trajectory constraints, like RMs or wheeled vehicles, where it is enough to have smooth trajectories up to the 3rd time derivative of

displacement. The notion of time and energy optimality is not used in a mathematics theory manner but in real life physically feasible engineering manner. The generated trajectory can be applied as parametrisation to any vector function defined path $\boldsymbol{f}(t)=(f_x(r(t)),f_y(r(t)),f_z(r(t)))$. When determining the constraints on trajectory derivatives, one has to take into consideration both the system limits and curvature properties of the desired path $\boldsymbol{f}(t)$ and its derivatives. $\boldsymbol{f}(t)$ has to be smooth at least up to the required smoothness of the trajectory. The same basic principle of accounting for the actuator dynamics when planning for system trajectories can be also applied to other than electro motor actuated system, by replacing equations (3) to appropriate ones, and then evaluating their transient behaviour. When the actuator dynamics and its relation to the system trajectory is known, one can use the algorithm and the method described in this paper to design trajectories of required transient dynamics and smoothness by replacing equation (4) to the appropriate one [23-45].

REFERENCES

[1] A. Nemes: *Synopsis of Soft Computing Techniques Used in Quadrotor UAV Modelling and Control*, Interdisciplinary Description of Complex Systems, Vol.13, No.1, pp.15-25, 2015.
[2] A. Rodić, G. Mester, I. Stojković: *Qualitative Evaluation of Flight Controller Performances for Autonomous Quadrotors*, in E. Pap (Ed.): Intelligent Systems: Models and Applications, Vol.3, pp. 115–134. Springer-Verlag, Berlin Heidelberg, 2013.
[3] N. Varminska, D. Chablat: *Optimal Motion of Flexible Objects with Oscillations Elimination at the Final Point*, Eucomes, Nantes, Springer, 2016.
[4] L.S. Pontryagin, V.G. Boltyanskii, R.V. Gamkrelidze, E.F. Mishchenko: *The mathematical theory of optimal processes*, Interscience Publishers, New York, 1962.
[5] J.T. Betts: *A survey of Numerical Methods for Trajectory Optimization, Mathematics and Engineering Analysis*, Boeing Information and Support Services, Washington, 1998.
[6] R. Zwahlen, T. Chang: *Feedforward Speed Control of Brushless DC Motors with Input Shaping*, The 33rd Annual Conference of the IEEE Industrial Electronics Society (IECON), Taipei, 2007.
[7] M. Murugan, R. Jeyabharath, P. Veena: *Stability Analysis of BLDC Motor Drive based on Input Shaping*, International Journal of Engineering and Technology, Vol.5, No.2, pp.1169-1177, 2013.
[8] G. Venu, Dr. S. T. Kalyani: *A New Topology for Speed control of Sensor less BLDC Motor with Reduced Commutator Switches and Improved Input Power Factor*, International Journal Of Engineering And Computer Science, Vol.3, No.11, pp. 9243-9247, 2014.
[9] J.E. Bobrow, S. Dubowsky, J.S. Gibson: *Time-optimal control of robotic manipulators along specified paths*, Int. J. Robotic Research, 4(3):3-17, 1985.
[10] Y. Bouktri, M. Haddad, T. Chettibi: *Trajectory planning for quadrotor helicopter*, 16th Mediterranean Conference on Control and Automation, Ajaccio, 2008.
[11] A. Naghash, M. Naghshineh, A. Honari: *Minimum Time Trajectory Optimisation for Flying a Quadrotor in an 8-shaped Path*, International Micro Air Vehicle Conference and Flight Competition (IMAV2013), Toulouse, 2013.
[12] A. Sanchez, V. Parra-Vega, O. Garcia, F. Ruiz-Sanchez, L. E. Ramos-Velasco: *Time-Parametrization Control of Quadrotors with a Robust Quaternion-based Sliding Mode Controller for Aggressive Maneuvering*, European Control Conference (ECC), Zürich, 2013.
[13] M. A. Olivares-Mendez, I. F. Mondragón, P. Campoy, L. Mejías, C. Martinezm: *Aerial Object Following Using Visual Fuzzy Servoing*, in Proceedings of the 1st Workshop on Research, Development and Education on Unmanned Aerial Systems (REDUAS 2011), Centro Avanzado de Tecnologías Aeroespaciales (CATEC), Seville, Spain, pp. 61-70, 2011.
[14] T. Fraichard A. Scheuer: *From Reeds and Shepp's to continuous-curvature paths*, IEEE Trans. on Robotics and Automation, 20(6):1025–1035, 2004.
[15] R. Lozano: *Unmanned Aerial Vehicles*, ISTE Ltd, London, 2010.

[16] D. Mellinger, V. Kumar: *Minimum snap trajectory generation and control for quadrotors*, IEEE International Conference on Robotics and Automation (ICRA2011), pp. 2520 –2525, 2011.
[17] A. Nemes: *Tools for Efficient Soft Computing Modelling and Feasible Optimal Control of Complex Dynamic Systems, Multi-Rotor Unmanned Aerial Vehicle Navigation with Obstacle Avoidance*, PhD Thesis, Óbuda University, Doctoral School on Safety and Security Sciences, Budapest, 3rd October, 2016.
[18] A. Nemes: *Continuous Periodic Fuzzy Logic Systems and Smooth Trajectory Planning for Multi-Rotor Dynamic Modeling*, Acta Polytechncia Hungarica, 2016, in press.
[19] A. Nemes: *Fuzzy-Genetic Control of Quadrotors Unmanned Aerial Vehicles*, Interdisciplinary Description of Complex Systems, Vol.14, No 2, pp.223-235, 2016.
[20] A. Nemes: *Genetic Algorithm-Based Adaptive Fuzzy Logic Systems for Dynamic Modeling of Quadrotors*, Proceedings of the 3rd International Conference MechEdu, pp.96-103 Subotica, 2015.
[21] A. Nemes: *Genetic Fuzzy Identification Method for Quadrotor UAVs*, Annals of Faculty of Hunedoara – International Journal of Engineering, Tome XIII, Fascicule 3, pp. 257-264, 2015.
[22] A. Nemes, G. Mester: *Unconstrained Evolutionary and Gradient Descent-Based Tuning of Fuzzy partitions for UAV Dynamic Modeling*, FME TRANSACTIONS, Vol.45, No.1, pp.1-8, paper No: 16 – 136, 2017, in press.
[23] C. Richter, A. Bry, N. Roy: *Polynomial Trajectory Planning for Quadrotor Flight*, Proceedings of the International Symposium of Robotics Research (ISRR), 2013.
[24] A. Nemes, B. Lantos: *Genetic Algorithms-Based Fuzzy Logic Systems for Dynamic Modeling of Robots*, Periodica Polytechnica Electrical Engineering, Vol. 43, No. 3, pp.177-187, 1999.
[25] A. Nemes, B. Lantos: *Optimization of Fuzzy Logic Systems for Gray-Box Dynamic Modeling of Robot Manipulators by Genetic Algorithms*, Proceedings of IEEE INES'99. pp. 353-358, 1999.
[26] A. Nemes, B. Lantos, *Training Data Reduction for Optimisation of Fuzzy Logic Systems for Dynamic Modelling of Robot Manipulators by Genetic Algorithms*, Proceedings of IEEE Instrumentation and Measurement Technology Conference, Vol.3, pp. 1418-1423, 2001.
[27] G. Mester: *Distance Learning in Robotics*, Proceedings of The Third International Conference on Informatics, Educational Technology and New Media in Education, pp.239-245, Sombor, 2006.
[28] G. Mester: *Improving the Mobile Robot Control in Unknown Environments*, Proceedings of the Conference YUINFO' 2007, pp. 1-5, Kopaonik, 2007.
[29] G. Mester, A. Rodic: *Modeling and Navigation of an Autonomous Quad-Rotor Helicopter*, E-society Journal: Research and Applications, Vol.3, No.1, pp.45-53, 2012.
[30] G. Mester, A. Rodic: *Navigation of an Autonomous Outdoor Quadrotor Helicopter*, 2nd Int. Conference on Internet Society Technology and Management, pp. 259-262, Kopaonik, 2012.
[31] G. Mester, A. Rodic, J. Stepanic: *Nonlinear Control of Aerial Robotics*, Modern Approach to Product Development and Business Improvement, Balatonfüred, 2013.
[32] G. Mester, A. Rodic: *Négyrotoros robothelikopter modellje és irányítása*, A Magyar Tudomány Napja a Délvidéken, Vajdasági Magyar Tudományos Társaság, Újvidék, pp.469-476, 2013.
[33] G. Mester, A. Rodic: *Simulation of Quad-rotor Flight Dynamics for the Analysis of Control, Spatial Navigation and Obstacle Avoidance*, Proceedings of the 3rd International Workshop on Advanced Computational Intelligence and Intelligent Informatics, pp.1-4, Shanghai, 2013.
[34] G. Mester: *Backstepping Control for Hexa-Rotor Microcopter*, Acta Technica Corviniensis – Bulletin of Engineering, Tome VIII, Fascicule 3. pp. 121-125, 2015.
[35] G. Mester: *Modeling of Autonomous Hexa-Rotor Microcopter*, Proc. of the 3rd Int. Conference and Workshop Mechatronics in Practice and Education, pp.88-91, Subotica, 2015.
[36] A. Rodić, G. Mester: *Modeling and Simulation of Quad-Rotor Dynamics and Spatial Navigation*, Proceedings of the SISY 2011, 9th IEEE International Symposium on Intelligent Systems and Informatics, pp.23-28, Subotica, 2011.

[37] A. Rodić, G. Mester: *Remotely Controlled Ground-Aerial Robot-Sensor Network for 3D Environmental Surveillance and Monitoring*, invited talk, TAMOP 422 Workshop, Szeged, 2011.
[38] A. Rodić, G. Mester: *The Modeling and Simulation of an Autonomous Quadrotor Microcopter in a Virtual Outdoor Scenario*, in Acta Polytechnica Hungarica, Vol. 8, No. 4, 2011, pp. 107-122
[39] A. Rodić, G. Mester: *Control of a Quadrotor Flight*, Proceedings of the ICIST Conference, pp.61-66, Kopaonik, 2013.
[40] L. Cveticanin, M. Kalami-Yazdi, H. Askari: *Analytical approximations to the solutions for a generalized oscillator with strong nonlinear terms*, Journal of Engineering Mathematics, Vol. 77, No. 1, pp. 211-223, 2012.
[41] L. Cveticanin: *Application of homotopy-perturbation to non-linear partial differential equations*,
Chaos, Solitons & Fractals, Vol. 40, No. 1, pp. 221-228, 2009.
[42] J. Sárosi, J. Gyeviki, G. Szabó, P. Szendrő: *Laboratory investigations of fluid muscles*, International Journal of Engineering, Annals of Faculty of Engineering, Vol. 8, No. 1, pp. 137-142, 2010.
[43] T. Szépe, J. Sárosi: *Matlab models for pneumatic artificial muscles,* Scientific Bulletin of the Politehnica, University of Timisoara, Transactions on Mechanics, pp. 1224-1227, Romania, 2009.
[44] B. Kuljić, J. Simon, T. Szakáll: *Pathfinding based on edge detection and infrared distance measuring sensor*, Acta Polytechnica Hungarica, Vol. 6, No. 1, pp. 103-116, 2009.
[45] I. Matijevics , J. Simon : Advantages of Remote Greenhouse Laboratory for Distant Monitoring, Proceedings of the Conference ICoSTAF, pp. 1-5, 2008.

INTERNATIONAL SCIENTIFIC CONFERENCE ON
ADVANCES IN MECHANICAL ENGINEERING
13-15 October 2016, Debrecen, Hungary

DESIGN CONSIDERATIONS OF HARMONIC TRACTION DRIVES

[1]NÉMETH Géza, [2]PÉTER, József PhD

[1]*University of Miskolc*
E-mail: machng@uni-miskolc.hu
[2]*University of Miskolc*
E-mail: machpj@uni-miskolc.hu

Abstract
The harmonic gear drives are well known gears with high transmission ratio, produced in series with large variety. They are accurate and have high power density. There are researches at the field of such traction drives. The authors of present paper want to contribute to this work by entering some new design considerations, acknowledging the existing disadvantages comparing to the harmonic gear drives. However the simplicity and the hoped capability of the traction type drive encourage the effort for developing drives which incorporate unusual elements and perhaps cheaper solutions, too. This paper is a continuation of a previous one of ours where the potential for enlarging the compressive force between the mating friction elements were analysed. The transmission ratio of the drive is independent of the number of deflection waves but the compressive force depends on it. These propose a greater number of deflection wave. The authors suggest mechanical solutions for the wave generator where the load carrying capacity is the maximum one at a given geometry.

Keywords: *harmonic traction drive, hydrodynamic bearing, deflection wave, wave generator.*

1. INTRODUCTION

The harmonic traction drives are suitable mainly for kinematic drives, e.g. for dives with very low power transmission and where the load carrying capacity or the efficiency is not the most essential point of view. *Figure 1* shows one of the best known solutions. The first stage is an epicyclic drive and the second one is a harmonic drive. The annular ring 4 is relatively thick but elastically deformable. This element assure the compressive force both between itself and the flexible thin cup shaped element 3 and also between the loosely jointed roller (or planet wheel) 2 and the sun wheel 1. The highly flexible element 3 is fixed to the stand, to be maintained an unambiguous relation between the input shaft 1 and the output shaft 4 of the drive. The planet carrier k and the arm of the wave generator g is the same element.

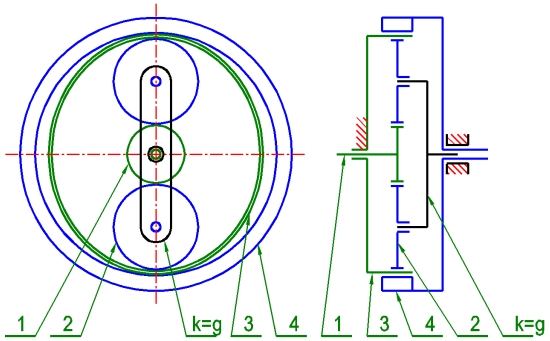

Figure 1 Roller type harmonic traction drive

The ratio of the drive can be very high. Considering the radii of the contacting elements at unloaded condition and both the inner and outer surfaces of the highly elastic element 3 (3i and 3o) taking into account as $r_1 = 3mm, r_2 = 11mm, r_{3i} = 25mm, r_{3o} = 26mm, r_4 = 26.1mm$ the ratio of the first and second stages are

$$i_{1k}^{(3)} = 2\left(1 + \frac{r_2}{r_1}\right) \text{ and } i_{k4}^{(3)} = \frac{r_4}{r_4 - r_{3o}} \quad (1)$$

respectively, and the whole ratio is around 2400.

2. OTHER SOLUTIONS

There are problems requiring not so high ratios. The diameter of roller 2 can be greater than the half diameter of highly elastic element 3. The solution at *Figure 2* seems to be simpler. The huge axial dimension assures more power transmission. One of the advantages of the drive is the better fit between the wave generator and the flexible wheel 3 due to the greater disk diameter. The disks can be accurately fit to their axes. Beside the elasticity of the annular wheel 4 the arms of the disk carrier also can be modified towards the proper elastic behaviour as shown in *Figure 3*.

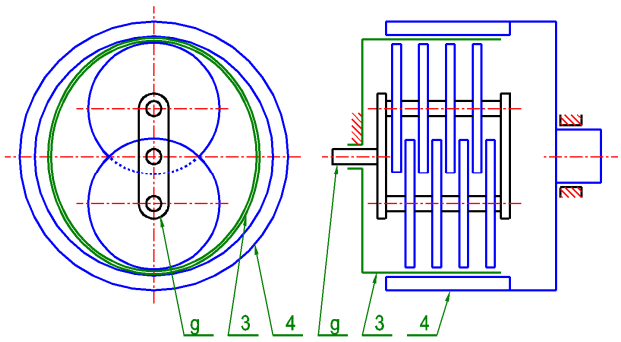

Figure 2 Disk type harmonic traction drive

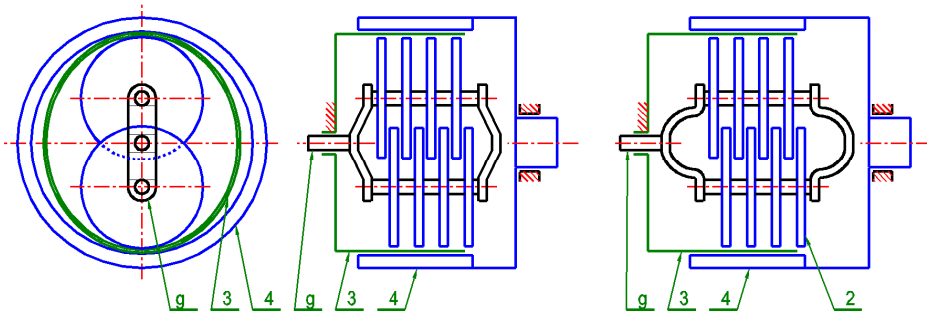

Figure 3 Disk type harmonic traction drives with elastic disc carrier

Both the contacting surfaces of the highly flexible wheel 3 and the annular wheel 4 are smooth and so the susceptibility of the rings for fatigue is low. Another method to decrease the fatigue behaviour of the annular wheel is its substitution with helical torsion spring. *Figure 4* shows this solution. The bending stiffness of spring should be high enough not to wrap totally around the highly flexible cup shaped wheel 3, like a rope or like in the spring type freewheel clutches [1]. The torsion spring may be produced also by manufacturing, and this make it possible to combine the

spring and the output shaft in one machine element. The proper contact between the flexible wheel 3 and the annular wheel 4 is assured by installing extra supporting rollers 5 opposite to the disks 2.

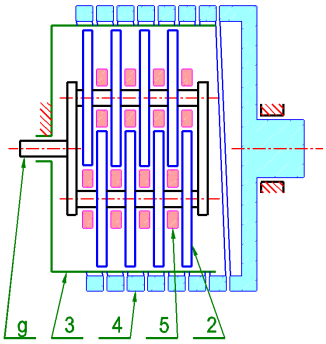

Figure 4 Disk type drive with torsion spring and supporting rollers

Figure 5 demonstrates a solution where the disk type wave generator is the same as it is used in some harmonic gear drive [2]. The disks 2 are installed to the shaft of the wave generator g eccentrically. The disks are supported by rolling bearings.

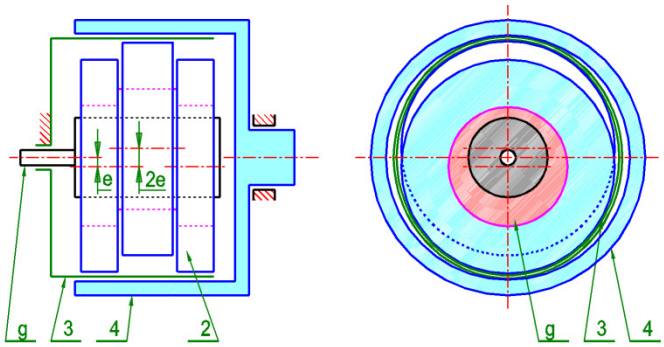

Figure 5 Conventional disk type drive

3. WAVE GENERATOR WITH SLIDING BEARINGS

In harmonic gear drives the shape closing connection does not require too large radial loads. In contrast the harmonic traction drive is force closing and requires great radial load to transmit sufficient tangential force. The tangential force could be increased by greater number of contact point around the circumference. The greater the number of deflection wave the less bending moment loads the annular wheel, so the force is increasable. The greater number of disks should be narrower, too, and the roller bearings cannot fulfil this problem. The narrow sliding bearings are also unusual but the *Figure 6* suggest a prosperous idea.
The eccentric disks are made of sheet metal by laser cutting and are keyed to the spline shaft of the wave generator. The bearings are hydrodynamic journal types and they are lubricated by the traction lubricant developed especially for traction drives with metal surfaces. The bearings are narrow ones, the sufficient pressure in the lubricant is developed with the axially located elastic side washers containing slots to supply lubricant in the gap between the eccentric disk and the roller. The side washers are also lubricated by the radially flowing lubricant from the radial bearing. The pressure of this flowing out liquid will push away the thin side washer ($b_{sw} = 0.1mm$) in the necessary grade. Considering the bearing diameter $d = 30mm$, the bearing width $b = 1mm$, the

radial load $F = 240N$, the angular velocity $\omega = 160s^{-1}$ beside a fixed annular wheel (slightly greater than that of the input shaft $\omega_g = 151s^{-1}$), the bearing type is full ($\beta = 360°$) at the point of view of the hydrodynamic lubrication, the operating temperature $\vartheta = 80℃$, the lubricant consumption is $q = 1.5cm^3/min$ of the *ISO VG* 68 type and the natural cooling is sufficient. The necessary fit of the bearing is $\phi 30H7/f7$. The volume of the tinny lubricant tank is $= 2{,}6mm^3 > V_{necess} = 1mm^3/rev$.

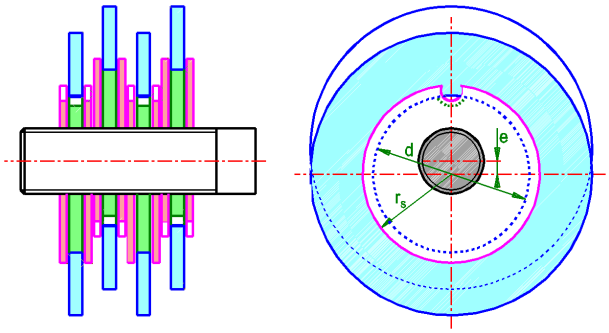

Figure 6 Sliding type bearings in the wave generator

CONCLUSIONS

The authors had ascertained the constraints of the greater tangential force in harmonic traction drive. Accordingly to the highly elastic thin walled cup shaped element has smooth surface and there is no danger for fatigue from bending. In contrast, the thick circular wheel is overtaken to bending. The traction drive require great compressive forces between the elements and this can be assured by greater number of disks and so greater number of deflection waves. The problem is hoped to be solved by narrow hydrodynamic bearings supplied by axially supported highly elastic side washers.

ACKNOWLEDGMENTS

The research work presented in this paper/study/etc. based on the results achieved within the TÁMOP-4.2.1.B-10/2/KONV-2010-0001 project and carried out as part of the TÁMOP-4.1.1.C-12/1/KONV-2012-0002 project in the framework of the New Széchenyi Plan. The realization of this project is supported by the European Union, and co-financed by the European Social Fund.
The research work was supported by the Hungarian Scientific Research Found grants OTKA 29326 and Fund for the Development of Higher Education FKFP 8/2000 project.

REFERENCES

[1] Wiebush, C. F., Dial Clutch of the Spring Type, Bell System Technical Journal, Volume 18, Issue 4, October 1939, p. 724–741.
[2] Volkov, D. P., Krainev,A. F., Stupakov, A. A., Bondarenko S. V., Harmonic Gear Reduction Unit, US Patent no. 4003272, 1977.
[3] Németh, G., Németh, N., Péter, J., Strength Calculation of Elastic Elements in Epicyclic Traction Drive (in Hungarian), In: Bodzás Sándor (ed.), Műszaki Tudomány az Észak - Kelet Magyarországi Régióban 2015 Konferencia előadásai, Debreceni Akadémiai Bizottság Műszaki Szakbizottsága, 2015, pp.213-219, ISBN 978-963-7064-32-6.
[4] Németh, G., Péter, J., Németh, N., A New Type of Epicyclic Traction Drive, Advances in Mechanical Engineering, 1:(1), 2013, p.137-142, ISBN 978-963-473-623-3.

THE SITUATION OF MAINTENANCE SERVICES IN AGRICULTURE

OLÁH Béla

Department of Economics and Science of Organisations, GAMF Faculty of Engineering and Computer Science, Pallas Athene University
E-mail: olahb@szolf.hu

Abstract
Maintenance is gaining more and more importance nowadays; in spite of this fact it is regrettable that sufficient information is hardly available on the state of the domestic maintenance services particularly in agriculture. I carried out the survey by means of a questionnaire within the sphere of the small- and medium-scale agricultural companies operating in the eastern region of Hungary. The scientific research gives an account of this survey and the experiences of its evaluation, especially of the utilization and supply of the maintenance services in the field of machine repair and diagnosis, as well as compares these assessments with results of earlier projects carried out by colleagues of the Department of Maintenance at the Agricultural College Faculty of Tessedik Sámuel College in Mezőtúr.

Keywords: *maintenance, services, agriculture, small- and medium-scale companies, regional survey*

1. INTRODUCTION

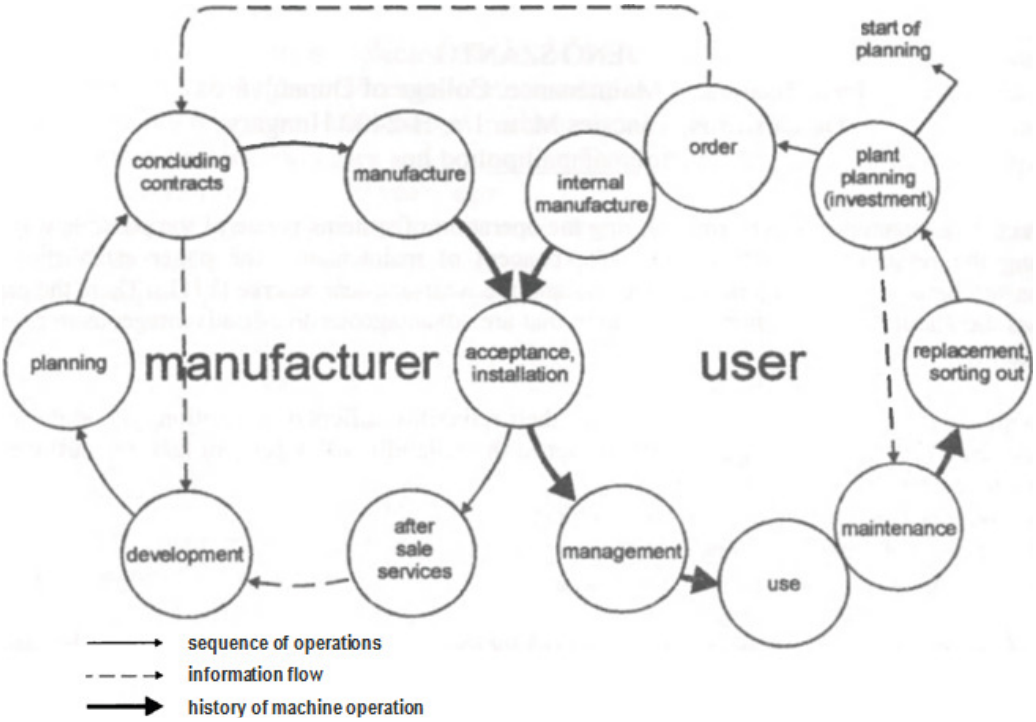

Figure 1 Dual-circuit model of the service life of machines [9]

The failures of machines and other equipment cannot be totally eliminated by the application of modern, preventive maintenance strategies and methods, either. There are errors and off-times.

These often cause great losses [12]. The standard of maintenance by means of the available instruments has an influence on the use of energy and materials of production, on the quality of products, on the trend of rejects, and on the quality of waste among other things [1]. It is not by accident that the importance of maintenance is growing. The technical-economic development also requires the improvement of maintenance services [11].
Maintenance is part of the service life of machines (*Figure 1*) from the investment up to sorting out [10].
The maintenance covers the entirety of measures aimed at preserving and restoring functionality as well as evaluating the actual state. The precondition of functional ability is that the machine is provided with reserve – the so-called wear and tear reserve – necessary for fulfilling its function. The changes in this reserve are shown in *Figure 2* from the start of planning up to the time of putting out of service [9].

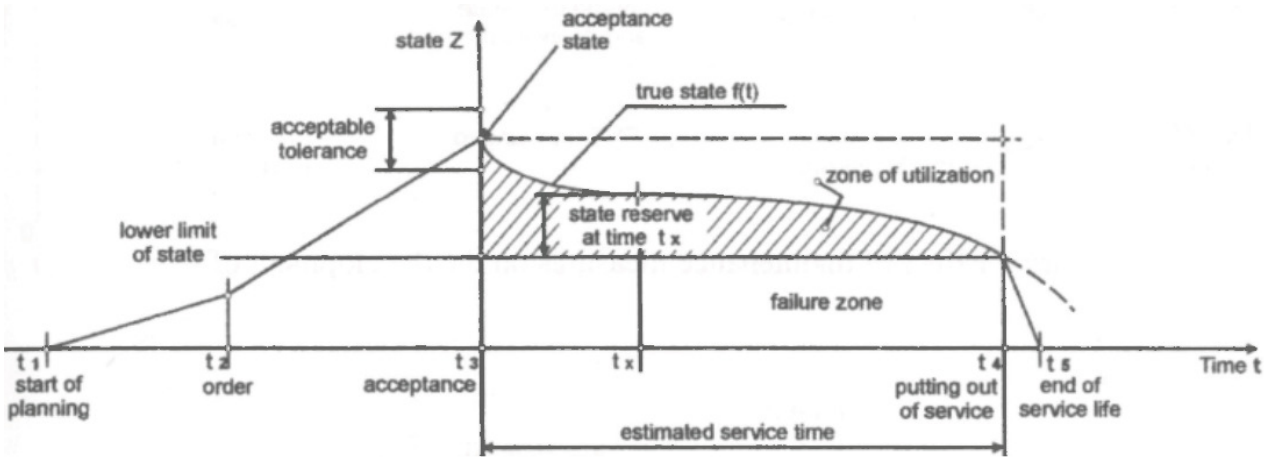

Figure 2 Changes in the state of the machine during its life history [4]

Maintenance is fundamentally a service activity carried out with internal (own) resources or external (foreign) organisation. Although it seems that there is evidence of internal marketing of the maintenance services too [8], in respect of the topic, I argue for the importance of the external, purchased services. National reports about the situation of maintenance services are rarely published [3], therefore I would like to examine this in the eastern region of Hungary, first of all in the Great Hungarian Plain.

2. METHODS

Within the compass of the possibilities, I decided on the completion of a survey aided by questionnaire sent by mail. Some business units were surveyed with the help of the students were studying at the College of Szolnok in the specialisation of Mechanical Engineering in the Agriculture and Food Industry at the speciality of Machine Stock Maintenance, who completed the questionnaires via face-to-face interviews with business units. The questions were about the data of the enterprise; the whole maintenance of machines and their service condition; some fields of repair, the quality, the logistics, the environment and its projects – relating to services – in the future [5].

The whole process of investigation is shown in *Figure 3*.

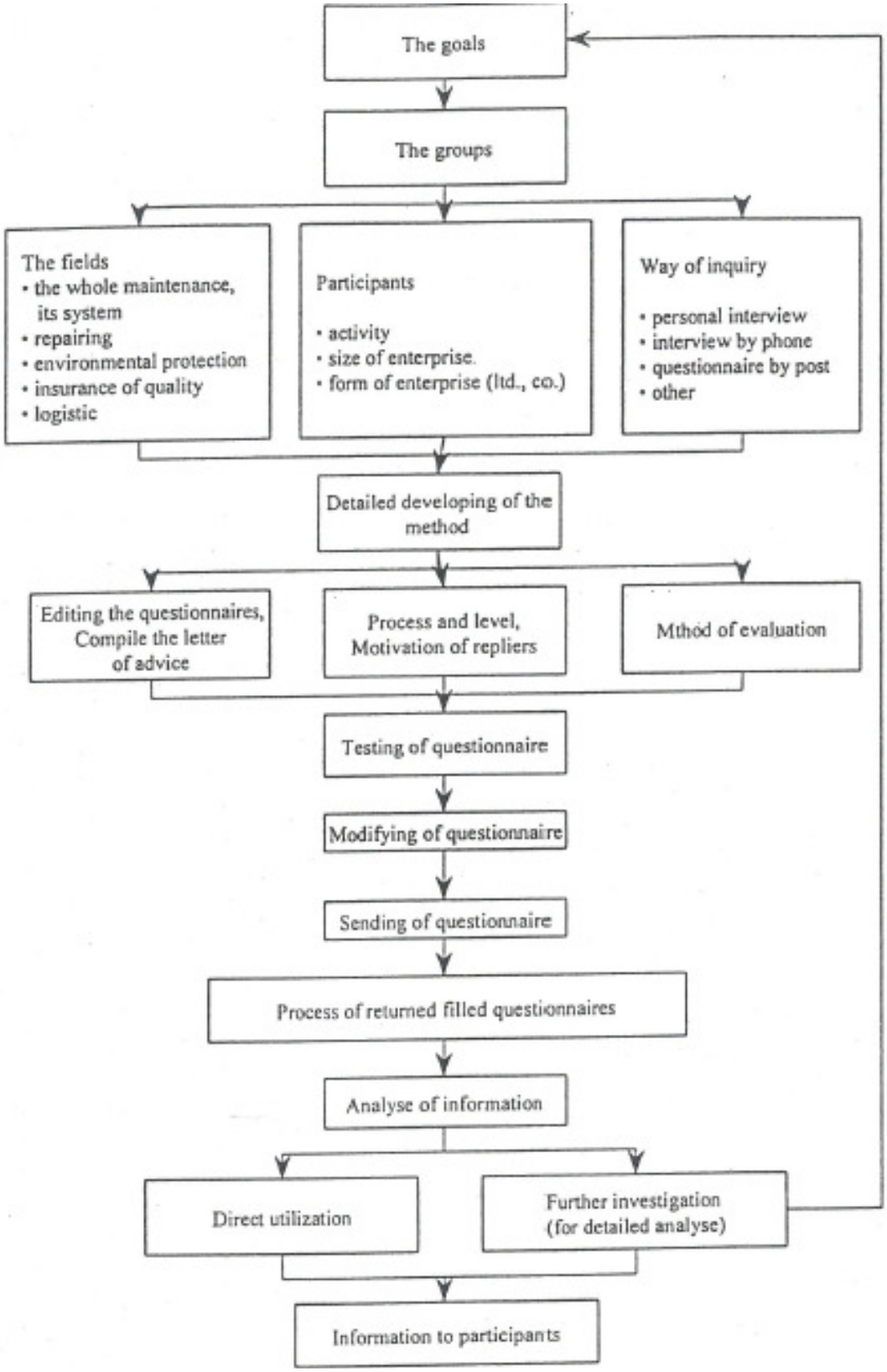

Figure 3 The process of the questionnaire survey [2]

3. RESULTS

3.1. Some characteristics of the firms that replied

36 enterprises returned the completed forms, all operating in the eastern region of Hungary [5]. These firms are producers, respectively productive-services. All of them deal with agriculture. A quarter of these are primary producers, 30.6 percent of the firms are family farm businesses, as well as 7 private companies 6 limited liability companies and 3 co-operatives also sent back the completed questionnaires. Half of the enterprises deal with only crop production, 13 firms deal with animal husbandry, too. The average agricultural area is 1,077 hectares (the average size of the land cultivated by companies is 2,883 hectares while this is 28 hectares in the case of the primary producers and the average family farm size is 130 hectares). 58.3% of the agricultural producers that replied have fewer than 10 employees. All the private holdings (primary producers and family farms) are in this category. The ages of the main machines and equipment are very different, in the family farms almost 25% of the tractors are under 10 years, while in the companies this value is more than 45%. The situation is a little bit better in the case of combine harvesters, 37% of them are less than 10 years old [6].
It can be seen in *Figure 4* that in the respondents' opinion the services utilized by them are significant (ascertained by 38.5% of them), important (claimed by also 38.5%), unimportant (stated by 15.4%); the services given by them are very important (declared by 33.3% of them), significant (claimed by 44.4% of them), unimportant (stated by 11.1% of them) from the view of the whole business [7]. At the enterprises the rate of the repairmen of all employees is 11.6%, and the yearly cost of maintenance is 6.2% of the whole value of instruments.

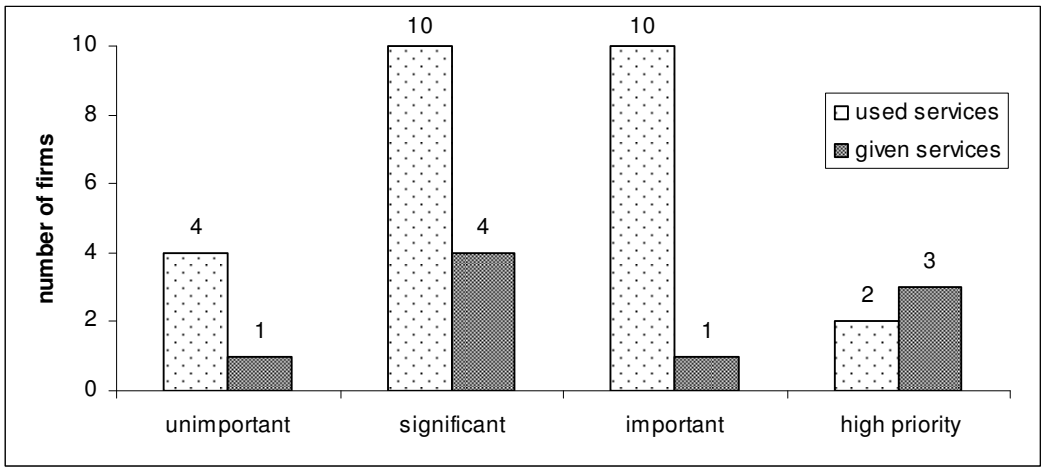

Figure 4 Importance of the present services from the point of view of the firms [7]

3.2. Research on overall maintenance

36.1% of the investigated firms follow a cyclic or periodic (preventative) maintenance system (*Figure 5*), 11.1% of them do corrective repair (this rate was 35.5 per cent in the survey carried out in 2004/2005 [14], so it was three times higher than now), 19.5% of them use the condition based (predictive) maintenance strategy and 33.3% of them have got a mixed maintenance system.

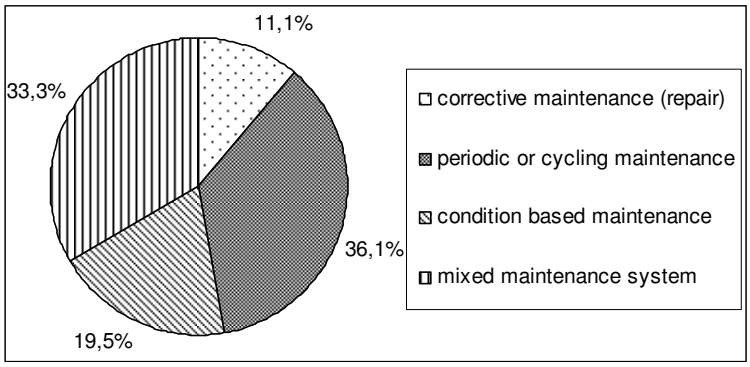

Figure 5 Proportion of applied maintenance philosophies [Source: own editing]

In general, all business units use external maintenance services, because (*Figure 6*) it is compulsory (35.5%), more economical (3.2%), they do not have enough professional skills (38.7%) (it is higher by 16.2 percentage point than in 2004 [14]) or enough instruments (16.2%) or capacity (3.2%) (it is lower by 16.6 percentage point than 10 years ago [14]).

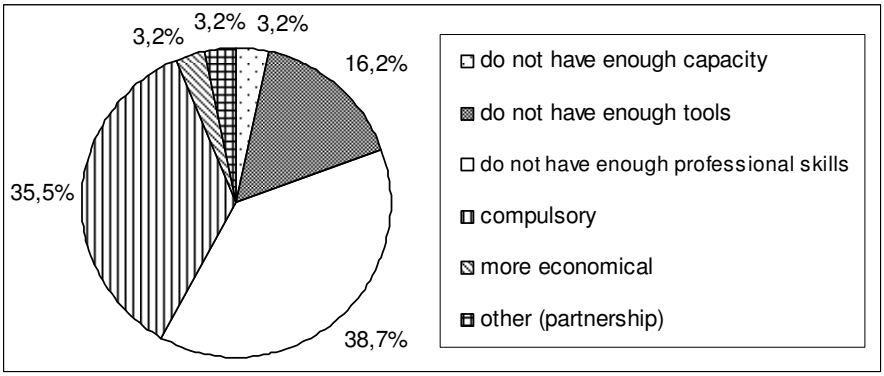

Figure 6 Proportion of causes of the services employed [Source: own editing]

It can be stated from *Figure 7* that about 23.8% of the services employed deal with special repair, 20.6 percent of them are warranty repair, 11.1-11.1% engage in technical diagnostics or repair of unexpected errors, 12.7% of them deal with overhaul and 9.5 percent aim at installation. The cost of the external maintenance services employed are 18% of the total maintenance cost (which is less by one fifth than in 2003 [2, 12]), but this rate was between 10%-26.6%.

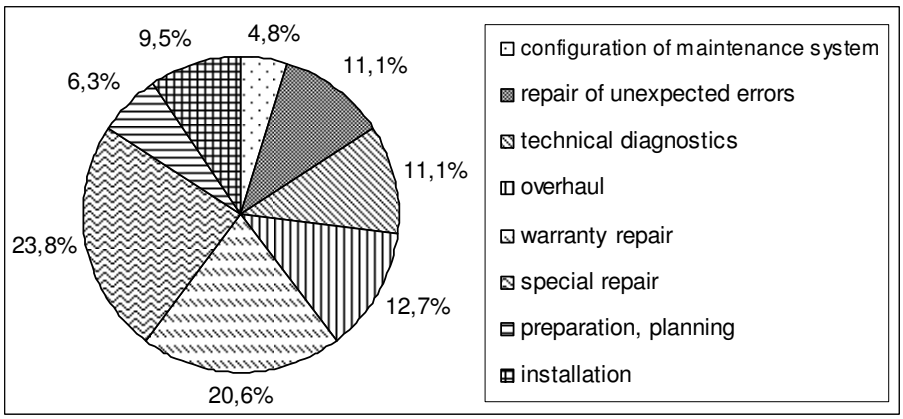

Figure 7 Proportion of types of the maintenance services employed [Source: own editing]

Only one quarter of the enterprises under investigation provide services [7] either because of partnership (50%) or appointed service (25%), and (only 8.3%) do so owing to financial reasons. 13.8% of the services provided are special repair, 27.7% make up for repairs of unexpected errors. The operators do 56.2% of their own repair, 26.2% in external service. In 87% of the firms the tasks of machine storage are made by the operators themselves or together with the yard persons or repairmen (it is similar to that in 2004) [6, 15]. All the firms protect against corrosion with their own instruments and employees as it was the case ten years ago [13, 14].
Five (55.6%) agricultural companies would like to introduce or extend the analysis of their customers' satisfaction in relation to maintenance services performed by them.

CONCLUSIONS

Some conclusions from the findings and evaluations of the investigations are:

- it seems that the enterprises do not manage the maintenance according to its weight, but the cost of maintenance and the number of employees are important;
- most agricultural companies do not operate up-to-date maintenance systems;
- it seems that the pressure (specifications, shortages) are felt on both areas; the employed and provided services, and the quality, and the economy are motivating factors only to a small degree, the demands of market do not predominate [11];
- the whole maintenance process needs development; the reasonable areas are: the introduction of maintenance systems, the problems of own or external maintenance.

REFERENCES

[1] Berger, J.: *Wissen erhöht Verfügbarkeit. Optimierte Planung und Instandhaltung von Produktionsanlagen.* VDI-Zeitschrift Integrierte Produktion, 144 (6), 67-69., 2002.
[2] Györki, J. et al.: *The situation of maintenances services – beginning results of an investigation.* 8th International Scientific Symposium, Quality and Reliability of Machines, Nitra, 200-203., 2003.
[3] Janik, J. et al.: *Topical questions of stock maintenance of agricultural machines*. 27th Research and Development Conference of the Hungarian Academy of Sciences, Agricultural-Technical Committee, Gödöllő, 2003. (in Hungarian)
[4] Kakuk, Gy., Zsoldos, I., Janik, J.: *Gépek életciklusának modellezhetőségi jellemzői*. Gépgyártás, 44. (5-6), 11-17., 2004.
[5] Oláh, B.: *Survey of the current state of the machine maintenance in agriculture*. 21st International Student Conference on Environmental Protection and Rural Development, In: ECONOMICA, Scientific Publications of the College of Szolnok, 8 (3), 258-265., 2015. (in Hungarian)
[6] Oláh, B.: *The state of storage of agricultural machines nowadays*. 9th International Scientific Day of Land Management in the Great Hungarian Plain, In: ECONOMICA, Scientific Publications of the College of Szolnok, 8 (4/1), 35-44., 2015. (in Hungarian)
[7] Oláh, B.: *Managing maintenance services in agriculture in eastern Hungary*. Fórum Manažéra, Trnava, 12 (1), 42-47., 2016.
[8] Röben, D. F. O.: *Internes Marketing von Instandhaltungsdienstleistungen*. IO Management-Zeitschrift Industrielle Organisation, Zürich, 70 (3), 51-55., 2001.
[9] Szántó, J.: *Reliability-based maintenance*. Production Processes and Systems, Vol. 1, 169-175., 2002.
[10] Vermes, P., Herbály, L., Vas, F.: *Plant maintenance*. (Edited by: Vermes, P.) Gödöllő

University of Agricultural Sciences, Agricultural College Faculty, Mezőtúr, college textbook. 1996. (in Hungarian)

[11] Vermes, P.: *Market aspects of maintenance services*. 26th Research and Development Conference of the Hungarian Academy of Sciences, Agricultural-Technical Committee, Gödöllő, 152-156., 2002. (in Hungarian)

[12] Vermes, P. et al.: *The situation of maintenances services – beginning results of an investigation*. 27th Research and Development Conference of the Hungarian Academy of Sciences, Agricultural-Technical Committee, Gödöllő, 248-252., 2003. (in Hungarian)

[13] Vermes, P.: *Részjelentés „A mezőgazdasági gépüzemfenntartás fejlesztése, a gépek optimális üzemben tartásának meghatározása" című kutatási témához*. Mezőtúr, TSF MFK, 2004.

[14] Vermes, P., Vas, F.: *A gépkarbantartás helyzete és megoldások a mezőgazdaságban*. Műszaki Tudomány az Észak-Alföldi Régióban, Nyíregyháza, 5-22., 2006.

[15] Oláh, B.: *Survey of the current situation of storing agricultural machines*. Hungarian Economy and Society in the Globalization World of the 21st Century. International Scientific Conference. Békéscsaba. 2016. (Conference proceedings under publication)

INTERNATIONAL SCIENTIFIC CONFERENCE ON ADVANCES IN MECHANICAL ENGINEERING
13-15 October 2016, Debrecen, Hungary

IMPROVEMENT OF TILLAGE ELEMENTS OF AGRICULTURAL MACHINERY

[1]PÁLINKÁS Sándor PhD, [2]FAZEKAS Lajos PhD, [3]GINDERT-KELE Ágnes PhD, [4]MOLNÁR András, [5]HAGYMÁSSY Zoltán PhD, [6]KONYHÁS Dávid

[1,2,3,6]Department of Mechanical Engineering, Faculty of Engineering, University of Debrecen
E-mail: palinkassandor@eng.unideb.hu, fazekas@eng.unideb.hu, battane@eng.unideb.hu, konyhas900309@gmail.com
[4]Department of Mechanical Technology, Faculty of Mechanical Engineering and Informatics, University of Miskolc
E-mail: a.molnar2007@gmail.com
[5]Institute of Land Use, Technology and Regional Development, Faculty of the Agricultural and Food Sciences and Environmental Management, University of Debrecen,
E-mail: hagymassy@agr.unideb.hu

Abstract
The efficiency of agricultural activity is significantly influenced by the condition of power machines used in the agricultural production. Among others, the formation and maintenance of suitable soil-conditions play a very important role in obtaining the desired harvest yield. The implement tools of tillers are exposed to an extraordinary high load and a significant wear, therefore it is necessary to investigate the relationship between their active layer and durability. The purpose of our research work is to change the old, worn cultivator tines to tines having a longer durability; different heat-treatment technologies have been developed moreover hot metal powder spray fusing has been used in order to realize our aim. The products made by us will be used in the agricultural production in the future therefore the type of heat treatment- or layer build-up technology to be used during the production can be determined. As a cultivator is equipped with a lot of cultivator tines, the expenses can significantly be decreased by the use of cultivator tines made by a well-chosen layer build-up technology and a higher yield/agricultural area can be obtained during the cultivation. On the basis of the investigations performed till now one can forecast that it seems to be efficient to use Ni-alloyed metal powders for layer build-up by a subsequent (hot) melting.

Keywords: *hot metal powder spray fusing, increase of durability, agricultural implements*

1. INTRODUCTION

The size-decrease or breaking as well as the surface quality of parts exposed to significant wear and load can be improved by building up a new surface by using the traditional surface-layer welding [1] and the different metal powder spray fusing technologies [3]. By this, the construction of machine elements can be simplified and it is significant from economical point of view as well as it is not necessary to replace the whole workpiece [2]. A lower specific flame intensity is used during the surface-layer welding; the seams are not deep but they are wide instead.
A significant wear of machines used in the different fields of agriculture can be experienced (*Figure 1*). As a significant part of people living in Hungary deals with agriculture, it is very important to know how to ensure the cost-efficiency and the efficient agriculture. During the recent period of our research work, the heat treatment and hot metal powder spray fusing of cultivator tines made experimentally by free-forming forging has been performed in order to investigate their durability.

Corn-stalk crushing knife and disc of corncob-breaking adapter of corn combine harvester

Cultivator tine used on combinators and cultivators

Figure 1 Worn agricultural machine parts

2. HEAT TREATMENT OF CULTIVATOR TINES

The production and heat-treatment of cultivator tines made for experimental purposes were shown in detail on the 3rd International Scientific Conference on Advances in Mechanical Engineering (ISCAME 2015). 10 samples were made by free forming forging and 5 of them were heat treated by using different heat-treatment methods (see in *Table 1*). The complete heat-treated workpieces can be seen in *Figure 2*.

Table 1 The performed heat-treatment methods

No. of sample	Performed heat treatment methods
1.	Normalizing heat treatment
2.	Hardening of edges
3.	Tempering of edges
4.	Hardening of the entire surface
5.	Tempering of the whole surface

Figure 2 The complete heat-treated workpieces

3. HOT METAL POWDER SPRAY FUSING OF CULTIVATOR TINES

Hot metal powder was built up on the surface of four of the samples which had been made preliminary for experimental purposes and a traditional surface-layer welding was used in case of one sample (see in *Table 2*). Our experiments were performed in the Welding Laboratory of Technical Faculty of University of Debrecen.

Table 2 Performed Layer Build-up

No. of Sample	Performed Layer Build-up
6.	Traditional surface-layer welding
7.	Hot metal powder spray fusing by using Deloro powder
8.	Hot metal powder spray fusing by using N40 powder
9.	Hot metal powder spray fusing by using N50 powder
10.	Hot metal powder spray fusing by using N60 powder

The metal powder was sprayed by using an UTP variobond type hot spraying gun as shown in *Figure 3*. The hot metal powder spray fusing is a layer build-up method which is based on heating of the initial material up to a liquid or plastic state then it is powdered, accelerated to a certain velocity and delivered to the workpiece – to the basic metal – by means of flame (spraying).

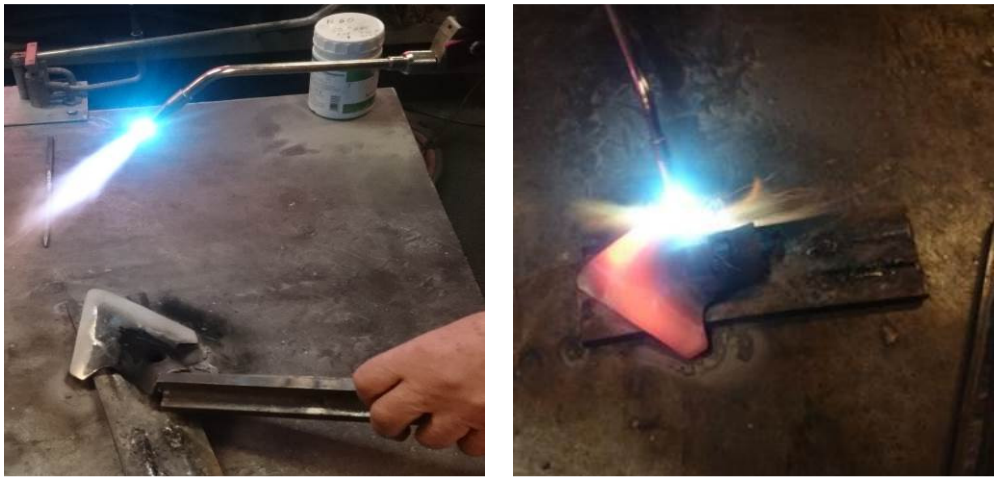

Figure 3 The layer-build-up of alloy powder by means of hot metal powder spray fusing

In the course of the flame spraying method, the material (wire, rod or powder) placed in the spraying device (gun, burner, etc.) melts or it becomes plastic, passes through the flame and dashes to the surface of workpiece; by this a coherent layer develops. The selection or breaking into particles of the spraying material (rod, wire, powder, etc.) and the increase of their kinetic energy are promoted by a kind of accelerating gas – usually by means of compressed air - it means that the source of thermal energy is the gas flame developing during burning of the oxygen-combustible gas (acetylene, natural gas, propane-butane, hydrogen) mixture [6].

3.1. The process of hot metal powder spray fusing

It is very important to prepare the specimen as no proper bond can develop between the two different materials in case if even a minor contamination can be found on the material. First of all, the impurities were removed from the surface by using an angle grinder. Then the workpiece was heated to a temperature of around 250-300^{o}C. It is called a wetting process. The proper choice of basic material is very important in order that a suitable bond can develop between the powder and workpiece during the hot metal powder spray fusing. During the hot metal powder spray fusing, the workpieces are in a high temperature range therefore the character of cooling is very important in order to ensure the suitable hardness – in our case the workpieces are cooled in open air. The complete workpieces can be seen in *Figure 4*.

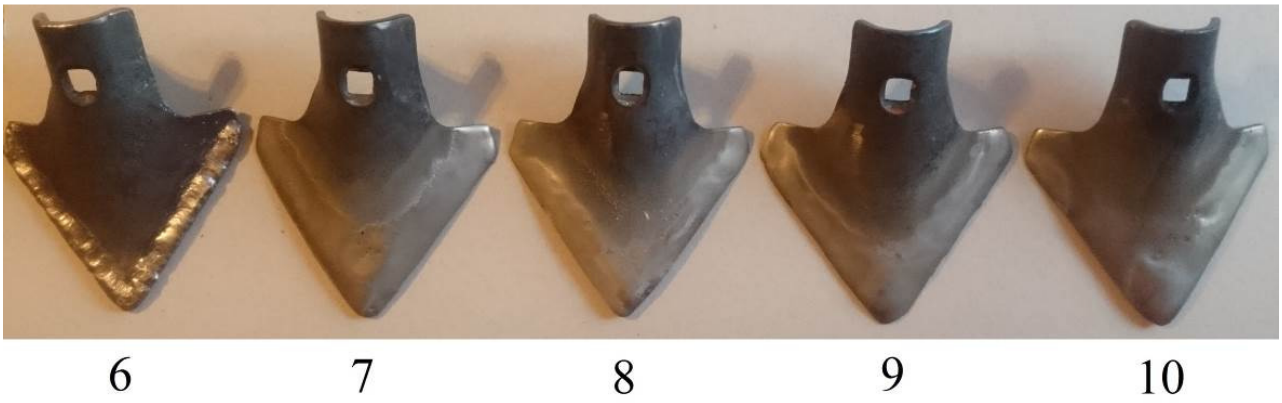

Figure 4 The complete sprayed workpieces

3.2. Investigation of the build-up layer by a Scanning electron microscope

The basic material of cultivator tines is a C60 grade hot-rolled steel plate. In the course of the hot metal powder spray fusing, the different layers were built up on a steel plate the grade of which corresponded to the material-grade of cultivator tine by this a specimen was made in order to investigate the intermediate layer developing between the build-up layer and the basic material. A sample was taken from the specimen; this sample was imbedded in synthetic resin then it was grinded, polished and etched and investigated by a Scanning electron microscope (*Figure 5*). Then a photo was taken in order to determine the grain diameter of the applied alloy-powder (*Figure 6*).

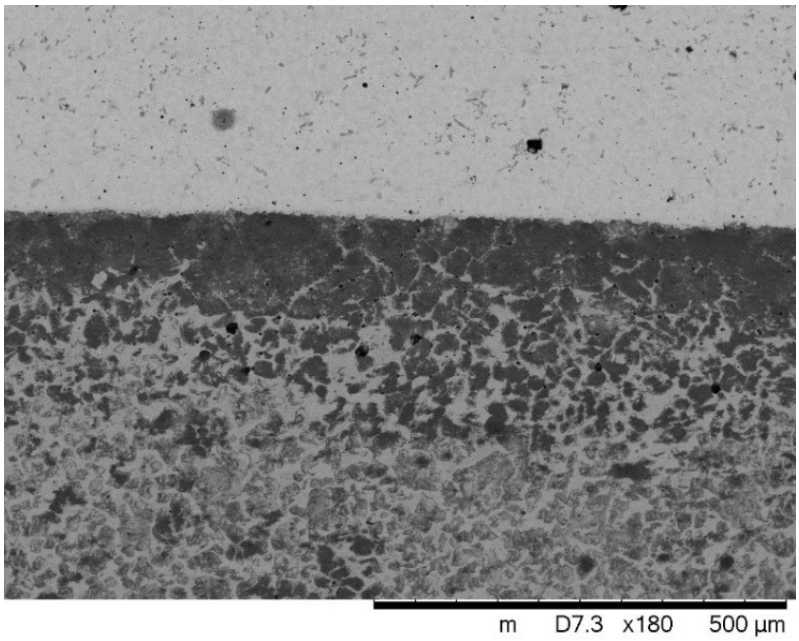

Figure 5 Investigation of the intermediate layer in case of sample No. 8. Magnification: 180x

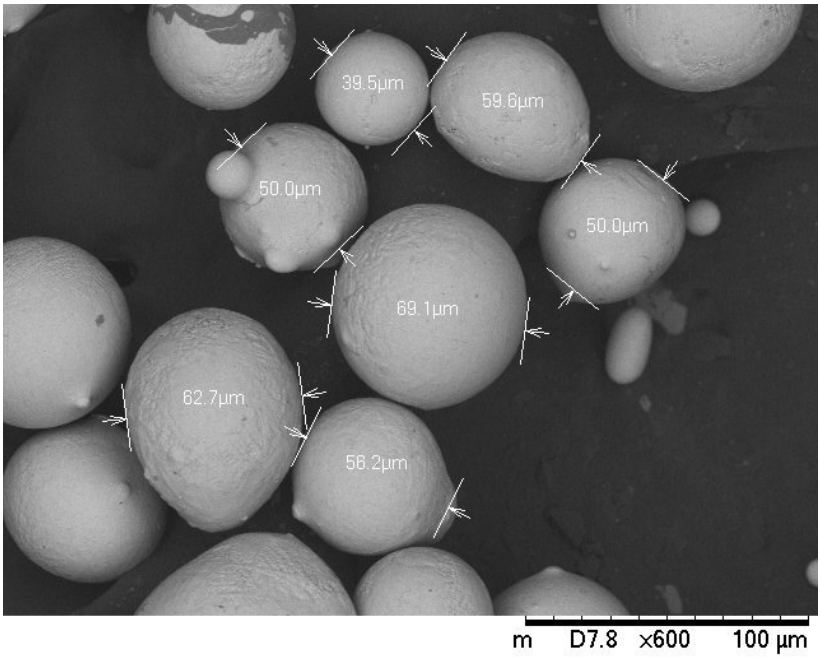

Figure 6 Investigation of the alloy powder (N40). Magnification: 200x

4. THE USE OF COMPLETE WORKPIECES FOR SOIL PREPARATION

The experimental workpieces were given to János Illyés agricultural entrepreneur in Hajdúszovát who mounted them on the combinator seen in *Figure 7* and performed the soil-preparation of a land of 200 hectare.

Figure 7 Agricultural machine equipped with cultivator tines

The mass of tines was measured both before using them and after the soil-preparation of the land of 200 hectare. The obtained results are demonstrated in *Table 3*.

Table 3 The mass of cultivator tines before and after use

No. of sample	Performed procedures	Mass of workpiece [g]		
		Before use	After use	Difference
1.	Normalized	226,44	118,42	108,02
2.	Edges hardened	232,85	163,34	69,51
3.	Edges tempered	230,74	157,72	73,02
4.	Entire surface hardened	234,93	142,32	92,61
5.	Entire surface tempered	231,63	119,71	111,92
6.	Surface-layer welding	252,68	134,78	117,9
7.	Spray welding by using Deloro powder	247,23	153,54	93,69
8.	Spray welding by using N40 powder	244,58	167,35	77,23
9.	Spray welding by using N50 powder	240,25	169,06	71,19
10.	Spray welding by using N60 powder	249,43	206,08	43,35

The worn experimental workpieces are shown in *Figure 8*. It can be stated that the material-loss of heat-treated pieces is the lowest in case of samples No. 2 and No. 3 while the wear of workpiece No. 10 treated by hot metal powder spray fusing is the lowest. This result could exactly be expected in case of samples treated by layer build-up as this powder was of the highest hardness (60 HRC). However, the results obtained in case of the heat-treated samples cannot be explained by the theoretical background of scientific field as the material loss was higher than expected at these samples. This contradiction could be caused by more different factors. One of the reasons is that the heat treatment was not performed in controlled circumstances in the forge-shop. The other one is that the load of cultivator tines mounted on the agricultural machine was not equal; the tines overlap each other and the tines working in the tractor wheel track were exposed to a higher abrasive power owing to the compression of soil.

Figure 8 The experimental workpieces after use. Heat-treated pieces (upper row) and the sprayed pieces (bottom row)

CONCLUSIONS

The pre-experiments of long-term research work performed at the Department of Mechanical Engineering of Technical Faculty of University of Debrecen are described in our present paper. In the course of our earlier research work, cultivator tines were made by means of free-forming forging for experimental purposes. A part of the cultivator tines were heat treated by different methods and a wear-proof layer was developed on the other part of tines by means of the hot metal powder spray fusing. In order to investigate the durability of these tines, they were given to an agricultural entrepreneur who used them for soil-preparation in real circumstances. By utilizing the results obtained during our present experiments, our research work will be going on in the future as well. Different alloy-powders will be built up on 9 pieces of cultivator tines by using the hot metal powder spray fusing method moreover layers will be built-up on 3 workpieces by means of manual arc-fusion welding. The workpieces produced such a way will be used in agricultural circumstances as well in addition the metallographic investigations of these workpieces will also be performed. The research work aiming at the increase of agricultural productivity is of an extraordinary significance as the topsoil is of an excellent quality in Hungary and the agriculture plays a determining role in the economic life of our country.

REFERENCES

[1] Ember, M., Jánossy, GY., Szíjjártó O.: *Mezőgazdasági gépek javítása.* Mezőgazdasági Kiadó. Budapest, 1983.
[2] Hartmann, V., Felker, J., Kalmár, V., Horváth, G.: *Mezőgazdasági gépalkatrészek felújítása.* Mezőgazdasági Kiadó, Budapest, 1986.
[3] Tóth E.: *Felületi rétegek technológiája.* Műegyetemi Kiadó Budapest, 1993.
[4] Aschenbrenner J.: *Fémötvözetek tulajdonságainak megváltoztatása hőkezeléssel.* Nemzeti Szakképzési és Felnőttképzési Intézet, Budapest, 2008.
[5] Davis J. R. (Ed.): *Handbook of Thermal Spray Technology.* ASM International, 2004.
[6] Bach, F.W., Möhwald, K., Laarmann, A., Wenz, T.: *Modern Surface Technology.* 1st ed., WILEY-VCH Verlag, Weinheim, 2006.

INTERNATIONAL SCIENTIFIC CONFERENCE ON ADVANCES IN MECHANICAL ENGINEERING
13-15 October 2016, Debrecen, Hungary

ARC WELDING AS A CONTROL SYSTEM

[1]PODRŽAJ Primož PhD, [2]SIMONČIČ Samo PhD

[1]University of Ljubljana, Faculty of Mechanical Engineering
Askerčeva 6, 1000 Ljubljana, Slovenia
E-mail: primoz.podrzaj@fs.uni-lj.si
[2]University of Ljubljana, Faculty of Mechanical Engineering
Askerčeva 6, 1000 Ljubljana, Slovenia
E-mail: samo.simoncic@fs.uni-lj.si

Abstract
In this paper a brief overview of arc welding control is presented. In the introduction the basic physics of arc welding is explained and a subdivision into several categories of arc welding is given. Each of them is also briefly explained. The main part of the paper explains the main challenges of arc welding from control engineering point of view. Some previous solutions to these problems are given as well. In control engineering the main property of the close loop control system is a feedback signal. In this paper a special emphasis is given on control systems, which apply machine vision based systems for obtaining feedback signal.

Keywords: *Arc welding, Overview, Control Systems, Machine vision*

1. INTRODUCTION

In general welding can be described as joining of two (or more) pieces of material (usually called weldpieces) by the application of heat. From historical perspective the first type of welding was forge welding, where the weldpieces are first heated and then hammered or pressed together to remove slag and oxides and enable the bonding of the surfaces. An alternative is the so called fusion welding, where enough heat input must be intense enough to locally melt the two weldpieces. In the case of a surface heat source the minimum rate of energy release per unit area P required to maintain a molten weld pool of radius r is approximately [1]:

$$P = \frac{AkT_m}{r} \tag{1}$$

where k is thermal conductivity, T_m is melting temperature and A is a factor dependent on welding speed, weld size and thermal diffusivity. The weld pool size is of course limited by practical considerations. The typical values are within 10-20 mm range, which for steels results in the required power density of around 10^7 W/m^2. As shown in Fig. 1 this is a typical value of power density provided by arc welding sources. This is one of the reasons for its widespread usage.

An arc refers to strong electric fields that cause gas to induce an electric breakdown and continuous discharge of plasma [2]. Thus, the current passes through insulation media in a manner similar to air. In general arc welding can be defined as a type of welding where the heat needed to melt the material is provided by an arc between the electrode and the weldpiece(s). The welding current can be DC or AC and the electrode can be consumable or non-consumable. In many cases the welding region is protected by a shielding gas.

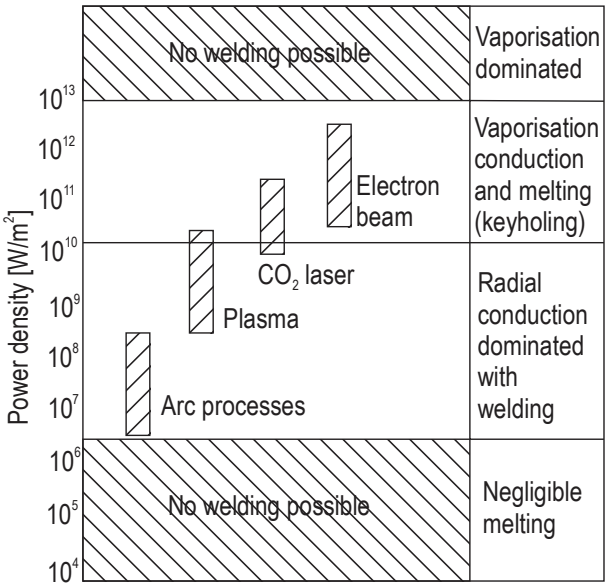

Figure 1 Power density for various welding processes [1]

The electrons in the arc are being released from the cathode by a thermionic emission. The current density is J is given by the following formula [3]:

$$J = AT^2 \frac{\phi e}{kT} \tag{2}$$

where the constant A is approximately 6×10^5 A/m^{2}K^2 for most metals, ϕ is the work function of the cathode surface, e is the charge on an electron, k the Boltzmann constant, and T temperature of the cathode surface. Before the arc is started, the electrode is too cold to release enough electrons to form the arc. Three methods may be used to ignite the arc: high voltage and high frequency, high-voltage impulse, and cathode preheating. An arc ignited by means of the first two methods is established by field emission, where a high voltage up to 20 kV is used [3].

A schematic representation of arc welding is shown in Fig. 2.

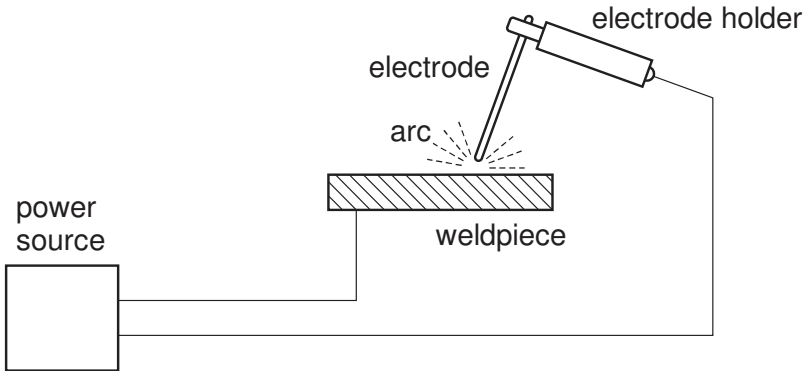

Figure 2 Schematic representation of arc welding

In general arc welding can be subdivided into the following procedures [4]:

- Shielded Metal Arc Welding (SMAW) is an arc welding process where an electric arc that is maintained between the tip of a covered electrode and the surface of the base metal produces

the heat required for joining (see Fig. 1).

- Gas Tungsten Arc Welding (GTAW) is an arc welding process that uses the arc between a non-consumable tungsten electrode and the weld pool with a shielding gas (see Fig. 3).

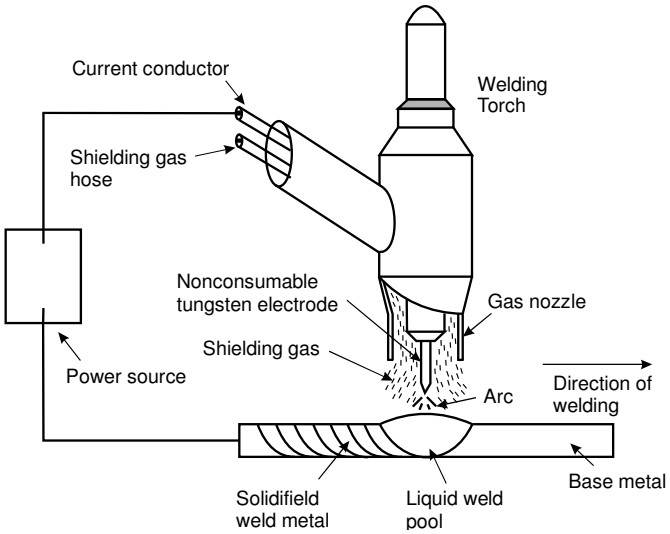

Figure 3 GTAW or TIG welding process

- Gas Metal Arc Welding (GMAW) is an arc welding process that uses an arc between a consumable electrode and the welding pool with a shielding from externally supplied gas without any application of pressure (see Fig. 4).

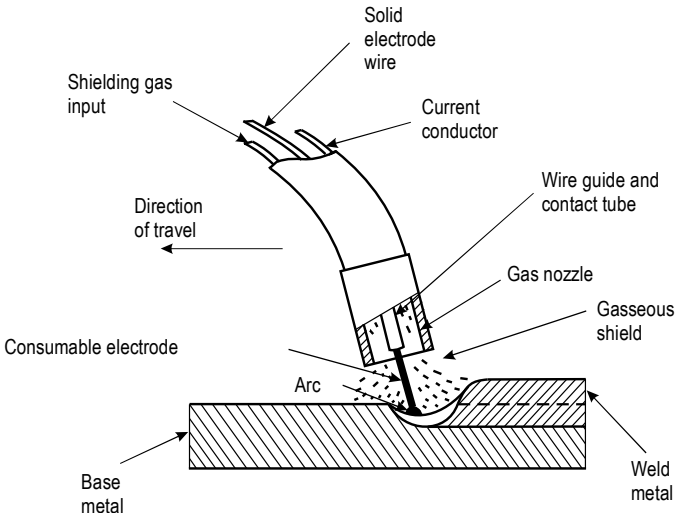

Figure 4 GMAW welding proces

In Europe, GMAW is also called metal inert gas (MIG) or metal active gas (MAG) welding.

- Flux-Cored Arc Welding (FCAW) is an arc welding process that uses an arc between the consumable electrode and the weld pool with a shielding from a flux contained within the tubular electrode with or without additional shielding from an externally supplied gas.
- Submerged Arc Welding (SAW) is an arc welding process that produces joining of metals by heating them with an arc between a metal electrode and the work piece. The arc and the molten metal are "submerged" in a flux on the work piece.
- Electro-gas Welding (EGW)is an arc welding process that uses an arc between a consumable

electrode and the weld pool, using auxiliary gas shielding around a flux-cored electrode.

- Plasma Arc Welding (PAW) is an arc welding process that produces coalescence of metals by heating them with an arc between an electrode and the workpiece with shielding from an ionized gas.

Of all the procedures, the first three seem to be the most often applied ones. That's also the reason, why they will be focused on, when discussing the control aspect of welding systems.

2. MODELLING AND CONTROL

From the control aspect point of view arc welding can be divided into two categories [5]. The first one is where the wire-feed rate is constant. It implies automatic regulation of the arc length. The second on is characterized by the wire-feeding rate being controlled by the arc voltage. The control system should include all of the mechanical or electrical devices that affect the welding arc. It is shown schematically in Fig. 5.

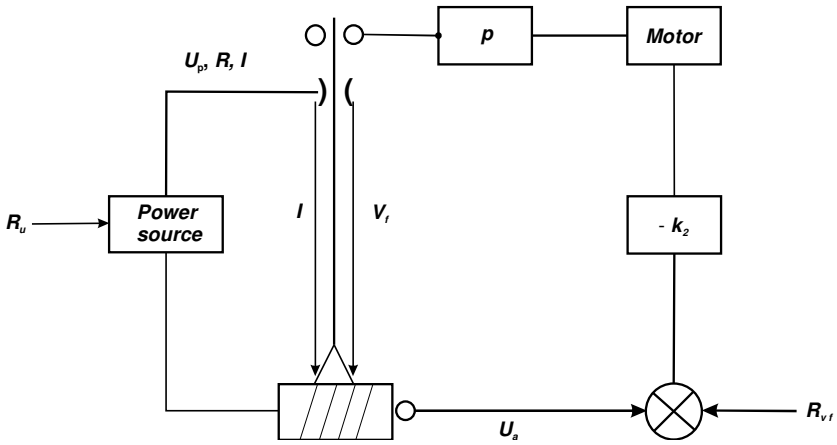

Figure 5 Schematic representation of arc welding [5]

For the electrical circuit of the welding process we can write the following equation

$$U_p = L\frac{di}{dt} + Ri + U_a \tag{3}$$

where U_p is the output voltage of power source, L the inductance of the welding loop, R its resistance, i the welding current and U_a the arc voltage. The arc voltage is determined by equation:

$$U_a = k_a l_a + k_p i + U_c \tag{4}$$

where l_a is the arc length, and k_a, k_p and U_c the parameters of the arc characteristics [5]. For the wire melting rate, we can write:

$$v_m = k_m i \tag{5}$$

where v_m is the wire melting rate, and k_m the coefficient of the wire melting rate. For the arc length, we write the equation

$$v_m - v_f = \frac{dl_a}{dt} \tag{6}$$

where v_f is the constant wire feeding rate. For the power source, we can write

$$U_p = k_0(r_u + k_1 i) \tag{7}$$

where r_u is the reference input of the power source, k_0 the gain of the power source, and k_1 the feedback gain. After performing the Laplace transform Eqs. 3-7 can be used to design the block diagram shown in Fig. 6.

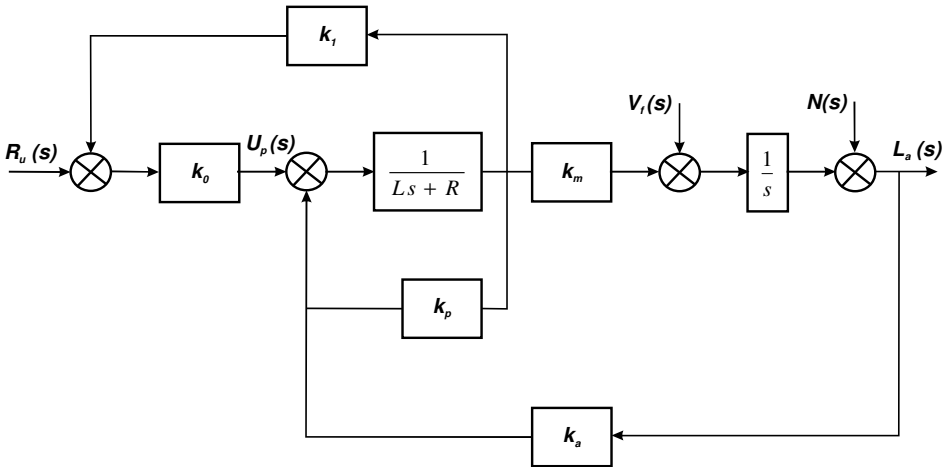

Figure 6 Block diagram of an arc welding system (constant wire feeding rate) [5]

This block diagram can serve as a basis for discussion regarding arc welding control systems. There is however continuous improvement being made in this regard. One possibility is to use gain scheduling to maintain optimum gain in the feedforward loop of the arc length control system [6]. With its application constant arc length can be maintained over a wide set of welding currents. A pseudogradient adaptive algorithm used to self-tune a proportional-integral (PI) controller is presented in [7]. In 1994 a system which uses arc temperature for feedback was presented [8].

3. MACHINE VISION BASED CONTROL SYSTEMS

A typical machine vision based arc welding control system is shown in Fig. 7.

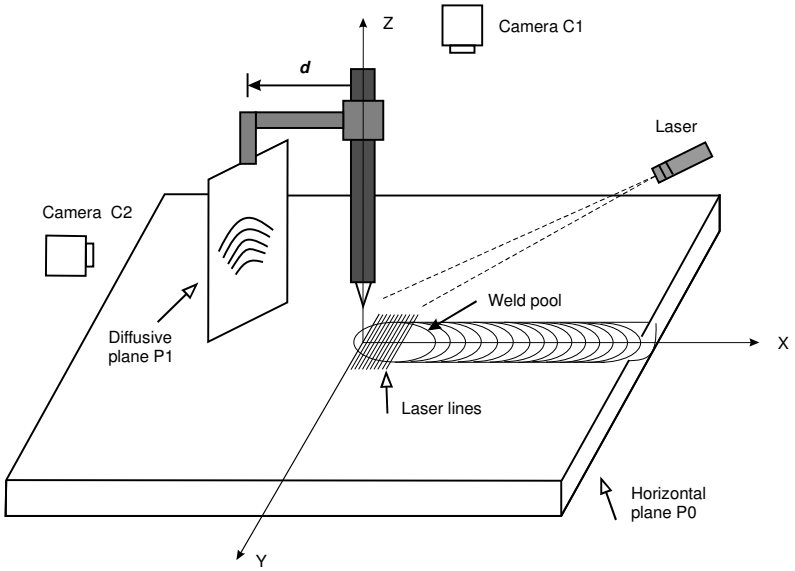

Figure 7 Machine vision based arc welding control [9]

It uses a laser light source, which makes it possible to observe the weld region even in the case of very strong light coming from the weld region.

CONCLUSIONS

Based on the amount of papers dealing with arc welding control it can be concluded that despite being a quite old technology it is still an area of vivid research.

REFERENCES

[1] John Frederick Lancaster. The physics of welding. Physics in technology, 15(2):73, 1984.
[2] Jian-Min Wang and Sen-Tung Wu. A novel inverter for arc welding machines. IEEE Transactions on Industrial Electronics, 62(3):1431–1439, 2015.
[3] Yizhang Liu, George E Cook, R Joel Barnett, and James F Springfield. PC-based arc ignition and arc length control system for gas tungsten arc welding. IEEE transactions on industry applications, 28(5):1160–1165, 1992.
[4] S Ozcelik and K Moore. Modeling, sensing and control of gas metal arc welding. Elsevier, 2003.
[5] Jiluan Pan. Arc welding control. Elsevier, 2003.
[6] Jon B Bjorgvinsson, George E Cook, and K Andersen. Microprocessor based arc voltage control for gas tungsten arc welding using gain scheduling. IEEE transactions on industry applications, 29(2):250–255, 1993.
[7] DE Henderson, PV Kokotovic, JL Schiano, and DS Rhode. Adaptive control of an arc welding process. IEEE Control Systems, 13(1):49–53, 1993.
[8] DV Nishar, JL Schiano, WR Perkins, and RA Weber. Adaptive control of temperature in arc welding. IEEE Control Systems, 14(4):4–12, 1994.
[9] ZhenZhou Wang. Monitoring of gmaw weld pool from the reflected laser lines for real-time control. IEEE Transactions on Industrial Informatics, 10(4):2073–2083, 2014.

INTERNATIONAL SCIENTIFIC CONFERENCE ON ADVANCES IN MECHANICAL ENGINEERING
13-15 October 2016, Debrecen, Hungary

INVESTIGATION OF MAINTENANCE PROCESS WITH MARKOV MATRIX

[1]POKORÁDI László CSc, [2]DUER Stanisław PhD

[1]Óbuda University, Institute of Mechatronics and Vehicle Engineering
E-mail: pokoradi.laszlo@bgk.uni-obuda.hu
[2]Politechnika Koszalińska, Wydział Mechaniczny, Poland
E-mail: stanislaw.duer@tu.koszalin.pl

Abstract
The operation is one of the most important territories of the engineering practice. From the mathematical point of view, maintenance is a discrete state space stochastic process without after-effects, so it can be modelled as a Markov-chain. After determination of probabilities of changes of operational states and setting up the transition probability (Markov) matrix, a matrix-algebraic method can be used for investigating these processes with systems approach analysis. This paper is aimed to show the first result of Authors on maintenance process modelling with Markov matrix that is a background their future scientific research related to this field of applied mathematics and maintenance modelling.

Keywords: *Maintenance; Stochastic modelling; Markov-processes.*

1. INTRODUCTION

The Operation (maintenance) is one of the most important territories of practical engineering [9]. It is a stochastic process based upon the used equipment, their maintenance, their preparation, and also based upon the personnel carrying out their repair, and upon the regulations. This process is set of events that happen to equipment, or to one of its systems from its manufacturing to its discarding, is a random in time and frequency succession of states of operation.
As leaving a certain state of operation does not depend on the previous states, or their succession, that is the process has not after-effects, maintenance can be considered as a mathematically continuous time, discrete state space Markov-process. Such stochastic process can be approximated with a Markov-chain.
Decisions concerning an operation system, and its control-efficiency respectively, can be made on the basis of certain characteristic features. During the study of the operation process such characteristic features can be established through the system approach, by means of the continuous-time, discrete-state space Markov-, or Semi-Markov models of the operation process.
There is a vast literature on maintenance and Markov processes, including many articles and books. The mathematical background of Markov-processes is discussed in books of Bharucha-Reid [1], Karlin and Taylor [4] and Ushakov [10]. The purpose of Jardine and Tsang's book is to provide readers with the tools needed for making data-driven decisions [3]. Duer presented a modelling method of the operation process of repairable technical objects of various classes [2]. Duer's paper also included theoretical grounds of the modelling process of the operation of objects in the form of the following models: mathematical (analytical), graphical and descriptive ones. Book of Manzini et.al. identifies the role of maintenance in a production system and the capability of guaranteeing a high level of safety, quality, and productivity in a proper way [5].
The paper of Nguyen et.al. has highlighted the importance of considering maintenance actions at the

tactical level [6]. Shu and Zhao presented a simplified three-step Markov analysis approach that avoids building large Markov models [8]. Their approach simplified the modelling and calculating of Markov-based safety integrity level verification without loss of accuracy. A case study was performed and the results prove that the proposed approach can simplify Markov modelling without loss of accuracy if a proper common cause failure model was adopted.
Pokorádi showed the possibilities of the use of Markov matrix in the case of stationary maintenance processes, and proposed a well-algorithmizable method for mathematical modelling of stationary stochastic industrial process [7]. This modelling method can be used for estimating maintenance cost and the time of availability of equipment.
The paper is shows first result of Authors on maintenance process modelling that is a background their future scientific research related to this field of applied mathematics and maintenance management.
The remainder of this article is structured as follows: Chapter 2 shows the theoretical background of Markov-processes. Section 3 presents theoretical background of maintenance process modelling. Section 4 shows results of stationer and non-stationer Markov-modelling of an investigated maintenance process. The closing part of the paper is a summary.

2. MARKOV-PROCESSES

Stochastic processes, whose development in the future is influenced by their development in the past only through their development in the present that is stochastic processes without after-effects, are called Markov-processes.
If process $\eta(\tau)$ during the study period can have an X value at any moment, it is called a continuous-time process. If η can only have some value at certain moments, the process is called a discrete-time process. A stochastic process is considered to be of discrete state space, if the possible values of parameter η constitute a finite set or a count non-finite set.
Finite or count non-finite stochastic process, that is the discrete state space one with no after-effects, is called Markov-chain. In this case the hypothetical probability

$$P_{ij} = P\left\{\eta(\tau_{n+1}) = X_j \middle| \eta(\tau_n) = X_i\right\} \tag{1}$$

is called transition probability. Having N number of states, P_{ij} transition probabilities are usually arranged in matrix

$$\mathbf{P}_{NxN} = [P_{ij}] \tag{2}$$

For the sake of further analyses it is advisable for us to consider the case a transition where after $\Delta\tau$ time period the value of $\eta(\tau)$ will be the beginning one again. So the determination of variables in the main diagonal of the matrix is carried out as follows:

$$P_{ii} = 1 - \sum_{\substack{j=1 \\ j \neq i}}^{N} P_{ji} \tag{3}$$

as the total space means that the object of operation enters into a new state or it remains in the beginning one. Using the Markov-matrix, the change in time of the probability of staying in different states can occur according to the equation

$$\mathbf{p}(\tau + \Delta\tau) = \mathbf{P}^T \mathbf{p}(\tau) \tag{4}$$

where $\mathbf{P}^T$ is the transposed matrix of $\mathbf{P}_{NxN}$ [1].

3. MAINTENANCE PROCESS

Maintenance process can be described with the so called operational chain, which is, from mathematical point of view a Markov-chain (see Fig. 1).

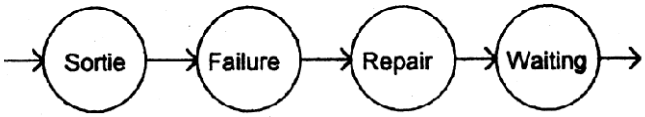

Figure 1 An Operational Chain

When analysing operational processes with the system approach, the actual succession of single states for each aircraft is no concern of ours. It is rather complicated to describe the whole operational process with an operational chain. In order to achieve a clearer survey it is advisable to describe the operational process as a directed graph. Within the graph of operation states are represented by another are represented by the directed edges of the graph (see Fig. 2).
Analysing the operational chain or the type graph, we assume that states are clearly marked, and transitions occur during zero time. For characterization of transitions from one state to another we use their transition probability.
The limit of transition probability P_{ij} below is called transition probability density, and marked with

$$\beta_{ij} = \lim_{\Delta\tau \to 0} \frac{P_{ij}(\Delta\tau)}{\Delta\tau} \tag{5}$$

where $\Delta\tau$ is the length of the time interval.
Naturally these transition probability densities β_{ij} can be arranged in matrix analogously to equations (2) and (3):

$$\mathbf{B}_{NxN} = [\beta_{ij}] \tag{6}$$

During our investigation maintenance process of the equipment used in a large number four different (***A***, ***B***, ***C***, ***D***) types component-related failures have been distinguished. The feature of the repairs of equipment (except ***C*** type failure) is a long – approximately 45 day (1080 hours) – period because of logistical matters. This investigation is done from point of view of end-user; therefore the repairs are characterized by Mean Repair Turnaround Times (MRTT). Additionally it can be established that the time of replacement of faulty equipment is negligible. So these times are not taken into account during simulation modelling.

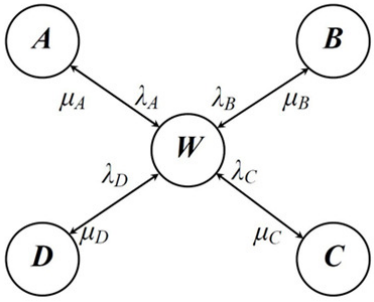

Figure 2 The Graph Model of Investigated Maintenance Process

The main data of the failures and their repairs are included in Table 1. The Fig. 2 shows weighted directed graph of the process. In the graph, the weights of the edges show probability densities

(failure or turnaround rates) of changes of operational states.
The failure rate λ_i is equal to the probability of the i^{th} failure in a unit time interval given that no failure has occurred before it [7]. The turnaround rate μ_j can be interpreted analogically. The system of differential equations of this process that describes the changes in time of the probability densities can be determined as

$$\mathbf{B}=\begin{bmatrix} 1-(\lambda_A+\lambda_B+\lambda_C+\lambda_D) & \mu_A & \mu_B & \mu_C & \mu_D \\ \lambda_A & 1-\mu_A & 0 & 0 & 0 \\ \lambda_B & 0 & 1-\mu_B & 0 & 0 \\ \lambda_C & 0 & 0 & 1-\mu_C & 0 \\ \lambda_D & 0 & 0 & 0 & 1-\mu_D \end{bmatrix} \tag{7}$$

Table 1 Essential Data of Statistical Analysis

Failures	***A***	***B***	***C***	***D***
Mean Time Between Failures *MTBF* [hour]	183627	162059	152800	179789
Failure Rate λ [hour^{-1}]	5.446 10^{-6}	6.171 10^{-6}	6.545 10^{-6}	5.562 10^{-6}
Mean Repair Turnaround Time *MRTT* [hour]	1080.8	1081.1	167.13	1079.8
Turnaround Rate μ [hour^{-1}]	9.252 10^{-4}	9.250 0^{-4}	5.983 10^{-3}	9.261 10^{-4}

3. RESULTS

In case of stationary processes, using the property of unit matrix **E**, the following matrix equation can be set up

$$\mathbf{p}(\tau+\Delta\tau)=\mathbf{P}^T\mathbf{p}(\tau)=\mathbf{E}p(\tau) \tag{8}$$

which can be transformed into the following formula

$$[\mathbf{P}^T-\mathbf{E}]\mathbf{p}=\mathbf{0} \tag{9}$$

In this case the problem is that the numerical algorithms provide the trivial solution. It is obvious that our concern is the solution different from the trivial one. The equation with N unknowns (9) has been transformed into an equation with $N+l$ unknowns. The $N+l^{th}$ equation is:

$$\sum_{i=W}^{E} P_i(\tau)=1 \tag{10}$$

which expresses that the equipment has to stay only in one of six states (in the present case, the state space consists of them). Then on the basis of equations (9) and (10) stochastic model of the investigated stationary operation process can be depicted as the following matrix formula:

$$\begin{bmatrix} & & & \vdots & 1 \\ \mathbf{P}^T & - & \mathbf{E} & \vdots & \vdots \\ & & & \vdots & 1 \\ \cdots & \cdots & \cdots & \cdots & \cdots \\ 1 & \cdots & 1 & \vdots & 0 \end{bmatrix}\begin{bmatrix} 1 \\ \vdots \\ 1 \\ \cdots \\ 1 \end{bmatrix}=\begin{bmatrix} 1 \\ \vdots \\ \vdots \\ \vdots \\ 1 \end{bmatrix}. \tag{11}$$

The methodology of setting up of the model mentioned above can be known profoundly by publication [7]. Table 2 consists of results of equation (11) that is stochastic model of maintenance process using nominal values of Table 1.

Table 2 Results of Stationary Model

$P_W = 9.7399\ 10^{-1}$	$P_A = 1.1452\ 10^{-3}$	$P_B = 2.0551\ 10^{-3}$
$P_C = 1.5562\ 10^{-3}$	$P_D = 5.1048\ 10^{-3}$	$P_E = 5.8403\ 10^{-3}$

In case of non-stationary maintenance processes the probabilities of staying in different states can be determined with equation (9).
Using the dynamic Markov model, we determined the change of probabilities of staying in different states depending on time. These results are shown in figure 3. The diagrams contain the probabilities of staying in states during an 8760-hour (1 year) period. The initial state was:

$$P_W(0) = 1 \; ; \; P_A(0) = P_B(0) = P_C(0) = P_D(0) = 0 \; . \tag{8}$$

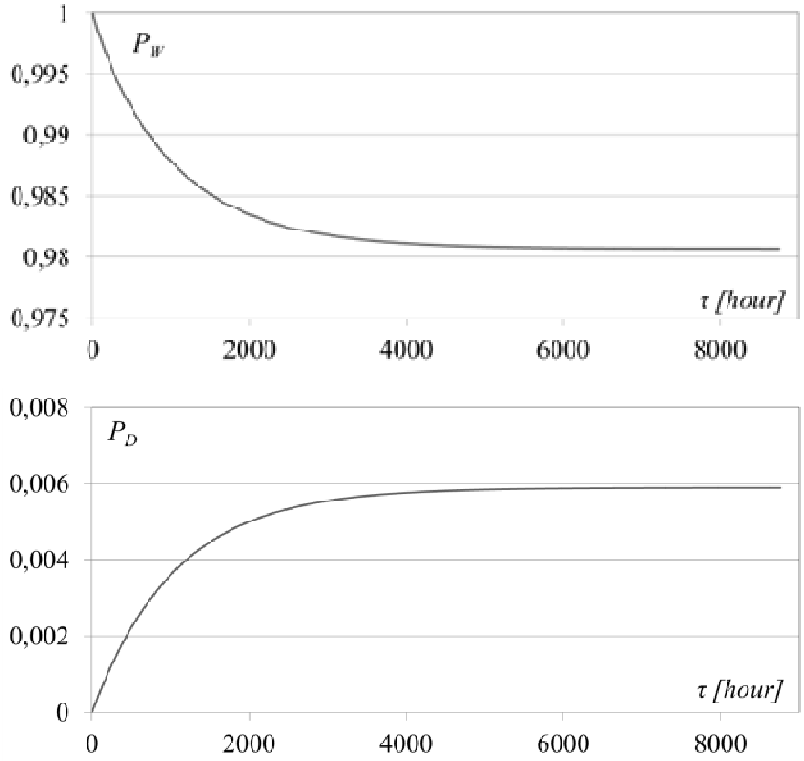

Figure 3 Results of Non-Stationary Model

From the results, the following conclusions are made:

- The proposed simulation methods can be used to analyse maintenance processes.

The results of the simulations show that the investigated maintenance system contains complex interconnections and effects. It is possible that using "linear approach", these relationships cannot be depicted and decision makers draw erroneous conclusions and make inaccurate decisions.

- The results of dynamic model approach the stationary model's ones asymptotically.

These results verify the models.

- The proposed simulation methods can be developed.

For example, knowing production proceeds, the revenue can be determined. (Due to the lack of data we have waived in this study.)
Parametrical uncertainties maintenance systems and processes can be analysed by Dynamic Monte-Carlo Simulation of Markov-Processes.

CONCLUSIONS

From mathematical point of view, the maintenance is a discrete state space stochastic process without after-effects so it can be approximated with a Markov-chain. After setting up of Markov (transition probability) matrix analysis of maintenance process with system approach can be investigated with matrix-algebraically. This paper was aimed to show the possibilities of use of Markov matrix in case of stationary or non-stationary maintenance process.
The Authors' planed prospective scientific research related to this field of applied mathematics and maintenance management includes elaborating methodologies of mathematical tools for example Dynamic Monte-Carlo Simulation to analyse maintenance systems and processes.

REFERENCES

[1] Bharucha-Reid, A.T.: Elements of Theory c of Markov Processes and Their Applications. New York: Mc Graw-Hill Book Company, 1960.
[2] Duer, S.: Modelling of the operation process of repairable technical objects with the use information from an artificial neural network. Expert Systems with Applications, 38, 5867-5878., 2011.
[3] Jardin, A.K.S., Tsang, A.H.C.: Maintenance, Replacement, and Reliability: Theory and Applications. Taylor & Francis, New York, 2006.
[4] Karlin, S., Taylor, H.M.: A First Course in Stochastic Processes. Academic Press, London, 1985.
[5] Manzini, R., Regattieri, A., Pham, H., Ferrari, E.: Maintenance for Industrial Systems. Springer-Verlag, New York, 2010.
[6] Nguyen, T., Castanier, B., Yeung, T.: Maintaining a system subject to uncertain technological evolution. Reliability Engineering and System Safety, 128, 56-65., 2014.
[7] Pokorádi, L.: Availability Assessment Based on Stochastic Maintenance Process Modelling. Debreceni Műszaki Közlemények 1, 37-46., 2013.
[8] Shu, Y., Zhao, J.: A simplified Markov-based approach for safety integrity level verification. Journal of Loss Prevention in the Process Industries, 29, 262-266., 2014.
[9] Szabó J.Z.: Műszaki diagnosztikai módszerek. Óbudai Egyetem, Bánki Donát Gépész és Biztonságtechnikai Mérnöki Kar, Budapest, 2015.
[10] Ushakov, I.A.: Handbook of Reliability Engineering. John Wiley & Sons, Inc., New York, 1994.

INTERNATIONAL SCIENTIFIC CONFERENCE ON ADVANCES IN MECHANICAL ENGINEERING
13-15 October 2016, Debrecen, Hungary

DETERMINATION OF DRYING RATE AT HERBS DRYING WITH AMBIENT AIR

[1]POÓS Tibor PhD, [2]VARJU Evelin, [3]SEBESI Viktória, [4]SZABÓ Viktor

[1]Budapest University of Technology and Economics, Faculty of Mechanical Engineering, Department of building Services and Process Engineering, poos@mail.bme.hu
[2]Budapest University of Technology and Economics, Faculty of Mechanical Engineering, Department of building Services and Process Engineering, varjuevelin93@gmail.com
[3]Budapest University of Technology and Economics, Faculty of Mechanical Engineering, Department of building Services and Process Engineering, sebesi.viki@gmail.com
[4]Budapest University of Technology and Economics, Faculty of Mechanical Engineering, Department of building Services and Process Engineering, szabo.viktor@mail.bme.hu

Abstract
The key element in herbs and spices processing is drying. The required low moisture content of medicinal plants to storage can be achieved only by applying drying equipment at Hungarian climatic conditions. The extent of the dryer capacity defines the processing capacity of the factory. During the daily operation can easily occur bottleneck, when large amount of herbs are transported to the factory, which is above the drying capacity - various plants unexpected simultaneous flowering, weather emergency, extraordinary collecting, etc. Our aim is determination of operational data at herbs pre-drying with low temperature air by measurements. This work defines the drying rate for various medicinal plants at drying with ambient air.

Keywords: *herb, convective drying, drying rate, moisture rate.*

1. INTRODUCTION

The role of medicinal plants in therapy is changed in different ages, closely linked to the state of the level of the therapy. No doubt that synthetic drugs have played a vital role in the enhancement of human living standards during the past century; herbal medicine has regained its momentum once again in recent years. Long-term ailments cannot typically be cured by injection or consumption of a single medicine. Instead of focusing only on curing an illness, people are paying more attention nowadays to improve the whole body immune system so as to prevent the attack of diseases. Besides their traditional pharmaceutical usage, herbs have also become one of the important sources for drug discovery and production. Herbal medicine plays an important role in healthcare in many regions of the world [1, 2].
The special active agent content makes suitable herbals for healing and health preservation. A significant number of medicinal plants are pharmaceutical raw materials, which from the active agent can be extracted by various procedures. These materials are marketed after determination of the exact active agent content, or by further processing are used for raw materials of drugs or combinations of drugs [3].
The aim of medicinal plants processing is turning the herbs to drug, some drugs form, pure active agent or medicine. Primary processing is called the collecting or harvesting, cleaning, drying, qualification etc. The moisture content of harvested plants is generally very high, around 60-80%. %. If the moisture content is not significantly reduced, it enables maturation of harmful biological processes. Because of this valuable active agent of herbs can be destroyed and the external properties of the drugs can become unfavourable. The fundamental requirement to prevent the

harmful processes is the reduction of moisture content as quickly as possible [3, 4].
During our research work five herbs (Achillea collina, Solidago gigantea, wormwood, walnut leaf and Daucus carota) were investigated. One of the aims of our work was the determination of drying rate at a given air velocity for different medicinal plants. Another aim was to determine the drying rate for a given herb at different air velocities.

2. METHODS

During the measurements was used the equipment that is found at the Department of building Services and Process Engineering (*Figure 2*). The measurement begins by filling the herbs into the drying chamber (7). First of all, the initial weight (m_0) and initial height (H_0) of plants were measured, and the herbs initial moisture content (x_0, X_0) is determined by small sample experiment.

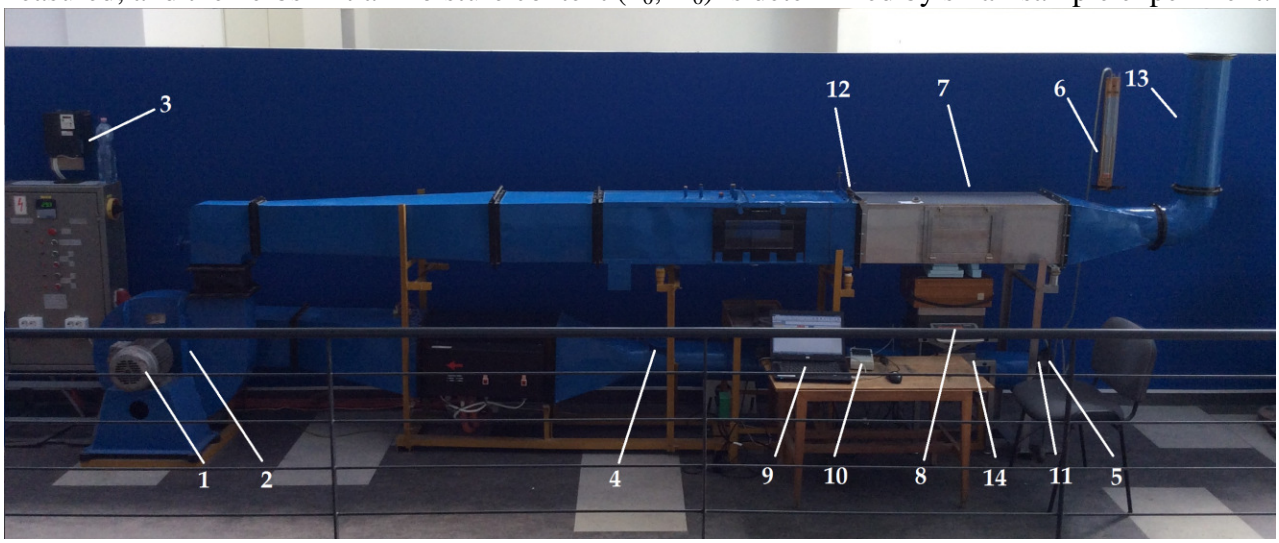

Figure 2 Experimental apparatus and main parts (1 – electric motor, 2 – centrifugal fan, 3 – frequency converter, 4 – butterfly valve, 5 – orifice flow meter, 6 - U-tube manometer, 7 – drying chamber, 8 - scales, 9 – software on computer, 10 – data logger, 11 – measuring temperature and absolute humidity of ambient air, 12 – measuring inlet air temperature, 13 – outlet pipe, 14 - elevator)

The drying chamber is applied on the scale (8) and raised from the bottom into the dryer by the elevator (14). Later the centrifugal fan (2) is started, that is driven by an electric motor (1), and the flow rate can be modified by the frequency converter (3) and butterfly valve (4). A U-tube manometer (6) measures the pressure difference (Δh) on the orifice flow meter (5), that from the air velocity (v_G) is can be calculated. During the measurements the registered values by the data logger (10) are: temperature (T_{am}) and absolute humidity (Y_{am}) of ambient air by a hygrometer (11), inlet temperature (T_G) of drying gas by T-type thermometer (12) and the varying weight (m) of plants by the scales. The measured values are registered with 1 minute sampling by the software (9). The measurement takes about six to eight hours depending on the herb. The humid gas leaves the system through an outlet pipe (13) to the ambient. The measurement ends by stopping the fan and taking out the drying chamber from the dryer. The final weight (m_1) and final height (H_1) of plants are measured, then herbs final moisture content (x_1, X_1) is determined by small sample experiment.

3. RESULTS

During drying the velocity of drying gas was almost the same, which is chosen to 0,5 m/s by previous research [1]. This air velocity results sufficient drying rate with relatively small energy

consumption. Furthermore, this velocity had to be below the minimum fluidization velocity not to carry away the herb parts by pneumatic transport. During measurements the parameters are described in chapter 2 was registered. *Table 1* shows initial data and measurement results at various medicinal plants, where Δm_{water} is the weight of water that is evaporated to the drying gas. the During measurements Achillea collina and Solidago gigantea dried up the most, almost 23% moisture content decreasing. Varying of moisture content at Daucus carota is 15%, while wormwood and walnut leaf showed the smallest moisture content decreasing, only 6-8 %.

Table 1 Initial data and measurement results of the studied medicinal plants

		Achillea collina	Solidago gigantea	Wormwood	Walnut leaf	Daucus carota
t	[min]	397	414	442	378	312
m_0	[kg]	2,917	2,721	1,603	3,481	1,996
m_1	[kg]	1,5995	1,897	1,273	2,897	0,899
Δm_{water}	[kg]	1,318	0,824	0,330	0,584	1,097
x_0	[%]	71,2	66,0	63,6	62,7	83,3
x_1	[%]	47,6	42,4	57,0	54,4	68,1
X_0	[kg/kg]	2,47	1,945	1,749	1,681	4,996
X_1	[kg/kg]	0,91	0,736	1,326	1,192	2,131
H_0	[mm]	240	250	280	280	270
H_1	[mm]	200	230	250	260	130
V_0	[m^3]	0,0252	0,0263	0,0294	0,0294	0,0284
N_V	[kg/h/m^3]	7,9015	4,5493	1,5237	3,1530	7,4413
$\overline{T}_{am}$	[°C]	29,30	29,70	28,06	25,17	25,64
$\overline{Y}_{am}$	[g/kg]	9,2	10,4	11,2	8,7	8,6
$\overline{T}_G$	[°C]	31,2	31,4	30,2	27,7	28,0
v_G	[m/s]	0,5				

An avarage drying rate (N_V) can be determined that is related to the volume of material, what is valid at given moisture content range, temperature and absolute humidity of drying air:

$$N_V = \frac{\Delta m_{water}}{t \cdot V_0} \tag{1}$$

where t is length of drying, V_0 is the initial volume of plants. Characteristics of drying air and the initial volume of herbs were nearly the same each measurement. Drying rate of Achillea collina and Ducus carota were the highest, followed by Solidago gigantea, walnut leaf and wormwood.

Figure 3 shows the weight decreasing of Achillea collina and absolute humidity of drying gas in the function of time. The diagrams were similar to the other medicinal plants too.

The drying process can be characterized by drying rate curves, where the moisture rate is plotted in the function of time. The moisture rate can be determined the following equation:

$$MR = \frac{X - X^*}{X_0 - X^*} \tag{2}$$

where MR is moisture rate (1), X is the currently moisture content of the herbs (kg/kg), X_0 is the final moisture content of herbs (kg/kg), X*is the equilibrium moisture content of herbs (kg/kg) that is neglected in this case.

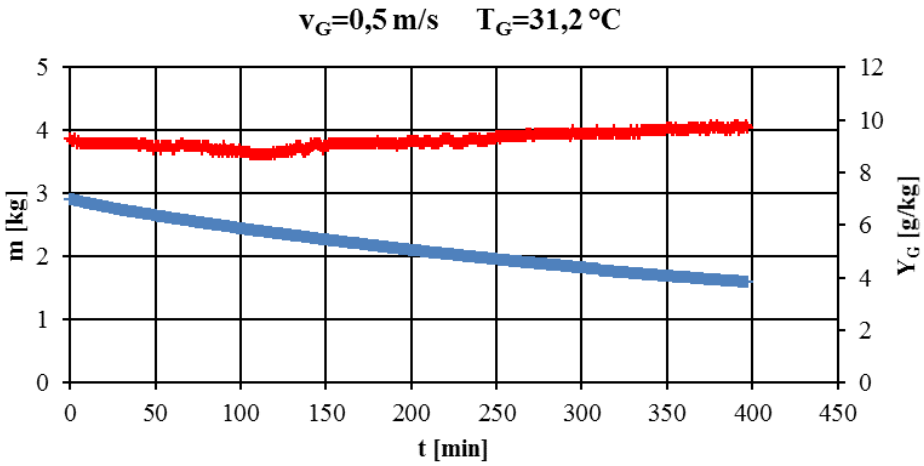

Figure 3 Weight decreasing (blue) and absolute humidity of air (red) in the function of time at Achillea collina

Figure 4 shows the moisture rate in the function of time by the studied medicinal plants. It can be observed that the greater the gradient of the linear, the more moisture lost the plants. The Daucus carota, Acillea collina and Solidago gigantea lost the most moisture during drying compared with the initial state, while the walnut leaf and wormwood lost less.

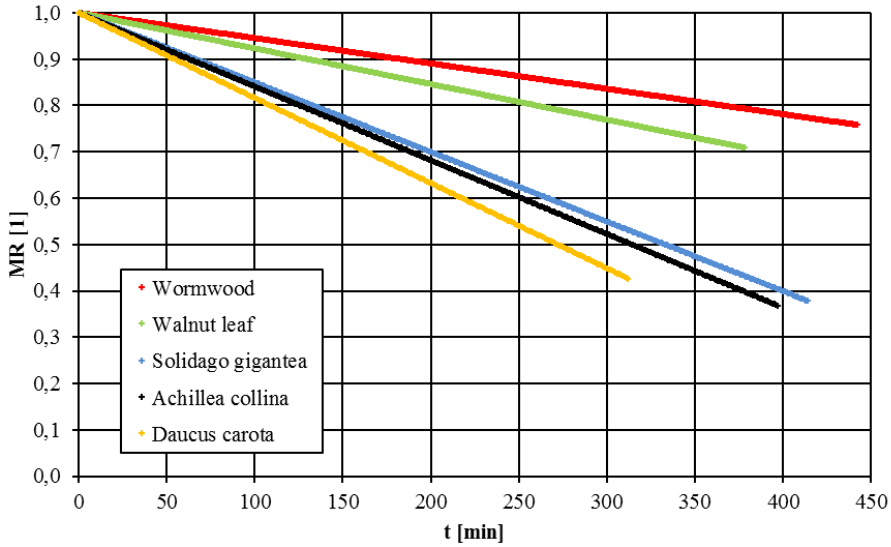

Figure 4 The moisture rate in the function of time by the studied medicinal plants.

The temperature of drying air is nearly constant so the variable parameter during measurements is only the air velocity that influence the drying rate. That is why several measurements were occurred for Solidago gigantea at different air velocities to determine the influence of air velocity to drying rate. The air velocities beyond 0,5 m/s are 1; 0,25; 0,1 m/s and natural convection (0 m/s).
During measurements the parameters are described in chapter 2 was registered. *Table 2* shows initial data and measurement results for Solidago gigantea at various air velocities.
There is a minimum air velocity, which is not worthy to go below, because it would reach the same result if the herbs dry with ambient air at natural convection. In addition, there is a maximum air velocity, which is not worthy to go above, because it does not cause significant improving during drying and occurs pneumatic transport of the medicinal plants. There is an optimum velocity what

can be achieved the highest level of drying with, but to determine the actual air velocity further measurements and economic calculations would be needed.

Table 2 Initial data and measurement results for Solidago gigantea at various air velocities

v_G	[m/s]	1	0,5	0,25	0,1	0
t	[min]	432	414	443	329	399
m_0	[kg]	2,605	2,721	2,073	1,94	0,82
m_1	[kg]	1,826	1,897	1,348	1,606	0,749
Δm_{water}	[kg]	0,779	0,824	0,725	0,334	0,071
x_0	[%]	58,0	66,0	58,6	54,0	52,9
x_1	[%]	45,5	42,4	38,4	44,4	40,0
X_0	[kg/kg]	1,381	1,945	1,416	1,174	1,124
X_1	[kg/kg]	0,835	0,736	0,625	0,8	0,667
H_0	[mm]	270	250	280	270	150
H_1	[mm]	270	230	260	260	150
V_0	[m^3]	0,0284	0,0263	0,0294	0,0284	0,0160
N_V	[kg/h/m^3]	3,8164	4,5493	3,3399	2,1486	0,6690
$\overline{T}_{am}$	[°C]	25,62	29,70	26,86	25,84	27,89
$\overline{Y}_{am}$	[g/kg]	11,1	10,4	10,1	10,5	10,5
$\overline{T}_G$	[°C]	27,4	31,4	29,9	27,4	27,9

Figure 5 shows the weight decreasing of Solidago gigantea and absolute humidity of air in the function of time at 0,25 m/s air velocity. The diagrams were similar at the other air velocities too.

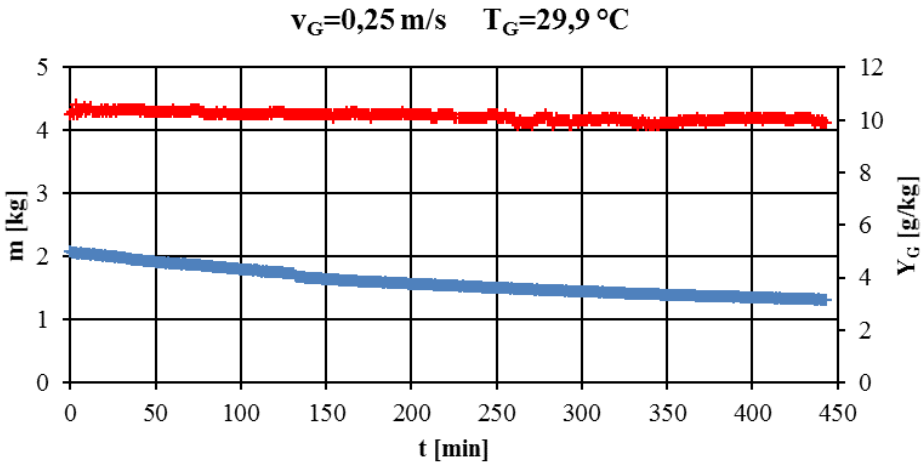

Figure 5 The weight decreasing (blue) of Solidago gigantea and absolute humidity of air (red) in the function of time at 0,25 m/s air velocity

Characteristics of drying air and the initial volume of herbs were nearly the same each measurement. Unlike the anticipation at the 1 m/s air velocity was not the greatest drying rate, but 0,5 m/s, however there was smaller amount of herbs and the period of drying was also shorter, but

the temperature of drying gas was higher with 4°C. Regardless of this, the other measurements were corresponding to the expected results, that the lower the velocity of the drying gas, the lower the drying rate.

Figure 6 shows the moisture rate in the function of time for Solidago gigantea at different air velocities. In this case the results were surprisingly different compared to the drying rates. The greatest moisture rate decreasing was at 0,5 and 0,25 m/s air velocities, while the results at 1; 0,1 and 0 m/s air velocities were nearly the same.

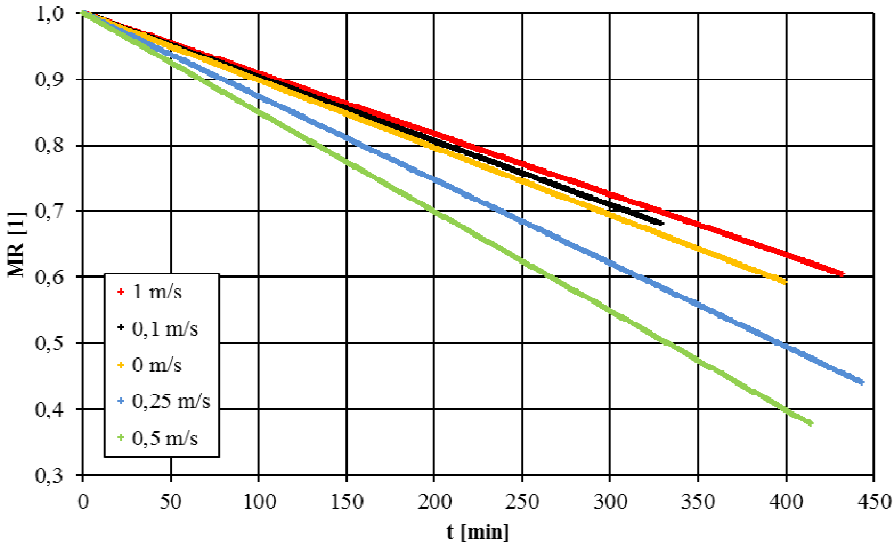

Figure 6 The moisture rate in the function of time for Solidago gigantea at different air velocities.

CONCLUSIONS

During drying the moisture content decreasing was investigated at constant air velocity and from this an average drying rate was determined that is related to the volume of the material. The average drying rate of Achillea collina and Daucus carota were the highest, followed by Solidago gigantea, walnut leaf and wormwood. The air velocity how influences the moisture content decreasing was also investigated. These measurements were made for Solidago gigantea. The air velocities were 1; 0,5; 0,25; 0,1 m/s and natural convection (0 m/s). The required air velocity can be determined by measurements for a particular process, which the effective drying can be achieved beyond economical operating. During drying the moisture rate in the function of time was investigated, which can characterize the efficiency of drying.

ACKNOWLEDGEMENTS

Special thanks for Dr. Mária Örvös for her helps in this work. This paper was supported by Gedeon Richter's Talentum Foundation (H-1103 Budapest, Gyömrői str. 19-21, Hungary), and by Hungarian Scientific Research Found (OTKA-116326).

REFERENCES

[1] Arun S. M.: *Handbook of Industrial Drying*, Fourth Edition, 2015.
[2] Szőke É. et al: *Knowledge of Herbal and Drugs Pharmacognosy – Phytochemistry, the use of Herbals*, 2012.
[3] Borbélyné H. É., Kutasy E.: *Cultivation and processing of herbs*, Debrecen, 2012.
[4] http://trebag.hu/tudasbazis_cikk/92/gyogynovenyek_termesztouzemi_feldolgozasa (*Medicinal plants processing at growing factory*, 2016.09.24.)

INTERNATIONAL SCIENTIFIC CONFERENCE ON ADVANCES IN MECHANICAL ENGINEERING
13-15 October 2016, Debrecen, Hungary

DETERMINATION OF VOLUME DECREASE AND AIR VELOCITY AT HERBS DRYING WITH AMBIENT AIR

[1]POÓS Tibor PhD, [2]VARJU Evelin

[1]Budapest University of Technology and Economics, Faculty of Mechanical Engineering, Department of building Services and Process Engineering, poos@mail.bme.hu
[2]Budapest University of Technology and Economics, Faculty of Mechanical Engineering, Department of building Services and Process Engineering, varjuevelin93@gmail.com

Abstract
The special active agent content makes suitable herbals for healing and health preservation. The key element in herbs and spices processing is drying. The required low moisture content of medicinal plants to storage can be achieved only by applying drying equipment at Hungarian climatic conditions. The aim of the manuscript is to determinate operational data at herbs pre-drying with low temperature air by measurements. This work defines the volume decrease and drying air velocity for various medicinal plants at drying with ambient air.

Keywords: *herb, convective drying, volume decrease, fluidization.*

1. INTRODUCTION

A significant number of medicinal plants are pharmaceutical raw materials, which from the active agent can be extracted by various procedures. These materials are marketed after determination of the exact active agent content, or by further processing are used for raw materials of drugs or combinations of drugs. The aim of medicinal plants processing is turning the herbs to drug, some drugs form, pure active agent or medicine. Because of the high moisture content the freshly harvested raw plant parts are not suitable for storage and should be preserved in some way. Primary processing is called the collecting or harvesting, cleaning, drying, qualification etc. [1].
The moisture content of harvested plants is generally very high, around 60-80%. If the moisture content is not significantly reduced, it enables maturation of harmful biological processes. The fundamental requirement to prevent the harmful processes is the reduction of moisture content as quickly as possible. The moisture content of the medicinal plants at the end of the herbs drying must be 10-14%. With this moisture content most of the drugs can be storage for a longer period of time without damage of the plants [2].
During our research work five herbs (Figure 1) were investigated. One of the aims of our work was the determination of the maximum air velocity at which the particular plant is still not fluidized during pre-drying or ventilation. This limit value is called the minimum fluidization velocity.

If air flows through a bed of solid particles in upward direction with the velocity which greater than the settling velocity of the particles, the solid particles will expanding and large instabilities with bubbling and channeling of gas are observed. At this state, solid bed looks like a boiling liquid, the particles blend and bump to each other, therefore this phenomenon called as fluidized state [3, 4]. *Figure 2* shows the fluidization diagram. In the section A-B the pressure drop can be described by quadratic equation of the Reynolds number. However this is only valid as long as the particles are at rest. In the section B-C the particles start to float and arrange in the direction of the least resistance. In the section C-D the resistance is higher by increasing the air velocity, but smaller extent and at the point C reaches a maximum. This is due to the loosening already reduces the

resistance in greater extent, than the increasing of the air velocity would do. The section D-E is the fluidized state, where further air velocity increasing will not cause pressure drop increasing.

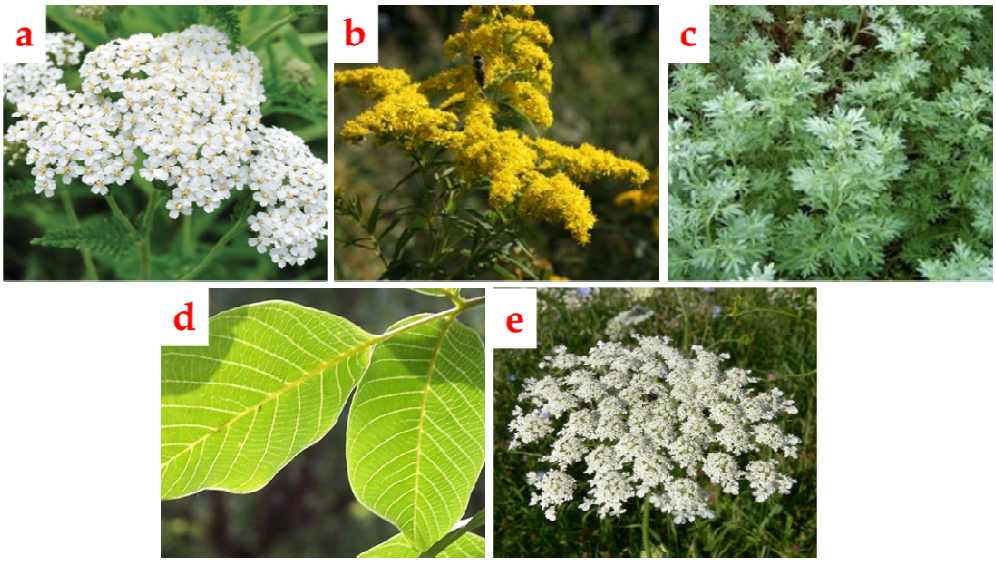

Figure 1 The studied medicinal plants (a – Achillea collina, b – Solidago gigantea, c - Wormwood, d – Walnut leaf, e –Daucus carota)

Point D is the fluidization starting point. Ideally, the fluid velocity among the paricles is constant, because at higher volume flow rate the voids volume increases. From the point E with increasing the air velocity, after reaching the upper limit of gas flow rate, the gas stream the whole congeries carries away; this is called pneumatic transport [4, 5].

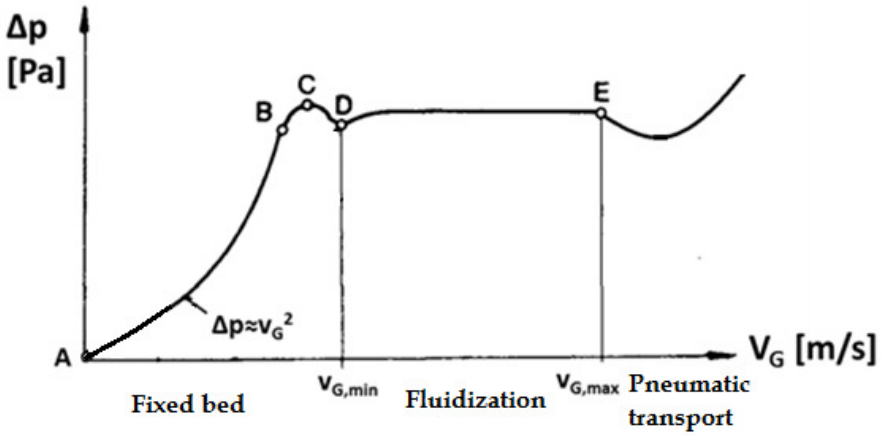

Figure 2 The differential pressure in the function of air velocity in the empty cross section

Another aim of our work was to determine the volume decrease in the function of time and moisture content. The measurement results would be used for planning of a medicinal plants pre-drying, ventilation technology.

2. METHODS

The measuring equipment – a pilot plant fluidized bed dryer – which is located at the Department of Building Services and Process Engineering. The *Figure 3* shows the equipment. To the examination

of the phenomenon of fluidization the needed air flow provides a ventilator (1), where the flow rate can be modified by the knife gate valve (2), and be measured by the orifice flow meter (6) from the pressure difference. Before the measurement the studied plants through an upper opening are charged into the central part of the measuring system, the vertical positioned chamber (4) with the diameter 100 mm ($d_{chamber}$). During measurement the differential pressure of the chamber (7), the inlet gas temperature (3), the differential pressure of the orifice flow meter (8), the absolute humidity of ambient air (9), are measured. The measured values are registered with a self-developed software (5) by a data logger (10).

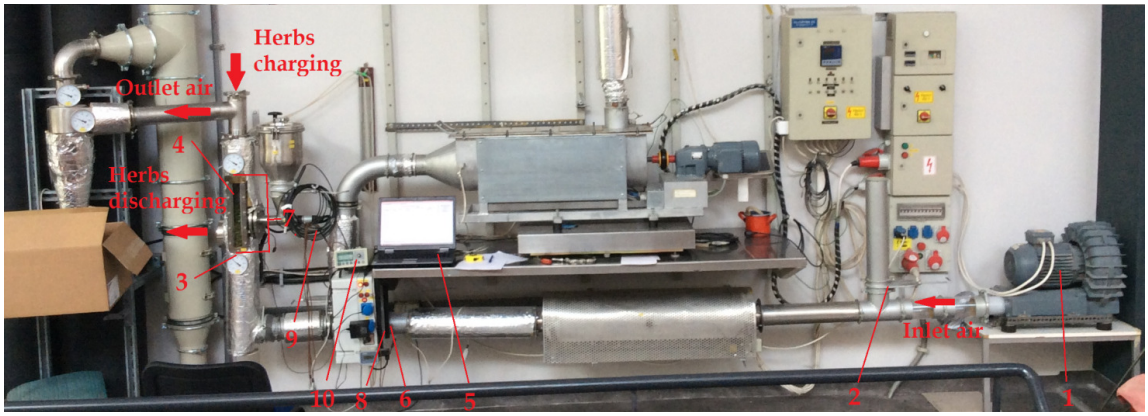

Figure 3 The fluidized bed dryer (1 – ventilator, 2 – knife gate valve, 3 – inlet temperature measuring, 4 – chamber, 5 –analysis software, 6 – orifice flow meter, 7 – measuring of pressure drop of chamber, 8 – measuring of pressure drop of orifice flow meter, 9 – measuring of absolute humidity of ambient air, 10 – data logger)

2.1 Minimum fluidization velocity

űThe measurement begins by the chopping of the medicinal plants to help the placement in the chamber. The chopped plants is charged manually through the upper opening into the chamber, and the initial height of plants (H_0) is measured before the measurement. Before measuring, the herbs initial moisture content is determined by small sample experiment (x_0). The next step is starting the ventilator while the knife gate valve is completely open. The air velocity is raised by gradually closing the knife gate valve, while the measured values are registered with 10 seconds sampling by the software: differential pressure of orifice flow meter (Δp_{ofm}) and air temperature (T_{ofm}), differential pressure of the chamber ($\Delta p_{chamber}$), inlet temperature of air (T_G) and absolute humidity (Y_{am}) and temperature (T_{am}) of ambient air. The measurement is continued until we reach the adge of the fluidized state, which is the minimum fluidization velocity, where the herbs are just not fluidized. At this point the knife gate vale is opened, the ventilator is stopped and the plants are removed through the opening on the left side of the chamber from the system.

2.2 Volume decrease

The measurements require the same preparations such as chapter 2.1., then starting the ventilator while the knife gate valve is completely open. During the measurements the measured values are the same parameters that are registered the data logger at the determination of the minimum fluidization velocity, but the sampling time is 1 minute. In addition, in every half hour is recorded the height of the plants during drying. The measurement is continued until the varying the height of the material is negligible. Then the ventilator is stopped and the plants are removed through the

opening on the left side of the chamber from the system. After the measurement the herbs final moisture content is determined by small sample experiment (x_1).

3. RESULTS

During the determination of the maximum allowable air velocity, after some days spent in the laboratory the medicinal plants significantly dried, so they had low moisture content. Instead of the high moisture content which is 60-70%, the herbs were only 10-20%, which resulting lower snatching velocity, so in terms of discharge a more critical state were investigated. The varying of the moisture content of the herbs is negligible, because the short time measurement of determination of the minimum fluidization velocity. During the measurement air velocity was increased until the plants moved in the chamber, so we reached the fluidized state. From the measurement results calculated an average ambient temperature, inlet air temperature and absolute humidity of ambient air. These results can be seen in *Table 1*.

Table 1 The initial data and results of the studied medicinal plants

		Achillea collina	Solidago gigantea	Wormwood	Walnut leaf	Daucus carota
t	[s]	830	1020	990	580	990
H_0	[mm]	270	270	255	265	250
$\overline{T}_G$	[°C]	37,50	34,81	35,24	32,49	36,04
$\overline{T}_{am}$	[°C]	28,9	26,6	27,1	28,1	28,5
$\overline{Y}_{am}$	[g/kg]	10,1	10,5	10,6	10,5	10,4
x_0	[%]	14,6	21,7	17,7	10,1	12,5
$v_{G,max}$	[m/s]	1,8	1,9	2,1	1,8	2,2

Figure 4 shows the differential pressure of the chamber per one meter material in the function of air velocity in the case of Achillea collina. Diagram shows that the minimum fluidization velocity is 1,8 m/s in the case of Achillea collina. The maximum air velocity was determined similarly for the other herbs.

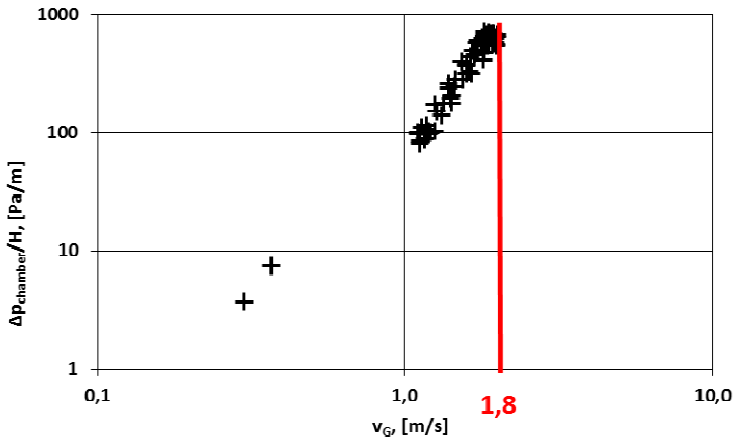

Figure 4 The differential pressure of the chamber per one meter material in the function of air velocity in the case of Achillea collina

The available five herbs were alike dry state and the measurements were happened in similar circumstances. It found that the maximum air velocity for each medicinal plants were between 1,8 and 2,2 m/s.

After this volume decrease is examined in the function of time and moisture content. Measurements were accomplished like described in chapter 2.2.. The initial data and measurement results of the studied medicinal plants are shown in Table 2.

During measurements the height of material (H) was recorded in every half hour, which from was determined the volume of the material (V) by the following equation:

$$V = H \cdot \frac{d_{chamber} \cdot \pi}{4} \tag{1}$$

In order to simplify comparing the measurement results a percental decreasing was calculated in every measuring points:

$$V_{\%} = \frac{V}{V_0} \cdot 100 \tag{2}$$

Table 2 The initial data and measurement results of the studied medicinal plants

		Achillea collina	Solidago gigantea	Wormwood	Walnut leaf	Daucus carota
v_G	[m/s]	1,74	1,83	1,44	1,41	1,55
t	[min]	242	373	304	205	195
H_0	[mm]	220	215	285	265	270
$\overline{T}_G$	[°C]	40,1	40,1	37,6	35,0	36,7
$\overline{T}_{am}$	[°C]	30,55	30,58	30,20	27,23	27,93
$\overline{Y}_{am}$	[g/kg]	8,6	9,8	11,1	8,2	8,3
x_0	[%]	71,2	66,0	63,6	62,7	84,1
x_1	[%]	40,3	23,9	53,0	37,3	36,2

Figure 5 shows the results of all measurements in one diagram, the volume decrease in the function of time. In the volume of wormwood and Achillea collina do not happen too much varying during drying. The varying of volume at walnut leaf and Solidago gigantea are similar, while volume decrease of Daucus carota compared to the other herbs is really intense.

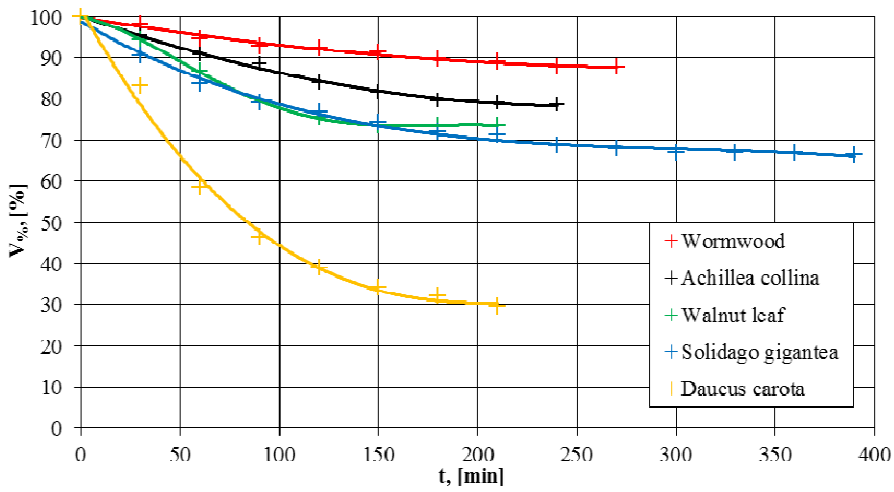

Figure 5 The volume decrease in the function of time at studied herbs

Figure 6 shows the volume decrease in the function of moisture content at studied herbs. The initial moisture content of the Daucus carota was the highest and the final moisture content had become the smallest, while the volume decrease of the herb was the highest during drying. The varying of the moisture content at Solidago gigantea was also high, but the plant is less collapsed during drying. The walnut leaf and Achillea collina showed similar varying during measurements, while wormwood reached the smallest volume decrease and moisture content varying.

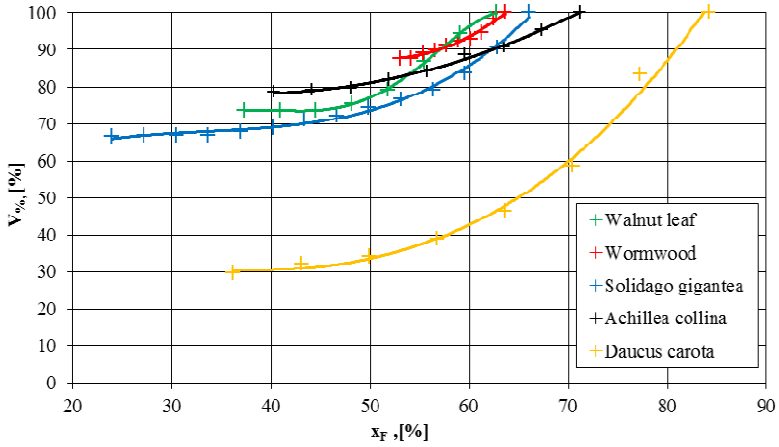

Figure 6 The volume decrease in the function of moisture content at studied herbs

CONCLUSIONS

The maximum air velocity was determined by the fluidized bed dryer, which is located at the Department, when the medicinal plants was just not in fluidized state and the gas stream did not carry away the material. The available five herbs were alike dry state and the measurements were happened in similar circumstances. It found that the maximum air velocity for each medicinal plants were between 1,8 and 2,2 m/s. The volume decrease was determined in the function of time and moisture content. The initial moisture content of the Daucus carota was the highest and the final moisture content had become the smallest, while the volume decrease of the herb was the highest during drying. The varying of the moisture content at Solidago gigantea was also high, but the plant is less collapsed during drying. The walnut leaf and Achillea collina showed similar varying during measurements, while wormwood reached the smallest volume decrease and moisture content varying.

ACKNOWLEDGEMENTS

Special thanks for Dr. Mária Örvös for her helps in this work. This paper was supported by Hungarian Scientific Research Found (OTKA-116326).

REFERENCES

[1] Borbélyné H. É., Kutasy E.: *Cultivation and processing of herbs*, Debrecen, 2012.
[2] http://trebag.hu/tudasbazis_cikk/92/gyogynovenyek_termesztouzemi_feldolgozasa (*Medicinal plants processing at growing factory*, 2016.09.24.)
[3] Leva, M.: *Fluidizáció (Fluidization),* Műszaki Könyvkiadó, 1964.
[4] http://technologia.chem.elte.hu/hu/muvelettan/Vegyipari_Muvelettan_teljes.pdf (*Chemical Operations*, 2016.09.30.)
[5] http://www.tankonyvtar.hu/en/tartalom/tamop412A/2011-0013_hodur_biologiai_rendszerek/52_fluidizci.html (*Technical processes of biological systems*, 2016.09.30.)

INTERNATIONAL SCIENTIFIC CONFERENCE ON ADVANCES IN MECHANICAL ENGINEERING
13-15 October 2016, Debrecen, Hungary

DIMENSIONLESS EVAPORATION RATE AT TUBULAR ARTIFICAL FLOW

[1]POÓS Tibor PhD, [2]SEBESI Viktória, [3]VARJU Evelin, [4]SZABÓ Viktor

[1]Budapest University of Technology and Economics, Faculty of Mechanical Engineering, Department of Building Services and Process Engineering, poos@mail.bme.hu
[2]Budapest University of Technology and Economics, Faculty of Mechanical Engineering, Department of Building Services and Process Engineering, sebesi.viki@gmail.com
[3]Budapest University of Technology and Economics, Faculty of Mechanical Engineering, Department of Building Services and Process Engineering, varjuevelin93@gmail.com
[4]Budapest University of Technology and Economics, Faculty of Mechanical Engineering, Department of Building Services and Process Engineering, szabo.viktor@mail.bme.hu

Abstract
Besides building services employments and swimming pools there are many industrial facilities with free surface water reservoir for different technological purposes. On the free surface heat transfer and diffusion occur, whereby the vapour diffuses into the ambient air. Therefore, the water loss should be replaced. There are many empirical correlations for calculating the quantity of evaporated water which methods largely differ from each other. The evaporation rate can be varied depending on attendance of clear humidity-based driving forces between gas and liquid or in addition attendance of temperature-based driving forces too. At the literary models another problem is that different correlations should be used depending on the temperature and velocity of ambient air and the temperature of the evaporating liquid. Furthermore the range of interpretation of these correlations in many cases is often not known. In our work dimensionless equations will be described the evaporation rate for natural and forced convection taking into account the direction of the two driving forces.

Keywords: *evaporation rate, Sherwood number, heat- and mass transfer.*

1. INTRODUCTION

In the contact surface of a free water surface with air, heat- and mass transfer process occurs [1, 2], when from the saturated surface of water vapor diffuses to the unsaturated air. This phenomenon is called evaporation.
The vapor from the water surface diffuses to the unsaturated air, which can be described by the molecular evaporation rate:

$$N_{H2O} = k_G M_{H2O} \left(p_{v,f} - p_{v,G} \right). \quad (1)$$

Evaporation from free liquid surface occurs commonly in everyday-life and industrial processes e.g. open air reservoirs, pools and swimming pools. There are two mechanisms of the air movement: forced convection by ventilation indoor or by wind outdoor, or natural convection based on concentration or temperature differences. Evaporation intensity can differ in case of still or rippling surfaces. A number of publications discuss the measurement of surface evaporation; their results are based on experiments.
Based on the experiments, correlations to best describe the phenomenon were identified by regression analysis; in general, they can be applied only in limited conditions. According to special sources, Dalton was the first in 1802 to discuss the issue and to describe the problem of evaporation

by empirical hydrodynamic approximation. He concluded that the intensity of evaporation is proportional to the partial pressure difference of the liquid surface and the main stream of air and the velocity of air flow.
The equations for evaporation rate of the researchers are valid in various interval (different gas and liquid temperature, surface area) and conditions (natural or forced convection), which reduces their usefulness. In addition, these equations are correct only for water, but in the industry there are several cases, where other, volatile components (e.g. ethanol used for cleaning, boric acid solution in power plant) can evaporated to the ambient. In this paper measurement results and evaporation rates are presented for the first and second categories.

2. METHODS

A describe and sketch of the equipment and measurements can be seen in our previous work [3].

3. RESULTS

During measurements velocity of air (v_{dG}), temperature of air (T_{dG}) and temperature of water – thereby the temperature of water surface - were adjusted. The temperature based driving force (ΔT) could, the absolute humidity based driving force (ΔY) could not have modified from the two evaporation driving forces through measurements. During research from the four cases of evaporation the first three cases were investigated. The convective heat flow direction was different, while the mass flow direction was the same.

1: $T_G > T_f$; $Y_f > Y_G$ (the water temperature is lower than the air temperature)
2: $T_G < T_f$; $Y_f > Y_G$ (the water temperature is higher than the air temperature)
3: $T_G = T_f$; $Y_f > Y_G$ (the air and the water temperature are equal)

During measurements water is being evaporated at different air flow rate and water temperature. The measurements were carried out at four different air velocities at forced convection. The weight of evaporated water in function of time is shown in Fig 1. On the diagrams can be clearly seen the effect of the water temperature and the air velocity on the evaporation rate.

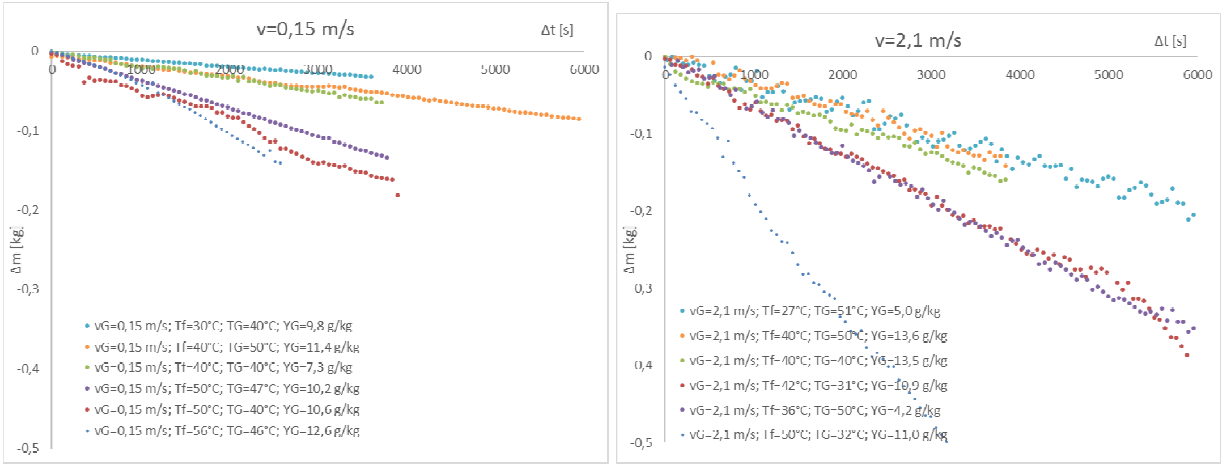

Figure 1 The weight of evaporated water at different temperature-based driving forces in function of time

The summary of measurements results is shown in Table 1, where the first, second and third cases were investigated. The measurements are marked by different colours at different heat flow direction or if there is not heat flow. The results are demonstrated by the air velocity. During

measurements the air velocity, temperature, humidity and water characteristic temperature were constant. The varying parameter was only the weight of water. It can be determined the weight decrease of the water by fitting a lineal to the plotted points (dm_{H2O}/dt).

Table 1 Summary of measurements results (light grey: 2nd; dark grey: 3rd; white: 1st case)

v_G	T_G	φ	Y_G	dm_{H2O}/dt	D	T_{H2O}	T_f	Y_f	N_{H2O}	σ	k_c	Re	Ra	Sh	Direction of heat flow
m/s	°C	%	g_{H2O}/kg_{dG}	g/s	m^2/s	°C	°C	g_{H2O}/kg_{dG}	$kg/(m^2h)$	$kg/(m^2s)$	m/s	[1]	[1]	[1]	
0	22,8	54,6	12,2	-0,126824	0,0000226	69,6	65,2	204,6	4,683	0,0068	0,0058		179622	19,9	$T_G<T_f$
	26,1	60,1	12,7	-0,063785	0,0000225	57,6	54,6	106,7	2,355	0,0070	0,0059		181041	20,5	$T_G<T_f$
	25,7	57,0	11,7	-0,044343	0,0000226	52,6	49,9	81,1	1,637	0,0066	0,0056		181037	19,3	$T_G<T_f$
	25,9	47,1	9,8	-0,034969	0,0000227	48,3	45,9	64,2	1,291	0,0066	0,0056		181109	19,3	$T_G<T_f$
	23,9	45,2	8,3	-0,016400	0,0000226	38,4	36,4	38,5	0,606	0,0056	0,0048		181895	16,4	$T_G<T_f$
	30,5	56,8	14,2	-0,010681	0,0000236	41,2	39,8	45,9	0,394	0,0035	0,0030		178393	9,9	$T_G<T_f$
	27,5	37,7	8,5	-0,005142	0,0000231	28,3	27,3	25,2	0,190	0,0032	0,0027		180723	9,2	$T_G=T_f$
	40,4	53,6	14,6	-0,013220	0,0000250	41,3	40,0	46,2	0,488	0,0043	0,0039		174174	12,0	$T_G=T_f$
	48,4	54,8	14,3	-0,012362	0,0000261	41,5	39,8	45,8	0,456	0,0040	0,0037		170955	11,1	$T_G>T_f$
	18,9	38,8	5,2	-0,002086	0,0000222	19,0	17,4	16,7	0,077	0,0019	0,0016		184781	5,5	$T_G>T_f$
0,15	46,1	49,5	12,6	-0,053661	0,0000258	58,8	56,2	117,3	1,981	0,0053	0,0048	3222	9708987	56,0	$T_G<T_f$
	39,9	42,1	10,6	-0,040620	0,0000249	52,0	50,1	81,6	1,500	0,0059	0,0053	3269	9879735	63,5	$T_G<T_f$
	39,8	31,6	7,3	-0,017065	0,0000249	41,2	39,9	46,0	0,630	0,0045	0,0001	3276	9924917	0,8	$T_G=T_f$
	46,9	45,9	10,2	-0,034241	0,0000260	52,5	50,2	82,2	1,264	0,0049	0,0045	4560	9719152	47,5	$T_G=T_f$
	46,9	47,6	9,8	-0,008331	0,0000250	31,5	30,0	28,3	0,308	0,0046	0,0041	4560	9719152	47,5	$T_G>T_f$
	49,6	42,2	11,4	-0,012672	0,0000263	41,7	40,3	47,1	0,468	0,0036	0,0034	3191	9697875	38,5	$T_G>T_f$
0,26	40,1	41,5	10,8	-0,041383	0,0000250	51,9	50,2	82,2	1,528	0,0059	0,0053	4616		64,2	$T_G<T_f$
	50,0	47,0	11,9	-0,062253	0,0000264	61,9	59,9	147,2	2,299	0,0047	0,0044	4517		49,9	$T_G<T_f$
	40,0	30,0	7,1	-0,017634	0,0000249	41,6	39,9	46,1	0,651	0,0046	0,0042	4629		50,1	$T_G=T_f$
	46,9	44,6	10,3	-0,030827	0,0000259	51,8	49,9	81,1	1,138	0,0045	0,0041	4560		47,5	$T_G=T_f$
	46,9	51,5	10,6	-0,011185	0,0000250	31,7	30,2	28,6	0,413	0,0064	0,0057	4560		47,5	$T_G>T_f$
	40,3	49,4	13,5	-0,015668	0,0000264	41,2	39,9	46,1	0,579	0,0046	0,0043	4503		48,9	$T_G>T_f$
0,6	50,2	36,8	6,5	-0,102377	0,0000264	66,2	62,1	168,3	3,780	0,0065	0,0060	9121		68,6	$T_G<T_f$
	50,0	31,0	5,7	-0,076196	0,0000264	59,9	57,4	126,3	2,813	0,0065	0,0060	9118		68,5	$T_G<T_f$
	50,0	40,0	6,3	-0,052259	0,0000264	53,3	49,8	80,4	1,930	0,0072	0,0067	9156		76,5	$T_G=T_f$
	50,0	20,3	3,6	-0,051013	0,0000264	50,0	47,6	70,8	1,884	0,0078	0,0072	9120		82,4	$T_G>T_f$
	50,1	29,2	5,1	-0,026758	0,0000264	40,0	38,0	41,6	0,988	0,0075	0,0070	9126		79,5	$T_G>T_f$
	50,1	21,7	3,5	-0,014248	0,0000264	30,0	27,9	25,9	0,526	0,0065	0,0061	9142		69,1	$T_G>T_f$
	50,0	30,9	7,2	-0,012648	0,0000264	26,8	27,3	25,2	0,467	0,0072	0,0067	9054		76,0	$T_G>T_f$
1,1	49,9	38,3	7,2	-0,153087	0,0000263	68,3	62,5	172,3	5,652	0,0095	0,0088	17052		100,5	$T_G<T_f$
	50,0	30,6	5,6	-0,110594	0,0000264	60,0	56,1	117,0	4,083	0,0102	0,0095	17054		107,6	$T_G<T_f$
	50,1	36,0	6,1	-0,079441	0,0000264	54,6	49,9	81,0	2,933	0,0109	0,0101	17092		114,9	$T_G=T_f$
	50,1	35,3	6,3	-0,064368	0,0000264	50,0	46,6	66,8	2,377	0,0109	0,0101	17066		115,2	$T_G>T_f$
	50,1	28,9	5,3	-0,037078	0,0000264	40,0	37,2	39,9	1,369	0,0110	0,0102	17054		116,1	$T_G>T_f$
	49,9	30,1	5,8	-0,020676	0,0000264	29,9	27,6	25,5	0,763	0,0107	0,0100	17032		113,6	$T_G>T_f$
	50,0	44,0	6,8	-0,013108	0,0000264	21,2	25,1	23,1	0,484	0,0082	0,0077	17139		87,1	$T_G>T_f$
1,7	50,1	30,7	5,6	-0,149729	0,0000264	60,0	54,8	107,9	5,528	0,0150	0,0139	27913		158,5	$T_G<T_f$
	50,1	41,1	7,2	-0,112903	0,0000264	55,9	50,2	82,2	4,169	0,0155	0,0144	27940		163,2	$T_G=T_f$
	50,0	31,7	5,8	-0,089740	0,0000264	50,0	45,8	63,7	3,313	0,0159	0,0148	27912		168,1	$T_G>T_f$
	50,0	22,7	4,0	-0,050730	0,0000264	40,0	36,5	38,5	1,873	0,0150	0,0140	27942		159,1	$T_G>T_f$
	49,9	21,6	3,7	-0,030543	0,0000264	30,0	27,3	25,2	1,128	0,0146	0,0135	27976		154,0	$T_G>T_f$
	49,8	30,3	5,5	-0,025083	0,0000263	25,8	22,7	20,9	0,926	0,0168	0,0155	27922		177,1	$T_G>T_f$
2,1	31,5	55,1	11,0	-0,146989	0,0000238	55,9	50,1	81,8	5,427	0,0213	0,0187	37557		235,4	$T_G<T_f$
	31,0	55,1	10,9	-0,063148	0,0000237	45,7	41,8	50,9	2,332	0,0162	0,0142	37614		179,4	$T_G<T_f$
	40,3	49,4	13,5	-0,041916	0,0000250	43,2	40,1	46,6	1,548	0,0130	0,0117	35542		140,1	$T_G=T_f$
	50,1	23,9	4,2	-0,059833	0,0000264	40,0	36,2	38,0	2,209	0,0181	0,0168	33834		191,6	$T_G>T_f$
	50,7	36,8	5,0	-0,032343	0,0000265	29,5	26,7	24,6	1,194	0,0169	0,0158	34031		178,6	$T_G>T_f$
	50,2	47,4	13,6	-0,033585	0,0000264	43,2	40,2	46,8	1,240	0,0104	0,0096	33666		109,6	$T_G>T_f$

In Table 1 the dimensionless number are shown that are determined from the measurements results. At natural convection the Rayleigh-number, at forced convection the Reynolds-number is the relevant. Since the Sherwood-number is the dimensionless number of the mass transfer, it was expected, when the mass transfer coefficient is the highest the Sherwood-number is also the highest.

For describing the phenomenon of evaporation at natural convection insufficient measurements are made to determinate the Sh-Re equations. Therefore further measurements are needed to the representation of this case and the determination of the equations of fitted curve.

CONCLUSIONS

In the course of our work, evaporation from a water surface was examined based on laboratory measurements. A measurement method has been developed and a measurement station has been established for testing heated fluid vessel, suitable for identifying evaporation processes increased by heat sources in the course forced convection. The velocity and the temperature of the humid gas and the temperature of the water can be regulated in a wide interval. Therefore, the tests were investigated not only in natural evaporation, but helping with heated water too. In the cases examined, evaporation was not only consequent upon environmental impacts, but it was also assisted by the heat source of the water. This case has been discussed deficiently by literature on the description and calculation of evaporation.
Our equipment is suitable to research the first, second and third evaporation categories, which appears the evaporation in traditional sense. Measurements were carried out for two cases: the temperature of the gas is higher than the water's, and for the opposite case. The measurement objectives are to determine vapor evaporation in various flow conditions, and to calculate the evaporation coefficient. The measurement results are plotted on diagrams. Our future plan is to establish an equation system, which can describe the phenomenon of evaporation in wide range of interpretation, taking into account the different categories.

ACKNOWLEDGEMENTS

Special thanks for Dr. Mária Örvös for her helps in this work. This paper was supported by Gedeon Richter's Talentum Foundation (H-1103 Budapest, Gyömrői str. 19-21, Hungary), and by Hungarian Scientific Research Found (OTKA-116326).

REFERENCES

[1] S. Szentgyörgyi, K. Molnár, M. Parti, Transzportfolyamatok, Budapest: Tankönyvkiadó, 1986.
[2] E. R. Treybal, Mass-transfer operations, Third Edition, USA: McGraw-Hill Company, 1981.
[3] T. Poós, V. Evelin, „Determination of evaporation rate at free wtaer surface," in *8th International Symposium on Exploitation of Renewable Energy Resources*, Subotica, Szerbia, 2016, pp. 66-71.

OPTIMIZATION METHODS OF THE DRIVES FOR MECHANICAL PRESSES

[1]POP-SZOVÁTI Anton-Georghe, [2]GYENGE Csaba DSc, [3]BORZAN Marian PhD, [4]POP-SZOVÁTI Jusztin Ágoston

[1,2,3,4] Departament Industrial Enginering, Faculty of Manufacturing Enginering, Tehnical, Tehnical University of Cluj-Napoca
E-mail: anton_pops@yahoo.com, csaba.gyenge@tcm.utcluj.ro, marian.borzan@tcm.utcluj.ro, justin_90_07@yahoo.com

Abstract
Presses due to their technical functionality characteristics and kinetic energy that it develops processes the semi-finished sheet metal through stamping or blanking in the semis with predetermined shapes and properties. The mechanical presses driving systems synchronizes functioning parameters (movement, speed, force) to transmit energy to the executor. Our research team has studied the main drive with serrated wheel gearing of mechanical presses at Electrolux-Satu Mare company specialized in manufacturing of household cookers.

Keywords: presses, main driver, serrated wheel gearing, the press ram, servo presses

1. INTRODUCTION

Strong development of the industry in general, the construction industry, and, in particular, has brought in a considerable increase in the number of types of presses for plastic deformation by cold pressing of sheet metal. The redaction of this work has been given particular importance to the theoretical part, based on the results of investigations and on the experience of our team of advanced researchers at the Electrolux company of Satu Mare. The object of research from the study on the role of the serrated wheel gearings in main drive of the mechanical presses. The requirements that have to meet by the subassemblies which make up the presses, in general the difference from a press to another which led to the development of a fairly large number of types of presses covering a wide range of needs.

2. CONVENTIONAL DRIVE METHODS FOR MECHANICAL PRESSES

Classification of mechanical presses type by transmission reports of the developed force required, required tools mounted on the press which can be drived with: flywheel, flywheel and reducer with gearings with a step, flywheel and reducer with gearings with two steps, double action presses. The electric motor rotates the flywheels that store kinetic energy which it is used to activate the mechanism *(Figure 1).* The involvement of the ram in a double race cycle consumes about 10-15% of the kinetic energy of the flywheel created by reducing the speed. The electric engine restores the flywheels speed thus the press is ready for the next cycle. In case that the percentage of 15% is exceeded due to the large number of double races per minute the electric motor will not have enough time to compensate for the lost energy.
Presses with a connecting rod, the length of the race can be controlled with a side-mounted eccentric bushing eccentric crank shaft, which directly influence the speed of the ram so at small racing speed the speed of the ram is smaller and in the higher racing speeds the speed of the

ram is higher. In the case of presses with two connecting rods (*Figure 2)* with the main drive gears without the flywheel with safety clutch-brake assembly mounted at one end of the eccentric shaft or at the middle of the eccentric shaft. Pressing energy is provided by the mass and speed of the flywheel and drive belt.

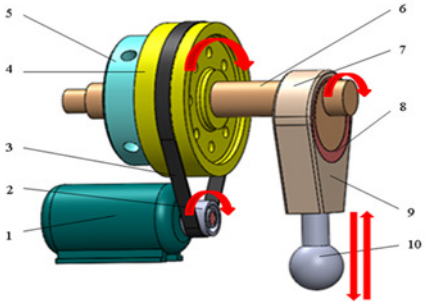

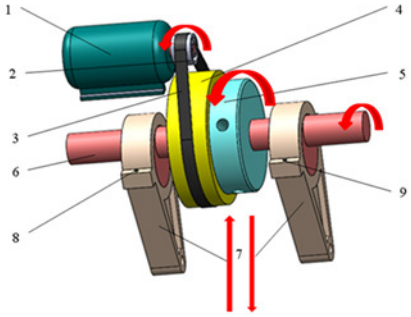

Figure 1 *Figure* 2

Figure 1 Direct drive press with open frame shaped,,C"
1 -main electric motor; 2 -belt pulley; 3 –transmission belt; 4 -flywheel; 5 -whole clutch-brake; 6 - eccentric shaft; 7 -connecting rod; 8 - eccentric bushing; 9 -connecting rod; 10 - screws with spherical head

Figure 2 Direct drive presses with closed-shaped frame,,O"
1 -main electric motor; 2 -belt belt pulley; 3 –drive belt; 4 -flywheel; 5 -whole clutch-brake; 6 - two eccentric shaft; 7 -connecting rods; 8 and 9 -studs with nuts for belt tension of the two sides of the connecting rod.

Presses with one notch *(Figure 3)* may have shaped machine frame,,C". In the case of presses with symmetrical gear-shaped frame ,,O" may be substantially perpendicular to the shaft on the front (*Figure 4 and 5*) of the press and parallel to the front *(Figure 7 and 8)* of the press. Compared presses operated by electric motor and flywheel energy presses Geared transmission ensures maintaining a constant connection between the drive gearing mechanism and the ram and is more rigid for the presses with two connecting rods. By including a gear reducer with the main drive *(Figure 4)* presses become slower but the pressing force increases, ranging between 1600kN and 12000kN.

Presses with one notch are used to outline cuts with long, drawn from half-finished sheet metal which makes it hard to deform, because the energy that emerges from the reducer is greater than in the case of presses operated only by flywheel. Average number of 30 cycles per minute favors equipping the presses with transfer devices, processing of sheet roll with progressive tools, it is possible the manual handling of blanks, automation or robotics manufacturing process increases the life of the machine considerably. The smaller number of cycles per minute of the ram enables the flywheel to maintain a constant velocity values, such energy that acts on the blanks in each double race is constant.

Mechanical presses with two stage (Figure 5) are recommended for large production series are of rigid construction and are used in operations that require large pressing force, technological time takes longer. These types of presses connection between the actuating mechanism and main ram is usually achieved with two rods. These types of presses can be equipped with devices to transfer because the number of 40 cycles per minute is favorable for transferring the blanks. On these presses tools can be mounted for progressive stamping operations, drilling, cutting, embossing. The disadvantage of this pressure comes from the eccentric shaft length which is solicited strongly in the middle portion of the torsion.

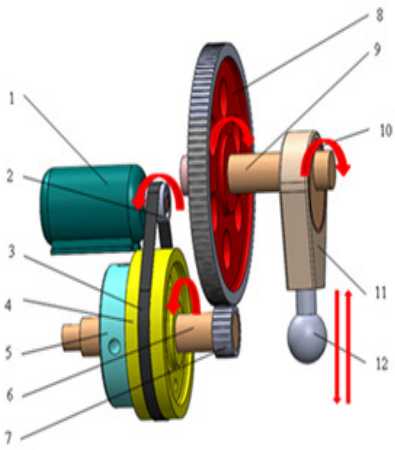

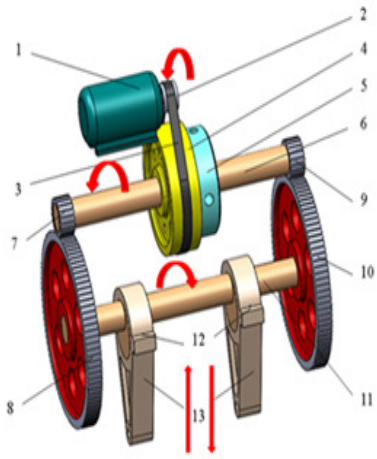

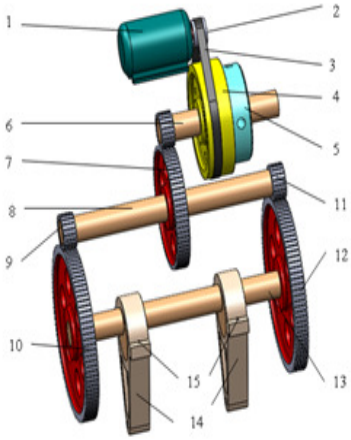

Figure 3 *Figure 4* *Figure 5*

Figure 3 Driven by a gear reducer presses with open frame shaped ,,C"
1 -the main electric motor; 2 -belt belt pulley; 3 –drive belt; 4 -flywheel; 5 - whole clutch-brake; 6 - drive shaft; 7 and 8 -gearing; 9 -crank; 10 -eccentric bushing; 11 -connecting rod; 12 -screw ball

Figure 4 Presses closed-shaped frame ,, O " driven with symmetrical reductor with one notch gear
1 -the main electric motor; 2 -belt belt pulley; 3 –drive belt; 4 -flywheel; 5 -whole clutch-brake; 6 -drive shaft; 7 and 8 -gears; 9 and 10 - gears; 11 - two eccentric shafts; 12 -bolts with nut; 13 -connecting rods

Figure 5 Presses closed-shaped frame ,,O"operated with symmetrical two-stage gearboxes
1 -main electric motor; 2 -belt belt pulley; 3 –drive belt; 4 -flywheel; 5 -whole clutch-brake; 6 - sprocket; 7 -idler gear; 8 -intermediate shaft; 9 and 10 - gear; 11:12 - gear; 13 - two eccentric shafts; 14 - rod; 15 - bolts with nut

Generally presses with two connecting rods perpendicular to the main shaft at the front of the press *(Figure 7 and 8)* is integral with an eccentric gear of the main drive mechanism. These types of presses are used in operations where required racing up to 300-400 mm wide and the distance between the active surface of the rams weight to be greater in order to favor higher installation tool. The two wheel gears are mounted on eccentric shafts with different leading to a lower precision compared to the second rod presses the main shaft parallel to the front where the eccentrics are processed on the same shaft.

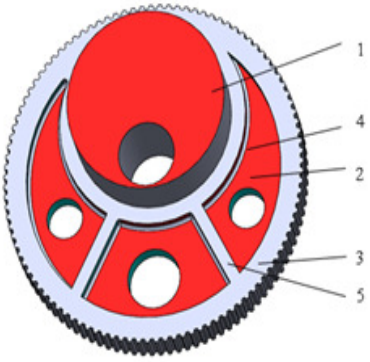

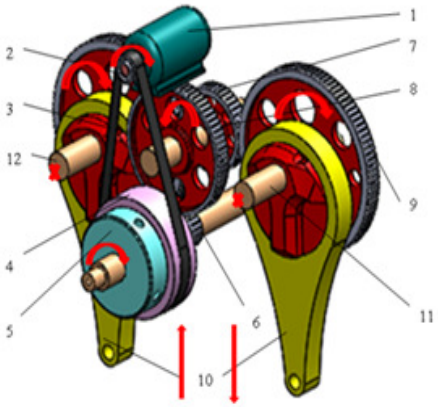

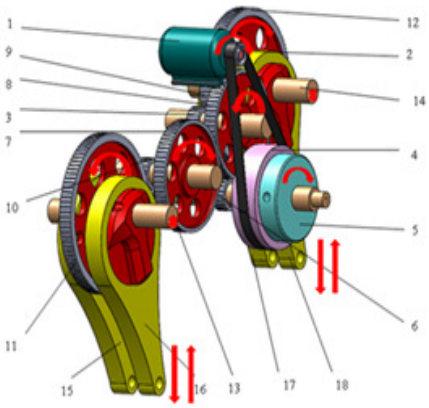

Figure 6 *Figure 7* *Figure 8*

Figure 6 Gear eccentric built

1- block; 2 - intermediate part; 3 - ring gear; 4 - weld; 5 - strengthening ribs of the ensemble
Figure 7 Presses closed-shaped frame ,,O“ driven by the second gear symmetric reducers
1 -the main electric motor; 2-belt pulley; 3 -drive belt; 4 -flywheel; 5 -clutch-brake assembly; 6 and 7- shafts; 8 -intermediate gear wheel; 9 -incorporated eccentric gear ; 10 -rods; 11and12 - axles
Figure 8 Presses closed-shaped frame ,,O"operated with symmetrical two-stage gearboxes
1-main electric motor; 2 -belt pulley; 3 –drive belt; 4 -flywheel; 5 -clutch-brake assembly; 6 - sprocket; 7 and 8 –idler: 9 and 10 - pinion; 11 and 12 - two eccentric gears incorporated; 13 and 14 -axles; 15 and 16 -connecting rods to the right; 17 and 18 -connecting rods to the left.

These types of presses are used in operations where required racing up to 300-400 mm wide and the distance between the active surface of the rams weight to be greater in order to favor higher installation of the tools. The two gearings are mounted on the eccentric shafts with different leading to a lower precision compared to the second rod presses the main shaft parallel to the front where the eccentrics are processed on the same shaft.
To generate large forces for processing through plastic deformation of the metal in the construction of the presses with knuckle joints operated by servo motors were included intermediate mechanisms of action through the drive belts and ball screws*(Figure 9)* to transform rotational movement in motion translation. Rotational movement of the servo-motor is transmitted using drive belt transmission shaped for perfect synchronization of the two drives that drives simultaneously the ball screws that connects to the ram. The rams press is trained to translate the motion of the ball screw or alternative to ball screws that are driven in synchronous servomotors through two drive belts profiled. Maximum pressing force is available at any point in the rams stroke, but it is limited by the capacity of transmission timing of the servo-motor the ratio of the drives belt and the power factor of the servo-motor. The movement of the ram controlled by programming the linear transducers and corrected by controlling the movement of rotation of each servo-motor individually as required. Thus, it is possible to maintain the parallelism and non-proportional in the case of applications distributed on the table surface or active surface of the ram.
In figure 10 is shown the driving mechanism of a press with knuckle joint-shaped frame ,, C "acted directly by a servo-motor. Reciprocating motion of the ram can be changed by reversing the direction of rotation of the servo-motor not needing to achieving a complete stroke of the ram. *Figure 11* shows the construction of a press with knuckle joint-shaped frame ,, O ", which is driven with ball screws on both sides. By screwing screws and unscrewing them through a mecanism with knuckle joints, operating the ram in reciprocation it is led by four guides. The two servo-motors via software controls the parallelism between the active surface of the press table and the rams arrangement for misalignment or disproportionate tools.

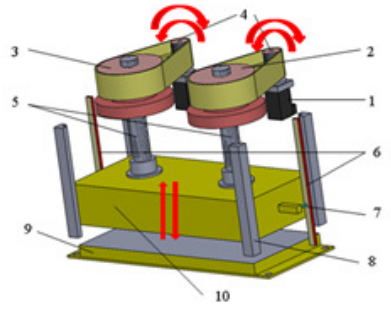

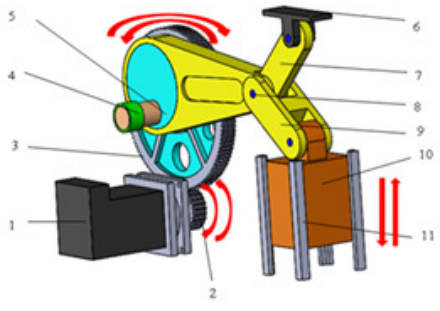

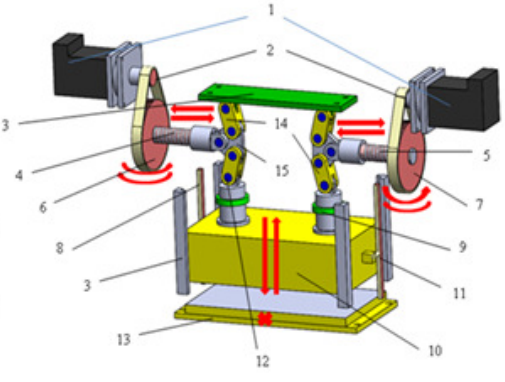

Figure 11 *Figure 9* *Figure 10*
Figure 9 Driving the ram with transmission through belts profiled with servo-motor.

1 –servo-motor; 2 and 3 - profiled driven belt pulley; 4 -profiled leading belt pulley; 5 -Ball screw; 6 -linear transducer; 7 -sensor; 8 - guides; 9 - the press table; 10 – ram

Figure 10 The drive of the press with knuckle joints

1 –servo-motor; 2 -pinion; 3 -Eccentric gear incorporated; 4 -hole for axle; 6 –fixed frame support; 7 and 9 -rocking 10 -ram; 11 –guides

Figure 11 The main drive of a press with two symmetrical mechanisms with knuckle joints and with two servo-motors.

1 -servo-motors; 2 -sprocket belt profiled; 3 -fixed support frame; 4 and 5 -ballscrew; 6 and 7 -profiled belt pulley; 8 -linear transducer; 9 -plunger; 10 –ram; 11 -sensor; 12 -bolt; 13-press table; 14 -sticks; 15 –triangular connecting elements

The latest developments regarding the operation of mechanical presses kinetic energy of the flywheel is replaced by presses with servo-motors. Servo-motors have been developed so that at low-speed the transmission developers great moments which through the servo-motor pinion shaft directly drives the gear and engages the press gear*(Figure 12 and 13)* with the eccentric. Thus, there is no need for drive belt and belt pulley therefore no need gripping supports. Direct drive of a high power servo-motor, replaces the pinion shaft that was fitted to the flywheel and clutch-brake, and routers for the drive (compressed air, oil) of their. This type of drive is convenient because it is economical, environmentally friendly by eliminating several transmission components of the operating mechanism, reduces costs for maintenance or replacement.

The construction shown in figure 14 which is a press operated by a servo-motor developing large transmission moments.

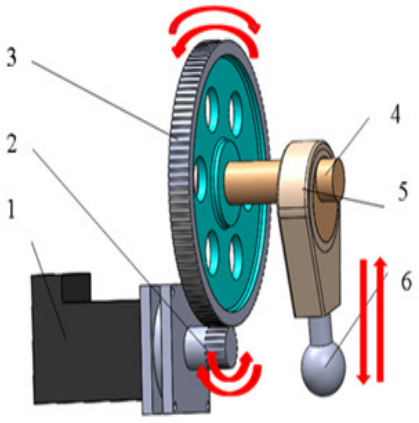

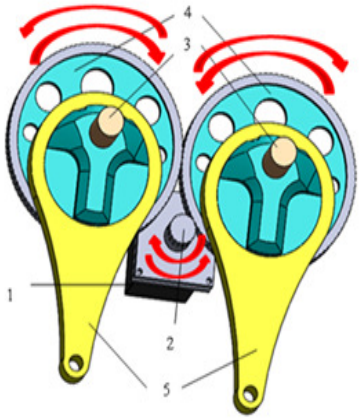

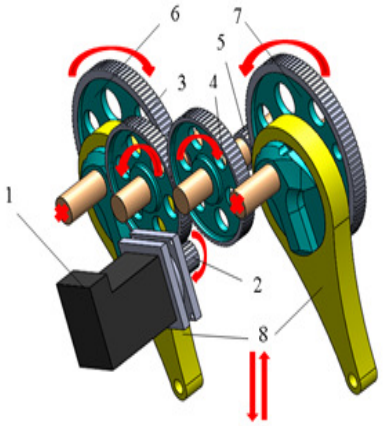

Figure 12 *Figure 13* *Figure 14*

Figure 12 Driving directly with the servo-motor mechanism of a press geared mainly by one notch

1 -servomotor; 2-pinion; 3 -gear; 4 -connecting rod; 5 -rod; 6 - screw ball

Figure 13 Driving directly with the servo-motor mechanism of a press geared mainly symmetrically by one notch

1 -servomotor; 2 -pinion; 3 -axles; 4 -symmetrical gear; 5 -rod.

Figure 14 The main press drive gear units with a symmetrical with two stage notch with a direct servo-motor

1 -servo-motor; 2 -pinion; 3 and 4 -idler gears; 5 - pinion; 6 and 7-gears with eccentric built; 8 - connecting rod

CONCLUSIONS

1. Increased productivity in the case of blanking operations where necessary to reduce the speed during the critical technological time to avoid tearing of the semi-finished products the rest of the cycle can be accelerated. Compared with the conventional mechanical presses with flywheel, where the cycle follows the speed of drawing of the blank, the productivity can be increased by 150%. The rams race can be changed and every tool minimized. If the press with a fixed race (frame closed with two rods or four rods) the processing of semi-finished products which are smaller there a useless race of the rams press that when operating presses with servo-motors during a double race can be shortened by reversing the rotation of the servo-motor by pivoting movement of the press ram.
2. Lower cost for maintenance of the blanking and stamping tools since you can program to minimize contact speed to any tool or phase in the case of combined tools. By reducing contact speed in addition to the direct effect in preventing drawing and stamping tool wear is reduced and the level of noise and vibration pollution.
3 The number of mechanical components is lower in servo-motor drive presses, proportional decreases maintenance costs. . There is no need for a mechanical battery of kinetic energy (flywheel), clutch-brake overall, reduce the number of gears and couplings connecting the transmission of movements between different machine parts. Travel speed of the ram can reduce any portion of the trajectory of a double race because it does not depend on the speed of the flywheel. Servo-motors replace complex mechanisms for which deliver the rams speed.
4. Provides a wide range of length adjustment of the ram race by reversing the direction of rotation without having the crank shaft rotation complete.
5. It can be programmed to stop the rams race in situations where during the plastic deformation of the material is large in order to increase the time to restore the ties between the materials crystals subject to the stamping processing. To materials arching subject to the stamping operation, bending, embossing which does not retain its final form after the first pressing, it is possible that during the same race to be able to return a second time for the total deformation.
6. Energy consumption reduced by 60% compared to traditional mechanical presses where much of the energy it is consumed for the driving of the flywheel. Much of the energy is consumed in maintaining the rotating movement of the flywheel and to build up kinetic energy, energy that is used only during movement of the ram.

REFERENCES

[1] Altan, T., Groseclose, A.: Servo-Drive Presses – Recent Developments, 2009.Komatsu, I., Murakami, T.: Practical Use of Servo Press, TheNikkan Kogyo Shimbun, Ltd., 48-49, 2009.
[2] Pop, A., Gyenge, Cs., Borzan, M.: Dynamic analyisis of vibration and noise metal forming presses. Debreceni műszaki közlemények 2014/2.
[3] Pop , A., Gyenge, Cs, Borzan, M.: Specific achievements in the direction of the automated assembly through adhesion of household machines. ANNALS of Faculty EngineeringHunedoara–International Journal of Engineering, Tome XIII [2015]– Fascicule 4 [November] ISSN:1584-2673.
[4] Pop , A., Gyenge, Cs, Borzan, M.: The study of mechanical presses drives using cold plastic deformation. Proceedings of the 3 rd International Scientific Conference on Advances in Mechanical Engineering (ISCAME 2015) 19 November, 2015 Debrecen, Hungary.

INTERNATIONAL SCIENTIFIC CONFERENCE ON ADVANCES IN MECHANICAL ENGINEERING
13-15 October 2016, Debrecen, Hungary

GEOMETRICALLY NONLINEAR MODELING OF A SNAP FITTING PROCESS

[1]RÓNAI László, [2]SZABÓ Tamás PhD

[1]Robert Bosch Department of Mechatronics, University of Miskolc
E-mail: ronai.laszlo@uni-miskolc.hu
[2]Robert Bosch Department of Mechatronics, University of Miskolc
E-mail: szabo.tamas@uni-miskolc.hu

Abstract
Elastic modeling of the snap fitting of an electrical contact is discussed in this paper. A snap fit phenomenon is appearing during assemble. The contact element is modeled by beams. A large displacement analysis is used to describe the mounting process of the beam. The contact problem between the plastic workpiece and the electrical contact element is treated with kinematical contact method. The simulation program has been written in Scilab software.

Keywords: *beam, large displacement, contact problem*

1. INTRODUCTION

During many assembling processes the snap fit phenomenon can be experienced. These processes are usually show instability. The phenomenon can be detected by measuring and recording the load-deflection curve.
The description of the snap fit phenomenon is important to use in the haptic concept of robotics. The expression of haptic is derived from the ancient Greek word meaning “sense of touch” [5]. In haptic robotics, it is necessary to sense the forces arising in closing mechanism of the end effectors.
The main purpose of this paper to model an elastic metal electrical contact element, which is characterized by the above mentioned phenomenon. In the purposed model, large elastic displacements are assumed.
Usually the updated Lagrangian [4] and the total Lagrangian [3], [4] descriptions are used to setup nonlinear problems [4]. In case of small strains but large displacement the treatment of rotations is essential. One of the efficient method is the so called corotational [1], [2] concept, which is practically the updated Lagrangian method. In this paper the corotational formulation [1] was used to solve the modeling of the mounting process. The rigid body motions and the deformations can be separated by the local coordinate systems. In this local system only small rotations are present.
The kinematical contact method is based on the kinematical contact condition, i.e., kinematical load is applied to those nodes, which are below the contact surface. The contact node will be pushed to the contact surface. The contact conditions are handled in local coordinate systems, which are defined by the normal vector of the contact surface. This means that the coordinates are transformed to normal and tangent components.

2. LARGE DISPLACEMENT ANAYLSIS

In this section, the corotational method has been described [1], [2]. Three necessary steps are required to use this formulation. The determination of the angle of the rotation, the relationship

between the local and global coordinates are the first two steps. The last objective is the creation of the tangent stiffness matrix [1].
The rotations and translations are rigid body motions. These motions are separated from the deformations of the loads at local element level by using the corotational formulation. Alignment and creation of a local coordinate system to an element is necessary. Thus with the local coordinate system, the rotations and translations are depend only the deformations. The angles, coordinate systems and deformations of a beam are shown in Figure 1.

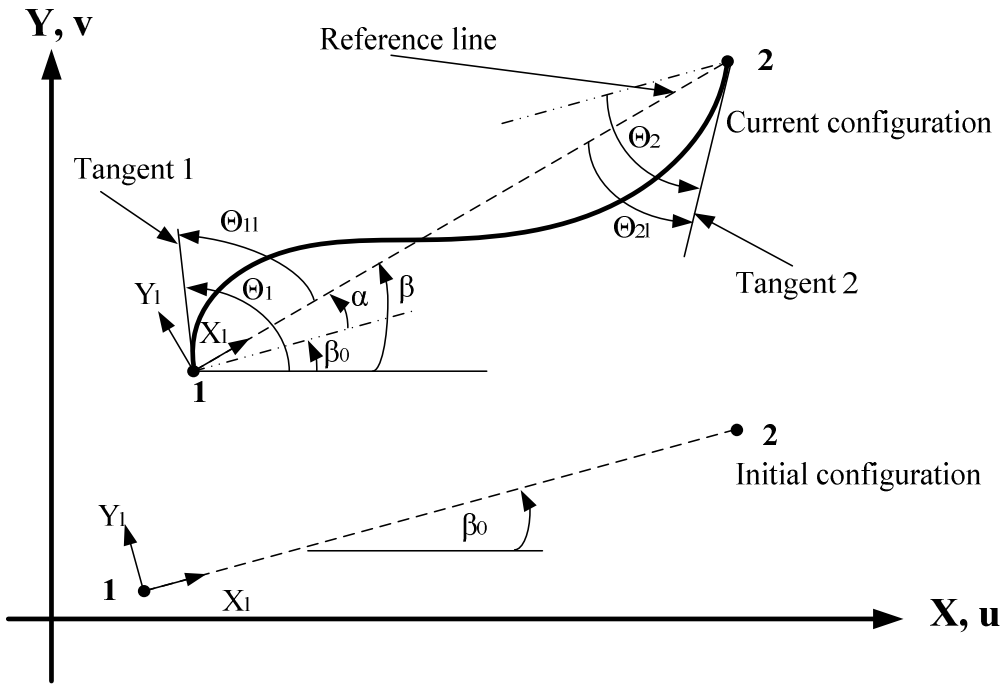

Figure 1 Deformation of a beam

The notations in Figure 1 are as follows: α angle measured from the initial configuration, Θ_1, Θ_2 global nodal rotations, Θ_{1l}, Θ_{2l} local nodal rotations, β_0 angle of the initial configuration, β angle of the deformed configuration.
According to Souza [2] the local nodal rotations can be determined

$$\Theta_{1l} = \operatorname{atan}\left(\frac{\sin(\Theta_{1l})}{\cos(\Theta_{1l})}\right) = \operatorname{atan}\left(\frac{\cos(\beta)\sin(\beta_1) - \sin(\beta)\cos(\beta_1)}{\cos(\beta)\cos(\beta_1) + \sin(\beta)\sin(\beta_1)}\right), \quad (1)$$

$$\Theta_{2l} = \operatorname{atan}\left(\frac{\sin(\Theta_{2l})}{\cos(\Theta_{2l})}\right) = \operatorname{atan}\left(\frac{\cos(\beta)\sin(\beta_2) - \sin(\beta)\cos(\beta_2)}{\cos(\beta)\cos(\beta_2) + \sin(\beta)\sin(2)}\right), \quad (2)$$

where $\beta_1 = \Theta_1 + \beta_0$ and $\beta_2 = \Theta_2 + \beta_0$. The advantage of these formulae that those provide appropriate values any range of rotation of the element.

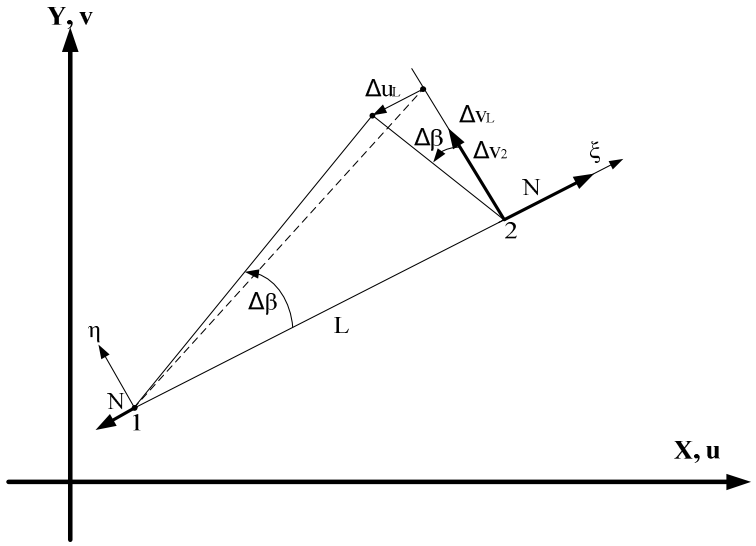

Figure 2 Rotations of the element with linear and nonlinear approaches

The rigid body motion of the linear finite element is examined in nonlinear concept. In Figure 2, the dashed line represents the linear concept.

$$\Delta u_L = tg(\Delta\beta)\Delta v_L. \tag{3}$$

Due to this fact in addition to the linear stiffness matrix, geometry stiffness matrix is a part of the tangential stiffness matrix to treat the rigid body rotation. The so called updated Lagrangian method is used to formulate the necessary finite element matrices. Let us assume that the system is in equilibrium at time t. The principle of the virtual work is given at time $t + \Delta t$:

$$\int_{V^t} \delta\varepsilon_\xi^{t+\Delta t}\, \sigma_\xi^{t+\Delta t}\, dV = \delta R^{t+\Delta t}, \tag{4}$$

where $\varepsilon_\xi^{t+\Delta t}$, $\sigma_\xi^{t+\Delta t}$ are the strain and stress in axial direction of the beam at $t + \Delta t$, and δ denotes the virtual change. The Green-Lagrange axial strain is given as:

$$\varepsilon_\xi^{t+\Delta t} = \frac{du^{t+\Delta t}}{d\xi} + \frac{1}{2}\left(\left(\frac{du^{t+\Delta t}}{d\xi}\right)^2 + \left(\frac{dv^{t+\Delta t}}{d\xi}\right)^2\right). \tag{5}$$

The quantities in (4) can be written by incrementally:

$$u^{t+\Delta t} = u^t + \Delta u, \quad v^{t+\Delta t} = v^t + \Delta v, \tag{6}$$

$$\varepsilon_\xi^{t+\Delta t} = \varepsilon_\xi^t + \Delta\varepsilon_\xi, \quad \Delta\varepsilon_\xi = \Delta\varepsilon_\xi^L + \Delta\varepsilon_\xi^{NL}, \tag{7}$$

$$\delta\varepsilon_\xi^{t+\Delta t} = \delta\Delta\varepsilon_\xi^L + \delta\Delta\varepsilon_\xi^{NL}, \tag{8}$$

$$\sigma_\xi^{t+\Delta t} = \sigma_\xi^t + \Delta\sigma_\xi, \quad \Delta\sigma_\xi \cong E\Delta\varepsilon_\xi^L. \tag{9}$$

Substituting (6)-(9) into (4), we obtain the incremental form of the virtual work. The linear terms provide load vectors and the quadratic terms give stiffness matrices and the third order term in increment will be neglected.

$$\int_{V^t} \delta\Delta\varepsilon_\xi^L E\, \Delta\varepsilon_\xi^L dV + \int_{V^t} \delta\Delta\varepsilon_\xi^{NL}\sigma_\xi^t dV = \delta R^{t+\Delta t} - \int_{V^t} \delta\Delta\varepsilon_\xi^L \sigma_\xi^t dV. \tag{10}$$

$$\Delta\varepsilon_\xi^L = \frac{d\Delta u}{d\xi} + \eta\frac{d^2\Delta v}{d\xi^2}, \qquad \Delta\varepsilon_\xi^{NL} = \frac{1}{2}\left(\left(\frac{d\Delta u^{t+\Delta t}}{d\xi}\right)^2 + \left(\frac{d\Delta v^{t+\Delta t}}{d\xi}\right)^2\right). \tag{11}$$

$$dV = Ad\xi = d\xi d\eta d\zeta. \tag{12}$$

Substituting (11) and (12) into (10) one can obtain integrals to provide the linear and the geometric stiffness matrices and the external and internal force vectors:

$$\int_{L^t}\left(\delta\frac{d\Delta u}{d\xi}EA\frac{d\Delta u}{d\xi} + \delta\frac{d^2\Delta v}{d\xi^2}EI_\zeta\frac{d^2\Delta v}{d\xi^2}\right)d\xi = \delta\Delta\boldsymbol{q}^T\boldsymbol{K}^L\Delta\boldsymbol{q}, \tag{13}$$

$$\int_{L^t}\left(\left(\delta\frac{d\Delta u^{t+\Delta t}}{d\xi}\right)\left(\frac{d\Delta u^{t+\Delta t}}{d\xi}\right) + \left(\delta\frac{d\Delta v^{t+\Delta t}}{d\xi}\right)\left(\frac{d\Delta v^{t+\Delta t}}{d\xi}\right)\right)\sigma_\xi^t A d\xi = \delta\Delta\boldsymbol{q}^T\boldsymbol{K}^G\Delta\boldsymbol{q}, \tag{14}$$

$$\delta R^{t+\Delta t} = \delta\Delta\boldsymbol{q}^T\boldsymbol{f}^{ext}, \tag{15}$$

$$\int_{L^t}\delta\frac{d\Delta u}{d\xi}N^t d\xi + \int_{L^t}\delta\frac{d^2\Delta v}{d\xi^2}M^t d\xi = \delta\Delta\boldsymbol{q}^T\boldsymbol{f}^{int}, \tag{16}$$

where $N^t = AE\frac{du_l^t}{d\xi}$ is the axial force and $M^t = I_\zeta E\frac{d^2v_l}{d\xi^2}$.

3. KINEMATICAL CONTACT METHOD

To treat the problem of mechanical contact one should introduce the terms of gap (d) and the contact pressure (p), which measured in normal direction to the contacting surfaces. When two bodies are contacting in a point, the contact pressure $p \geq 0$ and the gap $d = 0$. Otherwise in non-contact case $p = 0$ and $d > 0$. In order to treat the contact conditions the use of local coordinate system is advantageous.

The displacements of the contacting nodes are transformed to a local coordinate systems with basis vectors tangential and normal directions to the contact surfaces. One of the coordinate system is shown in Figure 3. The blue colored contact surfaces and the left side beam are displayed. The normal and tangential unit vectors are denoted $\boldsymbol{n}$ and $\boldsymbol{t}$. The $\boldsymbol{t}^v$ is a vector between the node 6 and the end node of the beam. The vector of $\boldsymbol{t}^t$ represents the projection of the $\boldsymbol{t}^v$ to the contact surface, and S_{56} is the length of the actual contacting surface along the meridian.

If $|\boldsymbol{t}^t| < S_{56}$ the contact is taking place on S_{56}, when $\boldsymbol{t}^t > S_{56}$, this means that the contact point will be on S_{45}.

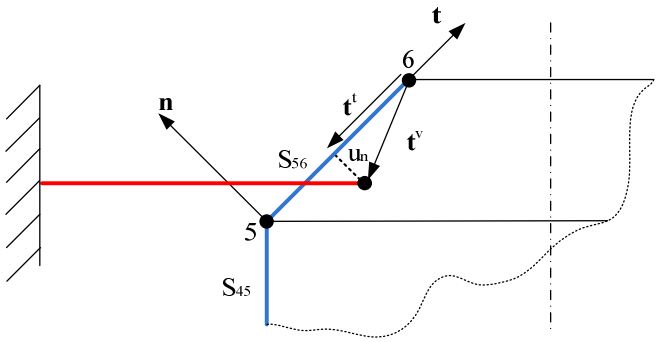

Figure 3 Kinematics of the contact condition

To fulfill the contact conditions, the contact node of the beam is pushed by kinematic loads to the contact surface by applying the calculated displacement in normal direction. The formula of the necessary displacement:

$$u_n = \boldsymbol{n} \cdot \boldsymbol{t}^v = n_x t_x^v + n_y t_y^v. \tag{16}$$

The dot product between a unit vector and a general vector gives the perpendicular projection of the general vector in the direction of the unit vector. The algorithm is recognizing contact, when the end node of the beam is below the contact surface, i.e., $u_n < 0$.

4. SIMULATION

The snap fit process and the plastic protruding surface are shown in Figure 4. The material of the protruding surface is Acrylonitrile butadiene styrene (ABS) and the material of the beam is a type of steel. The value of the friction coefficient is $\mu = 0{,}2$, the area of the cross section is $A = 0{,}4\,mm^2$, the area moment of inertia is $I = \frac{1}{750}\,mm^4$, the young's modulus is $E = 2{,}1 \cdot 10^5\,MPa$. The vertical force, which is pushing the electrical contact element downwards is calculated by the program is shown in Figure 5.

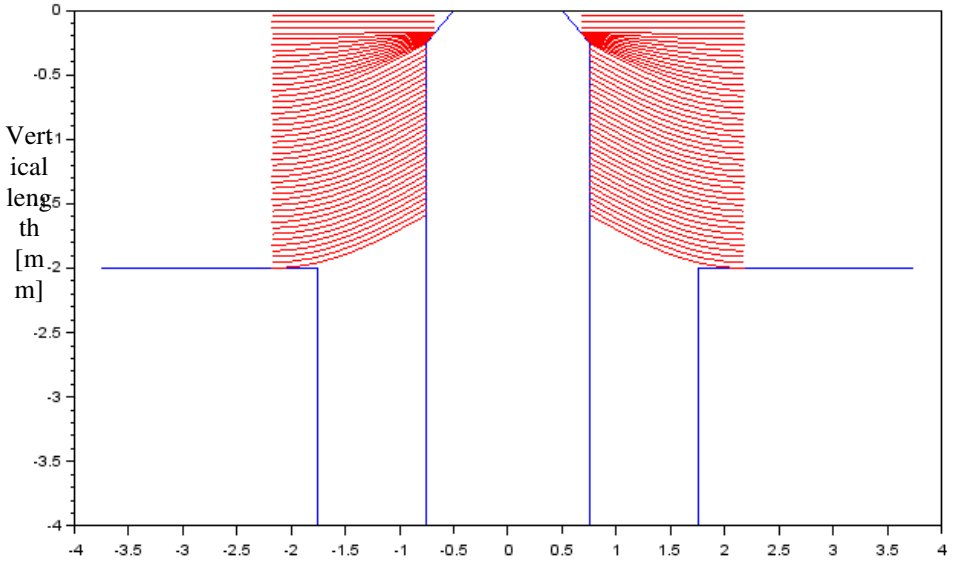

Plastic protruding workpiece

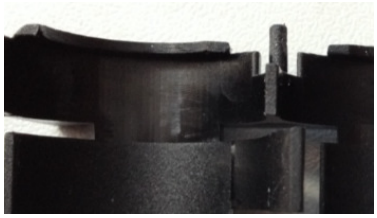

Figure 4 The snap fit process and the plastic protruding workpiece

The total displacement of the electrical contact element is $2\,mm$. The beam was modeled by 8 straight element. The total $2\,mm$ displacement is applied in 45 load increments. There were no contact in the first four load steps.

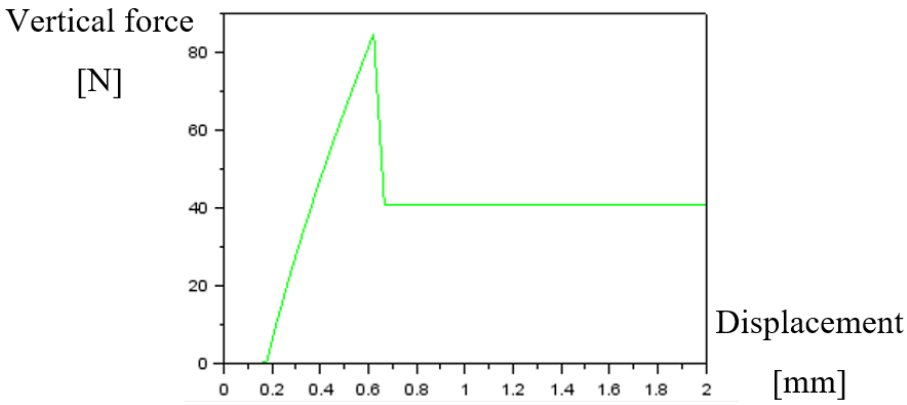

Figure 5 The calculated results

One can see in Figure 5 that the vertical load is increased while the contact node is located on the upper plastic protruding surface and jumped to a lower value when it appears on the circular surface of the protrude. It means that a snap through buckling phenomenon is taking place.

CONCLUSIONS

Elastic modeling of a snap fit contact element has been investigated. The so called corotational method has been used to describe the kinematics of the beam. Material- and geometric stiffness matrices have been determined.
A simulation program has been written in Scilab freeware software. The phenomenon of the snap fit process has been modeled via the kinematical contact analysis. The necessary force to perform the assembly is increasing gradually at the first stage, but later it is falling back to a lower level.
In haptic robotics such a snap fit phenomenon is recognized and the process is controlled according to the force feedback.

ACKNOWLEDGEMENT

This research was carried out in the framework of that Center of Excellence of Mechatronics and Logistics at the University of Miskolc.

REFERENCES

[1] Louie L. Yaw: *2D Corotational Beam Formulation*, 2009.
[2] Remo Magalhaes de Souza: *Force-based Finite Element Analysis of Solids and Structures*, John Wiley & Sons Ltd., England, 1991
[3] P. Nanakorn, L. N. Vu: *A 2D field-consistent beam element for large displacement analysis using the total Lagrangian formulation*, Sciencedirect, 2006
[4] K.-J. Bathe, H. Ozdemir: *Elastic-Plastic Large Deformation Static and Dynamic Analysis*, Computers & Structures, 1976
[5] M. A Srinivasan: *What is Haptics*, The Touch Lab, MIT, 2005

INTERNATIONAL SCIENTIFIC CONFERENCE ON ADVANCES IN MECHANICAL ENGINEERING

13-15 October 2016, Debrecen, Hungary

CYCLE TIME ADAPTATION OF STOCHASTIC ASSEMBLY LINE

[1]RUPPERT Tamás, [2]ABONYI János DSc

[1]University of Pannonia
E-mail: ruppertt@fmt.uni-pannon.hu
[2]University of Pannonia; Institute of Advanced Studies Kőszeg
E-mail: janos@abonyilab.com

Abstract
A wire harness assembly conveyor line consists of manual workstations (tables) linked by a conveyor. The tables are rotating in each cycle. The stochastic nature of the activity times makes difficulties since the operators have to finish their operations before the cycle time. Although minor delays can be handled as the workers can temporarily follow the table to work off their backlogs, the conveyor has to be stopped when the accumulated delays achieve a certain limit. The aim of the adaptation of the cycle time is to minimise the risk of stopping the process. The algorithm estimates the activity times based on a Brownian motion model and calculates the cycle time that guarantees that the delay of the operators will not exceed a certain limit.

Keywords: *Modular production, Cycle time, Stochastic processes*

1. INTRODUCTION

The wire harness is the vascular system of the car. Wire harness assembly conveyors are frequently applied in the automobile industry. These modular assembly lines consist of manual workstations (tables) linked by a conveyor (see Figure 1). The optimisation and the cost estimation of these processes is an economically significant problem [1]. Schraft and Schlaich from Fraunhofer Institut published a survey and compared manual and automatized processes [2]. Pil and Holweg studied the effect of product variety [3]. Xiaobo and Ohno developed unit flow and worker movement diagrams [4] and developed an algorithm for sequencing in JIT production [5].
Our goal is, to develop an algorithm that continuously sets the cycle time to maximise the productivity meanwhile avoiding the stopping of the line. The algorithm estimates in every cycle step the necessary cycle time needed to ensure that all of the operators will be able to finish his/her define our job. This calculation is based on the database of theoretical activity times. This database defines the time required for a given operator for given task based on the information related to a modular type of product. The algorithm continuously monitors the activities of the operators and based on the detected delays adapts the cycle time of the conveyor in every step to ensure process improvement.
To validate this concept, we developed a complex simulation model based on the analysis of wire harness assembly lines [6][7][8][9][10]. In the second session we will describe the model of the assembly line and its parameters. The third session shows the developed algorithm and the results of its application.

Figure 1 The wire harness assembly conveyor

2. STOCHASTIC MODEL OF THE PRODUCTION LINE

The wire harness assembly conveyor is operated by human operators working at tables, and the tables are moving similarly as a conveyor belt. The movement of these tables has a certain speed which is referred as cycle time. This time is related to the complexity of the product. After the cycle step every table moves to the next station, the operators can work on the next product, but many times when the operator do not finish her/his job and she/he can move with the table and try to work of the backlog if it is necessary. In the other case, when the operator finishes the job before the end of cycle time, in that case, she/he can work ahead (see on Figure 2 and 3)

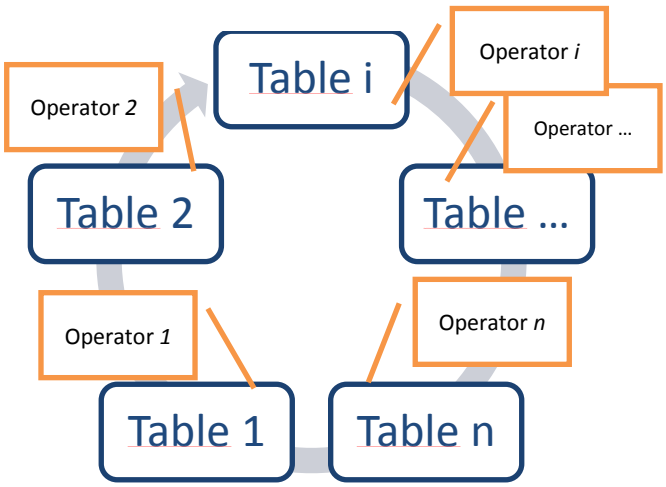

Figure 2 Model of assembly line in the first step

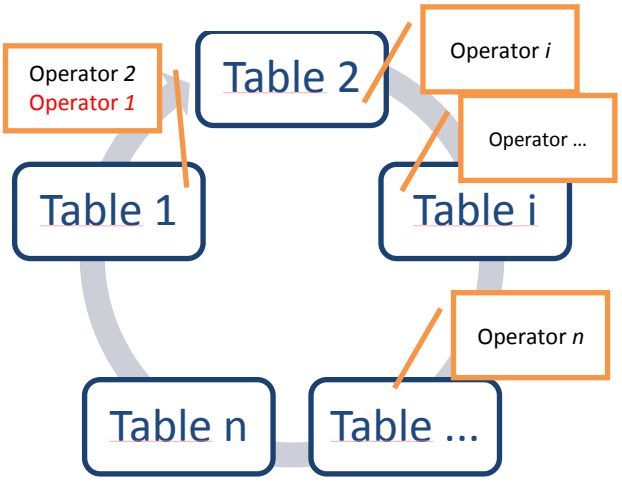

Figure 3 Model of assembly line in the next step

We formalize the model in the following ways and developed an algorithm for the dynamic cycle time calculation. Every table has two assembly times, first is the measured times (T), secondly the theoretical times ($\tilde{T}$). These times assign to the type of product.
Figure 4 shows the parameters on assembly line:

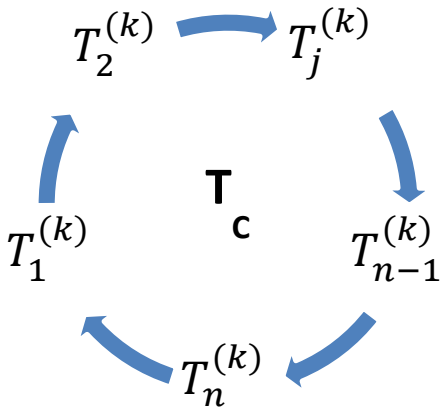

Figure 4 The parameters of model

The k-th cycle begins at the $t^{(k)}$-th time instant and ends after the $T_C^{(k)}$ cycle time, $t^{(k+1)} = t^{(k)} + T_C^{(k)}$. In this period the *i*-th operator starts his/her activity at $t_i^{(k)}$. We modelled the activity times as normally distributed variables $t_i^{(k+1)} = t_i^{(k)} + N(T_i, \sigma_i)$, parametrized by the T_i mean and σ_i variance. The $\Delta_i^{(k)} = t^{(k)} - t_i^{(k)}$ difference shows how the operator is ahead or delayed related to the cycle time. This difference should be smaller than a given percentage of the activity time, in our case 50%, so when $\Delta_{cr} = 0.5T_i < \Delta_i^{(k)}$ the process should be stopped. We also constrain how much the operator may not work ahead. This should be no more than the 25% of the normal activity time $\Delta_{ah} = 0.25T_i > \Delta_i^{(k)}$. In this case the operator should wait at least for a $w_i^{(k)} = \Delta_i^{(k)} - 0{,}25T_i^{(k)}$.

3. THE ADAPTIVE OPERATING STRATEGY AND APPLICATION EXAMPLE

In each cycle before the production the product barcode is scanned and the system calculates theoretical assembly times for each tables based on the complexity of the product. In the next step, the algorithm estimates the maximum assembly times for each tables and selects the biggest one to that minimises the risk of archiving critical delay that requires the stopping of the system.

$$T_C^{(k+1)} = max\left(\tilde{T}_{i,j}^{(k+1)} - t^{(k)}\right) \quad (1)$$

$\tilde{T}_{i,j}^{(k+1)}$ is estimated based on the previously measured differences $\Delta_i^{(k-1)}$.

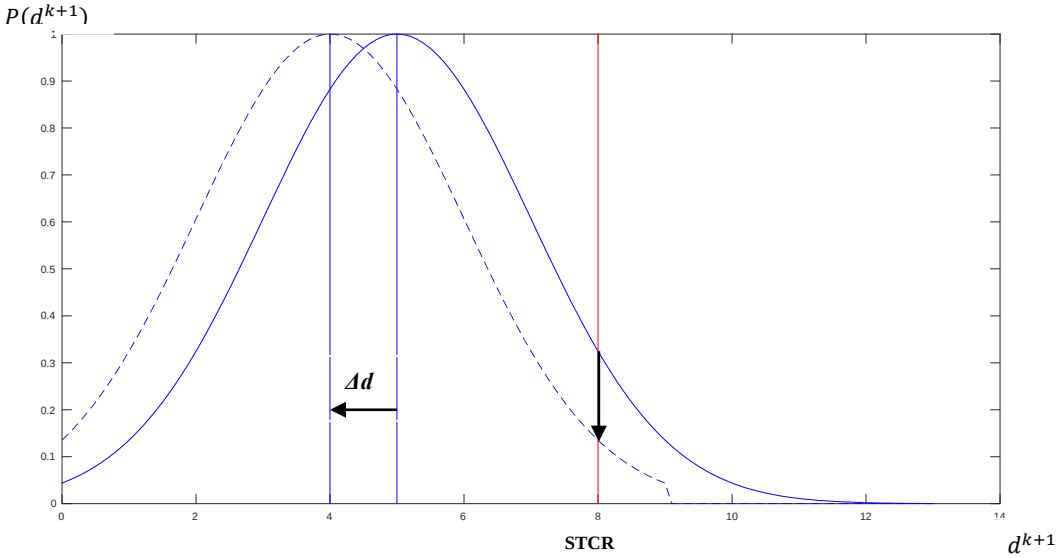

Figure 5 The concept of the robust cycle time adaptation. We modify the cycle time to ensure that the accumulated difference will not exceed the critical stopping time with a given probability.

We developed a Matlab program to simulate the proposed stochastic model of the assembly line. In this study only one product is produced. The conveyor consists of ten stations. The process is assumed to be well balanced, so every operator activity is modelled as a $T_i = N(10,0.3)$.

Figure 6 and 7 show the accumulated times ($\Delta_i^{(k)}$) without and with the application of the proposed algorithm.

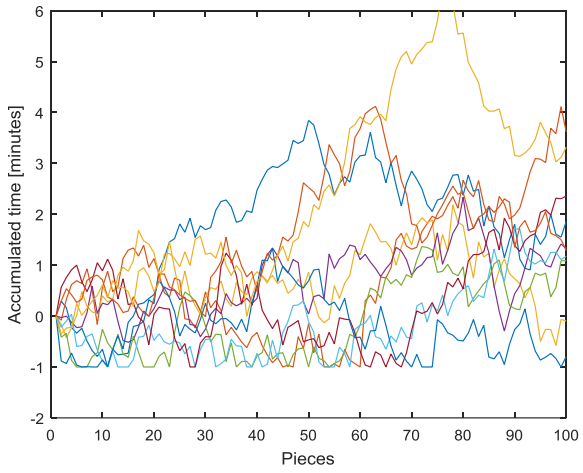

Figure 6 The accumulated times without the application of the proposed algorithm

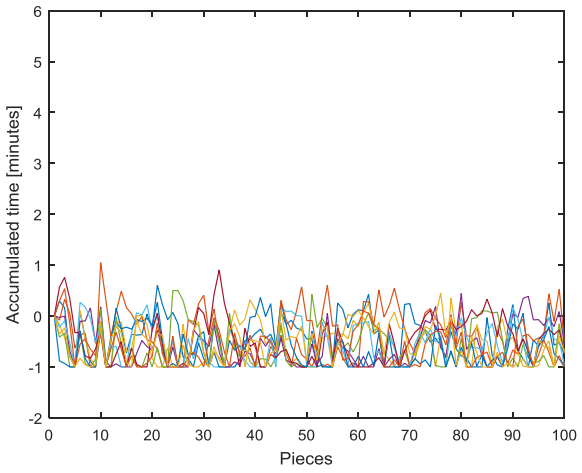

Figure 7 The reduced accumulated times achieved with dynamic cycle times

We can notice in Figure 7 with the application of the proposed algorithm the accumulated times become shortened, so we can avoid the stopping of the process, which reduces the downtimes.

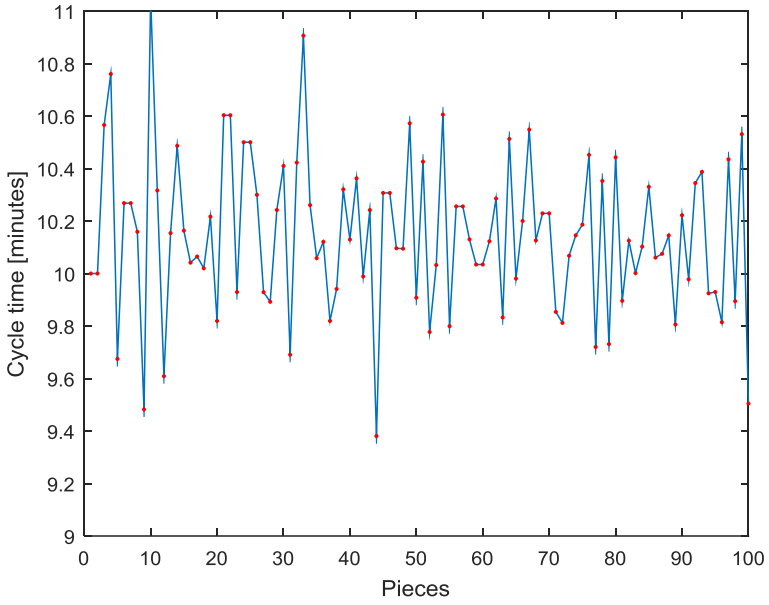

Figure 8 The dynamic cycle times

CONCLUSIONS

We developed an algorithm for the cycle time control of a special stochastic assembly line. in every cycle step The proposed algorithm calculates the necessary cycle time. The critical thing is the general assembly times because the system calculates the new cycle time based on this information. We can prove with this algorithm that the production will be more balancing with the changing cycle times and we can avoid the downtime on the assembly line.

ACKNOWLEDGEMENT

The research has been supported by the National Research, Development and Innovation Office - NKFIH, through the project OTKA-116674 (Process mining and deep learning in the natural sciences and process development)

REFERENCES

[1] E. Aguirre, B. Raucent: *Performances of Wire Harness Assembly Systems.* Industrial Electronics, 6, 292-297. 1994
[2] R.D. Schraft, G. Schlatch: *A survey of the assembly of wire harnesses in industry.* Assembly Automation, 4, 29-32. 1988
[3] F. K. Pil, M. Holweg: *Linking Product Variety to Order-Fulfillment Strategies.* Interfaces, 10, 394-403. 2004
[4] Z. Xiaobo, K. Ohno: *Properties of a sequencing problem for a mixed model assembly line with conveyor stoppages.* European Journal of Operational Research, 11, 560-570. 1998
[5] Z. Xiaobo, K. Ohno:. *Algorithms for sequencing mixed models on an assembly line in JIT production system.* Computers ind. Engng, 10, 47-56. 1997
[6] E. Cevikcan, M. B. Durmusoglu, *An integrated job release and scheduling approach on parallel machines: An application in electric wire-harness industry.* Computers & Industrial Engineering, 15, 318-332. 2014

[7] J. Tilindis, V. Kleiza, *The effect of learning factors due to low volume order fluctuation in the automotive wiring harness production*. Procedia CIRP, Volume 19, 6, 129-134. 2014

[8] N.S. Ong, G. Boothroyd, *Assembly times for electrical connections and wire harnesses.* The International Journal of Advanced Manufacturing Technology, 25, 155-179. 1991

[9] C. da Cunha, B. Agard, A. Kusiak, *Improving manufacturing quality by re-sequencing assembly operations: a data-mining approach.* 18th International Conference on Production Research, 6. 2005

[10] K. Okamura, H. Yamashina, *A heuristic algorithm for the assembly line model-mix sequencing problem to minimize the risk of stopping the conveyor*. International Journal of Production Research, 16, 233-247. 1979

INTERNATIONAL SCIENTIFIC CONFERENCE ON ADVANCES IN MECHANICAL ENGINEERING
13-15 October 2016, Debrecen, Hungary

MACHINING OF ENGINEERING POLYMERS

[1] SARANKÓ Ádám, [2] KERESZTES Róbert PhD, [3]KALÁCSKA Gábor DSc

[1]Szent István University, Institute for Mechanical Engineering
E-mail: saranko.Adam@gmail.com
[2]Szent István University, Institute for Mechanical Engineering Technology
E-mail: kresztes.Robert@gek.szie.hu
[3]Szent István University, Institute for Mechanical Engineering Technology
E-mail: kalacska.Gabor@gek.szie.hu

Abstract
In the engineering applications polymers are widely used not only in injection moulded or formed versions but in machined finishing. The producers mainly support the end-users by general recommendations for the applicability and machining in broad ranges and tolerances. To set more precise machining features of many semi-finished engineering polymers we developed a measuring system for CNC lathe machine. Nowadays, CNC machining centres are the most widely used devices for machining, so we performed tests on NCT CNC lathe by changing the relevant parameters, while measuring the feed force and the main cutting force. We used the results to determine generally adaptable cutting parameters.

Keywords: *force measuring, lathe, turning force components*

1. INTRODUCTION

These days, it is becoming more and more widespread to use technical plastic parts in the practice of mechanical engineering. These plastic machinery components, depending on the number of units, are mainly produced by injection moulding or machining. Injection moulding technology is economically favourable only above a very high volume production. For smaller volumes, the parts are produced by some sort of machining process. One of the most commonly used devices for machining is lathe. That is why plastics manufacturers publish catalogues, in which they indicate the recommended values within the ideal interval for cutting parameters of different materials. These values are mostly defined empirically, and are practice-proven. However, they have become less reliable lately, as every company wants to produce their goods in the shortest possible time, and in the maximum possible amount. This process can be sped up by, among other things, increasing the cutting speed. Relatively high speeds are available for the manufacturers by modern CNC machining centres, although these materials have not been studied at such a machining speed range before [3], [4].
One of the aims of our research is to examine the surface roughness of the machined material, calculate cutting forces under high-speed cutting conditions, and determine the type and tensile strength of the produced chip. Based on the results, we learn which cutting parameters should be used in case of various plastic materials, thus allowing for faster machining.

2. METHODS

In order to get the desired shape of a workpiece while machining, a suitable tool is used for this purpose, forming the piece by removal of material. The resulting, redundant layer of material is

called polymer chip, of which a few more important details will be discussed in the following paragraphs [5].

2.1. The equipment used in the experiment

The tests were run on a type NCT EUROturn-12B CNC machine. The device is located in the workshop of the Institute for Mechical Engineering Technology at Szent István University. The first figure illustrates the measured forces during the machining. The yellow arrow shows the direction of rotation of the workpiece, the red arrow points to the main cutting force, and the blue one shows the feed force [1], [2]. The arrangement shown on the image is a proper illustration of the actual arrangement.

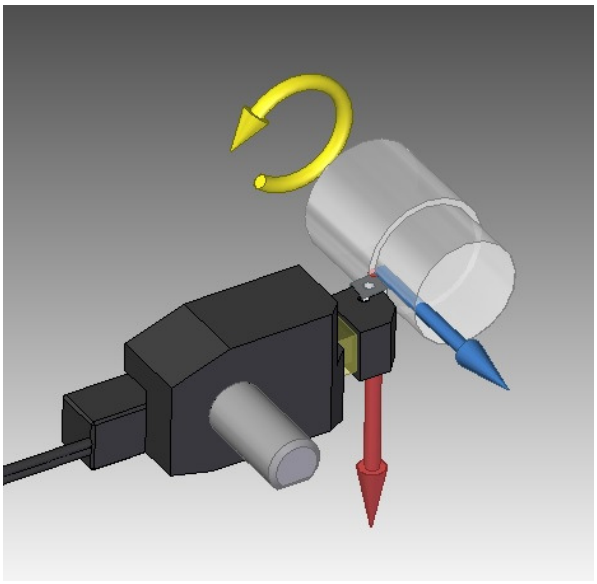

Figure 1 Illustration of the main cutting force (red arrow) and the feed force (blue arrow)

The second figure shows some elements of the implemented measuring system, such as the workpiece clamped in the chuck and the turning tool clamped in the tool post.

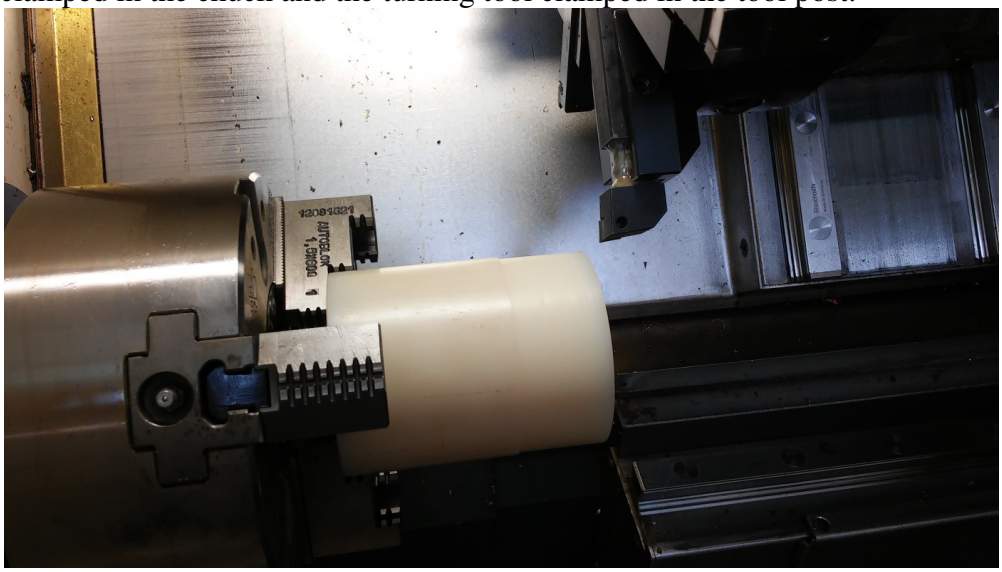

Figure 2 The workpiece clamped in the chuck and turning tool clamped in the tool post

The turning tool used for measuring forces is clamped in a radial tool post, the shaft of the tool being eased up at a certain section. This process is necessary to ensure that the strains will be the largest on this part. The so-called strain gauges, which are also to be found here, are fixed to the shaft with a special glue.
The third figure shows the 3D image and a photo of the turning tool clamped in a tool post.

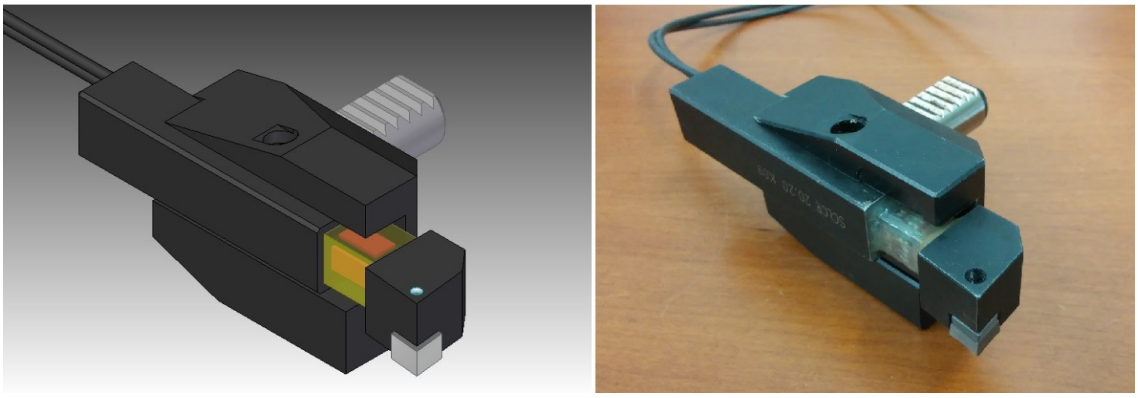

Figure 3 3D illustration and photo of the clamping

The tool post had to be designed from a DIN69880-standard based type B7-20x16x30 tool post, since normally only 16x16-sized tools can be inserted in it, but the force measuring tool is 20x20 in size. Using adequate milling of the surface, the instrument has been centred. We calibrated the force measuring system using a pressure cell, with which we carried out successful test runs.
During the test I examined the main cutting force (in tangential direction) and the feed force (in axial direction). The strain gauges found on the tool and the type Spider 8 measuring amplifier are connected by wire, converting the analogue signals to digital, which are then transmitted to the computer. I achieved the chart-like visualization of the digital signals with a software called Catman 3.1. The measurement and data collection are both of 50 Hz frequency.
The properties of the polymer chip vary by a large extent accordingly to certain parameters. During machining, elementary rotation is favourable, while fast-flowing chip is the least desirable. This type gets curled up and stuck in between other parts of the processing machine very easily, and can even cause fracturing of tools and smaller workpieces, not to mention that while spinning, the hands or clothing of the operator may be caught, which can be fatal . For safety reasons, we decided to saw a specimen across to the middle, making the flowing chips break at each rotation. The measurement results were not affected by this. The fourth figure below shows the specimen.

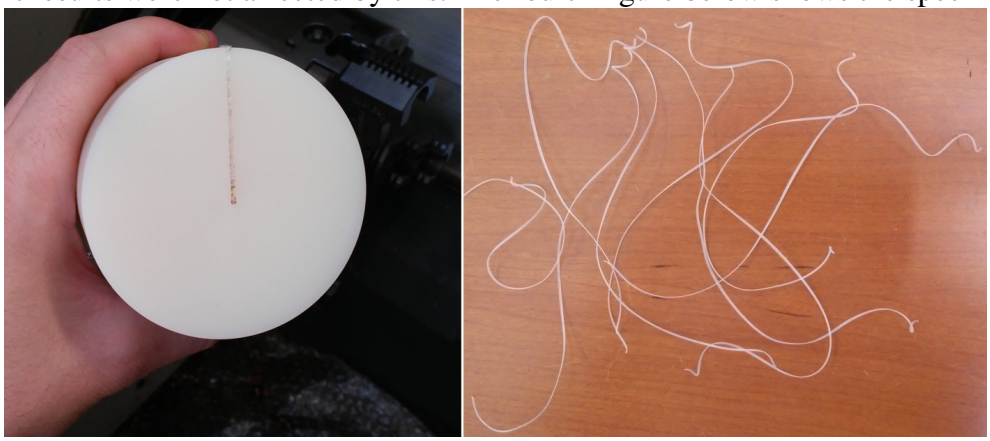

Figure 4 The test piece and the polymer chip produced during the process

2.2. Materials used in the research

The tested materials are mainly the most common polymers used in the technological sector, such as PA, POM C, HDPE [6]. However, the test program may include a variety of environmentally friendly composites,and self-lubricating polymers,using the aforementioned high cutting speeds [3].

2.3. Sample chart

During this research, we expect diagrams structured comparable to the following chart (fig.5), which is from a previous, similar study of the Institute for Mechanical Engineering Technology.

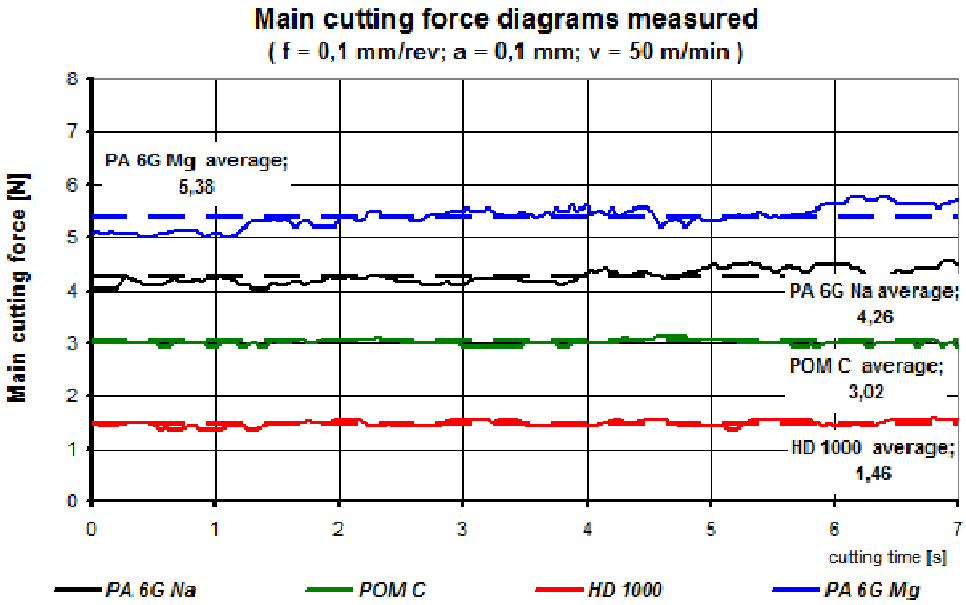

Figure 5 Sample chart of a similar research

SUMMARY

As a result of the research program, a measuring system is developed and we expect to see if it is economically beneficial to deviate from the cutting speed and other parameters recommended in the catalogues published by manufacturers. Different parameters result in varying surface quality, so it is recommended to examine these surfaces.

REFERENCES

[1] Angyal B., Dobor Lné., Palásti K. B., Sipos S. – A Forgácsolás és Szerszámai – Műszaki Könyvkiadó, Budapest, 1988
[2] Frischerz, Dax, Gundelfinger, Häffher, Itschner, Kotsch, Staniczek – Fémtechnológiai Táblázatok – B+V Lap- és Könyvkiadó Kft., 1997
[3] Dr. Kalácska Gábor – Műszaki polimerek és kompozitok a gépészmérnöki gyakorlatban, 3C-Grafika Kft., Gödöllő, 2007
[4] Dr. Kalácska Gábor - Műszaki Műanyag Féltermékek Forgácsolása - Quattroplast Kft., Gödöllő, 2005.
[5] Nagy P. S. – Szerszámgépek, gyártórendszerek – BDMF jegyzet, Budapest, 1997
[6] www.quattroplast.hu

INTERNATIONAL SCIENTIFIC CONFERENCE ON ADVANCES IN MECHANICAL ENGINEERING

13-15 October 2016, Debrecen, Hungary

GENETIC ALGORITHM BASED PARAMETER OPTIMIZATION OF 3 CONTROL METHODS OF PNEUMATIC POSITIONING SYSTEM

[1]SÁRKÖZI Eszter, [2]FÖLDI László PhD

[1]Szent István University Institute for Mechanical Engineering Technology
E-mail: sarkozi.eszter@gek.szie.hu
[2]Szent István University Institute for Mechanical Engineering Technology
E-mail: foldi.laszlo@gek.szie.hu

Abstract
In this paper three different control methods –PID, Status feedback controller and Sliding mode controller- were studied in a position controlled pneumatic linear drive. As the examined system is complex and nonlinear optimal tunings of controllers are complicated. With genetic algorithm based optimization near-optimal control parameters were found and the three control methods were evaluated. From technical viewpoint after proper tuning the three control methods behave similar during positioning.

Keywords: *Pneumatic drive, Position control, Optimization, Genetic algorithm*

1. INTRODUCTION

Evaluating different control methods of a certain drive system the used optimization method of control parameters has great impact on the overall performance. There are several proven optimization methods for PID controller (as Ziegler-Nichols, Tyreus Luyben) and for sliding mode controller (as Lyapunov method), but these methods have limitations in pneumatic systems as the behavior of pneumatics is non-linear due to piston friction and the characteristics of compressed gas flow. In this paper three different control methods were applied (PID, status feedback controller and chattering-free sliding mode control), each parameters were optimized by the same algorithm. Therefore genetic algorithm (GA), a general-purpose, heuristic search and optimization method was chosen, which is suitable for optimization of all controller types if a proper objective function (a fitness function) is defined. Genetic algorithm uses the principles of biological evolution, it searches for the best individual with crossover, selection and mutation.

2. PNEUMATIC LINEAR SERVO DRIVE SYSTEM

As an actuator a Festo DGPL-25-450-PPV-A-KF-B cylinder was used with 450mm stroke length, to which we attached a Festo MLO-POT-0450-TLF analogue displacement encoder, which has a 0,01 mm travel resolution. The applied way-valve was an MPYE-5-1/8-LF-010-B 5/3 proportional valve. The controller was a modular NI CompactRIO™ (cRIO 9073) programmable automation controller, out of its modules we used the analogue-to-digital converter (NI 9201). We controlled the proportional solenoid valve with the help of the analog output module (NI 9472). The circuit diagram of the pneumatic positioning system is presented on figure 1.

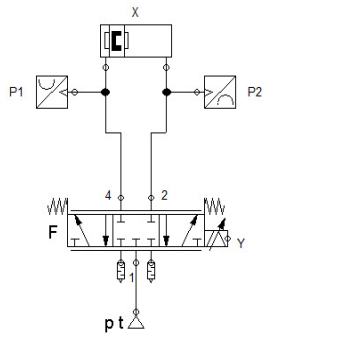

Designation	Description
F	Proportional 5/3-way directional valve
pt	Compressed air supply
x	Cylinder without piston rod
	Electrical connection 24V
	Electrical connection 0V
X	Displacement encoder
Y	Proportional valve solenoid, position controlled
P2	Analog pressure sensor
P1	Analog pressure sensor
P1	Analog pressure sensor
P2	Analog pressure sensor
NI cRIO 9037	Logic module

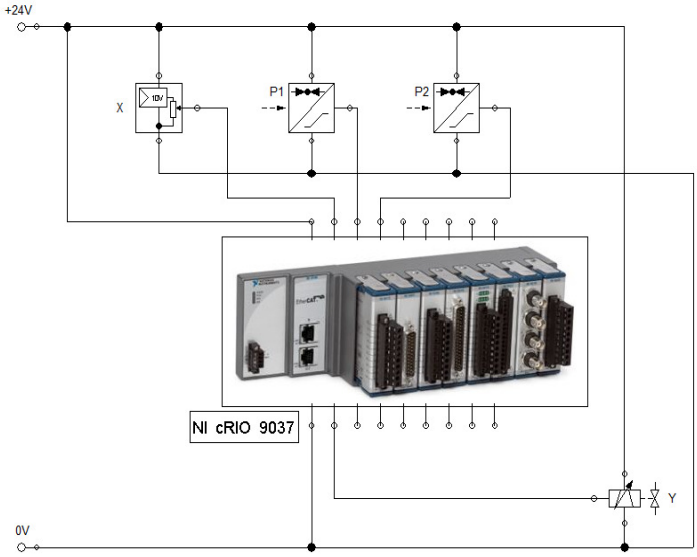

Figure 1 The pneumatic and electric circuit diagram

2. METHODS

In the first step a block-oriented model of pneumatic linear drive system was built, after it's identification, the three controller (PID, status and sliding mode controller) was connected individually to the system model. Then we have specified the fitness function, the parameters of the genetic algorithm (GA) solver and run the GA solver. With the results an fminsearch was run as well in order to find the local minimum in the neighbourhood of the GA's result. During modelling MATLAB Simulink was used, the optimisation processes was run with MATLAB Optimization Toolbox 7.2.

2.1. Block-oriented model of pneumatic linear drive system

To create mathematical model of double-acting pneumatic cylinder three main mathematical formulas have to be declared: the descriptive equation of the flow mass rate flowing through an orifice, the force equation and a container filling eqaution. After some simplification, as we consider the flowing gas as ideal gas, and neglecting the effect of the temperature change, the following equation was used (*Figure 2*.).

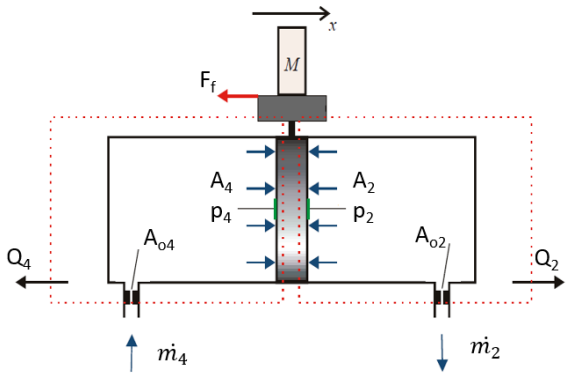

Figure 2 Outline of the cylinder

The mass flow rate through an orifice due to the pressure difference is:

$$\dot{m} = A_o * p_u * \sqrt{\frac{2*\kappa}{(\kappa-1)*R*T} * \left(\left(\frac{p_d}{p_u}\right)^{\frac{2}{\kappa}} - \left(\frac{p_d}{p_u}\right)^{\frac{\kappa+1}{\kappa}}\right)} \quad (1)$$

The mass flow rate in function of p_d/p_u has a maximum value at $p_d/p_u=0.528$, so this pressure ratio is called critical pressure ratio. Below the critical pressure ratio the velocity of flow is maximal, and this velocity is the speed of the sound at exhausting temperature. Above the critical pressure ratio the velocity of flow is lower than the speed of sound, the value of it depends on the current pressure ratio. The force equation of the cylinder is:

$$m * \ddot{x} = A_4 * p_4 - A_2 * p_2 - F_f - F_l \quad (2)$$

The container filling equation:

$$R * T * \dot{m} = V * \dot{p} + \dot{V} * p \quad (3)$$

In the Equation (2), the friction force is defined with the use of Stribeck friction as follows:

$$F_f = \begin{cases} F_{str,} & v \geq 0{,}001 \text{ m/s} \\ \min(F_b, |\sum F_i|) * \text{sign}F_i, & v < 0.001 m/s \end{cases} \quad (4)$$

where $F_i = p_4 * A_4 - p_2 * A_2 - F_l$, and Stribeck friction is:

$$F_{Str} = \left(F_C + (F_{br} - F_C) * \exp(-c_v * |v|)\right) * \text{sign}(v) + f * v \quad (5)$$

To create mathematical model of the proportional valve, equation (1) is also used defining mass flow rates through the valve. Considering the physical construction of 5/3 proportional valve, as it can be interpreted by the application of four orifices.

2.2. Control methods

2.2.1. PID controller

The algorithm calculates the control variable as a function of the difference of the process output and the setpoint. This algorithm modifies the error (e) through three channels: via the proportional channel, the integral channel and the derivative channel. PID controller is popular because it is reliably able to fulfill the prescribed control requirements in most industrial applications despite of it's relatively simple structure.

2.2.2 Status controller

The status controller is based on the classic proportion controller with the addition that it takes into account the first and second derivative of the feedback signal. In positioning the controlled variable is the position, the first derivative is the velocity, the second derivative is the acceleration. So the status controller takes into consideration the motion parameters. The velocity and the acceleration have negative impact, so they are a dampings proportionally to the velocity and the acceleration. Typical field of application of the status controller is the positioning of pneumatic linear drives.

2.2.3 Chattering free sliding mode control

One element of the non-linear controllers is the so-called sliding mode controller. The design of the sliding mode controller contains three main steps. The first step is the design of the sliding surface. The second step is to select a control law, which forces the trajectory of the state variables on the sliding surfaces and then keeps them there. The third is the most important step, it is the chattering free implementation [Gyiveki, 2007].

2.3. Optimization

The control objective of the system was a positioning task: the cylinder should move from 0 mm to 360 mm position. Genetic Algorithm solver of MATLAB Optimization Toolbox 7.2 was used to minimize a value of an objective function. The applied objective function (a fitness function) of the optimization was Integral of the Time weighted Absolute Error (ITAE) criteria:

$$ITAE = \int_0^\infty t|e(t)|dt. \quad \text{(n)}$$

The settings of Genetic Algorithm solver:

- number of variables: 3 (PID: P, I, D; State controller: Kx, Kv, P; sliding mode controller: u_{max}, λ, s_k),
- population size: 10 with 10 subpopulation in each population,
- initial range: 0…1;
- fitness scaling function: rank,
- selection function: stochastic function,
- stopping criteria: max. 500 generations.

As genetic algorithm had found a near-optimal parameter set, a gradient optimization tool (fminsearch) was used to find the local optimal set of parameters in the neighbourhood of the GA optimized parameter set.

3. RESULTS

With every control method 20 optimization processes were performed. From it's results, based on the calculated ITAE values, the 10 best control parameter sets of each control methods were chosen. Implementation of positioning tasks by the three control methods with the best parameter set is illustrated on *Figure 4-6*.
After optimization the following criteria were evaluated: ITAE value, steady-state error, overshoot, setting time with best parameter set and the average of the 10 best parameter sets *(Table 1).*

Table 1 Positioning results

	ITAE value [-]		Steady-state error [mm]		Overshoot [mm]		Setting time [s]	
	Best	**Average of 10 best**	**Best**	**Average of 10 best**	**Best**	**Average of 10 best**	**Best**	**Average of 10 best**
PID controller	0.19053	0.193474 ±0.00379	0.009879	0.0313 ± 0.0535	0	4.7508 ±10.5481	0.201	0.2212 ±0.0359
State controller	0.19056	0.198715 ±0.00699	0.009651	0.0089 ± 0.0018	1.004533	2.6832 ±3.9943	0.201	0.2031 ± 0.0037
Sliding mode c.	0.197448	0.204314 ±0.00679	0.010344	0.00963 ±0.00110	0.08552	2.685707 ±8.350474	0.217	0.2338 ±0.027051

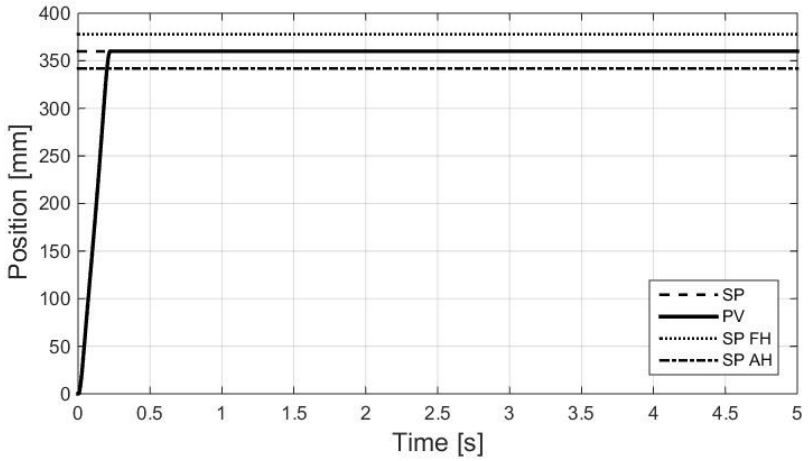

Figure 4 Positioning from 0 to 360 mm by PID controller with the best GA optimized parameters

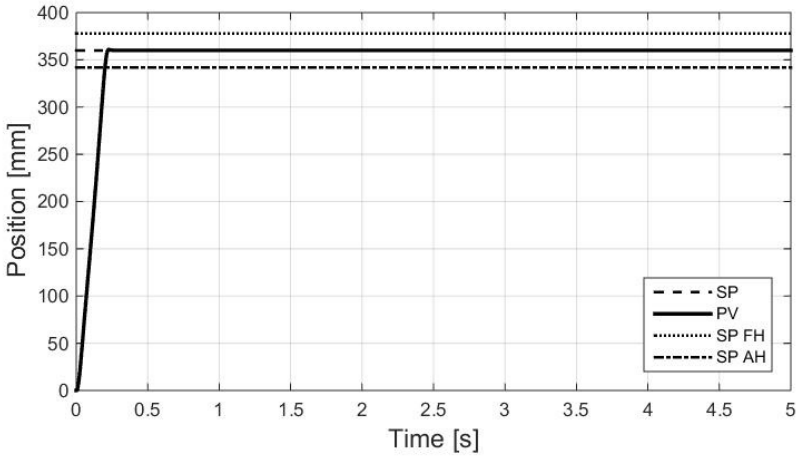

Figure 5 Positioning from 0 to 360 mm by State controller with the best GA optimized parameters

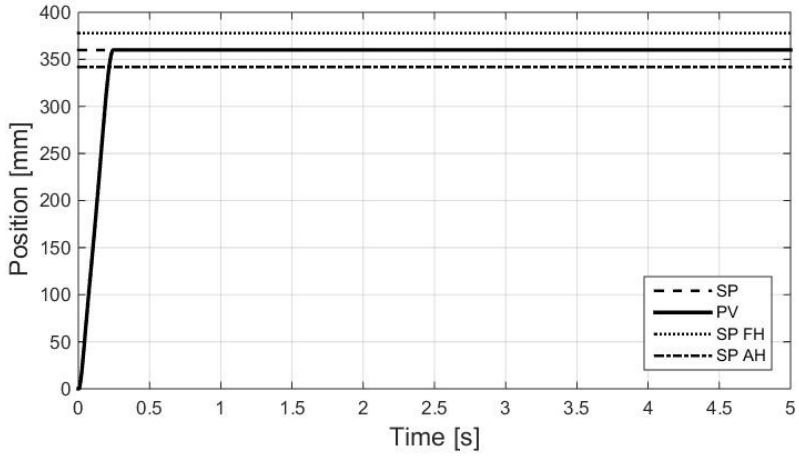

Figure 6 Positioning from 0 to 360 mm by Sliding mode controller with the best GA optimized parameters

CONCLUSIONS

As genetic algorithm uses random populations and it is not an exhaustive search method, it may not find the global optimum of the function. In our case, as the system model is complex and because of pneumatics it is non-linear, during repeated solver runnings it is revealed that the used GA (with combination of fminsearch) cannot find the global optimum. But considering the results from technical viewpoint (as accuracy of positioning) and taking into account the resources (time and CPU capacity), it can be stated that genetic algorithm is a proper universal optimization algorithm for all three examined control methods (PID, status and chattering free sliding mode control) and there are only slight differences between the three control methods during the 0 to 360 mm positioning task.

REFERENCES

[1] Ahn, K., Yokota, S. (2005) *Intelligent switching control of pneumatic actuator using on/off solenoid valves*, Mechatronics vol. 15, 683–702.
[2] Czmerk, A. (2015). *Pneumatikus rendszerek dimanikájának és beállási pontosságának a javítása*. PhD Thesis. BME Budapest.Hamiti, K; Voda-Besanqon, A.; Roux-Buisson H. (1996): Position control of a pneumatic actuator under the influence of stiction, Control Engineering Practice, Vol. 4. pp. 1079-1088
[3] Földi, L.; Sárközi, E.; Jánosi, L. (2015) *Positioning algorithms of pneumatic cylinders*, Mechanical Engineering Letters R and D: Research and Development, Vol. 12. p. 50-60.
[4] Gyeviki, János (2007) *Szervopneumatikus pozícionálás pontosságának növelése DSP alapú csúszómód szabályozással*, PhD Thesis, Debreceni Egyetem Mezőgazdaságtudományi Kar, Debrecen
[5] Madarasz Istvan, Szendro Peter (2008). *Applying genetic algorithm to agricultural machine mechanisms*. 7th Youth Symposium on Experimental Solid Mechanics, 14.05.-17.05.2008., Wojcieszyce, Poland
[6] Nguyen, T., Leavitt, J., Jabbari, F., Bobrow, J.E. (2007) *Accurate Sliding-Mode Control of Pneumatic Systems Using Low-Cost Solenoid Valves*, IEEE/ASME Transactions on mechatronics, 12(2), p. 216-219.
[7] Rahmat, M. F. (2011). *Review on modeling and controller design in pneumatic actuator control system*. Vol. 4., Nr. 4.
[8] Xiang, F., & W. J. (2004). *Block-oriented approximate feedback linearization for control of pneumatic actuator system.* Control Engineering Practice, pp. 387–399.
[9] Yi-Chang Tsai, A.-C. H. (2008). *Multiple-surface sliding controller design for pneumatic servo systems*. Mechatronics, Vol. 18. pp. 506–512.
[10] Yong-Soo Jeon, Chung-Oh Lee, Ye-Sun Hong (1998) *Optimization of the control parameters of a pneumatic servo cylinder drive using genetic algorithms*, Control Engineering Practice 6 pp. 847-853

INTERNATIONAL SCIENTIFIC CONFERENCE ON ADVANCES IN MECHANICAL ENGINEERING
13-15 October 2016, Debrecen, Hungary

INFLUENCE OF DIAMETER AND LENGTH ON FORCE DEVELOPED BY PNEUMATIC MUSCLE ACTUATOR

SÁROSI József PhD

University of Szeged, Faculty of Engineering, Technical Institute
E-mail: sarosi@mk.u-szeged.hu

Abstract
Pneumatic cylinders, pneumatic motors, pneumatic stepper motors and pneumatic bellows are widely used in industrial environment due to their power/weight ratio, power/volume ratio, strength, compactness, simplicity, reliability and cost. Disadvantages of pneumatic actuators can be summarized as follows: difficult to control accurately, air compressibility, compliance and noisiness. Relatively new type of the pneumatic actuators is the pneumatic artificial muscle (PAM) or pneumatic muscle actuator (PMA). Fluidic Muscle made by Festo Company is one of the most investigated commercially available PMA. These muscles can be used in industrial environment as well as in prosthesis or rehabilitation devices. In this paper Fluidic Muscles with different geometric parameters (length, diameter) are compared experimentally.

Keywords: *pneumatic muscle actuator, Fluidic Muscle, experimental setup, force-contraction characteristics.*

1. INTRODUCTION

History of PMAs dates back to 1930s. Unfortunately, due to lacks in technology the production was limited. In 1950s, Joseph L. McKibben was the first who designed an artificial muscle for practical use in medicine. McKibben is often mentioned as the pioneer in PMA. In 1980s, engineers in Bridgestone Company in Japan produced the so called Rubbertuator PMA. Recently, the most often applied is the Fluidic Muscle and also the Shadow Air Muscle (SAM) produced by the Shadow Robot Company.
The structure of the most PMAs can be divided into two main parts: a flexible membrane (e.g. latex, silicone rubber or chloroprene) and a load carrying element (e.g. nylon, fiberglass or aramid). On the basis of their connection, Daerden in [1] discriminates braided muscles, netted muscles and embedded muscles. The difference between netted and braided muscles is in the density of the threads in the braided mesh shell (network of load carrying element) surrounding the membrane: it is higher for the braided muscles. In embedded muscles the loaded threads are settled into the elastic tube. In the paper this type of muscles is considered (Fig. 1).

Figure 1 Fluidic Muscles (as embedded muscle) with different nominal length and diameter [2]

Working principle of PMAs is simple: when a PMA is pressurized, the flexible membrane tends to increase its volume against the braided mesh shell which is non-extensible, therefore the actuator will be shortened and a pulling force will be produced if the muscle is connected to a load.
This flexible actuator shows similarity to human muscle, because the force and motion generated by PMA are linear and unidirectional. For two-direction motion an antagonistic pair of PMAs or a spring returned PMA has to be used. Typically, one muscle moves the load, while the other serves as a brake. During the motion in opposite direction the mechanisms commute their action. These serially connected muscles are named antagonistic pair: the muscle for motion is a flexor while the braking muscle is named an extensor or antagonist [3].
PMAs differ from general pneumatic cylinders as they have no inner moved parts and there is no sliding on the surfaces. The main disadvantages are nonlinear and time variable behaviour, existence of hysteresis and step-jump pressure. This is why number of control schemes and static and dynamic models can be found in the literatures [4], [5], [6], [7], [8], [9], [10] and [11].
Pneumatic muscle actuator can be used for totally different fields: lifting aid, tab punching, robotic prosthesis, wearable exoskeleton robot or jumping robot (Fig. 2).

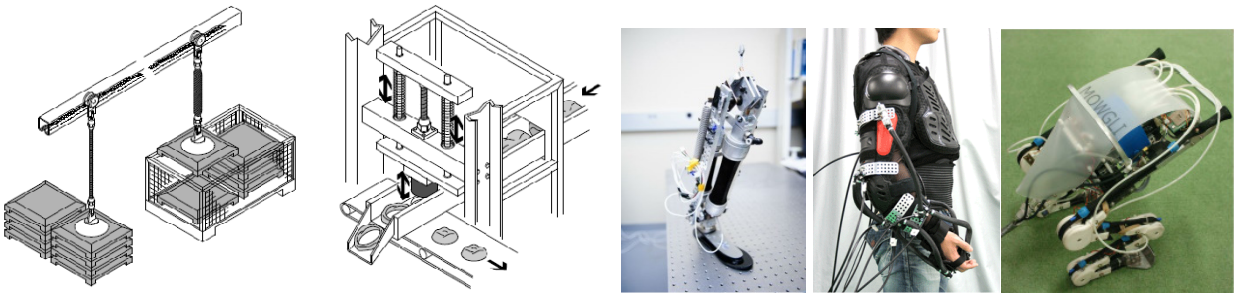

Figure 2 Applications of PMAs [2], [12], [13], [14]

This paper is organized in 4 sections. After Introduction, in Section 2 the applied experimental setup and the experimental measurements are described. The experimental results and the comparisons of Fluidic Muscles are presented in Section 3. The paper ends with Conclusions (Section 4).

2. EXPERIMENTAL SETUP FOR MEASURING FORCE, PRESSURE AND POSITION

For investigation of key features of PMAs, force, pressure and position (displacement) must be measured by an experimental setup (Fig. 3) that is well described in [15]. It illustrates the Fluidic Muscle is built horizontally into the test bed. One of ends of PMA is fixed while the other is movable. The free end of PMA is connected with a spindle which is connected with an accurate position measuring instrument. The setup consists of the following sensors and regulator:

- proportional pressure regulator (PPR) (VPPM-6L-L-1-G1/8-0L6H-V1N-S1C1),
- incremental encoder (LINIMIK MSA 320),
- load cell (Kaliber 7923),
- pressure sensor (Motorola MPX5999D).

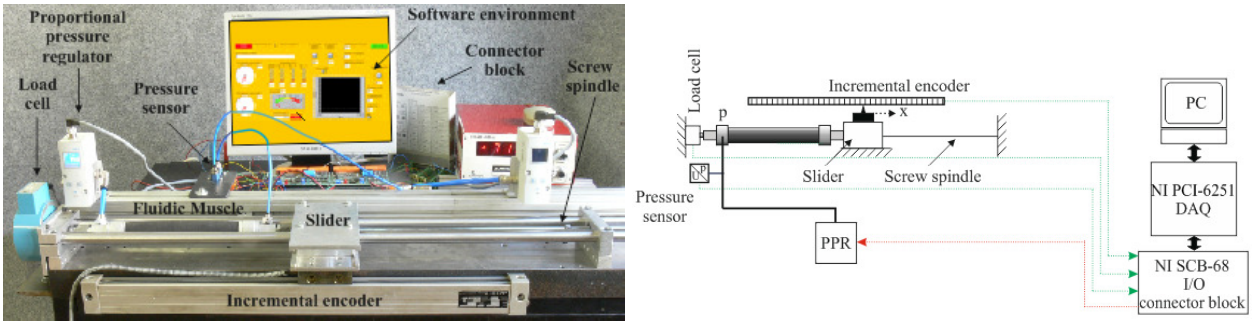

Figure 3 Experimental setup for measuring force, pressure and position

With the help of it, five Fluidic Muscles (DMSP-10-100N-RM-RM, DMSP-10-250N-RM-RM, DMSP-20-200N-RM-RM, DMSP-20-400N-RM-RM and DMSP-40-200N-RM-RM) are investigated - where DMSP means pressed end caps and integrated air connectors, first number defines the inside diameter in mm, second number defines the nominal length in mm and RM means radial pneumatic connection at both ends. Based on values in 30 points of PMAs measured for various compressions the force-contraction curve is plotted. Measuring at every point is repeated for 5 times and statistically averaged. For acquisition and monitoring of measured data a LabVIEW program is developed.

3. COMPARISON OF STATIC FORCE DEVELOPED BY DIFFERENT FLUDIC MUSCLES

Firstly, the force-contraction function of Fluidic Muscles type DMSP-20-200N-RM-RM and DMSP-20-400N-RM-RM are measured at a temperature of 25 °C. The applied pressure is kept at a constant value (0, 100, 200, 300, 400 and 500 kPa, respectively), while the length of PMA is changed by the screw spindle (see Fig. 3). The pulling force decreases with increasing contraction. At maximal contraction the volume reaches its maximum value and the force drops to zero. It means that contraction has an upper limit at which there is no force developed by PMA. The characteristic is nonlinear. In Fig. 4, the characteristic curves in the interval of 0-500 kPa with increase for 100 kPa are plotted. The maximal force of 2048,32 N and the maximal contraction of 25,88% (200 mm length), furthermore the maximal force of 2060,44 N and the maximal contraction of 27,18% (400 mm length) are measured on the pressure of 500 kPa.

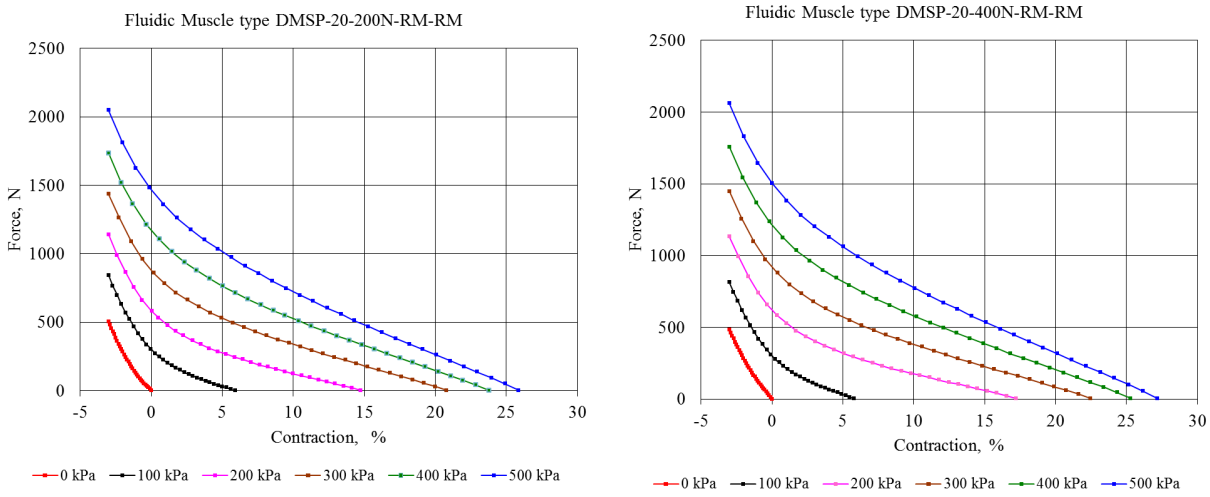

Figure 4 Force as a function of contraction (DMSP-20-200N-RM-RM, DMSP-20-400N-RM-RM)

Comparison of Fluidic Muscles having the same diameter but different length is presented in Fig. 5.

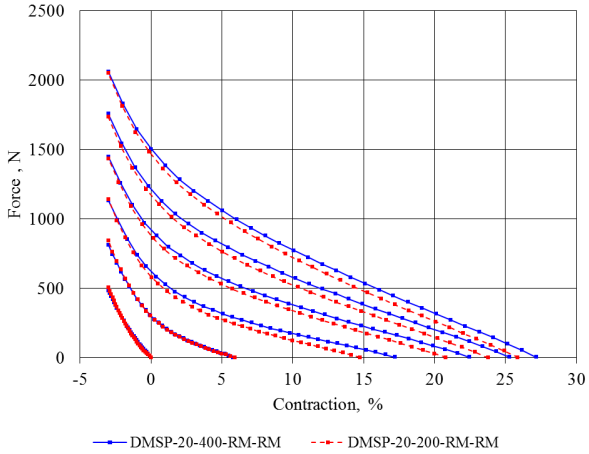

Figure 5 Comparison of Fluidic Muscles having the same diameter

Secondly, the measurement is repeated with Fluidic Muscles type DMSP-10-100N-RM-RM and DMSP-10-250N-RM-RM. In these cases, the maximal force of 768,28 N and the maximal contraction of 18,29% (100 mm), furthermore the maximal force of 811,06 N and the maximal contraction of 20,03% (250 mm length) are also measured on the pressure of 500 kPa (Fig. 6). This significant difference attributes to the shorter effective length of DMSP-10-100N-RM-RM.

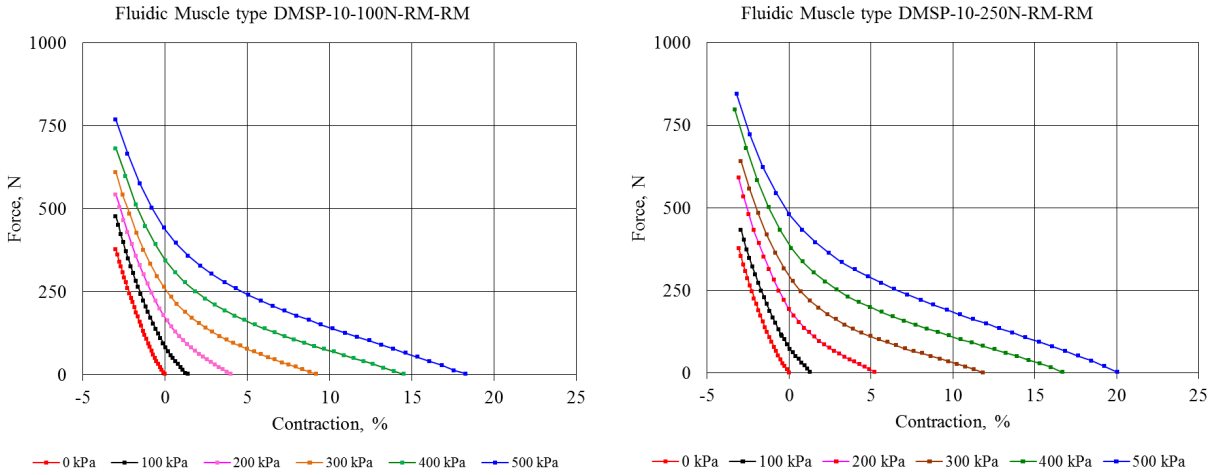

Figure 6 Force as a function of contraction (DMSP-10-100N-RM-RM, DMSP-10-250N-RM-RM)

Finally, DMSP-40-200N-RM-RM is investigated: the maximal force of 7273,78 N and the maximal contraction of 28,85% are measured on the pressure of 500 kPa (Fig. 7).

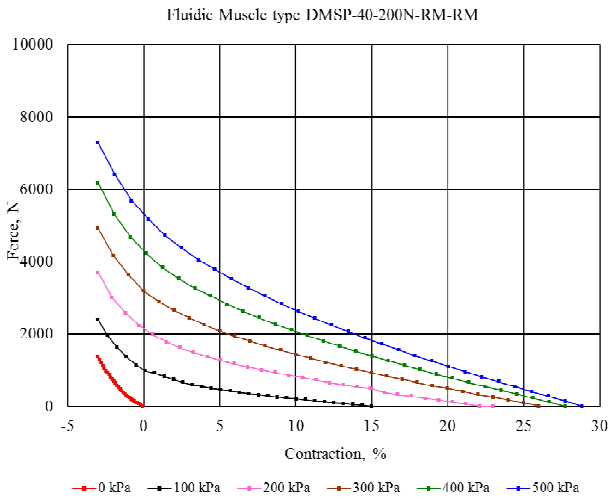

Figure 7 Force as a function of contraction (DMSP-40-200N-RM-RM)

CONCLUSIONS

Based on some investigations the following is concluded: An important difference between pneumatic cylinders and PMAs can be noticed: while the force at cylinders is only a function of pressure and piston size meaning that at constant pressure the force does not change with position in the case of PMAs the force is influenced by displacement. The force produced by PMAs increases with increasing inside diameter and the force depends not only on inside diameter but also length.

REFERENCES

[1] Daerden, F., Lefeber, D.: *Pneumatic Artificial Muscles: Actuator for Robotics and Automation*. European Journal of Mechanical and Enviromental Engineering, 47(1), 11-21, 2002.
[2] Festo: *Fluidic Muscle DMSP/MAS.* Festo product catalog, 36 p., 2005.
[3] Enoka, R.M.: *Neuromechanics of Human Movement.* Human Kinetics Publishers, Champaign, United States, 2008
[4] Mukhtar, M., Akyürek, E., Kalganova, T., Lesne, N.: *Implementation of PID, Bang-bang and Backstep-ping Controllers on 3D Printed Ambidextrous Robot Hand*. In Studies in Computational Intelligence, Springer, 21 p., 2016.
[5] Cao, J., Xie, S.Q., Zhang, M., Das, R.: *A New Dynamic Modelling Algorithm for Pneumatic Muscle Actuators.* Proceedings of Intelligent Robotics and Applications (7th International Conference (ICIRA)), Guangzhou, China, 8918, 432-440, 2014.
[6] Tothova, M., Pitel, J.: *Dynamic Simulation of Pneumatic Muscle Actuator in Matlab/Simulink Environment.* Proceedings of the 12th International Symposium on Intelligent Systems and Informatics (SISY 2014), Subotica, Serbia, 209-213, 2014.
[7] Tothova, M., Pitel, J., Hošovský, A., Sárosi, J.: *Numerical Approximation of Static Characteristics of McKibben Pneumatic Artificial Muscle*. International Journal of Mathematics and Computers in Simulation, 9, 228-233, 2015.
[8] Sárosi, J.: *New Approximation Algorithm for the Force of Fluidic Muscles*. Proceedings of the 7th IEEE International Symposium on Applied Computational Intelligence and Informatics (SACI 2012), Timisoara, Romania, 229-233, 2012.
[9] Shi X., Zhang H-T.: *Modeling of Pneumatic Muscle Actuators Based on Hammerstein System*. 35th Chinese Control Conference (CCC), Chengdu, China, 2279-2284, 2016.
[10] Al-Ibadi A., Nefti-Meziani S., Davis S.: *Valuable Experimental Model of Contraction*

Pneumatic Muscle Actuator. 21st International Conference on Methods and Models in Automation and Robotics (MMAR), Miedzyzdroje, Poland, 744-749, 2016.

[11] Veale A.J., Xie S.Q., Anderson I.A.: *Modeling the Peano Fluidic Muscle and the Effects of Its Material Properties on Its Static and Dynamic Behavior*. Smart Materials and Structures, 25 (6), 65014-65029, 2016.

[12] Wu, M., Driver, T., Wu, S-K., Shen, X.: *Design and Preliminary Testing of a Pneumatic Muscle-actuated Transfemoral Prosthesis.* ASME Journal of Medical Devices, 8(4), 7 p., 2014.

[13] http://www.biorobotics.gatech.edu - Muscle Control Project, Accessed on: 2016-10-03

[14] Niiyama, R., Nagakubo, A., Kuniyoshi, Y.: *Mowgli: A Bipedal Jumping and Landing Robot with an Artificial Musculoskeletal System.* Proceedings of IEEE International Conference on Robotics and Automation, Roma, Italy, 2546-2551, 2007.

[15] Toman, P., Gyeviki, J., Endrődy, T., Sárosi, J., Véha, A.: *Design and Fabrication of a Test-bed Aimed for Experiment with Pneumatic Artificial Muscle.* International Journal of Engineering, Annals of Faculty of Engineering Hunedoara, 7(4), 91-94, 2009.

OPTIMIZATION OF DISASSEMBLY OF THEPRODUCTS BASED ON GENETIC ALGORITHM

ŠEBO Juraj PhD

Department of Industrial Engineering and Management, Faculty of Mechanical Engineering, Technical University of Košice
E-mail: juraj.sebo@tuke.sk

Abstract
The paper focuses on practical application of optimization methodology based on genetic algorithm with the maintaining precedence relationships. The goal of our paper is to examine the methodology through real mobile phones disassembly optimization case(s). We found 3 major problems in application of the optimization methodology on mobile phones disassembly: in some cases product structure diagram fail to exactly describe real product structure, the system of selection of group(s) of switchable genes is not set, and the fitness function does not reach same maximum (resp. global maximum) in any attempt.

Keywords: *genetic algorithm, disassembly, optimization, product*

1. INTRODUCTION

In the literature in the wider topic of disassembly planning is often included the disassembly sequence optimization. We can find articles about different algorithms for optimization of disassembly sequence as linear programing, genetic algorithm (GA), petri nets, neural networks and other [1].
In the following paper we focus on practical application of genetic algorithm (GA) with the maintaining precedence relationships on mobile phone disassembly sequence optimization. Applied GA methodology is based on the article of Kongar and Gupta (see [2]). The goal of the paper is examine GA based optimization methodology through real disassembly cases of different models of mobile phones and find out problems and also how differences in mobile phones influence optimization when it is applied subsequently for particular mobile phones from the group.

2. GENETIC ALGORITHM (GA)

Genetic algorithm (GA) belongs to search heuristics that mimic natural selection. This heuristic is normally used to generate useful solutions to optimization and search problems [3]. Genetic algorithm belongs to the class of evolutionary algorithms that are used to solve optimization problems through techniques inspired by natural evolution, such as inheritance, mutation, selection and crossover [4].
In the practical application of GA we have followed the methodology of Kongar and Gupta in these steps (adapted from [5]):
1. Based on experimental disassembly of the mobile phone we created a product structure diagram (from which we identified disassembly order precedence), disassembly directions (x,y,z), disassembly methods (D-destructive, N-non-destructive) and based on component material we also identified whether or not is demand for the particular component (D-demand, N- no-demand).
2. We created an original population of 10 individuals (each individual is composed of 15

genes), so that each individual had a different order of genes.
3. We calculated the fitness function of the current population which is depending on demand for component, directional changes and method changes. Higher fitness of individual means better disassembly sequence it represents.
4. We chose the 5 individuals with the highest level of fitness from the current population which we clone and thus receive 10 parents (individuals).
5. We applied the genetic operators (crossover and mutation) on current population and thus we created a new generation (10 children).
6. We continue with step 3 of algorithm until we generate 40th generation. Then we stop algorithm. (Remark: we ignore one "stop" condition ("ratio" indicator) of original methodology to see how the algorithm behave in long run)
7. The individual with the highest achieved value of fitness across all generations represents the optimal disassembly sequence.

3. IDENTIFICATION OF PROBLEMS IN THE GENETIC ALGORITHM (GA) BASED DISASSEMBLY OPTIMIZATION OF DIFFERENT MOBILE PHONES

Disassembly case study: GA based disassembly sequence optimization of Nokia 1101
Step 1: Problem #1: In construction of the product structure diagram, is not possible to design the situation that for next disassembly step (resp. reaching lover level on diagram) we need to disassemble only subassembly SUB1. In this diagram for reaching lover level we have to disassemble particular component (not subassembly). So only possibility is to describe real situation like we did in our diagram (*Figure 1*) where the component 3 is taken as substitute for SUB1 on which disassembly of further components is depending, and component 2 we can disassemble any time.

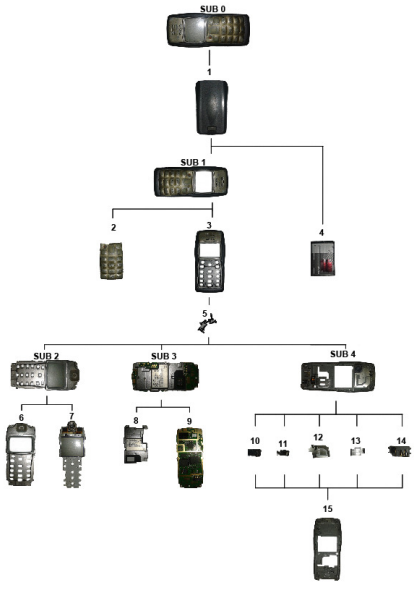

Figure 1 Product structure diagram of Nokia 1101 [6]

Step: 2, 3 and 4: no problem
Step 5: Problem #2: Application of mutation in a GA based disassembly optimization is a bit complicated part of GA application. One reason is, that we cannot mutate in a way that we just change gene (component) to another gene (component). We have to use only mutation, which is

switching two genes (components) position, because each our individual represents sequence of components and every component have to be just once in the sequence. It implies that before we can run a mutation we have to know if genes (components) could be mutated and if yes, which genes (components) they could be interchanged with. In this case study we have found that some of components could not be mutated, because if we mutate them we will not maintain precedence conditions. Considering this idea, we were looking for answer of question: How to identify genes (components) which we can switch without breaking the precedence conditions. We think, we can switch the genes (components), if they are at the same vertical level of product structure diagram and are under the same node of product structure diagram (Remark: the node is equal to component or subassembly in the product structure diagram). On the base of these assumptions we have created for this disassembly case one group of switchable genes (components) (6,7,8,9,10,11,12,13,14). After this we were able to apply mutation operator in a following way. First we randomly set a number of mutated genes (components) (resp. pairs of genes (components)) for each generation from the interval 1 to 4 (Remark. this interval is set on the fact that we have 9 switchable genes (components), what means maximum 4 possible pairs of genes (components)). Then we applied mutation operator on first 4 individuals (children) (Remark. this number („4“) is taken from mentioned methodology of Kongar and Gupta. This number of mutated individuals is fixed for all generations.) and thus we created new generation after mutation.

Step 6: Problem #3: The development of maximum fitness from first to last (40th) generation does not have standard upward trend and does not reach same maximum (resp. global maximum) in any attempt (*Figure 2* and *Figure 3*).

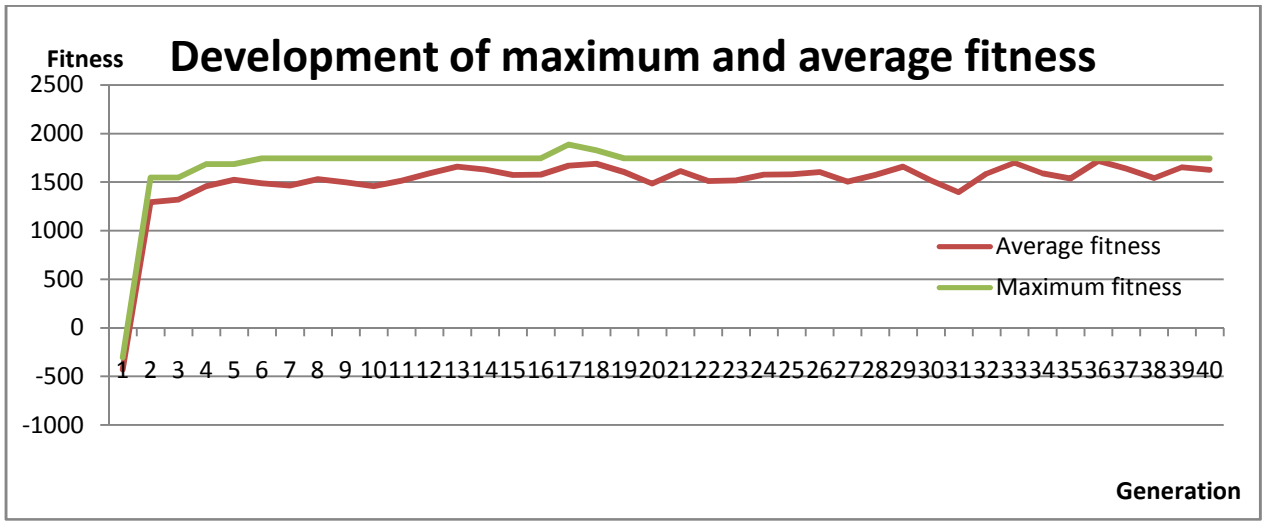

Figure 2 Development of maximum and average fitness of Nokia 1101 – attempt 1

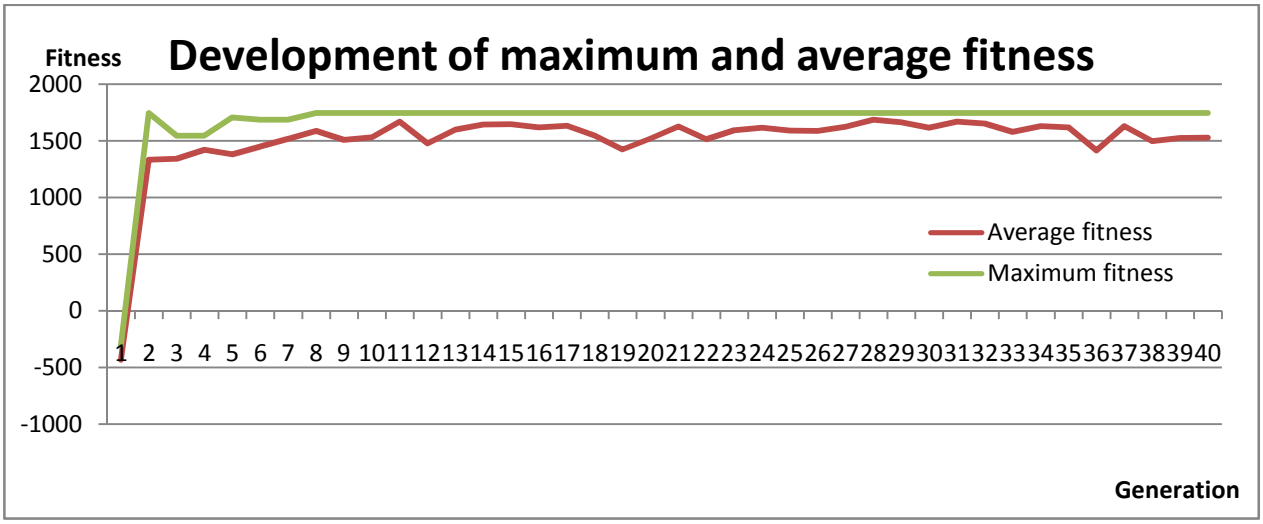

Figure 3 Development of maximum and average fitness of Nokia 1101 – attempt 2

Step 7: no problem

CONCLUSIONS

During application of the mentioned disassembly sequence optimization methodology on particular mobile phone(s) we have found following problems, develop our solution and define challenges:
Problem 1: Product structure diagram used in the methodology of Kongar and Gupta is not able exactly describe some real case product structure. Our solution was to substitute subassembly by component. The challenge is to find out why the product structure diagram is not possible to exactly describe some real case product structure and its improvement.
Problem 2: The system of selection of group(s) of switchable genes is not set. Our solution was "manual" selection of group(s) of switchable genes based on assumption, that we can switch the genes (components), if they are at the same vertical level and under the same node of product structure diagram. The challenge is to find out strong automated mechanism for selecting group(s) of switchable genes.
Problem 3: The fitness function does not reach same maximum (resp. global maximum) in any attempt. Our solution was, that in the disassemble cases we did more optimization attempts and chose highest maximum fitness from all attempts. The challenge is to set the GA characteristics (fitness constants, selection criteria and mutation criteria) in a way it would give in any attempt global maximum of fitness.

ACKNOWLEDGEMENT

This article was supported by the state grant agency VEGA research grant 1/0853/16 "New projecting technologies for design and implementation of the factories of the future".

REFERENCES

[1] Šebo, J.: *Appropriateness of genetic algorithm use for disassembly sequence optimization.* Journal of Production Engineering, 18(2), 89-95., 2015.

[2] Kongar, E., Gupta, S.M.:*Genetic Algorithm for Disassembly Process Planning.* Proceedings of the SPIE International Conference on Environmentally Conscious Manufacturing II, Newton

(Massachusetts), 2001.

[3] Mitchell, M.: *An Introduction to Genetic Algorithms*. Cambridge: MIT Press, 1996.

[4] Wikipedia, "Genetic Algorithm," [Online]. Available: https://en.wikipedia.Org / wiki / Genetic_algorithm. [Accessed 2015].

[5] Šebo, J., Szabóová, V., Kováč, J.: *Testing the genetic algorithm suitability for disassembly sequence optimization in a case of recycling of obsolete mobile phones.* International Journal of Industrial Engineering and Management, 6(3), 93-99, 2015.

[6] Vaňo, D.: *Optimalizácia demontáže vybraného výrobku s využitím netradičných algortimov.* TUKE, Košice, 2016.

INTERNATIONAL SCIENTIFIC CONFERENCE ON ADVANCES IN MECHANICAL ENGINEERING
13-15 October 2016, Debrecen, Hungary

NON-CONTACT MONITORING OF FATIGUE CRACK GROWTH VIA DIGITAL IMAGE CORRELATION METHOD

[1]SEDMAK Simon, [2]MILOVIC Ljubica PhD, [1]JOVICIC Radomir, [1]DJORDJEVIC Branislav, [1]DZINDO Emina, [2]ZRILIC Milorad PhD, [3]MANESKI Tasko

[1]Innovation Center of Faculty of Mechanical Engineering, Kraljice Marije 16, 11120 Belgrade
[2]Faculty of Technology and Metallurgy, University of Belgrade, Karnegijeva 4, 11120 Belgrade
[3]Faculy of Mechanical Engineering, University of Belgrade, Kraljice Marije 16, 11120 Belgrade
E-mail: simon.sedmak@yahoo.com

Abstract
The aim of this paper is to present the possibilities of application of digital image correlation (DIC) method in measuring crack propagation in a welded joint specimen with a notch. For this purpose, specimens were taken from butt welded plates, made of P460NL1 micro-alloyed steel, which is typically used in manufacturing of pressure vessels, such as pipelines and storage tanks. Solid wire FILTUB 12M was used as additional material for the welded joints. Fatigue pre-cracking of three-point bending specimens was done on the hydraulic testing machine 1332 INSTRON-100 kN by introducing fatigue crack in the weld metal region of the welded joint.
After that specimens were analysed using digital image correlation software ARAMIS. This optical measuring system, in addition to the software also includes two cameras, which were used to record images of crack propagation in three dimensions, as well as the strain field.

Keywords: *Digital image correlation, Fatigue, Crack propagation, Welded joint*

1. INTRODUCTION

In the recent years, there is an increasing trend in use of digital image correlation method in determining of displacement and strain fields, as well as in measuring of fracture mechanics parameters [1]. This method has a number of advantages, such as high accuracy and its non-contact nature, as well as some disadvantages, and presented in this paper, are the results obtained with it, for a notched specimen with a welded joint, subjected to three-point bending. The digital image correlation system used for this experiment consisted of two cameras (for the purpose of a 3D analysis) and ARAMIS software (GOM, Braunschweig).
Prior to three-point bending, a tensile test was performed in order to determine the mechanical properties of the weld metal which were required for the purpose determining the dimensions of the test specimen, as well as for introducing a fatigue crack. Mechanical properties of the parent material were taken from previous work [2].
Optical measuring via digital image correlation was focused on the area around this fatigue crack, and its corresponding strain distribution. With this method, it was possible to monitor the development of plastic strain during the loading, by capturing images of the deformed specimen for different values of force, which was gradually increased until its maximum value.

2. MATERIALS AND METHOD

For this paper, a welded joint specimen was cut from a welded plate made of P460NL1 steel, wherein FILTUB 12M solid wire was used as the additional material. The specimen was notched, wherein the notch was made in the middle of the weld metal area. Fatigue pre-cracking of three-

point bending specimens was done on the hydraulic testing machine 1332 INSTRON-100 kN by introducing a fatigue crack in the weld metal region of the welded joint. The length of the initial crack was 3 mm, wherein the depth of the notch was 7 mm. The geometry and dimensions of the notched specimen are given in figure 1 below, along with the position and initial length of the fatigue crack.

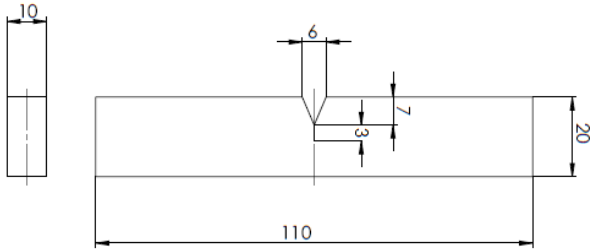

Figure 1 The dimensions of the test specimen, including the fatigue crack.

The mechanical properties of both materials, which were required for the fatigue crack and dimensioning of the specimen, are shown in table 1. It should be mentioned that the properties of the parent material were known from previous research, whereas the properties of the weld metal were determined based on a series of tensile tests, using load-displacement diagrams. The effective yield strength of the weld metal was determined according to ASTME 18-20 standard, as the mean value between the yield strength for plasticity of 0.2 and the ultimate tensile strength, wherein the average value for three specimens was adopted. The chemical composition of the materials used is given in table 2 [2, 3].

Table 1 Mechanical characteristics of parent and additional materials

Material	Yield stress (MPa)	Ultimate tensile strength (MPa)	Elongation (%)
P460NL1	460	620	19
FILTUB 12M	535	580	24

Table 2 Chemical composition of parent and additional materials

Material	C	Si	Mn	P	S	Al
P460NL1	≤ 0.20	0.40	1.45	≤ 0.02	≤ 0.02	≥ 0.020
FILTUB 12M	0.05	0.55	1.40	-	-	-

Digital image correlation was performed during the three point bending test. A DIC system records the surface structure of a non-deformed measured object in form of series of digital images, and then assigns coordinates to every pixel in the image. Specimens are prepared for recording by applying a layer of white paint to the surface, which is then covered by finely dispersed black paint, creating a mesh of dots, which serve as pixels. Additional images were made while the load was being applied and were then compared with the initial (undeformed) one and in this way, displacement and strain of characteristic points or parts of the specimen were calculated [4]. These images also provided insight into the propagation of the initial fatigue crack. In addition to the cameras, two light sources were used, in order to obtain better quality images. However, calculations are limited to local level displacements that are tangent to the surface, and the strain in the direction perpendicular to it is considered constant, which represents a disadvantage of the method, and should be taken into account. In addition, the cameras must be calibrated before recording, to ensure that the obtained results are as accurate as possible.

The experimental setup used for tensile and three point bending tests is shown in figure 2, along with the specimen after it was prepared for digital imaging, and the tensile test machine (1332 INSTRON-100 kN). A detailed view of the prepared test specimen can be seen in figure 3.

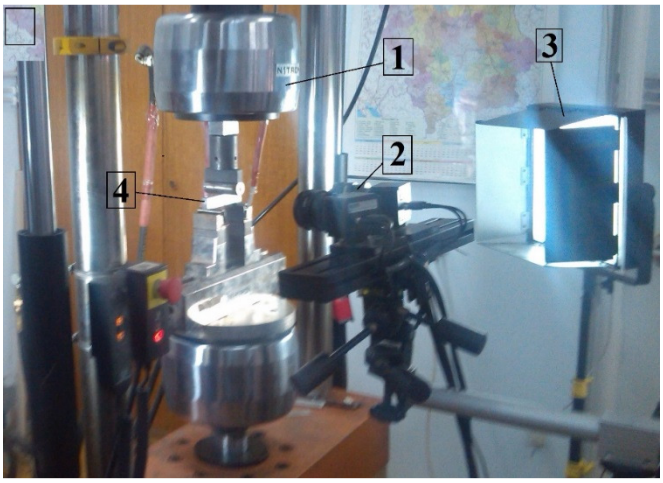

Figure 2 The experimental setup - 1) 1332 INSTRON - 100 kN test machine, 2) Cameras, 3) Light source 4) The specimen

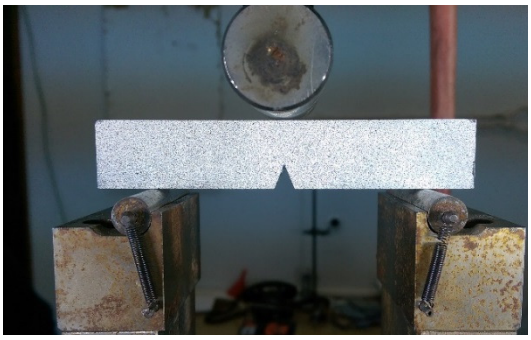

Figure 3 The prepared specimen, prior to loading

Digital image correlation was performed in 49 stages (including the initial stage), for various load levels, including the point at which maximum force was reached, as well as the points where it started decreasing. The values of force for each stage are shown in the table below. Stage 10 was omitted due an error during the recording, which did not affect the other results.

Table 3 Force values at digital image recording stages

Stage	Force (N)	Stage	Force (N)	Stage	Force (N)	Stage	Force (N)	Stage	Force (N)
0	0	11	7870	21	9200	31	9400	41	8500
1	965	12	8010	22	9310	32	9320	42	8400
2	1880	13	8210	23	9350	33	9250	43	8300
3	3030	14	8370	24	9400	34	9150	44	8170
4	4370	15	8505	25	9450	35	9100	45	8100
5	4850	16	8705	26	9500	36	9000	46	8000
6	5570	17	8850	27	9550	37	8900	47	7800
7	6400	18	8900	28	9550	38	8800	48	7600
8	6570	19	9000	29	9500	39	8700	49	7400
9	6920	20	9100	30	9460	40	8600		

Shown in fig. 4 below is the result of three-point bending testing, in form of a force-displacement diagram.

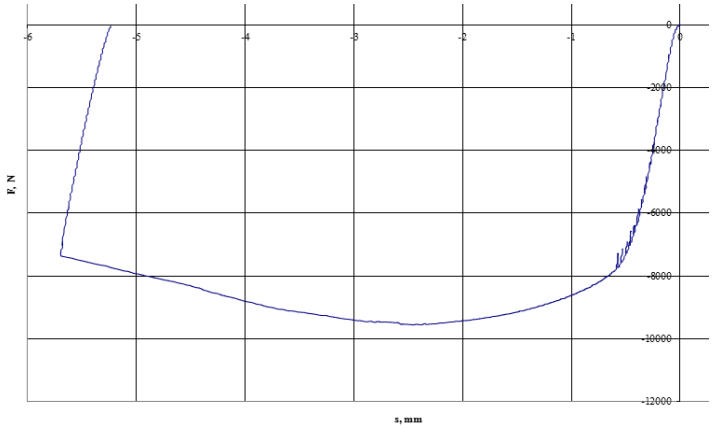

Figure 4 Force displacement diagram for the specimen

3. RESULTS

Shown in this section of the paper are the results for strain distribution obtained by digital image correlation. Due to a large number of recorded stages, only some of the results are presented in the figures 5-8 below.

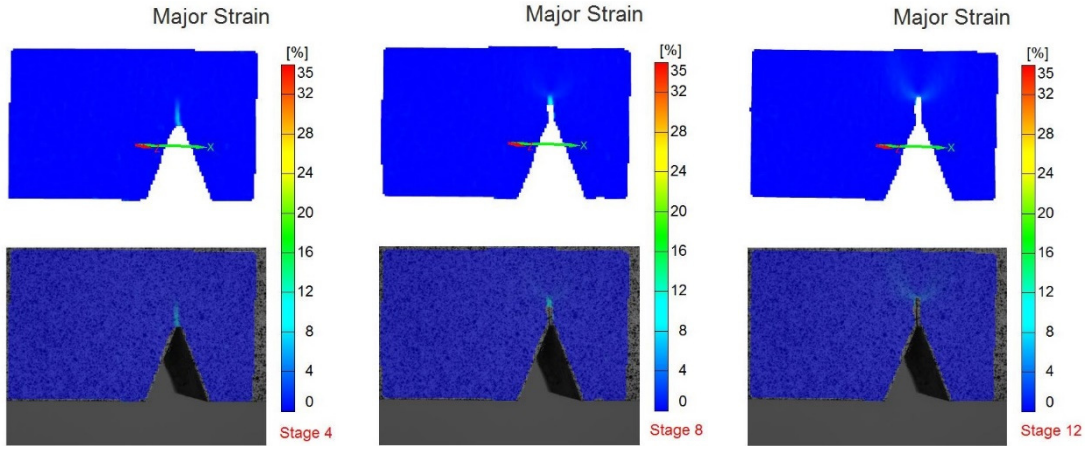

Figure 5 Strain results obtained by DIC (Stages 4, 8, 12)

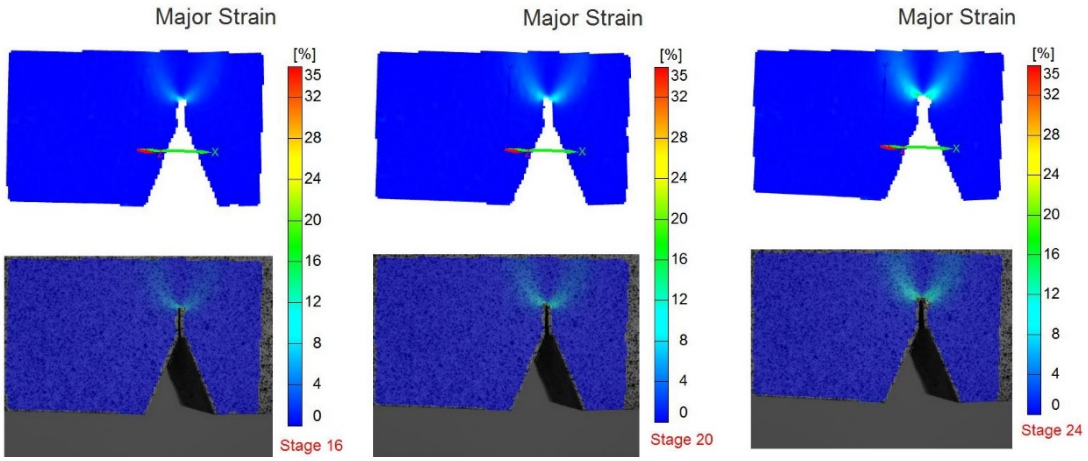

Figure 6 Strain results obtained by DIC (Stages 16, 20, 24)

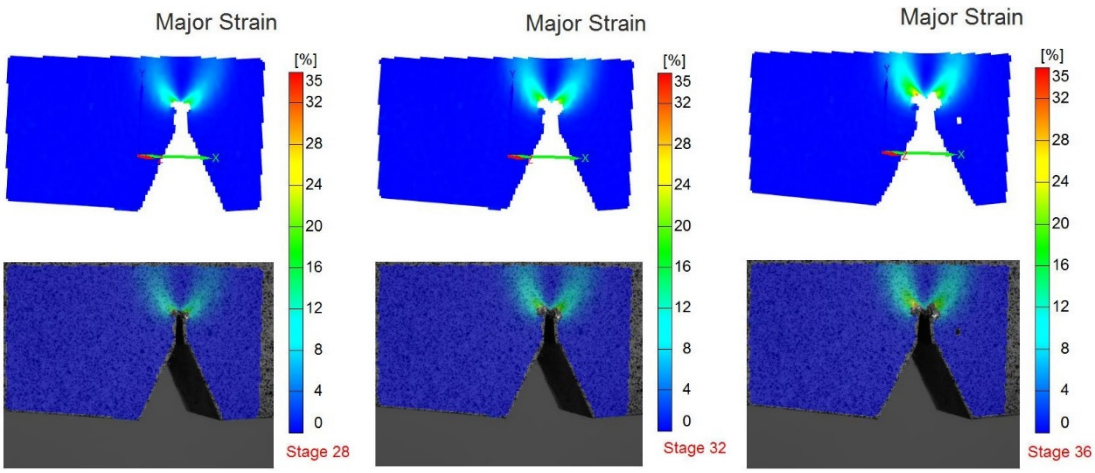

Figure 7 Strain results obtained by DIC (Stages 28, 32, 36)

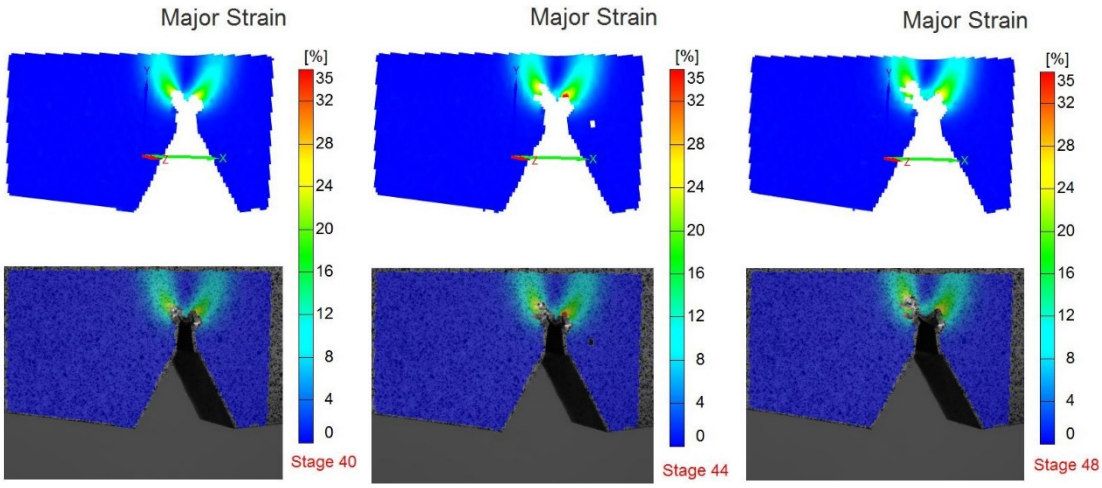

Figure 8 Strain results obtained by DIC (Stages 40, 44, 48)

A more detailed view of one of the stages (where maximum plastic strain has occurred) is shown in figure 9, along with the geometry of the propagated crack.

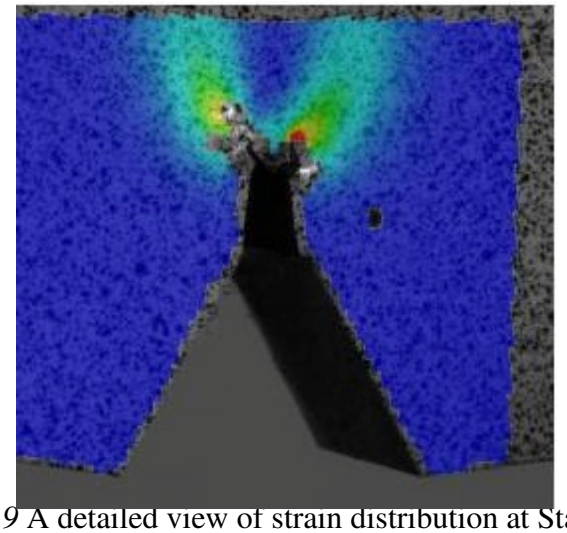

Figure 9 A detailed view of strain distribution at Stage 44.

4. DISCUSSION

From the images shown in the previous figures, the crack propagation can be clearly seen. The crack itself can be observed at the beginning of the loading, denoted by a slightly different color compared to the surrounding area in the early stages (fig. 4). As expected, the strain was concentrated near the crack tip, as indicated in the later stages, as the crack propagation takes place (figs. 5-7). As can be seen from table 3, Stage 28 corresponds to the maximum force of 9550 N. The homogeneous appearance of the strain field in the images (homogeneous in this case refers to the fact, that there are barely any empty points, such as the one in Stages 36 and 44). This suggests that the specimen has been exceptionally well prepared for DIC optical measuring. This, in combination with camera calibration which was performed prior to the testing, resulted in the obtaining of accurate and representative results.
Strain which corresponded to the maximum force was determined to be around 15%, which corresponded to the value from the load-displacement diagram obtained by the experiment (vertical displacement at maximum force was 2.55 mm, i.e. the strain was ~13% since the specimen height was 20 mm). Maximum strain obtained by DIC was 35%, wherein the experimentally measured strain was around 29% (corresponding to a force of 7400 N), hence there was a bigger difference in this case, compared to the values at maximum force (of ~18% compared to 13% for maximum force).

CONCLUSION

Based on the results obtained by both digital image correlation and presented in this paper, it can be concluded that DIC can be used to measure the strain distribution of welded joint specimens subjected to three point bending load, with a satisfying level of accuracy. It should be pointed out, however, that this accuracy decreases after the maximum force is reached, and the load starts to decrease. The method also provided detailed insight into the propagation of the crack, by recording its various stages, and providing a clear digital representation, from the initial to the final stage.
Additionally, it can be concluded that the preparation of the specimen itself, along with proper calibration of the cameras, represent important factors in the accuracy and quality of the obtained results. These factors should always be taken into account in order to avoid possible errors during optical measuring.
The next step in this research should involve the development of a numerical model in order to compare different methods of determining the strain field in a three-point bending specimen, along with their corresponding crack propagations.

ACKNOWLEDGEMENTS

The authors of this paper acknowledge the support from Serbian Ministry of Education, Science and Technological Development for projects TR35040 and TR35011.

REFERENCES

[1] McNeill SR, Peters WH, Sutton, MA. Estimation of stress intensity factor by digital image correlation, Engineering Fracture Mechanics, Vol. 28, No. 1, 1987.
[2] Jovičić, R., Sedmak, S., Tatić, U., Lukić, U., Walid, M.: Stress state around the imperfections in welded joints, Integritet i Vek Konstrukcija, Vol. 15, No. 1, 2015
[3] http://www.honex.rs/sites/default/files/jesenice/elektrode_web.pdf
[4] Đordjević B., Tatić U., Vučetić F., Milošević M., Sedmak S., Effect of DIC equipment calibration on deformation measuring errors, Second International Conference on Modern Methods of Testing and Evaluation in Science, Belgrade (Serbia), 14-15.12.2015,

INTERNATIONAL SCIENTIFIC CONFERENCE ON ADVANCES IN MECHANICAL ENGINEERING

13-15 October 2016, Debrecen, Hungary

APPROACH TO DEVELOPMENT, MEASUREMENT AND EVALUATION THE INTELLECTUAL CAPITAL OF THE COMPANY IN ITS INDUSTRIAL PROCESSES

[1]SEFCIKOVA Miriam PhD

[1]Institute of Industrial Engineering and Management, Faculty of Materials Science and Technology, Slovak University of Technology in Bratislava
E-mail: miriam.sefcikova@stuba.sk

Abstract
The theory of management is used term "intellectual capital" undertaking is the most important component of human capital. Development of human potential, its measurement and evaluation can be observed from two main aspects - economic (financial benefit) and personal (individual benefits). Both aspects need to be taken into account equally and therefore the paper discusses possible approaches that can be used in both respects. The paper discusses the significance and importance of intellectual capital, while attention is also focused on the one part, and the human capital as the potential value creation of the company. A significant part of the paper is focused on the measurement and evaluation of intellectual capital that comes into its possession. Terms of both financial and non-financial models that contribute to the management of intangible assets.

Keywords: *intellectual capital, measuring, value creation potential*

1. INTRODUCTION

In the financial management of the company one of the major problems is the identification and evaluation of intellectual capital of the enterprise as a whole. This capital includes the value contained in employee skills, organizational operation, in relation to the company and the customer. The most commonly used models for the measurement and evaluation emphasize that non-financial rate must be complemented with just the financial value. Most of these models is considered the intellectual capital as something "invisible", which is based on knowledge and experience "stored" in the people - employees who after working hours go home, carrying it with you. Stated component assets is important for businesses because it offers better opportunities for business success in the future. Minds of employees and performances they produce, the share of corporate intellectual capital. It forms each employee 'controller' most important assets owned by the company, despite the fact that these assets are not recognized in the financial statements of the company.
Globally, businesses in order to increase its capital solvency, gradually moves away from the base of physical capital and shifting the focus just on intangible assets property, which represents the company just the more substantial part of the economic benefits. Today, the heads of companies those that have managed to create a space for the creation of intangible assets, preserve and protect it. The valuable object of intangible asset is its rapid progress and "power", which contributes to the benefit not only businesses, but by the whole society. On the other intangible assets is an important part of business risk due to the fact that the value of intangible assets is inconsistent and depends on the stability of the company, a process for the recovery and maintenance of economic benefits resulting therefrom.

2. THE IMPORTANCE OF INTELLECTUAL CAPITAL

The interest on this type of activity originally arose from the considerable differences between the market value of companies and their book value, which was based on the level of their physical assets. While financial capital shows the history of the transformation process and the achievements of the past, the intellectual capital represents the hidden potential for future growth. The relationship between the different components of capital corresponds to the classification model Skandia navigator [1)], which is based on market value of the company.

A summary of all the definitions of human capital it can say that is a combination of knowledge, skills, innovation ability of individuals to perform tasks with the inclusion of individual values, culture and philosophy. It also includes the knowledge, wisdom, expertise, intuition and the ability of individuals to realize the value creating tasks and objectives.

The structural capital is the knowledge of other assets, i.e. those that remained after considering their non-inclusion in human capital. Structural capital refers to things such as property software systems, distribution network and supply channels. They include the organizational capital and customer capital (*also known as the capital market*). Unlike human capital, structural capital can be owned enterprises and can deal with it. Based on the above, part of the capital is called market capital, which represents the value "stored" in respect of the company and its customers. This relationship enhances the ability of value creation and exploitation of knowledge.

Organizational capital refers to skills such as organizational structure, hardware, software, databases, patents, trademarks, and everything else that promotes innovation and productivity by sharing and knowledge transfer. Practitioners refer to this kind of capital as a comprehensive global-scale enterprise and provided a multiple power efficiency and absolute monetary measure of intellectual capital. [2)]

Organizational capital consists of two components and the process of capital and capital reconstruction and development. Process capital is a process, activities and associated infrastructure for creating, sharing and dissemination of knowledge to contribute to individual knowledge employee productivity. It is defined in terms of non-life "warehouses" knowledge assets "stored" in the technology, information and communication systems represented laboratory and organizational structure with the promotion and implementation of human capital output. Capital reconstruction and development is a component of intellectual capital, which reflects competence and current investments for future growth, such as research and development, patents, trademarks, and start-ups, which can be considered as determinant of competence in the future.

Define the different components of intellectual capital, according to OECD studies, we can once again say that while financial capital shows the history and achievements of the past, then

- process and capital market are the components on which is based the current operation
- capital reconstruction and development provides, as the company is ready for the future
- human capital is embodied in the leadership, expertise and people of learning and It allows the creation of value in all other components of intellectual capital.

In other special literature [3)] it can be found easier to divide intellectual capital, human capital (*human values such as intellect, experience, skill, creativity, and work under way.*), organizational capital (*companies own tools such as systems, intangible assets, processes, databases, values, culture, ...*) And relational capital (*external relations with customers, suppliers, business partners, distribution network, and the regulation of trade.*)

Mentioned breakdown is a guideline to the individual components of intellectual capital, which are combined with one another and the interacting with traditional unit of capital (*physical*) and each is unique in its own way to the establishment, and their combination for it to create value. Mentioned could be represented by the following formula:

company's market value = book value of the company + intangibles assets value

However, the equation is challenged in particular in view of the fact that it contains accounting errors and that the right side of the equation can not be determined by the same unit as virtual and real money can not be added together.

3. HUMAN CAPITAL AS THE COMPANY'S VALUE CREATION POTENTIAL

When we look to the recent past, a larger portion of unidentifiable intangible asset was classified in accounting policy as goodwill and human capital was part of goodwill. Traditional accounting does not provide methods for identifying and measuring of this "new" type of intangible assets in the company. The answer can only be found in the new model for measuring and evaluating the intellectual capital which advises businesses to access synthesis financial and non-financial aspects of the company making up its value.
Human capital is the property of individuals. It includes human resources within the company as well as customers and suppliers of the company. This wealth is multifaceted and includes knowledge about facts, laws, and principles, as well as less definable knowledge specialization, teamwork, and communication skills. Ratios should include the quality and quantity of each "stock" of knowledge and collectively "stocks" in the working groups and teams. [1)] The next decade will be 70-80% of the growth and competitiveness of enterprises based on new knowledge (*According to a study IPTS - Institute for Prospective Technology Studies*).
The needs of the development of human potential is defined by the practice. The key skills for managers include a wide range of capabilities and features. In addition to more industry-specific expertise and methodological skills and analytical and systemic thinking, including specific competencies related to information development, these include mainly social and personal competences. This applies to communication skills, listening, empathy, as well as sensitivity to the dynamics of the group or team work. In addition to general language training, knowledge of the social, economic and political context is also required knowledge of other cultures to adapt to international conditions. The most important component is Special competence, the ability to take initiative and responsibility challenges and to realize the goals set out in the immediate practice of management.
Human capital you can imagine how "human values" and its evaluation is in itself a paradox at the level of ethics and morality. However, there are efforts on its assessment, the main aim of this evaluation is on the one hand, the 'economic' (*quantitative*) expression in numbers, on the other hand also a qualitative statement to the effect search reserves and its development possibilities**.** as part of the development of intellectual capital of the company.
The development of human capital is essential to create the model, whereby it would be possible to show respective characteristics, abilities and skills of man. This option offers labor potential of man**,** which is derived from the creative potential of the employee (*prof. E. Weisbier Vienna Academy of creativity*). Potential labor can be expressed by the formula: **PP = SP + LP**
PP - potential worker, it´s "value" is contingent upon what the worker is as a man and how it manifests itself externally by behaves.
SP - potential behavior of workers - Expresses the course of action and behavior of the employee, including:

- open and flexible attitude - the ability to accept new things, not to deny them, prove them to consider and feel.
- way of communicating with others,
- thoroughness and conscientiousness at work,
- methods of conflict resolution,
- ability to analyze problems, define the problem, to withdraw from the problem and so on.

L'P - Human (personality) potential consists of two components:
IQ - intelligence potential - it discloses a method for evaluation of the level of human intelligence (known as intelligence quotient) which is more or less exactly measured. In addition to more industry-specific expertise and methodological skills and analytical and systemic thinking, here, also includes the specific knowledge relating to the development of information, general language education, knowledge of social, economic and political context, and also learn about other cultures.
EQ - emotional potential it is referred to as emotional intelligence and its importance and development in the past decade begins steeper than ever. Reviews for the opportunity to exactly measure this component are different personalities. Emotional intelligence it is made up of several components, which can be summarized in the following five areas of innovation processes in the enterprise:

- self-awareness of own emotions, their own mental states,
- self control - managing these emotions, frustration tolerance, patience,
- motivation and self-motivation
- empathy
- the ability to think, work and communicate in painting and abstraction.

4. MEASUREMENT AND EVALUATION OF INTELLECTUAL CAPITAL

Developing models of measurement and recording of intellectual capital comes from the individual making the request of the individual components within the enterprise and also to improve its understanding and finding out what it consists of business value as well as the management of those components that create this value. The models then provide input for the process of valuation. [1)]
In the case of physical capital comparing current and future revenue by using a discount factor and expenses are measured using the established value adjustments. In case knowledge-based assets, There is no way back calculation of income and expenses for any period except just for the period. For this reason, to take the necessary adjustment to the chart of accounts so that in the current financial year to capture a movement in relation to the use of these assets directly to a designated revenue and expense accounts. There is however a prerequisite to realizing the business use of those assets and appropriately adjust their overall operation.
Economic uncertainty characterizing the decision as to use an asset or to invest, growing precisely in the case of knowledge assets. In the classical financial accounting intellectual capital is accompanied by specific features and immateriality, uncertainty, almost impossibility to measure it and incompatibilities with the conventions that guide everyday transactions recorded financial accounting and reporting. [1)]
The obvious approach to manage and measure the effort to preserve as much of the accuracy and robustness of conventional accounting treatment of traditional tools. Support for this view and beliefs, its proponents have not decided on the creation of new measurement models, but support in the form of conventional accounting. The alternative is a waiver of accounting and establish measurement and control of the values obtained Modifiers economic activity of each company. The question is whether at least one of these two approaches may be to some extent meet the needs of controllability, usability and reliability. There are a wide range of available methodologies of measuring intellectual capital. In order to be able to determine the relative effectiveness of different approaches measurement and management, it is necessary to define certain criteria that may be considered: [4)]
The method in question is verifiable and credible? If managers assess the progress and results of measurements, then they need assurance that they can rely on the information they receive. Even if the interpretation of this information may vary for individual managers, but the source must be reliable.

Intellectual capital is not inherently complement the overall transformation process and its assessment is still subject to resolution and the establishment of relevant measurement systems. It is now generally accepted that non-financial measurement systems can achieve the same degree of accuracy as a theory based on a financial basis. The key requirement is that the system and its constituent elements are within the full screen, a unique overlap is preferred independence with respect to the other, are observable and measurable.

The method is easy to use? It requires a high price? This is a very difficult point, because if we start from the very nature of the measurement process, immediately appears a threat of increasing the cost of information collection. These costs will far exceed the benefits of providing the information and the measurement approach becomes ineffective.

Facilitate strategic and tactical management? Managers can impact the performance of their operations on two levels. First, the organizational level, which affect the processes of value creation, which are interconnected in a company. The second method is the ability to support improvements in individual and group processes at the operational level. An example of the first is the formation of strategic alliances, while the second example, investments in intangible assets of the company.

It creates the information necessary for investors and shareholders? To be able to communicate with shareholders outside the company, we have the information and they must be in the form and language in which shareholders can understand. Over a long period, the shareholders provided a kind of information that seemed to them necessary. This information was reported in a standardized form and in many businesses, it was mainly business performance in financial terms. In the area of knowledge, or even the concept of shareholder value for the shareholder has moved beyond simple financial measures and there exists a critical change. Communicate with shareholders now requires a deeper understanding of the attribute value in terms of a group of shareholders.

An example of such requirements is to create a model of monitoring of knowledge assets and the more holistic approach of value HVA (*Holistic Approach Value*). The model acts as an extended and customized research and database system for financial and intangible assets, which is also called as a Business Value Model (*enterprise value model*). It is a multi-dimensional accounting system that combines measures and financial and intangible contributions using the value idea individuality of all shareholders.

For the initial identification of key stakeholders and to provide a review of strategic organizational objectives is primarily required input from senior management. Subsequently, the development of value hierarchy can be complete only by the operational level, which requires support economic activity. This activity is then used to identify the two sets of variables of each shareholder: the first is a set of scales that describe the relative importance of the objective of each shareholder, the latter's behavior and measure performance. The output of this process is the "navigator", which is visible as a value in the company actually formed. [2)]

Model transformation process as a value creator is an essential prerequisite for understanding exchange relationships between different forms of value and cost. Business models assessing economic activity and its outputs as value generators and distinguish between the value of internally generated just by the business operations and value realized from the outside. General business creates value internally using the quality of its management, efficiency of intellectual capital efficiency output of activities, quality complying with regulatory measures. An important measure of the size and cost which is an impairment, and must be monitored and the size of capital and operating expenses throughout the value created internally, the cost of information to and from the external environment and the negative impact of costs and social environment.

External environment affects the value using the income from the sale of goods and services, value-added customer after the sale (*during the product's life*), Value-added employees after receipt of wages and financial benefits, the added value of the shareholders, the valuation legislation and

professional interests, especially financial analysts, valuation of environmental impacts and social environment arising from the existence of the company, media reports and reactions from the public. Internal and external values are then associated in the definition of the total, aggregate value. It consists of two main categories - financial and non-financial values. [2)]

The advantage of such approach is that the model of HVA, the instrument has a very wide scope of application. Nevertheless, even here, there are many documented differences between the economic activities of businesses in different countries. These differences arise from the culture of the country values of business, relations between business and of course the national accounting rules and principles, insofar as they are adopted by the International Accounting Standards Board, which seek to harmonize accounting between countries.

In terms of our practice is to perform the valuation of intangible assets of the company revised with legislation. It has been compiled in accordance with the harmonization with international valuation standards (*IVS*). In the sequence of intangible assets was subject to international steering of valuation report no. 4 "(*International Valuation Guidance Note no. 4*), concerning the valuation of intangible assets. Commission for IVS (*IVSC*) this report was adopted to improve the consistency and quality of the valuation of intangible assets within the international community to support the users of financial statements and users of its assessment.

Using any suitable method (*expert procedure shall apply mutatis mutandis practice in other fields or other procedure that corresponds to the state of scientific knowledge in this field, taking into account the specificities and the technical and economical determination of the constituents listed property*) The resulting value, which is known as the universal value of the property, which means the resulting objectified value of the property is an expert estimate of the most likely prices of the asset at the date of valuation in a given place and time, which he should reach the market in terms of competition; at an honest sale, the buyer and seller will act with due awareness and caution and assume that the price is not affected by undue consideration.

The particular model for the recognition of intellectual property is subject to the condition under which the valuation exercise. Each model and approach indicates its classification adapted to the nature of the monitoring scheme established intellectual capital. Model needs to be examined to see whether it provides an overview of historical data, and is focused demonstrate the future operation - business venture. Particularly preferred are predictive methods, because they provide information that can be incorporated into the decision making process, while retrospective reporting does not provide for such a possibility.

Among the most commonly used methods include the following [1)]:

Scandinavian navigator

It is a model best known measurement of knowledge assets, which was developed in Sweden. It is based on the premise that intellectual capital is the difference between market and book value of the company. The initial conceptualization of this model was aimed equally at the five regional improvements: financial, customer, process, reconstruction and development, and human capital. Model analyzes each component separately intellectual capital to ensure greater focus. Intellectual capital is measured by analysis of up to 164 metric Peace (91 intellectually based and 73 traditional peace) covering the above-mentioned five basic components, which is then subject to the reporting of intellectual capital. Said statement is generally made up of state variables as model uses a balance sheet approach, which provides a statistical picture and fails to capture the A flow area in the company. But still used, parameters such as income, expenses, earnings, return on equity and assets below. Then, the variables are further treated, such as expenses that are divided for example. number of employees and the result is then analyzed already outside the financial sector.

Balanced Scorecard (BSC)

BSC model was created in order to provide managers transfer direction of the company and its strategy to aggregate the set of measures that provide working framework for a strategic

measurement and management system. [3] About this model in contemporary literature, many have reported on the development of strategic management. It is a balance between short-term and long-term objectives, between financial and non-financial scale, ie a balanced measuring system. BSC is trying to find a balance between rates of external shareholders and customers, and Internal Rate of critical operational activities, innovation, education and growth.

Classical accounting model, ie the application of financial accounting in the management company should at least be supplemented by items comprising intangible assets and intellectual capital, such as. high quality products and services, motivated and experienced staff, flexible and predictable internal processes, satisfied and loyal customers, and so on. These assets are for business information age is very important and it is necessary to know their value. If they could easily identify those assets, valued and recorded on conventional accounts of accounting, businesses would be able to inform them of its shareholders, creditors and the public future. Their management would be demonstrable. But in fact, the valuation of such assets such as distribution channels, workflow, employee skill, motivation and flexibility, and enterprise database systems by their very nature problematic, so the balance sheet almost can not recognize. This is despite the fact that their existence is currently of great importance to gain a competitive advantage in the market. [3]

Compared to other instruments, this model provides a comprehensive focus on the management and measurement of knowledge assets. It is one of the primary tools that developed an integrated vision measuring systems for management with a focus on financial and non-financial indicators relevant to business operations. Model in their reporting includes both the state and the flows, so it is appropriate support for other models used in the valuation of the intellectual capital of the company. BSC supplements the information provided by other instruments with a focus on specific activities in relation to the outcome of the transformation process.

Monitor intangible assets (IAM)

Otherwise called as Sveibyho monitor was developed based on work experience and observation that traditional corporate financial statements do not provide the necessary information relating to knowledge of the assets that carry a larger portion of the market value of the company. The model defines three types of intangible assets, corresponding to the difference between the book value and the market value of the company in its valuation. Balance that does not match the book value is assigned to the individual responsibility of employees, internal structure and external structure.

While Scandinavian navigator handles the culture and management philosophy as part of human capital, this approach it is classified as internal structure. With its primary focus on people, this model is based on the premise that people are the only real source of the company and all aspects of internal and external structures are embodied in human action. The application of this model is very context-specific indicators and are used as pole descriptor (How good or bad). This is specific to the related subjects, which may be located on different interpretations of the various management levels in the company. [1]

IAM is actually a statement that records the amount of financial and non-financial peace. Management selects indicators based on the strategic goals of the company in order to measure four aspects of the creation of the intangible assets and growth, renewal, efficiency and stability. The report is composed mainly of state variables, but may also include flows, such as revenue growth and sales growth of the number of employees at a certain management level and below.

Index of intellectual capital (IC Index)

IC index consolidates all individual indicators into a single index, in contrast to previous models, which provide valuation isolated components of intellectual capital.

IC index aims to monitor the dynamics of intellectual capital. It provides an index composed of several indicators based on the correlation of changes in intellectual capital with changes in the market. Indices are: relational capital, human capital, innovation capital and infrastructure capital. By consolidating all the indexes representing the intangible assets are obtained by one index. Then

changes in the index are compared with changes in the market valuation of the company. Into account the performance achieved in the past and may be modified major changes that have emerged in recent years.

The above models are based on scorecard methods in which the various components are identified and intellectual capital indicators obtained are recorded in the "Accounts" and in the graphs. Their advantage is that they can provide a more comprehensive analysis of business performance than other approaches based on financial measures. These models allow measurement closer to current inputs, processes, outputs and reporting can therefore be faster. It is therefore particularly well suited to address the issues of failure and bug fixes in the guidance inputs and processes to outputs. Indicators capture contextual variations and result in a "rich" analysis, from which it is possible to make any useful insights for the development of enterprise policy. The said advantages, which make them particularly effective, on the other hand can be interpreted in terms of inefficiencies. Data received by indoor observation on deep analysis may not be effective under conditions of rapid analysis and do not easily provide simple standard numerical or financial indices based. [1)]

Technology Broker model

In other words, it is the intellectual capital audit. The model divides enterprise knowledge-based assets into four categories - market assets personally targeted assets, operating assets and infrastructure assets. Each component of the model is examined by the audit questionnaire about specific variables related to the specific asset categories. The value of corporate intellectual capital is determined using a diagnostic analysis of the company. The first 20 sets of questions need to strengthen intellectual capital and subsequent audit of 158 questions concerning the above four categories.

The weighted average value of patents

Technological factor is calculated based on patents developed businesses. Intellectual capital is measured by calculating parameters such as. number of patents, the amount of cost of sales turnover that characterize corporate patents.

Inclusive valuation method (IVM)

It refers to the relationship between the value of the company, intellectual capital and monetary rate in order to carry out the all-inclusive valuation of the company. It uses three categories of values: (1) The intrinsic value represents the internal efficiency of operations, (2) the external value is measured using the supplied business efficiency and (3) a useful value reflects the impact of competitive environment. It attempts to provide a total enterprise value on the amount of intellectual capital and corporate cash flow. The combined value added of the monetary added value in combination with the added value of intangible assets.

The Value Explorer

It regards the accounting methodology serving to estimate the value of intellectual capital corresponding to the principal object of business. It is based on the following allocation of the value of intangible assets: assets and grants, skills and "soft" skills, the set of values and standards, technology and explicit knowledge, production and management practices.

These models are based on the direct method of intellectual capital, ie estimated financial value of intangible assets by identifying its various components. Some of these models are of limited use for the evaluation and analysis of specific knowledge-based assets. They can be used in conjunction with the scorecard methods when the aim is to derive composite standard financial indicators. These standards should be adopted with caution in relation to ensuring the validity and reliability of the measurement comparison. The advantage is that it allows the evaluation of individual components of intellectual capital allow a combination of monetary and non-monetary valuation, provide a comprehensive view of the intellectual wealth of the company. This is a randomly-based measurements and therefore it is appropriate to combine them with financial measures. The

disadvantages of those models are that far obtained are specific to individual companies and are difficult to compared and tested between undertakings.

Tobin's q

Indicator q, The value of capital in relation to its replacement cost. The indicator was developed as a measure of forecast investment decisions independent of macroeconomic factors such as. interest rate. During the development of intellectual capital measurement models it began to be used as an indicator in this respect. This method is similar to the market-to-book value, among other things because it replaces the carrying amount of the replacement cost of fixed assets. Enterprises with q greater than 1 and greater than the q competition is expected to show higher profits resulting from the assumed and benefits of intellectual capital.

Investors establishing market value (IAMV)

Value of the company considered its fair value and makes it into proportion with the sum of physical capital and intellectual capital realized, wear and sustainable competitive advantage. The model is based on market capitalization, ie to determine the value of intellectual capital as the difference between the market capitalization of the company and the capital of undertakings.

The value of the ratio of the market price of shares and equity per share

Market-to-book value

The method is based on the difference between the market capitalization of the company and its book value. The main assumption is that the market value is the true value of the company holding the value of tangible assets as well as the value of intellectual capital. It is a commonly accepted method of accounting.

The above models are based on market capitalization, ie provide intellectual capital as the difference between the company and the market capitalization of the company capital. An advantage of it is good to see the financial value of the capital and are suitable for internal benchmarking within the industry. Also contain negative aspects and that they do not provide information about individual parts of the capital, monetary targeting gives only a partial view. They are not suitable for human capital development approaches.

Economic Value Added (EVA^{TM})

That method is not a new discovery. It is used in enterprises to measure their performance in addition to, or instead of profitability indicators, in particular, is an indicator ROE (return on equity). In this case the EVA^{TM} based on a calculation made by adjusting corporate profits by expenses of intangible assets. Changes in EVA^{TM} indicate whether corporate intellectual capital is productive or not.

Financial theory emphasizes that the company creates value (ie it maximizing their market value, which is one of the fundamental goals of the enterprise) If revenues exceed the cost of the total capital of the company. Said method we talk about economic profit, which expresses the after tax profit after deduction of recognized costs of capital, added to create those gains. Calculation of economic profit derived from the profit from operations is not easy and requires a lot of changes (as expenditure on research and development for the company in the concept of classical financial accounting costs when calculating economic profit becomes activated costs until the time of the economic income of the said research and development).

In conclusion, the main objective of EVA^{TM} Method is to bring revenues and income to compare the return on the capital base, which is also expressed in cash equivalent concept. [3)]

Market value added MVA

MVA method, as well as the EVA^{TM}, it has its origins in deriving economic profit. MVA is the difference between the market value of the company and the value of the capital that has been inserted into the company creditors (loans) and shareholders (paid-in capital, retained earnings). Then MVA is a measure of the difference between "Proceeds", Ie investments in businesses and "Expenditure", Ie those which could get creditors and shareholders by selling its assets and shares.

If this difference is positive, i.e. the company increased its value (ie the value of the capital entrusted to it) and thus increase the welfare of the investor. We can imagine what happens if it is negative.

Budget and accounting of human resources (HRCA)

Calculates the hidden impact on human resources in relation to the costs that reduce profits. Intellectual capital is measured by calculating the ratio of the benefits of human activities-owned enterprises to capitalized staff costs.

Calculated intangible value

Overrun calculates the return on fixed assets using the scheme as a basis for determining the ratio of return on intangible assets. It can be used as an indicator of the profitability of investments in the knowledge assets.

Revenues knowledge capital

The method is based on a calculation of such income as part of the standard yields in excess of expected returns for asset accounting.

The added value of intellectual coefficient (VAIC)

It measures the extent to which and how effective intellectual and physical capital together create value.

These models are based on the rate of return on plan assets of the company. The indicator is calculated by the ratio between the company's income before taxes and average assets Tangible and then compared with the average for the sector. The difference is then multiplied by the corporate average tangible assets to calculate the average annual income of intangible assets. Dividing those of average incomes corporate average cost of capital or interest rate makes the value of corporate intellectual capital. The advantage is that they are suitable for the industry and benchmarking to show the financial value of intellectual capital. They are based on traditional accounting principles and rules and these form the basis for easy communication between accountants. On the other hand, contain information on the components contributing to the development of the capital. Monetary exclusive focus provides only a partial view. Not suitable for human development approaches. [1)]

CONCLUSIONS

The significance of intellectual capital and demonstrate various recent studies that focus on the individual components and analyze to what extent they contribute to senior corporate objectives and to maximize its market value. I recently conducted analysis, according to a study by Accenture [3)], It is currently the biggest problem of recruitment and retention of employees, which is for top managers top priority this year. Up to 35% of surveyed executives at the highest levels is a top priority for attracting and retaining experienced staff. For comparison, the increase in shareholder value is a priority for only 27% of top managers.

The aim of this article was to contribute to an expanded view of the importance of intellectual capital that you should be aware of every business and so also access it. An overview and breakdown is different view on this issue as we know it in terms of our businesses. Wealth business depends only on how intensive use of all its available resources, and it is this rate makes businesses viable and competitive and above all it is their task to create a foundation that would enable more transparent information for investors outputs.

ACKNOWLEDGEMENT

The described work was carried out as part of a project supported by the Ministry of Education, Science, Research and Sport of the Slovak Republic VEGA Nr. 1/0218/16: The model of the implementation of controlling as a management tool.

REFERENCES

[1] Malhotra, Y.: *Measuring Knowledge Assets of a Nation.* Knowledge Systems for Development, State of Research 2003-2004, United Nations Advisory Meeting, http://www.kmnetwork.com/KnowledgeManagementMeasurementResearch.pdf
[2] Pike, S., Roos, G.: *Intellectual Capital Measurement and Holistic Value Approach.* http://www.works-i.com
[3] Vyhláška MS SR Z. č. 492/ 2004 Z.z. o stanovení všeobecnej hodnoty majetku
[4] Berg, H. A.: Models *of Intellectual Capital valuation.* A Comparative Evaluation, http://business.queensu.ca/knowledge/consortium2002/ModelsofICValuation.pdf
[5] Kaplan, R., Norton, D.: *Balanced Scorecard.* Management Press, Praha, 2002.
[6] Mlkva, M., Vanová, J., Šefciková, M., Dóza, P.: *The use of selected concepts of measuring enterprise performance in industrial enterprises in Slovakia.* Upravlenije ekonomikoj: metody, modeli, technologii : 14. meždunarodnaja naučnaja konferencija, Ufa - Krasnousoľsk, 9 - 11.10.2014. Sbornik naučnych trudov. Tom 2. 1. vyd. Ufa : Ufimskij gosudarstvennyj aviacionnyj techničeskij universitet, 211-214., 2014.
[7] Šefciková, M.: *Manažérske kompetencie v rámci riadenia nehmotného majetku podniku. Managerial competences within corporation intangible assets managing.* Obchod, jakost a finance v podnicích - determinanty konkurenceschopnosti VI. : Sborník příspěvků z mezinárodní vědecké konference, 16-17.dubna 2008, Praha. 1. vyd. Praha : Česká zemědělská univerzita v Praze, 218-220., 2008.
[8] Šefciková, M.: *Intelektuálny majetok ako zdroj ekonomických prínosov.* Finanční a logistické řízení v kontextu vstupu České republiky do Evropské unie : Sborník referátů. 1.díl. Ostrava : Vysoká škola báňská - Technická univerzita v Ostravě, 226-230., 2003.
[9] Šefciková, M.: *Postup stanovenia likvidačnej hodnoty podniku.* Procedure of the company liquidating value determination. In CO-MAT-TECH 2000 : 8. medzinárodná vedecká konferencia. Časť 3.: Manažment priemyselných podnikov a kvalita. Bratislava : STU v Bratislave, 277-282., 2000.
[10] Šefciková, M.: *Ohodnocovanie podniku.* In Trendy v systémoch riadenia podniku : 4. medzinárodná vedecká konferencia. Košice : TU, 179-183., 2001.

INTERNATIONAL SCIENTIFIC CONFERENCE ON ADVANCES IN MECHANICAL ENGINEERING

13-15 October 2016, Debrecen, Hungary

MODIFIED INVERSE COMPOSITIONAL ALGORITHM FOR APPLICATIONS WITH SIGNIFICANT LIGHTING VARIATIONS

[1]SIMONČIČ Samo PhD, [2]PODRŽAJ Primož PhD

Faculty of Mechanical Engineering, Aškerčeva cesta 6, 1000 Ljubljana, Slovenia
[1]E-mail:samo.simoncic@fs.uni-lj.si
[2]E-mail:primoz.podrzaj@fs.uni-lj.si

Abstract
Measurement of displacements and corresponding deformations based on digital images captured by digital camera have become the most dominant and widely accepted non-contact technique for characterization of material's structure and properties. In the field of experimental mechanics, it is well-known as digital image correlation (DIC) where one of the most frequently used sub-pixel registration approaches is certainly the forward additive matching strategy using Newton-Raphson (FA-NR) numerical procedure. Recently, it has been receiving a lot of attention from the theoretical and practical point of view. However, its significant drawback lies in the fact that the Hessian matrix has to be re-calculated and inverted at each iteration. Furthermore, the original FA-NR procedure is extremely sensitive to lighting variation through the sequence of deformed images. Therefore, these facts have major impact on computational complexity which are usually reflected in higher execution time. To overcome this concern, the modified inverse compositional matching strategy using Newton-Raphson (IC-NR) is addressed, where the parametric sum of square difference correlation criterion (PSSD) is used. This modification makes it possible to use the proposed procedure in applications where lighting variations are not controlled. In addition, the Hessian matrix is only calculated once per each subset and therefore it is constant during the optimization procedure, which is according to the nature of inverse compositional matching strategy.

Keywords: *Inverse compositional Newton-Raphson algorithm, parametric sum of square difference correlation criterion, digital image correlation.*

1. INTRODUCTION

The basic idea of digital image correlation (DIC) was presented for the first time in the early 1980s [1] and has since then been vastly improved especially in terms of sub-pixel registration accuracy [2], computational efficiency [3], robustness [4] and application scope [5]. One of the main fields of science where the DIC has received a lot of attention is certainly experimental mechanics where it is well known as non-contact (optical) method for full-field motion, deformation and shape measurement [6]. In essence, DIC is numerical procedure which compares the template (reference) subset with the target (deformed) one. To be as accurate as possible, the similarity between both subsets has to be estimated by predefined correlation criterion. The deformed subset which has highest or lowest (depends on type of correlation criterion) value of correlation coefficient presents the best match in comparison to the actual template subset. It is worth mentioning, that as the criteria are getting more advanced (e.g. they can be successfully used in an environment with significant lighting variation) they are usually also more and more computationally demanding and consequently difficult to implement for real time application. Due to this fact, the efficiency of the DIC method is one of the most challenging steps, since the complexity is getting even higher when

the sub-pixel displacement accuracy is required. The algorithms used for this kind of application are usually termed as sub-pixel registration algorithms in which the forward additive matching strategy is most frequently applied. In this case, the correlation criterion is used directly in the optimization procedure which implies that the numerical approach becomes non-linear. Definitely, the forward additive Newton-Raphson (FA-NR) algorithm belongs in this group. It was proposed by Bruck, et. al. [7] in 1989 and since then it has been extensively improved by various researchers [8]. The major drawback of this method lies in the fact that the Hessian matrix and its inverse have to be calculated at each iteration. This step is also by far the most significant part of the entire approach from computational complexity point of view. As a consequence, it is interesting to try use strategy, in which the Hessian matrix and its inverse are not needed to be re-calculated at each iteration. This kind of strategy would represent a significant improvement.
It is worth mentioning, that the inverse compositional matching strategy using Gauss-Newton numerical procedure (IC-GN) presents such an improvement and it has been realized by Baker and Matthews [9] in 2001. Moreover, the authors proved that the IC-GN is equivalent to the forward additive matching algorithm [9] and without great effort this equivalence can be derived for the FA-NR algorithm as well. One of the main advantages of the inverse compositional matching strategy lies in the fact that its Hessian matrix has to be calculated only once, at first iteration, which enormously enlarges the set of possible real-time applications. Due to this fact, the modified IC-GN approach together with parametric sum of square difference (PSSD) correlation criterion is presented in this paper. Based on the PSSD correlation criterion, the lighting variation parameters are included directly in the optimization procedure which enhance robustness of the proposed novelty. This ensures that it is invariant to lighting variation through the sequence of deformed images.

2. MODIFIED INVERSE COMPOSITIONAL NEWTON-RAPHSON ALGORITHM

In order for the standard IC-NR algorithm to be insensitive to linear lighting variation, the simple sum of square difference (SSD) correlation criterion was replaced by more sophisticated PSSD correlation criterion. Since the PSSD correlation criterion is invariant to linear variation it consequently means that the robustness of the entire IC-NR is actually enhanced. If affine warping function $\mathbf{W}(\mathbf{x};\mathbf{p})$ is assumed between reference and deformed subset the following expression holds:

$$\sum_{x}[\Delta a T\big(\mathbf{W}(\mathbf{x};\Delta\mathbf{p})\big)+\Delta b-aI\big(\mathbf{W}(\mathbf{x};\mathbf{p})\big)-b]^2, \tag{1}$$

where $\mathbf{x}=(x,y,1)^T$, a is the gain and b the offset of lighting intensity in the target image $I(\mathbf{W}(\mathbf{x};\mathbf{p}))$, Δa the gain variation and Δb the offset variation in template image $T(\mathbf{W}(\mathbf{x};\Delta\mathbf{p}))$. Based on the Eq. 1, it can be seen that the PSSD correlation criterion has two additional parameters a and b which implies that initial guess vector $\mathbf{p}$ has to be extended into the following vector $\mathbf{p'}=(p_1,p_2,p_3,p_4,p_5,p_6,a,b)^T$. Thus the modified warping function $\mathbf{W'}(\mathbf{x};T(\mathbf{x});\mathbf{p'})$ gets the following form:

$$\mathbf{W}'(\mathbf{x},T(\mathbf{x});\mathbf{p}')=\begin{pmatrix}1+p_1 & p_3 & p_5 & 0\\ p_2 & 1+p_4 & p_6 & 0\\ 0 & 0 & b & a\end{pmatrix}\begin{pmatrix}x\\ y\\ 1\\ \mathrm{T}(\mathbf{x})\end{pmatrix}. \tag{2}$$

The same procedure must be realized on the incremental warping function $\mathbf{W}(\mathbf{x};\Delta\mathbf{p})$ where the

modified warping function $\mathbf{W}'(\mathbf{x}, T(\mathbf{x});\ \Delta\mathbf{p}')$ is obtained and subsequently applied on the template subset. It should be noted, that the incremental parameter vector $\Delta\mathbf{p}$' is calculated by minimizing the parametric SSD correlation criterion given in Eq.1. Based on the applied minimization procedure, the incremental warp function $\mathbf{W}'(\mathbf{x}, T(\mathbf{x}); \Delta\mathbf{p}')$ is inverted and composed with the current estimated warping function $\mathbf{W}'(\mathbf{x}, T(\mathbf{x}); \mathbf{p}')$. The obtained result is the updated warping function $\mathbf{W}'(\mathbf{x}, T(\mathbf{x}); \mathbf{p}')$ of the target subset, from which the incremental parameter vector can be determined. The way of calculation of incremental parameter vector $\mathbf{p}'$ is the main difference in comparison to the regular forward matching strategy, in which the incremental parameter vector $\Delta\mathbf{p}$' is applied to the target subset $\mathbf{W}'(\mathbf{x}, T(\mathbf{x}); \mathbf{p}')$ and subsequently compared with the template subset. The entire derivation procedure of the incremental parameter vector $\mathbf{p}'$ is schematically shown in Figure 1. In left and right side of Figure 1 the backward and forward matching strategies at each iteration are schematically presented, respectively.

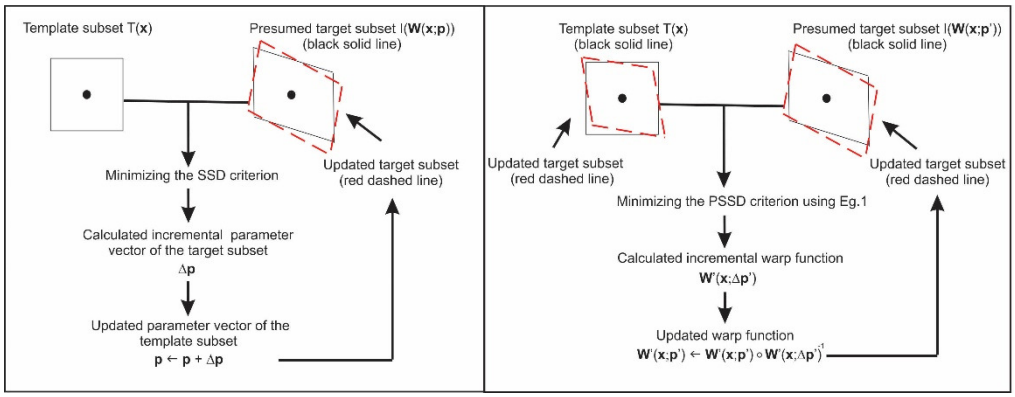

Figure 1 The forward matching strategy of the FA-NR algorithm (left) and the backward matching strategy of the modified IC-GN algorithm (right).

As already mentioned the derivation of the proposed algorithm is performed by the minimization of Eq. 1. In order to find the optimal solution for incremental parameter vector $\Delta\mathbf{p}$', the first-order Taylor expansion of the expression Eq. 1 with respect to the $\Delta\mathbf{p}$' is performed first and subsequently the minimization procedure is applied. The obtained solution is the well-known least square problem and can be written as:

$$\Delta\mathbf{p}' = \mathrm{H}^{-1} \sum_{x} \mathbf{h}^T [aI(\mathbf{W}(\mathbf{x}; \mathbf{p})) + b - T(\mathbf{x})], \tag{3}$$

where H is 8x8 Hessian matrix and vector $\mathbf{h}$ the column vector with 8 elements and defined by the following form:

$$\mathbf{h} = \left[\nabla T \frac{\partial \mathbf{W}}{\partial(\Delta\mathbf{p})} T(\mathbf{x})\ 1\right]. \tag{4}$$

For more interested readers, the deeper and more gradual derivation of the proposed approach is presented in Ref. [10].

3. RESULTS

The robustness of the proposed IC-GN algorithm was verified on a set of computer generated images with speckled patterns. As the images were prepared especially for this purpose, the intensity variation could easily be controlled. The speckled patterns of the template image were generated based on the algorithm presented in Ref. [11]. The template image consisted of 1500 randomly distributed speckle granules. The deformed images were modified by the inclusion of the simulated illumination intensity variation using 10% decrease in contrast followed by a 15 bit increase in brightness. In calculation procedure 40x40 evenly spaced calculation points were used. They were chosen automatically inside the region of interest (ROI). The distance between calculation points was 5 pixels in both horizontal and vertical directions. The size of the subset associated with each calculation point was equal to 31x31 pixels. As already mentioned, the proposed algorithm allows handling the difference in lighting variation between template and target subset. This variation is reflected in last two components of vector **p**' in the template subset and is denoted by *a* (gain*)* and *b* (offset). The obtained lighting variation parameters (*a* and *b*) for computer generated images are presented in Figure 2.

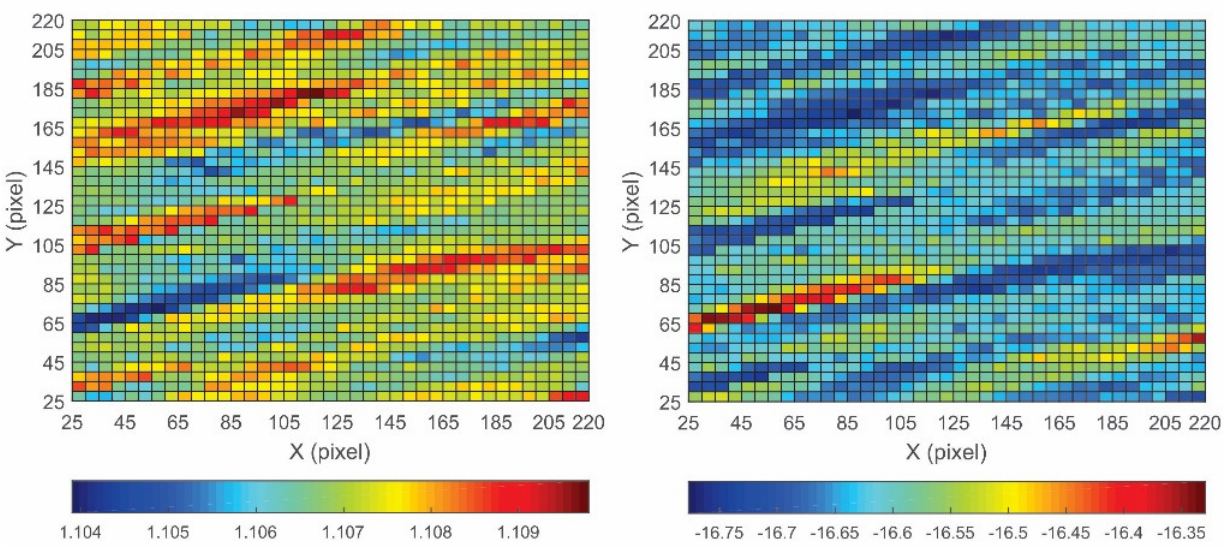

Figure 2 Calculated values of the contrast *a* and the brightness *b* for 40 x 40 target subsets are graphically presented on the left and the right side, respectively.

It can be seen that the average value of the contrast is approx. equal to 10% and the average value of the brightness to approx. -16 bits. These results correspond to the parameters used for modifying the template image. It must however be emphasized that due to the fact that now we are comparing target image with the template, the signs of the brightness change and the contrast values are the opposite of the ones used to modify the template image. It can also be seen that a positive variation of parameter *a* corresponds to a negative variation of parameter *b* and vice-versa, which is of course in accordance with the theoretical expectations.

CONCLUSIONS

The forward matching strategy is the most widely used method for tracking a set of pixels through a sequence of target images. As already mentioned, the major drawback of it lies in the fact that the Hessian matrix has to be re-calculated. To overcome this limitation the modified IC-NR algorithm

based on the PSSD correlation criterion was presented. The theoretical derivation thoroughly explained in the first part of this paper is followed by the experimental validation, which was performed on a set of computer generated images. Results show that the proposed method is insensitive to the linear intensity variation in the target image which enlarge applicability of the proposed approach.

REFERENCES

[1] Chu, T. C., Ranson, W. F., Sutton M. A.: *Applications of digital-image-correlation techniques to experimental mechanics*. Experimental mechanics, 25(3), 232-244., 1985.
[2] Huang, J., Pan, X., Peng, X., Yuan, Y., Xiong, C., Fang, J., Yuan, F.:. *Digital image correlation with self-adaptive gaussian windows*. Experimental Mechanics, 53(3), 505-512., 2013.
[3] Wang, Z., Hoang, T. M., Nguyen, D. A., Urcinas, A.C., Magro, J. R.: *High-speed digital-image correlation method comment*. Optics letters, 35(17), 2891-2891., 2010.
[4] Simončič, S., Klobčar, D., Podržaj, P.: *Kalman filter based initial guess estimation for digital image correlation*. Optics and Lasers in Engineering, 73, 80-88., 2015.
[5] Abshirini, M., Soltani, N., Marashizadeh, P.: *On the mode i fracture analysis of cracked brazilian disc using a digital image correlation method*. Optics and Lasers in Engineering, 78, 99-105., 2016.
[6] Pan, B.: *Recent progress in digital image correlation*. Experimental Mechanics, 51(7), 1223-1235., 2011.
[7] Bruck, H. A., McNeill, S. R., Sutton, M. A., Peters III, W. H.: *Digital image correlation using newton-raphson method of partial differential correction*. Experimental Mechanics, 29(3), 261-267., 1989.
[8] Pan, B., Wang, Z., Lu, Z.: *Genuine full-field deformation measurement of an object with complex shape using reliability-guided digital image correlation*. Optics express, 18(2), 1011-1023., 2010.
[9] Baker, S., Matthews, I.: *Equivalence and efficiency of image alignment algorithms*. In Computer Vision and Pattern Recognition. Proceedings of the 2001 IEEE Computer Society Conference on, volume 1, pages I-1090. IEEE, 2001.
[10] Simončič, S., Podržaj, P.: *An improved digital image correlation calculation in the case of substantial lighting variation*. Experimental Mechanics, in review.
[11] Zhou, P., Goodson, K. E.: *Subpixel displacement and deformation gradient measurement using digital image/speckle correlation (disc)*. Optical Engineering, 40(8), 1613-1620, 2001.

INTERNATIONAL SCIENTIFIC CONFERENCE ON ADVANCES IN MECHANICAL ENGINEERING
13-15 October 2016, Debrecen, Hungary

NANO MODIFICATION OF HARD COATINGS WITH IONS

[1] SKORIC Branko PhD, [1]MILETIC Aleksandar PhD, [1]TEREK Pal PhD, [1]KOVACEVIC Lazar PhD, [1]KUKURUZOVIC Dragan
[1]University of Novi Sad, Center for Surface Engineering and Nanotechnology
21000 Novi Sad, Trg D. Obradovic 6, Serbia
E-mail: skoricb@uns.ac.rs

Abstract
In this paper, we present the results of a study of TiN films which are deposited by a Physical Vapor Deposition and Ion Beam Assisted Deposition. In the present investigation the subsequent ion implantation was provided with N^{5+} ions. The ion implantation was applied to enhance the mechanical properties of surface. The film deposition process exerts a number of effects such as crystallographic orientation, morphology, topography, densification of the films. A variety of analytic techniques were used for characterization, such as scratch test, calo test, SEM, AFM, XRD and EDAX.

Keywords: Hard coatings, ion implantation, synthesis, microstructure, nanohardness

1. INTRODUCTION

The film deposition process exerts a number of effects such as crystallographic orientation, morphology, topography, densification of the films. The optimization procedure for coated parts could be more effective, knowing more about the fundamental physical and mechanical properties of a coating. In this research are present the results of a study of the relationship between the process, composition, microstructure and nanohardness of duplex TiN coatings and modified with ion implantation.
A duplex surface treatment involves the sequential application of two surface technologies to produce a surface composition with combined properties [1]. A typical duplex process involves plasma nitriding and the coating treatment of materials. In the paper are presented characteristics of hard coatings deposited by PVD (physical vapor deposition) and IBAD (ion beam assisted deposition). The synthesis of the TiN film by IBAD has been performed by irradiation of Ar ions. Subsequent ion implantation was provided with N^{5+} ions.
Thin hard coatings deposited by physical vapor deposition (PVD), e.g. titanium nitride (TiN) are frequently used to improve tribological performance in many engineering applications [2]. In many cases single coating cannot solve the wear problems [3]. The combination of nitriding and hard coating allows the production of duplex coatings, which are distinguished by a high resistance against complex loads, since the advantages of both individual processes are combined here.
In the nanoindentation technique, hardness and Young's modulus can be determined by the Oliver and Pharr method [4], where hardness (H) can be defined as: $H = \frac{P_{\max}}{A}$, where P_{max} is maximum applied load, and A is contact area at maximum load. In nanoindentation, the Young's Modulus, E, can be obtained from:

$$\frac{1}{E_r} = \frac{1-\nu^2}{E} + \frac{1-\nu_i^2}{E_i} \quad (1)$$

Where v_i=Poisson ratio of the diamond indenter (0.07) and Ei=Young's modulus of the diamond indenter.
On the other hand, in the Vickers micro hardness tester, the hardness can be calculated by measuring the residual indent area with the help of an optical microscope and the value is fully dependent on the visual resolution of the indentation
Therefore, in recent years, a number of measurements have been made in which nanoindentation and AFM have been combined.

2. METHODS

The substrate material used was high speed steel type S 6-5-2. Prior to deposition the substrate was mechanically polished to a surface roughness of 0.12 μm (R_a). The specimens were first austenized, quenched and than tempered to the final hardness of 850 HV. In order to produce good adhesion of the coating, the substrates were plasma nitrided at low pressure (1×10^{-3} Pa), prior to deposition of the coating. The PVD treatment was performed in a Balzers Sputron installation with rotating specimen. The gas flow into the deposition chamber was controlled by mass flow meters and the partial pressures of argon and nitrogen were measured. The other samples were produced with IBAD technology in DANFYSIK chamber. The IBAD system consists of an e-beam evaporation source for evaporating Ti metal and 5-cm-diameter Kaufman ion source for providing argon ion beam. Deposition rate was a_D=0.05–0.25 nm/s. Quartz crystal monitor was used to gauge the approximate thickness of the film.
A pure titanium intermediate layer with a thickness of about 50nm has been deposited first for all the coatings to enhance the interfacial adhesion to the substrates. After deposition, the samples were irradiated with 120 keV, N^{5+} ions at room temperature (RT). The Ion Source is a multiply charged heavy ion injector, based on the electron cyclotron resonance effect (ECR). The implanted fluencies were in the range from 0.6×10^{17} to 1×10^{17} ions/cm^2.
The mechanical properties on coated samples were characterized using a Nanohardness Tester (NHT) developed by CSM Instruments, Switzerland. Nanoindentation testing was carried out with applied loads in the range of 10 to 20 mN. The nanohardness tester was calibrated by using fused silica samples for a range of operating conditions. A Berkovich diamond indenter was used for all the measurements. The tip radius of the indenter was approximately 50 nm and the displacement resolution of the machine was 0.03 nm. The data was processed using proprietary software to produce load–displacement curves and the mechanical properties were calculated using the Oliver and Pharr method. The Nano-Hardness tester uses an already established method where a Berkovich indenter tip with a known geometry is driven into a specific site of the material to be tested, by applying an increasing normal load. The analysis of the indents was performed by Atomic Force Microscope (AFM). The analyzed AE signal was obtained by a scratching test designed for adherence evaluation. The steadily increasing contact load causes tensile stress behind the indenter tip and compressive stress ahead of the cutting tip. Detection of elastic waves generated as a result of the formation and propagation of microcracks. The AE sensor is insensitive to mechanical vibration frequencies of the instrument. This enables the force fluctuations along the scratch length to be followed, and the friction coefficient to be measured. The scratch tester equipment with an acoustic sensor (CSM-REVETEST) was used.
X-ray diffraction studies were undertaken in an attempt to determine the phases present, and perhaps an estimate of grain size from line broadening. The determination of phases was realized by X-ray diffraction using PHILIPS APD 1700 X-ray diffractometer. The surface roughness was measured using stylus type (Talysurf Taylor Hobson) instruments. The most popular experimental XRD approach to the evaluation of residual stresses in polycrystalline materials is the $\sin^2\psi$

method. For each selected (hkl) crystallographic direction, diffraction data are collected at different ψ tilting angles. The method requires a θ-2θ scan for every ψ angle around the selected diffraction peak and, in order to emphasize the peak shifts, it is important to work at the highest possible 2θ angle.

3. RESULTS

The nitrogen to metal ratio, EDX, table 1, is stoichiometries for IBAD technology and something smaller from PVD. For sample with additional ion implantation, value is significantly different, smaller. It is possibly diffused from the layer of TiN to the interface. The TiN coatings only show a golden surface and after ion implantation the color is dark golden.

Table 1 Atomic ratio N/TI in coatings

	Coating	Ratio N/Ti (atomic)
1	IBAD	1.00
2	PVD	0.98
3	PVD/III	0.89

The analysis of the indents was performed by Atomic Force Microscope (Figure 1a).It can be seen, from cross section of an indent during indentation, that the indents are regularly shaped with the slightly concave edges tipically seen where is significant degree of elastic recovery.(Figure 1b).

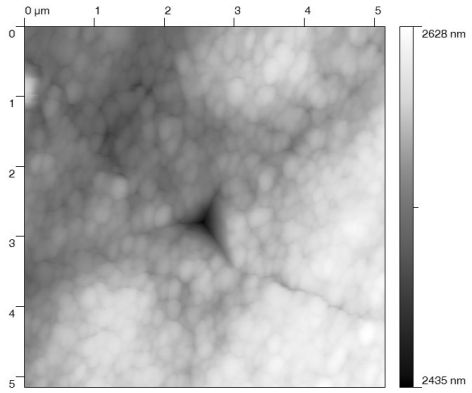

Figure 1a AFM image of a nanoindentation

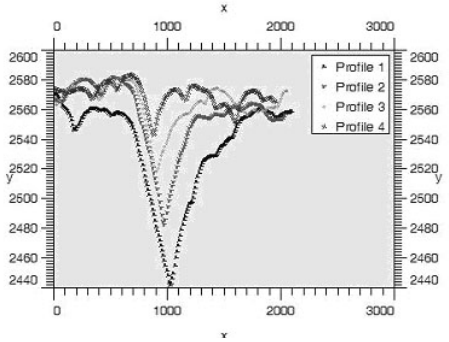

Figure 1b Cross-section of the indentation

All the results of nanohardness are obtained with the Oliver & Pharr method and using a supposed sample Poisson's ratio of 0.3 for modulus calculation.
The nanohardness values and microhardness are shown in table 2.

Table 2 Surface microhardness (HV0.03) and nanohardness (LOAD-10MN).

Unit	pn/IBAD	PVD	pn/PVD/II	Fused Silica
Vickers	2007	3028	3927	943
GPa	21.6	32.6	42.6	10,1

For each measurement, the penetration (Pd), the residual penetration (Rd), the acoustic emission (AE) and the frictional force are recorded versus the normal load. The breakdown of the coatings was determined both by AE signal analysis and optical and scanning electron microscopy.
AE permits an earlier detection, because the shear stress is a maximum at certain depth beneath the surface, where a subsurface crack starts. Critical loads are presents in Table 3.

Table 3 Critical load for different type of coatings

	pn/TiN(IBAD)	pn/TiN(PVD)
Lc1	-	23
Lc2	100	54
Lc3	138	108

It was found that the plasma-nitriding process enhanced the coating to substrates adhesion. In some places of hard coatings cohesive failure of the coating and the delamination of the coating was observed (Figure 2).

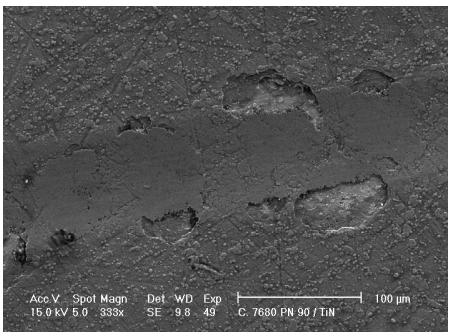

Figure 2 SEM morphology of scratch test: pn/TiN(PVD).

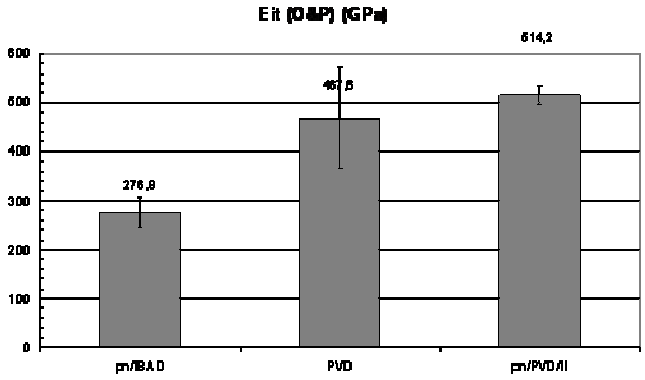

Figure 3 Young's elastic module.

The nanoindentation elastic modulus was calculated using the Oliver–Pharr data analysis procedure. The individual values of E are the different for all measurements, figure 3.

The errors related to the measurements and estimations were different and for duplex coating with ion implantation is less than 4%. Good agreement could be achieved between the E_c values and nanohardness.
The tribological behaviour of the coatings was studied also by means of pin-on-ring contact configuration in dry sliding conditions, described elsewhere [5]. The friction coefficient of sample with duplex coating with additional ion implantation, is presented in Fig. 4.

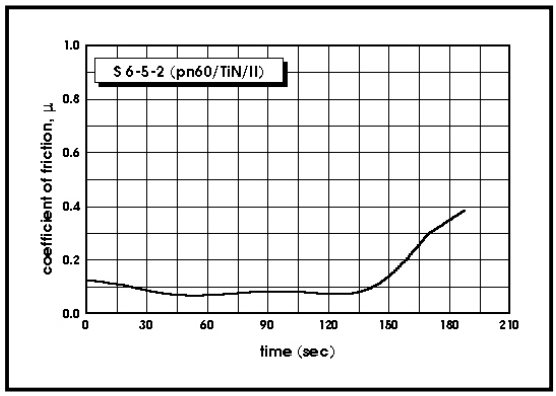

Figure 4 Friction Coefficient of pn/TiN/II

The width of column is derived from the width of the diffraction peaks, (λ=0.154nm, θ=62.5^o and β=0.056rad), and it is 70 nm.

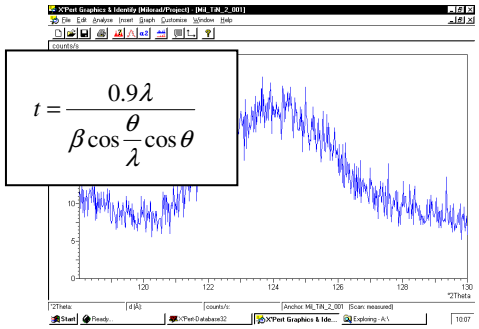

Figure 5 XRD diffraction peak of TiN(422).

The stress determination follows the conventional $\sin^2\psi$ method. Stress determination was performed using a PHILIPS XPert diffractometer. The (422) diffraction peak was recorded in a 2θ interval between 118^o and 130^o. A typical result for compact film, with residual stresses σ = -4.28Gpa, has TiN(PVD).

CONCLUSIONS

It was concluded that the formation of a plasma nitrided layer at low pressure, beneath a hard coating, is important in determining the use of hard coating.
The experimental results indicated that the mechanical hardness is elevated by penetration of nitrogen, whereas the Young's modulus is significantly elevated. Nitrogen ion implantation leads to the formation of a highly wear resistant and hard surface layer.
The present coating method can produce dance structures, high hardness and the high critical load values can be achieved. Tribological tests confirm that these composite coatings are wear resistant and provide very low friction coefficient

The above findings show that deposition process and the resulting coating properties depend strongly on the additional ion bombardment.

ACKNOWLEDGMENT

The authors gratefully acknowledge the financial support Science and Technological Development of Autonomous Province of Vojvodina

REFERENCES

[1]. J.C.A. Batista, C. Godoy and A. Matthews, A. Leyland, *Developments Towards Producing Well Adherent Duplex PAPVD Coatings*, Surface Engineering, 9, 37-43.,2003.
[2]. Y. Sun and T. Bell, *Plasma surface engineering of low alloy steel,* Mater. .Sci. Eng., A 140**,** 419-434.,1991.
[3]. H. Haufmann,, *Industrial applications of plasma and ion surface engineering,* Surface and Coatings Technology, 74-75, 23-28..1988.
[4]. Pharr, G.M., Oliver, W.C., Brotzen, F.R., *On the generality of the relationship among contact stiffness, contact area, and elastic modulus during indentation*, J. Mater. Res., 7, 613.,1992.
[5]. B. Škorić and D. Kakaš, *Influence of plasma nitriding on mechanical and tribological properties of steel with subsequent PVD surface treatments*, Thin Solid Films, 317, 486-489.,1998.
[6]. L. Combadiere, J. Machet, *Reactive magnetron sputtering deposition of TiN films* ,Surface and Coating Technology, 88, 17-27.,1996.

INTERNATIONAL SCIENTIFIC CONFERENCE ON ADVANCES IN MECHANICAL ENGINEERING
13-15 October 2016, Debrecen, Hungary

PARAMETERS AND STRATEGIES THAT INFLUENCE THE QUALITY OF THE MOLD SURFACE IN HSC PROCESS

[1]SOÓS Noémi Rita, [2]SOÓS Ödön János

[1,2]Technical University of Cluj Napoca
E-mail: noemi_soos@yahoo.com; soosodon@yahoo.com

Abstract
The mold manufacturing has a direct influence on the lead time, cost and quality of the plastic parts. For the mold industry the most commonly used manufacturing process is the milling and turning. Due to some limitation of this operations, in function of the part surface requirement, the surface roughness of the mold requires frequently hand finishing and polishing. Even using the latest technologies such as High Speed Milling, which improves the machine surface quality, the hand finishing is still required and it brings some negative influences to the process such as costs, time and geometrical errors. Nowadays, any CAM software has a variety of different tool paths strategies to milling complex geometrical surfaces. However, the programmer must have the know – how to choose the strategy according to the surface geometrical complexity. The current paper investigates different tool path strategies of a mold cavity finishing on a CNC milling machine. Different molds were manufactured using multiple strategies and the results shows the influence on the circle time and the surface roughness.

Keywords: *surface quality, mold, HSM.*

1. INTRODUCTION

The mold industry represents a key branch of the manufacturing chain. The current market requires that manufacturing companies to deliver their products as soon as possible respecting the high quality standards and a low manufacturing price. According to Fallböhmer [1], the automotive industry is the greatest consumer of molds, followed by the electronic industry. 60% of the mold manufacturing time is the machining of the functional parts of the mold such as the cavity.
The process of the mold manufacturing is composed by two elementary stages: the mold design in a CAD software, the programing in a CAM software and machining it on the CNC machine. After this processes the mold is not usually ready to go to the production line, because not all the time the surface finish is good enough. Therefore the mold core and cavity has to be finished by hand operation, polishing. According to Rigby [2], the hand finishing operation of a mold for the automotive industry is responsible for about 38% of total labor costs and the total manufacturing time is deeply influenced by this process limitation. Due to this amount of wasted time the manufacturing cost of a mold are a lot higher. In general 20 ~ 30 % of the mold manufacturing is hand finishing, polishing.
This paper has its objective of study the impact of different milling strategies on the surface roughness of the mold. During this study it will be analyzed the surface quality of the mold manufactured with different milling strategies and the impact of the manufacturing time. The main of this paper is to find out if hand finishing can be eliminated from the manufacturing equation.

2. CASE STUDY

The goal of this paper is to find an optimal programing method using CAM software to reduce the time of the hand finishing operation. The study is made on a kitchen bowl mold which has to have a shiny surface. For the programing stage we will use the MasterCAM 2017 software and after that the part will be milled on a Haas VF3 custom made for mold machining, with a spindle of 24000 rpm. The focus of this paper is on the finishing operation of the mold and the previous operation of roughing are not specified. On the image below [*Figure 1*] it can be seen a circular tool path with constant depths of cut. For this operation we will use a 16 mm diameter ball nose end mill. The tool path strategy from MasterCAM is a surface finish contour with a maximum step-down of 0.3 mm using a 50 mm ramping length/ contour. The cutter is in permanent tangential contact with the surface of the mold. This strategy type reduces cycle time because the repositioning time of the tool is eliminated from the process.

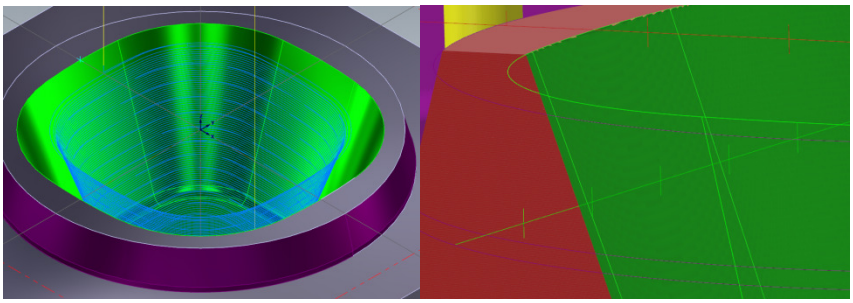

Figure 1 Tool path motion & simulation result

Input values: material type of the cavity - 1.2738; speed and feed s=4600 rpm, f=600 mm/min; tungsten ball nose end mill with a diameter of 16 mm' coolant –synthetic oil.

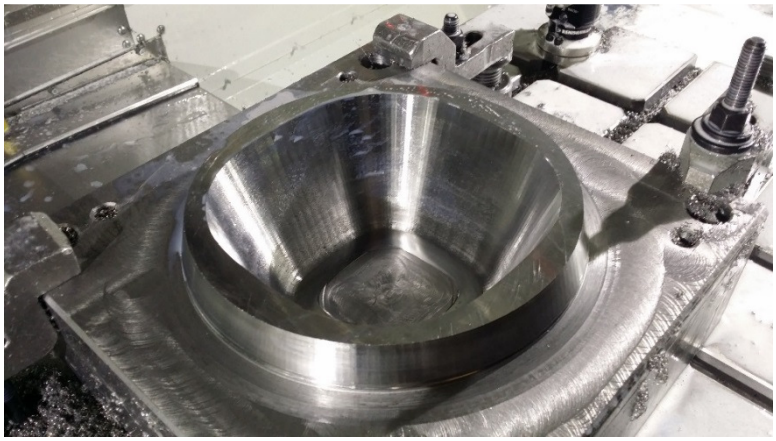

Figure 2 Machining result

In Figure 2 it can be notice that the surface of the mold is not like expected. The cause of this is that the evacuation of the chips from the cavity was not made adequately and therefore the surface of the mold was scratched. To cure the situation, a high feed surface tool path, called "waterline" was used. The effect of this strategy was that the surface quality has improved but not enough to be considered good for production.
To improve the quality of the surface and to minimize the hand polishing time, for this mold a special made ball nosed "grinding mill" was used. Future on a different strategy was implemented

to shown in figure 3. This strategy had the purpose to grid the surface of the mold perpendicularly on the previous tool trajectory and in a 20 degree sloping angle. In this way the surface scallop is reduced significantly and the quality of the part is much better.

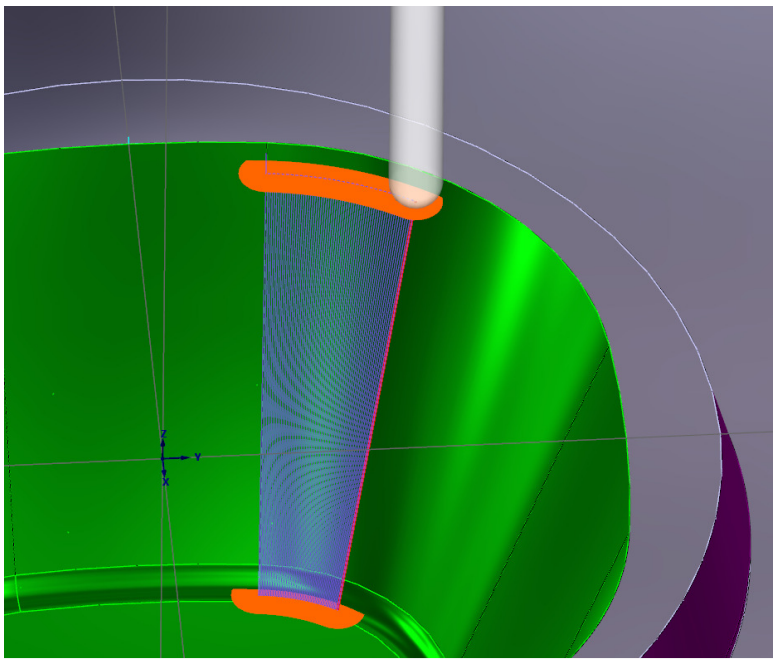

Figure 3 20 degrees slope angle machining

Figure 4 Surface after re-machining with abrasive tool in a slope angle of 20 degrees

The strategy used for this operation is a HSM tool path named “Flow line” in which the tool follows the machined surface in the programed angle given by the programmer. The mill-grinding parameters are: spindle speed s= 20000 rpm, feed F= 2500 mm/min, stepdown ap= 0.15 mm and the tool is a special grinding ball nosed end mill with a diameter of 10 mm.
The result can be seen on figure 4 with the specification that after this operation the mold was polished further on by hand with a 2 micron polishing pasta but for a shorter amount of time.

CONCLUSIONS

The purpose of this study was to reduce as much as possible the mold manufacturing process time. During this experiment the conclusion of using HSM strategies are the following:

- Reduced machining time up to 20%;
- Higher surface quality;
- Longer tool life;
- A larger surface of the tool is used, not only the tip, and this is more cost efficient.

To get the best results from the manufacturing operation all the parameters of process must be in perfect harmony, starting from the adequate tool use, the feeds and speeds of the machining process, the coolant viscosity etc.

In conclusion, to get a good surface quality of the mold and reduce hand finishing operations, the combination of the adequate process and tooling leads to the right solution. In some cases the human factor (hand polishing process) can be eliminated but in major cases is necessary, the only thing that we can do is to manufacture the surface with the highest quality possible to reduce the hand polishing operation time.

REFERENCES

[1] Fallböhmer P, Altan T, Tönshoff H, Nakagawa T. *Survey of the die and mold manufacturing industry*, Journal of Material Processing Tecnology,1996; v.59, p.158-168.

[2] Rigby P. *High speed milling in the mold and die making industries*. In:DIAMOND AND CBN ULTRAHARD MATERIALS SYMPOSIUM,1996, Ontario.

[3] G. Menges, W. Michaeli, *How to make injection moulds*, Hanser Gardner Publications Inc., Cincinnati, 2000, p. 208.

[4] V. Brutans, T. Torims, P. Rosado Castellano, R.Torres, S.C. Gutierrez Rubert, *The impact of high speed milling on 3D surface roughness parameters*, 8th International DAAAM Baltic Conference "Industrial engineering" – 19-21 April 2012, Tallinn, Estonia, 4 pg.

[5] Hamdan, A., Sarhan, A. A. D., Hamdi, M., 2012, "*An optimization method of the machining parameters in high-speed machining of stainless steel using coated carbide tool for best surface finish*", International Journal of Advanced Manufacturing Technology.

[6] M. Kumermanis, J. Rudzitis, N. Mozga, A. Ancans, A. Grislis, "*Investigation into the accuracy of 3D surface roughness characteristics*", Latvian Journal of Physics and Technical Sciences, Nr. 2, DOI: 10.2478/lpts-2014-0013, 2014, pg. 55-59.

[7] M. Held, C. Spielberger, "*Improved spiral high-speed machining of multiply-connected pockets*", Computer-Aided Design & Applications, Vol. 11 Issue 3, DOI: 10.1080/16864360.2014.863508, 2014, pg. 346-357.

[8] Souza AF, Coelho RT. *Experimental investigation of feed rate limitations on high speed milling aimed at industrial applications*, Int J Adv Manuf Technol; 2007,

[9] Souza AF, Diniz AE, Rodrigues AR, Coelho RT, *Investigating the cutting phenomena in free-form milling using a ball-end cutting tool for die and mold manufacturing*, Int J Adv Manuf Technol. 2013.

[10] Pessoles, X., Tournier, C.. *Automatic polishing process of plastic injection molds on a 5-axis milling center*, Journal of Materials Processing Technology 2009.

INTERNATIONAL SCIENTIFIC CONFERENCE ON ADVANCES IN MECHANICAL ENGINEERING

13-15 October 2016, Debrecen, Hungary

DESIGN OF A CNC ROUTER THAT CAN BE MOUNTED ON AN EDM EQUIPMENT FOR ON BOARD ELECTROD MACHINING

[1]SOÓS Ödön János, [2]SOÓS Noémi Rita
[1,2]Technical University of Cluj Napoca
E-mail: soosodon@yahoo.com, noemi_soos@yahoo.com

Abstract
In this paper is shown a specialized CNC router concept that is used for electrode machining for EDM erosion. The main goal of this project is to build a CNC milling machine that is capable of manufacturing electrodes from copper and graphite that can't be used for mold manufacturing on electrical discharge machines. The author had the concept of manufacturing and building a low cost equipment that can be afforded by small companies to be able to manufacture their own parts and products. Another objective during the modelling and designing of the project was that the built equipment that can't be transformed and mounted on EDM machines for rehabilitant and correcting the shapes of the wear electrodes without the removal of it from the machine. In this way it is eliminated the possibility of erroneous positioning of the electrode after the re-machining and remounting of it on the EDM machine.

Keywords: *CNC equipment, mold, EDM, machining.*

1. INTRODUCTION

EDM and ECM processes is advanced manufacturing technologies with unique capabilities due to their non-mechanical material removal principles can be found in different areas of application in industry offering a better alternative or sometimes the only alternative in generating accurate 3D complex shaped macro, micro and nano features and components of difficult to machine materials. Typical as well as innovative examples of application for the most important areas of application – die and mold manufacturing, turbo-machinery component manufacture, tooling and prototyping and medical engineering.
In all areas of application, the final surface integrity defines the later part performance. Therefore, the machining processes have to be designed and executed in such a way that the specific operation demands are fully met by the remaining surface modifications of the machined part. From application point of view different manufacturing processes could only compete with each other when providing at least the same part functionality and therefore similar material modifications.
To obtain the necessary form and shape of the electrode you need a machine that can drill, mill or turn your part into the adequate shape that you need. For this it shaping the electrode to the correct form nowadays computer controlled machines are used. To buy such a machine, it is a big investment for small companies. The alternative to this solution is to manufacture yourself a machine that is capable of machining complex geometrical forms in a relative tight tolerance and with a good surface finish, because the final product after erosion is directly influenced of the electrode quality.

2. THE CONCEPT OF THE CNC ROUTER

The main idea for this machine was the following: to be able to machine electrodes with complex geometrical forms; simultaneous machining on all three axes and the possibility of mounting the

forth axis on the table of the machine; a high spindle rpm for high surface quality finish; reduced cost for the design and manufacturing of the equipment; easy maintenance and interchangeable parts; an ergonomic and rigid design; easy handling and programming; high accuracy and repeatability in the manufacturing process.

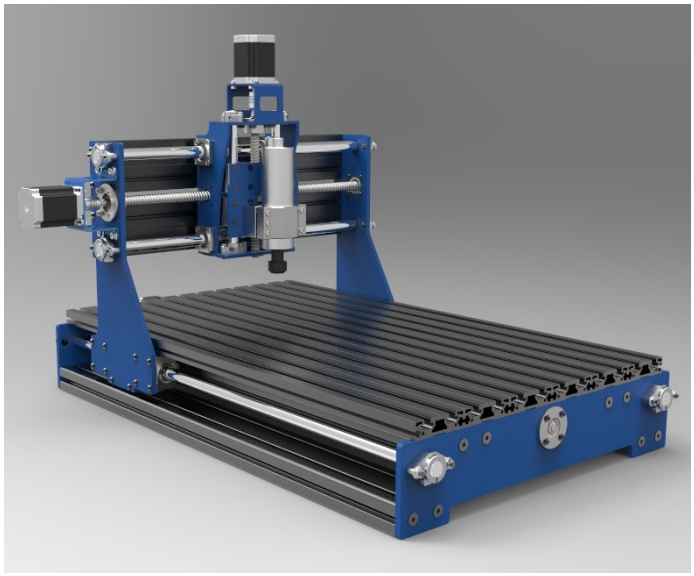

Figure 1 Design of the CNC router

Input values: Table size – 1200x1200 mm; travel on the Z axes 120 mm; water cooling spindle of 2,2 kw; spindle rpm 24000;

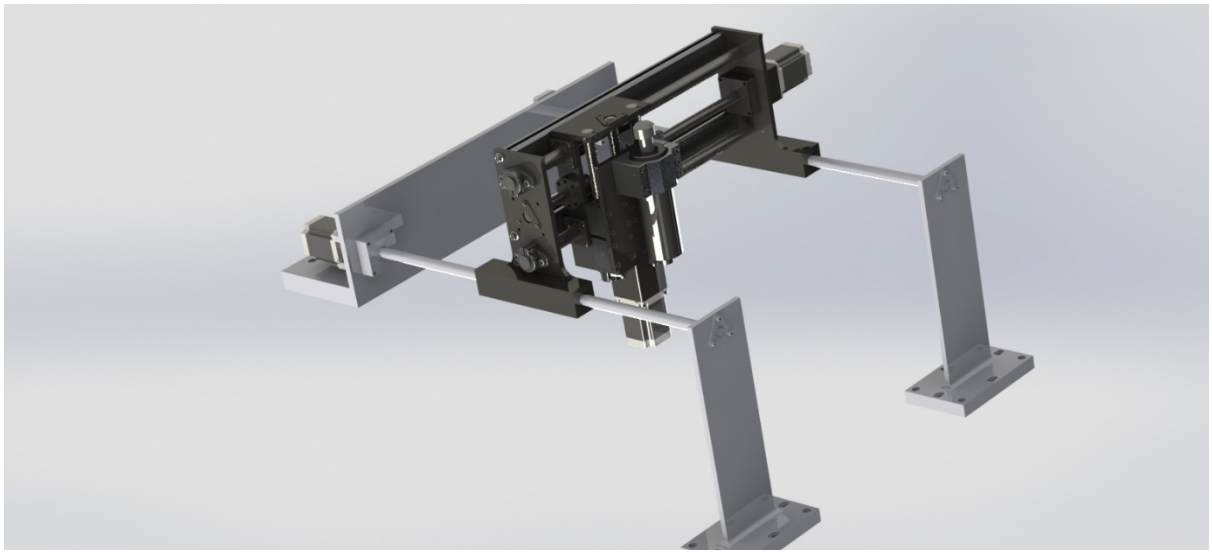

Figure 2 Device of mounting the CNC router had on an EDM machine

In *Figure 2* it can be seen a slit modification to the CNC router. In this modification the possibility is offered to transform the CNC equipment in a device that can correct electrodes directly on an EDM machine. This is done with mounting the right side of the equipment on the table and fixing the left side of it on the edge of the EDM machine. All the functions of a normal CNC machine is available with this modification only it has some limitations. The height of the elected is limited to the Z axes travel, the head of the EDM machine has to be fixed to offer rigidity.

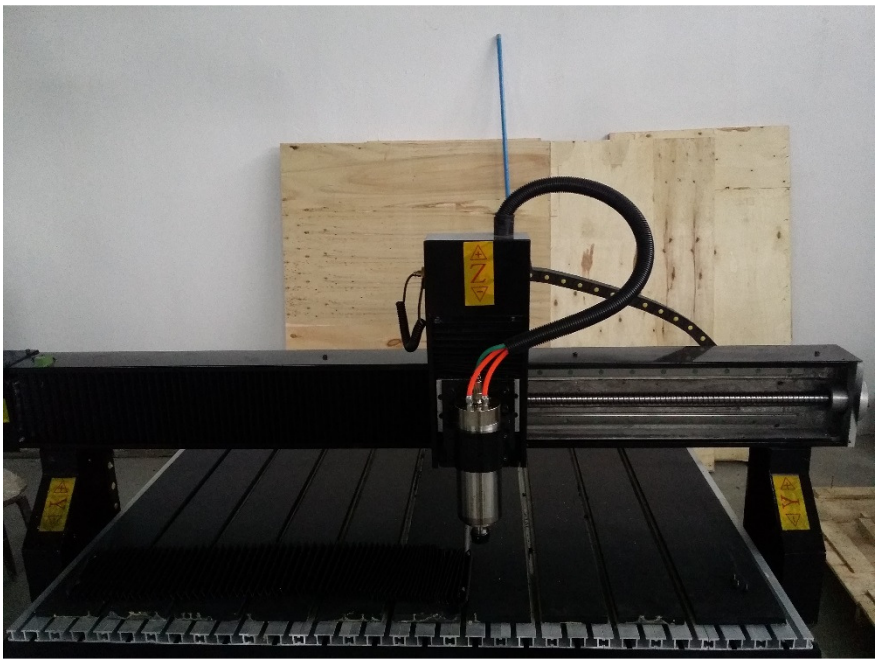

Figure 3 The CNC router after manufacturing

Precision and repeatability of the machine:

- The accuracy of manufacturing ±0.05 mm;
- The positioning and repositioning repeatability accuracy ±0.03 mm.

3. COST COMPARE OF THE CNC ROUTER AND MACHINES READY TO BUY

On the global market there are a variety of CNC machines that are available for users to buy. This machines are at a price that not all of the small factories and manufacturers can buy. A comparison of a bought machine and a self-manufactured machine is, percentage 30% more efficient to manufacture and build such a machine than to buy one with the same specifications shown above.

CONCLUSIONS

The conclusion of this paper is the following: for small companies and home businesses is more cost efficient to manufacture and build a CNC router that can machine copper and graphite electrodes than to buy a similar machine from the market. The amount of money invested in this machine is 30% less than the amount of a bought machine. To be able to design and build a good machine dimensioning and force, load, torque calculations are necessary. The precision and accuracy of the machine depends on the guide rails, ball screws and the structure of the CNC router.

REFERENCES

[1] Rahman M, Heikkala J, Lappalainen K. *Modeling measurement and error compensation of multi-axis machine tools*, International Journal of Machine Tools and Manufacture 2000; 40(10):

[2] Zhu D Z, Ren L, Liu H L. *Balance compensation system for spindle box of floor type CNC boring & milling machine and its adjustment*, Manufacturing Technology & Machine Tool 2006

[3] Liu W Z. *Finite element analysis and deformation conpensation technology of CNC horizontal milling machine,* Modern Manufacturing Engineering 2008
[4] Parag V, Aydin N, Sanjeev K, Stephen TN. *A Unified Manufacturing Resource Model for representing CNC machining systems,* Robotics and Computer-Integrat 2009;
[5] Palanisamy, P., Rajendran, I., Shanmugasundaram, S., 2007. *Optimization of machining parameters using genetic algorithm and experimental validation for end-milling operation*
[6] Denkena B, Köhler J, Mörke T, Gümmer O. *High-Performance Cutting of Micro Patterns*, Procedia CIRP 20
[7] Mayer, J. et al., 2012 (in press). *Thermal issues in machine tools*, Annals of the CIRP
[8] Uhlmann, E. et al., 2008. *Compensation of Thermal Deformations at Machine Tools using Adaptronic CRP-Structures*, in "Proceedings of 41st CIRP Conference on Manufacturing Systems: Manufacturing Systems and Techniques for the New Front"
[9] Ghionea, A., Constantin, G., Catrina, D., Vintilescu, A., Popa L.C. (2008). *Configurations and modularization grade of some CNC turning machines*, Proceedings of the 17th International Conference on Manufacturing Systems – ICMaS, Edit. Academiei Române,
[10] Ghionea, A., Constantin, G., Popa, C.L.,(2010). *Kinematic structures and machining possibilities of some CNC machine tools*, *Scientific Bulletin,* Serie C, Volume XXIII, North University of Baia Mare, Romania,2010.

INTERNATIONAL SCIENTIFIC CONFERENCE ON ADVANCES IN MECHANICAL ENGINEERING

13-15 October 2016, Debrecen, Hungary

OPTIMIZATION OF MIXED-FLOW GRAIN DRYERS BASED ON THERMAL ANALYSIS

[1]SPEISER Ferenc PhD, [1]ENISZ Krisztián PhD

[1] Institute of Mechanical Engineering, Faculty of Engineering, University of Pannonia
E-mail: speiserf@almos.uni-pannon.hu , eniszk@almos.uni-pannon.hu

Abstract
The drying process is the key element of the technology for secure storage of the harvested grain. Economic significance is appreciable and it affects the effectiveness of many other sectors (e.g. food industry, animal production). However, grain-drying is a flammable technological process. The secure warehousing and the quality of the harvested grain and feeds are important segment of the environmental protection; hence, the quality of the feeds significantly affects the excellence of the animal origin products. The improper drying-process leads to troubles during the warehousing (microbes, dust). But how do we know that the drying-technology is working on an optimal level? This paper introduces a novel measurement method which gives detailed overview of the drying process. There are 15-20 main type of grain driers in Hungary, this paper gives an overview of thermal analysis of the most popular types using a measurement system based on a Hungarian patent. Based on the data from the measurement system precision drying – a new level of efficient drying – will be introduced.

Keywords: precision drying, grain dryer, optimization, thermal analysis, Videokontroll

1. INTRODUCTION

A grain-dryer is built for the next 20-30 years. What are the market needs: reduced costs, efficient operation and control, besides better monitoring of temperature and speed parameters, and one of the most important requirement is the fire prevention. The grain dryer is an expensive investment; therefore, the owners want to establish the most efficient technology. It is worth to use the most innovative devices and solutions to achieve the optimal drying-process. Essential requirement is the optimal moisture distraction in the dryer and the simple fine tuning possibilities during the installation. The modern grain dryers mostly have 5-6% deviation of the moisture content in one discharge of grain-mass [5], even though generally it should have homogenous moisture content distribution. By exploring the factors and solving the problems of the significant deviation of moisture content, energy saving and better grain-quality can be achieved, which means easier warehousing.
Optimal drying process realizes slow and gentle vaporization of water from the grain. The process takes only the necessary amount of water from the grain that is needed for the secure warehousing, while the technology prevents the locally overheating and over-drying of the grain mass. This process protects the quality of the grain while the energy consumption is kept on minimum level. Neither the modern grain-dryers give sufficient information about the drying-process for the operators. But most of the dryers can be fine-tuned using the precision drying methodology (some of them need small interventions, for others structural modifications are necessary after the problem identification). The precision drying is based on modern information technology (IT) devices, new data processing methods and it supplies much more information on the drying process than any other device before. It gives tight control of the drying process; hence, preserving of the grain

quality is important from the point of view the plant improvement, plant production and animal production also.
Besides preventing grain quality the moisture distraction practically should be gentle but maximum efficiency. Experience has shown that the precision drying principle based developments increased the performance and efficiency in most of the cases.
Scientific research has shown that if the mass temperature is over 50°C then unfavourable processes get started, and these causes the deterioration of the inner values of the grain (denatures proteins, oxidizes vegetable fats, inactivates enzymes and vitamins). The higher the mass-temperature, the risk of degradation of the grain quality will be higher too. It is very important to take into consideration this limitation during the development of the drying-process. Every outlet temperature and mass-temperature that is higher than 50°C causes loss during the operation of the grain dryer.
To realize precision drying more condition should be kept near to its optimum:

- homogenous heat-load over the surface of the tower,
- homogenous grain-mass speed everywhere in the dryer shaft,
- constant air-pressure over the surface of the tower [3].

More than 1500 grain-dryers works in Hungary during the harvesting period of the year. The investigation highlighted the fact that, most of the currently operating grain-dryers (even the newest ones) not satisfying the minimum requirements of precision drying. Most of them are not able to work on an optimal level, and achieve precision drying without some structural modifications.

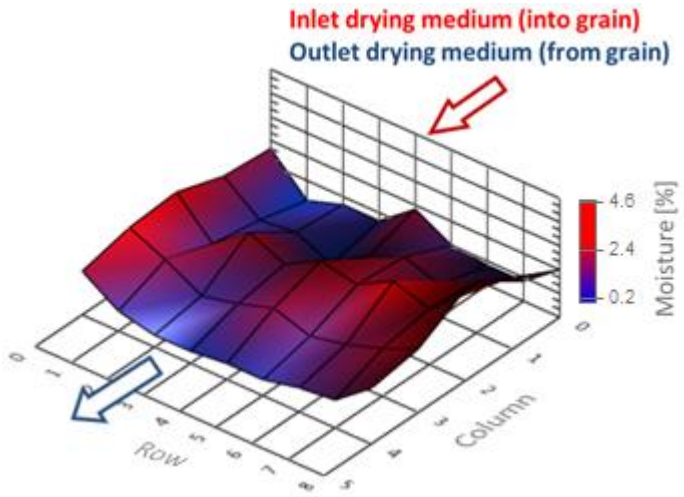

Figure 1 Moisture content decrease (%) horizontally in the dryer, when the grain-mass steps out from the drying zone

The moisture divergence in the discharged grain-mass is not caused by the big moisture content difference in the harvested grain, but the interference of physical effects in the tower (*Figure 1*). The cause of the previously mentioned significant difference (5-6%) in one discharge is more complex. The drying medium (homogenous temperature hot air) from the burner is evenly distributed through the product, which is slowly warming up the unique seeds from 8-10°C to 48-55°C during the water-distraction process (*Figure 2*).
In the Constant drying-speed section (1. section) all the heat given to the product goes for the vaporization of the moisture, the drying-speed (dx/dt) and the product temperature (t_m) are constant. When the moisture decreases in the grain (x), the capillaries shrinks, the evaporation zone contracts to the centre of the grain, the mass temperature is increasing while the drying speed is decreasing (2. section). In the 3. section the drying speed is still decreasing, the mass temperature still increasing and the average moisture content is under the “secure storage minimum” in theory.

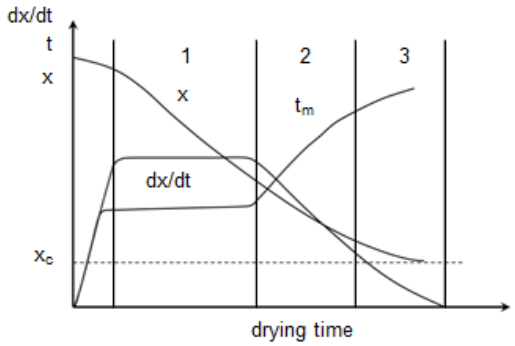

Figure 2 Warm up of the grain-mass, „t_m" theoretical diagram

A real measurement can be seen in *Figure 3*, which has been taken during maize drying. Left of the figure shows an optimal drying-process in the drying section of a tower. The grain enters on the top (cca. 20°C, designated by blue) as it flows down by gravity it slowly warming up to 50°C (designated by purple). During the gentle warming, the water evaporates from the grain. There are no red spots on the temperature distribution, which means there is no over-heating.

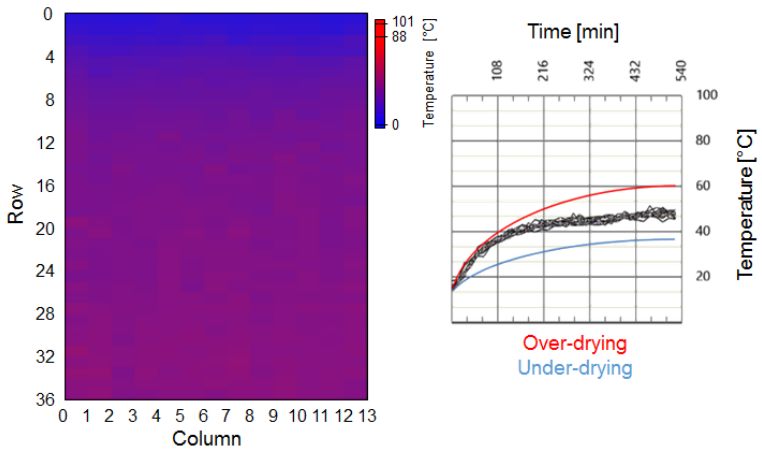

Figure 3 Warm up of the grain-mass, „t_m" measured diagram

The difference easily can be seen between the theoretical and the measured diagram, principally in the second section. The drying-speed (*dx/dt*) is not constant in the second section, but continuously increasing by the decrease of the moisture of the grain. There is no constant temperature section even over-drying is applied for some reason, in this case the mass temperature will be higher at the end of the drying section. The decrease of moisture content of the grain in *Figure 3* is similar to the "*x*" curve on *Figure 2*.

2. METHODS

We need a method to gain precise data from the outlet air-ducts of the grain-dryer, which can be used to identify the configuration of the dryer (temperature distribution, heat intensity, grain flow). Videokontroll is an industrial temperature measurement system that is able to measure air-temperature more than 500 measurement-points parallel. It measures the temperature of hot air all over the surface passing through the mass of grain at the time of exit (*Figure 4*). The system is able to point out the divergence of measurable parameters of grain driers form the optimal level. These parameters are: homogenous temperature and speed of the grain flow [2]. In case of divergence, the

grain may get stuck creating jams, get fire, be over-heated (in this case the grain becomes fragmented and lose inner-values) or under-heated (in this case grains flow too fast and do not lose enough moisture, generating mold). The sensors can identify grain jams and measure the intensity of heat inside the dryer-shaft.

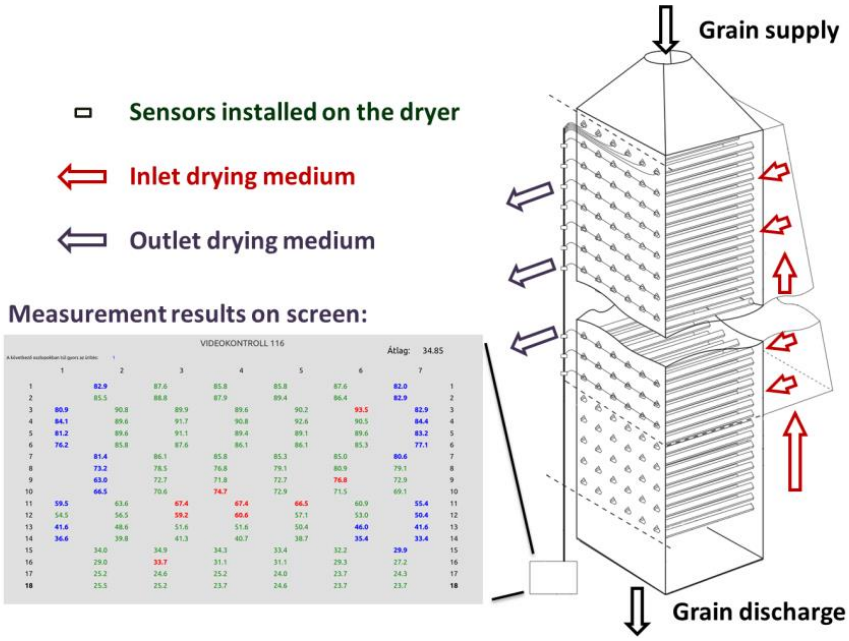

Figure 4 Videokontroll measurement method

The system measures temperature of hot air passing through the mass of grain at the time of exit from the outlet airducts, there is a strong correlation between the drying air temperature and the moisture content of the grain (the higher the temperature, the lower the moisture content of the grain). Using this information, we can get a so-called "thermal map" (*Figure 5*) about the vertical drying surface of the dryer shaft in front of the outlet airducts (the "cold-side" of the dryer).

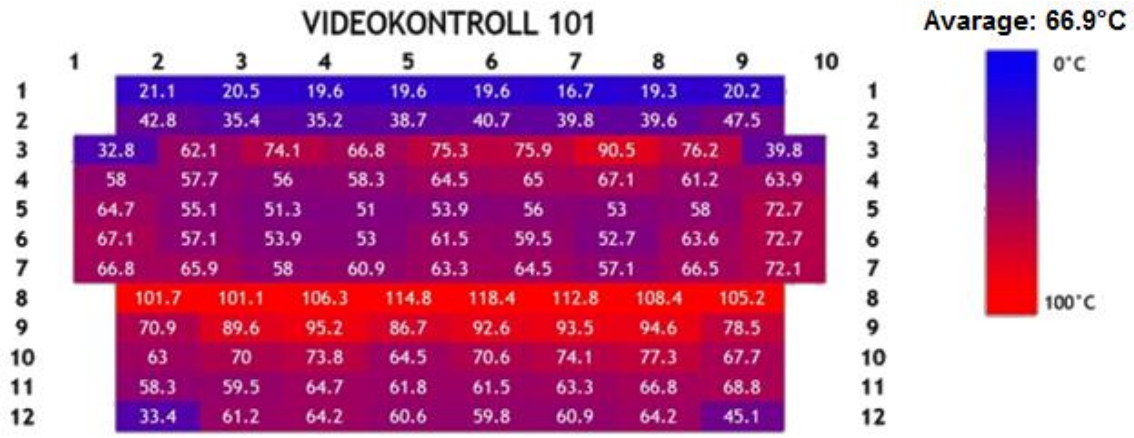

Figure 5 Thermal map of a grain-dryer during maize drying (web-interface)

A diagnosis can be set up based on the thermal map of the dryer, conclusions can be drawn about the configuration of the hot-side of the dryer (burner functionality, distribution of hot air in the air tunnel and on the surface, saturation of the air) and the dryer shaft (structural problems, air speed). If the problem is identified a solution can be elaborated upon it.

3. RESULTS

The main problems that were found at the grain dryers by the investigation in Hungary (most of them are modern dryers from the European Union) will be introduced in this part. Thermal maps sign the hot air by red, cold air by blue, 1st row and 1st column is always the upper left outlet air duct on the dryer column in the cold-side of the tower.

I. Asymmetry of heat load in the dryer section

The asymmetric heat load in the dryer section can be caused by the asymmetry of the gas-burner and the inconvenient configuration of air tunnel over the burner.

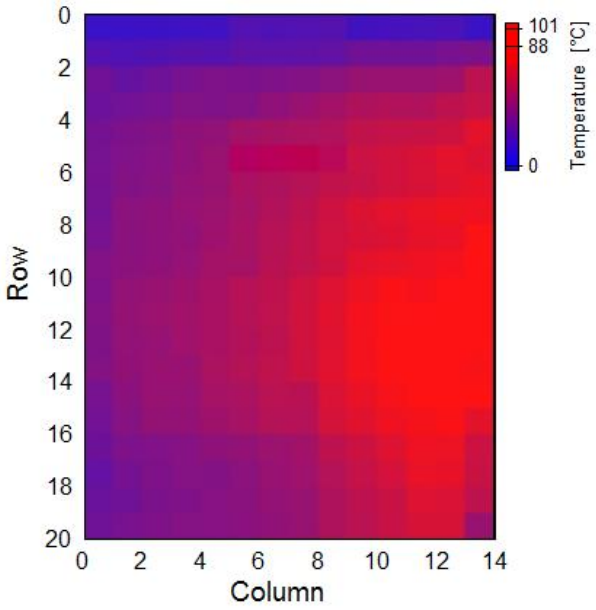

Temperature matrix [°C]

20,5	21,1	21,4	22	22,3	29	27,8	29,3	29,9	23,7	24,9	25,2	27	21,1
29	27,8	28,7	30,2	29,6	33,7	33,1	33,1	34,6	39,6	39,6	39	42,5	43,1
39,6	35,4	38,4	42,5	44,8	43,1	44,2	45,7	49,2	53	53,6	53	55,4	65,9
37,2	40,4	41,9	45,7	44,8	46,3	50,4	53,6	57,1	61,2	62,4	61,5	66,5	68,8
40,7	43,9	46	49,8	51,3	56,5	58,9	60,1	62,1	67,7	68,8	69,4	72,1	80
41,6	45,1	46,6	50,1	53,3	56,5	58,9	60,1	62,1	70,9	72,9	75,6	79,4	77,1
41,3	46	47,2	51,3	53,3	59,5	61,2	63	67,4	69,4	73,2	74,7	78,5	81,2
40,7	49,2	49,8	52,1	54,5	57,7	62,4	65,9	71,5	76,8	79,7	81,7	84,4	84,1
41,9	48,3	49,8	50,7	55,1	59,2	63	67,7	72,4	75,6	77,1	80,6	81,4	88,5
45,7	48,9	49,8	52,4	57,1	58	64,7	68	71,8	79,7	82	83,5	85,5	90,5
44,5	51,3	53	55,4	59,2	63,9	66,2	72,7	77,6	83,2	87,6	85,8	90,8	90,2
46	51,9	54,5	56,8	59,5	63	67,1	73,2	78,8	85,5	88,2	89,4	94,3	93,5
44,8	51	52,1	56	59,2	62,4	65,9	72,7	77,9	85,3	89,9	91,1	95,2	88,8
46	50,4	53,6	53,6	59,8	63	67,1	72,1	78,5	85,3	89,6	91,4	95,5	87
41,6	48,6	53,3	52,4	57,4	60,1	65,6	64,5	76,5	81,7	86,7	90,8	92,3	89,1
40,4	47,2	51,9	51,6	55,4	58,3	63,6	63,3	74,1	78,2	84,1	85,8	87,6	80
38,1	43,9	45,1	46,6	49,8	51,9	54,2	56,8	66,2	71,2	77,3	82,9	82,6	71,2
34,6	41,3	44,5	46,6	46	49,2	53,6	56	63,6	68,8	73,8	82	80,9	69,7
37,2	39,6	43,7	44,2	46,9	48,3	51,9	53	60,9	65,9	69,7	77,6	76,5	66,2
39,3	42,2	44,5	46,6	46,6	48,9	50,4	53,3	60,9	65,6	69,4	75,3	75	53

Figure 6 Thermal map of a grain-dryer during maize drying (°C)

On the right side of the drying shaft instead of 40°C, 90°C can be measured in whole season that can cause enormous energy waste, over-drying and problems during warehousing (5-6% difference of moisture content within one discharge cycle) (*Figure 6*). This deflection can be corrected by optimizing the configuration of the hot-side of the tower. During this process appropriate air flaps are installed over the gas burner to force the air to mix to gain homogenous temperature before it enters into the dryer shaft. Figure 3 shows the thermal map of the dryer shown in Figure 5 after the optimization process.

II. Asymmetry of the discharge mechanism

A physical phenomenon can be seen in *Figure 7*. The grain pouring into the dryer centre trickles clearly faster than the layers at the side walls, where the wall friction is retarding the flow [1]. Thus a grain column in the dryer shaft centre is clearly faster delivered than the remaining part in the shaft. The discharging mechanism should be corrected here to slow the grain flow in the shaft centre.

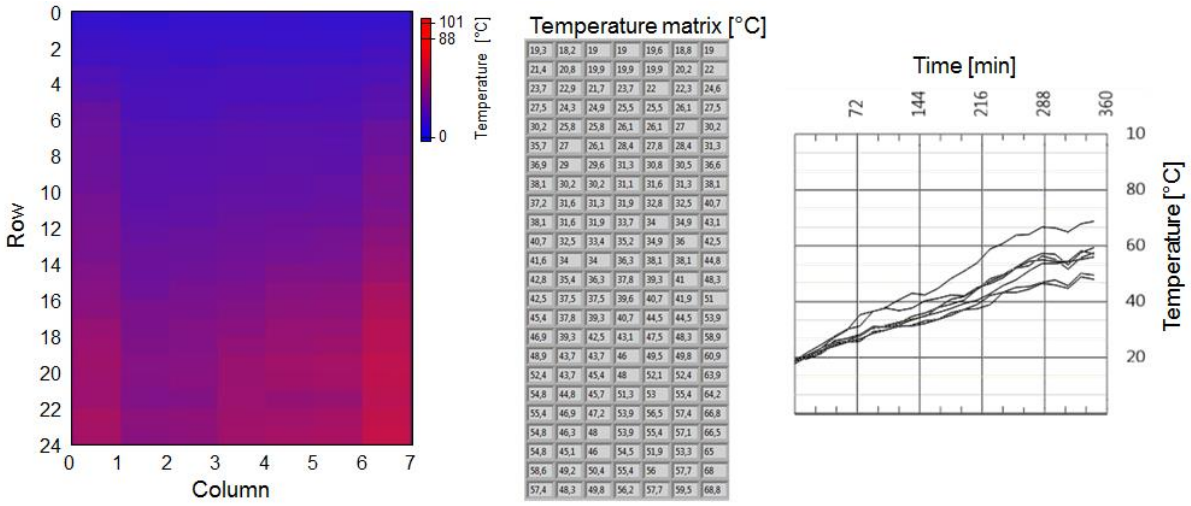

Figure 7 Asymmetry of discharge is shown in 1st and the 7th column

III. Pressure parameters are unbalanced on the drying surface

Unfortunately this is the main problem in most of the cases (*Figure 5*). The condition of the homogenous pressure is the homogenous structure of air ducts. If the air ducts are not distributed uniformly on the surface of the drying shaft, that will cause difference in air speeds and in drying efficiency also (*Figure 8*).

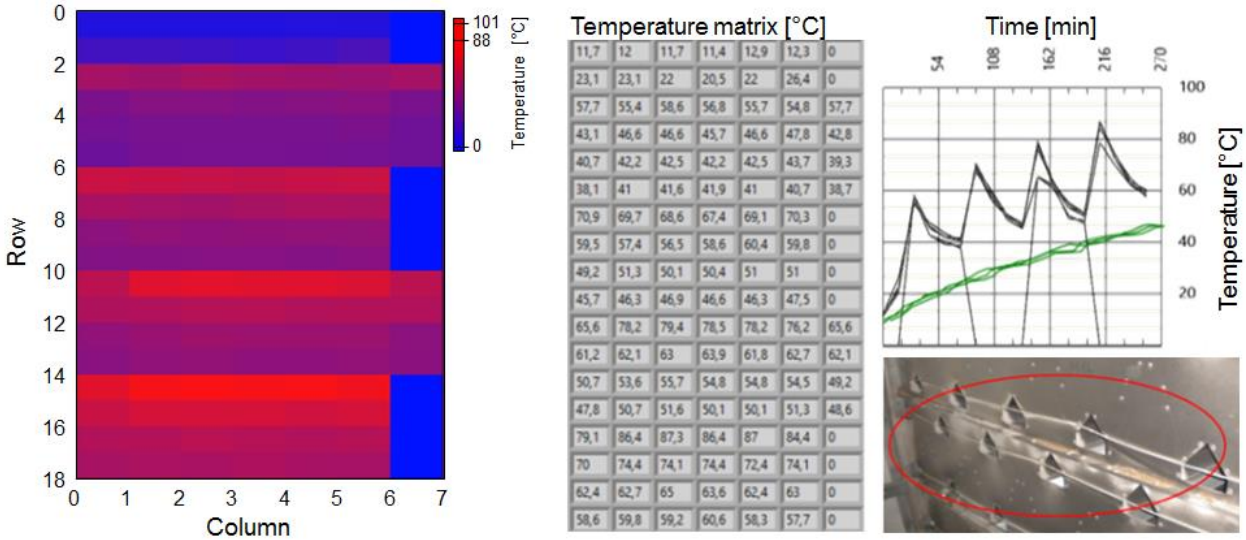

Figure 8 Air ducts are not distributed uniformly on the surface (right), over-heating is present at every double line (left), the optimal process designated by green, the reality is by black (top-right)

The over-heated horizontal lines exists because of the nonuniform distribution of airducts, at the irregular places the air-speed increase, even the maize is pulled out by the airflow from the dryer. The red lines means energy-loss, if the overheating can be ceased, then up to 20% energy saving can be realized. Correction of this problem is possible it requires disassemble the dryer and re-assemble the dryer shaft with an appropriate distribution of the airducts. The correction is a good investment, it retains in the first year.

CONCLUSIONS

Precision drying makes the drying process transparent and more secure, that results better quality of the dried grain. The data set were collected on 12 different types of grain dryers, which covers the most generally used dryer types in Hungary and the European Union. The investigation determined that most of the dryers in Hungary need some modification to work on an optimal level. Through precision drying the drying process can be optimized, which can generate considerable cost reduction each year for the agricultural holdings. The transparent drying process ensures better quality of dried grain (proteins, vitamins not destructed), more secure drying process (reduced fire hazard) and warehousing (no microbes, no dust) and less energy consumption, less CO_2 emission.

REFERENCES

[1] Kocsis, L., I. Keppler, I., Herdovics, M., Fenyvesi, L., Farkas, I., *„Investigation of moisture content fluctuation in mixed-flow dryer”,* Agronomy Research, Biosystem Engineering Special Issue, pp. 99-105, 2011.
[2] K. L. Iroba, F. Weigler, J. Mellmann, T. Metzger, and E. Tsotsas, *„ Residence Time Distribution in Mixed-Flow Grain Dryers”* Drying Technology, 29 pp. 1252–1266, 2011.
[3] K. Gottschalk, *„A model for air flow control in a mixed-flow grain dryer”,* IFAC Proceedings Volumes Volume 43, Issue 26, 2010, Pages 101–104
[4] Weigler, F. , Scaar, H., Mellmann, J., Kuhlmann, H., Grothaus, A., *„Increase of homogeneity and energy efficiency of mixed-flow grain drying”*.
[5] Mellmann, J., Iroba, K.L., Metzger, T., Tsotsas, E., Mészáros, C., Farkas, I., *Moisture content and residence time distributions in mixed-flow grain dryers,* Biosystems Engineering 109 (2011) pp. 297-307.

INTERNATIONAL SCIENTIFIC CONFERENCE ON ADVANCES IN MECHANICAL ENGINEERING

13-15 October 2016, Debrecen, Hungary

OPTIMALIZATION OF THE PREVENTIVE MAINTENANCE PLAN OF TECHNICAL EQUIPMENTS

[1]STRAKA Ľuboslav PhD, [2]HAŠOVÁ Slavomíra

[1]Technical University of Kosice, Slovakia
E-mail: luboslav.straka@tuke.sk
[2] Technical University of Kosice, Slovakia
E-mail: slavomira.hasova@tuke.sk

Abstract
The basic strategy in design, innovation up, and operation of equipment is increasing, respectively, maintaining the required level of reliability. Higher reliability of technical equipment in the design and innovation can be achieved by appropriate selection and arrangement of individual structural elements. In the operation phase, the targeted preventive maintenance comes across as the effective option. By determining the appropriate preventive maintenance plan can be hold the reliability of technical equipment at the required level. Moreover, the adverse consequences arising disorders can prevent by timely and effective maintenance intervention. This paper describes a procedure for determining the optimal plan for preventive maintenance of technical equipment.

Keywords: *Technical equipment, preventive maintenance, reliability, life time.*

1. INTRODUCTION

Reliability of technical equipment is determined by the reliability and the configurations of the individual elements on the 60 to 70%. [1,2] To increase the reliability of technical equipment in the operation phase is quite difficult. It can be achieved by replacing the weakest element in the system instead of elements with higher reliability or to back them up. [3] Many times in practice it is not necessary to increase the reliability of technical equipment. Rather, it requires the maintenance of reliability on a certain appropriate level and it can be achieved by suitable operation mode with appropriate preventive maintenance. [4]

2. PREVENTIVE MAINTENANCE OF TECHNICAL EQUIPMENT

In general, preventive maintenance can be characterized as a combination of all activities aimed at the maintenance of technical equipment in fault free conditions or returned to the state in which it can perform a required function. It is generally carried out at certain regular intervals or according to the current state of individual elements of technical equipment. In the case of carrying out the preventive maintenance at regular time intervals it is spoken about periodic preventive maintenance. If the preventive maintenance is carried out according to the current technical condition of individual elements of equipment, it is called the age preventive maintenance. Both types of preventive maintenance are aimed for eliminating the probability of failure formation of technical equipment or for degradation characteristics of its individual elements. [5] From the above it evident that the periodic preventive maintenance is less effective than maintenance that respect period the use of technical equipment. Moreover, in relation with increasing requirements of the operators of technical equipment, the emphasis is primarily on optimizing of individual maintenance interventions throughout the life time of technical equipment. [6]

3. OPTIMIZATION OF THE PREVENTIVE MAINTENANCE PLAN OF TECHNICAL EQUIPMENT

One of the basic criteria in optimization preventive maintenance plan is to maintain reliability of technical equipment to the level required for the economic efficiency of its operation. [7, 8] Optimization of the preventive maintenance is principally based on cost analysis of lifecycle of the equipment which examines the influence of the applied system of maintenance to the total lifecycle costs. Input parameters in this analysis are the financial costs associated with the acquisition of technical equipment and financial costs required to restore the operability of technical equipment, i. e. removing its failure. [9] The aim of optimization preventive maintenance plan is to find such a moment during the operation of technical equipment, which made recovery ensures the achievement of minimum average unit costs for its operation, respectively, for restore operability throughout life time.

Optimization of the preventive maintenance is considering the fact that:

- reliability of technical equipment is determined by two state model,
- the current state of technical equipment is known, i.e. whether it is in serviceable or in fault condition,
- maintenance not only intact, but also disturbed elements of technical equipment, i.e. fault removal can be performed immediately after its formation,
- time to the failure of technical equipment is a random variable, wherein the failure rate of its individual components over time is growing due to aging degradation of material properties or wear.

As described above, the time to failure of technical equipment is a random variable with increasing intensity of failures of elements. Simultaneously it holds that indicators of failure free and maintenance indicators have probabilistic nature. [10,11] Consequently, these are able to be analysed with use of continuous and discrete random variables, the probability parameters distribution and statistical distribution. For statistical analysis of maintenance characteristics it is used a much smaller number of statistical distribution such as the analysis of indicators of failure free operation.

Basic information necessary for optimization the preventive maintenance of technical equipment:

- ✓ probability of occurrence of failure of technical equipment, depending on the interval of preventive maintenance $F(t_p)$,
- ✓ the financial costs incurred to restore the operating condition of technical equipment after failure Np,
- ✓ financial costs associated with preventive maintenance of technical equipment Nu,
- ✓ financial losses caused by an emergency failures of technical equipment Ns defined as the difference between the costs incurred for maintenance after failure Np and costs of preventive maintenance Nu the technical equipment according to equation (1),

$$Ns = Np - Nu, \tag{1}$$

- ✓ functional dependence of the central interval of preventive maintenance of technical equipment on a simple interval of its preventive maintenance $\bar{t}(t_p)$ according to equation (2)

$$\bar{t}(t_p) = \frac{1}{n}\left[\sum_{i=1}^{m(t_p)} t_i(t_p) + \sum_{j=1}^{n-m(t_p)} t_j(t_p)\right] \tag{2}$$

where:

$t_i(t_p)$ - is operation time of the i-th element, operative in a state t_p,
$t_j(t_p)$ - is operation time of the i-th element which in state t_p is inoperative,
$m(t_p)$ - is the number of elements operating at state t_p,
n - is the number of all monitored elements of a given type,

- ✓ functional dependences of median cumulative financial costs $N_{Pu}(t_p)$ incurred for the operation of technical equipment caused by degradation or increasing wear of various elements observed functional surfaces of the components and groups depending on the interval of preventive maintenance,
- ✓ functional dependences of median cumulative financial costs $N_{Pd}(t_p)$ incurred to operate the technical equipment in relation to the monitoring or diagnostics of technical condition depending on the interval of preventive maintenance.

Based on the above parameters using the theory of opposing cost trends in their unit formulation can be determined the optimal value of an interval of preventive maintenance of the technical equipment according to the relation (3):

$$u(t_p) = \frac{N_u + N_s \cdot F(t_p) + N_{Pu}(t_p) + N_{Pd}(t_p)}{\bar{t}(t_p)} \tag{3}$$

4. DETERMINING THE OPTIMAL PLAN FOR PREVENTIVE MAINTENANCE OF TECHNICAL EQUIPMENT

In determining the optimal plan of preventive maintenance is necessary to consider that there is a real opportunity to follow the technical equipment in the two-state model. It is also necessary to be able to continuously monitor and detect the corresponding value of the diagnostic signals of the individual elements in the technical equipment and on the basis thereof provide the required reliability indicators. [12] Current values of diagnostic signals can be in practice obtained using non-destructive diagnostic methods using modern measuring instruments and equipment. Based on these data can be determined by various trends of the current status of its major components with the definition of critical values. *Figure 1* shows trends in the reliability of the individual components of technical equipment to the definition of critical values, i.e. probability of failure formation. Their coordinates are given by diagnosed parameter *S*, respectively, by technical life time.

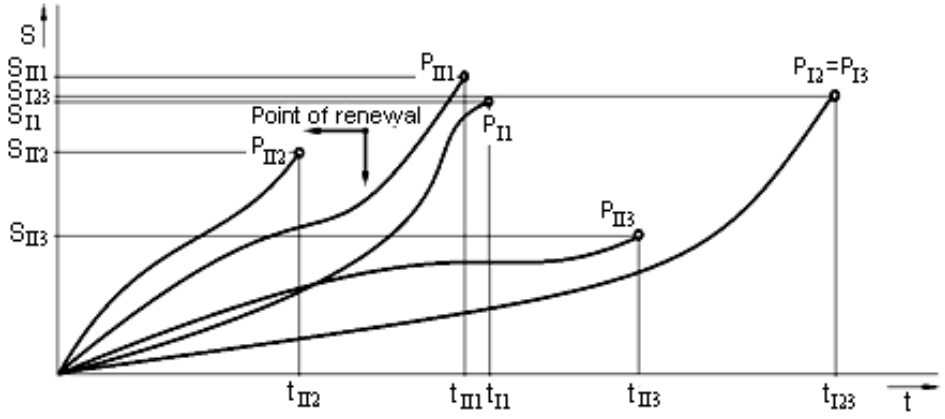

Figure 1 e of the

In the case of major system components of technical equipment may be considered with elements, respectively, set of elements in which is the most assumption for the failure existence. In general, the important thing is to consider in design of optimal preventive maintenance plan with only those

elements of the technical equipment where maintenance can prevent emergency failure, respectively, prevent large material damage. [13, 14]

In the design of the optimal preventive maintenance plan is expected to restore individual elements of technical equipment will be carried out either at the moment of failure, after established period of operation t_p, or when reaching the critical value of diagnostic signal S_p whichever event occurs first. t_p indicates the time interval for recovery and S_p diagnostic signal recovery. The optimized parameters t_p respectively S_p then they depend on the economic and operating conditions of the specific technical equipment.

From *Figure 2*, in the design of the optimal plan for preventive maintenance of technical equipment, based on the values share of medium cost c and shape function parameter m can be determined standardized optimum maintenance interval z.

Ratio of the average financial costs c is calculated according to (4)

$$c = \frac{N_p}{N_u} \tag{4}$$

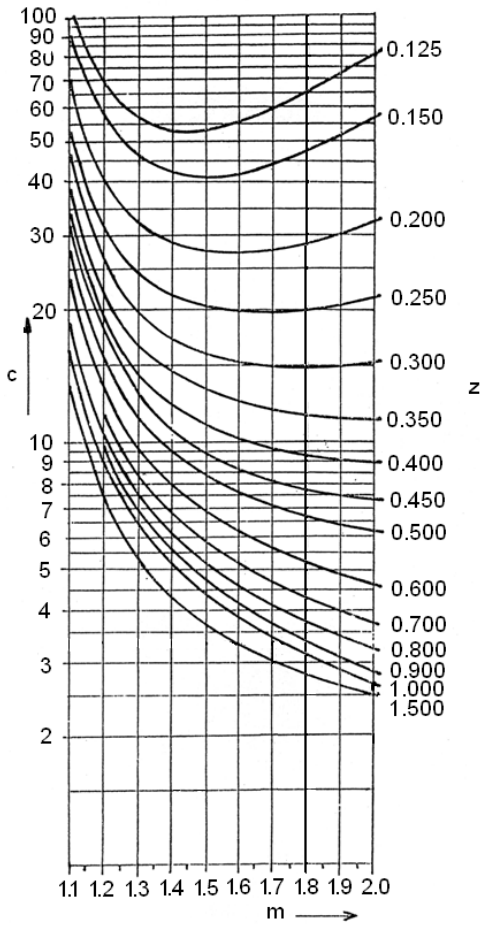

Figure 2 Dependence of standardized optimum maintenance interval z on the share value medium costs c and shape parameters m

Standardized optimum maintenance interval can be calculated from:

$$z = \frac{u^x}{Q(t)} \tag{5}$$

Mean time to failure of technical equipment T_s then is calculated as follows (6):

$$T_s = \beta \cdot \Gamma\left|1+\frac{1}{m}\right|, \tag{6}$$

while the gamma function $\Gamma\left|1+\frac{1}{m}\right|$ can be determined from *Table 1* based on the parameter of probability of failure *p*.

Table 1 Gamma function $\Gamma\left|1+\frac{1}{m}\right|$

Shape parameter	Probability of failure formation *p*								
m	0.00	0.01	0.02	0.03	....	0.06	0.07	0.08	0.09
1.6	0.8966	0.8961	0.8956	0.8951	....	0.8938	0.8934	0.8930	0.8926
1.7	0.8922	0.8919	0.8916	0.8912	....	0.8903	0.8901	0.8898	0.8895
1.8	0.8893	0.8891	0.8888	0.8886	....	0.8880	0.8878	0.8877	0.8875
1.9	0.8874	0.8872	0.8871	0.8869	....	0.8866	0.8865	0.8964	0.8863
2.0	0.8862	0.8861	0.8861	0.8860		0.8858	0.8858	0.8858	0.8857

The optimal interval maintenance of technical equipment $u=u^x$ can be calculated from (7):

$$u^x = z \cdot T_s \tag{7}$$

CONCLUSIONS

In general, in the first hours of operation of the technical equipment may be expected to the increased possibility of failure because of the production and installation errors. After this initial period, followed by a relatively long period of settled (steady) state operation. The occurrence of failures of the period is relatively low for a longer period. For maintaining the technical equipment in this period as long as possible for the preventive maintenance should be carried out according to a predetermined plan. Its aim is to design a control plan, whose task is cleaning, alignment, lubrication, replacement of worn parts, and so on. In order to be preventive maintenance not only effective, but also efficient, i. e. that the costs do not exceed the costs of removing emergency failure, it is necessary optimal preventive maintenance plan. The optimal plan of preventive maintenance of technical equipment must be chosen according to the power parameter. It characterizes the progress of wear of the component parts (elements). The basis for optimization of the preventive maintenance of the database by the period of operation of the individual elements of technical equipment to their physical limit state. This is a condition where part (element) of technical equipment loses the ability to perform a required function, for example, due to wear, fracture, corrosion and so on. The paper aimed to describe how to design an optimal plan of preventive maintenance of technical equipment in order to achieve the efficient operation of the equipment with a view to minimize the failure downtime during the entire of the desired life time.

REFERENCES

[1] Dhillon, B.S.: *Reliability, Quality, and Safety for Engineers*. CRC Press, 240., 2004.
[2] Fabian, S., Straka, Ľ.: *Operation of production systems. Prevádzka výrobných systémov (in Slovak)*. Edícia vedeckej a odbornej literatúry, FVT TU v Košiciach so sídlom v Prešove, Prešov 2008, 252 s., ISBN 978-80-8073-989-8.
[3] Fabian, S., Straka, Ľ.: *Theory of products reliability and systems in application examples. Teória spoľahlivosti výrobkov a systémov v aplikačných príkladoch (in Slovak)*. TU Košice FVT Prešov, 106., 2007.

[4] Famfulík, J., Míková, J., Krzyžanek, R.: *Theory of maintenance. Teória údrž*by. (in Slovak). VŠB TU Ostrava, 237., 2007.
[5] Hrubec, J.: *Quality control. Riadenie kvality (in Slovak).* SPU Nitra, 203., 2001.
[6] Kahancová, E.: *Reliability and Diagnostics. Spoľahlivosť a diagnostika (in Slovak).* ES VŠT Košice, 1989.
[7] Kreidl, M., Šmíd, R.: *Technical diagnostics. Technická diagnostika (in Slovak).* Praha, 2006.
[8] Legát, V., Jurča, V., Horáková, A.*: Quality, reliability and renewal of machinery. Jakost, spolehlivost a obnova strojů (in Czech)*. ČZU Praha, 219., 2006.
[9] Mrkvicka, T., Petrášková, V.: *Introduction to Probability Theory. Úvod do teorie pravděpodobnosti (in Czech).* PF JU České Budějovice, 2008.
[10] Mykiška, A.: Safety and reliability of technical systems. Bezpečnost a spolehlivost technických systémů *(in Czech).* ČVUT Praha, 206., 2006.
[11] Novák, M., Šebesta, V., Votruba, Z.: *Safety and reliability systems. Bezpečnost a spolehlivost systémů (in Czech).* ČVUT Praha, 195., 2003.
[12] Straka, Ľ. Fabian, S.: *Modelling of selected reliability indicators of prototype PAM equipment*. Applied Mechanics and Materials, 460, 91-98., 2014.
[13] Straka, Ľ., Gerková, J., Hašová, S.: *Proposal of preventive maintenance plan of experimental equipment.* Key Engineering Materials, 669, 523-531., 2016.
[14] Straka, Ľ.: *Operational reliability of mechatronic equipment based on pneumatic artificial muscle.* Applied Mechanics and Materials, 460, 41-48., 2014.
[15] Straka, Ľ., Fabian, S.: *Modelling of selected reliability indicators of prototype PAM equipment.* Applied Mechanics and Materials, 460, 91-98., 2014.

INTERNATIONAL SCIENTIFIC CONFERENCE ON ADVANCES IN MECHANICAL ENGINEERING
13-15 October 2016, Debrecen, Hungary

INFLUENCE OF DIELECTRIC FLUID ON THE SURFACE QUALITY AFTER DIE-SINKING EDM

[1]STRAKA Ľuboslav PhD, [2]HAŠOVÁ Slavomíra

[1]Technical University of Kosice, Slovakia
E-mail: luboslav.straka@tuke.sk
[2] Technical University of Kosice, Slovakia
E-mail: slavomira.hasova@tuke.sk

Abstract
Die-sinking EDM is one of the progressively growing machining technologies of electrical conductive materials. In practice, it is usually used as a final technology for machining the materials of high strength mostly complicated shapes. It is used in the manufacture of moulds for die casting, cutting tools and so on. The resulting quality of machined surface after die-sinking EDM depends on many factors, but primary on setting of the main technological, process and operating parameters. The paper deals with the influence of dielectric fluid as one of the operating parameters in die-sinking EDM. It was assessed its influence on material removal rate (MRR) and surface roughness quality in terms of surface roughness parameter Ra.

Keywords: *Dielectric fluid, surface quality, die-sinking EDM, surface roughness, material removal rate (MRR).*

1. INTRODUCTION

The technology die-sinking EDM currently represents a significant position between unconventional machining methods. Continuous universal development for many years had got this advanced technology to a level from which it can compete with very precise machining technology of metals. [1] In practice, it is mainly used as the final machining technology that solves important issues of tool room practice.[2,3] Since it is a final machining technology, the high quality machined surface plays a key role. For its assessment are used methods and the parameters that define applicable standard STN ISO 4287. Surface roughness quality after die-sinking EDM affect the main technological parameters (peak current I, pulse on-time t_{on} and with associated with it pause for renewal of the discharge channel, called pulse off-time t_{off}, and voltage of discharge U) and operating parameters relating to the tool electrode and dielectric fluid. [4,5]

2. DIELECTRIC FLUID

The dielectric fluid means a fluid with a high electrical resistance. It is a fluid which does not conduct current very little, or not at all.

Dielectric fluid in die-sinking EDM performs three main tasks:
1. it ensures the necessary deionizing of discharge channels between the tool electrode and the workpiece in electroerosion,
2. it removes from the working space *gap* eroded material particles,
3. it cools the electrode tool, workpiece and gap.

3. THE BASIC PROPERTIES OF DIELECTRIC FLUIDS USED IN DIE-SINKING EDM

Dielectric fluid significantly influences the entire electroerosion process therefore demanding requirements on its quality must be necessarily complied with.

Selected properties of dielectric fluids used in die-sinking EDM:
- sufficient aggressiveness which will provide the desired resistance between the anode and cathode, such that the current transmission between the electrodes will result in discharge, [6,7]
- low viscosity and good wettability for the rapid restoration of isolation the *gap* between electrical discharges,
- chemical neutrality for the minimization of corrosion,
- sufficiently high flash point to avoid auto ignition,
- during electroerosion shall not release any toxic gases or unpleasant odour,
- it must be chemically stable and must not interfere with the integrity of the workpiece surface neither tool electrode,
- it must be easy manufactured and be affordably priced.

In die-sinking EDM is as dielectric fluid often used deionized (demineralized) water, and selected types of oils which meet almost all the features. [8,9] An advantage of dielectric fluid based on deionized water are ecological usage, low price, low viscosity, flame resistance, and chemical stability. A disadvantage, however, is the necessity of using ionizing equipment. Simultaneously, deionized water causes corrosion of machined surfaces during machining. Therefore, currently come into prominence Therefore, currently come into prominence dielectrics oil-based dielectrics. Using oil- based dielectric is possible to prevent corrosion of workpiece during machining. Its main disadvantage is high operating costs and lower speed of machining due to its high viscosity. Using high-intensity generators may be achieved for fine finishing operations with the use of dielectric oil almost comparable cutting speeds, as when using deionized water. [10,11]

Figure 1 describes the dependence of influence of MRR using the dielectrics based on deionized water and oil at different temperatures in the range of 20 to 80°C.

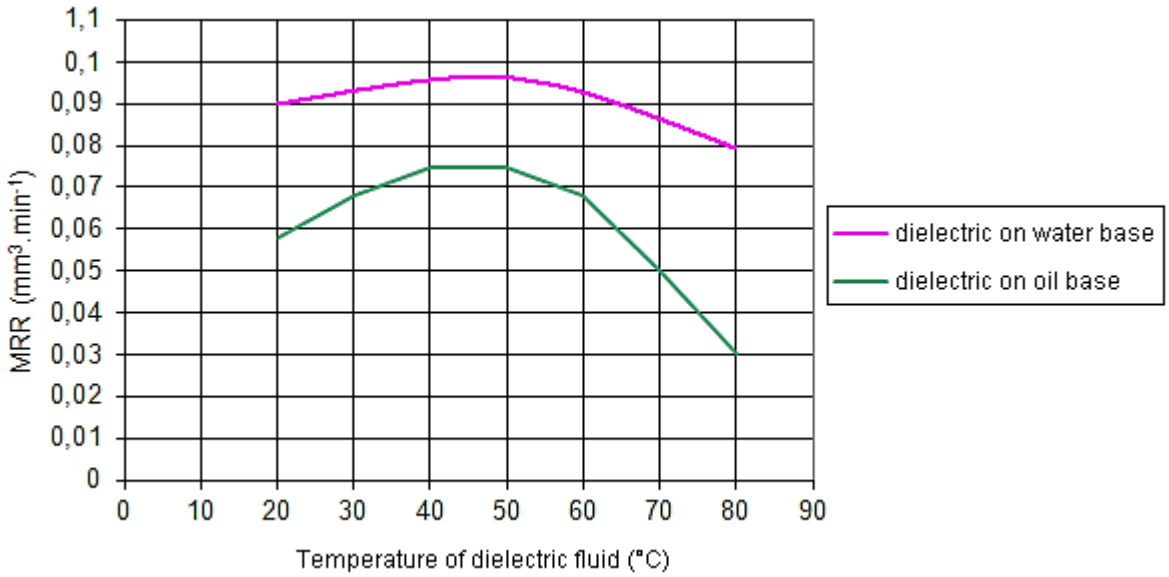

Figure 1 Dependence of MRR on temperature changes of dielectrics based on water and oil

Due to the maintenance of the required dielectric properties of water based during the electroerosion process is necessary its continuous deionization and filtration. Pollution due to particles of eroded material and tool electrode at the level of 4 to 6 % leads to the decrease of MRR up to 30 to 40%. This adverse effect is especially true at greater depths and complex shaped tool electrode where the removing metal particles from eroded surface is harder. [12,13] This causes the decrease in MRR. In certain cases, it may leads to the complete stop of electroerosion process due to pollution. [14,15] On the process of removing eroded metal particles from the workpiece also has a significant influence a flushing pressure of dielectric. [16] With the increasing value of the flushing pressure of the dielectric is growing MRR and quality of machined surface in terms of surface roughness parameters *Ra* and *Rz*. However, increase of flushing pressure only makes sense to some extent. From a certain flushing pressure of the dielectric fluid the MRR and roughness of machined surface are varying only slightly. Too low flushing pressure values result in a temperature increase in the gap, thereby it significantly leads to the heat-affecting of the subsurface layers of eroded surface. [17]

As mentioned above, the quality of machined surface after fine finishing by die-sinking EDM with regard to the roughness parameters is almost identical to the use of deionized water and oil-based of the dielectric. On *Figure 2* can be observed the dependence of MRR and roughness parameters of machined surface *Ra* on the time of machining in fine finishing by die-sinking EDM using of the oil dielectric and deionized water.

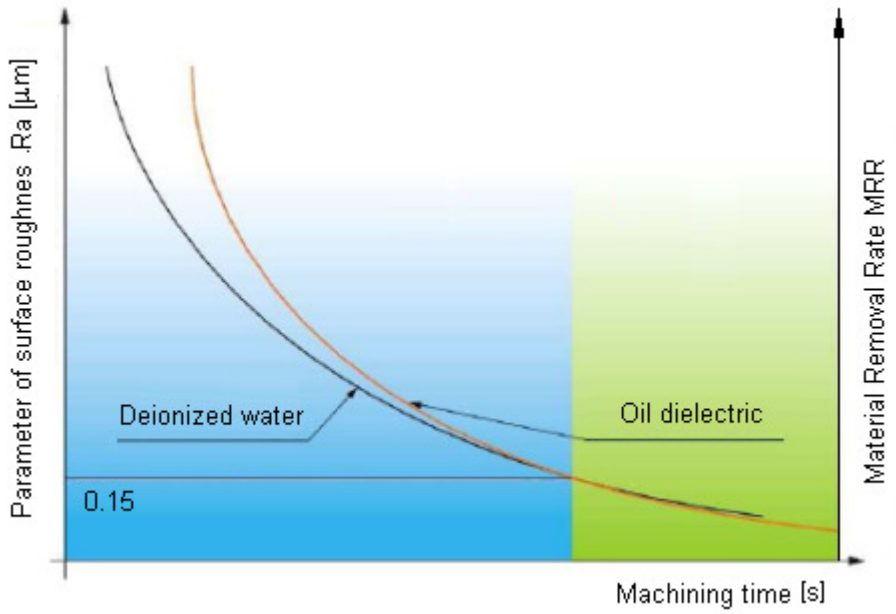

Figure 2 Influence of dielectric based on deionized water and oil on the quality in terms of machined surface roughness parameters in fine finishing by die-sinking EDM [18]

From above graphic dependence can be observed that in surface roughness of machined surface Ra<0.15µm is the machining speed almost identical using oil-based dielectric and also deionized water dielectric.

SUMMARY

Quality of machined surface in die-sinking EDM in terms of roughness parameters is an important factor in choosing the suitable dielectric fluid. Unsuitable choice of dielectric fluid parameters in terms of physical and chemical properties has a negative impact not only on the quality of the machined surface in respect of roughness parameters, but also in terms of heat affecting and shape accuracy. A substantial increase not only the quality of machined surface after die-sinking EDM, but also the efficiency of electroerosion process can be achieved by appropriate choice of parameters relating to the dielectric fluid, i.e. flushing pressure, temperature, purity, and so on. The paper aimed to highlight the importance of correct choice of the type of dielectric for particular operations in die-sinking EDM and describe the impact of influence of selected dielectric parameters on the quality of the machined surface in terms of MRR and roughness parameters Ra. The paper presents also concrete recommendations for the correct choice of flushing pressure and temperature to achieve the required quality and performance requirements during die-sinking EDM.

REFERENCES

[1] Abbas, N.M., Solomon, D.G., Bahari, M. F.: *A review on current research trends in electrical discharge machining EDM.* International Journal of Machine Tools & Manufacture, 47, 1214–1228., 2007.
[2] Čada, R., Zlámalík, J.: *Materials comparison of cutting tools functional parts for cutting of electrical engineering sheets*. Transactions of the VŠB, Technical University of Ostrava, Mechanical Series, LVIII/1, 1892., 2012.
[3] Das, C.S.: *Simulation of Fluid Flow in the Vicinity of the Electrode and the Workpiece in the Wire-EDM Process*. Journal of Materials Processing Technology, 125-131., 2002.
[4] Fenggou, C., Dayong, Y.: *The study of high efficiency and intelligent optimization system in EDM sinking process*. Journal of Materials Processing Technology, 149, 83–87., 2004.
[5] Kiyak, M., Cakir, O.: *Examination of machining parameters on surface roughness in EDM of tool steel, Journal of Materials Processing Technology*. Journal of Materials Processing Technology, 1-3, 141-144., 2007.
[6] Mathew, S., Varma, P.R.D., Kurian, P.S.: *Study on the Influence of Process Parameters on Surface Roughness and MRR of AISI 420 Stainless Steel Machined by EDM*. International Journal of Engineering Trends and Technology (IJETT), 2, 54-58., 2014.
[7] Singh, H., Kumar, P.: *Tool wear optimization in turning operation by Taguchi method.* Indian Journal of Engineering and Materials Sciences, 2, 25-30., 2004.
[8] Saha, S.K., CHaudhary, S.K.: *Experimental investigation and empirical modeling of the dry electrical discharge machining process*. International Journal of machine tools and manufacturing, 49, 297-308., 2009.
[9] Sidhom, H. et al.: *Effect of electro discharge machining (EDM) on the AISI316L SS white layer microstructure and corrosion resistance*. The International Journal of Advanced Manufacturing Technology, 1-4, 141-153., 2012.
[10] Singh, S., Maheshwari, S., Pandey, P.C.: *Some investigations into the electric discharge machining of hardened tool steel using different electrode materials*. Journal of Materials Processing Technology, 149, 272–277., 2004.
[11] Singh, S., Maheshwari, S., Pandey, P.C.: *An experimental investigation into abrasive electrical discharge machining (AEDM) of Al2O3particulate reinforced Al-based metal matrix composites.* Journal of Mechanical Engineering, , 7/1, 13–33., 2006.

[12] Straka, Ľ., Čorný, I., Mižáková, J.: *Analysis of heat-affected zone depth of sample surface at electrical discharge machining with brass wire electrode*. Strojarstvo journal for Theory and Application in Mechanical Engineering, 51/6, 633-640., 2009.
[13] Straka, Ľ.: *Analysis of Wire-Cut Electrical Discharge Machined Surface, Study of Heat-Affected Zone Depth in Wire-Cut Electrical Discharge Machined (WEDM) Surface with Brass Electrode*. LAP LAMBERT Academic Publishing, Saarbrücken, 108., 2014.
[14] Straka, Ľ., Čorný, I.: *Heat Treating of Chrome Tool Steel before Electroerosion Cutting with Brass Electrode.* Acta Metallurgica Slovaca, 15/3, 180-186., 2009.
[15] Straka, Ľ., Čorný, I.: *Quantification of Functional Dependencies of Machined Surface Quality Parameters at Electroerosion Cutting of Tool Steel X210 Cr12*. Operation and Diagnostics of Machines and Production Systems Operational States, RAM – Verlang, Lüdenscheid, Germany, 42 – 49., 2010.
[16] Straka, Ľ., Čorný, I.: *Mathematical model of infuence of cutting current on machined surface roughness at electro-erosion cutting*. Operation and Diagnostics of Machines and Production Systems Operational States, RAM – Verlang, Lüdenscheid, Germany, 71-77., 2009.
[17] Su, J.C., Kao, J.Y., Tarng, Y.S.: *Optimization of the electrical discharge machining process using a GA-based neural network*. Journal of Advance Manufacturing Techology, 24, 81–90., 2004.
[18] http://www.bedra.com/index_ger.html.

IMPROVEMENT OF SELECTED PROCESSES ON A PRODUCTION LINE

[1]SUJOVÁ Erika PhD, [1]ČIERNA Helena PhD

[1]Technical University in Zvolen, Faculty of Environmental and Manufacturing Technology, Department of Manufacturing Technology and Quality Management, Slovak Republic,
E-mail: erika.sujova@tuzvo.sk, cierna@tuzvo.sk

Abstract
The article deals with improvement and optimization of test processes on a production line. It analyzes options for improving capacity, availability and productivity of processes of an output test by using modern technology available on the market. We have focused on analysis of operation times before and after optimization of test processes at specific production sections. By analyzing measured results we have determined differences in time before and after improvement of the process. We have determined a coefficient of efficiency OEE and by comparing outputs we have confirmed real improvement of the process of the output test of cylinder heads.

Keywords: *Production Line, Test process, Output test, Coefficient of efficiency OEE*

1. INTRODUCTION

Efficiency of the process generally determines efficiency of input resources and benefits that they bring. It is a proportion of the output and input of a given activity or a system. From a management of company point of view, it determines a proportion of quality of final products and amount of resources input into the production process. It is the, so called, use of resources, which can reach maximum volume of production and quality of products and reduction of human work in production. Only healthy companies have a chance to succeed in this highly competitive environment. Customers expect companies to deliver their orders in the shortest time, at the lowest price and with the highest quality, which can be achieved only by increasing productivity and efficiency of a company [1].
The article discusses the subject of increasing efficiency of test processes at a production line of cylinder heads of engines in a production company operating in the automotive industry. Production of castings of heads of cylinders belongs to high-tech components with complex technological parts. Customers‘demands and demands for high quality of products in the above-mentioned industry are only increasing. The goals of increased competition are decreasing production costs, which are directly projected on the price of the final product. After analysis of the production process, we suggest a new arrangement of the production line for the final test of products by implementing a new measuring device. Our suggestion will simplify the entire process, manipulation of castings; will simplify manipulation of the process and will add financial savings.

2. METHODS

2.1. Defining Overall Equipment Efficiency – OEE

Measuring overall equipment efficiency has an irreplaceable role when evaluating efficiency of production equipment, production lines, technological results, or of entire production companies. Overall Equipment Effectiveness (OEE) is a recognized coefficient, which is a comparable

parameter around the world. OEE takes into consideration availability, equipment performance and produced quality. It can be expressed in percentages as part of effective use of equipment in relation to time when equipment is available for product production (Textbook, Čierna et al.).
OEE is a tool that evaluates overall efficiency of a production line calculated by adding three factors: availability, performance, quality. Overall equipment efficiency takes into consideration three parameters that describe a state of a production process, which are availability (A), performance of equipment (P) and produced quality (Q):

1. **availability (use) of equipment (A-vailability) –** compares times when the equipment was in production and when it could be in production;
2. **performance of equipment (P-erformance)** – compares actually produced amounts with amounts set by a norm;
3. **quality of production (Q-uality) –** compares number of produced pieces of required quality with the final number of products.

Calculation of the OEE coefficient is based on the following relationship:

$$OEE = A * P * Q \quad (1)$$

Final data portray clear and unbiased comparison between how each individual production equipment is utilized or not utilized. By monitoring efficiency, we can increase efficiency not only in jumps, but also systematically. It allows for optimization of production processes, increase in productivity of production processes, use of human resources and use of materials. Cost optimization and optimization of interval maintenance are also significant [2].

2.2 Description of production of cylinder heads of engines

2.2.1 Technological process of production

The analyzed company predominantly produces castings of cylinder heads for various automotive producers. A cylinder head can be considered a fundamental part of each reliable engine. It has a difficult shape since it consists of numerous channels for cooling, for air intake and output of exhaust, and more. Cylinder heads are made by the gravitational casting method. The principle of gravitational casting is based on filling a form using gravity [3].
The technological process commences by selection of cores, preparation of the metal, casting into metal forms. Following is cleaning of separating planes and removal of sand, which creates cavities in the casting, sawing of technological fillings. The following heat process adds the casting structure and hardiness. Some of the final procedures include work with the CNC equipment – finishing centers. A very important final step of the production process of cylinder heads for engines is output testing [4].

2.2.2 Characterization of the output test process

Output testing is the final part of the production cycle. It is an operation or a group of operations that control a produced part – casting before packaging and shipment to the end customer. The test process checks on the casting whether is conforms to specified norms and production documentation as well as specific norms specified by the customer. These norms differ, depending on customer, automobile manufacturer [6].
Examples of specific norms are allowed errors, insufficiencies defined by a specific place, number of defects and more. In addition to a visual check, other important components of the casting need to be verified. These are for example:

- passability of the water core,
- presence of openings of a water core,

- dimensional accuracy of position of the burning area and opening that composes the exhaust and suction area,
- tightness of openings for the water and oil areas as well as other places that could possibly lose pressure and fluids that would render the engine dysfunctional,
- other inclusions need to also be checked, such as shavings from finishing, which could render the engine dysfunctional.

2.2.3 Operations of the output test process before improvement

1. Control of tightness of the water and oil areas. The main principle is to check the casting under water for visible loss of air in form of bubbles rising to the surface. The advantage of the method is accurate detection of the place of leak and technological possibility to remove this defect based on accurate localization and statistical occurrence in this specific area.
2. Checking for existing openings – the casting, on the burned side, a mold which in places of openings have pegs of various dimensions depending on the actual openings. This mold is freely placed on the casting and all pegs need to fall into openings.
3. Passability of openings of the water area is checked by the „needle“ test. Part of the oil core and core for a water pump are checked „ tape“ test. The needle test consists of checking openings of the water area by inserting a wire from flexible steel into all openings and directions of the water area.
4. During visual check a casting is checked for casting and surface errors, mechanical damage, outstanding impurity, check of air intake and outtake area, presence of all markings, that confirm specific checks and errors, which could affect performance [6].

2.2.4 Operations of the output test process after improvement

For tightness test of the water and oil areas we suggest automatic equipment, which works based on an air-air system. Specific amount of air is forced into the casting, which creates certain pressure. The pressure is continuously measured until it reaches approximately 15s. If there is no decrease in pressure, the casting is declared to be pressure tight. If there is decrease in pressure, there is a gap causing this loss of pressure and the casting is declared as not tight. The same process is repeated also for pressurizing other areas. Everything takes place in one equipment which moves the casting between sections, automatically on a precise trajectory placed in one appliance. After a successful completion of the tightness test, the results are indicated and the casting is marked with letters W and O. The equipment also checks the area of the water area –Flow test.
Datalan a.s. invented and patented equipment for testing passability and presence of openings Light Thru. The unique project started with cooperation with Neman Slovak s.r.o. Light Thru equipment is used to test integrity of the water area of castings and other products, predominately of cylinder heads for the automotive industry. The equipment is capable of detecting broken integrity of a water lining, impenetrable cooling liquid, which renders the casting defective= inconsistent part. Figure 1 portrays a principle of activity of the equipment by the passing channel (a) in case when there is debris in the channel (b). The equipment works on the principle of optical fibers, which send light into channels. The fibers also absorb reflected light and direct it to the measuring device. If the light from the channel is blocked by debris, which is in the channel (broken core, CNC splitting, dirt from the core, etc.), the light will reflect from the debris into the original measuring device of the optical fiber.

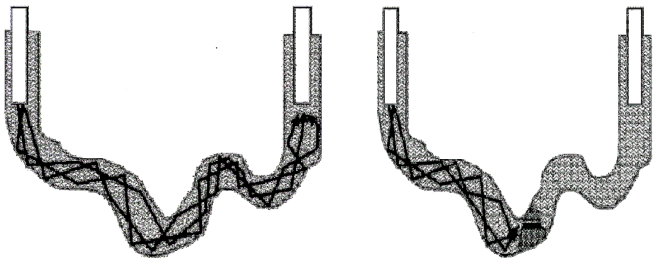

a b

Figure 1 Portrayal of a passable channel (a) and not passable channel (b) [5]

A device for checking presence of openings, that includes a camera, which will record the casting, is an additional device to the Light Thru system. Based on color distinction, black/white, it prepares an outline of the opening, which is compared to a mathematical model. By comparing the picture and a model we evaluate presence of openings and evaluate the correct shape of defined openings.

3. RESULTS

3.1 Results of evaluation of performance of the output test process before improvement

Pressurizing of the water area is usually selected as the first test. With this method of testing, after evaluating availability, performance and quality with the current cycles, we calculated, with the help of measured time, 157.2 pieces of castings per one work shift.
Pressurizing of the oil area is usually selected as the second test. This method of testing was after evaluating availability, performance and quality with current cycles, calculated, with the help of measured time, 227.5 pieces of casting per one work shit.
The output test is the final operation before packaging and shipping to the customer. This test checks presence of openings, visual check for defects, marking of previous tests. At the end of this visual "check-up" a marking will be put on the casting and it will be packed info packaging material specified by the customer. The table portrays aforementioned individual times of tests. We have determined performance of a process of 161.4 pieces of casting per work shift based on times received during tests and by using OEE [6].

3.2 Results of evaluation of performance of the output test process after improvement – after integration of testing activities in one production line

After integrating testing activities into one production line and implementation of a test of tightness, device for testing passability and presence of openings with the help of Light Thru, we measured cyclical times and have indicated measured time in Table 1 - the blue color indicates parallel operations. From these times and taking into consideration OEE, we have expressed performance of the process as 336.8 pieces of castings as a change. We have not added into the cyclical time performance of a robot, test of the pressure device or test with Light Thru. These are in the "background" because these are taking place parallel to the tests of the casting.

Table 1 Time stamp of a productions line after improvement [6]

Product: Cylinder head		
Workpleace: Output test, test of casting + pressurization, camera, light thru		
	List of activities	**Average time of activity (sec.)**
Production of one piece	Placing of casting on the conveyer belt	2.4
	Pressurizing of casting Koster	74.0
	Camera test to determine presence of openings + light thru	70.0
	Visual check of casting for possible defects	14.7
	Cleaning mechanical sander	17.1
	Cleaning by shinning	17.5
	Mechanical cleaning	3.8
	Identifing by symbol	2.3
	Placement into GTB	5.2
	Final time of test	56,3
	Total time of cycle (sec)	63.0
	Total time of cycle (min) - CCC	1.1
	Number of pieces in 60 minutes	57.1
Pieces per shift	Number of pieces per shift (480 minutes)	456.9
	Availability A = 480*90%/CCC	411.2
	Performance P = A*91%	374.2
	Quality Q = P*90%	336.8
	OEE = A*P*Q	74 %
	Real number of pieces per shift	**336**

3.3 Evaluation of results of an integrated cell

Results calculated in Table no. 1 are actual pieces only if ideal cyclical time is calculated from individual measurements. These values do not offer an accurate overall picture about expected volume. In terms of reality of these results, we have adjusted the values using coefficient of Overall Equipment Efficiency, OEE, the following way:

1) availability – 10% is deducted from the total measured time of 480 minutes; this way we get number of pieces produce during 90% of working time.
2) performance – during production, we need to be prepared for lower performance, which will be calculated from availability decreased by 9%. The result is 91% availability.
3) quality– is also a parameter decreasing total availability of the production line. It is calculated from performance decreased by 10%. The result is 90%.

In Table 2 we indicate the final value of the overall time that a test lasts per one casting for a process of internal test before improvement and after adjustment with coefficient OEE. The total time of the check per one casting is expressed from values of performance of the output test process before improvement (chapter 3.1) [6].

Table 2 Calculation of final value of total time of testing per one casting during the output test process before improvement [6]

Activity	**Pressurization of water area**	**Pressurization of oil area**	**Visual output test**
Min/piece	3.05	2.11	2.97
∑	8.13		

Table 1 shows that the real number of products after calculation with OEE, which during one shift (480 minutes) go through an output test process on an improved production line with integrated processes, is 336 pieces. We can express from this the final time of duration of a test per one casting for an output test process after improvement, which is 1.43 minutes. Table 3 shows comparison of achieved results.

Table 3 Comparison of achieved results [6]

Total time of testing of one casting during the output test process before improvement	**Total time of testing of one casting during the output test process after improvement**	**Percentage by which the time of the output test process was decreased after improvement**
8.13 min	1.43 min	82.5 %

CONCLUSIONS

The goal of the article was to suggest improvement of efficiency of the output test process. Through integration of three test activities with automated technologies and a new measuring device, the output test became more effective by 82.5 %. Another advantage of the solution is increase in quality of tested activities. This advantage, which protects the customer, cannot be evaluated. It is very important, because customer trust and satisfaction is achieved by prevention before possible risk of shipping incompatible pieces. In no circumstances can we think only about increase of performance by expressing volume of tested casting, but also through unification and reliability of test activities. Finally, by realizing our suggestion, operators of the output test process will find their work easier. An unwritten benefit, however one that cannot be overseen, is also benefit for the customer and that is protection of the customer from receiving incompatible pieces.

REFERENCES

[1] ČIERNA, H., SUJOVÁ, E., ŤAVODOVÁ, M. *Vybrané aspekty manažmentu pre technikov*. Zvolen: TU Zvolen, FEVT, 2015. ISBN 978-80-228-2733-1
[2] BOLEDOVIČ, Ľ. *CEZ (OEE)* [online], Žilina 2007. IPA Slovakia [cit 27.11.2015] available on: http://www.ipaslovakia.sk/sk/ipa-slovnik/cez-oee
[3] BANHARD, J. et al. *Cellular Metals and Metal Foaming Technology,* MIT-Verlag, Bremen, 2001.
[4] YAMAGATA H, 2003: *The Science and Technology of materials in automotive engines*. CRC Press, Cambridge, England, 2003, ISBN 10-0-8493-25854.
[5] KOČIŠ, I., et al. *Vyhne ´12: Produktivní řízení slévárny*. Brno-Trnitá: Česká slévarenská společnost, 2012. 148 p. ISBN 978-80-02-02403-3.
[6] DEKÝŠ, T. *Návrh zefektívnenia postupu výstupnej kontroly odliatkov hláv valcov v spoločnosti Nemak slovakia s. r. o.* Bakalárska práca. Zvolen: Technická univerzita vo Zvolene. Fakulta environmentálnej a výrobnej techniky. 2016.

INTERNATIONAL SCIENTIFIC CONFERENCE ON ADVANCES IN MECHANICAL ENGINEERING

13-15 October 2016, Debrecen, Hungary

STIMULATION OF NERVE PATH FOR MEDICAL USE

SVOBODA Antonin, SOUKUP Josef CSc

J. E. Purkyne University in Usti nad Labem, Faculty of Production Technology and Management, Department of Machinery and Mechanics, Usti nad Labem
E-mail: svoban@email.cz

Abstract
This solution describes methods of stimulation of nerve paths for medical use. Medical doctors need stimulate nerve paths and nerve endings patients after injury of spine. These methods are destined for tetraplegic and paraplegic patients specially for men. For this request was developed device and mechanism for vibrostimulation of nerve paths and nerve endings. In develop of construction has been taken of the safety of mechanism. Next were taken into account the construction of other devices, especially their shortcomings in the operation on the battery. For mains powered vibrators 230 (110) Volt were assessed for safety and noise vibrating mechanism. The sum of all failures was proposed structure described below. The success rate of this vibration method is reported mostly between 60-80%. Higher percentage is in patients with total spinal cord injuries, injuries over Th8 (thoracic vertebra) for spastic patients (upper motoneuron lesion) the loss of perception of heat in the dam and the glans penis and testicle squeezing perceived inability.

Keywords: *crank mechanism, excenter, amplitude, frequency, DC engine*

1. INTRODUCTION

According to available information, and clinical test have mechanisms to induce ejaculation reflex for the collection of genetic material (sperm) in affected males for several years. These methods proved to be reliable with relatively high efficiency. As the most effective method of obtaining genetic material in men can be called surgical sperm collection. This method is performed under general anesthesia, which limits patient. Performance is preceded by internal examination, ECG, blood biochemistry and other examinations according to the patient's condition. Behind this method it is then electrostimulation, which again is performed under general anesthesia by electrical stimulation of the prostate. This method, however, requires a great practical experience of the doctor, as it can cause a burn or burns intestine of the patient. At least stressful method for the patient is vibrostimulation. The doctor or also informed patient stimulates via vibration nerve endings in the penis prescribed amplitude and frequency. After injury of spine are medical doctors ready to help tetraplegic and paraplegic patients return them back normal or near normal life. Most man patients after injury of spine are no able to have got children and family. This status is for most men traumatic and stressful [4]. At least stressful method for the patient is vibro-stimulating. The doctor or also informed patient vibration stimulates nerve endings in the penis specified amplitude and frequency. To induce ejaculation is after approximately eleven minutes of stimulation, but it is necessary to observe the procedure three series of stimulation after three minutes and a minute break between every three minutes. Another way to evokes reflection in paraplegics and another way in tetraplegic. Paraplegic person is paralyzed legs, and then the person tetraplegic paralyzed on all four limbs. This method describes ways to return back to life without minimum patient's stresses. One of no stress method is vibro-stimulating of nerve paths. Our developed mechanism is generating vibrations – amplitude and frequencies between effective ranges. After consultations

injury doctor specialists, we can presuppose amplitude of the range between 1 – 3 mm and frequencies between 80 – 100 Hz. For optimal frequency and amplitude, we can take information from doctor's injury and convalescence specialists. Finally, we can make a proposal optimal frequency and amplitude [1]. For the best solution we can mark range between 80 – 120 Hz and 1 – 4 mm [2]. To achieve the desired frequency range between 80 – 120 Hz, it is necessary to convert frequency to DC engine speed:

$$f = \frac{n}{T}\ [Hz] \Rightarrow n = f \cdot T \Rightarrow n = f \cdot 60 \tag{1}$$

where is f - frequency, n – DC engine speed, T – time

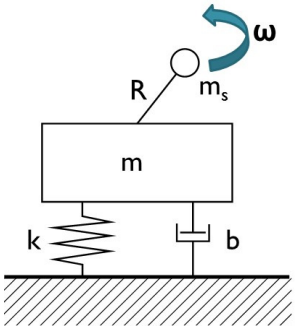

Figure 1 Forced damped vibration system with one degree of freedom

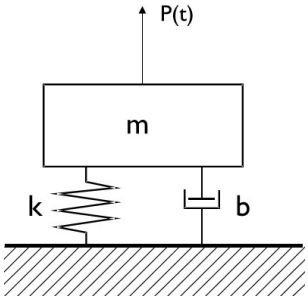

Figure 2 Forced damped vibration system with one degree of freedom

where is m_s - weight of particles, m – weight, R – eccentricity, ω – angular velocity, b – coefficient of shock absorber, k – stiffness of the spring
Equation of motion

$$m\ddot{x} + b\dot{x} + kx = P(t) \tag{2}$$

Where is x – the displacement from the static equilibrium of position, $P(t)$ – the excitation of power

$$m\ddot{x} + b\dot{x} + kx = P(t) \tag{3}$$

Another form of motion of equation

$$\omega^2 = \frac{k}{m} \tag{4}$$

Angular frequency
Harmonic oscillation is characterized by harmonic waveforms

$$y = y_0 \sin(2\pi f) = y_0 \sin(\omega t) \tag{5}$$

$$a = \frac{dv}{dt} = -\omega^2 y_0 \sin(\omega t) = a_0 \sin(\omega t) \tag{6}$$

$$v = \frac{dy}{dt} = y_0 \cos\omega \tag{7}$$

where is ω – angular velocity, y_0 – amplitude of displacement, a_0 – amplitude of acceleration
t – time.

2. VIBRATION GENERATOR IN SEVERAL VARIANTS

The mechanism was designed in several variants. Solution can be effective via analytics method, method of final points and experimental measurement. For the best solution can be mark experimental measurement. For making these test of experimental measurement was designed vibro-generator in several variants. In all variants was used electrical engine SPEED 400 with maximum 12000 rpm and powered between 6 – 12 Volts. For our needs are effective rpm between 4800 – 7200 @ 3,32 – 4,81 Volts.

2.1. Construction with the crank mechanism

Crank mechanism (*Figure 1*) is very hard for production in this very small sizes. Is necessary to take into consideration more difficult assembly of mechanism and device [2].
Advantages: Precisely adjustable amplitude shift crankshaft, separation of amplitude from frequency - with increasing of the engine speed (frequency) is the amplitude constant. Disadvantages: Miniature parts of the crank mechanism - higher demands on production and assembly [5].

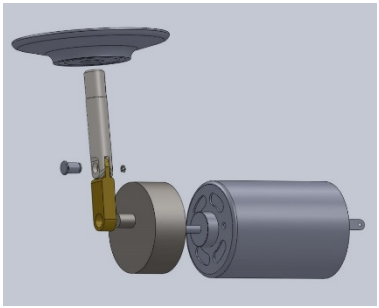

Figure 3 Crank mechanism

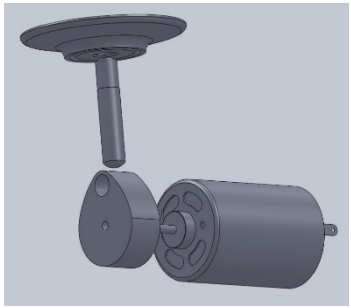

Figure 4 Construction with the cam

2.2. Construction with the cam

A cam mechanism (Figure 2) provides the distinct advantage the simplicity of design [7], the lower cost of the assembly apparatus, than the variants with the crank mechanism [3]. Advantages: Simplicity of design - lower assembly costs and assembly of device mechanism. Disadvantages: Complicated of cam production, noise. When using a cam mechanism, it is necessary to take into account unbalance cam which causes the vibration of the whole mechanism. In this case, unbalance works in favour of the final oscillation amplitudes, but to the detriment of engine bearings and the entire device. At the prescribed speed in the range 4800 – 7200 rpm occurs due to imbalance even more options, so-called own auto oscillations [3].

2.3. Construction with an eccentric

Eccentric is probably the simplest design of solution, bringing in low manufacturing costs. Experimental measurements with eccentric showed higher noise of the device. Advantages: Simplicity of design. Disadvantages: Higher load of engine's bearings, noise.

2.4. Construction with the unbalance

Unbalance (Figure 4 and 5) is the simplest solution, however, the fundamental problem depending engine speed (frequency) vs. amplitude. Advantages: Simplicity of design. Disadvantages: Higher load of engine's bearings, frequency dependence of the amplitude.

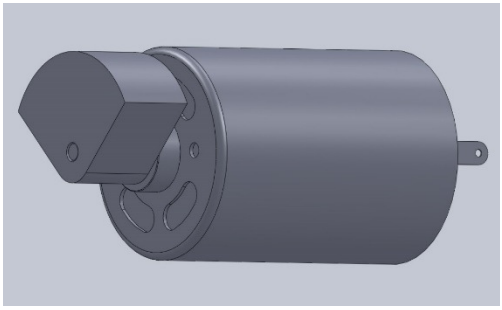

Figure 6 Construction with the unbalance

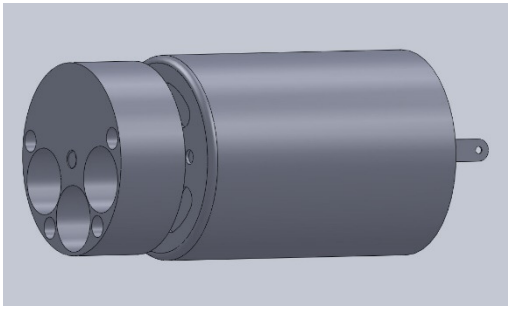

Figure 7 Constructions with drilled unbalance holes are simpler from a manufacturing point of view

3. RESULTS

With experimental measurements were found maximum values of amplitude at frequency. In the future, these results will be used for the final design of the device for generating vibrations. Unbalance method was verified in the laboratory (Figure 6). DC engine was powered by a stabilized source and were measured engine rpm, the electric current (A) and frequency (Hz).

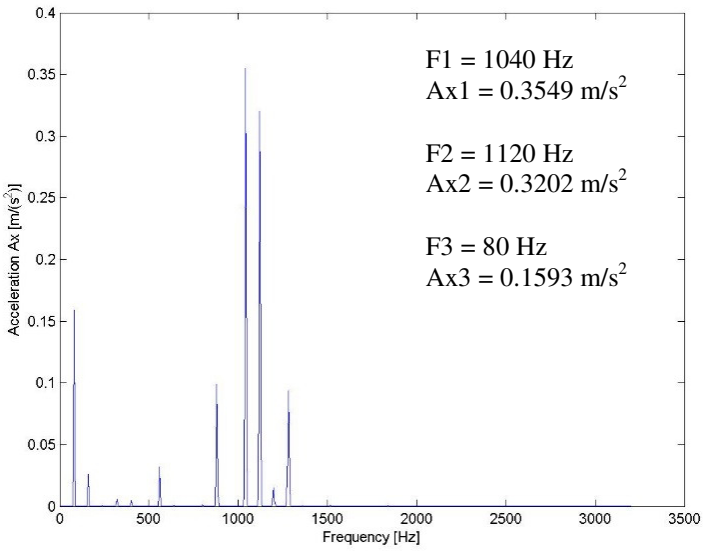

Figure 9 Acceleration in the x direction – measurements at speed 4800 rpm

In *Figure 9* was achieve the maximum of acceleration value 0.3549 m/s^2 in frequency 1040 Hz via 4800 rpm of DC engine. These values were recalculated to amplitude and later theoretically confirmed via Lagrange numerical mathematics method.

In *Figure 10* was achieve the maximum of acceleration value 9.1390 m/s^2 in frequency 172 Hz via 5160 rpm of DC engine. These values were recalculated to amplitude and later theoretically confirmed via Lagrange numerical mathematics method.
In *Figure 11* was achieve the maximum of acceleration value 0.3892 m/s^2 in frequency 52 Hz via 3060 rpm of DC engine. These values were recalculated to amplitude and later theoretically confirmed via Lagrange numerical mathematics method.

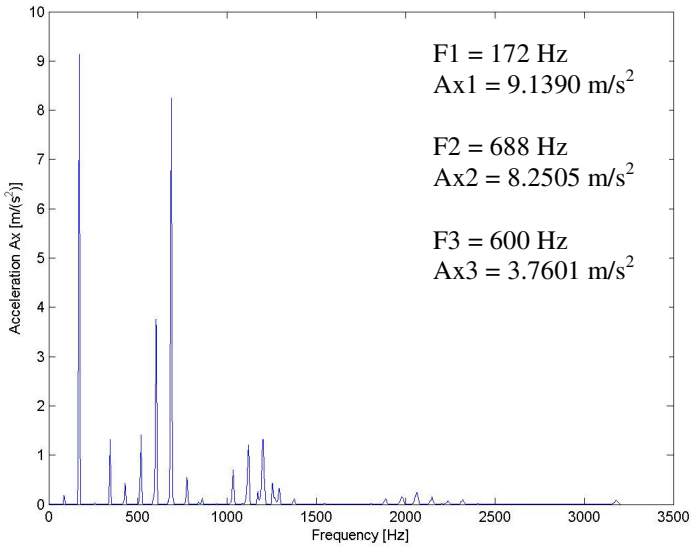

Figure 10 Acceleration in the x direction – measurements at speed 5160 rpm

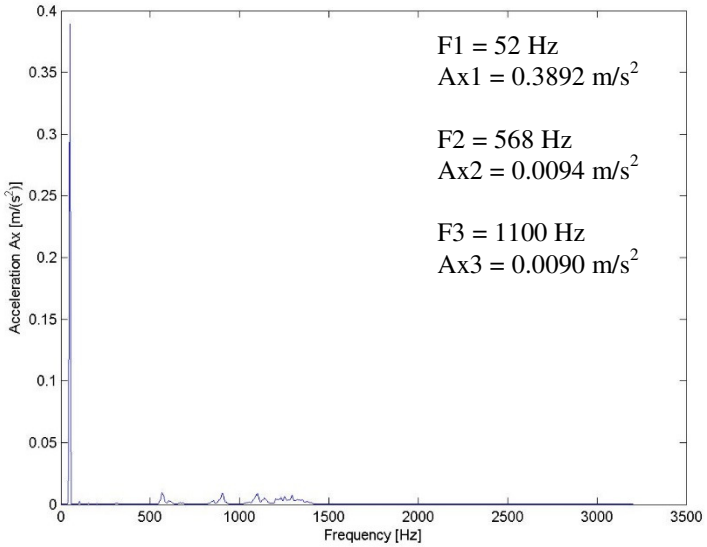

Figure 11 Acceleration in the x direction – measurements at speed 3060 rpm

CONCLUSIONS

For measurement of vibrations was designed special stand. In all cases of tests were used the same engine SPEED 400 powered by stabilized source. Rpm was taken via laser sensor and vibration was

measured via accelerometer. All measurement results were recalculating from acceleration to amplitude and was used numerical method Lagrange for verify this values. Next were processed via software MATLAB and converted to MS-EXCEL. In these methods described above were compared vibration exciter suitable mechanism design. Was selected the most appropriate method of construction equipment. This method was experimentally verified in laboratory. It will also be developed by the cheapest method of production and assembly device for vibration excitation and stimulation of nerve endings and paths. The result of this work will be quality and cheap device for stimulating a man patients.

ACKNOWLEDGEMENT

Special thanks to J. E. Purkyne University in Usti nad Labem, Faculty of Production Technology and Management for support of this project from SGS grant.

REFERENCES

[1] Šrámková T.: Poruchy sexuality u somatických nemocných a jejich léčba, Grada Publishing, 2013
[2] Dejl Z.: Konstrukce strojů a zařízení I. Spoje. Montanex, Ostrava, 2000
[3] Vejrosta V.: Konstrukce zdravotnických přístrojů, Česká společnost pro zdravotnickou techniku, June 1995
[4] Verbal presentation doctor of neurology Prim. MD. Marta Vachová, Head of neurology department hospital Teplice, on 10. 2. 2014
[5] Juliš K., Brebta R., a kol.: Mechanika I. – Statika a kinematika, SNTL Praha, 1986
[6] Brebta R., Půst L., Turek F.: Mechanické kmitání, Sobotáles, Praha 1994
[7] Benaroya H.: Mechanical vibration, Marcel Dekker, N.Y., 2004
[8] Svoboda, A.: Mechanický přístroj pro stimulaci nervových drah, Diplomová práce, Fakulta výrobních technologií a managementu UJEP v Ústí nad Labem, Ústí n. L., 2015, 53 str.

INTERNATIONAL SCIENTIFIC CONFERENCE ON ADVANCES IN MECHANICAL ENGINEERING
13-15 October 2016, Debrecen, Hungary

THERMAL MODELING OF A FLUIDIZED BED DRYER

[1] SZABÓ Viktor, [2]POÓS Tibor PhD, [3]VARJU Evelin, [4]SEBESI Viktória

[1]Budapest University of Technology and Economics, Faculty of Mechanical Engineering, Department of Building Services and Process Engineering, szabo.viktor@mail.bme.hu
[2]Budapest University of Technology and Economics, Faculty of Mechanical Engineering, Department of Building Services and Process Engineering, poos@mail.bme.hu
[3]Budapest University of Technology and Economics, Faculty of Mechanical Engineering, Department of Building Services and Process Engineering, varjuevelin93@gmail.com
[4]Budapest University of Technology and Economics, Faculty of Mechanical Engineering, Department of Building Services and Process Engineering, sebesi.viki@gmail.com

Abstract
Fluidized bed dryers are widely used in the chemical -, pharmaceutical industry, and agriculture. To scaling up, sufficiently accurate thermal models provide an opportunity to increase the effectiveness of dryers. Applying the mathematical model, the required size of a fluidized bed dryer can be defined. The work is aimed at developing mathematical model to investigate the influence of operating parameters in a fluidized bed dryer using volumetric heat transfer coefficient. After the defining the input parameters of the differential equations, the required entry length of the dryer which effective heat- and mass transfer between gas and particles takes place can be estimated. The correct estimation of the entry length is useful in optimal design of a fluidized bed dryer.

Keywords: *fluidized bed dryer, heat- and mass transfer, volumetric heat transfer coefficient, mathematical model*

1. INTRODUCTION

Since the middle of the 20th century, when the first commercial fluidized bed was installed, hundreds of fluidized bed dryers have been used worldwide to dry a wide range of materials, particularly granular materials which can be readily fluidized [1]. Despite the widespread application of fluidized bed dryers, the development of efficient and reliable modelling tools has been undermined by lack of systematic and well-documented data the literature [2].
The basics of the scaling up procedure is the determination of the required minimal entry length above the distributor plate of the fluidized bed. This is important in designing the dryer equipment to reduce the pressure drop of the fluidized bed and decreasing the power consumption in the process. In a fluidized bed, the gas-particle heat – and mass transfer takes place only up a certain length called the entry length [3]. Under steady state the hot gas enters the bed than cooled by the cold solids, and simultaneously, the entering dry gas absorbs moisture from the wet particles. Along the length of the fluidized bed, the temperature of gas continuously decreases, and the absolute humidity of the gas increasing, until reaching the saturation state. On the saturation state the temperature of drying gas tends to the wet bulb temperature, while the humidity tends to the saturation absolute humidity. Above this point the drying gas is not able to carry more moisture from the particles, so during the scaling up this length should be determined. The absolute humidity, and temperature profile of the drying gas along the fluidized bed represented in *Figure 1* under steady state. The required entry length marked with Z, the inlet temperature with $T_{G,in}$, the absolute humidity with $Y_{G,in}$, and the saturation (wet bulb) temperature is $T_{G,sat}$, and the saturation absolute humidity with $Y_{G,sat}$.

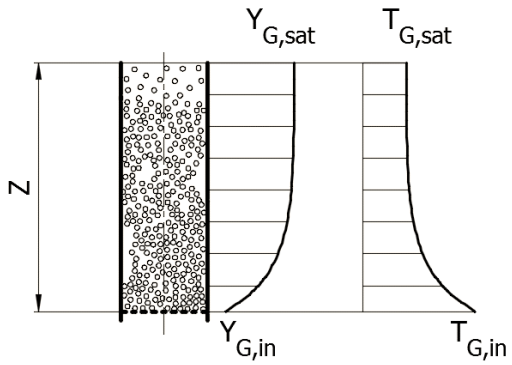

Figure 1 The absolute humidity and temperature profiles of drying gas along the length of the fluidized bed

In the literature there are number of methods to evaluate the entry length. Walton et al. [4] examined the heat transfer characteristics in a fluidized bed in batch operation. They assumed uniform bed temperature for the solid, and they neglected the heat loss through the walls. The slope of the temperature of drying gas can be calculated at any point through the length of the dryer:

$$\frac{dT_G}{dz} = -\frac{\alpha \cdot a}{c_G \dot{m}_{dG}}(T_G - T_P), \tag{1}$$

where dz is the elementary length coordinate, α is the heat transfer coefficient, a is the volumetric interfacial surface area, c_G is the specific heat of gas, $\dot{m}_{dG}$ is the mass flow rate of gas, T_G is the temperature of gas, and T_P is the temperature of material.

Roy et al. [3] determined the entry length of a fluidized bed granulator using Stanton number:

$$Z = -\frac{cd_P}{6St(1-\varepsilon)}, \tag{2}$$

where d_P is the particle diameter, St is Stanton number, and ε is the porosity of bed. Constant c is defined as the follow expression:

$$e^{-c} = \frac{T_G - T_P}{T_{G,in} - T_P}. \tag{3}$$

Ng et al. [5] optimized an industrial-scale fluidized bed dryer using Class 1 and Class 3 models, drying Geldart Type D nylon particles. Assuming plug-flow behavior and neglecting the influence of the bubble phase, the Class 1 model can be used. The minimum bed height needed to ensure that the moisture content in exit air is maximized, i.e. at adiabatic saturation can be calculated with the following equation:

$$Z = \frac{\rho_G c_G v}{\alpha \cdot a} ln\left(\frac{Y_{G,sat} - Y_{G,in}}{Y_{G,sat} - Y_G}\right), \tag{4}$$

where ρ_G is the density of gas, c_G is the specific heat of gas, v is the superficial gas velocity.

Using Class 3 model, the humidity content of the dense phase along the bed height:

$$\frac{dY_d}{dz} = \left(Y_{G,sat} - Y_d\right)\left(\frac{\alpha \cdot a}{\rho_G c_G v_d}\right) - \sigma_c \frac{6}{d_P}\frac{1}{u_b}(Y_d - Y_b), \tag{5}$$

where Y_d is the absolute humidity of dense phase, σ_c is the mass transfer coefficient between bubble and dense phase, v_d is the average velocity in dense phase, v_b is the velocity of bubbles, and Y_b is the absolute humidity of bubble phase.

The heat transfer coefficient between gas and particles is calculated in the literature dealing with the scaling-up is calculated from various *Nu=f(Re)* criterial equations. The heat transfer coefficient can

be calculated by making some simplifying assumptions, meaning to assume that the geometry of the particles is spherical, and the contact between the gas and the material is ideal, which means that during the drying process each particle is in contact with the drying gas, on its whole surface. With these assumptions, and in the knowledge of the total number of particles in the drying chamber, the contact surface of the material can be determined [6]. The volumetric interfacial surface area is calculated in those literatures knowing the porosity of particles, sphericity and assuming that the particles are spherical [7]:

$$a = \frac{6(1-\varepsilon)\Phi}{d_P}, \tag{6}$$

where Φ is the sphericity.

Application of a volumetric heat transfer coefficient (αa) and modified dimensionless numbers for mathematical models provides favorable opportunities to describe the drying process of wet particles, and eliminates the above mentioned uncertainties in the heat transfer area [8]. The mathematical models of fluidized bed drying require the volumetric heat transfer coefficient between the gas and particles. A volumetric heat transfer coefficient was applied for modeling fluidized bed dryers in our previous work. Based on our measurements and literature data a modified *Nu'=f(Re)* relationship was created for fluidized bed drying [9]:

$$Nu' = 6{,}4 \cdot 10^{-3} \cdot Re^{1{,}15}. \tag{7}$$

The purpose of our work is to determine the required entry length of the fluidized bed dryer using volumetric heat transfer coefficient as an input parameter to the mathematical model.

2. METHODS

The following assumptions are made in the development of model for determining the entry length:

- The fluidized bed is perfectly mixed, so the temperature (T_P) and moisture content (X) of the particles are constant along the dryer.
- The mass flow rate of the drying gas is constant during the operation.
- The heat loss and radiation are negligible.

The variation in the absolute humidity of drying gas along the length of the dryer can be calculated with the following equation:

$$\frac{dY}{dz} = \frac{\alpha a}{c_G}\frac{A_d}{\dot{m}_{dG}}\left(Y_{G,sat} - Y\right), \tag{8}$$

where A_d is the cross section of the dryer.

The temperature of drying gas for a section dz can be calculated:

$$\frac{dT_G}{dz} = -\frac{c_v}{c_G}(T_G - T_P)\frac{dY}{dz} - \frac{\alpha a}{\dot{m}_{dG}c_G} \cdot A_d \Delta T_{G-P}, \tag{9}$$

where c_v is the specific heat of vapour, $\Delta T_{G\text{-}P}$ is the logarithmic mean temperature difference.

The differential equations (8) and (9) can be solved numerically in every dz sections, in elementary i length scales. The simplest solving method is Euler-method [10]. The absolute humidity of gas in every elementary steps can be calculated with the following method:

$$Y_G^{i+1} = Y_G^i + dz\left(\frac{\alpha a}{c_G}\frac{A_d}{\dot{m}_{dG}}\left(Y_{G,sat} - Y\right)\right). \tag{10}$$

The temperature of drying gas can be evaluated for every steps with similar method. The calculating method represented in *Figure 2.* The calculation is finished when the saturated values are reached by 1% accuracy, when the drying process happens in the constant drying rate period.

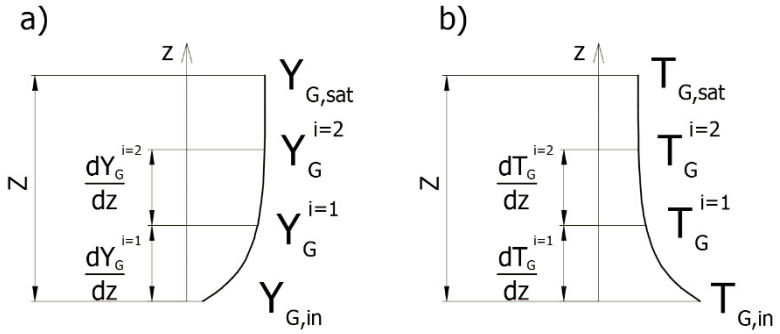

Figure 2 The calculating method. a; Determining the absolute humidity of gas in every steps, b; Determining the temperature of gas

Hereinafter the calculation process will be presented during an example. The input parameters of the model are listed in *Table 1*. The model makes it possible to calculate the temperature and absolute humidity of drying gas along the length of the fluidized bed dryer (*z*).

Table 1 Input parameters

Notations	Values	Units
D	0,1	m
$\dot{m}_{dG}$	0,027	kg/s
$T_{G,in}$	70	°C
$T_{P,in}$	20	°C
$Y_{G,in}$	0,0063	kg_{H2O}/kg_{dG}
Δz	0,01	m

In *Table 1 D* is the diameter of the dryer.
The saturation absolute humidity can be determined:

$$Y_F = \frac{M_{H_2O}}{M_{dG}} \frac{\varphi p_{v,sat}}{P - \varphi p_{v,sat}}, \tag{11}$$

where M_{H_2O} is the molecular weight of the water, M_{dG} is the molecular weight of drying gas, φ is the relative humidity of gas, P is the absolute pressure, and $p_{v,sat}$ is the saturation gas pressure, which in the function of the saturation temperature $T_{G,sat}$. The saturated temperature (and also the saturation absolute humidity) can be determined by using Mollier diagram knowing the inlet temperature $T_{G,in}$ and absolute humidity of gas $Y_{G,in}$. *Figure 3* shows the determination of satirated values on the Mollier diagram.

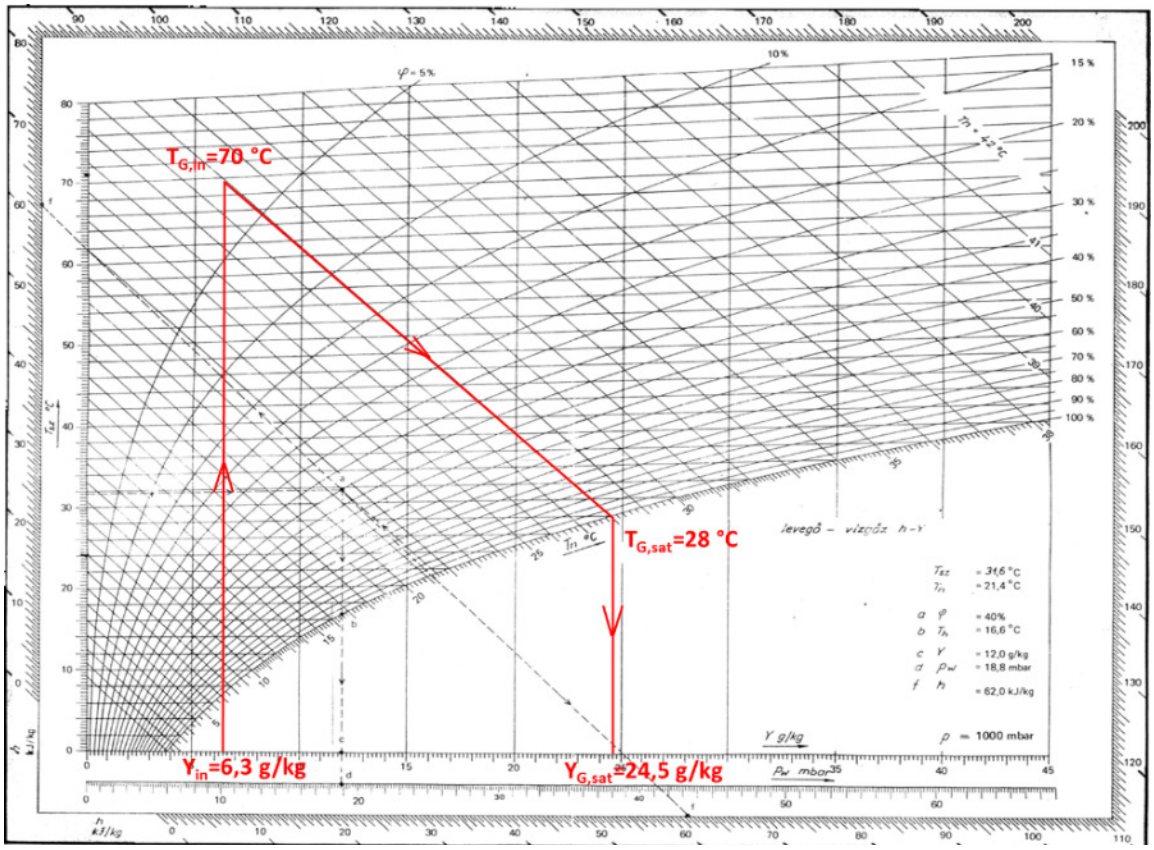

Figure 3 Determining the saturated values on the Mollier diagram

3. RESULTS

By repeating the calculation step by step (Δz=0.01 m) the absolute humidity and temperature curves can be created, and the required entry length can be determined. To avoid numerical failures, the calculation steps should be selected to an appropriate low resolution. *Figure 4* shows the humidity and temperature curves, and the saturated values (red line). The value of volumetric heat transfer coefficient was evaluated from Eq. (7). The value of the required entry length can be determined from the diagram.

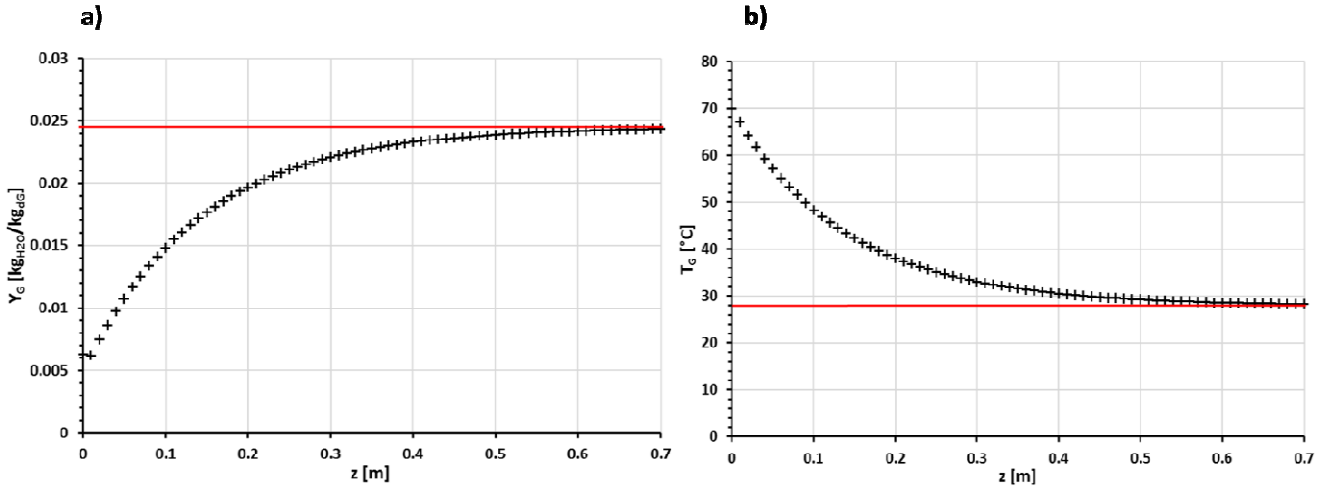

Figure 4 Calculating the required entry length. a; Absolute humidity of drying gas vs length, b; Temperature of drying gas vs length

CONCLUSIONS

The purpose of our work was to develop a mathematical model to determine the entry length for fluidized bed drying. Volumetric heat transfer coefficient is required in this model. The model made it possible to calculate the temperature and absolute humidity of drying gas versus the length of dryer. The goal of our work was to propose a new method for scaling up fluidized bed dryers using a volumetric heat transfer coefficient.

ACKNOWLEDGEMENT

This paper was supported by Richter Gedeon Talentum Foundation (H-1103 Budapest, Gyömrői str. 19-21, Hungary), and by Hungarian Scientific Research Found (OTKA-116326).

REFERENCES

[1] Zahed, A.H., Zhu, J.-X., Grace, J.R.: *Modelling and Simulation of Batch and Continuous Fluidized Bed Dryers.* Drying Technology, 13(1-2), 1-28., 2007.
[2] Burgschweiger J., Tsotsas E.: *Experimental investigation and modelling of continuous fluidized bed drying under steady-state and dynamic conditions*. Chemical Engineering Science, 57(24), 5021-5038, 2002.
[3] Roy, P., Vashishtha, M., Khanna, R., Subbarao D.: *Heat and mass transfer study in fluidized bed granulation—Prediction of entry length*. Particuology, 7(3), 215-219, 2009.
[4] Walton, J.S., Olson, R.L., Levenspiel, O.: *The partial coefficient of heat transfer in a drying* fluidized bed. Chem. Eng. Sci., 44, 1474-1480, 1952.
[5] Ng, WK., Tan, RBH.: Case study: *Optimization of an industrial fluidized bed drying process for large Geldart Type D nylon particles*. Powder Technology, 180(3), 289-295, 2008.
[6] Kumaresan R., Viruthagiri, T.: *Simultaneous heat and mass transfer studies in drying ammonium chloride in a batch-fluidized bed dryer*. *I*ndian Journal of Chemical Technology, 13(5), 440-447, 2006.
[7] Ciesielczyk, W.: *Analogy of Heat and Mass Transfer During Constant Rate Period in Fluidized Bed Drying*, Drying Technology, 14(2), 217-230, 1996.
[8] Alvarez, PI., Shene, C.: *Experimental determination of volumetric heat transfer coefficient in a rotary dryer*, Drying Technology, 12(7), 1605-1627, 1992.
[9] Poós T., Szabó V.: *Application of volumetric heat transfer coefficient on fluidized bed dryers*, 8th International Symposium on Exploitation of Renewable Energy Sources, 72-75, 2016.
[10] Kollár B.: *Numerical Solutions of Differential Equations*. University of Pécs, 2010.

INTERNATIONAL SCIENTIFIC CONFERENCE ON ADVANCES IN MECHANICAL ENGINEERING
13-15 October 2016, Debrecen, Hungary

CHANGE IN THE MECHANICAL PROPERTIES OF GLASS-REINFORCED VINYL ESTER RESIN UNDER CHEMICAL EFFECTS

SZAKÁL Zoltán PhD, SCHREMPF Norbert PhD, KORZENSZKY Péter PhD, KARI-HORVÁTH Attila PhD, PATAKI Tamás PhD

Szent István University, Faculty of Mechanical Engineering, Institute for Mechanical Engineering Technology, Gödöllő H-2100. Páter K. út 1.
E-mail: szakal.zoltan@gek.szie.hu

Abstract
In this project the mechanical properties of acid-treated glass fibre reinforced vinyl Ester resin sheets were tested. The plastic specimens have been exposed in chemicals for different time at room temperature. The liquids used for the test were acids and oils. The acids were nitric acid (HNO3), hydric chloride (HCl), phosphoric acid (H3PO4), and the oils were engine oil (5W40) and bio ethanol (E85). The specimens were attacked for 1 - 2 - 4 - 16 - 24 hour with the mentioned chemicals respectively. The goal of the tests was to clarify the deterioration of the mechanical properties of the glass-reinforced vinyl ester resin. Tensile and flexural tests were carried out. The used acids and oils ruined the structure of the polymer therefore the mechanical properties changed a lot. The trends of the different deterioration processes were set.

Keywords: acid, glass-fibre, resin, vinyl ester

1. INTRODUCTION

In this project we made some measure to determine the properties of Green Tech platter. Green Tech platter was made of glass fibre reinforced vinyl Ester resin. If a chemical tank wear through is used in the Green Tech platter. In this device can restrain the environmental disaster. It collect the flowing fluid from the tank, the chemical composition can't flow to the ground. The during the process effect different chemical material in different time for this Green Tech platter. During the working time the workers step on this material surface. In same time are the mechanical and chemical effects. The examination was in the SZIE lab. We simulated the step of the workers on the platter with tensile test and three point bending tests.
The standard is MSZ EN ISO 14125 for glass-reinforced resins. The tensile test machine was the Zwick Roell Z100. This machine use Test Expert II software.
Five times repeated the measure. This platter is available in the trade market. The plastic specimens have been exposed in chemicals for different time at room temperature. The liquids used for the test were acids and oils. The acids were nitric acid (HNO3), hydric chloride (HCl), phosphoric acid (H3PO4), and the oils were engine oil (5W40) and bio ethanol (E85). The specimens were attacked for 1 - 2 - 4 - 16 - 24 hour with the mentioned chemicals respectively.

2. EXPERIMENTAL

2.1. Material

Fibre reinforced plastic composites include two major constituents: resin matrix and the fibre reinforcement. Unlike blends, in composites its construction parts fibres and the matrix maintain

their identities and together produce properties that could not be achieved with either acting alone. The fibres are high strength and are normally responsible of the loadbearing properties of composites. The matrix resin keeps the fibres orientated. The load on a FRP composite material is distributed into the fibres through the resin matrix. The matrix is responsible of the shear properties, maximum operating temperatures and the chemical resistance of the compo site. Still the mechanical prope rties cannot be predicted straight from the components because the properties originate from various complex mechanisms. Fillers and reinforcements improve properties but may reduce or degrade other performances at the same time. Tailoring composite properties is basically development of the specific mixture of polymer, reinforcements and fillers.

Chemical

The vinyl ester resins are thermosetting resins that consist of a polymer backbone with an acrylate (R=H) or methacrylate ($R=CH_3$) termination. Although vinyl ester resins have sometimes been classified as polymers, they are typically diesters that (depending on the polymer backbone) contain recurring ether linkages. The backbone component of vinyl ester resins can be derived from an epoxide resin, polyester resin, urethane resin and so on, but those based on epoxide resins are of particular commercial significance.

Chemical characteristics

The vinyl esters resins can be used in a neat from or they can contain either a vinyl-type relative comonomer (e.g. styrene, vinyl toluene, and trimethylol propane triacrylate) or a nonreactive diluent (e.g. methyl ethyl ketone and toluene). Typically, the methacrylate vinyl ester resins contain styrene and are used in chemical-resistant fiberglass-rein-forced plastics, whereas the acrylate vinyl ester resins are supplied undiluted, with appropriate coreactants added during the formulation of ultraviolet coatings and inks. The physical and handing properties of vinyl ester resins depend on the source of vinyl termination (methacrylate or acrylate), the amount and type of coreactants, and the type and molecular weight of the resin backbone. Upon cure, the styrenated methacrylate vinyl ester resins exhibit excellent resistance to acids, based, and solvents. The acrylate vinyl ester resins are more susceptible to hydrolysis than the methacrylate vinyl ester resins and thus are not generally used in applications requiring premium chemical resistance.

Glass reinforced vinyl

The reinforcing phase of the composite provides the material with strength and stiffness. Reinforcements are usually fibres or particulates. Normally the reinforcement is harder, stiffer and stronger than the matrix material. Particulate reinforcements are spherical, platelets or other shapes or forms; their aspect ratio is clearly smaller than that of fibres. Particulate reinforced plastics tend to be much weaker than fibre reinforced composites, but they are usually much cheaper. Fibre reinforcements are made of continuous fibres or discontinuous fibres. This research focuses on continuous fiberglass reinforced plastic composites.

Glass is an amorphous material and is based on silica backbone with many oxide components to improve specific properties. Glass fibres are made of silica sand, limestone, boric acid and smaller amounts of clay, coal and fluorspar. There are many types of glass fibres with specific properties and compositions. E-glass is the most commonly used type with good electrical and weathering properties, dimensional stability, good strength and stiffness, moisture resistance and most of all low cost.

Mechanical Testing

Premium mechanical properties are the hallmark of vinyl esters, and high heat resistance is a key characteristic for novolac vinyl esters. Thus, physical testing is required as a part of this study to evaluate higher thermal performance novolac vinyl esters. The validation of these candidates mechanically begins with testing nonreinforced clear cast specimens. Clear casts were prepared by curing the resins with 1% TBPB and post curing as outlined in the experimentation section.
The laminates and clear cast specimens of the various resins were mechanically tested on an Zwick Roel Z series Universal Testing System via MSZ EN 6892 (tensile).

2.1. The strength tests of the bonded connections

We examine the specimens prepared for the experiment plan adequately on a tensile-test machine, according to DIN EN 1465 standard. Although the standard mentions more solutions onto the forming of the specimens, we elected the simple overlap joining. Its disadvantage, is tensile-tests that not clear shearing stress affects the gluing, identical forming is at disposal of all of the specimens at the same time. The knowledge of the absolute result is not necessary in the interest of the comparison because of this. We executed 5 repetitions in the course of our measurements. Thewas managed by a Zwick Roell Z100 tensile test machine (Fig. 1.). The maximum tensile load is 100kN of the tensile-test machine.

Figure 1 Zwick Roell Z100 tensile-test machine

Specimen

We made specimens for measure of the mechanical properties of Green Tech platter. The fig. 2 show the base dimensions. The "*h*" is the thickness of the specimen, this dimension was not had to work. This dimension is checked always.

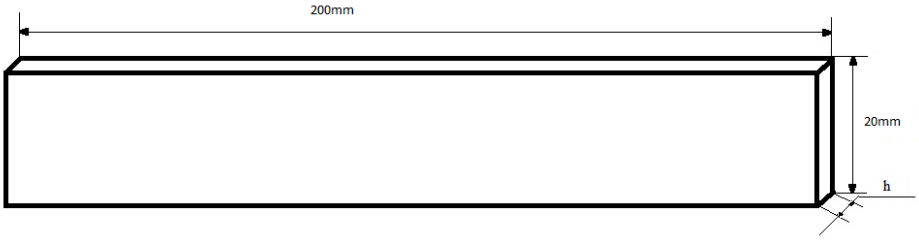

Figure 2 Dimensions of specimen

The specimens was made 5mm thickness material. We cut the specimens from plate. Produce tolerance is 0,2 mm in the dimensions of specimen. The fig. 3 show the specimens.

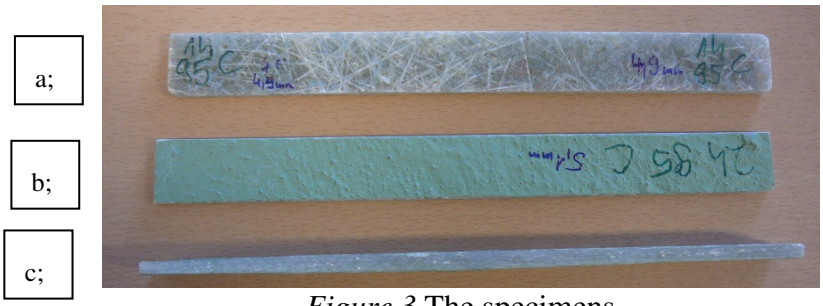

Figure 3 The specimens
a; the specimens back b; the specimen front c; the specimen axe

The measured material one side is without coating or another side is anti-sleep coating (green). The specimen consist 60 -70% glass fibre reinforced. The glass fibre has an irregular structure inside specimen.

3 RESULTS

In this project we made some measure to determine the properties of Green Tech platter. Green Tech platter was made of glass fibre reinforced vinyl Ester resin. If a chemical tank wear through is used in the Green Tech platter. In this device can restrain the environmental disaster. It collect the flowing fluid from the tank, the chemical composition can't flow to the ground. The during the process effect different chemical material in different time for this Green Tech platter. During the working time the workers step on this material surface. In same time are the mechanical and chemical effects.
The plastic specimens have been exposed in chemicals for different time at room temperature. The liquids used for the test were acids and oils. The acids were nitric acid (HNO_3), hydric chloride (HCl), phosphoric acid (H_3PO_4), and the oils were engine oil (5W40) and bio ethanol (E85). The specimens were attacked for 1 - 2 - 4 - 16 - 24 hour with the mentioned chemicals respectively. The goal of the tests was to clarify the deterioration of the mechanical properties of the glass-reinforced vinyl ester resin. Tensile and flexural tests were carried out. The used acids and oils ruined the structure of the polymer therefore the mechanical properties changed a lot. The trends of the different deterioration processes were set.
The H_2SO_4 acid form the examined fluid corroded the specimen just. Effect of the acid can be see. The first specimen's surfaces (1 hour long was in acid) was corroded by acid. The acid corroded the anti-slip surface. The glass fibre was undamaged. The glass fibre was damaged when the specimen was in acid in 16 hour long. The resin was vanished when the specimen was in acid in 24 hour long. The acid total damaged the specimen. Effect the acid show the fig. 4.

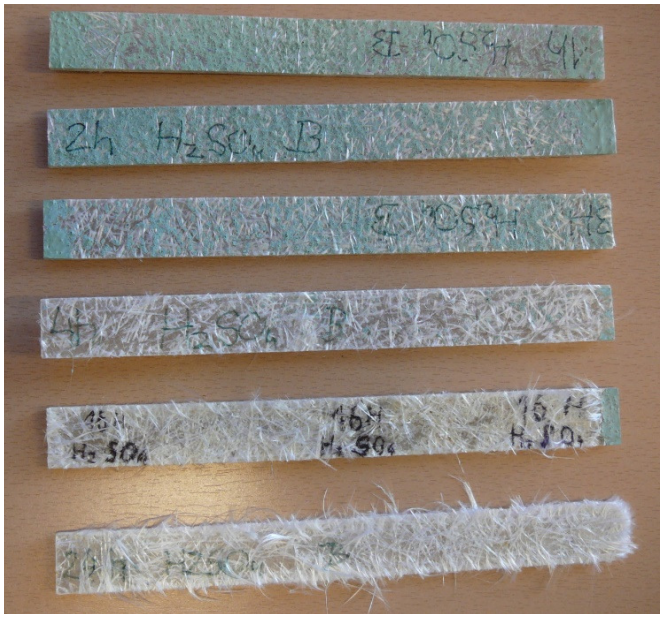

Figure 4 The etheched specimens

Mainly the acid damaged the resin. You can see the diagram that the effect of acid reduce the strength. The tensile force is 1800 N effected of 24 hour long acid.

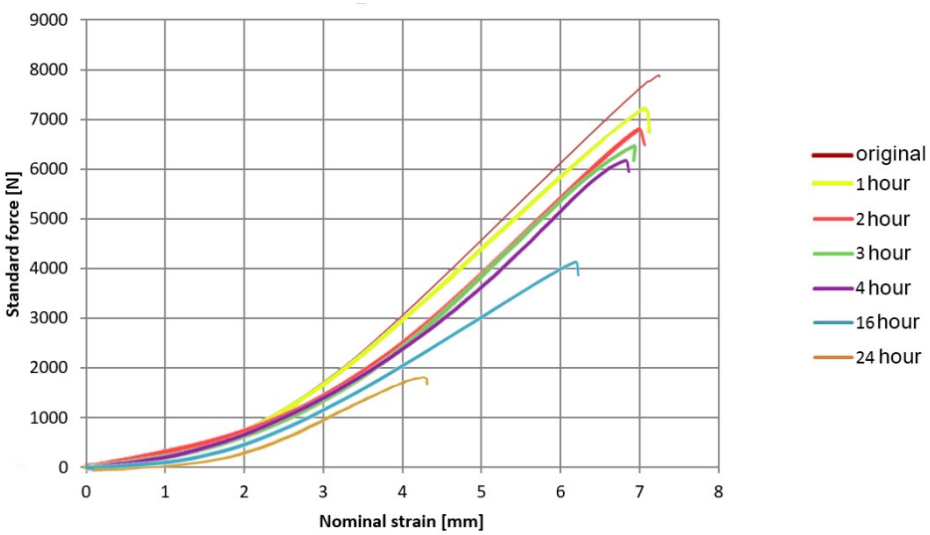

Figure 5 Result the tensile test

CONCLUSIONS

It is not to easy to compare the examinations because the material thickness is inhomogeneous. During the measure the „h" thickness was changed between 5,6-5,7 mm.
The streng test of polimer materials showed us, that in the case of the same material properties is the 10% standard deviation is normal. Only the H_2SO_4 acid from the examined fluid corroded the specimen. The specimens were damaged. The effect of acid is linear. If the specimen is in the acid for a long time, than the ulitimate tensile streng will low. After 16 hours reduced the strength of speciemens in half. The stregth of the test material reduced a short time if it reached acid H2SO4. The specimen surface was corroded after one hour later. This tools usually use in case of an accident, if the tools reach the acid than musnt use any more. Due to the acid for 24 hours did not

allow the liquid through the material. The strength is reduced, but the liquid solution inside. None of the other sample liquid does not damaged the material.

REFERENCES

[1] Metthew B. George Lubin, Handbook of composites, Houston, Texas, pp 38-49
[2] Kelly, Mark E. "Vinyl Ester Resins Applications." Unsaturated Polyester Technology. Ed. Paul F. Bruins. New York: Gordon and Breach, 1976.
[3] Zhanhu Guo, Kenny Lei, Yutong Li, Ho Wai Ng, Fabrication and characterization of iron oxide nanoparticles reinforced vinyl-ester resin nanocomposites, Composite Science and Technologies, Volume 68, Issue 6, P1513-1520
[4] A.L. Nazareth da Silva, S. C. S Teixeria, A.C.C WIdal, F.M.B CCoutino, Mechanical properties of polymer comosites based on commercial epoxy vynil ester resin and glass fiber, polimer Testing, Volume 20, Issue 8, p 895-899
[5] Edwin P. Plueddemann, Chemical of Silane Coupling Agents, Silance Coupling Agents, PP 31-54
[6] I.K. Varma, B. S. Rao, M.S. Choudhary, V. Choudhary, D.S. Varma, Effect of styrene on properties of vinil ester resin, Macromolecular Materials and Engineering, Volume 130 Issue 1, p 191 - 199

INTERNATIONAL SCIENTIFIC CONFERENCE ON ADVANCES IN MECHANICAL ENGINEERING
13-15 October 2016, Debrecen, Hungary

MEASUREMENT OF THE ELECTROMAGNETIC AND DYNAMIC CHARACTERISTICS OF A SERIES WOUND DC MOTOR

[1]SZIKI Gusztáv Áron PhD, [2]KISS János, [3]SZÁNTÓ Attila, [4]GÁL Tibor

[1]Department of Basic Technical Studies, Faculty of Engineering, University of Debrecen
szikig@eng.unideb.hu
[2]Debreceni Képző Központ
kissjanos.mano@gmail.com
[3]Department of Mechanical Engineering, Faculty of Engineering, University of Debrecen
szanto930922@freemail.hu
[4]Department of Electrical Engineering and Mechatronics, Faculty of Engineering, University of Debrecen
tiborgal991@gmail.com

Abstract
In our previous publication [1], we presented a model for serial wound DC motors and also described a simulation program that is based on this model and was developed in MATLAB environment. The present publication gives an insight into our experimental work in the course of which we measured the electromagnetic and dynamic characteristics (electric resistances, dynamic inductances, bearing resistance torque) of the above motor. From the measured characteristics, the program simulates the operation of the motor, calculating its torque, rpm and current intensity, as a function of time. To check the accuracy of the measured characteristics, and also the proper operation of our program, we carried out locked rotor response test measurements on the motor and compared their results with the simulated ones.

Keywords: *series DC motor, electromagnetic characteristics, dynamic simulation, MATLAB*

1. MOTOR MODEL

The motor model that we have presented in our previous publication [1] is based on the following differential equations [2]:

$$U_{táp} - \left(R_a + R_g\right) \cdot I - \left(L_a(I) + L_g(I)\right) \cdot \frac{dI}{dt} - L_{ga}(I) \cdot \omega \cdot I = 0 \qquad (1)$$

$$L_{ga}(I) \cdot I^2 - M_{terh}(\omega) - M_{ell}(\omega) = J_m \cdot \frac{d\omega}{dt} \qquad (2)$$

In the equations, $L_a(I)$, $L_g(I)$ and $L_{ga}(I)$ are the self dynamic inductances of the armature and main field winding respectively, and the mutual dynamic inductance [2]. All the above quantities depend on the intensity of current flowing through the motor. Quantities $M_{terh}(\omega)$ and $M_{ell}(\omega)$, are loading torques on the motor, which depend on its rpm. The former one comes from the motor moving the vehicle, while the latter one is the result of the bearing resistance of the rotor of the motor. Quantity J_m is the moment of inertia of the above rotor. Characteristics $L_a(I)$, $L_g(I)$, $L_{ga}(I)$ and $M_{ell}(\omega)$ have to be measured [2]. The value of J_m can be found in the catalogue of the motor, or it have to be measured. Characteristic $M_{terh}(\omega)$ is calculated by the program from the data of the vehicle driven by the motor. In *Figure 1*, we can see the block diagram of the simulation program created on the basis of differential equations (1) and (2).

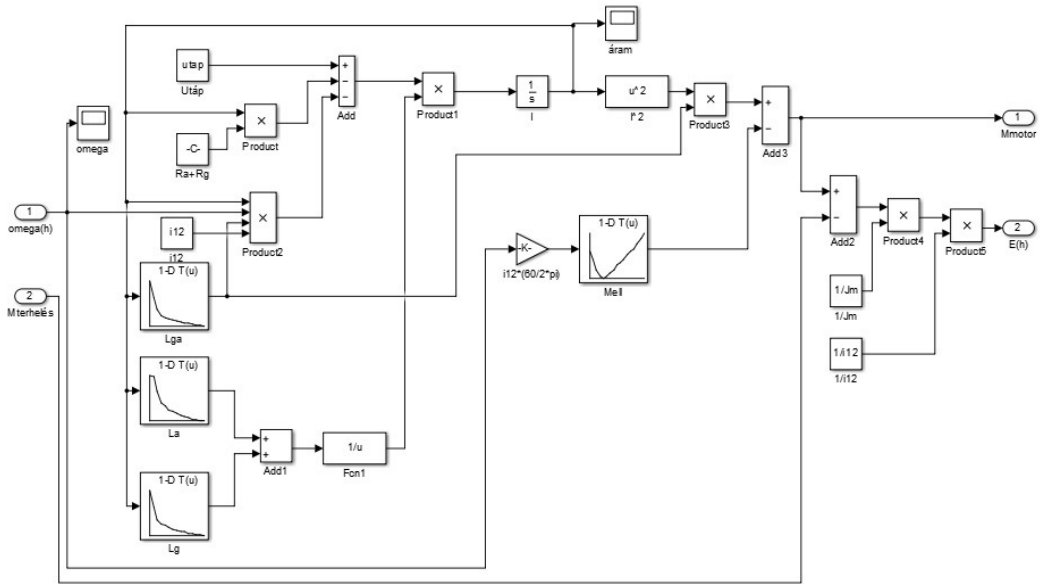

Figure 1 The block diagram of our motor model [1] created in MATLAB [3] environment.

The motor model can be connected to the vehicle model [1,4,5] through input and output ports 1 and 2. Electric resistances R_a and R_g are represented in the above block diagram as constants, while dynamic inductances $L_a(I)$, $L_g(I)$ and $L_{ga}(I)$ and bearing resistance torque $M_{ell}(\omega)$ in the form of „Lookup Tables". In the following we present the experimental set-up that was applied for measuring of the above electromagnetic and dynamic characteristics, and – as an example – we give the detailed description of the measurement process of electric resistances. In the case of dynamic inductances, bearing resistance torque and locked rotor response tests the above description – together with the obtained results – will be published elsewhere.

2. MEASUREMENTS

For the measurements the experimental set-up in *Figure 2* was used.

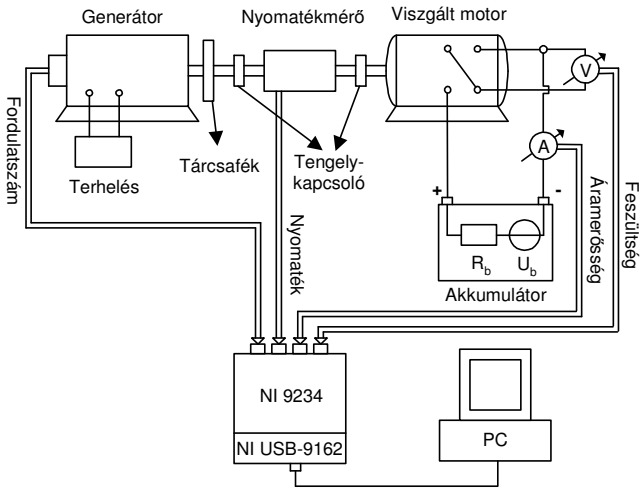

Figure 2 Experimental set-up that was applied for the measurements

Figure 3 shows the experimental arrangement that was applied for the measurement of electric resistances.

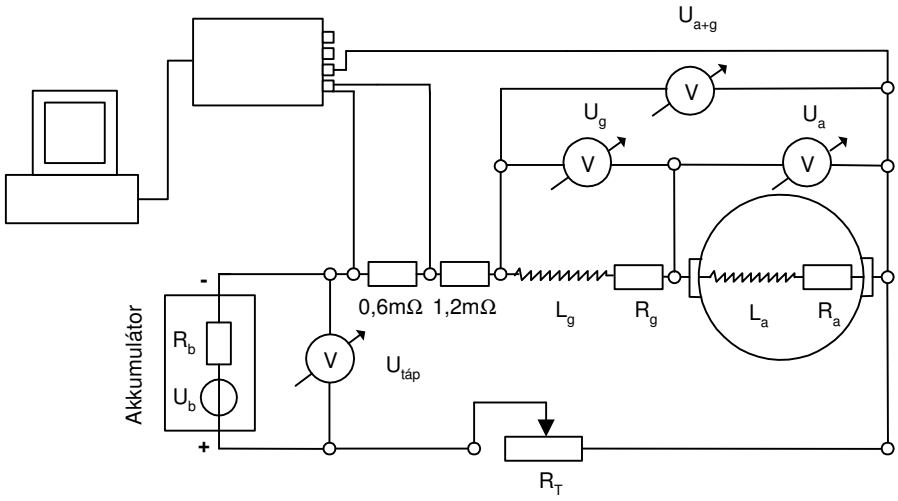

Figure 3 Experimental set-up for the measurement of electric resistances

During the measurements of electric resistances the rotor of the motor was fixed with a disc brake (*Figure 2*). As a DC supply, an accumulator with nominal voltage of 12 [V] was used. The intensity of current was varied in the 0-190 [A] range adjusting the resistance of the load resistor (R_T). The measurement of current intensity was realised as measurement of voltage on a shunt resistor (0.6 mΩ) with a NI 9234 dynamic signal acquisition module, which was connected to the PC through an NI USB-9162 Hi-Speed USB carrier. The voltage was measured on the main field and armature winding separately and also on the windings in a series connection with digital multimeters. In the later case the voltage was also measured with the NI 9234 device independently. The difference between the voltages measured with the two different devices was less than 1%. *Figure 4* shows voltages measured on the two windings separately and also in series.

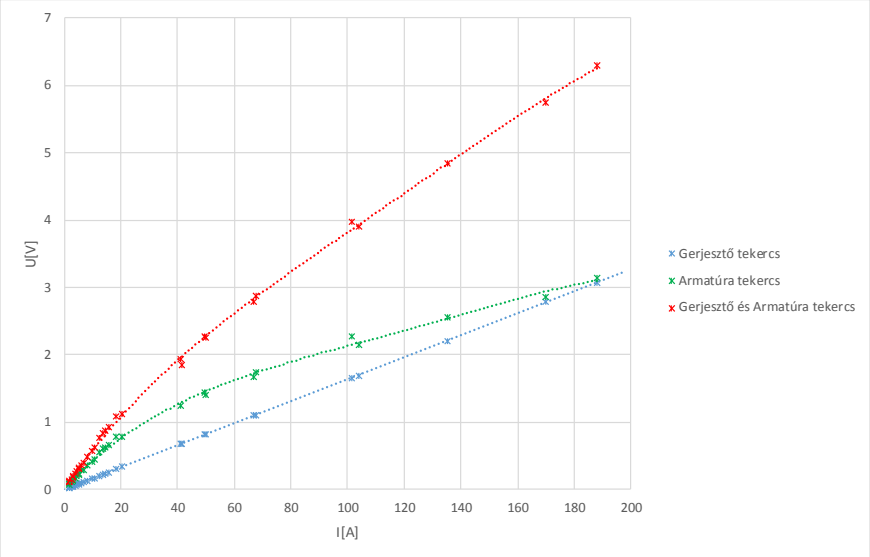

Figure 4 Voltages measured on the main field and armature windings separately and in series

The figure clearly shows that in case of the main field winding the connection between current intensity and voltage is linear, in accordance with Ohm's law, while in case of the armature winding it is nonlinear. It is important to emphasise hear that the multimeter was connected to the armature winding through carbon brushes. We suppose that the contact voltage between the copper segments

of the motor and the carbon brushes cause the above nonlinear behaviour. We intend to study the above phenomenon in details in the near future.

CONCLUSIONS

The electromagnetic and dynamic characteristics (electric resistances, dynamic inductances, bearing resistance torque) of a series wound DC motor were measured. These data are input parameters of our MATLAB program which has been developed for the dynamic simulation of the motor. The accuracy of the measured characteristics and also the proper operation of our simulation program were checked by locked rotor response tests. During the tests DC power was switched on the locked rotor motor, and the rise of current intensity and torque were measured and simulated. The difference between the measured and simulated data – in the case of saturation values – is less than 1%. In this brief publication we have given an insight into the above mentioned experimental work by presenting the applied experimental set-up for the measurements, and also the experimental arrangement and measurement process in the case of electric resistances. The same description and data for dynamic inductances, bearing resistances torque and locked rotor response tests will be published elsewhere.

REFERENCES

[1] Szántó, A., Szíki, G.Á., Hajdu, S.: *Soros gerjesztésű egyenáramú motorral hajtott versenyautó dinamikai modellezése*. Műszaki tudomány az Észak-Kelet Magyarországi régióban 2016, Debreceni Akadémiai Bizottság Műszaki Szakbizottsága, Debrecen, 406-414., 2016.
[2] Miralem, H., Matic, B., Bojan Š,, Ivan Z,: *Magnetically Nonlinear Dynamic Model of a Series Wound DC Motor.* Przeglad Elektrotechniczny (Electrical Review), ISSN 0033-2097, 87(12b), 2011
[3] Matlab 2014b, The MathWorks, Inc, Natick, Massachusetts, United States.
[4] Sziki, G.Á., Hajdu, S., Szántó, A.: *Vehicle Dynamics Modelling of an Electric Driven Race Car*. International Scientific Conference on Advances in Mechanical Engineering proceedings, Debrecen, Hungary, 2015.
[5] Szántó Attila: *Elektromos hajtású tanszéki versenyautó járműdinamikai modellezése.* TDK dolgozat, Debreceni Egyetem Műszaki Kar., 2015.

INTERNATIONAL SCIENTIFIC CONFERENCE ON ADVANCES IN MECHANICAL ENGINEERING
13-15 October 2016, Debrecen, Hungary

TRENDS AND DEVELOPMENTS ON THE SURFACE- AND EDGE QUALITY OF BIOCERAMICS

[1]TAKÁCS Annamária, [2]GYURIKA István Gábor PhD

[1]Institute: University of Pannonia
E-mail:takacs.annamari17@gmail.com
[2]Institute: University of Pannonia
E-mail:gyurika@almos.uni-pannon.hu

Abstract
Medical use of bioceramic materials is accepted more widely which stimulates science to continuously improve production technologies. As the number of implants implanted in a year increases rapidly, innovation of their lifespans and their roles is essential. These days it is hard to find an area in medical technology where prostheses are not used. Therefore the generic term includes a wide variety of products which need to satisfy quite distinct and unique requirements.
In this article an overview on the modern technical solutions through the presentation of the most frequently used prosthesis types are provided. The analysis in this article summarizes the main development directions in the individual fields. The test were made from the aspect of surface quality and edge quality. As a result the deficiencies of these technologies were disclosed. Eventually proposals were formulated to improve the affected production technologies in this field.

Keywords: *Bioceramic, prosthesis, surface quality, dental, rapid prototyping.*

1. INTRODUCTION

In the last two decades medical technology in respect of prostheses has shown a rapid development. One of the motivations for this is the varied complaints of the patients, as well as the improvement of the quality of life for the more and more often affected younger age group. For this reason not only do the prostheses need to supply an even more versatile function, but during design their lifetime is key as well.
Today's expectation towards an implant is that the patient can live with it without it needing to be replaced. One condition on this is that the prosthesis can resist the effects of the human body. Furthermore its material needs to be biocompatible so no toxic substances can be dissolved from it. After the implantation its role is performed, it does not move, it does not loose.
The progression of medical technology proceeds in the direction of implants that can cooperate with the human body. In this context many experiments are performed, and based on those it can be implied which conditions need to be satisfied by the different prostheses. It is important to note that the design parameters differ from prosthesis to prosthesis. No unified conditions can be formulated, so a complete mapping of functions is needed in order to adapt the prosthesis to the individual or to the project.
During the research prostheses made from bioceramic were examined. Many of the implants used in medical technology are in need of refinement where bioceramic materials are used. Such prostheses are made from bioceramic that are usually for replacement of joints and osteoplasts, so these limb prostheses will be discussed in another article.
Among the parameters examined surface and edge quality are the most important. These factors were tested for two main areas: prostheses made by chipping and made by rapid prototyping. In

case of the first area current scientific knowledge is going to be summarized in connection with dental prostheses. In case of the second area quality limits of surface quality of prostheses produced by additive proceedings were explored.

2. MEDICAL TECHNOLOGY APPLICATIONS OF BIOCERAMICS

During our research diversified literature on prosthesis material for bioceramic was found. Hip abrasion is one of the first problems which was solved by prosthesis. By the current scientific knowledge bioceramic-metal combined implants are implanted in the patients [2] [3]. Locking to femur is done with the stem that is made of titan but in most cases a bioceramic coating is also found on it. The cup is directly joined to the pelvis which matches the stem in its material compilation [1].
Another important joint related to a musculoskeletal is the knee. Here similar bioceramic-metal prostheses are used similar to the ones in the case of the hips [3]. The problems can come from the same reasons [4]. The more customized solutions are needed in the field of osteoplast. Due to unique formations complex geometric production is needed.
One of the implanted prosthesis that needs to be aesthetic is prosthetic dentistry. Thanks to this bioceramic materials have come into view [8] [10]. Most often zirconia is used because in appearance it resembles real teeth so much that it can be mistaken for it [9] [10]. Besides, it is important to note that this feature is kept which means that it resists the effects of the mouth. By modern prosthetic dentistry a zirconia crown is attached to a titan screw and it is placed in the patient's mouth. The titan screw is implanted in the jaw.

3. TECHNOLOGIES APPLIED BY PRODUCTION OF BIOCERAMIC JOINT REPLACEMENT AND OSTEOPLAST IMPLANTS

Processing of bioceramics can be divided into two groups. By the traditional subtractive technology material is subtracted from an existing block of green part. By the additive method there is no green part but the product is built from scratch.
Micro-cutting is classified as a subtractive technology of prostheses made from bioceramic. During this a 3D geometry planned by a CAD/CAM system is manufactured from a block of green part by micro-cutting with a CNC machine. The initial part is usually produced by powder metallurgy and is already sintered. Accordingly raw processing and hard processing is distinguished. By the former, additional heat treatment is required so the surface roughness peaks generated during processing would disappear. By the other method no further sintering is needed which means that there is no size change resulting uncertainty, however polishing could be required [5].
Those technologies belong to the additive group that build the products from layers. In the study of Kumar and his associates [6] a summary of these is found. In *Table 1* the technologies and their descriptions are listed with which bioceramic material can be produced [6] [7].

Table 1 Additive technology

Technology name		Short description
LCM	Litography-based Ceramic Manufacturing	Body shaping by ceramic suspension that solidifies due to UV light.
3DPP	3D Powder Printing	In the appropriate points of the given layer liquid binder is dosed that fixes the grains. For the fixing of the green part sintering is required.

3DPL	3D Plotting	A mixture of ceramic and polymer is extruded by the printhead then the melt is dosed in the proper place.
CIJ	Continuous Inkjet	Continuous fluid jetting printing where the liquid is mixed from ceramic and binder, the placement of streams is created by potential difference. For the fixing of the green part sintering is required.
DOD	Drop on Demand	Continuous fluid jetting printing where the liquid is mixed from ceramic and binder, the streams are placed in a mechanically controlled manner. For the fixing of the green part sintering is required.
EIJ	Electrostatic Inkjet	Continuous fluid jetting printing where the liquid is mixed from ceramic and binder, the streams are placed in an electrostatically controlled manner. For the fixing of the green part sintering is required.
	Bioprinting / Bioplotting / Biofabrication	Printing of such bioceramic materials during which different scaffolds can be found in the material to be printed. Scaffolds aid the tissue formation in the place of the implantation. In protection of the scaffolds these prints are executed at low temperature.
SLS	Selective Laser Sintering	Consolidation of ceramic dust layer by layer with laser.
FF	Freeze Foaming	Boiling of suspension in a way that the boiling point is offset towards the room temperature by decompression, then form fixing by sudden cooling.
	Ceramic thermal spray coating	Shaping of ceramic coating during which smouldering ceramic grains are sprayed on the surface to be coated.

4. RESEARCH RESULT REGARDING DENTAL IMPLANTS

Dental implants made by chipping was one the emphasized areas where a more detailed research was performed. The function of an implant: to cater to all the essential functions that eliminates all the restrictions caused by the not properly working organ. The following requirements are to be satisfied by dental implants: low surface roughness, wear resistance, adequate hardness against chewing, resistance against the environment in the mouth, biocompatible material composition for the human body, appropriate optical features.
Dental implants are made by micro-cutting. For this a green part is necessary made by powder metallurgy. Depending on the extent of sintering used on the material by micro-processing, raw processing and hard processing can be distinguished.
Goeuriot and associates [8] tested the resulting fragmentation measurements by different material composition, chipped enstatite as well as in the case of ordinary ceramics using a weight-load-cutting testing machine. Based on their research it was shown that the fragmentation rate is the lowest by the lowest chipping speed in the group of materials that have emphasized hardness. Their further conclusion was that on the surface of enstatite materials no macroscopic alterations occurred when effected by force input however by the glass-ceramic it occurred.
Mitov and associates [9] tested the wear of real teeth and prostheses in the case of finishing with the help of a chewing simulator. The surface roughness of the speciments and the wear effect was near proportional, the greatest damage was made by the roughest speciment. On the other side the glass-ceramic speciments wore and the zirconia speciments did not. Furthermore it is established that the finer the microstructure of the material is, the better the surface quality is that can be reached during polishing.

In Song and associates' research [11] a feldspar dentistric prosthesis processing-experiment was made using a diamond drill. In case of smaller depth of cut smaller surface quality was measured. It was observed that as the feed rate increases, the rate of ductile deformation decreases while more and more microcracks appear. It is proved that the depth of cut has a greater effect on the surface quality than the feed rate.

5. RAPID PROTOTYPING – TECHNOLOGICAL LIMITS

These days additive production technologies gain space at a rapid pace. The reason for this is that the machines and base materials required are at proximity access. Production of prostheses sharpen towards customized products. The palette of technologies is extensive, however there are still a lot of limiting factors.
In the research of Kumar and associates [6] a summary can be found on these technologies. Based on this summary belonging limits to the production of bioceramic implants were collected (see in *Table 2*) and it is found that in most cases they have a connection with the surface quality [6] [7].

Table 2 Limits to the additive technologies

Technology name		Technological limits	Advantages	Disadvantages	Processable materials
3DPP	3D Powder Printing	Layer thickness: 20-100 µm Smallest size: 350-500 µm	No supporter material in needed, cheap, fast	Sintering needed which leads to product shrinkage	Metal, ceramic, polymer
3DPL	3D Plotting	Layer thickness: 40-1000 µm Smallest size: 100 µm	Processing at room temperature or at physiological temperature	Production of overhanging structures	Ceramic mixed with polymer
CIJ	Continuous Inkjet	Drop size: >50 µm	High speed, productive	Continouos ink supply, recycled ink can be contaminated, limited accuracy	Ceramic suspension
DOD	Drop on Demand	Drop size: 10-100 µm	Better control of streams, impulse generated streams		Ceramic suspension
EIJ	Electrostatic Inkjet		High accuracy		Ceramic suspension
SLS	Selective Laser Sintering	Layer thickness: 76-100 µm Smallest size: 45-100 µm	No supporter material in needed, high accuracy, no additional heat treatment, good mechanical attributes	Processed at high temperature so no scaffolds can be injected in the product	Metal, ceramic, polymer

6. FORMULATION OF DEVELOPMENT RECOMMENDATIONS

During literature research it became clear that the products need to satisfy different requirements by each prosthesis type. That is also true about the surface quality. This way no distinct development direction can be established, but it should be done type by type.
In the case of teeth implants produced by chipping the aim is to reach the best possible surface quality. Depending on their material prostheses can wear the enamel which leads to the loss of the existing real teeth. For development a specification of the still missing damaging mechanism is necessary. Parallel with this such prosthesis needs to be produced which has a material composition and surface quality matching the requirements and has no wear effect.
Meiszterics Anikó and associates proved by research that by every metal-bioceramic prosthesis the binding between the ceramic and the bone tissue is more durable [12]. There is also a chance that the ceramic-metal connection deteriorates earlier than the connection between the bone tissue and the ceramic. This causes the implant to loose and a replacement is required. For this reason science proceeds towards total bioceramic prostheses. However the determination of those ceramic compositions that are capable of replacing the metal parts by their enough high solidity is still necessary.
According to Ahlhelm and associates [13] the future of osteoplast are the prostheses that resemble the structure of real bones the most. This means primarily the tissue structure. Outside a solid, hard shell can be found and inside there is a porous, shock absorbent structure. Another important viewpoint that regarding the material composition of the implant, it should resemble the structure in the human body as much as possible. From the perspective of porosity the research of those parameters is required whereby such a structure can be produced in which both living tissue and vasculature can be settled down. By combining two different proceedings (LCM + FF) an implant was produced with a structure largely resembling the structure of real bones.
In the case of additive production technologies the finer grainy powder is produced, the better surface quality is reached. Those technologies will gain space where only a minimum amount of rework is necessary. By the sintering resulted shrinkage such an uncertainty factor is brought in the system that is not acceptable for future development.

CONCLUSIONS

In this article bioceramics that are more and more suitable for joint replacement and osteoplast were discussed. Based on the existing professional literature among the most often implanted implants are hip, knee and teeth implants and osteoplast. During the research it became clear that for every type of prosthesis a different set of requirements exists.
For this, different kind of production technologies are needed. Two main technological groups are distinguished: subtractive and additive proceedings. In the case of the former we could read more on the micro-cutting of the teeth implants. Additive technologies are greatly diversified so we gave a short summary on the continuously expanding list.
In order to specify development trends dental implants were discussed in greater detail. During this it was shown that the surface quality in case of a prosthetic dentistry needs to be excellent so that the enamel of the real teeth would not be worn. During processing surface quality is greatly influenced by the variable feed rate and the depth of cut. As final result it can be established that the larger the feed rate or the depth of cut, the higher surface roughness is developed.
In case of the rapid prototyping the technological limits of the proceedings suitable for processing bioceramic were examined. As a result it can be said that an uncertainty is caused by additional heat treatment. The grain size of the powder base material influences the porosity, the hardness, the density and the surface quality achievable by additional polishing of the manufactured product.

REFERENCES

[1] V. A. Dubok, V. V. Lashneva: *New materials and processes for improvement of hip prostheses.* Powder Metallurgy and Metal Ceramics, 49 (9-10), 575-580, 2011.
[2] Besim Ben-Nissan, Giuseppe Pezzotti: *Bioceramics Processing Routes and Mechanical Evaluation.* Journal of the Ceramic Society of Japan, 110 (1283), 601-608, 2002.
[3] John Dumbleton, Michael T. Manley: *Hydroxyapatite-Coated Prostheses in Total Hip and Knee Arthroplasty.* The Journal of Bone and Joint Surgery, Inc. J Bone Joint Surg Am, 86 (11), 2526-2540, 2004.
[4] Ezzet, Kace; Hermida, Juan; Colwell, Clifford; D'Lima, Darryl: *Oxidized Zirconium Femoral Components Reduce Polyethylene Wear in a Knee Wear Simulator.* Clinical Orthopaedics & Related Research, 428, 120-124, 2004.
[5] Dr. Borbély Judit: *Fogászati kerámiák II. rész: Oxidkerámiák.* Fogpótlástani Klinika, Semmelweis Egyetem, Fogorvostudományi Kar, 2015.
[6] Alok Kumar, Sourav Mandal, Srimanta Barui, Ramakrishna Vasireddi, Uwe Gbureck, Michael Gelinsky, Bikramjit Basu: *Low temperature additive manufacturing of three dimensional scaffolds for bone-tissue engineering applications: Processing related challenges and property assessment.* Materials Science and Engineering: R: Reports, 103, 1–39, 2016.
[7] Brian Derby: *Additive Manufacture of Ceramics Components by Inkjet Printing*. Engineering, 1 (1), 113–123, 2015.
[8] D. Goeuriot, J.C. Dubois, D. Merle, F. Thevenot, P. Exbrayat: *Enstatite Based Ceramics for Machinable Prosthesis Applications.* Journal of the European Ceramic Society, 18 (14), 2045–2056, 1998.
[9] Gergo Mitov, Siegward D. Heintze, Stephanie Walz, Karsten Woll, Frank Muecklich, Peter Pospiech: *Wear behavior of dental Y-TZP ceramic against natural enamel after different finishing procedures.* Dental Materials, 28 (8), 909–918, 2012.
[10] Niko Bärsch, Stephan Barcikowski, Klaus Baier: *Ultrafast-Laser-Processed Zirconia and its Adhesion to Dental Cement.* JLMN-Journal of Laser Micro/Nanoengineering 3 (2), 2008.
[11] Xiao-Fei Song, Ling Yin, Yi-Gang Han, Hui Wang*: Micro-fine finishing of a feldspar porcelain for dental prostheses.* Medical Engineering & Physics, 30 (7), 856–864, 2008
[12] Szíjjártó Anita/ ELTE: *Fém implantátum helyett biokerámia*. National Geographic Magyarország, 2012.
[13] M. Ahlhelm, P. Günther, U. Scheithauer, E. Schwarzer, A. Günther, T. Slawik, T. Moritz, A. Michaelis: *Innovative and novel manufacturing methods of ceramics and metal-ceramic composites for biomedical applications.* Journal of the European Ceramic Societ, 36 (12), 2883–2888, 2016.

INTERNATIONAL SCIENTIFIC CONFERENCE ON ADVANCES IN MECHANICAL ENGINEERING
13-15 October 2016, Debrecen, Hungary

TECHNOLOGICAL AND ECONOMIC ANALYSES OF A DIFFERENT DESIGNS SOLUTIONS OF A PIPELINE SUPPORTING STRUCTURE

[1]TATIC Uros, [1]DJORDJEVIC Branislav, [1]SEDMAK Simon, [1]VUCETIC Filip, [1]ARANDJELOVIC Mihajlo

[1]Innovation Center of Faculty of Mechanical Engineering
E-mail:taticuros@gmail.com

Abstract
The main goal of this paper was to determine the technological and economic aspects of a pipeline supporting structure related to the selection of different steel beam profiles. For that purpose, numerical models were made in ABAQUS, using IPE and HEA profiles, and were subjected to wind loads in order to calculate stress and displacement fields, wherein the calculations were performed in the elastic area of deformation. Based on these results it was possible to determine the savings in terms of raw material costs, along with the weight reduction of the whole metal construction. From these results, it was concluded that the construction made of IPE profiles was the cost-effective solution, due to its smaller weight, which also suggests that such a construction would be easier to manufacture and manipulate.

Keywords: *Metal constructions, steel profiles, numerical simulation, pipeline,*

1. INTRODUCTION

Metal constructions represent structures that are partly or completely made of metal materials. Each structure can be observed as a group of parts with individual loadings that together constitute one functional unit or assembly. Construction can be divided according to design, production type, and their application into bridges, buildings, means of transportation (boats, airplanes, trains, vehicles) and industrial facilities constructions (cranes, supporting bridges, transporters, excavators, diggers, reservoir, supports etc.). Steels are the most commonly used materials in metal constructions. During installation and production, metal constructions are characterized by minor needs for machine processing and easy and fast joining of metal parts and profiles.
According to the shape and form of used elements and according to general metal construction type, metal construction can be also divided into:

- Steel frame structure,
- Sheet metal structure.

The basic problem of designing of metal constructions and performing strength calculations comes down to solving one unknown using the remaining two known parameters. Relations between these three parameters are shown in the *Figure 1*.

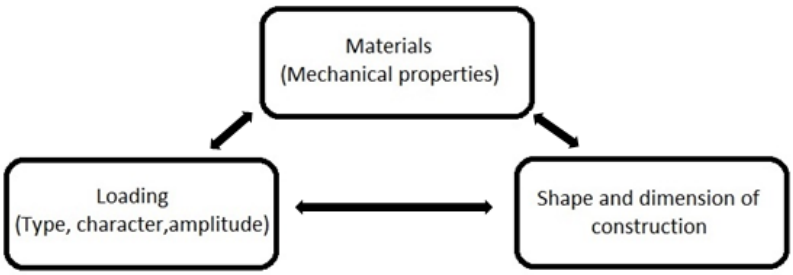

Figure 1 Relations used in metal construction calculation

The aim during each construction realization is the most economic utilization of materials that will satisfy construction purpose and loading conditions. Thus, used structural elements depend on these conditions.
These constructive elements can be divided into following groups:

- Lamellar and full cross-section beams
- Metal sheets
- Profile beams
- Complex profiles
- Cold sized profiles

Metal constructions have their own advantages and flaws. The main advantages include:

- The possibility of production of prefabricated whole constructions
- Minor machine processing (holes, grinding the edges, welding of joints)
- Easy adaptation to a new function
- Possibility of disassembling and shifting to a new location
- Possibility of combining different materials

Flaws of metal constructions include corrosion influence or other environmental influences that can cause fractures, delays etc. These fractures can cause economic losses, as well as human losses [1,2,3].
Results presented in this paper were obtained by numerical simulations used to perform optimization of a steel support structure in order to maintain best cost effectiveness, while using less material. It was designed as a steel frame construction made out of full cross-section beams and later reinforced during the design process with Profile beams in accordance with the results obtained during different stages of numerical simulations.

2. DESIGN SOLUTIONS

Initial design of a steel support structure is shown in *Figure 2*.X shaped cross beams were positioned only on the lateral sides as well as on the center hole on the top part. Structure is designed to be fixed to the ground using 2000mm x 2000mm plates with a use of four screws. Idea behind the design was to perform numerical simulations on both lateral, as well as vertical maximum loading in order to define week spots and areas of high stress concentration. Design was initially planned to be tested with different beam profiles in order to achieve maximumweight reduction and production savings [4]. Tube profiles denoted with A were designed to be eitherX shaped cross beams were positioned only on the lateral sides as well as on the center hole on the top part.

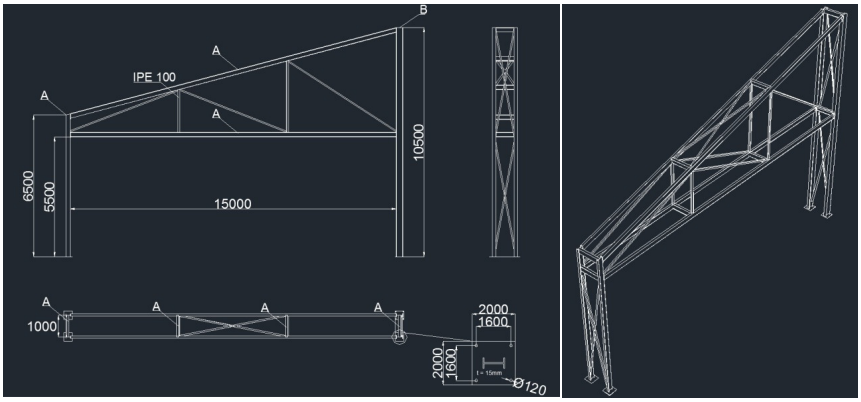

Figure 2 Initial design of a steel support structure

Structure is designed to be fixed to the ground using 2000mm x 2000mm plates with a use of four screws. Idea behind the design was to perform numerical simulations on both lateral, as well as vertical maximum loading in order to define week spots and areas of high stress concentration. Design was initially planned to be tested with different beam profiles in order to achieve maximum weight reduction and production savings. Tube profiles denoted with A were designed to be either IPE200 or HEA200, while lateral support beams denoted with B should be tested for IPE240 or HEA 240[5,6,7]. Technical specifications of the beam cross sections are shown in *Table 1*.

Table 1 Technical specifications of the beam cross section

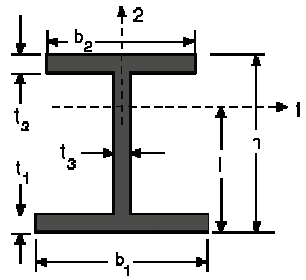	**IPE200**	**HEA200**	**IPE240**	**HEA240**
l [mm]	100	100	120	120
h [mm]	200	190	240	230
b1[mm]	100	200	120	240
b2[mm]	100	200	120	240
t1[mm]	8.5	10	9.8	12
t2[mm]	8.5	10	9.8	12
t3[mm]	5.6	6.5	6.2	7.5
A[cm^2]	28.5	53.8	39.1	76.8

Designed specifications require that in the case of using the HEA profile instead of IPE, it should be rotated by 90 degrees in order to obtain local orientation of the beams relative to the whole model. Initial idea was tested with a use of numerical simulation and it was determined that the design had a lot of weak points and insignificant rigidity. In order to perform adequate testing and evaluations, initial design was remodeled with added X shape stiffeners, as well as angular reinforcements. Wire frame of the adapted model with the boundary conditions can be seen in *Figure 3*, including a comparison with the original design.

X shaped reinforcements were also added with the use of IPE100 on all three hole sections at the top, as well as on the bottom two (on the edges). Angular reinforcements were created with a use of a rectangular tube profile with dimensions of 80mm x 80mm and wall thickness of 3mm. Resulting displacement of the initial model in comparison with the reinforced model (used in further testing), under the same transversal loading, can be seen in *Figure 4*. Applied loading to the model is transversal and has same value and distribution as the calculated loading defined by the third party manufacturer. Shown comparison is performed between models with IPE 200 and IPE 240 beams. Model without reinforcement has shown total magnitude of displacement of 107mm in the large area at the middle top hole. Already present X shape reinforcement within the middle hole has helped to add rigidity to the middle of the frame which resulted in additional stress of the top and bottom hole. Model with added reinforcement had shown displacement with a magnitude of 21 mm.

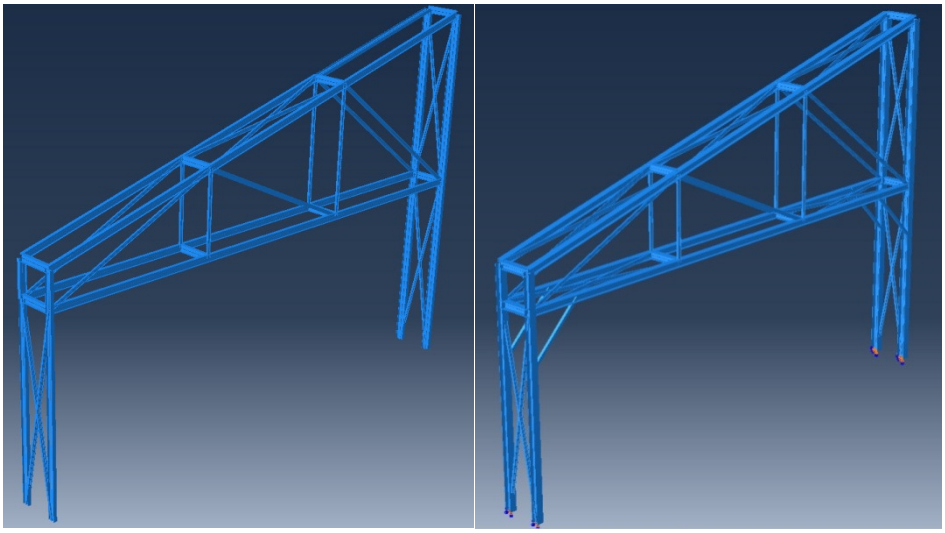

Figure 3 Initial design of a steel support structure (left), reinforced design of a steel support structure (right)

It is important to note that the displacement distribution has completely changed, and that the maximum displacement was now located at the middle of the reinforced holes in comparison to the area of the beam connection, and throughout two holes in the first model.

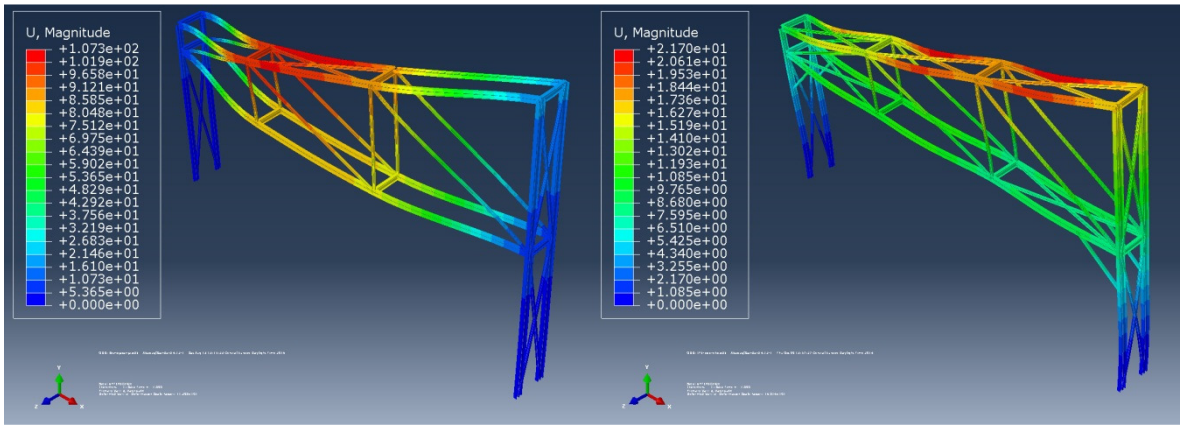

Figure 4 Displacement results of the initial model (left) in comparison to the reinforced model (right), under the same transversal loading

3. MATERIALS AND METHOD

Numerical simulation was performed within the boundaries of elastic deformation, with an Elasticity module of 210000 MPa and Poisson's ratio of 0.3 due to the fact that the biggest stresses in both of the models were below the yield stress. Aim of the simulations was not to determine which of the beams will provide sufficient structural resistance, but to determent what would be the difference in the both weight and the cost of each structure since both of the designs have shown passing results. After the modifications of the original designs were established two new models were created in order to assess the influence of different beam profiles used for the steel structure.
Model IPE was created with a use of IPE 200 beam profiles on the position A and IPE 240 beam profiles on the position B (*Figure 2*). Model HEA was created with a use of HEA 200 beam profiles on the position A and HEA 240 beam profiles on the position B (*Figure 2*). Rest of the beams were made using IPE 100 for the X shape reinforcements and rectangular tubes 80mm x 80 mm for

angular reinforcement on both of the models.
Loads applied on the model were determined by taking into account the extreme values of real wind loads [8]. Boundary conditions were defined as encastre at the bottom of vertical supports where model was fixed, anchored to the ground by 2000x2000 plates [9]. Depending on the position and direction of the beams the load was applied as uniformly distributed pressure acting along each beam, with values ranging from 0.08 to 0.425 kN/cm^2. These loads were defined by the third party manufacturer specification and were determined and calculated by taking into account the extreme values of real wind loads measured in the area where the structure will be used. Calculations were performed individually for the case of lateral, as well as longitudinal loading [10].
Obtained parallel results for the IPE and HEA models with reinforcements for both loadings can be seen in *Figures 5* and *6*.

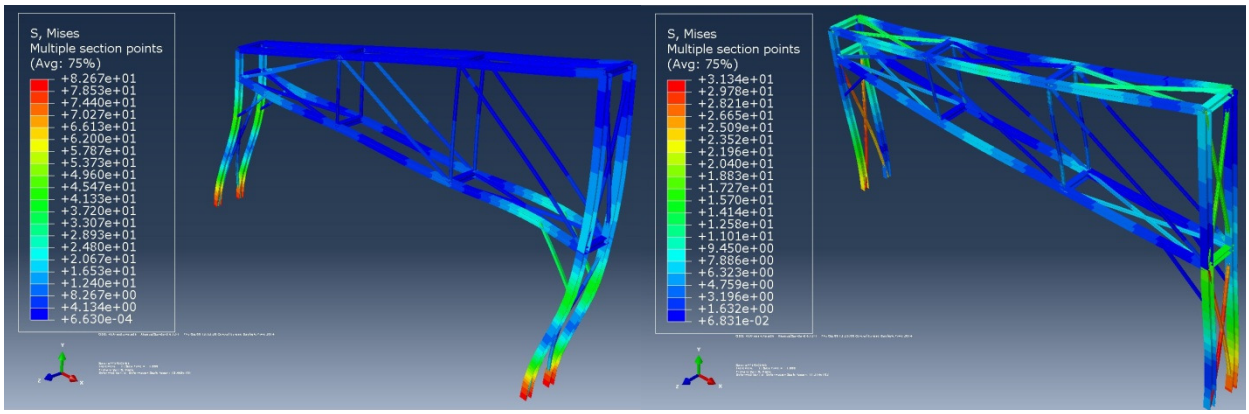

Figure 5 HEA model stress field caused by the longitudinal load (left),HEA model stress field caused by the lateral load (right)

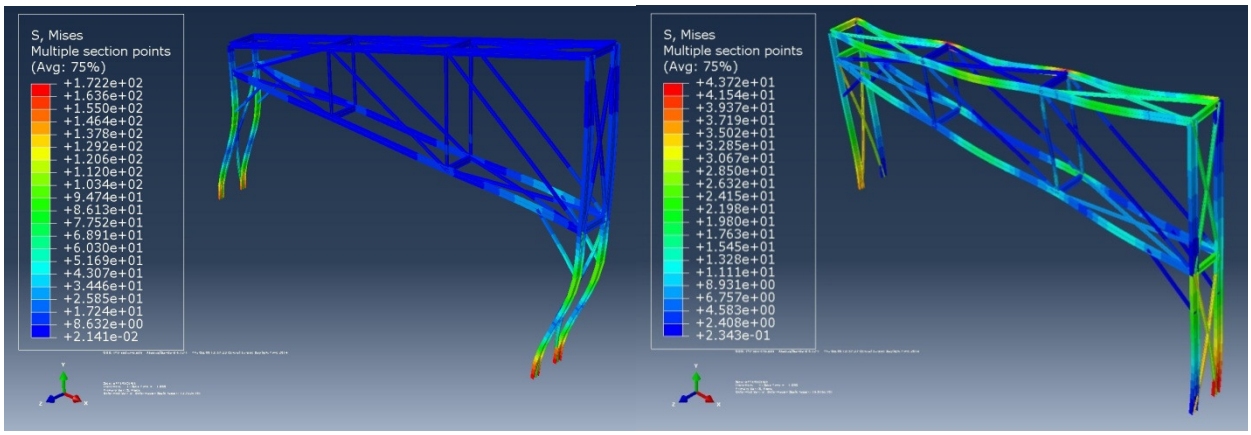

Figure 6 IPE model stress field caused by the longitudinal load (left),IPE model stress field caused by the lateral load (right)

Obtained results have shown smaller maximum stress values for the HEA model compared to IPE model. In a case of longitude loading maximum stress is located at the supporting beams near the encastre and has a value of 82MPa for the HEA model and 172MPa for IPE model. In a case of the transversal loading, the HEA model has shown maximum stress values of 31MPa, while the IPE had a maximum of 43MPa. It should be noted that both models have predicted stress levels significantly beneath the yield stress, but the interesting difference can be seen in the stress field on the supporting X structure reinforcements as well as on the A longitude top beams. In the case of the HEA model supporting X reinforcement represent the areas with a highest stress values, and in

the case of both models these values are approximately the same, around 30MPa.In the case of the IPE model the higher stress values are located at the top longitudinal beam and had a value of 41MPa. As a result of the profile used throughout the whole top section of the model, an increase in stress for the IPE profile can be noticed.
Maximum displacements for both models were calculated for the lateral loading. In a case of a HEA model, it was predicted at12mm and for the IPE, it was calculated to be 21mm.
HEA200 has a specific weight of 42.6 Kg/m while IPE200 has a specific weight of 22.4 Kg/m. HEA240 has a specific weight of 60.3 Kg/m while IPE240 has a specific weight of 30.7 Kg/m. It can be noted that the weight is two times less in the case IPE profiles. Total designed distance for A type of profiles is 81m and for B is 21m. By calculating global weights of the whole structure, it can be concluded that a use of IPE profiles will provide saving of 2257.8 kg.

CONCLUSION

Calculation has shown that the HEA model will have smaller stress values throughout, but the difference will be negligible considering that both of the models have shown maximum stress values significantly beneath the yield stress, and that both are expected to provide sufficient support under the load. Thorough inspection of the stress field has shown that depending on the design attention, maintenance should be focused on different areas of the model, supporting X reinforcement in a case of HEA and lateral beams in a case of IPE.
Both models will have sufficient structural support with small and insignificant maximum stress values. In the case of an IPE model, weight reduction can be expected to be around 2250 Kg. The use of IPE 200 and IPE240 profiles should not only provide weight reduction, but also reduce raw material costs, as well as provide better conditions for manipulation and positioning of the whole structure.
Although the calculations have shown adequate results for both models, and the IPE model was chosen for production, experience from the practice is always lead by the engineers on the constructions site who wanted to ensure sufficient safety. Finished model of a pipeline supporting structure can be seen in figure 7. Slight changes and modifications to the design were added. This practice is recommended due to the fact that without calculations some of the reinforcement can achieve over-rigidity in certain area which can result in stress concentration elsewhere. Simulations and calculations are performed in order to predict the behavior of the structure, and any changes on the site should be retroactively added to the numerical models.

Figure 7 Finished design of the pipeline supporting structure

ACKNOWLEDGEMENTS

The study was carried out within Projects TR – 35040, as well as TR – 35011, financed by the Ministry of Education, Science and Technological Development, Republic of Serbia.

REFERENCES

[1] Irwin, G. R. Fracture dynamics ASME,Cleveland 1948J.
[2] G. R. Irwin, A. Kies, Fracturing and fracture dynamics, Welding Journal. Res. Sup. 31(2) pp.95-100
[3] A. Sedmak, Primenamehanikelomanaintegritetkonstrukcija (monografija) Belgrade, Mašinski fakultet,2003
[4] Čosić, M.; Folić, B.; Folić, R.; Sedmak, S.:Performance based seismic analysis ofhighway E75 overpass at Kovilj, IntegritetI VekKonstrukcija, 17-28, UDK/UDC:625.745.12:624.042.7, ISSN: 1451-3749
[5] Zaric, B., Budjevac, D., Stipanic, B. Celicnekonstrukcije u gradjevinarstvu, 2007
[6] DIN 1025-2 : Hot rolled I-beams - Part 2: Wide flange I-beams, IPB-serie; dimensions, masses, sectional properties,1994
[7] DIN 1025-5: Hot rolled I-beams; medium flange I-beams, IPE-serie; dimensions, masses, sectional properties,1994
[8] European Committee for Standardisation (CEN). Eurocode 1. Action on structures, part 1-4: Wind load
[9] TaskoManeski, Kompjuterskomodeliranjei proracunkonstrukcja, Faculty ofMechanical Engineering , Belgrade 1998 ,ISBN 86-7083- 319-0
[10] M. Milovančević, N. Anđelić, Otpornost materijala, Beograd, Mašinski Fakultet, 2006

INTERNATIONAL SCIENTIFIC CONFERENCE ON ADVANCES IN MECHANICAL ENGINEERING

13-15 October 2016, Debrecen, Hungary

THE COMPARISON AND EVALUATION OF ADVANTAGES AND DISADVANTAGES BETWEEN CONVENTIONAL AND UNCONVENTIONAL CUTTING OF MATERIAL

[1]ŤAVODOVÁ Miroslava PhD, [1]KALINCOVÁ Daniela PhD, [2]SLOVÁKOVÁ Ivana PhD

[1]Faculty of Environmental and Manufacturing Technology, [2]The Institute of Foreign Languages, Technical University in Zvolen, Študentská 26, 960 53. Slovak republic.
E-mail: tavodova@tuzvo.sk, kalincova@tuzvo.sk, slovakova@tuzvo.sk

Abstract
The paper offers comparison of two technologies of material cutting. The first is a conventional way referring to cutting with a band saw and second one is unconventional referring to cutting by the means of plasma beam. Both equipments are placed in one plant. The fully-automated production process is of no great importance in a small-scale production or job-order manufacture. For that reason universal plasma cutting machine VANAD and band saw cutting from Pilana company are used. The difference of given material cutting technologies indicates that their use is different, too. We selected three criteria to compare the technologies given. They are as follows: utilization possibilities, cut surface quality and costs. In the conclusion we assessed the advantages and disadvantages of plasma cutting compared to conventional cutting method with a band saw according to selected criteria.

Keywords: *material cutting, plasma, band saw, roughness, costs.*

1. INTRODUCTION

The use of progressive technologies in mechanical engineering has brought new possibilities of material machining. They refer especially to the procedures of precise and highly precise dimension machining, micro-machining and nanotechnologies. These technologies meet demanding requirements of modern production not only in the area of automation but also from the viewpoint of energy, ecology and economy. It is necessary to emphasize that development of traditional machining technologies has not stopped and new cutting materials and abrasives and innovative machining technologies have been developed and used. To certain degree they address the problems of hard-to-machine materials [1].

2. METHODS

The technologies of material cutting by the means of band saw and plasma beam were selected to evaluate and compare the conventional and unconventional technology. Material cutting with band saw belongs to widely used technologies. The separation is based on mechanical principle by plastic material deformation, exceeding the Rm tensile strength. The process of material cutting by the means of plasma beam is defined as energy-beam cutting process. It uses heat energy provided by high-energy plasma beams as a primary source to reduce the material [1]. Both equipments are placed in one production plant.
The first machine refers to a plasma CNC cutting machine VANAD KOMPAKT with integrated material table (*Figure 1, left*). The second machine is band saw Pilana PMS 600/1500 VS, a vertical semi-automated band saw for metal used for cutting of large material blocks [2] (*Figure 1, right*).

Figure 1 VANAD Plasma equipment (left) a band saw Pilana PMS 600/1500 VS (right)

The best way how to compare two essentially different equipments for the same purpose is to compare the output. It can be evaluated for example by the means of the possibilities of utilization of single technologies and the quality of cut surface expressed by the means of roughness characteristics. The economic aspect, i.e. the costs is closely related with it. For comparison we selected following criteria:

- Utilization possibilities;
- Cut surface quality;
- Costs.

Cut material – chromium-nickel steel STN 17 240, appellation pursuant to DIN is X5CrNi18-10.

2.1 Utilization possibilities

Equipment data stated by the producer refer to one of the main factors affecting the purchase. Sometimes, however, one equipment cannot perform all required operations done in the production process and therefore, it is advantageous also to have second equipment that is able to perform the operations. Considering the fact that plasma cutting technology is based on thermal principle and cutting with a band saw is based on mechanical one, we shall use qualitative comparison of parameters. The aim of the comparison is to point out the differences in equal operation conditions (*Table 1*).

Table 1 Qualitative comparison of cutting parameters

VANAD Plasma equipment	Band saw Pilana PMS 600/1500 VS
Recommended materials	
Electrically conductive materials	All material types up to the hardness 65 HRC; not suitable for brittle materials
Thickness of material to be cut	
min. 0.5 mm - max. 30 mm – steel max. 20 mm – stainless steel	min. 1.5 mm - max. 600 mm
Possibilities of the equipment to accommodate to material thickness	
Replacing nozzle Current size setting	Setting of height of upper guide blocks, saw band tool replacement
Quality of edges after cutting	
Distinguishing satisfactory and unsatisfactory side, unsatisfactory side it is a scrap	Both sides are acceptable
Cut width	
for $h \leq 6$ mm 2.2 ÷ 3.5 mm for $h \geq 6$ mm 3.5 ÷ 4 mm	0.65 mm – 1.3 mm Conditioned by the saw band used

Cutting speed depending on material thickness; in band saw depending on the material hardness, too			
h = 2 mm h = 6 mm h = 10 mm	7.5 m.min^{-1} 4.3 m.min^{-1} 3.3 m.min^{-1}	h = 2 mm h = 6 mm h = 10 mm used material of the same hardness	1.5 m.min^{-1} 0.8 m.min^{-1} 0.5 m.min^{-1}
Restrictions for product designing			
It is not possible to make small roundness of cutting edge or narrow grooves; holes min. Ø1.5 x h		Shape cutting conditioned by the width of saw band; curvature radius: min. 3 mm	
Shaping possibilities of cut material			
It is possible to cut planar material in the form of a sheet only		Planar material, material bundles, profiles, bars, beams, material of variable thickness	
Working environment			
dustiness, fumes, UV radiation		Risk of slipping on the cooling emulsion	
Noise level			
The noise level rises proportionately to increased current		small	

2.2 The quality of cut surface

In plasma cutting the satisfactory and unsatisfactory side shall be determined (*Figure 2, left*) due to whirling motion of plasma gas. Inclination of one side is approximately 3° and second side even 15°. The fact may be partially influenced by gases of higher quality and a burner with water jet washing. However, it cannot be removed absolutely. The cut surface roughness is stated in the range of Ra=10÷30 µm. Molten material is usually taken from the cut spot by a high-flow-rate gas resulting in formation of a clean smooth surface on the left side of the cut. There is a heat affected zone (HAZ) whose thickness is stated in the range 0.25 ÷ 1.25 mm under this smooth surface layer. Considerable cooling of the cut zone causes creation and spreading of small cracks behind the heat affected zone, often till the depth of 1.6 mm [1], [3]. This fact affects the need of further machining of the cutting edge.

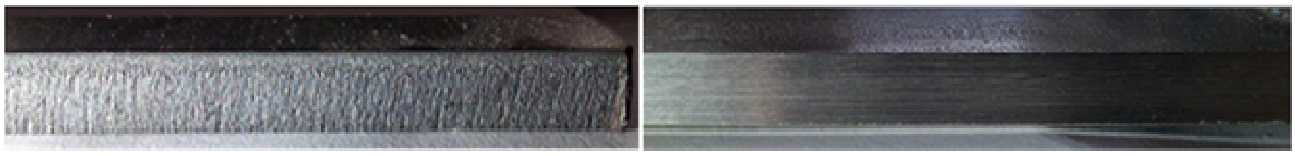

Figure 2 Material cut by the means of plasma beam (left) and with band saw (right)

The edge perpendicularity with the deviation of maximum 0,5 mm (*Figure 2, right*) is achieved after cutting with a band saw. Surface roughness depends on chip formation and the toll used. When using a bimetal saw band with wave gearing, then Ra=25µm is achieved. Achieved cut precision and roughness is sufficient for common use, therefore cut material is often not further machined. There are mean values of measured roughness parameters Ra, Rz and Rq of cut material X5CrNi18-10 in the *Table 2*. The measurement was done on a touch roughness gauge SURFCOM 130A.

Table 2 Surface roughness parameter values for plasma cutting and cutting with band saw

Technology	Roughness characteristics values (µm)		
	Ra	Rq	Rz
Plasma	5.36	6.59	25.07
Band saw	2.29	2.74	9.99

Ra, Rz and Rq roughness characteristics are compared in the chart in the *Figure 3*.

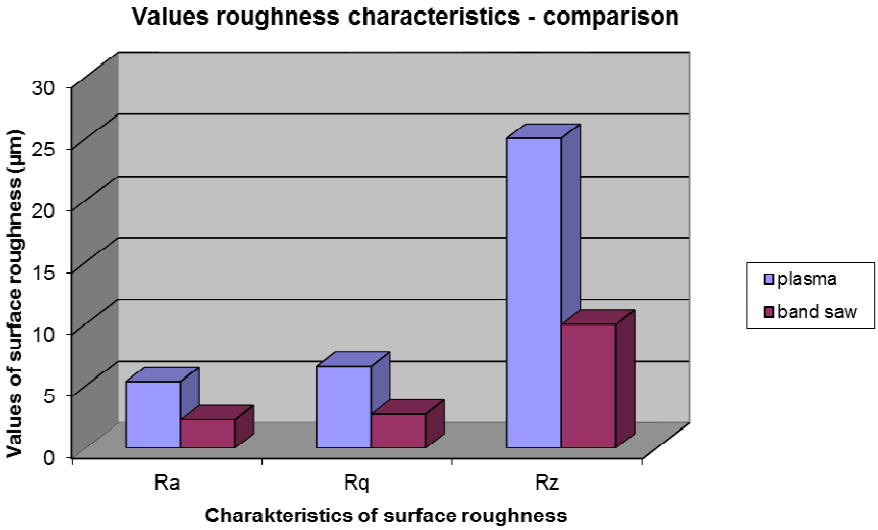

Figure 3 Comparison of roughness values for both technologies

2.3 Costs

Current cutting equipments are much more reliable and require less maintenance and service compared to the equipments used several years ago. The maintenance costs and production equipment repair costs are often determined as a coefficient from the production equipment price. Further, they can be determined by the means of a qualified estimation or as a real consumption of spare parts and consumption parts determined on the basis of internal records and book-keeping [4]. Economic aspects can be divided into partial groups and subgroups. However, the most significant aspects that must be taken into account in the optimization of such a technology are definitely investment costs (the volume of financial means connected with purchase of specific cutting machine). Further, there are operating costs (electricity consumption, working media and other related costs) that affect the final decision on purchase of such a technology in the production plant to a large extent [5].
The costs for operation are in fact real expenses affected by equipment operation (*Tables 3 and 4*). These expenses can be divided into two main groups:

- service and maintenance costs;
- costs of cutting.

The prices are based on real costs; cutting costs was determined according to the energy prices and gas price for one month.

Table 3 Costs - plasma

Investment costs		113 800 € without VAT
Service costs per year		2 876 €
Material thickness	Hole burnout/arch start	Price for one running meter of cut
3 mm	0.05 €	0.40 €
10 mm	0.05 €	0.75 €
20 mm	0.10 €	1.75 €
35 mm	0.15 €	2.50 €

Service and maintenance costs: ventilation filter, grate exchange, annual inspection of electric appliances, a set for lubrication of CNC machines, annual service inspection by the supplier.
Costs of cutting: plasma gases, protective gases, electricity, worn and torn parts (nozzles, electrodes), labour costs.

Table 4 Costs – band saw

Investment costs		74 237 € without VAT
Service costs per year		1 274 €
Material thickness	Price for one running meter of cut without cooling	Price for one running meter of cut with cooling
3 mm	0.65 €	0.70 €
10 mm	1.05 €	1.15 €
20 mm	2.10 €	2.25 €
35 mm	4.00 €	4.35 €

Service and maintenance costs: coolant filters, coolant, annual inspection of electric appliances, lubricants, disposal of hazardous waste.

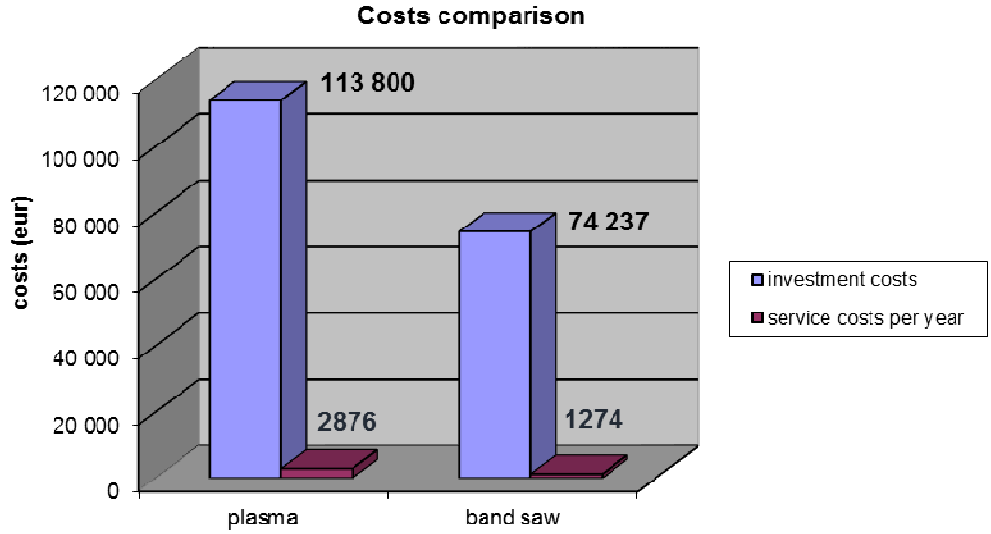

Figure 4 The ratio of investment costs and operating costs

Costs of cutting: electricity consumption, coolant consumption, wear and tear of the saw band, labour costs.
The chart (*Picture 4*) shows the ratio of investment costs and operating costs. The chart (*Figure 5*) compares the cut price for one running meter of cut for both technologies of material cutting.

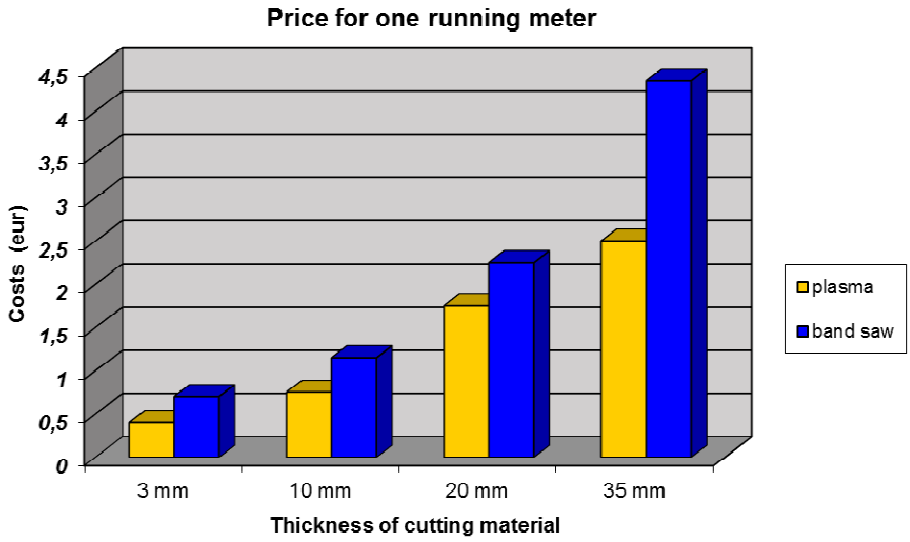

Figure 5 The comparison of cut price for one running meter of cut for both technologies

3. RESULTS

Plasma cutting is a low-cost possibility how to cut electrically conductive planar material in the form of sheets and plates up to the thickness of 35 mm as for steel and up to the thickness of 20 mm as for stainless steel and aluminium. The cutting process performed on CNC machines predetermined it for cutting of complicated shapes when following elementary conditions are met:

- Satisfactory cut side is the left side only,
- Hole diameter refers to 1.5 multiple of the material thickness; however, not less than 8 mm;
- Space between cut parts refers to min. 9 mm.

The controlled cutting process on a CNC machine fully automates the cutting process, thus simplifying serial production. Thus, STN EN ISO 9013 standard is met with an accuracy of 0.1 mm, in repeated cutting of 0,05 mm and cutting edge inclination of 2˚-4˚ (roughness Ra=10–30μm) [6]. The automated process reduces demands imposed on equipment operation. As the cutting process is controlled by a program, it requires another position of CNC machine programmer. Considering high productivity of plasma cutting, the total costs are low (costs for equipment operation and wage costs). Therefore, this way of cutting is predetermined for preferred use.

Cutting with vertical band saw is a universal way of material cutting with no high demands on operation. It allows to cut all types of material up to the hardness of 65 HRC. Exceptions are only very brittle material types that may crack as a consequence of vibrations or impacts caused by penetrating cutting wedge. Complicated shapes are conditioned by auxiliary holes what prolongs the production process to a large extent and it gets more complicated. The possibility to cut material up to the thickness of 600 mm and cut profiled material of various thicknesses refers to an appreciable advantage. We can separate material of big lengths, however up to the width of 1500 mm and height of 600 mm.

In common practice plasma cutting is used for cutting of sheets up to the thickness of 35 mm; the exception is only stainless steel quenchable in the air when the thermal process of cutting is not suitable and cutting with a band saw is used. The band saw is used in cutting of material exceeding the thickness of 35 mm. Main advantage is cutting of material bundles when the productivity per cycle is increased by the amount of pieces in a bundle. One of the main disadvantages of cutting with band saw is the necessity to change the saw band when material hardness or material thickness is changed. In plasma cutting it is sufficient to change the nozzle that is assembled by quick clamping.

CONCLUSIONS

The aim of each enterprise is to reduce costs related to production process and therefore it is useful sometimes even unnecessary to choose such a processing technology whose process is the least costly. The development in the field of plasma cutting is heading in the direction towards increased source output for cutting of thicker materials. Another innovation refers to variable burner head for cutting of bevels and profile-cutting rotator marked as 3D plasma cutting. Recently, the development of cutting with band saws has been focused on increased quality of saw band material and application of equipment automation.

REFERENCES

[1] Maňková, I.: *Progresívne technológie*. Košice. ISBN 80-7099-430-4 10. 275., 2000.
[2] Pásové píly na kov [online], PMS 600/1500 [cit. 2016.04.09.] http://www.pilanametal.sk/14/kategorie/47/Pasova-pila-na-kov-PMS-6001500- VS 21.
[3] McGeough, J.A.: *Advanced Methods of Machining*, Chapman and Hall, London, 1.ed., 1988.
[4] Vidová, J. *Transfer inovácií 10/2007: Model hodnotenia nákladov nekonvenčných technológií.* VEGA 1/2193/05, Technická univerzita v Košiciach, pp. 204-209., 2007.
[5] Chrappa, R., Mičietová, A., Pilc, J.: *Možnosti optimalizácie plazmového rezania*. Strojárstvo 5/2004, pp. 93.
[6] STN EN ISO 9013:2004: Thermal cutting. Classification of thermal cuts. Geometrical product specification and quality tolerances.

INTERNATIONAL SCIENTIFIC CONFERENCE ON ADVANCES IN MECHANICAL ENGINEERING

13-15 October 2016, Debrecen, Hungary

RECOMMENDATIONS FOR IMPROVING THE PRECISION OF NOISE-MEASURING OF ROLLING-CONTACT BEARINGS

[1]TIBA Zsolt PhD, [2]FEKETE-SZŰCS Dániel

[1]University of Debrecen, Faculty of Engineering
E-mail: tiba@eng.unideb.hu
[2]AFT Soft Ltd.
E-mail: fszdani@unideb.hu

Abstract

In this paper we make a proposal for developing an up-to-date bearing noise-measuring appliance based on a common one in order to eliminate its inherent measuring errors. The developed appliance provides the technical background to find the correlation between the different types of bearing failures and the measuring results. Measurements are conducted with defect-free bearings and those with known failures (cracked rings, cracked cage, lack of roller, reversed roller, defective roller and raceways, jamming cage, falling-apart-bearing because of the faulty pressing). Being in possession of reference measuring results for different bearing failures, an unknown bearing may be qualified by a comparative measuring.

Keywords: *bearing noise-measuring, excited vibration, low- and high-pass filters, bearing failures*

1. INTRODUCTION

Noise-measuring is one of the most important means of quality-control of assembled rolling-contact bearings. The noise-measuring implemented satisfactorily is capable of detecting many failures of the assembled bearings such as:

- Not appropriate assembling of the bearing cage unit; defective pressing of the inner ring and the assembled cage unit in the case of conical roller bearing. These problems result either in jam of the bearing or in bobbing of the assembled cage unit on the inner ring.
- Not good finish of raceways (grinding, superfinishing).
- Form error of rolling elements due to improper finish.
- Lack of bearing rollers or reversed assembly of bearing rollers in the case of conical rolling bearing.
- Cracked bearing rings and cages are applied at assembling.

The noise-measuring as the indispensable means of quality assurance is required by the big customers (motor-car industry) from the manufacturer in the order contract specifying the allowed noise level in dB for the particular bearing type. The demand of the motor-car industry shows the importance of the topic, as well. Another important aspect of the quality assurance process is that the noise-measuring shall be implemented with automatic devices eliminating the human factor as a work station of the bearing unit assembling typically before the stamping. In this paper we introduce briefly the main parameters of the measure and measuring device and focus on the inherent errors of measurement. We set forth the measuring process for single row tapered roller bearing. Our statements gained this way apply to radial loaded bearings (single- and double-row deep grooved ball bearings, self-aligning ball and roller bearings). However, they cannot be applied either to cylindrical roller bearings or thrust bearings. On the basis of conventional method of measurement we make a suggestion for constructing a measuring device providing a more precise measuring result. We analyze the process in detail on the basis of which the manufacturing defects

may be concluded from the disorder displayed by the noise-measuring device, whereby the effectiveness can be increased and the number of waste products may be decreased.
We propose eventually a measuring set-up appropriate for conducting the measurement more accurate. More and more precise information may be acquired about the actual reasons for the disorders induced by the errors.

2. THE COMMON METHOD AND DEVICES OF NOISE-MEASURING

As mentioned in the introduction we set forth the measuring process for tapered roller bearings. However, the statements are valid for other bearing types, as well. The factors influencing the measuring results (lubrication, gauging pressure) detailed for different bearing types are compiled in local directives of the plants. The construction and later on the operating operation of the appliance shall provide the appropriate measuring circumstances. Fig. 1 shows the set-up of the noise-measuring appliance and the measuring process.

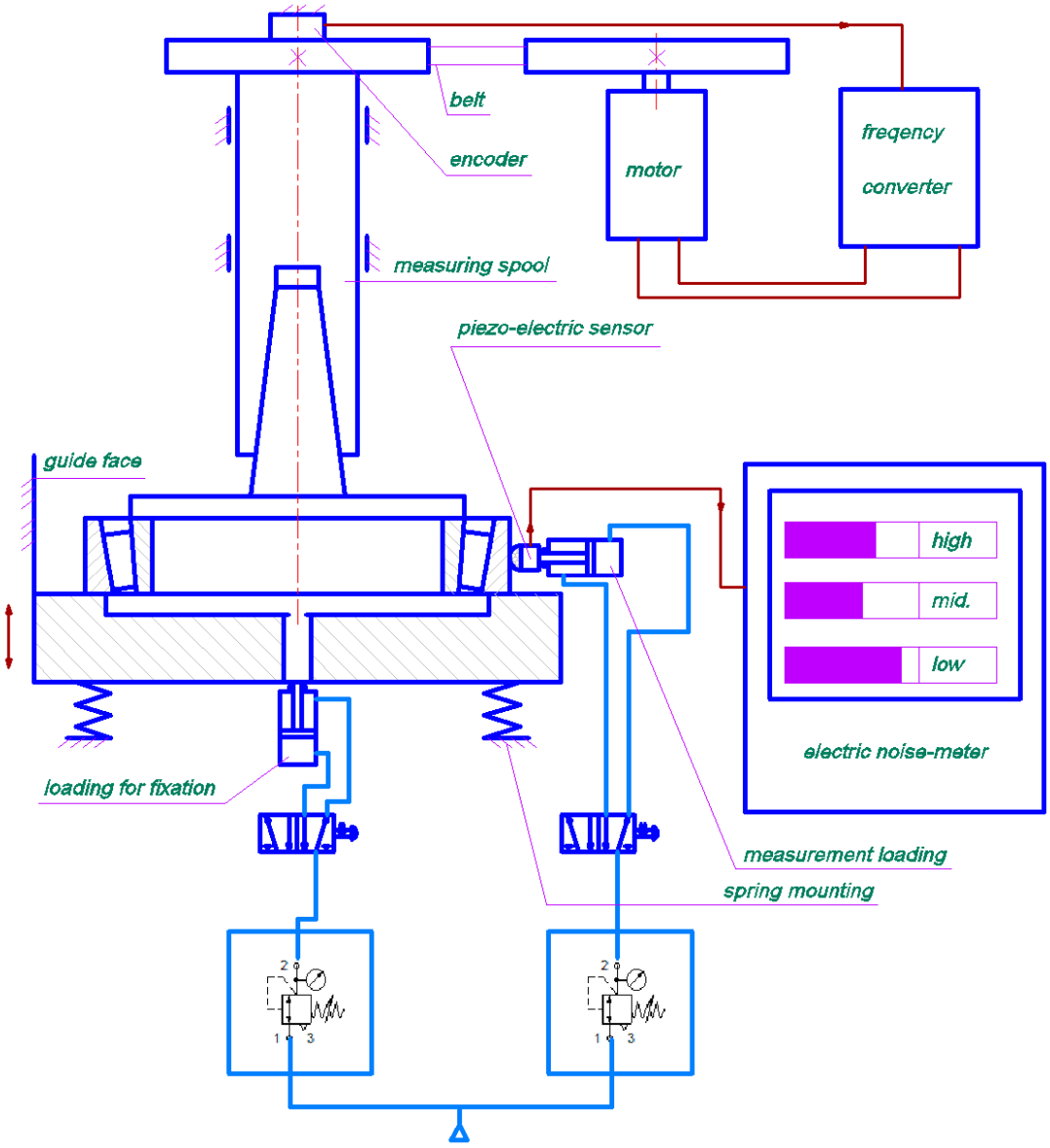

Figure 1 Set-up of the noise-measuring appliance

When measuring, a measuring pin is pressed into the inner ring of the bearing. The flange of the pin bears up on the big side of the inner ring. The shank of the measuring pin is Morse tapered fixing it in the measuring unit and transmitting the driving torque. During the measuring the roller bearing has to be positioned with its big side of the outer ring seating on the appliance's table. The gauging pressure (simulating the working load) between the measuring pin flange and the big front of the inner ring has to be kept accurately.
When measuring, the inner assembled unit of the roller bearing is rotated with the prescribed RPM while a piezo-electronic sensor is attached by a contact force to the outer surface of the standing outer bearing ring. By this means the contact force and the gauging pressure is specified, as well. When rotating the assembled inner unit, the standing outer ring vibrates inducing the consecutive distortion of the quartz crystal pressed to it. The generated electrical signal induced by the distortion (piezoelectric effect) is amplified and transmitted on low-pass and high-pass filters. The amplifier and the filters are contained in the noise-measuring electronics as a self-contained unit. The supplied electrical signal is divided into three frequency ranges and displayed on the screen of the instrument in a column graph, see Fig. 2.
The measuring is comparative. The measuring electronics qualifying the bearings may be calibrated for "proper" or "not proper" noise level. The calibration is implemented by means of measuring results of bearings qualified in another way as a proper bearing or a noisy one. The roller bearing has to be qualified as a noisy one, hence a waster if the noise level measured on the bearing exceeds the allowed one of the divided noise levels either in the low, in the mean or in the high frequency range. The measuring electronics has a binary input and output (start of the measuring, end of the measuring, noisy or not), by means of which the instrument communicates with the PLC the appliance. Usually, there are other instruments as well installed in the noise-measuring appliance providing data before or during the noise-measuring, such as:

- measuring the height of the assembled unit with inductive displacement instrument,
- detection of the lack of bearing rollers or reversed assembly of bearing rollers by means of measuring the intensity of the laser beam projected and reflex from the big side of the roller row.

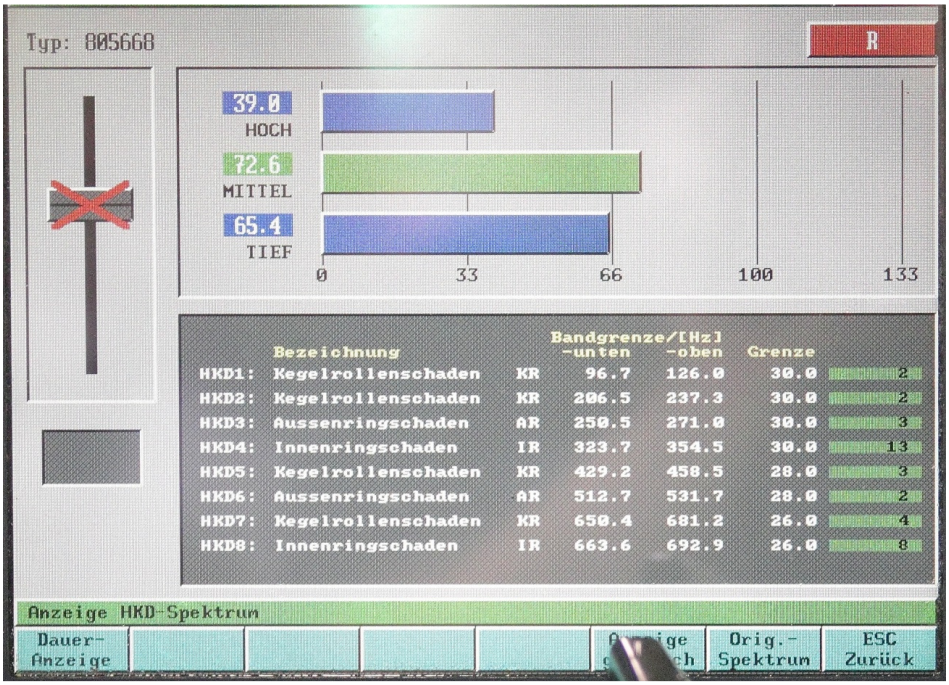

Figure 2 The screen of the instrument displaying the measuring results

By means of dividing the noise into three frequency rages not only can it be determined, whether the bearing is noisy or not but the reason for the failure as well, analyzing the measured frequency exceeding the noise limit.

- If the failure occurs in the high-frequency range, the noise is induced by defective rolling elements.
- If the bearing is noisy in the mean frequency range, it refers to the machining failure of the inner ring raceway.
- If the noise is in the low-frequency range, it indicates the failure of the outer ring.

The construction and production of the appliance have to be done with respect to the noise and vibration insulation between the working appliance and the roller bearing.

3. THE FAILURES OF THE COMMONLY APPLIED APPLIANCE

The appliance and measuring system shown in Fig. 2 cause numerous errors endangering the success of measuring in spite of the most carefully assembling. The main source of the problem is the electric motor and the gear driving the measuring unit. It may be seen in the figure that the measuring unit is driven by short-circuited asynchronous motor through a belt drive.
The desired RPM is adjusted with a frequency converter. Majority of the occurring failures may originate in it. We would not like to classify the constructors of the common appliances, though, we have to note that the development of the power electronics and the electric motors nowadays allow the implementation of better constructions.

3.1. Dimensions In Question

The frequency converter, the short-circuited asynchronous motor, measuring unit and its bearing house satisfying the stiffness requirements, the pulleys and the belt, driving the measuring unit constitute a voluminous appliance. The main problem is not the big space demand of it but the troubleshooting when moving the drive in vertical direction. Since the measuring pin has to be pushed into the inner bearing ring and after measuring it has to be pulled out, the mechanism of the appliance has to provide relative displacement facility of the roller bearing and the measuring unit in vertical direction. If the measuring unit cannot be moved because of the voluminous dimensions, the measuring table has to be moved on which the roller bearing lies. Apart from the difficulty relating to satisfying the material handling requirements, it causes other problems. The measuring table must be positioned in vertical direction by self-aligning supporting, otherwise the arising supplementary forces will excite the measuring assemble modifying the measuring circumstances. Unfortunately, the fixation of the table may swing which motion can be modelled with difficulty. Therefore, when measuring, its effect can be taken into account with difficulty. The self-aligning fixation may cause other problems. If the rolling bearing is positioned inappropriately, the measuring unit cannot be pushed into the inner ring damaging the bearings of the measuring unit and the drive gear. Another problem is the disadjustment of the additionally installed height measuring device. For this there are several examples in practice.

3.2. Drive Gear

It is well-known that belt drives may be described as a vibrational system. The vibration is induced by the inherent feature of the belt (tractive element) transversal and longitudinal flexible deformation. The vibration absorber feature of belts made of advanced viscoelastic material (above

all flat belt, syncronous belts) is accepted. However, it is well known as well that the vibrations of the simplified system shown in Fig. 3 are not linear basically due to the non-linearity of the belt material. Obviously, the vibration of the drive-belt transmitted to the measuring unit, indirectly to the inspected roller bearing. It is also known that the non-linear vibrations may be described with stochastic model in which the random effect cannot be eliminated. Consequently, if the vibration is stochastic, the way and measure of the vibration transmitted to the inspected roller bearing may be described inexact, degrading the accuracy of the measuring results which makes it impossible to find correlation between the bearings operating under measuring and working circumstances. We give the motion equation of the driving belt on the basis of Fig. 3.

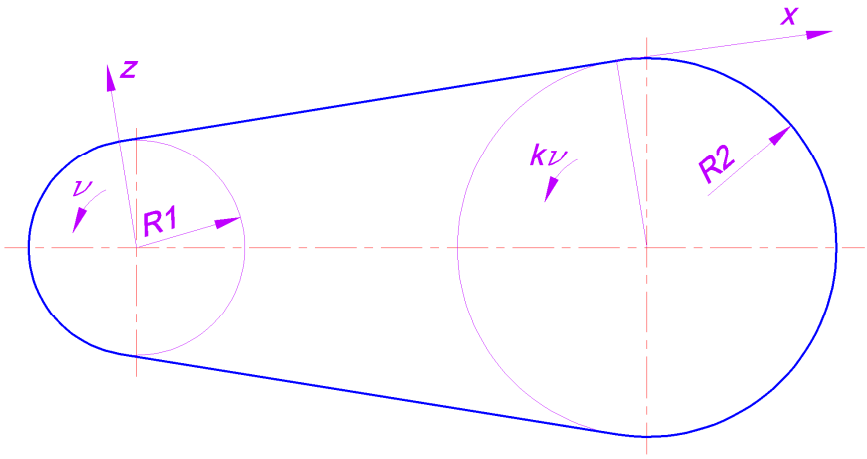

Figure 3. Belt drive, coordinate system

When modeling, the non-linear feature of the belt material has to be taken into consideration, the spring characteristics of the belt may be approximated with third-degree function polynomial: To show the motion equation we take the following into consideration:

- The belt displaces only in xz plane.
- The strain of the belt is low.
- The cross-section area of the belt is constant, its material properties do not change along the x axis.
- The viscoelastic material model is ignored in this phase of the inspection, however, a more accurate approximation may be applied [5].

The specific strain of the belt by means of the approximation from [4]:

$$\varepsilon_{x0} = \frac{\partial u}{\partial x} + \frac{1}{2}\left(\frac{\partial w}{\partial x}\right)^2 \tag{1}$$

The motion equation system applying the Hamilton-principle [6] without the intermediate calculations:

$$\rho A\frac{\partial^2 u}{\partial t^2}-\frac{\partial}{\partial x}\left\{AE\left[\frac{\partial u}{\partial x}+\frac{1}{2}\left(\frac{\partial w}{\partial x}\right)^2\right]+\right.$$
$$+\beta\left\{A\left[\frac{\partial u}{\partial x}+\frac{1}{2}\left(\frac{\partial w}{\partial x}\right)^2\right]^3+\right.$$
$$\left.\left.+3I_y\left[\frac{\partial u}{\partial x}+\frac{1}{2}\left(\frac{\partial w}{\partial x}\right)^2\right]\cdot\left(\frac{\partial^2 w}{\partial x^2}\right)^2-I_{3y}\left(\frac{\partial^2 w}{\partial x^2}\right)^3\right\}\right\}=0$$

$$\rho A\frac{\partial^2 w}{\partial t^2}-\frac{\partial}{\partial x}\left\{\frac{\partial w}{\partial x}\left\{AE\left[\frac{\partial u}{\partial x}+\frac{1}{2}\left(\frac{\partial w}{\partial x}\right)^2\right]+\beta\left\{A\left[\frac{\partial u}{\partial x}+\frac{1}{2}\left(\frac{\partial w}{\partial x}\right)^2\right]^3+\right.\right.\right. \tag{2}$$
$$\left.\left.\left.+3I_y\left[\frac{\partial u}{\partial x}+\frac{1}{2}\left(\frac{\partial w}{\partial x}\right)^2\right]\cdot\frac{\partial^2 w}{\partial x^2}-I_{3y}\left(\frac{\partial^2 w}{\partial x^2}\right)^3\right\}\right\}\right\}+$$
$$+\frac{\partial}{\partial x^2}\left\{\frac{\partial^2 w}{\partial x^2}\left\{I_y E+\beta\left\{3I_y\left[\frac{\partial u}{\partial x}+\frac{1}{2}\left(\frac{\partial w}{\partial x}\right)\right]-\right.\right.\right.$$
$$\left.\left.\left.-3I_{3y}\left[\frac{\partial u}{\partial x}+\frac{1}{2}\left(\frac{\partial w}{\partial x}\right)^2\right]\frac{\partial w}{\partial x}+I_{4y}\left(\frac{\partial^2 w}{\partial x^2}\right)\right\}\right\}\right\}=0$$

where: ρ is the density of the belt material,
A is the cross section area of the belt

The solution of Eq. 2 in closed form is not known yet. The simplified formula may be used rather in engineering practice can be gained by applying the approximation based on the Kirchhoff's energy principle which assumes the member expressing the longitudinal vibration can be ignored in proportion to the transversal one. Applying the above mentioned simplifications, the motion equation system of the belt is the following:

$$\frac{\partial}{\partial x}\left\{AE\left[\frac{\partial u}{\partial x}+\frac{1}{2}\left(\frac{\partial w}{\partial x}\right)^2\right]\right\}=0$$

$$\rho A\frac{\partial^2 w}{\partial t^2}+\frac{\partial}{\partial x^2}\left[I_y E\left(\frac{\partial^2 w}{\partial x^2}\right)\right]- \tag{3}$$
$$-\frac{\partial}{\partial x}\left\{\frac{\partial w}{\partial x}\left\{AE\left[\frac{\partial u}{\partial x}+\frac{1}{2}\frac{\partial^2 w}{\partial x^2}\right]\right\}\right\}=0$$

It may be seen in Eq. 3 that the strain of the centre line of the belt is independent from the x variable but depends on the time. Because of the extent limitation, ignoring the intermediate calculations, we

note that the displacement-time function according to the Galerkin method may be sought by means of trigonometrical series from which the displacement may be solved numerically.

$$\rho A \ddot{q}_i + r\dot{q}_i + \frac{i^2\pi^2}{L^2}\left\{\frac{i^2\pi^2}{L^2} I_y E - \rho A \mathrm{v}^2 + \right.$$
$$\left. + \frac{AE}{L}\left[u(L,t) - u(0,t) + \frac{\pi^2}{4L}\sum_{k=1}^{\infty}\left(k^2 q_k^2\right)\right]\right\} q_i -$$
$$- \frac{2\mathrm{v}}{L}\sum_{\ell=1}^{\infty(\ell\neq i)}\left\{\ell\cdot\left(2\rho A\dot{q}_\ell + r q_\ell\right)\frac{i\left[1-(-1)^{i+\ell}\right]}{i^2-\ell^2}\right\} = 0 \qquad (4)$$
$$(i = 1,2,3,\ldots)$$

Returning to the main object of the paper, on the basis of Eq. 4 a computer program can be elaborated with which the vibrations may be modeled transmitted to the pulleys and hereby to the measuring unit and directly to the bearing in question. Analyzing the Eq. 2 it can be realized agreeing with our experiences that there are RPM ranges where a so-called stability loss of the belt may occur. It may manifest itself in significant transversal vibration amplitude of the belt. This phenomenon deteriorates the accuracy of the noise-measuring very much and gives an explanation why the noise-measuring appliance does not give appraisable result for particular bearing types at particular RPM's even if they could be qualified properly in terms of noise limit. The nonlinearity feature of the viscoelastic material is not considered in the model, however, it may be seen that the failures caused by the belt vibration should be eliminated. The application of a gearbox was considered. Obviously, the vibration induced by the mashing gear pair is more detrimental than the one generated by the belt drive, hence it is not a solution. Another facility is the direct drive of the measuring unit. The short-circuited asynchronous motor available as a commercial product is not appropriate because of its big dimensions, the inevitable production and assembly failures and the out-of-balance effects of the rotor. This is why this solution is not recommended. It may be seen that the stochastic vibrations result in undependable appliance. It means that the measuring based on the comparison with an etalon would classify as a good bearing for noise and - what is more disagreeable - a wrong one for appropriate.

3.3. Correlations Between Measuring Results And Reasons For Failures

The measuring system shown in chapter 2 does not shift out the following failures:

- Falling apart of the bearing because of unsuccessful pressing.
- Bearing sticking because of the wrongly produced or improperly assembled inner unit of the bearing and cage, respectively.

In order to eliminate the above mentioned failures individual appliances are needed working on customary principles (torque-measuring machine and appliance detecting the falling-apart of the inner assembly of the bearing). The purchase, the deployment and operation of these machines are very expensive. If we want to carry out the quality assurance procedure of the roller bearings without the mentioned appliances, we have to confide the inspections to the skilled worker at the assembly cell. However, it contradicts the principle, namely human factor should be excluded at quality control. For the following failures cannot be concluded directly from the measuring results gained by a common noise-measuring device:

- Build in of cracked cage at assembly

- Lack of roller
- Cracked (but not broken) bearing rings

The lack of roller may be shifted out by automatic image discrimination systems and the previously mentioned laser technique, however, the two other failures may be detected with difficulty.

4. PROPOSAL FOR ELIMINATING FAILURES MENTIONED IN CHAPTER 3

In the case of roller bearings of premium category it is a common practice that before building in the bearings are not inspected anymore. The perfect quality product is expected from the manufacturer. If there can be errors in the quality assurance procedure described in chapter 3 and for this reason the user will build in a defective product, the consequences may be very serious for both sides. On the one hand, we shall make a proposal for the implementation of a noise-measuring appliance being simpler in design, cheaper, smaller and more precise than the common one. On the other hand, we revise the common way of noise-measuring and introduce a measuring set-up eliminating basically the errors of the common one.

4.1. Noise-Measuring Appliance Having Direct Drive Of The Measuring Unit

The essential problem of the common construction is the feature of the belt drive of the measuring unit, see Fig. 3. Fortunately, the three-phase servo-motors are available due to the innovation intervened recently in the electrical drive techniques (see Fig. 4).

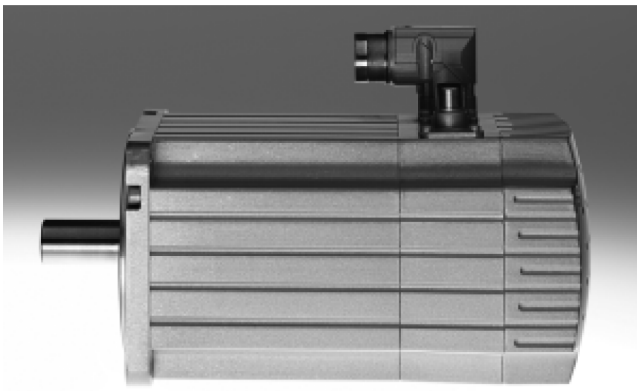

Figure 4 FESTO EMMS-AS three-phase servo-motors [2]

Advantageous features of *three-phase* servo-motors:

- Compact, small size and weight.
- High performance in proportion to its size.
- Precise, well-balanced, hence low-vibration operation.

The servo-motor is set up on the principle of building modules, such as driving and control electronics providing the following facilities:

- Its control techniques operating together precisely with the PLC of the measuring unit may be configured in a wide range.
- Keeping RPM accurately, wide RPM range.
- Reliable protection against overload.

Applying the building modules principle, the associated parts may be purchased (axial set, couplings) with which the servo-motor may be installed into the drive train satisfying the ultra precision requirements. Fig. 5 shows the axial set with the coupling.

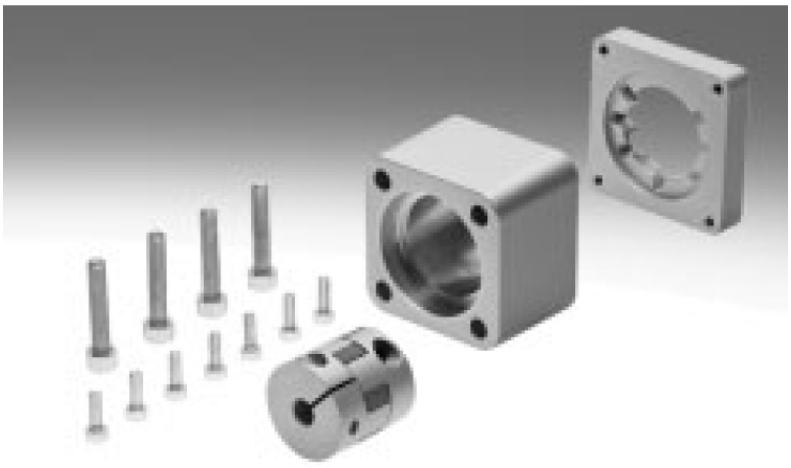

Figure 5 The axial set with the coupling [2]

In compliance with it a measuring unit with direct drive, a measuring unit house and a frame holding them may be implemented in small size and relatively cheap with favorable vibration features which do not have the problems mentioned in chapter 3. In terms of control technique, applying the well-handleable controller, the functions (stopping, controlling and maintaining the RPM, protection against overload) may easy be programmed. Utilizing these facilities we designed a measuring unit-house system making the material handling inside the appliance possible.
The set-up and the construction are shown in Fig. 6.
Aspects of design with special respects

- The thrust bearing of the measuring unit is implemented with two pieces of ultra-precision angular-contact ball-bearings installed opposed. It provides high-running accuracy and load-bearing capacity.
- The upper bearing of the measuring unit is a sliding bearing providing a vibrationless operation. This sliding bearing does not require independent lubrication because of its small borehole diameter and operating in a house fulfilled with oil. The narrow annulus between the measuring unit and the house and the lubrication in the house have a vibration isolator effect, as well.
- The measuring unit has to be machined carefully and balanced dynamically in order to avoid the continuum vibrations.
- Since the measuring unit and the house are robust, hence overstressed, they are not susceptible for vibration.
- The outer surface of the measuring unit including the tapered hole connecting the measuring pin have to be nitrided to avoid the wear because of the frequent tool change.
-

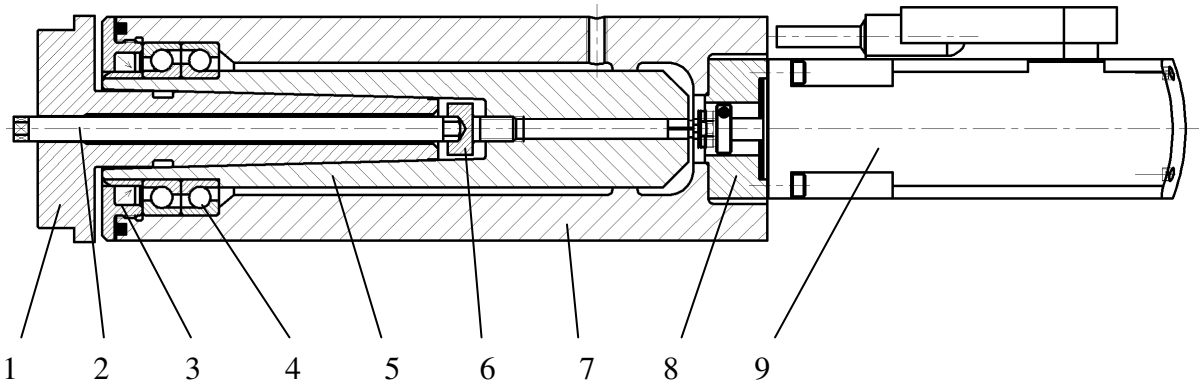

1: measuring pin
2: withdrawing device
3: bearing block cover with sealing and "O" ring
4: ultra-precision angular contact ball-bearing
5: measuring unit
6: withdrawing socket head cap screw
7: measuring unit house
8: axial fitting piece with the coupling
9: EMMS-AS servo-motor

Figure 6 The direct driven measuring unit and house

Ensuring the above mentioned, the bearing is subjected to low-vibration level. Another important problem is that vibration can be described with stochastic model does not occur, hence there is no incidental factor in qualifying the bearing. Eventually the technical requirement at the construction of the appliance it is very important that the measuring unit with its house and the electric motor move together in one unit. This way there is no flexible fixation used. In the introduction we mentioned that the precondition of the accurate measuring is the simulation of the operation load by adjusting the gauging pressure between the inner ring of the bearing and the measuring pin. It is ensured by moving the bracing with pneumatic carriage having no piston rod and the air supply of the pneumoelements and the working pressure is controlled by pressure-control valves. It is essential that the gauging pressure changes from bearing to bearing. It is ensured by the control module installed in the PLC of the appliance working together with the pressure-control valve. The upper bracing with the guiding and moving pneumatic carriage and with the measuring unit house is shown in Fig. 7.

Naturally, we have to have regard for the isolation of the vibration transmitted to the appliance from the environment and the duly stiff execution of the fixation and the lower bracing. Because of space limitations, we do not go into details. Eventually we succeed in executing the very stiff compact appliance can be controlled easy from informatics point of view and eliminating the problems induced by stochastic vibration. It is not negligible that the appliance does not require inner material handling system for moving the bearing, by this means low-cycle time may be achieved.

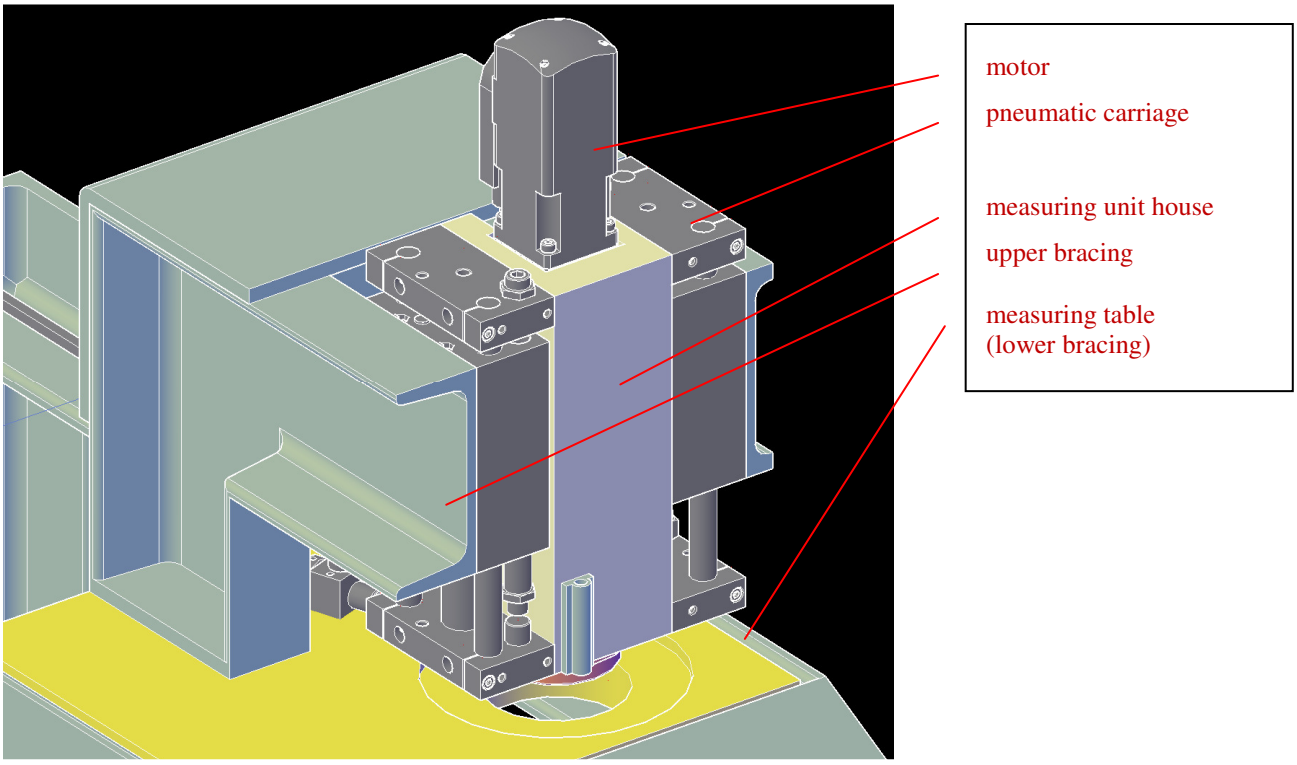

Figure 7 Moving the measuring unit house

4.2. Recommendation For The New Method Of Noise-Measuring

In chapter 3.3 we ascertained that the common way of noise-measuring is not appropriate for detecting certain bearing failures. It may be important when considering not only the achievement of defect-free bearings but searching the correlation between measuring results and possible failures (for e.g. manufacturing errors, improper appliance adjustment).
It means that we cannot ensure the detection of the waste product when manufacturing the semifinished product. Therefore, we cannot take measures to suspend the production and decrease the number of waste products. In the following we introduce a measuring system eliminating the insufficiency of the common one. This system is based on a new measuring technique and for the time being it is a recommendation for testing it in laboratory. Our aim at the moment is to check the accuracy of the measuring method and find the limits of its application. Accordingly, the method is not appropriate for satisfying the requirements of the mass production, however, if it is applicable we will design and implement an appliance for industrial application, as well.
The basic principle is to excite vibration of the bearing rings without rotating the inner unit and detect the answer signal. From the feature of the answer signal, such as its form and displacement, hopefully we can conclude not only the suitability of the bearing but by chance the cause for the failure. Thus, the method is appropriate not only for qualifying the bearing but for detecting failures which were not detectable with the common noise-measuring and it gives information regarding the missoperation of the production line. The operation of the appliance may be traced in Fig. 8.

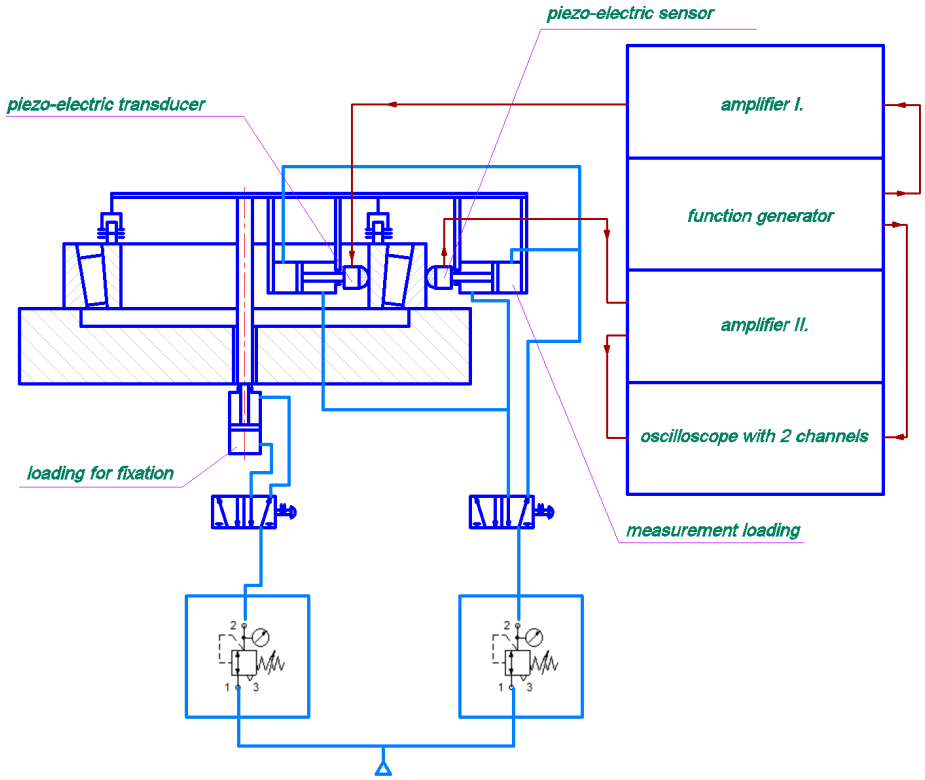

Figure 8 Noise-measuring on the basis of forced vibrations

The bearing is dogged down with a pivotal arm to the isolated table. Pneumatic press is applied controlled by manual pressure-control valve. The inner side of the arm is instrumented with piezoelectric vibration generator, while the outer side of it is instrumented with piezoelectric probe for measurements. The shape of the excitation signal, the frequency and the amplitude of the vibration may be adjusted by the function generator and amplifier. The contact pressure of the vibration generator and the probe is implemented by pneumatic pressure and controlled by manual pressure-control valve. There may be two measuring principles.

4.2.1. Inspecting Based On The Graphic Answer Signal

The answer signal is amplified and modulated by low- and high-pass filters and both the excitation and the answer signal are displayed on oscilloscope. Swinging the arm on the bearing, the answer signal is analyzed in terms of shape and amplitude. To find out the correlation between different types of bearing failures and measuring results. Measurements are conducted with defect-free bearings and those with known failures (cracked rings, cracked cage, lack of roller, reversed roller, defective roller and raceways, jamming cage, falling apart bearing because of faulty pressing). Being in possession of reference measuring results for different bearing failures, an unknown bearing may be qualified by comparative measuring.

4.2.2. Inspection By Analyzing Natural Frequencies

The disadvantage of the method set forth in chapter 4.2.1 is that the automatic analysis of the signals in industrial conditions may be tiresome and the automation of graphical analysis requires sophisticated software technology background. The realization of the natural frequencies may not be so difficult than the analysis of the signals and carried out with simpler computer program. It is

well known that in the case of damped-excited vibrations, natural frequency may be found where the phase-angle deviation between the excitation and the answer signal is 90°. This phase-angle deviation may be measured with the commercial two-channel measuring apparatuses available. The frequency of the excitation signal has to be adjusted with function generator so that the angle deviation has to be 90^{o}. Like in the previous chapter bearings are inspected with known failures at different measuring arm angular positions in order to realize that the failure in which position and in which direction modifies the natural frequency from which the failure and its type may be concluded.

SUMMARY

In this paper we make a proposal for developing an up-to-date bearing noise-measuring appliance based on a common one in order to eliminate the measuring errors. In addition to this the innovated appliance shall be faster, more accurate, more reliable, cheaper and smaller. The measuring system drafted in chapter 4.2 approaches the measuring task with a new aspect. It requires further research analysis and we hope that it reveals the reasons for different failures.

REFERENCES

[1] FESTO Part Solution Manager 2016, FESTO GMBH.
[2] FESTO Part Catalogue 2016, FESTO GMBH.
[3] Patkó Gy.: *Dinamikai eredmények és alkalmazások a géptervezésben habilitációs tézisek.* Miskolci Egyetem, 1998.
[4] Kauderer, H.: *Nichtlineare Mechanik*. Berlin-Göttingen-Heidelberg: Springer Verlag, 1958.
[5] Fekete-Szücs D.: *Lemez dinamikai viselkedésének szimulációja és anyagállandóinak kísérleti meghatározása viszkoelasztikus anyagmodell esetén.* ETH Zürich, 1992.
[6] Kirchhoff, G.: *Mathematische Physik*. Leipzig: Teubner Verlag, 1876.

INTERNATIONAL SCIENTIFIC CONFERENCE ON ADVANCES IN MECHANICAL ENGINEERING

13-15 October 2016, Debrecen, Hungary

EFFECTS OF HIGH CONCENTRATION HYDROGEN DURING GMA WELDING OF DUPLEX STAINLESS STEEL

[1]VARBAI Balázs, [2]MÁJLINGER Kornél PhD

[1]Budapest University of Technology and Economics, Department of Materials Science and Engineering, E-mail: varbai@eik.bme.hu
[2]Budapest University of Technology and Economics, Department of Materials Science and Engineering, E-mail: welding@att.bme.hu

Abstract
In our research the effects of high concentration hydrogen (argon + 13.5 % to 15.0 % hydrogen) in the shielding gas was compared to pure argon in case of gas metal arc welding of LDX 2404 lean duplex stainless steel. The hydrogen in the shielding gas increased the weld bead width, penetration depth and the average arc voltage too. In the microstructure and hardness distribution no significant differences were observed with the addition of hydrogen in the argon shielding gas.

Keywords: *duplex stainless steel, gas metal arc welding, hydrogen, arc voltage, weld geometry*

1. INTRODUCTION

Duplex stainless steels (DSS's) are one type of corrosion resistant stainless steels which contain approximately equal amount of ferrite and austenite phases. One special type of DSS's called lean duplex stainless steel (LDX), which has got the expression "lean" after their reduced nickel and molybdenum content. The reason of development of LDX's was the extensive fluctuation of nickel and molybdenum prices on the metal stock market experienced at the beginning of the 21st century [1]. Nowadays, beside the extensive spreading application of high strength steels in automotive industry [2, 3] the development of LDX's has a great attention and lean duplex started replacing regular austenitic (e.g. AISI 316 and 304) grades [4-7]. The welding of DSS's is often related with complex issues due to their double phase microstructure, however nowadays it can be stated DSS's generally demonstrate decent weldability [8]. During the gas metal arc (GMA) welding of DSS's, 1-2 % active component (CO_2 or O_2) or higher concentration of helium (up to 30 %) beside argon (Ar) is recommended to be used as shielding gas [9]. In some cases smaller concentration (1-5 %) of nitrogen is also recommended because of nitrogen's strong austenite forming ability [10-14]. One of the biggest challenges during welding of DSS's is to keep the phase balance in the weld metal (WM) and heat affected zone (HAZ). The usage of hydrogen (H_2) in the shielding gas in welding of austenitic stainless steels is widely used (mainly during gas tungsten arc (GTA) welding) [15-17], however the usage of hydrogen during the welding of DSS's is generally not recommended because of the possibility of hydrogen embrittlement or hydrogen cracking [18-19]. The interaction between hydrogen and duplex stainless steel is based on a complex mechanism, which can be originated from the dual phase microstructure of DSS's. The diffusivity of hydrogen is much higher in ferrite, than in austenite. The effective diffusivity of hydrogen in duplex steel containing 44 % austenite is reduced 400 times in comparison with fully ferritic steel [20]. This means the transport of hydrogen through DSS's occurs mainly through the ferrite matrix and austenite works as a hydrogen trap. It also means the transport paths of hydrogen in the ferrite phase are not straight because they must pass around the austenite grains [20]. The shapes of these paths are more complicated in case of the weld metal. The duplex weld microstructure consists of Widmanstätten austenite leading to more

tortuous paths [21]. On the other hand hydrogen-associated degradation of mechanical properties is much higher in ferrite, than in austenite [21]. In order to investigate the effects of hydrogen from the shielding gas Ogawa and Miura [22] performed GTA welding on different DSS's with shielding gas hydrogen content varies from 0 to 10 % in argon. With higher ferrite ratios cracking occurred during welding with 2-10 % hydrogen content, however preheating to 200°C and solution heath treatment were confirmed to be effective for crack prevention. Kordatos et al. investigated [23] the effect of 10 % hydrogen (beside 90 % argon) in shielding gas during GTA welding of 2507 type (EN 1.4410) super duplex stainless steel. The ferrite content increased due to the decreasing atomic nitrogen content in the weld metal. The hardness of the weld metal increased to the effect of hydrogen and hydrogen addition had a deleterious effect to the pitting corrosion. In case of usage of hydrogen in the backing gas, Westin et al. [24] experienced the best pitting corrosion resistance with using 90 % N_2 +10 % H_2 backing gas besides the mechanical properties had no significant change.

2. EXPERIMENTAL METHODS

The used base metal (BM) was 3 mm thick 2404 type (EN 1.4662) lean duplex stainless steel plate (*Figure 1*) with low nickel and molybdenum, however high nitrogen content (*Table 1*). The plate was welded in solution annealed condition as came from the manufacturer. The used filler material for bead-on-plate run welds was G 22 9 3 NL type (AWS A5.9 ER2209) duplex stainless steel welding wire with the diameter of 1.2 mm.

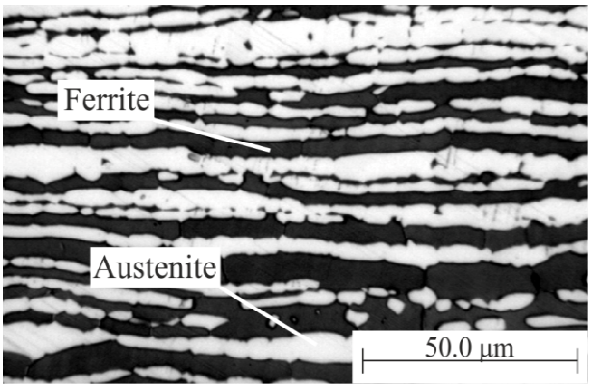

Figure 1 Microstructure of LDX 2404 base material (colour etched)

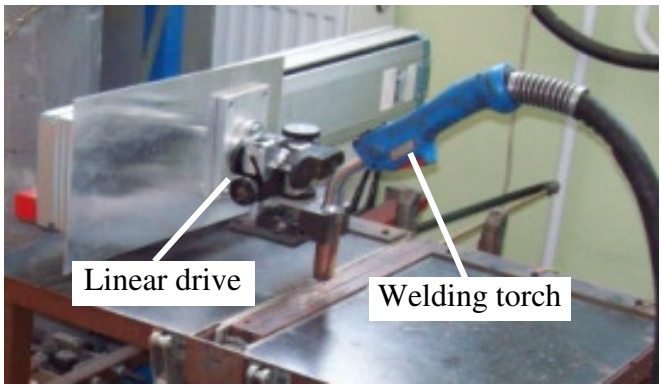

Figure 2 The automated assembly with the welding torch and linear drive

Table 1 The nominal chemical compositions of the LDX 2404 plate and the ER2209 welding wire

	Chemical composition of the used materials, nominal values (wt.%)						
Material	**C**	**N**	**Cr**	**Ni**	**Mo**	**Others**	**Fe**
LDX 2404	0.02	0.27	24	3.6	1.6	3Mn Cu	Bal.
ER 2209	<0.015	0.15	22.5	8.8	3.2	2Mn	Bal.

The welding process was performed on a Rehm Megapuls 300 type machine automated with a Yamaha F1405-500 type linear drive (*Figure 2*). The linear drive ensured the constant welding speed and constant nozzle gap. The fixed parameters of the welding processes are as follows: welding speed=4.7 mm·s^{-1}, wire feed speed=3.6 m·min^{-1}, current=130 A, arc voltage=20.7 V, shielding gas volume=12 l·min^{-1} and the nozzle distance=10 mm. The welding was performed with direct current, wire positive (DC+). The steel plates were cleaned with acetone just before welding. The position of the plates was fixed by a clamp device. On one plate 100 mm long weld seams were

made. Before the next welding sequence the plates were cooled down to room temperature on air. The welding process variables were the 5 different shielding gas mixtures with hydrogen content; 0 %, 13.5 %, 14.0 %, 14.5 %, 15.0 % next to argon (specimens designated as H0, H13.5, H14.0, H14.5 and H15.0, respectively). High concentration of hydrogen in shielding gas was used in order to investigate the effects which can be originated only from the hydrogen in the shielding gas and to get major differences compared to pure argon. The external weld geometry measurements were done using a calliper in 10 points. For metallographic examination sections perpendicular to the weld seams were saw cut under constant cooling. The cross section were mounted into epoxy resin and grinded up to 2400 grit paper and after polished with 3µm diamond suspension. The used etchant contained 100 ml distilled water, 18 ml hydrogen chloride (HCl) and 1 g potassium pyrosulfite ($K_2S_2O_5$). This etchant makes the ferrite phase appear darker and the austenite phase lighter because of the sulphide layer. The used optical microscope was Olympus PMG3 and the stereomicroscope was Olympus SZX16. For Vickers hardness measurements (HV10) KB Prüftechnik KB750 type equipment was used. The hardness measurements were performed in cross sectional specimens along a line 1 mm deep from the plate surface. The ferrite content measurement of the BM and WM was done using JMicroVision 1.2.7 image analyzer software on 10 metallographic images e.g. *Figure 1* with ~ 0.36 mm^2 areas typical to the microstructure.

3. RESULTS AND DISCUSSION

During all the welding processes smoke and soot formation were experienced. In case of hydrogen in the shielding gas metal splashes and unstable electric arc were observed. The unstable electric arc leaded to big differences in the weld geometry.

3.1 Changes in the weld seam geometry

Compared to pure argon (H0) the high concentration of hydrogen increased the weld bead width and penetration depth and decreased the height *(Figure 3 and Figure 5)*.

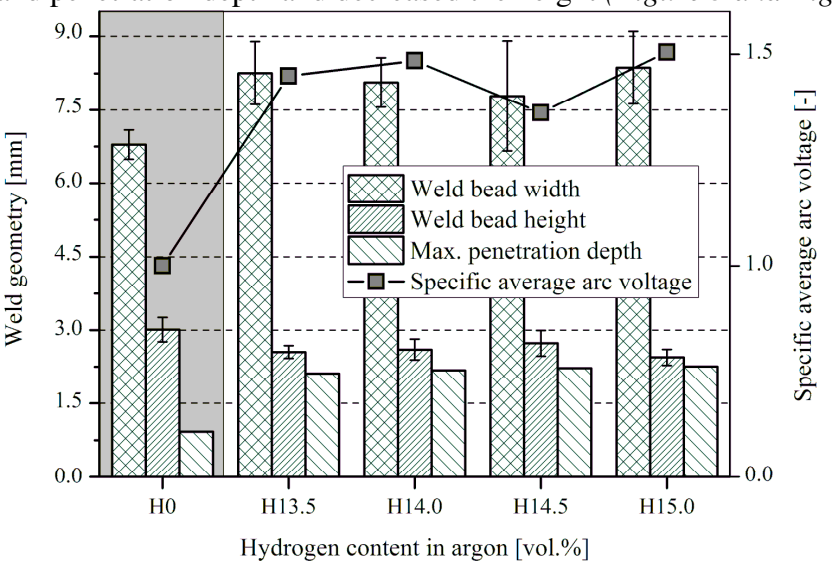

Figure 3 Weld geometry and average arc voltage values as a function of the H_2 content in the shielding gas

The biggest increase (compared to H0) in the average weld bead width is 23 % and the biggest increase in the penetration depth is 244 %, which were measured with H15.0 shielding gas. These values are in good correlation with the increasing average arc voltage, registered by the welding equipment. Compared to H0 shielding gas the arc voltage increased by 51 % in case of H15.0. The increasing arc voltage resulted in the bigger penetration depths and wider weld beads. The changes in the weld geometry and penetration depth occur in the changes of the form factors. The external form factor can be calculated as the ratio of bead width and the height and the internal form factor as the width over the penetration depth *(Figure 4)*. With high concentration in the shielding gas the external form factor increased with 28-52 % and

the internal form factor decreased with 47-52 %.

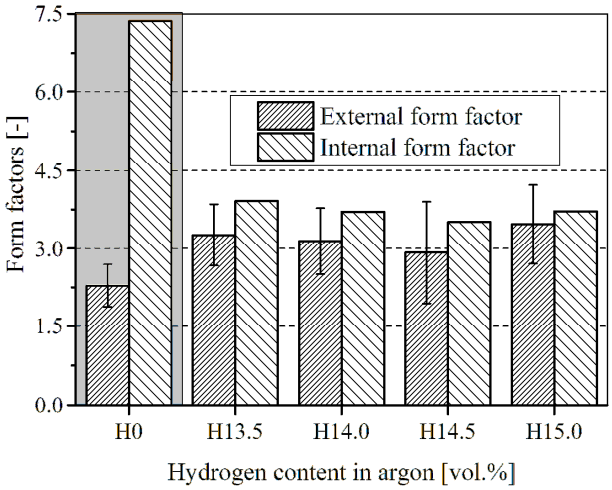

Figure 4 External and internal form factors as a function of hydrogen in the shielding gas

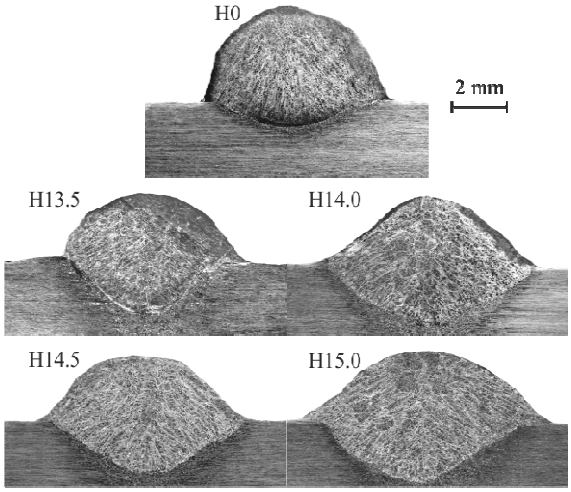

Figure 5 Macro images of the etched cross sections of the welded specimens

3.2 *Changes in the hardness distribution and the microstructure of the welds*

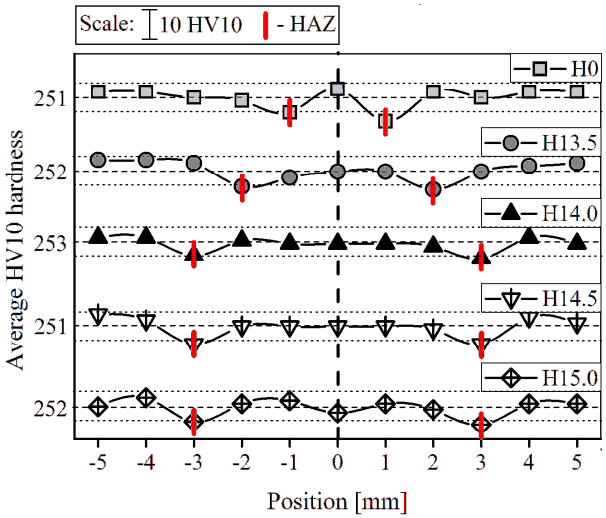

Figure 6 Hardness distribution in the different shielding gas welded WM and HAZ

The average hardness values have not changed to the effect of hydrogen in the shielding gas *(Figure 6)*. The average hardness of the LDX 2404 base material is 252±5 HV10 which is the same in the WM with all of the shielding gases. Also in all cases a small decrease (5 HV10 average) in the hardness was experienced in the HAZ. In the microstructure no significant differences can be discovered as a function of the applied shielding gas. In the WM oblong, radial ferrite grains can be seen symmetric to the centre line *(Figure 7)*. In the HAZ coarse ferrite grains are formed. The maximum width of the HAZ is about 1000 µm in case of H15.0.

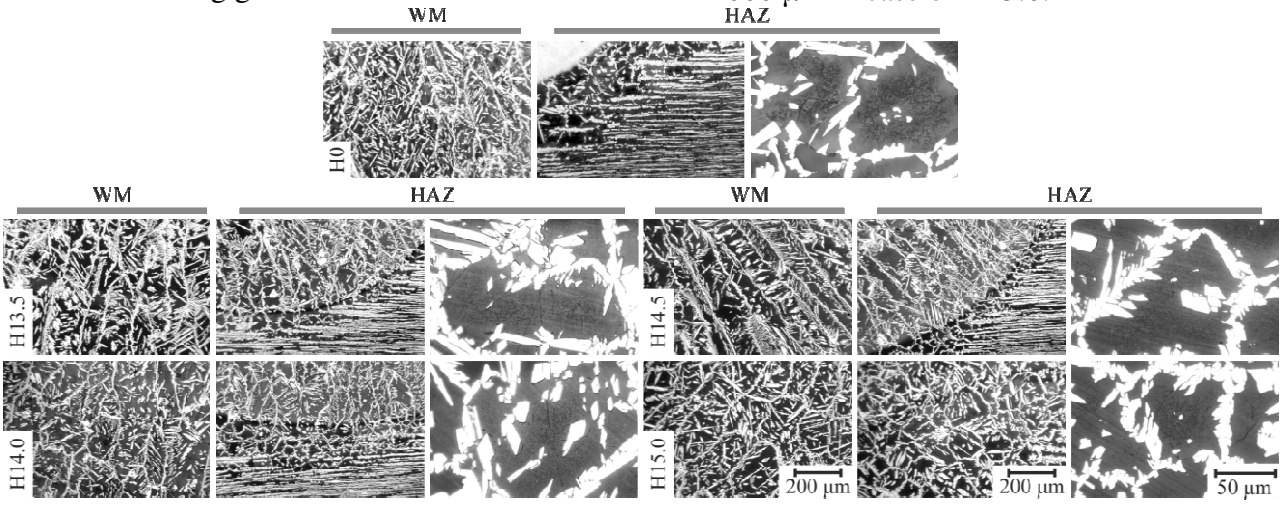

Figure 7 Microstructure of the WM and HAZ of the specimens

The ferrite content in the LDX 2404 base material is 49±2 in area %. The measured ferrite contents of the welds are as follows: H0=55±2 area %, H13.5=51±2 area %, H14.0=50±2 area %, H14.5=50±2 area % and H15.0=51±2 area %. With hydrogen in the shielding gas the ferrite content of the WM is similar to the BM but in case of argon shielding gas the ferrite content is slightly bigger. The lower ferrite content in case of H0 shielding gas can be originated from the lower heath input during welding (lower arc voltage value) as every DSS solidifies as δ-ferrite.

CONCLUSIONS

In our research LDX 2404 lean duplex stainless steel was welded with GMA technique with different shielding gas mixtures containing high concentration of hydrogen. The welding parameters stayed constant during the experiments, the hydrogen content beside argon varied from 0 % to 15.0 %. The effects to the welding process, weld geometry, hardness distribution, ferrite content and microstructure were investigated. The following conclusions can be drawn:

- hydrogen in the shielding gas increased the weld bead width (max. 23 % in case of H15.0) and the penetration depth (max. 244 % in case of H15.0),
- hydrogen in the shielding gas increased the average arc voltage during welding (max. 51 %),
- hydrogen increased the external form factor (28-52 %) and decreased the internal form factor (47-52 %),
- the hardness values did not change with the hydrogen in the shielding gas and remained near the BM's hardness which is 250±5 HV10,
- in the HAZ the hardness values decreased in all cases with average 5 HV10,
- in the microstructure no significant differences can be seen as a function of the hydrogen content in the shielding gas,
- the ferrite content was the biggest, 55±2 area %, in case of pure argon (H0) shielding gas, in all other cases the ferrite content in the WM is similar to the BM's, which is 49±2 area %.

ACKNOWLEDGEMENTS

This paper was supported by the János Bolyai Research Scholarship of the Hungarian Academy of Sciences grant number: BO/00294/14 and by The Hungarian Research Fund, NKTH-OTKA PD 120865 (K. Májlinger).

REFERENCES

[1] Charles, J.: *Past, present and future of duplex stainless steels*. Duplex Conference, Grado, Italy, 18–20 June, 2007

[2] Scavino, G., Federici, S., Maggi, S., Lamontanara, J., D´Aiuto, F., Matteis, P., Chiarbonello, M., Mortarino, G.M.M., Russo Spena, P., Firrao, D.: *Applications of innovative trip and twip steels to automotive body structures*. In: European congress and exhibition on advanced materials and processes, European congress and exhibition on advanced materials and processes, Nurnberg, Germany 10-13/09/2007

[3] Dobosy, Á., Gáspár, M.: *Welding of quenched and tempered high strength steels with heavy plate thickness*. In: & (szerk.) microCAD 2013, M: XXVII. microCAD International Scientific Conference. Konferencia helye, ideje: Miskolc, Magyarország, 2013.03.21-2013.03.22. Miskolc: Miskolci Egyetem, 2013. Paper M7. Mechanikai technológiák, Material Processing Technologies

[4] Gagnepain, J.: *Duplex Stainless Steels : Success Story and Growth Perspectives*. Stainless Steel World, December, 31–36 (2008).

[5] Boillot, P., Peultier, J.: Use *of stainless steels in the industry: Recent and future developments.*

in Procedia Engineering 83, 309–321 (2014).
[6] Charles, J., Chemelle, P.: *The history of duplex developments, nowadays DSS properties and duplex market future trends.* Eight Duplex Stainless Steel Conference, Beaune, France, 2010.
[7] Chater, J.: *Strength and corrosion resistance attract customer to duplex.* Stainless Steel World, June, 3–6 (2015).
[8] Pramanik, A., Littlefair, G., Basak, A. K.: *Weldability of duplex stainless steel.* Materials and Manufacturing Process. 30, 1053–1068 (2015).
[9] Valiente Bermejo, M. A. A. et al.: *Effect of shielding gas on welding performance and properties of duplex and superduplex stainless steel welds*. Welding in the World 59, 239–249 (2015).
[10] Hertzman, S.: *The influence of nitrogen on microstructure and properties of highly alloyed stainless steel welds*. Isij International 41, 580–589 (2001).
[11] Westin, E. M., Johansson, M. M. & Pettersson, R. F. A.: *Effect of nitrogen-containing shielding and backing gas on the pitting corrosion resistance of welded lean duplex stainless steel LDX 2101((R)) (EN 1.4162, UNS S32101).* Welding in the World 57, 467–476 (2013).
[12] Keskitalo, M. et al.: Laser *welding of duplex stainless steel with nitrogen as shielding gas.* Journal of Materials Processing Technology 216, 381–384 (2015).
[13] Migiakis, K. & Papadimitriou, G. D.: *Effect of nitrogen and nickel on the microstructure and mechanical properties of plasma welded UNS S32760 super-duplex stainless steels*. Journal of Material Science 44, 6372–6383 (2009).
[14] Dobránszky, J., Lőrinc, Zs., Gyímesi, F., Szigethy, A., Bitay, E.: *Laser welding of lean duplex stainless steels and their dissimilar joints*. 8th European Stainless Steel and Duplex Stainless Steel Conference, Graz, Austria, pp. 138-147 (2015).
[15] Gülenç, B., Develi, K., Kahraman, N. & Durgutlu, A.: *Experimental study of the effect of hydrogen in argon as a shielding gas in MIG welding of austenitic stainless steel.* International Journal of Hydrogen Energy 30, 1475–1481 (2005).
[16] Tušek, J. & Suban, M.: *Experimental research of the effect of hydrogen in argon as a shielding gas in arc welding of high-alloy stainless steel*. International Journal of Hydrogen Energy 25, 369–376 (2000).
[17] Suban, M., Tušek, J. & Uran, M.: *Use of hydrogen in welding engineering in former times and today*. Journal of Materials Processing and Technology 119, 193–198 (2001).
[18] Nirosta, K. T.: *Practical Guidelines for the Fabrication of Duplex Stainless Steels*. International Molybdenum Association 1–68 (2014). Available at: www.imoa.info. (Accessed: 2nd September 2016)
[19] Avesta Welding AB.: *How to weld duplex stainless steels*. Document 10601EN-GB. Avesta, Sweden (2006).
[20] Owczarek, E., Zakroczymski, T.: *Hydrogen transport in a duplex stainless steel.* Acta Materialia. 48, 3059–3070 (2000).
[21] Mente, T., Bollinghaus, T.: Modeling *Of Hydrogen Distribution in a Duplex Stainless Steel*. Welding in the World 56, 66–78 (2012).
[22] Ogawa, K., Miura, M.: *Hydrogen cracking in duplex stainless steel weldments*. Welding International 5, 691–696 (1991).
[23] Kordatos, J. D, Fourlaris, G., Papadimitriou, G.: *The Effect of Hydrogen and Cooling Rate on the Mechanical and Corrosion Properties of SAF 2507 Duplex Stainless Steel Welds.* Materials Science Forum Vols. 318-320, 615-620 (1999).
[24] Westin, E. M., et al.: *Effect on microstructure and properties of super duplex stainless steel welds when using backing gas containing nitrogen and hydrogen*. Welding in the World 58, 347–354 (2014).

INTERNATIONAL SCIENTIFIC CONFERENCE ON ADVANCES IN MECHANICAL ENGINEERING
13-15 October 2016, Debrecen, Hungary

DIGITAL IMAGE ANALYSIS OF METAL FOAM SPECIMENS

[1]VARGA Tamás Antal, [2]KAPUSI Tibor

[1]Department of Mechanical Engineering, Faculty of Engineering, University of Debrecen
[1]E-mail: varga.tamas@eng.unideb.hu
[2]Department of Computer Graphics and Image Processing, Faculty of Informatics, University of Debrecen

Abstract
The development of an efficient procedure for 3D modeling and finite element simulation of metal foams is one of the greatest challenges to engineer researchers nowadays. Creating 3D CAD model is alone a demanding engineering task due to its extremely complex geometry, and the proper finite element analysis process is still in the center of the research. The aim of this project is to analyze the related literature and to adapt the results may be considered.

Keywords: *metal foam, modeling, 3D reconstruction, finite element method*

1. INTRODUCTION

Metal foams are relatively new and advanced materials with high stiffness to weight ratio, good thermal conductivity, good acoustic insulation and excellent energy absorption capability which make them ideal materials for a variety of applications. Therefore, they have increasingly been employed for a wide range of applications, such as structural elements, automotive parts, sound and vibration absorbers or even biomedical implants. Basically, the mechanical properties of metal foams are influenced by three dominating factors, namely the property of the solid phase, the relative density of the solid phase and the spatial arrangement, that is, the structure of the metal foam (cell distribution, cell shape). To understand the structure property correlations in metal foams is required for optimizing its mechanical performance for a given application.
Although metal foams are popular they are still not sufficiently characterized thanks to its extremely complex structure which is highly stochastic in nature. In the last few years, several researchers focused on the finite element modeling of metal foams with more or less success, but it is still one of the greatest challenges. Instead of modeling the complex internal structure directly, idealized structural approaches (unit cell, statistical models, etc.) are often used where the cells are represented by miscellaneous two- or three dimensional models according to the structure behaviour. 3d model created by the help of X-ray tomography (beam model, voxel and tetrahedral element methods) is another possibility. In detail, different numerical approaches for the simulation of metal foams were proposed. This article attempts to describe the metal foam modeling opportunities available in international technical literature.

2. MODELLING OPPORTUNITIES OF METAL FOAM

Geometric modeling of metal foam can be achieved through two strategies. The first one is building an idealized model, generated from statistic data by computed tomographic shots, which reacts to load the same way as the original. The other opportunity is constructing the real geometric model based on the CT shots of the manufactured metal foam. Both processes have their pros and cons. The advantage of the idealized model is that we are able to construct a model from predefined data,

but the big downside is that we can only estimate the metal foam's reaction as the 3D model doesn't exactly match the manufactured sample. The CT shot's huge advantage is that we can examine the same 3D geometry as the examined metal foam. The disadvantage is that we can only provide information about the actual metal foam structure due to the low reproducibility stemming from the manufacturing technology. To conclude, both technologies require expensive equipment that is not available everywhere.

3. PROCESSING THE RESULTS OF THE CT ANALYSIS

The CT device is a unique measurement tool with which we can not only determine the topology of the outer surface of the analyzed component with great accuracy, but provide data about its inner structure, inhomogeneity as well [1]. Nowadays CT devices are used for various examinations. One of the most well-known are of application is medicine, still it has numerous mechanical uses as well. The CT device takes a 2D shot of the given component then turns the component together with the table in a certain angle and takes another shot *(Figure 1).* This goes on until the given component turns around entirely. The detector positioned at the opposite side of the component detects the different x-ray radiation intensity. After the examination is concluded we will have a 2D picture after every turn of angle.

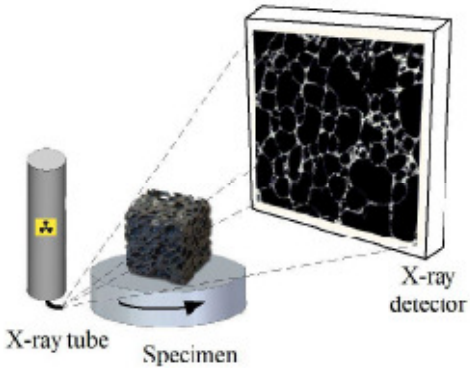

Figure 1 The operation of an industrial CT inspection system

The numerous 2D shots are composed into a 3D model by the software that comes with the CT device. These 3D models have .stl extension which are composed of voxel pieces and are only capable of visual display. The voxel is a three-dimensional picture element which extends to all three axis and as a volume-imaging tool it is standardized in medical diagnostics. Conversely the mechanical practice uses a web that describes surface (.dxf) or volume element (.iges) so the original voxel model needs to be converted. Nevertheless there are mistakes, noises on these CT shots which have to be erased from the shots. Furthermore the constructed model is not homogenous so it needs reconstruction. These changes can be made with various software.
Michailidis and his co-authors examine open cell aluminum and nickel foam in [2]. As the first step of reconstruction they modify the CT shots on which they remove the dots smaller than 70µm. After this they create a 3D volume model (.iges extension) which is composed of volume elements. Unfortunately they do not mention the software used for reconstruction in the article. The size of the 3D model is 7.3x6.1x1x4 mm, which due to the large change of form they use the NGLEOM function of the Ansys finite element software.
The authors examine a closed cell aluminum in [3]. They reconstruct the 2D shots made by the CT with MATLAB software. As the first step of the reconstruction they make binary pictures of the CT shots then remove the falsely sensed dots. Following this they define the borderlines of the cells thus punctuating the pictures. In this article they work with 2D models, while in [4] they conduct

their examinations on a Ø14x5 mm large model. They use the ABAQUS software for their finite element test.
Ramirez and his co-authors also examine open cell aluminum in [5]. They used the trial version of MIMICS for the reconstruction of CT shots. After this they generate a finite element web with the help of the ABAQUS software with which they carry out the finite element test. They use a narrow piece of the sample.
In [6] an open cell M-Pore® and a closed cell Alporas® is being examined. The 3D reconstruction is done with the phoenix datos|x software then the finite element test is done by the MSC.Marc software. The size of the generated models is 14x14x14 mm and 28x28x28 mm.
A closed cell ALPORAS aluminum foam is examined in [7]. The Octopus 8.1 software is used for reconstruction. For the finite element test they use 50x50x5.5 mm and 50x50x13.5 mm sized models.
A closed cell ALPORAS aluminum foam is examined in [8]. The TRI/3D-BON of Ratoc System Engineering Co. Ltd software was used for the reconstruction of the CT shots. After this the x-ray films were patched together using RapidForm of INUS software from which they created a 3D surface model. After this the finite element web was created with the PATRAN of MSC software. The finite element test was carried out with ABAQUS software. The finite element test was conducted on 5x5x5 mm models.
From the above information we can see that there are various opportunities to model metal foams and numerous software can be used successfully. We can also notice that most small size models are most likely used as the reconstruction and finite element simulation of such a model takes a long time. Our current research focuses on developing a reconstruction method with which we can construct a finite element web from a CT shot. Please see an example of a model reconstruction on Figure 2.

Figure 2 Model reconstruction

CONCLUSIONS

There are various options to model metal foam. During the strategy phase of the modeling we have to decide whether we use an idealized model constructed from statistical data or we try to construct the actual model. The scientists at the University of Debrecen have made significant achievements in geometric modeling of metal foams and their numeric stiffness tests.

ACKNOWLEDGEMENT

Supported through the New National Excellence Program of the Ministry of Human Capacities.
EMBERI ERŐFORRÁSOK MINISZTÉRIUMA

REFERENCES

[1] Kozma, I.: A *komputertomográf ipari alkalmazásai.* A jövő járműve járműipari innováció, Győr, Hungary, 5/(3-4), 8–11., 2006.
[2] Michailidis, N., Stergioudi, F., Omar, H., Papadopoulos, D., Tsipas, D.N.: *Experimental and FEM analysis of the material response of porous metals imposed to mechanical loading.* Colloids and Surfaces A: Physicochem. Eng. Aspects, 382, 124–131., 2011.
[3] Zhu, X., Ai, S., Fang, D., Liu, B., Lu, X.: *A novel modeling approach of aluminum foam based on MATLAB image processing.* Computational Materials Science, 82, 451–456., 2014.
[4] Zhu, X.,Ai, S., Lu, X., Ling, X., Zhu, L., Liu, B.: *Thermal conductivity of closed-cell aluminum foam based on the 3D geometrical reconstruction.* International Journal of Heat and Mass Transfer, 72, 242–249., 2014.
[5] Ramírez, J.F., Cardona, M., Velez, J.A., Mariaka, I., Isaza, J.A., Mendoza, E., Betancourt, S., Fernández-Morales, P.: *Numerical modeling and simulation of uniaxial compression of aluminum foams using FEM and 3D-CT images.* Procedia Materials Science, 4, 227–231., 2014.
[6] Veyhl, C., Belova, I.V., Murch, G.E., Fiedler, T.: *Finite element analysis of the mechanical properties of cellular aluminium based on micro-computed tomography.* Materials Science and Engineering, A 528, 4550–4555., 2011.
[7] Saadatfar, M., Mukherjee, M., Madadi, M., Schro¨der-Turk, G.E., Garcia-Moreno, F., Schaller, F.M., Hutzler, S., Sheppar, A.P., Banhart, J., Ramamurty, U.: *Structure and deformation correlation of closed-cell aluminium foam subject to uniaxial compressionm.* Acta Materialia, 60, 3604–3615., 2012.
[8] Jeon, I., Asahina, T., Kang, K., Im, S., Lu, T. J.: *Finite element simulation of the plastic collapse of closed-cell aluminum foams with X-ray computed tomography.* Mechanics of Materials 42, 227–236., 2010.

INTERNATIONAL SCIENTIFIC CONFERENCE ON ADVANCES IN MECHANICAL ENGINEERING
13-15 October 2016, Debrecen, Hungary

DESIGN OF SEVERE ACCIDENT MANAGEMENT SYSTEMS FOR PAKS NPP

[1,2]KATONA Tamás János DSc, [3]VILIMI András

[1]University of Pécs – Professor
E-mail: bata01@t-online.hu
[2]MVM Nuclear Power Plant Paks Ltd. – Scientific Advisor
E-mail: bata01@t-online.hu
[3]MVM Nuclear Power Plant Paks Ltd. – Senior Technical Advisor
E-mail: vilimi@npp.hu

Abstract
Paks Nuclear Power Plant identified the post-Fukushima actions for mitigation and management of severe accidents caused by external events that include updating of some hazard assessments, evaluation of capacity / margins of existing severe accident management facilities, and construction of some mew systems and facilities. In all cases, the basic question was, what level of margin has to be ensured above design basis external hazard effects, and what level of or hazard has to be taken for the design. Paks Nuclear Power Plant developed certain an applicable in the practice concept for the qualification of already implemented and design the new post-Fukushima measures that is outlined in the paper. The concept and practice is presented on several examples.

Keywords: *design, earthquake, hazard, vulnerability, severe accident.*

1. INTRODUCTION

2011 the comprehensive safety assessment ("stress tests") of the Paks Nuclear Power Plant has been performed, and the safety issues and actions related to the mitigation and management of severe accidents caused by severe external events have been identified. Actually, the most important measures for severe accident mitigation / management have been identified via Level 2 PSA well before 11th of March 2011, i.e. independent from the lessons learned from Fukushima accident. Design and implemented of these measures have also been started before 11th of March 2011. These are the installation of Severe Accident Hydrogen Management System, implementation of In-vessel Retention via External Vessel Cooling by reactor cavity flooding, ensuring the autonomous power supply to designated consumers by Mobile Severe Accident Diesel Generators, installation of Severe Accident Measurement System, reinforcement of Spent Fuel Pool Cooling System.
The post-Fukushima action plan of Paks NPP [1] is aimed at improving the design basis capabilities and establishing effective severe accident management and mitigation capabilities. The plan covers the following actions:

- Updating of some hazard assessments
- Evaluation of relevant beyond design basis external hazard consequences
- Definition of margins of existing systems, structures and components (SSCs) for severe accident management (SAM)
- Review and updating of seismic classification
- Re-assessment of seismic interactions
- Construction of some new SSCs and facilities.

According to the action plan, the extreme wind and tornado hazard, and other meteorological extremes have been re-evaluated on the basis of [2] and [3].
As it had been recognized early nineties, that the soil beneath the plant is susceptible to liquefaction. Hence the soil improvement below the operating plant seemed to be impractical, liquefaction is considered as beyond design basis hazard. A comprehensive evaluation of liquefaction hazard and analysis of the consequences of a possible liquefaction have been performed in frame of the action plan, Katona et al [4].
Capacity and availability of existing SAM facilities have been evaluated, e.g. barrack of the fire brigade, protected command center for emergency management staff.
The possibility of seismic interactions has also been re-evaluated. For example, the demineralized water tanks at Units 3 are installed beside the laboratory and service building that is not safety related. Since the damage of the tanks due to damages of service building can't be completely excluded, fixing of the service building has been decided. Seismic housekeeping has also been improved.
Review and updating of seismic classification resulted in the enhancing the seismic class and subsequent upgrading of several SSCs of the Safety Class 3 and those SSCs that have severe accident mitigation/management functions. For example, the high-voltage substations were non-safety classified and not qualified for design base seismic loads. Seismic qualification and reinforcement of the substations have been done as they may play an important role in cross-connections from one unit to another. Due to this measure emergency power supply of all units can additionally be ensured from one of the four units operated at reduced power level, i.e. the plant could be operated in "island mode", separate from the national power grid.
Construction of new SAM facilities has also been decided at the plant, e.g. installation of super-emergency diesel generator and a back-up shelter for SAM command center.
Obviously, the design of the dedicated SAM SSCs and facilities shall provide an adequate margin to protect items ultimately necessary for prevention of large or early radioactive releases in the case of beyond design basis natural hazards. Consequently, in all cases mentioned above, the basic question was, what level of external hazard has to be accepted for the design of new SAM facilities, and what level of margin is acceptable in case of existing ones?
There are some international examples to be considered while answering this question. For the seismic design of new NPPs, the existing practice is to use a 10^{-4}/a mean for the design basis and a safety margin of either 1.4 for all seismic Category 1 SSCs (approach of European Utility Requirement Document – EUR) or a 1.67 for the plant HCLPF (US approach). In order to comply with the post-Fukushima requirements, an additional margin seems to be needed for the selected SSCs required for severe accident mitigation/management functions.
In [5] and [6] adaptation of "seismic practice" is recommended for all external hazards. It is proposed that the existing margin for selected SAM items should further be increased by 50 %. This means that a margin of 1.6 for the selected SSCs will be applicable (EUR approach) and a HCLPF of 2.0 will be required for the selected SSCs (US approach). However, the features of particular hazards have to be accounted for, e.g. predictability, possibility of protective actions and time available for the protective actions, potential for causing cliff-edge effects and the physically realistic combinations.
In the paper the concept and practice of definition of external hazard design basis for design and upgrading of plant facilities and plant SSCs needed for severe accident management are presented. The concept is based on the adaptation and generalization of "seismic practice" for all external hazards. The concept takes into account the above advises and international practice, and the specific situation at the Paks NPP plant as well as the specific site features. The concept includes the definition of external hazard design basis, acceptance criteria and justification of the performance goal for the post-Fukushima measures

2. BACKGROUND OF THE CONCEPT

Basic requirements

According to the Hungarian Safety Regulation [7] the cumulative core damage frequency for the operating plant has to be less than 10^{-4}/a and the cumulative frequency of early large release has to be less than 10^{-5}/a. However, the licensee obliged to implement all reasonable practicable measures for decreasing the core damage frequency as well as for converging the frequency of early large releases to the 10^{-6}/a level. The Regulation allows specific considerations in case of earthquake and sabotage.
The Hungarian Regulation defines two levels of design extension conditions:
The Design Extension Conditions 1 (DEC1) is consequences of complex sequences not accounted for in the design basis. The DEC1 should not result in core damage and the plant can be brought into safe shutdown condition.
Design Extension Conditions 2 (DEC2) are severe accidents with core damage. However the heat removal from the core should be established in DEC 2 and the releases from the containment have to be limited.
Selected SSCs to be functional under design extension conditions can be designed by realistic or best estimate methods. However the term "realistic and best estimate" is not clearly defined either in Hungarian [7] or in the international regulation [8].
The Regulation requires avoidance of the cliff-edge effect, i.e. certain deviation from design basis plant parameters or effects of external hazard should not result in severely abnormal plant behavior.
The qualification of existing and the design of new SAM SSCs and facilities have to aim at the compliance with the above requirements, i.e. the mean annual frequency of unacceptable performance that is specified as a target should be less than 10^{-5}/a, and it tends to desirable $<10^{-6}$/a for ensuring the desirable frequency10^{-6}/a for early large releases.
There are new international requirements regarding Design Extension (DEC) and Beyond Design Basis External Event capabilities (WENRA/RHWG Guidance Documents: Issue T: Natural Hazards; Issue F: Design Extension of Existing Reactors). According to this: "It shall be demonstrated that SSCs (including mobile equipment and their connecting points, if applicable) for the prevention of severe fuel damage or mitigation of consequences in DEC have the capacity and capability and are adequately qualified to perform their relevant functions for the appropriate period of time…."When assessing the effects of natural hazards included in the DEC analysis, and identifying reasonably practicable improvements related to such events, analysis shall, as far as practicable, include: (a) demonstration of sufficient margins to avoid "cliff-edge effects" that would result in loss of a fundamental safety function;…"

Scope of the works

The scope of SSCs and facilities to be qualified or newly designed are as follows:
Containment

- Severe Accident Hydrogen Management System – implemented, new system
- In-vessel Retention via External Vessel Cooling (by reactor cavity flooding) – implemented, new system

Alternative Power supply

- Autonomous power supply to designated consumers by Mobile Severe Accident Diesel Generators – implemented, new

- Super-emergency Diesel generator – new

Measurement and Control systems

- Severe Accident Measurement System – implemented, new

Heat removal to the ultimate heat sink

- Reinforcement of Spent Fuel Pool Cooling System – implemented, new

Facilities that have to be available for SAM

- Protected Command Center – existing
- Backup Command Center – new
- Barrack of Fire Brigade – existing

The tasks to be performed:

- Regarding the already existing items the margins above design basis has to be evaluated, and the possibility of cliff-edge effects has to be checked.
- Regarding newly designed SAM SSCs and facilities the design basis external hazard parameters have to be defined and the margins have to be evaluated. The cliff-edge effects have to be avoided by the design.
- It has to be demonstrated that these items have the necessary performance level for ensuring the desired limit for early large releases.

Preconditions to be accounted for:

- The safety and seismic classified SSCs have already been upgraded to withstand the effects of design basis external hazards. In the frame of periodic safety review the code deterministic evaluations for all design basis external hazards have been reviewed and updated.
- The Level 1 and 2 probabilistic safety assessments (PSA) and the Level 1+ containment seismic PSA [9] are available.
- The newly implemented SAM SSCs have been designed for the design basis external hazards.
- Structural integrity of the containment, structures and piping to the ultimate heat sink, as well as emergency power supply have been evaluated and justified for possible effects of liquefaction.

The implemented SAM modifications were costly and difficult to implement measures, therefore, any further effort should be carefully optimized.

3. ASESSMENT OF THE MARGINS

Generalization of the "seismic practice"

Code Deterministic Margin Assessment methodology is applicable for quantitative evaluation of seismic margin. In case of existing NPPs the acceptable lower limit for the plant High-Confidence-of-Low-Probability-of-Failure (HCLPF) is HCLPF$\geq$ 1.4 × SSE.
The HCLPF is by definition the following [10]:

$$HCLPF = \frac{C-D_{NE}}{D_E+\Delta C_E} F_\mu a_{RLE}. \quad (1)$$

Where C is overall load-bearing capacity, D_E is earthquake induced load and simultaneous operational load D_{NE}, F_μ is ductility factor, and ΔC_{NE} is capacity for simultaneous loads of external events, if there is any (e.g. simultaneous shear and tension in reinforced concrete braced walls). The

D_E earthquake induced load is calculated for review or reference-level earthquake with PGA equal to a_{RLE}. The component's failure probability associated to its HCLPF is lower than 5%, with a confidence of ≥95%. The HCLPF is an appropriate measure of margin above the design basis hazard parameter (e.g., PGA). For example, if the HCLPF=0.35g there is 95% of confidence that the probability of failure is less than 5%, if the PGA≤0.35g. The system HCLPF can be calculated via min-max method.

The concept of the HCLPF can easily be generalized for evaluation of margin with respect to the effects of hazards other than earthquake. In this case the variables in Eq. (1) have to be calculated for the load case of given hazard (wind, extreme temperature).

The requirements regarding other external hazard effects are not so explicit. Therefore, the same criterion as for earthquake is accepted.

A supplemental requirement is introduced: The already existing plant systems and structures having SAM functions should have a minimum safety margin that covers the 10^{-5}/a hazard parameters.

Considerations made on the basis of hazard curves – Earthquake hazard

Hazard curves for the site external hazards have been defined up-to 10^{-7}/a level. According to the Hungarian Regulation the mean hazard curve has to be considered for definition of design basis hazard parameters. For avoiding the cliff-edge effect, slope of the hazard curves has to be evaluated. Slope is defined as ratio between the hazard parameters corresponding to 10^{-5}/a and 10^{-4}/a annual none-exceedance probabilities that indicate the possibility of sudden increase of the hazard parameter while reducing the probability of exceedance by one order of magnitude.

In case of earthquake, the slope factor of the hazard curve A_R is given by the following equation

$$A_R = SA_{0,1H_D}/SA_{H_D}\ . \tag{2}$$

Here the SA_{H_D} is the spectral amplitude at the required level of exceedance for design basis (H_D) and the $SA_{0.1H_D}$ is the spectral amplitude at $0.1H_D$.

For Paks site, a systematic analysis of the seismic hazard curves, the ground motion response spectra and Design Response Spectra has been performed in accordance with ASCE/SEI 43-05. It has been found that the $DRS \approx UHRS$, i.e. the design spectra can be approximated by the *UHRS* at free field.

Since the safety and seismic classified SSCs, including the already installed SAM systems have been designed or upgraded in compliance with relevant standards for the 10^{-4}/a earthquake, the statement of ASCE/SEI 43-05 on the factor of safety for the 10% conditional probability of failure can be validated, i.e. the conditional probability of failure is ≤10%, if the peak ground acceleration is 1.5 times larger than the design basis PGA. In the Paks case the design basis maximum horizontal acceleration at free field, PGA_{DB} is equal to 0.25g, and $1.5*PGA_{DB}$=0.375g. The PGA=0.375g corresponds to the annual exceedance probability $5*10^{-6}$/a.

Consequently, the SSCs designed for 10^{-4}/a design basis earthquake in compliance with relevant standards will have sufficient margin for performing their intended safety function even if an extreme low, $5*10^{-6}$/a annual probability earthquake will hit the plant. Otherwise, a margin of 40% above design basis earthquake for the whole facility will cover the 10^{-5}/a (mean) exceedance probability earthquake effects (see Figure 1):

$$\frac{PGA\ at\ 10^{-5}/a}{PGA\ \ at\ 10^{-4}/a} \approx 1.4. \tag{3}$$

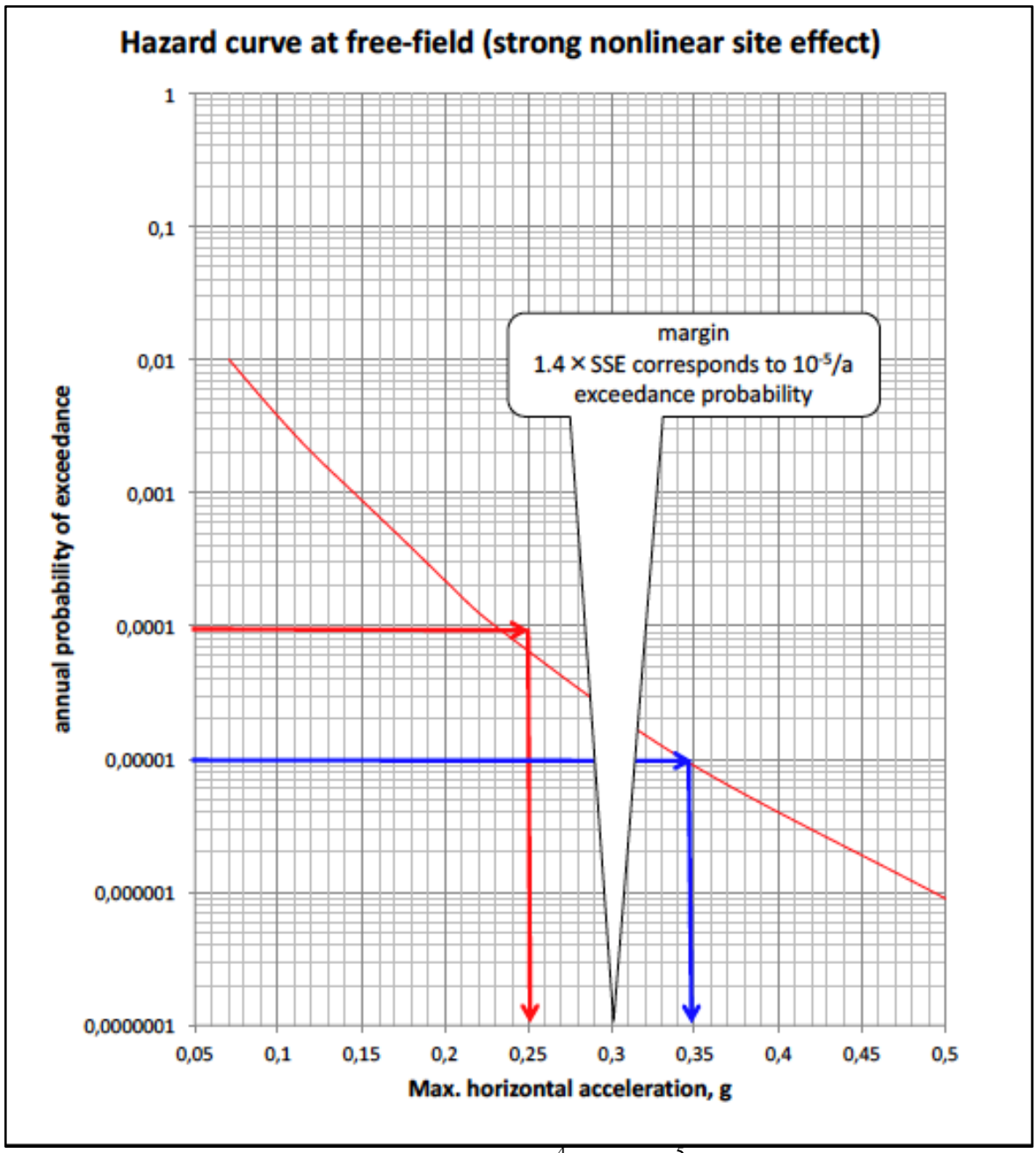

Figure 1 Seismic hazard curve. The values at 10^{-4}/a and 10^{-5}/a are indicated.

Hazards other than earthquake

As an example for hazards other than earthquake, let's consider the meteorological hazards. The extreme meteorological parameters are shown in the Table 2 for 10^{-4}/a and 10^{-5}/a annual exceedance probabilities.
It is obvious from the table, that the change of extreme values is practically negligible while the probability of exceedance is decreased by an order of magnitude, see Figure 2 where are shown the wind and maximum temperature hazard curves and increase of the parameters are only 14% and 6% while the frequency is decreased to 10^{-5}/a.
Moreover, the meteorological extremes are predictable, and a due time warning could allow effective protection.

Table 2 Extreme meteorological parameters

	Annual probability of exceedance		Slope $\frac{\text{value at } 10^{-5}/a}{\text{value at } 10^{-4}/a}$
	10^{-4}/a	10^{-5}/a	
Maximum temperature, °C	45.3	48.2	1.06
Minimum temperature, °C	-47.9	-55.7	1.16
Snow, kPa	1.5	1.8	1.20
Wind, m/s	41.5	47.3	1.14
Extreme daily precipitation, mm	132	155.7	1.18

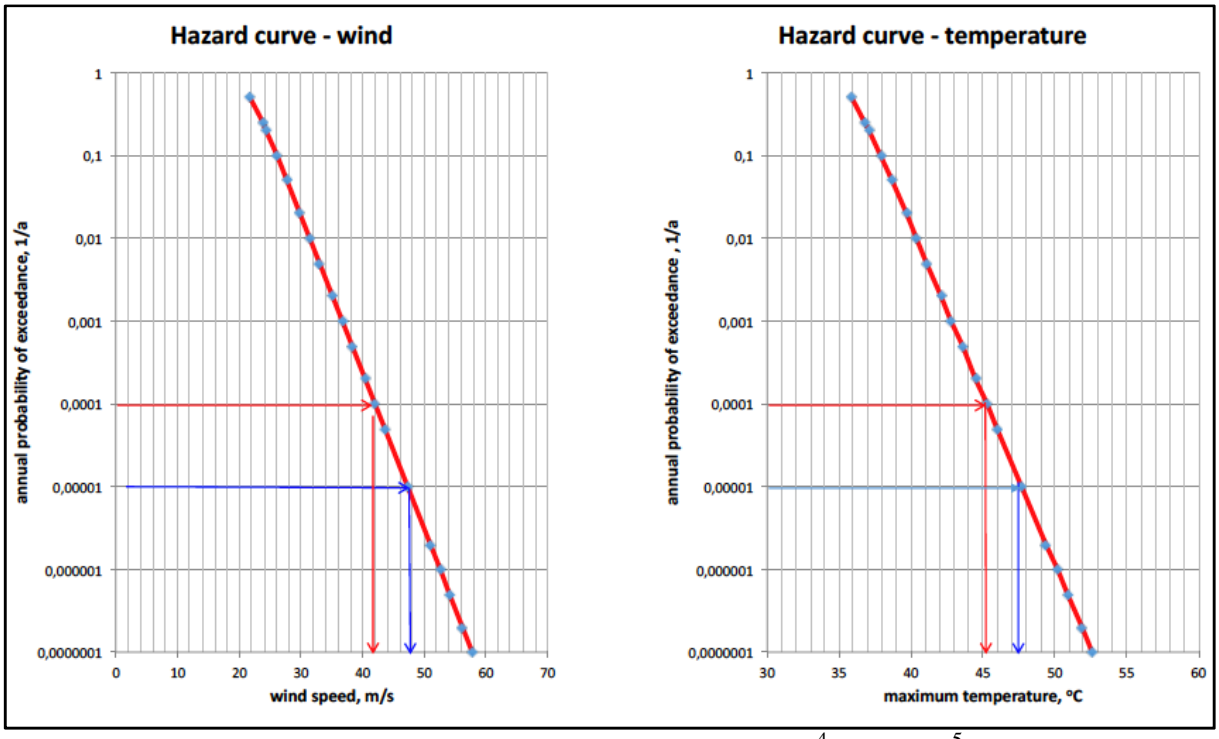

Figure 2 Meteorological hazard curves. The values at 10^{-4}/a and 10^{-5}/a are indicated.

4. VULNERABILITY OF SAM SSCS

The vulnerability of SAM SSCs has been assessed either by deterministic or probabilistic methods.

For example, the HCLPF seismic margin has been evaluated for the shelter of the protected command center. A margin of 40% above design basis earthquake loads for the whole facility has been assumed to be acceptable hence this margin will cover the earthquake vibratory effects of 10^{-5}/a (mean) exceedance probability; see Eq. (3). Moreover, building a backup command center is decided.

Probabilistic method has been applied for the definition of fragility of plant structures with respect to seismic and meteorological hazards.

The fragility of SSCs and the possibility of cliff-edge effect with respect of earthquake have been analyzed already in the frame of seismic PSA [9] and the identified vulnerabilities have been analyzed and weak items had been already eliminated. The remaining open issues are part of the post-Fukushima action plan.
It is very important that the containment has very high median capacity of 0.53g with respect to earthquake ground motion that is much higher than the maximum horizontal acceleration of a 10^{-5}/a earthquake. In the frame of stress test, the combinations of events have also been analyzed, e.g. the simultaneous loss of emergency power supply and leakage of the containment.
Fragility analysis of the plant structures has been made for extreme temperatures, wind and extreme precipitation after the stress test; see [11]. It was found that the plant civil structures have median capacity close or over to the 10^{-5}/a level meteorological extremes. For example, the median capacity of the No 2 diesel generator building with respect to the wind load is about 61 m/s that is well above the wind speed corresponding to the 10^{-5}/a level. In case of snow load the fragility curves of some structures are rather steep. The extreme snow load can be combined with high wind as well. However in case of extreme snow there is an obvious possibility for forecasting and prevention.
The evaluation of plant condition for beyond design basis liquefaction has been also performed by deterministic methods [4]. It was found that the uneven settlement due to liquefaction is the dominating damaging effect. The condition of the containment and main building complex housing the safety systems, also the communications (piping, cables) between the buildings, especially the piping of the emergency service water system can survive the effects caused by liquefaction. Criteria for the evaluation of the condition of the structures have been developed on the basis of IAEA Safety Guide NS-G-1.10, EUROCODE 8 Part 3, FEMA-356, ASCE-31, ASCE-41 and NUREG/CR-6926, etc.

5. DESIGN BASIS FOR NEW SAM FACILTIES

From the considerations above it is obvious, that the SSCs designed for 10^{-4}/a annual exceedance hazard parameters in accordance with relevant standards and have sufficient margin, and these SSCs remain functional even if the hazard parameter would exceed the design basis value. Analysis of the hazard curves have shown that this margin covers the hazard parameters with annual probability of exceedance one order of magnitude less than the design basis one.
Despite of above finding, a 10^{-5}/a annual probability of exceedance has been set for design basis hazard level for the newly designed super-emergency diesel generator and the shelter for backup protected command center. The reason for this decision is more practical rather than fundamental. The design is a straightforward process starting with definition of design input parameters and applying the rules of codes and standards. Evaluation of the margins and justification of the adequacy of the design for a beyond design basis actions is a rather complex exercise that is performed a posteriorly. Considering the site specific hazards at Paks it is simpler and even more cost-effective to design the mentioned above facilities for the actions of external hazard with 10^{-5}/a annual probability of exceedance, rather than to design for 10^{-4}/a and justify the sufficiency of margin.
Specific consideration is required regarding liquefaction hazard while designing alternative or super-emergency diesel station and backup command center. The possibility of liquefaction has to be excluded by soil improvement or appropriate foundation design.

CONCLUSION

The safety and seismic classified SSCs at Paks NPP are upgraded and qualified for 10^{-4}/a design basis annual probability of exceedance hazards. All these SSCs, including those needed for the severe accident mitigation and management have sufficient margins that ensure function and availability for the level of exceedance probability of hazard parameters one order of magnitude less than the design basis one. Demonstration of the margin excludes the possibility of cliff-edge effect, too.

For the design of the new SAM systems and facilities the external hazards of 10^{-5} annual probability are accounted for. The reason of this decision is practical. From the analysis of site-specific hazards it seems to be simple and cost-effective to design for enhanced hazard parameters rather than for a prescribed margin.

The concept developed for Paks NPP can guarantee the compliance with the safety targets for core-melt and early large release set by the Regulations.

REFERENCES

[1] HAEA, 2012, "National Action Plan of Hungary", Hungarian Atomic Energy Authority, Budapest, December 2012, http://www.ensreg.eu/EU-Stress-Tests/Country-Specific-Reports/EU-Member-States/Hungary

[2] IAEA, 2012, "Meteorological and Hydrological Hazards in Site Evaluation for Nuclear Installations", Safety Standards No. SSG-18, International Atomic Energy Agency; Vienna, November 2011

[3] NRC, 2007, "Design-Basis Tornado and Tornado Missiles for Nuclear Power Plants", Regulatory Guide 1.76, US Nuclear Regulatory Commission, March 2007

[4] Katona, T. J., Győri, E., Bán, Z., Tóth, L., 2015, "Assessment of Liquefaction Consequences for Nuclear Power Plant Paks", *Transactions, SMiRT-23*, Manchester, United Kingdom - August 10-14, 2015, Division VII, Paper ID 125

[5] Gürpinar, A., Godoy, A.R., Johnson, J.J., 2015, "Considerations for Beyond Design Basis External Hazards in NPP Safety Analysis", *Transactions, SMiRT-23,* Manchester, United Kingdom - August 10-14, 2015, Division IV, Paper ID 424

[6] IAEA, 2015, "Considerations on the Application of the IAEA safety Requirements for design of NPPs" (Draft TECDOC), IAEA, Vienna

[7] HAEA, 2011, Nuclear Safety Regulations, Volume 3, Govt. Decree 118/2011. (VII.11.) Korm. Hungarian Atomic Energy Authority, Budapest, 2011

[8] IAEA, 2012a, Safety of Nuclear Power Plants : Design, SSR-2/1, International Atomic Energy Agency, Vienna, 2012, ISBN 978–92–0–121510–9

[9] VEIKI, 2002, "Paks Seismic PSA – Summary of Results", VEIKI Technical Report No. 22.52 921/7, Issue 2, July 2002

[10] EPRI 1991. "A Methodology for Assessment of Nuclear Power Plant Seismic Margin", (Revision 1), EPRI NP-6041-SL, Rev. 1. Electric Power Research Institute, Palo Alto, California

[11] Bareith A., Karsa Z., Siklóssy T., 2011, "Development of the PSA methodology for external hazards – Fragility analysis", in Hungarian, Research Report of the Nuclear Safety Research Institute, Budapest, No 221-010-00/3

INTERNATIONAL SCIENTIFIC CONFERENCE ON ADVANCES IN MECHANICAL ENGINEERING
13-15 October 2016, Debrecen, Hungary

PACKAGING PRACTICES IN AUTOMOTIVE ENGINE SUPPLY CHAINS

VÖRÖSKŐI Kata

Széchenyi István Universtity, Department of Logistics and Forwarding
E-mail: voroskoi.kata@sze.hu

Abstract
Actors of a traditional supply chain usually consist of manufacturer company, wholesaler, retailer and customer at the end of the chain. But, automotive groups have special supply chain in terms of that engine producers sell their products for firms of the same ownership. This situation significantly influences on the decision of what type disposable and/or returnable packaging should be chosen. In this paper automotive industrial packaging used in practice for engines will be reviewed, focusing on engine companies, which is one of the main elements of the vehicle industry. Recent trends like active and intelligent packaging will also be presented.

Keywords: *supply chain, automotive packaging, engine*

1. DEFINING AND CATEGORISING OF SUPPLY CHAINS

This chapter shows a short review on trends and classification in the supply chain management concerning packaging implication. A supply chain (SC) involves the flow of goods and information among the actors: suppliers, manufacturers, distributors, retailers, logistics providers and customers (at the end of the chain). Material management and physical distribution are the two main business processes within the supply chain. Material management supports the internal control of production materials, manages the acquisition and storage of raw materials, parts, and supplies. On the other hand, physical distribution comprises the outbound logistics activities, for example transportation and customer service. Unlike the denomination, a supply chain usually does not mean a linear chain between businesses, rather a network of multiple companies on the different levels.[1]
Fisher classifies supply chains according to the demand patterns of the products they produce, which are either functional or innovative. Functional products satisfy basic needs, have predictable demand and long life cycles. At the same time this stability causes competition, which often leads to low profit margins. Although innovation can make higher profit margins possible, the demand for these innovative products is unpredictable and their life cycle is short. In case of functional products companies mainly focus on physical costs (like cost of production, transportation and inventory storage). Another characteristic of them is the one month or six week schedules for assembling finished goods and the usage of manufacturing-resource-planning (MRP) software to minimize inventory and maximize production efficiency. The flow of information occurs among suppliers, manufacturers and retailers. This strategy does not work for innovative products, because the uncertain market reaction increases the risk of shortage or excess supplies. It is important to consider daily sales numbers and to react quickly. Crucial information flows not only within the chain, but also from the marketplace to the chain. The critical decisions are not about minimizing cost but about where to place inventory and production capacity in the chain. Suppliers should be chosen rather for their flexibility, not for low cost. Fisher describes cars as products can be offered as a basic functional product or also in an innovative form: “A lean, efficient distribution channel is exactly right for functional cars but totally inappropriate for innovative cars, which require inventory buffers to absorb uncertainty in demand”.[2]

The goal of an integrated supply chain is to ease the seamless flow of material, money, resources and information. Another type of SC approaches when the lean and agile manufacturing paradigms are integrated in the total supply chain at the same time, it is called 'leagility' in the literature. Another term should be introduced here, the decoupling point. It is a separation point (or points in some cases) within the supply chain between the part oriented to orders and the part of the SC based on preliminary planning. The reason why these two parts need to be separated is the difference between the paradigms. The point of lean manufacturing is to eliminate all non-value adding processes and in the most optimal case with minimum inventory. However agile manufacturing also has the same goal (to eliminate as many non-value adding activities as possible), but this system considers stock and capacity requirements carefully in order to ensure robustness and the flexible response to changes of the SC. In other words the downstream part of the SC from the decoupling point is market driven, while the upstream part is initially forecast driven.[3]
Another term we should be familiar with is 'demand chain'. Demand chain management coordinates the supply chain from end-customers backwards to suppliers[4]. It requires extended integration between all business partners. These type of connection is only possible recently due to the web-based technologies, which enables real-time demand information and inventory visibility. Demand driven supply chains not only allow companies to meet existing customer's expectations better but also to win customers in new markets. Frohlich et al. model shows, that the higher the level of integration the greater the performance.[5] In other words a "demand chain is a supply chain that emphasizes market mediation to a greater degree than its role of ensuring efficient physical supply of the products"[6].

2. AUTOMOTIVE PACKAGING

Packaging is a significant element in any logistics system; it is listed among the key logistical activities[7]. The functions of packaging can be classified as follows: (1) product and environmental protection (physical, safety, natural deterioration, waste reduction), (2) logistics containment and handling (unit, bulk, pallet, containers), (3) information (logo, description)[8].
Packaging can be divided into three types as automotive industry also uses:

- primary packaging (consumer packaging)
- secondary packaging (retail packaging)
- tertiary packaging (transportation packaging).[9]

The best packaging solutions for automotive packaging are those that beside the optimal cost levels can maximize the use of packaging space so that all the products can easily be packed and stacked, at the same time reduce packaging waste (for example boxes, folding cartons, customized trays, foldable containers, etc.)[10]. This way the following packaging system are the most popular used in automotive industry: one-way and returnable. Former is only suitable for one use as far as reusable containers and packaging are loaded with products and shipped to the destination, then the empty container is sent back to the supplier, refilled with products and this cycle is repeated over and over again as a closed-loop system In some cases it is an open-loop system, or in many cases reusable packaging is collected at a centralised return handling centre, where it is cleaned, stocked, and distributed for refilling[11]. Returnable packaging materials can be classified as a Returnable Transport Item (RTI) and they are usually part of a closed-loop supply chain in the automotive industry[12].

3. AUTOMOTIVE SUPPLY CHAIN VERSUS PACKAGING SUPPLY CHAIN

The automotive industry includes a wide range of companies and organizations involving the activities of design, development, manufacturing, marketing, and the sale of vehicles. This part of

the industry is one of the world's most significant economic sectors by its revenue. However, the automotive market is very concentrated, namely the 10 largest automotive groups share almost 80% of the market[13].

The most important actors of an industrial packaging supply chain (PSC) are suppliers, assembly factories[1] and packaging collectors (if returnable packaging is used). Packaging producers are also important, but choosing the right packaging for the product belongs to the competency of the factories, their suppliers or both together.

The role of OEM (Original Equipment Manufacturer) in the automotive supply chain (ASC) is to acquire the components and to integrate them into the ready-made new vehicle. Therefore the major OEMs are mainly focus on core competencies. This means that the OEMs have shifted their focus from handling a large number of parts toward the assembly of entire modules, which are delivered directly from a significantly smaller number of suppliers than before[14]. Based on the trend of focusing on core competencies, suppliers have an increasingly important function in the ASC. We shall also mention that the four main roles of suppliers have been classified by Veloso, Henry, Roth, and Clark (2000) as follows: (1) systems integrator, (2) global standardiser/systems manufacturer, (3) component specialist and (4) raw material supplier[15]. This paper concentrates on the engine producers and their place in the ASC. The above-mentioned classification is applied to a supply chain where the engine producer is in the focus. *(Figure 1 – left)*

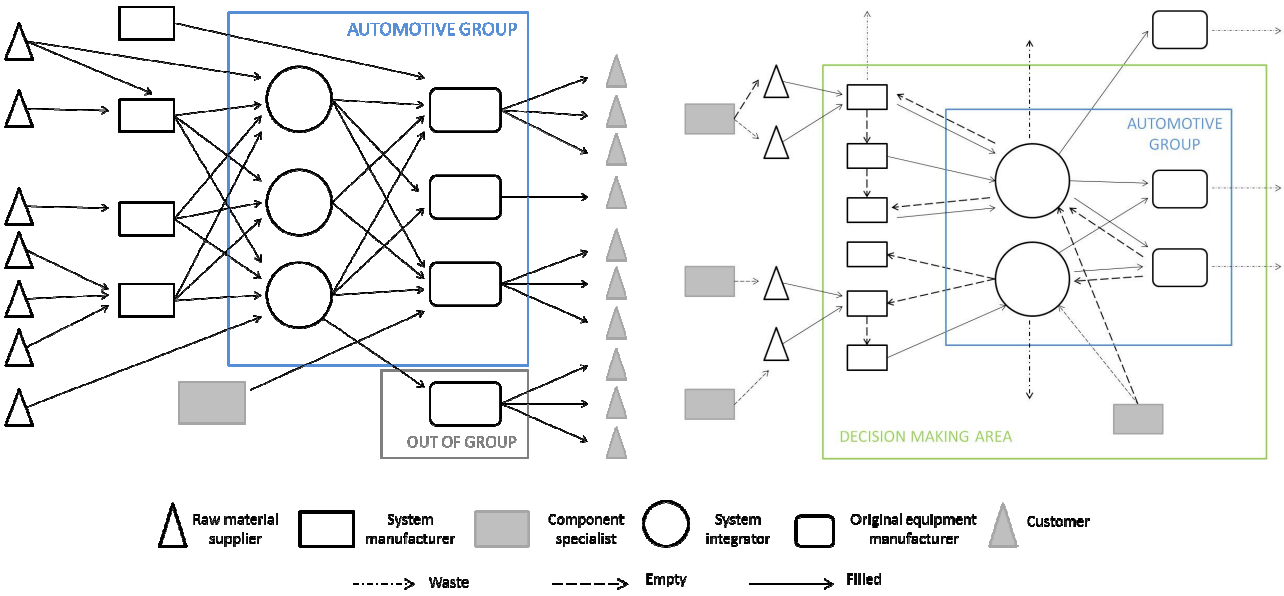

Figure 1 Left: Automotive supply chain Right: Automotive engine packaging supply chain

In this case, the engine company plays the role of system integrator, then the OEM complies with the vehicle-assembling factory. It has to be highlighted that the engine producers of the automotive industry usually belong to the same ownership group as the OEM. This way the largest part of their products is sold for the concern or group subsidiaries. Furthermore, a part of their suppliers is shared with other engine producers and the OEMs also within the group. Because of this special ownership structure, the ASC should be organised differently from any other industries, and packaging decisions will also be significantly affected. *(Figure 1 – right)* Returnable packaging is more common on the outbound flow of the engine companies. Decision-making on choosing the

different types of packaging exceeds the “borders” of the automotive group companies and usually the suppliers “suffer” its consequences.

4. AUTOMOTIVE ENGINE PACKAGING IN THE PRACTICE

In the automotive industry the primary function of packaging is the protection of products and parts optimised by the total costs of logistics. This way, even if shipping is performed on land or sea, by rail, trucks, vessels or multi-mode shipping, the distribution environment and logistics costs together define the possible form of packaging, and then determine the final solution from disposable to returnable packaging and systems.[16][17] Returnable packaging has been frequently used, for example, in the US automotive industry, in order to reduce waste, costs, transport damages and to enable JIT deliveries[18]. Standardised shipment materials are usually used as returnable packaging in the ASC, like the EUR/-EPAL pallets, racks, containers and specialty bins for certain types of parts[19].
To store and transport the finished engines, special steel racks are mainly used. These ensure safe and reliable transport and storage. The column is usually collapsible in order to save place while return back as empty transportation. The posts are supposed to keep the engine in place, but these can be also collapsed. *(Figure 2)*

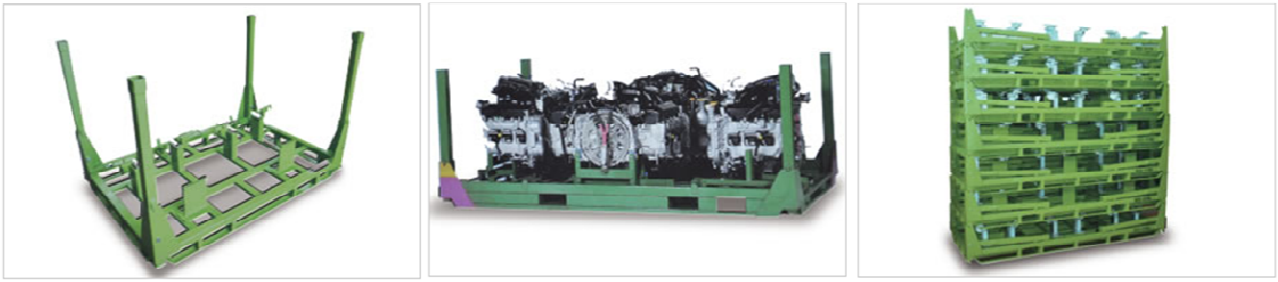

Figure 2 Returnable stillage for engine transportation: empty, loaded with engines and folded[20]

There are other ways, Suzuki for example uses transport boxes and DS Smith produces wooden tools. *(Figure 3)*

Figure 3 Other engine disposable (one-way) packaging solutions[21]

5. ACTIVE AND INTELLIGENT PACKAGING

During the past decades, several new or improved packaging technologies have emerged to satisfy the needs of the market, especially those relating to active and intelligent packaging. Active packaging involves advanced technologies that actively change the internal conditions of the package to extend product shelf life. Intelligent packaging involves the use of smart package

devices (such as RFID tags, time temperature indicators, and biosensors) to track product, sense the environment inside or outside the package, monitor product quality, and improve efficiency.[11] Demand for active and intelligent packaging in the US is forecast to increase 7.3 percent per year, stimulated by the need to develop more advanced packaging to suit products with sensitivity to moisture, temperature, or chemicals[22]. Market growth is expected for active packaging with leading shares of moisture absorbers, oxygen scavengers, microwave susceptors and antimicrobial packaging[23]. Although some cases using thermal monitoring in the automotive application can be found[24], it is more commonly applied for food transportation. But for example radiofrequency identification could be used more to inspect returnable containers[25].

CONCLUSIONS

Returnable packaging is dominant in the automotive packaging supply chain. Both disposable and returnable packaging is used, but returnable is preferred especially in the deliveries between the engine producer and the OEM even if the destination is over sea. Although several forms of returnable devices can be observed in practice, their function is built up from the same conceptual structure. Disposable solution appears only if the engine producers cannot dominate the supplier's decision on packaging strategies or the OEM is out of same automotive group. But it is expected that using of intelligent packaging will increase in the automotive industry in the near future.

REFERENCES

[1] Hokey Min, Gengui Zhou: *Supply chain modeling: past, present and future*. Computers & Industrial Engineering, 43, 231-249., 2002.
[2] Marshall L. Fisher: *What is the right supply chain for your product?* The Harward Business Review, March-April, 1997.
[3] J. Ben Naylor, Mohamed M Naim, Danny Berry: *Leagility: Integrating the lean and agile manufacturing paradigms in the total supply chain.* International Journal of Production Economics, 62, 107-118., 1999.
[4] Vollmann T.E., Cordon C., Heikkila J.: *Teaching supply chain management to business executives*. Production and Operations Management 9 (1), 81-90., 2000.
[5] Markham T. Frohlich, Roy Westbrook: *Demand chain management in manufacturing and services: web-based integration, drivers and performance*. Journal of Operations Management, 20, 729-745., 2002.
[6] Suzanne de Treville, Roy D. Shapiro, Ari-Pekka Hameri: *From supply chain to demand chain: the role of lead time reduction in improving demand chain performance*. Journal of Operations Management, 21, 613-627., 2004.
[7] Stock J R, Lambert D M: *Strategic Logistics Management*, New York: McGraw-Hill Higher Education, 2001.
[8] Böröcz P, Mojzes Á: *The importance of packaging in logistics*. Transpack, 8 (2), 28-32., 2008.
[9] F.T.S. Chan, H.K. Chan, K.L. Choy: *A systematic approach to manufacturing packaging logistics*. The International Journal of Advanced Manufacturing Technology, 29, 1088-1101., 2006.
[10] http://www.mjspackaging.com/blog/what-are-the-best-packaging-solutions-for-automotive-packaging/ (access on 05. 10. 2016)
[11] Yam K L: *The Wiley encyclopedia of packaging technology*. Wiley, USA, 2009
[12] Böröcz P, Singh SP, Singh J.: *Evaluation of Distribution Environment in LTL Shipment between Central Europe and South Africa.* Journal of Applied Packaging research, 7 (2), Paper 3, 2015.

[13] Lowry W: *A must-know investor's guide to Ford Motor Company*, 2014. http://marketrealist.com/2014/05/must-know-investors-guide-ford-motor-company/ (access on 11. 04. 2016)
[14] Doran D: *Supplying on a modular basis: an examination of strategic issues*. International Journal of Physical Distribution & Logistics Management, 35 (9), 654-663., 2005.
[15] Veloso F, Henry C, Roth R, Clark J: *Global Strategies for the Development of the Portuguese Autoparts Industry*, 2000. http://in3.dem.ist.utl.pt/labpolicy/docs/part_b5_4.pdf (access on 12. 15. 2016)
[16] Böröcz P, Vastag Gy: *Good Vibrations: Lessons from Packaging for the Global Supply Chain*, POMS 26th Annual Conference, Washington, USA, Production and Operations Management Society, pp. 1318, 2015
[17] Böröcz, P, Singh SP.: *Measurement and Analysis of Vibration Levels in Rail Transport in Central Europe*. Packaging Technology and Science, 2016
[18] Witt C E: *Are reusable containers worth the cost?* Material Handling Management, 55 (7), 75., 2000.
[19] Boysen N, Emde S, Hoeck M, Kauderer M: *Part logistics in the automotive industry: Decision problems, literature review and research agenda*. European Journal of Operational Research, 242 (1), 107-120., 2015.
[20] http://china-rollcontainer.com/product-6-1-engine-transport-stillage.html/138065 (access on 03. 10. 2016)
[21] http://www.directindustry.com/prod/ds-smith/product-124295-1425623.html (access on 03. 10. 2016)
[22] http://www.prnewswire.com/news-releases/us-active--intelligent-packaging-market-300273480.html (access on 04. 10. 2016)
[23] Carolina E. Realini, Begonya Marcos: *Active and intelligent packaging systems for a modern society*, Meat science, 98, 404-419., 2014.
[24] J.L. Merino, S.A. Bota, A. Herms, J. Samitier, E. Cabruja, X. Jorda, M. Vellvehi, J. Bausells, A. Ferre, J. Bigorra: *Smart temperature sensor for on-line monitoring in automotive applications*, On-Line Testing Workshop, 2001.
[25] Taebok Kim, Christoph H. Glock: *On the use of RFID in the management of reusable containers in closed-loop supply chains under stochastic container return quantities*, Transportation Research Part E, 64, 12–27., 2014.

SUPPORTING COMPANIES

THE ISCAME 2016 CONFERENCE AND THE 4th MECHANICAL ENGINEERING INDUSTRIAL EXHIBITION, DEBRECEN

Company name	Website	Location
Aventics Hungary Kft.	www.aventics.hu	Eger
Coloplast Hungary Kft.	www.coloplast.com	Nyírbátor
Diehl Aircabin Hungary Kft.	www.diehl.com	Nyírbátor
Eagle Ottawa Hungary Kft.	www.eagleottawa.com	Szolnok
eCon Engineering Kft.	www.econengineering.com	Budapest
Electrolux Lehel Kft.	www.electrolux.hu	Nyíregyháza
Enterprise Communications Magyarország Kft.	www.enterprise-group.hu	Budapest
Eurosolid Kft.	www.eurosolid.hu	Budapest
FAG Magyarország Ipari Kft.	www.schaeffler.hu	Debrecen
Flexiforce Hungary Kft.	www.flexiforce.com	Debrecen
FlexLink Systems Kft.	www.flexlink.com	Budapest
Grimas Kft.	www.grimas.hu	Budapest
HAJDU Cégcsoport	www.hajdurt.hu	Téglás
Hoya Szemüveglencse Gyártó Magyarország Zrt.	www.hoya.com	Mátészalka
Lego Manufacturing Kft.	www.lego.com	Nyíregyháza
MSK Hungary Gépgyártó Bt.	www.msk.hu	Nyírbátor
Nyomda-Technika Kft.	www.nyt.hu	Debrecen
Robert Bosch Automotive Steering Kft.	www.bosch.hu	Eger
Seco Tools Kft.	www.secotools.com	Budapest
SPM Instrument Budapest Kft.	www.spminstrument.com	Budapest
Szimikron Kft.	www.szimikron.com	Kecskemét
Takata Safety Systems Hungary Kft.	www.takata-miskolc.hu	Miskolc
T-Drill Oy	www.t-drill.fi	Laihia, FIN
Teva Gyógyszergyár Zrt.	www.teva.hu	Debrecen
Tranzit-Food Kft.	www.goldenfood.info.hu	Debrecen
Trumpf Hungary Kft.	www.trumpf.com	Vecsés
Unilever Magyarország Kft.	www.unilever.hu	Nyírbátor
Ventifilt Légtechnikai Zrt.	www.ventifilt.hu	Hajdúnánás
ZF Hungária Kft.	www.zf.com/hu	Eger

AVENTICS HUNGARY KFT.

Address: 3300 Eger, Bánki D. u. 3.
Phone: +36 36 531 600
Webpage: www.aventics.hu

Main activity: Manufacturing and sales of pneumatic equipments
References: In commercial vehicle manufacturing: MAN, Daimler, Scania, Volvo, DAF, TATA;
In parts manufacturing: ZF, EATON, GT
Products and services:
Mechanically-, electrically- and pneumatically operated valve systems, quick-relief valves, single-acting cylinders, clutch valves, integrated actuators, spare parts, air preparation systems, hoses, connectors
Certifi cates: ISO TS 16949, ISO 14000, ISO 9001, MEBIR MSZ 28001:2008
Founded in: 2014

ABOUT THE COMPANY

A former subsidiary of the Bosch Group, AVENTICS has been operating independently as a manufacturer of pneumatic systems since 2014 and is currently one of the world's leading suppliers. Its products are used among others in food and beverages industry, packaging and print techniques, as well as metal machining.
Aventics Hungary Kft. is one of the most prominent companies of Heves county. It has a leading position in cylinder manufacturing and assembly and produces valves and marine parts. It is also a supplier of driveline solutions and valve control systems for commercial vehicles. The company pays special attention to the integration of electronic systems in pneumatic components and off ers configured and tailor-made solutions in addition to its established product line. As opposed to largeseries manufacturers, AVENTICS is capable of fulfilling orders for small batch orders with short deadlines, selling over 25,000 different types of products every year to more than 10 thousand customers.

COLOPLAST

Webpage: www.coloplast.com

About Coloplast

Coloplast is a Danish international company that develops products and services that make life easier for people with very personal and private medical conditions. Working closely with the people who use our products, we create solutions that are sensitive to their special needs. We call this intimate healthcare.
Our business includes ostomy care, urology and continence care, and wound and skin care. We operate globally, employing more than 10,000 people. According to Forbes, Coloplast is among the 35 most innovative company in the world! We employ over 10,000 people from 100+ countries. In 2017 we expect to be 11,000 people globally.

Our mission, vision and values

Closeness to all customers makes this possible. We listen to better understand needs, and respond by finding new ways to do things better together. We lead the way by bringing the best ideas first and fast to market in the form of medical devices and service solutions. Deeply private and personal medical conditions are our focus. Our passion to make a real difference to people's lives is what drives and unites us. Our culture supports high ambitions, and releases the full potential of our own people to achieve them. We welcome the broader responsibility that comes with leadership - a responsibility to the environment, to society, to our shareholders, and to act with integrity in all we do.
Coloplast was built on the fundamental ability to listen and respond. Nurse Elise Sørensen listened to her sister's concerns, she understood her needs, and responded by inventing the world's first disposable ostomy bag. An invention that has made life easier for thousands of people. Ever since, listening and responding has been an integral part of all we do. Only by listening, can we understand the world of our consumers and act accordingly by developing the right products and services. Over decades, we have gained invaluable knowledge through working directly with healthcare professionals and the people who use our products.
We will be a trusted guide for consumers in a world of information overload – and a stronger partner with clinicians who are the experts in caring and healing. At Coloplast, we strive to be a greater resource for everyone by setting the global standard for listening and responding.
Our values define the way we think and act, both as individuals and as a company.

Coloplast in Hungary

Coloplast employs more than 3000 people in Hungary. There are 2 factory sites in Tatabánya and Nyírbátor and Postponement and Distribution Center in Tata. We are continuously growing! Join us!
When you get a job here, you get much more than just that – you get a career! We'll push you, stretch you and reward you. Performance here goes a long way, you drive your own career development. Be ambitious and deliver results, and you'll thrive.

Coloplast Hungary Kft Tatabánya
2800 Tatabánya, Búzavirág u. 15.
34/520-500

Coloplast Hungary Kft Nyírbátor
4300 Nyírbátor, Coloplast u.2.
42/886-300

Coloplast PDC Tata
2890 Tata Barina u.1.

DIEHL AIRCABIN HUNGARY KFT.

Address: H-4300 Nyírbátor, Ipari Park utca 9.
Phone: +36 42 510 720
Webpage: www.diehl.com

Welcome to Diehl Aircabin Hungary Kft.

Diehl Aircabin Hungary Kft. is a 100% subsidiary of Diehl Aircabin Gmbh., based in Laupheim Germany, and a member of the Diehl Aerosystems syndicate through the parent company.
Diehl Aircabin has established itself as a preferred partner in the international aviation industry. With its cabin modules, crew rest compartments, and air ducting, Diehl Aircabin provides an array of highly specialized aviation solutions under the general umbrella of Diehl Aerosystems.
The area of expertise of Diehl Aircabin GmbH includes product and process development, design, predevelopment, construction, and the production and qualification of cabin elements. The integration of system components such as in-flight entertainment, oxygen systems, and electrical equipment also forms an important part of the company's broadly based portfolio.
The story of the Hungarian company started in February 2011, when the growing pace of the German parent company made it necessary to establish a new production plant, where they could move a portion of the existing Single Aisle and Long Range airplane part manufacturing. After analyzing multiple sites globally, they choose Hungary: more precisely, Nyírbátor.
In its Nyírbátor plant, Diehl Aircabin Hungary Kft. manufactures three important parts of the passenger cab for the Airbus A319/320/321, A340, A350 and A380 planes: the sidewalls, the door doorframe casing and the air-conditioning pipes that provide the air supply. In our plants, we employ 450 employees. This August we opened our second and brand new production hall in our plant. Till 2018 our headcount will nearly double. Currently, 75% of our employees work in production.
For the production of these mostly handmade parts, the production of which can also be called almost “manufactorial”, a highly special knowledge is required which cannot be matched completely with any current school education. Therefore, beginning with the 2016/2017 school year, our company will also join the Dual Vocational Training system which, according to our plans, will provide education linked to practice in professions that we specifically need. At the same time, the training aims at improving the best skills and abilities of the individual. Students who graduate with good results can count on stable, long term employment. For engineers and people with a higher level of education, we offer more than fix and stable work: we offer a career opportunity. Positions in important areas such as production preparation, process engineering, quality assurance, logistics and economy-finance are expanding in size and responsibility. When launched, our comprehensive trainee program will be adjusted to our future improvements. Our headcount will nearly double after the construction of the new plant hall, and the range of product will widen. As the first step of this process, we would like to fill the engineering positions mentioned above. We are simultaneously hiring entrant engineers, trainees and more experienced colleagues. Moreover, we are counting on colleagues with unique qualifications, such as airplane designers or engineers who have the special certification required for airplane manufacturing. We hope we have been able to increase your enthusiasm for the airplane industry.

Fly with us to the safe future!

EAGLE OTTAWA HUNGARY KFT.
Address: 5000 Szolnok, Piroskai út 12.
Phone: +36 56 889524
Email: toborzas@eagleottawa.com
Webpage: www.eagleottawa.com

Why work for Eagle Ottawa?

We are large enough for your career, yet small enough to care!

We are part of Lear Corporation, which is the 154th largest company in the US stock exchange and the largest supplier to the Automotive Industry.
Eagle Ottawa Hungary is the largest private employer in Szolnok. Over 2,000 people work in our two plants.

At our Hungary plants, we produce premium quality seat leather for models of BMW, Jaguar, Land Rover, Mercedes, Toyota, Volvo and many others.

Leather is unique. It's luxurious, extremely durable, and a wonderful canvas for creativity. Through tightly controlled production processes, Eagle Ottawa makes the best automotive leather in the world for enhancing the driving experience.

We have customers in all of Europe and North Africa. Many of our production team members enjoy business travel to our customers.
We have sister plants in America, Thailand, China, Mexico and Brazil. Many of our staff travel to those international locations to learn and provide support.
We have two plants at Szolnok. One built in 2004 and expanded twice, one built in 2015. Our plants are modern, safe, and with good facilities.

Our equipment is state of the art. For example, our team leaders operate, and are responsible for a million euro finishing line.

We offer competitive wages and benefits – from new entry team members, through engineers and managers. We offer training courses and development opportunities.

Career growth is important to us. Over 80% of managers promoted from within company. Our four plant and production managers all started at Eagle Ottawa as engineers or logistics specialists.

We care for the environment and our surroundings. We sponsor local activities such as youth streetball competition, environmental clean up and donate used computers and pallets (to make outdoor furniture) to local schools.

eCon Engineering Kft.

Address: 1116 Budapest, Kondorosi út 3. IV. emelet
Phone: +3612790320/101
Webpage: www.econengineering.com

SOFTWARE SALES AND SUPPORT:

eCon Engineering Kft. was established in 2002. We emphasize our mission on the distribution of advanced engineering simulation technologies by representing such products as ANSYS, Moldex3D and Cast-Designer.

Beside the distribution of these software products we also provide solid mechanical-, fluid dynamical-, thermal- and electromagnetic analyses, injection moulding simulations, moulding optimisation and metal casting simulations during the product and design development of our customers.

The 46 years of experience and the thousands of developers worldwide are the guarantees for the market leader position of ANSYS, which was earned by its wide variety of solvers, easy operability and reliability of engineering simulations in the fields of solid mechanics, thermodynamics, fluid dynamics and electromagnetics. The ANSYS software family offers outstanding possibilities for Simulation Driven Product Development, which is indispensable in today's modern and cost-effective engineering.

The leading injection moulding simulation software provides product designers, designers/producers of moulding tools and manufacturers with the capability of predicting the outcome of their work. This way the injection moulding technology and the quality of the final product becomes much more reliable.

A practical cast designer and simulation software that enables the investigation of the cast parameters and eliminates the possible failures of the casting process during the design phase. It's a reliable tool for product and casting tool designers for cost- and time-effective cast design and production.

ANALYSIS:

Finite Element Method Analysis based development fits into the profile of eCon. With valuable experiences in the field of FEM development we offer engineering solutions for our partners.

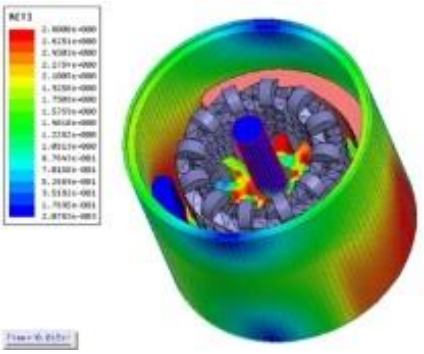

A skilled team of 50 engineers with a wide spectrum of knowledge in the fields of mechanics, optimisation, durability and fatigue analysis, analysis of composite frames, hydrodynamics, thermodynamics, correlation analysis, dynamics, vehicle construction, medical technology and turbine physics. It's very important for us to provide our customers with a complex solution on the most professional level.

We don't only focus on just a single problem, we aim analyse the whole spectrum of possible problems and provide a comprehensive solution.

SINGLE-PURPOSE MACHINES:

Our company also produces special single-purpose machines, assembly lines, testers for the car and the IT industry, according to the customer's needs.

Projects include the whole production process, from the development of technology to the execution procedure, concluding with onsite installation. Guarantee servicing and full-scale project management are also included.
Our quality policy is to use our experience, developments and knowledge to fulfil and to exceed our customer expectations.

ELECTROLUX LEHEL KFT.

Address: 4400 Nyíregyháza, Ipari Park
Phone: 426594-852
Webpage: www.electrolux.hu

ELECTROLUX
IN HUNGARY FOR 25 YEARS

Electrolux is a global leader in home appliances and appliances for professional use. Our company Electrolux Lehel Ltd. is one of the subsidiaries of the Swedish AB Electrolux. At Electrolux Lehel Ltd., the manufacturing operations are located in Jászberény and Nyíregyháza, while the sales and marketing organization and the Global Logistics Centre of Small Appliances can be found in Budapest. The company's main profile is the production of refrigerators, freezers, chest freezers and vacuum cleaners. The Jaszbereny and Nyiregyhaza sites are the company group's priority manufacturing base in Europe.

In Hungary, both medium and high category models are produced; primarily, to the European markets but products are also shipped to the United States of America, Brazil, Japan, and even to South-Korea. According to the TOP 200 survey comparing domestic companies, Electrolux Lehel Kft has become the 17th largest export company. In 2015, Electrolux reached the total turnover of 275,2 billion Hungarian Forints in Hungary.

Electrolux has 3,000 employees on average in Hungary and offers job opportunities to some other 2,500 people through its suppliers. As a responsible company, an integral part of the business strategy of Electrolux is sustainability. 100% of the electric energy used at its Hungarian sites comes from renewable energy resources, and they also use LED lighting and, in the course of production, recycled materials.

ENTERPRISE COMMUNICATIONS MAGYARORSZÁG KFT.

Address: H-1138 Budapest, Váci str. 117-119.
Phone: +36 (1) 471-2380 / ext. 2
Webpage: www.enterprise-group.hu

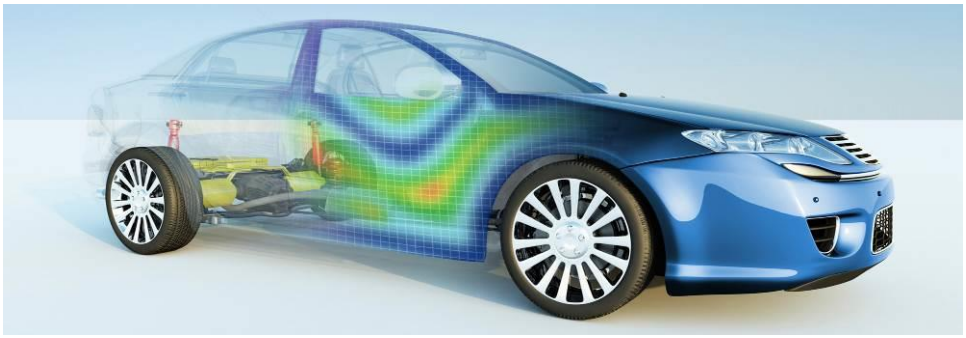

Enterprise Group PLM Business Unit – Engineering Solutions

CAD/CAM solutions and product lifecycle management (PLM) from design to implementation

Our PLM division provides complex engineering solutions and IT services for companies that operate in the field of industry. The market-leading solutions of Siemens PLM and Vero Software cover the entire lifecycle of products - from the original concept, through the design process, all the way to manufacturing - and also support product development and recycling. Our team of experts, with decades of experience in the industry, coupled with the stable corporate background of the Enterprise Group, ensures that our clients will always receive reliable solutions that are customised to meet their own particular requirements.

PLM is a complex process which facilitates the management of a product's entire lifecycle. It includes computer aided design (CAD) and manufacturing (CAM) solutions, but it is more complex than that, as it encompasses the full lifecycle of products. PLM offers advantages such as time-to-market acceleration, product quality improvements, prototype production cost reductions, rapid identification of potential sales opportunities and overall cost savings by recycling previously obtained data and by fully integrating engineering work processes.

Our PLM division supplies the well-known products developed by Siemens PLM Software, as well as their connected services. The division is ready to serve existing and future clients as a distributor of Solid Edge, NX, Tecnomatix Teamcenter and Femap.

With solutions from Vero Software, the world's largest CAM-oriented CAD/CAM developer, the division is capable of comprehensively satisfying all the requirements of manufacturing companies. Among these solutions, Edgecam is recommended for machining, Radan for sheet metal manufacturing tasks, and Alphacam for the wood and stone industries.

Besides supplying the market's well-known Siemens PLM products and solutions, Enterprise Group's PLM division also helps partners with the introduction of new software, as well as support and updates, training programs and constant availability. Our staff, consisting of experts with decades of experience in engineering, IT and industry related projects, can also call on the knowledge of Enterprise Group's other divisions and rely on the smooth operational background of the company when implementing their own projects.

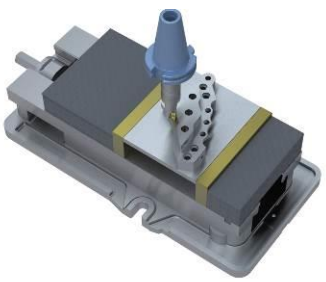

EUROSOLID LTD.

Address: Budapest, 1117 Szerémi út 7/B
Phone:+361 216 8661
Webpage: www.eurosolid.hu

EuroSolid Ltd. has been dealing with the introduction and installation of CAD/CAM/PLM/MDC systems, process optimization, education and support of technical, engineering and manufacturing softwares for almost 20 years. Since its foundation, our company was driven by one goal which is to help companies in product development and manufacturing fields in the most efficient way and at the highest professional standards to tackle their technical challenges.

Today EuroSolid Ltd is one of the market leaders and has more than 600 partners with references such as Michelin, Aloca, Coloplast, GE or Linamar.

Our company is the sole and exclusive distributor of SOLIDWORKS softwares in Hungary plus the only qualified education and support centre in the country. As the representative of SOLIDWORKS, our activities include professional client support, data management system installation, delivering and solving engineering tasks and performing different simulation tests with our softwares.

SOLIDWORKS is the market leading and the most integrated software system available. In the past 25 years the CAD software has grown out to became the foundation of a wide ranged product portfolio which not only includes engineering design and simulation but also electrical design, data management, quality management for inter- and post production processes, sheetless sketch creation, rendering, technical documentation modules and so much more.

Our goas is to deliver solutions with the excellent tools, quickly-to-adapt and easy-to-learn systems of SOLIDWORKS and with the new technologies supporting design and manufacturing that ensure profitable investment and increasing productivity with optimized workflow for our clients.

FAG MAGYARORSZÁG IPARI KFT.

Address: 1/D Határ Road/Street, 4031 Debrecen, Hungary
Phone: 00 36-52-581-700
Webpage: http://www.schaeffler.hu

A leading global technology company

The Schaeffler Group is a leading global integrated automotive and industrial supplier. The company stands for the highest quality, outstanding technology, and strong innovative ability. The Schaeffler Group makes a key contribution to Mobility for tomorrow with high- precision components and systems in engine, transmission, and chassis applications as well as rolling and plain bearing solutions for a large number of industrial applications. The company generated sales of approximately 13.2 billion Euros in 2015. With around 85,000 employees, Schaeffler is one of the world's largest technology companies in family ownership and, with approximately 170 locations in 50 countries, has a worldwide network of manufacturing locations, research and development facilities, and sales companies. As a global development partner and supplier, Schaeffler maintains stable long-term relationships with its customers and suppliers. The Schaeffler Group follows a growth strategy aimed at profitable above-market growth. At the core of this growth strategy are top quality, outstanding technology, and strong innovative ability, in doing business with customers as well as in the group's internal processes. Schaeffler identifies key trends early on, invests in researching and developing new, forward-looking products, takes them to volume production, and defines new technology standards.

Divisions and business divisions

Schaeffler develops and manufactures precision products for approximately 60 sectors around the world. Its technologically advanced components and systems are used in applications in vehicles, machinery, plants, as well as in aerospace applications. The group distributes its products and services to numerous auto- motive manufacturers and industrial customers.



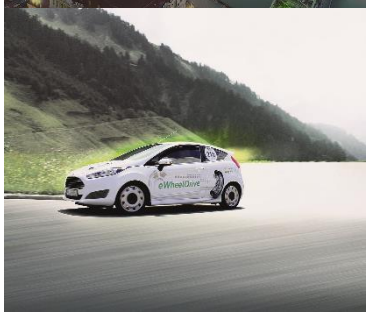


Mobility for tomorrow

Globalization, urbanization, digitalization, scarcity of resources, renewable energy, and the growing demand for affordable mobility are leading to changed, much more dynamic market requirements and business models. Based on these megatrends, the Schaeffler Group has developed its "Mobility for tomorrow" strategy concept, under which the company focuses on four areas across divisions and regions: eco-friendly drives, urban mobility, interurban mobility, and the energy chain.

Schaeffler plays an active part in shaping these focal areas through its own research and development activities and, as a leading expert in innovation and technology, offers an attractive product range to its customers and business partners.

The group's broad portfolio of products and services ranges from components and systems for automotive drive trains to products for high-speed trains and from rolling bearings for solar power plants to innovative solutions for aerospace applications.

FLEXIFORCE HUNGARY KFT.

Address: 4024 Debrecen, Medvefű u. 24.
Webpage: www.flexiforce.com

FLEXIFORCE – Everything (and more) for overhead doors

FlexiForce established in 1980 is an ambitious, multinational company with subsidiaries in the Netherlands, Hungary, Spain, Italy, Poland, China, Turkey, USA, Canada and the United Kingdom. We are specialized in offering hardware parts, automation, panels and hardware systems for residential (garage) and industrial overhead doors. We believe in the market opportunities of our worldwide customers: independent, often local or regional, door producers.

We support door companies in offering competitive door solutions. Our core competences lie not only in the design and quality of the products and systems, but even more in understanding the need for an efficient supply chain of products. Meaning to have each hinge, hardware set, industrial door opener and more, available within optimal lead-time and transport distance. This is facilitated through our production and warehouse facilities in Canada, United States of America, United Kingdom, the Netherlands, Spain, Hungary, Turkey, Italy, Poland and China.

In 2015 we have opened a new, state-of-art production plant of 15.000 m2 in the city of Debrecen in Eastern Hungary. The facility comprises warehouse, production and offices. Winding of torsion springs, spring assembly, roll forming of angles and tracks, bending of curves and assembly of industrial and residential hardware sets are the core of the production department. Out of FlexiForce Hungary we are ready to offer supply chain service in ISC (industrial) and RSC (residential) hardware sets to OEM-customers all over Europe. The local sales team serves customers in Hungary and surrounding countries.

Our “close to the costumer” strategy with local warehouses and local teams in place is helping our customers to successfully compete in their own market. In that way we grow our mutual business!

FLEXLINK SYSTEMS KFT.

Address: HU-1131 Budapest, Rokolya str. 1-13.
Phone: (+36) 20 666 7008
info.hu@flexlink.com

Webpage: www.flexlink.com

FlexLink is a world-class factory automation expert.

Working closely with global customers, we provide innovative, automated solutions to produce goods smarter, safer and at lower operating costs.

Headquartered in Gothenburg, Sweden, FlexLink has operating units in 30 countries and is represented in more than 60.

In 2015, FlexLink had 840 employees and a turnover of € 204 million.
.

The partner network has been an important strategic element of FlexLink's business model since the start in 1980, enabling the company to enhance efficiency at factories in more than 60 countries worldwide.

- 840 **employees**
- 30% of employees are **women**
- 50% have a **university degree**
- **Operating units** in 30 countries
- **Partner network** in more than 60 countries
- More than **8000 installations** worldwide;
  many for leading brands within FMCG,
  healthcare, automotive and electronics.

FlexLink is a company of COESIA Group. Coesia is a group of innovation-based industrial solutions companies operating globally, headquartered in Bologna, Italy and fully owned by Isabella Seràgnoli.

Coesia's companies are leaders in the sectors of:

- Advanced automated machinery and materials
- Industrial process solutions
- Precision gears

Coesia's customers are leading players in a broad range of industries, including Consumer Goods, Tobacco, Healthcare, Aerospace, Racing & Automotive and Electronics.

Coesia Group consists of fifteen companies:
ACMA, ADMV, CIMA, CITUS KALIX, EMMECI, FLEXLINK, G.D, GDM, HAPA, IPI, NORDEN, R.A JONES, SACMO, SASIB, VOLPAK. The Group has 91 operating units (55 of which with production facilities) in 33 countries, a turnover in 2015 of approx. 1,534 million Euro and 6,000 employees.

www.coesia.com

GRIMAS LTD.

Address: H-1214 Budapest, Puli stny. 2-4.
Phone: +3614205883
Webpage: www.grimas.hu

Trader of industrial material testing equipments and consumables since more than 20 years

Started at 1992 in Austria
Continued at 1993 in Hungary
Expanded at 2008 in Romania
Represented at 2014 in Serbia

23 years ago we started to deal with non-destructive testing equipments, and then slowly we began to deal with all areas of material testing methods, so for now we represent all of the material testing procedures in the field of machine industry. One year before the foundation of the Hungarian Grimas Ltd. our owner established a firm in Austria and five years ago we have a Grimas subsidiary in Romania as well. Our mission is to comply all needs of the field of machine industry-especially in the automotive industry- with material testing equipments, as requested by. To be prepared to fulfil these needs fast and without any trouble in accordance with the highest standards available in the market.

Our main references

Suppliers from automotive industry, auto part producers
- Vehicle producer companies
- Material testing service laboratories
- Educational institutes
- Research and development institutes and laboratories
- Foundries
- Heat treating companies
- Companies from oil-, chemical- and gas industry

Our main suppliers

Interesting facts about us

- we are present in three country, and our outsourced agencies are also working in a number of South East European countries
- in addition to the full spectrum of material testing, we have been dealing with the trade of JUTEC tube bending machines as well
- we have been in the market for over twenty years
- we have ISO 9001 certification
- more than fifty foreign suppliers are represented by our company
- we provide more convenient service to our customers with local repair service
- our colleagues assume a role in the development of the Hungarian material testing as board members of several professional organizations
- professional training courses are organized by us in the cooperation with the most prestigious Hungarian universities

Our sales team

Our six sales managers help to the customers to choose the material test methods and technologies in the field of destructive or non-destructive testing methods. They are mostly engineers who have been acquired their special knowledge and expertise regarding the latest testing technologies by the supplier companies. Every sales person has an own field of expertise, and each of them is a specialist.

HAJDU PUBLIC LIMITED COMPANY

Address: 4243 Téglás, külterület 135/9. hrsz.
Phone: +36 (52) 582-700
Webpage: https: //www.hajdurt.hu
Facebook: https://www.facebook.com/hajduzrt/

Company History

HAJDU Hajdúsági Ipari Zrt.'s forerunner Hajdúsági Iparművek was founded by the Hungarian government in 1952 for the purposes of military industry. In 1957 the company started to build household appliances whose assortment as well export were constantly growing. By manufacturing its own developed as well as licensed products and setting up corresponding machinery it managed to grow into a medium-sized enterprise by the 1980s. After 1998 – with a purpose of using up its free capacities – and after 2002 (primarily due to parts produced by sheet metal forming) the company also opened up to a car industry. In 1993 it was transformed into an incorporated company and in 1994 it was privatized by Hungarian investors. The ISO 9001 quality assurance certification was introduced in 1993, whilst the ISO 14001 environmental management certification was implemented in 2001. In October 2005 HAJDU Hajdúsági Iparművek Rt. split into three separate companies. HAJDU Hajdúsági Ipari Rt. continued to produce traditional products such as hot water storage tanks, washing machines, and spin dryers.

The other two companies

HAJDU Autotechnika Ipari Zrt. deals with metalworking – it characteristically manufactures metal sheet produced automobile parts – and designing as well as manufacturing machine tools.
HAJDU Infrastruktúra Szolgáltató Zrt. operates an Industrial Park which also hosts both of the other HAJDU companies. It occupies quite an extensive area and offers a number of services to the enterprises that have settled there.

In 2006 HAJDU Hajdúsági Ipari Rt. was transformed into a private limited company. In 2008 new branch of business was established, focusing on developing products that use renewable energy as well as launching them onto Hungarian market. This orientation has become one of the company's main strategies. In the same year the company began realizing a two-year investment program, partly financed by European Union, which enabled a significant technological development of the production process. Between 2010 and 2015 HAJDU brand received several awards thus getting recognition for the quality of its product development and business process.

Our mission, philosophy, plans

HAJDU Hajdúsági Ipari Zrt. meets customer demands by providing environmentally friendly household appliances and complex systems that offer a natural helping hand to families, public institutions as well as enterprises. Our goal is to strengthen HAJDU brand's position on regional market and to meet customer demands in Europe as well as in other parts of the World. In order to achieve that we have started following ISO 9001 quality assurance standards in 1993 and ISO 14001 environmental management standards in 2001. Excellent and constant quality of our products as well as their regular development are guaranteed by systematic on-site controls performed by various accredited – both domestic and international – testing institutes (TÜV Rheiland InterCert, VDE, LCIE, etc.) Our company puts a lot of emphasis on environment protection and on minimizing negative impact on the environment. We thus strive to employ an environmentally friendly technology and use resources (materials, energy) in an economical way.

HOYA LENS MANUFACTURING HUNGARY PRIVATE CO.

Address: H – 4700 Mátészalka, Ipari út 18.
Phone: +36-44-418-200
Webpage: www.hoya.com

HOYA Corporation is a diversified, multinational company and leading supplier of innovative and indispensable high-tech and healthcare products. HOYA is active in two main business segments: The Life Care segment encompasses health care areas such as eyeglass lenses and the operation of contact lens retail stores, as well as medical related areas such as intraocular lenses for cataract surgery, medical endoscopes, surgical equipment and artificial bones and implants. HOYA´s Information Technology segment focuses on electronics products for the semiconductor industry and LCD panels, glass disks for HDDs and optical lenses for digital cameras and smartphones. The HOYA Group comprises over 100 subsidiaries and affiliates and over 34,000 people worldwide.

Life Care

HOYA has diversified its business portfolio with its optical technologies providing indispensable products to people´s lives. We strongly believe that by providing enduring solutions that meet needs in areas closely connected to people's lives, such as endoscopes, eyeglass lenses and intraocular lenses, it will be able to bring about changes in the quality of those lives.

Life Care Segment, Health Care

HOYA provides products and services to care for that most important sensory organ- the eye. HOYA started manufacturing eyeglass lenses in 1962 and contact lenses in 1972. Based on the optical and material technologies acquired since 1941, HOYA continues to contribute quality high value-added vision products to people around the world.

Eyeglass lenses

As a global manufacturer of eyeglass lenses, HOYA has passionately driven optical technology innovation with the aim of finding only the best vision solutions.

HOYA´s unparalleled technology creates a profoundly clear vision experience for the progressive lens wearer.
Integrated Double Surface Design (iD), HOYA´s patented, award-winning design technology, separates the surface geometry of progressive lenses into two components: vertical and horizontal, positioned individually on each of the two lens surfaces. Thanks to this technology, HOYA´s premium progressive lenses can be individually designed; each patient´s unique visual and lifestyle requirements can be integrated in the lens design to provide them with the most comfortable and accurate vision, tailored to their individual needs.

HOYA Vision Care Company is a global organization covering 52 countries with a network of over 12,000 employees and over 64,000 active accounts globally.

HOYA Lens Manufacturing Hungary private Co., Mátészalka

HOYA Lens Manufacturing Hungary private Co. is the largest unit of Hoya group in Europe based on the headcount and production volume as well. The past of the company and the nearness of the European market give a geopolitical advantage and stabile future for the company. A Belgian investor bought 50% of Optikai Művek factory's unit in 1991. In 1994 with total ownership the enterprise with mass production has been called Buchmann Optical Művek for 8 years. Hoya has bought the Buchmann-group in 1994, so the plant in Mátészalka also became a member of the japan lens production company. By now the company do partial serving of all affiliated companies in Europe.

LEGO MANUFACTURING KFT.

Address: 4400 Nyíregyháza, LEGO utca 15.
Phone: 0642/505-000

Webpage: www.lego.com/careers

We produce the creative toys of the future in Nyíregyháza

The new LEGO factory in Nyíregyháza has been handed over in 2014, and provides a secure income for hundreds of families and brings joy to millions of children through the toys manufactured here. One of the five LEGO factories of the globe is situated at LEGO street 15 in Nyíregyháza – a site which is not only high-tech and extremely environment-friendly, but its look&feel reflects the world of LEGO toys as well.
The LEGO Group reached a global growth in return of more than 10% yearly in the last 12 years, year after year. This shows that the world is getting more and more open to high-quality creative play experiences, which moves the fantasy of kids and adults alike.
Our mission is to live up to the ever-growing demand, whilst ensuring the high quality we set for ourselves. As our motto since the 1930s says: Only the best is good enough!

Capacity extended

With our new factory we almost doubled our output – the number of moulding machines grew from 356 to 768, while our production area increased from 38 000 square meters to 122 000 m^2. As of today we have about 2 800 employees.
The biggest part of DUPLO toys have been produced at the Nyíregyháza site since years (we even can say to mould all the DUPLO bricks of the planet), but with the new factory, we do already produce LEGO boxes as well.
As demand rises quickly, we have to expand our capacity further. That is why we have already started to expand the factory to more than double size – the investment is scheduled to be finished by the end of 2018 and will add up to a 250 000 square meters manufacturing complex. The expansion will open up more than 1 600 additional jobs by 2020.

Green Factory

According to our 'Planet Promise' we think it is extremely important to preserve our environment for future generations, thus leave the smallest possible traces with our production activities. Several technological solutions help us save drinking water, electricity and make the environment of the factory and work conditions more liveable.

For detailed information about job opportunities at our factory,
please visit the LEGO career site at www.lego.com/careers.

MSK HUNGARY GÉPGYÁRTÓ BT.

Address: 4300 Nyírbátor, MSK tér 1.
Phone: +36 42 511 100
Webpage: www.msk.hu

MSK Covertech Group: The future is what we make it

Innovation is built on tradition. As a family managed business, MSK Hungary Bt, with a headcount of about 350 employees, is a team member of the MSK Covertech Group. MSK offers product-specific packaging and palletizing solutions to a number of industries.

All of our employees are respectful of our customers. We are positive that motivation and flexibility are the key components of successful participation in international competition and that is why we are one of the leading international manufacturers of heavy duty packaging machines and palletizing systems through our worldwide operations.

Value-orientation and an innovative spirit are two of the key factors that have kept the business of the Hannen family of Germany on a growth trajectory for the last 40 years. MSK offers its customers the treasure of its unique experience accumulated during the production of almost 5 000 units of packaging equipment sold. Driving innovation in our work requires us to keep expanding our current limits. MSK has experienced and creative project teams also in the field of product development who rely on their comprehensive industry competence to develop unique and outstanding packaging solutions. Owing to our state-of-the-art manufacturing methods (particularly at the central site in Nyírbátor) and continuous investments MSK stands for quality, productivity and relentess improvement.

MSK's factories count among the most modern in the industry. Accordingly, in 2010, we expanded the production area at the Nyírbátor site by approximately 5,000 m2 thus reaching 21,000 m2, we installed a modern and environment-friendly powder disperser unit and we consistently renewed our CNC equipment fleet. We have recently invested approximately HUF 1 billion including the purchasing of new manufacturing equipment and the extension of our office building. Further development projects, such as the enhancement of our production capacity and the construction of a modern training center, are in the pipeline. MSK is a pioneer in a number of areas demonstrated by the high number of international patens registered by us that are exemplary for the entire industry.

MSK Hungary Bt. – Nyírbátor: The magic of mechanical engineering

Our relentless search for quality, innovation and reliability has made MSK one of the leading international experts of packaging and logistics systems.

MSK means the following:

- customer-specific palletizing and packaging machines
- proprietary corporate software
- complete equipment and system solutions
- development, production, servicing: all from one supplier

Information about our most recent news, development initiatives and open positions is available at:

- www.msk.hu

NYOMDA-TECHNIKA KFT

Address: Debrecen , Böszörményi út 6.
Phone:+36 52 416-695

Webpage: www.nyt.hu

Our company deals with engineering and technical assistance which provides service for modernprinting production.We have gained our experience in Hungary's largest bookprinting factory, Alföldi Nyomda. Since 1991 we have estabilished working contacts with most Hungarian printing houses and also with those in surrounding countries.Apart from repair-work and maintenance we design and manufacture waste-paper handling systems, production monitors,and we are resellers of printing machinery and accessories.

Printing Machinery:

As part of our service we install second-hand printing machines, perform removal jobs, design and produce special equipment. We maintain and repair all kinds of machines in the printing and finishing processes.

Main tasks:

- Installation and commission of new printing and binding machinery and equipment
- Dismantling, repairing, overhauling, installation and commission of used printing and binding machinery and equipment
- Manufacturing spare parts
- Grinding and reconditioning guillotine and three-knife trimmer knives, milling tools.

Air-technical assistance:

Our company designs, manufactures and installs paper waste extraction systems. Over the last 19 years, we have installed more than 300 different sizes of waste-paper extraction systems in Hungary and aboard.

Main tasks:

Design ,Manufacture and Installation:

- Waste-paper handling systems, industrial extraction systems
- Noise-reducing coating,
- Dye supplier systems, energetic supplier systems.

Trade office:

We also deal with distribution of the printing accessories. Our profile includes resale of all kinds of accessories that are needed for priting houses.

Main tasks:

Resale of printing machinery and accessories for paper cutting:

- Cutting knives, cutting sticks
- Rubber products (suckers, trundle)
- Humidity and water threatment systems, paper waste baler machines adapted for customers' needs and requests.

ROBERT BOSCH AUTOMOTIVE STEERING KFT.

Address: H-3300 Eger, Kistályai út 2.
Phone: +36 36 510 930
Webpage: www.bosch.hu

As an automotive supplier, we produce steering gears, steering columns, I-shafts and reconditioned parts to 109 vehicle manufacturers worldwide, both for passenger cars and commercial vehicles.

Our company was operating in Eger between 2003-2014, under the name ZF Lenksysteme Hungária Kft. It has grown steadily in line with market demands and the ever-increasing order volume.

Since its foundation, the company was involved in the assembly and reconditioning of components. Based on our solid production results, in 2012, beyond hydraulic steering gears we were entrusted with new production tasks. In 2013, preparations started for the manufacturing and assembly of the EPSapa electric steering systems and their parts. A new site was built in Maklár, 10 km from Eger, also close to the motorway. The plant was opened in 2014. With this, we have expanded into a dual-based company.

The new manufacturing activities were set up at Maklár plant, while the hydraulic products stayed in Eger. 2014 was spent with the implementation of the production hall and also the installation and the alignment of machines. In May 2015 we started the serial production of racks and steering nuts for the electrical steerings. Beyond the traditional products, for year 2016 we planned the production of 1,1 mio steering systems, which quantity is expected to be growing in the next years.

In 2014 Bosch announced the acquisition of ZFLS group. Our company was registered as Robert Bosch Automotive Steering Kft. in April 2015.

SECO TOOLS KFT

Address: 1115 Budapest, Bártfai u. 54
Phone:+36-1-267-6720
Webpage: www.secotools.com

WHO WE ARE.

FOUNDED IN SWEDEN.

Our origins can be traced back to the Swedish mining industry, when Fagersta Bruks', a helve hammer, was established by the river Kolbäcksån in 1611.
The 400 years since were spent developing and applying expertise. In 1932, Fagersta Bruks AB introduced a new product called 'Seco', the Latin phrase for 'I cut'.
Four years later, Seco was established as a separate company unit and has since grown to become the global provider known in today's market. Since 2012, Seco has been part of Sandvik, a Swedish global engineering group dedicated to your productivity and profitability.

GLOBALLY SUCCESSFUL.

Seco operates in more than 40 countries, and with distributors and agents in an additional 35 countries, Seco has a truly global presence. And with 5,000 employees worldwide, it goes without saying that being close to you is the key to providing the advanced solutions you need.

A SYNONYM FOR ADVANCED METAL-CUTTING TECHNOLOGY.

We use our comprehensive know-how to provide advanced technology and tool solutions. On average, we invest approximately 3% of our turnover in R&D – which means that innovation is a part of our corporate culture. Our solutions enable you to succeed in your own markets by ensuring the optimisation and efficiency of your production processes.

A GLOBAL FAMILY

Seco is a global family present in more than 75 countries and originating from Fagersta in Sweden.

HOW WE THINK.

TOGETHER, WE MAKE IT EASIER.

We make things easier for you by being more than just a cutting-tool provider. We provide advanced products and services and are fully dedicated to understanding your operations, in order to deliver the best solutions for your specific needs.

CONTRIBUTING TO YOUR SUCCESS.

We understand that success in today's manufacturing environment requires more than a focus on tools. We are dedicated to also understanding and identifying with your challenges, and providing the unique personal engagement that results in a true and lasting partnership.

SHARED VALUES: UNITING THE SECO FAMILY.

5,000 people are members of the global Seco family, united by our shared values. First comes our family spirit. This means that we maintain an open and friendly workplace and share our knowledge. Next is a passion for you. Which means that we always focus on you, not us. And number three: personal commitment. This means that we ensure you always see our dedication in your individual Seco contact person.

TWO FACETS, ONE VISION

We always aim to combine the best of both worlds: the commitment to expertise and our advanced tool solutions.

WHAT WE PROVIDE.

PRODUCT PORTFOLIO.

With our extensive range of products, we provide solutions for all sizes and scopes of metal cutting applications. Our comprehensive offering includes solutions for milling, turning, grooving and parting off, threading, drilling, reaming, boring and advanced materials. And our array of toolholders provides optimum performance in every type of application through a variety of tooling solutions.

SERVICE PORTFOLIO.

Our advanced services ensure that we comprehensively meet all machining challenges. Component Engineered Tooling tailors solutions to your operations, while our Custom Products ensure that you always get the ultimate tool for your unique application. The Seco Technical Education Programme provides effective training to increase product-competences for every level of expertise. Additionally, the SecoPoint™ system supports you in managing your inventory. 'My Pages' puts the power of Seco at your fingertips. From product availability to cutting data to test reports, all of this information and more is available anytime, anywhere through this comprehensive digital portal.

COMPREHENSIVE SERVICES

Reaching your goals includes advanced services.

SPM INSTRUMENT-BUDAPEST KERESKEDELMI ÉS SZOLGÁLTATÓ KFT.

Address: 1173 Budapest, Búbosbanka u. 5/C
Phone: +3612560435
Webpage: www.spminstrument.com

About SPM Instrument AB
Since its 1970 inception, SPM Instrument has been at the frontline of technical development and has continuously presented new measuring techniques and instruments. Today, measuring equipment from SPM can be found in industries all over the world.
40 years ago, SPM created the original shock pulse method, True SPM®. This technique is commonly recognized as the best method for measuring bearing condition on rotating machinery.
Modern technology has made it possible to further develop True SPM® and so now SPM®HD enters the market. SPM Instrument is also the inventor of EVAM®, Evaluated Vibration Analysis Method, developed to enable large scale, cost-efficient condition monitoring of industrial machinery.
The SPM head office is located in Strängnäs, Sweden, where R&D as well as production and market support are found. Strängnäs also is the basis of the Swedish sales organization

About SPM Budapest Kft
Our company has been working in the Hungarian market since 1992. We introduced the SPM online and offline tools in the different areas of industry. Our references are in the ALCOA-KÖFÉM Ltd., Matra Power Plant Co., MOL Petrochemicals, BorsodChem Co., COCA-COLA, SAPA Profiles Ltd, Carl-Zeiss Vision Hungary Ltd. and etc,.

SPM Instrument presents HD ENV® - a new era in vibration monitoring

A new achievement in vibration monitoring technology, HD ENV® is an ideal complement to traditional vibration analysis. Capable of detecting at a very early stage such machine problems which are generally difficult to find in good time with conventional non-enveloping techniques - for example gear and bearing damages - the method utilizes cleverly engineered and patented algorithms for digital signal processing, preserving the true highest peak of the vibration signal. Signals buried in machine noise are revealed through high definition digital enveloping, extracting and enhancing the signals of interest from the overall machinery vibration signal.
Building on over four decades of experience and innovation, HD ENV® provides outstanding performance with the latest innovative technologies. The unit of measurement is HD Real Peak, a scalar value expressed in decibels. Representing the true amplitude levels found in the envelope signal, HD Real Peak is the primary value to use for determining the severity of a given damage. It is also used for triggering alarms. Using order tracking and symptom enhancement, applying FFT on the signal is very useful to determine the source of the signal. Spectrums and time signals are marvels of clarity, providing a snapshot of machine condition to give the maintenance department a heads-up on potential problems.

The setup of HD ENV® measurements in the diagnostic software is straightforward. A set of predefined filters are available for easy selection; each designed to detect damages or anomalies in different stages of development. HD ENV can be used to monitor applications in the 15-20,000 RPM range.

HD ENV® enables the detection of gear and bearing faults very early on in the damage process, making it possible to closely monitor the development throughout the stages. Significantly extending the planning horizon for predictive maintenance, the method is a boost to maintenance efficiency. The HD ENV® technique can be used with existing vibration transducer installations and thus quickly and easily integrates into existing industrial infrastructures.

HD Real Peak ***HD Time Signal*** ***HD Spectrum***

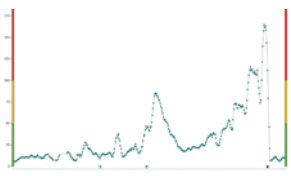
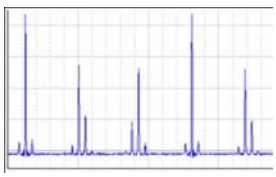
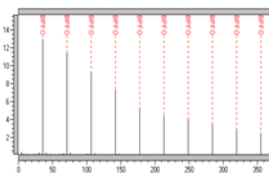

SZIMIKRON LTD

Address: H-6000 Kecskemét, Szegedi út 49. HUNGARY
Phone: +36 76 484 100
Webpage: www.szimikron.com

Szimikron ltd. designs and manufactures linear systems and ballscrews offering solutions for different sectors of industry, e.g. machine-tools, automotive, medical industry, automation.

BALLSCREWS

The ballscrew is the motion transmission unit of machine tools and several machinery structures, transforming the rotational motion into linear motion with a high rate of efficiency, ensuring in addition high accuracy, loadability, rigidity and durability.

TRAPEZOID SPINDLES – ACME SCREWS

Serving for the actuation duties at traditional machine tools and devices, for the general requirements of machine production, where simple and reliable motion transmission is required.

LINEAR MOTION SYSTEMS

Our compact modules are the most modern representatives of today's Linear Motion Systems. They can be integrated as a finished module without the effort usually needed for balancing the guide and drive element during installation into the machine. This ease of mounting applies to all our linear motion systems.

HYDRAULIC POWER CHUCKS

Patented innovation: **TAF…** type **programmable power chucks** are the result of a developement project led by Szimikron with Miskolc University machine-tool faculty according to the innovation of prof. Dr. Tajnafői.
The major advantages of the new automatic jaw adjustment chucks:

Novelty: no such hydraulic chucking machine has appeared on the market yet up to now that could safely perform these duties without the significant modifacion of the machine.

Automated: changeover to different diameters requires no manual interaction.

Fast: the adjustment of the three jaws takes place at the same time, so the operation requires three times less time as a minimum related to any previously applied methods.

Universal: the chuck makes automatic changeover possible within its entire diameter range.

Interchangeable: it is simply installable into the place of other traditional hydraulic chucks, the necessary additive elements are provided together with the chuck.

Productive: the dynamically balanced chucks make high cutting speed possible.

TAKATA SAFETY SYSTEMS HUNGARY KFT

3516 Miskolc, Takata út 1.
06-46-407-900
www.takata-miskolc.hu
www.takata.com

Our dream

At Takata, we dream of a world with zero fatalities from traffic accidents. We understand the importance of every individual and hope to one day experience a global community where everyone recognizes the true value of human life.

Takata is a leading global supplier of automotive passenger safety systems (products include steering wheels, airbag systems, seat belts, electronics, sensors, interior trim, child restraint systems) and supplies all major automotive manufacturers in the world. Headquartered in Tokyo, Japan, Takata is currently operating 57 plants in 20 countries and employs more than 50,530 people, every one of whom is committed to turning innovative ideas into reality.

Our common goal is to reduce the number of fatalities in road traffic accidents to zero. We develop and manufacture products that help keep people safe when travelling on today´s roads, aiming to provide optimum safety on the move, with a range of products for occupant and pedestrian protection. For many decades, we have been pioneering innovative technologies – producing our first seat belts in 1952 and starting the development of airbags as early as 1969. TAKATA's mission is the development of innovative products according to high quality standards, which helps to meet the highest satisfaction of the customers.

„Our mission – your safety."
There is no end to thinking about safety in today's automotive society. As a company that makes seat belts, airbags, child seats and other products that protect life, we are aware of our responsibilities to society and want to contribute to attaining the goal of creating a world that is safe. To do this, we will continue creating and further evolving safety products and systems that people can rely on. At Takata, we would be delighted developing our safety products in a world where they never had to be used, where traffic accidents do not occur anymore. That is the dream that drives us every day.

TAKATA at Miskolc
The latest step toward realizing our dream has been the establishment of Takata Safety Systems Hungary Kft. in October, 2013. This new plant is our first in Hungary and the 17th in Europe and it is located in the city of Miskolc, at the Miskolc South Industrial Park. Takata Safety Systems Hungary Kft. started production of airbag technology at this new facility in October 2014. The company's investment in the new plant is € 68.3 M, with a 25 hectares big ground and up to 60.000 sqm built-in area.

The number of the new employees at Miskolc is already more than 1000, who produce lifesaving automotive technology products, such as complete airbag modules, airbag components and inflators for car manufacturers across whole Europe. The new facility also features state-of-the-art systems for product development, testing, quality control and customer service.

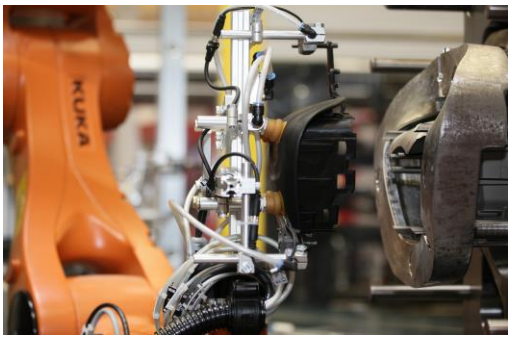

T-DRILL OY

Address: Ampujantie 32 FI-66400 Laihia Finland
Phone: +358 6 475 3333
Webpage: http://www.t-drill.fi/

T-DRILL is the world-class supplier of tube and pipe fabrication solutions. T-DRILL machinery consists of both industrial solutions for several customer segments as well as portable solutions for mechanical contractors and plumbers. In short, T-DRILL is there whenever the machine tools of a tried and trusted supplier are needed.
One of T-DRILL's cornerstones is the ability to foresee customers' needs and supply the right machine tools for their purposes. Supplying the right tools means that the special features of the tools meet the customers' special needs – a hand-operated machine tool for smaller purposes or an entire production line as a complete solution for industry.
We are glad to help you to find a solution for your tube and pipe manipulation requirements. In our webpage you may find some typical industries and applications, where T-DRILL machinery is used.
Our company is represented in Hungary by Gyula Szepessy, e-mail: szepessy@sbn.hu Phone:+36-30-9489377

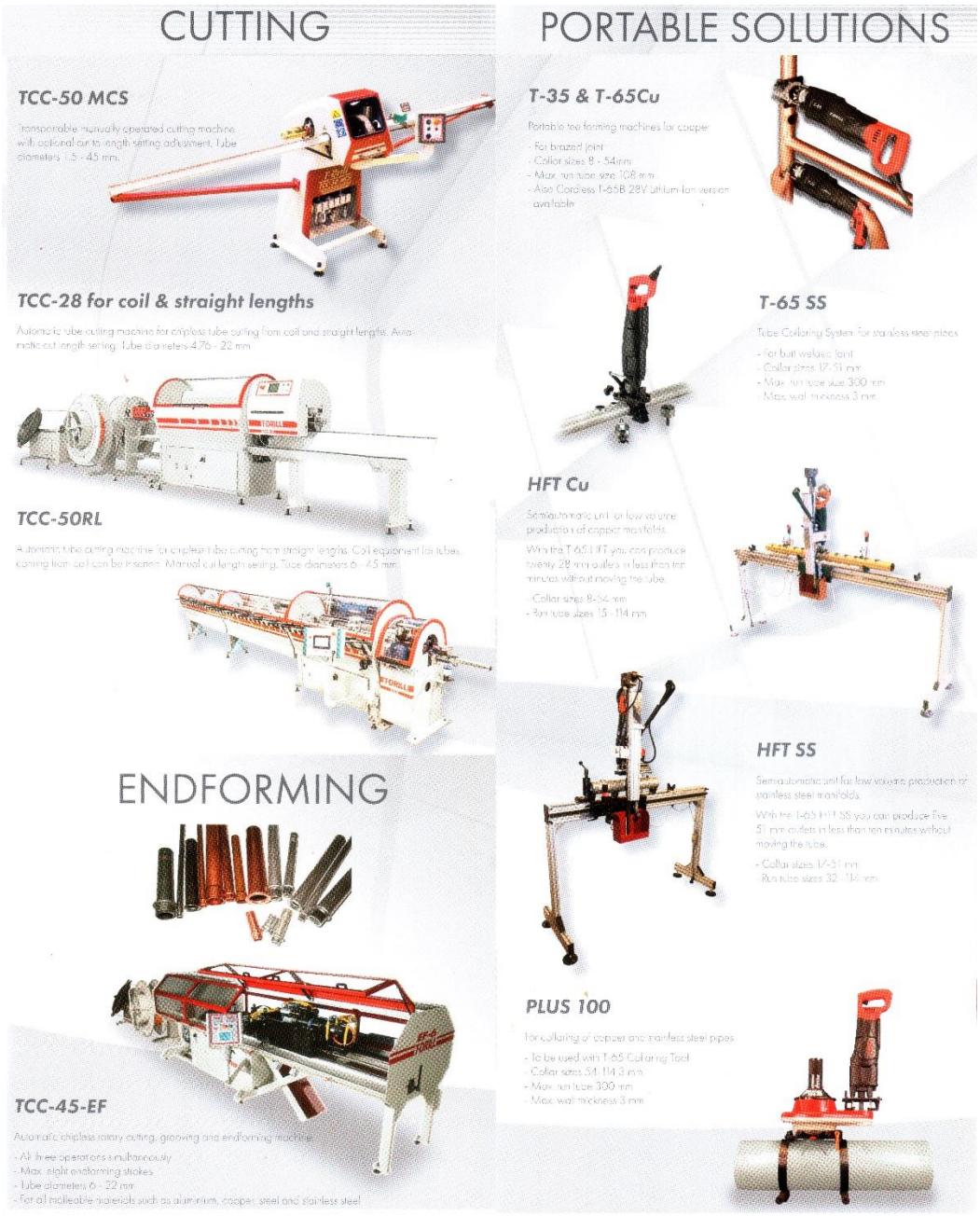

TEVA PHARMACEUTICALS LTD.

Address: H-4042, Debrecen, Pallagi út 13.
Phone: + 36 52 515 100
Webpage: http://www.teva.hu

In the Hungarian market, Teva is one of the pharmaceutical companies with the broadest product portfolios; its products of excellent quality help the treatment of cardiovascular, gastrointestinal, urulogic and oncologic conditions.

Teva has outstanding manufacturing capacity and world-class research activity in Hungary. The company produces both active pharmaceutical ingredients and finished dosage products at its Hungarian sites, in Debrecen, Gödöllő and Sajóbábony, furthermore its Budapest-based unit coordinates Hungarian pharmaceutical commerce.

TEVA's Debrecen site performs manufacturing and R&D activity. We produce tablets, gel-coated tablets, capsules and soft-gel products in considerable volume, which are sold on the Hungarian and mainly on foreign markets. Furthermore we produce high-quality pharmaceutical raw materials for our own use and also for export in large amounts. In addition to manufacturing, we carry out high-standard research and development in the fields of both generic and innovative products.

Our Sajóbábony site is engaged in manufacturing pharmaceutical raw materials.

TEVA's Gödöllő site manufactures parental pharmaceutical products – infusions and eyedrops etc.

Our Budapest site is responsible for the coordination of Hungarian commercial operations. We are working to make our world-class preparations available in Hungarian hospitals and pharmacies. We are proud that every seventh Hungarian patient is cured with Teva preparations.

TEVA Pharmaceuticals is considered one of the most stable employers of Hungary. TEVA is continuously improving its Hungarian production and packaging capacity and its research base through significant investments. Providing employment for 3000 people and offering competitive salary, a wide range of social benefits and other allowances to its employees, our company belongs to the largest and most attractive employers of the regions concerned.

The company operates a system of fringe benefits including a variety of items, and offers further exemplary allowances for its employees: variable salary depending on personal performance and company results, interest-free housing allowance, company resorts, etc.

We place great emphasis on the continuous development of our excellent professional staff, as we believe: a good expert represents the highest value.

With two affiliated university departments, a cooperative program and a professional practice program, we aim to provide the talented future career starters with assistance towards successful integration into the world of work.

TRANZIT-FOOD KFT

Address:H-426 Debrecen, Jókai u.1.
Phone:+36(42)269101
Webpage: www.goldenfood.info.hu

With 25 years of experience, we offer our premium meat Goose and Duck products from full vertical integration. The meat Goose (Golden Goose), which has its own genetic line, and the Cherry Walley Duck parent stock provides an adequate basis for high-quality Goldenfood brand. We produce 5million Ducks and 2 million Goose yearly.

Our Company is the largest waterfowl hatchery with modern technology in Central-Eastern Europe, which efficiently provides the ducklings and goslings needs of our 42 pcc own farms. We raise our meat Geese and Ducks with good care.

Our feed mill has a key roll in feeding both the parent- and the slaughter stock with proper quality feed, so the quality of the meat for consumption is fully provided.

Prime raw material results in prime final product, so as a part of the process we operate our own processing plant, where we produce further-processed products in addition to the primary processing, we organise the delivery from our own coldstore.

Our company, which employs more than a thousand people, gives a lot of attention to provide continuous qualification for our well-prepared and trained staff, so the market needs can be satisfied more and more.

We place a great emphasis on animal welfare and environment, we believe that our activities contribute to keep the ecological balance.

Thereby, we have the right tools and systems from the parent stock to the consumer, we guarantee the full traceability.

The Tranzit Food Ltd. is commited to development and progress. In the spirit of our long-term strategy,

and to fill the requirements of our Customers, Partners,we offer further processed products in our product range.

Additionally the traditional-pre-baked,boneless, halved rosted duck, we offer halved roasted goose, and marinated goose breast fillet.

We are more than happy to meat the requests of our Partners, our professional team is open to achieve all market-driven idea, and development.

TRUMPF HUNGARY KFT.

Address: H-2220 Vecsés, Lincoln u. 1.
Phone: +36 29 999 100

Webpage: www.trumpf.com

The high-technology company TRUMPF provides manufacturing solutions in the fields of machine tools, lasers and electronics. These are used in the manufacture of the most diverse products, from vehicles, building technology and mobile devices to state-of-the-art power and data storage. TRUMPF is the world technological and market leader for machine tools used in flexible sheet metal processing, and also for industrial lasers.

With around 11,000 employees, the company generated sales in the 2014/15 fiscal year of €2.72 billion. The company's development ratio in relation to sales of 9.8 percent is far above the average for the industry. The high value placed on research and development at TRUMPF and its long-term approach, characteristic of an independent, family-owned business, make it a guarantor of continuous innovative strength.

Machine tools for flexible sheet metal and tube processing form the core business of the TRUMPF Group. The product portfolio includes machines for bending, punching, combined punch and laser processing, laser cutting, and laser welding applications. Diverse automation solutions and a broad range of software round off the portfolio.

In the laser technology business field, TRUMPF provides high-performance CO_2 lasers, disk and fiber lasers, direct diode lasers, ultrashort pulse lasers, and also marking lasers and marking systems. The product range also features laser systems for the cutting, welding and surface treatment of three-dimensional components.

The product palette of the electronics business field includes DC, high and medium frequency generators for inductive material heating, surface coating and surface processing via plasma technology, as well as for laser excitation.

The family company is headquartered in Ditzingen near Stuttgart, Germany. The TRUMPF Group is represented by about 70 subsidiaries in all of the world's leading markets. Production facilities are located in Germany, France, Great Britain, Italy, Austria, Switzerland, Poland, the Czech Republic, the USA, Mexico, China and Japan.

UNILEVER HUNGARY

Address: 182. Váci street, 1138 Budapest
Phone: +36 1 465 93 00
Webpage: www.unilever.hu, www.unilever.hu/careers-jobs/

BRIGHT FUTURE - MADE BY YOU

LOVED THE WORLD OVER

Unilever is one of the largest fast-moving consumer goods (FMCG) companies in the world. We take care of the whole supply chain of our products, from development and sourcing right through to production, marketing and distribution. Over 169 000 employees around the world bring this operation to life – HR, Customer Management (Sales), R&D, Finance, Marketing, Supply Chain and more all working together towards a common vision. Our loved brands, like Dove, Axe, Lipton or Knorr, to name a few, are sold in 190 countries, and are used by two billion people daily.

AMBITIOUS – FOR THE PLANET

Unilever has a clear purpose: to build a brighter future for our world. We believe that being ambitious in business goes hand in hand with being ambitious for humanity and the environment. Business has a fundamental role in caring for the future of the planet. Unilever's vision is to double our size, while reducing our environmental footprint and increasing our positive social impact. Brands can be powerful influencers of behaviour and positive drivers of change. We can look deeply into what ours can mean for people and the world. This way it becomes not just about washing clothes, for example, but doing so using less water at lower temperatures. It is not just about how personal hygiene can make you clean and healthy, but how it can improve your self-esteem. Brands like Dove do exactly these things.

MAKE A DIFFERENCE

We have big ambitions about how our business can help create a bright future for our world, but to make it happen we need great people who can challenge the way things are done, bring new ideas, and dare to make big decisions. If you want to make a difference, Unilever is the place to come:

Unilever Future Leaders Programme (UFLP): The Unilever Future Leaders Programme is about developing tomorrow's leaders, today. It is designed to grow you into a manager, through hands-on learning alongside world-class experts. You'll be hired into a function and develop your leadership skills by working on live projects which offer you all the experience you need to become ready for your first management role.

Unilever International Internship Programme (UIPP): This is a world-class 6-month internship in one our Marketing, Finance, or Supply Chain functions.

Local Internship Programmes: We also offer local Internship Programmes across Europe in a broader range of functions: Marketing, Finance, Supply Chain Management, HR Management, Customer Management (Sales)

UNILEVER IN HUNGARY

Unilever was one of the first major international investors which appeared in 1991 in Hungary where it has three factories: the Nyírbátor household chemical factory, the Veszprém ice cream factory and the Röszke food factory. The company employs more than 1700 employees, its net sales last year exceeded HUF 51 billion, and its profit after tax in 2015 was over 6 billion Hungarian forints.

THE NYÍRBÁTOR HOUSEHOLD CHEMICAL FACTORY is one of Unilever's largest and most cost-effective European factories in the household chemical sector. 85% of the production, that is daily 50 truckloads of product is exported, shipped to a number of countries. Popular brands produced in Nyírbátor include, among others, Domestos, Cif, Floraszept or Coccolino. Local Internship Programmes open for university technical students throughout the year. https://www.unilever.hu/karrier/

VENTIFILT LÉGTECHNIKAI ZÁRKÖRŰEN MŰKÖDŐ RÉSZVÉNYTÁRSASÁG

Address: 4080 Hajdúnánás, Fürdő str. 2-4.
Phone: + 36 52 381 166
Webpage: www.ventifilt.hu

VENTIFILT Air Engineering Plc. is a market-leader industrial firm, which manufactures air engineering and environment appliances. Since 2010 the company is part of the **Videoton** Group (www.videoton.hu), a Hungary-based Central and Eastern European industrial group that offers manufacturing and manufacturing related services to industrial companies.

Our firm works since its establishment in mechanical engineering. Our main activities are: manufacturing of appliances for air engineering, air clearness, decrease environment-staining.
The product range of Ventifilt includes radial and axial fans, dust separators (cyclones, filters, washers) and pipelines.
We have got references in industrial branches (energetics, woodworking, cement, tobacco, food processing industries, environmental protection) and agricultural engineering.
Despite having own products, Ventifilt also works as a contract manufacturer for many well-known companies in industrial air engineering, especially on the export markets like Germany, Great-Britain, France, Austria etc. Here, the main advantage of Ventifilt over many other suppliers is the fact that Ventifilt is able to provide a significantly wider and higher level of service due to its background. We work together with our foreign partners in English and German languages.
We can receive documentation both in traditional form (paper) and in form of CAD systems per e-mail. Our designing department (working with design-system type Autodesk Inventor® 3D) and our ca. 140 experts support the manufacturing in high quality, short manufacturing date, and fulfilment of special customers' requirements, further manufacturing of goods in small and middle ranges.
Thanks its exceptionally stable financial background, Ventifilt is also continuously developing its manufacturing and engineering capabilities through various investments in order to further solidify its long-term competiveness on the market.

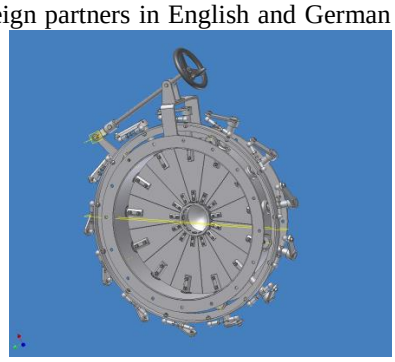

We work at our own site of 83 000 m^2 (inside areas: ca. 10 000 m^2). We manufacture our goods with modern, common & special CNC-driven machinery, technics from different materials (alloy steel, incorrodible, acid-proof, heat constant steels). We ourselves plan and produce the required individual tools & adjusting devices.
Our industrial textile confection makes confection of technical & filter textiles for special filters. We have special surfacings (galvanize, nickelize, chrome, eloxal processes) made by our reliable co-operation-partners, who confirm their competence by after years of co-operation for us & our clients.

Our vacant job can be found on this website: http://www.ventifilt.hu/index.php/hu/karrier
If you want to share in our success, let's join in it!

ZF HUNGÁRIA KFT.

Address:H-3300 Eger, Kistályai u. 2.
Phone: +36 36 520-100

Webpage: www.zf.com/hu

ZF HUNGÁRIA KFT.

ZF is a global leader in driveline and chassis technology as well as active and passive safety technology. The company acquired TRW Automotive on May 15, 2015, which was then integrated within the organization as the Active & Passive Safety Technology Division. The combined company reported sales of €29.2 billion in 2015 and now has a global workforce of around 135,000 with approximately 230 locations in some 40 countries. ZF annually invests approximately five percent of its sales in Research & Development (€1.4 billion in 2015) ensuring continued success through the design and engineering of innovative technologies. ZF is one of the largest automotive suppliers worldwide.

The company was founded in 1915 for the development and production of transmissions for airships and vehicles. Today, the group's product range comprises transmissions and steering systems as well as chassis components and complete axle systems and modules. As stockholders, the Zeppelin Foundation - which is administered by the City of Friedrichshafen - holds 93.8 percent and the Dr. Jürgen and Irmgard Ulderup Foundation Lemförder holds 6.2 percent of shares.

We have developed ZF Hungaria Kft. consistently in the years since its establishment in 1995. In our factory the parts are made on semiautomatic machining centers. We have one of the largest and most modern heat treatment shop in Hungary, one part of our capacity is utilised by other companies as well. On our new assembly lines a special IT system helps the employee in performing work processes precisely and in quality conrol. In the automatic high shelf warehouse of our logistic center we do storing in and storing out with robot technology. The material supplying is carried out in pull system, the delivery of parts is managed by the work rhythm of assembly work, so the whole process is in optimal rhythm. Parallel with modernization of production also the product development takes place in Eger. There are also an engineering centre, workshop and test-bench on the location, so the creations designed by engineers on the computer can be realized in practise and can be tested in laboratory and highway conditions. With our products and knowledge of our specialists we represent Hungary all over the world and with our purposeful improvements we provide for that, this representation should be high level and worthy of recognition.

DEPARTMENT OF MECHANICAL ENGINEERING
FACULTY OF ENGINEERING, UNIVERSITY OF DEBRECEN

2-4 Ótemető Debrecen, H-4028 Hungary

The Department of Mechanical Engineering is responsible for the mechanical engineering education on bachelor (BSc) and master (MSc) levels. The research activity of the department covers the mechanical engineering scientific area starting from the materials science to the specific fields (diagnostics, material handling, etc.). From 2015 we have introduced the dual training cooperating with 16 industrial partners.

Department staff:

Tamás MANKOVITS PhD head of department associate professor *mechanics* *finite element method* 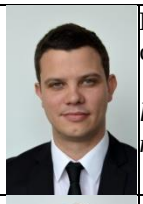	**Lajos FAZEKAS PhD** college professor *logistics,* *machine repairing* 	**Zsolt TIBA PhD** college professor *machine elements* 
Ágnes BATTÁNÉ GINDERT-KELE PhD associate professor *manufacturing,* *machine elements* 	**György JUHÁSZ PhD** associate professor *machine elements,* *hydraulics and pneumatics* 	**Sándor BODZÁS PhD** college associate professor *manufacturing,* *machine elements* 
Sándor PÁLINKÁS PhD assistant professor *materials science,* *manufacturing* 	**Sándor HAJDU** assistant professor PhD student *material handling,* *mechanics* 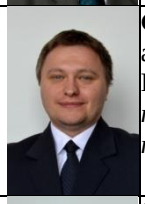	**Gábor BALOGH** assistant lecturer PhD student *materials science,* *manufacturing* 
Zsolt BÉKÉSI assistant lecturer PhD student *machine elements* 	**Krisztián DEÁK** assistant lecturer PhD student *diagnostics,* *mechanics* 	**József MENYHÁRT** assistant lecturer PhD student *process analysis,* *computer aided design* 
István SZÉKÁCS department teacher *manufacturing,* *technology* 	**Márton LÉVAI** department teacher *materials science,* *technology* 	**Péter BALSA** department engineer *manufacturing,* *machine elements* 
András GÁBORA department engineer PhD student *materials science,* *technology* 	**Dávid HURI** department engineer PhD student *mechanics,* *finite element method* 	**Gyula Dávid LOVADI** department engineer *manufacturing,* *technology* 
Tamás Antal VARGA department engineer *mechanics,* *computer aided design* 	**Judit BAK** administrative assistant 	

Contacts:

Department of Mechanical Engineering
Faculty of Engineering, University of Debrecen
2-4 Ótemető Debrecen, H-4028 Hungary

Tel.: +3652415155
E-mail: gepeszmernok@eng.unideb.hu
Website: www.eng.unideb.hu/userdir/gepesz

DEPARTMENT OF MECHANICAL ENGINEERING
FACULTY OF ENGINEERING, UNIVERSITY OF DEBRECEN
2-4 Ótemető Debrecen, H-4028 Hungary

Mechanical Engineering BSc Program
Automotive Production Process Control Specialization

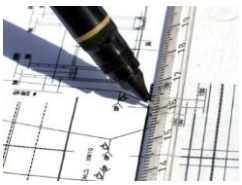

The aim of the teaching program includes preparing engineers to improve quality and use lean tools in the vehicle industry, enabling them to gain an understanding of the complete product development (from the supplier to the customer) and lead project teams. In cooperation with local vehicle suppliers students learn about completing cost estimation, utilizing computer software to solve manufacturing problems.

Our graduates will develop **competence or acquire knowledge** in the following areas:

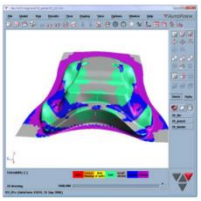

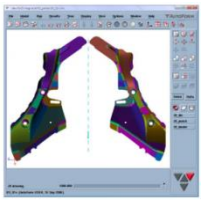

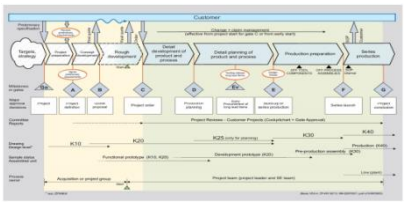

- introducing and applying modern technologies, computational engineering methods and systems (manufacturing technologies, CAE)
- operating and developing mechatronical systems (electrotechnics and electronics, measuring and automatics, hydraulics and pneumatics)
- designing and redesigning plant layouts, checking KPI systems robot technology, automation, etc.
- planning material handling and manufacturing processes
- analyzing, controlling and optimizing production processes
- applying modern manufacturing management philosophies (Lean management) in the vehicle industry

The **curriculum** contains the following **subject modules**:

Basic science subjects: 48 credits

- Mathematics, Technical Mechanics, Engineering Physics, Operation and Theory of Machines, Thermodynamics and Fluid Mechanics, Technical Chemistry

Economics and humanities subjects: 20 credits

- Economics for Engineers, Microeconomics, Basics of Quality Management, Management for Engineers, State Administration and Law, Introduction to Ethics

Professional subjects: 117 credits

- Informatics, Machine Elements, CAD and CAE, 3D Computer-Aided Design, Materials Science, Technology of Structural Materials, Electrotechnics and Electronics, Thermal and Fluid Machines, Manufacturing Processes, Logistics, Industrial Safety, Computational Engineering Methods and Systems, Measuring and Automatics, Hydraulics and Pneumatics, Mechanical System Engineering, Quality Management, Safety Engineering, Material Handling and Robotics, CAM, Manufacturing Planning, Maintenance Engineering, PLC.

Optional subjects: 10 credits

Thesis: 15 credits

Duration of studies: 7 semesters, Contact hours: 2.352
ECTS credits: 210, Internship: 6 weeks

Final exam:

- Defending the thesis (oral presentation and discussion)
- Exam in two subject areas chosen by the student
  - Production Process and Control, Production Optimization, Logistics
  - Assembling Technology, CAM, Quality Management

DEPARTMENT OF MECHANICAL ENGINEERING
FACULTY OF ENGINEERING, UNIVERSITY OF DEBRECEN
2-4 Ótemető Debrecen, H-4028 Hungary

Mechanical Engineering BSc Program
Operation and Maintenance Specialization

The aim of the teaching program is to train mechanical engineers who are able to operate and maintain machines and mechanical devices, introduce engineering technologies and apply them, organize and control work phases, mechanical developments, solve the general problems of research and planning as expected by the labor market. Those having completed the specialization have in-depth theoretical knowledge to continue their studies in the second cycle.

Our graduates will develop **competence or acquire knowledge** in the following areas:

- introducing and applying modern technologies and computational engineering methods and systems (manufacturing technologies, CAE)
- operating and developing mechatronical systems (electrotechnics and electronics, measuring and automatics, hydraulics and pneumatics)
- operating and maintaining machines and mechanical devices (mechanical system engineering, heat and fluid machines)

- organizing and controlling operational processes, mechanical developments
- planning the construction and designing of the machine parts, devices and apparatus (machine element, CAD, finite element method)
- solving the general problems of research and planning as expected by the labor market (studies of administration and law, basics of quality assurance, management for engineers, safety engineering)
- carrying out diagnostic testing, assessing the reliability of machines and devices (fracture mechanics, non-destructive testing and diagnostics)

The **curriculum** contains the following **subject modules**:

Basic science subjects: 48 credits
- Mathematics, Technical Mechanics, Engineering Physics, Operation and Theory of Machines, Thermodynamics and Fluid Mechanics, Technical Chemistry

Economics and humanities subjects: 20 credits
- Economics for Engineers, Microeconomics, Basics of Quality Management, Management for Engineers, State Administration and Law, Introduction to Ethics

Professional subjects: 117 credits
- Informatics, Descriptive Geometry, Technical Drawing, Machine Elements, CAD and CAE, 3D Computer-Aided Design, Materials Science, Technology of Structural Materials, Electrotechnics and Electronics, Measurements and Automatics, Thermal and Fluid Machines, Manufacturing Processes, Logistics, Industrial Safety, Steel Constructions, Hydraulics and Pneumatic Machines, Fracture Mechanics, Manufacturing Planning, Diagnostics, FEM, PLC, Material Handling and Robotics, Drivetrain Optimization, Machine Repairing, Maintenance Engineering.

Optional subjects: 10 credits

Thesis: 15 credits

Duration of studies: 7 semesters, Contact hours: 2.352
ECTS credits: 210, Internship: 6 weeks

Final exam:
- Defending the thesis (oral presentation and discussion)
- Exam in two subjects chosen by the student
  - Machine Repairing,
  - and one subject chosen by the student:
    - Material Handling and Robotics
    - *or* Maintenance Engineering

DEPARTMENT OF MECHANICAL ENGINEERING
FACULTY OF ENGINEERING, UNIVERSITY OF DEBRECEN
2-4 Ótemető Debrecen, H-4028 Hungary

Mechanical Engineering MSc Program
Production Engineering Specialization

The aim of the teaching program is to train engineers who are able to design and elaborate production processes and the conceptions of manufacturing technologies as well as can be responsible for modelling, designing, operating, maintaining, supervising and organizing production tasks. They are capable of providing the conditions of precise and up-to-date production and its processes (optimizing and developing production processes; designing and implementing devices and systems serving the production). The specialization considers the needs of the partner industrial companies.

Our graduates will develop **competence or acquire knowledge** in the following areas:

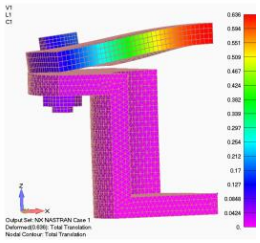

- applying modern computational engineering methods (CAD, CAM, CAE)
- supporting, optimizing and developing production systems and processes;
- designing of manufacturing and material handling systems,
- applying management methods and systems,
- supervising and organizing in production environment,
- applying expert systems (diagnostics and condition monitoring).

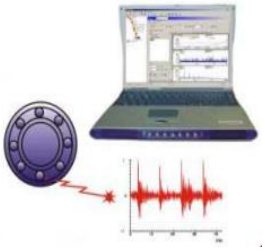

The **curriculum** contains the following **subject modules**:

Basic science subjects: 22 credits
- Mathematics, Applied Statistics, Modern Physics, Dynamics of Mechanical Systems, Thermodynamics and Fluid Mechanics, Advanced Material Science

Economics and humanities subjects: 16 credits
- Basics of Management, Quality Management, Financial and Advanced Economic Knowledge, Research Methodology

Professional subjects: 46 credits
- Measurement, Signal Processing and Electronics, Design of Engineering Structures, Engineering Modelling and Simulation, Manufacturing Equipments, Design and Quality Assurance of Manufacturing Processes, Assembly Automation, Design of Material Handling Systems, Production Logistics, Maintenance and Machine Repairing Technologies, Diagnostics and Condition Monitoring, Lean Production

Optional subjects: 6 credits
Thesis: 30 credits
Duration of studies: 4 semesters, Contact hours: 1.428
ECTS credits: 120, Internship: 4 weeks

Admission requirements for the Mechanical Engineering MSc program

Unconditional admission: Mechanical Engineering BSc:
Conditional admission by prescribing pre-master courses:
Materials Engineering BSc, Safety Engineering BSc, Energy Management BSc, Civil Engineering BSc, Industrial Design Engineering BSc, Vehicle Engineering BSc, Light Industrial Engineering BSc, Environmental Engineering BSc, Transportation Engineering BSc, Mechatronics Engineering BSc, Earth Science Engineering BSc, Technical Management BSc, Chemical Engineering BSc, Electrical Engineering BSc, Mechanical Engineering in Agriculture and Fodd Industry BSc

Final exam:
- Defending the thesis (oral presentation and discussion)
- Exam in two topics chosen by the student :
  - Production systems and processes (Design of Material Handling Systems, Production Logistics, Lean Production)
  - Manufacturing systems and processes (Manufacturing Equipments, Design and Quality Assurance of Manufacturing Processes)
  - Maintenance and operation (Maintenance and Machine Repairing Technologies, Diagnostics and Condition Monitoring)

PHOTO GALLERY OF THE ISCAME 2016 AND THE EXHIBITION

THE ISCAME 2016 CONFERENCE

PHOTO GALLERY OF THE ISCAME 2016 AND THE EXHIBITION

THE ISCAME 2016 CONFERENCE

PHOTO GALLERY OF THE ISCAME 2016 AND THE EXHIBITION

THE 4th MECHANICAL ENGINEERING INDUSTRIAL EXHIBITION

PHOTO GALLERY OF THE ISCAME 2016 AND THE EXHIBITION

THE 4th MECHANICAL ENGINEERING INDUSTRIAL EXHIBITION

PHOTO GALLERY OF THE ISCAME 2016 AND THE EXHIBITION

THE 4th MECHANICAL ENGINEERING INDUSTRIAL EXHIBITION

PHOTO GALLERY OF THE ISCAME 2016 AND THE EXHIBITION

THE 4th MECHANICAL ENGINEERING INDUSTRIAL EXHIBITION

Welcome in Debrecen for the

5th International Scientific Conference on Advances in Mechanical Engineering (ISCAME 2017)

and

5th Mechanical Engineering Exhibition

The Department of Mechanical Engineering
Faculty of Engineering, University of Debrecen